Realistic Evaluation Methodology for Large-Break LOCA of the APR1400

APR1400-F-A-TR-12004-NP-A

August 2018

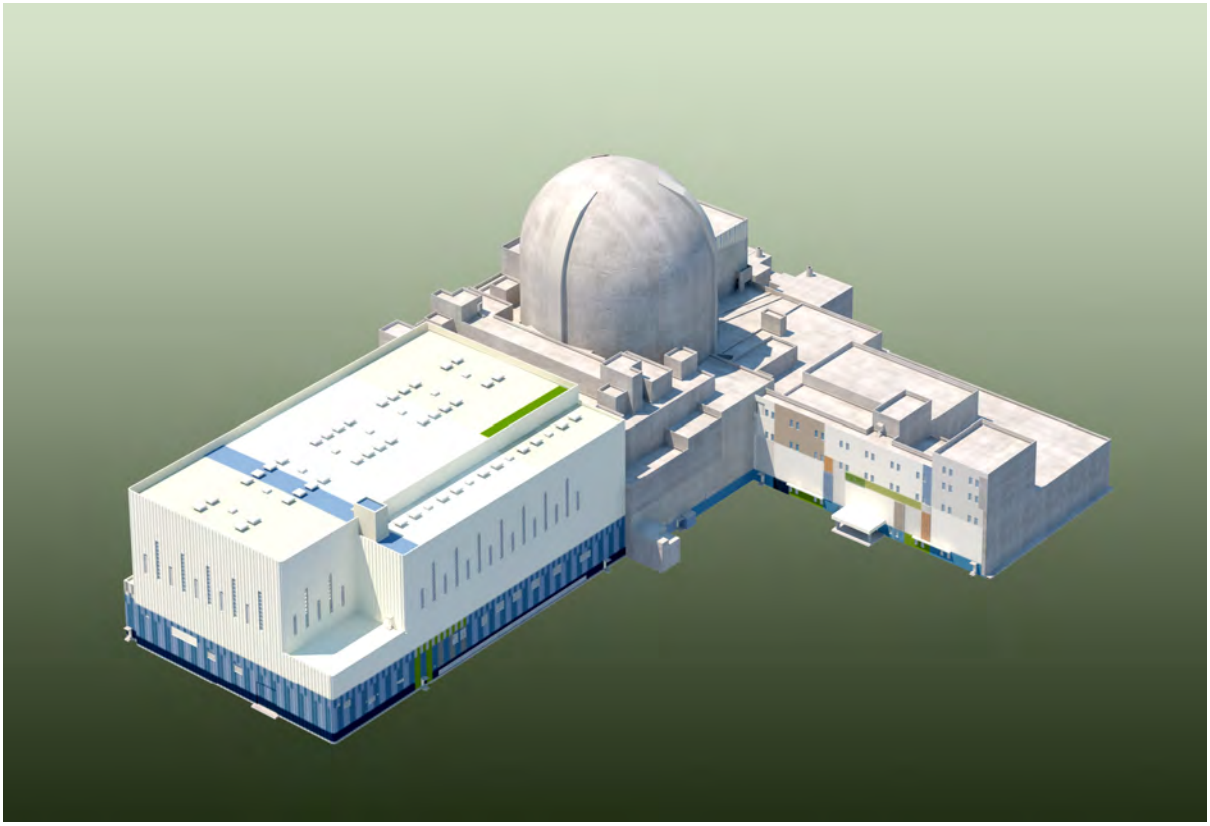

KOREA ELECTRIC POWER CORPORATION
KOREA HYDRO & NUCLEAR POWER CO., LTD

Non-Proprietary

CONTENTS

SECTION DESCRIPTION

Non-Proprietary

SECTION A

Page intentionally left blank

UNITED STATES
NUCLEAR REGULATORY COMMISSION
WASHINGTON, D.C. 20555-0001

July 31, 2018

Mr. Yun-Ho Kim, Project Manager
APR1400 Design Certification
Advanced Reactors Development Laboratory
Korea Hydro and Nuclear Power Co., Ltd.
70-1312-gil, Yuseong-daero
Yuseong-Gu, Daejeon
34101 Korea (Republic of)

SUBJECT: ADVANCED POWER REACTOR 1400 FINAL SAFETY EVALUATION FOR TOPICAL REPORT APR1400-F-A-TR-12004, REVISION 1, "REALISTIC EVALUATION METHODOLOGY FOR LARGE-BREAK LOSS OF COOLANT ACCIDENT OF THE APR1400"

Dear Mr. Kim:

The U.S. Nuclear Regulatory Commission (NRC) staff has prepared a final topical report (TR) safety evaluation (TRSE) for Topical Report APR1400-F-A-TR-12004, Revision 1, "Realistic Evaluation Methodology for Large-Break Loss of Coolant Accident of the APR1400." This TRSE is also valid for the non-proprietary version of the TR. This action is supported by the letter dated June 15, 2018 (Agencywide Documents Access and Management System Accession No. ML18166A269), whereby the Advisory Committee on Reactor Safeguards agrees with the NRC staff's conclusions, within the limits and conditions that are specified in the TRSE. This evaluation is in support of the review of the APR1400 design certification application submitted by Korea Hydro and Nuclear Power Co., Ltd. (KHNP) and Korea Electric Power Corporation on December 23, 2014.

The staff requests that KHNP publish the accepted enclosed proprietary and non-proprietary versions of this TR within one month of receipt of this letter. The accepted versions shall incorporate this letter and the enclosed final TRSE after the title page. Also, they must contain historical review information, including NRC requests for additional information and your responses. The accepted versions of the TR shall include an "-A" (designated accepted) following the report identification number.

If the NRC's criteria or regulations change such that its conclusion that the accepted TR is invalidated, KHNP and/or the applicant referencing the TR will be expected either to revise and resubmit its respective documentation or to submit justification for continued applicability of the TR without revision of the respective documentation.

Document transmitted herewith contains sensitive unclassified information. When separated from the enclosure, this document is "DECONTROLLED."

If you have any questions or comments concerning this matter, please contact me at (301) 415-7038, or via e-mail at William.Ward@nrc.gov.

Sincerely,

/RA/

William Ward, Senior Project Manager
Licensing Branch 2
Division of Licensing, Siting,
and Environmental Analysis
Office of New Reactors

Docket No. 52-046

Enclosure:
As stated

cc: w/o encl. see next page

SUBJECT: ADVANCED POWER REACTOR 1400 FINAL SAFETY EVALUATION FOR TOPICAL REPORT APR1400-F-A-TR-12004, REVISION 1, "REALISTIC EVALUATION METHODOLOGY FOR LARGE-BREAK LOSS OF COOLANT ACCIDENT OF THE APR1400" DATED: July 31, 2018

DISTRIBUTION:

D101	RidsNroLaCSmith	RidsOgcMailCenter Resource
Public	RidsNroOd	RidsACRS_MailCTR Resource
LB2 R/F	CLauron, NRO	SVrahoretis, OGC
RidsNroDnrl	WWard, NRO	RidsNroDnrlLb2
JGilmer, DSRA	JMonninger, NRO	RKaras, NRO
TDrzewiecki, DSRA	SLu, DSRA	

ADAMS Accession Nos.
Letter: ML18180A327 *via e-mail NRO-002

OFFICE	DLSE/LB2: PM	DLSE/LB2: LA	DLSE/LB2: PM
NAME	CLauron*	IBetts*	WWard
DATE	07/30/2018	07/24/2018	07/31/2018

OFFICIAL RECORD COPY

KHNP Mailing List

7/4/2018

Daegeun (Tony) Ahn
Director
KHNP Washington DC Center
8100 Boone Blvd, Suite 620
Vienna, VA 22182

E-mail

yunho.kim@khnp.co.kr [Yun-Ho Kim]
hansang.kim@khnp.co.kr [Hansang Kim]
dohwan.lee@khnp.co.kr [Do-Hwan Lee]
junghokim@khnp.co.kr [Jung-Ho Kim]
jiyong.oh@khnp.co.kr [Jiyong Andy Oh]
ahn.daegeun@khnp.co.kr [Daegeun Tony Ahn]
jksuh@khnp.co.kr [Jeong Kwan Suh]
hachewung@khnp.co.kr [Che Wung Ha]
kang.deogji@khnp.co.kr [Deog Ji Kang]
sunguk.kwon@khnp.co.kr [Sun Guk Kwon]
ptmaster300@kepco.co.kr [Hyun Chul Park]
sisk1rb@westinghouse.com [Rob Sisk]
robert.sweeney@consultant.aecom.com [Robert Sweeney]

FINAL SAFETY EVALUATION BY
THE OFFICE OF NEW REACTORS
(REVISED)
Topical Report APR1400-F-A-TR-12004-P
"Realistic Evaluation Methodology for Large-Break Loss of Coolant Accident of the APR1400"

Korea Hydro & Nuclear Power Co. Ltd

TOPICAL REPORT APR1400-F-A-TR-12004-P
"REALISTIC EVALUATION METHODOLOGY FOR LARGE-BREAK LOSS OF COOLANT ACCIDENT OF THE APR1400"

TABLE OF CONTENTS

LIST OF TABLES

LIST OF FIGURES

ACRONYMS AND ABBREVIATIONS

Acronym	Definition
ADAMS	Agency-wide Documents Access and Management System
AI	audit issue
APR	Advanced Power Reactor
ARO	all rod out
ASME	American Society of Mechanical Engineers
ATLAS	Advanced Thermal-hydraulic Test Loop for Accident Simulation
B&PV	Boiler and Pressure Vessel
BEMUSE	Best Estimate Methods - Uncertainty and Sensitivity Evaluation
BETHSY	Boucle d'Etudes Thermo-Hydraulique Système
BOC	beginning of cycle
CAMP	Code Applications and Maintenance Program
CAREM	code-accuracy-based realistic evaluation methodology
CCF	counter current flow
CCFL	counter current flow limitation
CCTF	Cylindrical Core Test Facility
CFR	Code of Federal Regulations
CHF	critical heat flux
CLI	cold leg injection
CLS	cold leg split
CSAU	Code Scaling Applicability and Uncertainty
CWO	core wide oxidation
DC	Design Certification
DCD	Design Control Document
DECLG	double ended cold leg guillotine
DOBO	downcomer boiling
DVI	direct vessel injection
ECC	emergency core cooling
ECCS	emergency core cooling system
ECCW	emergency core cooling water
EDG	emergency diesel generator
EM	evaluation model
EMDAP	evaluation model development and assessment process
FCT	fuel centerline temperature
FLECHT	Full Length Emergency Core Heat Transfer
FOM	figure of merit
HFP	hot full power
HTC	heat transfer coefficient
IET	integral effects test
INEEL	Idaho National Engineering and Environmental Laboratory
IRWST	in-containment refueling water storage tank
KHNP	Korea Hydro and Nuclear Power
KNGR	Korea Next Generation Reactor
L/D	length to diameter
LBLOCA	Large-break loss-of-coolant accident
LHGR	linear heat generation rate
LOBI	LWR Off-Normal Behaviour Investigation
LOCA	loss of coolant accident

Acronym	Definition
LOFT	Loss of Fluid Test
LOOP	loss of offsite power
LTCC	long term core cooling
MCO	maximum cladding oxidation
MIDAS	Multi-dimensional Investigation in Downcomer Annulus Simulation
MLO	maximum local oxidation
NA	not applicable
NEPTUN	Swiss LWR THTF facility for reflood experiments – see NUREG/IA-0040
NFI	Nuclear Fuel Industries
NRC	Nuclear Regulatory Commission
NSSS	nuclear steam supply system
PCT	peak cladding temperature
PIRT	phenomena identification and ranking table
PKL	PWR Integral System Test Facility
PWR	pressurized water reactor
QA	quality assurance
QAPD	Quality Assurance Program Description
RAI	request for additional information
RCP	reactor coolant pump
RCS	reactor coolant system
Ref.	Reference
RES	NRC Office of Regulatory Research
RG	Regulatory Guide
RPV	reactor pressure vessel
SEASET	Separate Effects and Systems Effects Tests
SER	Safety Evaluation Report
SET	separate effect test
SG	steam generator
SGS	steam generator simulator
SI	safety injection
SIP	safety injection pump
SIT	safety injection tank
SIT-FD	SIT Fluidic Device
SKN	Shin-Kori Nuclear Power Plant
SRP	Standard Review Plan
SRS	simple random sampling
TCD	thermal conductivity degradation
THTF	Thermal Hydraulic Test Facility
TR	Topical Report APR1400-F-A-TR-12004
UGS	upper guide structure
UO_2	uranium dioxide
UPTF	Upper Plenum Test Facility
VAPER	Valve Performance Evaluation Rig

1. INTRODUCTION

By letter dated January 7, 2013, Korea Hydro and Nuclear Power Company, Ltd. (the applicant) requested to the United States Nuclear Regulatory Commission (NRC) review and approval of Topical Report APR1400-F-A-TR-12004-P, Revision 0 (TR [1]) [Ref. 1] (see NRC's Agency-wide Documents Access and Management System (ADAMS)). By letter dated August 11, 2017 (Reference 13), the applicant submitted a revision to the TR which included updates to address the U.S. Nuclear Regulatory Commission (NRC) staff's requests for additional information (RAIs) [Refs. 7, 8, 9, 10] to which KHNP responded [Ref. 11]. This TR describes the applicant's evaluation methodology (EM) for the analysis of a large-break loss-of-coolant accident (LBLOCA) for the Advanced Power Reactor 1400 (APR1400) design. The applicant will reference the TR in future licensing actions, including the APR1400 Design Certification (DC) application.

The TR describes the applicant's calculation methodology used to evaluate the LBLOCA event for the KHNP APR1400 nuclear steam supply system (NSSS) during the blowdown, refill, and reflood stages. This TR does not address long term core cooling following such an event. The KHNP methodology for long-term core cooling is addressed separately in Technical Report APR1400-F-A-NR-14003-P, "Post-LOCA Long Term Cooling Evaluation Model" [Ref. 2].

As part of the NRC evaluation of the TR, the NRC staff identified a number of technical issues that were discussed with the applicant as Audit Issues (AI) [Ref. 3] to which KHNP responded [Ref. 4, 5, 6].[2] The NRC staff and KHNP subsequently discussed these RAIs and AIs during and following several NRC Audit Meetings [Ref. 12]. These discussions ultimately resulted in the issuance of TR Revision 1 [Ref. 13] by the applicant.

The objective of this Safety Evaluation Report (SER) is to provide an assessment of the technical adequacy of the methodology described in the TR for use in LBLOCA licensing calculations. The determination of technical adequacy is based on the NRC guidance and regulations as outlined in:

- NUREG-0800, "Standard Review Plan for the Review of Safety Analysis Reports for Nuclear Power Plants," Compiled 2007, (the SRP) - specifically Chapter 15 [Ref. 14]
- Title 10 *Code of Federal Regulations* (10 CFR) 50.46, "Acceptance criteria for emergency core cooling systems for light-water nuclear power reactors" [Ref. 15]
- Regulatory Guide (RG) 1.157 "Best-Estimate Calculations of Emergency Core Cooling System Performance," [Ref. 17]
- RG 1.203 "Transient and Accident Analysis Methods" [Ref. 18]
- NUREG/CR-5249, "Code Scaling, Applicability and Uncertainty" (CSAU) [Ref. 19]

[1] In this SER, TR refers to Topical Report APR1400-F-A-TR-12004, and is not used simply as an abbreviation.

[2] The attachments to Reference [3] contain material in the Korean language; however, the information contained in the also-attached English language documents was found to be adequate by the staff, and were relied upon for the purpose of the present review and assessment.

2. REGULATORY EVALUATION

Title 10 of the *Code of Federal Regulations* (10 CFR), Part 50, "Domestic Licensing Of Production And Utilization Facilities," Section 46, Paragraph (a) specifies that each boiling or pressurized light-water nuclear power reactor fueled with uranium oxide pellets within cylindrical Zircaloy or ZIRLO cladding must be provided with an Emergency Core Cooling System (ECCS) designed so that the calculated cooling performance following a postulated LOCA conforms to the criteria set forth in 10 CFR 50.46(b). The regulations in 10 CFR 50.46(a) also stipulate that the requirements can be met through an evaluation model (EM) for which an uncertainty analysis has been performed:

> *...the evaluation model must include sufficient supporting justification to show that the analytical technique realistically describes the behavior of the reactor system during a loss-of-coolant accident. Comparisons to applicable experimental data must be made and uncertainties in the analysis method and inputs must be identified and assessed so that the uncertainty in the calculated results can be estimated. This uncertainty must be accounted for, so that, when the calculated ECCS cooling performance is compared to the criteria set forth in paragraph (b) of this section, there is a high level of probability that the criteria would not be exceeded.*

The regulation 10 CFR 50.46(b) requires that:

- the Peak Cladding Temperature (PCT) shall not exceed 2200°F
- the calculated total oxidation of the cladding shall nowhere exceed 0.17 times the total cladding thickness before oxidation
- the calculated amount of hydrogen generated from chemical reaction of the cladding with water or steam shall not exceed 0.01 times the hypothetical amount that would be generated if all of the metal in the cladding surrounding the fuel, excluding the cladding surrounding the plenum volume, were to react
- calculated changes in core geometry shall be such that the core remains amenable to cooling
- calculated core temperature shall be maintained at an acceptably low value and decay heat shall be removed for the extended period of time required by the long-lived radioactivity remaining in the core.

The NRC has provided guidance on how these requirements can be met. RG 1.157 and NUREG/CR-5249 describe acceptable approaches that may be used to determine the uncertainty in the calculated parameters.

Additional guidance is provided in Standard Review Plan (SRP) Section 15.0.2, "Review of Transient and Accident Analysis Methods." Also, the guidance in RG 1.157 applies to the review of best-estimate methodology.

The information in the SRP is complementary to RG 1.203, which provides guidance to applicants on the standards expected by the NRC regarding transient and accident methods submittals. In SRP Section 15.0.2 and RG 1.203, the review of methods for the analysis of

transients and accidents includes a review of the submitted (or modified) EM consisting not only of the computer program(s) used in the analysis, but also of all associated aspects of the calculation framework, including mathematical models, assumptions, assignment of parameter values, and the treatment of input and output data. Both documents clearly delineate the items to be included in the submittal and the acceptance criteria upon which the applicant's documentation is evaluated.

RG 1.157 provides specific guidance for applicants regarding best-estimate accident analysis of emergency core cooling (ECC)[3] systems, which is clearly applicable to this TR. This review is conducted in accordance with the details in RG 1.157 and SRP 15.0.2.

As stated in SRP Section 15.0.2:

> *…licensees must analyze transients and accidents in accordance with the requirements of 10 CFR 50.34, 10 CFR 50.46, and where applicable, per NUREG-0737, "Clarification of TMI Action Plan Requirements." ... This section of the SRP describes the review process and acceptance criteria for analytical models and computer codes used by licensees to analyze accident and transient behavior… This review is independent of the type of application submitted (e.g., license amendment, topical report, design certification, or combined license application).*

This review documents the NRC staff evaluation of the applicant's TR, which describes a best-estimate ECCS Code-Accuracy-Based Realistic Evaluation Methodology (CAREM) and its associated EM.

SRP Section 15.0.2 lists six individual areas of review for transient and accident analysis methods. Discussed in each area are the criteria to be used to evaluate the submittal. These review areas are:

- Documentation
- Evaluation Model
- Accident Scenario Identification Process
- Code Assessment
- Uncertainty Analysis
- Quality Assurance Plan

The following sections provide an overview of how these six individual topics were considered in this evaluation.

2.1 Documentation

The SRP Section 15.0.2 states that the documentation must be scrutable, complete, unambiguous, accurate and reasonably self-contained in how it describes the codes and methods present in the EM. The SRP recommends that certain topics be specifically addressed:

- An overview of the methodology and associated EM

[3] The terms 'ECC', 'ECCS', and 'ECCW' are used interchangeably throughout this document, as well as in the applicant's documentation. All refer to the emergency core cooling system.

- A complete description of the accident scenario
- A complete description of the code assessment
- A determination of the code uncertainty
- A theory manual
- A user manual
- A quality assurance plan

Each of the applicable elements of the documentation must be accurate, complete, and consistent. The users' manuals in particular must provide clear and unambiguous guidance (on a scenario-specific basis, if applicable) for selecting or calculating all input parameters and code options.

Evaluation Model

The EM includes all computational and non-computational elements, including not only the computer program at the core of the methodology but also field equations, constitutive and closure relations, and simplifying assumptions used to perform the accident analyses. All of these parts of the methodology should be reviewed to determine their applicability, adequacy, and correctness.

2.2 Accident Scenario Identification Process

This review criterion recommends that applicants use a structured process for the identification and ranking of physical phenomena relevant to the accident scenarios to which the EM will be applied. This process is used to determine the importance of the phenomena by examining their effect upon the figures-of-merit (FOM) calculated. The guidance states that each accident scenario should include a complete and accurate description of its initial and boundary conditions. It should also be confirmed that phenomenological models present in the EM are consistent with the levels of importance attached to the phenomena.

2.3 Code Assessment

The guidance states that the assessment of the codes and code models present in the EM should be conducted over the full range of conditions to which they will be applied and use the same code options that would be employed in actual plant calculations. This assessment process should include separate effects testing, integral effects testing, code-to-code comparisons, and/or comparisons against the results of analytical models. Where applicable, the assessment process should also include scaling analysis to identify any non-dimensional parameters of the analysis, and should evaluate the impact of scaling upon the assessment. Comparisons should be sufficiently thorough such that the possibility of compensating errors is eliminated.

In the code assessment process, the review should confirm that the numerical solution conserves all important quantities and that code options are used appropriately.

Any closure relationships based on experimental data or more detailed calculations must have been assessed by the applicant over the full range of conditions expected to be encountered in the accident scenarios for which the EM will be used.

2.4 Uncertainty Analysis

The applicant should demonstrate in the submittal that all of the important sources of uncertainty in the codes, mathematical models, and experimental data comprising the EM are addressed. In addition, the combined uncertainty of the EM should be less than the design margin for safety of the resulting figures-of-merit. The process used should ensure that the resulting uncertainties in the EM do not exceed the design margins for the safety parameters of interest. Important sources of uncertainty should be identified using the accident scenario identification process.

2.5 Quality Assurance Plan

The guidance states that the applicant shall maintain the EM under a quality assurance program that meets the requirements of 10 CFR Part 50, Appendix B. The SRP guidance includes provisions to ensure that the documentation of the EM includes consideration of the issues of design control, document control, software configuration control and testing, and corrective actions and that independent peer reviews should be conducted at key steps in the development of the EM.

3. SUMMARY OF THE APPLICATION

A brief summary of the content of the TR is provided in this section.

3.1 Overview

In TR Section 1, the applicant introduced their LBLOCA methodology for APR1400, which is referred to as the code-accuracy-based realistic evaluation methodology (CAREM). According to the applicant, CAREM conforms to the guidance in RG 1.157, and consists of three elements and 14 steps as outlined in NUREG/CR-5249. An overall flow diagram of CAREM is shown in Figure 3-1, which is reproduced from TR Figure 1-1.

The TR states that one of the purposes of CAREM is to allow the applicant to quantify the uncertainties in the calculation of the acceptance criteria. This is accomplished in CAREM by propagating the uncertainty of each parameter deemed important for predicting the acceptance criteria. The TR states that CAREM utilizes the PCT, the maximum local oxidation (MLO), and the core-wide hydrogen generation as the LBLOCA acceptance criteria, which is consistent with the requirements of 10 CFR 50.46(b).

The TR states that CAREM is applied using modified versions of the RELAP5/MOD3.3 thermal-hydraulics code [Ref. 20] and the CONTEMPT4/MOD5 containment analysis code [Ref. 21] for the calculation of the APR1400 system thermal-hydraulics and containment back-pressure, respectively. The applicant performed and reported a demonstration calculation for the reference APR1400 plants, Shin-Kori Nuclear Power Plant (SKN) Units 3 and 4 using CAREM with these codes. In addition, the TR includes references to analyses performed by the applicant with previous RELAP5 versions, MOD2 [Ref. 22] and MOD3 [Ref. 23], which have their own unique characteristics, as described in the TR.

TR Section 1 provides a brief overview of the APR1400. It is a pressurized water reactor (PWR) design utilizing a direct vessel injection (DVI) system, a safety injection tank equipped with a fluidic device (SIT-FD), and an in-containment refueling water storage tank (IRWST). Otherwise, it retains the principal features of conventional 2-loop PWRs. Each loop consists of a hot leg, a steam generator (SG), two pump suction legs, two reactor coolant pumps (RCP), and two cold legs.

TR Table 1-1 lists the major system parameters of the APR1400. The core thermal power is 3,983 MW(t), and mass flow rates of the reactor coolant system (RCS) and core are 20,991 kg/s, and 20,361 kg/s respectively (with 630 kg/s through the core bypass region). The active core is 3.81 m long and consists of 241 fuel assemblies. Each fuel assembly utilizes the applicant's proprietary PLUS7 fuel design [Ref. 25], which employs a 16×16 lattice.

The TR states that certain key features of the APR1400 ECCS components and their design are directly relevant to the LBLOCA analysis. They include:

- Direct Vessel Injection (DVI) for all trains of ECCS components,
- Four independent trains of high-pressure safety injection pumps (SIPs),
- Four SIT-FDs,
- Elimination of low-pressure SIP due to the use of the fluidic device, and
- An IRWST which provides the water inventory (source) for the SIPs.

According to the TR, each of the four SIT-FDs and four trains of SIPs inject all the emergency core cooling water (ECCW) into the upper annulus of the reactor pressure vessel (RPV) through the respective DVI nozzles for each combination of SIT-FD and SIP. The four trains of the SIPs are designed to be mechanically and electrically independent. Four emergency diesel generators (EDG) independently provide the power to each SIP. According to the single failure analysis supplied in the TR, three SIPs are assumed operable. However, the analysis presented in the TR assumes that only two SIPs are operational for additional conservatism.

The TR describes the SIT-FD. The fluidic device controls the injection flow as a function of the water level inside the SIT. TR Figure 1-4 shows a schematic diagram of the fluidic device. It is a combination of a standpipe and a vortex chamber. The applicant states in the TR that the SIT-FD provides high injection flow, equivalent to that of a traditional SIT (i.e., accumulator) when the water level is higher than the top of the SIT standpipe. Once the water level falls at or below the top of the SIT standpipe, the SIT-FD provides low injection flow via the vortex chamber with performance that is similar to a conventional low-pressure SIP.

The TR states that refueling water, which is the source of the safety injection, is stored within a lower peripheral region of the containment building. This design is intended to eliminate the need for the traditional switchover from injection to recirculation, and eliminates the potential for breaks outside of containment through the ECCS pathways.

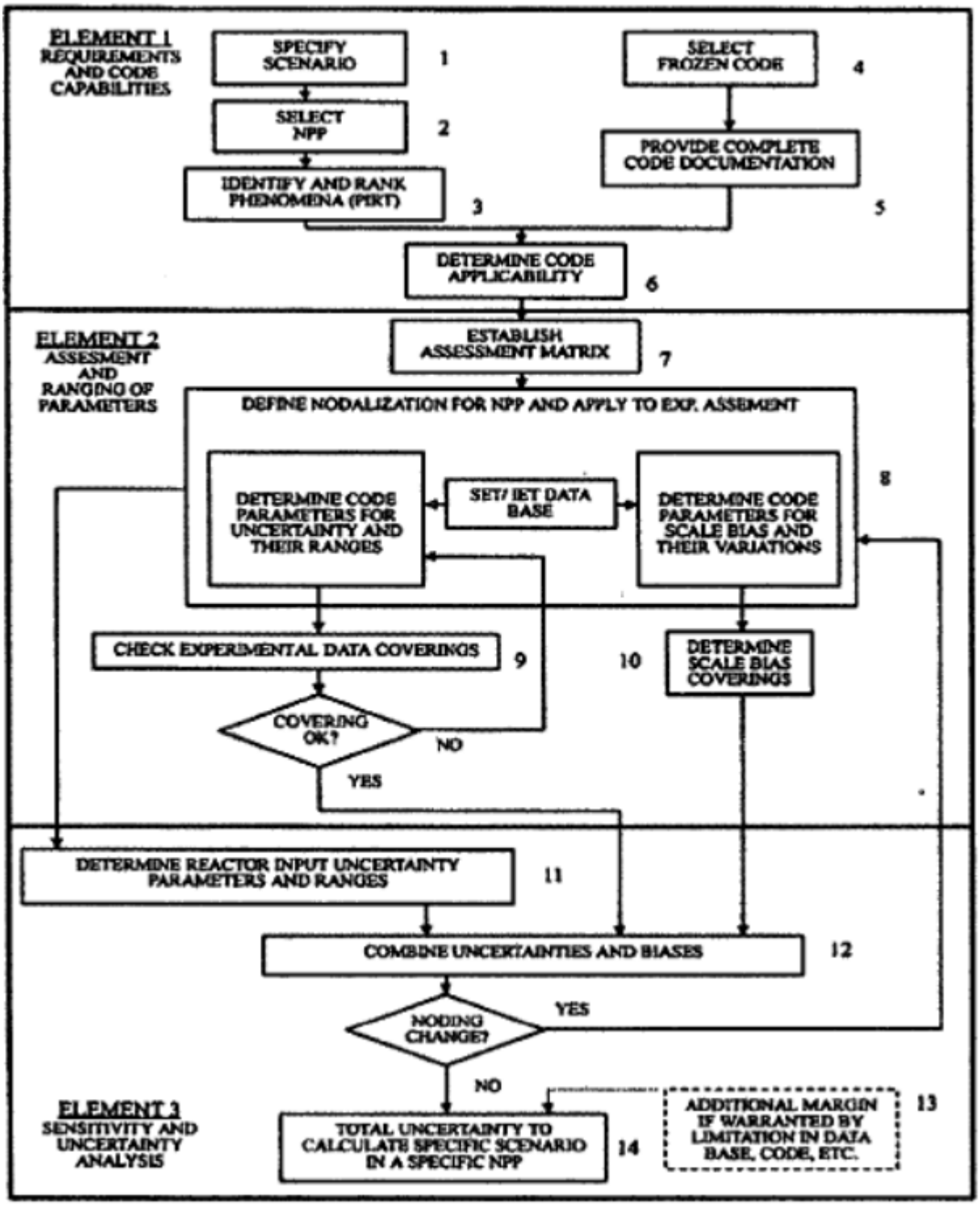

Figure 3-1 CAREM Flow Diagram

3.2 Method Roadmap

TR Section 2 describes the organization of the TR, as well as various features and steps associated with the CAREM methodology. This description states that the three elements of CAREM are described in subsequent sections. TR Sections 3 through 5 address each element of CAREM that is reproduced in Figure 3-1.

3.3 Requirements and Capabilities

TR Section 3 describes in detail the first element of CAREM, which is the specification of the requirements of the code capabilities and the determination of the code applicability. The first element consists of six steps and each one of these steps is discussed sequentially.

3.3.1 Scenario Specification (Step 1)

TR Section 3.1 discusses the scenario specification, which constitutes the first step in CAREM (see Figure 3-1). In order to determine the limiting scenario, the scenario that maximizes the impact on the FOMs, the applicant performed several pipe break sensitivity studies. The sensitivity studies covered the types of pipe breaks (double-ended guillotine breaks and split breaks), the locations of the breaks (i.e., cold leg, hot leg, and pump-suction leg), the break areas, and the assumptions employed. The applicant assumed that the loss-of-offsite power (LOOP) occurs coincident with the break, the RCPs coast down at the initiation of the accident due to LOOP, an emergency diesel generator (EDG) fails, and only credits the contribution of two of the four SIPs. The applicant uniformly used these assumptions in the sensitivity studies to determine the limiting break.

The applicant concluded that the highest peak cladding temperature (PCT) occurs in the case of the double ended guillotine cold leg break. This defines the limiting break type, location, and area. TR Sections 3.1.2 and 5.2.1.1 and Appendix K provide additional details.

The TR describes the scenario for the limiting break as being subdivided into four time-periods that characterize events during the accident. These time periods are (a) blowdown, (b) refill, (c) early reflood, and (d) the late reflood phases. These periods are defined by the water inventory in the reactor pressure vessel and the injection flow condition of the SIT-FD.

The TR defines the blowdown period as being from the occurrence of the break to the start time of the SIT-FD injection.

The TR defines the refill period as being from the start time of the SIT-FD injection to the time when the mixture level in the reactor vessel lower plenum reaches the bottom of the active core.

The TR defines the reflood period as being subdivided into early and late periods based on the time at which the SIT-FD depletes. This is to address the possibility of core heatup during the late reflood period since the APR1400 design does not include low pressure SIPs.

3.3.2 Nuclear Power Plant Selection (Step 2)

The applicant selected Shin-Kori (SKN) Units 3 and 4 as the reference plant in TR Section 3.2.

3.3.3 Phenomena Identification and Ranking Table (Step 3)

TR Section 3.3 introduces the phenomena identification and ranking table (PIRT) that is used to identify the major phenomena or processes that occur during the accident and to prioritize them according to their effects on the FOMs. The applicant stated that the PIRT for CAREM is derived from the Korea Next Generation Reactor (KNGR) PIRT. The KNGR PIRT was prepared by the Idaho National Engineering and Environmental Laboratory (INEEL) [Ref. 52], and KNGR is the name given during the developmental stage to what eventually became the APR1400 design.

TR Section 3.3 states that the KNGR and APR1400 PIRTs are both based upon the double-ended guillotine break of a cold leg with the same conditions as described above. These PIRTs consist of four characteristic time periods, however the definitions of time periods are different. APR1400 PIRT defines four characteristic time periods consisting of the blowdown, refill, early reflood, and late reflood. Each phenomenon or process considered in the KNGR and APR1400 PIRTs is ranked during each of the accident phases using 1 (low) to 5 (high) importance levels [Ref. 17]. The applicant modified some of the rankings in the KNGR PIRT when constructing the APR1400 PIRT to reflect the design finalization of APR1400 and new experimental data.

TR Table 3-2 provides the APR1400 PIRT. TR Appendix A provides details of the KNGR PIRT and the changes made to it resulting in the APR1400 PIRT.

As stated in TR Section 3.3, the distribution free statistical approach used in this methodology imposes no limitation on the number of uncertainty parameters. The ranking technique discussed in the TR ensures that those parameters that have a numerical rank of [[ ]] are used in the applicability and uncertainty analysis.

3.3.4 Frozen Code Selection (Step 4)

TR Section 3.4 states that the RELAP5/MOD3.3/K code used as the basis for the application is a modified version of RELAP5/MOD3.3 that is dynamically linked to the CONTEMPT4/MOD5 computer code by the applicant. This system of codes calculates the reactor system thermal-hydraulic conditions and the containment backpressure, respectively.

TR Appendix B documents several areas where the applicant modified the code to achieve certain improvements which include:

- [[
-
-
-]]
- and code failure due to [[ ]]

TR Appendix B displays the results from several cases demonstrating the degree of improvement achieved.

TR Appendix B also documents comparisons of RELAP5/MOD3.3/K calculations and Full-Length Emergency Core Heat Transfer for the Separate Effects and Systems Effects Tests (FLECHT-SEASET) measurements. This evidence of RELAP5/MOD3.3/K acceptability adds to the already substantial volume of comparisons from other RELAP5/MOD3.3/K assessments.

The TR continues by describing some of these assessments in the original RELAP5/MOD3.3 supporting documents [Ref. 20].

Volume III [Ref. d] documents "Developmental Assessment Problems" used to characterize RELAP5/MOD3.3 performance, and several classes of comparisons are documented therein. This assessment includes identification of some problem areas and limitations:

- Developmental Assessment Problems
- Phenomenological Problems
- Separate Effects Problems
- Integral Effects Problems

Volume 6 [Ref. g] documents the validation of RELAP5/MOD3.3 numerical techniques via a comprehensive battery of tests. Volume 6 comprehensively demonstrates the acceptability of the models employed, the domain of applicability, and the regions of solution stability. In addition, Volume 6 provides comparisons with several analytical solutions to support this validation.

Volume 7 [Ref. h] documents the wide variety of assessments that were accomplished independent of the NRC development and validation effort. A very diverse group of organizations, under the banner of the Organization for Economic Co-operation and Development and Nuclear Energy Agency (OECD/NEA), performed these assessments, and included:

- Code Applications and Maintenance Program (CAMP) members
- International Laboratories (e.g., Korea Institute of Nuclear Safety, Kurchatov Institute, etc.)
- Reactor vendors and licensees (e.g., Westinghouse, TRACTEBEL, STUDSVIK, Kraftwerk Union AG, etc.)
- Experimental facilities (e.g., BETHSY [Boucle d'Etudes Thermo-Hydraulique Système], LOFT [Loss of Fluid Test], FLECHT-SEASET, etc.)
- Independent researchers (e.g., Paul Scherrer Institute)

The Volume 7 assessment [Ref. h] pertains to an earlier version (i.e., version 3.0) of RELAP5 and it identified a number of deficiencies and areas for improvement. RELAP5/MOD3.3/K used by the applicant implements those improvements.

CONTEMPT4/MOD5 is a containment analysis code. As implemented by the applicant, it is used for calculating the LBLOCA containment backpressure utilizing input conditions supplied by RELAP5. This code includes models for the fan and spray cooling systems and the passive heat sinks (i.e., heat transfer to various containment structures) which are essential to the calculation of containment backpressure during a LBLOCA.

The application describes the merger of these two codes so that they may exchange information about the containment backpressure and the mass and energy release rate at every time step after a specific set of conditions are achieved.

3.3.5 Code Documentation (Step 5)

TR Section 3.5 provides a list of code manuals for RELAP5/MOD3.3 and CONTEMPT4/MOD5. The applicant asserts that because RELAP5/MOD3.3/K only includes relatively simple modifications to the original RELAP5/MOD3.3 code, the code manuals for RELAP5/MOD3.3 remain applicable [Ref. 20].

3.3.6 Code Applicability Determination (Step 6)

TR Section 3.6 discusses the analytical requirements of the code system. This section compares the features of RELAP5/MOD3.3/K and CONTEMPT4/MOD5 to these requirements by the applicant, where they conclude the following:

- *"The code system has the capability to simulate the four phases of blowdown, refill, early reflood, and late reflood of an APR1400 LBLOCA.*
- *The code system can approximate the multidimensional phenomena in the reactor pressure vessel by way of modeling multiple channels and their inter-connecting cross-flow junctions.*
- *The nonhomogeneous and non-equilibrium governing equations and the non-condensable gas transport equation, together with the constitutive relations of the code system can calculate such major phenomena as the critical flow at the break, dynamic characteristics of the centrifugal pump including the two-phase performance degradation, blowdown core heat transfer, penetration or bypass of ECC water in the downcomer, reflood core heat transfer, fuel rod quenching, droplet entrainment, two-phase pressure drop, containment backpressure, and so on.*
- *The code system contains a series of constitutive relations for all flow regimes.*
- *The code system contains important special component models for components such as the safety injection tank and separator.*
- *The code system can simulate plant geometry and control functions.*
- *The code system shows reasonable agreement qualitatively and quantitatively with various experimental data.*
- *Code assessment calculations performed against experiments at various scales can assure the scale-up capability of the code system to full-scale power plants.*
- *The frozen code system can be applied to the quantification of the calculational uncertainty, and is supported by a complete set of code documentation.*
- *Assessment calculations of the code system and their databases are available."*

3.4 Assessment and Ranging of Parameters

TR Section 4 states that the CAREM methodology evaluates the uncertainties of the models or correlations that it uses to simulate the major phenomena in PIRT. Further, uncertainty ranges

of individual parameters can be determined from information such as experimental data, reference documents, engineering judgments, code calculations, etc. The TR states that in some cases the uncertainty may be treated as a separate bias, bounding approach, or nodalization and for phenomena that are governed by the same model or correlation, the uncertainty is applied so as to ensure conservative predictions of PCT.

The TR defines code accuracy as a statistical difference (i.e., bias) and deviation obtained by comparing the calculated cladding temperature to that measured in experiments.

3.4.1 Establishment of Assessment Matrix (Step 7)

TR Section 4.1 describes the matrix of objectives used to select the separate effects tests (SET) and integral effects tests (IET) that establish the accuracy of various phenomena models, component performance attributes, and system behaviors. TR Section 4.1 states that the assessment matrix used for the APR1400 includes a combination of tests for traditional cold leg injection (CLI) plants, as well as those more specific to the APR1400 design. The tests for CLI plants are relevant because several phenomena that are expected to be important for the APR1400 LBLOCA are commonly important to CLI plants as well. However, it goes on to explain that since the APR1400 design also includes DVI, phenomena that occur in the downcomer region, such as ECC water bypass and void development in the downcomer region (i.e., downcomer boiling), can be significantly different from those in CLI plants. For this reason, the assessment matrix includes tests that investigate ECC water bypass and downcomer boiling phenomena:

- Multi-dimensional Investigation in Downcomer Annulus Simulation (MIDAS), Upper Plenum Test Facility (UPTF) 21D, which addresses the ECC water bypass phenomenon;
- Downcomer Boiling (DOBO), which addresses the downcomer boiling phenomenon;
- Advanced Thermal-hydraulic Test Loop for Accident Simulation (ATLAS), which addresses the general LBLOCA reflood behavior of the APR1400;
- Valve Performance Evaluation Rig (VAPER), which addresses the SIT-FD injection flow behavior.

3.4.2 Plant Nodalization and Experimental Assessment (Step 8)

3.4.2.1 Plant Nodalization (Step 8.1)

TR Section 4.2.1 discusses the nodalization of the APR1400 plant used in the CAREM for demonstration calculations and shows it graphically in TR Figure 4-1. The two hot legs and the four cold legs are modeled separately. The two loops are modeled identically except that the pressurizer is attached to one of the loops. The other loop contains the cold leg break between the pump and the reactor vessel which is the limiting break location. The noding for each loop describes the hot leg piping, U-tubes, and fluid volumes of the steam generator primary and secondary sides, two pump suction legs, two pumps, and two pump discharge cold legs.

The TR states that the reactor vessel nodalization of the APR1400 includes the downcomer, upper and lower plena, and the core regions. It states that the nodalization follows the typical

PWR approach except for the core and the downcomer components which include additional detail in the nodalization to allow calculations to capture the various thermal-hydraulic phenomena and multidimensional behaviors.

In TR Section 4.2.1 the reactor vessel downcomer is divided into [[ ]]. The applicant selected [[ ]] through sensitivity calculations that determined the number of channels required to prevent distortion of the phenomena, and to coincide with the loop piping connections. The [[ ]] are interconnected by cross-flow junctions. The channel form loss coefficient was modeled to reflect the geometric shapes as a function of the downcomer width, roughness, radius of curvature, and friction coefficients. The height of the upper annulus node to which the DVI nozzle is connected was selected to locate the node center at the DVI nozzle elevation. The TR states that the hot wall effect is acceptably simulated by modeling heat structures of the downcomer wall.

The TR states that the core is modeled with [[ ]]. The applicant determined that the active length of the fuel rod was acceptably modeled using [[ ]] axial nodes through the code assessment against the Thermal Hydraulic Test Facility (THTF) and FLECHT-SEASET tests.

3.4.2.2 Determination of Code Uncertainty Parameters and their Ranges (Step 8.2)

TR Section 4.2.2 describes the determination of RELAP5/MOD3.3/K input parameters that are selected for use under CAREM, what uncertainties and distributions the applicant believes are applicable to them, and why. This information is used to support the evaluation of overall calculation uncertainty for the plant sensitivity calculations. Plant input parameters and their uncertainties are discussed separately in TR Section 5.1.

TR Subsection 4.2.2.1.1 discusses how the fuel pellet thermal conductivity affects the initial stored energy. Using the CSAU approach, the applicant determined that the four dominant parameters affecting the fuel stored energy were the gap conductance, fuel rod peaking factors, fuel thermal conductivity and convective heat transfer coefficients. They determined that the gap conductance is dependent on the initial and transient fuel rod performance parameters of geometry, gap gas composition, burnup, etc. To address the effects of thermal conductivity degradation (TCD) in CAREM, the gap conductance is not treated as an uncertainty variable since the steady state fuel centerline temperature is adjusted to match fuel rod design information when the TCD effect is considered. The applicant determined a penalty which they apply to the fuel centerline temperature in the fuel performance design interface to account for TCD.

TR Subsection 4.2.2.1.1 discusses how the fuel pellet heat transfer is affected by the thermal conductivity of UO_2 pellets. The thermal conductivity of the fuel pellet is modeled by the modified Nuclear Fuel Industries (NFI) correlation to consider thermal conductivity degradation (TCD) as a function of burnup. The modified NFI correlation and related uncertainty is discussed in the FRAPCON-4.0 code document [Ref. 24].

TR Subsection 4.2.2.1.1 discusses how RELAP5/MOD3.3/K uses the Dittus-Boelter correlation to calculate turbulent convection heat transfer to single-phase liquid and vapor. The applicant referred to discussions in various references where 95 percent of the data have been

encompassed in an uncertainty range of [[ ]] percent. Consequently, for CAREM the applicant applied that as the uncertainty in the Dittus-Boelter correlation for prediction of single-phase liquid and vapor heat transfer and assumed the applicability of a normal distribution function for this uncertainty component.

TR Subsection 4.2.2.1.2 discusses how RELAP5/MOD3.3/K calculates the nucleate boiling heat transfer coefficient using the Chen correlation. According to the RELAP5 code manual, the average uncertainty is ± 21.1 percent in saturation nucleate boiling, and ± 40 percent in subcooled nucleate boiling. For CAREM, the applicant assumed a normal distribution with a standard deviation of [[ ]] percent for this parameter.

TR Subsection 4.2.2.1.2 discusses how RELAP5/MOD3.3/K calculates the critical heat flux (CHF) in the high-pressure and high-flow region using the Groeneveld lookup table. In TR Figure 4-2, a comparison of 1993 data points covering various test conditions, including those of high-pressure and high-flow, shows that the Groeneveld lookup table estimates the critical heat fluxes lower than the experimental data by 4.9 percent on average with a root-mean-squared error of 37.9 percent. The TR goes on to state that no comparison between the prediction from the lookup table and the data measured in only the high-pressure and high-flow condition is available. Therefore, for CAREM the applicant assigns the root-mean-squared error of [[ ]] percent as the standard deviation of the uncertainty of CHF in the high-pressure and high-flow region with a normal distribution.

TR Subsection 4.2.2.1.2 discusses how the CHF model of the RELAP5/MOD3.3/K code for the low-pressure and low-flow region is the modified Zuber correlation. The applicant demonstrated in TR Figure 4-3 that the modified Zuber correlation conservatively predicts 75 experimental data points. Furthermore, the correlation predicts 95 percent of the data in a range from [[ ]] percent. However, CAREM uses an uncertainty range for this correlation of [[ ]] percent, which is more conservative, and assumes a normal distribution.

TR Subsection 4.2.2.1.2 discusses how the reflood model in RELAP5/MOD3.3/K uses the maximum of the film boiling heat transfer coefficients calculated by the Bromley and the Forslund-Rohsenow correlations. Analysis using CAREM will select these two correlations as uncertainty parameters for film boiling heat transfer. The uncertainty in the Forslund-Rohsenow correlation in [Ref. 19] and code assessment results documented in TR Appendix C show that the uncertainty range for the Forslund-Rohsenow correlation is [[ ]]. The RELAP5/MOD3.3 manual states that the calculated film boiling heat transfer coefficients using the Bromley correlation covers all data within ±18 percent. The applicant cited a different study wherein the experimental data - which includes conduction, convection, and radiation heat transfer - are 12.1 percent higher than the RELAP5 predicted values on average, and the data are distributed within 0.37 to ~ 2.61 times of the predicted values. Based on these results, the applicant determined that for CAREM, the standard deviation of the Bromley correlation is [[ ]].

TR Subsection 4.2.2.6.1 discusses how the RELAP5/MOD3/K code uses the Ransom-Trapp critical flow model to predict critical flow rate. The applicant determined the uncertainty of this model using an assessment against the nine MARVIKEN tests. The assessment showed that the Ransom-Trapp critical flow model over-predicts the data by [[ ]] percent for the subcooled single-phase critical flow and under-predicts the data by [[ ]] percent for the two-phase critical flow. The predicted values agreed well with the data when the discharge coefficients of [[ ]] were applied to the subcooled single-phase and to the two-phase critical flow, respectively. As a result, the applicant selected these values of the

discharge coefficient for CAREM as the mean values of the normal distribution. The standard deviations of the discharge coefficients of the subcooled single-phase and the two-phase flow are [[ ]], respectively.

TR Subsection 4.2.2.6.2 discusses how the containment temperature and pressure history is calculated conservatively. [[

]]. The TR further states that, due to the conservatively chosen CONTEMPT4/MOD5 input parameters, the uncertainties in various containment-related parameters or phenomena are not subjected to sampling using uncertainty distributions. Since the APR1400 CAREM employs a mixture of best-estimate and conservative assumptions, for the post-blowdown containment backpressure calculation, the input parameters to the CONTEMPT4/MOD5 computer code are selected conservatively to result in a conservatively low containment backpressure.

TR Subsection 4.2.3.1, the applicant discusses how several phenomena of importance in the downcomer region that they attribute to the ECC water bypass behavior, such as condensation, multidimensional flow, steam velocity, entrainment, de-entrainment, inter-phase momentum transfer, and countercurrent flow. Since it is difficult to determine one specific code parameter that governs ECC water bypass, CAREM captures the combined uncertainties related to the ECC water bypasses as a bias.

TR Subsection 4.2.3.1 discusses how the applicant used code assessments to determine the ECC water bypass bias during the refill period. To accomplish this, the applicant conducted tests at the Upper Plenum Test Facility (UPTF) and the ATLAS. TR Appendix F describes the UPTF tests, while TR Appendix E describes the ATLAS tests. The applicant performed an assessment against a full-scale UPTF-4A test, and compared the predicted lower plenum inventory with the measured data. The UPTF-4A test simulated the bypass phenomena during the refill period of a LBLOCA in a plant with CLI configuration. According to the applicant, the thermal-hydraulic behavior that occurred in the reactor pressure vessel downcomer during the refill period of the APR1400 LBLOCA is similar to that experienced in a conventional CLI PWR. This justified the use of the UPTF-4A test data. The code assessment revealed that the water inventory in the lower plenum predicted at the end of the test exceeded the measured amount by several hundred kilograms. The applicant conservatively interpreted [[ ]] as a measure of the ECCW bypass during the refill period. For CAREM, the applicant chose to evaluate the bias in the prediction of the PCT due to ECCW bypass [[ ]].

TR Subsection 4.2.3.1 discusses how the applicant evaluated the code's ability to predict ECC bypass phenomena during the reflood period through code assessments against tests in the Multi-dimensional Investigation in Downcomer Annulus Simulation (MIDAS) facility and the UPTF-21 D, and ATLAS Tests 9, 11, and 15. ATLAS is an integral test facility simulating the APR1400, whereas MIDAS and UPTF-21 D tests are separate effects tests designed to investigate ECCW bypass during the reflood phase for DVI configurations. TR Appendices E and F provide details of the code assessment against the ATLAS tests, and the MIDAS and UPTF 21-D tests, respectively.

TR Subsection 4.2.2.2.1 states that the results of the code assessment studies against the above-mentioned tests showed that the RELAP5/MOD3.3/K code conservatively calculates ECC bypass during reflood. The TR asserts that, since the tests used in the code assessment

include a full-scale UPTF test, the conservative prediction of RELAP5/MOD3.3/K can be considered to be valid for full-scale APR1400 LOCA events. The conservative or favorable bias for ECCW bypass during the reflood phase is not credited by the applicant in the CAREM evaluation of the PCT bias of the plant sensitivity calculations. Therefore, the applicant did not determine the code parameters or measures necessary to evaluate the bias of the ECCW bypass during reflood. As a result, the applicant applies the ECCW bypass bias only during the refill phase of the accident.

TR Subsection 4.2.3.2 discusses the importance of accounting for the steam binding bias and the source of this concern. Steam binding results due to the vaporization of droplets entrained into the steam generator U-tubes. The droplets are vaporized by the heat transfer from the secondary side to the primary side during the reflood period. The amount of water droplets that enter the U-tubes is determined by the entrainment and de-entrainment in the upper plenum and hot legs. Water droplets entrained from the upper plenum by the steam exiting the core can be de-entrained by the mechanical structures in the upper plenum. This entrainment and de-entrainment phenomena occurring across the upper plenum is inherently multidimensional. RELAP5/MOD3.3/K does not include a specific model to predict the mechanical de-entrainment by the structures. The applicant assessed the two distinct phenomena of entrainment and vaporization of the droplets independently in order to determine the relevant biases in CAREM analyses.

TR Subsection 4.2.3.2 discusses the entrainment and de-entrainment in the upper plenum as assessed by the UPTF-10B test. The applicant cited a previous assessment of RELAP5/MOD3.1 against UPTF-10B, which showed that mass inventory of the upper plenum can be [[

]]. Based on these results, the applicant determined that [[

]] for CAREM analyses.

TR Subsection 4.2.3.2 discusses the decision for CAREM analyses to maximize the effect of the vaporization of the droplets in the U-tubes by [[

]] at the same time.

3.4.3 Check Experimental Data Coverings (Step 9)

In TR Section 4.3, the applicant discusses the experimental data used to ensure the validity of the selected code uncertainty parameters. Step 9 examines whether the simulation calculations using the uncertainty parameters from the previous steps can successfully encompass the acceptance criteria of the experiments. The applicant performed these calculations for all the experiments in which the cladding temperatures were measured.

3.4.3.1 Code Accuracy Evaluation (Step 9.1)

In TR Section 4.3.1, the applicant defines code accuracy as the statistical difference between calculated and measured PCTs. Even if the locations and the occurrence times of the PCTs are different from each other, the code accuracy is defined simply as the PCT difference regardless of the location and when it occurs (i.e., code accuracy is defined in terms of PCT predictability).

In TR Section 4.3.1 the applicant uses standard definitions of parameters such as the mean and standard deviation to determine the statistical code accuracy based on the difference between the predicted and measured PCT. They state that the code accuracy, or the ability of the code to predict the PCT, needs to be reproducible, even if the uncertainties in the models used to predict PCT are propagated. As a result, the applicant uses the code accuracy as a reference value. If the resulting PCT from simple random sampling (SRS) calculations using the parameter uncertainties is higher than the maximum value of the measurements, then the number and probability distribution functions of the uncertainty parameters are sufficient. If the resulting PCT of SRS calculations cannot cover the maximum value of the measurements, the applicant will then need to examine further whether the resulting PCT covers the 95 percent one-sided limit.

TR Section 4.3.1.1 discusses four separate effects tests (THTF-105, 151, 160, and 162) and four integral effects tests (LOBI [LWR Off-Normal Behaviour Investigation] A1-66, LOFT L2-2, L2-3, and LP-02-6) to determine the code accuracy for the blowdown PCT. The TR states that blowdown experiments in facilities with DVI configuration are unavailable, partly due to the fact that the blowdown phenomena are almost independent of the injection system and therefore the necessity of DVI blowdown experiments is low. As a consequence, the applicant evaluated the blowdown code accuracy against the above mentioned blowdown experiments, which are in facilities with a CLI configuration. TR Appendices C and D describe code assessment calculations against separate effects tests and integral effects tests.

TR Section 4.3.1.2 discusses the evaluation of the code accuracy for reflood PCT. The applicant performed this evaluation using data from 27 separate effects tests (i.e., 17 FLECHT-SEASET tests, 7 NEPTUN tests, and 3 ATLAS tests) and 7 integral effects tests (i.e., LOFT L2-2, L2-3, L2-5, LP-02-6, CCTF C2-4, PKL-IIB5 [PWR Integral System Test Facility], and Semiscale S-06-3). TR Appendices C and D describe code assessment calculations against separate effects tests and integral effects tests.

3.4.3.2 Check Data Covering (Step 9.2)

TR Section 4.3.2 discusses the need to ensure that the spectrum of data employed in the evaluation is sufficient to justify the analysis objectives and that distribution-free statistics are utilized. The applicant showed that using distribution-free statistics requires 181 simulations in order to obtain at least five samples that exceed the 95th percentile at a 95 percent confidence level. In subsequent discussions in this SER this is then termed the 95/95 criteria, condition, limit, objective, or value depending on usage. In the context of this SER it means that the three most common results, the highest maximum cladding oxidation (MCO), the highest core wide oxidation (CWO), and the third ordered peak cladding temperature (PCT) are drawn from the domain of 181 LBLOCA calculations and they are 95/95 values.

TR Section 4.3.2.1 states that SRS calculations are performed against the test data obtained from THTF, LOFT, and LOBI in order to determine whether the calculations encompass the measured blowdown PCTs. To accomplish the coverage check, the applicant sampled eight code parameters and their associated uncertainties, from a larger potential list, to examine the blowdown test results:

- the [[ ]],
- the [[ ]],
- the [[ ]],

- the [[ ]],
- the [[ ]], and
- the [[ ]].

The applicant selected some additional system parameters that are considered for these tests since the LOFT and LOBI tests are integral effects tests that cover the reflood period as well. The applicant stated that the effects of these additional code and system parameters selected for the reflood period on the blowdown PCT calculation are minimal. The additional parameters used are listed in Appendices C and D for the THTF, and LOBI and LOFT, respectively.

The applicant confirmed that the third highest value out of the 181 calculations encompasses the upper-bound of the blowdown PCT measurements in the abovementioned tests based on the 181 calculations and the use of a distribution-free statistical approach.

TR Section 4.3.2.1 states that the applicant evaluated reflood results against the ATLAS, FLECHT-SEASET, LOFT, NEPTUN, Semiscale, PKL, and CCTF tests. The applicant employed eight code uncertainty parameters:

- the [[ ]],
- the [[ ]],
- the [[ ]],
- the [[ ]],
- the [[ ]], and
- the [[ ]].

The applicant also employed the use of system parameters specific to each test facility. TR Appendices C lists the additional parameters used (for FLECHT-SEASET, NEPTUN, PKL, and CCTF), D (for LOFT and Semiscale), and E (for ATLAS).

The applicant concluded that the third highest value out of the 181 calculations encompasses the upper-bound of the reflood PCT measurements in the above mentioned tests.

3.4.4 Determination of Scale Bias Covering (Step 10)

TR Section 4.4 states that the total amount of the ECC is conservatively estimated. TR Section 4.2.3 states that the effect of the downcomer water level depression in the reflood phase is not considered. TR Section 4.4.2 states that the RELAP5 code does not include a model to describe mechanical de-entrainment due to the internal structures in the upper plenum, the entrainment amount is [[ ]] the experimental measurements. The steam binding bias is evaluated by assuming the [[ ]] in the U-tubes. In this manner steam binding is maximized. TR Section 5.2 evaluates the effects of the steam binding bias on plant calculations.

3.5 Sensitivity and Uncertainty Analysis

TR Section 5 discusses the determination of the uncertainty in those parameters that are plant inputs, rather than phenomenological variables. The CAREM methodology provides the results of the 181 SRS calculations for the APR1400 plant to determine the limiting PCT.

3.5.1 Determination of Plant Input Uncertainty (Step 11)

TR Section 5.1 discusses the probability distribution functions and uncertainties of plant condition parameters. The overall uncertainty of the LBLOCA transient, including peak cladding temperature behavior, which is one of the major acceptance criteria, depends on the initial and boundary conditions of the plant, as well as the code uncertainty parameters. Plant initial and boundary conditions include core power distribution, fuel parameters, reactor coolant pump performance, safety injection system capacity and availability, system pressures and system flow rates.

TR Section 5.1.5 discusses the loss coefficient (K-factor) for the SIT-FD during high and low flow injection. The uncertainty in that parameter is not included based on the separate-effects test (VAPER) and sensitivity studies performed by the applicant. TR Appendix H provides the details of the VAPER test and the sensitivity studies.

3.5.2 Combine Uncertainties and Biases (Step 12)

The applicant performed a base case LBLOCA calculation to illustrate overall APR1400 system behavior in TR Section 5.2.1. The base case calculation of the plant applied the best-estimate operating conditions for the limiting break type, location, and size. The applicant defined the best-estimate conditions as the mean values of plant operating parameters and then performed a time step sensitivity study to determine that the variation of PCT is minimal and that the numerical stability is ensured if the maximum time step is smaller than [[ ]] seconds. Therefore, the applicant has committed to using a maximum time step restriction of [[ ]] seconds for CAREM calculations.

The applicant used the results of the base case calculation, along with the figures showing key system parameters during the accident, to describe the system behavior during the four accident phases.

The applicant performed demonstration calculations that included uncertainty variation in [[ ]] selected parameters that are listed in TR Table 5-1. The 181 demonstration calculations use SRS and distribution-free statistics. The applicant provided the third highest value of the calculated PCT from the 181 cases as the licensing value, and compared it against the 10 CFR 50.46(b)(1) acceptance criteria. TR Appendix J lists the 181 simple random samplings of [[ ]] uncertainty parameters utilized. In addition, the applicant also used several of the sampled cases to evaluate the scale bias due to ECCW and steam binding.

3.6 Quantification of Total Uncertainties (Steps 13 and 14)

TR Section 6 describes how CAREM is used to determine the limiting PCT, the maximum local oxidation, and the maximum hydrogen formation for the demonstration case which the applicant compared against the acceptance criteria. Therein, the applicant evaluated uncertainties from sources other than the code models or plant operational conditions, such as the automatic time-step control function and the data reading frequency of RELAP5/MOD3.3/K. The applicant added a fixed value of 10 K to the limiting PCT due to the difficulty in discerning the effects of these sources from the calculated cladding temperatures. This bias is based on the applicant's experience with using RELAP5 to support licensing applications in Korea. The applicant compared the final results against the acceptance criteria to demonstrate that there is sufficient margin in the calculated APR1400 behavior.

3.7 TR Appendix A: Identification and Ranking of Phenomena and Processes

TR Appendix A discusses the development of the APR1400 PIRT. The actual PIRT is provided therein as Table 5. This PIRT is a derivative taken from the KNGR PIRT prepared by INEEL in 2001 [52]. KNGR was the name given to what subsequently became the APR1400 design.

The KNGR PIRT was also based on the double-ended guillotine break of a cold leg. The PIRT considered the same four characteristic time periods of blowdown, refill, early reflood, and late reflood. The KNGR PIRT ranked each phenomenon or process considered during each of the accident phases using one of five importance levels. The KNGR PIRT is documented in TR Appendix A, Table 3.

As stated in TR Appendix A.2, the KNGR PIRT was developed on [[

]].

The applicant divided the LBLOCA scenario of the APR1400 into four temporal periods and described them as:

- The blowdown period starts when the break occurs and ends when SIT injection initiates;
- The refill period ends when the liquid level in the vessel lower plenum approaches the core inlet and remains full thereafter;
- The early reflood period ends when the SITs are emptied; and
- The late reflood period continues after the SITs are emptied.

The applicant also adjusted the relative importance of certain phenomena or processes after modifying the definition of temporal periods to account for the finalization of the APR1400 design and related experiments.

The applicant only considered the high ranked phenomena from the KNGR PIRT (with a numerical ranking of [[ ]] in any accident phase) to develop the APR1400 PIRT or modify the rankings. The rationale stated in TR Appendix A.3.2 is that the high ranked phenomena or processes are necessary for appropriate assessment of uncertainties. The uncertainty parameters that are identified for these parameters are then included in plant calculations. In cases where the identification of uncertainty parameters is not possible, those phenomena or processes are either treated conservatively or appropriate biases are determined and applied. The medium ranked phenomena (with a numerical ranking of [[']] in any accident phase) can be modeled with moderate accuracy but corresponding uncertainty parameters are not determined. Phenomena or processes of low importance ranks (with a numerical ranking of [[ ]] in any accident phase) are not used to determine any uncertainties or biases.

Based on the above rationale, the applicant identified [[ ]] phenomena from the KNGR PIRT whose rankings were adjusted in response to the changes in the phase definitions. The result is the APR1400 PIRT listed in Table 5 of TR Appendix A.

3.8 Appendix B: Freezing of RELAP5/MOD3.3/K

TR Appendix B documents the changes made to the source code of RELAP5/MOD3.3 to develop RELAP5/MOD3.3/K. These include modifications for:

- the [[ ]],
- the [[ ]],
- the [[ ]],
- the [[ ]], and
- the [[ ]].

TR Appendix B.1 states that various assessments against SETs and IETs have revealed that the RELAP5/MOD3.3 code tends to predict that rod quenching occurs earlier than the experimental results. This tendency is mainly caused by the [[ ]].

TR Appendix B.1.1 describes changes to the RELAP5/MOD3.3 code to allow [[ ]]. The original implementation in RELAP5/MOD3.3 code allowed [[ ]], thereby resulting in earlier quenching. The modification is based on the [[ ]] in an older version (MOD3.1) of RELAP5. The predicted cladding temperature and quenching behavior after the modification show improved comparison against data from two FLECHT-SEASET tests.

TR Appendix B.1.1 describes how in RELAP5/MOD3.3 the calculation of the heat transfer coefficient to liquid during film boiling in bundles undergoing reflood is the maximum of the Forslund-Rohsenow correlation and the normal Bromley correlation. The final film boiling heat transfer coefficient is then obtained by adding the contributions from “the heat transfer coefficient to vapor” and “radiation to droplets” to the “heat transfer coefficient to liquid.” The applicant compared the heat transfer coefficients to liquid calculated by the three correlations (film coefficient, the Forslund-Rohsenow correlation, and the Bromley correlation) against corresponding data-derived values for two FLECHT-SEASET tests. The comparisons showed that the values predicted by [[ ]]. Thus, the film boiling heat transfer coefficient in RELAP5/MOD3.3/K is the maximum value between the [[ ]]. The predicted cladding temperature and quenching behavior predictions are improved using comparisons from two FLECHT-SEASET tests.

TR Appendix B.1.3 describes the detection of errors in the calculation of the [[ ]] in the RELAP5/MOD3.3 code. The applicant corrected these errors by modifying the source code.

TR Appendix B.1.5 describes modifications to RELAP5/MOD3.3/K to prevent calculational failures due to the manner in which RELAP5 models [[

]].

TR Appendix B.2.1 describes the improvements to the reflood model due to modifications of the [[ ]] calculation via comparisons against SET data. The assessment calculations used FLECHT-SEASET tests, 31504 and 31108. These tests are representative of low and high reflood rate tests, respectively. The comparisons illustrate the improvements in heated rod cladding temperatures and the differential pressure. The applicant concluded that the modifications to the reflood model improve the prediction of heated rod quenching time, and the effects of the modifications on system hydraulic behavior are insignificant.

The applicant investigated the effect of the modification of [[ ]] calculation through sensitivity calculations. The applicant compared [[ ]] predicted by the modified and unmodified versions of RELAP5/MOD3.3 against the values calculated by a previous version, RELAP5/MOD3.1. Since the [[ ]] has remained unchanged from the previous version (MOD3.1), the [[ ]] calculated without the modification was expected to be the same as the results from RELAP5/MOD3.1. The calculated values, however, show a difference due to a coding error identified by the applicant. After modification by the applicant, the calculated values are restored to the RELAP5/MOD3.1 values. The applicant showed that after the modification to the [[ ]] calculation, the blowdown PCT decreased by about 6 K and the reflood PCT decreases by about 35 K with no significant difference in the heated rod quenching time.

3.9 Appendix C: Assessment of RELAP5/MOD3.3/K against Separate-Effect Tests

TR Appendix C documents the capability of the RELAP5/MOD3.3/K code to predict various thermal-hydraulic responses during blowdown and reflood phases using SETs. The objectives of the assessment are to:

- examine the code ability to accurately predict experimental data,
- determine code accuracy,
- evaluate probability distribution functions of the uncertainty parameters, and
- confirm the adequacy of the uncertainty parameters and their ranges.

As a result of the abovementioned objectives, TR Appendix C is heavily cited in the assessment and ranging of parameters in TR Section 4.

TR Appendix C.1 states that code accuracy is the difference between the calculated and the measured PCTs. The applicant confirmed the ability of the code to predict the thermal-hydraulic phenomena and determined the uncertainty parameters. By adopting distribution-free statistic techniques, the applicant performed 181 calculations with SRS for each experiment. The applicant then confirmed that the PCT of the experiment was covered by the third highest value of PCT calculated.

TR Appendix C.1 states that the following SETs for code assessment, code accuracy evaluation and the experimental coverage check are used:

- seventeen FLECHT-SEASET tests,
- one Cylindrical Core Test Facility (CCTF) test,
- seven PWR reflood in bundle geometry (NEPTUN) tests,
- four THTF tests, and
- one Primary Coolant Loop (PKL) test.

The four THTF tests assess the capability of the RELAP5/MOD3.3/K code to predict the blowdown progression. The other tests assess the capability of the code to predict the reflood progression and reflood PCT.

Appendix C provides extensive details regarding each SET facility, the tests that are chosen, and a discussion of the comparison of the results from the code assessment and accuracy against the experimental data.

The SRS calculations for the seventeen FLECHT-SEASET, CCTF, and NEPTUN tests used [[ ]] code uncertainty parameters that are all related to reflood core heat transfer. These parameters are:

- the [[ ]],
- the [[ ]],
- the [[ ]],
- the [[ ]],
- the [[ ]], and
- the [[ ]].

In addition to these parameters, the applicant also considered system parameters specific to the FLECHT-SEASET test facility, such as the [[ ]] in the SRS calculations. The applicant did not consider system parameters specific to the CCTF and NEPTUN facilities in the SRS calculations.

SRS calculations performed against four THTF tests used [[ ]] code uncertainty parameters related to the core heat transfer. These parameters are:

- the [[ ]],
- the [[ ]],
- the [[ ]],
- the [[ ]],
- the [[ ]], and
- two code uncertainty parameters related to [[ ]].

SRS calculations performed against the PKL-IIB5 test used [[ ]] code uncertainty parameters related to the core heat transfer and [[ ]].

In TR Appendix C, Sections 2.4, 4.4, and 5.4, the applicant determined comparisons of the predictions against the measured data to quantify the code accuracy for prediction of blowdown and reflood PCT. The applicant presented the accuracy in terms of a bias and standard deviation on the PCT.

TR Appendix C, Sections 2.5, 3.4, 4.5, 5.5, and 6.4, state that the SRS calculations support the conclusion that the measured PCTs are covered by the calculated values and that the number and the probability distribution functions of the selected code uncertainty parameters used for the SRS calculations in TR Appendix C are sufficient to cover the measured PCT.

3.10 Appendix D: Assessment of RELAP5/MOD3.3/K Against Integral-Effect Tests

TR Appendix D documents the capability of the RELAP5/MOD3.3/K code to predict thermal-hydraulic responses during blowdown and reflood phases when assessed against IETs. The purpose and approach for the assessment against the IETs is identical to that used for the assessments against the SETs in TR Appendix C and is not repeated here.

The IETs used for the code assessment are:

- four LOFT tests (L2-2, L2-3, L2-5 and LP-02-6),
- one Semiscale test (S-06-3), and
- one LOBI test (AI-66).

TR Appendix D, Sections 2, 3, and 4 provide extensive details regarding each IET facility, the tests that the applicant chose, and a discussion of the comparison of the results from the code assessment and accuracy against the experimental data.

TR Appendix D, Section 2 discusses the 181 SRS calculations performed by the applicant for each LOFT experiment assessment. The assessment includes all [[ ]] uncertainty parameters listed in TR Appendix D, Table 2-2. Since the fuel rods are used in the LOFT tests, the parameters include those related to both blowdown and reflood phenomena as well as the nuclear fuel-related parameters, such as [[ ]]. In addition, the assessment also included three parameters specific to LOFT tests [[ ]]. The applicant used test-specific uncertainty ranges of these facility-related parameters in the SRS calculations for each test because the applicable uncertainty ranges of the [[ ]] for each test.

SRS calculations performed against the Semiscale Test S-06-3 used [[ ]] uncertainty parameters listed in TR Appendix D, Table 3-3 that are related to [[ ]]. SRS calculations performed against the LOBI test used [[ ]] uncertainty parameters listed in TR Appendix D, Table 4-3 that are related to [[ ]].

TR Appendix D, Section 5 states that the comparisons of the predictions against the measured data from the selected IETs allow the determination of the code accuracy for prediction of blowdown and reflood PCT. The applicant determined the accuracy in terms of a bias and

standard deviation based on the difference in the predicted and measured PCT. The SRS calculations support the conclusion that the calculated PCTs are sufficient to cover the measured PCTs.

3.11 Appendix E: Assessment of RELAP5/MOD3.3/K Against APR1400 Reflood Tests

TR Appendix E describes the assessment of RELAP5/MOD3.3/K code against the APR1400 LBLOCA tests performed in the ATLAS (Advanced Thermal-hydraulic Test Loop for Accident Simulation) test facility. Three tests are used to simulate a LBLOCA in the APR1400 design:

- LB-CL-09 (Test 09),
- LB-CL-11 (Test 11), and
- LB-CL-15 (Test 15).

The applicant used these tests to assess major phenomena related to the DVI of the ECCW, such as boiling of the downcomer inventory and ECCW bypass.

According to TR Appendix E.2.1, the ATLAS facility is an integral effects thermal-hydraulic test facility that uses ½ reduced height and 1/288 volume scaled test facility based on the design features of the APR1400. It also provides details about the design and configuration of the ATLAS facility, along with important scaling relations used in the facility design. TR Appendix E.5 provides a description of the results.

TR Appendix E.3 describes one aspect of the assessment which indicates that the ATLAS tests showed [[

]] during the APR1400 LBLOCA. The code simulations [[

]].

In the assessment, the applicant performed 181 SRS calculations for ATLAS Test 09 and Test 15 using the selected uncertainty parameters. The applicant did not perform SRS calculations for Test 11 because all fuel rods are quenched at the very beginning stage of the time period considered for the code assessment. The applicant used a total of [[ ]] uncertainty parameters in the SRS calculations. The uncertainty parameters considered in the SRS calculations are [[

]].

TR Appendix E.5 states that the RELAP5/MOD3.3/K code assessment against the ATLAS Test 09, 11, and 15 shows that the code correctly calculated the reflood thermal hydraulic behaviors, including the fuel rod cladding temperatures, and downcomer boiling phenomenon. Based on the results of these SRS calculations using the distribution free statistics approach, the applicant concluded that the selected uncertainty parameters, including the parameters related to [[ ]], are sufficient to cover the measured cladding temperatures.

3.12 Appendix F: Assessment of RELAP5/MOD3.3/K Against ECCW Bypass Tests

In TR Appendix F, the applicant addressed ECCW bypass during the late reflood period when only the SIP flow is available and examined the ability of the RELAP5/MOD3.3/K code to predict

this behavior. The assessment used the data obtained from tests conducted using the Multidimensional Investigation in Downcomer Annulus Simulation (MIDAS) and the Upper Plenum Test Facility (UPTF).

TR Appendix F.2 describes the MIDAS facility having a scale which is 1/5 in height, 1/24 in flow area, and 1/54 in flow rate as compared to APR1400. The temperature and pressure conditions of the MIDAS tests are prototypic to the APR1400 during the period of interest for the simulation. ECCW bypass tests allow the assessment of that phenomenon during the late reflood period. Only SIPs supply the ECCS injection during the late reflood period.

TR Appendix F.2.2.2 describes the assessment of the RELAP5/MOD3.3/K predictions of the ECCW bypass against MIDAS tests. This assessment shows that the code conservatively over-predicts the ECCW bypass fraction over the entire range. The degree of the over-prediction increases as the measured value decreases. RELAP5/MOD3.3/K also over-predicts the ECCW bypass fraction over the entire range of the steam flow rate. The over-prediction is stronger for the low steam injection flow rate condition. When the steam flow rate is high, the degree of over-prediction is reduced. The code-predicted condensation ratio is generally lower than measured, except for one test for which the code over-predicts the condensation ratio. TR Appendix F.2.2.2 states that even though RELAP5/MOD3.3/K typically over-predicts the ECCW bypass and under-predicts the condensation ratio, the code predicts the general trend of the bypass and condensation acceptably. It goes on to assert that the code prediction is conservative with respect to the availability of ECCS injection regardless of the number of available SIPs and their injection locations.

TR Appendix F.3 describes the assessment of RELAP5/MOD3.3/K predictions of ECCS bypass against UPTF Test 21-D where ECCW injection is through the two DVI nozzles in the downcomer. TR Appendix F.3.3 states that comparisons of key parameters of interest predicted by the code against the corresponding experimental data shows that RELAP5/MOD3.3/K reasonably predicts the major phenomena observed during the UPTF Test 21-D and conservatively over-predicts the ECCW bypass.

3.13 Appendix G: Assessment of RELAP5/MOD3.3/K Against Downcomer Boiling Tests

TR Appendix G describes the ability of RELAP5/MOD3.3/K to simulate downcomer boiling using assessments from the downcomer boiling (DOBO) test facility. TR Appendix G.2 describes the test facility which simulates the high temperature wall of the reactor pressure vessel annulus (downcomer) between the elevations of the cold leg and flow skirt. The test section has a heated rectangular cross-section with prototypic APR1400 dimensions. The circumferential length of the test section is 1/47.08 of the APR1400 under the assumption that there is no preference of downcomer boiling in the azimuthal direction. The simulated azimuthal angle of the test section corresponds to 7.65 degrees. Due to the small curvature of the simulated angle, the applicant neglected curvature, and used a rectangular channel for the test section. The downcomer wall is heated by the electrical heaters to achieve a steady-state constant heat flux condition. The test facility operates at prototypic APR1400 pressures during the period of interest. The injection nozzle of the emergency core cooling water is located at the upper part of the test section and the major parameters during the test were the wall heat flux, the water temperature, and the void fraction.

TR Appendix G.2.2 describes the results of the assessment of RELAP5/MOD3.3/K against experimental data from the DOBO facility. The code over-predicts the void fractions in all of the

axial nodes for all test cases. In addition, the measurements show subcooled water at the bottom of the test section, whereas the code calculations show almost no subcooling.

TR Appendix G. 3 concludes that RELAP5/MOD3.3/K conservatively predicts downcomer boiling using a single radial channel. Accordingly, in the TR, the applicant commits to using this model for APR1400.

3.14 Appendix H: Assessment of RELAP5/MOD3.3/K Against Fluidic-Device-Installed Safety Injection Tank Tests

TR Appendix H describes the assessment of the ability of RELAP5/MOD3.3/K to simulate the performance of safety injection tanks equipped with fluidic devices (SIT-FD). It states that the fluidic device is installed inside the SIT and passively controls the water injection flow rate from the SIT which injects water at a high flow rate during the blowdown and refill periods, and at a low flow rate during the reflood period.

TR Appendix H.1.1.1 describes the assessment facility, Valve Performance Evaluation Rig (VAPER) which consists of the SIT-FD, compressed air supply system, safety injection (SI) water discharge pipe line, SI water supply and recirculation system, stock tank, and a data acquisition and control system. The fluidic device is installed at the bottom of the tank. The fluidic device of the VAPER facility has a similar geometric shape and size as the in APR1400.

TR Appendix H.1.1.1 states that the major parameters measured in the tests are SIT water level, gas pressure and temperature, water level in the standpipe, and pressure drop across the fluidic device. The details of how the measurements are taken are detailed there.

The applicant uses four different modeling approaches to represent the SIT-FD. These models are:

- Model A: Modeling of SIT-FD with [[ ]]
- Model B: Modeling of SIT-FD with [[ ]]
- Model C: Modeling of SIT-FD with [[ ]]
- Model D: Modeling of SIT-FD with [[ ]]

Details regarding each of these modeling approaches are provided in TR Appendix H.1.2. The model assessment results show that models A, B, and C reasonably predict the injection flow rates, pressure drop in the tank, and water level behaviors during both the large and small flow injection periods. Air release behaviors predicted by these three models, however, show discrepancies from the test data. [[ ]].

TR Appendix H1.3 provides the assessment results. The assessment determines that the uncertainty range for the K-factors of large and small flow delivery can be determined using the results of VAPER tests and Model C is selected as the final SIT-FD model for the APR1400 LBLOCA analysis. The results also show that the K-factor selection shows little variation in downcomer/core level. The blowdown PCTs are the same in all calculations, because the blowdown PCTs occur before the SIT-FD injection. The maximum variation of reflood PCT and fuel rod quenching time, according to injection characteristics of the SIT-FD, is within 10 K and 75 s, respectively. The highest refllod PCT was predicted with [[

]].

3.15 Appendix I: Coupling RELAP5/MOD3.3/K and CONTEMPT4/MOD5

The RG 1.157 guidance states that the containment pressure should be used for evaluating cooling effectiveness during the post-blowdown phase of a LOCA. It goes on to state that the pressure should be calculated in a best-estimate manner and should include the effects of containment heat sinks and the operation of all pressure reducing equipment assumed to be available. However, TR Appendix I.1 states that the RELAP5/MOD3.3 code does not have the capability and thus, CAREM adopts the use of CONTEMPT4/MOD5 for this calculation. TR Appendix I.1.1 describes the coupling of CONTEMPT4/MOD5 to RELAP5/MOD3/K by utilizing the dynamic link library.

TR Appendix I.2 illustrates the use of this coupled code for calculation of a LBLOCA in the APR1400 and discusses the verification of the results. It states that the containment pressure calculated using the coupled code shows good agreement with the pressure calculated through iterative calculations exchanging the results of the separate calculations of RELAP5/MOD3.3 and CONTEMPT4/MOD5.

3.16 Appendix J: Sampled Uncertainty Parameter Values for 181 Plant Calculations

TR Appendix J provides the list of the sampled values for all the [[ ]] uncertainty parameters for each of the 181 plant calculations performed to determine the limiting PCT. The results of the calculations are described in TR Section 5.

3.17 Appendix K: Break and Burnup Sensitivity Study

TR Revision 1 provides Appendix K. This appendix provides the results of sensitivity studies for the break size, type, and location, in order to establish the limiting break for the nominal set of conditions. Since the effect of fuel TCD due to burnup affects the core stored energy, Appendix K also describes the results of sensitivity studies to determine the limiting time in life, i.e., the limiting burnup condition. Since the core stored energy can affect the limiting break size, the [[ ]] are performed for each of the three selected break discharge coefficients of 1.0, 0.8, and 0.6, for a total of [[ ]] cases. TR Appendix K also describes the process used to initialize the core stored energy that was specifically developed to address the TCD effect and that process is used to perform the 181 SRS calculations.

4. TECHNICAL EVALUATION

This review considers the compliance of the TR with the NRC regulatory requirements and applicable guidance documents for LBLOCA. It considers the technical soundness and merits of the statements made by the applicant in the TR and TR Revision 1.

Furthermore, this evaluation fully considers all of the material presented in responses to the AIs, information presented during the Audit Meetings, any supporting information addressing the AIs discussed during the Audit Meetings, as well as responses by KHNP to the RAIs. The NRC staff evaluated and satisfactorily resolved the issues raised in the AIs and RAIs, as described in this section.

During this review, the NRC staff identified certain Conditions and Limitations which must be met by the applicant for future licensing submittals that utilize the CAREM methodology. These Conditions and Limitations are discussed in this section and then are summarized in Section 5 of this SER.

4.1 Code Management

As discussed in SRP 15.0.2 Section 2, an EM consists of:

> *"one or more computer programs and other information necessary for application of the calculation framework to a specific transient or accident, such as mathematical models used, assumptions included in the programs, a procedure for treating the program input and output information, specification of those portions of the analysis not included in the computer programs, values of parameters, and other information necessary to specify the calculation procedure."*

The TR commits to using specific versions of RELAP and CONTEMPT that are dynamically coupled by the applicant. As discussed in TR Appendix B, the applicant obtained RELAP5/MOD3.3 through an international agreement and it has been rigorously maintained. During an inspection [Ref. 53], NRC staff verified that the codes are appropriately maintained under the KHNP QA program. In the EM, the applicant designated the modified code as RELAP5/MOD3.3/K.

KHNP's QA program is described in approved topical report APR1400-K-Q-TR-11005-NP-A, Revision 5, "KHNP Quality Assurance Program Description (QAPD) for the APR1400 Design Certification," April 2016, ADAMS Accession No. ML16123A406, [Ref. 54]. KHNP commits to follow ASME NQA-1-2008 and NQA-1a-2009 Addenda, "Quality Assurance Requirements for Nuclear Facility Applications," [Ref. 55], as endorsed by the NRC in RG 1.28, Revision 4. Subpart 2.7 of NQA-1, "Quality Assurance Requirements for Computer Software for Nuclear Facility Applications" provides requirements for the acquisition, development, operation, maintenance, and retirement of software. The KHNP QAPD governs the treatment of computer applications and digital equipment software when used in safety-related applications and designated non-safety-related applications. KHNP and its suppliers are responsible for developing, approving, and issuing procedures, as necessary, to control the use of such computer applications and digital equipment software.

In AI-26 [Ref. 3], the staff requested details of the quality assurance program applied to the LBLOCA Evaluation Model for the RELAP5/MOD3.3/K code, specifically for the changes made to the RELAP5 program. In response to AI-26, KHNP submitted their Design Control Procedure

DP-10-10, “Design Computer Code Control” [Reference 4]. The staff determined that the KHNP internal design control procedure is consistent with Subpart 2.7 of NQA-1.

Code Configuration Management

The guidance in SRP Section 15.0.2 states that the EM should be placed under a quality assurance program that meets the requirements of 10 CFR Part 50, Appendix B. The NRC staff conducted a separate limited scope software quality assurance inspection from February 29 through March 4, 2016 [Ref. 53], which included the RELAP5/MOD3.3/K code and other selected software. In the inspection, the NRC staff also examined the applicant’s implementation of a 10 CFR Part 21 [Ref. 15] program for reporting of defects and noncompliance. Since the applicant contracts design analysis activities to the various entities comprising KHNP, the inspection focused on the applicant’s oversight of these activities. The NRC inspection team found that, for the samples assessed, the applicant’s design controls are in compliance with the requirements of Criterion III, “Design Control” of Appendix B to 10 CFR Part 50. The oversight of contracted activities is consistent with the requirements of Criterion IV, “Procurement Document Control,” of Appendix B to 10 CFR Part 50.

On the basis of the applicant’s conformance with 10 CFR 50, Appendix B, the NRC staff finds that the applicant’s configuration management process for this EM is acceptable.

Code Changes

TR Appendix B documents the changes made to the source code of RELAP5/MOD3.3 to develop the RELAP5/MOD3.3/K code. Appendix B also includes excerpts showing the original source code and the modified version. The applicant provided the RELAP5/MOD3.3/K source code files [Ref. 26]. The NRC staff compared the changes to the source code described and shown in Appendix B against the actual source code provided in [Ref. 26].

In AI-75a [Ref. 3], the NRC staff requested the applicant to explain several code changes to the RELAP5/MOD3.3/K code and whether those changes were made under an acceptable system of controls that is consistent with Subpart 2.7 of ASME NQA-1. In response to AI-75a [Ref. 4] , the applicant explained that they implemented changes to allow improvements to the calculation of gas gap heat transfer and to edit the gap conductance data as well as the pellet radius as major edits to identify the current heat structure number. Similarly, the applicant modified the code to remove [[

]].

In AI-21 [Ref. 3], the NRC staff requested the applicant to characterize all of the changes made to RELAP5/MOD3.3 and include these in TR Appendix B. In response to AI-21 [Ref. 4], the applicant stated that TR Section 3.4 and Appendix B describe the model and error changes to RELAP5/MOD3.3/K which would affect the calculation results. The applicant stated that they transcribed and managed any other modifications to RELAP5/MOD3.3/K and CONTEMPT4/MOD5 in a separate report for each code controlled by the KHNP software management system. The NRC staff reviewed the documentation of code changes and the qualification records of persons making the changes during the software quality assurance inspection. The staff finds that the documentation is complete and in compliance with the requirements of 10 CFR 50, Appendix B, and that the personnel making the changes are qualified.

Based on the discussions above, including the response to AI-75, the staff considers the process used by the applicant in making modifications to the code and in maintaining code configuration acceptable, and therefore concludes that this issue is resolved.

CONTEMPT-RELAP Coupling

According to [Ref. 26] (page 7 of 23) for the APR1400 LBLOCA analysis,

> *"...TPEAK is set to 0 (zero) and CONTEMPT4/MOD5 dynamic-link library (contl.dll) is loaded when RELAP5/MOD3.3 starts reflood calculation (reflood heat structures enter to reflood mode). The coupled code sets TPEAK to the time reflood calculation starts."*

In AI-44 [Ref. 3], the NRC staff requested the applicant to explain how the containment backpressure is calculated and passed to RELAP5/MOD3.3/K for the accident period prior to the early reflood phase.

The applicant responded that [[

]] as described in Volume II, Section A10.1 [Ref. 20] of the code manual. [[
]]. The loading time is about 22 seconds after the break in the nominal calculation of the APR1400. Because the early reflood period begins at around 38 seconds, as discussed in TR Section 3.1.2.3, the applicant confirmed that CONTEMPT4/ MOD5 is loaded during the refill period. A representative containment pressure is used for LBLOCA analysis of the APR1400 before the start of the CONTEMPT4/MOD5 activation. The TR states that since the break flow remains critical to about 20 s, there should be no impact from containment pressure on break flow and thus reactor coolant system condition. Therefore, the NRC staff finds that the use of a "representative containment pressure" prior to activation of CONTEMPT4/MOD5 calculations is acceptable. Figure 2 in the response to AI-44 [Ref. 5] provides the value of the representative containment pressure used in the APR1400 analysis calculation and shows that it is lower than the Nominal Case containment pressure calculation.

The NRC staff finds that the applicant's treatment of CONTEMPT-RELAP5 coupling as described above is acceptable since it provides a conservative representation of the containment pressure response due to LBLOCA during the early reflood period, and therefore concludes that this issue is resolved.

RELAP/MOD3.1 Applicability

TR Section 4.2.3.2 cites results from a past assessment by the applicant using RELAP5/MOD3.1. That is not the code version that will be utilized in subsequent licensing submittals. In AI-48 Part a [Ref. 3], the NRC staff requested the applicant to indicate whether RELAP5/MOD3.3/K, the version that will be used in subsequent license submittals, has been used to confirm that the results cited are applicable. In response [Ref. 4], the applicant stated that the cited analysis has not been confirmed directly using RELAP5/MOD3.3/K; however, it is expected to be acceptable because of similar code predictability inferred from the code accuracy results, which were described in [Ref. 43] and [Ref. 44], where the RELAP5/MOD3.3/K predictions show similar or more conservative results. The applicant further stated that in order

to confirm the code applicability of RELAP5/MOD3.3/K, they performed an assessment against the UPTF-10B test. The results of the recent simulation are consistent with the results from RELAP5/MOD3.1, as shown in Figure 1 of the response.

The applicant stated that the RELAP5/MOD3.3/K has not been tested against data, except for UPTF-10B. They further stated that results using the RELAP5/MOD3.3/K code version have been shown to be "similar" or "more conservative" results.

The NRC staff finds that the applicant's assessment of the applicability of RELAP5/MOD3.1 to APR1400 is acceptable in this instance, since it provides similar or more conservative results as compared to experimental data, and therefore concludes that this issue is resolved.

Code Accuracy

The applicant defined code accuracy as the statistical difference between calculated and measured PCTs. The applicant used standard definitions of parameters, such as the mean and standard deviation, to determine the statistical code accuracy based on the difference in the code-predicted and the measured PCT. In AI-49 [Ref. 3], the NRC staff requested the applicant to clarify the one-sided 95 percent limit of blowdown PCT of [[ ]]. The applicant's response to AI-49 [Ref. 4] stated that the equation in the TR (i.e., [[ ]]) is correct as stated in the TR. However, the applicant corrected the numerical value to [[ ]] in TR Revision 1.

The NRC staff finds that the applicant's assessment of code accuracy is adequately justified in the response to AI-49, and on the basis of that information concludes that this issue is resolved.

4.2 Code Scaling, Applicability, and Uncertainty

TR Section 1 states that the CAREM methodology follows the Code Scaling Applicability and Uncertainty (CSAU) methodology [Ref. 19]. In the NRC staff assessment of the TR, the NRC staff raised a number of issues, which are further discussed in this section of the SER.

PIRT and Uncertainties

TR Section 3.3 states that the distribution-free statistical approach that is used in CAREM is superior to that of CSAU (NUREG/CR-5249). The TR states that, in contrast to the CSAU methodology, CAREM provides more freedom in the ranking of the phenomena in a PIRT, as evidenced by a large number (i.e., [[ ]]) of phenomena or processes that are ranked as [[ ]]. However, the application of the methodology, described in TR Section 5 states that only [[ ]] uncertainty parameters are utilized. In addition, the process used to arrive at the [[ ]]uncertainty parameters is not described. Therefore, in AI-14, Parts a and b [Ref. 3], the NRC staff requested the applicant to clearly describe the process that is followed to determine the number of uncertainty parameters that can be used. Further, the NRC staff also requested the applicant to explain and justify the approach used (i.e., conservative, or best-estimate values) for the remaining parameters not included as part of the uncertainty analysis.

The applicant responded [Ref. 5] that they described the entire process to determine the [[ ]] uncertainty parameters from the [[ ]] process/phenomena in the APR1400 PIRT in the presentation material provided during the January 2016 meeting [Ref. 1.a] and that they provided a revised PIRT in response to AI-15 [Ref. 3]. In the response to AI-14, Part a, Tables 1 through Table 3 describe the PIRT component, the related process/phenomena, and provides

a reference to a section in the TR or other sources of information. This information provides an additional roadmap to the location of the discussion of the process/phenomena. The response then describes the general process used to determine whether a parameter is treated through an uncertainty evaluation or is treated conservatively.

In response to Part b of AI-14, the applicant provided Table 1, Table 2, and Table 3 to justify excluding some parameters from the uncertainty analysis. In addition, the applicant noted that two phenomena were not included in the TR:

- [[
  ]],
- [[
  ]].

The applicant stated that they did not consider [[
]]. The applicant's statements at the June 2016 Audit Meeting argued that it is highly unlikely that [[
]]. Based on the results of the VAPER tests, consideration was given to various SIT parameters already included for uncertainty quantification, and the expanded geometry of the SI piping connection to the reactor coolant system (i.e., minimizing the potential for any impact from the pump flow on SIT injection). Therefore, the staff concludes that the applicant has provided sufficient justification and bases for the conservative treatment of both [[
]], such that further uncertainty considerations are not required. The staff considers this issue resolved.

In response to RAI 7-8567, Question No. APR1400-4, (ADAMS Accession No. ML16153A454), the applicant provided the same information also provided in response to AI-14, Part a [Ref. 5], but with a clear description of the process used to determine the phenomena that were treated by other uncertainty parameters, the parameters treated conservatively, and the phenomena treated as biases. The response to RAI 7-8567 discussed the phenomena treated conservatively in the response to AI-5 [Ref. 5], and was augmented by an additional discussion of phenomena treated by other uncertainty parameters and phenomena treated as biases. Table 1 in the response to RAI 7-8567 [Ref. 1.h] describes the PIRT component, the related process/phenomena, and provides a reference to a section in the TR or other sources of information. Table 2 in the response to RAI 7-8567 provides a list of the phenomena treated conservatively by CAREM. Table 3 provides a list of the modified APR1400 PIRT process/phenomena treated as biases. While not a clear and concise description of the process used to determine when a parameter is treated through uncertainty evaluation or is treated conservatively, the information in the response to RAI 7-8567 provides sufficient explanation to understand how each PIRT process/phenomena is treated.

The NRC staff finds that the applicant's RAI and AI responses and modification of the PIRT are acceptable and comply with the guidance as outlined in RG 1.203, and on the basis of that information concludes that this issue is resolved.

PIRT Source Information

TR Table 3-2 provides the PIRT used by the applicant as part of the CAREM methodology. The PIRT is used to identify the major phenomena or processes that occur during the accident and to prioritize the major phenomena according to their impact on the acceptance criteria. The PIRT is based on the KNGR PIRT [Ref. 52]. The applicant adjusted the relative importance of certain phenomena or processes in the KNGR PIRT after modifying the definition of temporal periods between the LBLOCA used for the KNGR PIRT and that for the APR1400 PIRT.

TR Appendix A provides details of the KNGR PIRT, but only shows the phenomena that have a numerical ranking of [[ ]] during any phase of the accident, i.e., only the phenomena determined to have a significant influence on the transient. A complete PIRT, as described in the guidance of NUREG/CR-5249 [Ref. 19] includes all the phenomena and their corresponding ranks. In addition, both the KNGR and the APR1400 PIRTs lack a ranking for the "state-of-knowledge" that is used to determine whether a particular phenomenon is well understood and can, therefore, be simulated accurately by the EM. In addition, according to RG 1.203 [Ref. 18], the PIRT generated to guide the EM development process should be adequately documented. Such documentation includes the discussion of the steps followed to generate the PIRT and the definition of each phenomenon that is ranked in the PIRT. Neither the original TR Section 3.3, nor its Appendix A provides a complete PIRT. In AI-15 [Ref. 3], the NRC staff requested the applicant to provide a complete PIRT that addresses the above-mentioned issues.

In response [Ref. 5], the applicant stated that it would revise the APR1400 PIRT to the document contained in Attachment 2 of the Revision 1 response to AI-15 [Ref. 6], which includes a brief rationale description for the assigned process/phenomena rankings and a brief state-of-knowledge column. In addition, TR Revision 1, Appendix A, documents that six experts in nuclear reactor research and operation peer reviewed the adjustments to the KNGR PIRT to arrive at the APR1400 PIRT.

The NRC staff finds that the information supplied satisfies the regulatory guidance in RG 1.203 [Ref. 18] and the approach originally documented in NUREG/CR-5249 [Ref. 19] for PIRT development, and is therefore acceptable. Since the additional information is included in the TR revision [Reference 11], the staff concludes that this issue is resolved.

Containment Pressure Analysis

Section 3.12.1 of RG 1.157 [Ref. 17] states that "...the containment pressure used for evaluating cooling effectiveness during the post-blowdown phase of a LOCA should be calculated in a best-estimate manner and should include the effects of containment heat sinks..." According to TR Section 3.4, the APR1400 best-estimate LBLOCA methodology calls for the coupling of RELAP5/MOD3.3/K with CONTEMPT4/MOD5. Consequently, containment phenomena need to be included in the PIRT, so as to determine the adequacy of, and uncertainty in, CONTEMPT4/MOD5. Table 3-2 contains and ranks generic processes such as "pressure history" and "temperature history" for the containment component. However, the NRC staff considers the ranking of such generic processes insufficient for adequacy determination. The NRC staff position is that individual phenomena that impact these general processes (e.g., "condensation heat transfer," "impact of non-condensable gases," "droplet heat and mass

transfer," etc.) should be included and ranked in the PIRT to determine code adequacy and uncertainty following the SRP Section 15.0.2, and NUREG/CR-5249. Therefore, in AI-16 [Ref. 3], the NRC staff requested the applicant to provide information regarding the PIRT, containment parameters and the process used for the statistical treatment of the containment calculations.

In response [Ref. 4], the applicant stated that CAREM does not treat the containment pressure analysis statistically through uncertainty variables and assessments, but performs a conservative analysis using conservative assumptions. The applicant provided the initial conditions, active heat removal systems assumptions, and the passive heat removal assumptions used to perform a minimum containment pressure analysis in response to AI-16 [Ref. 4]. A conservatively low containment pressure calculation based upon the initial conditions and heat removal assumptions will result in a conservative transient analysis in terms of the PCT.

The NRC staff finds that the explanation supplied by the applicant is acceptable, since an assumed low containment pressure will result in a conservative PCT prediction, so the pressure uncertainty need not be considered. The staff concludes that this issue is resolved.

Importance Adjustments

In Parts (a) through (i) of AI-17 [Ref. 3], the NRC staff requested the applicant to justify the rationale for the assignment of the importance ranking for several phenomena in the APR1400 PIRT presented in Table 3-2. The NRC staff requested the applicant to provide the basis for the stated importance rankings for the following phenomena:

- [[ ]]
- [[ ]]
- [[ ]]
- [[ ]]
- [[ ]]
- [[ ]]
- [[ ]],
- [[ ]], and
- [[ ]].

In response to AI-17 [Ref. 5], the applicant stated that modification of the KNGR PIRT to the APR1400 PIRT resulted in some errors, in large part due to the change in the definitions of various time periods. The applicant revised the PIRT in Revision 1 of TR Appendix A to correct the errors consistent with the definition of the time periods and provided a basis for the importance rankings.

The NRC staff finds that the applicant acceptably updated revisions to the importance rankings consistent with the guidance in RG 1.203 [Ref. 18] and the approach originally documented in NUREG/CR-5249 [Ref. 19]. Therefore, on the basis of that information concludes that this issue is resolved.

Applicable Phenomena

TR Table 3-5 lists the constitutive equations and models in the RELAP5/MOD3.3/K and CONTEMPT4/MOD5 computer codes that are used to predict important phenomena or processes for the APR1400 LBLOCA. Table 3-5 identifies the components, the key phenomena, or processes in each component based on the PIRT rankings and the models or correlations in the codes that participate in the prediction of each phenomenon.

TR Table 3-5 does not provide the entire picture of the presence of models and correlations in RELAP5/MOD3.3/K and CONTEMPT4/MOD5 that are necessary for phenomena prediction. The model for the phenomenon of "entrainment/de-entrainment" and "level" in the upper plenum component is specified as "interfacial drag" in TR Table 3-5. However, as pointed out in TR Section 3.6.1, RELAP5/MOD3.3/K cannot model de-entrainment on internal structures. As a result, the information in TR Revision 0, Table 3-5, can be confusing because the reader is left with the impression that the interfacial drag correlations in RELAP5/MOD3.3/K can predict de-entrainment, whereas in reality such a correlation does not exist in the code. The applicant did not mention any other biases that will be included in the uncertainty analysis in TR Section 3.6.1 or Table 3-5.

In AI-19 Part a [Ref. 3], the NRC staff requested the applicant to provide a clear statement of all the phenomena that are treated by biases in TR Section 3.6.1. In the Revision 1 response to AI-19, Part a [Ref. 4], the applicant stated that there are two types of biases in CAREM; (1) Steam Binding bias, described in TR Section 4.2.3.2, which consisted of de-entrainment bias in the upper plenum and a droplet evaporation bias in the steam generator U-tubes; and (2) ECC Bypass bias, described in TR Section 4.2.3.1, which the applicant divided into a ECC bypass bias during the refill and ECC bypass bias during reflood. The applicant provided Table 1, "Modified APR1400 PIRT treated by biases," in the response to AI-19, Part a, which summarized the processes / phenomena that are treated as biases. The applicant's discussion of the steam binding and the ECCS bypass bias along with the table that lists the PIRT phenomena that are treated by biases addresses the NRC staff's question in AI-19, Part a.

The response to RAI 7-8567, Question APR1400-4, (ADAMS Accession No. ML16153A454), includes for component "Reactor vessel upper plenum" a process/phenomenon and level as part of the Steam binding bias. Table 1 in the response to AI-19, Part a does not include this process/phenomenon. In addition, both tables include the process/phenomena flashing in the ECC bypass bias, which the applicant agreed in the June 2016 Audit Meeting should not be included in a bias discussion.

In Part b of AI-19 [Ref. 3], the NRC staff requested the applicant to consider modifying TR Table 3-5 to include a column providing the status of existence of a model ("yes/no") in

RELAP5/MOD3.3/K and CONTEMPT4/MOD5 for each of the listed phenomenon, following the approach utilized in NUREG/CR-5249.

In response [Ref. 4], the applicant stated that the second column of TR Table 3-5 shows important phenomena related to each component and that the third column shows the existing models in RELAP5/MOD3.3/K and CONTEMPT4/MOD5. Table 1 in the response to AI-19, Part a, provided information from the Modified APR1400 PIRT that showed which process/phenomena were treated as biases.

The NRC staff finds that the information supplied in response to AI-19 is acceptable, since it completes the expected PIRT information recommended in RG 1.203 [Ref. 18] consistent with the approach documented in NUREG/CR-5249 [Ref. 19]. The applicant incorporated this information in TR Revision 1, so the NRC staff concludes that this issue is resolved.

Uncertainty Parameters

In TR Section 4.3.1.2, the applicant demonstrates the variety, number, and ranges of the selected code uncertainty parameters that are appropriate for each licensing application of the CAREM methodology. In TR, Revision 1 [Ref. 13], Section 5.2.2, "Plant SRS Calculation," the applicant confirms that in license submittals they will utilize distribution-free statistics and 181 simulations in order to obtain at least three samples for the PCT, one for the MCO and one for the CWO for a 95/95 confidence level. The applicant will then choose appropriate uncertainty parameters for variation during each of the 181 calculations for each SET used in what is called the "coverage check" as described in TR Section 4.3.2.

According to the applicant, the 'coverage check' compares the uncertainty of [[ ]] parameters against SET data. In AI-50, Part a [Ref. 3], the NRC staff requested the applicant to explain the process for choosing the limited number of parameters for uncertainty variation in the blowdown and reflood "coverage check" from the list of all phenomena with [[ ]] during these periods. Also, in AI-50, the NRC staff asked the applicant to explain how it is ensured that inclusion of the additional uncertainty for parameters does not change the results and alter the conclusions of the 'coverage check'. Further, if such a demonstration has been accomplished, the NRC staff requested the applicant to describe the change in the limiting PCT in AI-50, Part b [Ref. 3].

In the response [Ref. 4], the applicant stated that all uncertainty parameters can be consistently considered for blowdown and reflood coverage check. The applicant further stated that it is not necessary to consider the uncertainty parameters related to reflood phenomena for blowdown coverage check, and vice versa.

The NRC finds that some uncertainty parameters involved with both blowdown and reflood phenomena are commonly used for the blowdown and reflood coverage check. In addition, both uncertainty parameters related to blowdown and reflood phenomena are considered for IETs. Furthermore, a larger number of uncertainty parameters results in wider uncertainty variation (i.e., higher cladding temperature).

However, in the view of the NRC staff, this explanation did not address the fact that many phenomena [[ ]], specifically for blowdown (APR1400 PIRT), are not used in the blowdown coverage check for the SET. This was discussed during the January 2016 Audit Meeting [Ref. 12], where the applicant confirmed that the number of parameters selected covers the applicable and appropriate phenomena [[ ]]. The applicant stated that the

phenomena that were not included in the coverage check for a specific SET were not applicable or appropriate for consideration based upon the APR1400 design and operating conditions, which precluded particular phenomena from occurring. Based upon the facility design detailed information in the TR, the NRC staff concurs that restricting the selection of parameters to those related to the blowdown phenomena in the specific SET coverage checks is appropriate. The NRC staff finds that the coverage check performed by the applicant is acceptable, and is consistent with the guidance in RG 1.203 [Ref. 18] and the approach documented in NUREG/CR-5249 [Ref. 19]; therefore, the determination of uncertainty parameters is also acceptable. On the basis of this information, the NRC staff concludes that this issue is resolved.

Simple Random Sampling Approach

TR Section 5.2.2 discusses the use of simple random sampling approach to perform 181 SRS calculations using the distributions of the uncertainty parameters listed in the TR Table 5-1. However, the TR does not discuss the model used to perform the random sampling. In AI-63 [Ref. 3], the NRC staff requested the applicant to describe the model or method that is utilized to perform the random selection of samples and to provide justification that the sampling process is unbiased.

The applicant's response [Ref. 4] referred to a report by Glaser, "BEMUSE Phase VI Report," [Ref. 40] that provides guidance which has been followed for CAREM:

> *"It is also important to note that the model outcome sample values $Y_1 \ldots Y_N$ from which the tolerance intervals/limits are determined must constitute a random sample of the model outcome Y in the statistical sense, i.e., they must be realizations of stochastically independent and identically distributed random variables $Y_1 \ldots Y_N$ from which the tolerance intervals/limits are determined must constitute a random sample of the model outcome Y in the statistical sense, i.e., they must be realizations of stochastically independent and identically distributed random variables $Y_1 \ldots Y_N$.. This is ensured if the underlying input parameter sample is generated according to the simple random sampling principle. Other types of parameter selection procedures like Latin Hypercube Sampling or Importance Sampling, etc. may therefore be appropriate for tolerance intervals or tolerance limits."*

The Glaser report also states:

> *"Simple random sampling should be used to derive tolerance intervals or one-sided tolerance limits."*

To get the random sample, the applicant used an open source computer program, LHS [Ref. 45]. Simple random sampling was performed using the option for "random sampling" in the LHS code that causes LHS to perform a pure Monte Carlo method to generate random samples.

The applicant demonstrated the use of distribution-free statistics for the APR1400 LBLOCA calculations in TR Section 5.2.2. The applicant chose the third highest PCT result of 181 calculations as the 95/95 value for PCT. In TR Section 5.2.2, the applicant presented the third highest result of 181 SRS calculations as the limiting PCT. In AI-64 [Ref. 3], the NRC staff requested the applicant to provide the values and plots for all three highest PCTs predicted in the SRS calculations. The applicant provided the requested information [Ref. 4], but the AI-64 response information was superseded by new calculations in TR Revision 1.

The NRC staff finds that the applicant's method for performing the random sampling is acceptable, as demonstrated by the revised calculations which utilize methods published in the peer-reviewed literature that meet Regulatory Position 4 (Estimation of Overall Calculational Uncertainty) of RG 1.157 [Ref. 17]; therefore, on the basis of that information, the staff concludes that this issue is resolved.

Basis for the Number of Cases

The applicant employs distribution-free statistics and uses 181 simulations to obtain at least five samples consisting of the highest maximum cladding oxidation (MCO), the highest core wide oxidation (CWO), and the third ordered peak cladding temperature (PCT) at a 95/95 confidence level. The applicant formally documented this approach in the response to AI-51, Parts a-d [Ref. 5]. In the response, the applicant states that the uncertainty evaluation method is third order with 181 runs based upon the theoretical background provided by the formulation of Guba, Makai, and Pál [Ref. 37], and the AI response details the parameter selection process and the number of cases that need to be run. The methodology continues to rely upon the work of Glaser [Ref. 40] to agree that more than 124 sample runs are necessary to meet the NRC's requirements on the interpretation for satisfying the 10 CFR 50.46 acceptance criteria under the order statistics approach. The response provides justification for the use of 181 cases and the selection of the third highest value of PCT, the highest value of the MCO, and the highest CWO selected from all of the SRS calculations. With this approach, the APR1400 CAREM methodology documented in TR Revision 1 remains largely the same as that in the original TR Revision 0, the only difference being that the number of SRS calculations would now be 181 instead of the previous 124.

The NRC staff finds that the applicant's use of distribution free statistics to determine that 181 cases satisfies Regulatory Position 4 (Estimation of Overall Calculational Uncertainty) of RG 1.157, since it is consistent with published peer reviewed statistical methods; therefore, on the basis of that information, the staff concludes that this issue is resolved.

Uncertainties in Initial and Boundary Conditions

As stated in TR Section 5, uncertainties in the initial and boundary conditions of the plant as well as those associated with modeling parameters govern the uncertainties associated with analysis of LBLOCA events. Plant initial and boundary conditions include [[

]]. TR Table 5-1 lists probability distribution functions and uncertainties of plant condition parameters, as well as code uncertainty parameters that are applicable.

The guidance in RG 1.157, Section 4, establishes acceptable controls for the estimation of uncertainties. In addition, NUREG/CR-5249 describes the process for formulation of uncertainty distributions. In CAREM, the uncertainties are propagated through the models using distribution-free (i.e., non-parametric) statistics to determine the limiting PCT based on the variation of key uncertainty parameters.

In AI-52 Part a [Ref. 3], the NRC staff requested the applicant to provide the justification for the use of the non-parametric distribution free statistical approach. The Revision 1 response to AI-51 [Ref. 6] provides the justification.

The NRC staff finds that the applicant's response to AI-51 provides an acceptable explanation to support the uncertainties employed to ascertain PCT, consistent with the guidance in Regulatory Position 4 of RG 1.157, and on the basis of that information concludes that this issue is resolved.

95/95 Methodology

The example of the CSAU process shown in NUREG/CR-5249 indicates that the mean value of the effect for each of the uncertainties on the blowdown and reflood portions is calculated. The sums of all the 95th percentiles, relative to the mean, are added to obtain the summed biases. The summed biases are then added to 95th percentile of the response surface produced from the calculation of the mean peak cladding temperatures from the uncertainty of high influence parameters. TR Revision 1, Tables 5-5 through 5-8, provide the determination of the biases for application in the CAREM process. In AI-52, Part b [Ref. 3], the NRC staff requested the applicant to describe how the CAREM process provides the 95th percentile for the bias determination.

In response [Ref. 4], the applicant stated that, although the bias evaluation in NUREG/CR-5249 appears to provide the 95th percentiles for the bias determination, it only considers the bias related to the hot channel. It further states that CAREM uses almost the same approach as NUREG/CR-5249. The applicant evaluated the biases in CAREM using [[ ]]. The applicant then observed the thermal-hydraulic conditions that can affect the PCT in the assessment of [[ ]]. The applicant considered the evaluated bias as shown in Tables 5-4 through 5-7 for practically all of the SRS cases. For example, [[ ]]. The 95th percentile of the bias does not need to be evaluated in CAREM because the bias is considered for practically all of the SRS cases. Therefore, for the final scaled bias evaluation, the applicant considers the maximum biases, which neglect the negative biases.

This response shows that the determination of biases in CAREM differs from the approach utilized in CSAU (NUREG/CR-5249), but the applicant argues that in the CAREM approach, the bias is considered conservatively, for a large number of SRS cases. Since the maximum impact of biases is in increasing the calculated 95th percentile of PCT, the applicant states that this approach is conservative.

RG 1.157 indicates that the uncertainty can vary over time during the transient, and it states that:

> *"In evaluating the code uncertainty, it will be necessary to evaluate the code's predictive ability over several time intervals, since different processes and phenomena occur at different intervals. For example, in large-break loss-of-coolant accident evaluations, separate code uncertainties may be required for the peak cladding temperature during the blowdown and post-blowdown periods. Justification for treating these uncertainties individually or methods for combining them should be provided."*

Since it was not clear to the NRC staff how the temporal differences in the bias and uncertainty are treated in the CAREM methodology, in AI-52, Part c [Ref. 3], the NRC staff requested the applicant to provide the basis and the process for determination and application of the bias and uncertainty during the blowdown and reflood (early and late) periods.

In response [Ref. 4], the applicant stated that the temporal difference in the biases is addressed by examining the importance rankings defined in the PIRT. If one bias is important for a certain period, the bias is activated for that period. The applicant concluded that the treatment of biases need not consider the uncertainties due to the application of the estimated biases. The estimated biases from test assessment are applied for practically all of the SRS cases, thus the methodology obtains the most conservative estimation of biases as the result of the final bias evaluation. The applicant restates that the assignment of biases in CAREM follows a conservative approach.

Furthermore, the response states that the temporal impact of biases considers the importance rankings in the PIRT. The applicant provided examples for ECC bypass, steam binding and steam generator U-tube heat transfer and vapor superheat to show the consideration of biases varies over intervals of time. The applicant provided these to show that the final bias evaluation is sufficiently conservative.

The NRC staff finds that the applicant's methodology for determining suitably conservative biases is acceptable, since it is consistent with Step 20 of RG 1.203 [Ref. 18] and the approach documented in NUREG/CR-5249 [Ref. 19]. Therefore, on the basis of that information, the staff concludes that this issue is resolved.

Uncertainty Distribution SRS for FLECHT-SEASET Tests

Table 2-2 in TR Appendix C shows the parameters and distribution functions used for SRS calculations for the FLECHT-SEASET tests. The system-specific parameters for the FLECHT-SEASET test facility include [[ ]]. However, the applicant did not provide an explanation for how the uncertainty in these parameters is determined. Therefore, in AI-77 [Ref. 3], the NRC staff requested information on the process followed to determine the uncertainty range and distribution for the flooding rate and power that are applicable to the FLECHT-SEASET facility. AI-77 also requested clarification regarding the importance of negative power and flooding rate and how they are handled in the calculations.

In response [Ref. 4], the applicant provided the measurement uncertainties of total power and volumetric flow rate at a one sigma level. Since the applicant's RELAP5 model uses the liquid phase velocity as a boundary condition using a time dependent junction, volumetric flow rate is changed to obtain velocity using the core area of 0.0156 m^2. Furthermore, the response stated that, in CAREM, the uncertainty ranges are calculated by [[ ]]. Therefore, the sample uncertainty ranges for power and liquid phase velocity (reflooding rate) are as follows:

[[

]]

These uncertainties for power and reflooding rate are used in conjunction with normal distribution functions for power and reflooding rate in common, since the measurement uncertainty data described in [Ref. 2-1] of TR Appendix C are the standard deviations for each measurement.

In the response, the applicant stated that the fuel rod power in TR Appendix C, Table 2-1, is the linear heat generation rate for a fuel rod, while the uncertainty associated with power shown above is the uncertainty associated with the total power. The response also stated that the unit

of flooding rates in Table 2-1 in Appendix C was given as cm/sec, and it should have been in mm/sec. In TR Revision 1, Appendix C, the correct information is listed.

The sampled values for power and reflooding rate are varied from their nominal values, which are boundary conditions of each test. Therefore, the sampled values are added to the nominal values of the total power and reflood rate.

The NRC staff finds that the applicant has provided sufficient information on the process to determine the uncertainty range and distribution for flooding rate and power, and on the basis of that information concludes that this issue is resolved.

Limits of the Uncertainty Distribution

The NRC staff determined that the limits of the uncertainty distribution utilized in CAREM (e.g., twice the standard deviation) used for the parameters with normal distribution during the SRS sampling in TR Appendix C, are not clearly specified. In AI-78 [Ref. 3], the NRC staff requested the applicant to clarify the uncertainty limits for parameters with a normal distribution during SRS sampling

In response [Ref. 4], the applicant stated that, for the SRS sampling of the uncertainty variables with normal distribution, the uncertainty range of [[ ]] is used in order to include a broad range in the uncertainty. On the one hand, for sampling with uniform distribution, the uncertainty range of [[ ]] is used. In this case, σ is the standard deviation, but μ is the deviation of one-sided limit.

The NRC staff finds that the applicant has clarified the uncertainty limits acceptably, and on the basis of that information concludes that this issue is resolved.

Negligible Uncertainties

In TR Section 4.5 of Appendix C, the applicant states that "...the selected code parameters and distribution functions for the NEPTUN test are the same as those used in the SRS calculations against FLECHT-SEASET tests." However, Table 4-5 of Appendix C lists only [[ ]] parameters compared with the [[ ]] parameters used for the FLECHT-SEASET tests. In AI-79 [Ref. 3], the NRC staff requested the applicant to clarify and confirm any inconsistencies.

In response [Ref. 4], the applicant referred to the response to AI-50, Part a, which commits to considering the effects of test-specific uncertainty, if not negligible. The response provided specific examples of these uncertainty factors in the FLECHT-SEASET tests, such as the [[ ]].

The NRC staff finds that the applicant's information concerning non-negligible uncertainties is acceptable, and on the basis of that information concludes that this issue is resolved.

4.3 Evaluation Model Assessments

According to TR Section 4.1, the applicant performed the EM assessment using SETs that investigate individual phenomena, and IETs that incorporate many or all of the important phenomena and components. Table 4-1 restates the type of assessments, facilities used, and where the test details are documented.

Table 4-1 APR1400 Separate Effects Tests

Assessment	Facility Tests	Documented in
reflood, system pressure, clad temperature, power refill & reflood reflood energy transport/transfer reflood	FLECHT-SEASET 31805, 31504, 31203, 31302, 31701, 34209, 32013, 30518, 30817, 34420, 31021, 34524, 31108, 32235, 32333, 33338, 34006 CCTF C2-4 NEPTUN 5025, 5036, 5049, 5050, 5051, 5052, 5056 THTF 105, 151, 160, 162 PKL IIB5	TR Appendix C
integral effects tests	LOFT L2-2, L2-3, L2-5, LP-02-6 Semiscale S-06-3 LOBI A1-66	TR Appendix D
DVI of ECCW, downcomer boiling, ECCW bypass	ATLAS 09, 11, 15	TR Appendix E
ECCW bypass	MIDAS, UPTF 21-D	TR Appendix F
downcomer boiling	DOBO 1, 2, 3, 4	TR Appendix G
SIT-FD	VAPER 01, 02, 03, 04	TR Appendix H

Certain tests raised issues during the review and were the subject of information requests to the applicant.

FLECHT-SEASET Reflood Tests

TR Section 3.4 and Appendix B discuss two modifications which the applicant made to improve the predictability of the time of fuel rod quenching. Figures 3 and 4 in TR Appendix B show only a small difference from the change in the PCT for [[ ]]. In AI-22 [Ref. 3], the NRC staff requested the applicant to discuss the impact of the code modification that was used to improve the fuel rod quenching time predictions. In response, the applicant provided figures illustrating the effect of [[ ]] on the simulation of FLECHT-SEASET low flooding rate tests 31805 and 34006, which showed delayed quenching and better agreement with the test data.

Additionally, as part of AI-23, the applicant clarified that RELAP5/MOD3.3/K predicts [[ ]] measured in FLECHT-SEASET tests 31805 and 34006. However, in a letter dated April 25, 2018, the applicant provided analysis results to demonstrate that the application of RELAP5/MOD3.3/K in accordance with the CAREM methodology results in conservatively high estimates for fuel temperatures and quench times for FLECHT-SEASET tests at all reflood rates (Reference 57). Based on the analyses presented in Appendix C of the TR and the supplemental information provided in Reference 4 and Reference 57, NRC staff finds that the application of RELAP5/MOD3.3/K in accordance with the CAREM methodology provides suitably conservative estimates for fuel temperature during reflood.

An initial version of this SER imposed Condition (1) here. This condition has been removed based on the additional information presented by the applicant. However, due to external references, the condition numbering is being kept for consistency.

Condition (1): Deleted.

ATLAS Integral Effects Tests

In TR Appendix E, the applicant shows that [[
]] than the ideal case using scaling relationships. This means that [[
]]. Therefore, the outer surface temperature of the lower downcomer wall (i.e., reactor vessel-wall below the cold leg elevation) of [[
]]. In spite of this, [[
]]. As a result, [[
]] in the APR1400. The initial temperature of the upper downcomer wall was [[ ]].

The applicant states that the results of three ATLAS tests showed [[
]] during the APR1400 LBLOCA events. Moreover, RELAP5/MOD3.3/K code is [[
]].

The scaling of the ATLAS facility is briefly discussed in TR Section 2.1 of Appendix E. It provides the major scaling relations used in the ATLAS facility design. Section 3.1 of Appendix E demonstrates that the downcomer wall heat transfer area of the ATLAS is about [[
]]. However, the applicant did not discuss the approach used to scale the metal mass to fluid volume ratio in order to correctly capture the stored energy release and downcomer boiling phenomena. In AI-82 [Ref. 3], the NRC staff requested the applicant to describe how the metal mass to fluid volume ratio was scaled in order to correctly capture the stored energy release and the downcomer boiling phenomena.

In the response to AI-82 [Ref. 4], the applicant provided descriptions of how the metal mass to fluid volume ratio was scaled in order to correctly capture the stored energy release and the downcomer boiling phenomena. The response stated that for the reactor pressure vessel downcomer with an annular shape, the metal mass to fluid volume ratio is proportional to volume ratio, and can be expressed by:

[[ ]]

where D_i and D_o are the downcomer inner and outer diameter, respectively. L is the height, and t is the vessel thickness. The ratio of metal mass to fluid volume can be expressed by:

[[ ]]

Here, G is the downcomer gap, defined as (D_o-D_i), and the subscript R indicates a ratio of model to prototype.

In order to preserve the stored energy release from the downcomer wall to fluid in the scaled-down model, the ratio $(t/G)_R$, should be equal to 1.0 However, in the as-built design of ATLAS, the downcomer diameter was intentionally enlarged to have a gap large enough to simulate the cap bubble rising in the downcomer region and the wall thickness was increased to be able to withstand the high pressure conditions using the guidance from the American Society of Mechanical Engineers Boiler and Pressure Vessel (ASME) (B&PV) Code, Section VIII, Division II. Consequently, the ratio $(t/G)_R$ of ATLAS becomes [[ ]]. As a result, the ATLAS downcomer wall has a larger stored energy per unit fluid volume than the APR1400 design by a factor of [[ ]]. The applicant provided a summary of the comparison of the major scaling values in Table 1 of the response to AI-82. The applicant concluded that these scaling conditions provide more conservative conditions, particularly when the downcomer boiling phenomena are simulated in the ATLAS facility.

TR Section 2.2 in Appendix E states that the conditions at the start of the reflood period of the APR1400 LBLOCA are given as the initial and boundary conditions for ATLAS Tests 9, 11 and 15. Presumably, the applicant determines these conditions based on code calculations. Therefore, in AI-83 [Ref. 3], the NRC staff requested the applicant to confirm this understanding and clarify whether it uses RELAP5/MOD3.3/K to determine the initial conditions.

The applicant stated [Ref. 4] that RELAP5/MOD3.3 patch 03 obtained the initial and boundary conditions for the ATLAS tests at the start of the reflood period of the APR1400 LBLOCA. However, the code prediction during blowdown and refill periods is not different from RELAP5/MOD3.3/K because, [[ ]]. Therefore, the applicant considered the code assessment for blowdown period in TR Appendices C and D to be valid in so far as the adequacy of code used in the determination of the initial condition for the ATLAS tests is concerned.

TR Figures 2-9 and 2-15 in Appendix E show the SIT-FD injection rate (high- and low-flow) for ATLAS Tests 9 and 11. The tests start from the reflood period and therefore, as shown in Figure 2-6 in Appendix E, the applicant does not consider a portion of the SIT-FD flow. In AI-84 [Ref. 3], the NRC staff requested the applicant to explain how the time at which SIT-FD injection, and therefore, the injection rate in the tests, is determined. In addition, the NRC staff also requested the applicant to explain the reason for the difference in the injection rate between the four SITs as seen in Figure 2-9 and especially in TR Figure 2-15.

In the response, the applicant stated that it determined the initial condition of the reflood test and the injection rate of the SIT-FD in the ATLAS tests using the [[ ]], which it then verified against measurements.

The applicant provided an explanation of the test initialization procedure. In the drainage step, the applicant explained that the power is linearly increased from 0 to a specified value when the water levels in the core and downcomer reach a specified value. Subsequently the power is maintained until the maximum heater rod temperature reached 450°C, at which point the SIT injection signal is triggered. [[ ]] and the power is decreased to follow 120 percent of the ANS-79 decay heat curve. The applicant attributed the differences noted in above in TR Figure 2-9 and Figure 2-15 of TR Appendix E to small differences in the orifice diameter and the behavior of the flow control valves.

The applicant asserts in TR Appendix E that [[ ]] in ATLAS Tests 9, 11 and 15 are not expected to occur in the APR1400 plant. However, the purpose of integral

tests is to demonstrate the expected behavior of the plant. Therefore, stating that certain phenomena observed in the tests are not expected in the plant defeats the purpose of the tests. In addition, the applicant's rationale for not expecting [[ ]] in the plant was unconvincing. As an example, [[

]] but, such flow will also exist in the test facility which does exhibit the temperature difference. In AI-85 [Ref. 3], the NRC staff requested the applicant to justify the use of the selected ATLAS tests for this assessment.

In response [Ref. 5], the applicant states that downcomer boiling can occur during the refill and reflood periods. The effects of downcomer boiling on the thermal-hydraulic behavior is relatively insignificant because a large amount of ECCW is injected during refill and early reflood periods, while thermal-hydraulic behavior during the late reflood period can be affected by downcomer boiling phenomena due to the small ECCW injection flow rate. [[

]]. The applicant selected two uncertainty parameters for downcomer phenomena in CAREM, and determined uncertainty parameter ranges and distribution functions based on the assessment of ATLAS tests.

In addition, the applicant states that the methodology treats the ECCW bypass phenomenon by bias because it is related to many complex phenomena as described in TR Section 4.4.1. Discussions during the January 2016 Audit Meeting and the response to AI-45, Part f [Ref. 5], and AI-85 described [[ ]] in the ATLAS tests as discussed above. Even though ATLAS Test 15 had better initial conditions than Tests 9 and 11, the initial conditions of Test 15 were also [[ ]]. Since the ATLAS tests were used to justify, with other tests, the treatment of ECC water bypass as a bias, the contribution of the ATLAS tests to the bias determination, and specifically which other tests determined the bias, needed to be provided by the applicant. This issue was again discussed in conjunction with AI-45, Part f [Ref. 5], at the June 2016 Audit Meeting. As noted before, some non-typical aspects of the facility in connection with the test initialization procedure resulted in some portions of the tests being unsuitable for use in the determination of the ECCS bypass bias. For the periods when the test was prototypical, the applicant described the information available to perform the code simulation, and for the period when the condition was deemed non-prototypical, a restart of the code was performed with the appropriate temperature input conditions to simulate the prototypical period in the test. The NRC staff agrees that the process of restarting the test simulation with the appropriate temperature data is acceptable.

Based upon the guidance in RG 1.203, the applicant followed the EMDAP process in Step 8(a) by evaluating the integral effect test distortion and utilized the appropriate information from the ATLAS test to meet the test and code simulation objectives for the period in which the test data was prototypical. The NRC staff finds that the applicant's information regarding the metal mass to fluid volume scaling is acceptable, and on the basis of that information concludes that this issue is resolved.

4.4 Biases and Uncertainties

Entrainment [[ ]] and Droplet Evaporation Biases

In [Ref. 26] (Slide 18 of 29) the applicant illustrates the implementation of the entrainment [[ ]] bias in RELAP5/MOD3.3/K, and states that the bias is activated [[ ]] period. However, it is unclear when this bias is activated during the simulation of the

UPTF-10B test and whether the system conditions during the test at the time of activation are similar to those in the APR1400 simulation during [[ ]] period.

In AI-48, Part c [Ref. 3], the NRC staff requested the applicant to clarify whether the [[ ]] implemented in RELAP5/MOD3.3/K is consistent with that used for the UPTF-10B test. In the response to AI-48 Part c [Ref. 4], the applicant stated that the de-entrainment bias activation time in the APR1400 simulation is different from that of the simulation of the UPTF-10B test. The time at which the entrainment [[ ]] bias is activated in the APR1400 simulation is at the [[ ]] period. The applicant stated that the purpose of the UPTF-10B simulation was to investigate the de-entrainment phenomena in the upper plenum during the reflood period, and the start of the reflood in the simulation of the UPTF-10B test corresponds to the start of the liquid injection time. Therefore, both the APR1400 calculation and the simulation of the UPTF-10B test use [[ ]]. The applicant stated that the [[ ]] for de-entrainment bias in the EM. Hence, the NRC staff finds that applicant's position on the bias activation time is acceptable because the bias should be and is active in the specific period of interest, and concludes that this issue is resolved.

The applicant describes in TR Section 5.2.3 the droplet evaporation bias. Selection of the activation time for this bias is different from that for the entrainment [[ ]] activation. According to TR Table 3-5, the APR1400 PIRT assigns its highest importance rank of '5' to [[ ]] in periods 3 and 4. In AI-48, Part d [Ref. 3], the NRC staff requested the applicant to justify the selected activation timing for the droplet evaporation bias because the steam binding effect is expected to be more important during the early reflood period due to the higher rates of flow and entrainment. In response [Ref. 4], the applicant stated that, due to the reasons described in the response to AI-71 [Ref. 4], the activation timing for droplet evaluation bias is [[ ]] because of the high flooding rate during the early reflood and excessive steam binding bias evaluation methodology.

The NRC staff finds that the applicant's information clarifying the activation times for the entrainment [[ ]] bias and the droplet evaporation bias are acceptable, and on the basis of that information concludes that this issue is resolved.

Best-Estimate vs. Conservative Assumptions

The applicant presented the CAREM approach in the TR as a best-estimate methodology. However, the actual implementation of the methodology incorporates a mixture of best-estimate analysis that also uses conservative values for some parameters selectively. The reason that some items are treated conservatively is identified only for certain parameters. Therefore, in AI-5 [Ref. 3], the NRC staff requested the applicant to provide the basis for the determination of when an item is to be treated by using conservative values instead of in a best-estimate manner.

In response to AI-5 [Ref. 5], the applicant provided Table 1 "Phenomena treated conservatively in CAREM" and provided a basis and justification for conservative treatment. For each of the components in Table 1, the applicant showed the process/phenomena and PIRT ranking. The applicant cited the guidelines provided by RG 1.157 regarding justification for the introduction of conservatism in a best-estimate model. For each of the process/phenomena, the applicant provided a justification for the conservatism and the category of conservatism in accordance with RG 1.157.

In response to RAI 7-8567, Question No. APR1400-4, [Ref. 1.i], the applicant described the parameters that are treated statistically by the uncertainty analysis, the parameters that are assigned conservative values, and the parameters that are biased. This response provides the basis for the applicant's determination of when a process/phenomenon is to be treated by a conservative approach and not in a best-estimate manner within CAREM.

The NRC staff finds that the applicant's information clarifying the basis for the determination of when an item is to be treated conservatively instead of in a best-estimate manner is acceptable, and on the basis of that information concludes that this issue is resolved.

ECCS Bypass

NRC RAI No. 7-8567, Question No. APR1400-4 [Ref. 10] requested the applicant to identify which phenomena are treated by other uncertainty parameters, which are treated conservatively and as biases. In Table 3, "Modified APR1400 PIRT treated by biases" of its response [Ref. 1.h], the applicant clearly designates which processes/phenomena are treated by biases. [[ ]], which the applicant stated was an intrinsic and appropriately calculated code parameter, there are [[ ]] processes/phenomena which are combined into the steam binding bias, and [[ ]] processes/phenomena which are combined into the ECCS bypass bias, as discussed in the response above. While the CSAU process discusses the combination of some processes/phenomena into the ECCS bypass bias determination, the basis and justification for the number of processes/phenomena combined into a single bias by the applicant in the CAREM methodology is not clear to the NRC staff. This question was posed in AI-40 [Ref. 3].

In the response to AI-40 [Ref. 5], the applicant stated that the cited process/phenomena are not included as part of the SRS uncertainty assessment process, but are treated as biases, as discussed in Section 4.2.3 of the Topical Report. The applicant noted that test facilities designed to scale power to volume can result in a bias due to scale distortions and that phenomena affected by these scale distortions should be treated as biases which are evaluated based on assessments against full-scale test data. In response, the applicant provided Table 1, "PIRT items treated by biases." This table indicated that it considered [[ ]] part of the ECC bypass bias, [[ ]] as part of the ECC bypass bias, and [[ ]] as part of the ECC bypass bias.

Table 1 in the response to AI-40 corresponds to Table 1 in the response to AI-19 Part a [Ref. 4], which as noted earlier, does not completely agree with Table 3 in the response to RAI 7-8567, Question APR1400-4. The applicant's response to AI-40 [Ref. 5] stated that the processes/phenomena are all included in the ECCS bypass bias. While in a different text format, Section 4.2.3 of TR Revision 1 lists the various phenomena that are evaluated by the applicant as biases, which therefore resolves the inconsistencies noted above.

The NRC staff finds that the applicant's information justifying the combination of bias terms into a single bias does not render the analysis results unrealistic and is consistent with the guidance in RGs 1.203 [Ref. 18] and 1.157 [Ref. 17] to incorporate biases in the analyses in absence of best-estimate models. Therefore, on the basis of that information, the staff concludes that this issue is resolved.

Dissolved Nitrogen

NUREG/CR-5249 [Ref. 19] explicitly addresses the bias due to the presence of dissolved nitrogen in the injected coolant. The RELAP5/MOD3.3 code does not model any dissolved nitrogen in the liquid, and therefore, the predicted reflood peak cladding temperature does not reflect the effect of dissolved nitrogen coming from coolant injected from the SITs. In AI-20 [Ref. 3], the NRC staff requested the applicant to provide an assessment of the effect of dissolved nitrogen on the PCT and transient results.

In the Revision 1 response to AI-20 [Ref. 6], the applicant stated that Section 5.2 of [Ref. 28] evaluated the dissolved nitrogen release from the SIT-FD. The applicant states that this reference conservatively estimates the mass and volume flow rate of dissolved nitrogen from the SIT-FD, and analyzes the effects on the fluidic device K-factors as shown in Figure 5.2-1 and Figure 5.2-2 of that document. The applicant states that the estimated mass and volume flow rate effect due to dissolved nitrogen is small compared with contribution of ECCW from the SIT-FD.

Furthermore, the applicant performed a sensitivity calculation to evaluate the dissolved nitrogen effects on the refill phase using APR1400 LBLOCA EM. In that calculation the amount of dissolved nitrogen assumed was based upon the following: (1) nitrogen gas is fully saturated in the water of SIT-FDs, (2) the amount of dissolved nitrogen in the water is proportional to the partial pressure of the nitrogen gas, and (3) all of the dissolved nitrogen is released when the water from SIT-FDs is discharged through the DVI nozzle. In that calculation, the applicant did not consider the pressure change in the tank, and larger amounts of dissolved nitrogen were released than in the evaluation in [Ref. 28] to make the effects of dissolved nitrogen more apparent. The applicant stated that it used four time-dependent volumes and junctions to simulate the dissolved nitrogen gas release and it installed each set of time-dependent volumes and junctions at the same position as the DVI. A control variable in RELAP5/MOD3.3/K that depends upon the mass flow rates of SIT-FDs controlled the amount of released nitrogen gas. The applicant stated that most of the LBLOCA analysis shows that the refill period ends at about 33 seconds after the break; therefore, the study focused on the timeframe between the initiation of the break and 50 seconds after. The applicant provided a figure showing the total dissolved nitrogen gas release rate from the four SIT-FDs as a function of time. The peak mass flow rate of dissolved nitrogen was about 2.7 kg/s, which exceeds the maximum value in [Ref. 28]. However, the amount of dissolved nitrogen compared to the discharged water mass flow rate from SIT-FDs is insignificant.

Figure 2, provided as part of the response, shows the core collapsed water level. The bottom of the active core is about 2.5 m and the collapsed water level reaches that elevation at about 35 seconds in both the nominal case and the case with the dissolved nitrogen. Therefore, the applicant concluded that the dissolved nitrogen gas has no effect on the duration of the refill phase. Since the discharged water mass flow rate from SIT-FDs is large, the dissolved nitrogen effects are negligible, and this result is consistent with the description in [Ref. 28].

The NRC staff concurs with the applicant's assessment that the effect of dissolved nitrogen on the PCT and transient results is insignificant. Therefore, this issue is resolved.

Hot Channel

Section 4.3.1.1 of NUREG/CR-5249 discusses the use of different nodalizations in the core to evaluate the hot channel bias. The TR does not document or discuss such sensitivity studies. In AI-27 Part e [Ref. 3], the NRC staff requested the applicant to provide the basis for the selected radial nodalization of the core and upper plenum.

The applicant stated in the response to AI-76 [Ref. 5], that the [[ ]] utilized by CAREM, in which [[ ]] is adequate to model the core and also includes some conservatism coming from using the higher F_r value for the hot assembly. In addition, the applicant stated that various code assessments confirmed the acceptability of the [[ ]] as described in TR Appendices, and therefore, no additional sensitivity studies for the multi-channel model of the core need to be performed. Furthermore, the applicant noted that due to the issues related to the modeling of the upper plenum during the reflood period related to the entrainment of liquid droplets, CAREM incorporates a conservative model as part of the determination of the steam binding bias.

In the June 2016 Audit Meeting, the applicant reiterated the position that the [[ ]] nodalization is adequate due to the confirmation provided by the code assessment studies provide in TR Appendices C, D, and E. Since the analysis utilized [[ ]]. Then, the applicant proceeded to present the results of a [[ ]]. The applicant believes that [[ ]]. This is discussed in response to AI-27 and AI-47 [Ref. 5]. Despite the [[ ]].

The NRC staff finds the applicant's basis for the radial nodalization of the core and upper plenum is acceptable, and on the basis of that information concludes that this issue is resolved.

Reactor Vessel Downcomer

TR Section 4.2.2.2.1 discusses the uncertainty parameters for important phenomena or processes that occur in the reactor vessel downcomer. The applicant attributes all except three such phenomena to the ECCW bypass and states that the ECCW bypass bias accounts for them. Therefore, the applicant determines the uncertainty for only three processes or phenomena of [[ ]] important phenomena identified in the APR1400 PIRT. Among the phenomena that the applicant lumps together with the ECCW bypass bias is [[ ]].

The NRC staff and the applicant discussed the issue of flashing in the downcomer in the June 2016 Audit Meeting as part of the discussion of the number of process/phenomena that are included in the biases in CAREM. The applicant presented the following information at the meeting:

Flashing uncertainty should be considered directly

1. *In RELAP5, flashing is not considered as a correlation, but as a result of governing equations and state equations.*

2. *The uncertainty of flashing is considered in CAREM is considered as other parameters*

3. *[[*

   ]].

4. *Initial system pressure may affect the subsequent flashing behavior*

The NRC staff notes the conflict between these facts and believes that flashing is a phenomenon associated with several components as stated in the TR PIRT. The applicant stated that flashing is a consequence of the solution of the mass and energy conservation equations through the equations of state, and therefore its treatment as one of the process/phenomenon lumped into a bias does not strictly correspond to the general approach for addressing biases in RG 1.157. The response to AI-39 described proposed changes to TR Section 4.2.2.2.1 to make the discussion of flashing in the downcomer consistent with the treatment in other components by stating that [[

]]." The details are then documented in TR Revision 1, Sections 4.2.2.6.1 and 5.1.7.

The NRC staff finds that the applicant's decision to modify the TR to provide consistency in the treatment of the phenomenon of flashing follows the guidance in RG 1.203, and on the basis of the information provided concludes that this issue is resolved.

Bias Grouping

In response to RAI 7-8567, Question APR1400-4, the applicant provided information regarding which processes/phenomena are treated conservatively, through a bias, through uncertainty representation or are considered as part of other parameters. In the response to RAI 7-8567, Question APR1400-4, Table 2 lists the processes/phenomena which are treated conservatively in CAREM and Table 3 provides a list of the processes/phenomena which are treated by biases.

In the responses to AI-14, AI-17, and AI-19 [Refs. 3 and 4], the applicant identified several processes/phenomena that are combined into a single bias. The applicant did not describe or justify the process and basis for combining multiple processes/phenomena using the guidance in RG 1.157 or NUREG/CR-5249. The CSAU approach discussed in NUREG/CR-5249 indicates that combining biases may be appropriate:

(1) when the data base is insufficient to judge the nodalization and therefore a separate bias for plant noding may be added to determine uncertainty;

(2) due to the difference between code-calculated and experimental data for important phenomena, although a more powerful and successful technique determines the individual uncertainty contributions;

(3) when the effects of scale must be combined with other uncertainty contributions; or

(4) when the absence of data may necessitate a bounding analysis.

RG 1.157 states:

> *"The effects of all important variables should be considered. If it is not possible or practical to consider a particular phenomenon, the effect of ignoring this phenomenon should not normally be treated by including a bias in the analysis directly, but should be included as part of the model uncertainty."*

RG 1.157 recognizes that a bias may be introduced when a particular model does not require a totally best-estimate calculation. In general, the APR1400 CAREM does not provide a justification or methodology for determining the single bias that is to be used to represent a combination of processes or phenomena. The NRC staff believes that such a justification is important when the processes or /phenomena are of high importance.

During the June 2016 Audit Meeting discussion the applicant provided presentation material which described the process of bias treatment and identified that power-to-volume scaled test facilities have components that cause bias due to scaling distortions. The applicant further identified that the one-dimensional modeling capability of RELAP5 is known to be inadequate for a complete best-estimate depiction of all the phenomena that are combined into the biases. By determining a conservative bias in the code prediction of the test facility response, the phenomena are effectively combined into a single bias consideration.

Regulatory Guide 1.157 states that conservatism may be introduced for several reasons, including: "…*2. The uncertainty of a particular model is difficult to determine, and only an upper bound can be determined. 3. The particular application does not require a totally best estimate calculation, so a bias in the calculation is acceptable*." The CSAU methodology discussed in NUREG/CR-5249 provides some clarification, stating: "*In the absence of a data base sufficient to quantify scaling effects in the form of biases and deviations, it may become necessary to perform a bounding analysis and employ the results as a separate bias (i.e., a penalty or benefit) in the total uncertainty statement*."

Based upon the information the applicant provided in response to AI-40, the information in the TR regarding the test simulations, and the clarifications in the June 2016 audit meeting, the NRC finds that the applicant follows the guidance provided by Regulatory Guide 1.157 and NUREG/CR-5249, and provides a reasonable method for representing multiple phenomena with a single bias. The NRC staff finds that the applicant's method for combining biases into a single bias is acceptable, and on the basis of the information provided concludes that this issue is resolved.

Containment

TR Section 4.2.2.6.2 discusses the applicant's uncertainty evaluation approach for the containment related parameters. Containment pressure history during LBLOCA is especially important during the reflood phase since it acts as the backpressure for reflooding the core.

Break mass flow rate and system pressure drop are dependent on the containment backpressure during the reflood phase. In CAREM, containment backpressure is calculated by CONTEMPT4/MOD5 when choked flow is stopped at the end of blowdown. Prior to that, a representative containment backpressure is used.

TR Section 4.2.2.7.2 states that relevant containment parameters are selected to ensure conservative results and containment backpressure is calculated conservatively. However, the applicant did not provide any description of the CONTEMPT inputs (e.g., for heat transfer surface area, the wall condensation model, etc.), nor any results of sensitivity calculations that demonstrate the conservatism of the selected inputs relative to the LOCA backpressure calculations. Therefore, in AI-43 [Ref. 3], the NRC staff requested the applicant to provide justification for the statements regarding conservatism in modeling the containment response.

The applicant's response to AI-16 [Ref. 4] provided some of the containment calculation input parameters and the type of values selected for the calculation of a minimum containment backpressure calculation. The applicant's response concluded that sensitivity calculations demonstrating conservatism are unnecessary. The NRC staff and the applicant discussed treatment of containment backpressure during the January 2016 Audit Meeting and agreed that lower containment pressures tend to result in lower core reflooding rates since break flow is increased. This is conservative from a PCT perspective.

The NRC staff finds that the applicant's information regarding CONTEMPT input and the results of sensitivity calculations that demonstrate the conservatism of the selected inputs relative to the LOCA backpressure is acceptable, and on the basis of that information concludes that this issue is resolved.

ECCW Bypass

According to the TR, the applicant relied upon code assessments to determine the ECCW bypass bias during the refill period. The code assessments revealed that the water inventory in the lower plenum predicted at the end of the test exceeded the measured amount by several hundred kilograms. According to the TR, the applicant conservatively uses [[ ]] of the ECCW bypass during the refill period. The applicant then chooses to evaluate the bias in the prediction of the PCT due to ECCW bypass [[ ]] during the refill period. Similarly, the applicant also used code assessments to determine the ECCW bypass phenomena during the reflood period. Results of those code assessments showed that the RELAP5/MOD3.3/K code conservatively calculates ECCW bypass during reflood. The applicant does not credit this conservatism for ECCW bypass during the reflood phase in the evaluation of the PCT bias in the plant sensitivity calculations. As a result, the applicant applies the ECCW bypass bias only during the refill phase of the accident. In AI-45 [Ref. 3], the NRC staff requested the applicant to clarify several concerns regarding the determination of the ECCW bypass bias that are discussed in TR Section 4.2.3.1:

- In AI-45 Part a [Ref. 3], the NRC staff requested the applicant to clarify the approach used to incorporate the ECCW bypass bias in the code during the blowdown, early reflood, and late reflood periods. In response to AI-45, Part a [Ref. 4], the applicant stated that [[ ]] to the code-calculated-ECC
- bypass and it is only for the refill ECC bypass. Separately from this, the ECC bypass during the early and late reflood periods is assessed based on the code assessment studies against MIDAS, UPTF-21D, and ATLAS test 9, 11, and 15. Results of the

code assessment using these reflood tests showed that the RELAP5/MOD3.3/K code conservatively calculates ECC bypass during reflood. Therefore, these studies justify the conservatism of the code without the need to apply a bias for the reflood ECC bypass. Following the guidance in RG 1.157 regarding comparisons to different tests to ensure that a reasonable estimate of the bias has been obtained, the NRC staff finds that the applicant's application of the ECC bypass refill bias is appropriate for that period and the reflood ECC bypass bias was appropriately determined for the reflood period based upon test assessments.

- In AI-45 Part b [Ref. 3], the NRC staff requested the applicant to provide comparisons from the simulation of the UPTF-4A test with and without the ECCW bypass bias applied to show that the selected bias is appropriate. The applicant stated [Ref. 4] "*The purpose of the UPTF-4A test assessment is not to confirm the appropriateness of bias, but to determine the value of the bias.*" The applicant did not expect to obtain good agreement with the test data when the bias was activated, due to the impact of the bias on local predicted core and downcomer levels. However, the applicant believes that it is important to get agreement with test data for global parameters, such as vessel inventory. The applicant included results in the response to AI-45, Part b, which showed the liquid mass through the breaks and the liquid mass extracted before and after activation of the refill ECC bypass. The run with bias showed slightly smaller break flow mass than the run without bias, but the difference was not significant. In the run with the bias, the applicant confirmed that the total liquid out of the vessel is larger than the test data, which is [[ ]]. Therefore, the applicant believes that, for the vessel inventory, the activation of ECC bypass is logically correct. The NRC staff examined the results of the requested analysis with and without the bias and determined a slightly different mass was extracted through the break with and without the bias. The NRC staff concurs that the applicant correctly followed the guidance in RG 1.157 for the application of the bias and that the key parameters meet the expected response, which addresses the concern.

- In AI-45, Part c [Ref. 4], the NRC staff requested the applicant to comment on the applicability of UPTF-4A to determine the ECCW bypass bias it initiates from a system pressure of 1200 kPa (i.e., 1.2 MPa) while the pressure in the refill period in APR1400 is approximately 6 MPa. The applicant stated:

  "*The initial conditions of UPTF-4A test were determined from the TRAC analysis of a US PWR and starts at 1.2 MPa, while the SIT injection in APR1400 starts at 6 MPa. The beginning of SIT injection is only dependent on the setpoint of SIT, hence is different due to the design differences between reference plant of UPTF-4A and APR1400. Although the SIT injection starts at 6 MPa, the RCS pressure still drops rapidly after the injection of SIT, and at about 25 seconds the RCS pressure becomes below 1.2 MPa which is consistent with the initial condition of UPTF-4A. The period between 6 MPa and 1.5 MPa still has the strong characteristic of blowdown and therefore not adequate to be considered as the ECC bypass for refill.*"

The applicant concluded that the difference in the initial conditions for UPTF-4 and the APR1400 minimally affected the ECCS refill period (e.g., period between 6 MPa and 1.5 MPa is considered to be representative of the blow-down period). Therefore, the applicant considers the UPTF-4A test is applicable for the selection of ECCS bypass

bias for the analysis. The NRC staff finds that the conditions of the APR1400 simulation and the UPTF simulation are somewhat different. The point at which the APR1400 SIT begins to inject at 6 MPa through the conditions at end of blowdown, with a pressure of approximately 1.5 MPa, are not appropriate for the calculation of ECC bypass during refill.

The appropriate conditions after the pressure has fallen below 1.5 MPa correspond approximately to the test conditions for the UPTF-4A test. Consequently the NRC staff concludes that the applicant correctly followed the guidance in RG 1.157 to utilize the appropriate test conditions to determine ECC bypass during the refill period, such that the concern is resolved.

- In AI-45, Part d [Ref. 3], the NRC staff requested the applicant to further justify the selection of UPTF-4A with cold leg injection for determination of the ECCW bypass bias over the tests with a configuration similar to that in APR1400. The applicant stated [Ref. 5] that the ECC bypass during the end-of-blowdown and refill period is mainly dependent on the flow mixing behavior below the bottom of the cold leg. Therefore, the ECC injection type is less important in comparison to the depressurization process. Also, the test configurations of UPTF-21A and -21B are not exactly the same as the LBLOCA conditions during the end-of-blowdown and refill period.

During the June 14, 2016, Audit Meeting [Ref. 12], the applicant presented information regarding the UPTF-21A, UPTF-21B and UPTF-4A tests to justify the selection of the UPTF-4A cold leg injection test for the determination of the ECCW bypass ratio for the APR1400 with DVI [Ref. 27]. As the applicant noted in prior responses:

- The ECC bypass during end of bypass and refill is mainly dependent on the flow mixing below the bottom of the cold leg and therefore the delivery process to that point is of less consequence,

- The depressurization process is more important to the bypass determination than the injection point,

- The cold leg injection configuration in UPTF-4A can be used to quantify the ECC bypass bias since it captures the important phenomena, and

- The large break LOCA conditions in tests UPTF-21A and UPTF-21B are not exactly the same as those expected in the APR1400.

In that same meeting, the applicant described the features of the UPTF-21A -21B tests that renders them less suitable for determination of the ECC bypass bias:

- The intentions of the tests were to investigate the steady state downcomer counter-current flow limitation (CCFL) and provide data only for certain flow rate conditions,

- The DVI configuration UPTF tests 21A and 21B were counter-part tests to the cold leg injection (CLI) configuration tests of UPTF-5, 6 and 7,

- The intact loops in the DVI configuration tests UPTF-21A and -21B were blocked to match the CLI configuration tests,

- The tests were at steady state conditions,

- The pressure was approximately 3 bar for the test UPTF-21A, and tests UPTF-21B-I, -II & -III were sensitivity tests,

- The DVI configuration test closest to the expected plant conditions was test UPTF-21A, which had steam injection through the core simulator and steam generator simulator (SGS),

- The DVI configuration test UPTF-21B-I had hot ECC fluid and test UPTF-21B-II and –III had no steam generator simulator.

The applicant stated that there were no other UPTF tests that are more representative of the end of bypass to refill period which had a representative DVI configuration. The closest DVI configuration test, UPTF-21A, shows only one state of the process and not the whole end of bypass to refill process. Consequently, the applicant concludes that this test cannot be used to quantify the bias due to the difficulty in converting the results into a bias. In contrast, the applicant stated that the CLI configuration test UPTF-4A can be used to determine the bias as the difference in the [[ ]] during the test. Since the DVI injection point in the APR1400 design is above the cold legs in the downcomer, the distance that the steam and ECC water are expected to be in contact until they go through the broken cold leg, is almost the same as that of the cold leg injection plants. Consequently, the applicant concluded that the ECC injection type was less important than the expected mixing flow behavior, for which the test UPTF-4A would be representative.

The NRC staff recognizes and acknowledges that there are no tests with the exact DVI configuration and test conditions that are appropriate to determine the ECC bypass bias. Based upon the information provided by the applicant regarding the inadequacy of the DVI configuration UPTF tests, and the fact that the UPTF-4a cold leg test conditions are appropriate to the conditions for which DVI ECC injection will occur in the APR1400, the NRC staff concurs that the test UPTF-4A provided the most representative conditions for assessment, and this resolved the concern.

- In AI-45, Part e [Ref. 3], the NRC staff requested the applicant to discuss the differences between the APR1400 and UPTF nodalizations and their impact on the conclusions drawn from the UPTF simulations. In response [Ref. 4], the applicant stated that, although the downcomer modeling of UPTF tests is not exactly the same at that of the AP1400, the principle idea employed in the modeling of the [[ ]]. The applicant explained that in modeling [[ ]]. In UPTF, there are four (4) hot legs and four (4) cold legs, while the APR1400 has two hot legs and four (4) cold legs. In order to preserve the [[ ]]. The difference in the

axial nodalization of the downcomer is mainly due to the geometrical difference between the APR1400 and the UPTF rig. The [[ ]] values are similar and also the connections to the cold legs are consistent in both nodalizations by having the same single-junction connections. RG 1.203 states that the modeling of the test facility should be consistent between the experimental facility and similar components in the nuclear power plant. Due to differences in the configuration of the UPTF test facility and the APR1400, the NRC staff finds that the modeling of the UPTF facility follows the modeling approach employed for the APR1400 and that the UPTF nodalization is acceptable, and therefore resolves the concerns.

The applicant stated that the upper plenum noding in UPTF in TR Appendix F is different from that of APR1400. The noding is based on the upper plenum noding scheme developed for the analysis of other nuclear power plants in Korea which have upper plenum injection. In this approach, every upper plenum structure is modeled using pipes and multi-junction components. The applicant stated that his noding scheme was employed because the upper plenum SI mixing phenomena were considered to be important in CAREM. However, in the APR1400 modeling, the detailed investigations on these phenomena were not necessary, and therefore, the multi-channel upper plenum noding scheme is not used. The UPTF nodalization is only used in the assessment of the test UPTF-21d. The scheme used in the assessment of the test UPTF-10B was performed using the simplified upper plenum noding, which is consistent with the APR1400 nodalization. See the response to AI-48, Part b [Ref. 4]. In the assessment of UPTF-21D, the impact of the modeling differences does not appear to be significant. The complicated upper plenum noding may only affect the flow behavior in the upper plenum, which would be very limited in the DVI injection test, such as UPTF-21D.

During the January 2016 Audit Meeting [Ref. 12], the NRC staff and the applicant agreed that it is important for KHNP to revise the UPTF nodalization and repeat the study. In TR Revision 1, the applicant revised the UPTF-21D nodalization to be consistent with the APR1400 nodalization and then re-ran that simulation. The applicant also performed an assessment of UPTF-21D with a simplified upper plenum noding. The results of the downcomer level and the break flow showed that the simulation results are slightly more conservative than the test results. The applicant determined that the conclusions from the assessment in the TR were unchanged. The revised simulation of UPTF-21D using the nodalization applied in the APR1400 showed slightly more conservative results and followed the guidance in RG 1.203 that there should be consistency between the modeling of the experimental facility and the modeling of the nuclear power plant. Therefore, the NRC staff finds the revised modeling of UPTF-21D acceptable, which resolves the concern.

In AI-45, Part f [Ref. 3], the NRC staff requested the applicant to provide justification for neglecting the non-conservatism shown in the first 200 seconds of ATLAS tests 9, 11 and 15 in the ECCS bypass prediction during the early reflood period. The applicant's response [Ref. 5] stated that, as discussed in TR Appendix E, the result of the initial period (the period before 200 seconds after the beginning of the test) of the ATLAS Tests 9 and 11 include [[ ]]. The applicant stated that the cited behaviors are due to [[ ]] during the reflood period of APR1400. During the January 2016 Audit Meeting, the applicant stated that the results of ATLAS Tests 9 and 11 could be [[ ]]. Since the potential for, and the effect of,

downcomer boiling is a function of the metal heat content of the vessel wall during the late reflood period of low safety injection flow, the NRC staff requested the applicant to describe the process by which the code metal heat content was adjusted, the process used to verify that the values corresponded to the metal heat content of the vessel wall in the ATLAS tests at the time of code restart, and how those values are prototypic of the expected behavior in the APR1400. In the June 2016 Audit Meeting, the applicant noted that there were sufficient measured data including wall temperatures to characterize the metal stored energy for setting the initial conditions for the ATLAS test simulations. In discussing the ATLAS IET earlier in this SER, the NRC staff found the restart of the simulation with the appropriate initial conditions for the simulation of the test data with prototypic plant conditions is an acceptable process, and concurred that this addressed the issue.

None of the descriptions of the models for APR1400, MIDAS, or UPTF used to determine the ECCW bypass bias mention the use of a CCFL correlation in the downcomer. The CCFL correlation can impact the prediction of ECCS bypass because such a correlation will reduce the amount of liquid penetrating downwards into the downcomer. In AI-45, Part g [Ref. 3], the NRC staff requested the applicant to clarify whether any such correlation was used, and if so, to describe the resulting impact on the ECCS bypass bias. The applicant's response [Ref. 4] indicated that a CCFL model was not used in any calculations since the model has a strong tendency to amplify numerical oscillations during reflood. The applicant noted that although it does not apply a CCFL model it conservatively calculated the results for test assessment (MIDAS and UPTF) without applying a CCFL model in terms of reflood ECC bypass; therefore, such a bias is not included. CCFL is discussed in detail later in this SER. The NRC staff finds that the applicant's information regarding CCFL on the tie plate and the observed calculated hydraulic phenomena are acceptable, and on the basis of that information concludes that CCFL does not need to be included, which resolves this issue.

TR Appendix F documents the assessment of the RELAP5/MOD3.3/K code against SETs in the MIDAS and UPTF facilities for determination of the ECCW bypass bias in the late reflood period. The expression for the bypass fraction defines that parameter as the ratio of the liquid flow rate discharged though the lower plenum to the total inflow from the safety injection and the condensate and the expression in Equation (1) was incorrect. TR Revision 1 [Ref. 13] incorporates the correct expression for the bypass fraction. The applicant also confirmed that they correctly calculated and compared Figures 2-4, 2-7, and 2-8.

Several concerns were raised regarding the determination of the ECCW bypass bias. The NRC staff has the following findings:

- The ECCW bypass bias determination during refill is appropriate,
- The ECCW bypass bias determination during reflood is appropriate,
- The application of the ECCW bypass bias resulted in the expected response in key parameters,
- The test conditions used to determine the ECCW bypass bias were appropriate, and
- The test nodalizations used to determine the ECCW bias were appropriate.

Therefore, NRC staff finds that the applicant's information regarding the several issues discussed above is acceptable, and on the basis of that information concludes that this issue is resolved.

Steam Binding

In AI-50, Part c [Ref. 3], the NRC staff requested the applicant to clarify whether the steam binding bias is included in the performance of the 'coverage checks' for the reflood period when compared to integral test data. In response [Ref. 4], the applicant stated that the purpose of the "coverage check" was to confirm the adequacy of the number of uncertainty parameters and the uncertainty range of each parameter. The purpose of the bias determination was to evaluate scale distortions, code deficiencies in prediction, or model deficiencies. The bias evaluations were only included in the plant calculations to quantify total uncertainty. The applicant justifies not including steam binding bias in coverage checks, believing that the proper place to examine biases is in the plant calculations that evaluate the total uncertainty, rather than in coverage checks of parameter uncertainties. The NRC staff confirms that this statement is correct according to CAREM, Step 10.

Following the guidance in RG 1.157, the applicant has justified the treatment of the uncertainties and methods for combining the uncertainties include the appropriate point for application of the bias. The NRC staff finds that the applicant's explanation of the interactions between "coverage check" and steam binding bias is acceptable, and on the basis of that information concludes that this issue is resolved.

Previous Experience and Scaling

The applicant, after performing the 181 demonstration calculations, evaluated scale biases for all cases that are expected to be limiting.

> *"Based upon previous experiences, [[*
> *]] are selected for scale bias calculation."*

In TR Revision 1, [[ ]] cases were selected for the evaluation of scale biases. In AI-65 [Ref. 3], the NRC staff requested the applicant to provide details of the referenced "previous experiences" and the basis for the selection of the cases. The NRC staff also requested the applicant to confirm that the case with the highest second peak is captured in the set that is used for the evaluation of the scale bias.

In response [Ref. 4], the applicant stated that 181 combinations of the uncertainty parameters are used to quantify the uncertainty of the PCT prediction. In those combinations, two cases with the highest PCT are not considered valid results and are therefore not considered for scale bias application. [[ ]] for the selection of the scale bias cases is based on "the previous experiences," for which the applicant explained that it means experience in exercising the code in development, sensitivity studies, and from licensing applications in Korea. The applicant stated that the potential for application of the bias to make a case more limiting is generally lower than [[ ]] as indicated in Table 5-8. In other words, once the limiting reflood PCT case has been selected, no other reflood PCT case has typically been found to become limiting with the application of the bias if the other cases are more than [[ ]] lower than the limiting reflood case. Consequently the applicant selected a conservatively high cutoff of [[ ]]. All reflood PCT cases within [[ ]] of the limiting reflood PCT case are selected for bias application to determine if they become the limiting reflood PCT case for comparison to the licensing limit. The first and second highest cases are neglected even if they are reflood peak PCT cases, since their use would exceed the 95/95 criteria. The NRC examined the reflood PCT cases in TR Revision 0 and TR Revision 1, and observed that a [[ ]] is

sufficiently conservative for the identification of reflood PCT cases for which the bias should be applied for evaluation.

The [[ ]] cases selected for bias evaluation are documented in TR Revision 1, Table 5-5. Four of the [[ ]] cases in TR Revision 1, namely cases 35, 43,142 and 162, do not show any influence of either of the [[ ]]. In AI-66 [Ref. 3], the NRC staff requested the applicant to elaborate on the reasons for the observed behavior. For the revised analyses in TR Revision 1 [Ref. 13], the zero bias values are the result of negative biases that are conservatively limited to a value of zero or are small such that round-off lists it as zero.

Based upon the applicant's response and information in the TR, the NRC staff finds that the applicant's information regarding "previous experiences" and the basis for the selection of the cases is acceptable, and on the basis of that information concludes that this issue is resolved.

4.5 Nodalization

Changes

The applicant states in TR Section 1 that the CAREM methodology described in the TR strictly follows the concept and philosophy of CSAU as documented in NUREG/CR-5249. Comparing Figure 1-1 in the TR to Figure 1 of NUREG/CR-5249, the NRC staff noted that the step that determines whether a noding change is necessary is different between the two figures. In the TR, the determination is made after all the uncertainties and biases have been determined. On the other hand, in NUREG/CR-5249, nodalization is established as part of the second element of the approach (i.e., assessment and ranging of parameters), while biases and uncertainties are determined as part of the third and last element of the process. In AI-4 [Ref. 3], the NRC staff requested the applicant to explain this discrepancy. During the January 2016 Audit Meeting, KHNP provided a presentation on the CAREM process [Ref. 27] describing how and when noding changes occur, stating that prior practice established the original nodalization, which was based upon separate effects tests. KHNP stated [Ref. 4] that they would revise the noding and repeat all of the process steps if changes were warranted to simulate test results or to capture important phenomena. This approach, although not strictly the same as that outlined in the CSAU (NUREG/CR-5249), is considered reasonable, since it provides a mechanism to revise the nodalization if important phenomena could not be captured.

The NRC staff finds that the applicant's information regarding how and when noding changes occur and that this process is based upon prior practice and the results from separate effects tests is acceptable and, on the basis of that information, concludes that this issue is resolved.

Core and Upper Plenum

The NRC staff expects that the predicted entrainment from the upper plenum will be a strong function of the nodalization of the core and the upper plenum. Therefore, in AI-48 [Ref. 3], the NRC staff requested the applicant to describe the nodalization of these components for comparison against UPTF-10B. In response [Ref. 4], the applicant provided the noding for the upper plenum in the APR1400 model and the upper plenum for the UPTF-10B test simulation. The model for the APR1400 upper plenum uses three volumes:

(1) the region above the [[ ]];

(2) the region above the [[ ]]; and

(3) the region above [[ ]].

The applicant explained that in UPTF, there is no such thing as the fuel alignment plate or UGS bottom plate. Therefore, the hot leg bottom and top line substitute for those plates because the vertical locations of those plates are similar with hot leg bottom and top lines. Consequently, the EM uses three volumes for the UPTF:

(1) the region above [[ ]];
(2) the region above [[ ]]; and
(3) the region above [[ ]].

The applicant stated that this makes the APR1400 upper plenum modeling consistent with UPTF-10B upper plenum model. The model does not include details of the upper plenum structures, [[ ]]. These are left as empty volumes in both the APR1400 and UPTF-10B models. The applicant explained that [[ ]]. The applicant provided the rationale for using the UPTF-10B nodalization for APR1400 during the January 2016 Audit meeting [Ref. 12]. The applicant explained that [[ ]].

The NRC staff finds that the applicant's information regarding the nodalization of the APR1400 and the UPTF-10B followed the guidelines of RG 1.203, step 14 which states: "In particular, nodalization and option selections should be consistent between the experimental facility and similar components in the nuclear power plant" and concludes that this issue is resolved.

TR Section 4.2 discusses the applicant's nodalization of the APR1400 plant for use in the CAREM methodology. The nodalization separately models the two hot legs and four cold legs, which are spaced equally, 60-degrees apart in the circumferential direction. The model includes two identically modeled loops, except that one of the loops includes the pressurizer and the other loop (i.e., the loop without the pressurizer) models the cold leg break between the pump and the reactor vessel. The nodalization for each loop contains the hot leg piping, the steam generator U-tubes, and the fluid volumes of the steam generator primary and secondary sides, two pump suction legs, two pumps, and two pump discharge cold legs.

The reactor vessel nodalization consists of the downcomer, upper and lower plenum, and the core regions. The reactor vessel downcomer is divided into six azimuthal downcomer channels according to the loop models and each channel has 10 axial volumes. The [[ ]].

The NRC staff developed several questions regarding the nodalization selected by the applicant. In AI-27 [Ref. 3], the NRC staff requested the applicant to respond to these questions. The NRC staff and the applicant discussed these questions during the January 2016

Audit Meeting [Ref. 12] and the discussion below characterizes the applicant's rationale behind each question.

TR Section 4.2.1 states that the APR1400 nodalization of the reactor vessel "...follows the typical pressurized water reactor nodalization..." However, the applicant did not provide any references or details to support this assertion or to demonstrate how the applicant determined "typical pressurized water reactor nodalization." Tables 7 and 8 in NUREG/CR-5249 provide the basis for the nodalization chosen in that study and compare the chosen nodalization to that used to represent several integral test facilities. The NRC staff requested the applicant to provide additional information supporting the assertion that the selected nodalization for APR1400 is "typical" using the content of Tables 7 and 8 in NUREG/CR-5249 as a guide. In AI-27, Part a [Ref. 3], the NRC staff requested the applicant to provide a reference for the documentation of the nodalization sensitivity studies that were performed to determine the CAREM nodalization that will be used to support license submittals.

In the response to AI-27, Part a [Ref. 4], the applicant stated that the APR1400 plant nodalization was based upon code assessments related to the nodalization, code assessments using SET and IET of the assessment matrix and nodalization examples and code user guidelines described in RELAP5/MOD3.3 Code Manual, Volume III and Volume V [Ref. 20]. Specific nodalization details for the upper guide structures are in [Ref. 30]. The applicant stated that the experimental assessments described in the appendices of the TR also confirmed the applicability of the selected nodalization.

The NRC staff finds that the applicant's information regarding the documentation of the nodalization sensitivity studies and the SETs and IETs follows the guidance provided in RG 1.203 and is consistent with industry practice, and on that basis concludes that this issue is resolved.

In the response to AI-27, Part c [Ref. 4], the applicant stated that [[ ]] were chosen to represent the downcomer based on [[ ]] However, the applicant did not provide any information as to what phenomena are investigated. Moreover, the applicant introduced the ECCW bypass as a bias that is not dependent on the nodalization of the downcomer. Therefore, the NRC staff requested the applicant to list the applicable phenomena considered. In AI-27, Part b, the NRC staff requested the applicant to provide information regarding the potential for distortion due to nodalization.

In the response to AI-27, Part b [Ref. 4], the applicant stated that the CAREM model uses a multi-channel downcomer modeling technique where [[ ]]. The NRC staff finds this approach is appropriate and consistent with industry practice. The applicant stated that the distortion of the phenomena that are addressed in the TR include ECCS bypass, the ECC bypass ratio, level at the downcomer, break flow, etc., and are the phenomena of concern. Since the applicant evaluated the ECC bypass bias against the UPTF and MIDAS tests, the bypass itself is somewhat dependent on the nodalization. The applicant stated that the downcomer nodalization in the UPTF and MIDAS test are consistent with that of the APR1400. The applicant stated that it is necessary to model the downcomer by azimuthally [[ ]] for the APR1400. The applicant provided a figure depicting the nodalization of the reactor vessel downcomer in the circumferential direction. The

applicant stated that the applicable phenomena considered relate to the ECC bypass. The applicant stated that the APR1400 modeling approach was based on the determination of biases using the assessment from the UPTF and MIDAS tests, which utilized a specific nodalization and therefore had some nodalization dependence. Therefore, it is reasonable to extend the bias determination to the APR1400 simulations. Based upon the information in the TR and the applicant's description of the phenomena investigated, the NRC staff finds that the ECCW bypass bias is dependent upon the nodalization inherent in the consistent use between the UPTF and MIDAS tests and the APR1400. Because of this, a condition is imposed upon the application of the APR1400 downcomer modeling.

The NRC staff imposes the following CAREM methodology application Condition (2):

> *Changes to the downcomer modeling shall require additional justification and NRC approval.*

The NRC staff finds that the applicant's information regarding the nodalization of the downcomer is acceptable, since it is justified by comparison to experimental benchmark tests with similar model nodalization, and on the basis of that information concludes that these issues are resolved, subject to Condition (2).

Plant Nodalization Using Code Assessment Studies

According to NUREG/CR-5249, the plant nodalization should be informed by, and to the extent possible, follow that used for the EM code assessment studies. The APR1400 plant shown in TR Figure 4-1, and the ATLAS facility shown in Figure 3-3 in TR Appendix E, show differences in the nodalization of the vessel. These differences include the nodalization of the downcomer, lower plenum, upper plenum, and the upper plenum to dome connection. In AI-27 Part m [Ref. 3], the NRC staff requested the applicant to explain the reasons for the differences.

In response [Ref. 5], the applicant explained that the lower downcomer to lower plenum noding differences resulted from geometric differences between the facility design for the APR1400 and design of the ATLAS test facility. Similarly, geometric differences in the lower plenum account for the differences in the nodalization in the lower plenum. The ATLAS test facility [[ ]] prototypical of the APR1400 design. The NRC staff determined that the deviation in the RELAP5 noding should not be the same, but reflect the actual designs for the test facility simulation and for the plant analyses.

For the upper plenum, the applicant noted that a [[ ]] for the APR1400 is utilized based upon sensitivity studies which indicate that it is conservative for blowdown quenching phenomena. Since the ATLAS facility was designed to assess the behavior during reflood, the detail desired for blowdown phenomena is not necessary for a reflood test. Consequently, a [[ ]] is utilized for the ATLAS facility. The applicant concluded that the thermal-hydraulic effects of the [[ ]]. However, the response to AI-5 [Ref. 5] showed a difference between the [[ ]]. This was discussed during the June 14, 2016, Audit Meeting where the applicant explained that the difference between the post-blowdown peak PCT response between the [[ ]]. Since the ATLAS facility would not experience the phenomena predominant during blowdown, the effects driving the difference during reflood would not be present. The NRC staff concludes that the lack of the blowdown forces would

result in an insignificant difference in the response of the ATLAS facility whether a [[ ]] is used. Consequently, the NRC staff finds that the [[ ]] ATLAS facility is sufficient for assessment purposes.

Furthermore, the NRC staff finds that the applicant followed the guidance in RG 1.203, which in step 14 states:

"In particular, nodalization and option selections should be consistent between the experimental facility and similar components in the nuclear power plant."

The differences between the noding utilized for the ATLAS facility and the APR1400 plant were determined to be due to facility design differences and differences in the prototypic conditions expected during reflood. The NRC staff finds that the applicant's information regarding the differences in nodalization between the APR1400 model and the model employed for the ATLAS facility for the downcomer, lower plenum, upper plenum, and the upper plenum to dome connection is acceptable, and on the basis of that information concludes that this issue is resolved.

Mixture Level

The NRC staff recognizes that the froth or mixture level is typically important in determining the quench front progression. The APR1400 nodalization, as described in the TR, uses [[ ]] control volumes in the core in the axial direction. Consequently, changing the axial nodalization may change the quench front uncertainty. As a result, in AI-27 Part g [Ref. 3], the NRC staff requested the applicant to explain the basis for the selected core axial nodalization and the level of accuracy that it provides.

The applicant's response to AI-27, Part g [Ref. 4], stated that the nodalization of the plant should be modeled in detail to simulate the design characteristic and the major phenomena. The modeling of core axial nodalization of CAREM is based on assessment against THTF and FLECHT-SEASET tests, of which the rod lengths are the same as the fuel rod of the conventional plant.

According to the applicant, the THTF and FLECHT-SEASET test facilities have the same core length as the plant and the assumption that the power-to-flow area ratio is similar to the value of the fuel assembly prevents the distortion of the thermal-hydraulic behavior in the core due to the scale down. Therefore, the measuring positions of the test facilities against axial direction of the core is an important reference in determining the noding for the plant. In CAREM, the active length of the fuel rod is modeled using [[ ]] axial nodes based upon the [[ ]] of FLECHT-SEASET. Therefore, in case of [[ ]]. CSAU modeling in NUREG/CR-5149 assumed 15 axial core nodes representing a nodal length of 9.6 in. The NRC staff does not consider the small difference between the FLECHT-SEASET tests and the APR1400 CAREM significant. As a test temperature probe is quenched, it is indicative that the fluid or two-phase mixture level has reached or surpassed the elevation of the temperature probe. The NRC staff finds that the APR1400 CAREM utilizes the same nodalization as the test simulations and the simulations of the THTF and FLECHT-SEASET temperature response and quenching times shows that the nodalization is sufficient to capture the mixture level response properly.

The applicant also provided results showing the comparison of the Courant limit and the time step for the plant calculation. This confirmed that the time step used in the plant calculation is always lower than the Courant limit for CAREM.

Based upon the test simulations and predictions of quenching times, the NRC staff finds that the applicant's model follows the guidance of RG 1.157 that the model should be "capable of calculating the two-phase level in the reactor during a postulated accident." The NRC staff finds that the applicant's information regarding the adequacy of the nodalization for mixture level tracking is acceptable, and on the basis of that information concludes that this issue is resolved.

Lower Plenum Nodalization

According to NUREG/CR-5249 (see Figure 18), analysis results from the simulation of a PWR LBLOCA showed that the lower plenum below the downcomer skirt requires at least two nodes to adequately model the sweep-out effect, which carries an [[']] in the APR1400 PIRT (TR Table 3-2). It appears that the APR1400 nodalization models [[ ]]. As part of the January 2016 Audit Meeting, in AI-27, Part h [Ref. 3] the NRC staff requested the applicant to justify the selected nodalization for the lower plenum.

The applicant provided a figure in the response to AI-27h [Ref. 4] showing the liquid temperature and the saturation temperature in the lower plenum as an indication that the vapor generation from flashing is limited to a short period of time, less than 30 seconds, after the break. In addition, the applicant performed a sensitivity study in which it utilized two-fluid nodes to represent the lower plenum below the flow skirt [[ ]]. It compared the vapor generation rate in the lower plenum for the EM noding and the vapor generation rate in the lower plenum for the two-node sensitivity study and showed very small differences in the calculated results. It also noted similar observations in comparing the temperature of the hottest fuel rod. Since the sensitivity study demonstrated only very small differences between the results obtained for [[ ]] lower plenum model, the NRC staff finds the applicant's response acceptable and considers the issue of noding of the lower plenum resolved.

Break Nodalization

According to Section 3.5 of RG 1.157, the break location and ECCS injection point are areas of high fluid velocity and complex fluid flow, and contain phenomena that are often difficult to calculate. The results of these calculations are often highly dependent on the nodalization in the vicinity of such points. As part of the January 2016 Audit Meeting, in AI-27, Part i [Ref. 3], the NRC staff requested the applicant to justify the nodalization selected for the APR1400 broken cold leg and provide results from relevant sensitivity studies to assess the impact of based on the Marviken data.

In the TR, the applicant provided a schematic illustrating the Marviken test nodalization. To determine the break nozzle nodalization, the applicant performed sensitivity studies, varying the number of volumes in the supplied report [Ref. 50]. The applicant stated that the two-phase critical flow rates are [[ ]]. Therefore, the [[ ]] was adopted for the nozzle. Using this noding, it performed an evaluation and determined the best-estimate discharge coefficients of [[ ]].

As noted in [Ref. 31], the length to diameter ratio of the nozzle was limited within the range of [[ ]] to minimize the impact on the critical mass flux under subcooled conditions in the Marviken tests. The applicant stated that the Marviken test nozzle is represented by [[and an L/D ratio of each volume is [[ ]].

To assess the noding in the vicinity of the break, the applicant performed a sensitivity study varying the L/D ratio from [[ ]] (see Figure 2 in the response to AI-27 Part i, [Ref. 4]). The applicant compared the result of the study in terms of the cladding temperature for the PCT.

The applicant noted that the [[ ]]. The applicant concluded, however, that the noding sensitivity shows that [[ ]].

In addition, the applicant provided a limited sensitivity study to justify the nodalization of the APR1400 in the vicinity of the break. The sensitivity study effectively subdivided one node on the RCP discharge pipe near the break, thereby changing the L/D ratio for that subdivided node and demonstrated only a small effect on the PCT.

Following the guidance of RG 1.157, which in Section 3.5 states: "*Sufficient sensitivity studies should be performed on the noding and other important parameters to ensure that the calculations provide realistic results*"; the applicant performed sensitivity studies on the nodalization near the break and determined the appropriate EM representation by assessing the simulation noding in comparison to test results. Other important parameters, such as the L/D, were assessed. Finally, the applicant performed sensitivity studies with the APR1400 model to validate the nodalization near the break. The NRC staff finds that the applicant's test comparisons and sensitivity studies are sufficient to justify the noding near the break, and on the basis of that information concludes that this issue is resolved.

ECCS Injection Point Nodalization

RG 1.157 Section 3.5 discusses nodalization near the ECCS injection point and states that "…sufficient sensitivity studies should be performed on the noding and other important parameters to ensure that the calculations provided realistic results." TR Appendix E discusses tests performed in the ATLAS facility to study direct vessel injection (DVI) performance relative to emergency core cooling water bypass and downcomer boiling. In AI-27, Part j [Ref. 3], the NRC staff requested the applicant to describe or reference the sensitivity studies performed to assess the selected nodalization near the ECCS injection point using the ATLAS test results.

The applicant described and justified the existing nodalization based on the downcomer geometry and DVI configuration [Ref. 4]. Subsequently, the applicant described the results of sensitivity analyses performed to assess the nodalization near the ECCS injection point. For ATLAS Test 15, the nodalization was varied [[ ]] by up to an order of magnitude. The sensitivity results indicated small variations in the integrated break mass flow rate. The calculated ECC bypass ratio showed only a small variation. The PCT variation was about 15 K (27°F), which is not significant as defined by 10 CFR 50.46. Based upon the results of the sensitivity studies, the NRC staff determined that variations in the noding and other parameters, such as [[ ]] a small effect on the calculations for the key parameters of integrated break flow, bypass ratio, and PCT.

The NRC staff finds that the applicant's information regarding nodalization near the ECCS injection point follows the guidance in RG1.157 and is acceptable, and on the basis of that information concludes that this issue is resolved.

Pressurizer Surge Line

TR Section 4.2.1 does not provide the description for the pressurizer surge line nodalization. According to the RELAP5/MOD3.3/K base model input deck, the surge line is modeled using a single inclined hydraulic component. Additionally, the code computes the loss coefficient though the surge line pipe, which neglects the turns and orientation changes in the line. In AI-27 Part k [Ref. 3], the NRC staff requested the applicant to justify the selected nodalization and loss coefficients, including references to nodalization sensitivity studies comparing the pressurizer flow into the upper plenum against available SET and/or IET data.

In response [Ref. 5], the applicant provided information regarding the modeling of the pressurizer surge line in the RELAP5/MOD3.3/K model. The model was used to simulate the pressurizer level response for LOFT test and Figure 2 in response to AI-27, Part k [Ref. 5], showed the comparison of the pressurizer level for the test simulation and the test data. Based upon the adequacy of this simulation, the applicant justified the use of this model for APR1400 plant calculations.

The applicant also stated that the turns and orientation changes in the surge line are represented by loss coefficients in the branch connections. The applicant performed a sensitivity study to determine the effect of the variation on the pressurizer depletion time. In addition, the applicant performed a sensitivity study in which the surge line was represented by multiple nodes instead of a single inclined node. The results of the sensitivity study showed a small effect on the rate of depressurization, collapsed liquid level, and mass flow rate through the surge line. However, there was an insignificant effect on the PCT during blowdown, while the PCT during the reflood phase was slightly lower for the more detailed surge line model. The applicant concluded that the effect of the variation of the loss coefficient and modeling was not significant.

Based upon the results of the sensitivity studies and the conservatism in the APR1400 surge line model, the NRC staff finds that the applicant's information regarding the justification for the nodalization and loss coefficients in the pressurizer surge line is acceptable, and on the basis of that information concludes that this issue is resolved.

Upper Guide Support Structure

The nodalization of the upper guide support structure region in the original TR showed a difference between the RELAP5/MOD3.3/K nodalizations shown in TR Figure 4-1 and that in Figure 17 in TR Appendix B. Therefore, in AI-27, Part i, [Ref 55], the NRC staff requested the applicant to justify the nodalization that will be used for LBLOCA licensing calculations.

In response [Ref. 5], the applicant stated that they will utilize the nodalization of TR Figure 4-1 for all licensing calculations and that it is reasonable to use the same nodalization for all sensitivity studies. The Revision 1 of TR Appendix B utilizes the LBLOCA licensing nodalization in Figure 17 and new sensitivity results are presented.

The NRC staff finds that the applicant's changes in Revision 1 of TR Appendix B that utilizes the LBLOCA licensing nodalization in Figure 17 are acceptable, and therefore concludes that this issue is resolved.

Radial Nodalization of Reactor Core

The guidance in NUREG/CR-5249, Section 2.0, discusses issues related to model nodalization. TR Figure 17 of Appendix B shows the nodalization of the primary system where the entire core is divided into [[ ]]. The NRC staff concern is that this nodalization may overestimate the cross-bundle core flow [[ ]]. In AI-76 [Ref. 3] the NRC staff requested the applicant to justify core radial nodalization from this perspective. If a different nodalization is to be used, the NRC staff requested the applicant to justify why it will provide conservative or realistic predictions of the core heat transfer behavior.

In response to the AI-76 [Ref. 5], the applicant stated, [[

]] Furthermore, it is stated "in CAREM, the conservative F_r (radial peaking factor) is applied to hot bundle." In the June 2016 Audit Meeting [Ref. 12], the NRC staff and the applicant discussed this in conjunction with the related topic in AI-27, Part e. The applicant provided a presentation [Ref. 27] showing the planar average power distribution a burnup of [[

]].

The applicant's presentation indicated that [[

]]. So, the same question of thermal channel cooling arises as in AI-27, Part e. In response to AI-27, Part e, the applicant performed a sensitivity study using [[

]]. In the presentation, the applicant also addressed questions regarding the radial peaking factors raised in AI-54 [Ref. 3] which the NRC staff finds justifies the peaking factor choices. The applicant's cross-flow model is discussed further in Section 4.9 below where the cross-flow loss coefficient calculations and uncertainty treatment are also acceptable.

The NRC staff finds that the applicant's information justifying core radial nodalization is acceptable because a conservative radial peaking factor is used, the cross-flow representation is appropriate, and the applicant demonstrated by sensitivity study that the model is conservative. On the basis of that information, the staff concludes that this issue is resolved.

4.6 Breaks

Spectrum

The TR describes the methodology for a LBLOCA and the applicant uses a representative scenario (termed the limiting large break) to demonstrate the methodology. Although the representative scenario is a double-ended guillotine break of a cold leg, approval of the

methodology is sought for any break that is a LBLOCA. However, the TR does not define the type of breaks that the applicant regards as LBLOCA, and therefore fall within the scope of the EM.

RG 1.157 specifies that breaks should be evaluated to include the range from "full double-ended" to small breaks. Furthermore, the guidance specifies that longitudinal breaks should also be considered. RG 1.157 also states that actual peaking factors and fuel conditions should be used. These will establish the limiting conditions applicable to subsequent design activities. The discussion in TR Section 3.1 did not include these and other details regarding the selection of the limiting break. As a result, in AI-3 and AI-6 [Ref. 3], the NRC staff requested the applicant to provide additional information. In the response to AI-3 [Ref. 4], the applicant stated that the requested information may be found in the response for AI-6, Part a.

In the response to AI-6 Parts a, c, d, and e [Ref. 4], the applicant stated:

- CAREM is applicable to the following spectrum of breaks:
    - Break location: primary loop piping, such as the RCP discharge leg (cold leg), RCP suction leg, hot leg.
    - Break type: guillotine, double-ended and longitudinal split.
    - Break size: From 0.5 ft^2 to 100 percent double ended[4].

This addresses the information requested in AI-3 and resolves the concern. In addition, the issues associated with AI-6 Parts a, c, d, and e are addressed as follows:

- TR Appendix K, which the applicant added to the TR in Revision 1, determines the limiting break and burnup conditions as follows:
    - Break location sensitivity: To determine the limiting break location
    - Break type sensitivity: To determine the limiting break type for the limiting break location
    - Pressurizer Location sensitivity: To determine the limiting location of the pressurizer (intact loop or broken loop)
    - Break size and burnup sensitivity: To determine the limiting break size for the limiting break location and type and limiting burnup condition since the burnup may affect the limiting break size

The applicant found that the limiting break location was the cold leg, the limiting break type was a double ended guillotine break, the limiting size was 100 percent, and the limiting time in life occurred for a burnup of 27,000 MWd/MTU. Based upon the studies in the TR and TR Revision 1, the NRC staff is able to conclude that the limiting location and type of break is a double ended guillotine break in the cold leg at a burnup of 27,000 MWd/MTU. The break size

[4] 100 percent break means 100 percent of pipe cross sectional area. Therefore, 100 percent double-ended guillotine break has a total of 200 percent break area of a pipe.

spectrum of 100 percent, 80 percent, and 60 percent in the TR and TR Revision 1 shows the 100 percent size to be limiting.

The NRC finds that the responses to AI-6 address the break spectrum and are acceptable because they clearly establish the break location, type, and size range for CAREM, they followed the guidance of RG 1.157, and are based upon the commitment made by the applicant in those responses.

The NRC staff imposes CAREM methodology application Limitation (1):

> *The CAREM methodology is limited to LOCA applications where the minimum break size is greater than or equal to 0.5 ft^2.*

Guillotine vs. Slot

In TR Revision 1, Appendix K, Figure 4 depicts the slot break model used in the break type sensitivity study. In this model of the split break in the cold leg, a single break valve is connected to pipe component 496-01 with an area 200 percent of the pipe cross sectional area. In contrast, the double ended guillotine break has one break valve connected to pipe component 491 and another break valve component connected to pipe component 496-01, both with areas of 100 percent of the pipe cross sectional area. The split break model also uses the Ransom-Trapp critical flow model with discharge coefficients of [[ ]] for single and two-phase flow respectively, which is the same critical flow model used for the double-ended guillotine breaks. When compared to the guillotine break, the slot break was less limiting as stated in Figure 5 in TR Revision 1, Appendix K.

In response to AI-61, Parts b-f [Ref. 4] discussed in further detail below, the applicant provided more detailed information regarding the slot break, including different models for representing the slot break and various sizes of the slot break ranging from 20 percent through 200 percent. The slot break model B shown in Figure 3 of the response to AI-61, Parts b through f is used in the TR and TR Revision 1 studies. Model A shown in Figure 3 in the response to Parts b through f of AI-61, may be a more representative slot break model. However, Figure 4 in the response to Parts b through f of AI-61 shows that results of both slot break models A and B are well below the PCT response resulting from the DECLG case.

The NRC staff finds that the applicant's information demonstrating that the guillotine break is more limiting in terms of PCT is acceptable, and on the basis of that information concludes that this issue is resolved.

Limiting Location

In the response to AI-6 [Ref. 4], the applicant clarified that they did not perform any sensitivity calculations to arrive at the location of the break in the cold leg and stated:

> *"Break location sensitivity in the cold leg is not performed because there is no additional pressure loss coefficient in the cold leg. Therefore, it can be thought that there is no significant difference in break location in the cold leg (pump discharge line). Moreover, it is widely accepted that the break location near the vessel is more limiting because it has more possibility to have ECC bypass or sweep-out of coolant than the other break locations in the cold leg. [[*
>
> *]]"*

The NRC staff notes that there is a slight increase in loss coefficient as the break is moved away from the cold leg nozzle. This slight increase would tend to mitigate the effects of ECCS bypass and downcomer water sweep-out, which would be beneficial to the calculation of PCT. The NRC staff also determines that a break further away from the cold leg nozzle would result in a slight increase in the downcomer water level and the associated driving head which would also tend to enhance core reflooding and mitigate increases in the cladding temperature. The slightly higher water level results from the "river" effect as the water must travel to the break location to spill into containment. The further the break is from the cold leg nozzle, the higher the water level would be.

The applicant performed a sensitivity study to determine the limiting location for the pressurizer. In TR Revision 1, Appendix K, the applicant summarized the results of two sensitivity calculations. In one case, the cold leg break was in the loop that did not contain the pressurizer, and in the second case, the cold leg break was in the loop containing the pressurizer. The applicant determined that the PCTs during the blowdown were similar in both cases, but that the reflood PCT is higher and quenching times are longer when the cold leg break is in the loop that does not contain the pressurizer.

The NRC staff finds that the applicant's information that a cold leg break further from the nozzle is less limiting and that based upon the sensitivity study the reflood PCT is higher and the quenching time is longer when the cold-leg break is not in the same loop as the pressurizer is acceptable, and on the basis of that information concludes that this issue is resolved.

Limiting Break Size and Elevation

TR Section 5.2.1.1 discusses the process followed by the applicant to determine the limiting break size. TR Section 5.2.1.1, citing Figure 5-9, states that the applicant selected the 100 percent guillotine break of the cold leg as the limiting case because its blowdown PCT is the maximum as compared to 80 and 60 percent breaks. However, Figure 5-9 shows that the reflood PCT for the 80 percent break is nearly the same as the blowdown PCT for the 100 percent break.

In AI-61 [Ref. 3], the NRC staff requested the applicant to address several concerns as briefly restated in the following Parts:

a. Provide the calculated PCT and corresponding elevation during the blowdown period and the reflood period for the 100 percent and 80 percent guillotine break cases.

b. Provide the basis for not examining the 90 percent and 70 percent guillotine break cases.

c. Describe the phenomena resulting in the 80 percent guillotine break case quenching before the 100 percent guillotine break case.

d. Provide information to justify that the 180 percent, 160 percent, 140 percent, etc., cold leg split (CLS) break PCT will be bounded by the guillotine break.

e. Provide evidence that the reflood PCT for the 80 percent guillotine break resulting from the application of distribution free statistics is not limiting.

f. Justify that the calculations performed are representative of the spectrum of break sizes and locations applicable and that split breaks are bounded by the limiting break.

In the response to AI-61, Part a [Ref. 4], the applicant provided the calculated PCT, and its location, for the 100 percent and 80 percent guillotine break cases for blowdown and reflood. Based on this information, the NRC staff is now able to better understand the blowdown PCT and reflood PCT transient response.

In the response to AI-61 Part c [Ref. 4], the applicant stated that fuel rod quenching occurred at about [[ ]] seconds for the 60 percent break case, while for the other break cases, fuel rod quenching occurred at about [[ ]] seconds. Furthermore, the different quenching response was mainly as a result of the elevation at which the PCT occurred. For the 60 percent case, the PCT occurred in heat structure node [[ ]], while the other cases had the PCT in heat structure node [[ ]]. The applicant stated that the fuel rod quenching in the 60 percent break case occurs at a later time, [[ ]] s, because the [[ ]] for the 80 percent and 100 percent cases. In the response to AI-61, Part c [Ref. 4], the applicant presented Figure 7 showing the collapsed core level for the 80 percent and 100 percent cases and stated that the collapsed water level for the 80 percent case is lower than the 100 percent case due to the delay in the time of SIT injection.

[[

]].

The NRC staff finds that the explanation for the quenching time is reasonable and therefore concludes that this part of the issue is resolved.

In the response to AI-61, Part d [Ref. 4], the applicant provided a break size sensitivity study for the split break cases. The applicant examined different models for representing the split break in RELAP5 and examined split break sizes ranging from [[ ]] percent. Based upon the split break sensitivity studies, the NRC staff concludes that the sensitivity study illustrates that the double ended guillotine break cases bound the split break cases of various sizes, and that the issues associated with AI-61, Parts d and f are resolved.

In the response to AI-61, Parts b, [Ref. 4], the applicant performed a SRS calculation utilizing the break area as one of the uncertainty parameters for a double ended cold leg guillotine break. The SRS calculations incorporated the break size as one of the uncertainty parameters assuming a uniform distribution of sizes from [[ ]] percent and Figure 6 of the response provided the calculation results. The third highest PCT of these SRS calculations resulted in a PCT of [[ ]] percent double ended cold line guillotine (DECLG) break. The third highest PCT from the SRS calculations in the TR was 1264 K. The third

highest PCT case in the TR (1264 K) occurred during blowdown, while the third highest of the SRS calculations which included break area as an uncertainty variable ([[ ]] K) occurred during reflood. Rod quenching for the TR case occurred later than for the SRS case with break area uncertainty. There were no other details of the study provided. The applicant concluded that the 100 percent DECLG break presented in the TR is in fact limiting as they had stated in the TR.

Appendix K in TR Revision 1 provides the results of sensitivity studies for the break location, break type, break size, and limiting time in life. The applicant found that the limiting break location was the cold leg, the limiting break type was a double-ended guillotine break, the limiting size was 100 percent, and the limiting time in life occurred for a burnup of 27,000 MWd/MTU. RG 1.157 states that "*the range of break sizes considered should be sufficiently broad that the system response as a function of break size is well enough defined so that interpolations between calculations, without considering unexpected behavior between break sizes, may be made confidently.*" Based upon the studies in the TR and TR Revision 1, the NRC staff is able to conclude that the limiting location and type of break is a double ended guillotine break in the cold leg at a burnup of 27,000 MWd/MTU. Based upon the studies performed in response to the audit issues, the NRC staff is able to conclude that the break size spectrum is sufficiently broad and that smaller break sizes are bounded by the spectrum analyzed. The break size spectrum of 100 percent, 80 percent, and 60 percent in the TR and TR Revision 1 shows that the 100 percent break size is limiting. The NRC staff finds that the applicant's information regarding the spectrum of break sizes, types, and locations meets the guidance of RG 1.157, and on the basis of that information concludes that this issue is resolved; however, the NRC staff imposes CAREM methodology application Condition (3):

> *The limiting break size shall be determined such that interpolation between break sizes would not result in a calculated peak cladding temperature that is significantly larger than 50° F, as specified by 10 CFR 50.46(a)(3)(i) for model changes.*

The NRC staff finds that the applicant's information supplied above to clarify the several issues regarding the determination of limiting LBLOCA breaks is acceptable, and on the basis of that information concludes that this issue is resolved, subject to Condition (3).

Long Term Core Cooling

The base case calculation of the APR1400 using the best-estimate operating conditions and nominal values is shown in TR Figures 5-12 through 5-28. The TR states that the water level in the reactor vessel is mainly determined by the balance of inlet (ECCS) and outlet (break) mass flow rates. In TR Revision 1, Figure 5-14 shows that during the late reflood period, ECCS water is supplied by the SIPs with a constant flow rate while the break flow, shown in Figure 5-13, decreases to almost zero beyond 225 seconds. From these results, one would expect continuous water level recovery in the reactor core region after 225 seconds. However, the water levels in the core and downcomer region, shown in Figure 5-15, are basically constant beyond 325 seconds. Therefore, in AI-62 [Ref. 3] the NRC staff requested the applicant to provide an explanation for the observed behavior. In TR Revision 1 [Ref. 13], the figures are extended to 400 seconds instead of being truncated at 250 seconds. The extended time scale in Figure 5-15 in TR Revision 1 shows that the downcomer and core collapsed water levels are stable and show a slow increasing trend, demonstrating that a continuous water level recovery results, which leads into the period of long term core cooling. Consequently, the transient behavior is more apparent and the previous NRC staff concerns associated with AI-62 are no longer present.

The NRC staff finds that the applicant's information supplied showing event progression out to 400 seconds is acceptable, and on the basis of that information concludes that this issue is resolved.

4.7 Thermal Conductivity

Thermal Conductivity Degradation

To address the impact of fuel pellet Thermal Conductivity Degradation (TCD), the applicant developed a procedure in which a penalty is applied to the fuel centerline temperature using results from the FATES-3B analysis. This method is described in TR Section 2.4.2 of Appendix K.

In applying this method, the applicant adjusts the heat structure inputs for the fuel in RELAP5/MOD3.3/K to match the interface data from the FATES-3B tests. This interface data includes the steady-state calculated fuel centerline temperatures (FCT) with an additional TCD penalty and the gap width. The applicant performs this calculation at the limiting burnup for several values of fuel rod linear heat generation rate (LHGR). Next, the applicant uses these calculations to develop functions that give fuel rod roughness as a function of LHGR, presented in Figure 27 and Figure 28 in TR Appendix K, for use in the 181 SRS calculations. Therefore, [[

]].

The NRC staff finds that the applicant's information on TCD describes an acceptable approach because it captures the best-estimate nature of the interface data while allowing for the sampling of thermal-conductivity during the SRS calculations, and on the basis of that information concludes that this issue is resolved.

Gap Conductance Model

TR Appendix B states that the applicant modified [[

]]. However, it was unclear what prompted this modification. In AI-24 [Ref. 3], the NRC staff requested the applicant to provide the basis for performing this modification.

In the response to AI-24 [Ref. 4], the applicant stated that [[

]].

The applicant demonstrated the effect of this modification to RELAP5/MOD3.3 using APR1400 plant simulations in TR Appendix B. The APR1400 simulations show the comparison of results before and after the applicant made this change. However, the applicant did not supply a comparison of results for either the APR1400 plant or an integral test using RELAP5/MOD3.3 and RELAP5/MOD3.3/K (i.e., with all changes present in the frozen version that is submitted for licensing). In AI-25 [Ref. 3], the NRC staff requested the applicant to provide the results of such a comparison.

In the response to AI-25 [Ref. 4], the applicant compared the cladding temperature for the high-power region using RELAP5/MOD3.3 and RELAP5/MOD3.3/K for LOFT Test L2-2. The applicant noted that the code inputs were the same except for the user input for [[ ]]. The applicant provided the calculation results, showing essentially no difference in the reflood PCTs, although the quenching time is delayed for both cases as compared to the test data. The applicant's comparison illustrated that the integral effect of this code modification is acceptable to the NRC staff.

The NRC staff finds that the applicant's information justifying the modification to return [[ ]] is acceptable, based on the results of the calculations provided by the applicant, and therefore concludes that this issue is resolved.

Transient Gap Conductance

TR Section 4.2.2.1.1 states that the uncertainty in the transient gap conductance is lumped with that of the [[ ]]" According to Volume 4, Section 9.3 of [Ref. 20], the gap conductance model in the code, derived from FRAP-T6, considers "...elastic deformation of cladding under the differential pressure..." A few lines later, the manual states that "...clad ballooning is not included in the [gap conductance] model." In AI-29, Parts a-f [Ref. 3], the NRC staff requested the applicant to address several concerns regarding the approach used to treat the uncertainty in transient gap conductance.

In the response to AI-29 [Ref. 4], the applicant described the RELAP5/MOD3.3/K dynamic gap conductance model which is a simplified deformation model generated from FRAP-T6. The clad ballooning model is the standard RELAP5 model. The response described how RELAP5/MOD3.3 captures the effect of clad ballooning on the transient gap conductance, but notes that the code cannot represent the effect of fuel pellet fragment relocation, so this effect is not calculated by RELAP5/MOD3.3/K, and thus is not considered in CAREM.

Accordingly, the NRC staff imposes CAREM methodology application Limitation (2):

> *The CAREM methodology may be used to predict the onset and potential for cladding deformation resulting from swelling, but may not be used in licensing calculations to predict flow blockage effects due to pellet relocation or hydraulic flow redistribution.*

The applicant stated that the geometry changes caused by ballooned cladding do not alter any other parameters which have any influence on the RELAP5/MOD3.3/K hydraulic solution. The applicant further stated that the effect of cladding swelling on gap conductance is reasonable and based upon the FRAP-T6 code model. The NRC staff considers the FRAP-T6 cladding deformation model reasonable and the model's effect on the geometric changes to the gap conductance are appropriate. Therefore the NRC staff finds the applicant's explanation of the effect of geometry changes on the hydraulic solution resulting from cladding swelling are acceptable within the constraints of Limitation (2).

The applicant stated that in CAREM, the steady state gap conductance data as calculated by the FATES-3B fuel performance code is used to set the initial condition of the fuel. The treatment of the initial gap conductance is discussed in Appendix K of TR Revision 1. The applicant stated that the gap width during the transient can change significantly compared with that of steady-state, and it can have a dominant effect on the transient gap conductance. The applicant noted that as discussed above, the gap width during transient is considered by [[

]] which is based upon FRAP-T6. The NRC staff considers the FRAP-T6 cladding deformation model reasonable and the explanation of the transient gap conductance acceptable because the deformation calculated by the cladding swelling model will directly govern the transient gap width. Therefore, the NRC staff finds this explanation acceptable within the constraints of Limitation (2).

The applicant described how cladding deformation can be divided into two categories: elastic and plastic deformation. The applicant stated that [[

]]. The applicant stated that the uncertainty of transient gap conductance is caused by the uncertainty in the steady-state gap width which is a dominant parameter in the transient gap conductance calculation. Consequently, the applicant concluded that the [[
]].

The NRC staff finds the explanation acceptable because [[

]], and therefore the NRC staff finds the explanation acceptable, and the issue is resolved.

The applicant stated that conservative gap conductance data was generated by [[
]], etc. Consequently, [[

]]. In the methodology to address the thermal conductivity degradation (TCD) issue, the [[
]]. The applicant does not directly account for [[

]].

The NRC staff accepts the applicant's assertions that the balloon/burst model in RELAP5/MOD3.3/K is acceptable for indicating the potential for ballooning or bursting. The NRC staff also agrees that the RELAP5 clad ballooning and burst models are not sufficient to actually determine the effect of such occurrences on the PCT. Therefore, CAREM may not be used in licensing calculations to predict flow blockage effects due to pellet relocation. Accordingly, the NRC staff imposes Limitation (2), which prohibits the use of CAREM for calculating the flow distribution and associated PCT following the predicted onset of clad ballooning.

4.8 Hydrodynamics

Multidimensional Effects

RG 1.157 states that "…one-dimensional approximations to three-dimensional phenomena will be considered if those approximations are properly justified." The core nodalization is [[ ]]. It is unclear how the methodology in the TR selects this nodalization over other options and how it can model multidimensional phenomena occurring within the core (e.g., "upper plenum to core CCW" in TR Table 3-2). Therefore, in AI-27, Part d [Ref. 3] the NRC staff requested the applicant to discuss any known multidimensional phenomena of importance to LBLOCA and justify the selected core radial nodalization.

In the response to AI-27, Part d [Ref. 5], the applicant stated that core nodalization of the APR1400 model and the SETs and IETs models also use [[ ]]. The response continues, stating that multidimensional flows can be broadly classified into two phenomena. First, higher vapor velocities and liquid entrainment occur in the higher power region of the core. The entrained liquid from the core is carried into the upper plenum where it is de-entrained forming a two-phase pool. The liquid from the pool can reenter the lower power region of the core due to the lower vapor velocities in those regions. [[ ]]. In CAREM, the applicant does not specifically model the multidimensional phenomena of the core, but it does consider the adverse conditions that may occur in the area around the hottest fuel rod. The applicant then stated that in the case of the APR1400 plant, multidimensional phenomena are not significant for the following reasons:

- [[ ]].
- [[ ]].
- [[ ]].

The applicant also considered the radial power profiles depicted in Figures 4.3-4 through 4.3-18 of the APR1400 Design Control Document (DCD) Tier 2 Chapter 4, Revision 1. The applicant compared the power in the lower power outer assemblies with the power in the central assemblies, neglecting one hot assembly. The comparison for the unrodded, full power equilibrium Xenon conditions indicated that the average power in the peripheral assemblies ranged from [[ ]] of the average power in the central assemblies.

In response to AI-47 [Ref. 5], the applicant discussed the CCFL condition based upon the Kutateladze number and stated that the Kutateladze number during the reflood period (70 seconds to 200 seconds) for AP1400 calculations was between 4.0 m/sec and 6.7 m/sec. The applicant also stated that the steam velocity between the core and upper plenum during the reflood period (70 seconds to 200 seconds) for the APR1400 RELAP5/MOD3.3/K calculation was approximately 40 m/sec. Consequently, the average core exit steam velocity would preclude any liquid flow from the upper plenum to the core.

In response to AI-60 [Ref. 4], the applicant provided liquid and vapor flow rates from the core to the upper plenum for the RELAP5/MOD3.3/K average assemblies and the hot assembly:

- Figure 17 shows the liquid mass flow rate [[ ]],
- Figure 18 shows the vapor mass flow rate [[ ]],
- Figure 19 shows the liquid mass flow rate [[ ]], and
- Figure 20 shows the vapor mass flow rate [[ ]].

The vapor mass flow rate during the reflood period (70 seconds – 200 seconds) shows upward flow into the upper plenum. However, [[

]], the NRC staff was concerned that the calculated behavior does not seem to be realistic. Furthermore, the liquid back flow into [[ ]] which would be non-conservative behavior.

Figure 1 of the response to AI-27, Part d [Ref. 5], shows the mass flow rate at [[ ]]. To assess the effect of limiting flow back into [[ ]], the applicant performed a sensitivity calculation in which it assumed the reverse K-factor of the junction connecting [[ ]] exit and upper plenum to be a very large value. Figure 2 compares the original mass flow rate at [[ ]] exit with the case with the very large reverse K-factor. The very large reverse K-factor prevented flow back into [[ ]], similar to the effect of including a CCFL model, except that it precluded all downward flow into [[ ]], while a CCFL model may have calculated negative liquid flow if the conditions were appropriate. Figure 3 shows that the heat transfer mode at the PCT location was nearly identical and Figure 4 shows that the PCT response is very similar. This tends to imply that the unrealistic effect of downward flow at [[ ]] exit has little effect on the result, and therefore, a better model (i.e., use of a CCFL) is not required.

In response to RAI 399-8510, Question 9, Part 10 [Ref. 1.g], the applicant performed a multi-dimensional sensitivity calculation to confirm that the liquid fallback phenomenon from upper plenum to the core does not occur when lower power outer assemblies are represented in a separate channel in the RELAP5/MOD3.3/K model. [[

]].

Figure 10-6 in the response to RAI 399-8510, Question 9, Part 10, [[

]].

Based upon the figure for the cumulative liquid mass rate at the core to upper plenum, the applicant concluded [[

]].

In the responses cited above, the applicant concludes that [[

]]:

- the SET and IET assessments,
- liquid fallback from the upper plenum to the low-power region is not expected for the APR1400,
- the conservative power peaking factors for the hot fuel rod and [[ ]] (See SER Section 4.14).

The NRC staff finds that the applicant's information regarding how nodalization is selected over other options and how it can model multidimensional phenomena occurring within the core is properly justified and therefore acceptable, and on the basis of that information concludes that this issue is resolved.

Cross-Flow Junctions

Cross-flow junctions are used in the model between [[ ]]. The flow through these junctions in the core depends on the associated flow areas and loss coefficients. In AI-27, Part f [Ref. 3], the NRC staff requested the applicant to explain the approach used to determine these parameters and how the uncertainties are affected.

In the response to AI-27, Part f [Ref. 4], the applicant stated that in the areas of the core, cross-flow junctions are determined by the reactor core geometry and that they did not statistically treat the uncertainty associated with the flow area. They also did not statistically treat the uncertainty of the cross-flow junction loss coefficient because the effect of cross-flow is insignificant based upon information from [Ref. 51] which states:

> *"The power of the peripheral bundles is lower than the power of central bundles. This radial core power profile causes so called chimney effect (refer to Figure 1) As a result of this chimney effect, heat transfer to flow is enhanced in the high-power region and degraded in the low-power region. However, since PCT occurs in the high-power region, the net effect is a decrease in the PCT."*

The applicant also provided additional information related to the loss coefficients for cross-flow junctions. The NRC staff reviewed the applicant's methodology for the calculation of cross-flow in the response to AI-27, part f and found that the methodology conforms to a reasonable and common practice in RELAP5 calculations. The NRC staff is also aware of the relative insignificance of the cross-flow demonstrated in the 2D/3D Program Work Summary Report [Ref. 51]. The relative insignificance reduces the importance for specifying the uncertainty

related to cross-flow. The applicant has followed the guidance in RG 1.157, which recognizes that in the best-estimate analysis approach, not all models are required to be best-estimate with the associated uncertainty evaluation. RG 1.157 states:

> *In practice, best estimate codes may contain certain models that are simplified or contain conservatism to some degree. This conservatism may be introduced for the following reasons: (1) The model simplification or conservatism has little effect on the result, and therefore the development of a better model is not justified*.

The NRC staff finds that he applicant's methodology for calculating the cross-flow loss coefficients follows the guidelines of RG 1.157 Section 3.1.1, and since the effect of cross-flow is insignificant, it is not necessary to consider this as part of the uncertainty quantification, which is consistent with the guidance in RG 1.157 Part C, Section 1, and on this basis, it is concluded that the issue is resolved.

The NRC staff finds that the applicant's information explains how cross-flow junction parameters are determined and why an uncertainty assessment is unnecessary, and on the basis of that information concludes that this issue is resolved.

Counter Current Flow Limitation

CCFL on the tie plate is a complicated hydraulic phenomenon that consists of three flow streams:

- the steam flow up from the core,
- water up flow from the core, and
- the water fallback into the core.

RELAP5/MOD3.3/K treats CCFL with a general model that allows the user to select the Wallis form, the Kutateladze form, or a form in between the Wallis and Kutateladze forms. Experiments on CCFL are well correlated with the Kutateladze number, as shown in Figure 1 of the applicant's response to AI-47 [Ref. 5]. The applicant showed calculations of the Kutateladze number at pressures of 1 bar and 3 bar for fluid conditions at 100°C and obtained Kutateladze flooding limits of 4.0 m/sec at 3 bar and 6.7 m/sec at 1 bar.

The applicant showed that the steam velocity at the tie plate for APR1400 in Figure 2 of the response to AI-47 [Ref. 5] is always greater than 6.7 m/sec during the reflood period between 70 seconds and 200 seconds. The steam and liquid flow at the tie plate are shown in Figure 3 of the response to AI-47. The liquid flow is generally upward in the reflood period except the time period between 170 ~ 250 s, which is consistent with the limiting gas velocity. Therefore, the applicant concludes that the code prediction of thermal-hydraulic behavior on the tie plate is reasonable even without using the CCFL model.

The applicant also noted that RELAP5/MOD3.3/K implements CCFL by a change in the momentum equations (refer to Volume 1, Section 3.4.7 [Ref. 20]). The NRC staff observes that the applicant's CCFL models are validated mainly through steady state experiments, but the flow during the reflood period is very oscillatory. Consequently, CAREM does not use the CCFL option on the tie plate junctions.

The applicant's response also noted that RELAP5/MOD3.3/K in CAREM applications tends to over-predict the water carry-over from the core to the upper plenum. This is shown in the

assessments of FLECHT-SEASET [Ref. 42], Appendix P Evaluation of Steam Binding Using UPTF and PKL Test, pp. P-11) and NEPTUN [Ref. 42], Appendix C, Section 4.3.4). The applicant observes that the flow regime in the upper plenum during the reflood period is mainly annular or annular/mist and there are no models for the de-entrainment by internal structures in the upper plenum. Therefore, liquid flow from the upper plenum to the hot leg depends on the liquid volume fraction of the upper plenum and it is usually over predicted. Consequently, liquid volume remaining in the upper plenum is typically under predicted. This is evident in the applicant's UPTF-10B simulation [Ref. 42]. As a result, liquid flow to steam generator is excessive and the ensuing steam binding is too high. [[

]].

In Summary, the applicant concluded that:

(1) the steam velocity at the tie plate is greater than CCFL limit velocity and there was no need to include the CCFL option on the tie plate junction in calculations;

(2) the RELAP5/MOD3.3/K over predicts the liquid carry-over rate from the core to the upper plenum, and this is a conservative approach with respect to PCT;

(3) [[

]]; and

(4) [[

]].

The NRC staff review of the radial power variation in the APR1400 core finds that the power in the low power peripheral assemblies could be as low as [[ ]] of the average assembly power. Since the steam flow from the assemblies is proportional to the assembly power, the NRC staff determines that the steam velocity exiting the low power peripheral assemblies would still exceed the Kutateladze flooding limit by at least a factor of 4. Since the applicant demonstrated that counter-current flow should be precluded at the core tie plate and since the applicant utilizes a conservative model for droplet vaporization in the steam generators, the steam binding is conservatively calculated because it maximizes the amount of vapor entering the steam generators. The bias applied for steam binding is therefore bounding because of the process for maximizing the vapor entering the steam generators. The NRC staff finds that the applicant's information regarding CCFL on the tie plate and the observed hydraulic phenomena calculated are acceptable because the steam velocities even in the low power assemblies exceeds the Kutateladze flooding limit by at least a factor of 4, and the steam binding bias is conservatively calculated. Therefore, on the basis of that information the NRC staff concludes that this issue is resolved.

4.9 Cladding Rupture

Section 3.2.5 of RG 1.157 states that "[f]or rods calculated to rupture their cladding during the loss-of-coolant accident, the oxidation of the inside of the cladding should be calculated in a best-estimate manner." In AI-30, Part b [Ref. 3], the NRC staff requested the applicant to discuss how this requirement is met in CAREM. In the response to AI-30, Part b [Ref. 4], the applicant stated that the reaction of zirconium and steam in RELAP5/MOD3.3/K code uses the correlation developed by Cathcart and described in Volume 1, Section 4.13 [Ref. 20]. The response also stated that the metal water reaction model is coupled with the fuel rod

deformation model so that if a fuel rod ruptures, the inside of the cladding can react with steam and the oxidation of the inside of the cladding is calculated.

RG 1.157 states: *"The data of Reference 11 are considered acceptable for calculating the rates of energy release, hydrogen generation and cladding oxidation for cladding temperatures greater than 1900°F."* Since Reference 11 in RG 1.157 is the Cathcart model, the applicant has followed the guidance set forth in RG 1.157, Section 3.2.5 for both the best-estimate model and the calculation of oxidation on the cladding inner surface in the event of a rupture of a fuel rod. The NRC staff finds acceptable the applicant's information that justifies the calculations of the fuel rods to rupture, including the oxidation of the inside of the cladding in a best-estimate manner, because it meets the guidance provided in RG 1.157 Section 3.5.2.

4.10 Loop Seal

Based on drawing 1-190-H-184-001C ("primary piping interfaces") provided in [Ref. 26], it appears that the loop seal elevation for APR1400 is close to the midpoint of the active core, creating the possibility of a loop seal during LOCA. As a result, in AI-2 [Ref. 3], the NRC staff requested the applicant to demonstrate that the peak cladding temperature remains within acceptable limits at all times. Furthermore, the applicant was requested to demonstrate the impact of having three (3) or four (4) trains of safety injection flow (as compared to the two trains assumed for the LBLOCA analysis in the TR) available during the long term reflood and LTCC phases under the above-described conditions.

RAI 143-8092, Question 15.06.05-1 [Ref. 8], is related to AI-2. In response to RAI 143-8092, Question 15.06.05-1 [Ref. 1.c], the applicant stated that the APR1400 pump design has an exit volute that is almost to the top of the cold leg, preventing backflow during blowdown or reflood. During the June 2016 Audit meeting [Ref. 12], the applicant stated that there would be no loop seal plugging, even when all trains of safety injection were available during a large break LOCA.

The staff reviewed the applicant's information and concluded that there is no potential for a loop seal plugging to occur. This is because the cold leg piping would need to be nearly liquid filled for fluid to flow back into the loop seal due to the RCP exit volute design, and a large break in the cold leg precludes the development of a significant liquid level. Therefore, the NRC staff, on this basis, concludes that this issue is resolved.

4.11 Loss of Offsite Power

TR Section 3.1.2.1 states that the reactor coolant pumps (RCPs) are assumed to be tripped upon loss of offsite power (LOOP). Since the operational RCPs may impact the peak cladding temperature as well as the coolant inventory, in AI-6, Part g [Ref. 3], the NRC staff requested the applicant to clarify whether the limiting break analysis included consideration of the location of the available safety injection pump trains with respect to the broken cold leg. In the response to AI-6, Part g [Ref. 4], the applicant provided a figure depicting the locations of the DVI lines relative to the cold legs and stated that two SIPs were assumed to be operating. The SIPs assumed to be operating were connected to DVI-2 and DVI-4, where DVI-4 is near the broken loop and DVI-2 is 180° opposite.

In the response to AI-6, Part g [Ref. 4], the applicant stated that:

- When the loss of offsite power (LOOP) is not assumed, [[

]].

- [[

]].

- The uncertainty ranges for [[

]].

- A figure provided as part of the response showed the calculated cladding temperatures with and without RCPs operating. The peak cladding temperatures (PCTs), with and without LOOP assumption, are [[ ]], respectively, and PCTs for both cases occur during the blowdown period. The reflood PCTs for both cases, with and without LOOP assumption, are [[ ]].

- The PCT with LOOP assumption occurred at heat structure node [[ ]], whereas PCT without LOOP assumption occurred at heat structure node [[ ]], which means the quenching time difference is caused by PCT elevation.

Therefore, the applicant concluded that the LOOP assumption is more conservative than the non-LOOP assumption. However, the applicant's finding indicated that [[

]]. Therefore, the NRC staff set forth Condition (4) on the use of CAREM requiring [[

]]. This condition is intended to apply when performing the scenario definition step (i.e., Step 1 of Element 1 of the CAREM iteration process).

The NRC staff finds that the applicant's information regarding the potential for the operational RCPs to impact the PCT as well as the coolant inventory for a LOOP coincident with the break is acceptable [[

]].

The NRC staff imposes CAREM methodology application Condition (4):

> *The limiting loss-of-offsite-power (LOOP) assumption shall be utilized and justified for the appropriate type of limiting PCT calculation, i.e., blowdown PCT or reflood PCT, while performing Step 1 of CAREM Element 1.*

4.12 Boiling in the Downcomer

The TR Revision 1 PIRT has [[
]]. During the June 2016 Audit Meeting, the applicant discussed this topic in a presentation to the NRC staff related to AI-17 [Ref. 1.a]. The applicant stated [[

]]:

"Downcomer level is sufficient to force coolant into lower plenum to begin refill."

The discussion stated that the appropriate calculations for heat transfer from structures to fluid and the potential for fluid vaporization were present in the calculation.

The NRC staff finds that the applicant's information regarding boiling in the downcomer during the refill period is acceptable because the heat transfer from the structures to the fluid is accounted for; and therefore concludes that this issue is resolved.

4.13 Flow Blockage

TR Appendix A, Revision 1, [[ ]]. Section 3.3.1 of RG 1.157 states that the calculation of the swelling and rupture of the cladding should be included in the analysis and should be performed in a best-estimate manner. The blockage may reduce the cladding temperature but that does not decrease the importance of the effect of blockage on the physical response. The calculated cladding temperature transient should reflect the cooling effects of clad swelling. In AI-72 [Ref. 3] the NRC staff requested the applicant to confirm that RELAP5/MOD3.3/K can calculate fuel cladding swelling and rupture. Furthermore, the NRC staff also requested the applicant to confirm that the calculated effect of swelling and rupture on fluid flow and cladding temperature calculations reflects the effect of fuel channel blockage.

In response [Ref. 5], the applicant stated that the RELAP5/MOD3.3 computer code has a model for cladding deformation described in Volume 1, Section 4.14 [Ref. 20]. The applicant incorporated an empirical cladding deformation model from FRAP-T6 [Ref. 41] into RELAP5/MOD3.3/K. This model estimates cladding strain by thermal, elastic, and plastic deformation and predicts rupture strain and blockage from NUREG-0630 [Ref. 33] data.

The applicant stated that RELAP5/MOD3.3 can calculate swelling and rupture effects based upon the FRAP-T6 [Ref. 41] code model. Further details are in the response to AI-29, Parts a through f [Ref. 4]. The calculation of gap conductance considers the effect of swelling, but does not directly calculate the effect of swelling on fluid flow blockage unless rupture occurs. When fuel rod burst is calculated to occur, the effect of flow channel blockage may be represented through additional loss coefficients in the neighboring junctions.

The NRC staff finds the applicant's clarifications on the impact of cladding deformation and rupture on flow blockage acceptable because it meets the guidelines set forth in RG 1.157

Section 3.11 and therefore concludes that this issue is resolved within the constraints of Limitation (2) cited above.

4.14 Power

Peaking Factors F_r/F_q

The guidance in RG 1.157, Section 4.3.1, establishes acceptable controls for the utilization of conservative parameters in best-estimate analysis. In AI-53, Part a [Ref. 3] the NRC staff requested the applicant to describe the determination of the [[ ]] in the LBLOCA analysis.

In the response to AI-53, Part a [Ref. 4], the applicant stated that [[ ]]. The applicant stated that the principle for CAREM is to use a value of the radial peaking factor which is bounding for the cycle-specific analysis.

The response also stated that [[ ]] using this methodology using sensitivity studies that consider the radial fall-off curve.

In AI-53, Part b [Ref. 3], the NRC staff requested the applicant to describe the process used to determine the power shape and peaking factor (F_q) for the base case plant calculation.

In the response to AI-53 Part b [Ref. 5], the applicant provided a [[ ]].

The applicant also stated that the LHGR limit is defined as the product of F_q and the core average LHGR. [[ ]].

The applicant stated [[ ]]. For the base case calculation, the power shape used is shown in Figure 7 of the response to AI-53, Part b.

Revision 1 of TR Section 5.1.1 reflects the clarification of the hot assembly power peaking factor as:

"[[

]]"

In response to AI-54 [Ref. 5], the applicant also provided the maximum peaking factors for the equilibrium cycles. The applicant stated that [[

]].

The NRC staff finds that the applicant's information justifying the use of peaking factors in a suitably conservative manner is acceptable, and on the basis of that information concludes that this issue is resolved.

Power Distributions

RG 1.157 states that individual best-estimate models should be compared to applicable experimental data to ensure that realistic behavior is predicted and that relevant experimental variables are included. It further states that uncertainty analyses should ensure that a major bias does not exist in the models and that the model uncertainty is small enough to provide a realistic estimate of the effect of important experimental variables. The analyses in the TR utilized a top-skewed power distribution. The applicant performed a significant number of comparison calculations to the FLECHT-SEASET test data that utilized a cosine power distribution. However, since the licensing calculation is based upon a top-skewed power distribution, the NRC staff noticed that the applicant did not consider the FLECHT-SESET top skewed power tests. In AI-80 [Ref. 3], the NRC staff requested the applicant to provide the basis for this observation.

In the June 2016 Audit Meeting, the applicant presented information regarding the FLECHT-SEASET skewed power distribution tests. The applicant stated that the skewed power shape in the FLECHT-SEASET skewed power tests is not representative of the top skewed power distribution used in the APR1400 CAREM analyses and that the FLECHT-SEASET cosine power distribution test provides a power distribution that is more representative of the expected APR1400 power distribution. The applicant discussed the integrated power from the bottom of the core to the PCT location in conjunction with the effect of power distribution on the flooding rate, fuel rod quenching and entrainment effects.

[[

]].

The NRC staff finds that the applicant's information regarding axial power distributions including comparisons to test data is acceptable, and on the basis of that information concludes that this issue is resolved.

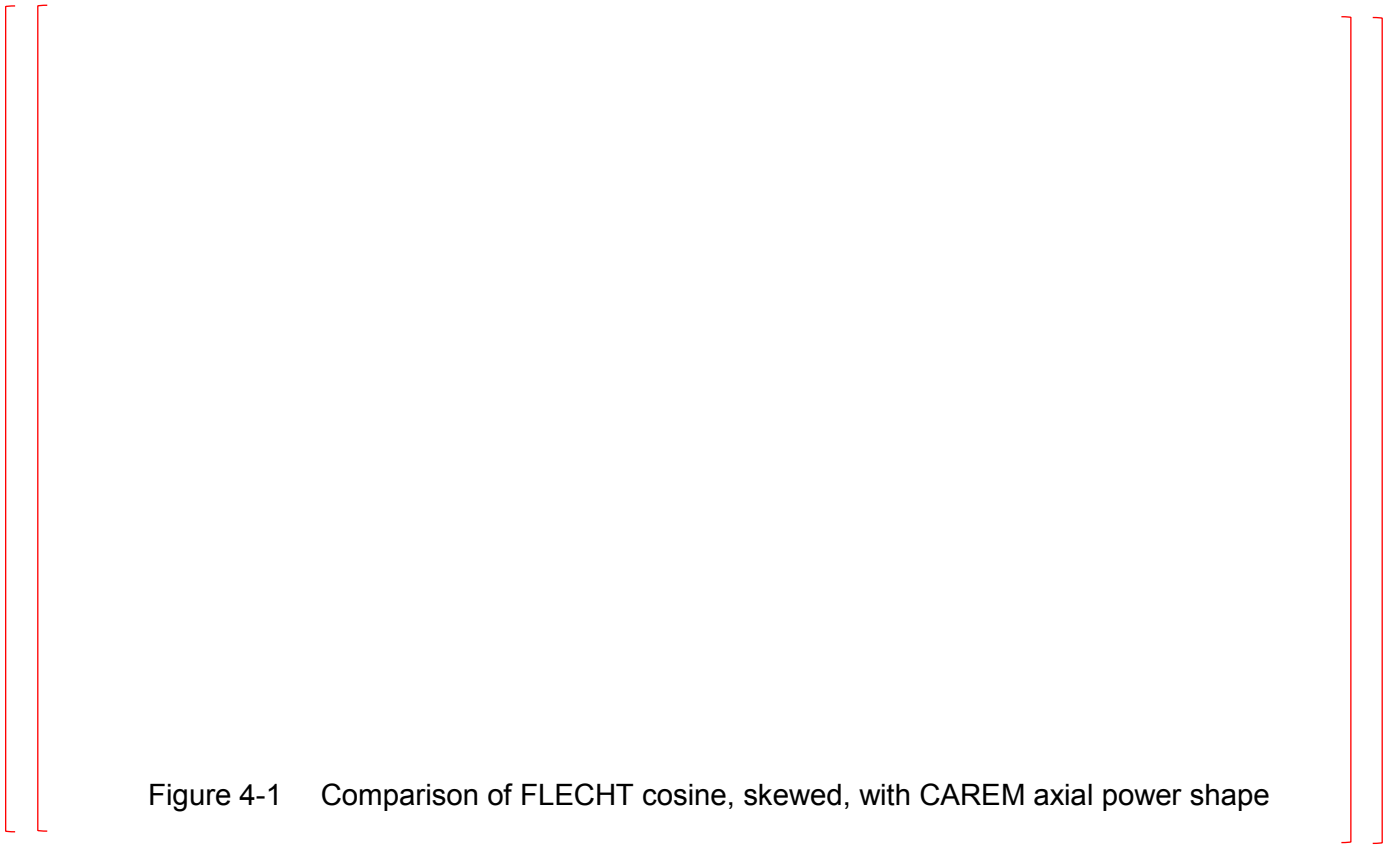

Figure 4-1 Comparison of FLECHT cosine, skewed, with CAREM axial power shape

4.15 Cladding Oxidation

The Cathcart model is used in RELAP5/MOD3.3 and RELAP5/MOD3.3/K to calculate cladding oxidation. TR Section 4.2.2.1.1 provides the uncertainty for the Cathcart model and page 4 of 23 [Ref. 26] describes the input for the uncertainty in the cladding oxidation reaction. The description implies that [[ ]]. However, the acceptance criterion applies to core-wide cladding oxidation and, in addition, RG 1.157 does not distinguish between oxidation in different fuel rods for best-estimate analysis. Therefore, in AI-30 [Ref. 3], the NRC staff requested the applicant to justify the basis for consideration of the uncertainty in cladding oxidation uncertainty [[ ]].

In the response to AI-30 [Ref. 4], the applicant stated that the core-wide cladding oxidation is related to the maximum hydrogen generation of 10 CFR 50.46(b). In CAREM, [[

]]. In the discussion of the reporting of the third highest PCT from the SRS as the licensing basis in AI-51, Part c [Ref. 3], the applicant clarified that it would determine the core wide hydrogen generation from the highest of all the SRS

calculations, not the third highest as in the case of PCT, to provide additional conservatism. In a revised response to AI-30, Part a [Ref. 4], the applicant provided Figure 1 showing the results of calculated hydrogen generation associated with [[ ]] for the results of the SRS calculations. Since the SRS cases include the range of PCTs including those for analyses with reflood peaks, the CAREM methodology is conservative.

The NRC staff finds that the applicant's justifications that the basis for consideration of the uncertainty in cladding oxidation uncertainty [[ ]] is acceptable, and on the basis of that information concludes that this issue is resolved.

5. CONDITIONS AND LIMITATIONS

The NRC staff evaluation of the applicant's CAREM large break LOCA analysis methodology finds that TR Revision 1, the underlying methodology, and the provided EM are acceptable to support APR1400 applications subject to the following Conditions:

(1) Deleted.

(2) Changes to the downcomer modeling shall require additional justification and NRC approval.

(3) The limiting break size shall be determined such that interpolation between break sizes would not result in a calculated peak cladding temperature that is significantly larger than 50° F, as specified by 10 CFR 50.46(a)(3)(i) for model changes.

(4) The limiting loss-of-offsite-power (LOOP) assumption shall be utilized and justified for the appropriate type of limiting peak cladding temperature (PCT) calculation, i.e., a blowdown PCT or a reflood PCT, while performing Step 1 of CAREM Element 1.

The NRC staff evaluation of the applicant's CAREM large break LOCA analysis methodology finds that TR Revision 1, the underlying methodology, and the provided EM are acceptable to support APR1400 applications subject to the following Limitations:

(1) The CAREM methodology is limited to LOCA applications where the minimum break size is greater than or equal to 0.5 ft^2.

(2) The CAREM methodology may be used to predict the onset and potential for cladding deformation resulting from swelling, but may not be used in licensing calculations to predict flow blockage effects due to pellet relocation or hydraulic flow redistribution.

6. CONCLUSIONS

TR Revision 1 presents the applicant's realistic, or best-estimate, LBLOCA analysis methodology for APR1400. A summary of the Application is provided in Section 3 of this SER.

Many issues were discussed during the NRC Audit Meetings and are described in the NRC Audit Summary Report [Ref. 12]. The review of the TR resulted in a number of AIs. A limited number of the issues could not be completely resolved during the Audit Meetings, which resulted in the NRC staff generating RAIs. The applicant responded to all of the AIs and RAIs and all of these were evaluated and dispositioned by the NRC staff. Those that contribute to the statements of acceptability issued by the NRC staff are documented in Section 4 of this SER.

TR Revision 1 complies with the regulatory criteria in 10 CFR 50.46 and the guidance in the SRP, Sections 15.0.2, Revision 0 and 15.6.5, Revision 3, RG 1.203, RG 1.157 and the CSAU methodology documented in NUREG/CR-5249. The review of the TR and the evaluation of the responses to AIs and RAIs resulted in several important technical observations that are as follows:

- The treatment of TCD is addressed in TR Revision 1.

- Liquid flow response from the core to upper plenum during reflood may be calculated in an unrealistic manner in the APR1400 RELAP5/MOD3.3K model. The applicant has provided information and calculations justifying that liquid penetration back into the core is prohibited due to the magnitude of core exit steam velocities. However, the APR1400 RELAP5/MOD3.3K calculations indicate significant liquid penetration back into the core from the upper plenum. Thus, calculations using a more detailed representation of the core and upper plenum may result in lower calculated PCTs.

The NRC staff concludes that the KHNP LBLOCA methodology, CAREM, as documented in TR Revision 1 is acceptable for analysis of the APR1400 LBLOCA subject to the Conditions and Limitations stated in Section 5 of this SER.

7. REFERENCES

1. APR1400-F-A-TR-12004-P Revision 0, “Realistic Evaluation Methodology for Large-Break LOCA of the APR1400,” December 2012, ADAMS Accession No. ML130230128.

2. APR1400-F-A-NR-14003-P, “Post-LOCA Long Term Cooling Evaluation Model,” Revision 0, ADAMS Accession No. ML15012A019 (Proprietary)/ ML15009A201 (Non-Proprietary).

3. APR1400 Large Break Loss of Coolant Accident Audit Issues, ADAMS Accession No. ML18011A393.

4. Response to Audit Issues, Topical Report APR1400-F-A-TR-12004, “Realistic Evaluation Methodology for Large-Break LOCA of the APR1400,” August 8, 2016 (ADAMS Accession No. ML16223A158).

5. Response to Audit Issues, Topical Report APR1400-F-A-TR-12004-P (Realistic Evaluation Methodology for Large-Break LOCA of the APR1400,” December 20, 2016 (ADAMS Accession No. ML17005A007).

6. Response to Audit Issues, Topical Report APR1400-F-A-TR-12004-P (Realistic Evaluation Methodology for Large-Break LOCA of the APR1400,” December 11, 2017, ADAMS Accession No. ML17345A958.

7. APR1400 Topical Report RAI No. 1-7425, Questions APR1400-1 through APR1400-3, ADAMS Accession No. ML14100A671, April 10, 2014.

8. APR1400 DCD RAI No. 143-8092, ADAMS Accession No. ML15221A006, August 7, 2015.

9. APR1400 DCD RAI 399-8510, ADAMS Accession No. ML16034A056, February 3, 2016.

10. APR1400 Topical Report RAI 7-8567, Questions APR1400-4 through APR1400-9, ADAMS Accession No. ML16098A098, April 7, 2016.

11. Korea Hydro & Nuclear Power Co., Ltd - Transmittal of Response to:

    a. RAI 1-7425, ADAMS Accession No. ML14113A325, April 10, 2014RAI 1-7425, ADAMS Accession No. ML14113A325, April 10, 2014

    b. RAI 143-8092, ADAMS Accession No. ML15246A531, September 3, 2015

    c. RAI 143-8092 Supplemental Response, ADAMS Accession No. ML16363A031, December 27, 2016

    d. RAI 399-8510, Question 6, ADAMS Accession No. ML16063A045, March 3, 2016

    e. RAI 399-8510, Question 7, ADAMS Accession No. ML17223A687, August 11, 2017

f. RAI 399-8510, Question 8, ADAMS Accession No. ML16063A045, March 3, 2016

g. RAI 399-8510, Question 9, ADAMS Accession No. ML16123A206, May 2, 2016

h. RAI 7-8567, 30-day response Questions APR1400 – 6, 7, 8, and 9, ADAMS Accession No. ML16116A446, April 25, 2016

i. RAI 7-8567, 45-day response Questions APR1400-4 and APR1400-5, ADAMS Accession No. ML16153A454, June 1, 2016

12. Audit Summary for APR1400 LBLOCA Topical Audit, ADAMS Accession No. ML17256B126, December 6, 2017.

13. Korea Hydro & Nuclear Power Co., Ltd - Transmittal of Topical Report APR1400-F-A-TR-12004-P, Revision 1, "Realistic Evaluation Methodology for Large-Break LOCA of the APR1400," Dated August 2017, ADAMS Accession No. ML17240A229 (Proprietary)/ ML17250A233 (Non-proprietary).

14. NUREG–0800, “Standard Review Plan for the Review of Safety Analysis Reports for Nuclear Power Plants,” Compiled 2007.

15. 10 CFR Part 21, “Reporting of Defects and Noncompliances,” 42 FR 28893, June 6, 1977.

16. 10 CFR 50.46, “Acceptance criteria for emergency core cooling systems for light-water nuclear power reactors,” 68 Federal Register 54142, September 16, 2003.

17. Regulatory Guide 1.157, “Best-Estimate Calculations of Emergency Core Cooling System Performance,” May 1989.

18. Regulatory Guide 1.203, “Transient and Accident Analysis Methods,” December 2005.

19. NUREG/CR-5249, "Quantifying Reactor Safety Margins," December 1989.

20. RELAP5 MOD3.3 supporting documents, (ADAMS Accession No. ML110330203):

a. RELAP5/MOD3.3 Code Manual Volume I: Code Structure, System Models, and Solution Methods, NUREG/CR-5535/Rev P4-Vol I.

b. RELAP5/MOD3.3 Code Manual Volume II: User’s Guide and Input Requirements, NUREG/CR-5535/Rev P4-Vol II.

c. RELAP5/MOD3.3 Code Manual Volume II: Appendix A Input Requirements, NUREG/CR-5535/Rev P4-Vol II App. A.

d. RELAP5/MOD3.3 Code Manual Volume III: Developmental Assessment Problems, NUREG/CR-5535/Rev P4-Vol III.

e. RELAP3.3 MOD3.3 Code Manual Volume IV: Models and Correlations, NUREG/CR-5535/Rev P4-Vol IV.

f. RELAP5/MOD3.3 Code Manual Volume V: User's Guidelines, NUREG/CR-5535/Rev P4-Vol V.

g. RELAP5/MOD3 Code Manual Volume 6: Validation of Numerical Techniques in RELAP5/MOD3.0, NUREG/CR-5535/Rev P3-Vol VI.

h. RELAP5/MOD3.3 Code Manual Volume VII: Summaries and Reviews of Independent Code Assessment Reports, NUREG/CR-5535/Rev P4-Vol VII.

i. RELAP5/MOD3.3 Code Manual Volume VIII: Programmers Manual,

j. NUREG/CR-5535/Rev P4-Vol VIII.

21. "CONTEMPT4/MOD5, A Multicompartment Containment System Analysis Program," NUREG/CR-4001, BNL-NUREG 51894, Brookhaven National Laboratory, 1984.

22. R.A. Dimmena, e. al., "RELAP5/MOD2 Models and Correlations," NUREG/CR-5194, EGG-2561-R4, 1988.

23. RELAP5/MOD3 Code Manual Vol.4, Models and Correlations (DRAFT)," NUREG/CR-5535, EGG-2596, 1990.06.

24. PNNL-19418, "FRAPCON-4.0: A Computer Code for the Calculation of Steady-State, Thermal-Mechanical Behavior of Oxide Fuel Rods for High Burnup," Vol.1, Rev.2, September 2015.

25. "KCE-1 Critical Heat Flux Correlation for Plus7 Thermal Design," APR1400-F-C-TR-12002-NP, Rev.0, KHNP/KNF, November 2012, ADAMS Accession No. ML14114A564.

26. Korea Hydro and Nuclear Power, Ltd., "KHNP Responses to Request for Additional Information No. 7425," APR1400-F-A-RA-14001-P, ADAMS Accession No. ML14112A432 (Proprietary)/ML14112A429 (Non-proprietary).

27. KHNP Presentation on CAREM, ADAMS Accession No.ML17228A819.

28. "Fluidic Device Design for the APR1400," KHNP APR1400-Z-M-TR-12003-P, Rev.0, December 31, 2012, ADAMS Accession No. ML130180120.

29. NUREG/CR-7024, "Material Property Correlations: Comparisons Between FRAPCON-3.4, FRAPTRAN 1.4, and MATPRO," 2011.

30. "Modification of LBLOCA Best-Estimate Evaluation Methodology of APR1400 Type 3 Nuclear Power Plants (2012)," KNF-TR-SGA-12005, KNF, September 2012.

31. EPRI-NP 2192 Project 14385-1, "Critical Flow Data Review and Analysis," S. Levy, Inc. January 1982.

32. NUREG/CR-0497, "MATPRO-Version 11(Rev. 1) A Handbook of Materials Properties for Use in the Analysis of Light Water Reactor Fuel Rod Behavior," 1980.

33. D.A. Powers, R.O. Meyer, "Cladding Swelling and Rupture Models for LOCA Analysis," NUREG-0630, U.S.NRC, March 1980.

34. Development of PCT Uncertainty Quantification Methodology Assessment of Separate Model and Construction of Thermal-Hydraulic Data Banks for Establishment of the Korean ECCS Evaluation Model," KINS/GR-011, 1990.12.

35. "Compendium of ECCS Research for Realistic LOCA Analysis," NUREG-1230, R4, December 1988.

36. "COBRA/TRAC - A Thermal-Hydraulics Code for Transient Analysis of Nuclear Reactor Vessels and Primary Coolant System, Volume 1, Revision 4," NUREG/CR-3046, PNL-4385, March 1983.

37. A. Guba, M. Makai, and L. Pál, "Statistical Aspects of Best Estimate Method-I," Reliability Engineering and System Safety, Vol. 80, Issue 3, pp.217-232, June 2003.

38. Korea Hydro and Nuclear Power, Ltd., "CAREM for LBLOCA Analysis of APR1400," APR1400-F-A-EC-13012- P, ADAMS Accession No. ML13239A464 (Proprietary)/ ML13239A343 (Non-Proprietary).

39. APR1400-F-A-NR-14002-P, Rev.0, "The Effect of Thermal Conductivity Degradation on APR1400 Design and Safety Analysis," September 2014.

40. H. Glaser, "BEMUSE Phase VI Report, Status report on the areas, classification of the methods, conclusions and recommendations," NEA/CSNI/R(2011)4, 28-Mar-2011; (https://www.oecd-nea.org/nsd/docs/2011/csni-r2011-4.pdf).

41. L.J. Siefken, C. M. Allison, M.P. Bohn, and S.O. Peck, FRAP-T6: A Computer Code for the Transient Analysis of Oxide Fuel Rods, EGG-CDAD-5410, Idaho National Engineering Laboratory, April 1981.

42. TR-33-002, 2002, "Topical Report for the Realistic Evaluation of Emergency Core Cooling System."

43. TR-KHNP-0018 (Proprietary), "Topical Report for LBLOCA Best Estimate Evaluation Methodology of APR1400 Type Nuclear Power Plants," 2010.8.

44. TR-KHNP-0008 (Proprietary), "Topical Report for Realistic Evaluation of Emergency Core Cooling System, Volume 1: Description of Best Estimate Methodology for Large Break LOCA," 2002.12.

45. G.D. Wyss, K.H. Jorgensen, "A User's Guide to LHS: Sandia's Latin Hypercube Sampling Software," SAND98-0210, February 1998.

46. KEPCO, KHNP, "APR1400 Design Control Document Tier 2," APR1400-K-FS-14002-NP, Rev.0, December 2014.

47. TR-KHNP-002, Topical Report "The best evaluation methodology for the Emergency Core Cooling System," KEPRI/KHNP, Dec. 2002.

48. M.J. Loftus, et al., "PWR FLECHT SEASET Unblocked Bundle Forced and Gravity Reflood Task Data Report," EPRI-NP-1459, NUREG/CR-1532, WCAP-9699, 1981.

49. APR1400-F-C-NR-12001-P, Rev.0, “Thermal Design Methodology,” July 2012.

50. KAERI/TR-437/94, “Uncertainty Quantification of RELAP5/MOD3/KAERI Critical Flow Model using Marviken Experimental Data,” S. Y. Lee, Oct. 1994.

51. NUREG/IA-0126, “2D/3D Program Work Summary Report,” June 1993.

52. “Phenomena Identification and Ranking Tabulation Korean Next Generation Reactor Large Break loss of Coolant Accident,” KINS/INEEL, 2001.

53. NRC Inspection of Korea Hydro & Nuclear Power Co., LTD, IR 05200046/2016201, April 8, 2016, ADAMS Accession No. ML16081A081

54. APR1400-K-Q-TR-11005-NP, Revision 5, “KHNP Quality Assurance Program Description (QAPD) for the APR1400 Design Certification,” April 2016, ADAMS Accession No. ML16123A406.

55. American Society of Mechanical Engineers (ASME) NQA-1-2008, “Quality Assurance Requirements for Nuclear Facility Applications,” New York, NY, March 2008.

56. Regulatory Guide 1.28, Revision 5, “Quality Assurance Program Criteria (Design and Construction), October 2017.

57. Submittal of Additional Information for the Condition (1) Regarding the APR1400 DCA – Safety Evaluation with No Open Items for Topical Report APR1400-F-A-TR-12004, April 25, 2018, ADAMS Accession No. ML18115A426.

Page intentionally left blank

Non-Proprietary

SECTION B

Page intentionally left blank

Realistic Evaluation Methodology for Large-Break LOCA of the APR1400

(Approved Version)

Non-Proprietary

August 2018

Abstract

This report describes a realistic evaluation method for the analysis of a large break loss-of-coolant accident (LBLOCA), and its demonstration application to APR1400. The method strictly follows the concept and the philosophy of “Code Scalability, Applicability, and Uncertainty (CSAU)” demonstrated by the United States Nuclear Regulatory Commission in NUREG/CR-5249 [1], “Quantifying Reactor Safety Margins” and conforms to the guidelines of Regulatory Guide (RG) 1.157 [2], “Best-Estimate Calculations of Emergency Core Cooling System Performance." Three elements and 14 steps of the method as in CSAU are explained in detail in NUREG/CR-5249. Statistical techniques used to quantify the overall uncertainty of the calculation are different from those of CSAU in order to accommodate the increased number of uncertainty parameters, but still conform to the requirements of RG 1.157.

A demonstration calculation was performed for the Shin-Kori (SKN) units 3 and 4, the first APR1400 type nuclear power plants. APR1400 is similar to, from the viewpoint of the LBLOCA analysis, conventional CE-type nuclear power plants except for the addition of direct vessel injection (DVI), which is a new safety injection system. All the emergency core cooling water in the safety injection tanks and pumps are delivered directly into the upper annulus of the reactor pressure vessel. In the APR1400, low-pressure safety injection pumps are removed. By installing a device to control the amount of injection flow in each safety injection tank, tank injection phases are divided into high- and low-flow injections, which are equivalent to the conventional safety injection tank flow and low-pressure safety injection pump flow, respectively. After emptying the safety injection tanks, high-pressure safety injection pumps take charge of ensuring emergency core cooling.

RELAP5/MOD3.3 and CONTEMPT4/MOD5 codes are used for the calculations of system thermal-hydraulics and containment backpressures, respectively.

The method evaluates the values to compare with the acceptance criteria of 10 CFR 50.46 (b) [3], but does not cover the so-called long term performance of an emergency core cooling system. The long term performance of an emergency core cooling system is covered by the other evaluation method described in reference [21]. Simple-random sampling calculations were performed 181 times adopting distribution-free statistics. And 95 % tolerance limit values of peak cladding temperature, peak local oxidation, and maximum hydrogen generation were evaluated and compared with the corresponding acceptance criteria.

Results of the demonstration calculations assured that the performance of the emergency core cooling system during an LBLOCA of APR1400 had enough margins to meet the acceptance criteria.

Table of Contents

Appendices

List of Tables

List of Figures

Acronyms

ACC	activation of the accumulators
AO	axial offset
BE	best-estimate
BOC	beginning of cycle
CAMP	code application maintenance program
CAREM	code-accuracy-based realistic evaluation methodology
CCDAS	computer-controlled digital data acquisition system
CCF	counter-current Flow
CHF	critical heat flux
CLI	cold leg injection
CSAU	code scaling, applicability and uncertainty
CWO	core wide oxidation
DG	diesel generator
DNB	departure from nucleate boiling
DOE	department of energy
DP	differential pressure
DVI	direct vessel injection
ECC	emergency core cooling
ECCS	emergency core cooling system
ECCW	emergency core cooling water
EDG	emergency diesel generator
EIR	Eidge institute fuer reaktorforschung
EOB	end of blowdown
EPRI	electric power research institute
FD	fluidic device
HPIS	high-pressure injection system
HPSI	high-pressure safety injection
HTC	heat transfer coefficient
ICAP	international code assessment and application program

IET	integral effect test
INEEL	Idaho national engineering and environment laboratory
INEL	Idaho national engineering laboratory
IRWST	in-containment refueling water storage tank
JAERI	Japan atomic energy research institute
JRC	joint research center
KAERI	Korea atomic energy research institute
KNGR	Korea next generation reactor
LBLOCA	large-break loss-of-coolant accident
LHGR	linear heat generation rate
LOCA	loss-of-coolant accident
LPCI	low-pressure coolant injection
LPIS	low-pressure injection system
LPSI	low-pressure safety injection
LPSIP	low-pressure safety injection pump
MSIV	main steam isolation valve
MSLB	main steam line break
MTC	moderator temperature coefficient
ORNL	Oak Ridge national laboratory
PCT	peak cladding temperature
PIRT	phenomena identification and ranking table
PLO	peak local oxidation
POSRV	pilot operated safety relief valve
PSI	Paul Scherrer institute
PWR	pressurized-water reactor
PZR	pressurizer
RCP	reactor coolant pump
RCS	reactor coolant system
RPV	reactor pressure vessel
SBLOCA	small break loss-of-coolant accident

SET	separate effect test
SG	steam generator
SGTR	steam generator tube rupture
SI	safety injection
SIP	safety injection pump
SIS	safety injection system
SIT	safety injection tank
SKN	Shin-Kori nuclear power plant
SRS	simple-random sampling
TCD	thermal-conductivity degradation
UGS	upper guide structure
UH	upper head
USNRC	United States nuclear regulatory commission
WH	Westinghouse corporation

1. Introduction

This report describes a code-accuracy-based realistic evaluation methodology (CAREM), for large-break loss-of-coolant accidents (LBLOCA) of APR1400. The method conforms to Regulatory Guide 1.157 [2], and consists of three elements and 14 steps as in “Code Scaling, Applicability and Uncertainty” (CSAU), NUREG/CR-5249 [1]. An overall flow diagram of CAREM is shown in Figure 1-1. It is also briefed in Chapter 2 and detailed throughout this report.

CAREM quantifies the overall calculational uncertainty by propagating the uncertainty of each parameter. Uncertainty parameters are basically determined by auxiliary calculations and through a survey of the literature, and are confirmed by checking experimental data coverings. To quantify the uncertainty at a 95 % probability with a 95 % confidence level, sampling calculations are performed 181 times adopting non-parametric statistics. CAREM “extrapolates” code accuracy, quantified as the difference between measured and calculated clad temperatures, to code uncertainty parameters that are to be applied to plant calculations. This is further explained in the following sections.

Modified versions of RELAP5/MOD3.3 and CONTEMPT4/MOD5 are used for the calculations of the system thermal–hydraulics and containment back-pressure, respectively. A detailed description of the modifications is presented in Appendix B.

Realistic evaluations of LBLOCAs for such nuclear power plants in Korea as Westinghouse 3-loop cold leg injection plants, Westinghouse 2-loop upper plenum injection plant, and OPR1000 plants which are conventional CE type plants have already been licensed and applied to reload designs. The purpose of this report is to describe the stepwise details and characteristics of the evaluation method and its applicability to APR1400. A demonstration calculation was done for the first APR1400, Shin-Kori (SKN) Units 3 and 4.

The APR1400 is an advanced pressurized water reactor (PWR) with a direct vessel injection (DVI) system; however, it retains the principal features of conventional CE type 2-loop plants. Each loop consists of a hot leg, a steam generator (SG), two pump suction legs, two reactor coolant pumps (RCP), and two cold legs. The major system parameters of APR1400 are given in Table 1-1. The rated core thermal power is 3,983 MWt. Mass flow rates of the reactor coolant system (RCS) and core are 20,991 kg/s, and 20,361 kg/s, respectively. The active core is 3.81 m long. In the core, 241 16 by16 type PLUS7 fuel assemblies are loaded. Detailed specifications of PLUS7 are presented in Table 1-2.

The features with respect to the LBLOCA analysis of the emergency core cooling system (ECCS) are as follows:

- DVI
- four independent trains of high-pressure safety injection pumps (SIP)
- safety injection tank equipped with a fluidic device (SIT-FD)
- elimination of low-pressure SIP (LPSIP)
- in-containment refueling water storage tank (IRWST)

All the emergency core cooling water (ECCW) of the four SIT-FDs and four SIPs is injected solely into the upper annulus of the reactor pressure vessel. The DVI nozzle is 2.1 m above the center of the cold leg (Figure 1-2); its azimuthal configuration is shown in Figure 1-3. The nozzles are 90° apart from each other. The four trains of the SIPs have been designed to be mechanically and electrically independent. Each of four emergency diesel generators (EDGs) independently provides

power source to each SIP. According to the worst single failure assumption, three SIPs are operable. However, only two SIPs are assumed to be operable in the present LBLOCA analysis for extra conservatism. The configuration is shown in Figure 1-3. The SIT-FD is equipped with a fluidic device, as shown in Figure 1-4, which controls the injection flow as a function of the water level [4]. The fluidic device is a combination of a stand pipe and a vortex chamber. The SIT-FD provides high injection flow, equivalent to that of a traditional SIT as far as the water level is higher than the top of the stand pipe; afterwards, the SIT-FD provides low injection flow equivalent to that of the LPSIP. Refueling water, which is the source of the safety injection, is stored within the bottom periphery of the containment building; the traditional switch-over to recirculation mode is eliminated.

CAREM provides three values (i.e., peak cladding temperature, peak local oxidation, and core-wide hydrogen generation) for the comparison with the acceptance criteria of 10 CFR 50.46(b).

Table 1-1 Major System Parameters of APR1400

Parameters	APR1400
Power, MWt	3,983
Coolant temperature - core inlet, °C (°F)	290.6 (555)
Coolant temperature - core average, °C (°F)	308.8 (587.8)
Coolant temperature - core outlet, °C (°F)	325.3 (617.5)
Operating pressure, MPa (psia)	15.51 (2,250)
Vessel flow rate, kg/s (106 lbm/hr)	20,991 (166.6)
Core flow rate, kg/s (106 lbm/hr)	20,361 (161.6)
Number of fuel assemblies	241
Number of fuel rods	56,876
Length of active core, m (ft)	3.81 (12.5)
RCS liquid volume including PZR, m^3 (ft^3)	403.9 (14,265)
RPV liquid volume, m^3 (ft^3)	163.5 (5,773)
Core liquid volume, m^3 (ft^3)	21.9 (773.1)
RPV inner diameter, m (in)	4.63 (182.3)
RPV outer diameter, m (in)	5.10 (200.6)
Downcomer gap width, m (in)	0.254 (10)

Table 1-2 Specifications of PLUS7 Fuel

Parameters	Value
Fuel assembly length, m (in)	4.5276 (178.25)
Active core length, m (in)	3.810 (150.0)
Fuel assembly pitch, m (in)	0.2078 (8.18)
Number of guide tubes per fuel assembly (outer + center)	5 (4+1)
Number of protective grids	1
Number of top Inconel grids	1
Number of bottom Inconel grids	1
Number of middle grids	9
Length of middle grid span, m (in)	0.3993 (15.719)
Number of fuel rods per fuel assembly	236
Fuel rod pitch, m (in)	0.01285 (0.506)
Clad material	ZIRLO
Fuel rod length, m (in)	4.0945 (161.20)
Fuel rod outer diameter, m (in)	0.0095 (0.374)
Clad thickness, m (in)	0.000572 (0.0225)
Pellet diameter, m (in)	0.008192 (0.3225)

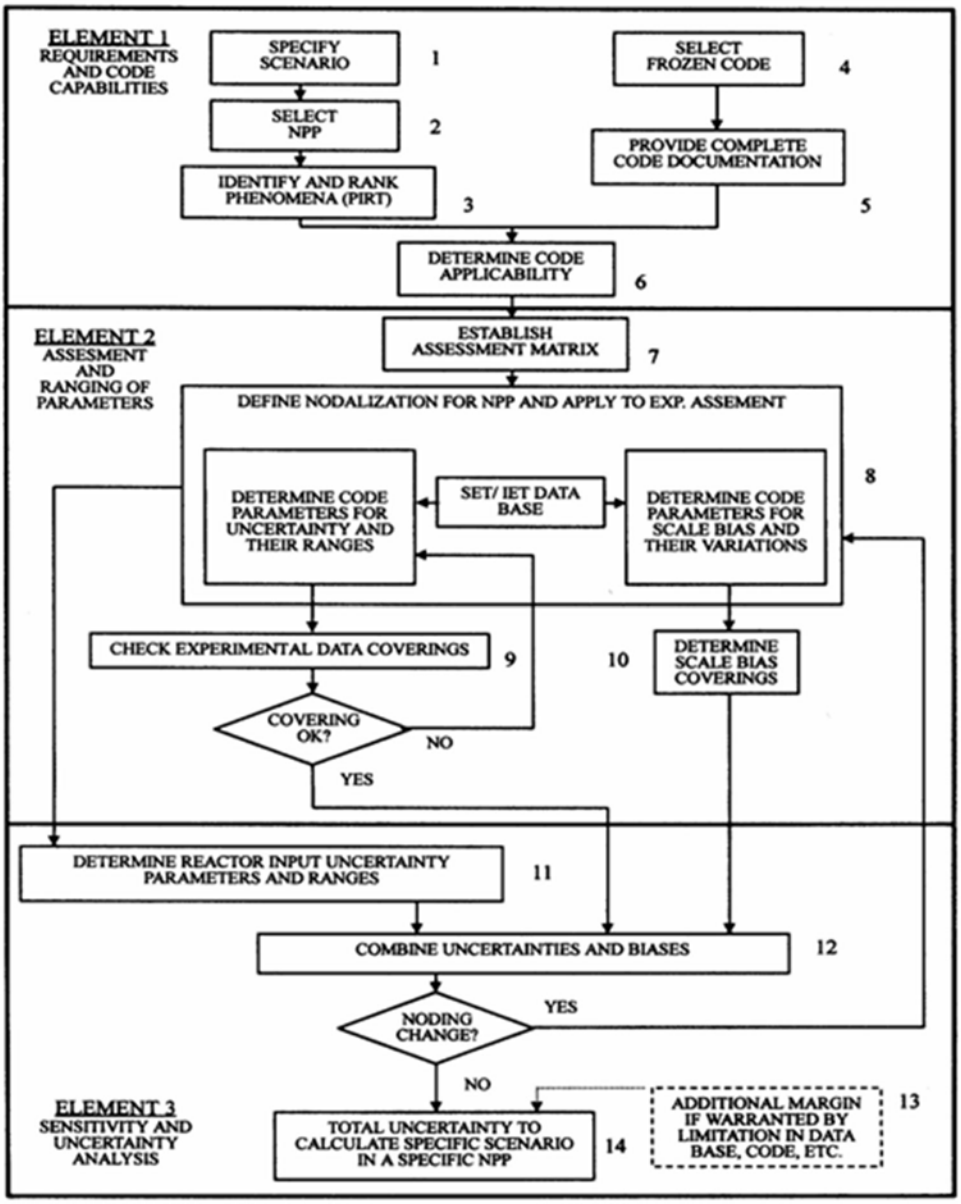

Figure 1-1 Diagram of CAREM

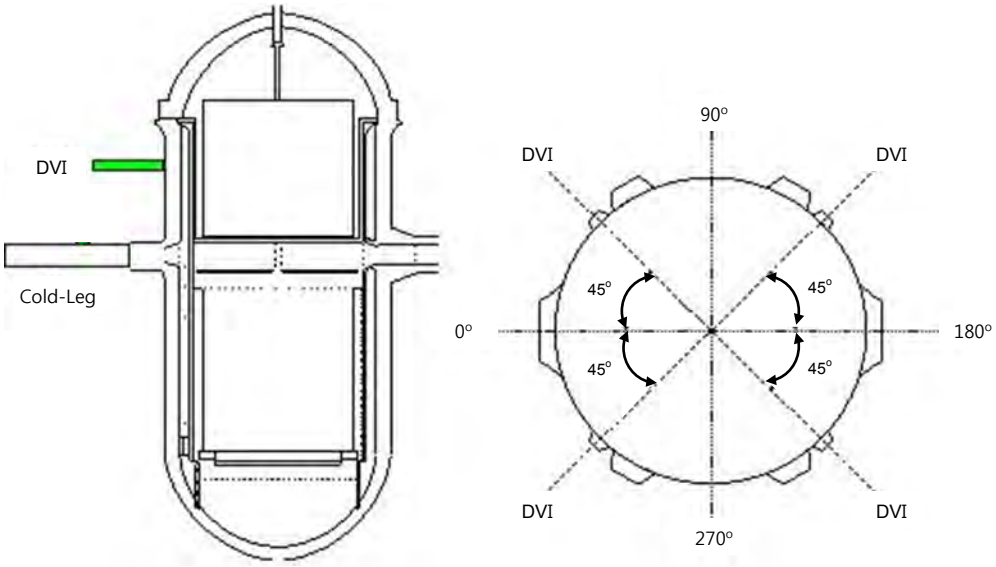

Figure 1-2 DVI Nozzle Location

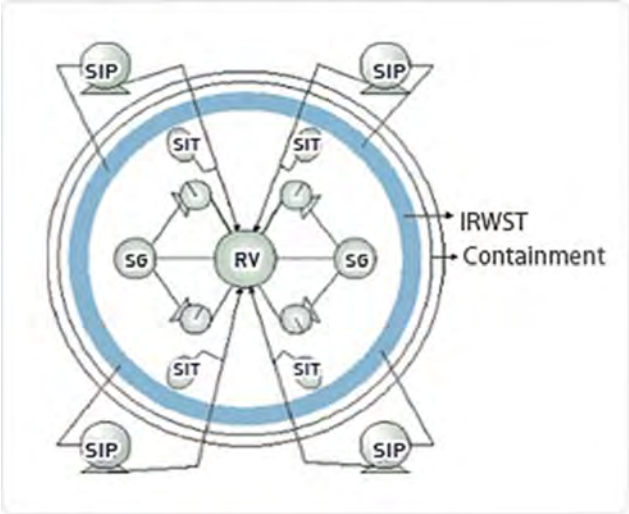

Figure 1-3 Configuration of the APR1400 Safety Injection System

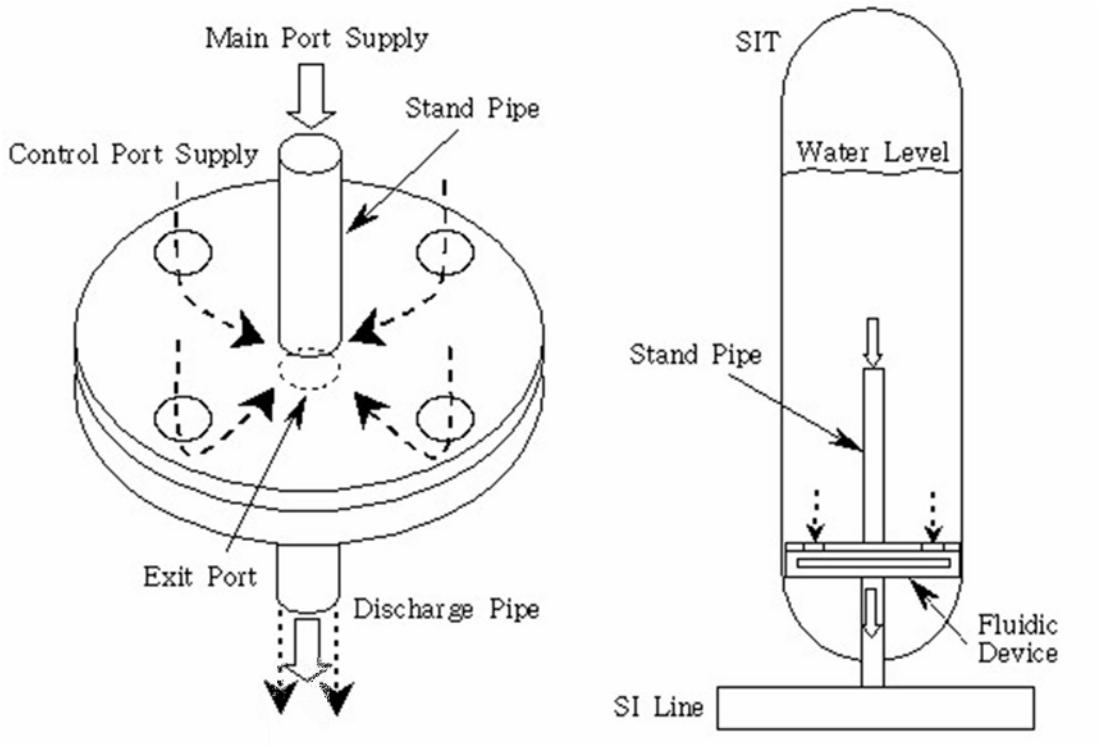

Figure 1-4 Schematic Diagram of Fluidic Device

2. Method Roadmap

Chapter 1 introduces the general overview of CAREM and the design features of APR1400 in view of LBLOCA. Chapter 2 is a description of the roadmap. Figure 1-1 shows the overall construction of the method. The three elements of CSAU are described in the following chapters, in sequence. Here in the roadmap, the principal concepts or techniques of each element and step are introduced.

Chapter 3 deals with the first element of the requirements and code capabilities, and consists of six steps.

- The first step is the specification of a scenario of LBLOCA on APR1400. SKN 3 and 4 are selected as a reference plant of APR1400 in the second step. The scenario is thoroughly studied according to the related systems, modules, components, and the time-advancement of the accident.

- The third step is the identification and ranking of phenomena or processes according to the scenario in Step 1. Important phenomena or processes are taken into consideration to identify governing uncertainty parameters.

- Apart from the physical scenario of the accident, computer codes used as tools to predict phenomena or processes are selected in Step 4. In order to study code capability to predict the accident, all code documents are provided in Step 5.

- By comparing the physical phenomena or processes occurring during the accident with the code capabilities, code applicability is determined in Step 6, which is the last step of the first element.

Chapter 4 provides for the code assessment and ranging of parameters. Through code assessment calculations against relevant experiments, the code capability to predict the accident is assured and the uncertainty parameters, which are necessary to quantify the overall uncertainty of the plant calculations, are determined in this second element.

- The first step of this element, Step 7, is the construction of an assessment matrix. Available experiments that can capture important phenomena or processes of the accident in the reference plant are included in the matrix. In order to assure scale-up capability of the code, tests of various scales are considered. In order to cover the transient behavior of the accident, tests of various initial and boundary conditions are included. Both separate-effect tests (SETs) and integral-effect tests (IETs) are considered.

- Step 8 is about the assessment calculations, according to the matrix, using a nodalization of the reference plant. Developmental assessments, other than the independent assessments performed in this report, are also utilized. Code accuracy, further detailed in Section 4.3.1, is quantified first, as the difference between measured and calculated values of cladding temperatures for all relevant experiments. In this quantification, the frozen code itself is applied and the probabilistic distribution functions of the parameters are not considered. Code accuracy is utilized to measure the sufficiency of the set of parameters in Step 9. Via these assessment calculations, the code's capability to predict the accident is further confirmed and the uncertainty parameters are determined in terms of probability distribution functions.

- Using the uncertainty parameters determined in Step 8, experiments are simulated again with respect to the prediction of cladding temperatures. By adopting a distribution-free statistics technique, calculations are performed 181 times for each experiment by varying the values of uncertainty parameters according to their distribution functions. And it is checked whether the peak cladding temperature of the experiment can be covered by the

third highest value of the calculations. In this way the sufficiency of the numbers and the ranges of the parameters are confirmed against SETs and IETs of various scales and conditions. And the sufficiency of the parameters for the prediction of plant behavior can also be assured. The uncertainty parameters are determined to result in the calculational uncertainty as much as the code accuracy. In Step 10 and later in Step 12, the uncertainty parameters used to quantify scale biases are addressed.

Chapter 5 describes the sensitivity calculations and uncertainty analysis of the plant. Plant operational uncertainty parameters other than the code uncertainty parameters are determined in Step 11. Step 12 describes the plant sensitivity calculations of 181 times and the quantification of the overall calculational uncertainties taking into account the effect of scale distortions of the experiment. By including an additional uncertainty quantified in Step 13, the total uncertainty of the plant calculation is determined in the Step 14.

Chapter 6 summarizes and concludes the applicability of CAREM to APR1400.

Appendices describe further details of the code assessment results and the treatment of related issues.

3. Requirements and Capabilities

3.1 Scenario Specification (Step 1)

Determination of code's applicability and uncertainty is very scenario-dependent because the major phenomena and safety parameters of interest differ from one scenario to another. Therefore, the scenario dictates the processes that must be addressed [1].

A scenario was constructed for a limiting break. The limiting break is defined as a break that results in the highest peak cladding temperature (PCT). In order to determine the limiting break, sensitivity studies on the location and size of the break were performed. Determination of the limiting location and limiting size are summarized in Sections 3.1.1 and 5.2.1.1, respectively. And detailed descriptions for the limiting break location, size, and burnup are presented in Appendix K. The scenario itself is described in Section 3.1.2.

3.1.1 Determination of the Limiting Break Location

Sensitivity studies were performed to determine the limiting or worst break location, in view of the PCT. Double-ended guillotine breaks were assumed in a cold leg, a hot leg, and a pump-suction leg. An EDG was assumed to fail for the worst single failure assumption and two SIPs were conservatively credited as operable as previously mentioned in Chapter 1. Except for the break location, all the conditions were set to be the same.

As shown in Figure 3-1, the cold leg break case showed the highest PCT, therefore, the limiting break location was determined as a guillotine break in a cold leg. As expected, the hot leg break case showed the most favorable results.

Pressurizer location was determined to connect intact loop hot leg based on sensitivity study described in Appendix K.

3.1.2 Scenario

The scenario is subdivided into four time periods that characterize events during the transient. These time periods, termed blowdown, refill, early reflood, and late reflood are defined by the inventory of the reactor pressure vessel and the flow condition of SIT-FD as shown in Figure 3-2. The major sequence of events for the LBLOCA scenario is presented in Table 5-3.

Blowdown is defined as the period from the opening time of the break to the start time of the SIT-FD injection. The refill period is defined as the period from the start time of the SIT-FD injection to the time when the mixture level in the reactor vessel lower plenum reaches the bottom of the active core. Definitions of these two periods are the same as those of the conventional LBLOCA scenario in PWRs. Unlike the conventional scenario, the reflood period is subdivided into early reflood and late reflood based on the time in which the SIT-FD becomes empty. This is to address any possibility of core heatup during the late reflood period in detail because there is no LPSIP available in APR1400.

3.1.2.1 Blowdown

The blowdown period starts when the break opens and it ends when a SIT-FD injection is initiated; blowdown lasts for approximately 15 s. During blowdown, the primary coolant is rapidly expelled into the containment through the break. The reactor coolant changes from a subcooled liquid to a two-phase mixture or pure steam, due to fluid flashing. A schematic diagram of the APR1400 shown in Figure 3-3 shows a two-phase primary coolant system 4 s after the break opens. By roughly 6 s, the core region begins to dry out as shown in Figure 3-4.

Initial break flow is very high, reflecting the subcooled critical flow at the break. Mass flow from the reactor vessel side of the break is larger than that from the pump side due to the higher hydraulic resistances of the pump and the steam generator. As the break flow develops, the core flow rapidly stagnates and then reverses shortly after the break occurs.

As the primary system depressurizes, flashing occurs first in the hot regions of the system, such as the upper plenum, hot leg, pressurizer, and core, and then proceeds to the relatively cold regions, such as the lower plenum, downcomer, and cold legs. Extensive voiding occurs in all areas of the reactor pressure vessel. Nucleate boiling develops in the core. Fission power, which is calculated by the kinetics model, drops to the level of decay heat due to the voiding in the core. The flashing also reduces the primary system depressurization rate.

When the critical heat flux (CHF) condition is reached in the core, heat transfer mode changes from nucleate boiling to post-CHF heat transfer regimes (i.e., transition boiling, film boiling, and forced convection to vapor). Fuel rod cladding temperatures increase rapidly due to the degrading rod-to-fluid heat transfer. The increase of the rod cladding temperatures during the early blowdown period is terminated by following reasons:

- The core power decreases rapidly due to the insertion of negative reactivity resulting from the voiding of the core.
- Rod-to-fluid heat transfer enhances due to the downward flow in the core after the flow stagnation.
- The large coolant inventory in the upper guide structures (UGS) and the upper head moves toward the top of the core by two paths; through the UGS drainage holes in the UGS bottom plate that is between the UGS and the upper plenum, and through the guide tube pipes that terminate in the upper inactive core.

Reactor coolant pumps (RCPs) are modeled to trip and coast down from the beginning of the accident assuming loss-of-offsite-power. As the primary system pressure continues to decrease, flashing develops in the cold regions of the system. Resultant voiding in the RCP degrades its pumping performance. Break flow rate decreases rapidly as the flow regime changes from subcooled to saturated critical flow at the break.

3.1.2.2 Refill

The refill period begins when SIT-FD injection flow is initiated and ends when the mixture level in the lower plenum reaches the bottom of the active core. Refill begins at around 15 s and ends at around 33 s.

Four SIT-FDs begin to deliver flow into the four DVI lines when the primary system pressure falls below their actuation set-point. The coolant flows through the DVI nozzles into the upper annulus and then begins to refill the reactor pressure vessel. The reactor coolant system keeps depressurizing because some of the coolant entering the upper annulus is swept out to the break along with entrained liquid from the lower plenum and the downcomer. Although the break flow remains high, sufficient flow in the excess of the bypass is delivered downward into the downcomer and increases the downcomer water level. Eventually, the coolant injected by the SIT-FDs reaches the lower plenum.

Reactor vessel walls and internals are large metal structures at temperatures above saturation. When subcooled ECC water comes into contact with the metal structures in the downcomer, steam is generated by nucleate boiling. This reduces the gravitational head of the fluid in the downcomer. The process of liquid penetration and sweep-out repeats in the downcomer and direct-contact condensation of steam on the subcooled ECC water continues in the upper annulus. Figure 3-5

gives a schematic of the two-phase primary coolant system 25 s after the break opens.

The depressurization of the system wanes as the differential pressure between the reactor coolant system (RCS) and the containment reduces. Owing to the gradual reduction of flashing and break flow, the rate of liquid penetration into the lower plenum increases. With the decreasing steam flow rate, ECCW bypass is insignificant and most of it flows downward to fill the downcomer and the lower plenum. At this stage, mixture levels in the downcomer and the lower plenum increase rapidly.

Heatup, which is almost adiabatic, continues in the core during this period because there is no inventory to cool the core.

The refill period ends when the mixture level in the lower plenum reaches the bottom of the active core and remains full thereafter and conditions are established for continuous core reflooding.

3.1.2.3 Early Reflood

The early reflood period begins when the mixture level in the lower plenum reaches the bottom of the active core and ends when the SIT-FD water is depleted. This period begins at around 33 s and ends at around 172 s. The early reflooding process is shown in Figure 3-6, Figure 3-7, and Figure 3-8. These figures respectively provide schematics of coolant distributions at 45 s when “high flow” is injected from the SIT-FDs, at 92 s and 150 s when “low flow” is injected from SIT-FDs. Modeling of SIT-FD is explained in Section 4.2.1. The “high flow” and the “low flow” of SIT-FD are exemplified in Figure 5-14 and further described in Section 5.2.1. Around the beginning of the early reflood period, SIPs begin to inject water.

Initially, the core reflood is quite rapid because:

- the downcomer remains filled with water by the ECC injection,
- the high flow injection of SIT-FD continues,
- loop steam flow rate is low and therefore the hydraulic resistance in the loop is low, and
- there is no severe steam binding.

Maximum SIT-FD injection flow is reached during this period at around 25 s after the break. High flow injection of the SIT-FD continues until around 45 s, then the flow through the stand-pipe becomes unavailable and only the flow through the control port of fluidic-device is possible. During the high flow injection, downcomer and core liquid levels increase rapidly. As the downcomer liquid level approaches the level of the cold legs, much of the coolant spills out of the break and the vessel side break flow tends to increase. When the water level in the SIT-FD decreases to below the top of the stand pipe, the low flow injection begins. Water levels in the downcomer and core decrease slightly but the levels increase again within around 5 s, maintaining downcomer water level around the level of the cold legs. It appears that the combined SIP and SIT-FD flows are sufficient to maintain the water level in the downcomer and to retard core heatup.

In the core, heat transfer regimes encompass the entire spectrum, such as single phase liquid convection, nucleate boiling, transition boiling, film boiling, and single phase vapor convection.

Due to droplet de-entrainment at the fuel alignment plate and spacer grids, local quenching could occur. Vapor velocities and liquid entrainment in the central region of the core are higher due to the higher power of this region. The entrained liquid could have a cooling effect on the upper region of the core. Some of the entrained liquid is de-entrained at the fuel alignment plate and the remainder is carried into the upper plenum forming a two-phase pool. Liquid from the pool can reenter the low powered regions of the core through the fuel alignment plate due to the lower vapor velocities in those regions. Therefore, a three-dimensional flow pattern can occur: water flows from low to high

powered regions in the core, while the flow is in the opposite direction in the upper plenum. Liquid from the upper plenum pool may be further entrained and carried over into the hot legs and steam generators.

As reflooding progresses upward from the lower core region, more liquid is entrained to the upper plenum and the level of the two-phase mixture in the pool can reach the hot leg. When the entrained liquid reaches the U-tubes of the steam generators, it is vaporized by reverse heat transfer from the secondary side to the primary side. Due to the vaporization in the U-tubes, hot side pressure increases and this causes steam binding which deteriorates the reflooding of the core. Because the steam generation rate in the core decreases due to the lower reflood rate, liquid entrainment and the steam binding effect decrease, causing the reflood rate to increase again. Through this cyclical process, the entire core eventually becomes reflooded. The increase of core pressure due to the steam binding causes manometric oscillations between levels in the downcomer and the core.

The early reflood period ends when SIT-FDs are emptied.

3.1.2.4 Late Reflood

The late reflood period begins when SIT-FDs are emptied. ECC water is supplied only by SIPs during this period.

The water level in the downcomer decreases somewhat as the SIT flow stops at the beginning of this late reflood, and falls below the level of the cold legs. Then, the core water level becomes stabilized. Liquid levels in the downcomer and core become balanced during this period as shown in Figure 3-2. Due to the decreased flow of coolant into the downcomer, liquid temperature in the downcomer can increase to near saturation temperature due to the residual heat of the metal structures, that is, vessel walls in the downcomer. Boiling can occur on the surface of the walls depending on the conditions. As enough ECCW is provided by two SIPs, the possibility of the downcomer boiling is successfully suppressed and the core is found to remain amenable to cooling.

Because the entire core is quenched and remains in a quenched state during this period, the steam generation in the core does not cause any severe ECCW bypass. The core is found to be kept in a coolable condition as shown in Figure 3-9.

3.2 Nuclear Power Plant Selection (Step 2)

SKN 3 and 4 were selected as a reference. The main features are described in Chapter 1.

3.3 Phenomena Identification and Ranking Table (Step 3)

Phenomena identification and ranking table (PIRT) is used to identify the major phenomena or processes that occur during the accident and to prioritize them according to their effects on primary safety concern.

The PIRT of APR1400 LBLOCA is based on “KNGR PIRT.” KNGR is initialism for “Korea Next Generation Reactor;” and it was APR1400’s name during its developmental stage. The PIRT was prepared by INEEL in 2001[5] for KINS. Four characteristic time periods of blowdown, refill, early reflood, and late reflood are summarized in Table 3-1. A numeric value is assigned to each phase as shown below:

1: Blowdown

2: Refill

3: Early reflood

4: Late reflood

The considered scenario is a double-ended guillotine break at a RCP discharge leg (i.e., a cold leg), with assumptions of the loss-of-offsite power and a single failure. The assumed single failure is the loss of one emergency diesel generator (i.e., one SIP failure); however, only two of the four SIPs are conservatively assumed to be available.

Reflecting the design finalization of APR1400 and the new experimental findings afterwards, modifications were made to the PIRT as described in Appendix A. Determined PIRT for APR1400 is shown in Table 3-2. Each phenomenon or process is ranked in five importance levels. Levels of importance are as follows:

5: highest degree of the high

4: high influence on safety criteria

3: moderate influence on safety criteria

2: low influence on (or important to) safety criteria

1: lowest of the low in importance

“NA” in Table 3-2 means the process or phenomenon is not active or present.

In contrast to the original idea of the ranking in CSAU, no limitation on the number of uncertainty parameters is necessary, in principle, in the distribution-free statistical approach. The original idea of the ranking in CSAU was to reduce the number of parameters as many as practicable. Thus, the importance of the ranking is whether the phenomena or processes are selected or not, rather than the ranking level itself when using the distribution-free statistical approach. Table 3-2 lists all the selected phenomena or processes with their rankings. [

]^{TS}. Selected, important phenomena or processes need to be addressed in terms of uncertainty parameters, biases, or conservatisms.

3.4 Frozen Code Selection (Step 4)

RELAP5/MOD3.3/K, which is a modified version of RELAP5/MOD3.3, and CONTEMPT4/MOD5 codes were selected to calculate system thermal-hydraulics and the containment back pressure calculations, respectively.

RELAP5/MOD3.3 is one of the most advanced best-estimate safety analysis codes to date. It was developed by USNRC and RELAP5/MOD3.3 (patch 03) is its latest version. Code manuals are introduced in the following section. The code has been widely applied to analyze system transients of pressurized water reactors, including the postulated LBLOCA. The film boiling heat transfer model of the reflood package of RELAP5/MOD3.3 was modified based on independent assessment calculations against FLECHT-SEASET data. The modified version was named RELAP5/MOD3.3/K. Details on the modifications including the circumvention of code failures caused by the injection of cold nitrogen gas from SIT-FD are described in Appendix B.

CONTEMPT4/MOD5 is a containment analysis code, especially used for calculating the containment backpressures in the case of a LOCA. This code includes the fan and spray cooling

system models and passive heat sink models which are essential to the calculation of containment backpressures of a LOCA. It also facilitates table input of the mass and energy release of primary system coolants. The code manual is introduced in the following section.

The two codes above are merged to exchange the containment backpressure calculated by CONTEMPT4 and the mass and energy release rate calculated by RELAP5, for every time step of RELAP5/MOD3.3. By way of the merging, errors which can be caused by the user's simplification of exchanged data, and which are unavoidable in case of tabulation inputs of exchanged data, are eliminated. Inter-code iterations between the two codes are also avoided. The merging was facilitated using a dynamic link library of a FORTRAN language.

3.5 Code Documentation (Step 5)

Code manuals for RELAP5/MOD3.3 and CONTEMPT4/MOD5 are listed in Table 3-3. Because RELAP5/MOD3.3/K is of simple modifications of RELAP5/MOD3.3 in relation to reflood film boiling heat transfer and code failures caused by non-condensable gas injection, code manuals for RELAP5/MOD3.3 are still applicable. The modified descriptions are available in Appendix B of this report.

In the case of RELAP5/MOD3.3, code details are explained in separate volumes, which group technical details. The contents of each volume are introduced in Table 3-3. Meanwhile in the case of CONTEMPT4/MOD5, all the descriptions are assembled in a single volume of Reference [6].

These code manuals are utilized in assessing code applicability.

3.6 Code Applicability Determination (Step 6)

Code applicability can be determined by examining code capabilities and limitations with respect to the scenario and the important phenomena and processes of LBLOCA. After the requirements of the code capabilities are determined by way of scenario specification and PIRT, the following items need to be assessed by utilizing code documents.

- applicability of the code system to the LBLOCA scenario
- applicability of the code system to the selected NPP
- limitations of models and correlations for the scenario
- deficiencies in the code system for the scenario

In order to assess the code's capability to address the requirements, overall features of the code system are reviewed first; then, constitutive equations and correlations, numerical solution methods, component models, and control functions are reviewed in sequence in the following sections. From this review the code applicability in comparison with the requirements derived from the scenario of the plant can be determined; then, code parameters to address the important phenomena and processes can be determined from a review of the constitutive equations.

3.6.1 Overall Code Capability

In order to determine whether RELAP5/MOD3.3/K has the capability to predict the four phases of blowdown, refill, early reflood, and late reflood of the scenario, the governing equations first need to be reviewed. Most of the important phenomena and processes of the PIRT require a two-fluid code system. Interface transport phenomena, such as steam generation and condensation, interface heat, and momentum transfer require the code system to address the unequal velocities and unequal temperatures of the fluid condition. Also, multidimensional behaviors occurring in the downcomer,

core, and upper plenum of the reactor pressure vessel need to be addressed. It should be possible to model the components such as SIT-FD, pump, and steam separator, whose mechanical and thermal characteristics require special treatment. These requirements and corresponding code models are compared in Table 3-4. The requirements are found to be able to be addressed by RELAP5/MOD3.3/K except local mechanical non-equilibrium. Localized mechanical non-equilibrium, which is required to model the phenomenon [

]^{TS}. The localized mechanical non-equilibrium is treated [

]^{TS}.

CONTEMPT4/MOD5 is equipped with the conservation equations of mass, momentum, and energy. It can calculate the mass and energy transfer due to the pressure difference between compartments. It also includes a state equation of non-condensable gas and can calculate humidity. Heat conduction of up to 99 heat structures can be modeled with diverse boundary heat transfer conditions.

3.6.2 Constitutive Equations

Several constitutive equations and correlations are necessary to solve the governing equations. The appropriateness of the constitutive equation is determined by the database on which it was developed. Code manuals listed in Table 3-3 include the descriptions of base data, applicable range, accuracy, and scalability for each constitutive equation or correlation.

As an example of constitutive equations; heat transfer between the wall and liquid or between the wall and gas; interface mass, energy and momentum transfer; spray system or fan cooling of the containment can be considered. These also require other constitutive relations of the flow regime map, boiling curves, and material properties. A proper constitutive equation or relation needs to be determined based on code assessment calculations against the database. Typical constitutive equations of the RELAP5/MOD3.3/K and CONTEMPT4/MOD5 are listed in Table 3-5 together with the related important phenomena and processes. Important phenomena and processes are found to be suitably modeled by the constitutive equations of RELAP5/MOD3.3/K and CONTEMPT4/MOD5. [6][7][8][9]

3.6.3 Numerical Solution

In order to obtain accurate and stable solutions of the governing and constitutive equations, consistency, completeness, and well-posedness should be theoretically established and justified through validation calculations. The validity of the numerical methods of RELAP5 and CONTEMPT4 were justified by the assessment calculations against various numerical problems, and by separate and integral effect tests. [6][7][8][9]

3.6.4 Component Models and Control Functions

Sometimes it is necessary to use special models to perform an accurate plant safety analysis. In order to predict the behavior of a safety injection tank or steam generator separator during LBLOCA, for example, it is more convenient to activate specialized component models. Such specialized component models are included in RELAP5/MOD3.3/K, and are activated for the convenience of modeling and for more accurate predictions. Such components as reactor pressure vessel, pressurizer, loop pipes, and so on can be modeled by code inherent models of PIPE, BRANCH, and so on of RELAP5/MOD3.3/K. Control functions are also available in RELAP5/MOD3.3/K to model reactor trip and reactor protection system signals and so on. The CONTEMPT4/MOD5 code is also equipped with necessary models for those kinds of special components and functions. The above discussion is summarized in Table 3-6.

3.6.5 Applicability of the Code System

As discussed, it is confirmed that the code system of this method has the capability to analyze an LBLOCA of APR1400. The confirmation can be summarized as follows:

- The code system has the capability to simulate the four phases of blowdown, refill, early reflood, and late reflood of an APR1400 LBLOCA.
- The code system can approximate the multidimensional phenomena in the reactor pressure vessel by way of modeling multiple channels and their inter-connecting cross flow junctions.
- The nonhomogeneous and non-equilibrium governing equations and the non-condensable gas transport equation, together with the constitutive relations of the code system can calculate such major phenomena as the critical flow at the break, dynamic characteristics of the centrifugal pump including the two-phase performance degradation, blowdown core heat transfer, penetration or bypass of ECC water in the downcomer, reflood core heat transfer, fuel rod quenching, droplet entrainment, two-phase pressure drop, containment backpressure, and so on.
- The code system contains a series of constitutive relations for all flow regimes.
- The code system contains important special component models for components such as the safety injection tank and separator.
- The code system can simulate plant geometry and control functions.
- The code system shows reasonable agreement qualitatively and quantitatively with various experimental data.
- Code assessment calculations performed against experiments at various scales can assure the scale-up capability of the code system to full-scale power plants.
- The frozen code system can be applied to the quantification of the calculational uncertainty, and is supported by a complete set of code documentation.
- Assessment calculations of the code system and their databases are available.

Table 3-1 Definition of Time Periods

Period (Number)*)	Starts at	Ends at
Blowdown (1)	Break initiation	Initiation of SIT injection
Refill (2)	End of blowdown	Initiation of core recovery (Mixture level at the bottom of the fuel rods)
Early Reflood (3)	End of refill	End of SIT injection
Late Reflood (4)	End of SIT injection	Stable core quench

*) The numbers indicated in parentheses are used as indices in the PIRT table to denote each phase in that table.

Table 3-2 Phenomena Identification and Ranking Table (1/3)

TS

Table 3-2 Phenomena Identification and Ranking Table (2/3)

TS

Table 3-2 Phenomena Identification and Ranking Table (3/3)

TS

Table 3-3 Code Documentation

RELAP5/MOD3 CODE MANUAL, NUREG/CR-5535, MARCH 2003

VOLUME 1: Code Structure, System Models, and Solution Methods

VOLUME 2: User's Guide and Input Requirements

VOLUME 3: Developmental Assessment Problems

VOLUME 4: Models and Correlations

VOLUME 5: User's Guidelines

VOLUME 6: Validation of Numerical Techniques in RELAP5/MOD3

VOLUME 7: Summaries and Reviews of Independent Code Assessments

VOLUME 8: Programmers Manual

CONTEMPT4/MOD4, NUREG/CR-3716, MARCH 1984

A Multi-compartment Containment System Analysis Program

CONTEMPT4/MOD5, NUREG/CR-4001, SEPTEMBER 1984

An Improvement to CONTEMPT4/MOD4 Multi-compartment Containment System Analysis Program for Ice Containment Analysis

Table 3-4 Field Equations and Models in RELAP5/MOD3.3/K and CONTEMPT4/MOD5

Scenario and PIRT Requirement	RELAP5/MOD3.3/K and CONTEMPT4/MOD5 Model Implementation	Field Equations and Models
Non-equilibrium two-phase flow	YES	Six equations, Unequal velocity, Unequal temperature
Non-condensable gas flow	YES	Gas mass transport in vapor flow field
Multidimensional flow capability	Partially YES	Multiple channels with multiple junctions
Separation due to gravity	YES	Horizontal flow with horizontal regime map
Interface exchange	YES	Mass and energy transfer between phases
Local mechanical non-equilibrium	NO	None

Table 3-5 Constitutive Equations and Models in RELAP5/MOD3.3/K and CONTEMPT4/MOD5

Component	Phenomena/Process	RELAP5/MOD3.3/K and CONTEMPT4/MOD5 Models
Fuel Rod	Initial stored energy Decay heat Oxidation Gap conductance Deformation, Burst Relocation	Fuel rod conduction model Point kinetics model Cathcart-Pawel model FRAP-T6 model Deformation model Fuel radial power distribution
Core	Post-CHF Rewet/Top Quench Heat transfer Reactivity feedback Entrainment/De-entrainment Multidimensional flow Vapor superheating Interfacial heat transfer	Full boiling curve Quench front tracking and heat transfer package Point kinetics Interfacial drag Multi-channel with multiple cross flow junctions Vaporization, Condensation, Mass exchange, Two-fluid equations
Upper Plenum	Entrainment/De-entrainment Level	Interfacial drag
Pressurizer	Flashing Level	Pressurizer model by nodalization
Steam Generator	Steam binding	Heat transfer, Vaporization
Pump	Two-phase performance Loss coefficient	Homologous curves with degradation curve
Downcomer	Stored energy Injection jet Condensation Entrainment/De-entrainment Multidimensional flow Non-condensable gas Dissolved Nitrogen	Heat structure conduction model Flow regime map, TMDPJUN Vaporization, Condensation Interfacial drag Multi-channel with multiple cross flow junctions SIT model Heat transfer degradation
Lower Plenum	Entrainment Boiling	Interfacial drag Wall heat transfer
Break	Critical flow Containment pressure/temperature	Critical flow model Wall condensation model Spray/Fan cooling model

Table 3-6 Component Modeling Requirements

Requirement	Code Component Models
Pressure vessel	Hydraulic volume & Junction
Hot leg	Hydraulic volume & Junction
Steam generator	Hydraulic volume & Junction
Pump	PUMP
Cold leg	Hydraulic volume & Junction
Pressurizer	Hydraulic volume & Junction
Surge line	Hydraulic volume & Junction
Safety injection tank	ACCUM
Emergency core cooling system	Hydraulic volume & Junction with nodalization
Valves	VALVE
Pressure boundary	VALVE with critical flow option CONTEMPT4/MOD5

TS

Figure 3-1 PCT Results of the Sensitivity Study on Break Locations

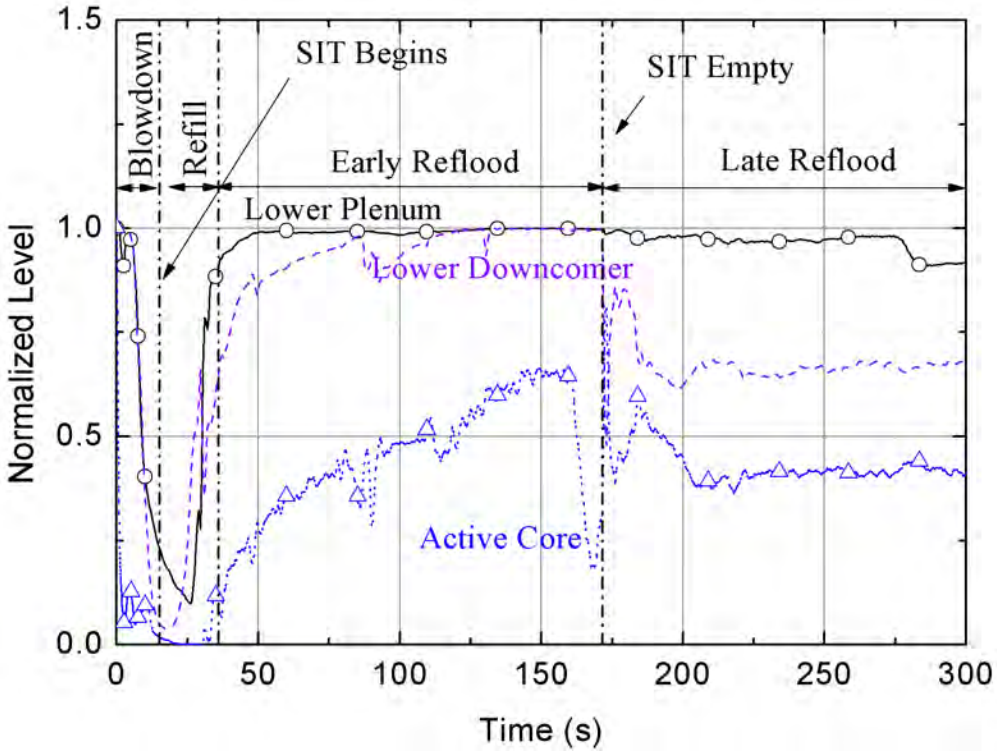

Figure 3-2 Normalized Collapsed Water Level in Downcomer and Core

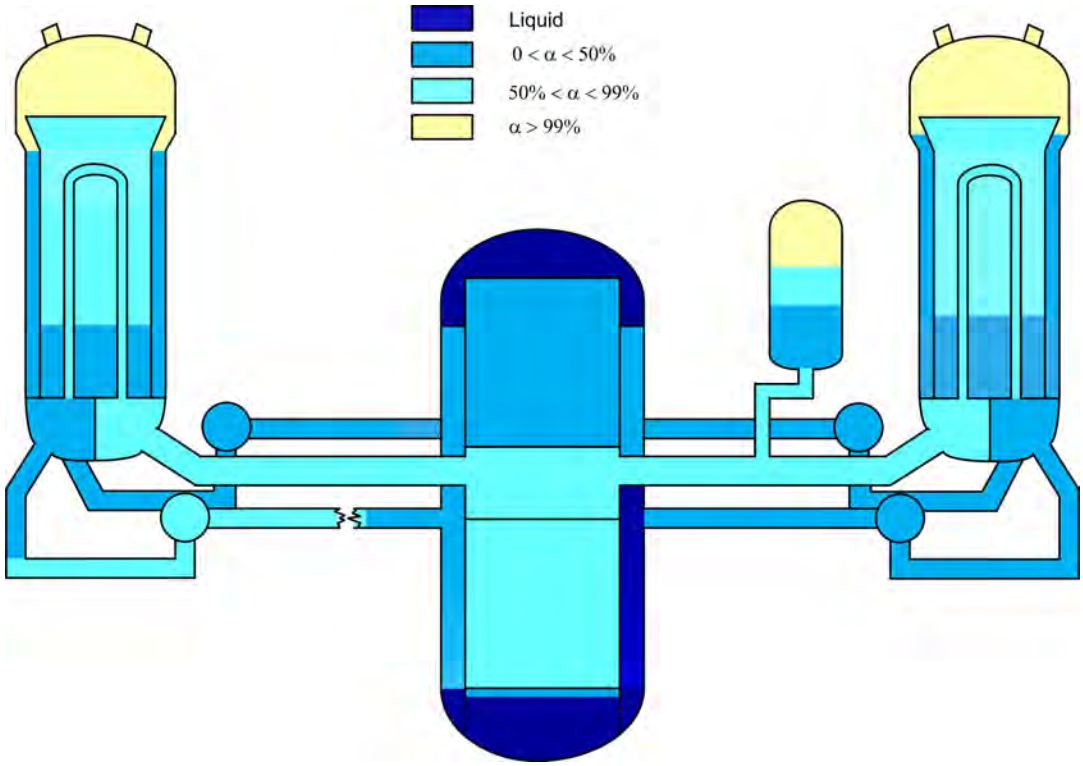

Figure 3-3 Calculated RCS Conditions, 4 s after the Break

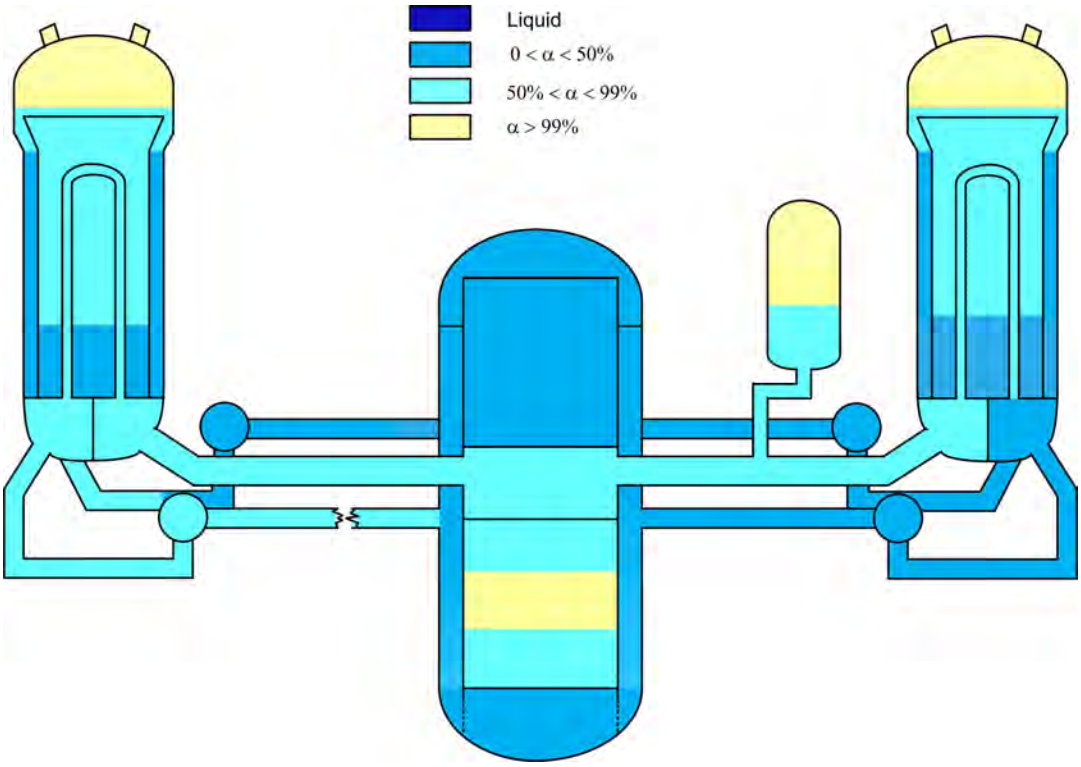

Figure 3-4 Calculated RCS Conditions, 6 s after the Break

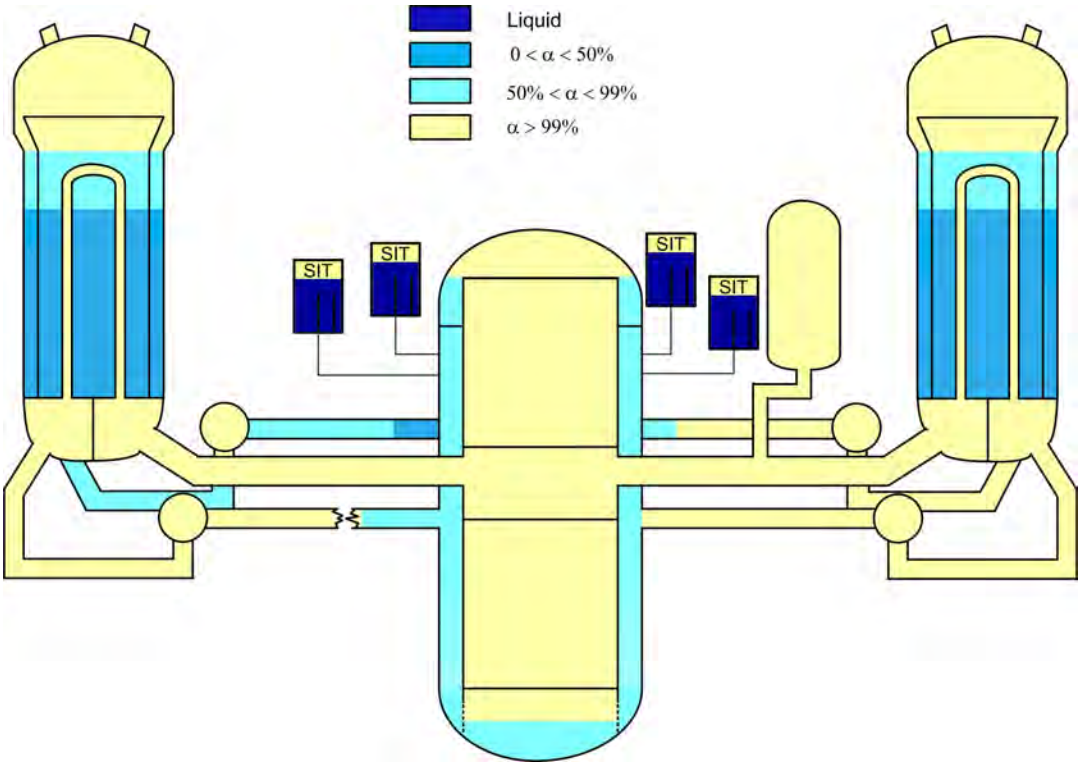

Figure 3-5 Calculated RCS Conditions, 25 s after the Break

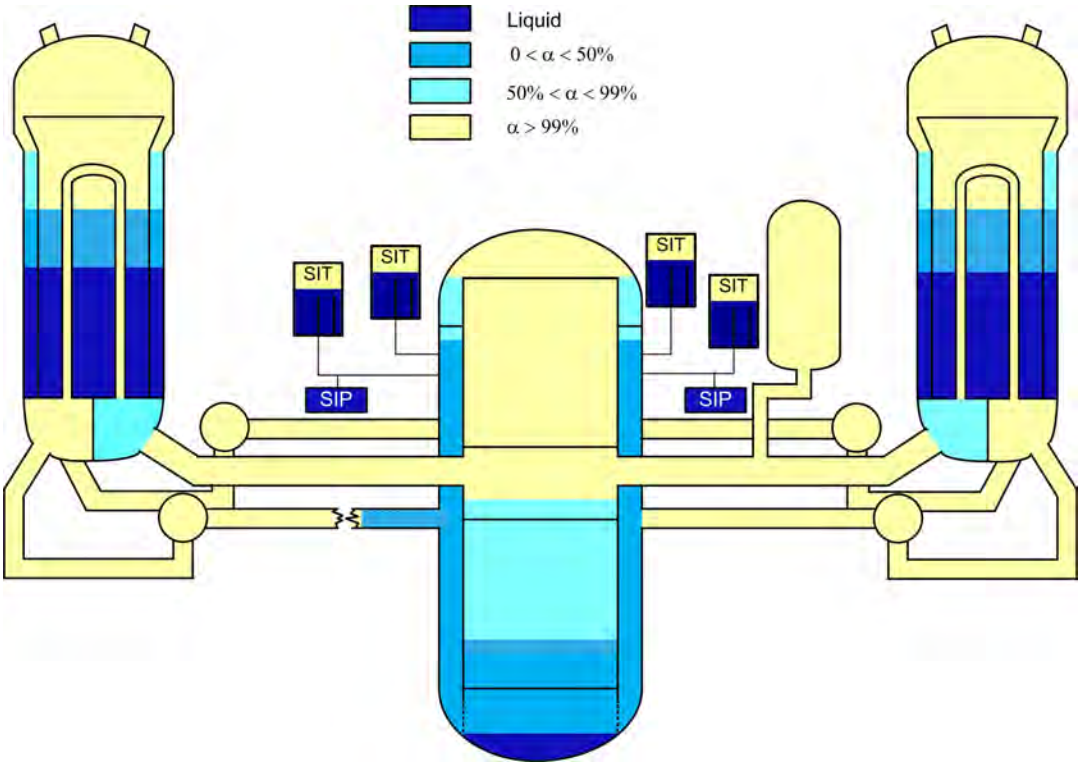

Figure 3-6 Calculated RCS Conditions, 45 s after the Break

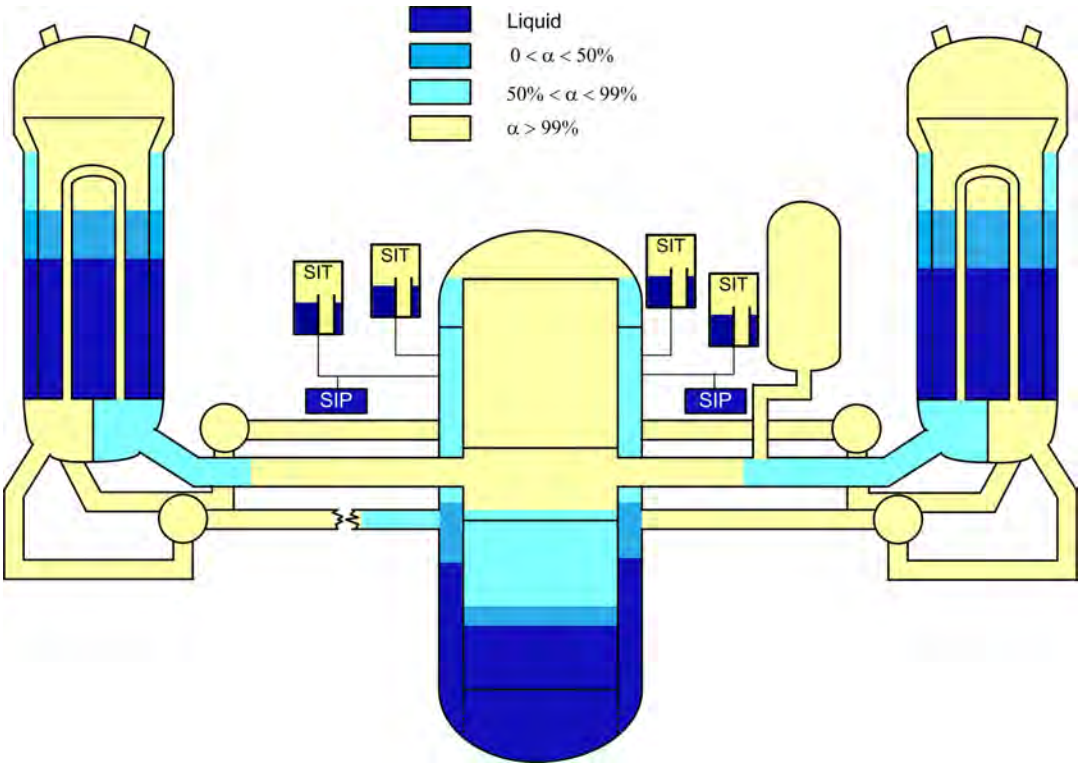

Figure 3-7 Calculated RCS Conditions, 92 s after the Break

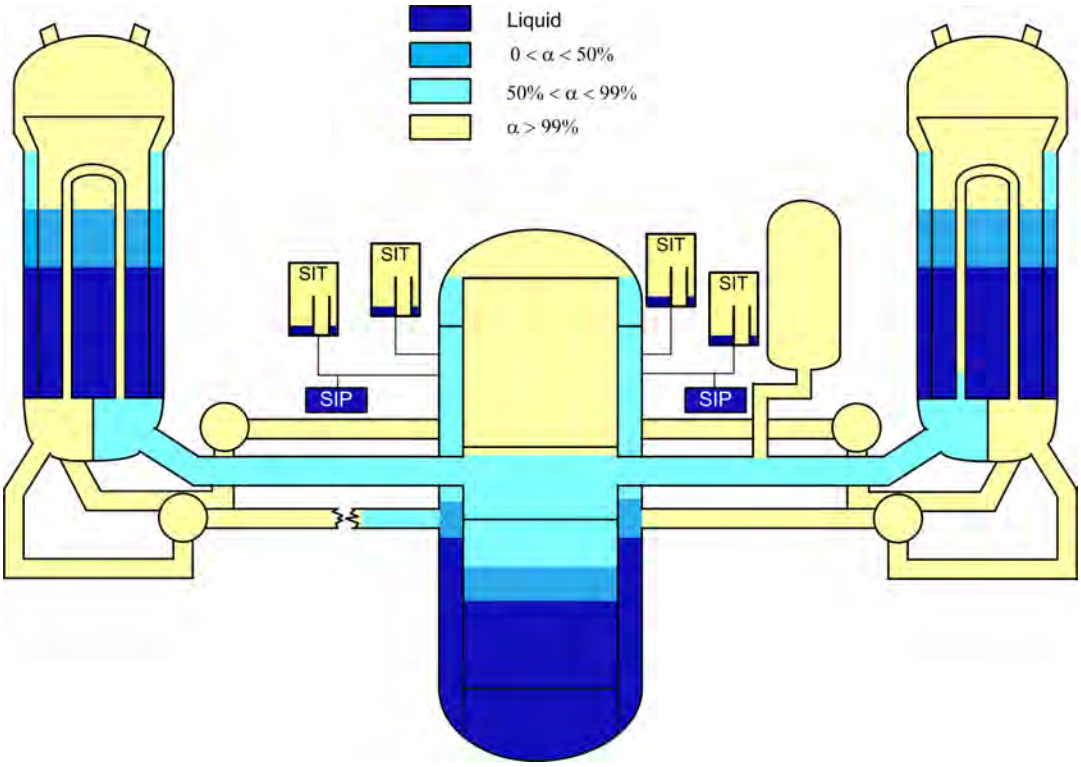

Figure 3-8 Calculated RCS Conditions, 150 s after the Break

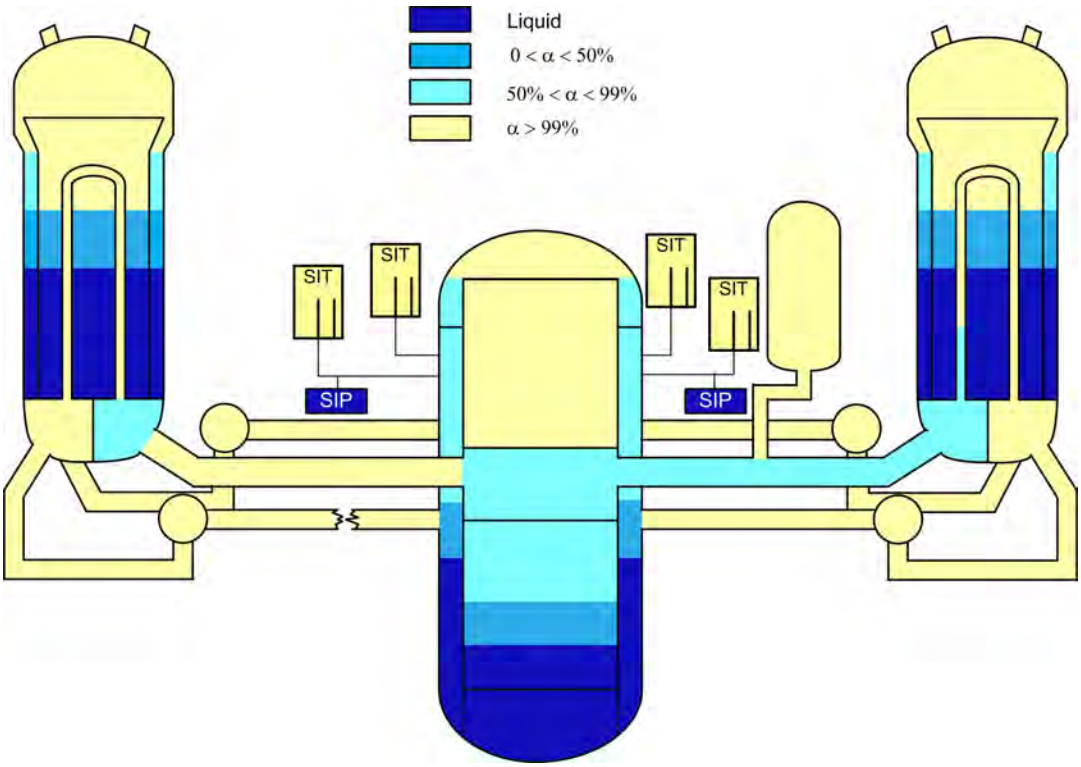

Figure 3-9 Calculated RCS Conditions, 350 s after the Break

4. Assessment and Ranging of Parameters

The second element, “Assessment and Ranging of Parameters,” consists of Steps 7, 8, 9 and 10. The main objectives of the second element are to specify the ranges of parameters, to quantify the code accuracy, and to obtain information for extrapolating the quantified code accuracy to the uncertainty of plant calculations.

A basic principle of CAREM is to evaluate the uncertainties of the models or correlations that are used to simulate the major phenomena in PIRT. Uncertainty ranges of individual parameters can be determined from information such as experimental data, reference documents, engineering judgments, code calculations, etc. However, in cases such as (a) phenomena that involve interaction of many processes, e.g., ECC bypass, (b) phenomena for which the database is insufficient, and (c) phenomena of which the uncertainty evaluation is not based on the test data, the uncertainty is treated in terms of a separate bias, bounding approach, or nodalization. For phenomena that are governed by the same model or correlation, the range of uncertainty of the model or correlation is determined by a representative phenomenon that would more significantly affect peak cladding temperature.

The code accuracy is defined as a statistical difference (i.e., bias) and deviation obtained by comparing the calculated cladding temperatures and the measured temperatures of the experiments. Because the code accuracy is defined in terms of the cladding temperature, it is not used as a measure of the ability of each code model to predict corresponding phenomenon. The procedures of extrapolating the code accuracy to the uncertainty of plant calculations are as follows:

- Establish an assessment matrix and determine the code accuracy through assessment calculations. These procedures are described in Sections 4.1 and 4.3.1.

- Determine the scalable code parameters from the reference information. Also, confirm the adequacy of the number of parameters and the uncertainty range of each parameter through the confirmation of experimental data covering. These procedures are described in Sections 4.2.2 and 4.3.2.

- Apply the code parameters and their uncertainty ranges, of which validities have been confirmed, to plant sensitivity calculations. This procedure is described in Section 5.2.2.

- Quantify the effect of scale distortions in the form of biases. The procedure to determine parameters to be used in bias evaluation is described in Section 4.2.3, and the quantification of the biases is described in Section 5.2.3.

4.1 Establishment of Assessment Matrix (Step 7)

The assessment matrix should be established to include separate effect tests (SETs), that investigate individual phenomena, and integral effect tests (IETs), that incorporate many or all of the important phenomena and components. The assessment matrix should be designed to provide a database for the evaluation of the following:

- code capability to predict important phenomena

- code accuracy

- code capability to scale-up the phenomena to NPP conditions

- nodalization

- parameters and their ranges

Because APR1400 adopts DVI, phenomena that occur in the downcomer region, such as ECC water bypass and void development in the downcomer region (i.e., downcomer boiling), could be different from those of traditional cold leg injection (CLI) plants. Thus, the assessment matrix should include tests that investigate ECC water bypass and downcomer boiling phenomena of the DVI plant. The assessment matrix which was used for CLI plants [11] is shown in Table 4-1. This matrix is applied to the APR1400 as well for the phenomena other than those specific to the DVI plant.

In addition to the tests referred to in Table 4-1, the following tests were selected to investigate ECC water bypass and the downcomer boiling phenomena of the APR1400.

- MIDAS, UPTF 21D: to address the ECC water bypass phenomenon
- DOBO: to address the downcomer boiling phenomenon
- ATLAS: to address the general LBLOCA reflood behavior of the APR1400
- VAPER: to address the SIT-FD injection flow behavior

MIDAS and DOBO experiments are separate effect tests performed to investigate the local phenomena of the APR1400. The reflood tests performed at the ATLAS facility were selected to address the general LBLOCA reflood phenomena, including the ECCW bypass and the downcomer boiling. ATLAS is the integral test facility that simulates all components of the APR1400. The assessment matrix for these tests is shown in Table 4-2.

Table 4-3 provides code models, parameters, and the related important phenomena/processes. Tests performed to assess these code models and parameters are listed in Table 4-4. Table 4-4 also includes the tests used for the model evaluation during the RELAP5/MOD3.3 development stage.

4.2 Plant Nodalization and Experiment Assessment (Step 8)

4.2.1 Plant Nodalization (Step 8.1)

Nodalization of the APR1400 is shown in Figure 4-1.

Two hot legs and four cold legs; which are spaced equally, 60° apart, in a circumferential direction, are modeled separately. The two loops are modeled identically except that (a) the pressurizer is attached to Loop 2 (Intact loop), and (b) Loop 1 (Broken loop) contains the cold leg break between the pump and the reactor vessel. The noding for each loop contains hot leg piping, U-tubes and fluid volumes of the steam generator primary and secondary, two pump suction legs, two pumps, and two pump discharge cold legs.

Reactor vessel nodalization consists of the downcomer, upper and lower plenum, and the core regions. Reactor vessel nodalization follows the typical pressurized water reactor nodalization, but the modeling of the core and the downcomer is remarkably detailed in order to capture the various thermal-hydraulic phenomena and multidimensional behaviors. [

]^{TS}.

Because nodalization should provide appropriate code options as well, code options are carefully selected following the code user's guidelines faithfully to avoid distortion of code results that could be caused by selecting inappropriate options.

Details of the nodalization are described below:

Hot Leg

Hot leg connects the reactor vessel to the steam generator inlet plenum. Hot leg is modeled with a [ ]TS. BRANCH components are utilized in connecting pressurizer surge line or the steam generator inlet plenum with the hot leg. On the junction connecting pressurizer surge line with the hot leg, [ ]TS.

Steam Generator

The inlet plenum of the steam generator is modeled with [ ]TS. The outlet plenum of the steam generator is [ ]TS. The U-tubes are modeled with [ ]TS. By designating both sides of the U-tubes as convective heat transfer boundaries, it is possible to simulate the heat transfer between primary and secondary sides. Reverse heat transfer during the transient, from the secondary side to the primary side, can also be calculated, as well as the steady-state heat transfer. Droplets entrained into the U-tubes can vaporize by the reverse heat transfer, resulting in the steam binding. The riser (i.e., boiling region) and economizer of the secondary side are modeled with [ ]TS. [

]TS. The [ ]TS are used to model the main feed-water flow which is supplied to the upper downcomer and to the lower region of the economizer.

Pump Suction Leg

The pump suction leg connecting the steam generator outlet plenum and the pump inlet is modeled with [ ]TS. The geometric shape of the pump suction leg is modeled appropriately with [ ]TS.

Reactor Coolant Pump

The RCP is modeled with a PUMP component. The PUMP component contains all the models that calculate the characteristics of the pump. Pump behavior during the steady state and transient can be simulated with the pump control input model. Degradation of pump performance due to the two-phase flow is simulated by the input of degradation multiplier tables for the pump head and torque.

Cold Leg

The pump discharge cold leg, connecting the pump and the reactor vessel, is modeled with a [ ]TS. [

]TS.

Safety Injection System

SIT-FD is modeled with an [ ]TS. When the SIT-FD water level is higher than the top of the stand pipe, a high flow rate is discharged. A low flow rate is discharged when the water level is lower than the top of the stand pipe. [

]TS. The SIT-FD injection start time is controlled by a [

]TS. The flow rate switching time from a high flow rate to a low flow rate is controlled by [ ]TS. The safety injection pump flow rate is modeled with a [ ]TS. [ ]TS. From the worst single failure assumption, the two SIPs are assumed to operate conservatively. The SIP located near the broken cold leg is assumed to operate because most of the ECC water injected from this SIP is expected to bypass the core. Another SIP located opposite side of broken cold leg.

Pressurizer

Because the core could be rewetted if the inventory in the pressurizer flows into the reactor upper plenum, the pressurizer emptying time could affect the fuel cladding temperature behavior. Based on the results of code assessments against the LOFT test, the pressurizer is modeled with [ ]TS in order to adequately simulate the emptying time of the pressurizer. [

]TS.

Reactor Pressure Vessel Downcomer

Geometrically, the downcomer is distinguished from the lower plenum by the flow skirt. The downcomer has four connections with the four cold legs and two structural penetrations of hot leg piping across the gap between the core barrel and the reactor pressure vessel. Each loop piping is spaced equally 60° apart azimuthally. The noding for the downcomer is configured to maintain consistency with the geometric boundary and to have six equal channels. [

]TS. [

]TS.

The axial noding of the downcomer has [ ]TS. The axial noding of the lower downcomer below the cold leg elevation consists of [ ]TS, and the axial noding for the upper annulus above the cold leg elevation contains [ ]TS. The height of the upper annulus node to which the DVI nozzle is connected has been determined to locate the node center at the DVI nozzle elevation. [

]TS.

[ ]TS.

Reactor Pressure Vessel Lower Plenum

The lower plenum noding consists of [ ]TS. The boundary of each volume is consistent with the geometric boundary of the lower plenum structures. [

]TS.

Reactor Pressure Vessel Upper Plenum

The upper plenum connects the core outlet to the hot legs and the upper guide structure (UGS). The control rod guide tubes are connected to the tie tubes in the upper plenum. The tie tube modeling provides a flow path from the top of the core to the UGS bottom plate. [

]TS.

Reactor Vessel Upper Head

The upper head is divided into the UGS and the top head. The UGS has two channels, and each channel contains [ ]^{TS}; the lowest volumes of each channel have a flow path to the upper plenum. The nodding for the top head is modeled with [ ]^{TS}

Reactor Core

The fuel region is divided into [ ]^{TS}, i.e., [ ]^{TS} [ ]^{TS}. The active length of the fuel rod is modeled using [ ]^{TS}, based upon the code assessment against the THTF and FLECHT-SEASET tests of which the rod lengths are the same as the fuel rod length of the conventional plant. Thus the length of each active core node for the APR1400, of which the core length is 3.81 m (150 in.), corresponds to [ ]^{TS}.

4.2.2 Determination of Code Uncertainty Parameters and Their Ranges (Step 8.2)

This section describes the determination of code uncertainty parameters and the range of their uncertainties. Code uncertainty parameters with their ranges determined in this step will be used for the evaluation of overall calculational uncertainty of the plant sensitivity calculations, if these parameters are confirmed to predict the experimental PCTs in Step 9. If these parameters are found to not be enough to encompass the experimental PCTs, the processes are iterated from Step 8.2 until all the experimental PCTs are successfully covered. The impacts of phenomena rated low by PIRT are examined indirectly through the evaluation of code accuracy and the confirmation of experimental PCT coverings. Plant input parameters are discussed in Section 5.1.

Determination of relevant uncertainty parameters or conservative treatment of each selected phenomenon or process is described in the following:

(Code uncertainty parameters which will be used for the evaluation of scale biases are described separately in section 4.2.3.)

4.2.2.1 Code Parameters and Their Ranges for the Phenomena in the Core/Fuel

4.2.2.1.1 Fuel Rod

Initial stored Energy Release

Following the importance evaluation of 16 parameters, which were identified as affecting the initial stored energy in the nuclear fuel rod, the same four dominant parameters as in CSAU were selected. They are gap conductance, rod peaking factors, fuel thermal conductivity, and convective heat transfer coefficients. The gap conductance is dependent on initial and transient fuel geometry, gas composition, burnup, and so on. The gap conductance of the steady state is not treated as an uncertainty parameter because the steady state fuel centerline temperatures, i.e., initial stored energy, are adjusted to match the design data considering UO_2 pellet thermal conductivity degradation (TCD) effects. The details of steady state fuel centerline temperature are described in Section 5.1 and Appendix K of this report. Transient gap conductance is discussed below.

Rod peaking factors are also discussed in Section 5.1. Fuel thermal conductivity is discussed below in “Fuel Pellet Heat Transfer” which was identified as an important phenomenon independently from initial stored energy. Convection heat transfer, important to the initial stored energy of the fuel rods,

is the heat transfer to liquid.

Fuel Pellet Heat Transfer

Fuel pellet heat transfer is represented by the [ ]TS. Thermal conductivity of fuel pellet is modeled by the modified NFI correlation to consider TCD effects. The uncertainty of the modified NFI correlation is determined based on the information in reference [12].

- Parameter; [

]TS

Gap Conductance during the Transient

Gap conductance during the transient is a strong function of the gap width between the pellet and the cladding. The transient gap width is mainly governed by cladding mechanical behaviors such as swelling and rupture. [

]TS Clad ballooning and burst is described below.

Clad Ballooning and Clad Burst

Deformation of the fuel cladding during the transient is mainly governed by the swelling and rupture behavior. RELAP5/MOD3.3/K code calculates the burst temperature, burst strain, and flow blockage as a function of the heatup rate using the model of NUREG-0630 [13]. [

]TS.

- Parameter; [

]TS

- Parameter; [

]TS

Liquid-phase Forced Convection Heat Transfer

RELAP5/MOD3.3/K uses Dittus-Boelter correlation to calculate turbulent convection heat transfer to liquid. By referring to the discussions of various references in which 95 percent of the data have

been encompassed if an error range of [ ]TS:

- Parameter; Dittus-Boelter correlation

  [ ]TS

Cladding Oxidation Reaction

Cathcart [14] model is used for the calculation of the cladding oxidation reaction in the RELAP5/MOD3.3/K code. The uncertainty of the Cathcart model was evaluated in Reference [14] and an excerpt from Reference [14] is described in Table 4-5. The maximum deviation is 4.9 % at 1,050 °C. Because this deviation was obtained at 90 % joint confidence intervals, the maximum deviation at a 95 % one-sided confidence interval is also 4.9 %, assuming normal distribution. On this assumption, the standard deviation is calculated to be [ ]TS. A similar method was used in Reference [15] to obtain the uncertainty of the cladding oxidation reaction.

- Parameter; Cathcart oxidation model

  Distribution function; normal

  Mean value; 1.0

  Standard deviation; [ ]TS

Fuel Relocation into the Clad-Ballooned Region

If the clad balloons and ruptures, fragmentation from the fuel pellet can move to the ballooned or ruptured region and increase the power generation there. This process occurs in a very limited region, though. And if the clad balloons or ruptures, the heat-transfer from the pellet to the cladding reduces because of widened gap widths. Therefore, the effect of fuel relocation is not critical. Therefore, fuel relocation is not treated as an uncertainty parameter.

4.2.2.1.2 Core

Nucleate Boiling Heat Transfer

Nucleate boiling heat transfer coefficient is calculated by Chen correlation. According to the code manual of RELAP5/MOD3.3, the average error is 21.1 % in saturation nucleate boiling, and ± 40 % in subcooled nucleate boiling. Most of the data are within these error ranges. In this report, the [ ]TS.

- Parameter; Chen nucleate boiling correlation

  [ ]TS

High-Pressure and High-Flow Critical Heat Flux

RELAP5/MOD3.3/K code calculates CHF in the high-pressure and high-flow region using the Groeneveld lookup table. KCE-1 CHF correlation [22] which was developed for PLUS7 fuel assembly is not used in this evaluation model because the applicable ranges of KCE-1 correlation do not cover whole LBLOCA conditions.

Figure 4-2 provides a comparison between the data and predicted CHF using the look up table. In this figure, 1,993 points are compared. The 1,993 data points cover all test conditions, including those of high-pressure and high-flow. As described in the RELAP5 manual, this figure shows a typical result of the comparison between the data and predicted values. As can be seen in the figure, the Groeneveld lookup table estimates the critical heat fluxes lower than the experimental data by 4.9 % on average with a root-mean-squared error of 37.9 %. Because these deviations were obtained using data covering all test conditions, the corresponding values obtained using the data measured only in the high-pressure and high-flow condition could exhibit differences.
[

]TS.

- Parameter; Groeneveld lookup table CHF

[

]TS

Low-Pressure and Low-Flow Critical Heat Flux

The CHF model of the RELAP5/MOD3.3/K code for the low-pressure and low-flow region is the modified Zuber correlation. This correlation predicts the CHF at the low-pressure and low-flow condition, by multiplying the liquid fraction, (1-α), to the Zuber's water boiling correlation. This method is the most representative correlation for the low flow regime region. Figure 4-3 shows that the modified Zuber correlation conservatively predicts 75 experimental data. [

]TS.

- Parameter; modified Zuber correlation

[

]TS

Film Boiling Heat Transfer

The reflood model of the RELAP5/MOD3.3/K compares film boiling heat transfer coefficients calculated by the Bromley correlation and the Forslund-Rohsenow correlation; it then uses the higher value. Therefore, for the film boiling heat transfer, two correlations have been selected as the uncertainty parameters and their ranges have been determined. According to CSAU [1], the uncertainty range for the Forslund-Rohsenow correlation, which was developed for the internal pipe flow, is 0.75 ~ 1.5 for their application to core fuel geometry. However, the distribution function is not known. Therefore, referring to the uncertainty variation of CSAU and code assessment results found

in Appendix C, the uncertainty range has been extended to [ ]TS.

As described in the RELAP5 manual, the calculated film boiling heat transfer coefficients using the Bromley correlation cover all data within ±18 %. Meanwhile, according to Reference [16], the experimental data which includes conduction, convection, and radiation heat transfer, are 12.1 % higher than the RELAP5 predicted values on average, and the data are distributed within 0.37 ~ 2.61 times of the predicted values. Based on these two conclusions, the standard deviation and the distribution function of the Bromley correlation are [ ]TS.

- Parameter; Forslund-Rohsenow correlation

[ ]TS

- Parameter; Bromley correlation

[ ]TS

Rewet Temperature or Minimum Stable Film Boiling Temperature

Rewetting is the process by which a liquid can penetrate the vapor layer on a hot surface to make initial contact with a surface. The temperature at which this occurs is called the minimum stable film boiling temperature (i.e., T_{min}). The reflood model of RELAP5/MOD3.3/K does not calculate T_{min}, but compares the heat flux calculated in the film boiling regime and the transition boiling regime; and uses the higher heat flux for transition boiling (or rewetting). Therefore, the uncertainty of rewetting is replaced by the uncertainties of film boiling and transition boiling heat transfer.

Transition Boiling Heat Transfer

RELAP5/MOD3.3/K uses the Weismann correlation [17] for the transient boiling heat transfer of rod bundles. According to Reference [17], a total of 273 data were used for the development of the Weismann correlation, and the correlation uncertainty has been evaluated as follows:

$$R = \frac{h_{measured}}{h_{predicted}} \qquad \text{where,} \quad h = \text{ heat transfer coefficient}$$

$\mu(R)$, average of R; 1.118

$\sigma(R)$, standard deviation of R; 0.618

The predicted values by the Weismann correlation against the experimental data are presented in Reference [17] and this indicates that most of the data can be covered [ ]TS

- Parameter; Weismann correlation

[

]TS

Single-Phase Forced Convection Heat Transfer to Vapor

RELAP5/MOD3.3/K uses the Dittus-Boelter correlation to calculate the convection heat transfer to vapor. By referring to the discussions of various references which show [

]TS:

- Parameter; Dittus-Boelter correlation

[

]TS

Radiation Heat Transfer to Surfaces, Vapor, and Liquid

[

]TS

Reactivity

Reactivity feedback due to the voiding of the moderator shown in Figure 4-4 is dependent on the core design of the NPP. Therefore, the uncertainty of reactivity feedback due to the voiding of the moderator is treated as a plant input parameter, and is discussed in Section 5.1.

Boron Reactivity Effect

Boron in the reactor coolant and the emergency core cooling water invokes negative reactivity. The Boron contents of the reactor coolant and safety injection water are dependent on the design and operation of the NPP. Therefore, the uncertainty of reactivity feedback due to the borated water is treated as a plant input parameter, and is discussed in Section 5.1.

Decay Power

The “ANSI/ANS-5.1-1979 standard model” [18] with “ANS79-1” and “GAMMA-AC” options of RELAP5 is used to calculate the decay heat in CAREM. The “ANS-79-1” option allows only the 1979 standard data for ^{235}U to be used, that is, it is assumed that the decay heat power from fission isotopes other than ^{235}U is identical to that from ^{235}U and the fission rate is constant over the operating history of the maximum power level. The “GAMMA-AC” option is applied to consider actinide decay with fission product decay. It is well known that this decay heat power calculation

method produces a conservative decay heat power in light water reactors in which the fuels contain a considerable amount of Pu. The uncertainty of the decay heat power has been determined [

]TS:

- Parameter; ANSI/ANS-5.1-1979 standard for decay heat in light-water reactors

[

]TS

Spacer Grid Heat Transfer Effects

The spacer grids of the fuel assembly usually have three effects on core cooling; (1) heat transfer enhancement by the agitation of the flow, (2) rewetting of spacer grids, and (3) breakup of entrained water drops into fine droplets. All three have favorable effects on core cooling. RELAP5/MOD3.3/K does not have a model to address these heat transfer enhancement effects of the spacer grids. The deficiency of the spacer grid model would result in a conservative prediction of the cladding temperatures.

Flashing

Because flashing is most pronounced during blowdown and significantly impacts vapor generation and voiding throughout the reactor coolant system, flashing was identified as an important phenomenon in various components such as the core, upper plenum, reactor vessel head, downcomer, pressurizer, etc. Flashing occurs if the system pressure is lowered to the saturation pressure of the coolant in the system. Flashing is a result of system depressurization. System depressurization is dependent on break size, critical flow, pressure resistances, initial system pressure, and so on. Therefore the uncertainty of the flashing phenomenon can be represented by the uncertainties of the break flow and the system initial pressure. The uncertainties of the break flow and the system initial pressure are described in Section 4.2.2.6.1 and Section 5.1.7, respectively.

Level

Water levels of the core, upper plenum, lower plenum, and downcomer have been identified as an important phenomenon. Water levels in these components are formed as a result of many processes such as break flow, ECCW injection, condensation, entrainment, de-entrainment, interfacial drag, multidimensional flow, core heat transfer, and wall heat transfer. There is no universal code parameter that characterizes the water level. Therefore no specific code parameter for the reactor vessel water level is identified on the premise that the water level is dependent on other phenomena or parameters. In other words, the water level is not a cause but a result of many other phenomena. And the uncertainty can be addressed by other uncertainties.

Interfacial Drag in Core

Entrainment of droplets as a result of interfacial drag in core is a major source of heat transfer for the fuel rods during the reflood period. Because there are many different correlations of entrainment (or interfacial drag) depending on the flow regime or hydraulic conditions, it is difficult to determine one governing parameter that is effective for all regimes. But it is well known that the interface drag as well as interface heat transfer is a strong function of droplet diameter which is determined by a Weber number. Therefore, CAREM has determined the [

]TS.

Multidimensional Flow

RELAP5/MOD3.3/K is a one-dimensional thermal-hydraulics code in principle, but it has a capability of two-dimensional approximation of multidimensional flow. [

]TS.

Vapor Superheating

The increase of the vapor temperature above the saturation temperature is governed by the heat transfer from the hot core structures. Vapor superheating is not a cause but a result of the core heat. Therefore the uncertainty of vapor superheating can be described by the uncertainties of core heat transfer parameters. Core heat transfer parameters are already described above. There is no need to determine an additional parameter for vapor superheating.

Interfacial Heat Transfer

Interfacial heat transfer is strongly dependent on the interface area between the phases. The volumetric interface area is often calculated as a function of droplet diameter. The droplet diameter is determined by the Weber number in RELAP5/MOD3.3. Selection of the [ ]TS as an uncertainty parameter for interfacial heat transfer is probable. And it has another advantage of describing the uncertainty of interfacial drag as well, because the drag is also dependent on the interfacial area. Therefore, the [ ]TS is selected as a code parameter to describe the uncertainty of interfacial drag and heat transfer. By referring to the code manuals of COBRA-TF and RELAP5, the uncertainty range of the [ ]TS has been determined. The maximum and minimum values of the [ ]TS, respectively. A [ ]TS.

- Parameter; [

]TS

Flow Phenomena at Top Nozzles

The flow redistribution phenomenon occurs at top nozzles during blowdown period. Except for the blowdown period, countercurrent flow is frequently calculated at the top nozzles of the fuel assemblies. At the top nozzles, steam flows upward while liquid flows downward. This countercurrent flow can affect the probable water accumulation at the upper plenum. Upflowing steam from the core can entrain the water in the upper plenum ultimately into the steam generator u-tubes. Because the steam generator secondary side is hotter than the primary side during reflood, the entrained droplets evaporate and the steam becomes superheated in the u-tubes. This droplet evaporation and steam superheating phenomena result in steam binding. The effect of steam binding on peak clad temperature is quantified as a separate bias in Section 4.2.3. Therefore, the uncertainty parameter for this countercurrent flow at the fuel assembly top nozzles is not determined.

4.2.2.2 Code Parameters and Their Ranges for Phenomena in the Reactor Vessel

4.2.2.2.1 Reactor Vessel Downcomer

As summarized in CSAU [1], the downcomer is one of the components where scale distortion is inevitable in scaled-down test facilities. Many facilities, especially when power-to-volume scaling is applied, preserve the height of the prototype but reduce the diameter of fluid volumes considerably. Due to a large height-to-diameter ratio, the facilities become tall and skinny. Consequently the downcomer not only has a narrow gap but also has a very large surface-to-volume ratio. These distortions will affect the ECC bypass process which is a consequence of many complex processes such as condensation, interface momentum transfer, entrainment, de-entrainment, single- and two-phase pressure drops. The ECC bypass is also affected by multidimensional and countercurrent flow phenomena in the downcomer. Therefore, the phenomena or processes observed in scaled facilities become atypical to those occurring in the full-scale power plant. Therefore, the observations cannot be directly applied to full-scale power plants. As there is no one code parameter that characterizes the ECC bypass phenomenon, it is necessary to evaluate the ECC bypass as a separate bias.

Except for these four processes or phenomena of "flashing", “vessel stored energy release,” “boiling in the downcomer,” and “non-condensable gas effect,” 12 among16 important processes or phenomena of the downcomer identified in Table 3-2 are treated in the evaluation of scale bias in Section 4.2.3.

Vessel Stored Energy Release and Boiling in the Downcomer

If enough cooling water is not supplied, the downcomer water would lose its subcooling and begin to boil. This is especially true in the late reflood period where SIPs only provide the emergency core cooling water. Therefore in order to describe the uncertainty of downcomer boiling, we need to consider the amount of ECCW supply and the wall stored energy. The SIP injection flow rate is treated as one of the plant parameters in Section 5.1.5. Wall stored energy can be described by material properties such as the heat capacity and conductivity. The material properties of the reactor vessel wall are dependent on the system design of the power plant. Therefore, the uncertainties of the material properties are described in Section 5.1.6.

[ ]^{TS}.

Direct Vessel Injection Jet Flow

DVI jet impingement produces dispersed droplets and affects the ECC bypass. This phenomenon is an attributor to the ECC bypass. Code parameter relevant to this phenomenon is not determined, and the effect is evaluated as a scale bias in Section 4.2.3.

Flashing

As described in Section 4.2.2.1.2, the uncertainty of the flashing phenomenon is represented by the uncertainties of the break flow model and system pressure.

Level

This phenomenon is an attributor to the ECC bypass. Code parameter relevant to this phenomenon is not determined and the effect is evaluated as a scale bias in Section 4.2.3.

Entrainment and De-entrainment

These processes are attributors to ECC bypass. Code parameters relevant to these processes are not determined and the effects are evaluated as a scale bias in Section 4.2.3.

Multidimensional Flow, Condensation, Countercurrent Flow, and Bulk Mixing

These processes or phenomena are attributors to ECC bypass. Code parameters relevant to these

are not determined and the effects are evaluated as a scale bias in Section 4.2.3.

Single- and Two-phase Pressure Drop

This phenomenon is an attributor to ECC bypass. Code parameter relevant to this phenomenon is not determined and the effect is evaluated as a scale bias in Section 4.2.3.

Non-condensable Gas Effect

Non-condensable gas in the downcomer is mainly nitrogen from SIT after the depletion of its water inventory. The nitrogen increases downcomer pressure because its pressure is higher than the downcomer pressure at its appearance time. The higher pressure pushes down the downcomer water column into the core and enhances core reflood. On the other hand, the nitrogen might affect the condensation in the downcomer. Ingression of the nitrogen into the core is not probable or considerable because of the existence of the water column in the downcomer. [

]^{TS}

The release of non-condensable gas from the SIT after the depletion of the SIT water is dependent on the SIT pressure, nitrogen volume and temperature. These SIT parameters are dependent on the safety system design of the NPP. Therefore, the uncertainties of these SIT parameters are treated as plant input parameters, and are discussed in Section 5.1.

4.2.2.2.2 Reactor Vessel Lower Plenum

As summarized in the CSAU [1], the lower plenum is one of the components where scale distortion is inevitable in the scaled-down test facilities. The phenomena or processes observed in scaled facilities become atypical to those occurring in the full-scale power plant. Therefore, it is necessary to evaluate the effects of the phenomena or processes except for those which code parameters can be determined.

Stored Energy Release and Boiling

The initial steady-state energy is released by conduction during the transient from the reactor vessel lower plenum walls. Consequently, boiling and vapor generation can occur in the lower plenum due to the energy release from the internal structures and the vessel wall. The parameters governing these phenomena are the material properties, such as heat capacity and conductivity, of the vessel lower plenum wall. The material of the reactor vessel lower plenum wall is dependent on the system design of the NPP. Therefore, the uncertainties of these governing parameters are treated as plant input parameters, and are discussed in Section 5.1.

Level

This phenomenon is an attributor to, or a result of, ECC bypass. Code parameters relevant to this phenomenon are not determined, and the effect is evaluated as a scale bias in Section 4.2.3.

Multidimensional Flow, Entrainment, and Bulk Mixing

Multidimensional flow, entrainment (i.e., sweep-out) and bulk mixing have an impact on the initiation time of core reflooding because these phenomena govern the water level in the lower plenum and the ECC bypass during the refill period. Therefore, the uncertainties of these phenomena can be described by a separate bias evaluation of the ECC bypass. Bias evaluation is described in detail in Section 4.2.3.

4.2.2.2.3 Reactor Vessel Upper Plenum

Flashing

As described in Section 4.2.2.1.2, the uncertainty of the flashing phenomenon is represented by the uncertainties of the break flow model and system pressure.

Level

As described in Section 4.2.2.1.2, no specific code parameter for the water level has been identified because the water level is dependent on all the other phenomena.

De-entrainment on Structures, and Multidimensional flow, Entrainment, Core to Upper Plenum Flow, Upper Plenum to Hot leg Flow, Core Counter-Current Flow

Liquid entrained from the upper plenum into the steam generator through the hot leg will vaporize by the heat transfer from the secondary side during the reflood period. The resulting steam pressure will reduce the core reflood rate. RELAP5/MOD3.3/K code does not have a specific model to calculate the de-entrainment on mechanical structures and all these phenomena are complex. These phenomena attribute to the steam binding and the effects are evaluated as an independent steam binding bias. Specific parameters are not determined for each of these phenomena. The evaluation of the steam binding bias is discussed in Section 4.2.3

4.2.2.2.4 Reactor Vessel Upper Head

Flashing

As described in Section 4.2.2.1.2, the uncertainty of the flashing phenomenon is treated through the uncertainties of the break flow model and system pressure.

Upper Head to Upper Plenum via Upper Guide Structure Support Plate Flow

Upper head flow down to the upper plenum and possibly into the core plays an important role to cool the core during the blowdown period. The major driving mechanism of the flow is the flashing of the upper head water during the blowdown period. Because the flow is a result of the flashing which is again the result of the system transient, no specific parameter is not determined.

4.2.2.3 Code Parameters and Their Ranges for Phenomena in the RCP

Pump Performance

RCP performance is dependent on the RCP design of the NPP. Therefore, the uncertainties of RCP performance are treated as plant input parameters, and are discussed in Step 11.

4.2.2.4 Code Parameters and Their Ranges for Phenomena in the Pressurizer

Flashing

As described in Section 4.2.2.1.2, the uncertainty of the flashing phenomenon is represented by the uncertainties of the system pressure, that is, the pressurizer pressure, and the break flow model. Because the pressurizer pressure is dependent on the system design, the uncertainty of the pressurizer pressure is treated as a plant input parameter, and is discussed in Step 11. The uncertainties of the break flow model are described in Section 4.2.2.6.

Pressure

Pressurizer pressure is dependent on the design of the NPP. The uncertainty of pressurizer pressure is treated as one of plant input parameters, and discussed in Step 11.

4.2.2.5 Code Parameters and Their Ranges for Phenomena in the Steam Generator

Vapor Superheating and Droplet Evaporation by Secondary-to-Primary Heat Transfer (Primary Side)

Heat transfer occurs from the steam generator secondary side to the primary side by way of steam generator U-tubes if the secondary side temperature becomes higher than the primary side temperature. As a result of this heat transfer through U-tubes, liquid droplets entrained to the steam generator U-tubes are vaporized and superheated, causing steam binding. The effect of steam binding is evaluated as a separate bias in CAREM. Thus the uncertainties of the above phenomena are treated as a bias evaluation and are discussed in Section 4.2.3.

Secondary-to-Primary-Heat-Transfer Induced Flow and Level (Secondary Side)

When the primary side temperature becomes lower than the secondary side temperature, the condensation heat transfer develops at the walls of the U-tubes in the shell side of the steam generators. As a result of the condensation, the two-phase level of the secondary collapses. The collapsed water level is an indicator of the heat source of the secondary-to-primary heat transfer, and directly affects the steam binding. The effect of the steam binding is evaluated as a separate bias in CAREM. Thus the uncertainties of the above phenomena are treated by a bias evaluation and are discussed in Section 4.2.3.

4.2.2.6 Code Parameters and Their Ranges for Phenomena in Break and Containment

4.2.2.6.1 Break

Critical Flow

RELAP5/MOD3/K code uses the Ransom-Trapp critical flow model to predict critical flow rate; code uncertainty of this model was obtained based on the code assessment against [

]TS.

[

]TS.

- Parameter; [

]TS

- Parameter; [

]TS

Cold Leg to Containment Flow Path, and Single- and Two-Phase Pressure Drop

The break mass flow rate is influenced by the pressure drop as well, which is caused by wall friction and geometric form loss of the break flow path. The pressure drop needs to be calculated according to the flow condition of single-phase or two-phase flow. It is also influenced by the configuration of the break plane. Depending on whether the break is a double-ended guillotine or a slot, the discharge flow rate and consequent blowdown behavior can develop in a different way. In this sense the limiting break type and area are first determined in CAREM with respect to resultant PCT. Plant sensitivity studies are performed assuming the occurrence of the limiting break. In this way the break configuration is conservatively bound. Determination of the limiting break is summarized in Section 5.2.1.1 and discussed in detail in Appendix K.

The pressure drop also influences the RCS flow rate thus, the uncertainty of pressure drop in the loop piping can be represented by the uncertainty of RCS flow rate. The uncertainty of RCS flow rate is described in Section 5.1.7 of this report.

Therefore, the uncertainty of “cold leg to containment flow path, and single- and two-phase pressure drop” is not treated separately.

4.2.2.6.2 Containment

Pressure and Temperature History

Containment pressure history during the transient of an LBLOCA is especially important during the reflood phase as it acts as backpressure for the core reflooding. Break mass flow rate and system pressure drop are quite dependent on the containment backpressure during the reflood phase. Containment backpressure is calculated by CONTEMPT4/MOD5 while the system thermal hydraulics is calculated by RELAP5/MOD3.3/K in CAREM. These two codes are coupled in order to exchange the mass and energy discharge flow rate and the containment backpressure between the system and the containment. The coupling of two codes and its validation are described in Appendix I. [

]^{TS}.

4.2.2.7 Code Parameters and Their Ranges for Phenomena in the Safety Injection System

4.2.2.7.1 Safety Injection Pump

Time Dependent Flow Delivery

Time dependent flow delivery from the safety injection pump (SIP) is dependent on the SIP design of the NPP. Therefore, the uncertainty of the flow delivery from the SIP is treated as a plant input parameter, and is discussed in Step 11.

4.2.2.7.2 Safety Injection Tank

Stored Energy Release, Pressure, Liquid Temperature, Gas Temperature, Level, Gas Discharge to Piping, and Fluidic Device K-factors for High Flow and Low Flow Deliveries

SIT related phenomena are dependent on the design of the safety injection tank and operation of the NPP. Therefore, the uncertainties related to the SIT are treated as a plant input parameter, and are discussed in Step 11.

4.2.2.7.3 In-Containment Refueling Water Storage Tank

Temperature

Water temperature of the in-containment refueling water storage tank (IRWST) is dependent on the IRWST design of the NPP. Therefore, the uncertainty of the IRWST water temperature is treated as a plant input parameter, and is discussed in Step 11.

4.2.3 Determination of the Code Parameters and Their Variations for Scale Bias (Step 8.3)

As discussed in NUREG-1230 [19], the downcomer, lower plenum, and upper plenum of the test facilities which are designed according to “power-to-volume” scaling, are known as the components that can cause bias due to scale distortions. These distortions may affect phenomena such as ECC bypass, multidimensional flow, entrainment, de-entrainment, and steam binding. The phenomena resulting from these distortions of the test facilities may not be representative of a full-scale plant response.

As discussed previously in Section 4.2.2, the uncertainties of the following phenomena are evaluated as separate biases.

Reactor Vessel Core Region

- flow phenomena at top nozzles

Reactor Pressure Vessel Downcomer

- direct vessel injection jet flow
- level
- entrainment and de-entrainment
- multidimensional flow
- condensation
- counter-current flow
- bulk mixing
- single- and two-phase pressure drop
- cold leg-downcomer flow
- downcomer-lower plenum flow
- DVI-downcomer flow

Reactor Pressure Vessel Lower Plenum

- level
- multidimensional flow
- entrainment or sweep-out
- bulk mixing

- lower plenum-core flow

Reactor Pressure Vessel Upper Plenum

- de-entrainment on structures
- multidimensional flow
- entrainment
- core-to-upper-plenum flow
- upper-plenum-to-hot-leg flow
- core countercurrent flow

Steam Generator

- vapor superheating
- secondary-to-primary heat transfer (primary side)
- secondary-to-primary heat transfer (secondary side)
- shell side level

Effects of above phenomena or processes are evaluated as biases. Two biases, the ECC bypass bias and the steam binding bias, are identified to describe above phenomena or processes. Phenomena of the reactor pressure vessel downcomer and lower plenum are included in the evaluation of the ECC bypass bias. Phenomena of the reactor pressure vessel upper plenum and steam generator are included in the evaluation of steam binding bias.

Determination of code parameters or measures for the evaluation of ECC bypass or steam binding bias is explained component-wise in the following sections. Evaluation of the biases in the plant calculation is described in Section 5.2.3.

4.2.3.1 ECC Bypass Bias

The ECC bypass phenomena involve many processes such as condensation, multidimensional flow, steam velocity, entrainment, de-entrainment, interphase momentum transfer, countercurrent flow, and so on. It is difficult to determine one specific code parameter governing ECC bypass. Therefore, the uncertainties of the ECC bypasses during the refill and reflood periods are treated as separate biases and the code parameters for evaluating the biases are described below.

ECC Bypass During the Refill Period

[

]^{TS}.

[

]TS

ECC Bypass During the Early and Late Reflood Periods

[

]TS.

[

]TS.

[

]TS.

4.2.3.2 Steam Binding Bias

[

]TS

[

]TS.

Code Parameters to Evaluate the Entrainment and De-entrainment in the Upper Plenum

[

]TS

Code Parameters to Evaluate U-tube Heat Transfer and Vapor Superheating

[

]TS.

4.3 Check Experimental Data Coverings (Step 9)

Step 9 ensures the validity of the code uncertainty parameters determined in Step 8. Step 9 examines whether the simulation calculations using the uncertainty parameters from the previous steps can successfully encompass the cladding temperatures of the experiments. These Step 9 calculations are performed for all the experiments in which clad temperatures are measured. If the calculations cannot cover the upper bound of the measured clad temperatures, it is presumed that the assumptions for those parameters are incorrect, or some other parameters are missing. In this case, Step 8 is referred to again and the assumptions are refined until the covering of the clad temperatures is confirmed. The uncertainty parameters and their ranges are determined to result in as much calculational uncertainty as the code accuracy. By way of this step, we can confirm the sufficiency of the number and the properness of the assumptions of the code uncertainty parameters against the experiments at various scales and conditions.

Step 9 consists of two sub-steps; code accuracy evaluation and an actual data covering check.

4.3.1 Code Accuracy Evaluation (Step 9.1)

Code accuracy is defined in this method as the statistical difference between calculated and measured PCTs. Even if the locations and the occurrence times of the PCTs are different from each other, the code accuracy is defined simply as the PCT difference regardless of the location and occurrence time. That is, code accuracy is defined in terms of PCT predictability. It is not used as a measure of the code's ability to predict each phenomenon.

[

]TS.

Bias and standard deviation of the difference are calculated as follows:

- PCT difference

$$\Delta PCT_{Zi} = PCT_{zi,cal} - PCT_{zi,\exp}$$

- PCT bias; difference between the averages of calculated values and measured values

$$Bias = M_{cal} - M_{\exp} \quad \text{or}$$

$$Bias = \frac{\sum_{j=1}^{n} (\Delta PCT_{zi})_j}{n}$$

- Standard deviation (σ)

$$\sigma = \sqrt{\frac{\sum_{j=1}^{n}\left\{\overline{\Delta PCT_{zi}} - (\Delta PCT_{zi})_j\right\}^2}{n}}$$

where, M_{cal} = the average value of code calculation,

M_{exp} = the average value of test data,

zi,cal = node elevation corresponding to measured elevation,

$zi,\exp$ = measured elevation,

n = total number of ΔPCT_{Zi}

One-sided 95 % limit is calculated in the code accuracy evaluation. Assuming a normal distribution function for the PCT difference, the one-sided 95 % PCT limit is calculated as:

$$95\%\ bound = 1.645\sigma + bias\ .$$

where, σ = standard deviation of ΔPCT_{Zi}.

This value is a reference value for the experimental data covering of Step 9.2. While all the code models or correlations are intermingled in the quantification of the code accuracy, we handle only a limited number of uncertainty parameters to quantify the overall calculational uncertainty. The code accuracy, or the degree of code capability to predict the PCT in other words, needs to be reproduced again, even we are propagating the uncertainties of the models to PCT. In this concept, the code accuracy is used as a reference value for the experimental data covering. Because the code accuracy covers the 95 percentile of PCTs, coverage of the 95 percentile, not the 100 percentile, of the data may be enough in the experimental data covering. But in order to provide conservatism and to enhance the practicality of the data covering, all the experiment data are covered. If the resulting PCT of simple random sampling (SRS) calculations is higher than the maximum value of the measurements, the number and probability distribution functions of the uncertainty parameters are confirmed to be sufficient. If the resulting PCT of SRS calculations cannot cover the maximum value of the measurements, it will be necessary to check further whether the resulting PCT can cover the 95 % one-sided limit. If the 95 percentile is covered by the SRS calculations, the number and probability distribution functions of the uncertainty parameters are confirmed to be sufficient.

4.3.1.1 Blowdown Code Accuracy

Blowdown experiments on DVI features are not available. This is partly due to the fact that the blowdown phenomena are almost independent of the injection system and therefore the necessity of the DVI blowdown experiments is relatively low. Henceforth, the blowdown code accuracy is evaluated against the blowdown experiments on the CLI features. Considered experiments consist of four separate effect tests of THTF105, 151, 160, and 162 and for integral effect tests of LOBI A1-66, LOFT L2-2, L2-3, and LP-02-6. Code assessment calculations against separate effect tests and integral effect tests are described in Appendices C and D, respectively.

Figure 4-7 shows the calculated code accuracy for the blowdown PCT. In the case of THTF, the measured PCT was obtained at 1.397 m (55 in.) or 1.957 m (77 in.) elevations. Cladding temperatures at these two elevations are very comparable. Cladding temperatures at these two elevations and their correspondents are used in the evaluation. From four THTF tests, [ ]^{TS} data

sets were obtained. In the case of LOBI, the data of measurement locations No. 5, 6, 7 and 8, of which elevations are 1.2, 1.7, 2.2, and 2.7 m from the bottom of the active core region, respectively, were obtained. Linear power and measured cladding temperatures at these elevations are very similar to each other. Two data sets were taken from each LOFT experiment. Cladding temperatures measured at the corresponding elevations to Nodes 4 and 5 were higher than other measured temperatures in case of L2-2 while cladding temperatures measured at the corresponding elevations to Nodes 3 and 4 were higher than others in case of the other LOFT experiments. Data from Nodes 4 and 5 or 3 and 4 are used for the LOFT experiments. Total data points for the IETs are [ ]^{TS}.

When all [ ]^{TS} data sets are considered, the RELAP5 code is found to over-predict the measured data by [ ]^{TS}. The one-sided 95 % limit of blowdown PCT is [ ]^{TS}.

4.3.1.2 Reflood Code Accuracy

In the evaluation of the reflood code accuracy, 27 separate effect tests (i.e., 17 FLECHT-SEASET tests, 7 NEPTUN tests, and 3 ATLAS tests) and 7 integral effect tests (i.e., LOFT L2-2, L2-3, L2-5, LP-02-6, CCTF C2-4, PKL-IIb5, and Semiscale S-06-3) are considered.

The maximum clad temperatures of NEPTUN were measured at various locations of No. 3, 4, and 5 in general depending on experimental conditions. These locations correspond to 0.512 m, 0.744 m, and 0.976 m elevations from the bottom of the 1.68 m effective length. The two highest measurements from each NEPTUN test and their calculational correspondents are considered in this evaluation. Code assessment calculation against NEPTUN is described in Appendix C. In the case of FLECHT-SEASET, three data sets, one at a PCT location and two at neighboring measurement locations, are considered. Calculated temperatures are taken from the results given in Appendix C. Measurements of the FLECHT-SEASET experiments are concentrated at the central part of the core. Three elevations correspond to one or two nodes in the calculation.

In the case of ATLAS, the three highest measurements from each test and their correspondents are considered. ATLAS Tests 9 and 15 showed the three highest temperatures at 1.066 m, 1.271 m, and 1.329 m elevations from the bottom of the 1.905 m active core, while they were measured at 0.953 m, 1.066 m, and 1.329 m elevations in Test 11. Corresponding node numbers are 12, 14, and 15 for test 9 and 15, and 11, 12, and 15 for Test 11. Calculated values are taken from calculations in Appendix E. In the case of CCTF C2-4, the measured peak value at 2.44 m (96 in.) and its correspondent are considered. In the case of PKL-IIb5, the measured peak value at 2.5 m (98 in.) elevation and a comparable peak value at 1.95 m (77 in.), and their correspondents, are considered. In the case of Semiscale S-06-3, the measured peak value at 0.74 m (29 in.) and the neighboring measurement at 0.71 m (28 in.) are selected and compared with their calculational correspondents.

Figure 4-8 shows the reflood code accuracy evaluated using [ ]^{TS} data sets. The code over-predicts the clad temperatures by [ ]^{TS}.

4.3.2 Check Data Covering (Step 9.2)

Data covering is checked to confirm the variety, number, and ranges of code uncertainty parameters. If the code uncertainty is quantified using all the code uncertainty parameters in accordance with the bottom-up approach of NUREG-1230 [19], this checking process may not be necessary. In the top-down approach, however, it is necessary to confirm the number of uncertainty parameters with respect to the practicality of the method. Identification and ranking of the phenomena and subsequent selection of uncertainty parameters are dependent on the subjective decision of experts in the field. Accordingly, the objective basis of the determination of the number and the ranges of the parameters needs to be provided.

In principle, this covering check is performed for all the experiments considered in the code accuracy evaluation, especially for the cases where code predictions are lower than the measured peak values. A set of uncertainty parameters confirmed by this covering check can produce the uncertainty encompassing code accuracy.

CAREM uses the non-parametric order statistics to estimate the uncertainty propagation.

CAREM provides three values (i.e., peak cladding temperature, peak local oxidation, and core-wide hydrogen generation) for the comparison with the acceptance criteria of 10 CFR 50.46(b). As a results, there are three code output parameters of interest.

As described in reference [23], the equation used to determine the number of computer code runs needed for three parameters, assuming a one-sided tolerance interval is given below

$$\beta = \sum_{j=0}^{N-p} \binom{N}{j} \gamma^j (1-\gamma)^{N-j} \quad (4\text{-}1)$$

where, β: confidence level

γ: probability

N: number of computer code runs

p: number of output parameters

For the case where p=3, and a 95 % probability and 95 % confidence level, the number of computer code runs (N) becomes 124. In this case, the extreme values (rank=1) are used as upper tolerance limits. However, the application of extreme values would cause following issues [24];

- The extreme values are subject to large variability.
- The sensitivity results will be less reliable.

Based on the above arguments, CAREM adopts p=5 instead of p=3 with 3rd order PCT, 1st order PLO, and 1st order CWO. Inserting p=5, γ=0.95, and β=0.95 to Equation 4-1 yields the necessary sample size which is 181.

Consequently, 3rd order value for PCT and 1st order values for CWO and PLO of 181 SRS calculations are chosen for licensing values in CAREM.

4.3.2.1 Check Blowdown Covering

SRS calculations were performed against the test data obtained from THTF, LOFT, and LOBI in order to check whether the calculations can cover the measured blowdown PCTs.

The eight code uncertainty parameters used for checking the blowdown covering against the THTF tests are: [

]TS. Because the LOFT and LOBI tests were integral effect tests performed for whole transients of the LBLOCA, other code parameters, which are used during the reflood period, and some system parameters are additionally considered for these tests. The effects of additional code parameters on the blowdown calculation are minimal. Uncertainty parameters used for checking the covering against each test are listed in Appendices C and D for the THTF, and LOBI and LOFT, respectively.

A set of uncertainty parameters is randomly sampled 181 times along their probability distribution functions, and the same numbers of calculations are performed. SRS calculations and measured data from the THTF Test 105 and Test 160 are compared in Figure 4-9 and Figure 4-10, respectively. Out of four sets of THTF SRS calculations in Appendix C, the above two are excerpted for examples, as they have the highest and the lowest rod power. Squared markings represent the upper-bound of the measurement. It is confirmed that the third highest value out of the 181 calculations covers the upper-bound of the measurements.

Because the results of the base case calculations of the LOFT experiments, except L2-5, already over-predicted their measured PCTs, SRS calculations of the other three experiments are not necessary in principle. However, since the LOFT experiments are very important integral effect tests conducted using nuclear fuel rods, SRS calculations were performed for all four LOFT experiments in order to check the reflood performance of the code. The results are shown in Figure 4-11 to Figure 4-14 for L2-2, L2-3, L2-5, and LP-02-6, respectively. The covering of the measured PCTs are confirmed through these figures.

Against the LOBI A1-66 experiment, the results of the SRS calculations cover the measured PCT, as shown in Figure 4-15.

4.3.2.2 Check Reflood Covering

Reflood covering is tested against the ATLAS, FLECHT-SEASET, LOFT, NEPTUN, Semiscale, PKL, and CCTF tests. Eight code uncertainty parameters related to reflood core heat transfer, such as [

]^{TS} used in all SRS calculations of the tests above. In addition to the eight parameters, [ ]^{TS} were also considered in the SRS calculations of each test. The uncertainty parameters used for checking the covering against each test are listed in Appendices C (for FLECHT-SEASET, NEPTUN, PKL, and CCTF), D (for LOFT and Semiscale), and E (for ATLAS).

Out of the three sets of ATLAS SRS calculations in Appendix E, SRS calculations and measured data of ATLAS Test 15 are compared representatively in Figure 4-16. For the ATLAS SRS calculations, [

]^{TS}. It is confirmed that the third highest value out of the 181 calculations covers the upper-bound of the measurements. The data coverings for the other two sets of SRS calculations against the ATLAS Test 9 and 11 were also confirmed, as described in Appendix E.

The 17 FLECHT-SEASET tests are divided into five groups in order to investigate the effects of the reflooding rate, system pressure, initial rod temperature, bundle power, etc., as listed in Table 4-6. Out of these 17 tests, 12 tests are needed to confirm data covering, because the results of the base calculations of these tests under-predict the measured PCTs as marked in the last column of Table 4-6. For the purpose of investigating the effects of uncertainty parameters and their ranges, however, SRS calculations were performed for all 17 tests. Test specific uncertainties of such aspects as [ ]^{TS} were additionally considered in SRS calculations. Representative results of the SRS calculations of Test 31504 from the “reflooding rate group,” Test 32013 from the “system pressure group,” Test 30817 from the “initial rod temperature group,” Test 34524 from the “bundle power group,” and Test 33338 from the “group made up of the other conditions”, are compared with the measured PCTs, as shown in Figure 4-17 to Figure 4-21. Results of the SRS calculations for the other tests are presented in Appendix C. The results of all 17 sets of SRS calculations are confirmed to cover the measured PCTs.

For the entire LOFT tests considered in this report, the calculated reflood cladding temperatures are

sufficiently higher than the measured cladding temperatures, as shown in Figure 4-11 to Figure 4-14. This is due to combined effects, such as the complexity of the system and propagation of the uncertainties of the blowdown calculation. The results of SRS calculations for NEPTUN 5050 and 5036 are shown in Figure 4-22 and Figure 4-23, respectively. Out of the seven sets of NEPTUN SRS calculations shown in Appendix C, the above two are excerpted as examples as they have the highest and the lowest reflooding rates, 15 cm/s and 1.5 cm/s, respectively. The results of all seven sets of the SRS calculations are confirmed to cover the measured PCTs. Results of SRS calculations for the Semiscale S-06-3, PKL-IIb5, and CCTF C2-4 tests are shown in Figure 4-24, Figure 4-25, and Figure 4-26, respectively. Data covering is confirmed for all of these tests.

4.4 Determination of Scale Bias Coverings (Step 10)

4.4.1 ECC Bypass Covering

4.4.1.1 ECC Bypass during the Refill Period

The total amount of the ECC bypass is conservatively estimated as [ ]^{TS} as described in Step 8.3. [ ]^{TS}. The effect on plant calculations is evaluated in Step 12.

4.4.1.2 ECC Bypass during the Early and Late Reflood Periods

As described in Step 8.3, the effect of the [ ]^{TS}.

4.4.2 Steam Binding Covering

As the RELAP5 code does not include a model to describe mechanical de-entrainment due to the internal structures in the upper plenum, [ ]^{TS} on plant calculations are evaluated in Step 12.

Table 4-1 Test Matrix

TS

Table 4-2 Test Matrix of the APR1400 Tests

TS

Table 4-3 Code Models and Parameters

TS

Table 4-4 RELAP5/MOD3.3 Model and Tests Used for the Assessment

RELAP5 MOD3.3 Model / Parameter	Tests
Gap conductance	Power burst
Core decay heat model	1979 ANS Standard for Decay Heat Power in Light Water Reactors
Critical flow model	Marviken
Two-phase pump head multiplier	CE pump, CREARE, Semiscale pump, W_pump, LOFT pump, Byron-Jackson, B&W
Two-phase pump torque multiplier	Semiscale
Critical heat flux, Vapor generation, Non-equilibrium heat transfer	Bennet experiment 5358, 5294, 5394 Royal Institute of Technology (RIT) Test 261 ORNL Bundle CHF Test 3.07.9B, 3.07.9N, 3.07.9W
Subcooled boiling	Christensen Subcooled boiling Test 15, Shoukri Subcooled Boiling Experiment
Dittus-Boelter Liquid/Vapor HTC	McAdams-Frost, Larsen and Ford, Kreith, Heineman, Morris-Whitman, Slecher-Rouse
Chen nucleate boiling HTC	Dengler-Addoms, Schrock-Grossman, Sani, Bennett et al, Wright
Chen transition boiling heat flux	B&W, Bennett, Bennett & Kearsey, Bertoletti, Bishop, Era, Jansson, Herkenrath
Bromley film boiling HTC	ADI data[1)]
Pressurizer model	MIT Pressurizer Test ST4
Interphase drag model	Dukler Air-Water Tests, FROJA, FRIGG, CISE, Kasai et al, ORNL TLTA, GEC TLTA, Hall et al, FLECHT-SEASET※), THETIS, FIST, Hughes, Carrier, ORNL THTF※), AERE Harwell, GE, Marviken, Petrick
Accumulator model	LOFT Accumulator blowdown test, VAPER※)
ECC bypass	UPTF※), CREARE, MIDAS※), ATLAS※)
Downcomer boiling	DOBO※), ATLAS※)
Steam generator heat transfer	ATLAS※)
Overall reflood phenomena	FLECHT-SEASET※), NEPTUN※), CCTF※), PKL※), ATLAS※)
Overall blowdown phenomena	THTF※)
Overall LOCA phenomena	LOFT※), Semiscale※), LOBI※)

※) Tests used for the code assessment conducted in this report.

1) Data tables are on file with the American Documentation Institute, Washington, D.C. Test conditions are described in page 132 of Reference [20].

Table 4-5 Joint 90 % Confidence Intervals for the Parabolic Rate Constants for Oxide Layer Growth

Percent Deviation from Expected Value at		
1,500 °C	1,250 °C	1,050 °C
+4.3 -4.1	+2.5 -2.4	+4.9 -4.7

Table 4-6 Test Matrix of FLECHT-SEASET

Group	Run	System Pressure (MPa)	Rod Temp. (°C)	Rod power (kW/m)	Flood rate (mm/s)	Coolant Temp (°C)	Radial power distribution	Prediction (Appendix C)
Flooding rate	31203(1)	0.28	872	2.3	38.4	52	Uniform	Under-predicted
	31302	0.28	869	2.3	76.5	52	Uniform	Under-predicted
	31504(2)	0.28	863	2.3	24.6	51	Uniform	Under-predicted
	31701	0.28	872	2.3	155.0	53	Uniform	Over-predicted
	31805	0.28	871	2.3	21.0	51	Uniform	Under-predicted
System pressure	31504	same as (2)						Under-predicted
	32013	0.41	887	2.3	26.4	66	Uniform	Under-predicted
	34209	0.14	889	2.4	27.2	32	Uniform	Over-predicted
Initial clad Temperature	30518	0.28	256	2.3	38.9	52	Uniform	Under-predicted
	30817	0.27	531	2.3	38.9	53	Uniform	Under-predicted
	31203	same as (1)						Under-predicted
	34420	0.27	1119	2.4	38.9	51	Uniform	Over-predicted
Bundle power	31021	0.28	879	1.3	38.6	52	Uniform	Under-predicted
	31203	same as (1)						Under-predicted
	34524	0.28	878	3.0	39.9	52	Uniform	Under-predicted
Others	31108	0.13	871	2.3	79.0	33	Uniform	Over-predicted
	32235	0.14	888	2.3	165.8/24.9/15.7	31	Uniform	Under-predicted
	32333	0.28	889	2.3	162/21	53	Uniform	Under-predicted
	33338	0.28	871	2.3/1.3	5.9/0.807 kg/s	52	Hot/cold	Over-predicted
	34006	0.27	882	1.3	15	51	Uniform	Under-predicted

TS

Figure 4-1 RELAP5/MOD3.3/K Nodalization of the APR1400

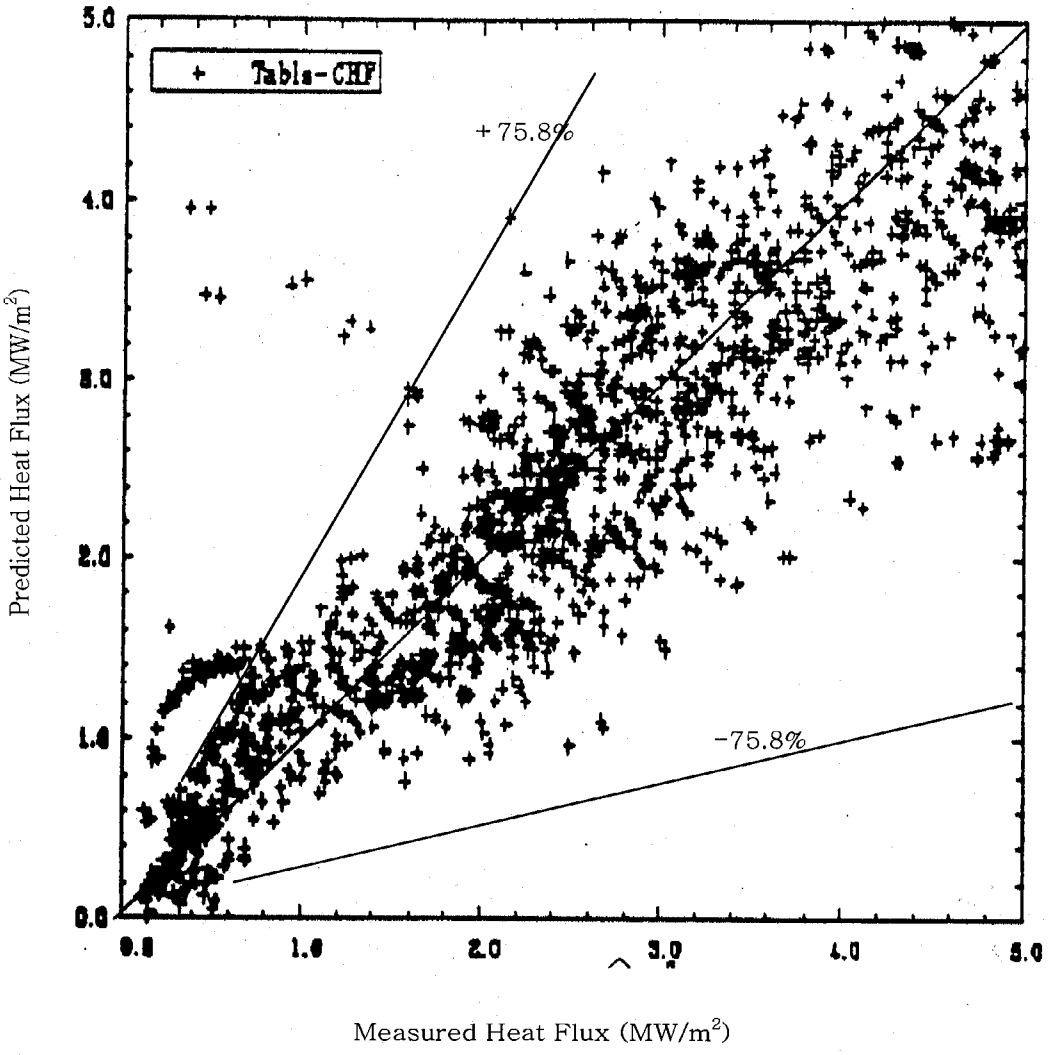

Figure 4-2 Comparison between the Data and the Predicted CHF Using the Lookup Table

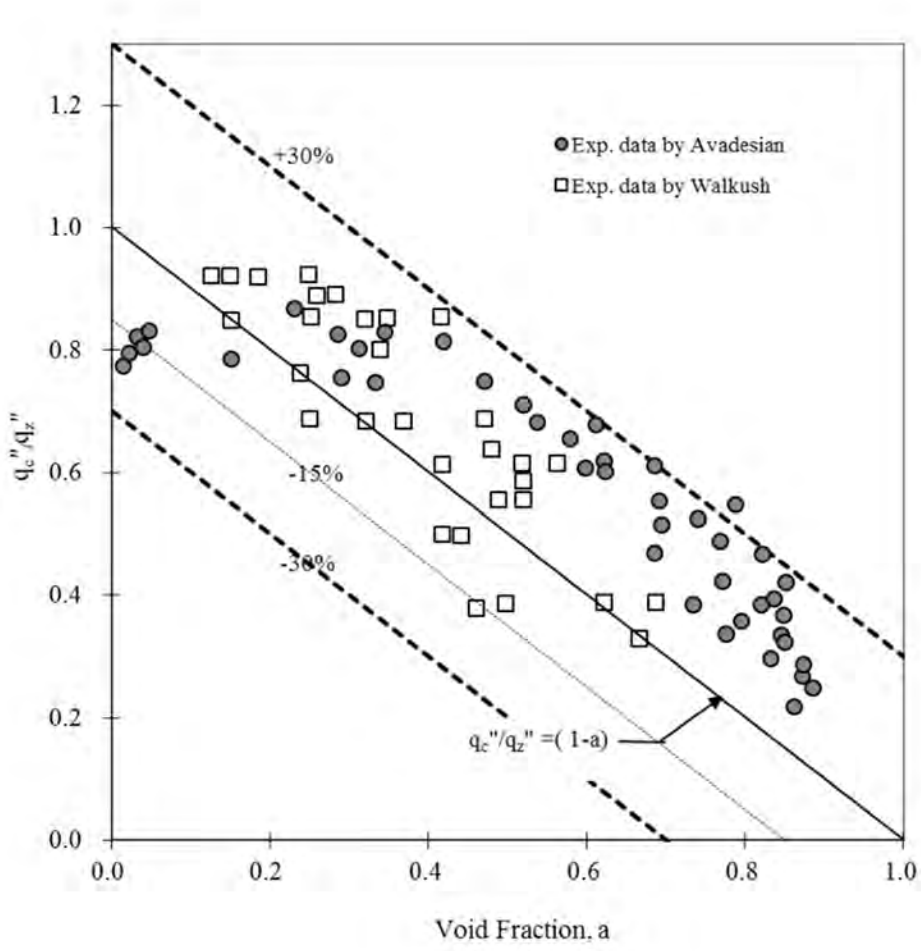

Figure 4-3 Uncertainty Ranges of the Modified Zuber Correlation

TS

Figure 4-4 Density Reactivity Change According to the Moderator Density Change

TS

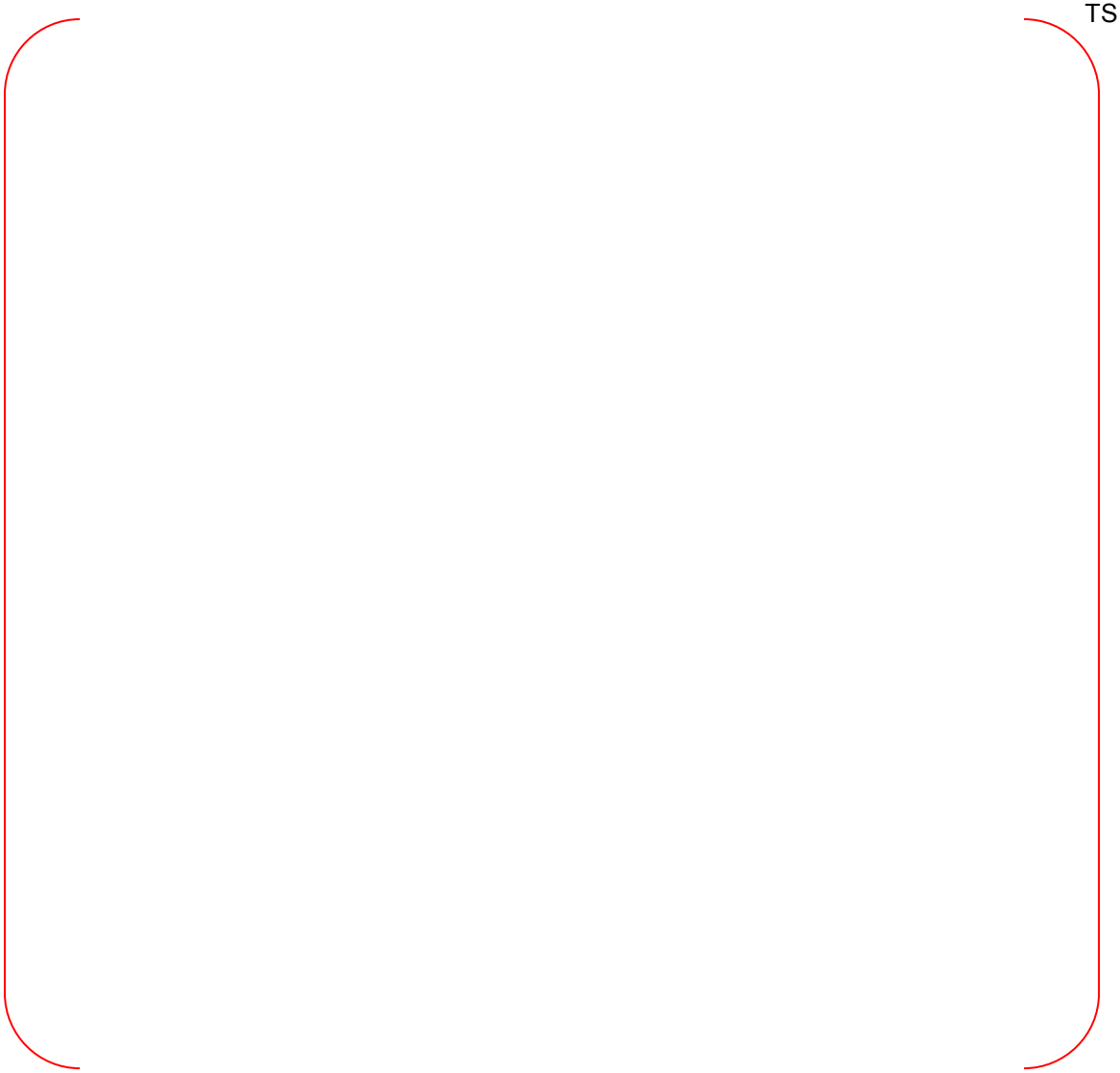

Figure 4-5 [ ]TS

TS

Figure 4-6 [ ]TS

TS

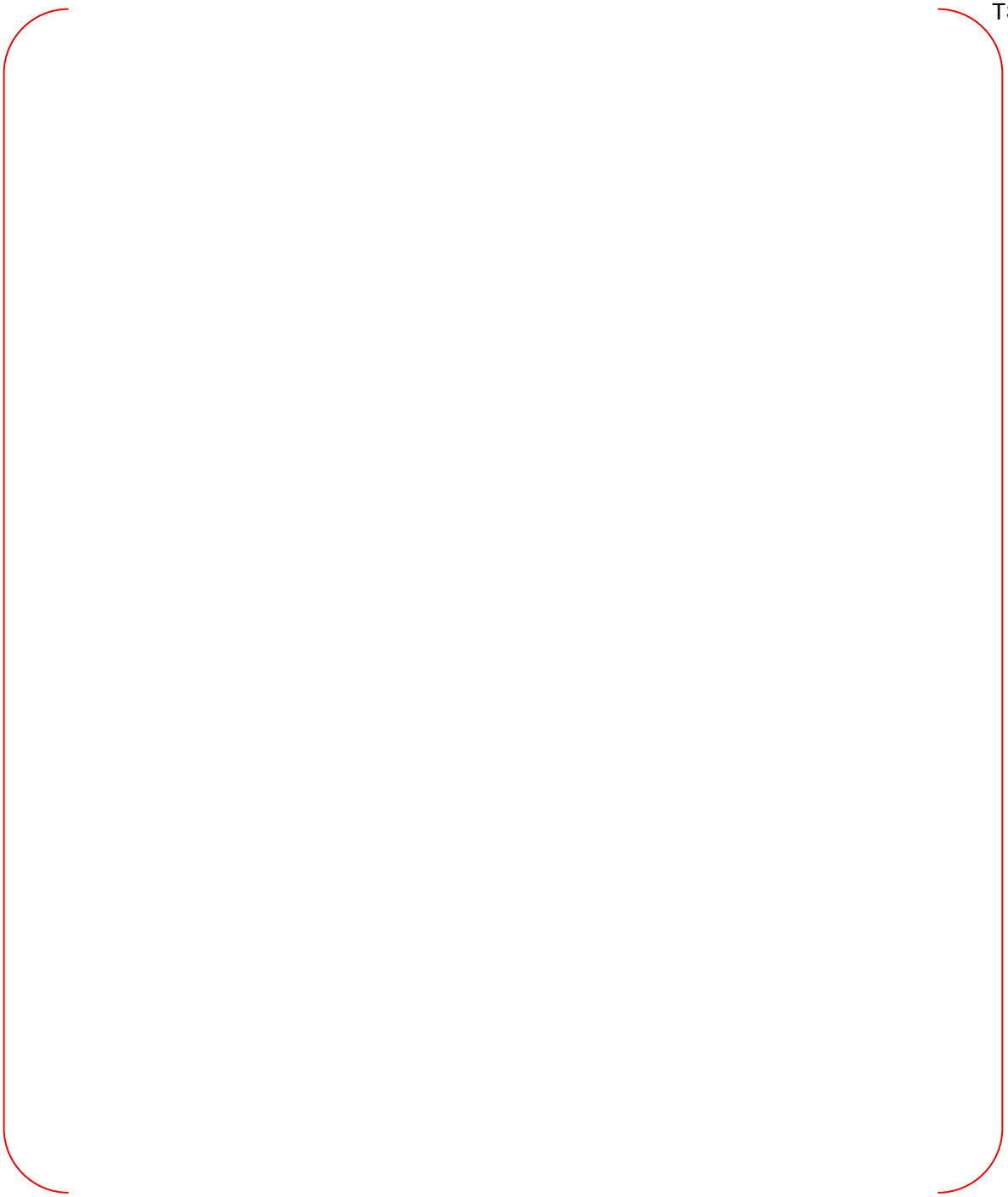

Figure 4-7 Code Accuracy during Blowdown Phase

TS

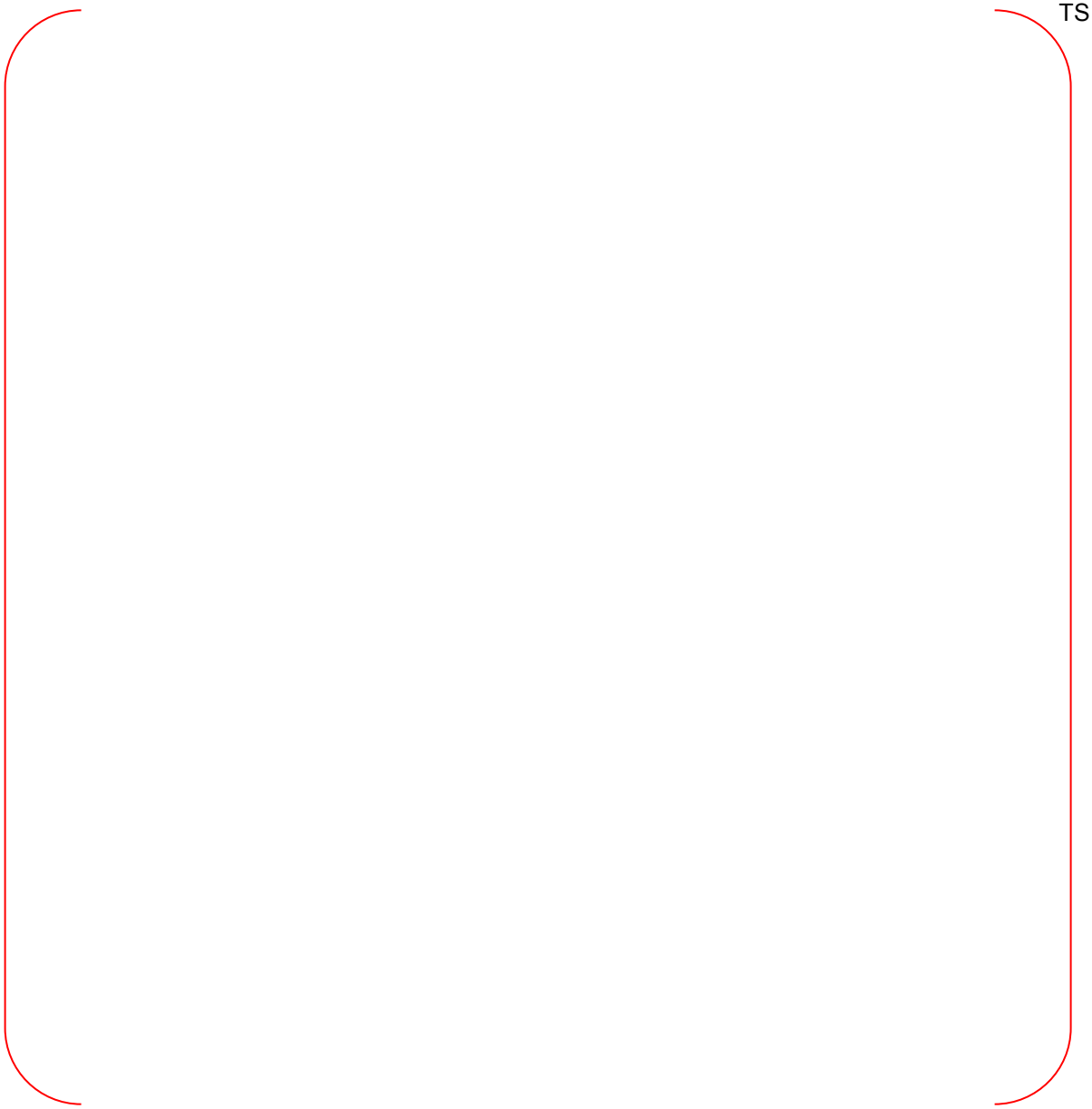

Figure 4-8 Code Accuracy during Reflood Phase

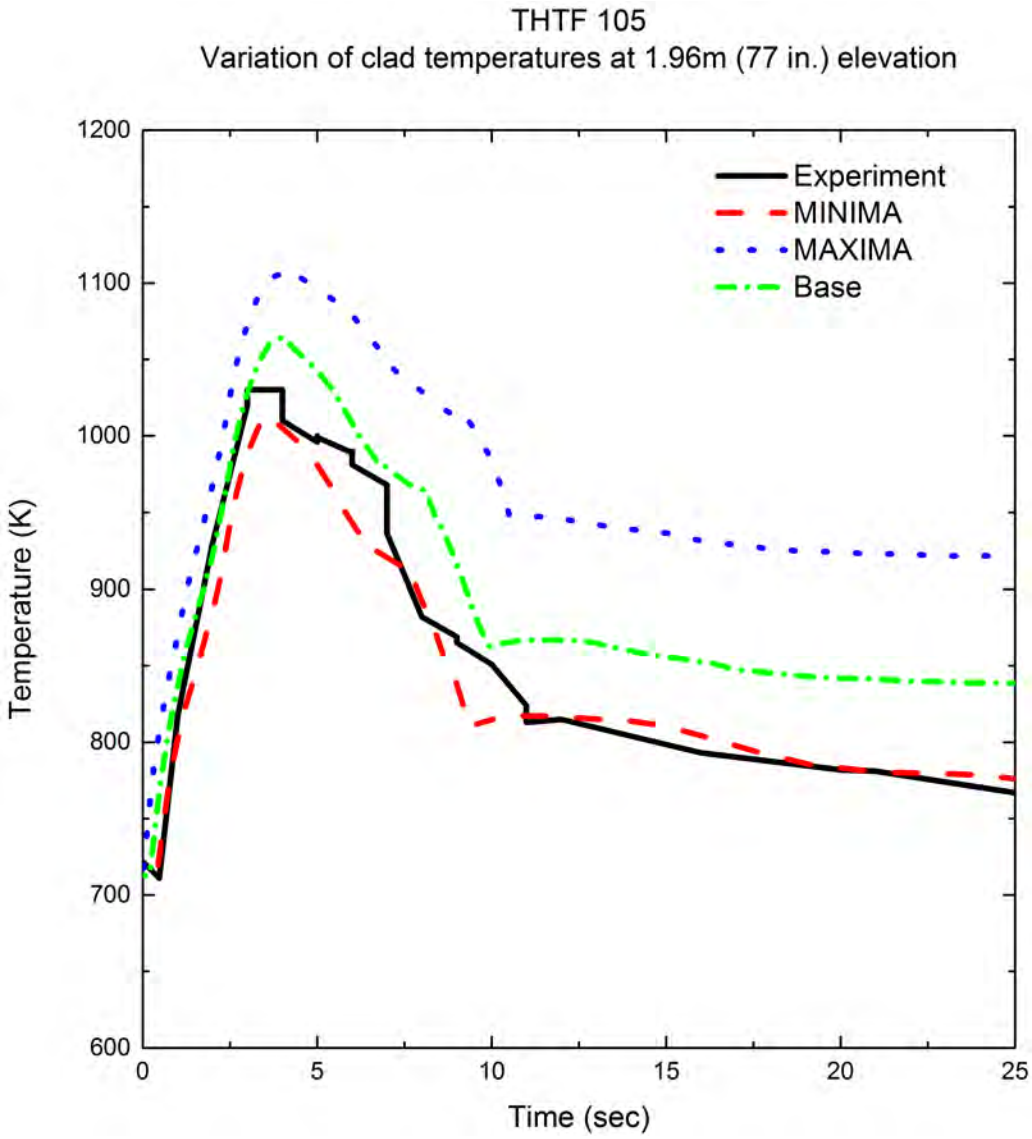

Figure 4-9 Results of the SRS Calculations for THTF 105

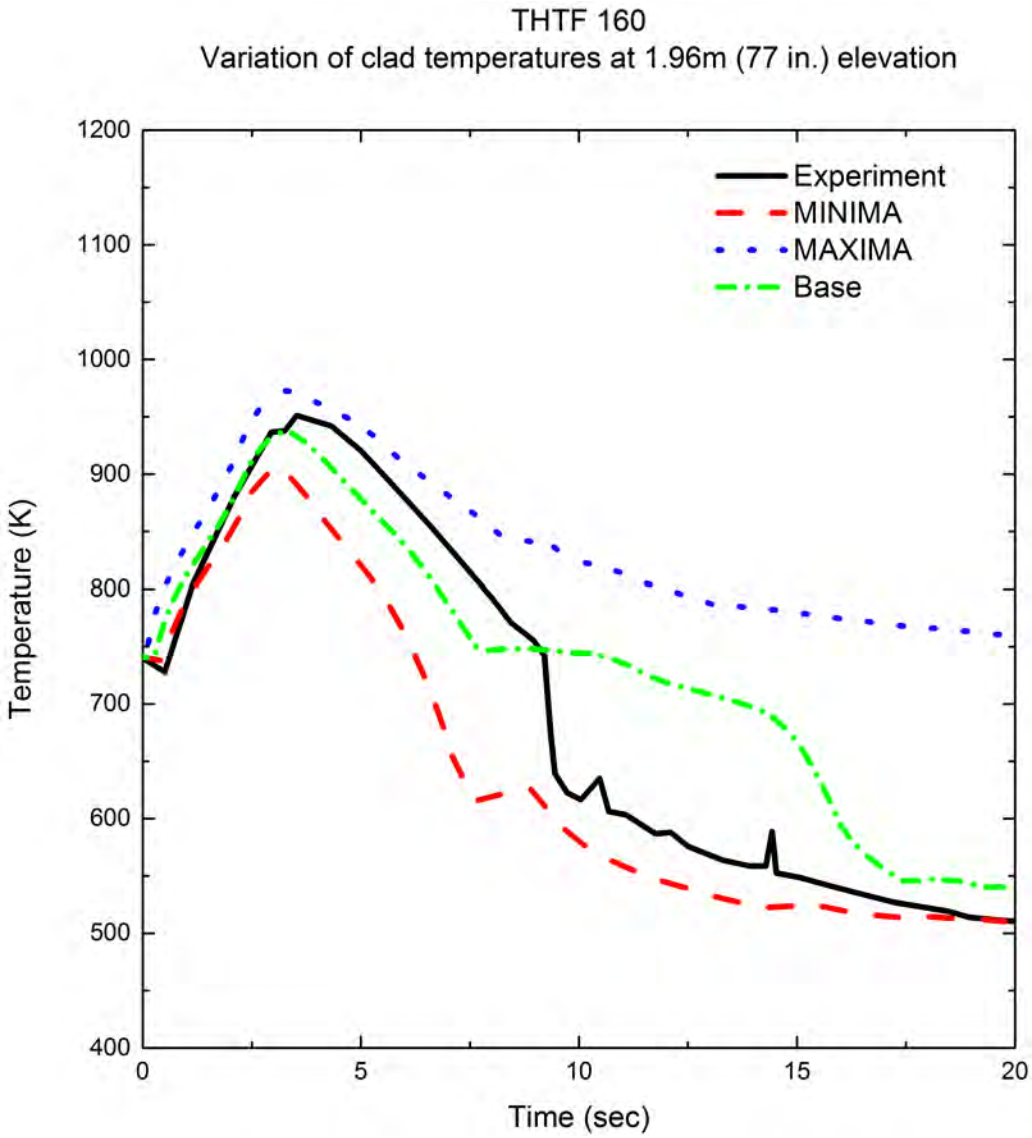

Figure 4-10 Results of the SRS Calculations for THTF 160

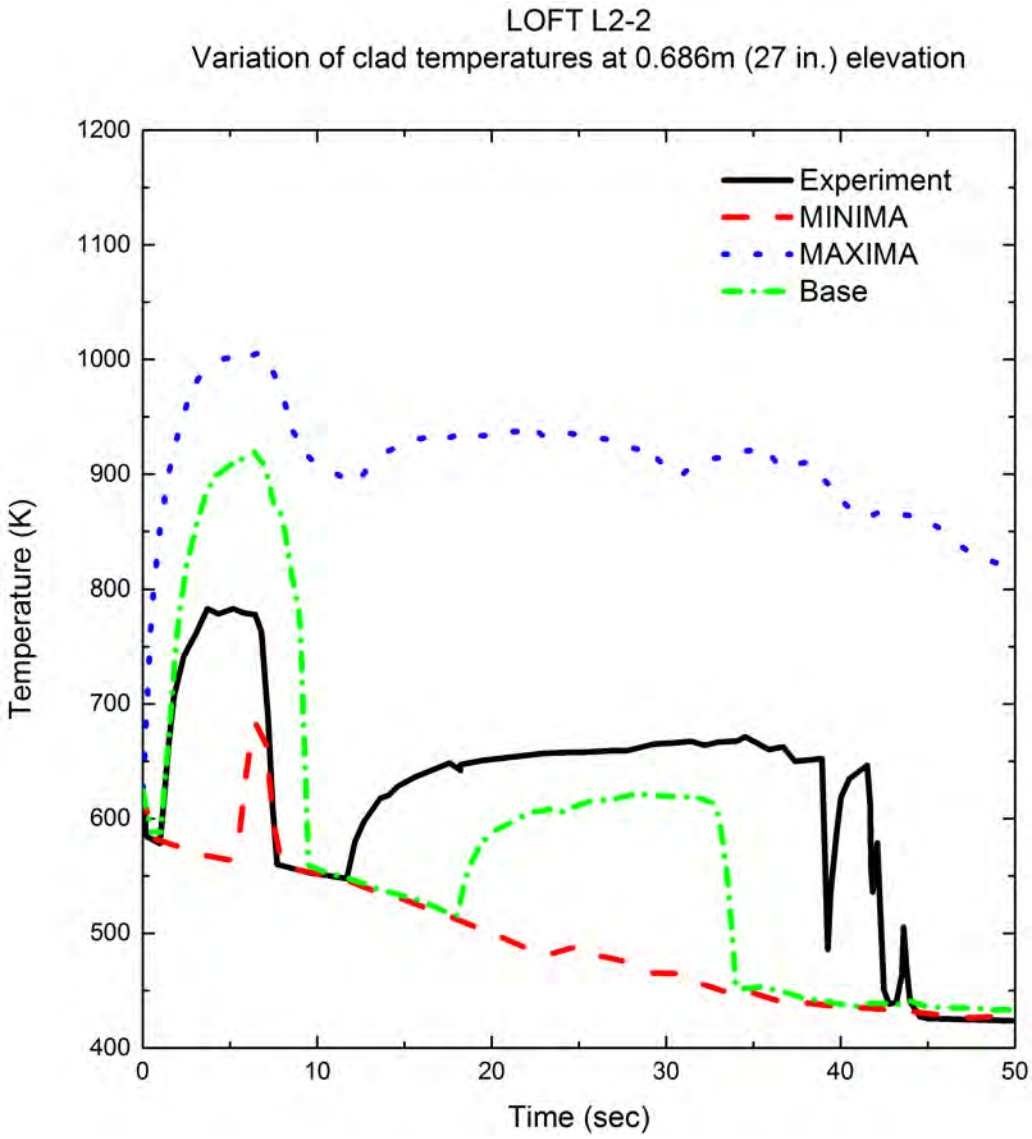

Figure 4-11 Results of the SRS Calculations for LOFT L2-2

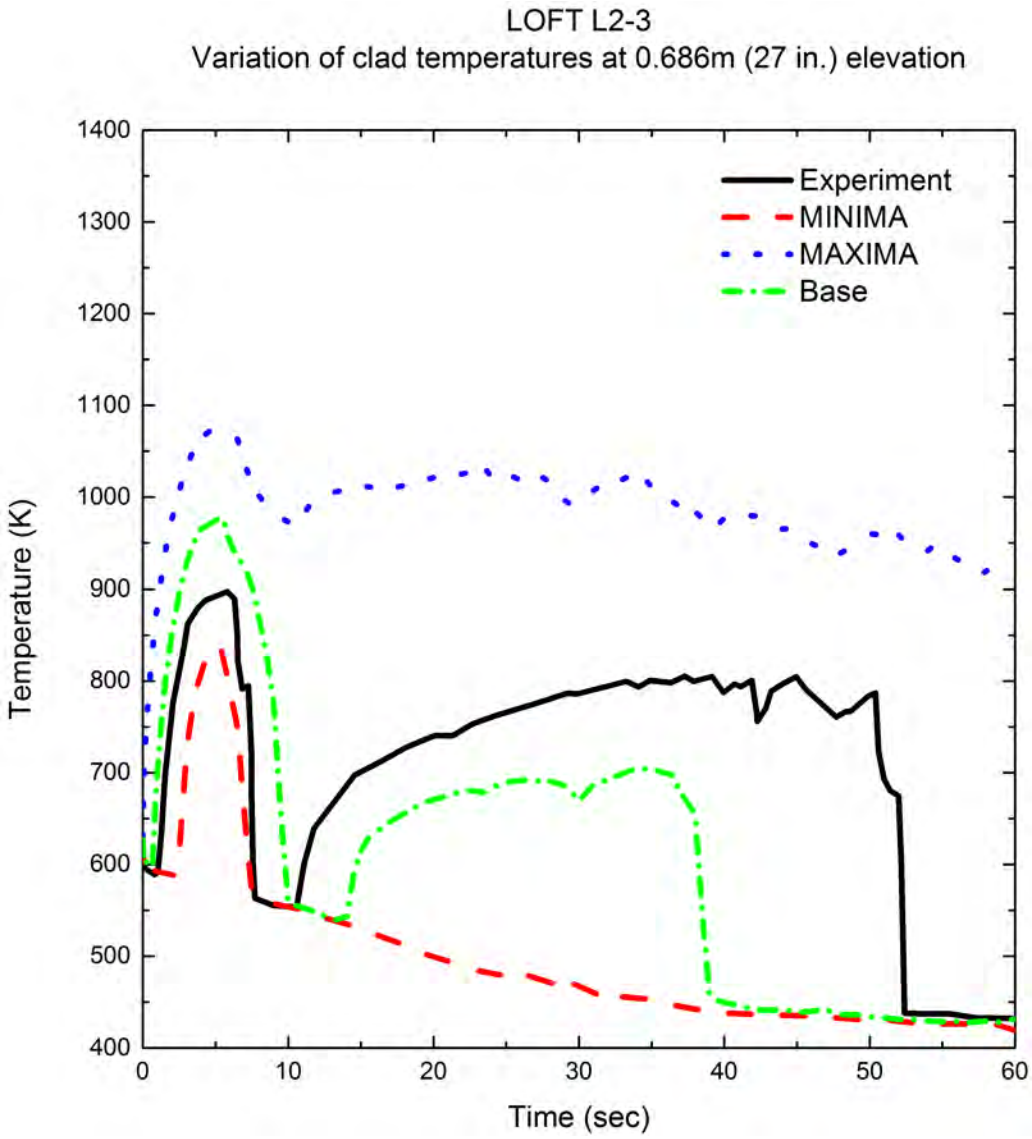

Figure 4-12 Results of the SRS Calculations for LOFT L2-3

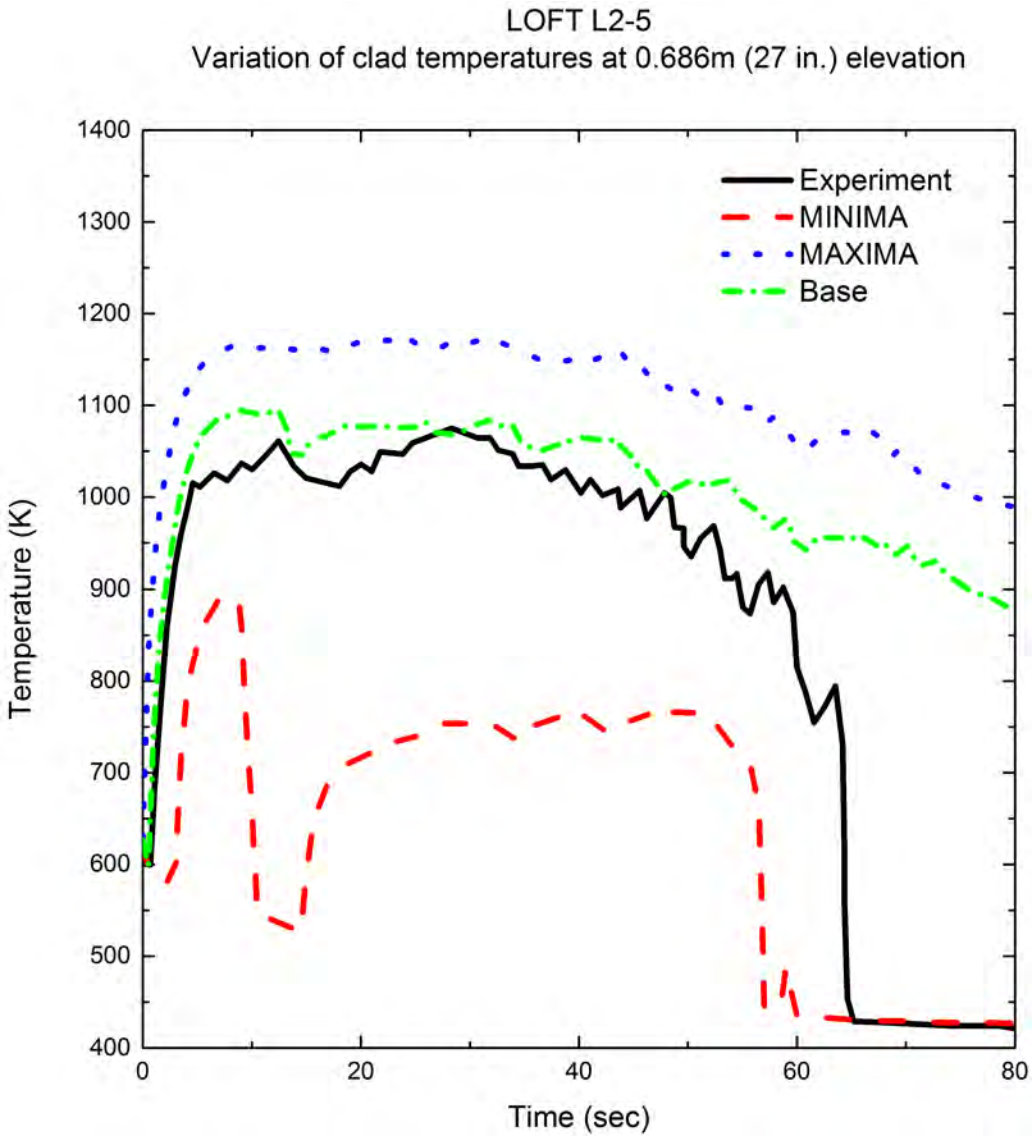

Figure 4-13 Results of the SRS Calculations for LOFT L2-5

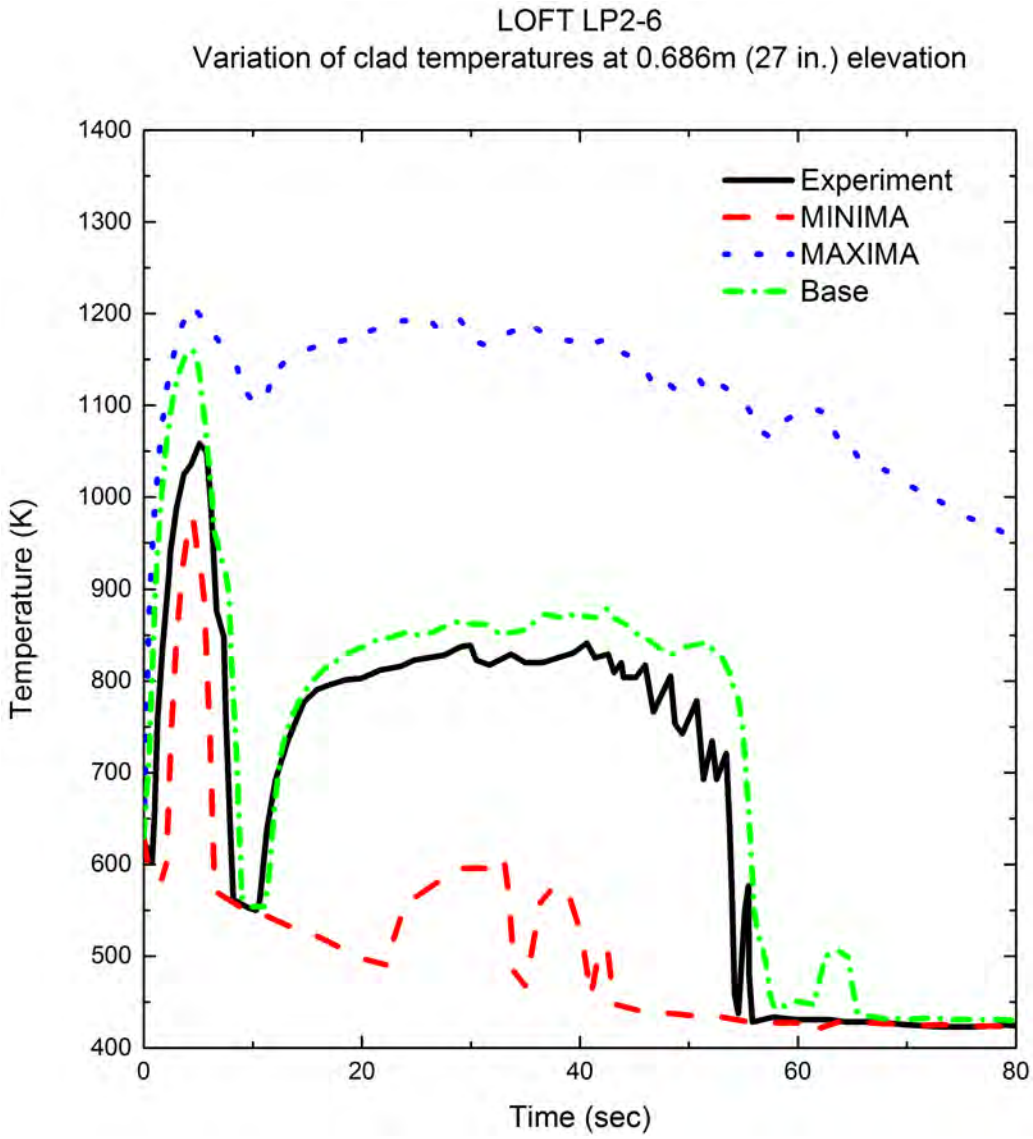

Figure 4-14 Results of the SRS Calculations for LOFT LP-02-6

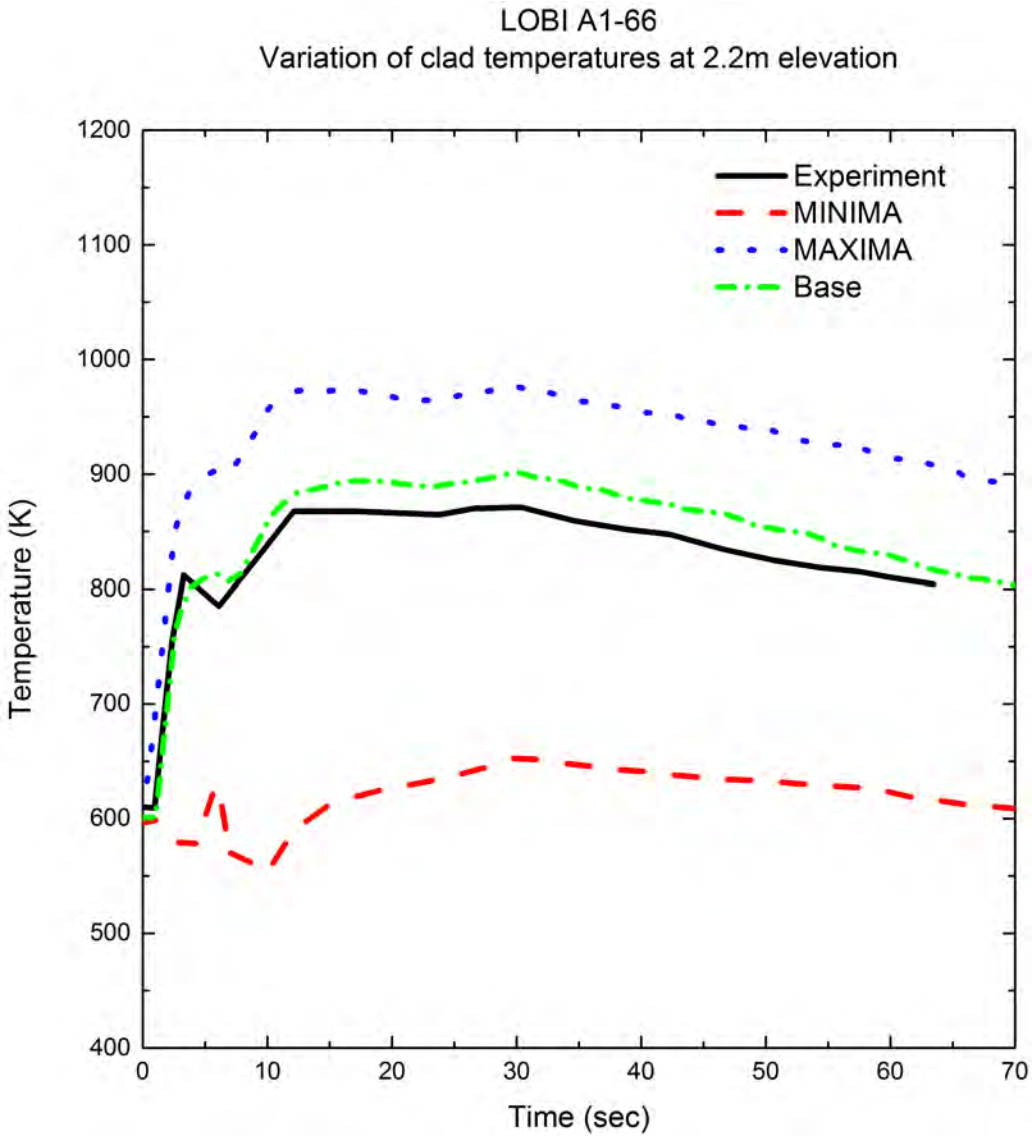

Figure 4-15 Results of the SRS Calculations for LOBI A1-66

TS

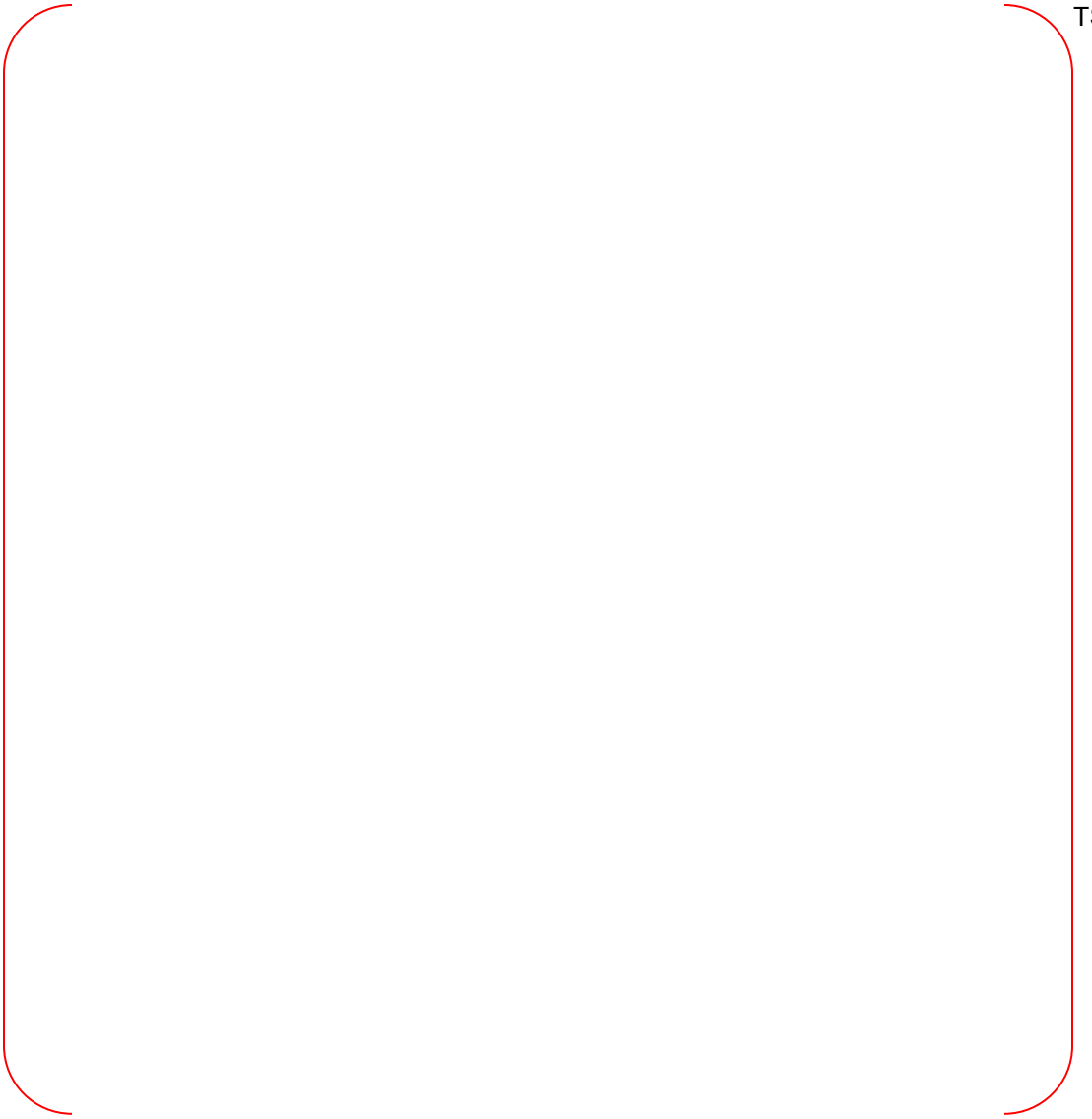

Figure 4-16 Results of the SRS Calculations for ATLAS 15

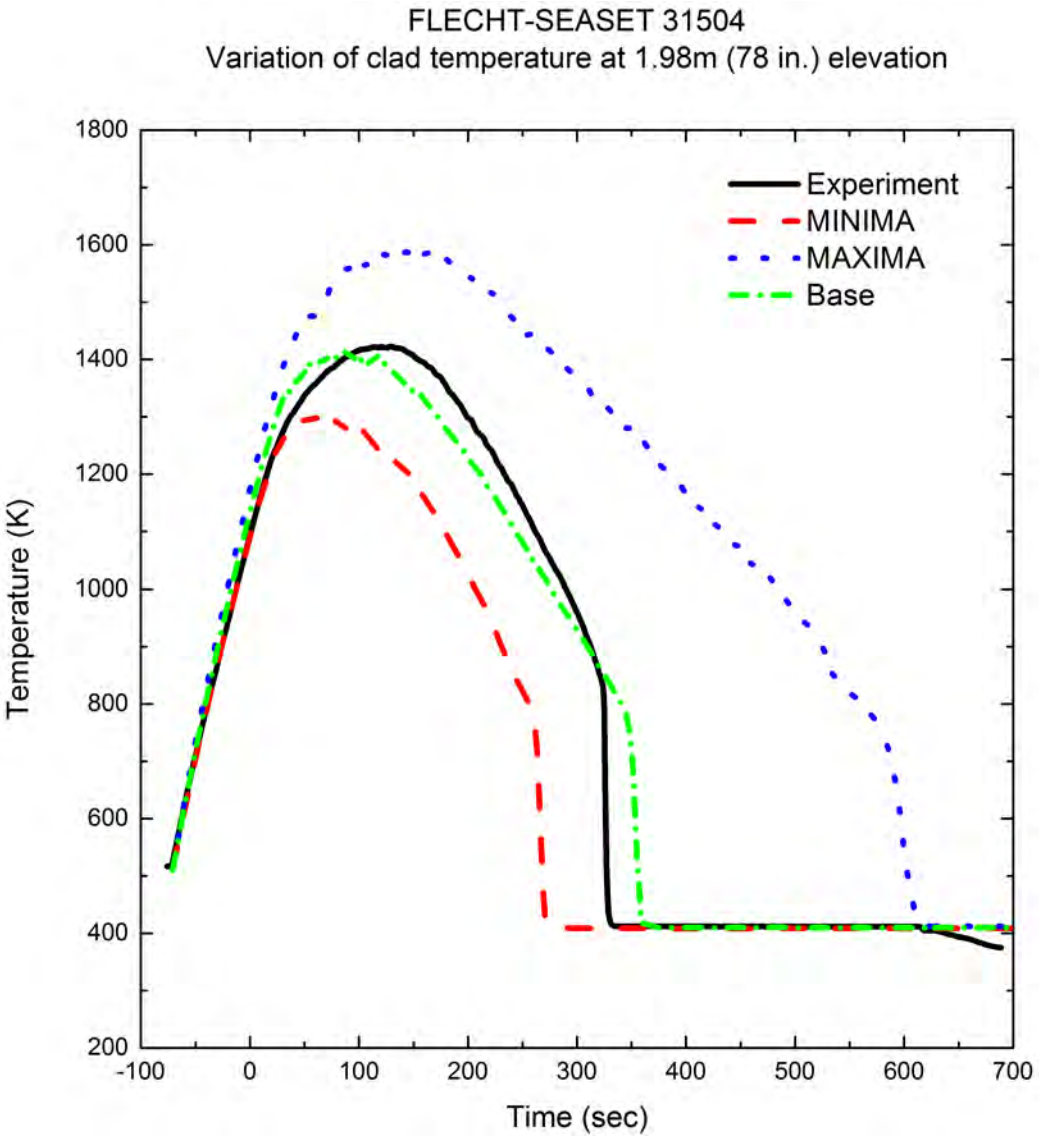

Figure 4-17 Results of the SRS Calculations for FLECHT-SEASET 31504

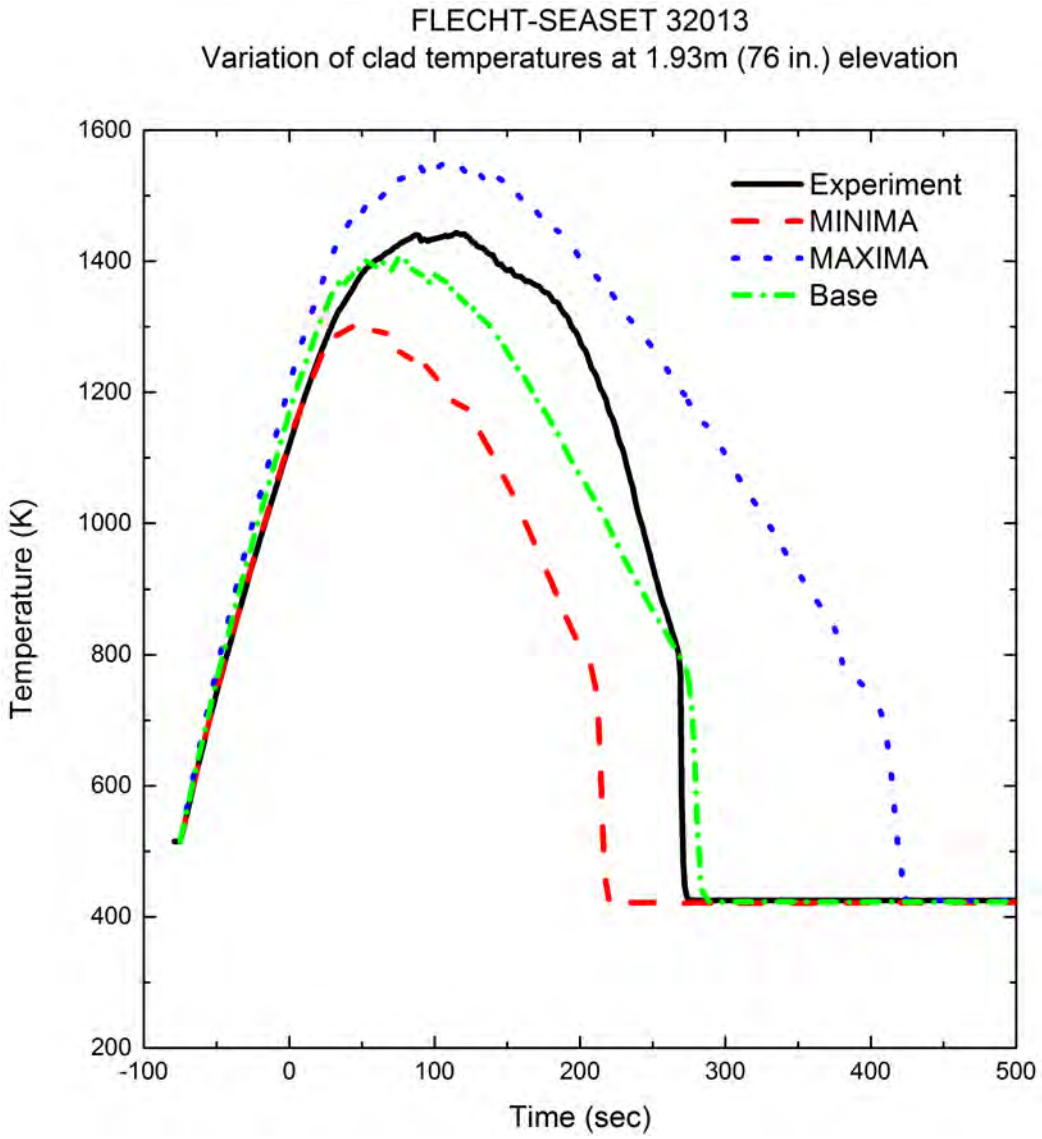

Figure 4-18 Results of the SRS Calculations for FLECHT-SEASET 32013

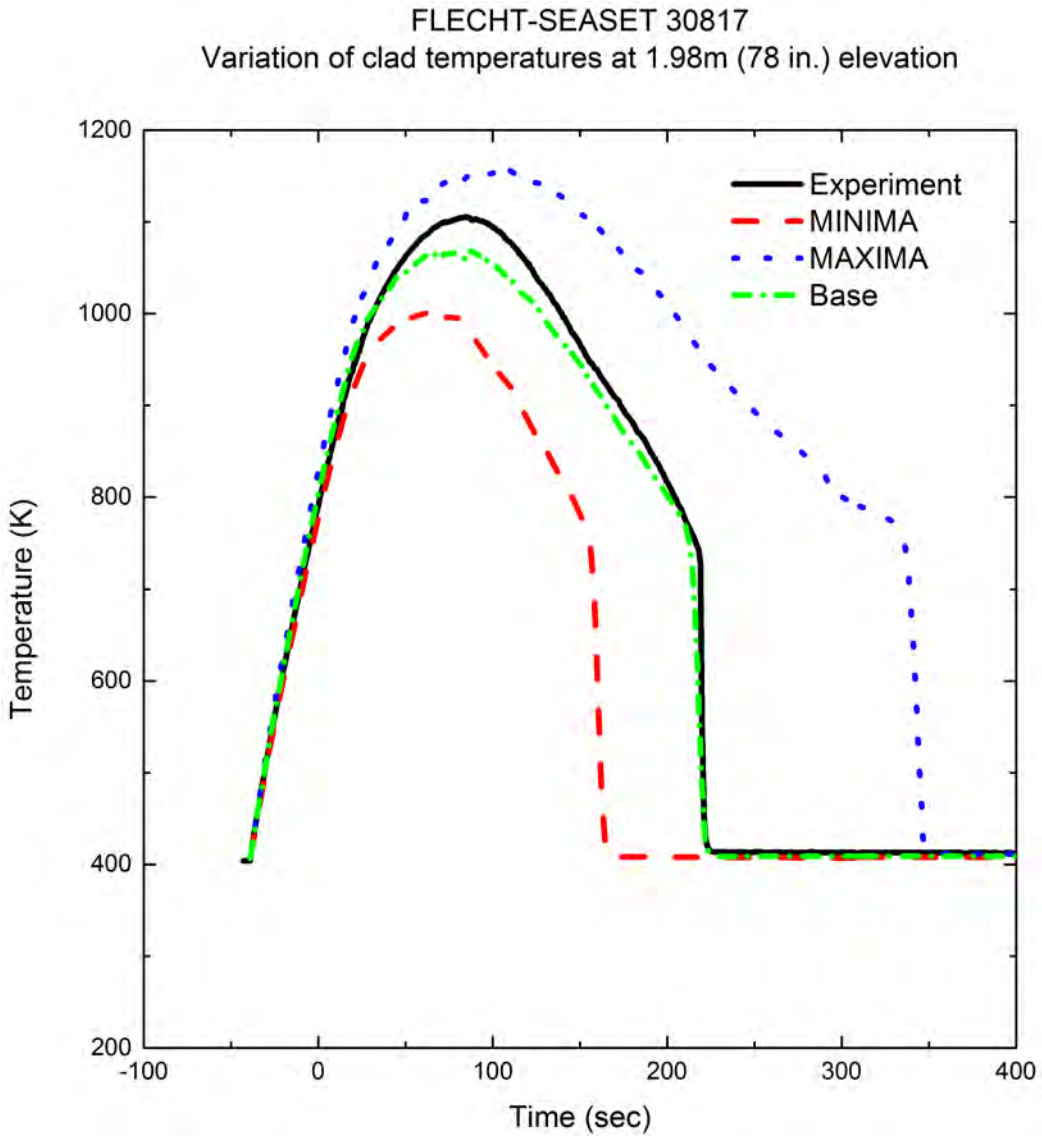

Figure 4-19 Results of the SRS Calculations for FLECHT-SEASET 30817

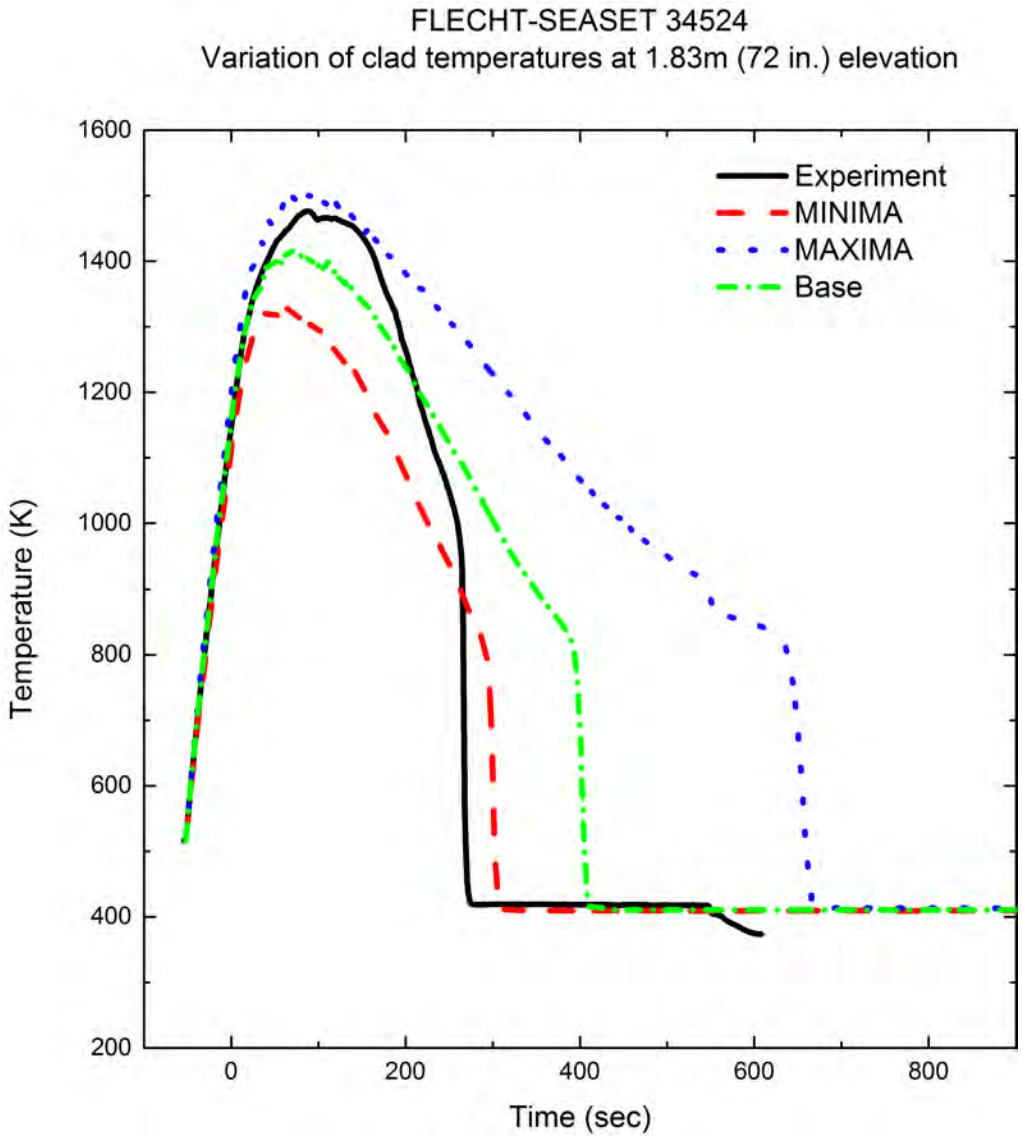

Figure 4-20 Results of the SRS Calculations for FLECHT-SEASET 34524

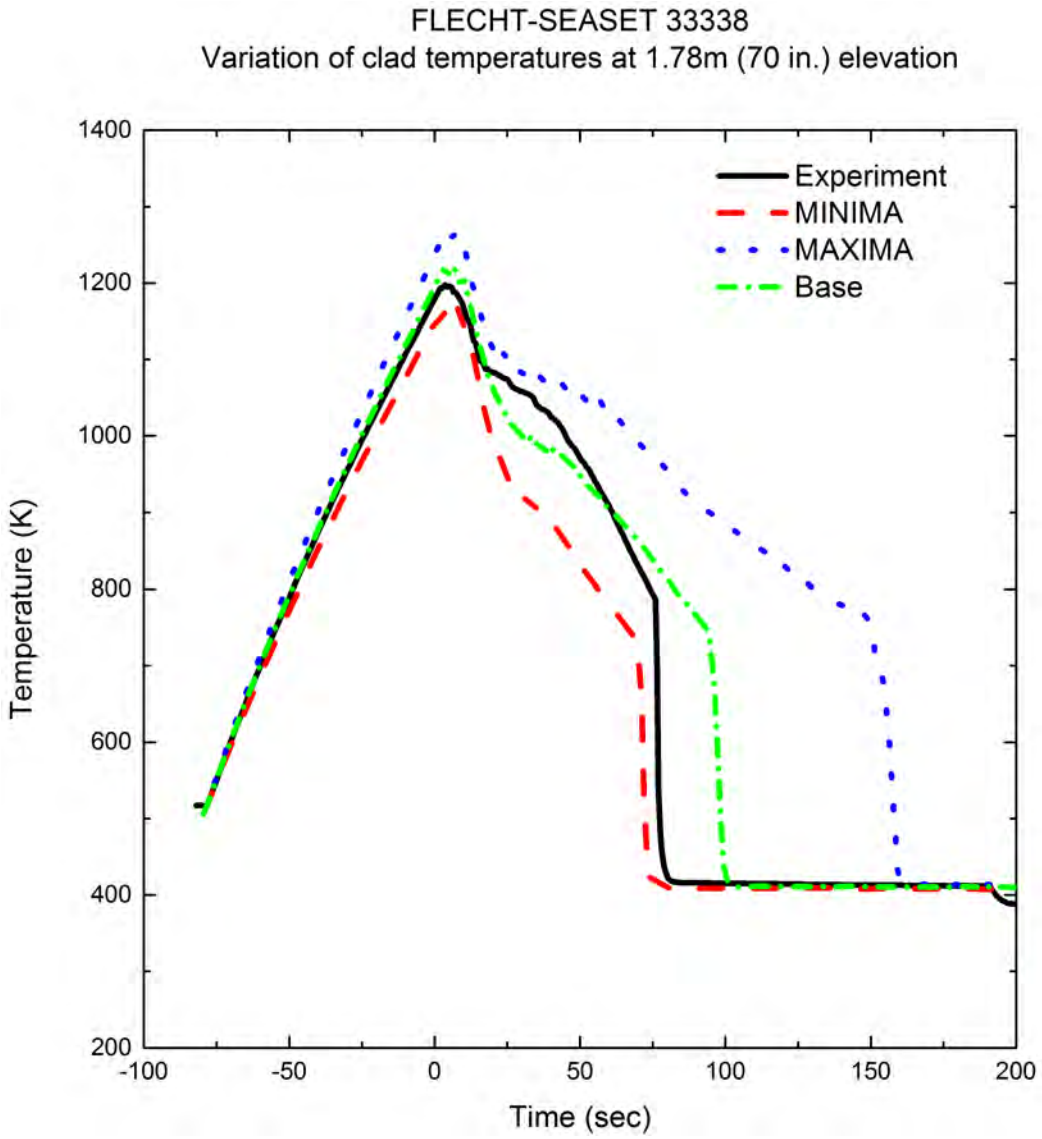

Figure 4-21 Results of the SRS Calculations for FLECHT-SEASET 33338

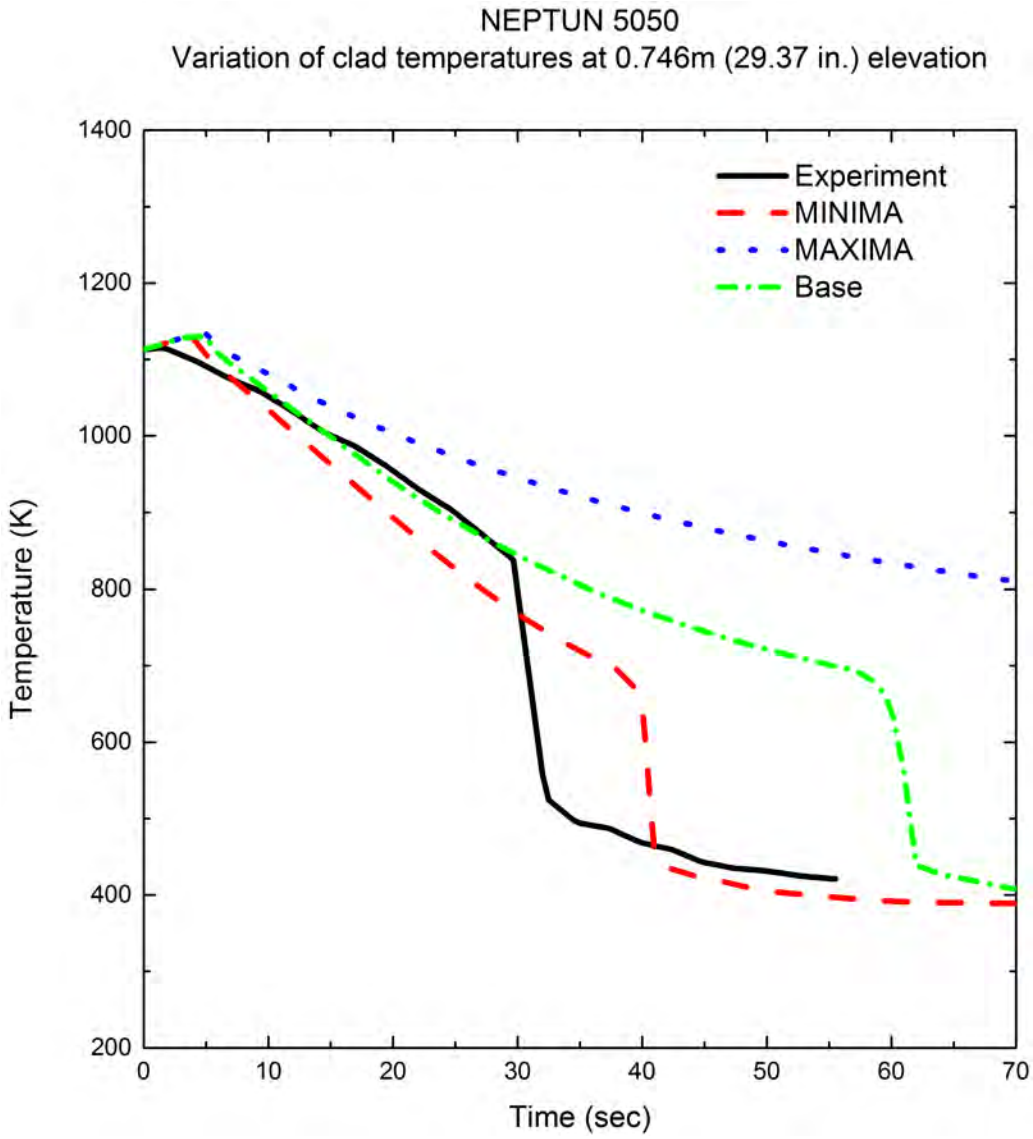

Figure 4-22 Results of the SRS Calculations for NEPTUN 5050

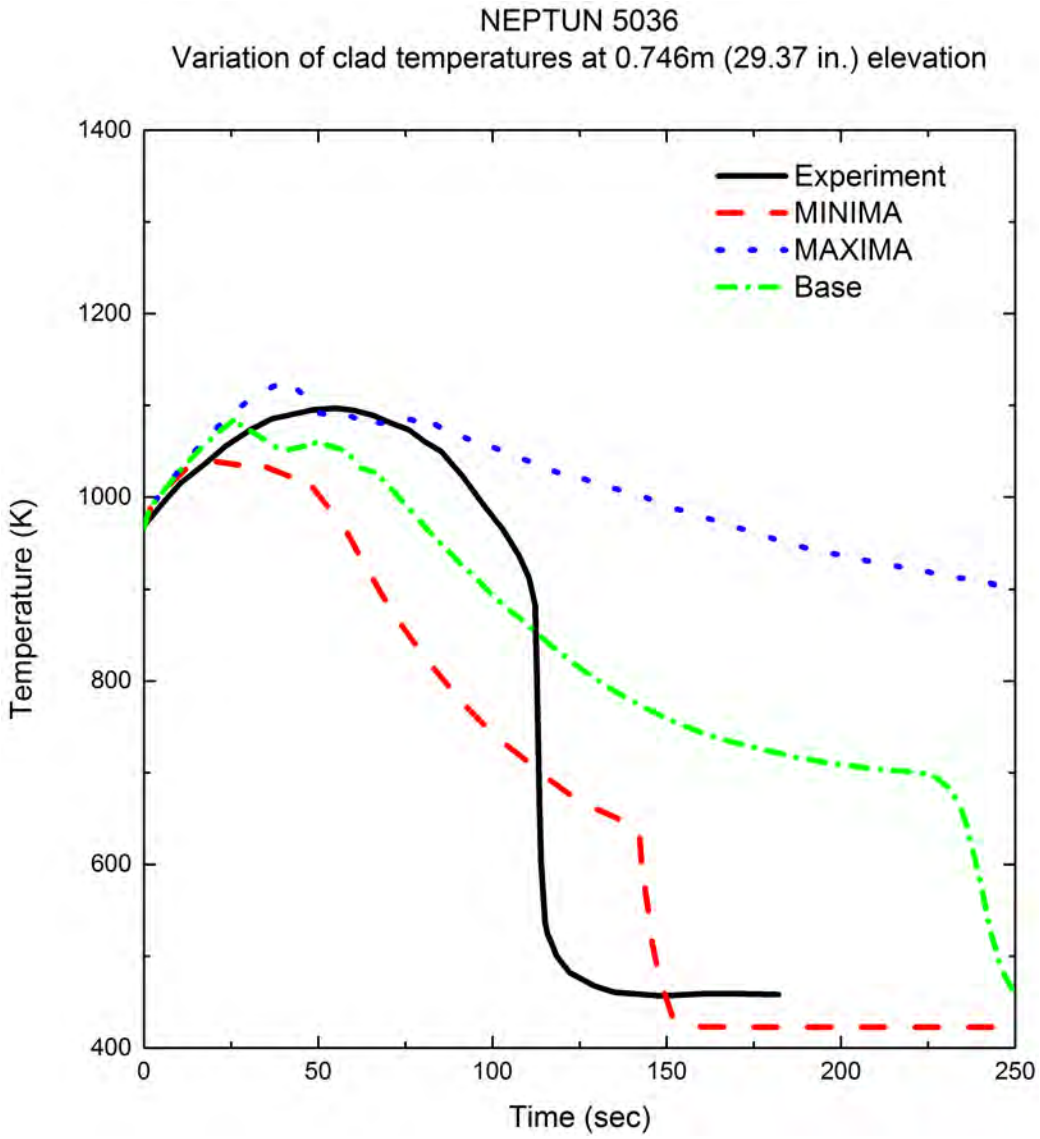

Figure 4-23 Results of the SRS Calculations for NEPTUN 5036

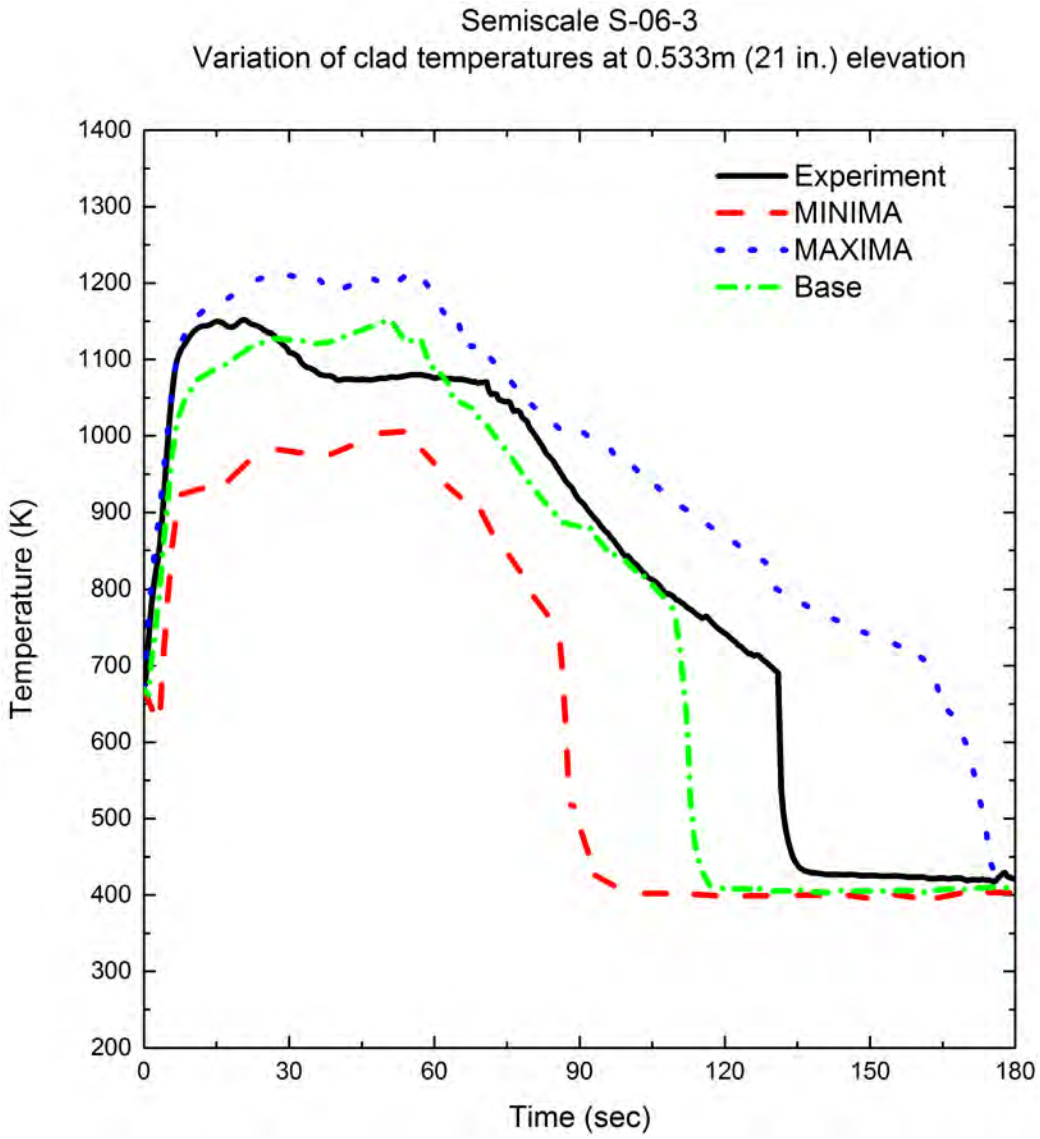

Figure 4-24 Results of the SRS Calculations for Semiscale S-06-3

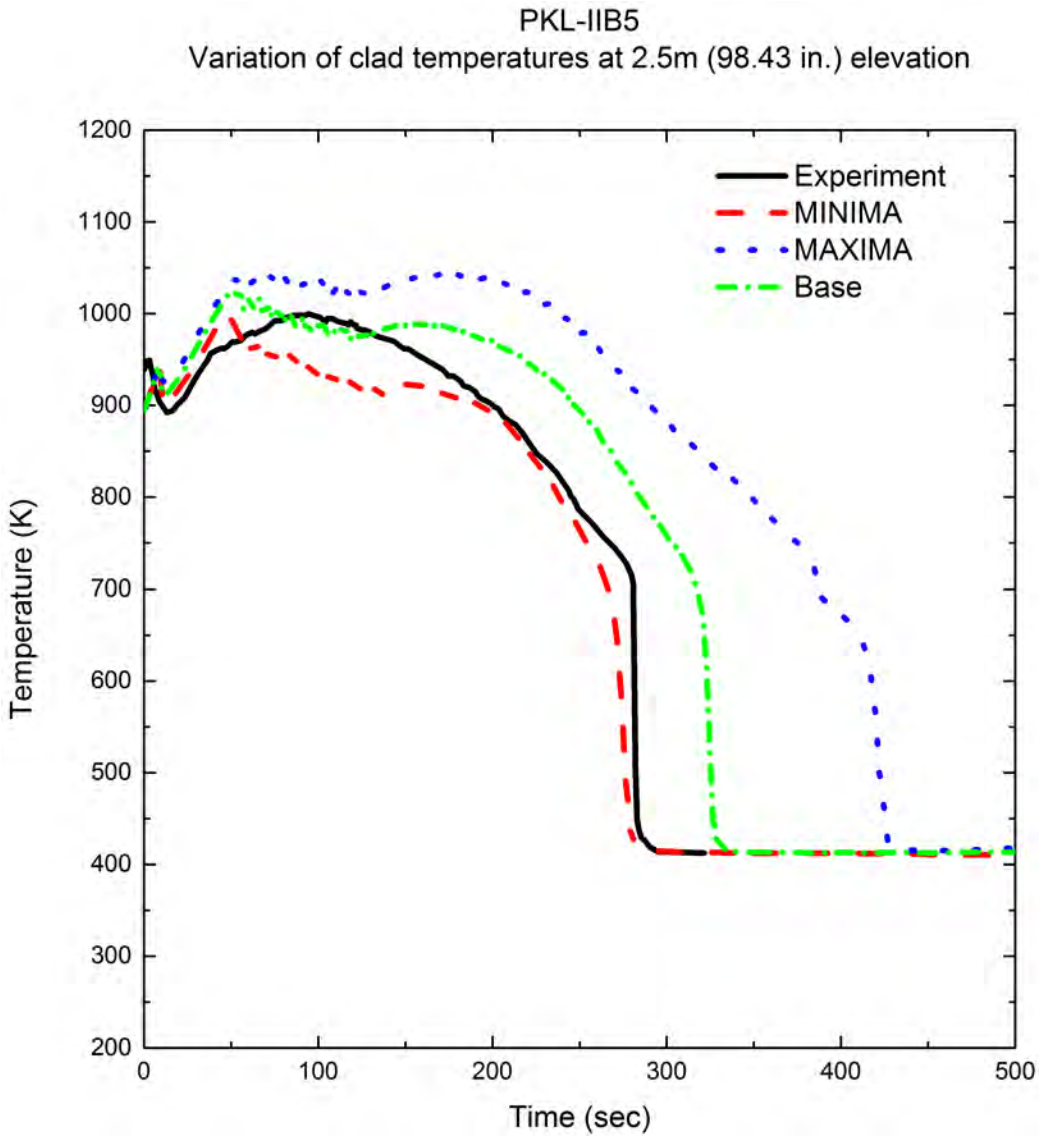

Figure 4-25 Results of the SRS Calculations for PKL-IIb5

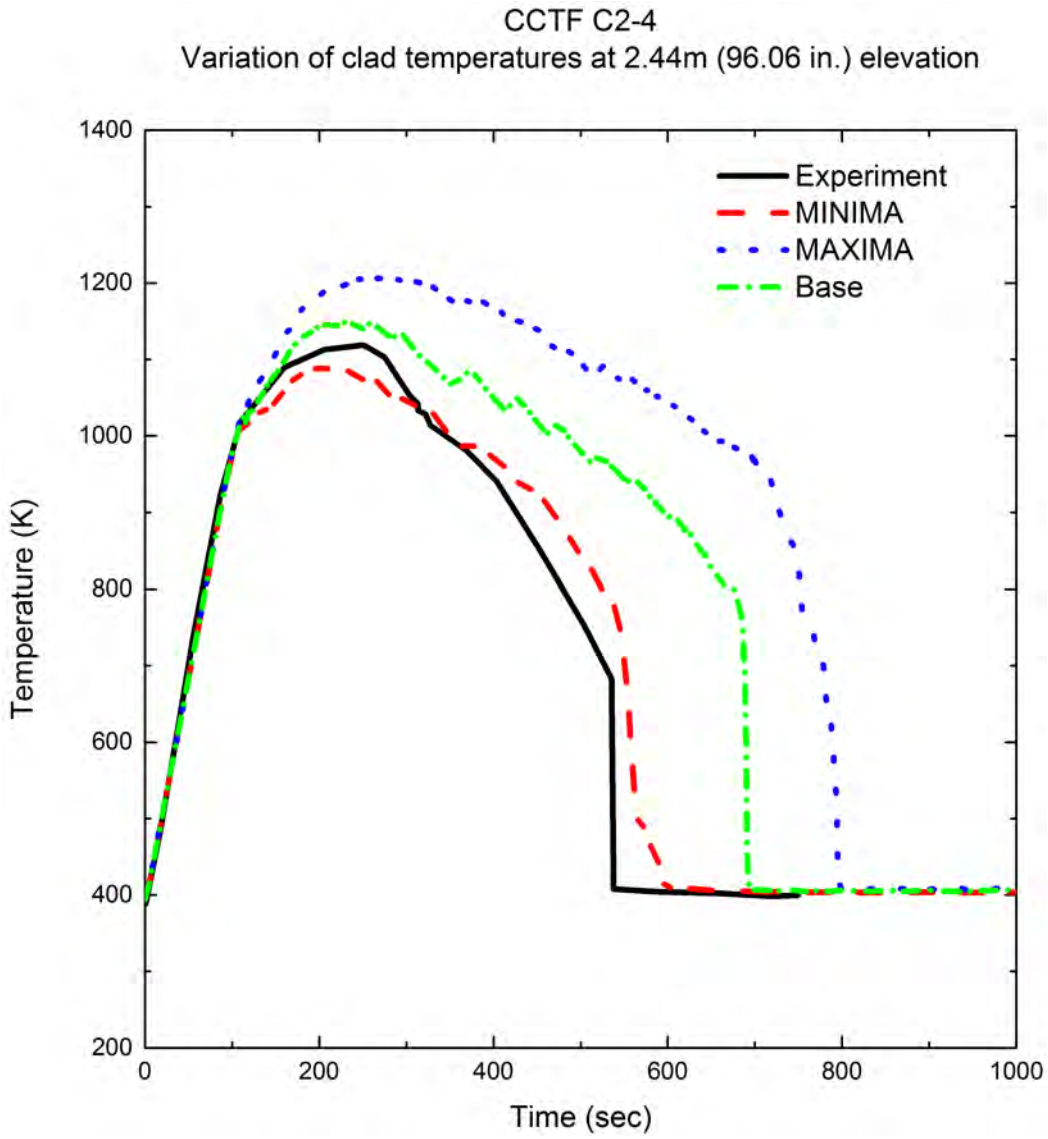

Figure 4-26 Results of the SRS Calculations for CCTF C2-4

5. Sensitivity and Uncertainty Analysis

5.1 Determination of Plant Input Uncertainty (Step 11)

The overall uncertainty of the LBLOCA transient, including peak cladding temperature behavior, which is one of the major safety criteria, depends on the initial and boundary conditions of the plant as well as on the code uncertainty parameters. Plant initial and boundary conditions include core power distribution, fuel parameters, reactor coolant pump, safety injection system, system pressures, system flow rates, and so on. Probabilistic distribution functions and uncertainties of plant condition parameters are listed in Table 5-1 with code uncertainty parameters. A detailed description for each of the plant parameters is given in the following sections.

5.1.1 Core Power Distribution Related Parameters

Three-dimensional distribution of the core power is described in general as a combination of radial and axial distributions, owing to their response rates. While the change of radial power distribution is slow in time and is not so sensitive to power level, xenon concentration or burnup; the axial distribution change is sensitive to burnup, control rod position, xenon concentration and power level. So, the three-dimensional power distribution is described separately in this method.

Core Power

Core thermal power is assumed to have a normal distribution function with [

]TS.

- Parameter; core power

[

]TS

Axial Power Distribution

Power peaking factor (Fq) is expressed as a product of axial peaking factor (Fnz) and radial peaking factor (Fr). [

]TS

[

]TS.

[

]TS

[

]TS

Hot Assembly Power

[

]TS

[

]TS

Hot Pin Power Peaking Factor

[

]TS

The technical specifications of the SKN 3 and 4 prescribe the LHGR limit as one of the limiting conditions for operation. The LHGR limit is defined as the product of Fq and the core average LHGR. The average LHGR at rated power is 5.602 kW/ft. The Fq corresponding to the LHGR limit 13.6 kW/ft is 2.428 (i.e., 13.6 kW/ft divided by 5.602 kW/ft). Therefore the range of Fq is extended to the limit of the technical specification of 2.428. The distribution function of Fq is conservatively assumed to be uniform.

- Parameter; hot pin power peaking factor (Fq)

  Distribution function; uniform

  Mean value; 2.184

  Minimum value; 1.940

  Maximum value; 2.428

[

]TS

5.1.2 Reactivity Feedback Related Parameters

Void Reactivity

The negative reactivity of the moderator rapidly reduces reactor power during the transient. Because the RELAP5/MOD3.3/K models the moderator density reactivity which corresponds to the void reactivity, it is necessary to treat the uncertainty of the moderator density reactivity. The moderator density reactivity is dependent on the moderator temperature coefficients (MTC); MTC

involves various core parameters. This means that there is no one code parameter that characterizes the moderator density reactivity. Therefore, the uncertainty of the moderator density reactivity is treated conservatively. The core design provides two conservative moderator density reactivity curves for the LOCA analysis as shown in Figure 4-4. [

]^{TS}.

Boron Reactivity

The boron reactivity depends on the boron density of the coolant flowing into the core. Negative reactivity effects of the borated water are not modeled in CAREM, in order to conservatively bound the uncertainty of the boron reactivity.

5.1.3 Fuel Rod Related Parameters

Gap Conductance

Accurate simulation of gap conductance at the steady state is required because it is a major parameter for the determination of the initial stored energy, which is an important heat source of the LBLOCA. The gap conductance, calculated by the fuel performance analysis code at the limiting burnup, would be applied to the hot pin and hot assembly rod, and the gap conductance calculated at core-average burnup would be applied to the average rods. However, the RELAP5 code does not accommodate direct input of the gap conductance variation.

Therefore, this methodology directly simulates the design data of steady state fuel centerline temperatures, i.e., the initial stored energy, instead of treating the uncertainty of gap conductance at the steady state. The design data of steady state fuel centerline temperatures includes the TCD effects as described in reference [25]. The uncertainty of the gap conductance at the steady state is not considered separately, since the uncertainty of the fuel centerline temperature is treated via the other parameters such as fuel conductivity and rod peaking factors. The details of RELAP5 simulation of steady state fuel centerline temperature are described in Appendix K of this report.

5.1.4 Reactor Coolant Pump Behavior Related Parameters

Pump two-phase degradation is expressed via two-phase multiplier curves. The two-phase head multiplier curves can be grouped into two, as can be seen in Figure 5-8: One is for such pumps as the Byron-Jackson pump, 1/5 CE pump, LOFT pump, and CREARE/CE pump, whose head multiplier values are relatively lower at low void fractions; the other is for such pumps such as the B&W pump, CREARE air/water pump, Semiscale pump, and the pump used for CE evaluation model, of which head multiplier values approach nearly 1.0 above the 30 % void fraction. Sensitivity studies were performed using the Byron-Jackson and the Semiscale pump data. These data are the representative pump data of each pump group. [

]^{TS}. [

]^{TS}

- Parameter; pump two-phase degradation multiplier

[

]TS

5.1.5 Safety Injection System Related Parameters

Parameters associated with the safety injection system can be divided into SIT parameters and SIP parameters. SIT parameters include water volume, water temperature, and nitrogen gas pressure. SIP parameters include IRWST water temperature and injection flow rate.

[

]TS

- Parameter; [

]TS

- Parameter; [

]TS

- Parameter; [

]TS

- Parameter; [

]TS

Note) The uncertainty of the [

]TS

- Parameter; [

]TS

- Parameter; [ ]TS

A Fluidic Device (FD) is installed inside the SIT to control the discharge flow rate passively. The FD provides a higher pressure drop by forming a vortex. The SIT-FD injects high-flow if the water level in SIT-FD is above the top of the stand pipe; it injects low-flow if the level in SIT-FD drops below the top of the stand pipe. The SIT injection flow rate is governed by the SIT pressure, water volume (or level) and flow resistances (K-factor) of the fluidic device and the safety injection line between the SIT injection nozzle and the DVI nozzle. [

]TS

Korea Atomic Energy Research Institute (KAERI) has performed several full-scale tests to investigate the characteristics of SIT-FD. However, the number of tests performed is not sufficient to quantify the uncertainties of the two K-factors and their distributions statistically. [

]TS

[

]TS

[

]TS

5.1.6 Downcomer Boiling Related Parameters

[ ]TS of the vessel wall have been selected as the uncertainty parameters for the downcomer boiling and for the vessel stored energy. Through the evaluation of the ATLAS Test 09, [ ]TS are found to be enough to cover the uncertainty of the vessel wall temperature and its effects on the downcomer boiling phenomenon. Therefore, the upper limit of each uncertainty range is determined as [ ]TS, respectively. Each range is assumed a [ ]TS The code evaluation results for the ATLAS experiments are described in detail in Appendix E.

- Parameter; [

[ ]TS

- Parameter; [

]TS

5.1.7 Reactor Coolant System Related Parameters

Pressurizer Pressure

The pressurizer pressure is assumed to have a [ ]TS

- Parameter; pressurizer pressure

[

]TS

RCS Flow Rate

The loop flow is affected by RCS pipe friction, form losses, and pump K-factor. Thermal design flow and the increased flow due to its measurement uncertainty are considered as the minimum and the maximum flow rates. In this method, loop flow uncertainties including friction and form losses of loop are [ ]TS. When a [

]TS.

- Parameter; [

]TS

5.2 Combine Uncertainties and Biases (Step 12)

Prior to the plant SRS calculations, a base case calculation is necessary for the overall system

behavior analysis. The following two subsections describe the results of the base case calculation and the plant SRS calculations.

5.2.1 Base Case Calculation

The base case calculation of the plant was performed by applying the best-estimate operating conditions for the limiting break location and size. The limiting break was obtained from the sensitivity calculations. Plant operation parameters are described in Section 5.1.

5.2.1.1 Limiting Break Location, Size, and Burnup

As described in Section 3.1.1, a cold leg break is found to be the most limiting with respect to the peak cladding temperature. In order to determine the limiting break size and burnup, a guillotine break spectrum of 100, 80, and 60 % break area at various burnups was studied. Sensitivity study for determination of the limiting break size and burnup is described in Appendix K. As can be seen in Figure 5-9, the blowdown PCT is the maximum when the break area is 100 % of the cold leg cross-sectional area and burnup of hot rod and hot assembly rods are 27,000 MWd/MTU. Therefore, the 100 percent break size at 27,000 MWd/MTU burnup is chosen as the limiting break size and burnup.

In the case of the 100 % guillotine break, the total break area is two times that of the cold leg cross-sectional area. In Figure 5-10, the cladding temperature for the case of a 200 % slot break is compared with that of the 100 % guillotine break. A 200 % slot break showed similar PCT in the blowdown period. The PCT of the reflood phase is lower than that of the guillotine break and the fuel quenching is earlier. Henceforth, the 100 % double-ended guillotine break in a cold leg is determined to be the limiting case.

5.2.1.2 Timestep Size

A set of timestep sensitivity study was performed. The timestep in the study ranged from [ ]^{TS}. [

]^{TS}

5.2.1.3 Base Case Calculation

The determined limiting break location, size, and burnup are applied to the base case calculation. The best-estimate operating conditions with the maximum Fq within Fq uncertainty range are applied to the base case calculation. The best-estimate conditions are defined as the combination of the mean values of plant operating parameters. The major plant conditions used in the base case calculation are summarized in Table 5-2.

The core power is 100 % of the rated thermal power of 3,983 MWt. The maximum value of 2.428 is used for the power peaking factor. The axial power distribution is shown in Figure 5-11. The ANSI/ANS 5.1 1979 standard model is used for the calculation of the decay heat assuming infinite operation at rated power.

The loop flow rate of the base case is the flow rate increased by a standard deviation amount over TDF, assuming 10 % plugging of the SG U-tubes. Nominal pressure of 155.1 bar is applied as the primary side pressure. The pressurizer is modeled at an intact loop based on the sensitivity calculations, even if its sensitivity was minimal. Nominal values of 52.63 m^3, 302.6 K and 42.45 bar are used for the water volume, water temperature, and nitrogen gas pressure of the SIT-FDs, respectively. A value of 302.6 K is used for the IRWST water temperature. The single failure assumption explained in Section 3.3 is applied.

The containment building conditions are reflected in the input of CONTEMPT4/MOD5. Major inputs include the free volume of the building, heat transfer area, and condensation heat transfer coefficients. All these inputs are prepared in a conservative manner.

5.2.1.3.1 Thermal Hydraulic Behavior of the Plant

Blowdown Period

Blowdown is defined as the period of time until one of the SIT-FDs begins the injection. Rapid depressurization of the primary system following the break opening is shown in Figure 5-12, comparing it with the secondary system pressure. As the secondary side pressure is kept higher than the primary side pressure after 6 s, the steam generator loses its function of removing heat. Therefore no effective heat sink is available except for the blowdown flow through the break until the SIT-FD actuation time. If the pressure decreases to the saturation pressure, violent vapor generation is caused by the flashing of subcooled water. The core experiences flow-stagnation, void generation, and coolant depletion. Accompanied by the degradation of the core heat transfer, a rapid heatup of the fuel follows during this stage. Core power falls down to the level of decay power within approximately one second because of the negative reactivity insertion by the core voiding. Meanwhile the depressurization rate of the primary system is decreased by the flashing in the primary system. SIT-FDs provide high flow rate injection for 15 to 45 s, and then they provide low flow rates up to about 172 s.

Figure 5-13 shows the break flow rates of the vessel side and the pump side of the break. Early in the accident, the break flow rate is very high. The mass flow from the reactor vessel side is much higher than that from the pump side because of the high hydraulic resistances of the pump and the steam generator piping. Break flow starts to decrease rapidly experiencing a transition from the subcooled to the mixture condition.

When primary system pressure decreases to 42.45 bar, SIT-FDs begin the injection. Figure 5-14 shows the total injection flow rates of the ECCS. Due to the stand pipe and fluidic device in the safety injection tank, the high flow rate injection continues up to 45 s, and then the low flow rate injection is maintained up to about 172 s. Subcooled water injected into the reactor vessel downcomer condenses the steam by way of direct contact condensation.

Collapsed water levels of the core and the reactor vessel lower downcomer are shown in Figure 5-15. The rapid decrease of core level at the initiation of the accident is due to the high amount of the break flow. Afterward, the rapid decrease of the core water level more or less halts due to the incoming flows from the upper plenum, the head of the reactor pressure vessel and the pressurizer. As blowdown continues, the core eventually becomes almost empty.

Rapid depressurization of the reactor pressure vessel early in the blowdown causes core boiling, which decreases the core power and the heat transfer between the fuel cladding and coolant. Rapid heatup of the cladding is mainly caused by the initial stored energy and the degradation of core heat transfer. Clad temperature reaches the peak of 1,170 K at 7.2 s and then decreases very rapidly.

Refill Period

Refill period is defined as the time period after the beginning of SIT-FD injection up to the time when the mixture level reaches the inlet of the active core. Refill begins with the SIT-FD injection but a considerable portion of the injection flow bypasses to the break and only a small amount penetrates the downcomer.

Subcooled ECCW condenses the steam in the downcomer, and a portion of it contacts the hot walls resulting in vapor generation. Due to the combined effect of this condensation and the generation of steam, water penetration and sweep-out repeats in the refill period. As the primary pressure

decreases and the vapor generation decreases due to the cooling of the walls, penetration of the ECCW starts to increase and finally fills the lower plenum completely.

Downcomer water level repeats its decrease and more or less increases, as shown in Figure 5-15; overall, the level increases during this period. As the downcomer level increases rapidly at about 30 s, the coolant begins to enter the core and the refill period ends. The clad experiences adiabatic heating after about 23 s because no core flow is available. Clad temperature continues to increase until core-wide cooling is available in the reflood phase.

As can be seen in Figure 5-16, the downward liquid velocity at the core inlet begins to halt at about 13 s and to increase again until 23 s due to the second heatup of the fuel. Integration of the core inlet flow is shown in Figure 5-17. No coolant enters the core during the refill period. After 33 s, core reflood begins and the integrated mass that has entered the core continues to increase.

Early Reflood Period

This period is defined as the time period from the end of refill to the emptying of the SIT-FDs at about 172 s. After the filling of the lower plenum, a huge amount of SIT-FD injection makes the downcomer water level increase and core insurge flow begins. The core insurge flow cools the lower part of the core and results in the generation of steam. The vapor entrains some amount of water to the upper part of the core. The entrained water enhances the cooling of the upper core. A part of the entrained water accumulates in the upper plenum; the other parts accompanied by the steam go through the hot leg, steam generator, pump suction leg, and finally into the containment via the break. Water entrained into the steam generators vaporizes by reverse heat transfer from the secondary side of the steam generators causing a pressure increase in the upper plenum. The pressure increase reduces the reflooding rate. This phenomenon is known as steam binding. If the insurge flow at the core inlet decreases, the steam binding effect also decreases. This results in the reduction of the upper plenum pressure, and causes the core insurge flow to increase again. This kind of insurge and outsurge of core flow repeats in the early reflood period.

As shown in Figure 5-15, the downcomer water level begins to increase after about 15 s. The pressure difference between the downcomer and the core builds up as the downcomer water level increases and causes the flow to enter the core after 33 s. The downcomer water level increases to over 6 m during the high-flow injection period of SIT-FDs. As the SIT-FD injection changes from high-flow injection to low-flow injection, the downcomer water level decreases, however the level maintains around the cold-leg elevation until the SIT-FDs become empty. The sudden decrease of the downcomer water level after about 172 s is due to the discharge of nitrogen gas at a pressure relatively higher than the primary system pressure.

Clad temperature behaviors are shown in Figure 5-23 to Figure 5-25 for the hot pin, hot assembly rod, and core average rods, respectively.

Late Reflood Period

This period is defined as the period after the emptying of the SIT-FDs. The ECCW is provided only by the safety injection pumps. As can be seen in Figure 5-17, the temporal decrease of the core inlet flow is caused by the level decrease of the downcomer after the emptying of the SIT-FDs. After around 200 s, the core inlet flow continues to increase gradually. The entire core quenches and maintains quenched state in this period. As can be seen in Figure 5-15, the water levels of the downcomer and the core are kept at lower elevations than the early reflood period.

Containment Pressure

Figure 5-18 shows the containment pressure behavior calculated using the conservative input parameters listed in Table 5-2. The peak pressure reaches 0.28 MPa at 20 s after the break. Figure

5-19 shows the containment wall condensation heat transfer coefficients calculated using the Tagami-Uchida correlation.

5.2.1.3.2 Core Thermal Behavior

Figure 5-20 shows the heat transfer coefficient at the PCT location. Figure 5-21 provides a temperature comparison between clad and steam at the PCT location. The PCT of the base case calculation occurs at the elevation of 2.76 m, which is equivalent to 72 % of the elevation of the active core. The calculated PCT is 1,170 K (1,646 °F) at 7.2 s. At this location the fuel rod quenches at around 275 s. On opening of the break the heat transfer coefficient suddenly drops to a few hundredths, and shows a value of 250 – 300 W/m^2-K at around 6.0 s. The increase of the heat transfer coefficient from 6.0 s is due to the rapid outsurge of the core flow and the influx of the upper head flow through the top of the core. Because the active core is uncovered and is exposed to steam after 11 s, the heat transfer coefficient rapidly drops and this results in the second heatup of the rod. As the hottest spot quenches at around 275 s, the heat transfer coefficient increases again and remains stable there.

The transition of the heat transfer modes at the PCT location is shown in Figure 5-22. It can be seen that the single phase vapor convection mode prevails until the reflood begins at about 33 s. As the reflood begins, film boiling develops, and the non-condensable gas that was sucked into the vessel from the containment at the end of blowdown begins to appear in the core. However, a very small amount of non-condensable gas is found to remain in the core. Between 270 and 310 s, the heat transfer mode changes from the saturated and subcooled film boiling to the transition boiling and the fuel rod quenches. Since then, the core maintains stable nucleate boiling.

Figure 5-23 to Figure 5-25 show the axial variation of clad temperatures for the hot pin, hot assembly rod, and core average rod, respectively. PCTs are calculated at 1,170 K (1,646 °F), 1,126 K (1,568 °F), and 895 K (1,152 °F) for each rod, respectively.

5.2.2 Plant SRS Calculation

The SRS calculations of 181 cases are performed adopting distribution-free statistics. In the case of 181 calculations, the highest three values of PCT exceed the 95 percentile at 95 % confidence level when the highest PLO and CWO are considered; the third highest value of PCT, the highest PLO and CWO are provided as licensing values with which the acceptance criteria will be compared. The 181 simple random samplings of [ ]^{TS} uncertainty parameters are listed in Appendix J. The appendix consists of sampling inputs, sampling results, and probability distribution diagrams.

The 179 hot spot clad temperatures excluding the first and the second highest cases of 15 and 179 are shown in Figure 5-26, and their PCTs are listed in Table 5-4 with the peak local oxidation and hot rod hydrogen generation results. The maximum PCT was obtained in Case 132, with value of 1,283 K at 83.5 s. Figure 5-27 and Figure 5-28 show the local clad oxidation and the hot rod hydrogen generation, respectively. The peak local oxidation and the maximum hot rod hydrogen generation are evaluated at 6.30 % and 0.25 % in Case 15.

[

]^{TS}

5.2.3 Evaluation of Scale Biases

Scale biases are evaluated for all the cases that have been expected to be able to be limiting when

the biases are additionally counted. Based on previous experiences, [ ]TS are selected for the scale bias calculations. [ ]TS

The code biases in the prediction of ECC bypass and steam binding are evaluated separately. The steam binding bias is evaluated by combining the results of two separate bias evaluations of droplet de-entrainment in the upper plenum of the reactor vessel and droplet evaporation in the steam generator U-tube.

The highest PCT obtained from bias evaluations combining all the biases is compared with the third highest PCT of SRS calculations. The difference of these two values is defined as total bias. The negative bias is not considered in total bias for the conservatism. The resultant PCT of scale bias evaluations is obtained by adding total bias to the third highest PCT of SRS calculations.

5.2.3.1 ECC Bypass Bias

[ ]TS

5.2.3.2 Steam Binding Bias

Upper Plenum De-entrainment Bias

[ ]TS

U-tube Droplet Evaporation Bias

[ ]TS

5.2.3.3 Results of the Scale Bias Evaluation

Summed scale biases are shown in Table 5-9. Biases of the upper plenum de-entrainment and the U-tube droplet evaporation are combined into a steam binding bias. Negative biases of the ECC bypass and the steam binding are conservatively neglected.

Total bias is evaluated as +9.8 K. This total bias is added to the third highest PCT of SRS calculations. The peak local oxidation and hot rod hydrogen generation are confirmed not to increase by the scale bias calculations.

Thus, the peak cladding temperature, peak local oxidation, and core-wide hydrogen generation combining all the biases are as follows:

- Peak cladding temperature = 1,283 + 9.8 = 1,293 K
- Peak local oxidation = 6.30 % + 0 = 6.30 %
- Maximum hydrogen production = 0.25 % + 0 = 0.25 %

Table 5-1 Distributions and Ranges of the Uncertainty Parameters

TS

Table 5-2 Major Input Parameters for the Base Calculation

Plant Parameters	Reference Conditions
Core	
1. Core power	3,983 MWt
2. Power peaking factor	2.428
3. Fuel type	16 x 16
4. Power output pattern	Figure 5-11
5. Decay heat	ANS79 model
Reactor Coolant System	
1. Loop flow	5,274 kg/s (Cold leg)
Pressurizer	
1. Pressure	155.1 bar
Steam Generator	
1. Feedwater temperature	505.23 K
2. Tube plugging rate	10 %
Safety Injection System	
1. Safety injection tank coolant volume	52.63 m^3
2. Safety injection tank gas pressure	42.45 bar
3. Safety injection tank coolant temperature	302.6 K
4. FD K-factor for high injection flow (including piping K)	10.0
5. FD K-factor for low injection flow (including piping K)	80.0
6. IRWST temperature	302.6 K
Containment Building	
1. Initial pressure	0.98 bar
2. Initial temperature	283.15 K
3. Free volume	97,239 m^3
4. Number of spray	2
5. Delay time for spray actuation	0 s
6. Spray flow rate (2 pumps)	10,000 gpm

Table 5-3 Major Sequence of Events for the Selected LBLOCA Scenario

Major Events	Time (s)
Start	0.0
Reactor Trip Occurrence	9.5
Safety Injection Actuation Time (SIAS) Occurrence	9.5
Safety Injection Tank Operation Time - SIT-1 (Broken Cold Leg) - SIT-2 (Broken Loop Intact Cold Leg) - SIT-3 (Intact Loop Intact Cold Leg 1) - SIT-4 (Intact Loop Intact Cold Leg 2)	14.5
Core Level Recovery Initiation	32.5
Safety Injection Pump Operation	48.0
PCT Occurrence	83.5
Safety Injection Tank (SIT) Empty - SIT-1 (Broken Cold Leg) - SIT-2 (Broken Loop Intact Cold Leg) - SIT-3 (Intact Loop Intact Cold Leg 1) - SIT-4 (Intact Loop Intact Cold Leg 2)	172.0
Quenching Time of PCT Node	272.5
Quenching Time of All Axial Hot Pin Nodes	315.6

Table 5-4 Shin-Kori Units 3 and 4 SRS Calculation Results (1/6)

TS

Table 5-4 Shin-Kori Units 3 and 4 SRS Calculation Results (2/6)

TS

Table 5-4 Shin-Kori Units 3 and 4 SRS Calculation Results (3/6)

TS

Table 5-4 Shin-Kori Units 3 and 4 SRS Calculation Results (4/6)

TS

Table 5-4 Shin-Kori Units 3 and 4 SRS Calculation Results (5/6) TS

Table 5-4 Shin-Kori Units 3 and 4 SRS Calculation Results (6/6)

TS

Table 5-5 Cases Selected for Bias Evaluation

TS

Table 5-6 [ ]TS

TS

Table 5-7 [ ]TS

TS

Table 5-8 [ ]TS

TS

Table 5-9 [ ]TS

TS

TS

Figure 5-1 [ ]TS

TS

Figure 5-2 [ ]TS

TS

Figure 5-3 [ ]TS

TS

Figure 5-4 [ ]TS

TS

Figure 5-5 [ ]TS

TS

Figure 5-6 [

]TS

TS

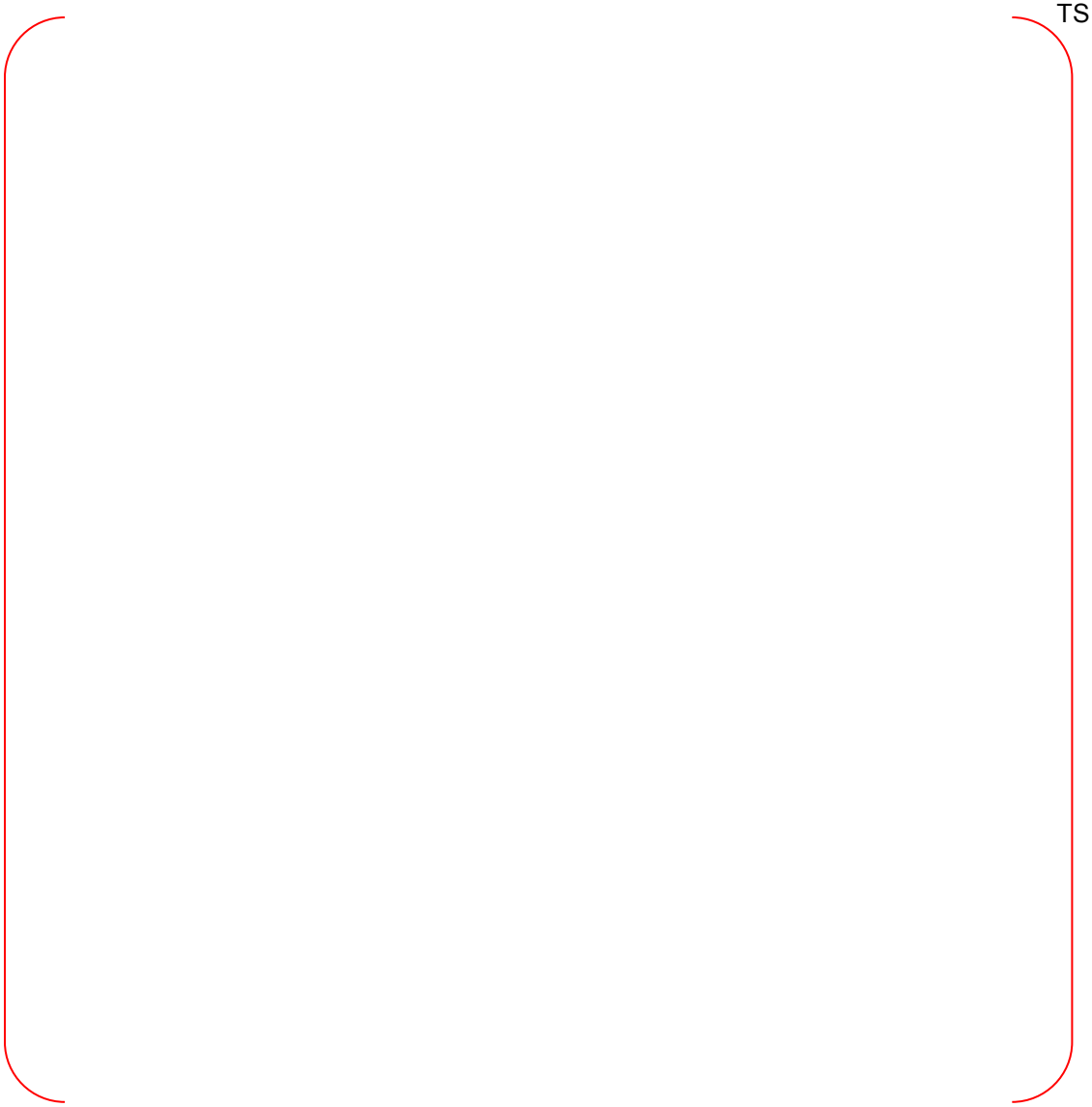

Figure 5-7 [ ]TS

TS

Figure 5-8 [ ]TS

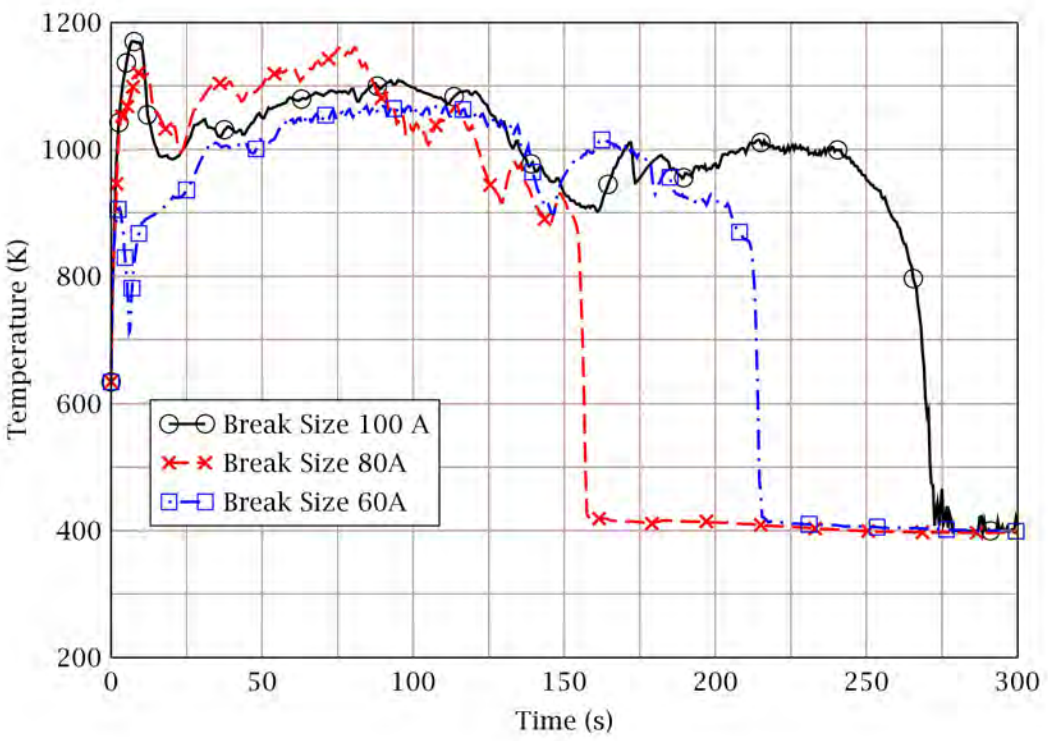

Figure 5-9 Comparison of PCTs Calculated for Various Break Sizes

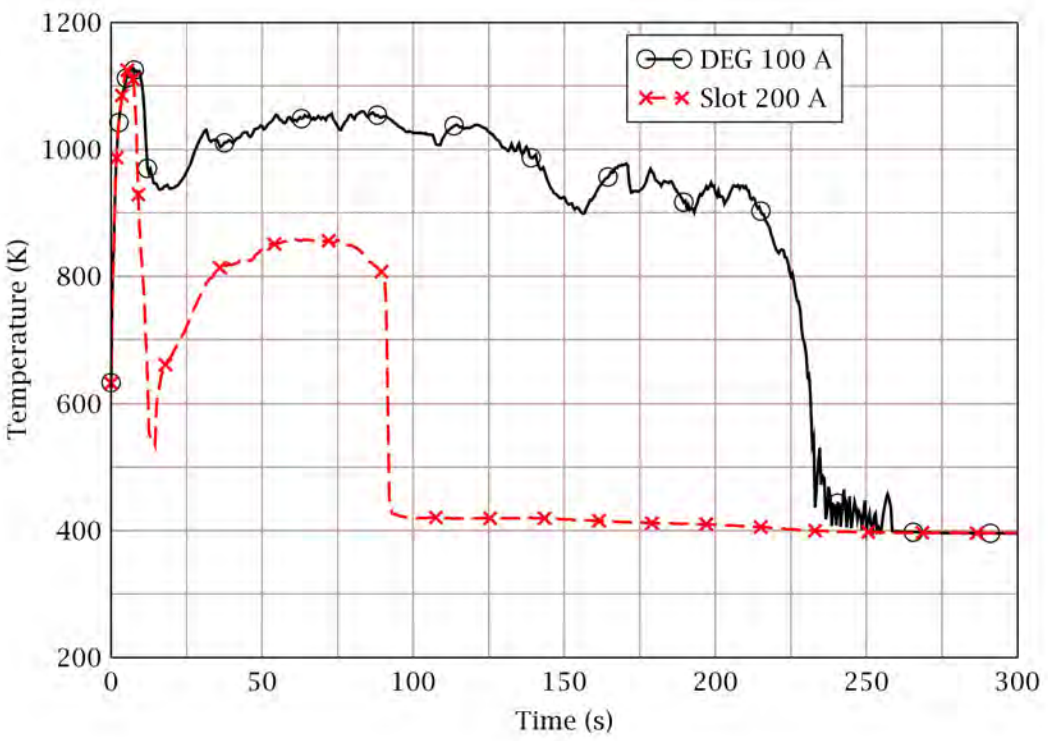

Figure 5-10 Comparison of PCTs Calculated for Break Plane Shapes

TS

Figure 5-11 [ ]TS

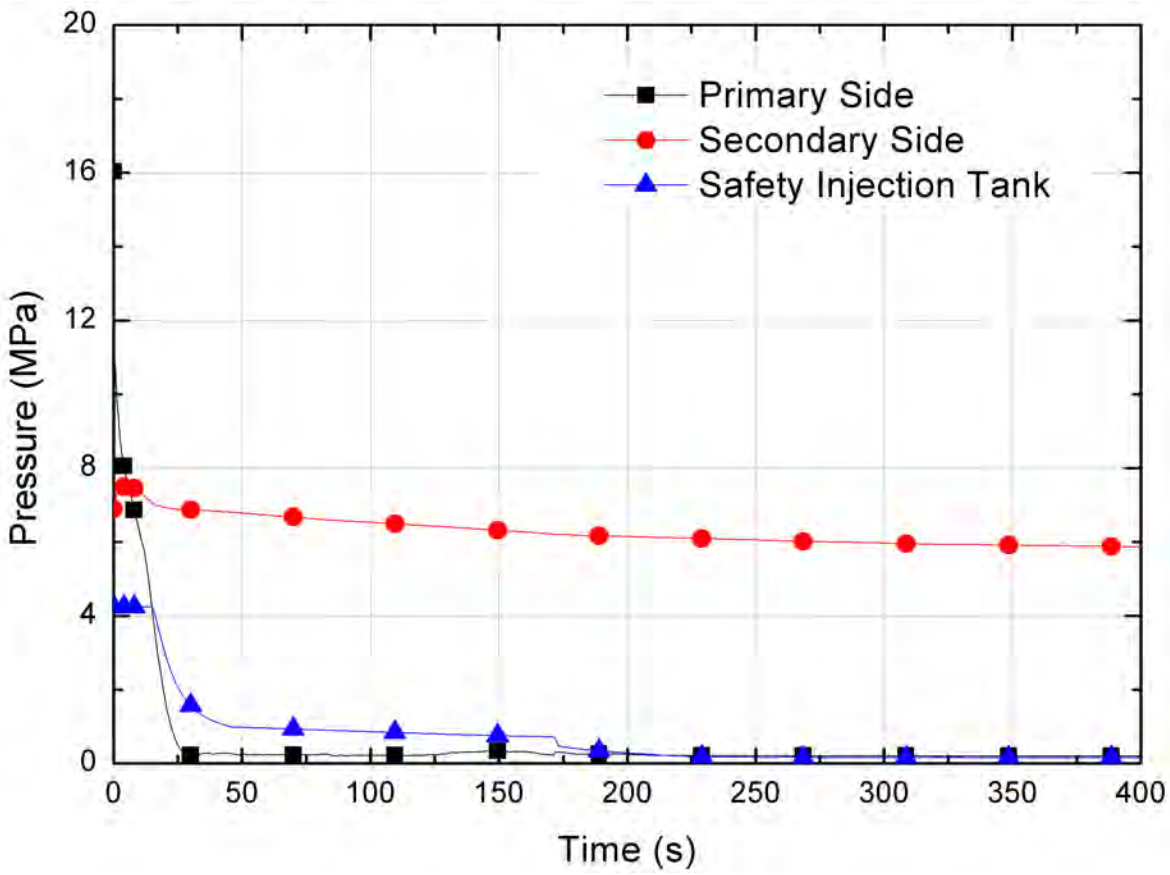

Figure 5-12 Pressure Behavior of Reactor Coolant System; Base Calculation

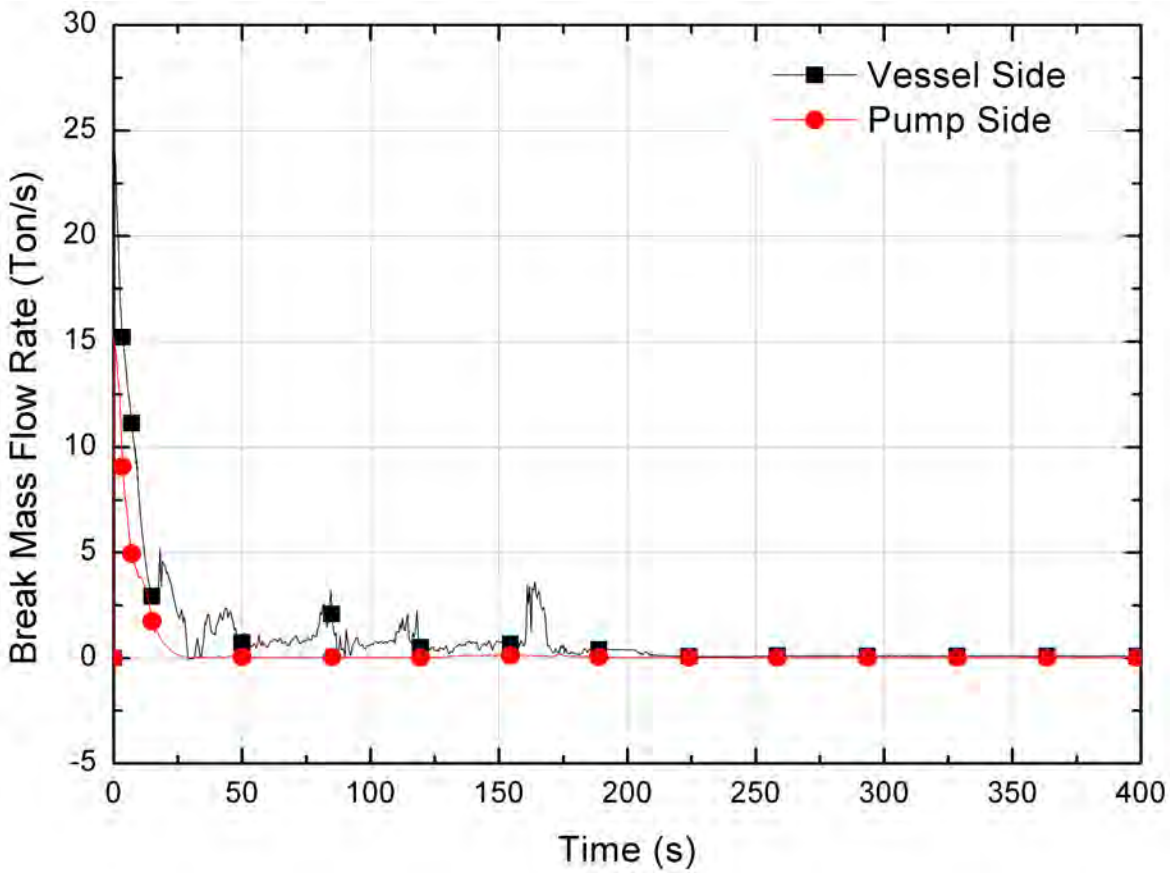

Figure 5-13 Break Flow Rate; Base Calculation

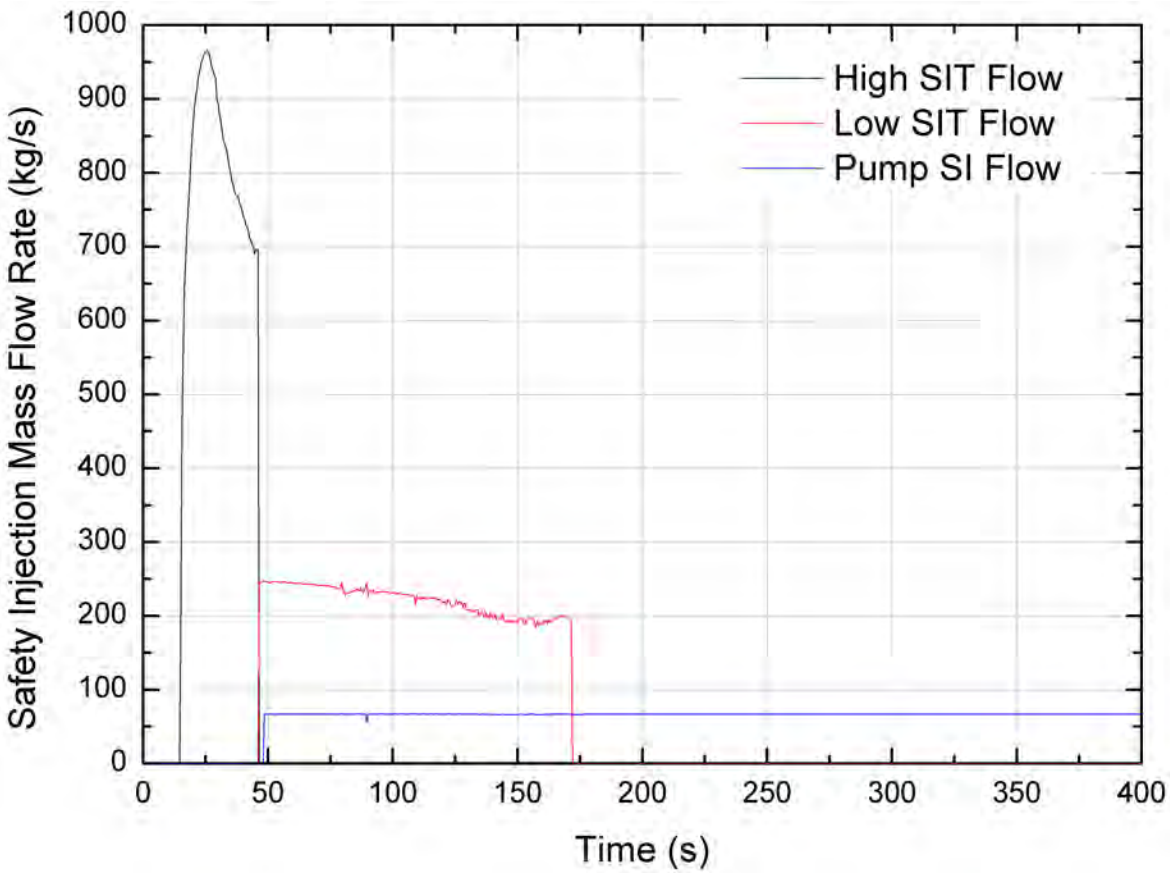

Figure 5-14 Safety Injection Flow Rates; Base Calculation

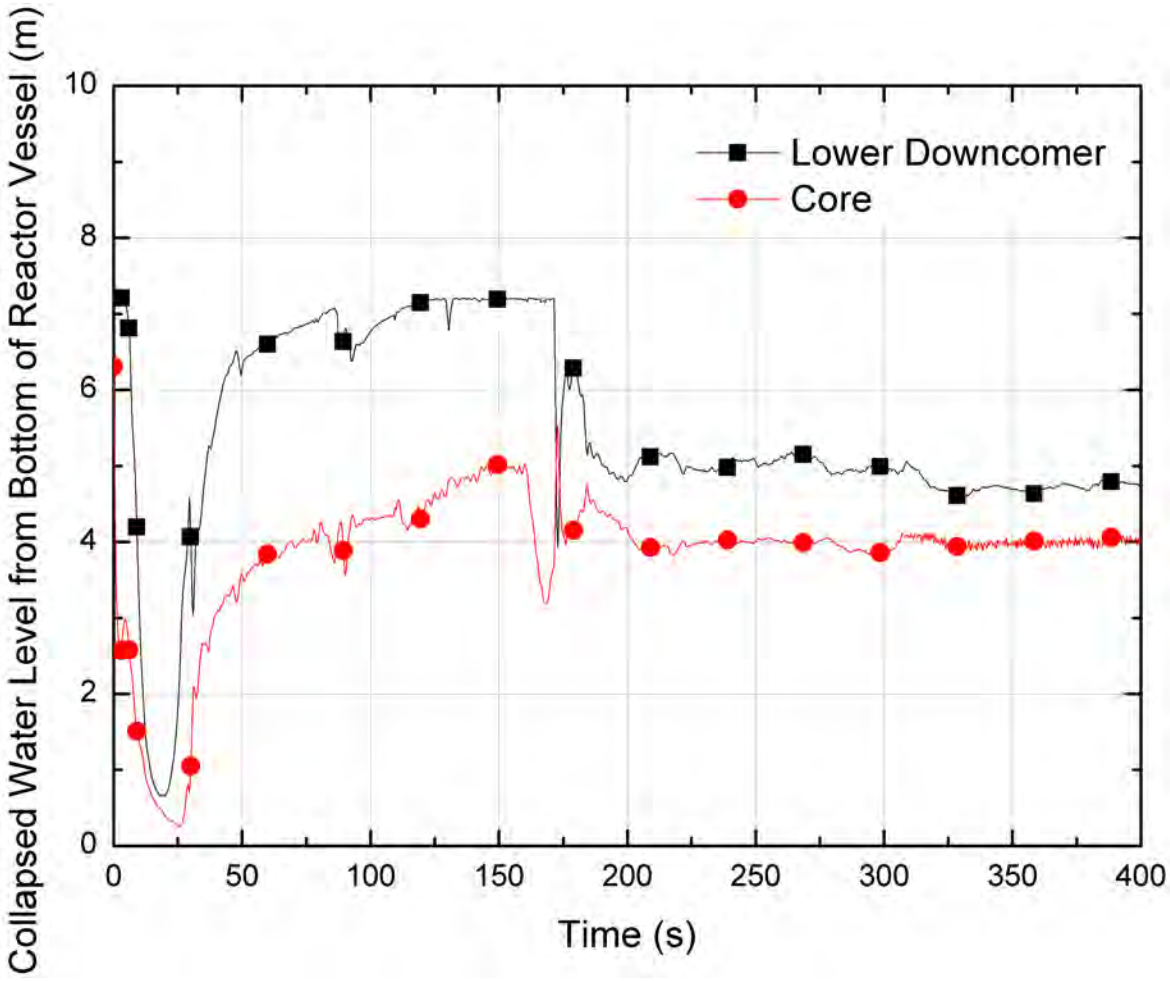

Figure 5-15 Water Levels in the Downcomer and the Core; Base Calculation

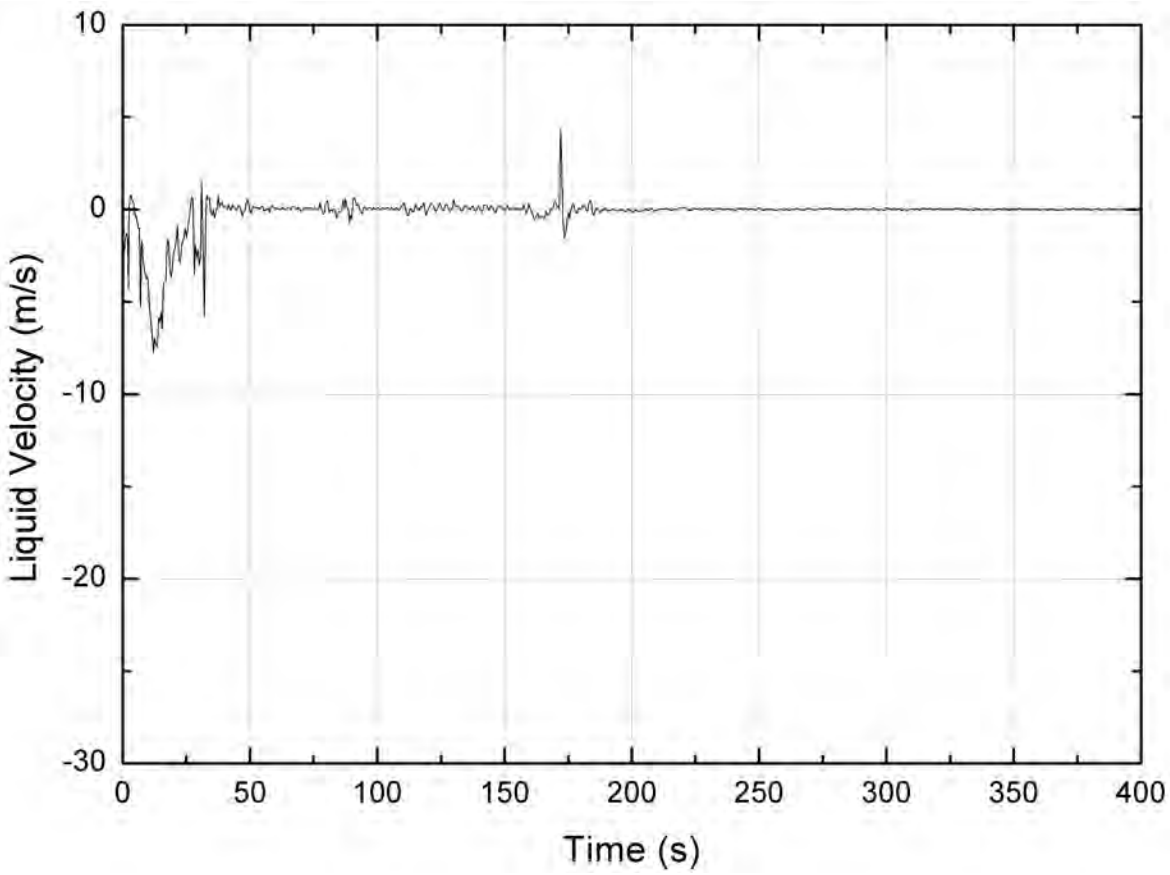

Figure 5-16 Liquid Velocity at the Core Inlet; Base Calculation

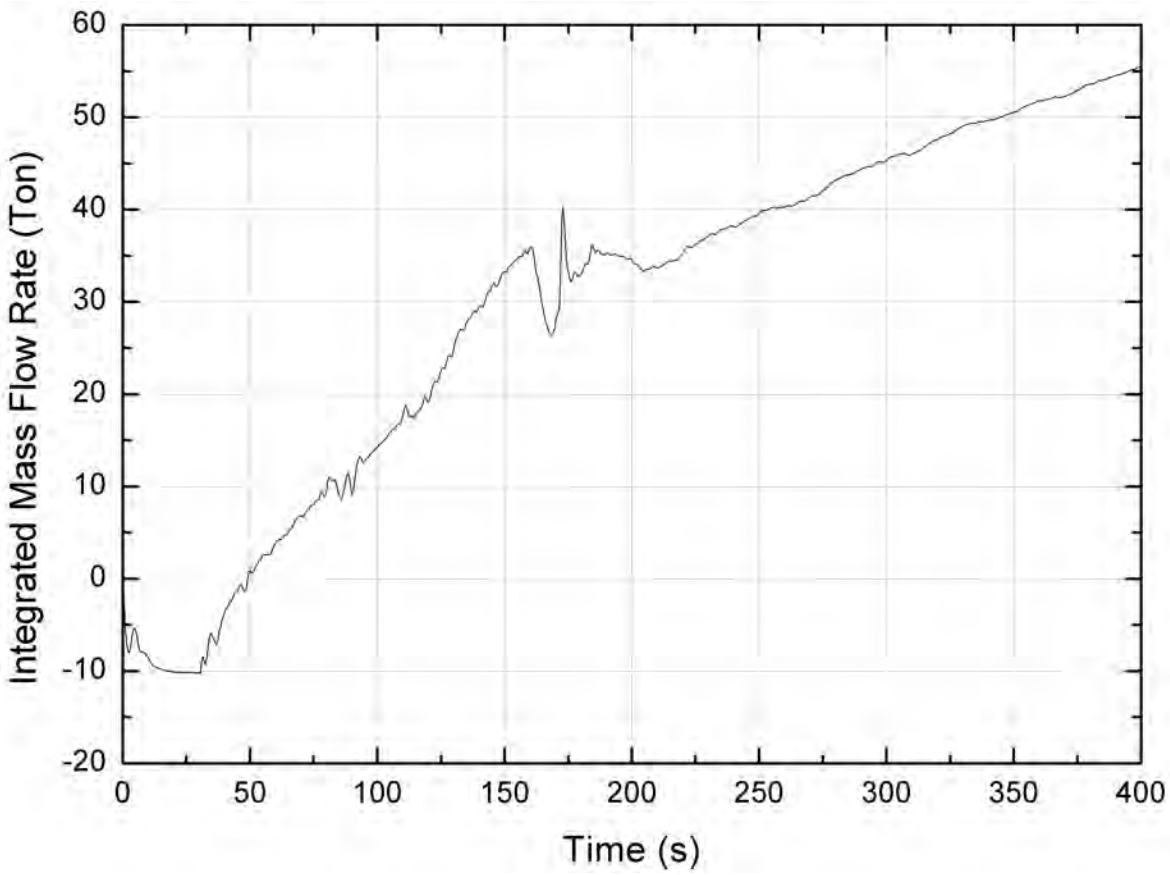

Figure 5-17 Integrated Mass of Core Inlet Flow; Base Calculation

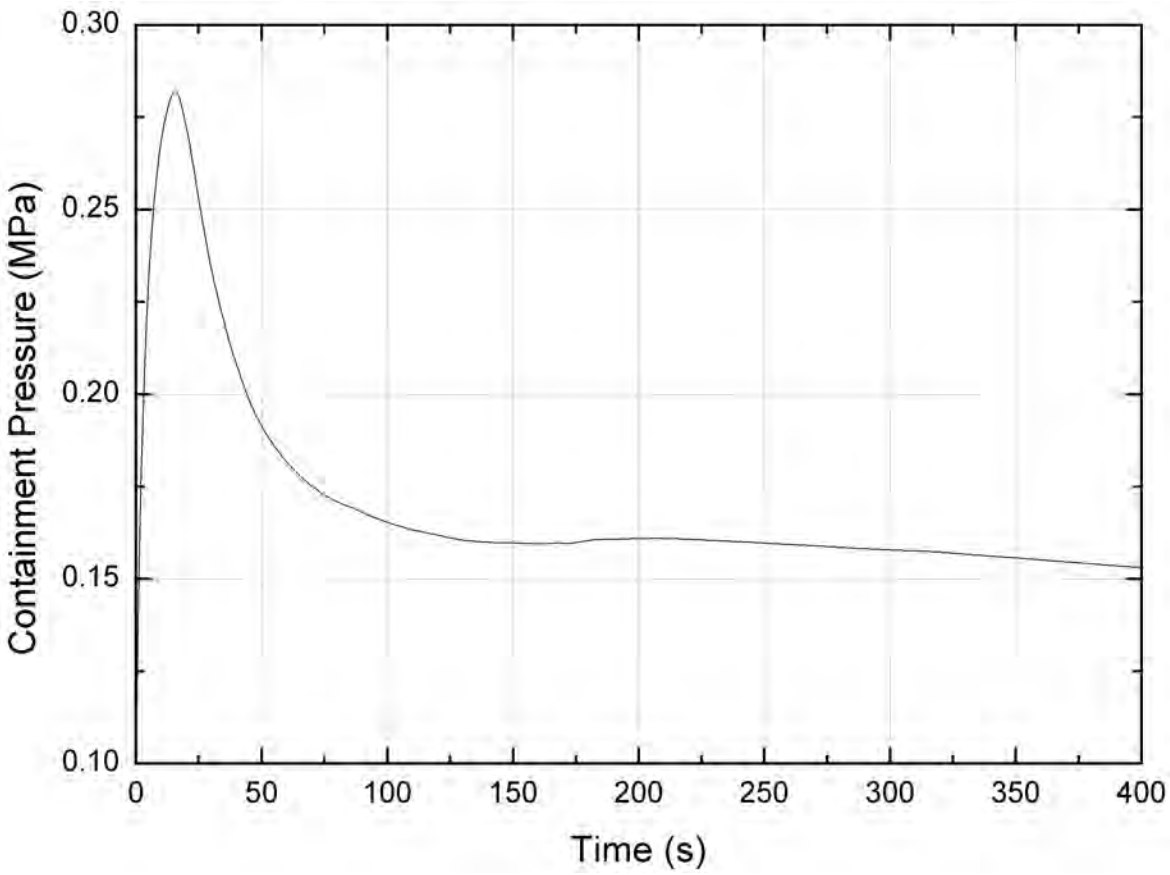

Figure 5-18 Containment Pressure; Base Calculation

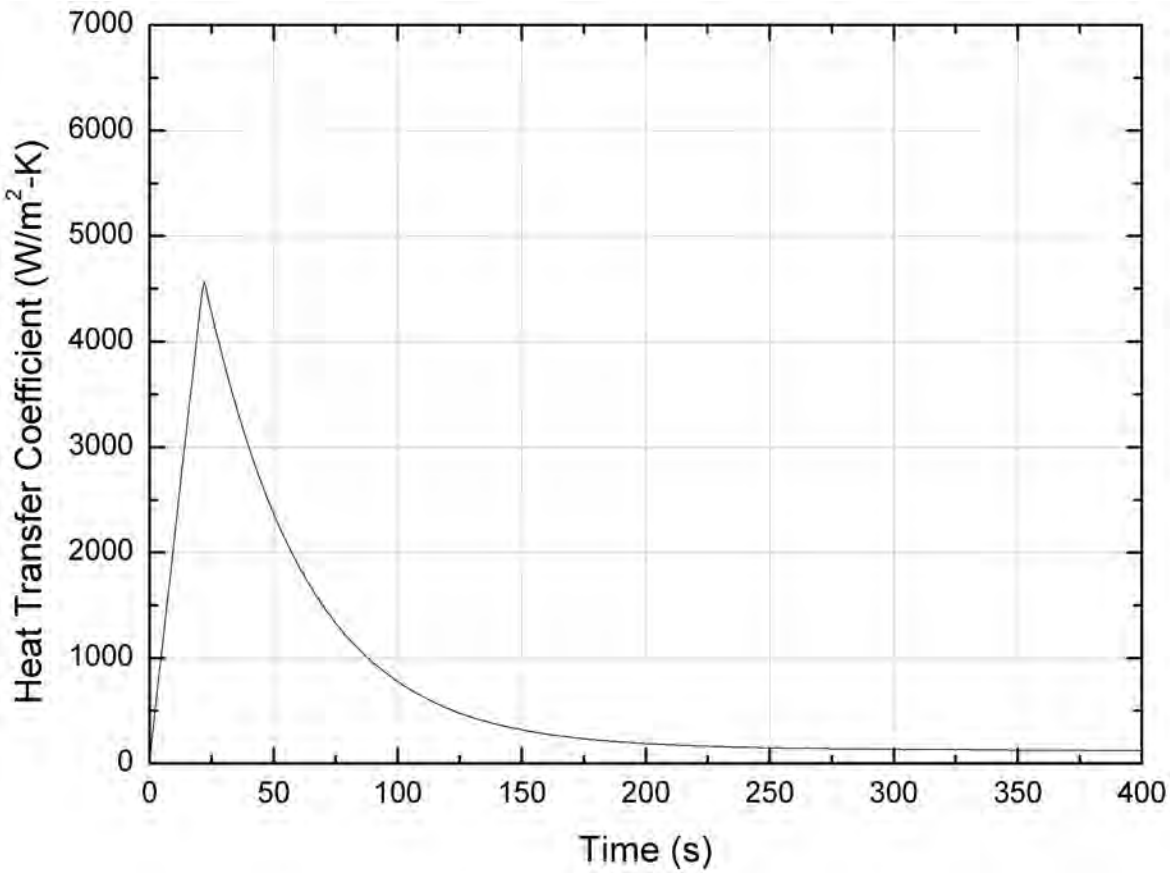

Figure 5-19 Containment Wall Condensation Heat Transfer Coefficients; Base Calculation

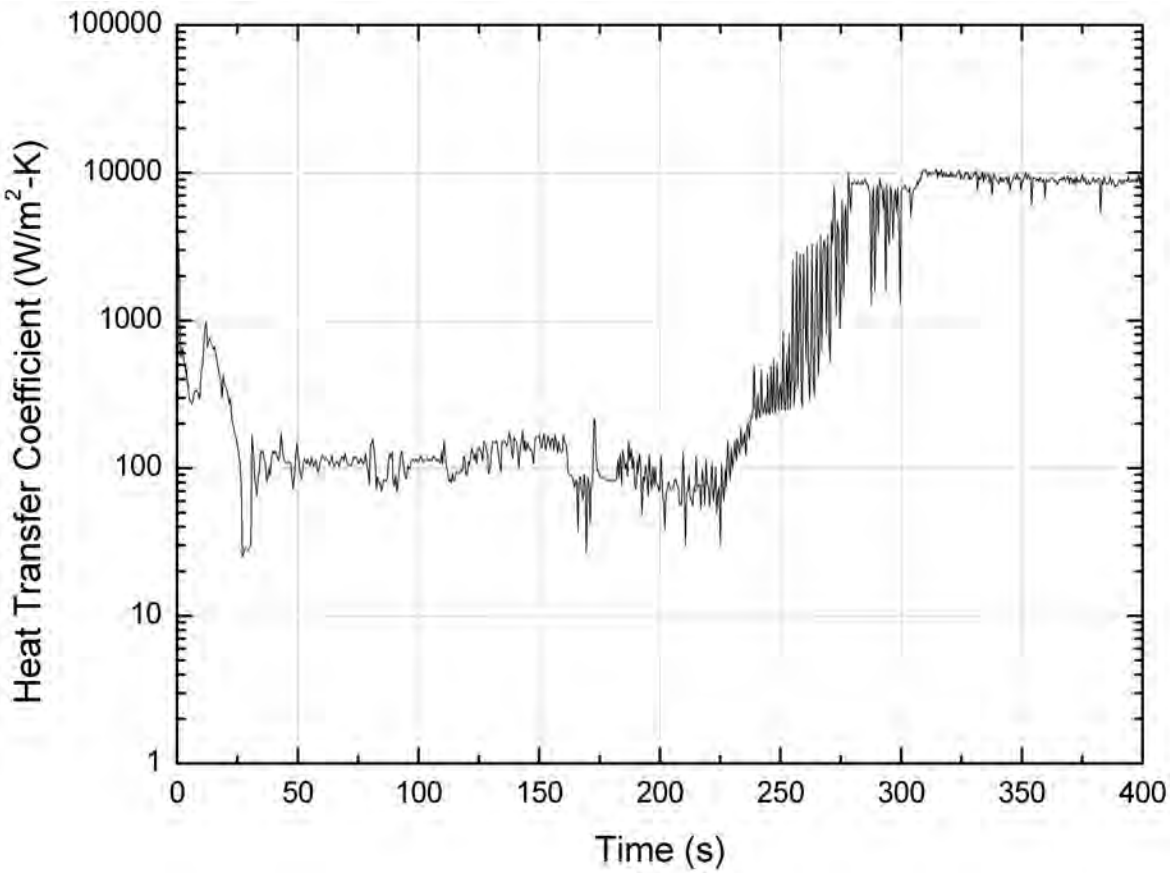

Figure 5-20 Hot Spot Heat Transfer Coefficients; Base Calculation

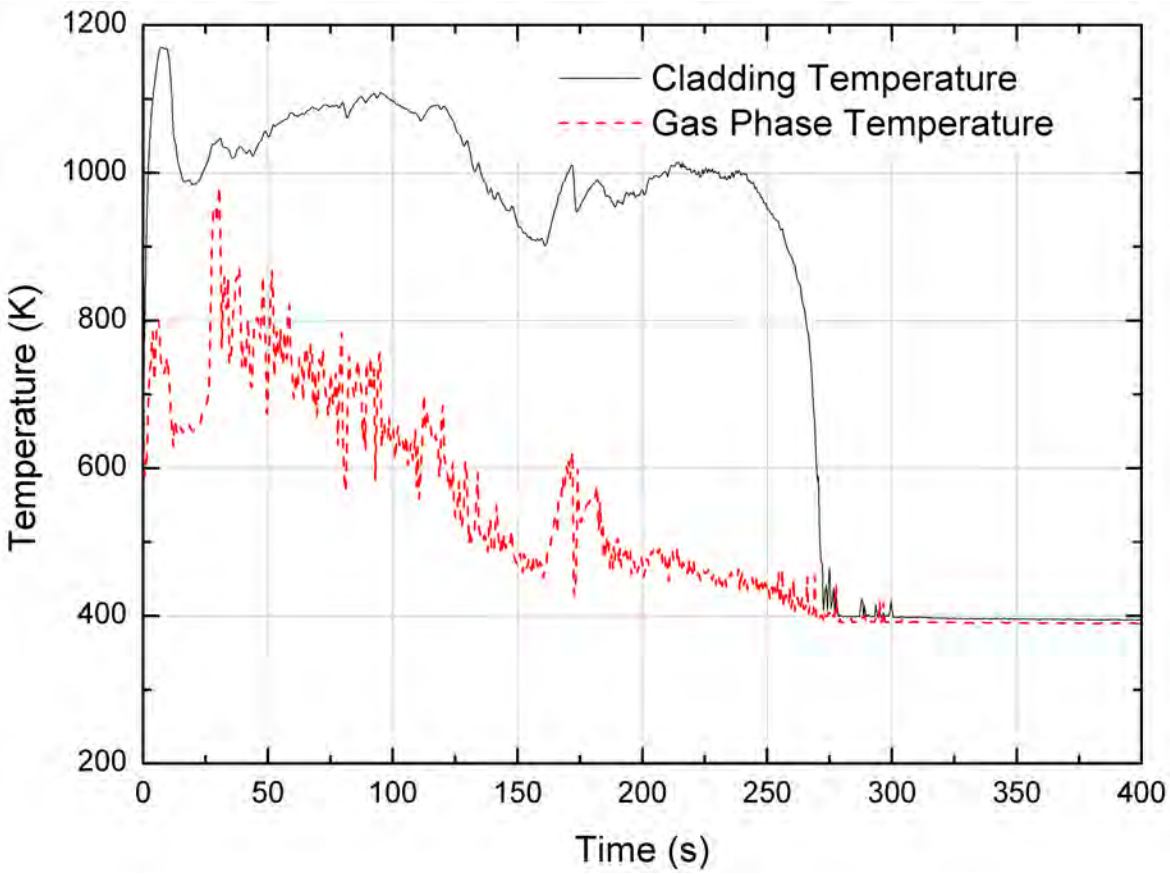

Figure 5-21 Hot Rod Cladding Temperature; Base Calculation

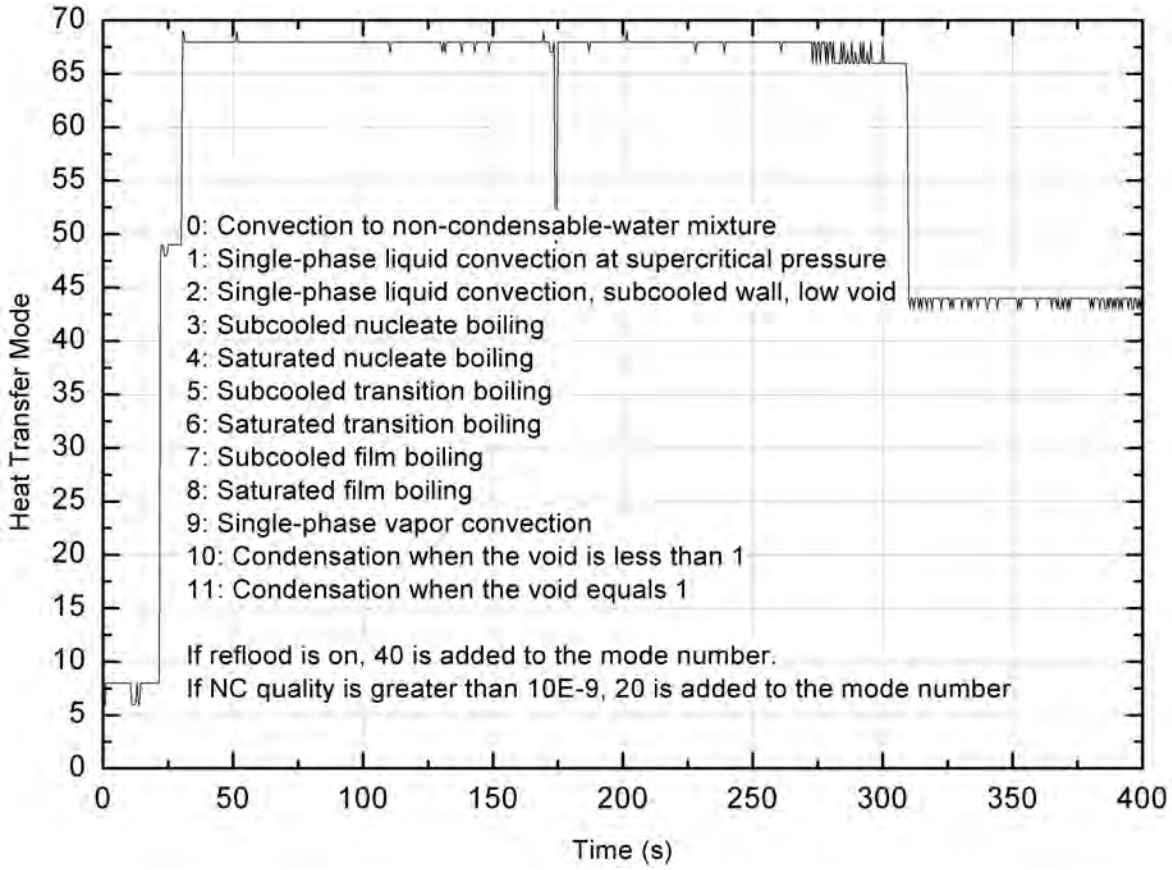

Figure 5-22 Change of Heat Transfer Modes at the PCT Location; Base Calculation

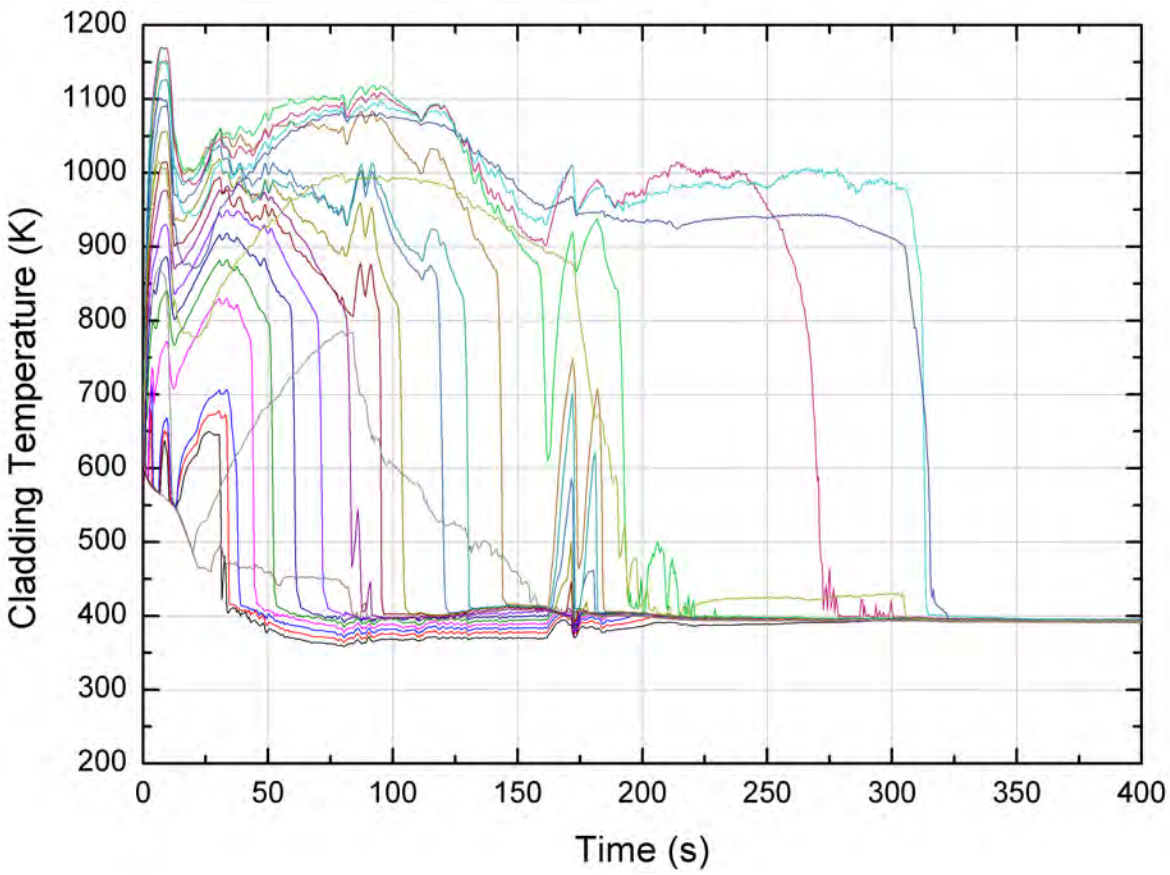

Figure 5-23 Cladding Temperatures at [ ]^{TS} of [ ]^{TS}; Base Calculation

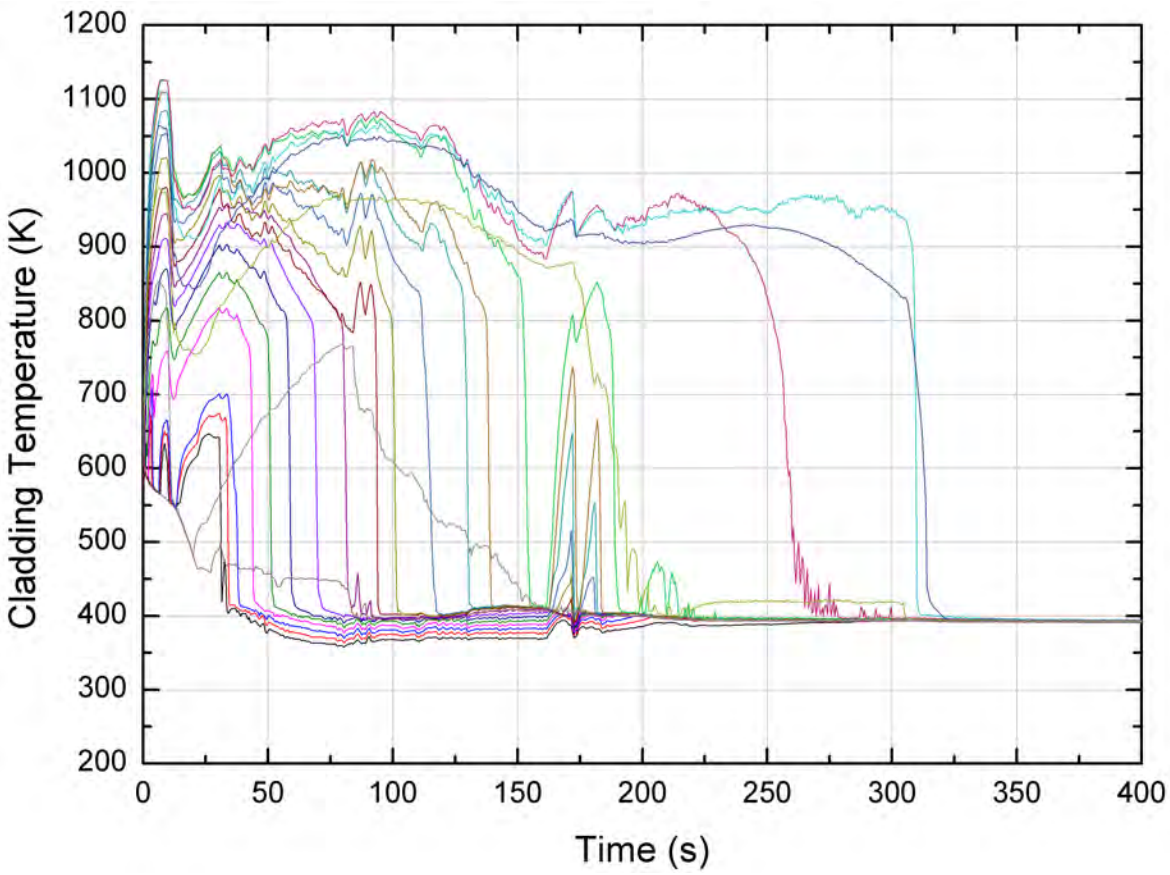

Figure 5-24 Cladding Temperatures at [ ]^{TS} of [ ]^{TS}; Base Calculation

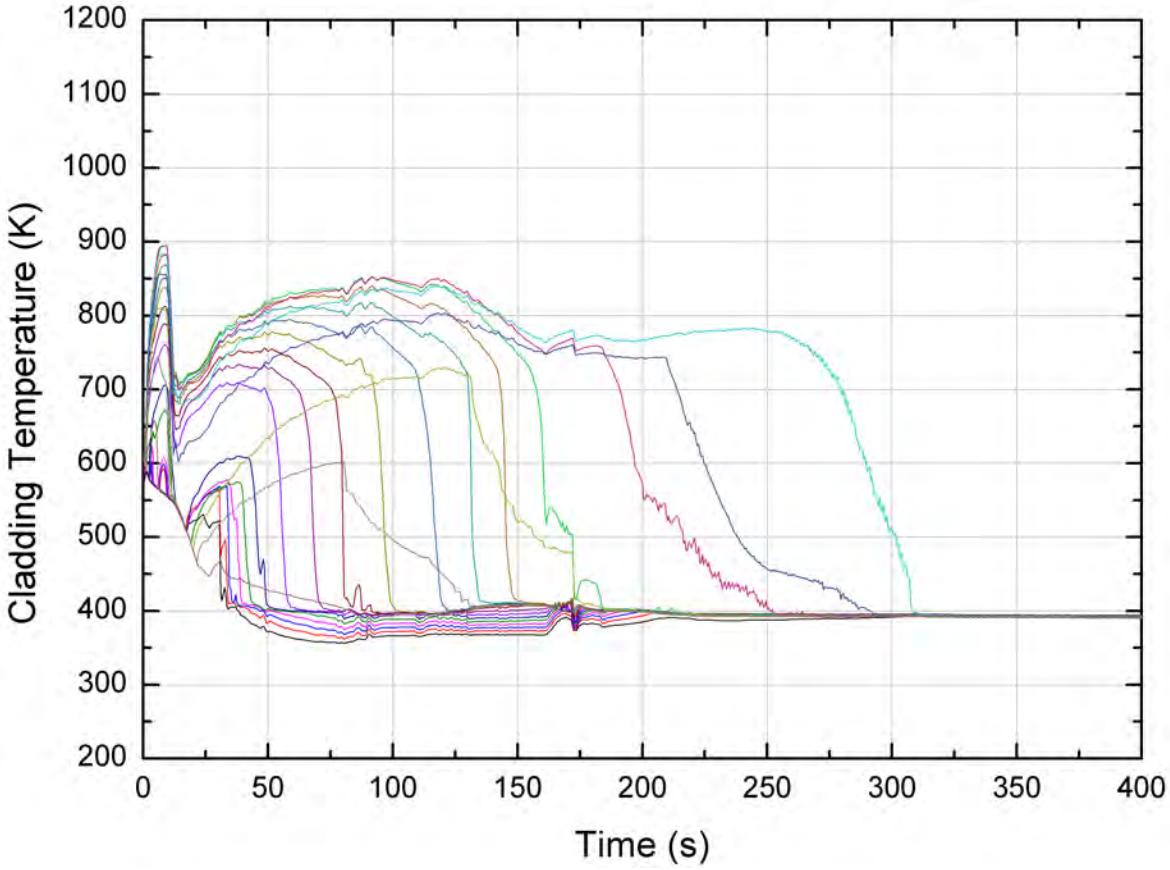

Figure 5-25 Cladding Temperatures at [ ]^{TS} of the [ ]^{TS}; Base Calculation

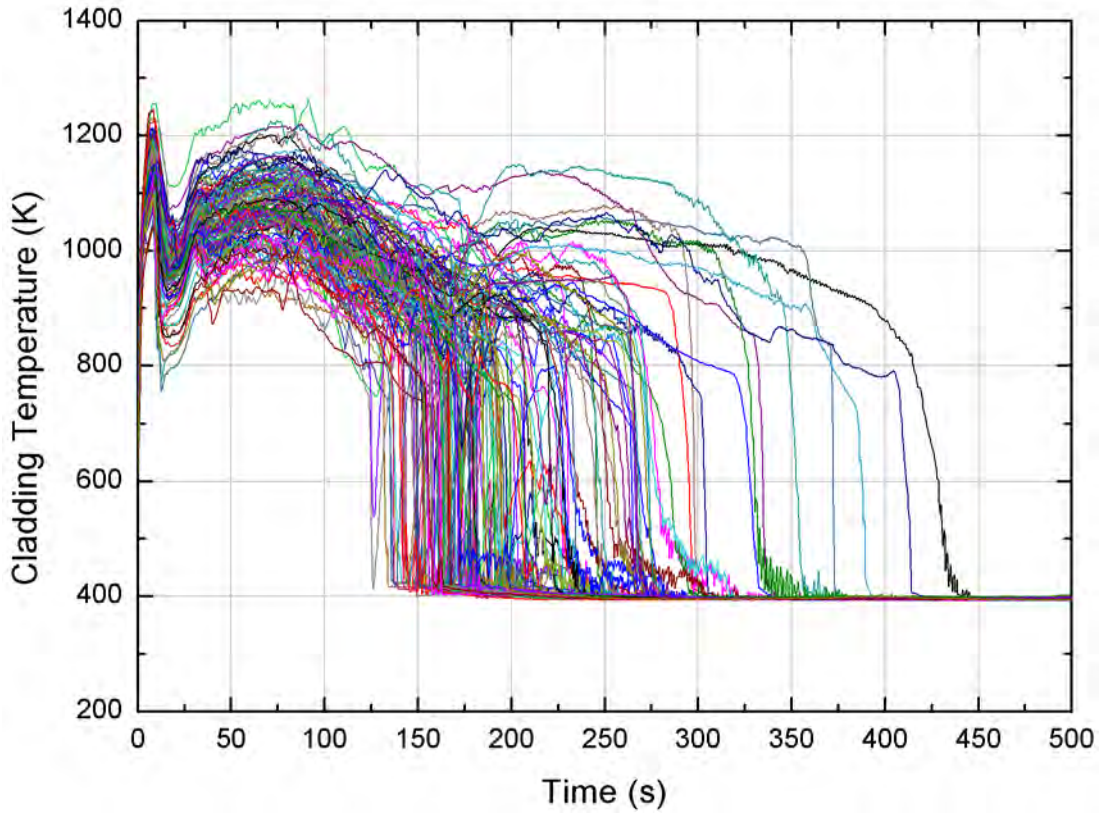

Figure 5-26 PCT Results from the SRS Calculations for Shin-Kori Units 3 and 4

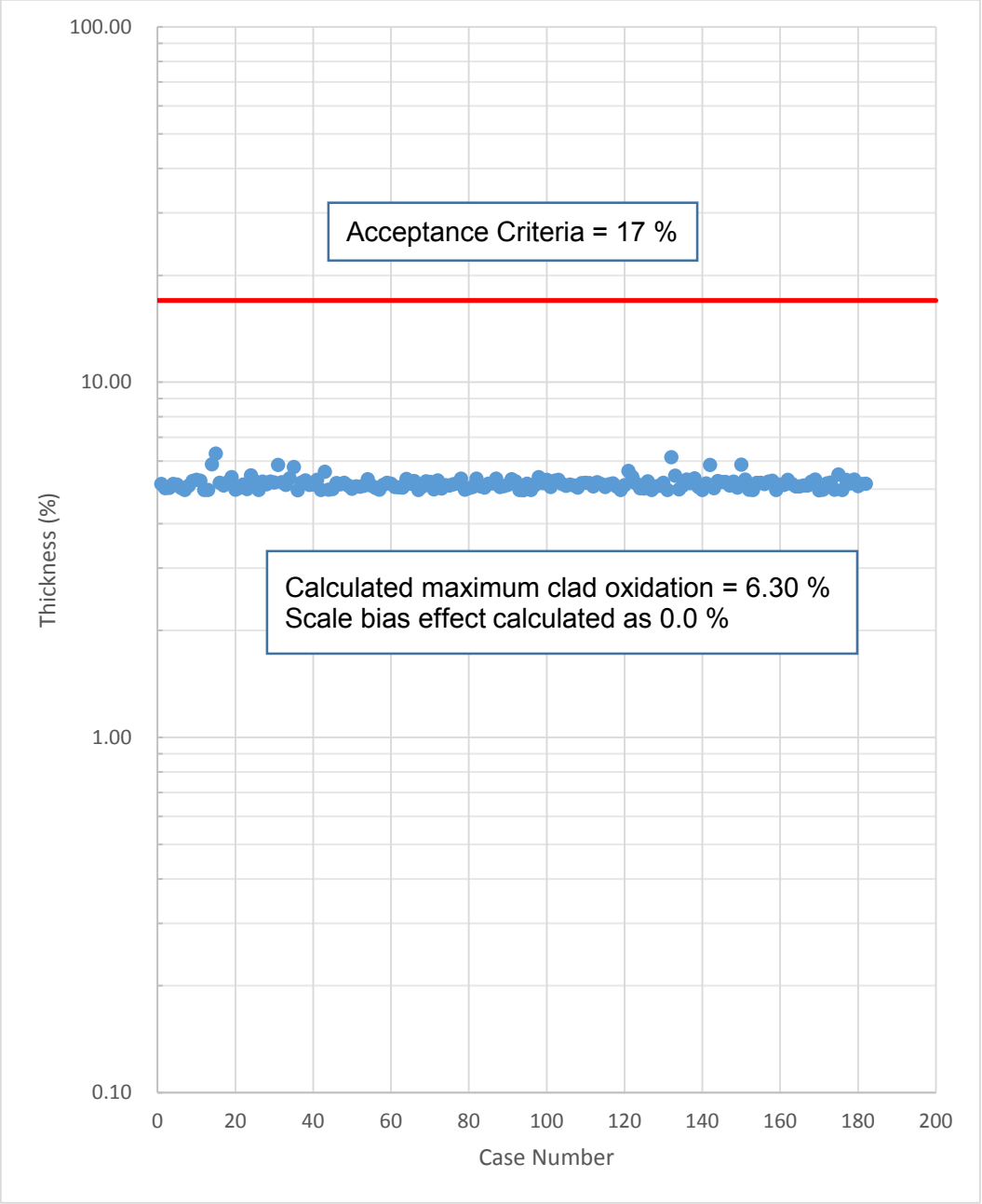

Figure 5-27 Peak Local Oxidation Results from the SRS Calculations for Shin-Kori Units 3 and 4

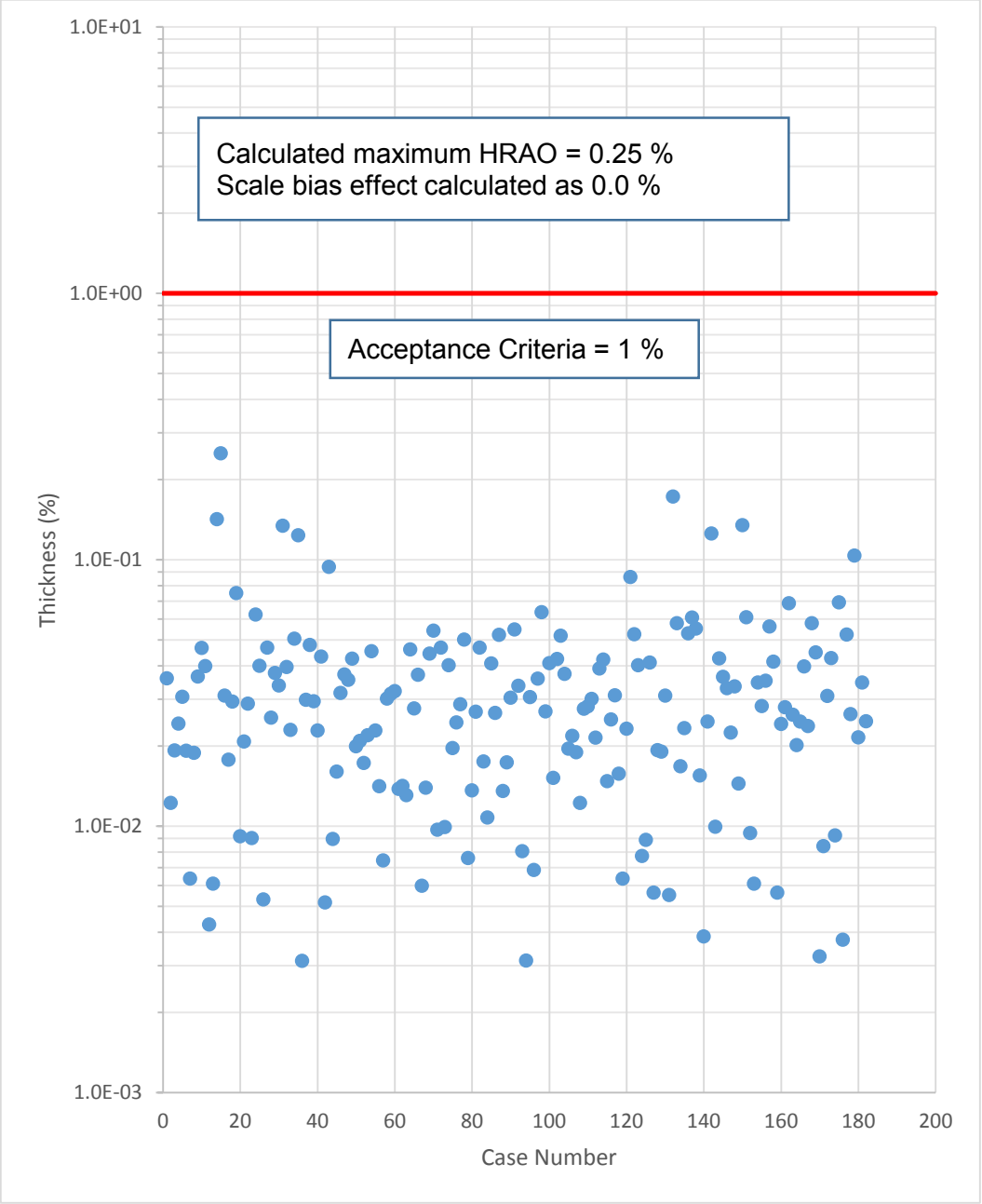

Figure 5-28 Hot Rod Hydrogen Generation Results from the SRS Calculations for Shin-Kori Units 3 and 4

6. Quantification of Total Uncertainties (Steps 13, 14)

Uncertainties from the sources other than the code models or plant operation conditions, such as the automatic time-step control function and the data reading frequency of RELAP5, need to be evaluated. It is, however, very difficult to discern the effects of these sources from the calculated clad temperatures. So, an error of 10 K was estimated based on the experiences with RELAP5, and thus 10 K is added to the results of the previous step PCT. The final results, with which the acceptance criteria are to be compared, are found below, and it is shown that these results satisfy the acceptance criteria with a sufficient margin for SKN 3 and 4.

Peak clad temperature = 1,293 + 10 K

= 1,303 K (1,885 ^{o}F) < 1,477 K (2,200 ^{o}F)

Peak local oxidation = 6.3 % < 17 %

Maximum hot rod hydrogen generation = 0.25 % $\ll$ 1%

7. Conclusion

This report described CAREM, a realistic evaluation method for the analysis of an LBLOCA in APR1400, and demonstrated its application to Shin-Kori units 3 and 4 (the first APR1400 type nuclear power plants).

The method strictly follows the concept and the philosophy of “Code Scaling, Applicability, and Uncertainty (CSAU) [1]” demonstrated by the United States Nuclear Regulatory Commission and conforms to the guidelines of Regulatory Guide (RG) 1.157, “Best-Estimate Calculations of Emergency Core Cooling System Performance [2]." Three elements and 14 steps of the method as in CSAU are explained in detail in this report. Statistical techniques used to quantify the overall uncertainty of the calculation are different from those of CSAU in order to accommodate the increased number of uncertainty parameters, but still conform to the requirements of RG 1.157. The method evaluates the values to compare with the acceptance criteria of 10 CFR 50.46 (b) [3], but does not cover the so-called long term performance of an emergency core cooling system.

CAREM uses the modified RELAP5/MOD3.3 and CONTEMPT4/MOD5 for the calculations of the system thermal hydraulics and the containment backpressure, respectively. All 14 specific steps of this method, including the determination of the code applicability, the evaluation of the code accuracy, and the confirmation of the experimental data covering etc. were performed. Code assessment against SETs and IETs confirmed the applicability of the modified RELAP5 to the LBLOCA analysis of APR1400 type plants.

A demonstration calculation was performed for the Shin-Kori (SKN) units 3 and 4, the first APR1400 type nuclear power plants. The APR1400 type plant is a two-loop PWR with 1400 MWe. It adopts a new design concept of ECCS with direct vessel injection, four trains of mechanically and electrically independent safety injection pumps, fluidic device-installed safety injection tanks, and an in-containment refueling water storage tank. Simple-random sampling calculations were performed 181 times adopting distribution-free statistics. And 95 % tolerance limit values of peak cladding temperature, peak local oxidation, and maximum hot rod hydrogen generation were evaluated and compared with the corresponding acceptance criteria.

Results of the demonstration calculations assured that the performance of the emergency core cooling system during an LBLOCA of APR1400 had enough margins to meet the acceptance criteria.

References

[1] "Quantifying Reactor Safety Margins; Application of Code Scaling, Applicability and Uncertainty Evaluation Methodology to a Large Break Loss of Coolant Accident," NUREG/CR-5249, Technical Program Group, October 1989.

[2] "Best-estimate calculations of emergency core cooling system performance," Regulatory Guide 1.157, May 1989.

[3] United States Code of Federal Regulations, Title 10, Section 50.46.

[4] "Performance Verification Test for APR1400 Fluidic Device," A03NJ02, KAERI, February 2005.

[5] "Phenomena Identification and Ranking Tabulation Korean Next Generation Reactor Large Break Loss of Coolant Accident," KINS/INEEL, 2001.

[6] C. C. Lin, C. Economos, "CONTEMPT4/MOD4, A Multicompartment Containment Analysis Program," NUREG/CR-3716, BNL-NUREG-51754, US.NRC, March 1984.

[7] "CONTEMPT4/MOD5: An improvement to CONTEMPT4/MOD4 multi- compartment containment system analysis program for ice containment analysis," NUREG/CR-4001, BNL-NUREG-51894, Brookhaven National Laboratory, 1984.

[8] V. H. Ransom, "The RELAP5 Two-Fluid Model and Associated Numerical Methods," Purdue Univ., June 1994.

[9] "RELAP5/MOD3 Code Manual Vol. 6, Validation of Numerical Techniques in RELAP5/MOD3.0," NUREG/CR-5535 Revision 1, December 2001.

[10] None

[11] Topical Report, "The best evaluation methodology for the Emergency Core Cooling System," TR-KHNP-002, KEPRI/KHNP, December 2002.

[12] "FRAPCON-4.0: A Computer Code for the Calculation of Steady-State, Thermal-Mechanical Behavior of Oxide Fuel Rods for High Burnup," PNNL-19418, Vol.1, Rev.2, September 2015.

[13] D. A. Powers, R. O. Meyer, "Cladding Swelling and Rupture Models for LOCA Analysis," NUREG-0630, US. NRC, March 1980.

[14] J. V. Cathcart, "Zirconium Metal-Water Oxidation Kinetics IV. Reaction Rate Studies," ORNL/NUREG-17, July 1977.

[15] L. D. O'Dell, "Realistic LB-LOCA Methodology for PWR," Framatome, EMF-2103(NP) Revision 0, 2001.

[16] "Development of PCT Uncertainty Quantification Methodology, Assessment of Separate Models and Construction of Thermal-Hydraulic Data Banks for Establishment of the Korean ECCS Evaluation Model," KINS/GR-011, December 1990.

[17] Weismann et al., "Studies of Transition Boiling Heat Transfer with Saturated Water at 1.4 Bar," NP-1899, Research Project 688-1, June 1981.

[18] American National Standard Decay Heat Power in Light Water Reactors, ANSI/ANS-5.1-

1979.

[19] D. F. Ross et al., “Compendium of ECCS Research for Realistic LOCA Analysis,” USNRC, NUREG-1230, April 1987.

[20] “RELAP5/MOD3.3 Code Manual Volume 4: Models and Correlations,” NUREG/CR-5535 Rev P3, March 2006.

[21] “Post-LOCA Long Term Cooling Evaluation Model,” APR1400-F-A-NR-14003-P, Rev.0, September 2014.

[22] “KCE-1 Critical Heat Flux Correlation for PLUS7 Thermal Design,” APR1400-F-C-TR-14003-P, Rev.0, November 2012.

[23] Reliability Engineering and System Safety, Vol. 80, Issue 3, pp.217-232, June 2003.

[24] H. Glaser, “BEMUSE Phase VI Report, Status report on the area, classification of the method, conclusions and recommendations,” NEA/CSNI/R(2011)4, March 2011.

[25] Topical Report, "PLUS7 Fuel Design for the APR1400,” APR1400-F-M-TR-13001-P-A, August 2018.

Appendix A

Identification and Ranking of Phenomena and Processes

Non-Proprietary

August 2018

Table of Contents

List of Tables

List of Figures

1. Introduction

Phenomena identification and ranking table (PIRT) is used to identify major phenomena that occur during relevant accidents of the reference plant, and to prioritize the phenomena according to their effects on major safety parameters. PIRT is essential to understand the phenomena or processes that occur during the accident, and to determine code capability and uncertainty parameters.

The PIRT for a large-break loss-of-coolant accident (LBLOCA) of APR1400 was developed based on the LBLOCA PIRT for "Korea Next Generation Reactor (KNGR)" by Wilson et al. 2001 [1]. KNGR was the name for APR1400 at its early developmental stage. KNGR PIRT was prepared by Idaho National Engineering and Environment Laboratory (INEEL) for Korea Institute of Nuclear Safety (KINS), the regulatory body of Korea. APR1400 PIRT has been established by adopting KNGR PIRT and reflecting the final design features of APR1400 and the results of the experiments specific to APR1400.

This appendix explains KNGR PIRT and its modifications. KNGR PIRT is explained in Chapter 2 and the adjustments of the rankings are explained in Chapter 3. All the adjustments were reviewed by the peer review group consisting of six experts in nuclear reactor research and operation. The determined APR1400 PIRT is provided in Chapter 4.

2. PIRT for "Korea Next Generation Reactor"

KNGR PIRT was prepared through 15 processes starting with defining the purpose of the PIRT and finishing with documenting the final PIRT. Figure 1 shows the development process of KNGR PIRT. The PIRT process used for KNGR is similar to those used in other preceding PIRT developments. Examples of prior PIRT efforts can be found in other references [2]-[8]. Applications of the process have repeatedly demonstrated that the collective knowledge of experts group significantly increase the probability of phenomena or processes of importance being identified. The KNGR PIRT panel has about 150 man-years of collective experience in nuclear reactor research and operation. The panel members were:

Dr. Brent E. Boyak (Los Alamos National Laboratory)

Dr. Bub-Dong Chung (Korea Atomic Energy Research Institute – KINS Representative)

Dr. Lawrence E. Hochreiter (Pennsylvania State University)

Dr. Jose N. Reyes (Oregon State University)

Mr. Gary E. Wilson (Idaho National Engineering and Environmental Laboratory – Panel Chairman)

The scenario selected for KNGR PIRT was an LBLOCA of a double-ended guillotine break in a cold leg with the assumptions of loss of off-site power and failure of one diesel generator. The assumptions led to the availability of only one, out of two, hydraulic division of the safety injection system. Each division included two safety injection pumps; and only two, out of four, safety injection pumps were credited in the scenario.

The relative importance of phenomena is time-dependent as an accident progresses. For KNGR PIRT, the panel divided the LBLOCA scenario into four temporal periods. These periods, termed blowdown (1), refill (2), reflood (3), and long-term cooling (4) were defined by the core and lower plenum liquid mass fractions as delineated in Table 1. The numbers in parentheses were used as indices of the periods in the PIRT. The blowdown period begins when the break occurs and ends when the lower plenum begins to refill. The refill period ends when the liquid level in the vessel lower plenum approaches the core inlet and remains full thereafter. The reflood period ends when the

entire core is quenched, that is, all fuel rod cladding temperatures are at or slightly above the coolant saturation temperature. The long-term cooling period continues after quenching. The first three time periods are standard for most PWR PIRTs. The last time period recognizes the possibility of fuel rod reheating after the depletion of safety injection tanks with no low-pressure safety injection pumps available.

The panel divided the plant into systems, components, and sub-components. The high-level systems selected for KNGR PIRT were the containment system, safety injection system, reactor coolant system, steam generator system, and reactor vessel. Each high-level system was partitioned into components and their sub-components; and then phenomena and processes occurring in the sub-components were identified. By dividing the plant into smaller elements and focusing on local phenomena, the panel ensured that no phenomena or processes were omitted. The figure-of-merit used to judge the relative importance of systems, components, phenomena, and processes was peak cladding temperature for the blowdown, refill, and reflood periods. Given there was some possibility of fuel rod reheat following initial quenching in reflood, stable core quenching was used as the figure-of-merit for the long-term cooling period.

The panel used a ranking scale of one to five to indicate the relative importance of systems, components, and phenomena or processes. Rank 1 indicates the lowest importance whereas rank 5 represents the highest importance. The ranking scale for relative importance of systems, components, and phenomena or processes is provided in Table 2.

KNGR PIRT is presented in Table 3. The table is constructed in the context of systems, components, phenomena or processes, and their ranks in four temporal periods.

3. Modification of PIRT for APR1400

The scenario employed for KNGR PIRT was based on the results of the code simulations of RELAP5/3D, RELAP5/MOD3.2.2-gamma, and TRAC-M. Two RELAP5 calculations and their brief comparisons with TRAC-M calculation are discussed in Appendix C of Reference [1]. [

]^{TS}

The difference between the SIT flow rate in the RELAP5 calculations and that of the TRAC-M calculations resulted in differences in calculated plant behaviors. [

]^{TS}

[

]^{TS} KNGR PIRT was developed based on the [

]^{TS} A more general criterion is necessary to distinguish the reflood from the long-term cooling period.

In this context, the four temporal periods and consequent ranking of the phenomena or processes in each period had to be modified. Definitions of the temporal periods in “Code Scaling, Applicability

and Uncertainty" by B. Boyack et al. 1989 [3] were referenced. Sections 3.1 and 3.2 explain the modification of the four temporal periods and subsequent adjustment of the ranking, respectively.

3.1 Definition of Time Phases

The LBLOCA scenario of APR1400 is divided into four temporal periods. The definitions of each period are described in Table 4. The periods are termed blowdown (1), refill (2), early reflood (3), and late reflood (4). The numbers indicated in parentheses are used as indices in the PIRT to denote each period.

(1) The blowdown period starts when the break occurs and ends when SIT injection initiates.

(2) The refill period ends when the mixture level in the vessel lower plenum approaches the core inlet and remains full thereafter.

(3) The early reflood period ends when SITs are emptied.

(4) The late reflood period continues after SITs are emptied.

3.2 Adjustment of the Rankings

It is necessary to adjust the relative importance of phenomena or processes after modifying the definition of temporal periods. In addition, finalization of the APR1400 design and the findings of the experiments and code simulations, which have been performed after the development of KNGR PIRT, need to be reflected.

The same ranking scale used for the relative importance of phenomena or processes of KNGR PIRT, described in Table 2, is used for APR1400 PIRT. It should be ensured that the phenomena or processes of [ ]^{TS} are considered in the calculation. For these phenomena or processes, relevant uncertainty parameters were identified and their uncertainties were reflected in plant calculations in principle. In cases where the identification of uncertainty parameters was not probable, [ ]^{TS} Relevant uncertainty parameters for [ ]^{TS} were not identified. As described in Table 2, [ ]^{TS} allow modeling of the phenomena or processes with inaccuracy or moderate accuracy. As the RELAP5 code has best-estimate features, those phenomena or processes [ ]^{TS} can be modeled with moderate accuracy if the phenomena or processes are not ignored in the calculation. Modeling of these phenomena or processes includes [ ]^{TS}, and so on. Phenomena or processes of ranks lower than [ ]^{TS} are paid no attention.

Among the phenomena or processes of KNGR PIRT, those phenomena or processes, of which the importance ranking is equal to or higher than [ ]^{TS} in any temporal period, are considered when adjusting the rankings. This selection criterion was established in order to prevent omitting significantly important phenomena or processes. Phenomena or processes of [ ]^{TS} can be modeled by applying the models and correlations as they are in the code or by the nodalization capability of the RELAP5 code. The uncertainty of all the other phenomena or processes, or the combined effect of not-considered low ranked phenomena or processes can be accounted for in [ ]^{TS} of this method.

Modifications on KNGR PIRT are described below, item-by-item, along with the rationale. The indices for each time period used in the following tables are "1" for the blowdown, "2" for the refill, "3" for the early reflood, and "4" for the late reflood periods as described earlier.

TS

TS

TS

TS

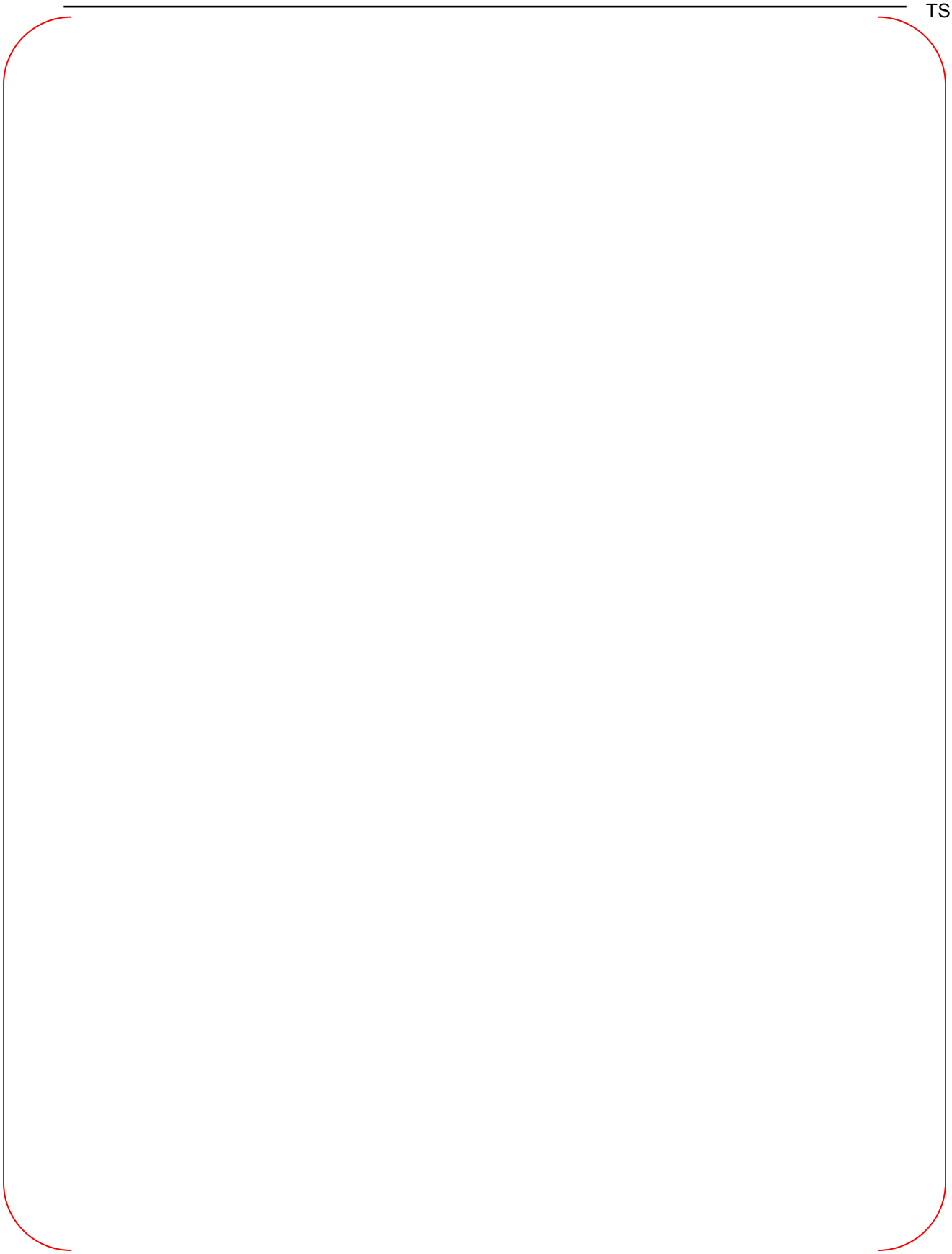

TS

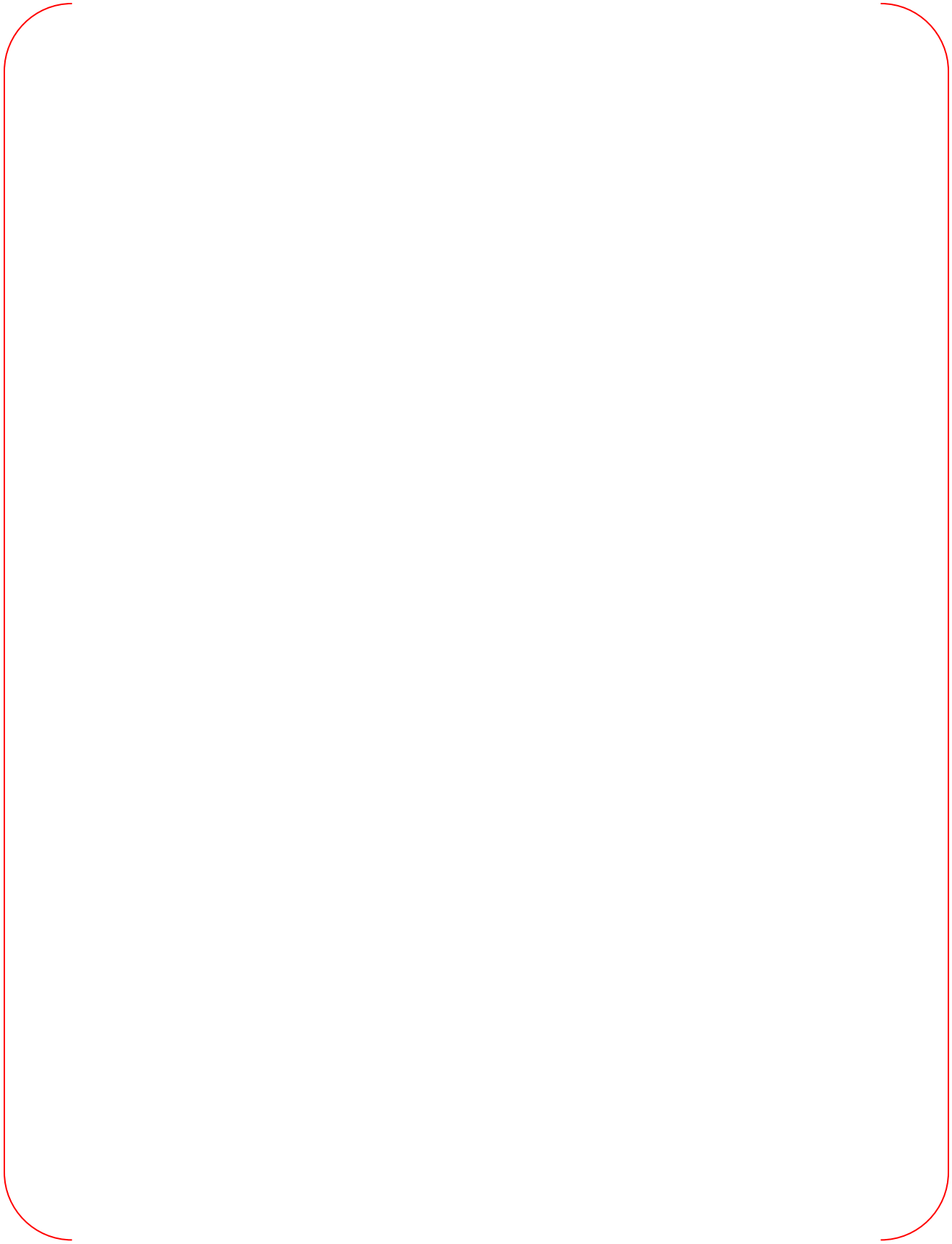

TS

TS

TS

TS

4. PIRT for APR1400

APR1400 PIRT is described in Table 5. Findings from further code simulations and experiments performed after the preparation of KNGR PIRT are incorporated. Final features of the APR1400 design are also reflected. [ ]^{TS} phenomena or processes from [ ]^{TS} components are ranked as important. The number of phenomena or processes for each component is as follows:

TS

TS

5. Conclusion

The APR1400 LBLOCA PIRT was developed based on the initial PIRT which was prepared at the developmental stage of APR1400, in this appendix. The APR1400 PIRT was established by reflecting the final design features of APR1400 and the results of the experiments specific to APR1400.

This PIRT was used as basis for the demonstration of code applicability, the determining uncertainty parameters, and the uncertainty quantification.

Table 1 Definition of Time Phases for KNGR PIRT

Phase (Number)*)	Starts at	Ends at
Blowdown (1)	Break initiation	Initiation of lower plenum refill
Refill (2)	End of blowdown	Initiation of core recovery (liquid level at bottom fuel rod heated length)
Reflood (3)	End of refill	Initial core quench
Long-term cooling (4)	Initial core quench	Stable core quench

*) The numbers indicated in parentheses are used as indices in the PIRT to denote each phase in that table.

Table 2 Ranking Scale for Relative Importance

Rank	General Descriptors
5	- **Highest of the high** - Experimental simulations and analytical modeling, with a high degree of accuracy, are critical.
4	- **High influence on safety criteria** - Needs to be experimentally present and/or analytically modeled with a high degree of accuracy. - Approximately one-half the importance of rank 5.
3	- **Moderate influence on safety criteria** - Needs to be experimentally present and/or analytically modeled with a moderate degree of accuracy. - Approximately one-half the importance of rank 4.
2	- **Low influence on (or importance to) safety criteria** - Needs to be experimentally present and/or analytically modeled, but [ ]^{TS} - Approximately one-half the importance of rank 3.
1	- **Lowest of the low in importance** - Very low influence on (or importance to) safety criteria. - Approximately one-half the importance of rank 2.
IS	A system, component or process/phenomena may be active; however, its influence on the safety criteria is insignificant and may be ignored
NA	A system, component or process/phenomena is not active or present

Table 3 KNGR PIRT (1/8)

TS

Table 3 KNGR PIRT (2/8)

TS

Table 3 KNGR PIRT (3/8)

TS

Table 3 KNGR PIRT (4/8)

TS

Table 3 KNGR PIRT (5/8)

TS

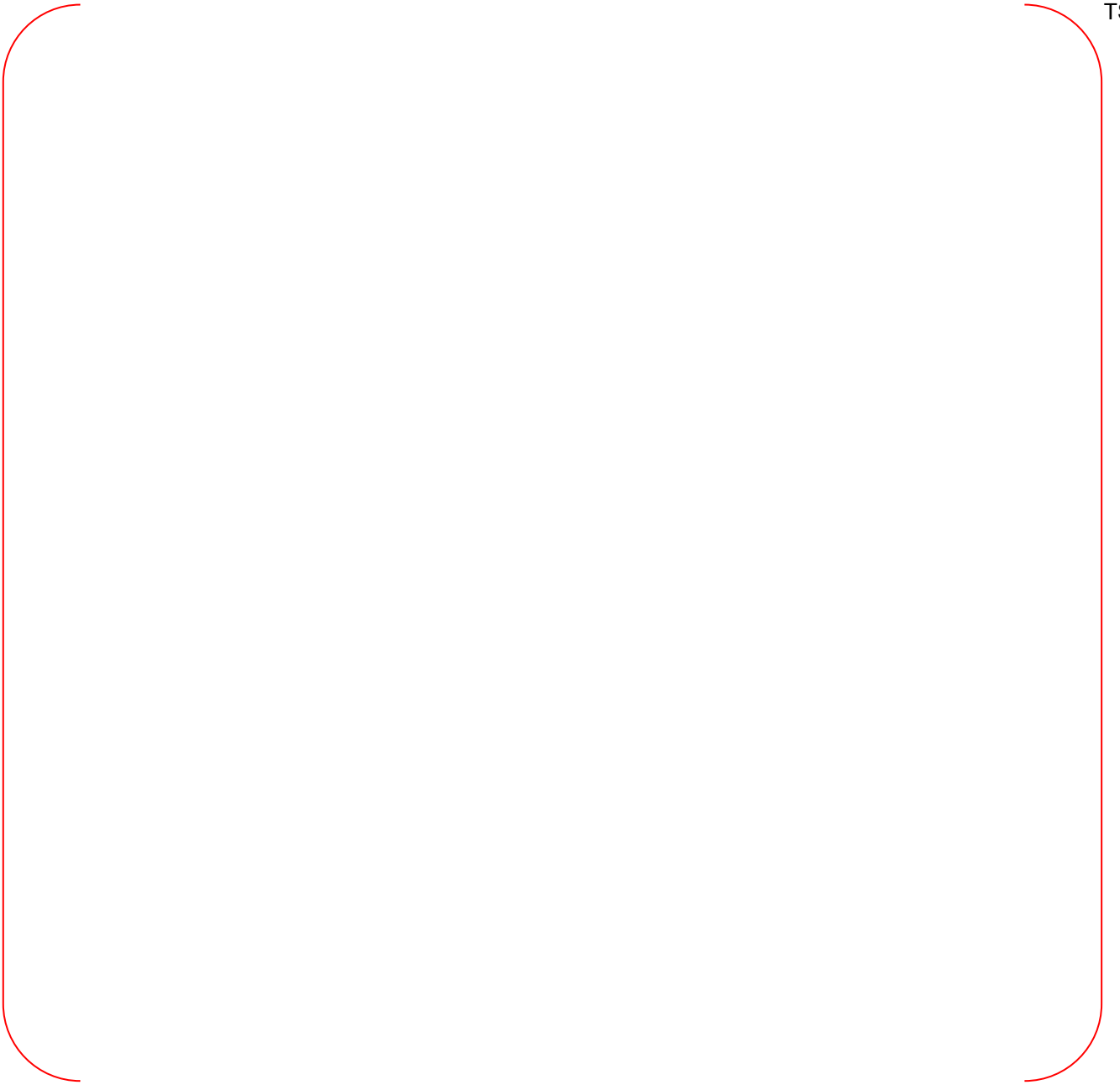

Table 3 KNGR PIRT (6/8)

TS

Table 3 KNGR PIRT (7/8)

TS

Table 3 KNGR PIRT (8/8)

TS

Table 4 Definition of Time Phases for APR1400 PIRT

Phase (Number)*)	Starts at	Ends at
Blowdown (1)	Break initiation	Initiation of SIT injection
Refill (2)	Initiation of SIT injection	Initiation of core recovery (Mixture level at bottom fuel rod heated length)
Early Reflood (3)	Initiation of core recovery	End of SIT injection
Late Reflood (4)	End of SIT injection	Stable core quench

*) The numbers indicated in parentheses are used as indices in the PIRT to denote each phase in that table.

Table 5 APR1400 PIRT (1/3)

TS

Table 5 APR1400 PIRT (2/3)

TS

Table 5 APR1400 PIRT (3/3)

TS

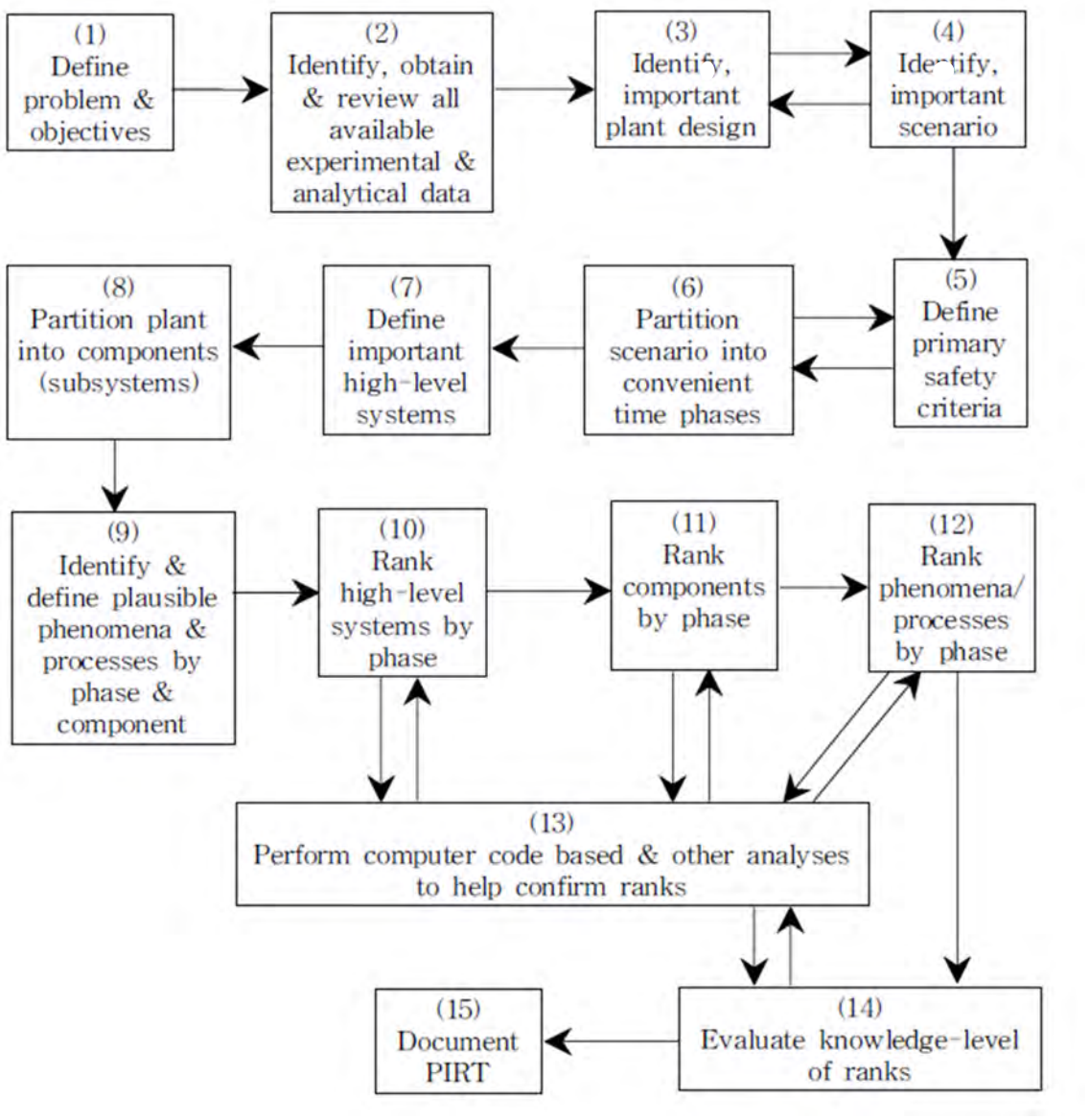

Figure 1 KNGR PIRT Process Flow Diagram

References

[1] "Phenomena Identification and Ranking Tabulation, Korean Next Generation Reactor Large Break Loss of Coolant Accident," WFO861702, KINS/INEEL, January 2001.

[2] R. A. Shaw, T. K. Larson and R. K. Dimenna, "Development of a Phenomenal Identification and Ranking Table (PIRT) for Thermal-hydraulic Phenomena during a PWR LBLOCA," NUREG/CR-5074, EG&G Idaho Inc., 1988.

[3] TPG (Technical Program Group), "Quantifying Reactor Safety Margins: Application of Code Scaling, Applicability, and Uncertainty Evaluation Methodology to a Large-Break, Loss-of-Coolant Accident," NUREG/CR-5249, EG&G Idaho Inc., 1989.

[4] TPG (Technical Program Group), "Quantifying Reactor Safety Margins: Application of Code Scaling, Applicability, and Uncertainty Evaluation Methodology to a Large-Break, Loss-of-Coolant Accident," Nuclear Engineering and Design, Vol. 119, pp. 1-117, 1990.

[5] M. G. Ortiz and L. S. Ghan, "Uncertainty Analysis of Minimum Vessel Liquid Inventory During a Small-Break LOCA in a B&W Plant – An Application of the CSAU Methodology Using the RELAP5/MOD3 Computer Code," NUREG/CR-5818, EG&G Idaho Inc., 1992.

[6] B. E. Boyack, "AP600 LBLOCA Phenomena Identification and Ranking Tabulation," LA-UR-95-2718, Los Alamos National Laboratory, 1995.

[7] G. E. Wilson et al., "Phenomena Identification and Ranking Tables for Westinghouse AP600 Small Break Loss-of-Coolant Accident, Main Steam Line Break, and Steam Generator Tube Rupture Scenarios," NUREG/CR-6541, Idaho National Engineering and Environmental Laboratory, Lockheed Idaho Technologies Company, June 1997.

[8] G. E. Wilson and B. E. Boyack, "The Role of the PIRT Process in Identifying Code Improvements and Executing Code Development," Proceedings of the OECD/CSNI Workshop on Transient Thermal-Hydraulic and Neutronic Codes Requirements (November 5-8, 1996), NUREG/CP-0159, Scientech, July, 1997.

[9] "Compendium of ECCS Research for Realistic LOCA Analysis," NUREG-1230, R4, Division of Systems Research, Office of Nuclear Regulatory Research, NRC, December 1988.

Appendix B

Freezing of RELAP5/MOD3.3/K

Non-Proprietary

August 2018

Abstract

The best-estimate code selected for CAREM is RELAP5/MOD3.3. The light water transient analysis code, RELAP5, was originally developed at the Idaho National Engineering Laboratory (INEL) for the U.S. Nuclear Regulatory Commission (NRC). RELAP5/MOD3.3 was developed jointly by the U.S. NRC, a consortium of several countries, and U.S. organizations that were members of the International Code Assessment and Application Program (ICAP) and its successor organization, Code Application and Maintenance Program (CAMP). This version has been preceded by many code versions and several new models, improvements to existing models, and user conveniences have been added to the current version. RELAP5/MOD3.3 is supported by a set of documentations.

The results of a broad assessment effort, however, showed that this code version has a tendency to predict quenching to occur earlier than actual occurrence. It was also found that this code version had some coding errors. Therefore, a part of the code's reflood model has been modified to improve the prediction of rods quenching time and to correct coding errors.

In many plant calculations, the code frequently fails when nitrogen gas is released from the safety injection tanks. This code failure is mainly due to the thermodynamic property error resulting from the interaction between very low temperature nitrogen gas and water. Thus, the code has been modified to improve code stability by adjusting [ ]^{TS}

The modifications on the reflood model were assessed against various separate effect tests (SETS) and integral effect tests (IETs); and the effect of the fixed coding errors was confirmed by the APR1400 large break loss of coolant accident (LBLOCA) calculation. Details on code modifications and the results of the assessment against representative reflood tests, FLECHT-SEASET tests, and the APR1400 LBLOCA calculation are presented in this appendix. The validity of the modifications can also be confirmed in Appendix C (Assessment of RELAP5/MOD3.3/K against Separate-Effect Tests) and Appendix D (Assessment of RELAP5/MOD3.3/K against Integral-Effect Tests) of this topical report.

Table of Contents

List of Figures

1. RELAP5/MOD3.3 Code Modification

The best-estimate code selected for CAREM, the realistic evaluation methodology of the APR1400 large break loss of coolant accident (LBLOCA), is RELAP5/MOD3.3. This code version is the latest version of RELAP5 and adopts a modified reflood heat transfer model, which was developed by the Paul Scherrer Institute (PSI) in Switzerland.

The PSI reflood model was developed to improve quench front behavior during the reactor core reflood process. The PSI reflood model was assessed against FLECHT-SEASET Test 31504 and 31701 during the developmental stage, and it has been demonstrated that improvements to the models in the code have strengthened the code's ability to calculate more accurately the thermal-hydraulic phenomenon associated with low and high rate reflood [1]. Through the various assessments against SETs and IETs, however, it was found that the RELAP5/MOD3.3 code tends to predict rods quenching to occur earlier than the experiment results. This tendency is mainly caused by the [ ]TS

It was also found that RELAP5/MOD3.3 has coding errors in [ ]TS For plant calculations, the code run frequently fails after nitrogen gas was released from safety injection tanks (SITs). This code failure is mainly due to the thermodynamic property error resulting from the interaction between very low temperature nitrogen gas and water.

Therefore, the reflood model was improved, coding errors were corrected, and code stability was enhanced before freezing the code to use for the APR1400 LBLOCA evaluation. In addition, the coding for [ ]TS

Section 1.1 and Section 1.2 describe the details of code modifications on [ ]TS Section 1.3 describes the correction of coding errors in [ ]TS Section 1.4 describes modification of the coding for [ ]TS Section 1.5 describes the modification for enhancing code stability when nitrogen gas is released from SITs.

The verification and effects of the above modifications are presented in Chapter 2 and conclusions of this appendix are presented in Chapter 3.

1.1 Modification of [ ]TS

[TS

[ ]TS

1.2 Modification of [ ]TS

[ ]TS

TS

[TS

1.3 Correction of [ ]TS

[TS

[ ]TS

1.4 Modification of [ ]TS

[ ]TS

TS

1.5 Modification to Prevent Code Failure due to [ ]TS

TS

TS

The effect of this code modification on the system behavior is described in Chapter 2.

2. Effect of Modifications

This chapter describes the effects of the modifications addressed in Chapter 1. All the modifications described in Chapter 1 have been incorporated into the modified RELAP5/MOD3.3, named RELAP5/MOD3.3/K. The effects of the modifications have been investigated using the RELAP5/MOD3.3/K code.

The effect of the modified reflood model addressed in sections 1.1, 1.2, and 1.3 is described in Section 2.1. The effect of the modification of [ ]^{TS} is described in Section 2.2. The effect of code modification to prevent a code failure on the system behavior is described in Section 2.3.

RELAP5/MOD3.3/K has been also assessed against other various separate effect tests (SETs) and integral effect tests (IETs). The validity of the modifications described in Chapter 1 can also be confirmed through these assessments. The details of assessment against SETs and IETs are described in Appendix C and Appendix D of this topical report, respectively.

2.1 Modifications of Reflood Model

The modifications on the reflood model include modification of [ ]^{TS} The effect of the modified reflood model is investigated through assessment calculations against two FLECHT-SEASET tests, 31504 and 31108. The FLECHT-SEASET tests 31504 and 31108 are representative low and high reflood rate tests, respectively. These tests were used to check the effect of each modification in Chapter 1.

Heater rod cladding temperatures calculated by the current version, RELAP5/MOD3.3, and the modified version, RELAP5/MOD3.3/K, are compared with the data at the elevation where peak cladding temperature was measured as shown in Figure 11 and Figure 12. The data in these figures are those of the rod with peak cladding temperature. The peak cladding temperatures calculated by both codes are almost the same in both figures. However, RELAP5/MOD3.3/K shows an improvement in rod quenching time prediction compared to the current version. RELAP5/MOD3.3/K predicted rod quenching time match data fairly well for Test 31108. For Test 31504, RELAP5/MOD3.3/K conservatively over-predicts rod quenching time.

The heat transfer coefficients calculated using rod cladding temperatures in Figure 11 and Figure 12 are shown in Figure 13 and Figure 14, respectively. In both the test data and the code calculations, the heat transfer coefficients were obtained using the definition in Equation 9. The heat transfer coefficients calculated by RELAP5/MOD3.3/K match well the data or are slightly lower than the data, showing significantly improved prediction in film boiling heat transfer coefficient compared to the current version.

Differential pressures calculated by RELAP5/MOD3.3 and RELAP5/MOD3.3/K are compared with the data for the entire core region in Figure 15 and Figure 16. Since accelerational and frictional pressure losses are insignificant, differential pressure can be directly converted to the mass of liquid in the core. The differential pressure for the entire core calculated by RELAP5/MOD3.3/K is very similar to that of the RELAP5/MOD3.3 calculation. The differential pressures calculated by both codes match the data fairly well. This means that both codes predict a correct amount of liquid in the core, which implies that the predicted amount of liquid carried out from the bundle would be the same as the data. These figures show that the effect of the modified reflood model on system hydraulic behavior is insignificant.

Based on the above results, it is confirmed that the modifications on the reflood model can improve the prediction of rod quenching time and the effect of the modifications on system hydraulic behavior is insignificant.

2.2 Modification of [ ]TS

The effect of the modification of [ ]TS is investigated through the APR1400 calculation. The RELAP5/MOD3.3/K input model for APR1400 is shown in Figure 17. The results of the calculation are shown in Figure 18 through Figure 21. In these figures, two RELAP5/MOD3.3/K results are compared; one before and one after modifying [ ]TS

The [ ]TS results of two RELAP5/MOD3.3 calculations are compared with those calculated by a previous version of RELAP5/MOD3.1, as shown in Figure 18. Since [ ]TS has remained unchanged from the previous version, [ ]TS calculated without the modification (i.e., before modification) should be same as the results from RELAP5/MOD3.1. The calculated value, however, shows a difference from RELAP5/MOD3.1 due to a coding difference described in Section 1.4. Meanwhile, the calculated values with the modification on [ ]TS (i.e., after modification) match well the result of RELAP5/MOD3.1. This confirms that the coding for [ ]TS is properly modified in RELAP5/MOD3.3/K.

Figure 19 shows the comparison between peak cladding temperatures. After modification on [ ]TS, the blowdown peak cladding temperature decreases about 6 K and the reflood peak cladding temperature decreases about 35 K. Quenching time is decreased about 7 s. These differences come from initial stored energy difference of fuel, which is caused by the [ ]TS.

Figure 20 and Figure 21 show the cladding temperatures of [ ]TS axial nodes of the hottest rod calculated with and without the modification, respectively. It also shows the same tendency as Figure 19.

Based on the above results, it is confirmed that the coding for [ ]TS has been modified properly.

2.3 Modification to Prevent Code Failure [ ]TS

The effect of the modification to prevent code failure [ ]TS is investigated through the APR1400 calculations. The RELAP5/MOD3.3/K input model for APR1400 is shown in Figure 17. The results of the calculations are shown in Figure 22 through Figure 27. In these figures, two RELAP5/MOD3.3/K-calculated results are given, one with and one without [ ]TS In the APR1400 calculation, nitrogen gas released from the safety injection tank (SIT) begins to flow into the downcomer through the direct vessel injection (DVI) nozzle at around 173 s.

Figure 22 shows the calculated [ ]TS in surgeline volume of SIT-FD. According to the modification, the result of the calculation without using [ ]TS As shown in Figure 23, the [ ]TS of the same nodes in both calculations, however, is nearly zero while nitrogen is released. Therefore, it is obvious that the effect of the modification on the other parameters is negligible.

Figure 24 shows the calculated [ ]TS in an upper downcomer volume to where the DVI nozzle is connected. In both calculations, [ ]TS in the node at around 173 s, but it is regained in about 176 s. The results of both calculations show little difference. Liquid and vapor temperatures at the same node also show little differences between the calculations, as shown in Figure 25.

The collapsed water level in the downcomer also shows little difference between the calculations, as presented in Figure 26. This means that [ ]TS does not significantly affect system hydraulic behaviors.

Figure 27 shows a comparison of the cladding temperature behavior of the hottest rod. The cladding temperature behavior during the nitrogen release period is enlarged in the lower part of the figure. The cladding temperature behaviors in the two calculations are almost identical.

Based on the above results, it is confirmed that the effect of the modification to prevent code failure [ ]TS on the system thermal-hydraulic behavior is negligible. The code failure, however, has been significantly improved by [ ]TS

3. Conclusion

Through the various assessment results of the RELAP5/MOD3.3 code, it was found that this version of the code predicts [ ]^{TS} This is mainly due to [ ]^{TS} Thus [ ]^{TS} have been modified to improve the capability of predicting [ ]^{TS} The improved capability of RELAP5/MOD3.3/K in predicting [ ]^{TS} has been confirmed through the code assessment against various SETs and IETs, as described not only in this appendix but Appendix C and Appendix D of this topical report.

In addition to the above modifications, the coding for [ ]^{TS} was modified to eliminate coding error and [ ]^{TS} was modified to maintain consistency with previous versions. Through the evaluation calculations, it is confirmed that the modifications are performed properly.

Modifications to prevent code failure due to [ ]^{TS} were also made for the plant calculations. Code failure has been significantly reduced by [ ]^{TS}

All the modifications described in this appendix have been incorporated into the modified RELAP5/MOD3.3, named RELAP5/MOD3.3/K, for a frozen code version. As guided in CSAU [4], this frozen code has been rigorously maintained in order to ensure that changes to the code after an evaluation has been completed do not impact the conclusions and that changes occur in an auditable and traceable manner.

TS

Figure 1 Modification of [ ]TS

TS

Figure 2 Modification of [ ]TS

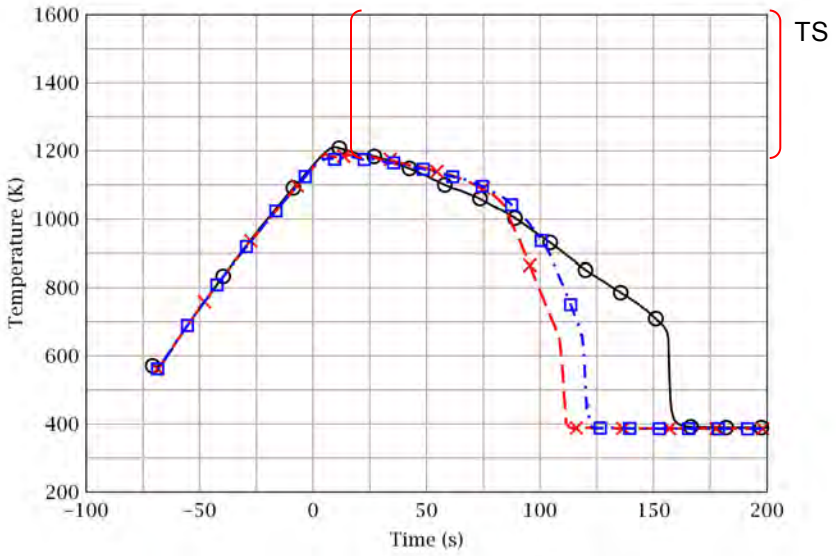

Figure 3 Effect of Modified [ ]^{TS}; FLECHT-SEASET 31108

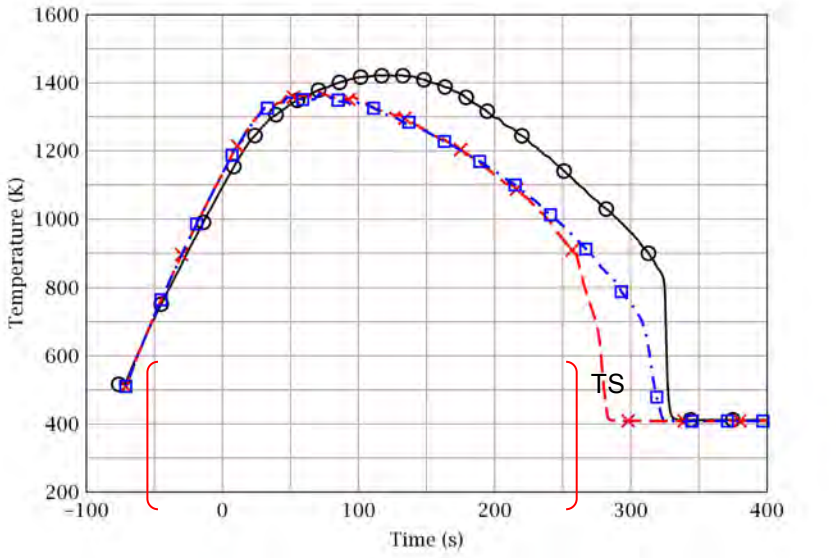

Figure 4 Effect of [ ]^{TS}; FLECHT-SEASET 31504

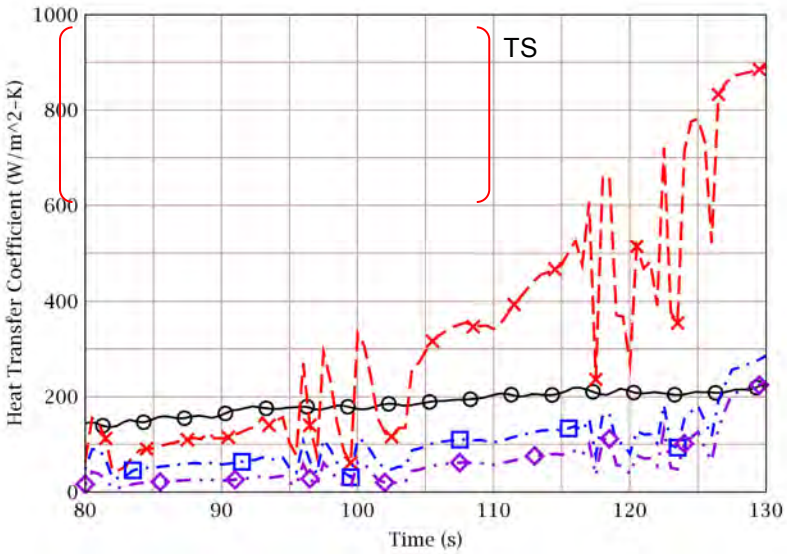

Figure 5 [ ]^{TS}; FLECHT-SEASET 31108

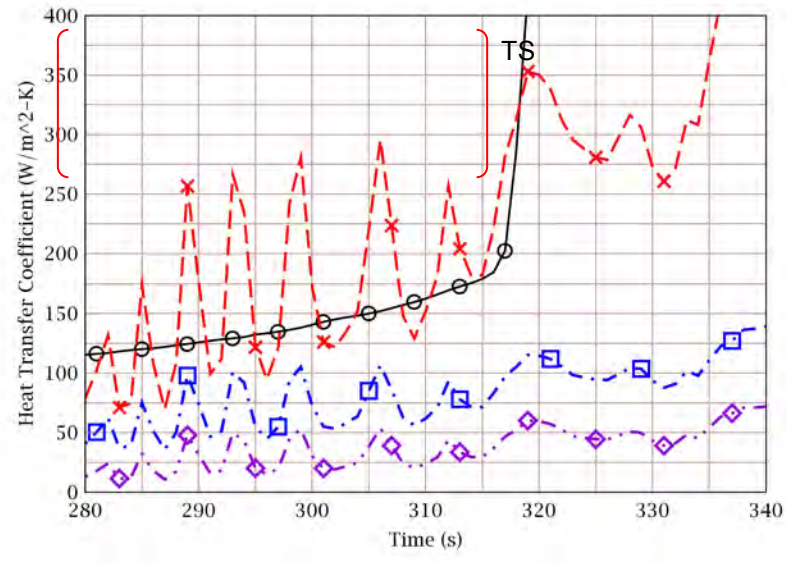

Figure 6 [ ]^{TS}; FLECHT-SEASET 31504

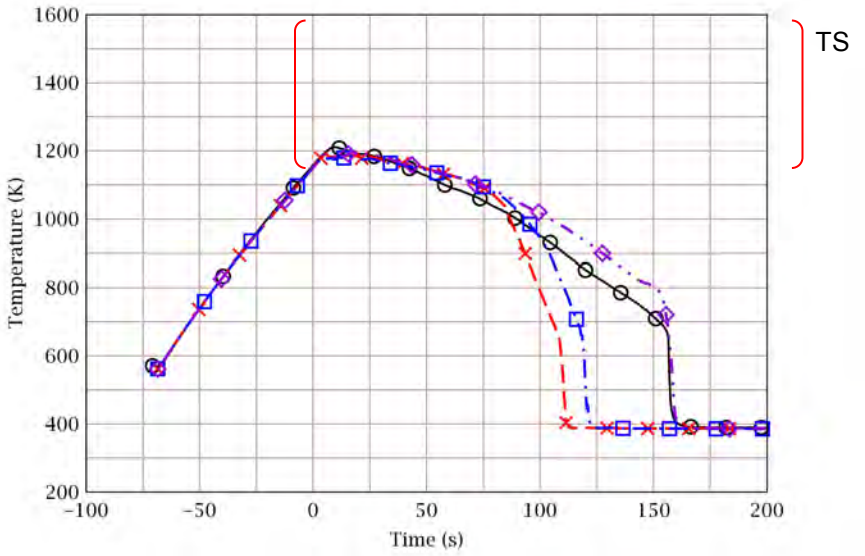

Figure 7 [ ]TS; FLECHT-SEASET 31108

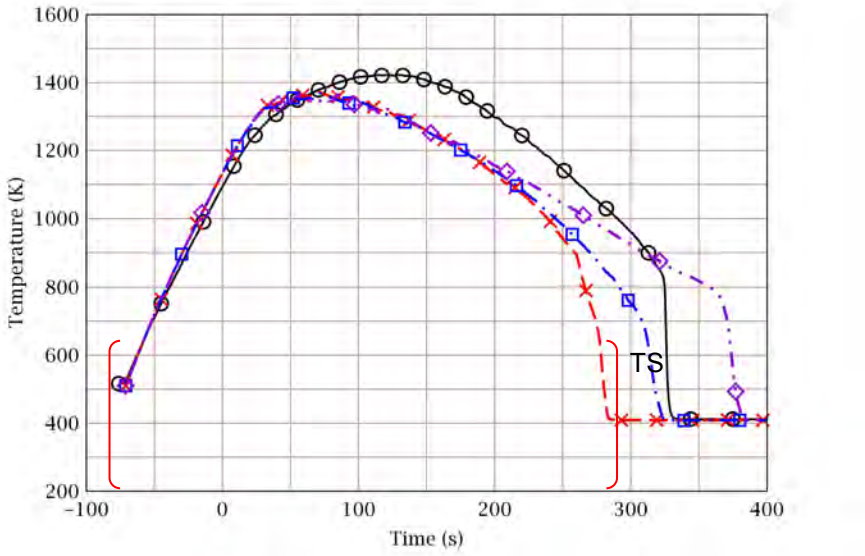

Figure 8 [ ]TS; FLECHT-SEASET 31504

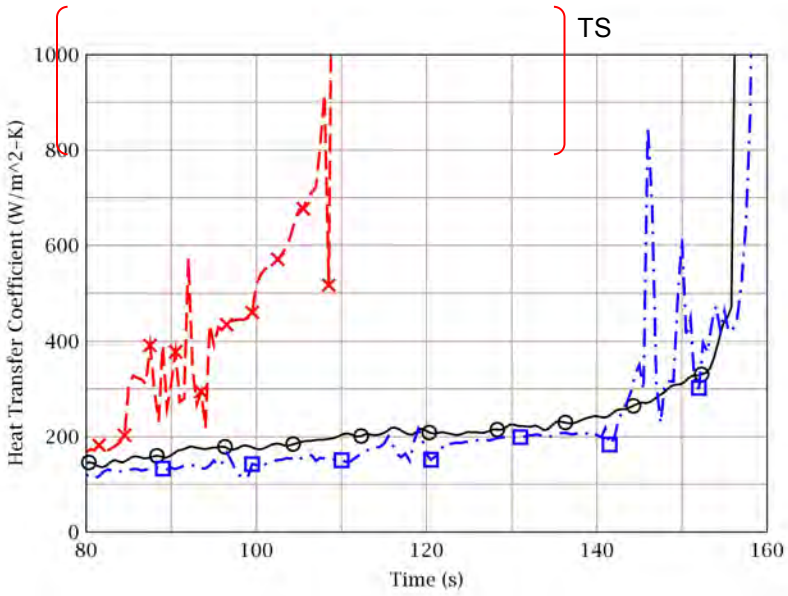

Figure 9 [ ]TS; FLECHT-SEASET 31108

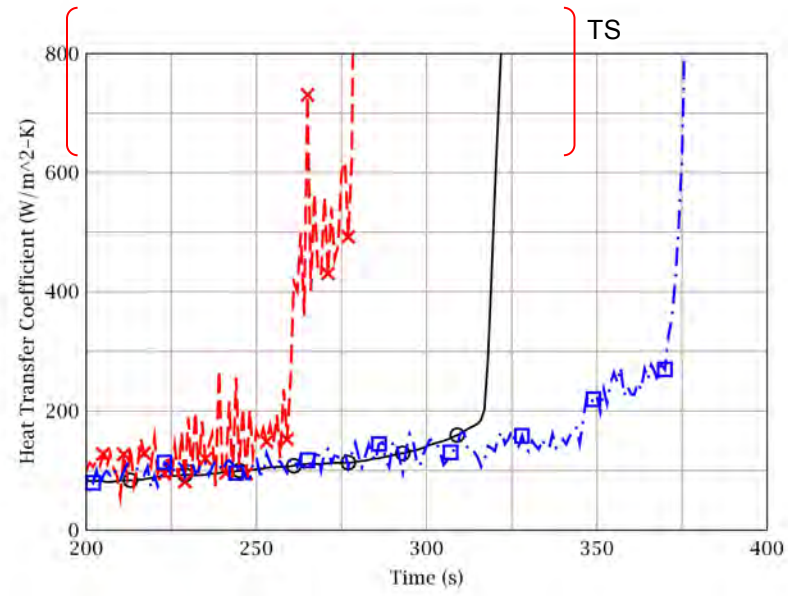

Figure 10 [ ]TS; FLECHT-SEASET 31504

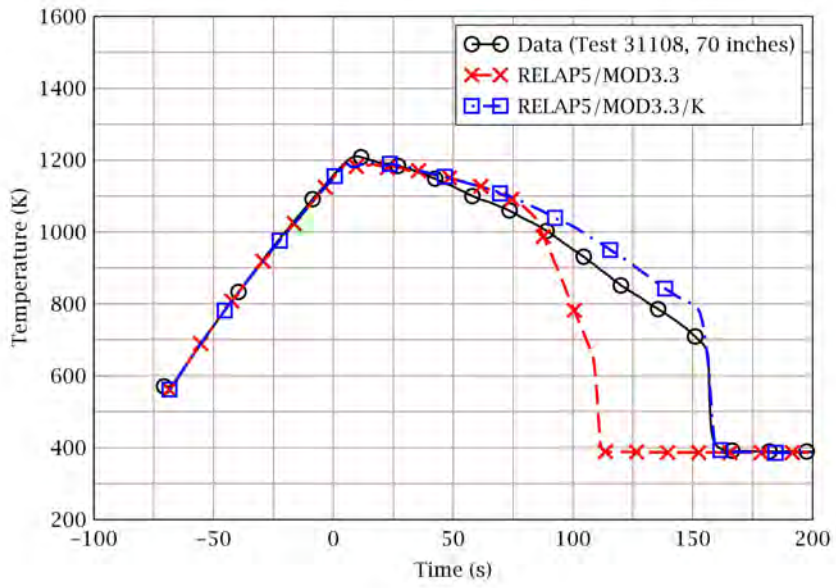

Figure 11 Comparison of Rod Cladding Temperature; FLECHT-SEASET 31108

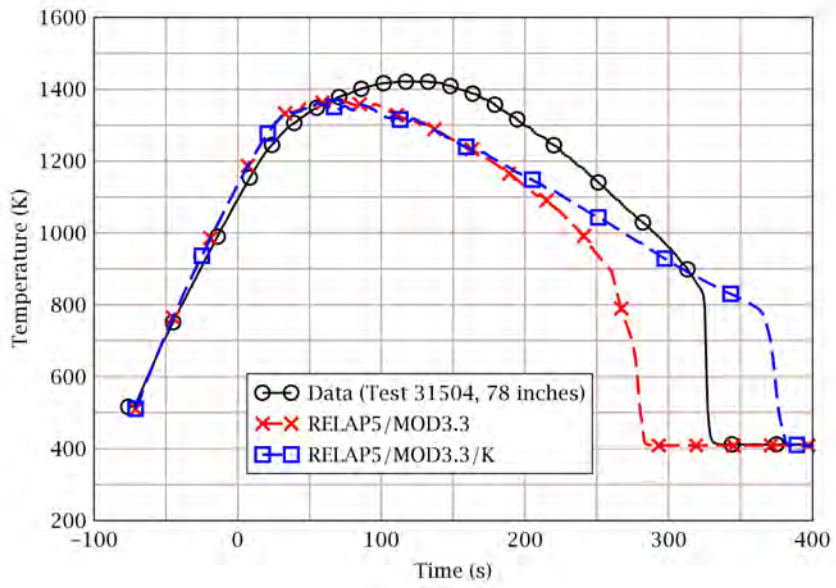

Figure 12 Comparison of Rod Cladding Temperature; FLECHT-SEASET 31504

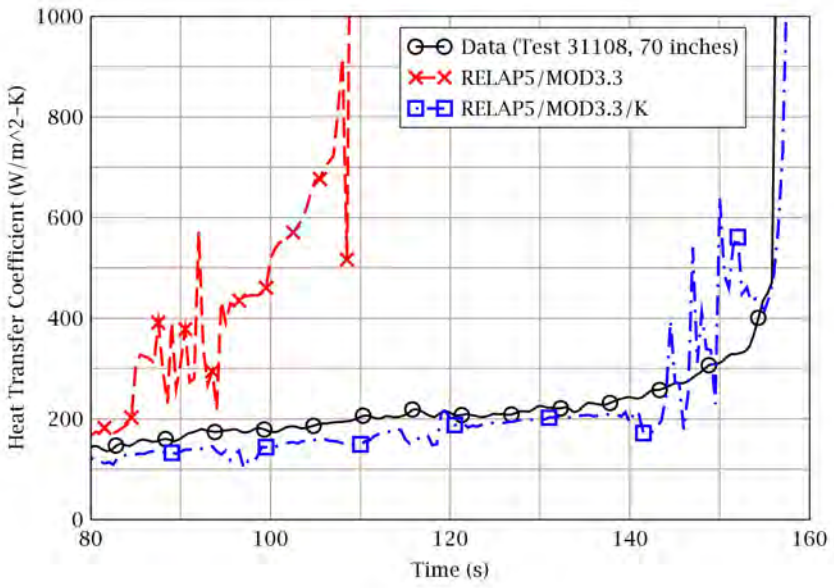

Figure 13 Comparison of Heat Transfer Coefficient; FLECHT-SEASET 31108

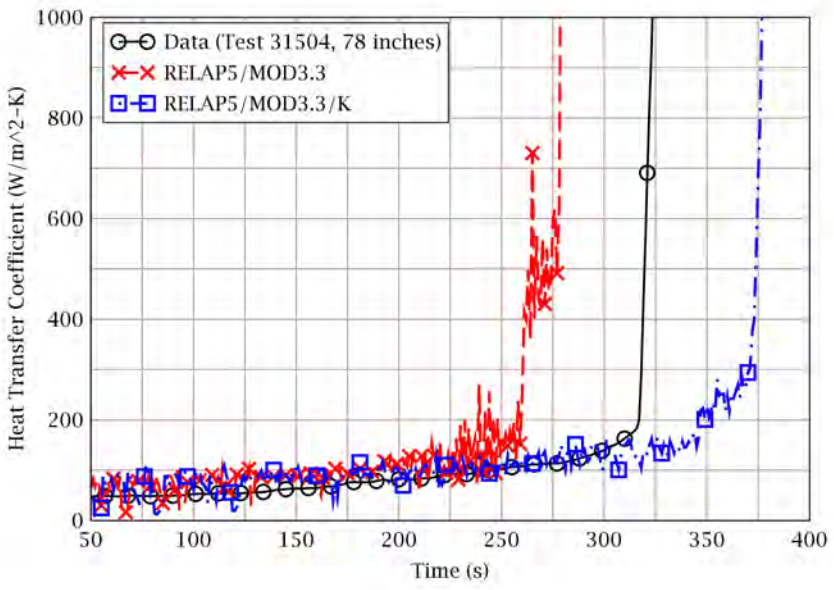

Figure 14 Comparison of Heat Transfer Coefficient; FLECHT-SEASET 31504

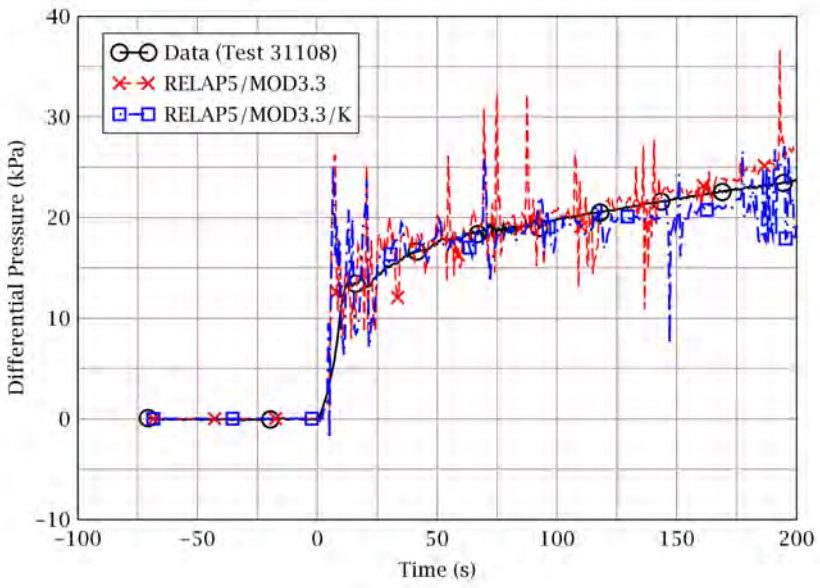

Figure 15 Comparison of Differential Pressure for the Entire Core; FLECHT-SEASET 31108

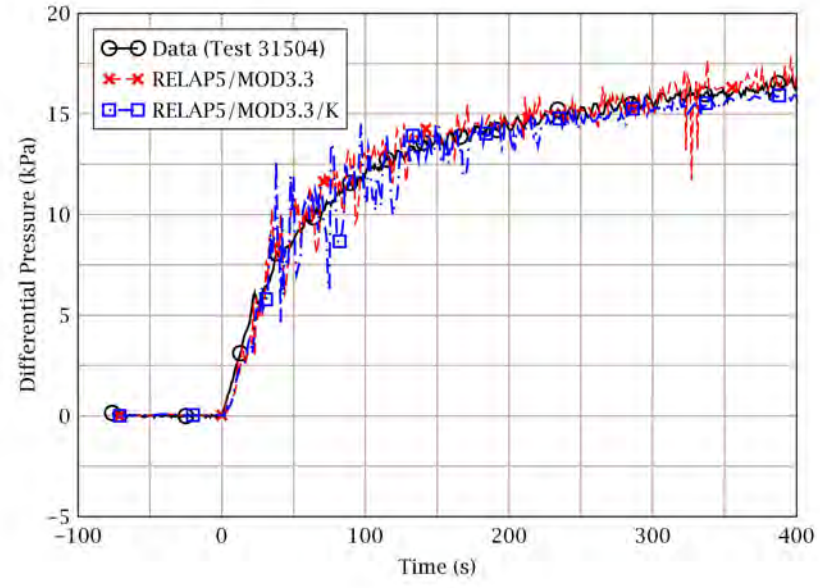

Figure 16 Comparison of Differential Pressure for the Entire Core; FLECHT-SEASET 31504

Figure 17 RELAP5 Noding Diagram for APR1400

[ ]TS

Figure 18 Comparison of [ ]TS

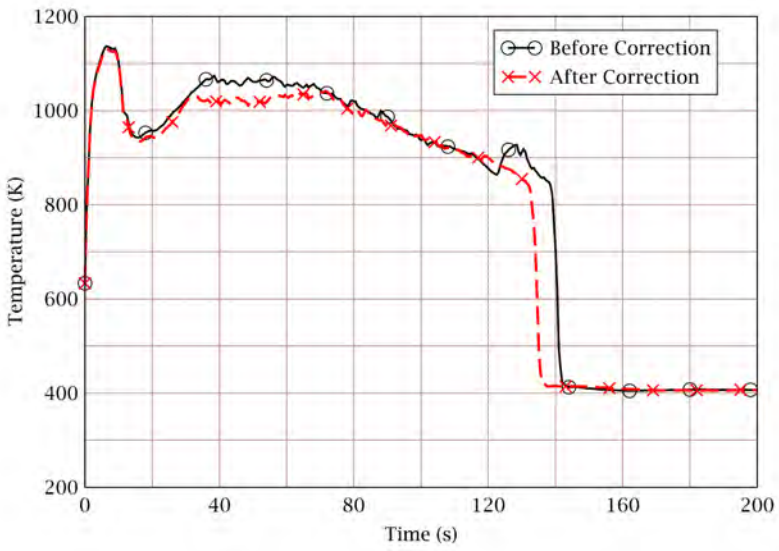

Figure 19 Effect of the [ ]TS

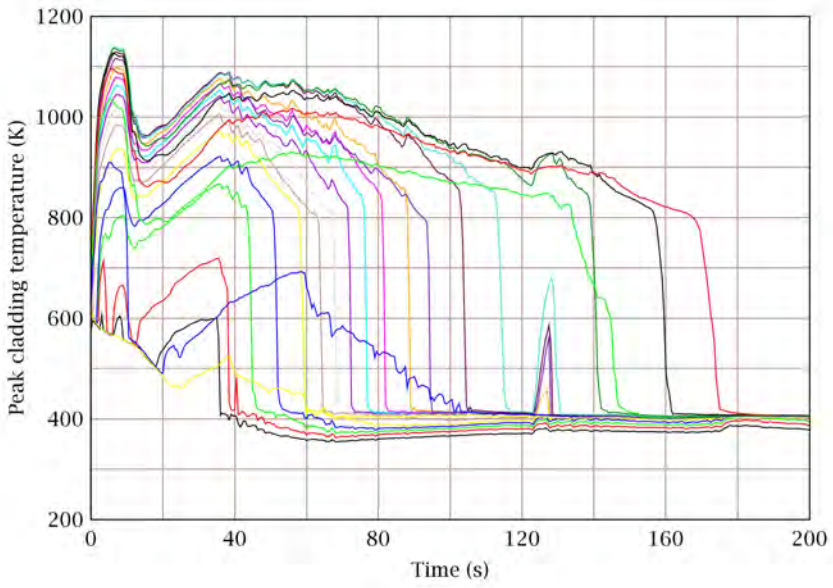

Figure 20 Cladding Temperatures at [ ]^{TS} Axial Nodes of the Hottest Rod; Before Modification

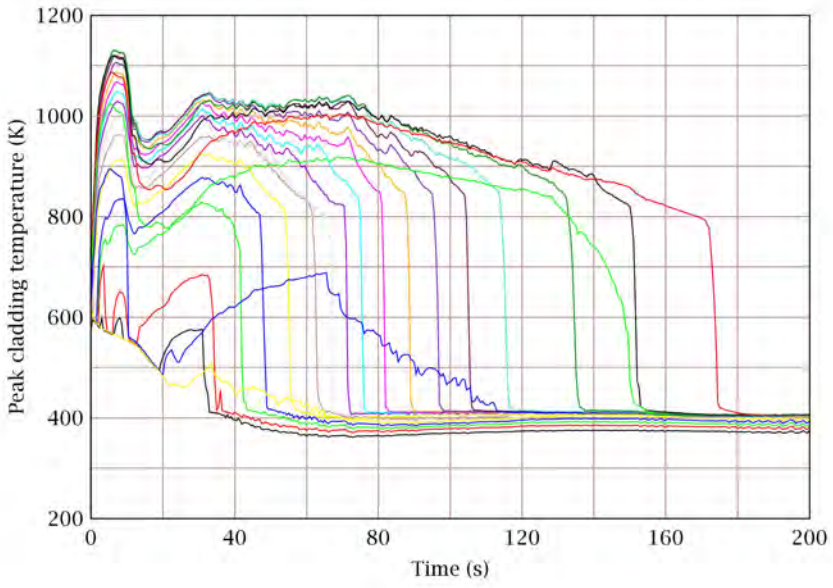

Figure 21 Cladding Temperatures at [ ]^{TS} Axial Nodes of the Hottest Rod; After Modification

TS

Figure 22 [ ]TS in the Surge-line of SIT-FD

TS

Figure 23 [ ]TS in the Surge-line of SIT-FD

TS

Figure 24 [ ]TS in an Upper Downcomer Node

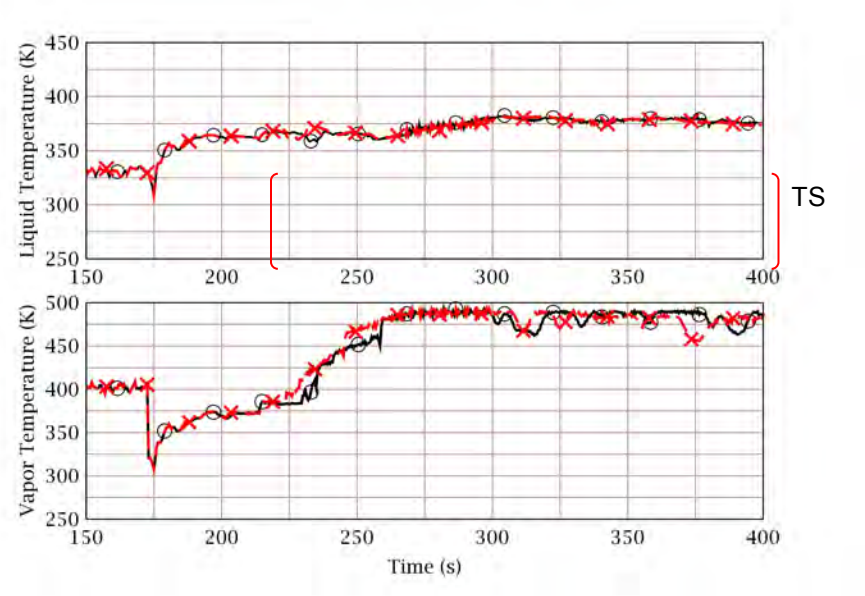

Figure 25 Liquid and Vapor Temperatures in an Upper Downcomer Node

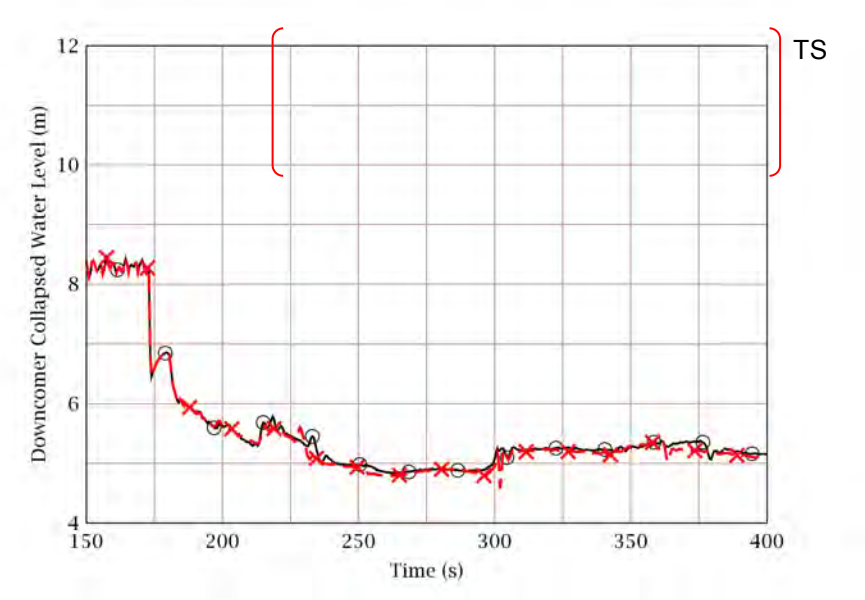

Figure 26 Collapsed Water Level in the Downcomer

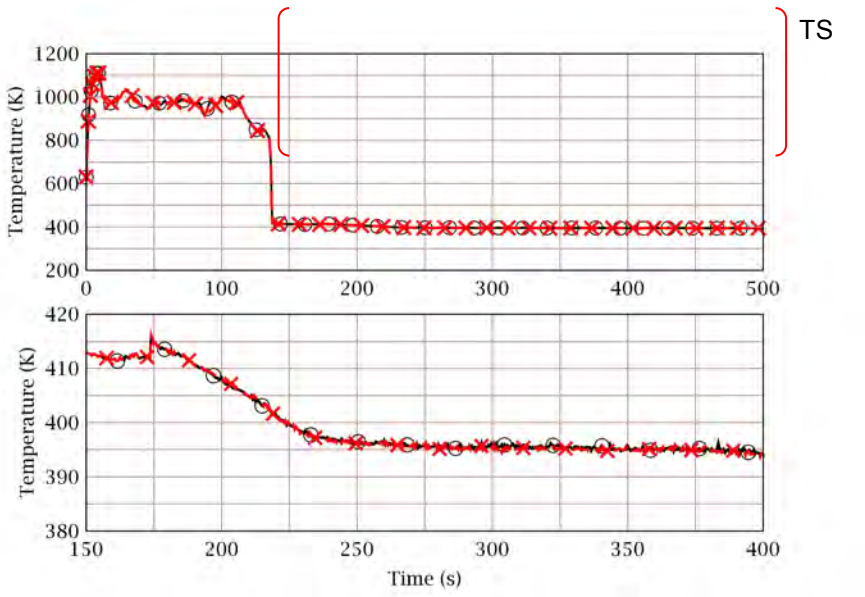

Figure 27 Comparison of the Cladding Temperature of the Hottest Rod

References

[1] “RELAP5/MOD3.3 Code Manual Volume III: Developmental Assessment Problems,” Nuclear Systems Analysis Division, March 2006.

[2] “RELAP5/MOD3.3 Code Manual Volume VIII: Programmers Manual,” Nuclear Systems Analysis Division, March 2006.

[3] G. Th. Analytis, “Developmental assessment of RELAP5/MOD3.1 with separate effect and integral test experiments: model changes and options,” Nuclear Engineering and Design 163 (125 ~ 148), 1996.

[4] "Quantifying Reactor Safety Margins; Application of Code Scaling, Applicability and Uncertainty Evaluation Methodology to a Large Break Loss of Coolant Accident,” NUREG/CR-5249, Technical Program Group, October 1989.

Appendix C

Assessment of RELAP5/MOD3.3/K against Separate-Effect Tests

Non-Proprietary

August 2018

Table of Contents

List of Tables

List of Figures

1. Introduction

The capability of the RELAP5/MOD3.3/K code to accurately predict the detailed thermal-hydraulic phenomena was assessed against various separate effect tests (SETs), and integrated effect tests (IETs).

In this appendix, the capability of the RELAP5/MOD3.3/K code to predict various thermal-hydraulic responses during blowdown and reflood phases are assessed against SETs. The purposes of the assessment are a) to examine the code's capability to accurately predict experimental data; b) to determine code accuracy; c) to determine probability distribution functions of the uncertainty parameters; d) to confirm the adequacy of the numbers of uncertainty parameters and their ranges, through checking the experimental data covering.

Code accuracy is defined in this methodology as the statistical difference between the calculated and the measured peak cladding temperatures (PCTs). Even if the locations and the occurrence times of the PCTs are different from each other, the code accuracy is defined simply as the PCT difference regardless of the location and the occurrence time. That is, the code accuracy is defined in terms of the capability to predict PCT. It is not used as a measure of the code's ability to predict each phenomenon. The frozen code itself is applied, and the probabilistic distribution functions of the uncertainty parameters are not considered for the code accuracy calculations.

While a sufficient amount of data is necessary in order to make the statistical treatment meaningful, only one value of the PCT is obtained from each experiment. Because the number of PCT experiments is not sufficient and there will be some discrepancies in the prediction of PCT locations, [

]^{TS} in order to obtain meaningful statistical code accuracy.

Bias and standard deviation of the differences are calculated as follows:

- PCT difference

$$\Delta PCT_{Zi} = PCT_{zi,cal} - PCT_{zi,\exp}$$

- PCT bias: the difference between the average of the calculated values and the measured ones

$$Bias = M_{cal} - M_{\exp} \quad \text{or}$$

$$Bias = \frac{\sum_{j=1}^{n} (\Delta PCT_{zi})_j}{n}$$

- Standard deviation (σ)

$$\sigma = \sqrt{\frac{\sum_{j=1}^{n} \left\{ \overline{\Delta PCT_{zi}} - (\Delta PCT_{zi})_j \right\}^2}{n}}$$

where, M_{cal} = the average value of code calculation

M_{exp} = the average value of test data

zi,cal = node elevation corresponding to measured elevation

$zi,\exp$ = measured elevation

n = total number of ΔPCT_{Zi}

The code accuracy is used as a measure of the sufficiency of the set of parameters. Via the code assessment, the capability of the code to predict the thermal-hydraulic phenomena is further confirmed and the uncertainty parameters are determined in terms of probability distribution functions. By adopting distribution-free statistic techniques, 181 times of simple random sampling (SRS) calculations are performed for each experiment, varying the values of the uncertainty parameters according to their distribution functions. Then it is checked whether the peak cladding temperature of the experiment can be covered by the third highest value of the calculations. In this way, sufficiency of the numbers and the ranges of the parameters are confirmed.

The SETs considered in the assessment are:

- 17 FLECHT-SEASET tests
- One CCTF test
- Seven NEPTUN tests
- Four THTF tests
- One PKL test

Four THTF tests are selected to assess the capability of the RELAP5/MOD3.3/K in predicting the blowdown progression. The other tests are selected to assess the capability of the code in predicting the reflood progression.

2. Code Assessment against FLECHT-SEASET

The Full-Length Emergency Core Heat Transfer - Separate Effects And System Effects Test (FLECHT-SEASET) facility was constructed mainly for reflood experiments as a joint project among the NRC, the Electric Power Research Institute (EPRI), and the Westinghouse corporation (WH). The FLECHT-SEASET data represents important data sources for reflood tests because the facility was large and well instrumented and tests were run at high temperatures the licensing limit of 1,204 ^{o}C (2,200 ^{o}F) in some cases. 17 tests are selected to assess the capability of RELAP5/MOD3.3/K in predicting the reflood progression, as provided in Table 2-1.

2.1 FLECHT-SEASET Test Facility Description

The FLECHT-SEASET facility [2-1] consisted of the following major components:

- Cylindrical test section consisting of a lower plenum, low-mass housing containing the heater rod bundle and an upper plenum
- Cooling water injection system
- Entrained liquid separation tank
- Carry-over liquid collection tank
- External pipe downcomer
- Steam boiler for back-pressure control to get the desired bundle pressure

The facility layout and the cross-sectional view of the bundle are shown in Figure 2-1 and Figure 2-2, respectively.

The heater rod bundle of the FLECHT-SEASET facility contained 177 rods which consisted of 161 heater rods and 16 thimble rods. These rods were placed in a cylinder of 0.194 m (7.625 in) diameter with a square lattice array similar to the typical 17×17 fuel assembly design of the WH. The bundle contained eight spacer grids, 12 steam probes, and 8 solid triangular fillers which were used to reduce the excess flow area near the housing wall. The heated part was 3.66 m (12 ft) long. The thimble rods were hollow and not heated. The heater rods were heated with a Kanthal heater coil which was imbedded in boron nitride encased with stainless steel cladding. The heater rod had the outside diameter of 9.5 mm (0.374 in), the wall thickness of 0.64 mm (0.025 in), as shown in Figure 2-3. Each rod had a cosine axial power profile, as shown in Figure 2-4. The radial power distribution was uniform.

The low-mass housing was designed to minimize the wall effect. An external pipe downcomer was connected to the bundle housing lower plenum for the gravity reflood tests. The upper plenum was expanded to a diameter bigger than the heated section, and the heated section housing wall was extended into the upper plenum to prevent the de-entrained liquid from falling back into the heated section. It also served to collect the liquid and drain it into a collection tank. The detailed description of the FLECHT-SEASET facility is described in reference [2-1].

2.2 RELAP5/MOD3.3/K Model Description

The RELAP5/MOD3.3/K input models of the FLECHT-SEASET facility is shown in Figure 2-5 and Figure 2-6. Input models in Figure 2-5 and Figure 2-6 are used to model forced and gravity reflood tests, respectively.

The FLECHT-SEASET facility is simplified to the extent necessary for simulating the reflood process in the bundle test section. The test section is divided into [ ]^{TS} Each channel is divided into [ ]^{TS} axial nodes. [ ]^{TS} channels are connected [ ]^{TS} in order to simulate cross flows between channels. The lower and upper plenums are modeled explicitly.

For the 16 tests except test 33338, because the radial and azimuthal power distributions are uniform, [ ]^{TS} For test 33338, the test bundle consisted of 52 hotter rods and the other 109 rods. Thus, [ ]^{TS}

The measured inlet flow rates are set [ ]^{TS} The measured upper plenum pressure is also set [ ]^{TS}

In order to simulate gravity reflood tests, the downcomer and the connection between the downcomer and the lower plenum are explicitly modeled, as shown in Figure 2-6.

2.3 RELAP5/MOD3.3/K Simulation

17 tests are selected for the RELAP5/MOD3.3/K assessment as indicated in Table 2-1. 12 tests are divided into five groups based on the variation of the test parameters. The flooding rate varies from 2.10 cm/s (0.83 in/s) to 15.50 cm/s (6.10 in/s), the system pressure from 0.13 MPa (19 psia) to 0.41 MPa (60 psia), the initial clad temperature from 256 ^{o}C (493 ^{o}F) to 1,119 ^{o}C (2,046 ^{o}F), and the initial rod peak power from 1.3 kW/m (0.40 kW/ft) to 3.0 kW/m (0.91 kW/ft). The other five tests grouped “Others” are selected to assess the capability of the RELAP5/MOD3.3/K in predicting reflood progression under various conditions which are not covered by the test conditions of the other groups.

The test conditions shown in Table 2-1 are nominal values, and the actual values vary with time. Thus, the actual inlet flow rates and temperatures and the upper plenum pressures are all approximated [ ]^{TS} Because the rod power decreases with time according to the Appendix K formula, [ ]^{TS} Initial conditions are set based on measured values.

Detailed results of the assessment are given in the following sections for each test in the five groups. The RELAP5/MOD3.3/K predicted values are presented and compared with data in the following order:

- Heater rod clad temperatures at 1.22 m (48 in) from the heated rod bottom
- Heater rod clad temperatures at 1.83 m (72 in) from the heated rod bottom
- Heater rod clad temperatures at 2.44 m (96 in) from the heated rod bottom
- Vapor temperatures at the 1.83 m (72 in) from the heated rod bottom
- Differential pressure for the entire 3.66 m (12 ft) of the core

For the rod clad and vapor temperature comparison, the calculated temperature at a specified elevation is obtained by interpolating the node center values near that elevation. The rod clad temperature obtained by interpolation sharply decreases twice after the turn-around time, because one of the two node center temperatures quenches later than the other one. For the differential pressures (DP) comparison, because accelerational and frictional pressure losses are insignificant, DP for the entire core can be directly converted to the mass of liquid in the core. Thus, no

differences between the predicted and measured DP for the entire core implies that the predicted amount of liquid carried out of the bundle would be the same as the data.

2.3.1 Flooding Rate Variation

The five tests of different flooding rates are presented from 2.10 cm/s (0.81 in/s) to 15.50 cm/s (6.10 in/s).

2.3.1.1 Simulation of Test 31805

The reflooding rate of test 31805 is 2.10 cm/s (0.83 in/s).

Figure 2-7, Figure 2-8, and Figure 2-9 show a comparison of measured and calculated values of rod clad temperatures at 1.22 m (48 in), 1.83 m (72 in) and 2.44 m (96 in) from the heated rod bottom, respectively. The RELAP5/MOD3.3/K slightly over-predicts the clad temperature, based on a comparison between the calculated value and the average measured value at a given elevation. This tendency becomes weaker at the middle and high elevations. However, the RELAP5/MOD/3.3/K reasonably predicts the clad temperature, at all elevations. At 2.44 m, the calculated temperatures tend to turn around and decrease faster than the data. Below 2.44 m, the calculated turn-around time matches the data very well. The RELAP5/MOD3.3/K slightly over-predicts rod quench time, at all elevations. The quench time difference between the calculations and the data becomes smaller as the elevation decreases. As described before, the rod clad temperature obtained by interpolation shows the quenching behavior twice. Considering the average value of the two quench times, the RELAP5/MOD3.3/K predicts well rod quench time for all elevations.

Vapor temperature calculated by the RELAP5/MOD3.3/K is compared with the data at 1.83 m (72 in) from the heated rod bottom, as shown in Figure 2-10. Between 100 s and 230 s after the reflood initiation, the predicted temperature is slightly lower than the data. The temperature decrease rate is also faster than the data during this time period. The RELAP5/MOD3.3/K, however, reasonably predicts vapor temperature considering that the vapor temperature measurements may have a large uncertainty.

Figure 2-11 shows a comparison of the predicted and the measured differential pressure (DP) for the entire 3.66 m (12 ft) core. The predicted DP matches the data fairly well. This means that the RELAP5/MOD3.3/K predicts fairly well the amount of liquid being accumulated in the core and the amount of liquid carried out of the bundle.

2.3.1.2 Simulation of Test 31504

The reflooding rate of test 31504 is 2.46 cm/s (0.97 in/s).

Figure 2-12, Figure 2-13, and Figure 2-14 show a comparison of measured and calculated values of the rod clad temperatures at 1.22 m (48 in), 1.83 m (72 in) and 2.44 m (96 in) from the heated rod bottom, respectively. The RELAP5/MOD3.3/K slightly over-predicts the clad temperature, based on a comparison between the calculated value and the average measured value at a given elevation. This tendency becomes weaker as the elevation increases. However, the RELAP5/MOD/3.3/K predicts clad temperatures very well, in all elevations. The predicted values are within the data spread range overall. At 2.44 m, the calculated temperatures tend to turn around and decrease faster than the data. Below 2.44 m, the calculated turn-around time matches the data very well. The RELAP5/MOD3.3/K slightly over-predicts the rod quench time at higher elevations. The quench time difference between the calculations and the data, however, becomes smaller as the elevation decreases. The calculated quench time at 1.22 m matches the data fairly well.

Vapor temperature calculated by the RELAP5/MOD3.3/K is compared with the data at 72 in from the heated rod bottom, in Figure 2-15. The RELAP5/MOD3.3/K reasonably predicts vapor temperature considering that vapor temperature measurements may have a large uncertainty.

Figure 2-16 shows a comparison of the predicted and the measured differential pressure (DP) for the entire 3.66 m (12 ft) core. The predicted DP matches the data fairly well. This implies that the RELAP5/MOD3.3/K predicts fairly well the amount of liquid being accumulated in the core and the amount of liquid carried out of the bundle.

2.3.1.3 Simulation of Test 31203

The reflooding rate of test 31203 is 3.84 cm/s (1.51 in/s).

Figure 2-17, Figure 2-18, and Figure 2-19 show a comparison of measured and calculated values of the rod clad temperatures at 1.22 m (48 in), 1.83 m (72 in) and 2.44 m (96 in) from the heated rod bottom, respectively. The RELAP5/MOD3.3/K slightly over-predicts the clad temperature, based on a comparison between the calculated value and the average measured value at a given elevation. For the lower elevation of 1.22 m (48 in), the predicted value is higher than the maximum temperature of the data. For the higher elevations, the RELAP5/MOD/3.3/K predicts clad temperatures very well. The predicted values are within the data spread range, overall. The tendency of over-prediction of the clad temperatures becomes weaker as the elevation increases. At 2.44 m, the calculated temperatures tend to turn around and decrease faster than the data. Below 2.44 m, the calculated turn-around time matches the data very well. The RELAP5/MOD3.3/K slightly over-predicts the rod quench time at higher elevations. The quench time difference between calculation and data, however, becomes smaller as the elevation decreases. The calculated quench time at 1.22 m is slightly shorter than the data.

Vapor temperature calculated by the RELAP5/MOD3.3/K is compared with the data at 72 in. from the heated rod bottom, in Figure 2-20. Between 50 s and 120 s, the RELAP5/MOD3.3/K under-predicts vapor temperatures. However, the RELAP5/MOD3.3/K reasonably predicts vapor temperature considering that vapor temperature measurements may have a large uncertainty.

Figure 2-21 shows a comparison of the predicted and the measured differential pressure (DP) for the entire 3.66 m (12 ft) core. Even though the predicted value is oscillatory during about 30 s through 160 s, the average value is reasonably close to the data. After around 200 s, the RELAP5/MOD3.3/K slightly under-predicts DP for the entire core. The predicted DP matches the data fairly well, in general. This implies that the RELAP5/MOD3.3/K predicts fairly well the amount of liquid being accumulated in the core and the amount of liquid carried out of the bundle.

2.3.1.4 Simulation of Test 31302

The reflooding rate of test 31302 is 7.65 cm/s (3.01 in/s).

Figure 2-22, Figure 2-23, and Figure 2-24 show a comparison of measured and calculated values of rod clad temperatures at 1.22 m (48 in), 1.83 m (72 in) and 2.44 m (96 in) from the heated rod bottom, respectively. The RELAP5/MOD3.3/K over-predicts the clad temperature at all elevations. The predicted values are higher than the maximum temperatures of the data. The calculated turn-around time match the data well, at all elevations. The RELAP5/MOD3.3/K slightly under-predicts rod quench time. The quench time difference between calculation and data, however, is not significant.

Vapor temperature calculated by the RELAP5/MOD3.3/K is compared with the data at 72 in. from the heated rod bottom, in Figure 2-25. Before reflood initiation time (i.e., time 0), the predicted vapor temperature is higher than the data. During this time period, the predicted temperature is close to

rod temperatures at the same elevation. After reflood initiation time, however, the RELAP5/MOD3.3/K reasonably predicts vapor temperature considering that vapor temperature measurements may have a large uncertainty.

Figure 2-26 shows a comparison of the predicted and the measured differential pressure (DP) for the entire 3.66 m (12 ft) core. Even though the predicted value is very oscillatory during the reflood period, the average value is reasonably close to the data. After around 100 s, the RELAP5/MOD3.3/K slightly under-predicts DP for the entire core. The predicted DP matches the data fairly well in general, based on a comparison between the average calculated value and the measured value. This implies that the RELAP5/MOD3.3/K predicts well the amount of liquid being accumulated in the core and the amount of liquid carried out of the bundle.

2.3.1.5 Simulation of Test 31701

The reflooding rate of test 31701 is 15.50 cm/s (6.10 in/s).

Figure 2-27, Figure 2-28, and Figure 2-29 show a comparison of measured and calculated values of rod clad temperatures at 1.22 m (48 in), 1.83 m (72 in), and 2.44 m (96 in) from the heated rod bottom, respectively. The RELAP5/MOD3.3/K over-predicts the clad temperature at all elevations. The predicted values are higher than the maximum temperatures of the data. The calculated turn-around time match the data well, at all elevations. The RELAP5/MOD3.3/K over-predicts rod quench time, at all elevations.

Vapor temperature calculated by the RELAP5/MOD3.3/K is compared with the data at 72 in from the heated rod bottom, in Figure 2-30. Before reflood initiation time (i.e., time 0.0 s), the predicted vapor temperature is higher than the data. During this time period, the predicted temperature is close to rod temperatures at the same elevation. After reflood initiation time, however, the RELAP5/MOD3.3/K predicts well the trend of vapor temperature behavior considering that vapor temperature measurements may have a large uncertainty.

Figure 2-31 shows a comparison of the predicted and the measured differential pressure (DP) for the entire 3.66 m (12 ft) core. Even though the predicted value is oscillatory during the reflood period, the average value is reasonably close to the data. After around 10 s, the RELAP5/MOD3.3/K slightly over-predicts DP for the entire core. This implies that the RELAP5/MOD3.3/K under-predicts the amount of liquid carried out of the bundle, after around 10 s. Even though the RELAP5/MOD3.3/K over-predicts the amount of liquid being accumulated in the core, the predicted temperatures are higher than the data. This is mainly because that the RELAP5/MOD3.3/K conservatively under-predicts heat transfer between the heater rods and fluids, for high reflooding tests.

2.3.2 System Pressure Variation

The three tests of different system pressure are presented from 0.14 MPa (20.3 psia) to 0.41 MPa (59.5 psia).

2.3.2.1 Simulation of Test 34209

The system pressure of test 34209 is 0.14 MPa (20.3 psia).

Figure 2-32, Figure 2-33, and Figure 2-34 show a comparison of measured and calculated values of rod clad temperatures at 1.22 m (48 in), 1.83 m (72 in), and 2.44 m (96 in) from the heated rod bottom, respectively. The RELAP5/MOD3.3/K over-predicts the clad temperature, based on a comparison between the calculated value and the average measured value at a given elevation. The predicted value is higher than the maximum temperature of the data, at all elevations. The calculated turn-around time matches the data well. The RELAP5/MOD3.3/K over-predicts rod

quench time at higher elevations. The tendency of over-prediction of rod quench time becomes stronger as the elevation increases.

Vapor temperature calculated by the RELAP5/MOD3.3/K is compared with the data at 72 in. from the heated rod bottom, in Figure 2-35. Before reflood initiation time (i.e., time 0.0 s), the predicted vapor temperature is higher than the data. During this time period, the predicted vapor temperature is close to rod temperatures at the same elevation. After reflood initiation time, the RELAP5/MOD3.3/K under-predicts vapor temperature. The predicted vapor temperature turns around as soon as reflood initiates, whereas the measured vapor temperatures turn around after 100 s.

Figure 2-36 shows a comparison of the predicted and the measured differential pressure (DP) for the entire 3.66 m (12 ft) core. Even though the predicted value is very oscillatory until around 200 s, the average value is reasonably close to the data. After around 130 s, the RELAP5/MOD3.3/K slightly under-predicts DP for the entire core. This implies that the RELAP5/MOD3.3/K over-predicts the amount of liquid carried out of the bundle, after around 130 s.

2.3.2.2 Simulation of Test 31504

The system pressure of test 31504 is 0.28 MPa (40.6 psia).

The simulation of test 31504 is presented in the previous section 2.3.1.2.

2.3.2.3 Simulation of Test 32013

The system pressure of test 32013 is 0.41 MPa (59.5 psia).

Figure 2-37, Figure 2-38, and Figure 2-39 show a comparison of measured and calculated values of rod clad temperatures at 1.22 m (48 in), 1.83 m (72 in), and 2.44 m (96 in) from the heated rod bottom, respectively. For the lower elevation of 1.22 m (48 in), the predicted value is higher than the maximum temperature of the data. However, the predicted clad temperature falls within the data spread for the elevation of 1.83 m (72 in). For the 2.44 m (96 in) elevation, the predicted rod temperature is slightly higher than the data until 80s, then it's lower than the data. The RELAP5/MOD3.3/K over-predicts the clad temperature, based on a comparison between the calculated value and the average measured value at a given elevation. The calculated temperatures tend to turn around faster than the data for all elevations. This tendency becomes stronger as the elevation increases. The RELAP5/MOD3.3/K over-predicts rod quench time at middle and high elevations. The tendency of over-prediction of rod quench time also becomes stronger as the elevation increases.

Vapor temperature calculated by the RELAP5/MOD3.3/K is compared with the data at 72 in. from the heated rod bottom, in Figure 2-40. Before reflood initiation time (i.e., time 0.0 s), the predicted vapor temperature is close to rod temperatures at the same elevation. After reflood initiation time, the RELAP5/MOD3.3/K predicts the vapor temperature well.

Figure 2-41 shows a comparison of the predicted and the measured differential pressure (DP) for the entire 3.66 m (12 ft) core. Even though the predicted value is oscillatory until around 130 s, the average value matches the data fairly well. This implies that the RELAP5/MOD3.3/K predicts fairly well the amount of liquid being accumulated in the core and the amount of liquid carried out of the bundle.

2.3.3 Initial Clad Temperature Variation

The four different tests of initial clad temperature are presented from 256 ^{o}C (529 K, 493 ^{o}F) to 1,119 ^{o}C (1,392 K, 2,046 ^{o}F).

2.3.3.1 Simulation of Test 30518

The initial clad temperature of test 30518 is 256 ^{o}C (529 K, 493 ^{o}F).

Figure 2-42, Figure 2-43, and Figure 2-44 show a comparison of measured and calculated values of rod clad temperatures at 1.22 m (48 in), 1.83 m (72 in), and 2.44 m (96 in) from the heated rod bottom, respectively. For the lower elevation of 1.22 m (48 in), the predicted value is higher than the highest measured temperature. However, the predicted rod quench time is considerably shorter than the data. For the middle elevation of 1.83 m (72 in), the predicted rod temperature matches the data well before the turn-around time. After the rod temperature turn-around time, the predicted value is slightly lower than the data. The calculated rod quenching time is shorter than the data, showing the same tendency at the lower elevation. For the higher elevation of 2.44 m (96 in), the RELAP5/MOD3.3/ K over-predicts the clad temperature, based on a comparison between the calculated value and the average measured value, before the rod temperature turn-around time. After that, the predicted value is within the data spread. The predicted rod quenching time is slightly longer than the data, contrary to the quenching time prediction for the middle and lower elevations.

Vapor temperature calculated by the RELAP5/MOD3.3/K is compared with the data at 72 in. from the heated rod bottom, in Figure 2-45. In most tests, vapor temperatures begin to increase when the rods begin to heat-up before the reflood initiation time. Whereas, for test 30518, the measured vapor temperatures began to increase after the reflood initiation time. The RELAP5/MOD3.3/K predicts that vapor temperature starts to increase if the rod heat-up begins before reflood initiation time. The behavior of the predicted vapor temperature differs a lot from the data. However, because the data are not considered to be very accurate, the extent of deviation in the figure may not present the reality.

Figure 2-46 shows a comparison of the predicted and the measured differential pressure (DP) for the entire 3.66 m (12 ft) core. The RELAP5/MOD3.3/K reasonably predicts DP for the entire core. The predicted value matches the data fairly well until around 100 s. After then, the RELAP5/MOD3.3/K slightly under-predicts the DP. This implies that the RELAP5/MOD3.3/K over-predicts the amount of liquid being accumulated in the core and the amount of liquid carried out of the bundle, after 100 s..

2.3.3.2 Simulation of Test 30817

The initial clad temperature of test 30817 is 531 ^{o}C (804 K, 988 ^{o}F).

Figure 2-47, Figure 2-48, and Figure 2-49 show a comparison of the measured and calculated values of rod clad temperatures at 1.22 m (48 in), 1.83 m (72 in), and 2.44 m (96 in) from the heated rod bottom, respectively. For the lower elevation of 1.22 m (48 in), the predicted value is higher than the highest measured temperature. However, the predicted rod quench time is shorter than the data. For the middle elevation of 1.83 m (72 in), the predicted rod temperature matches the data fairly well. As described before, the rod clad temperature obtained by interpolation shows quenching behavior twice. Considering the average value of two quench times, the RELAP5/MOD3.3/K closely predicts the rod quench time for the middle elevation. For the higher elevation of 2.44 m (96 in), the RELAP5/MOD3.3/ K closely predicts the clad temperature before turn-around time, after that, it slightly over-predicts the clad temperature. The predicted rod quenching time is slightly longer than the data.

Vapor temperature calculated by the RELAP5/MOD3.3/K is compared with the data at 72 in. from the heated rod bottom, in Figure 2-50. In most tests, vapor temperatures begin to increase when the rods begin to heat-up before the reflood initiation time. Whereas, in test 30817, the measured vapor temperatures begin to increase after reflood initiation time. The RELAP5/MOD3.3/K predicts that vapor temperature starts to increase when the rod heat-up begins before reflood initiation time. Between 25 s and 110 s, the RELAP5/MOD3.3/K reasonably predicts vapor temperature. However, the general behavior of the predicted vapor temperature differs from the data. Because the data are not considered to be very accurate, the extent of deviation in the figure may not present the reality.

Figure 2-51 shows a comparison of the predicted and the measured differential pressure (DP) for the entire 3.66 m (12 ft) core. Even though the predicted value is very oscillatory between 25 s and 100 s, the average value is reasonably close to the data. After around 100 s, the RELAP5/MOD3.3/K slightly under-predicts the DP for the entire core. This implies that the RELAP5/MOD3.3/K over-predicts the amount of liquid carried out of the bundle, after around 100 s.

2.3.3.3 Simulation of Test 31203

The initial clad temperature of test 31203 is 872 ^{o}C (1,145 K, 1,602 ^{o}F).

The simulation of test 31203 is presented in the previous section 2.3.1.3.

2.3.3.4 Simulation of Test 34420

The initial clad temperature of test 34420 is 1,119 ^{o}C (1,392 K, 2,046 ^{o}F).

Figure 2-52, Figure 2-53, and Figure 2-54 show a comparison of measured and calculated values of rod clad temperatures at 1.22 m (48 in), 1.83 m (72 in), and 2.44 m (96 in) from the heated rod bottom, respectively. For all elevations, the RELAP5/MOD3.3/K over-predicts clad temperatures and rod quench time, based on a comparison between the calculated value and the average measured value. The predicted rod temperature is higher than the highest measured temperature, and the predicted rod quench time is longer than the data, at a given elevation.

Vapor temperature calculated by the RELAP5/MOD3.3/K is compared with the data at 72 in. from the heated rod bottom, in Figure 2-55. Even though the general behavior of the predicted vapor temperature differs from the data, the RELAP5/MOD3.3/K reasonably predicts vapor temperature considering that vapor temperature measurements may have a large uncertainty.

Figure 2-56 shows a comparison of the predicted and the measured differential pressure (DP) for the entire 3.66 m (12 ft) core. Even though the predicted value is very oscillatory until around 150 s, the average value is reasonably close to the data. After around 150 s, the RELAP5/MOD3.3/K slightly under-predicts DP for the entire core. This implies that the RELAP5/MOD3.3/K over-predicts the amount of liquid carried out of the bundle, after around 150 s.

2.3.4 Initial Rod Peak Power Variation

The three tests of different initial rod peak power are presented from 1.3 kW/m (0.40 kW/ft) to 3.0 kW/m (0.91 kW/ft).

2.3.4.1 Simulation of Test 31021

The initial clad temperature of test 31021 is 1.3 kW/m (0.40 kW/ft).

Figure 2-57, Figure 2-58, and Figure 2-59 show a comparison of measured and calculated values of rod clad temperatures at 1.22 m (48 in), 1.83 m (72 in), and 2.44 m (96 in) from the heated rod

bottom, respectively. At the lower elevation of 1.22 m (48 in), the predicted value is higher than the highest measured temperature. At 1.83 m, the RELAP5/MOD3.3/K predicts well the clad temperature behavior. The predicted clad temperature is slightly higher than the highest measured value. At 2.44 m, the predicted highest temperature matches the highest measured value well. However, the turn-around time of the predicted clad temperature is faster than the data. The tendency of under-prediction of the turn-around time is weaker as elevation decreases. At all elevations, the RELAP5/MOD3.3/K slightly under-predicts rod quench time.

Vapor temperature calculated by the RELAP5/MOD3.3/K is compared with the data at 72 in. from the heated rod bottom, in Figure 2-60. The RELAP5/MOD3.3/K predicts well vapor temperature considering that vapor temperature measurements may have a large uncertainty.

Figure 2-61 shows a comparison of the predicted and the measured differential pressure (DP) for the entire 3.66 m (12 ft) core. Even though the predicted value is very oscillatory, the average value is reasonably close to the data. Up to around 130 s, the RELAP5/MOD3.3/K slightly over-predicts DP for the entire core, based on a comparison between the average calculated value and the measured value. After 130 s, the predicted value is quite close to the data. The DP comparison shows that the RELAP5/MOD3.3/K reasonably predicts the amount of liquid carried out of the bundle.

2.3.4.2 Simulation of Test 31203

The initial clad temperature of test 31203 is 2.3 kW/m (0.70 kW/ft).

The simulation of test 31203 is presented in the previous section 2.3.1.3.

2.3.4.3 Simulation of Test 34524

The initial clad temperature of test 34524 is 3.0 kW/m (0.91 kW/ft).

Figure 2-62, Figure 2-63, and Figure 2-64 show a comparison of measured and calculated values of rod clad temperatures at 1.22 m (48 in), 1.83 m (72 in) and 2.44 m (96 in) from the heated rod bottom, respectively. The RELAP5/MOD3.3/K over-predicts the clad temperature and rod quench time, based on a comparison between the calculated value and the average measured value at a given elevation. At the lower elevation of 1.22 m and the higher elevation of 2.44 m, the predicted value is higher than the highest measured temperature. At 1.83 m, the highest predicted value falls within the data spread range. However, the predicted value is higher than the average value of the data through the entire period.

Vapor temperature calculated by the RELAP5/MOD3.3/K is compared with the data at 72 in. from the heated rod bottom, in Figure 2-65. The RELAP5/MOD3.3/K reasonably predicts vapor temperature falls within the data spread. However, the general behavior of the predicted vapor temperature differs from the data. The predicted vapor temperature decreases gradually until the end of calculation time, whereas the measured temperatures do not vary much until around 150 s, then after that they decrease sharply. However, because the data are not considered to be very accurate, the deviation in the figure may not present the reality.

Figure 2-66 shows a comparison of the predicted and the measured differential pressure (DP) for the entire 3.66 m (12 ft) core. Even though the predicted value is very oscillatory until around 130 s, the average value is reasonably close to the data. After around 130 s, the RELAP5/MOD3.3/K slightly under-predicts DP for the entire core.

2.3.5 Others

2.3.5.1 Simulation of Test 31108

Initial test conditions of test 31108 are a reflooding rate of 7.9 cm/s (3.11 in/s), system pressure of 0.13 MPa (19 psia), rod peak power of 2.3 kW/m (0.70 kW/ft), rod temperature of 871 ^{o}C (1,144 K, 1,600 ^{o}F), and inlet liquid temperature of 33 ^{o}C (306 K, 91 ^{o}F), as shown in Table 2-1.

Figure 2-67, Figure 2-68, and Figure 2-69 show a comparison of measured and calculated values of rod clad temperatures at 1.22 m (48 in), 1.83 m (72 in) and 2.44 m (96 in) from the heated rod bottom, respectively. At all three elevations, the RELAP5/MOD3.3/K over-predicts clad temperatures. The calculated rod temperature is higher than the highest measured temperature at a given elevation. The predicted rod temperature turn-around time matches the data well at 1.22 m. Above 1.22 m, however, the predicted rod temperature turns around later than the data. The RELAP5/MOD3.3/K predicts well quench time at the middle elevation of 1.83 m. At 1.22 m, the RELAP5/MOD3.3/K predicts the rod quench time to occur later than the data whereas at 2.44 m, the predicted quench time is earlier than the data.

Vapor temperature calculated by the RELAP5/MOD3.3/K is compared with the data at 72 in. from the heated rod bottom, in Figure 2-70. Before reflood initiation time (i.e., time 0.0 s), the predicted vapor temperature is close to rod temperatures at the same elevation. After reflood initiation time, the RELAP5/MOD3.3/K reasonably predicts vapor temperature considering that vapor temperature measurements may have a large uncertainty.

Figure 2-71 shows a comparison of the predicted and the measured differential pressure (DP) for the entire 3.66 m (12 ft) core. The predicted value is very oscillatory for the entire reflood period. However, the average predicted value is reasonably close to the data. After around 100 s, the predicted value is slightly lower than the data. The DP comparison shows that the RELAP5/MOD3.3/K reasonably predicts the amount of liquid carried out of the bundle.

2.3.5.2 Simulation of Test 32235

Initial test conditions of test 32235 are a system pressure of 0.14 MPa (20 psia), rod peak power of 2.3 kW/m (0.70 kW/ft), rod temperature of 888 ^{o}C (1,161 K, 1,630 ^{o}F), and inlet liquid temperature of 31 ^{o}C (304 K, 88 ^{o}F), as shown in Table 2-1. The reflooding rate of this test varies from 16.58 cm/s (6.53 in/s) to 2.49 cm/s (0.98 in/s) then to 1.57 cm/s (0.62 in/s).

Figure 2-72, Figure 2-73, and Figure 2-74 show a comparison of measured and calculated values of rod clad temperatures at 1.22 m (48 in), 1.83 m (72 in) and 2.44 m (96 in) from the heated rod bottom, respectively. The RELAP5/MOD3.3/K over-predicts clad temperatures and rod quench times, based on a comparison between the calculated value and the average measured value at a given elevation. After 200 s when the reflooding rate changes to the lowest value of 1.57 cm/s, the tendency of over-prediction of clad temperature and rod quench time becomes stronger. This over-prediction tendency also becomes stronger as the elevation increases. At the elevation 1.83 m and 2.44 m, the predicted clad temperature is higher than the data and the predicted rod quench time is fairly later than the data.

Vapor temperature calculated by the RELAP5/MOD3.3/K is compared with the data at 72 in. from the heated rod bottom, in Figure 2-75. Before reflood initiation time (i.e., time 0.0 s), the predicted vapor temperature is close to rod temperatures at the same elevation. Between reflood initiation time and 180 s, the RELAP5/MOD3.3/K reasonably predicts vapor temperature considering that vapor temperature measurements may have a large uncertainty. After 200 s, the predicted value is much higher than the data mainly because of the over-prediction of clad temperature.

Figure 2-76 shows a comparison of the predicted and the measured differential pressure (DP) for the entire 3.66 m (12 ft) core. The predicted value is very oscillatory for the entire reflood period. The average predicted value is slightly lower than the data. However, the predicted value is reasonably close to the data. The DP comparison implies that the RELAP5/MOD3.3/K slightly over-predicts the amount of liquid carried out of the bundle.

2.3.5.3 Simulation of Test 32333

Initial test conditions of test 32333 are a system pressure of 0.28 MPa (40.6 psia), rod peak power of 2.3 kW/m (0.70 kW/ft), rod temperature of 889 ^{o}C (1,162 K, 1,632 ^{o}F), and inlet liquid temperature of 53 ^{o}C (326 K, 127 ^{o}F), as shown in Table 2-1. The reflooding rate of this test varies from 16.2 cm/s (6.38 in/s) to 2.1 cm/s (0.83 in/s).

Figure 2-77, Figure 2-78, and Figure 2-79 show a comparison of measured and calculated values of rod clad temperatures at 1.22 m (48 in), 1.83 m (72 in) and 2.44 m (96 in) from the heated rod bottom, respectively. At all elevations, the RELAP5/MOD3.3/K over-predicts the clad temperatures and rod quench times, based on a comparison between the calculated value and the average measured value. At 2.44m, the predicted clad temperature is higher than the data before the turn-around time; after that the predicted value is slightly lower than the data until around 400 s, based upon a comparison between the calculated value and the average measured value. At all three elevations, the RELAP5/MOD3.3/K over-predicts the rod quench time. The predicted clad temperature turn-around time is faster than the measured time at 1.83 m and 2.44 m. The RELAP5/MOD3.3/K predicts well the turn-around time at 1.22 m.

Vapor temperature calculated by the RELAP5/MOD3.3/K is compared with the data at 72 in. from the heated rod bottom, in Figure 2-80. Before the reflood initiation time (i.e., time 0.0 s), the predicted vapor temperature is close to rod temperatures at the same elevation. After reflood initiation, the RELAP5/MOD3.3/K reasonably predicts vapor temperature considering that the vapor temperature measurements may have a large uncertainty.

Figure 2-81 shows a comparison of the predicted and the measured differential pressure (DP) for the entire 3.66 m (12 ft) core. Even though the predicted value is oscillatory until 200 s, the average value matches the data fairly well. The DP comparison implies that the RELAP5/MOD3.3/K predicts fairly well the amount of liquid carried out of the bundle.

2.3.5.4 Simulation of Test 33338

Test 33338 was a gravity reflood test. The test bundle consisted of 52 hotter rods, plus the other 109 rods. The initial test condition has a system pressure of 0.28 MPa (40.6 psia), a rod temperature of 871 ^{o}C (1,144 K, 1,600 ^{o}F), a rod peak power of 2.3 kW/m (0.70 kW/ft)/1.3 kW/m (0.40 kW/ft) for hotter/the other rods, and inlet liquid temperature of 52 ^{o}C (325 K, 126 ^{o}F), as shown in Table 2-1. The rod peak power varies from 2.3 kW/m (0.70 kW/ft) to 1.3 kW/m (0.40 kW/ft). The flow rate of injected water for the reflood varies from 5.9 kg/s (13 lb/s) to 0.807 kg/s (1.78 lb/s).

Figure 2-82, Figure 2-83, and Figure 2-84 show a comparison of measured and calculated values of rod clad temperatures at 1.22 m (48 in), 1.83 m (72 in) and 2.44 m (96 in) from the heated rod bottom, respectively. The measured values at the hotter rods are compared with the calculated value. At all three elevations, the RELAP5/MOD3.3/K over-predicts the clad temperatures and rod quench times. The predicted cladding temperature is higher than the highest measured value at a given elevation. After the injection flow rate was decreased to 0.807 kg/s at 15 s, the measured values decreased slowly. The predicted value also follows this tendency.

Vapor temperature calculated by the RELAP5/MOD3.3/K is compared with the data at 72 in. from the heated rod bottom, in Figure 2-85. Before reflood initiation time (i.e., time 0.0 s), the predicted

vapor temperature is close to the rod temperatures at the same elevation. Between the reflood initiation time and about 10 s, the RELAP5/MOD3.3/K reasonably predicts vapor temperature. After about 10 s, the predicted value is fairly higher than the data. However, because the data measurement is not considered to be very accurate, the deviation in the figure may not present the reality.

Figure 2-86 shows a comparison of the predicted and the measured differential pressure (DP) for the entire 3.66 m (12 ft) core. The predicted value is very oscillatory for the entire reflood period. The average predicted value is close to the data until it reaches about 15 s. Between 15 s to 27 s, the predicted value is higher than the data. After 27 s, the RELAP5/MOD3.3/K under-predicts the entire core DP. This is mainly due to that the RELAP5/MOD3.3/K over-predicts the amount of liquid carried out of the bundle after 27 s. However, the RELAP5/MOD3.3/K reasonably predicts the core DP, overall.

2.3.5.5 Simulation of Test 34006

The initial test conditions of test 34006 have a reflooding rate of 1.5 cm/s (0.59 in/s), a system pressure of 0.27 MPa (39 psia), a rod peak power of 1.3 kW/m (0.40 kW/ft), a rod temperature of 882 ^{o}C (1,155 K, 1,620 ^{o}F), and an inlet liquid temperature of 51 ^{o}C (324 K, 124 ^{o}F), as shown in Table 2-1. The reflooding rate of this test is the lowest among the 17 tests.

Figure 2-87, Figure 2-88, and Figure 2-89 show a comparison of measured and calculated values of rod clad temperatures at 1.22 m (48 in), 1.83 m (72 in) and 2.44 m (96 in) from the heated rod bottom, respectively. The measured values at the hotter rods are compared with the calculated value. At all three elevations, the RELAP5/MOD3.3/K over-predicts the clad temperatures and rod quench times. The predicted value follows well the measured value at a given elevation. At 1.22 m, the predicted value is higher than the data; however the predicted quenching time matches well the data. At 1.83m, the predicted cladding temperature and quenching time match well the data. The predicted value is slightly lower than the data at 2.44 m. The general trend of the predicted value follows well the measured data, in all elevations.

Vapor temperature calculated by the RELAP5/MOD3.3/K is compared with the data at 72 in. from the heated rod bottom, in Figure 2-90. The RELAP5/MOD3.3/K under-predicts vapor temperature. However, because the vapor temperature measurements may have a large uncertainty, the deviation in the figure may not present the reality.

Figure 2-91 shows a comparison of the predicted and the measured differential pressure (DP) for the entire 3.66 m (12 ft) core. The RELAP5/MOD3.3/K predicts the entire core DP fairly well, based on a comparison between the average calculated value and the measured value. This implies that the RELAP5/MOD3.3/K predicts fairly well the amount of liquid carried out of the bundle.

2.3.6 Assessment Results Summary

The predictive capability of the RELAP5/MOD3.3/K was assessed against data from 17 FECHT-SEASET tests. The capability is summarized in terms of several important variables.

2.3.6.1 Rod Clad Temperatures and Rod Quench Time

Rod clad temperatures are compared between the data and the RELAP5/MOD3.3/K predicted values at three different axial elevations such as 1.22 m (48 in), 1.83 m (72 in), and 2.44 m (96 in) from the heated rod bottom.

In all 17 cases except Test 32013, the RELAP5/MOD3.3/K over-predicts rod clad temperatures at a given elevation, based on a comparison between the calculated value and the average measured

value. For Test 32013, the predicted clad temperature at 2.44 m (96 in) is slightly lower than the average measured value. In most cases, the predicted rod quench time is longer than the data. The over-prediction tendency of rod quench time becomes stronger as the elevation increases at a given test. The predicted rod heat-up rates are higher than the data in most cases. The rod heat-up rate is mainly dependent on the material properties of the heater rod. Thus the rod heat-up rate will be lowered if the accurate material properties of the heater rod, especially with boron nitride, are modeled.

The reflooding rate variation tests cover the reflooding rate from 2.10 cm/s (0.83 in/s) to 15.50 cm/s (6.10 in/s). The measured clad temperatures decrease as the flooding rates increase. The RELAP5/MOD3.3/K predicts well the effect of reflooding rate on the clad temperature. In all four tests, the RELAP5/MOD3.3/K over-predicts rod clad temperatures at a given elevation, based on a comparison between the calculated value and the average measured value. For high reflooding rate tests such as Test 31302 and Test 31701, the predicted value is higher than the highest measured value at all elevations.

The initial system pressure variation tests cover the initial system pressure 0.13 MPa (19 psia) to 0.41 MPa (60 psia). The initial conditions of these tests are almost the same except for the inlet coolant temperature. Even though the inlet coolant temperature is different, the subcooling of the inlet liquid is almost the same at about 80 ^{o}C (144 ^{o}F). The measured values show that the effect of the system pressure on the rod clad temperature is insignificant. However, rod quench time becomes shorter as the system pressure increases. The RELAP5/MOD3.3/K predicts well the effects of the system pressure on the rod clad temperature and the rod quench time.

The initial clad temperature variation tests cover the initial clad temperature from 256 ^{o}C (493 ^{o}F) to 1,119 ^{o}C (2,046 ^{o}F). Both RELAP5/MOD3.3/K predicted clad temperatures and measured clad temperatures increase as the initial clad temperatures increase. In all tests selected for the initial clad temperature variation, the RELAP5/MOD3.3/K over-predicts the clad temperature at a given elevation, based on a comparison between the calculated value and the average measured value. The RELAP5/MOD3/K tends to over-predict the clad temperature as the initial clad temperature increases. In the cases of low initial clad temperature tests such as Test 30518 and Test 30817, the predicted rod quench times are earlier than the data at the 1.22 m (48 in) and 1.83 m (72 in), whereas the RELAP5/MOD3.3/K over-predicts the rod quench time at 2.44 m for all the initial clad temperature variation tests. The RELAP5/MOD3.3/K tends to over-predict the rod quench time as the initial clad temperature increases.

The rod peak power variation tests cover the rod peak power from 1.3 kW/m (0.40 kW/ft) to 3.0 kW/m (0.91 kW/ft). Both the RELAP5/MOD3.3/K predicted and the measured clad temperatures increase as the initial rod peak power increases. In all three tests, the RELAP5/MOD3.3/K over-predicts the rod clad temperatures at a given elevation, based on a comparison between the calculated value and the average measured value. The RELAP5/MOD3.3/K tends to over-predict the rod clad temperature and the rod quench time as the initial rod peak power increases.

For the “Others” group, the RELAP5/MOD3.3/K over-predicts the rod clad temperature and the rod quench time, based on a comparison between the calculated value and the average measured value. In the cases of Test 32235, Test 32333, and Test 33338, the RELAP5/MOD3.3/K clearly predicts the effect of the reflooding rate change on the clad temperature behaviors. The clad temperature and rod quench time behaviors of the gravity reflood test, Test 33338, are predicted reasonably well by the RELAP5/MOD3.3/K.

2.3.6.2 Vapor Temperature

The vapor temperature is compared between the data and the RELAP5/MOD3.3/K predicted values at 1.83 m (72 in) from the heated rod bottom. In most cases, the RELAP5/MOD3.3/K reasonably

predicts the vapor temperature considering that vapor temperature measurements may have a large uncertainty.

2.3.6.3 Differential Pressure (DP) for the Entire Core

Differential pressure for the entire 3.66 m (12 ft) core is compared between the data and the RELAP5/MOD3.3/K predicted value. Even though the predicted value is oscillatory, the RELAP5/MOD3.3/K predicts the entire core DP well, based on a comparison between the average calculated value and the measured value. The RELAP5/MOD3.3/K predicts the DP fairly well during the entire reflood period for six of the 17 tests; slightly over-predicts it during the entire reflood period for one test; and slightly under-predicts it for ten tests during the late reflood period. Overall, the RELAP5/MOD3.3/K predicts reasonably well the DP for the entire core. This means that the RELAP5/MOD3.3/K reasonably predicts the amount of liquid being accumulated in the core and the amount of liquid carried out of the bundle.

2.4 Code Accuracy

Three data sets obtained from 17 tests in Table 2-1, [ ]^{TS} Since clad temperature measurements of the FLECHT-SEASET experiments are crowded at the central part of the core, [ ]^{TS} in the calculation. Data points are compared with the calculated values at corresponding elevations.

Figure 2-92 shows the code accuracy evaluated using [ ]^{TS} FLECHT-SEASET test data. The RELAP5/MOD3.3/K over-predicts the clad temperature by [ ]^{TS}

2.5 SRS Calculations

SRS calculations were performed against 17 FLECHT-SEASET tests in Table 2-1. [ ]^{TS} The uncertainty parameters and their distribution functions used for the SRS calculations are listed in Table 2-2.

Figures from Figure 2-93 to Figure 2-109 show the results of the SRS calculations against 17 FLECHT-SEASET tests. In all the SRS calculations, the third highest values of the calculated clad temperatures are higher than the measured PCTs confirming the data covering. Therefore, the number and the probability distribution functions of the selected code parameters and the test facility specific parameters are confirmed to be sufficient.

2.6 Conclusion

The capability of the RELAP5/MOD3.3/K in predicting the reflood progression was assessed against 17 FLECHT-SEASET tests. The assessment results show that the RELAP5/MOD3.3/K is capable of calculating the reflood process correctly, in general. The RELAP5/MOD3.3/K over-predicts the rod clad temperature as confirmed by the evaluation of code accuracy. The RELAP5/MOD3.3/K over predicts the clad temperature by [ ]^{TS} on average, with a standard deviation of [ ]^{TS} The tendency of over-prediction of the clad temperature is stronger at higher

elevations of the core. This may be caused by lack of a spacer grid model in the RELAP5/MOD3.3/K.

In all of the SRS calculations against 17 FLECHT-SEASET tests, the data covering was confirmed. This implies that the number and the probability distribution functions of the selected code parameters for the reflood heat transfer are sufficient to cover the measured PCTs.

References

[2-1] M.J. Loftus, et al., “PWR FLECHT SEASET Unblocked Bundle, Forced and Gravity Reflood Task Data Report,” EPRI NP-1459, NUREG/CR-1532, WCAP-9699, 1981.

Table 2-1 FLECT-SEASET Tests Used for RELAP5/MOD3.3/K Assessment

Group	Run No.	System Pressure	Rod Tem-perature	Rod power	Flood-ing rate	Coolant Inlet Temperature	PCT* Elevation	PCT	Radial power distribu-tion
		MPa	K	kW/m	mm/s	K	m (in)	K	-
Flooding rate	31203 (1)	0.28	1145.15	2.3	38.4	325.15	1.93, (76)	1310.15	Uniform
	31302	0.28	1142.15	2.3	76.5	325.15	1.70, (67)	1205.15	Uniform
	31504 (2)	0.28	1136.15	2.3	24.6	324.15	1.98, (78)	1423.15	Uniform
	31701	0.28	1145.15	2.3	155	326.15	1.78, (70)	1196.15	Uniform
	31805	0.28	1144.15	2.3	21	324.15	1.98, (78)	1505.15	Uniform
System pressure	31504	same as (2)							
	32013	0.41	1160.15	2.3	26.4	339.15	1.93, (76)	1444.15	Uniform
	34209	0.14	1162.15	2.4	27.2	305.15	1.98, (78)	1434.15	Uniform
Initial clad tempera-ture	30518	0.28	529.15	2.3	38.9	325.15	1.98, (78)	926.15	Uniform
	30817	0.27	804.15	2.3	38.9	326.15	1.98, (78)	1105.15	Uniform
	31203	same as (1)							
	34420	0.27	1392.15	2.4	38.9	324.15	1.83, (72)	1480.15	Uniform
Initial rod peak power	31021	0.28	1152.15	1.3	38.6	325.15	1.78, (70)	1214.15	Uniform
	31203	same as (1)							
	34524	0.28	1151.15	3	39.9	325.15	1.83, (72)	1477.15	Uniform
Others	31108	0.13	1144.15	2.3	79	306.15	1.78, (70)	1211.15	Uniform
	32235	0.14	1161.15	2.3	165.8/24.9/15.7	304.15	1.98, (78)	1419.15	Uniform
	32333	0.28	1162.15	2.3	162/21	326.15	1.93, (76)	1421.15	Uniform
	33338	0.28	1144.15	2.3/1.3	5.9/0.807 kg/s	325.15	1.78, (70)	1198.15	Hot/cold
	34006	0.27	1155.15	1.3	15	324.15	1.98, (78)	1436.15	Uniform

* PCT: Peak Cladding Temperature

Table 2-2 Parameters and Distribution Functions Used for SRS Calculations: FLECHT-SEASET

TS

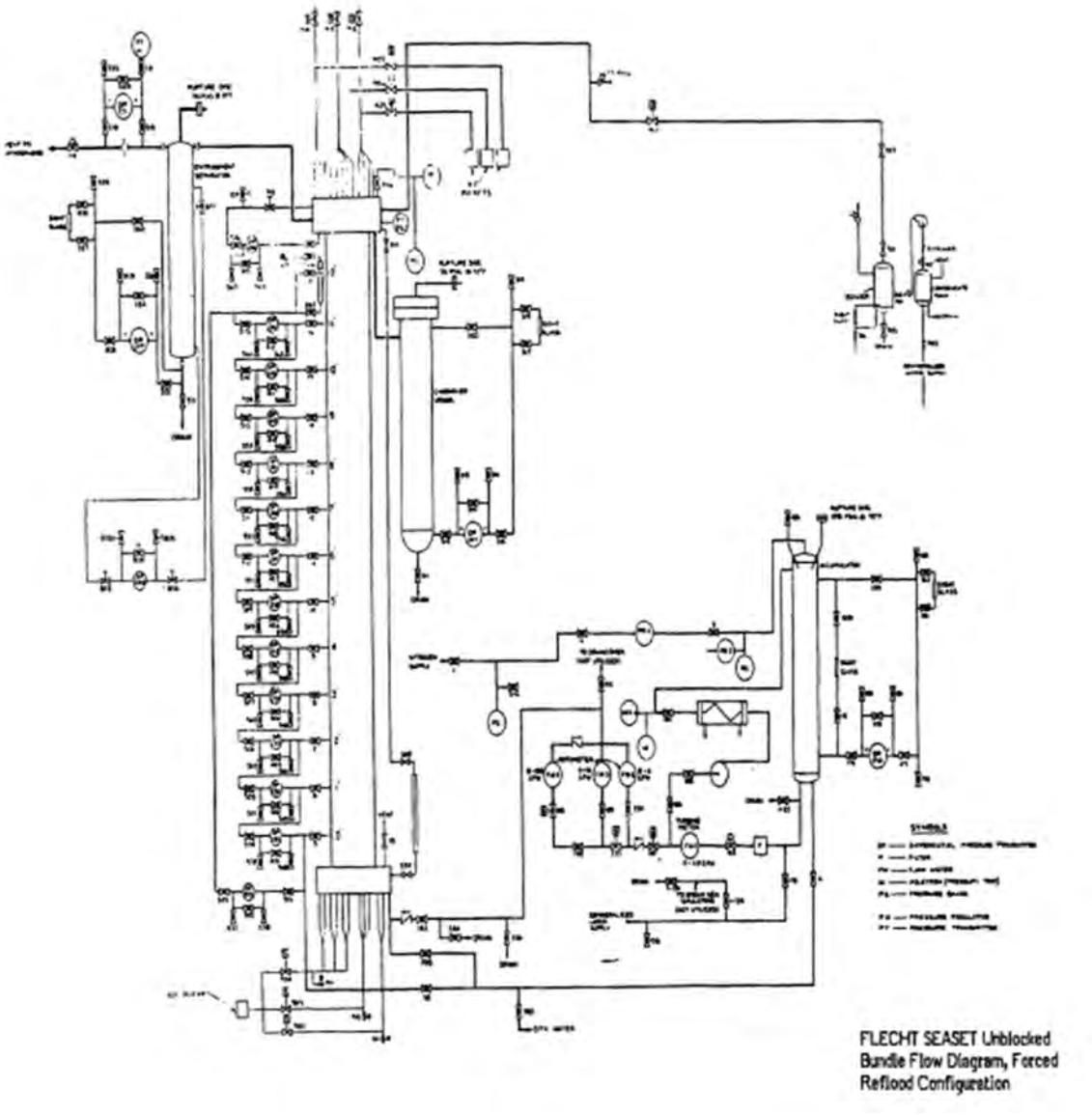

Figure 2-1 FLECHT-SEASET Facility Flow Diagram for Forced Reflood Tests

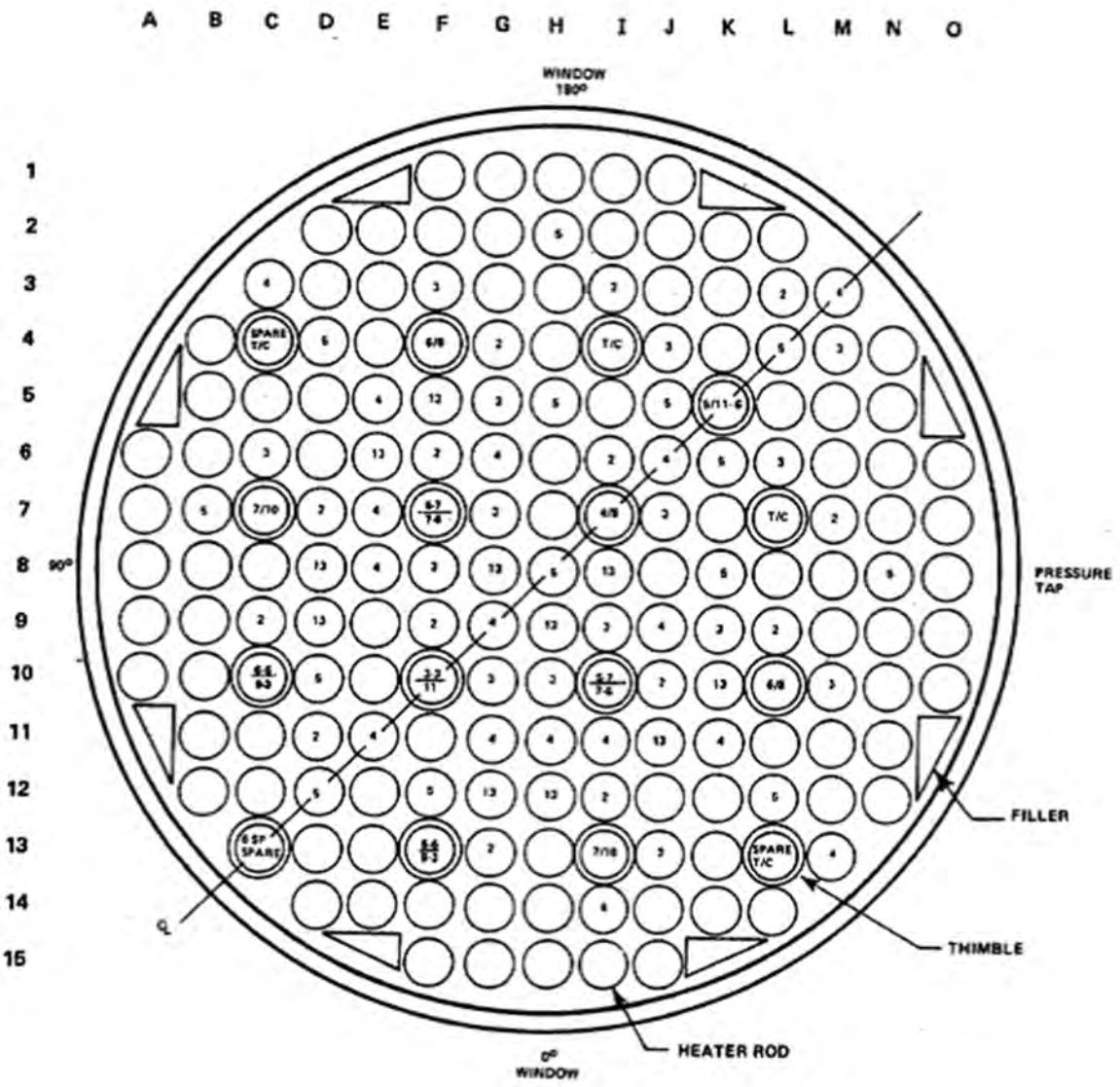

Figure 2-2 Cross-sectional View of the FLECHT-SEASET Bundle Heated Section

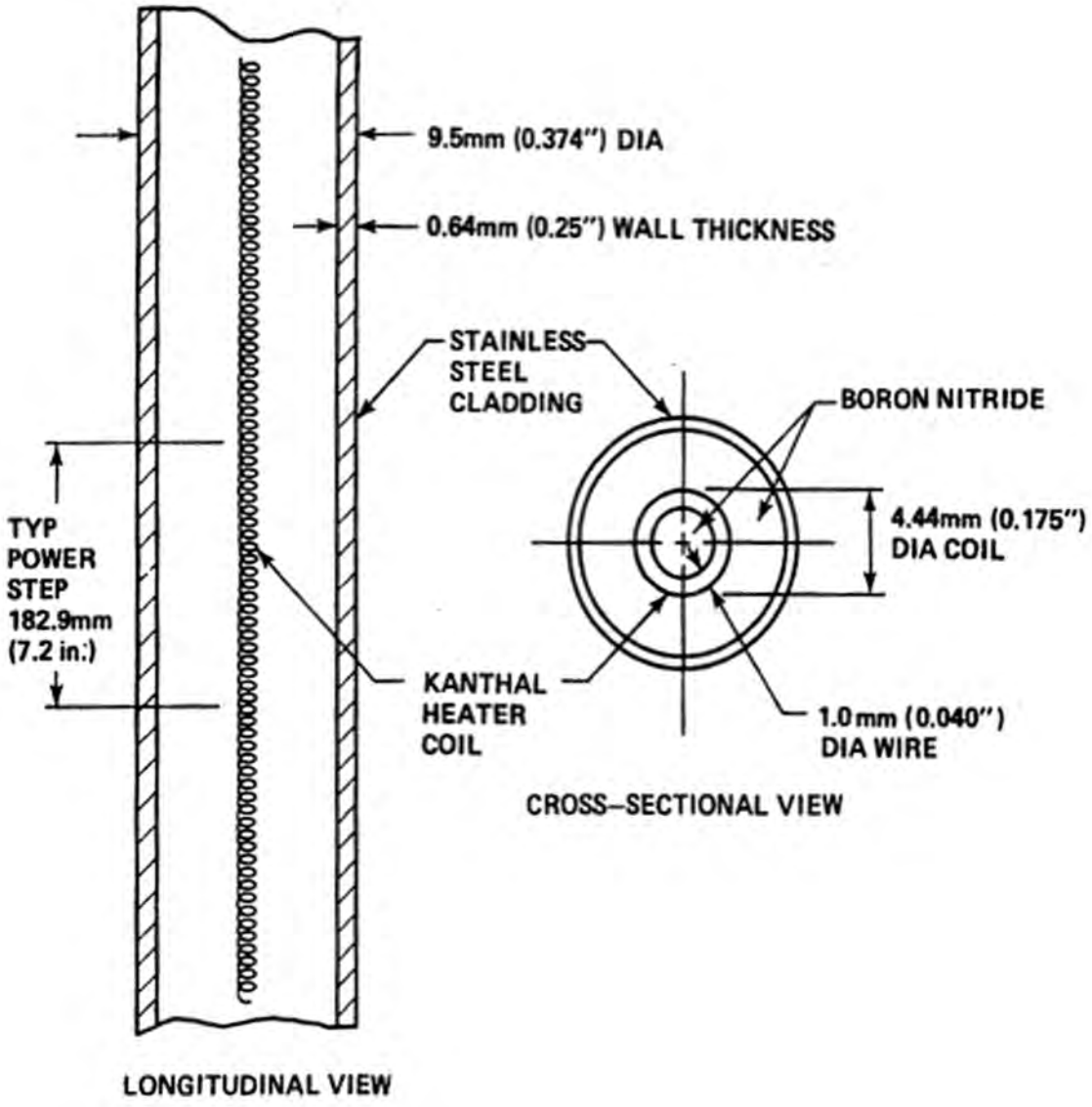

Figure 2-3 Heater Rod Schematic Diagram

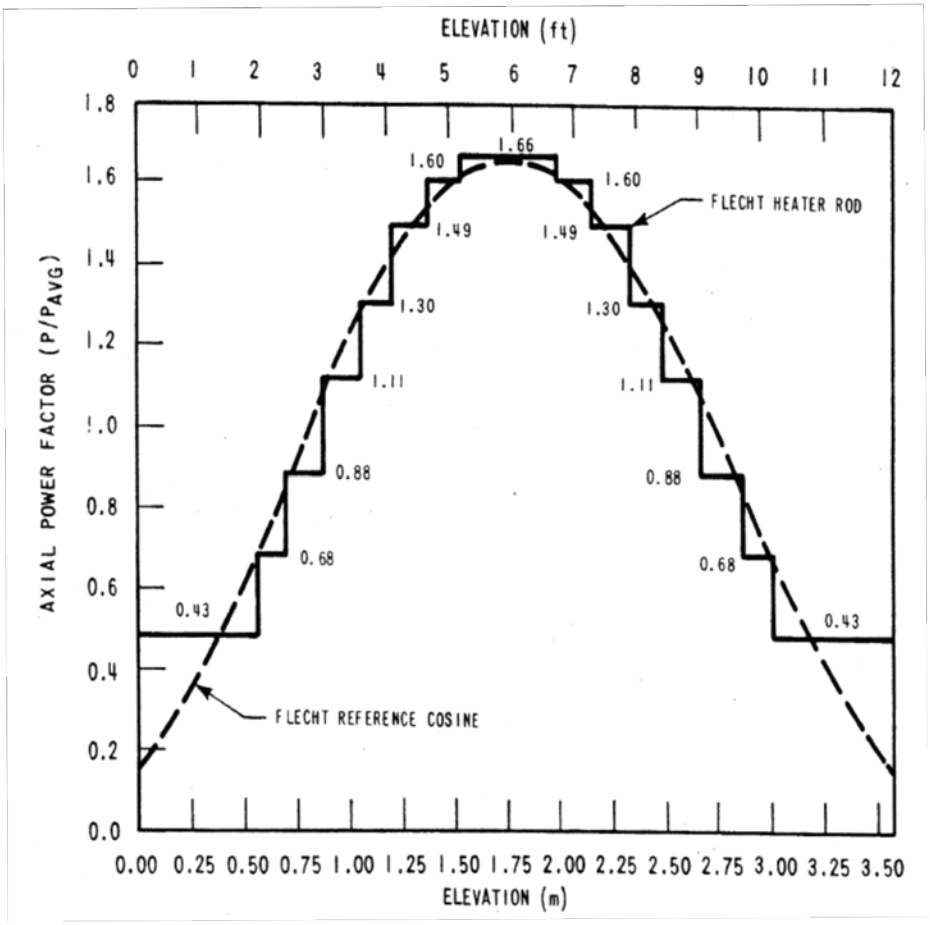

Figure 2-4 Axial Power Profile of the Heater Rods

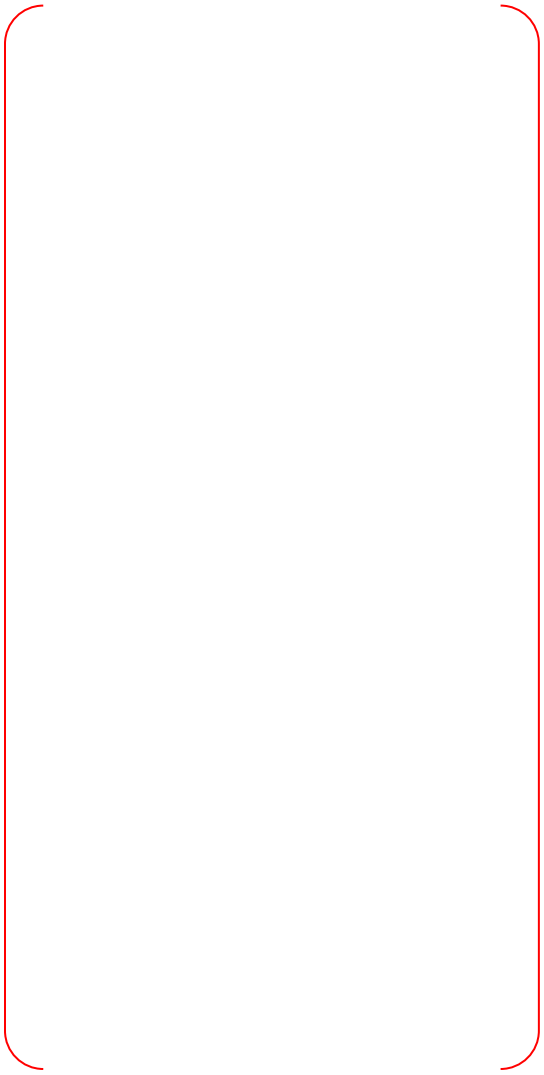

Figure 2-5 FLECHT-SEASET RELAP5/MOD3.3/K Noding Diagram for Forced Reflood Tests

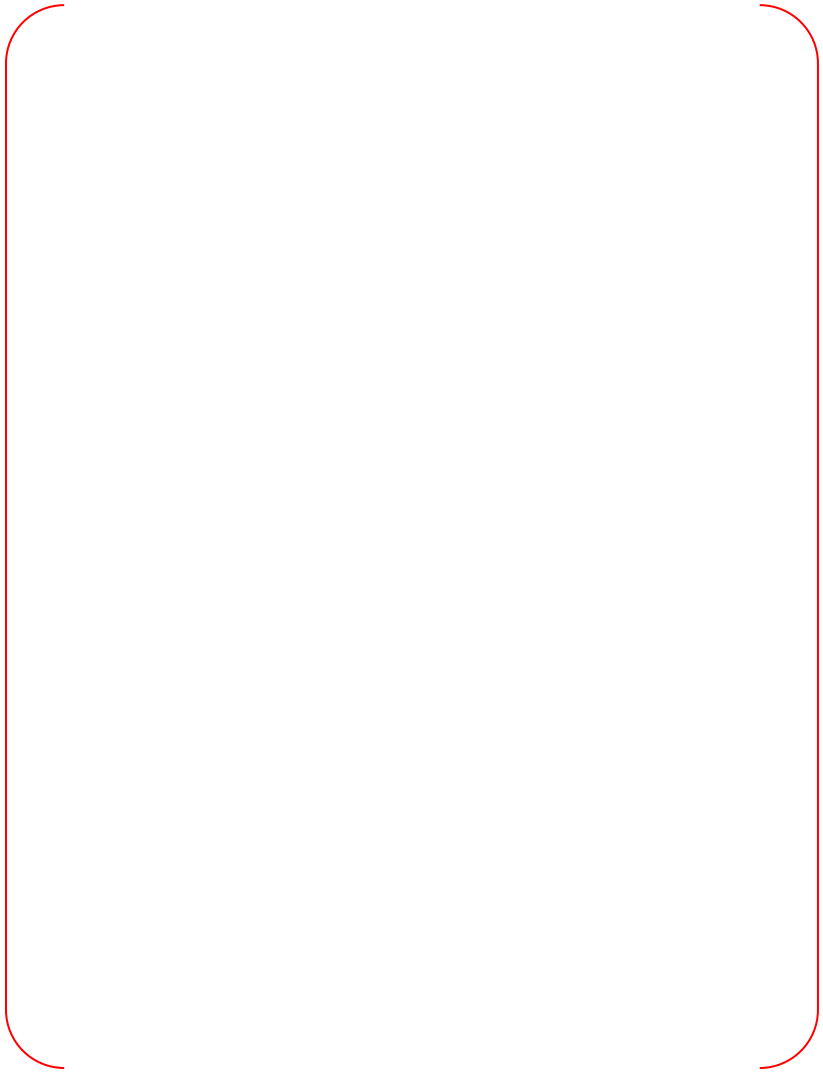

Figure 2-6 FLECHT-SEASET RELAP5/MOD3.3/K Noding Diagram for Gravity Reflood Tests

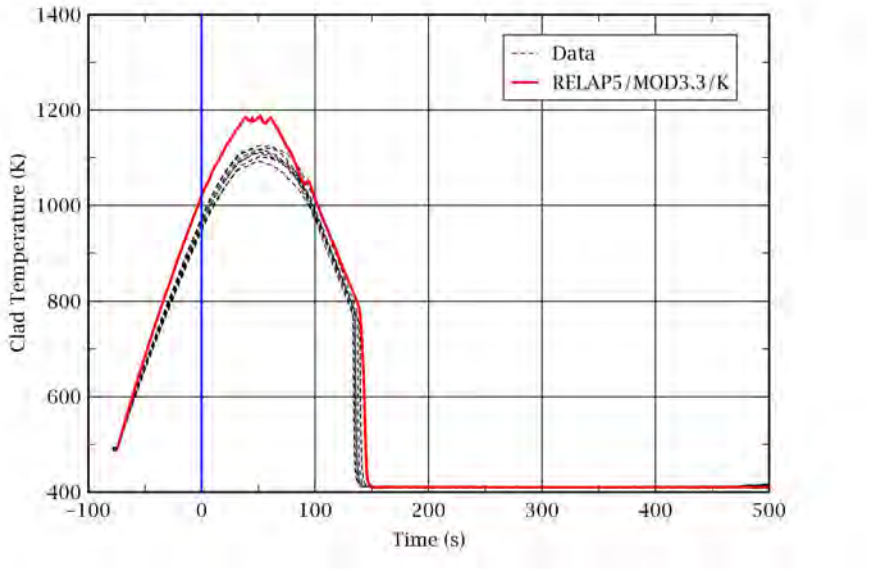

Figure 2-7 Rod Clad Temperatures at 48 in. from the Heated Bottom: Test 31805

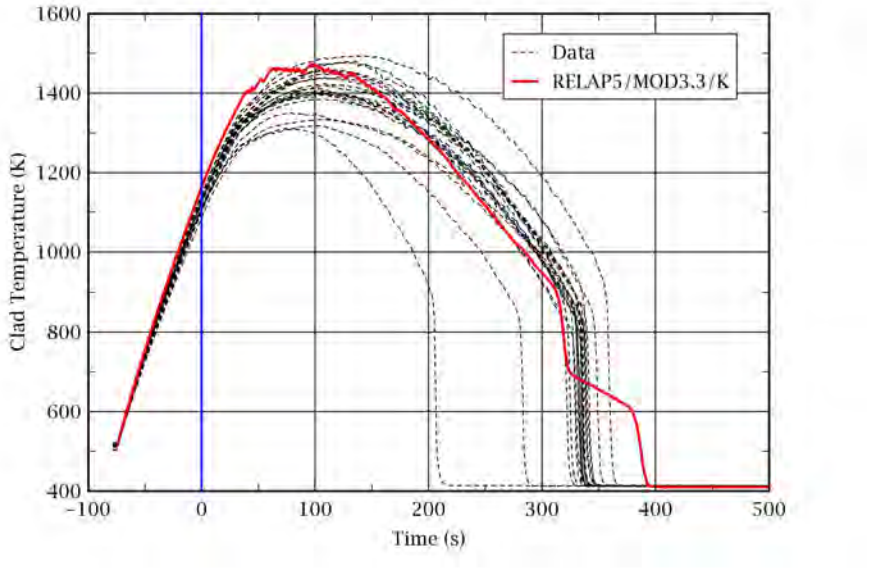

Figure 2-8 Rod Clad Temperatures at 72 in. from the Heated Bottom: Test 31805

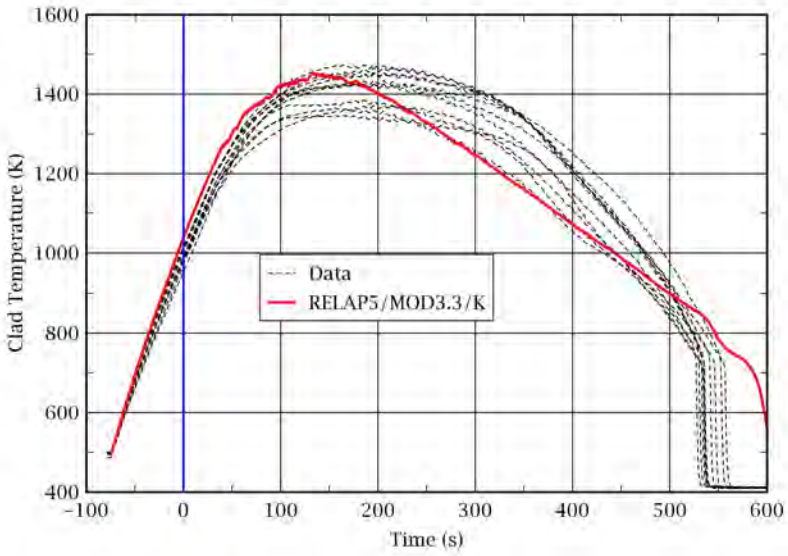

Figure 2-9 Rod Clad Temperatures at 96 in. from the Heated Bottom: Test 31805

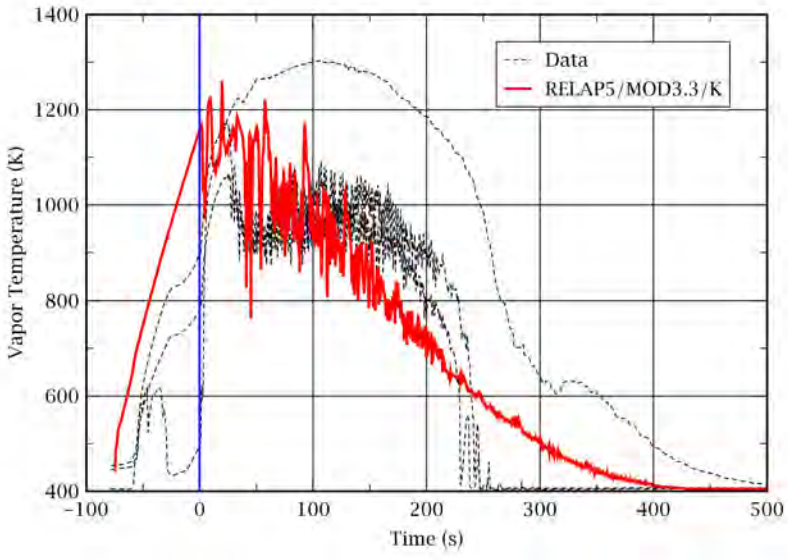

Figure 2-10 Vapor Temperatures at 72 in. from the Heated Bottom: Test 31805

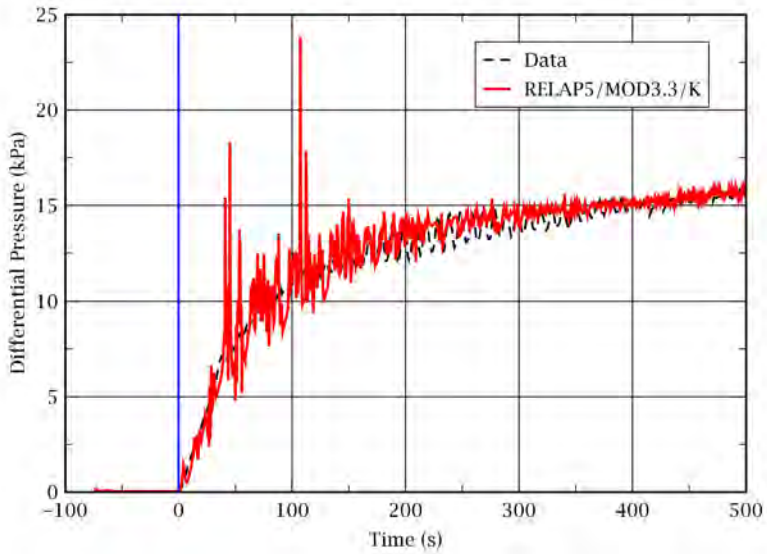

Figure 2-11 Differential Pressure for the Entire 12 ft Core: Test 31805

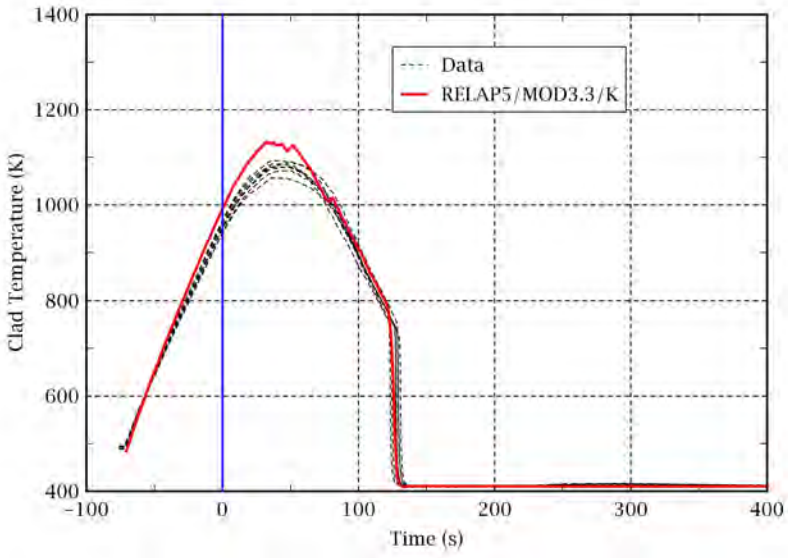

Figure 2-12 Rod Clad Temperatures at 48 in. from the Heated Bottom: Test 31504

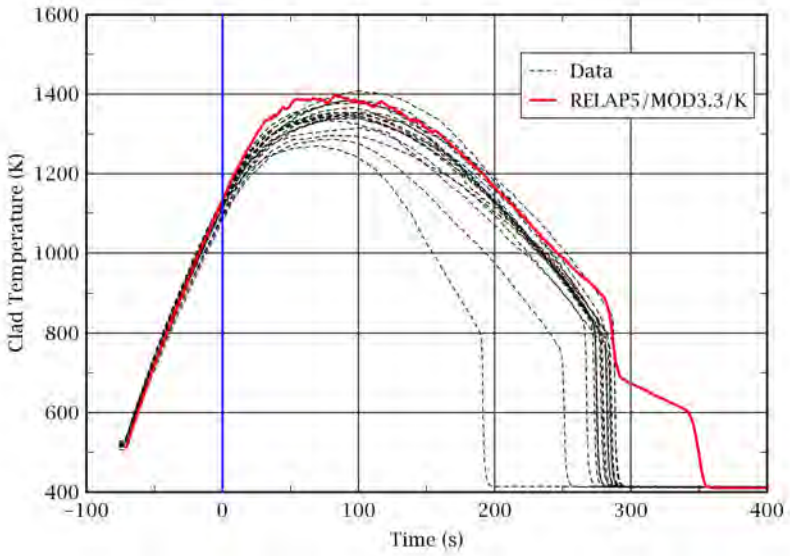

Figure 2-13 Rod Clad Temperatures at 72 in. from the Heated Bottom: Test 31504

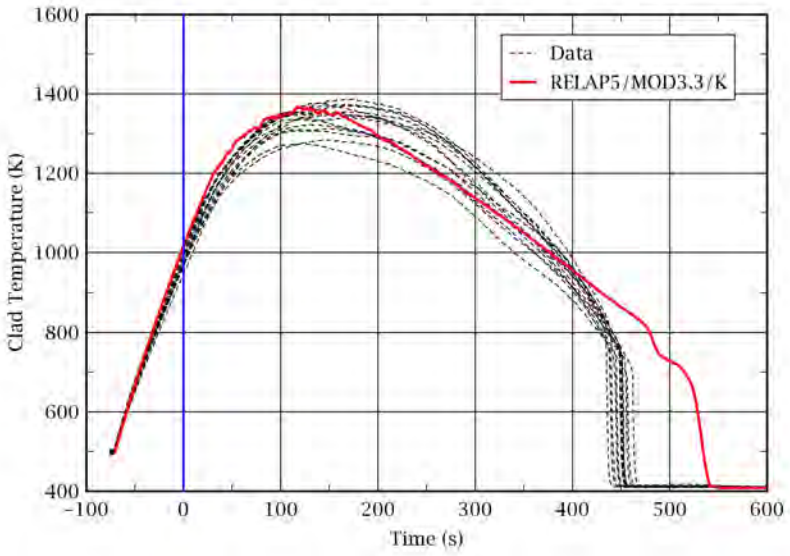

Figure 2-14 Rod Clad Temperatures at 96 in. from the Heated Bottom: Test 31504

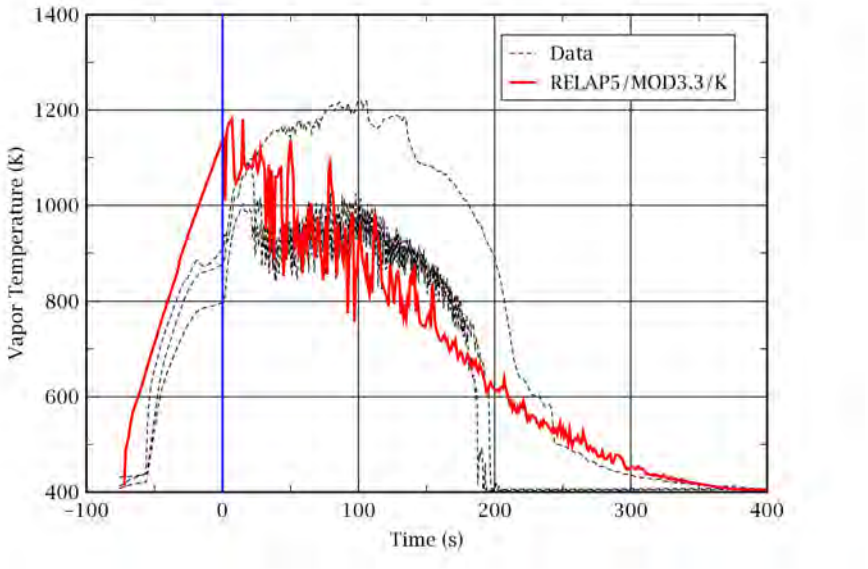

Figure 2-15 Vapor Temperatures at 72 in. from the Heated Bottom: Test 31504

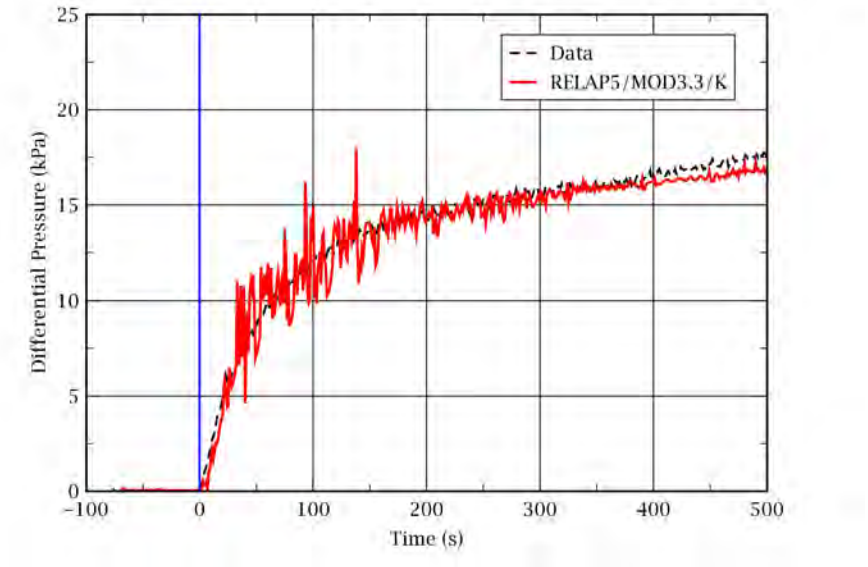

Figure 2-16 Differential Pressure for the Entire 12 ft Core: Test 31504

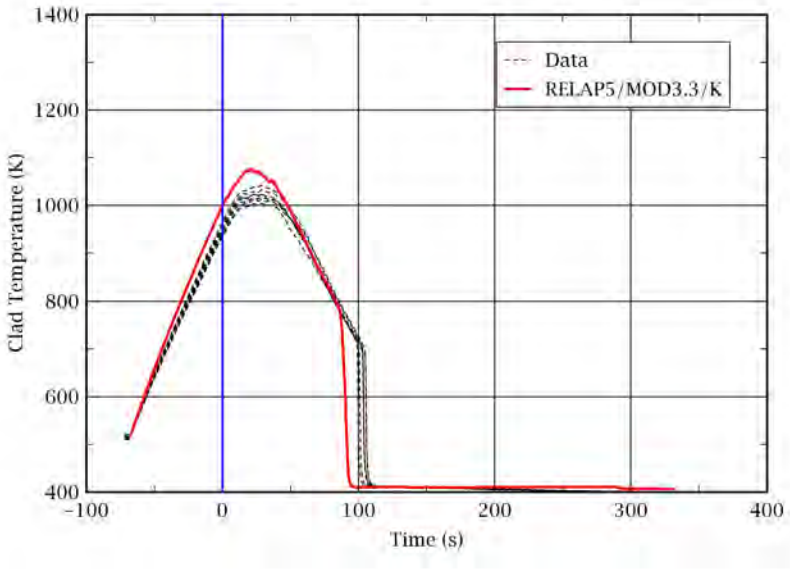

Figure 2-17 Rod Clad Temperatures at 48 in. from the Heated Bottom: Test 31203

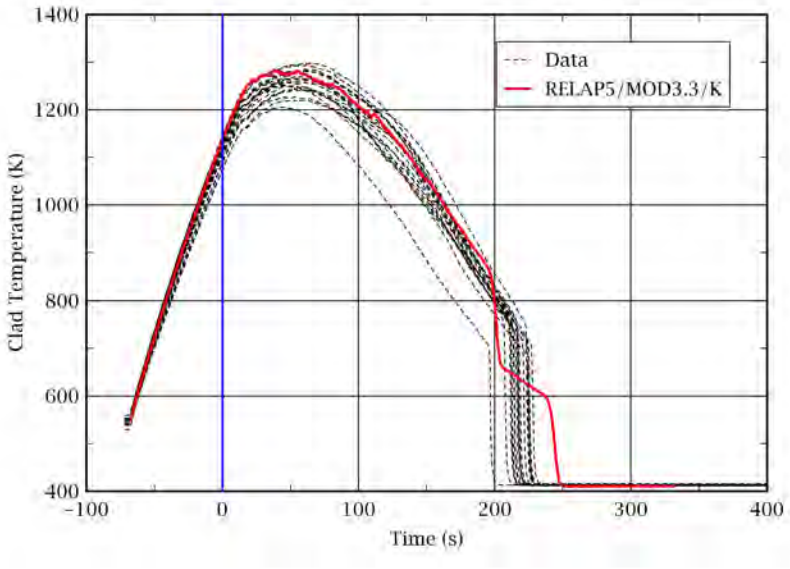

Figure 2-18 Rod Clad Temperatures at 72 in. from the Heated Bottom: Test 31203

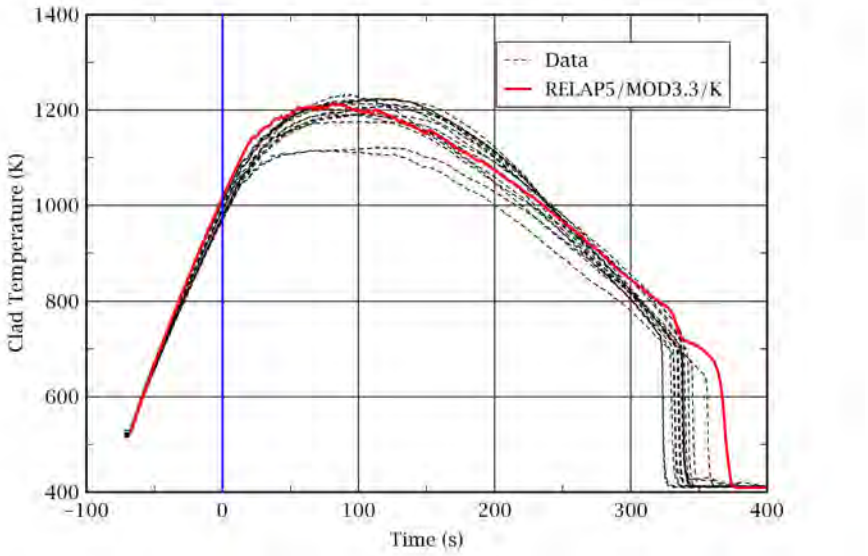

Figure 2-19 Rod Clad Temperatures at 96 in. from the Heated Bottom: Test 31203

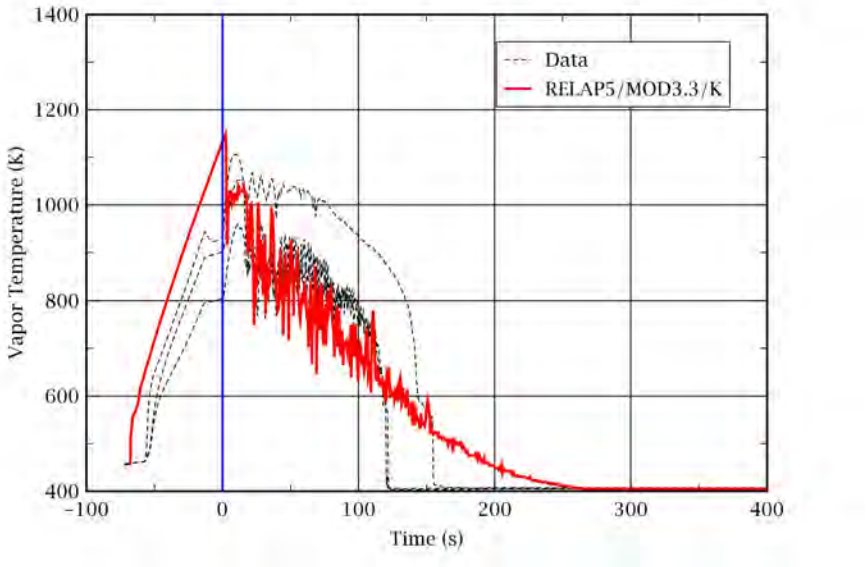

Figure 2-20 Vapor Temperatures at 72 in. from the Heated Bottom: Test 31203

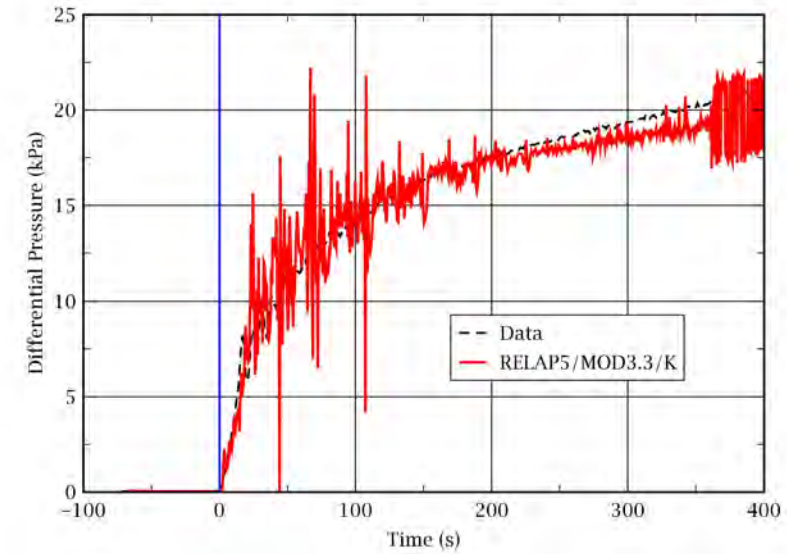

Figure 2-21 Differential Pressure for the Entire 12 ft Core: Test 31203

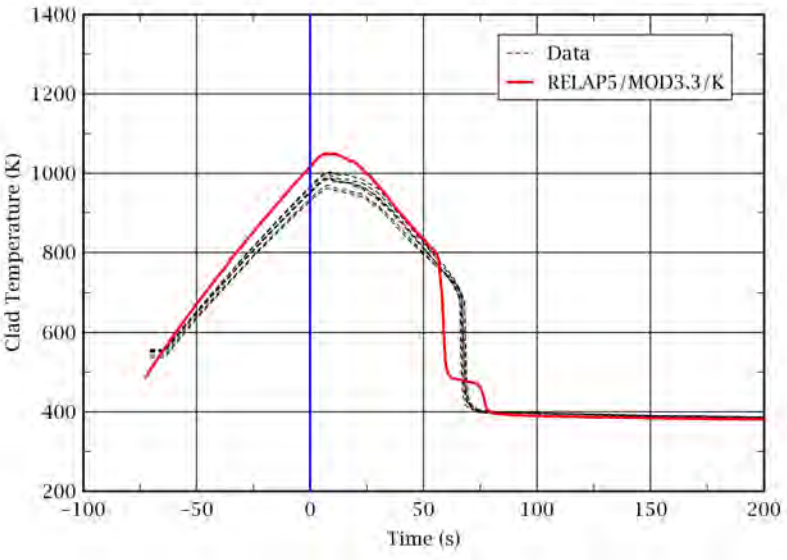

Figure 2-22 Rod Clad Temperatures at 48 in. from the Heated Bottom: Test 31302

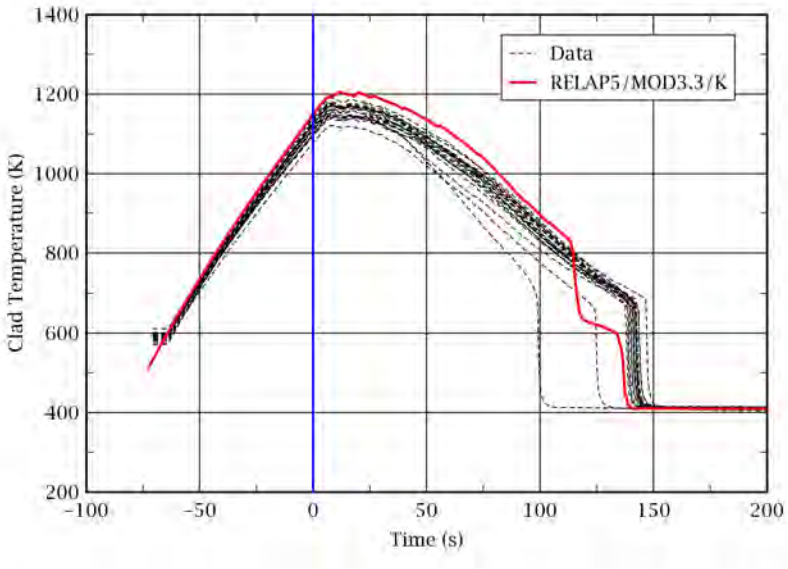

Figure 2-23 Rod Clad Temperatures at 72 in. from the Heated Bottom: Test 31302

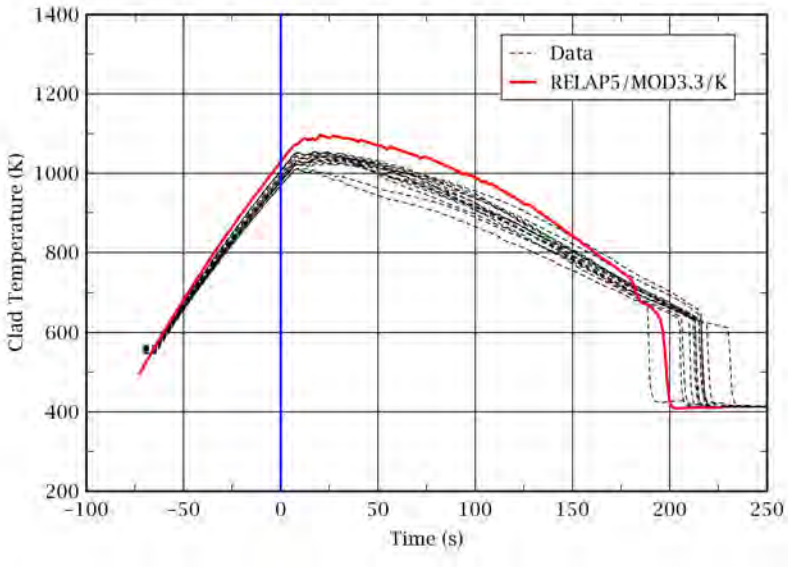

Figure 2-24 Rod Clad Temperatures at 96 in. from the Heated Bottom: Test 31302

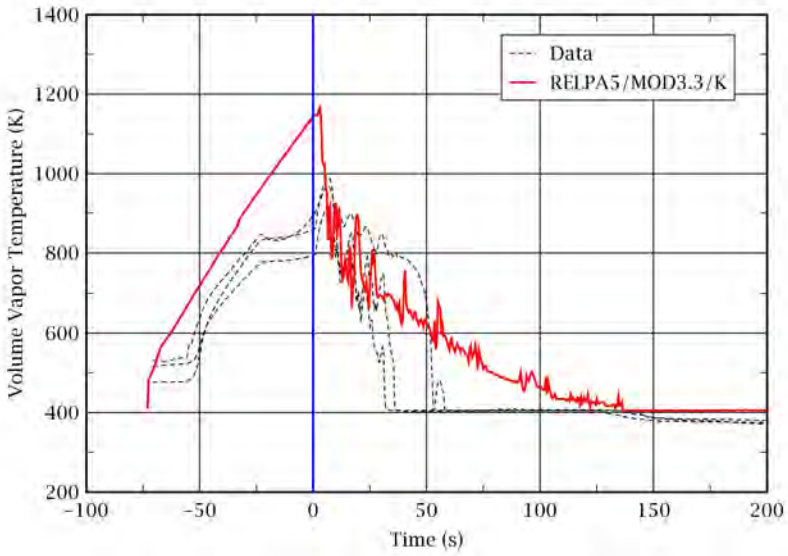

Figure 2-25 Vapor Temperatures at 72 in. from the Heated Bottom: Test 31302

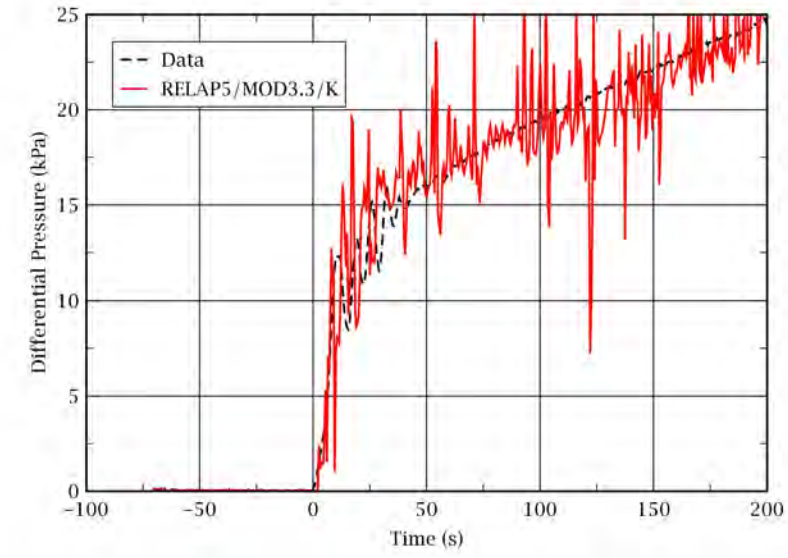

Figure 2-26 Differential Pressure for the Entire 12 ft Core: Test 31302

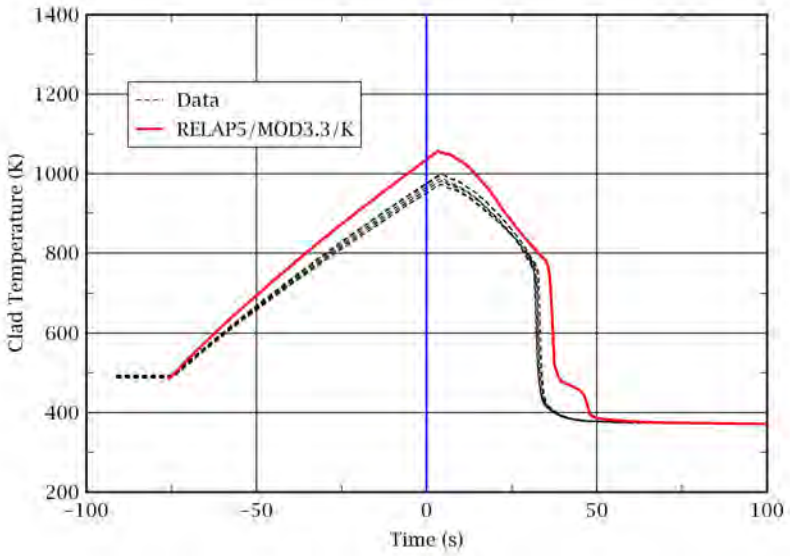

Figure 2-27 Rod Clad Temperatures at 48 in. from the Heated Bottom: Test 31701

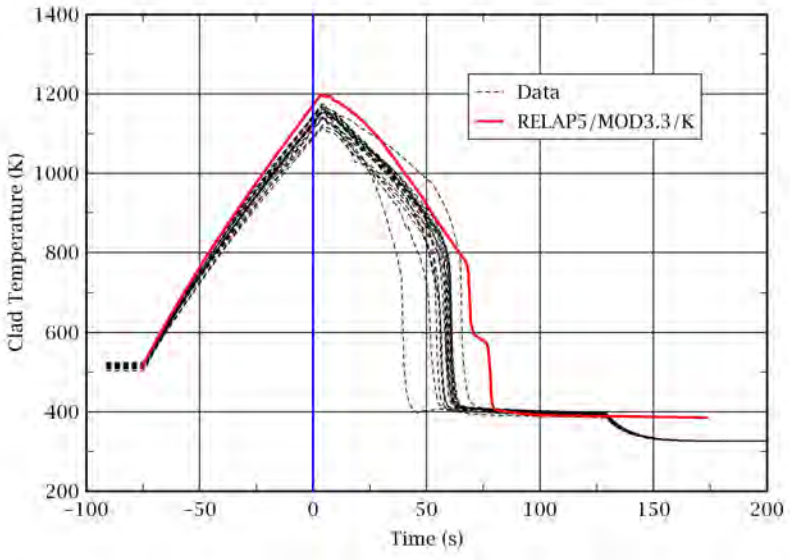

Figure 2-28 Rod Clad Temperatures at 72 in. from the Heated Bottom: Test 31701

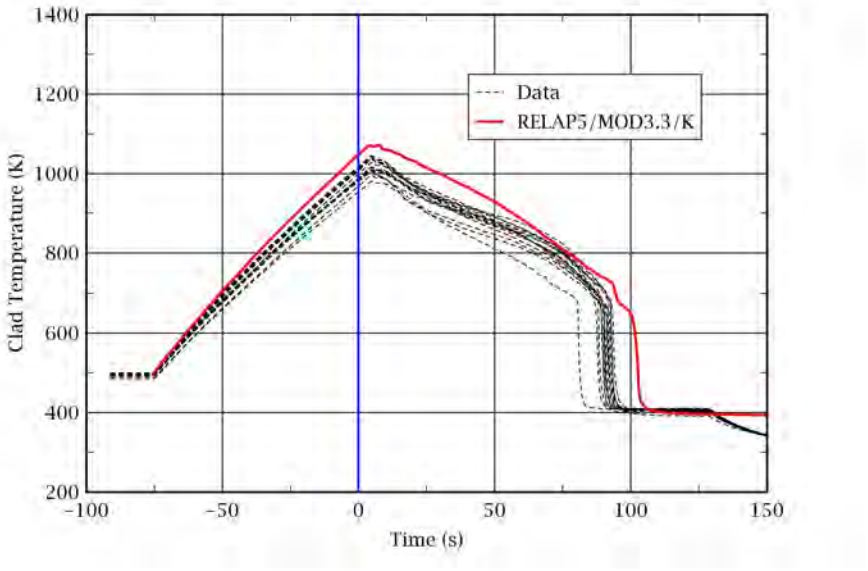

Figure 2-29 Rod Clad Temperatures at 96 in. from the Heated Bottom: Test 31701

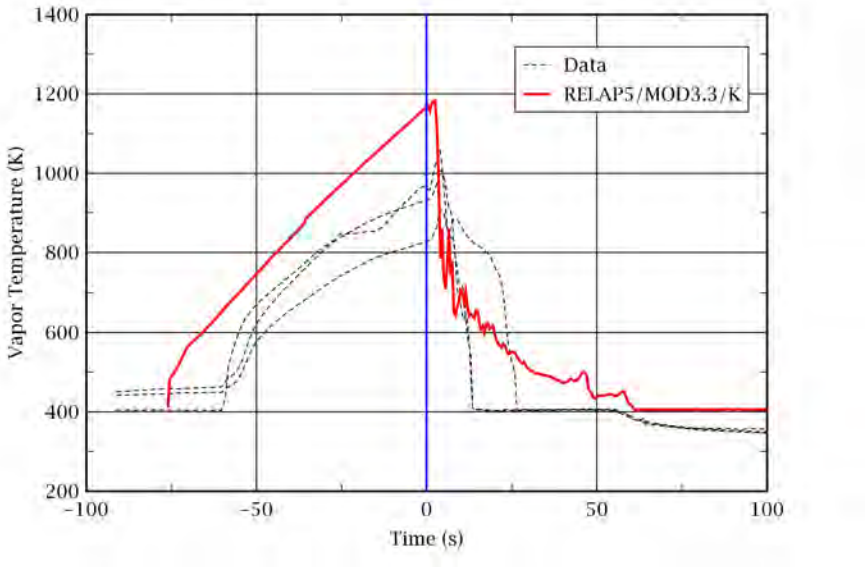

Figure 2-30 Vapor Temperatures at 72 in. from the Heated Bottom: Test 31701

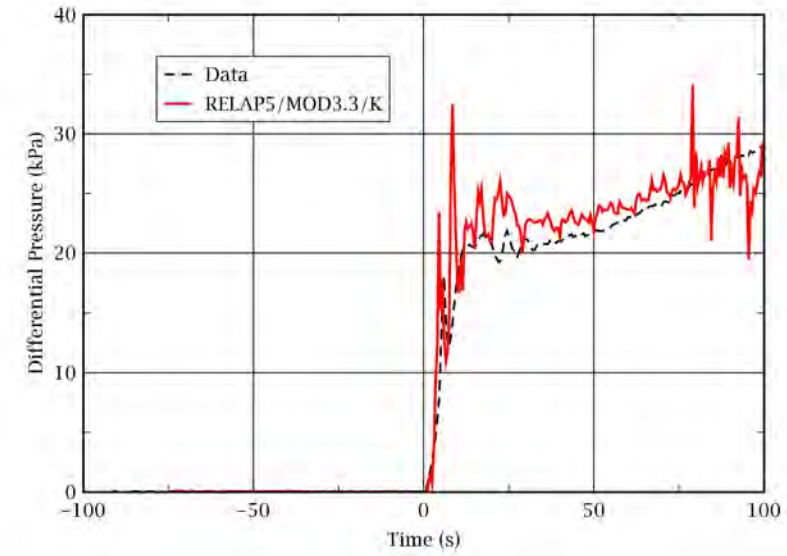

Figure 2-31 Differential Pressure for the Entire 12 ft Core: Test 31701

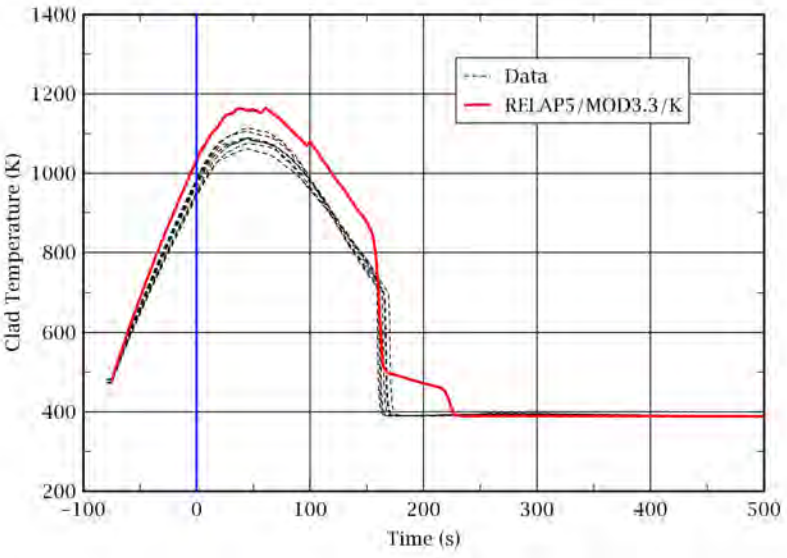

Figure 2-32 Rod Clad Temperatures at 48 in. from the Heated Bottom: Test 34209

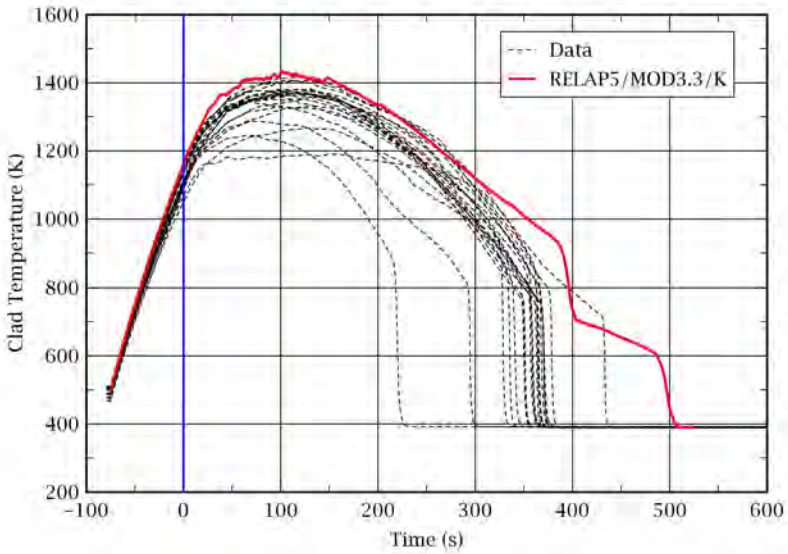

Figure 2-33 Rod Clad Temperatures at 72 in. from the Heated Bottom: Test 34209

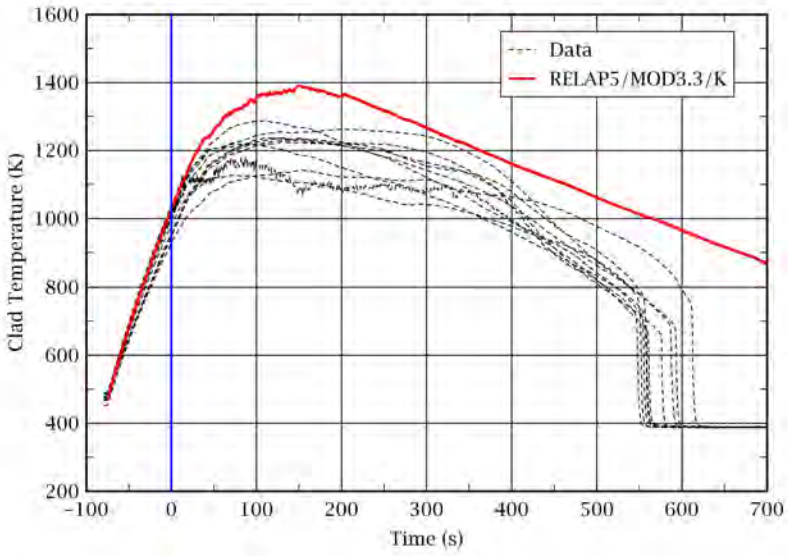

Figure 2-34 Rod Clad Temperatures at 96 in. from the Heated Bottom: Test 34209

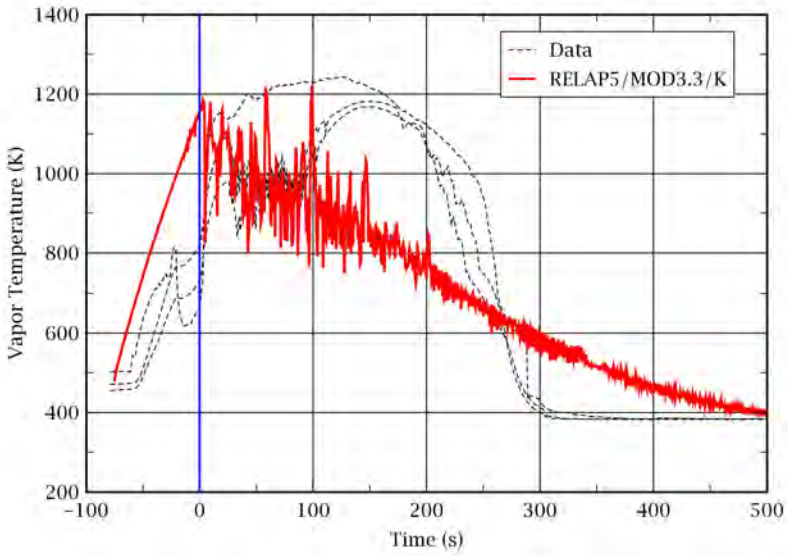

Figure 2-35 Vapor Temperatures at 72 in. from the Heated Bottom: Test 34209

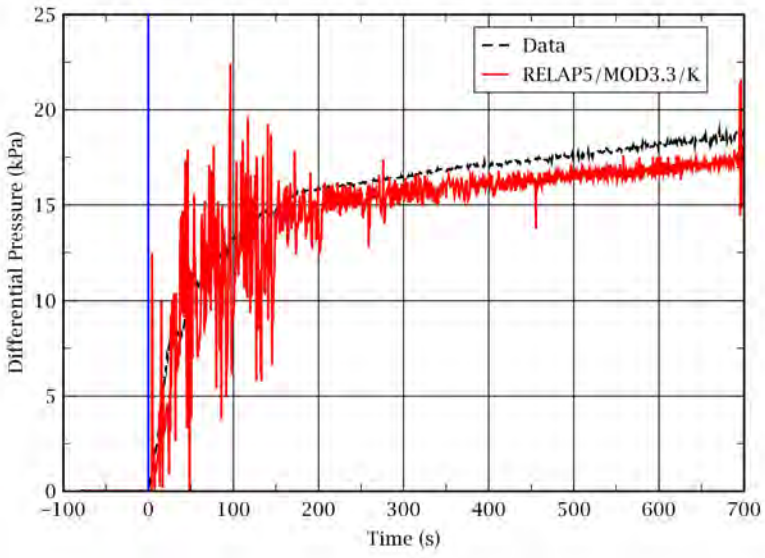

Figure 2-36 Differential Pressure for the Entire 12 ft Core: Test 34209

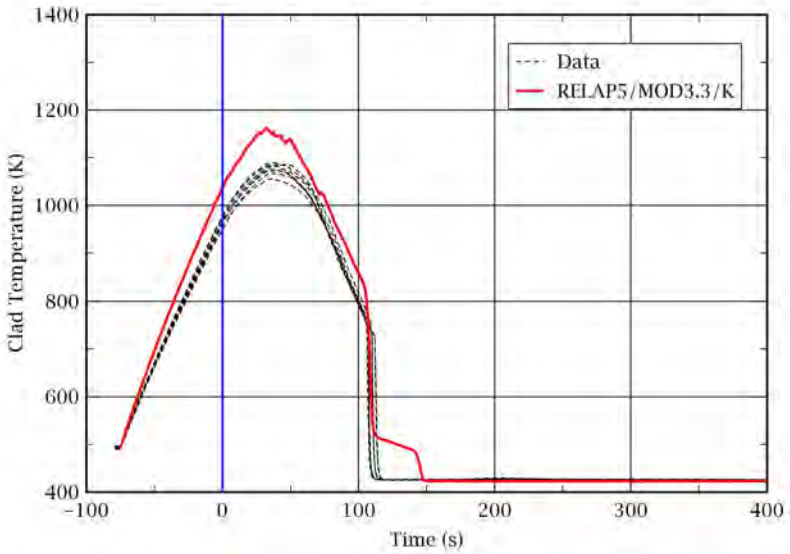

Figure 2-37 Rod Clad Temperatures at 48 in. from the Heated Bottom: Test 32013

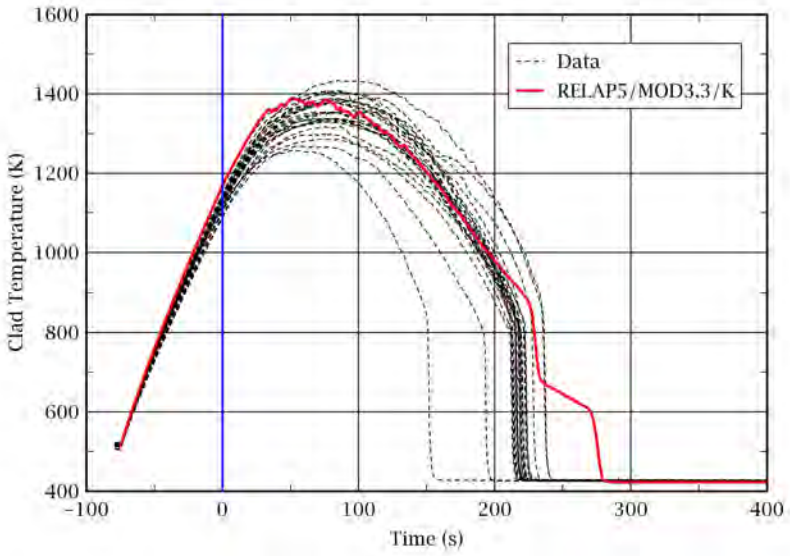

Figure 2-38 Rod Clad Temperatures at 72 in. from the Heated Bottom: Test 32013

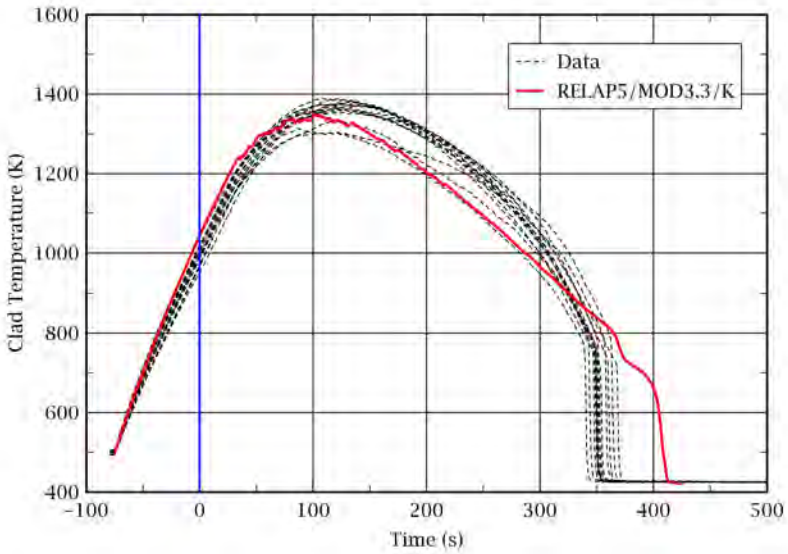

Figure 2-39 Rod Clad Temperatures at 96 in. from the Heated Bottom: Test 32013

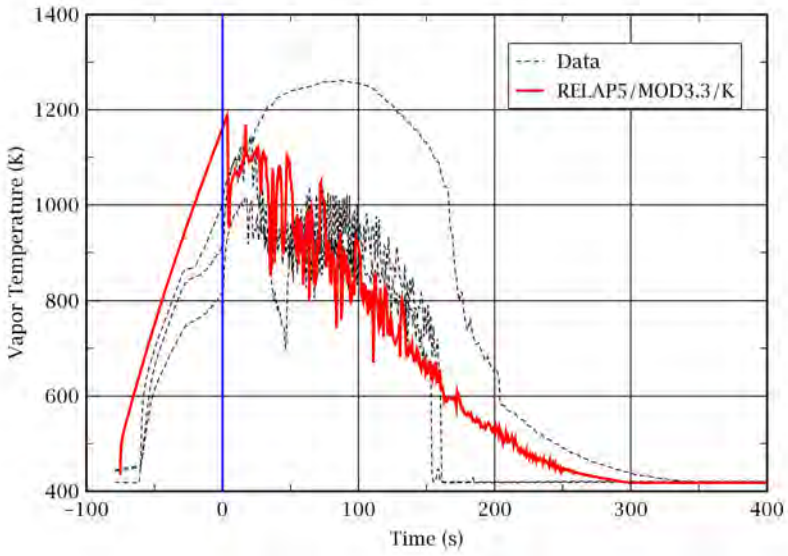

Figure 2-40 Vapor Temperatures at 72 in. from the Heated Bottom: Test 32013

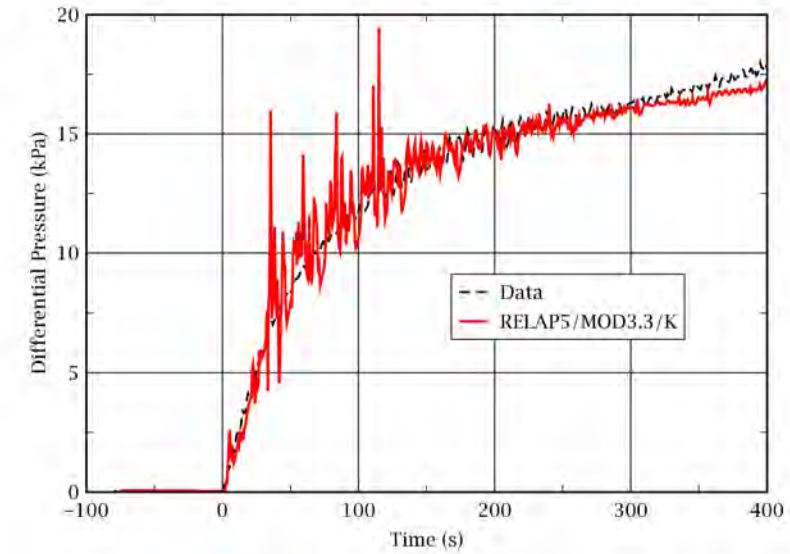

Figure 2-41 Differential Pressure for the Entire 12 ft Core: Test 32013

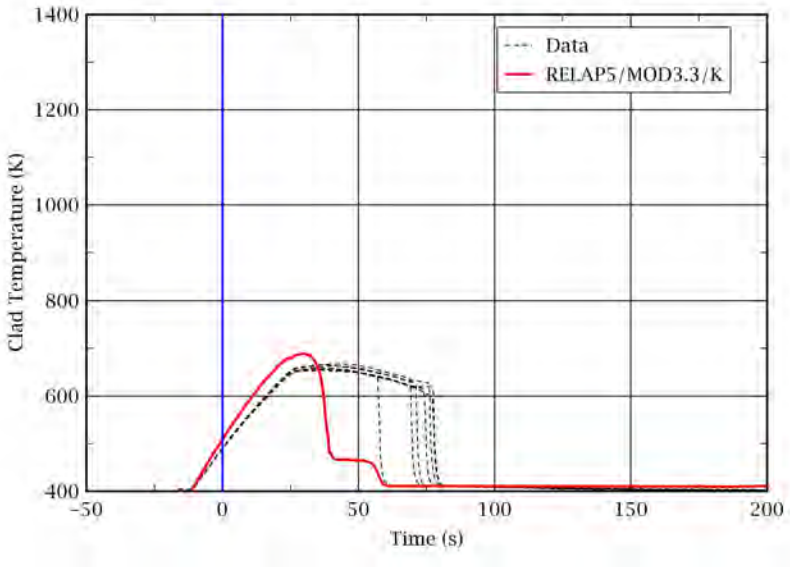

Figure 2-42 Rod Clad Temperatures at 48 in. from the Heated Bottom: Test 30518

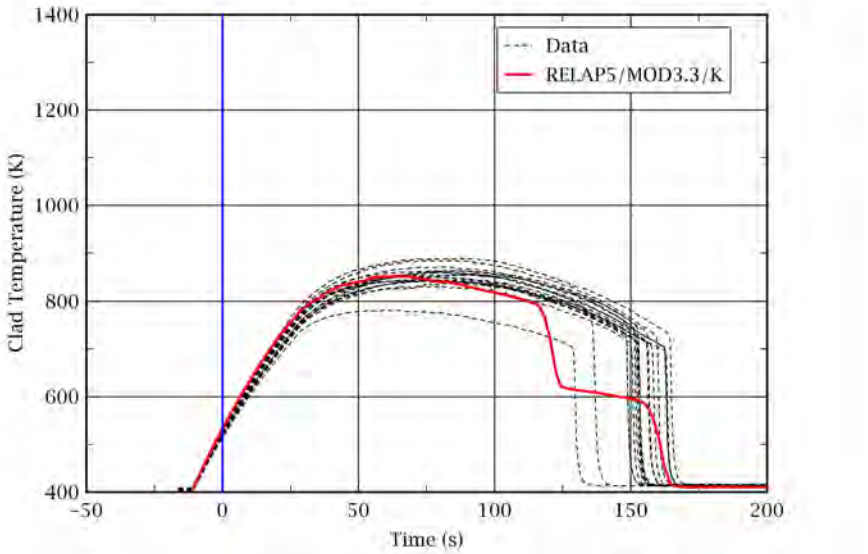

Figure 2-43 Rod Clad Temperatures at 72 in. from the Heated Bottom: Test 30518

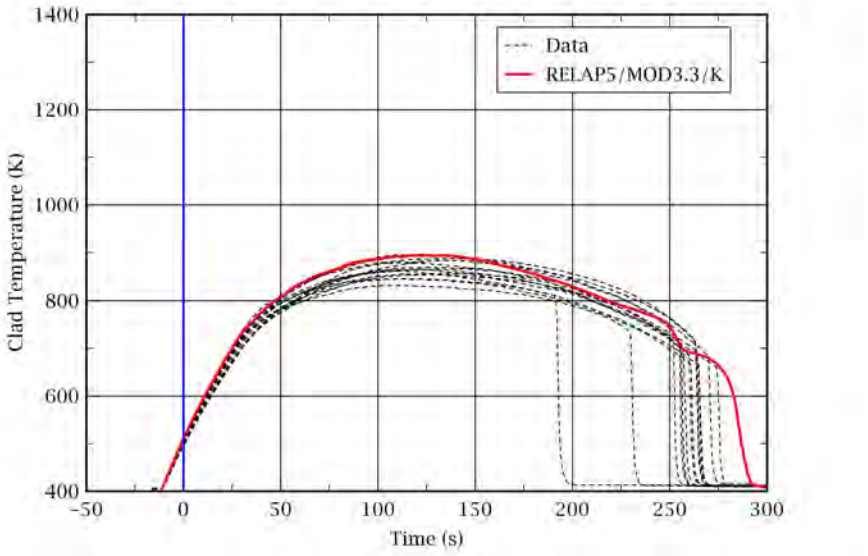

Figure 2-44 Rod Clad Temperatures at 96 in. from the Heated Bottom: Test 30518

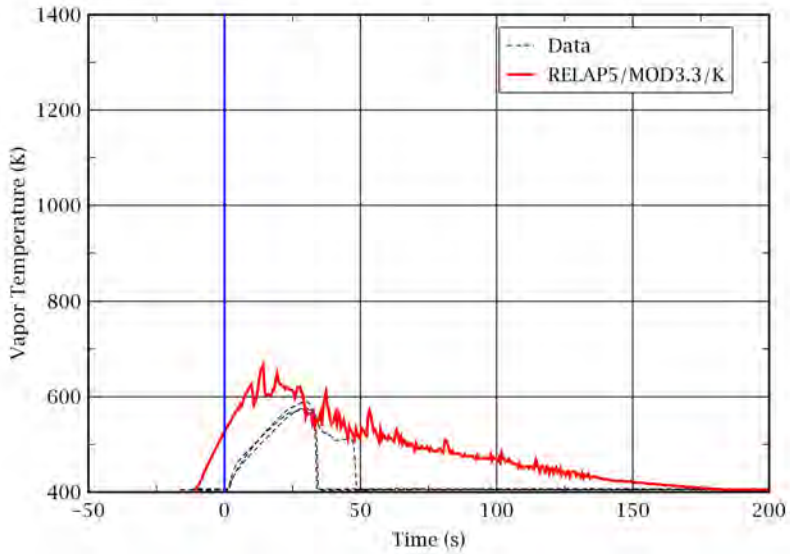

Figure 2-45 Vapor Temperatures at 72 in. from the Heated Bottom: Test 30518

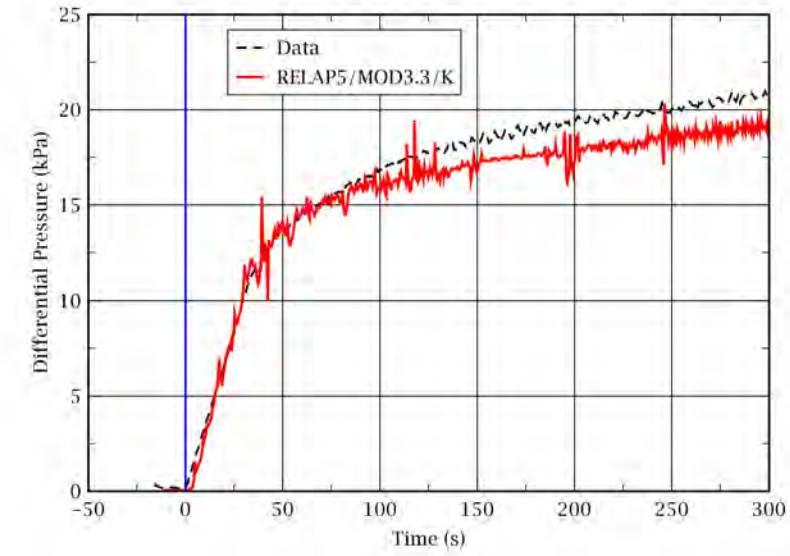

Figure 2-46 Differential Pressure for the Entire 12 ft Core: Test 30518

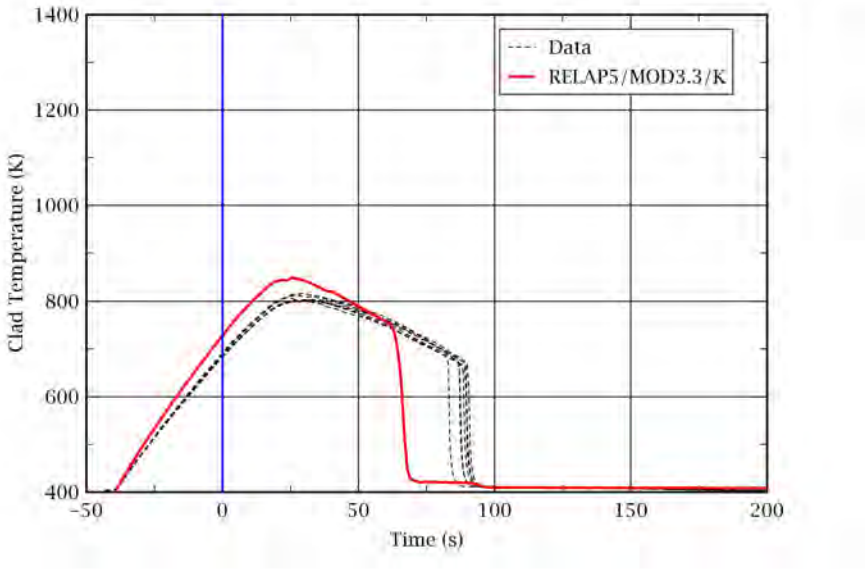

Figure 2-47 Rod Clad Temperatures at 48 in. from the Heated Bottom: Test 30817

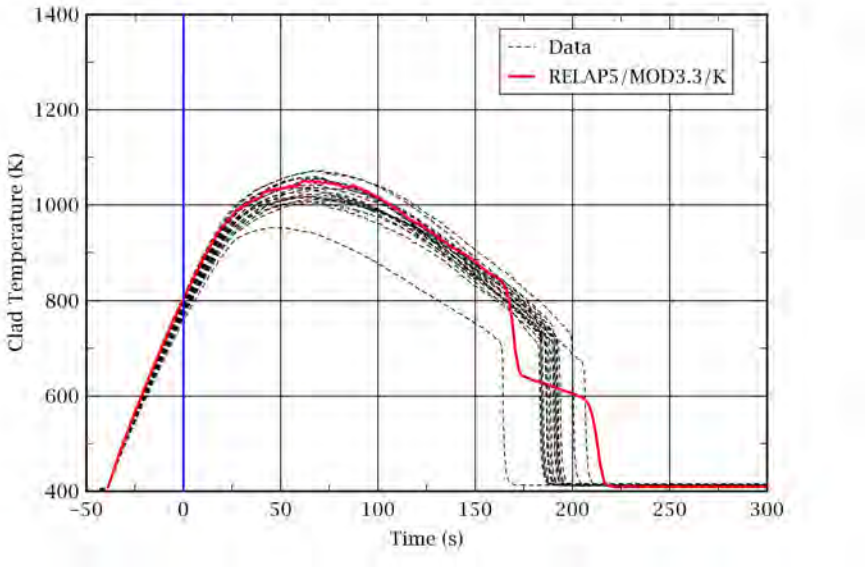

Figure 2-48 Rod Clad Temperatures at 72 in. from the Heated Bottom: Test 30817

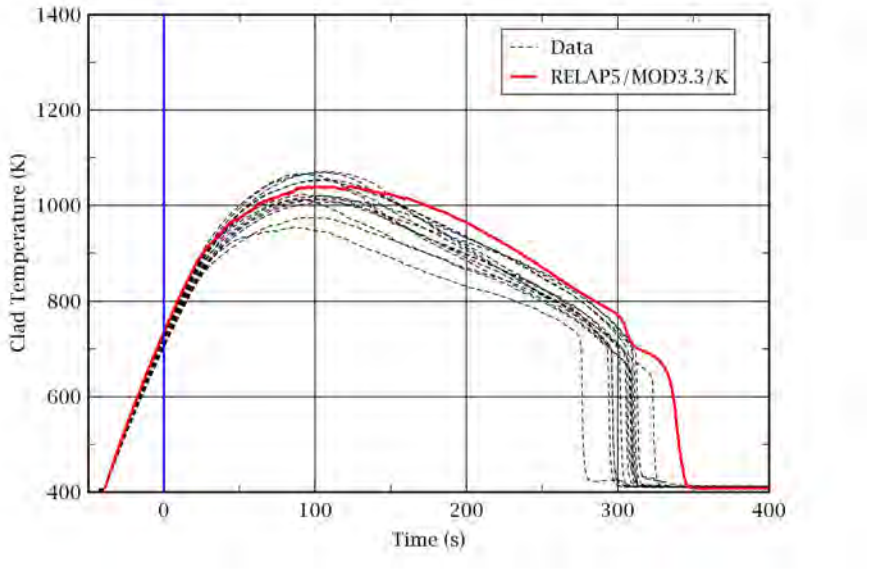

Figure 2-49 Rod Clad Temperatures at 96 in. from the Heated Bottom: Test 30817

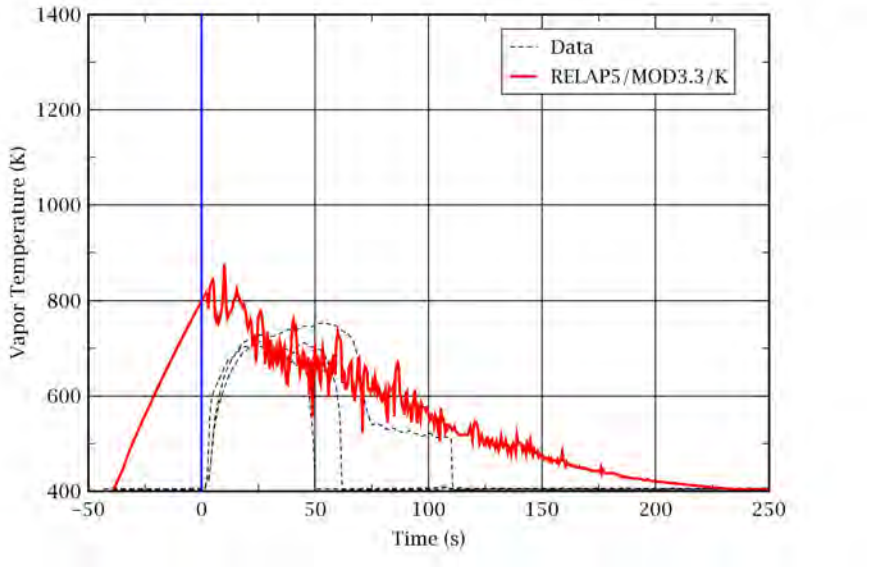

Figure 2-50 Vapor Temperatures at 72 in. from the Heated Bottom: Test 30817

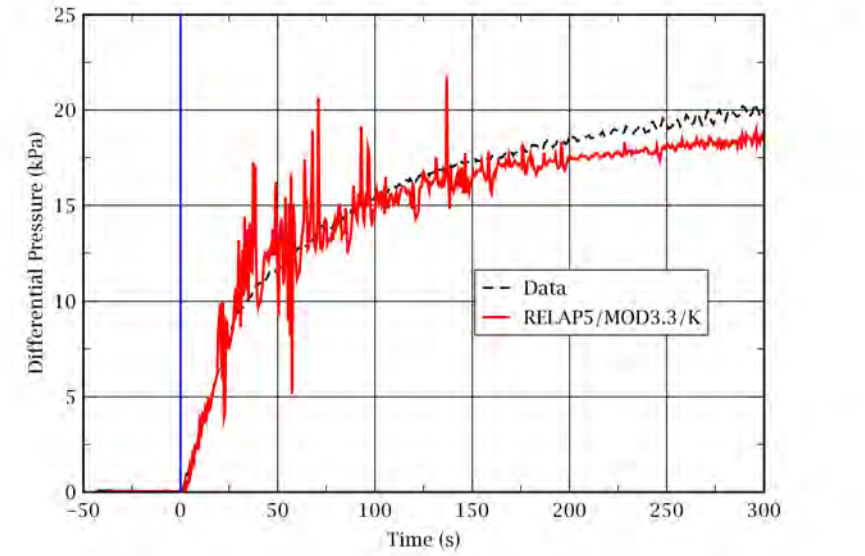

Figure 2-51 Differential Pressure for the Entire 12 ft Core: Test 30817

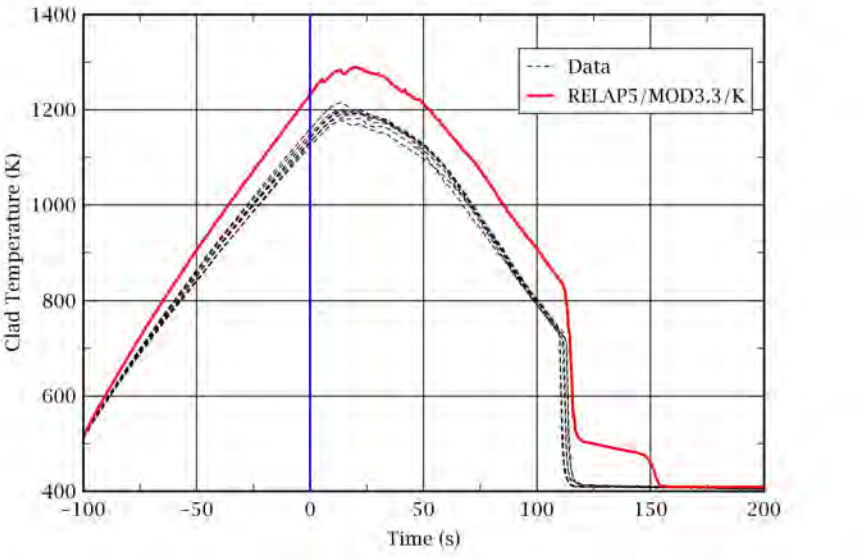

Figure 2-52 Rod Clad Temperatures at 48 in. from the Heated Bottom: Test 34420

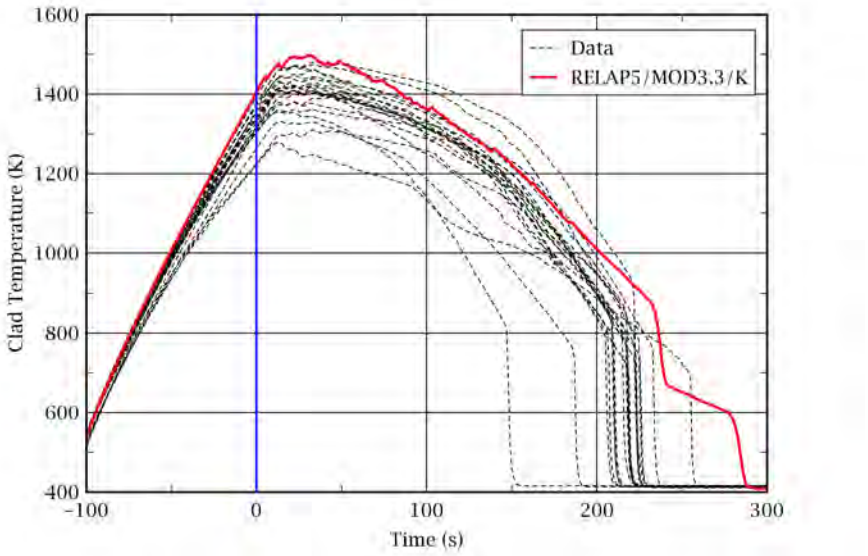

Figure 2-53 Rod Clad Temperatures at 72 in. from the Heated Bottom: Test 34420

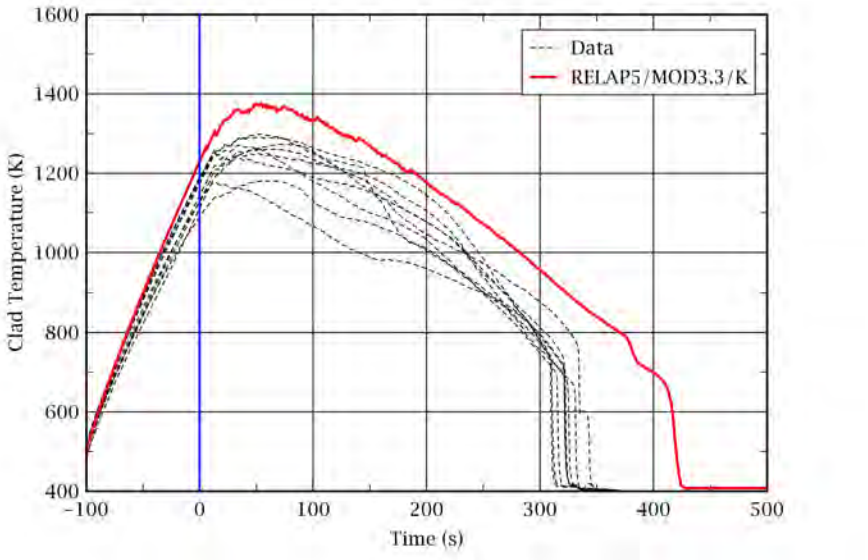

Figure 2-54 Rod Clad Temperatures at 96 in. from the Heated Bottom: Test 34420

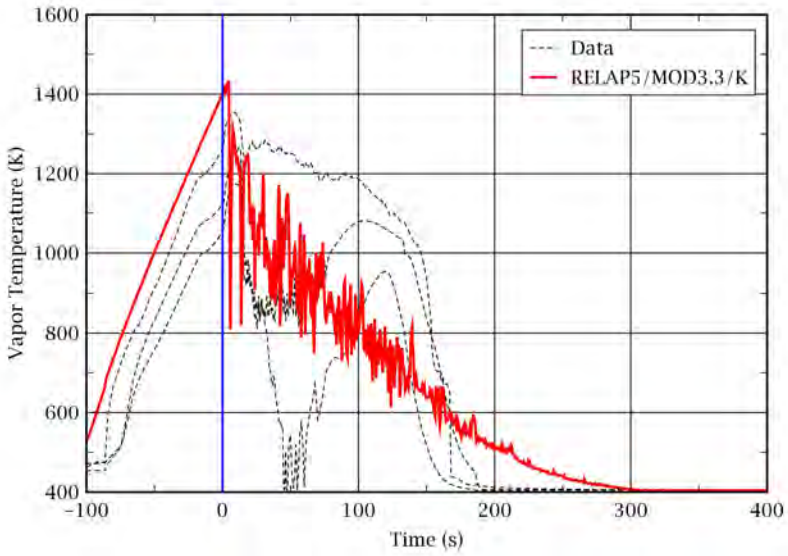

Figure 2-55 Vapor Temperatures at 72 in. from the Heated Bottom: Test 34420

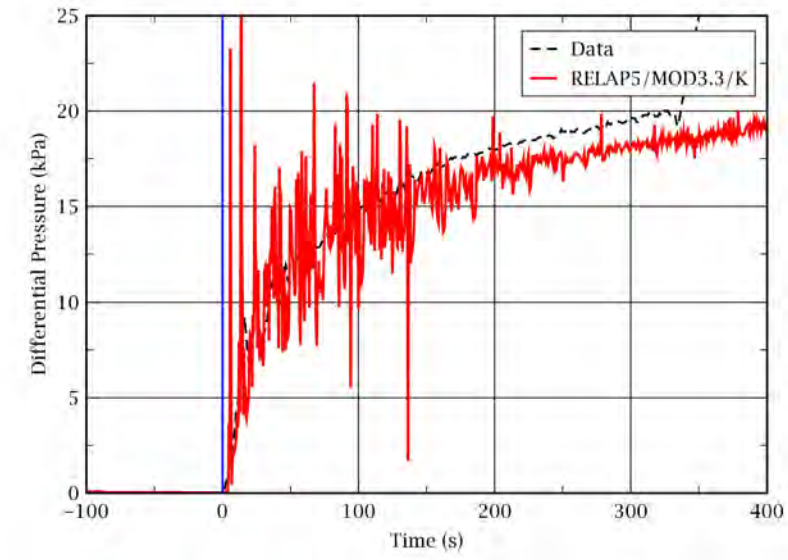

Figure 2-56 Differential Pressure for the Entire 12 ft Core: Test 34420

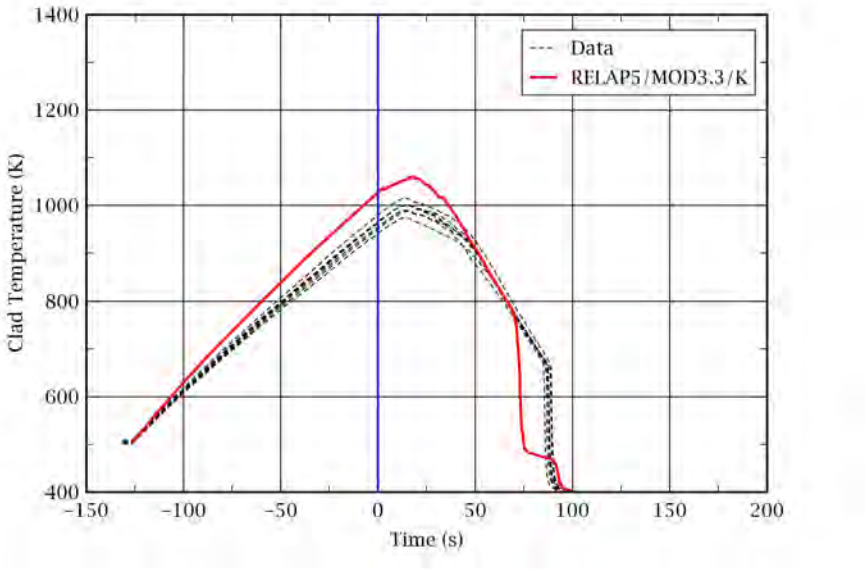

Figure 2-57 Rod Clad Temperatures at 48 in. from the Heated Bottom: Test 31021

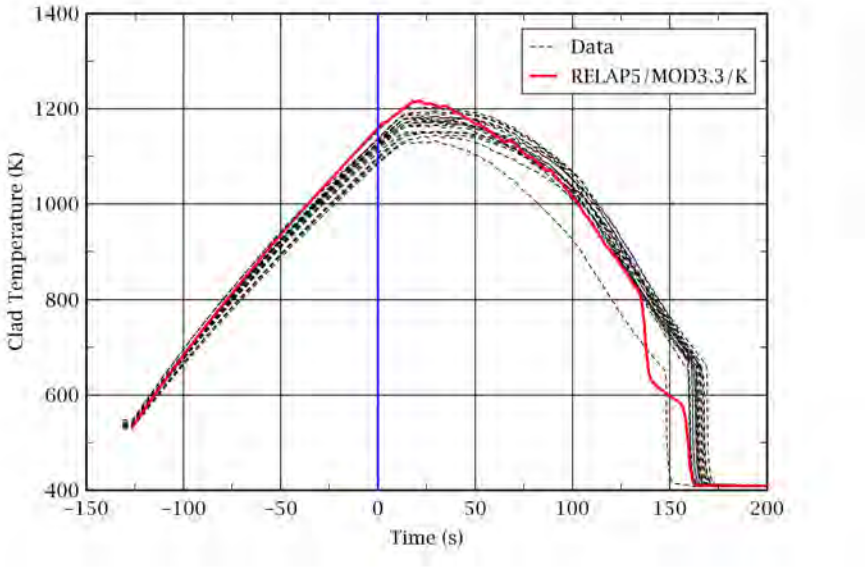

Figure 2-58 Rod Clad Temperatures at 72 in. from the Heated Bottom: Test 31021

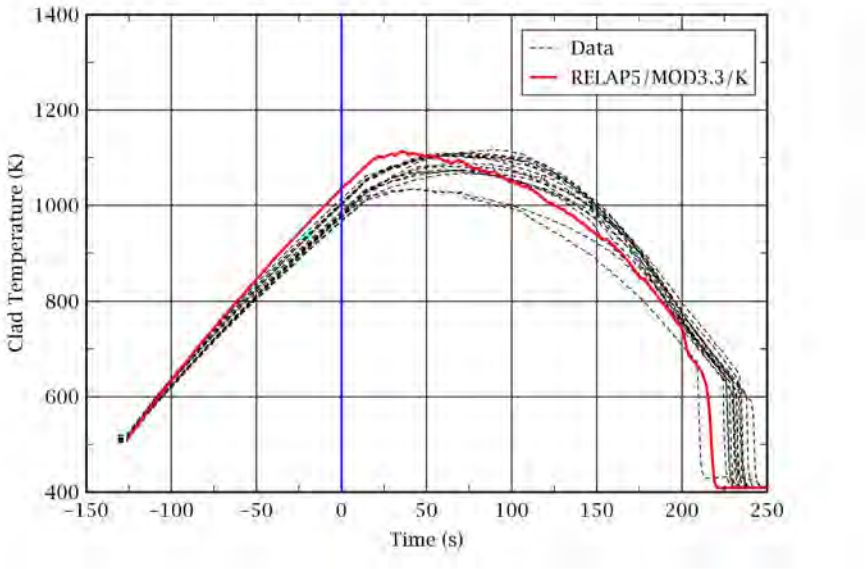

Figure 2-59 Rod Clad Temperatures at 96 in. from the Heated Bottom: Test 31021

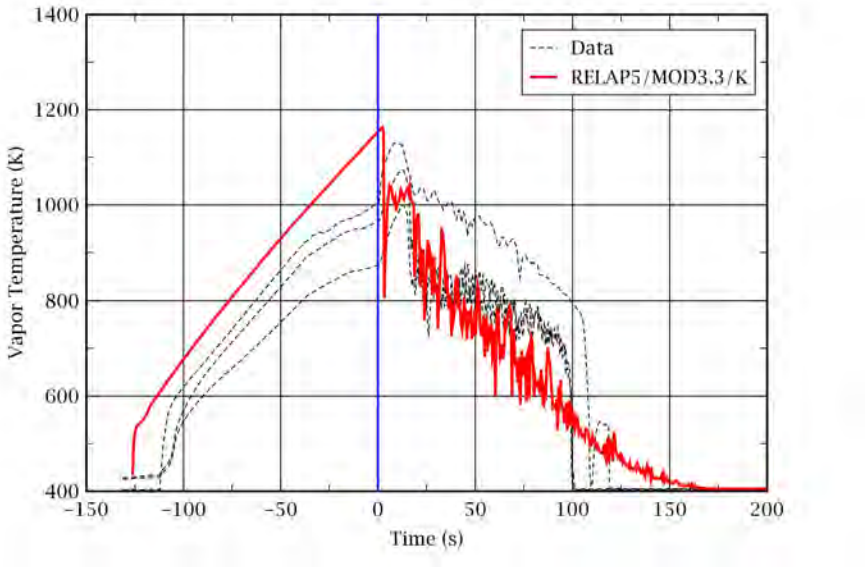

Figure 2-60 Vapor Temperatures at 72 in. from the Heated Bottom: Test 31021

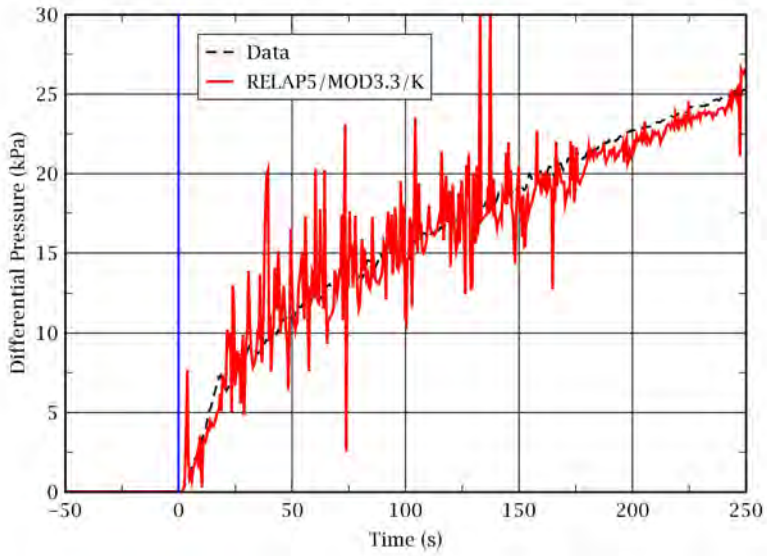

Figure 2-61 Differential Pressure for the Entire 12 ft Core: Test 31021

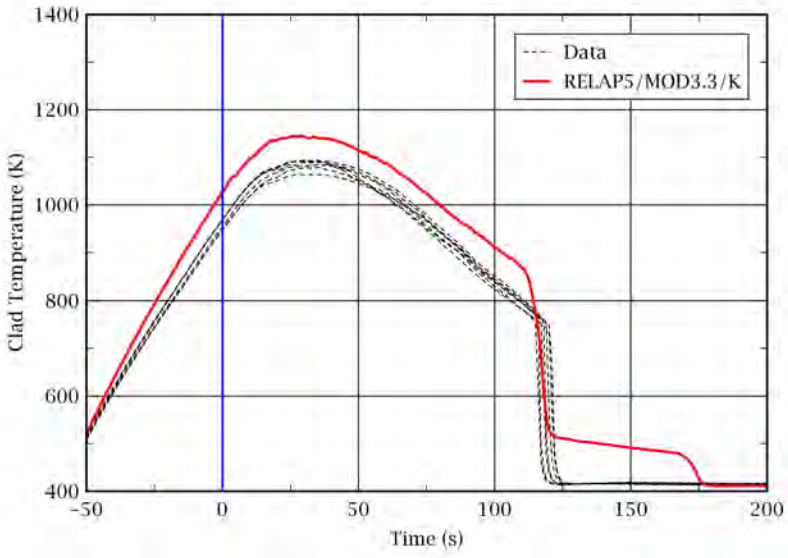

Figure 2-62 Rod Clad Temperatures at 48 in. from the Heated Bottom: Test 34524

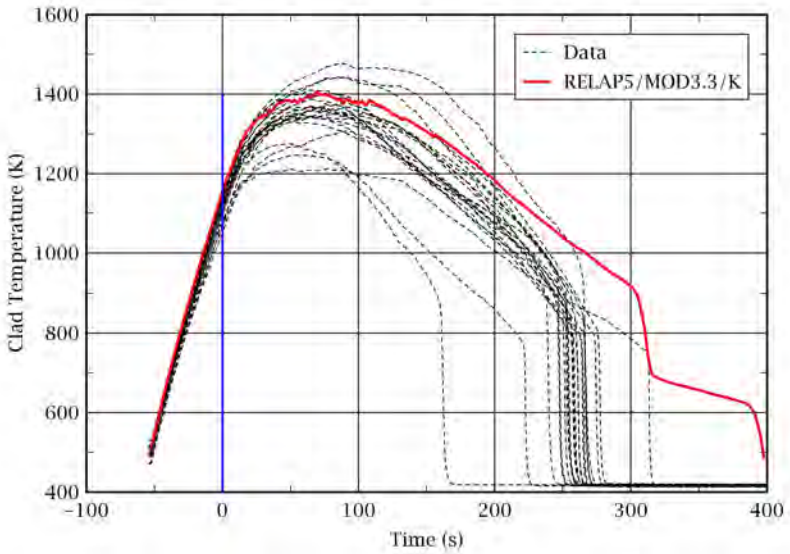

Figure 2-63 Rod Clad Temperatures at 72 in. from the Heated Bottom: Test 34524

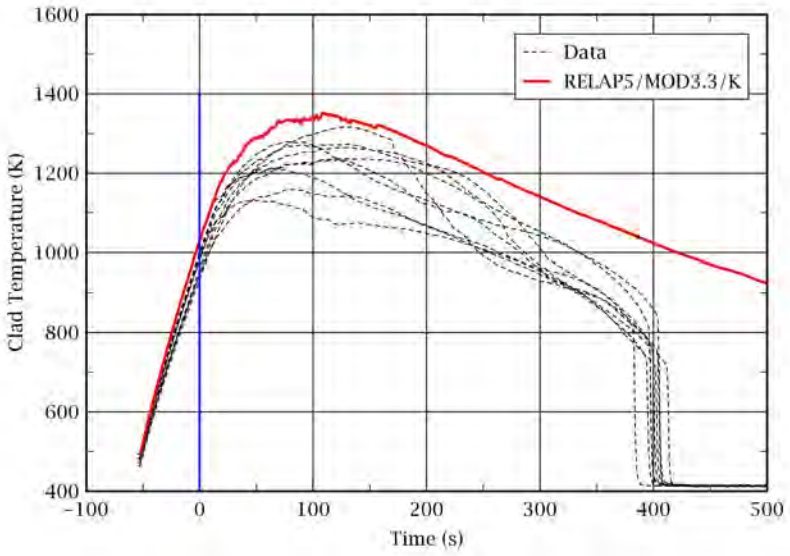

Figure 2-64 Rod Clad Temperatures at 96 in. from the Heated Bottom: Test 34524

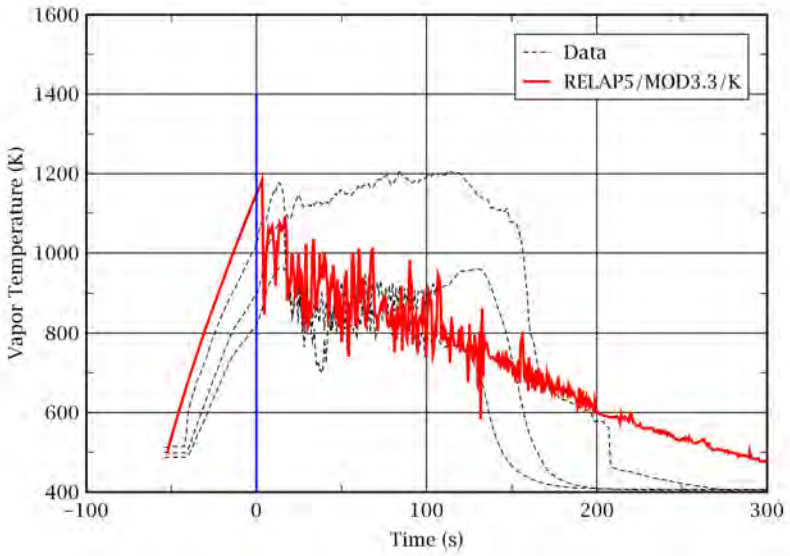

Figure 2-65 Vapor Temperatures at 72 in. from the Heated Bottom: Test 34524

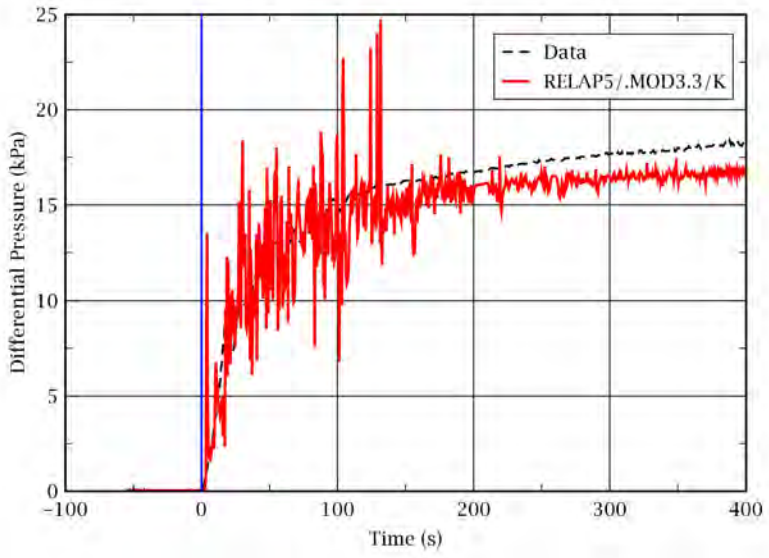

Figure 2-66 Differential Pressure for the Entire 12 ft Core: Test 34524

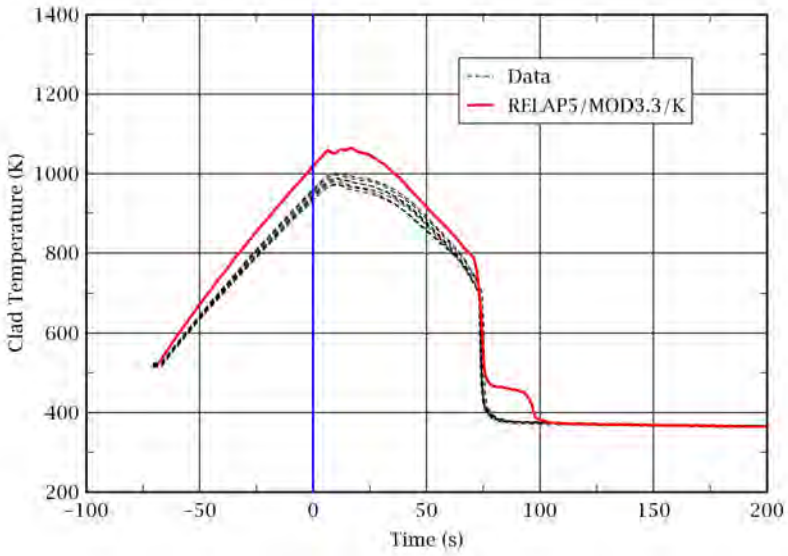

Figure 2-67 Rod Clad Temperatures at 48 in. from the Heated Bottom: Test 31108

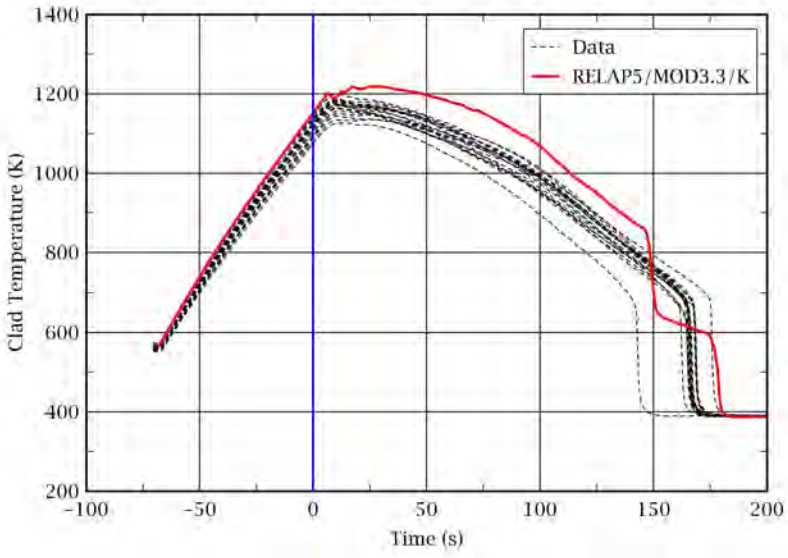

Figure 2-68 Rod Clad Temperatures at 72 in. from the Heated Bottom: Test 31108

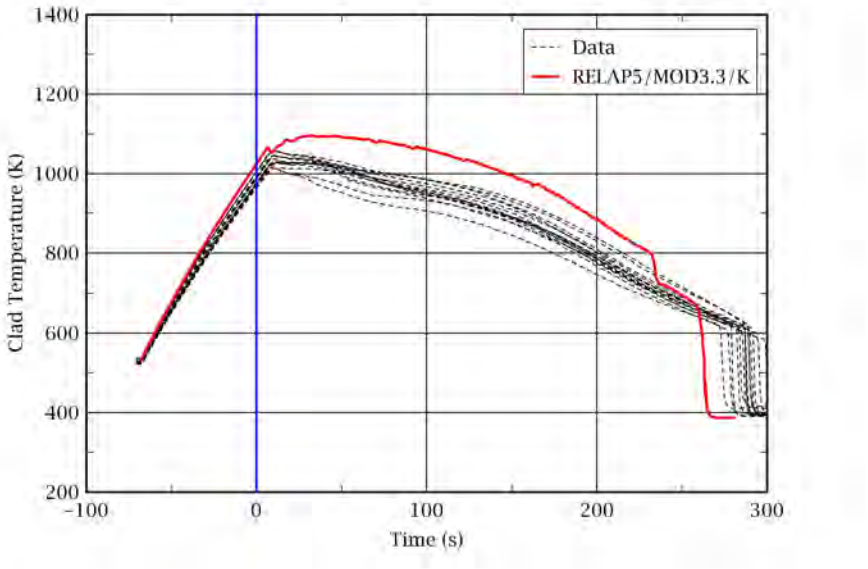

Figure 2-69 Rod Clad Temperatures at 96 in. from the Heated Bottom: Test 31108

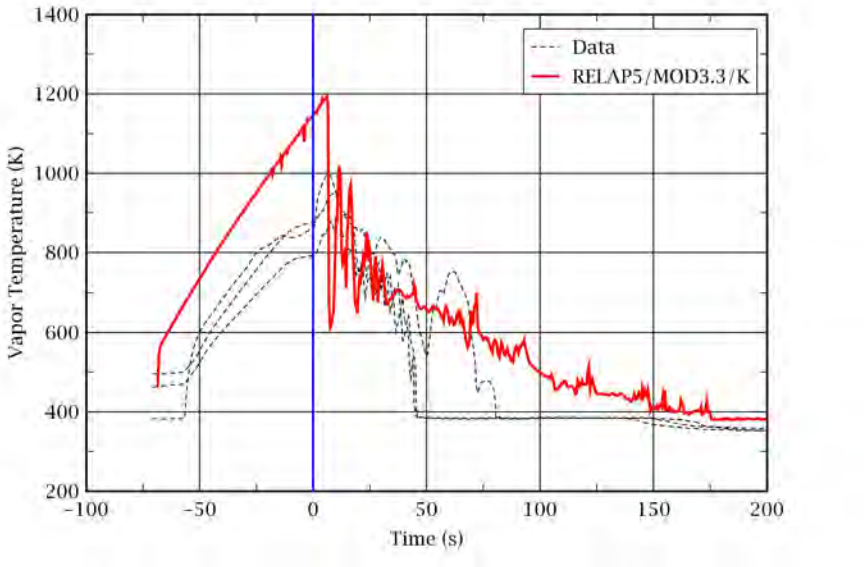

Figure 2-70 Vapor Temperatures at 72 in. from the Heated Bottom: Test 31108

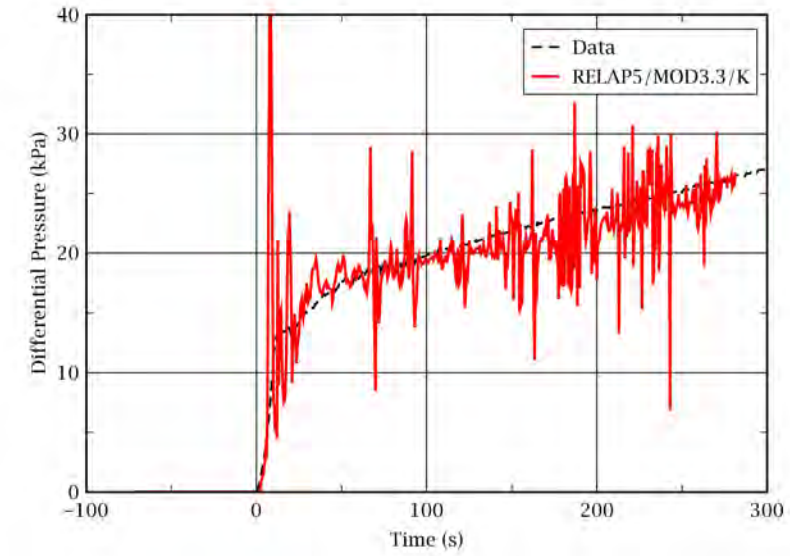

Figure 2-71 Differential Pressure for the Entire 12 ft Core: Test 31108

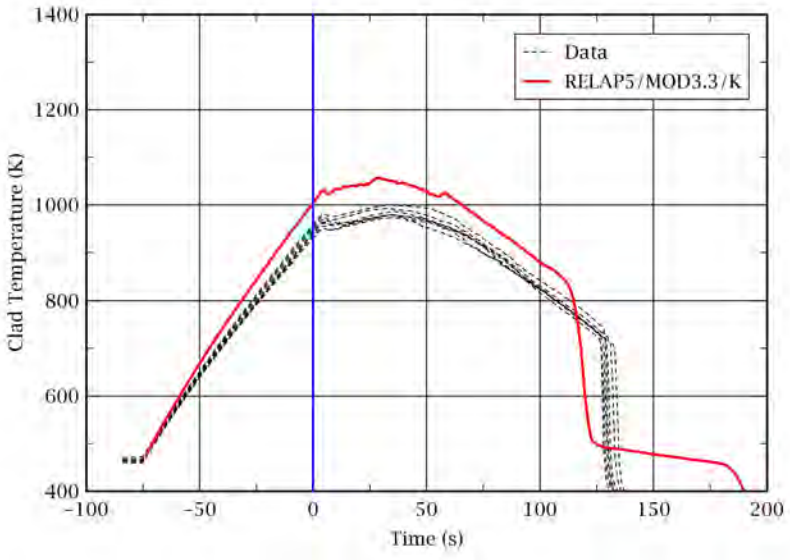

Figure 2-72 Rod Clad Temperatures at 48 in. from the Heated Bottom: Test 32235

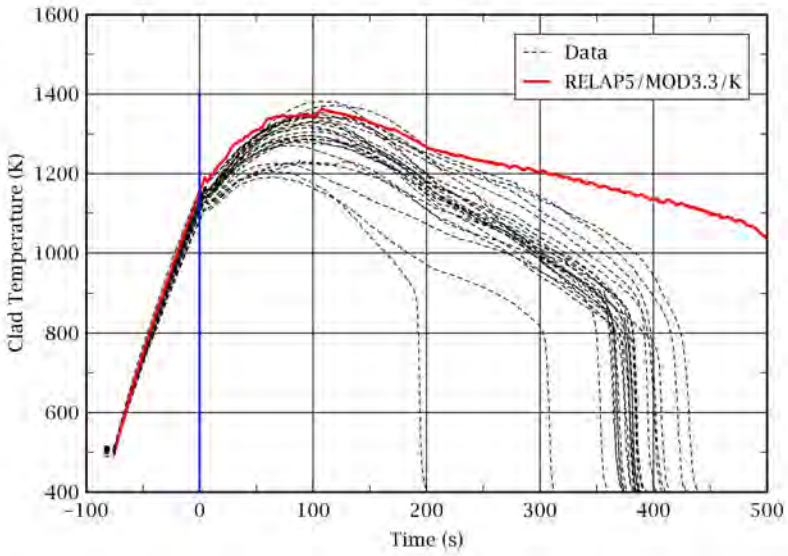

Figure 2-73 Rod Clad Temperatures at 72 in. from the Heated Bottom: Test 32235

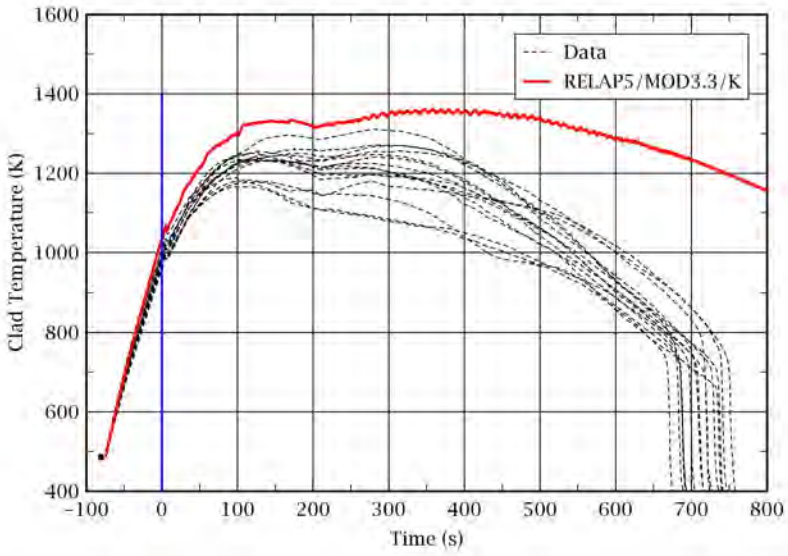

Figure 2-74 Rod Clad Temperatures at 96 in. from the Heated Bottom: Test 32235

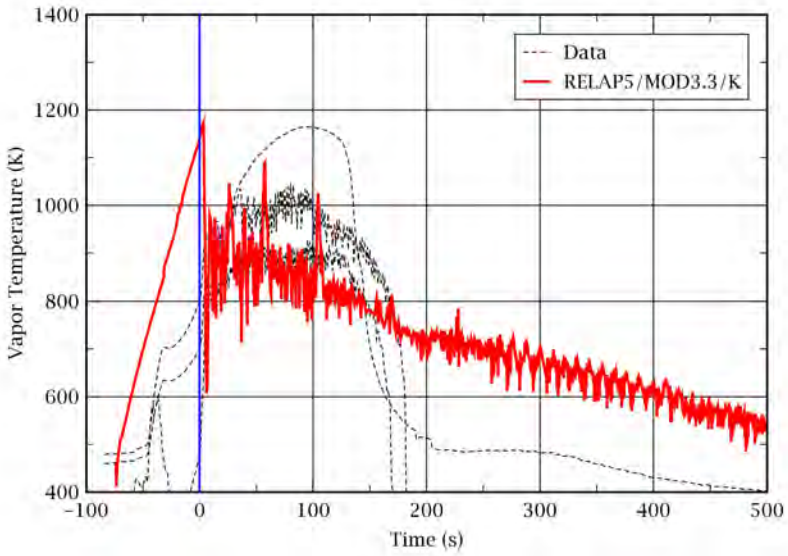

Figure 2-75 Vapor Temperatures at 72 in. from the Heated Bottom: Test 32235

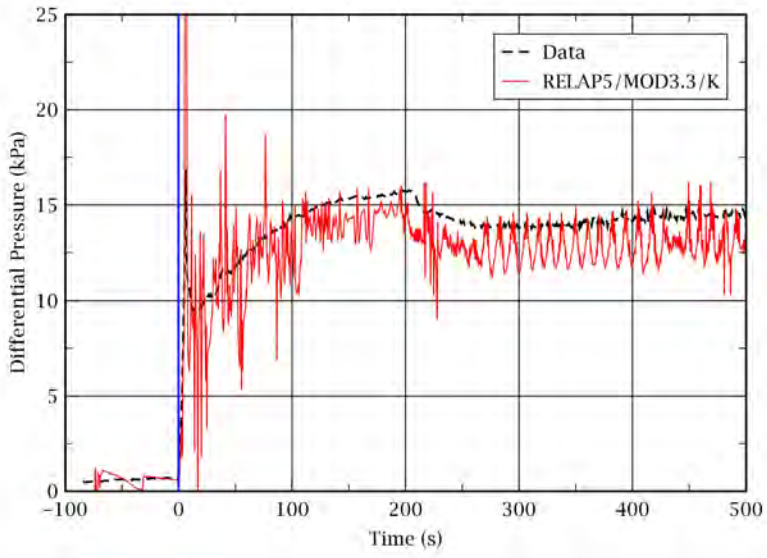

Figure 2-76 Differential Pressure for the Entire 12 ft Core: Test 32235

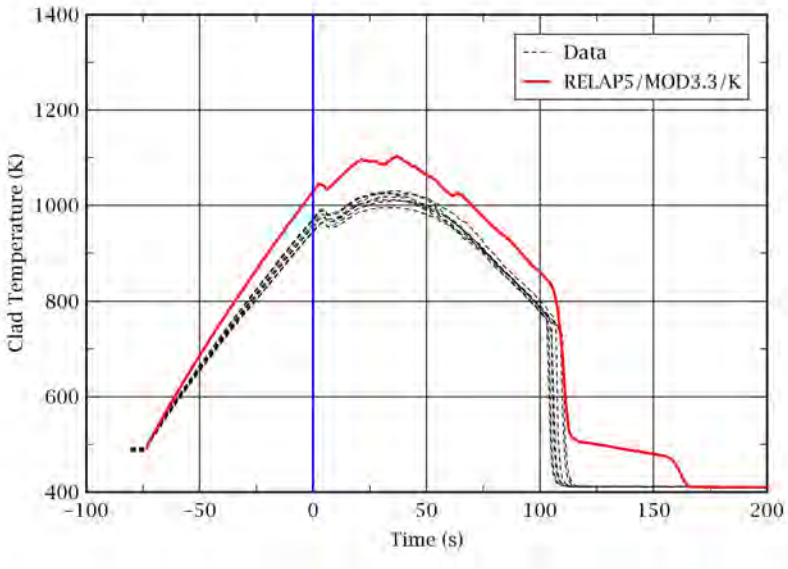

Figure 2-77 Rod Clad Temperatures at 48 in. from the Heated Bottom: Test 32333

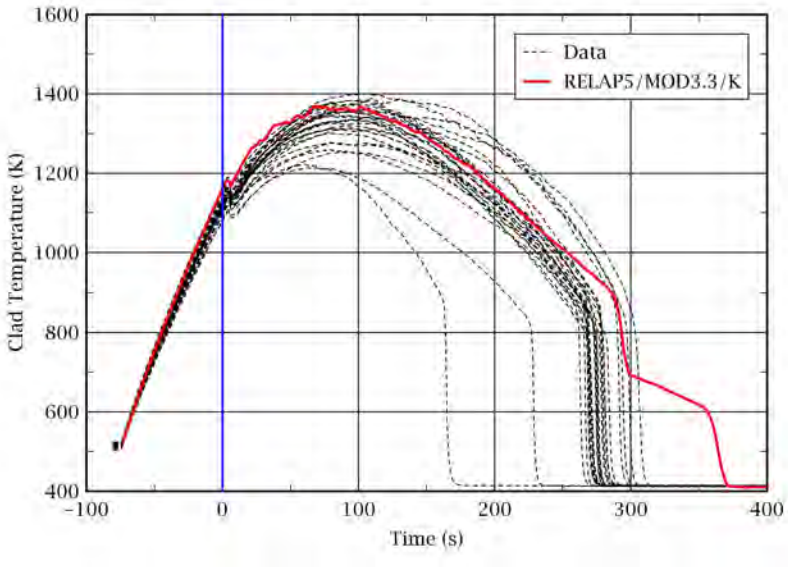

Figure 2-78 Rod Clad Temperatures at 72 in. from the Heated Bottom: Test 32333

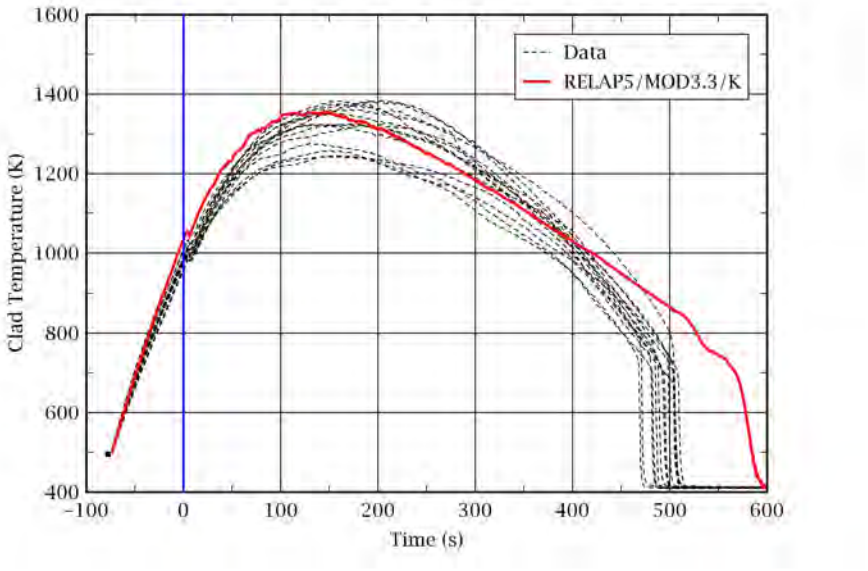

Figure 2-79 Rod Clad Temperatures at 96 in. from the Heated Bottom: Test 32333

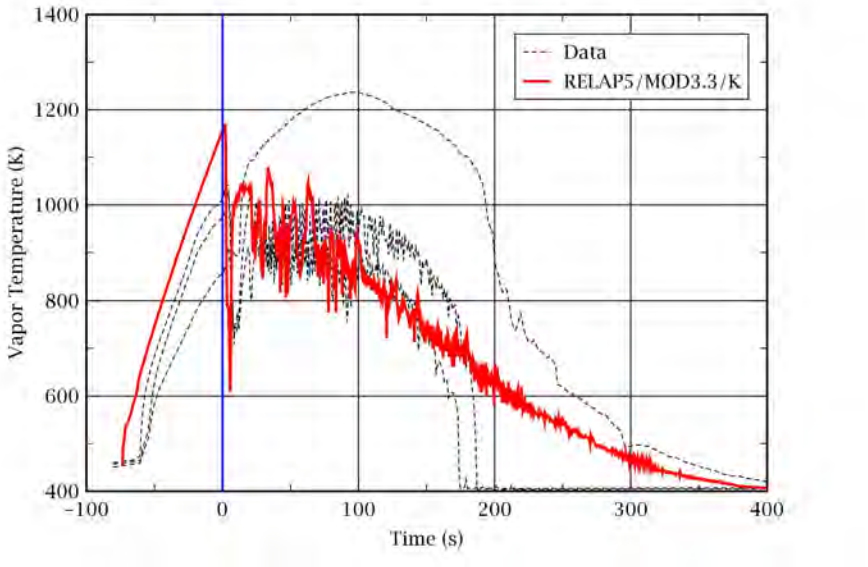

Figure 2-80 Vapor Temperatures at 72 in. from the Heated Bottom: Test 32333

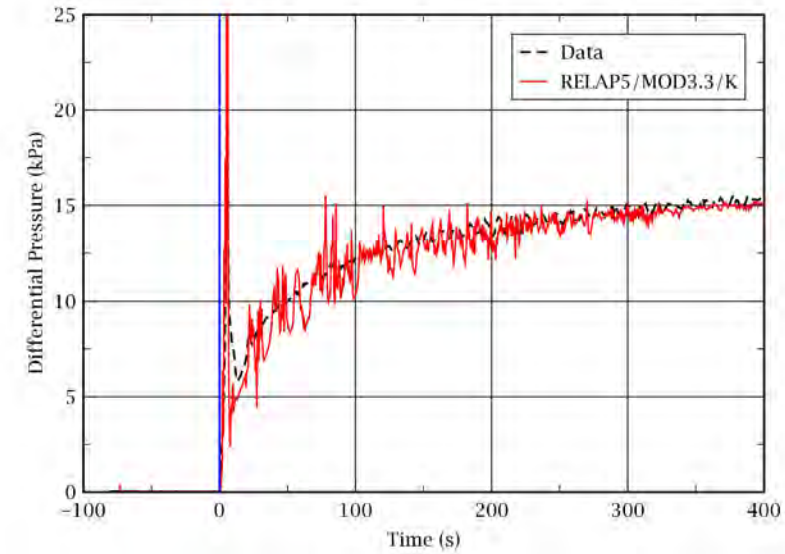

Figure 2-81 Differential Pressure for the Entire 12 ft Core: Test 32333

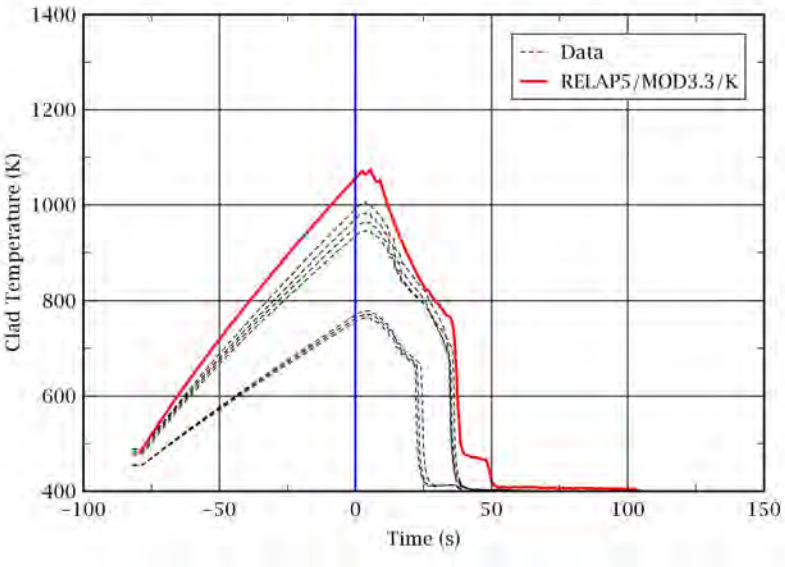

Figure 2-82 Rod Clad Temperatures at 48 in. from the Heated Bottom: Test 33338

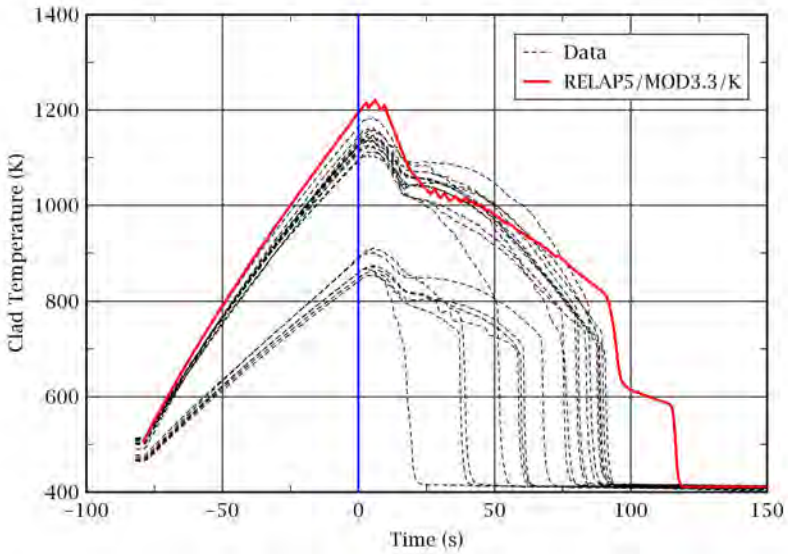

Figure 2-83 Rod Clad Temperatures at 72 in. from the Heated Bottom: Test 33338

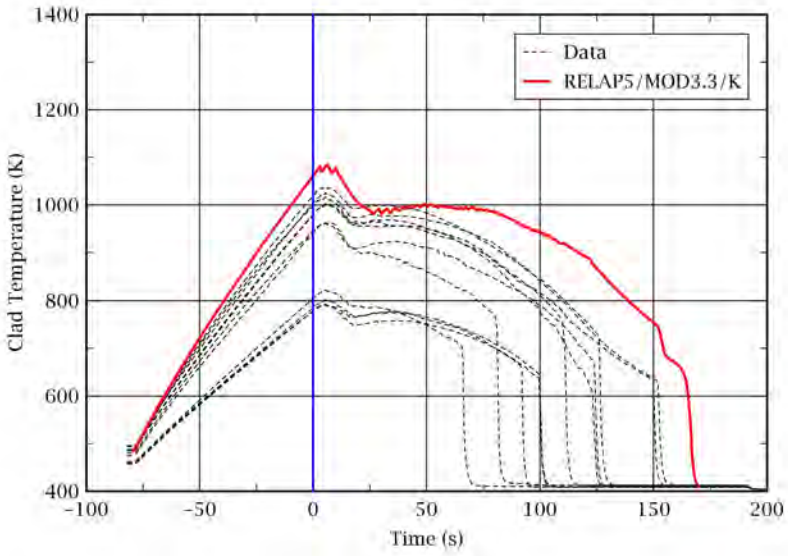

Figure 2-84 Rod Clad Temperatures at 96 in. from the Heated Bottom: Test 33338

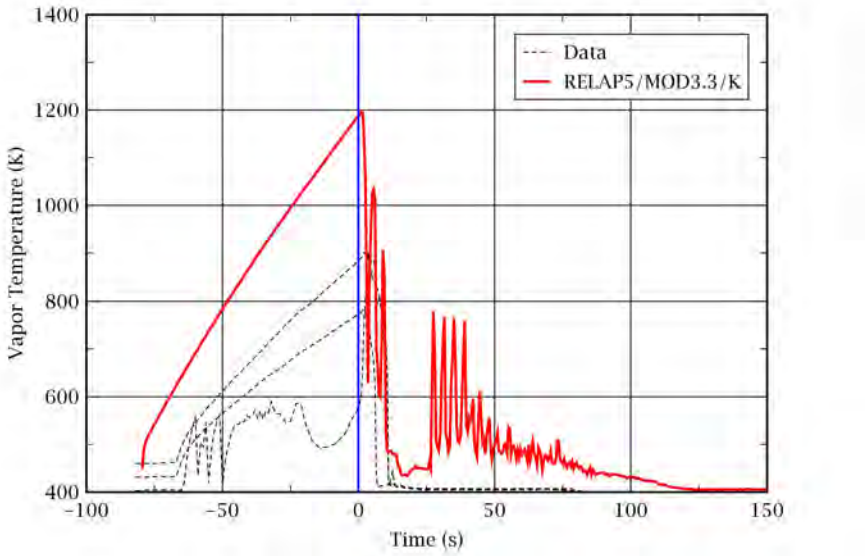

Figure 2-85 Vapor Temperatures at 72 in. from the Heated Bottom: Test 33338

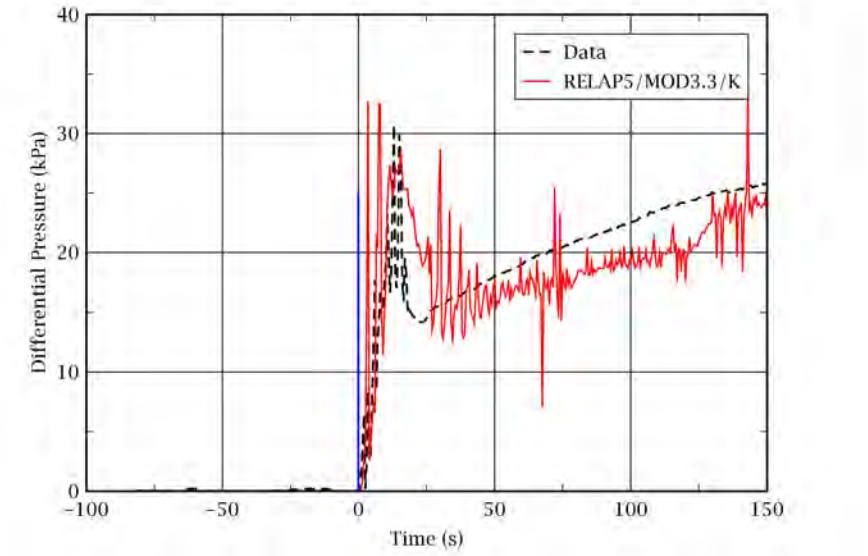

Figure 2-86 Differential Pressure for the Entire 12 ft Core: Test 33338

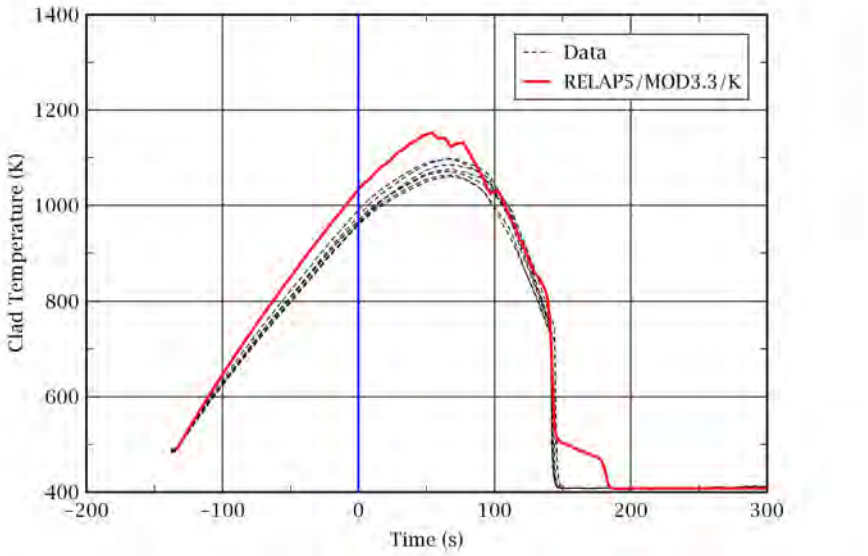

Figure 2-87 Rod Clad Temperatures at 48 in. from the Heated Bottom: Test 34006

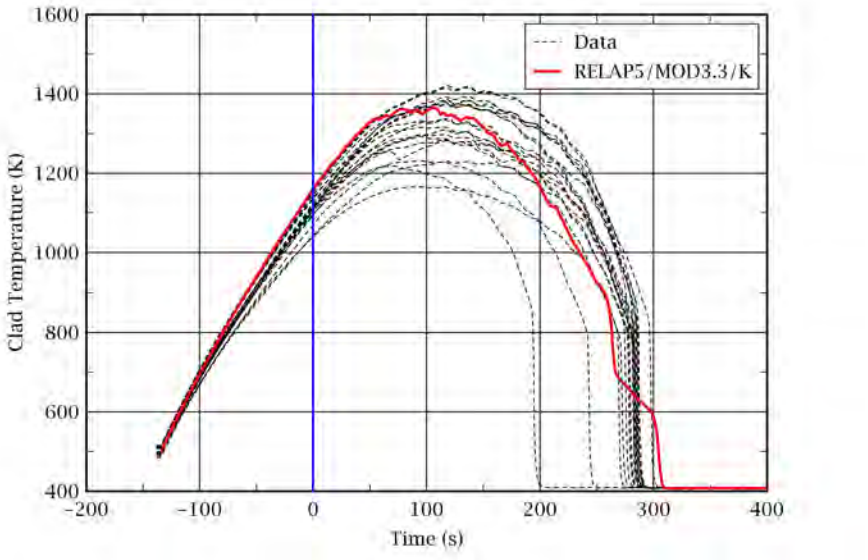

Figure 2-88 Rod Clad Temperatures at 72 in. from the Heated Bottom: Test 34006

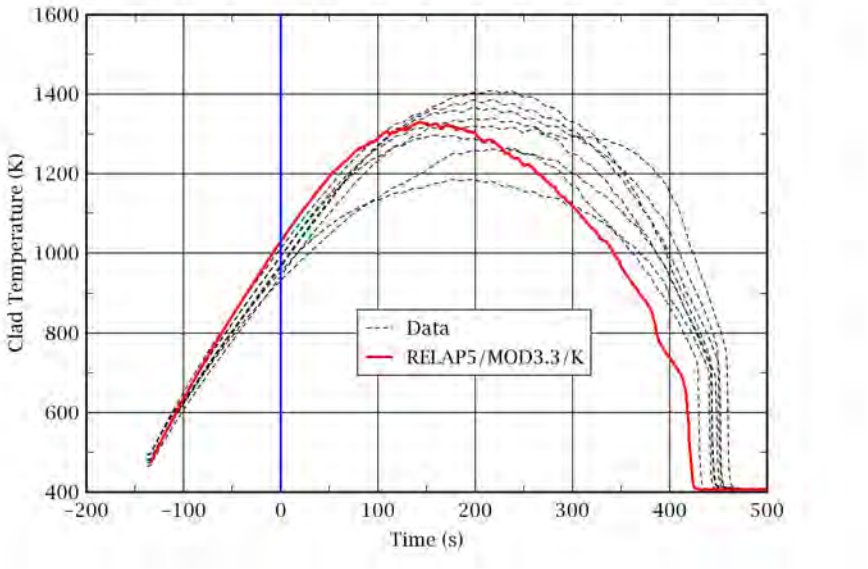

Figure 2-89 Rod Clad Temperatures at 96 in. from the Heated Bottom: Test 34006

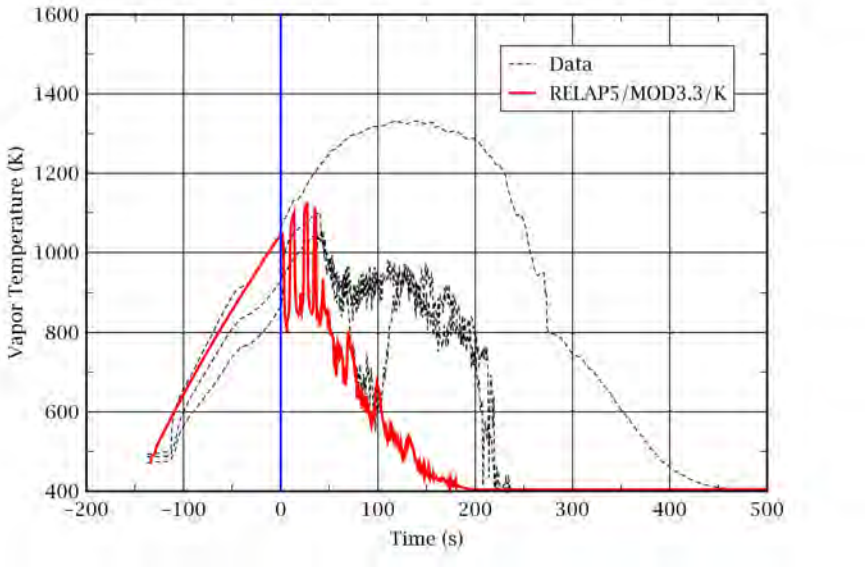

Figure 2-90 Vapor Temperatures at 72 in. from the Heated Bottom: Test 34006

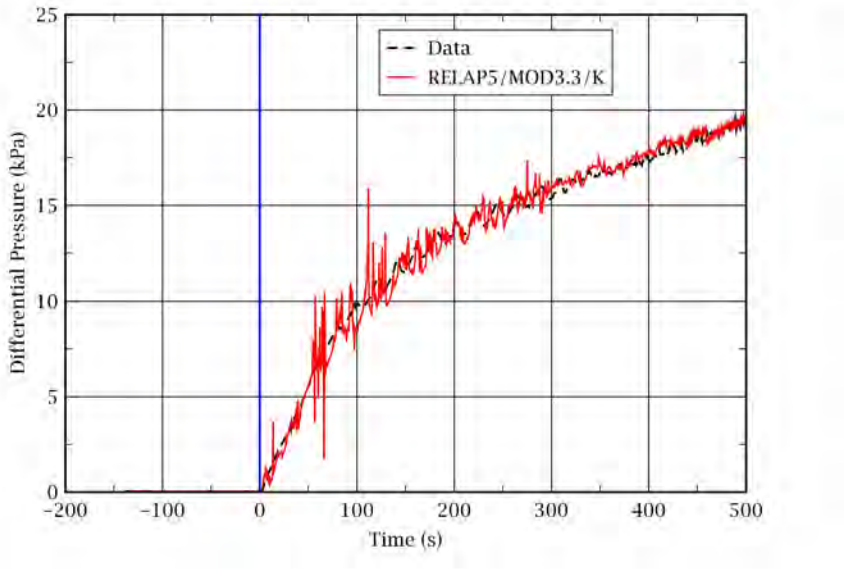

Figure 2-91 Differential Pressure for the Entire 12 ft Core: Test 34006

TS

Figure 2-92 Code Accuracy Calculated Using FLECHT-SEASET Test Data

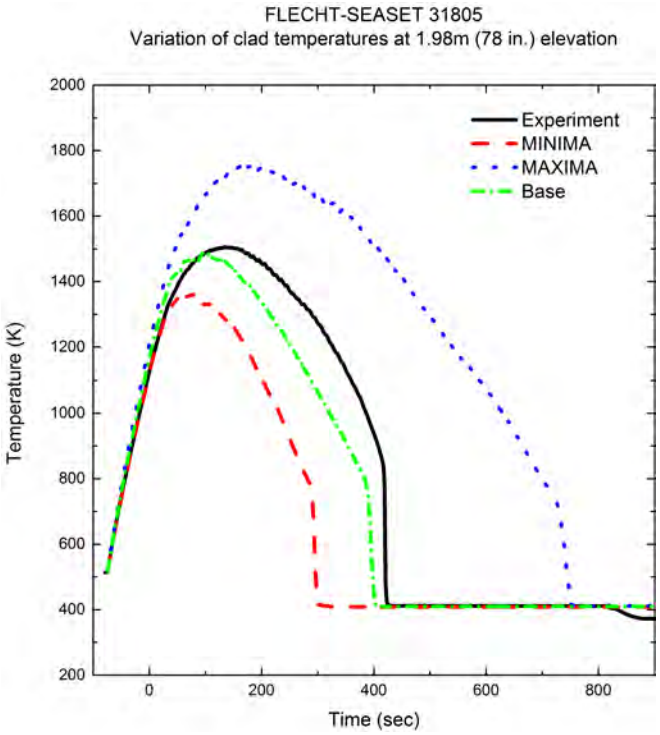

Figure 2-93 The Results of the SRS Calculations: Test 31805

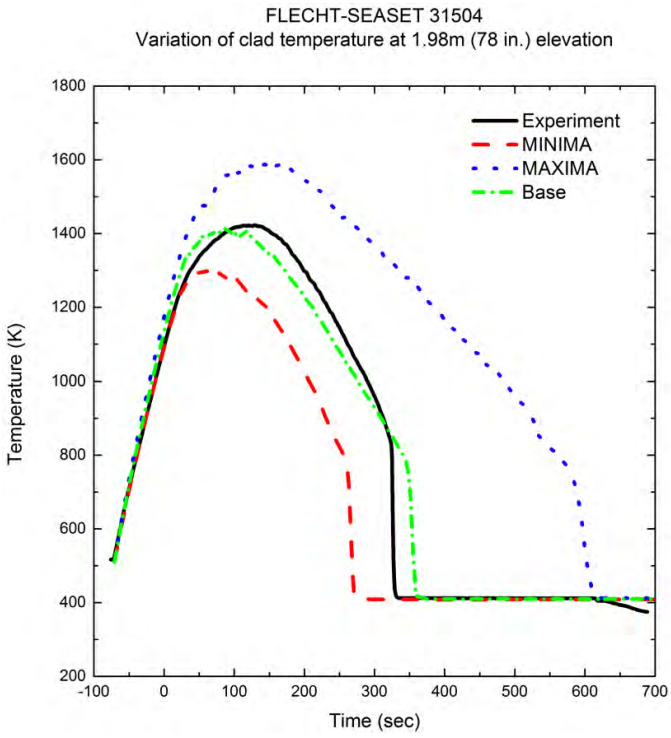

Figure 2-94 The Results of the SRS Calculations: Test 31504

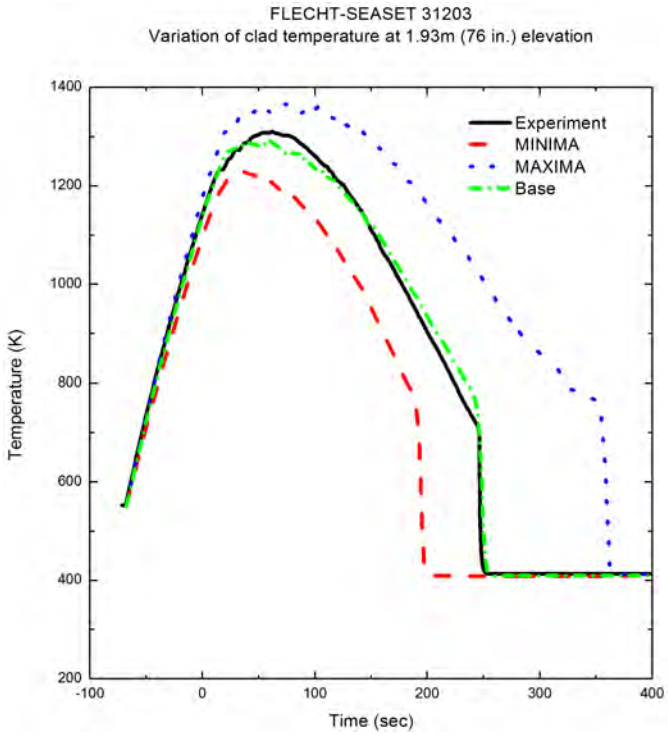

Figure 2-95 The Results of the SRS Calculations: Test 31203

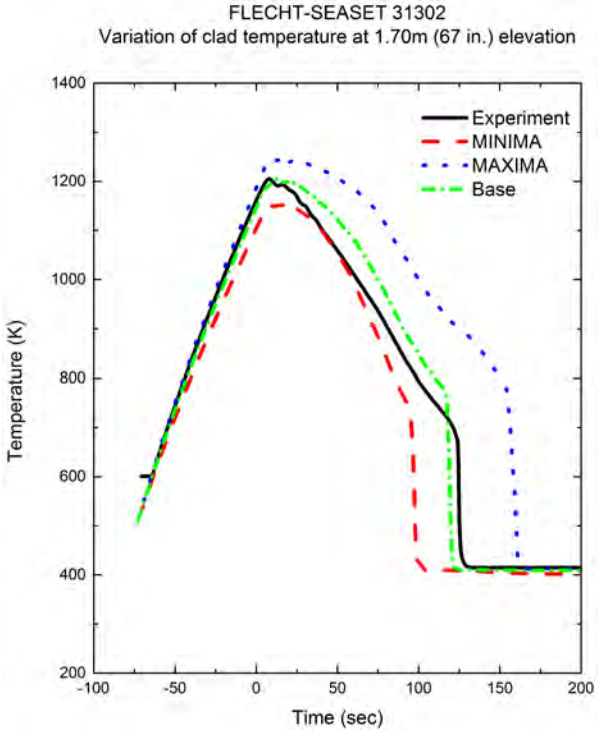

Figure 2-96 The Results of the SRS Calculations: Test 31302

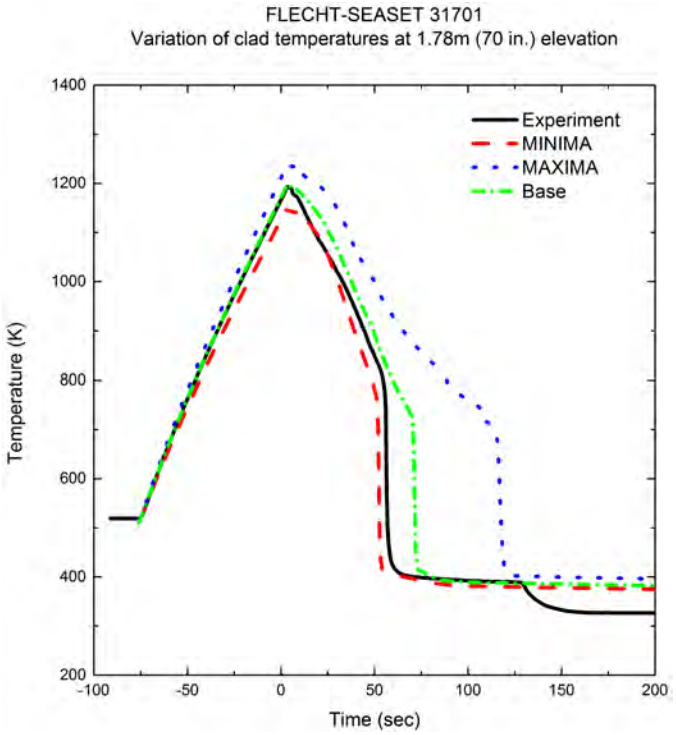

Figure 2-97 The Results of the SRS Calculations: Test 31701

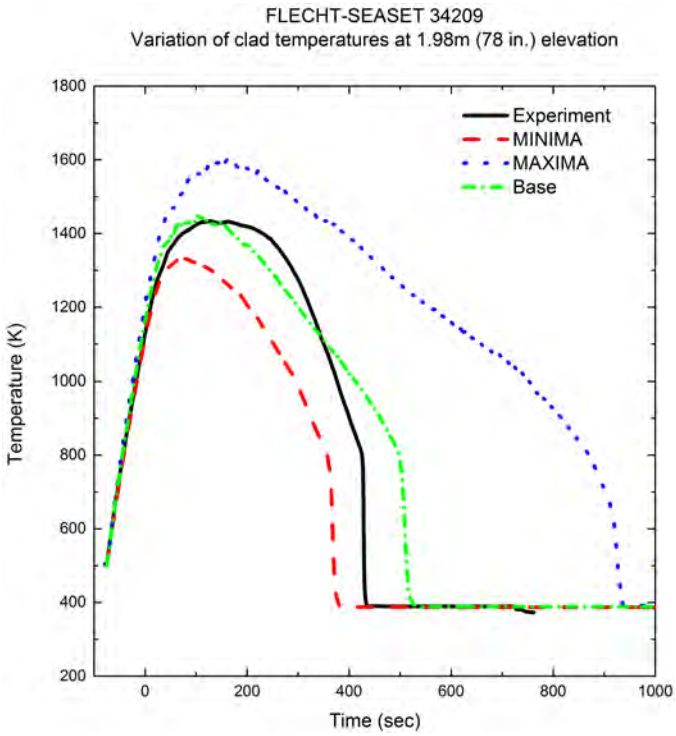

Figure 2-98 The Results of the SRS Calculations: Test 34209

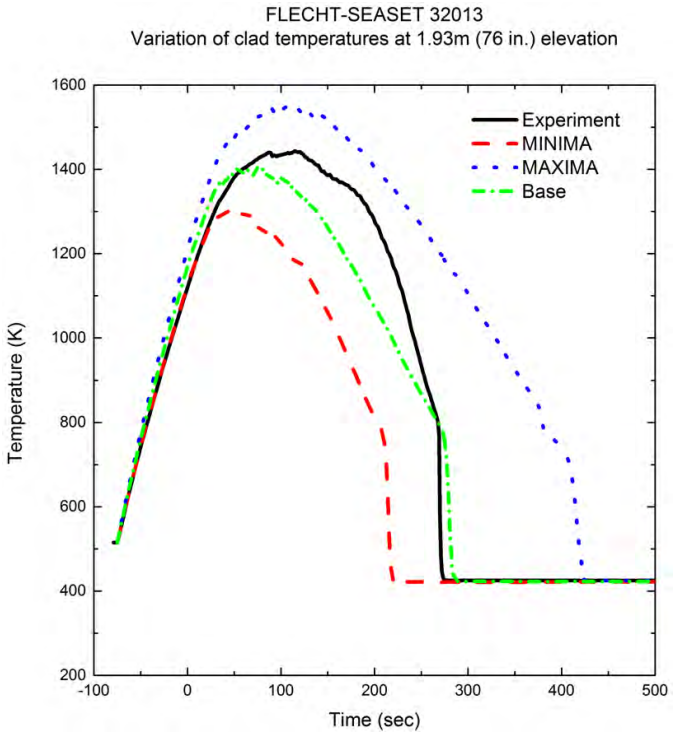

Figure 2-99 The Results of the SRS Calculations: Test 32013

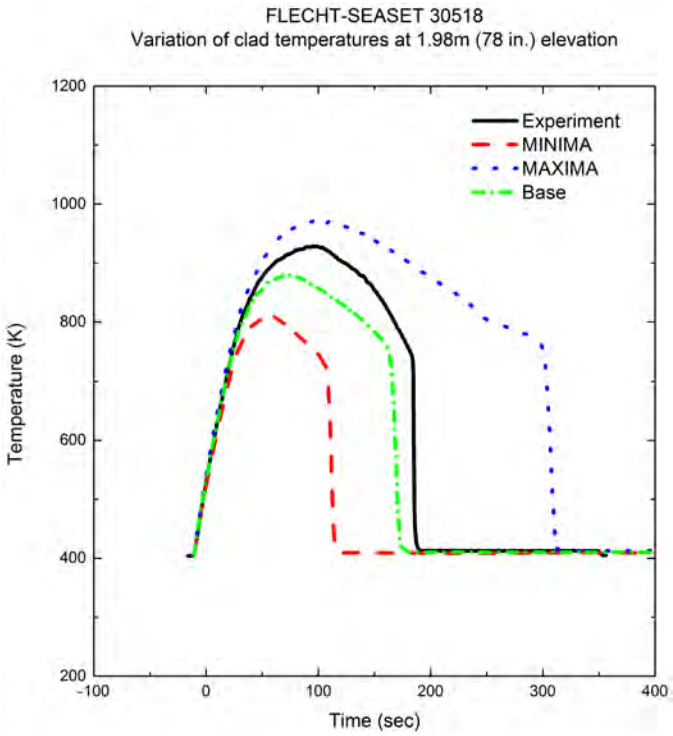

Figure 2-100 The Results of the SRS Calculations: Test 30518

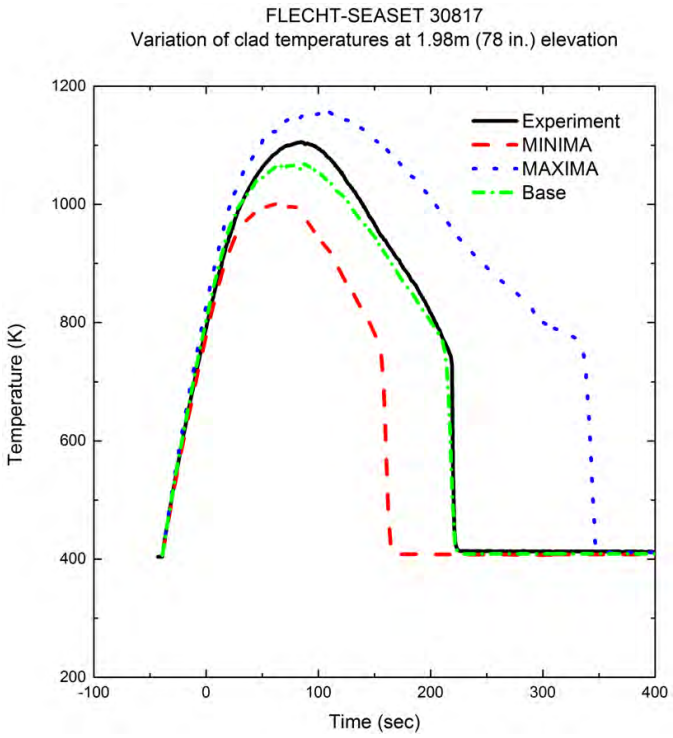

Figure 2-101 The Results of the SRS Calculations: Test 30817

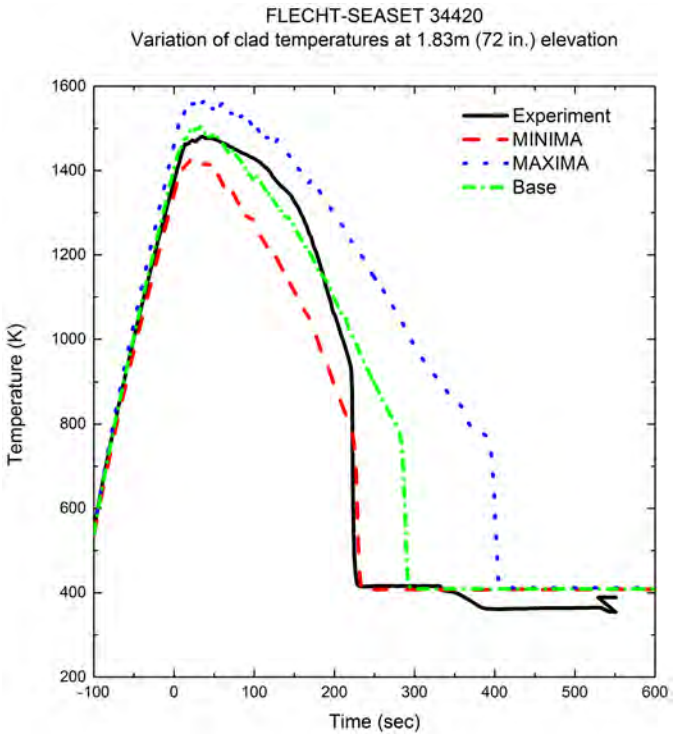

Figure 2-102 The Results of the SRS Calculations: Test 34420

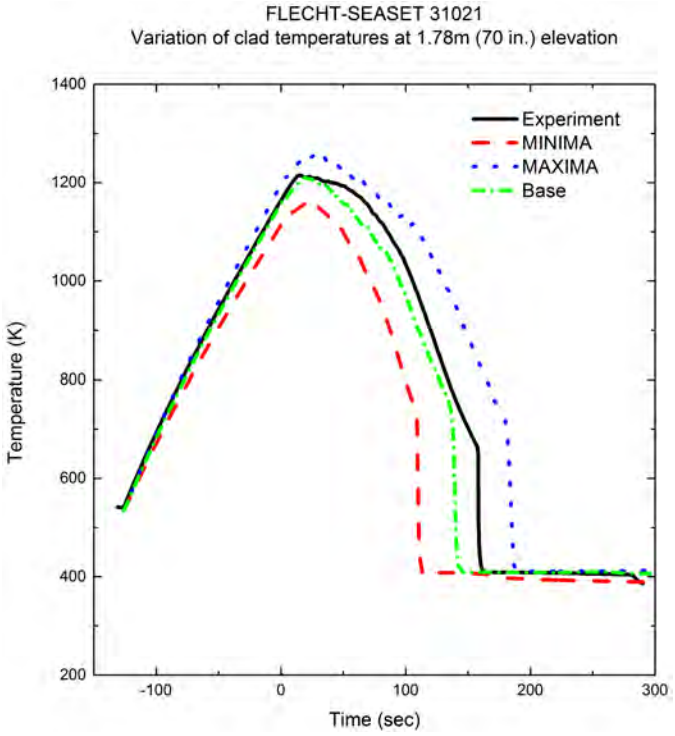

Figure 2-103 The Results of the SRS Calculations: Test 31021

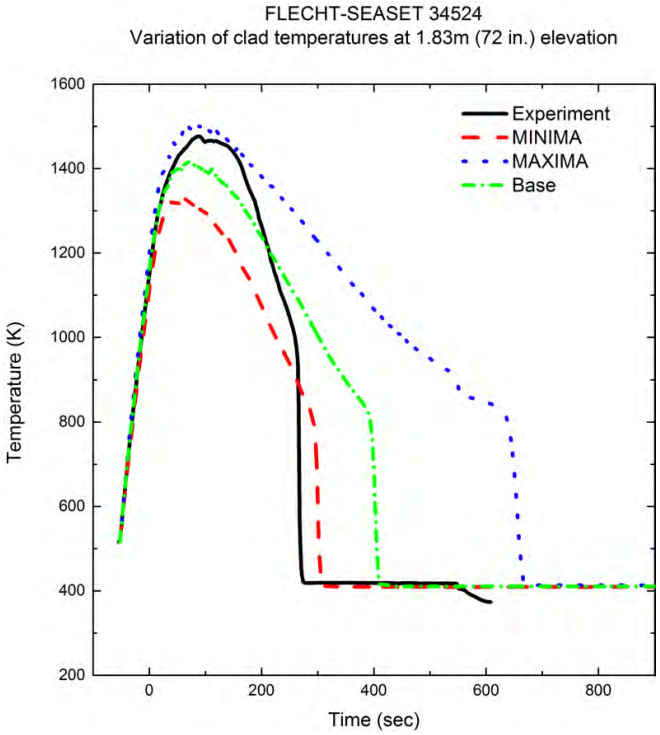

Figure 2-104 The Results of the SRS Calculations: Test 34524

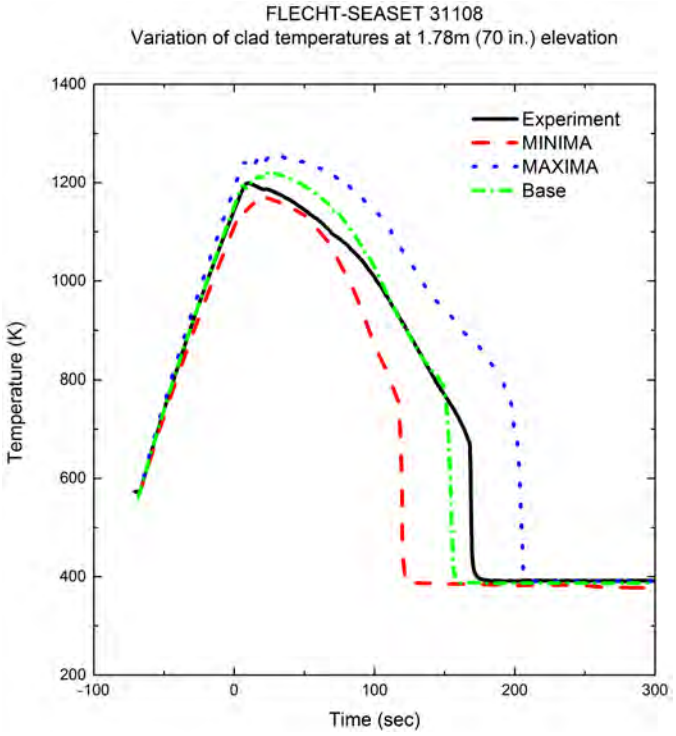

Figure 2-105 The Results of the SRS Calculations: Test 31108

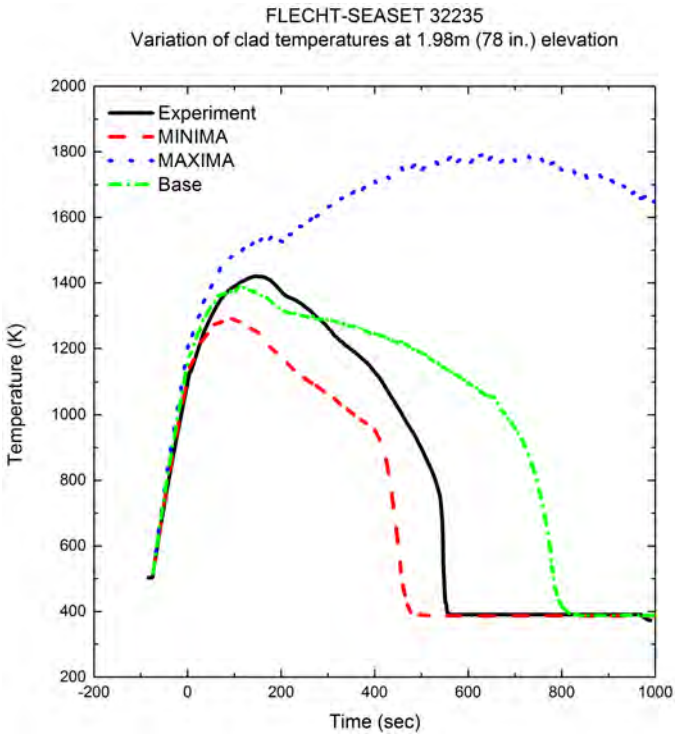

Figure 2-106 The Results of the SRS Calculations: Test 32235

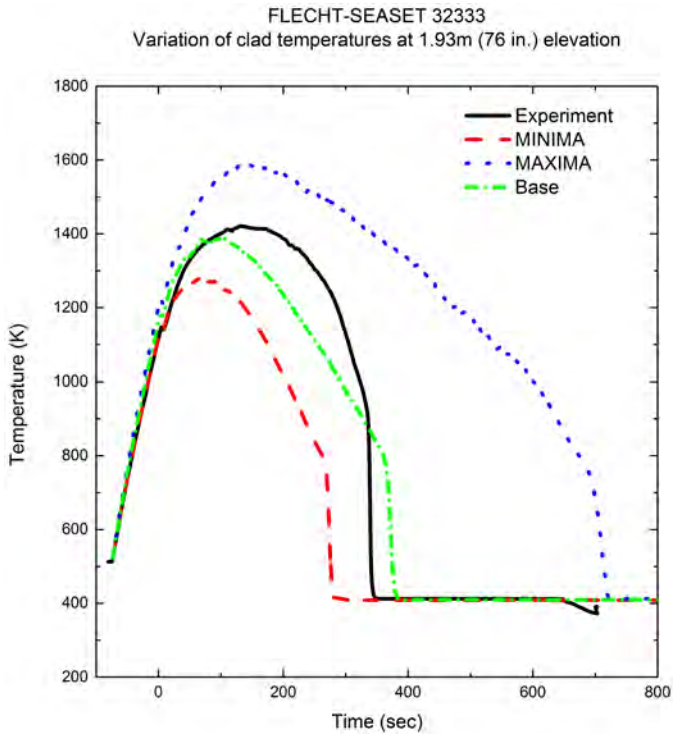

Figure 2-107 The Results of the SRS Calculations: Test 32333

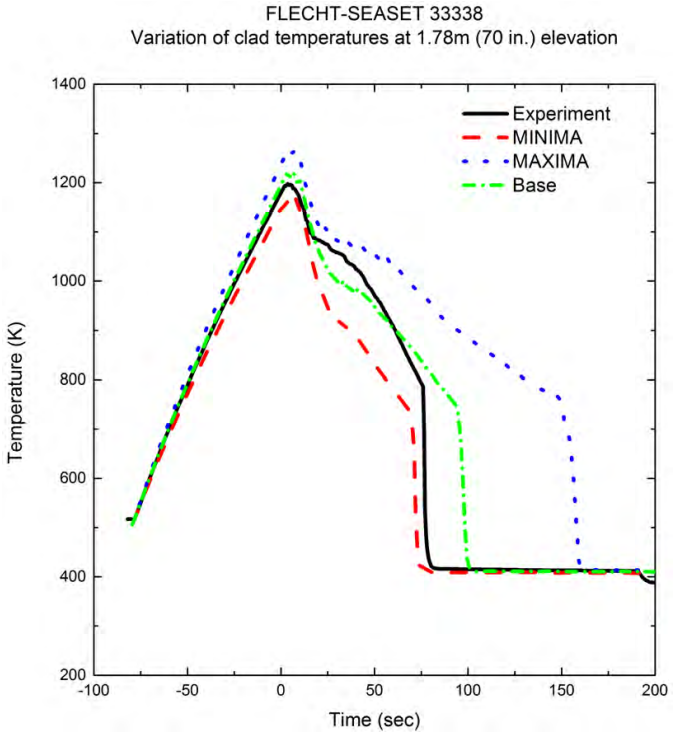

Figure 2-108 The Results of the SRS Calculations: Test 33338

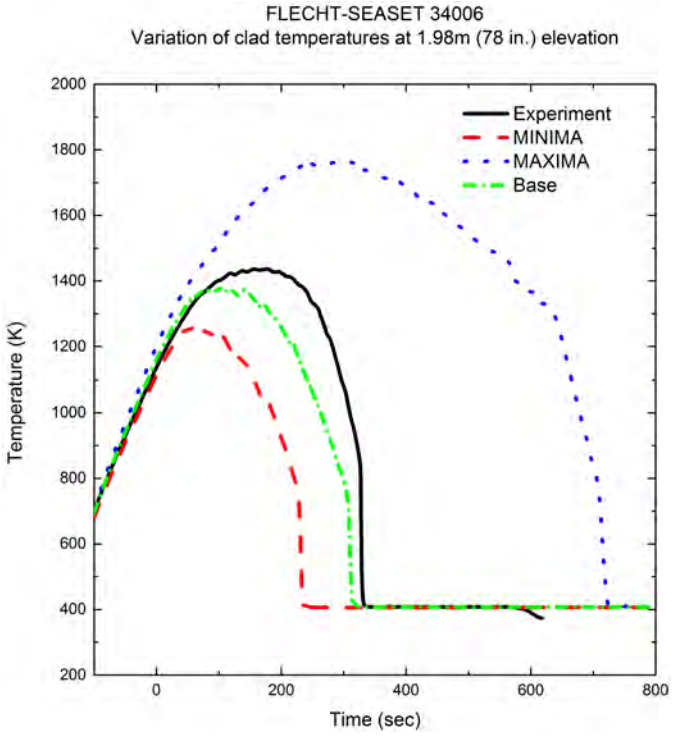

Figure 2-109 The Results of the SRS Calculations: Test 34006

3. Code Assessment against CCTF C2-4

The RELAP5/MOD3.3/K is assessed against Test C2-4 (Run 62) conducted at the Japan Atomic Energy Research Institute (JAERI) using the Cylindrical Core Test Facility (CCTF). Test C2-4 was one of the Core-II test series and conducted to confirm reproducibility of Test C2-SH1 (Run 53) [3-1]. The objectives of the CCTF tests were to a) demonstrate ECC behavior during refill and the reflood period, b) verify reflood analysis codes, and c) collect data sources and information to improve thermal-hydraulic models.

3.1 CCTF Test Facility Description

The CCTF was designed to model a full height core and four primary loops with components of a four-loop PWR. This experimental facility was used to provide information on fluid behavior in the core, downcomer, and upper plenum, including steam water carry-over and integral system effects during refill and the reflood periods of a hypothetical LOCA in a PWR. The facility layout and the configuration of the test vessel are shown in Figure 3-1 and Figure 3-2, respectively.

The test vessel consisted of a downcomer, lower plenum, upper plenum, and core region. The core of CCTF consisted of 32 rod bundles. The bundles were arranged in a cylindrical array. The 8x8 array of heater rods were made to simulate a 15x15 fuel assembly design of the WH. Each rod bundle contained 57 heater rods and seven non-heater rods. The configuration of the core and heater rod is shown in Figure 3-3 and Figure 3-4, respectively. The heater rods had a cosine axial power profile, as shown in Figure 3-5.

The primary loops consisted of three intact loops and a broken loop. Each loop consisted of a hot leg, a cold leg, a steam generator, and a pump simulator. The steam generator u-tubes of the two loops were contained in a single shell assembly. The containment of a PWR was simulated by two tanks. The broken cold leg was connected to two containment tanks.

The ECCS consisted of two accumulators and a low pressure coolant injection (LPCI) system. The injection points were at each cold leg and at the lower plenum. The upper plenum injection (UPI) and the downcomer injection (DVI) were also available.

3.2 RELAP5/MOD3.3/K Model Description

The RELAP5/MOD3.3/K input model of the CCTF is shown in Figure 3-6.

The core region is divided into [ ]^{TS} channels, the [ ]^{TS} Each channel is divided into [ ]^{TS} axial nodes. [ ]^{TS} channels are connected [ ]^{TS} [ ]^{TS}

Each loop is explicitly modeled. The downcomer is divided into [ ]^{TS} channels considering the azimuthal distance between cold legs. The [ ]^{TS} channels are connected each other using [ ]^{TS}

3.3 RELAP5/MOD3.3/K Simulation

3.3.1 Test Procedure and Initial Conditions

The system was heated to the specified temperatures with pre-heaters and pressurized to the specified pressure. After the initial pressure and temperature of the test were established, the saturated water was injected to the lower plenum until the desired initial level was obtained. Injection

of the saturated water was to simulate the fluid conditions of the test vessel during the initial reflood phase. After the lower plenum water level reached the specified level, the electric power was supplied to the heater rods. When the clad temperature reached the target value, the test was begun by injection of the accumulator water into the lower plenum. The system pressure was maintained at the specified value throughout the test by controlling the outlet valve of the containment tank. Decay power input to the heater rods was programmed to begin when the water reached the bottom of the heated region of the core.

The accumulator injection port was switched to the three intact cold leg ECC injection ports when the water level in the lower plenum reached a specified level. After the time of the core bottom recovery, the accumulator injection was switched to the LPCI injection. The LPCI injection was maintained throughout the remainder of the test.

The chronology and initial conditions for Test C2-4 are shown in Table 3-1 and Table 3-2, respectively. The reflood test was started at 93.5 s when the power decay initiated. The accumulator injection was initiated 9 s before the test was started. Four seconds after the reflood test initiation, the accumulator injection port was switched to the three intact cold leg ECC ports. The initial pressure and power for this test was 0.2 MPa (29.0 psia) and 9.34 MW, respectively.

3.3.2 Assessment Results

Test C2-4 is simulated from the reflood initiation time using the RELAP5/MOD3.3/K. Thus, the reflood initiation time of 93.5 s corresponds to the time 0.0 s in the simulation. The measured ECC flow rates are set as a function of time. The measured containment pressure is also set as a function of time.

Figure 3-7 shows a comparison of the measured and predicted upper plenum pressure. The measured upper plenum pressure begins to increase as the reflood test starts, whereas the calculated value is considerably lower than the data until around 22 s. This is mainly due to steam condensation occurring during the accumulator injection. The accumulator injection begins nine seconds before the reflood initiation. After 22 s, the RELAP5/MOD3.3/K over-predicts the upper plenum pressure throughout the remaining time. The main contributor to the over-prediction of the upper plenum pressure is the over-prediction of the core inlet fluid temperature as shown in Figure 3-8. Thus the predicted core inlet fluid temperature is less subcooled than the predicted value as shown in Figure 3-9. This results in more steam generation in the core and consequently a higher upper plenum pressure than the data.

Figure 3-10 shows a comparison of the measured and predicted differential pressure (DP) in the intact loop between the upper plenum and the cold leg nozzle. Even though the predicted value is oscillatory, the average predicted value matches the data well.

Figure 3-11 shows a comparison of the measured and predicted values of the rod clad temperature at 1.015 m (40 in) from the heated rod bottom. The measured temperature begins to decrease as soon as the reflood initiates, whereas the heat-up of the rods lasts longer than the data in the calculation. The predicted peak temperature matches the data fairly well. The predicted rod quench time, however, is earlier than the data. The measured and predicted temperature at the rod quench time is around 650 K and 800 K, respectively. Figure 3-12 shows a comparison of the measured and predicted heat transfer coefficients (HTCs) at the same elevation with the rod clad temperature measurement. Even though the predicted value is very oscillatory, the average predicted value is reasonably close to the measured value until the rod is quenched.

Figure 3-13 shows a comparison of the measured and predicted values of rod clad temperature at 1.83 m (72 in) from the heated rod bottom. The heat-up of the rod lasts longer than the data in the calculation. The RELAP5/MOD3.3/K over-predicts the rod clad temperature after turn-around time.

However, the predicted peak temperature and quench time match the data fairly well. The predicted HTC at this elevation is compared to the data in Figure 3-14.

Figure 3-15 shows a comparison of the measured and predicted values of rod clad temperature at 2.44 m (96 in) from the heated rod bottom. The highest rod clad temperature was measured at this elevation. The RELAP5/MOD3.3/K over-predicts the clad temperature throughout the transient. The predicted peak temperature is higher than the data. The predicted turn-around time match the data well, whereas the predicted quench time is later than the data because the predicted temperature is higher than the data and it decreases slowly after the turn-around time.

Figure 3-16 shows a comparison of the measured and predicted values of the rod clad temperature at 3.05 m (120 in) from the heated rod bottom. The RELAP5/MOD3.3/K over-predicts the clad temperature until around 480 s. After 480 s, the predicted value is lower than the data because the predicted quench time is earlier than the data. The predicted peak temperature is higher than the data. At the time of rod quench, the predicted value shows a slower temperature decline, whereas the data shows a sharp temperature decline.

Overall, the RELAP5/MOD3.3/K reasonably predicts the reflood progression of Test C2-4. The code over-predicts the rod clad temperatures at the upper part of the core. The predicted rod clad temperature is higher than the highest measured value. These assessment results show the conservative capability of the RELAP5/MOD3.3/K in predicting the rod clad temperature.

3.4 SRS Calculations

SRS calculations were performed against the CCTF C2-4. [

]^{TS} The uncertainty parameters and their distribution functions used for the SRS calculations are listed in Table 3-3.

Figure 3-17 shows the results of the SRS calculations against the CCTF C2-4. Time zero in the figure corresponds to the heater rod heat-up initiation time. The third highest value of the calculated clad temperatures is higher than the measured PCT confirming the data covering. Therefore, the number and the probability distribution functions of the selected code parameters are confirmed to be sufficient.

3.5 Conclusion

The capability of the RELAP5/MOD3.3/K in predicting the reflood progression was assessed against the CCTF C2-4. The assessment results show that the RELAP5/MOD3.3/K is capable of calculating the reflood process correctly. The RELAP5/MOD3.3/K over-predicts the rod clad temperatures at the upper core where the PCT occurred. The result of the SRS calculations against the CCTF C2-4 shows that the measured PCT is covered by the calculated value. This implies that the number and the probability distribution functions of the selected code parameters for the reflood heat transfer are sufficient to cover the measured PCT.

References

[3-1] Jun Sugimoto, et. al., “Evaluation Report on CCTF Core-II Reflood Tests C2-AC1(Run 51) and C2-4(Run-62) – Investigation of Reproducibility,” JAERI-M85-026, 1985.

[3-2] Tsutomu OKUBO, et al., “Evaluation Report on CCTF Core-II Reflood Tests C2ACL(Run 51) and C2-4(Run 62) – Effect of Initial Clad Temperature,” JAERI-M-84/026, Febrary 1984.

Table 3-1 Chronology of the CCTF C2-4 Test

Event	Time (s)
Test initiated (Heater rods power on)	0.0
Accumulator injection initiated	84.5
Power decay initiated	93.5
Bottom of core recovery	94.0
Accumulator injection switched from lower plenum to cold legs	97.0
Low pressure safety injection initiated	120.0
All heater rods quenched	652.0

Table 3-2 Initial Conditions for the CCTF C2-4 Test

Parameters	
Total Power (MW)	9.34
Average Linear Power (kW/m)	1.40
Radial Power Distribution (A:B:C)	1.36:1.20:0.76
Containment Pressure (MPa)	0.20
Steam Generator Secondary Pressure (MPa)	5.2
Downcomer Wall Temperature (K)	467
Primary Piping Wall Temperature (K)	394
Steam Generator Secondary Temperature (K)	539
Peak Clad Temperature at 2.44 m elevation (K)	
At ECC Initiation	910
At Reflood Initiation	971
Lower Plenum Filled Water Temperature (K)	394
ECC Water Temperature (K)	308
Lower Plenum Water Level (m)	0.80
Steam Generator Secondary Water Level (m)	7.4
Accumulator Injection Rate (m^3/s)	
Into Lower Plenum	0.11
Into Cold Leg	0.09
Low Pressure Safety Injection Rate (m^3/s)	0.001

Table 3-3 Parameters and Distribution Functions Used for the SRS Calculations: CCTF C2-4

TS

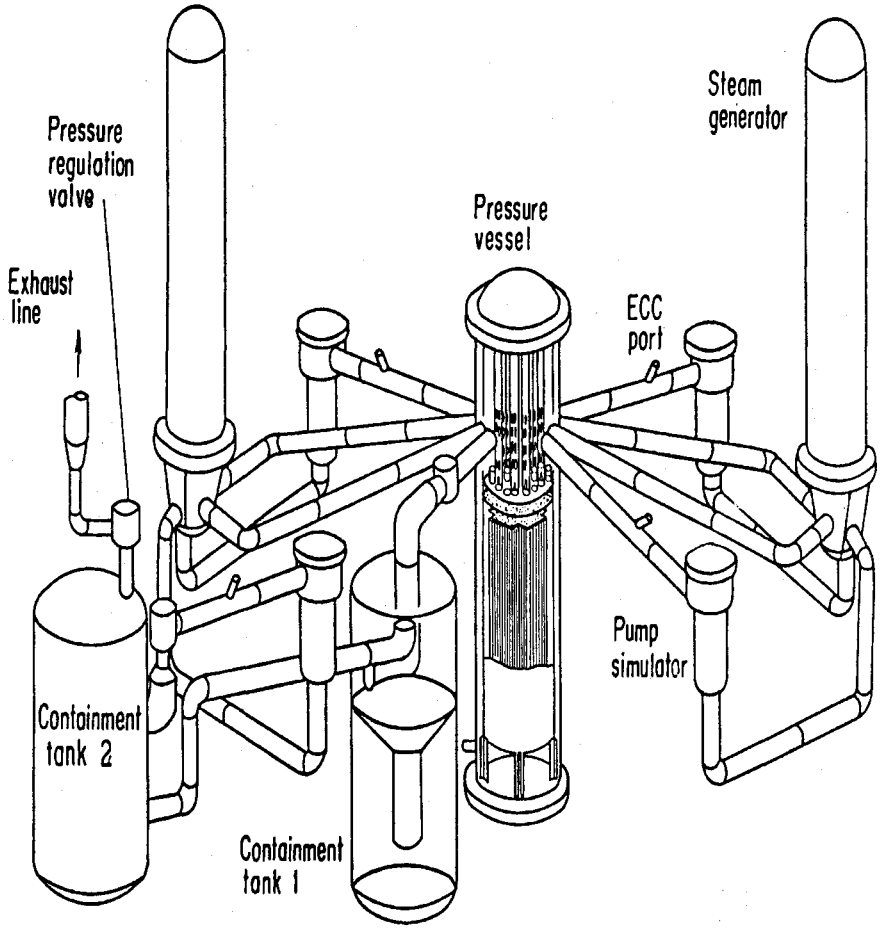

Figure 3-1 Configuration of the CCTF

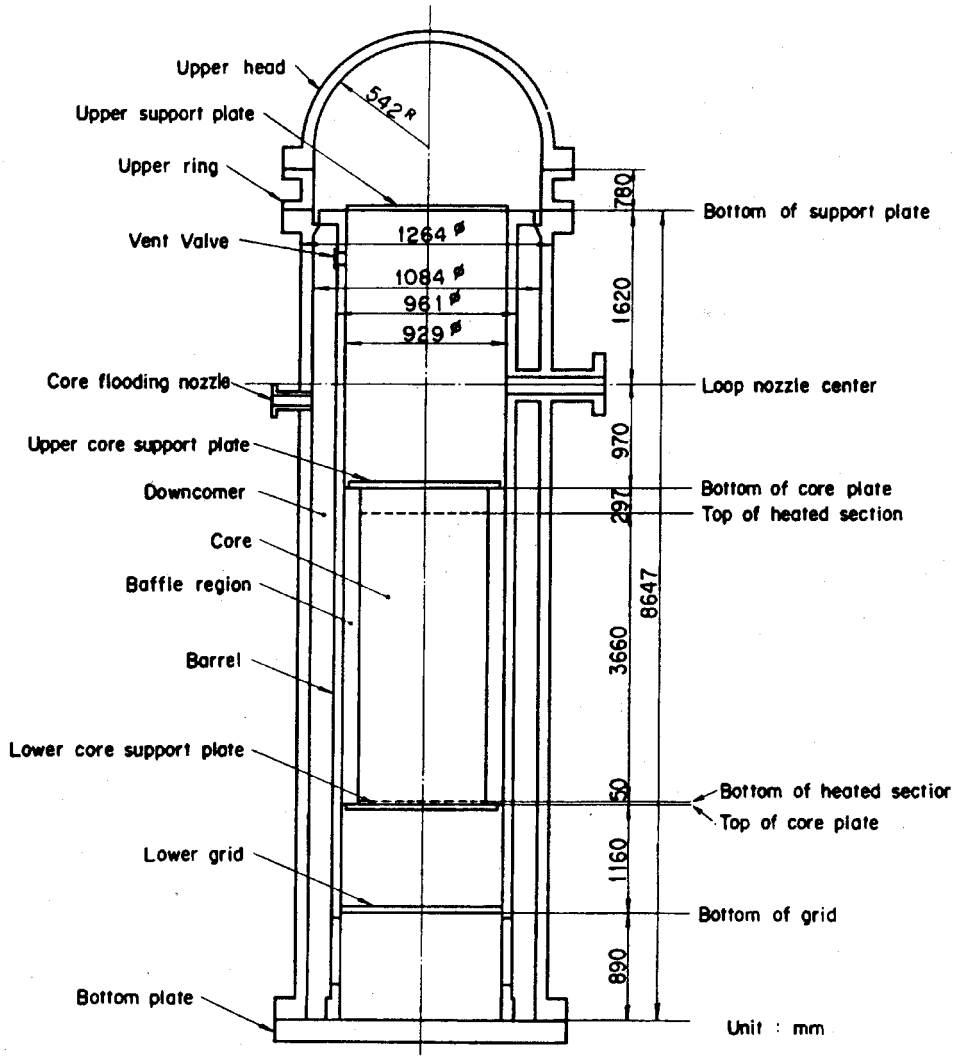

Figure 3-2 Reactor Vessel of the CCTF

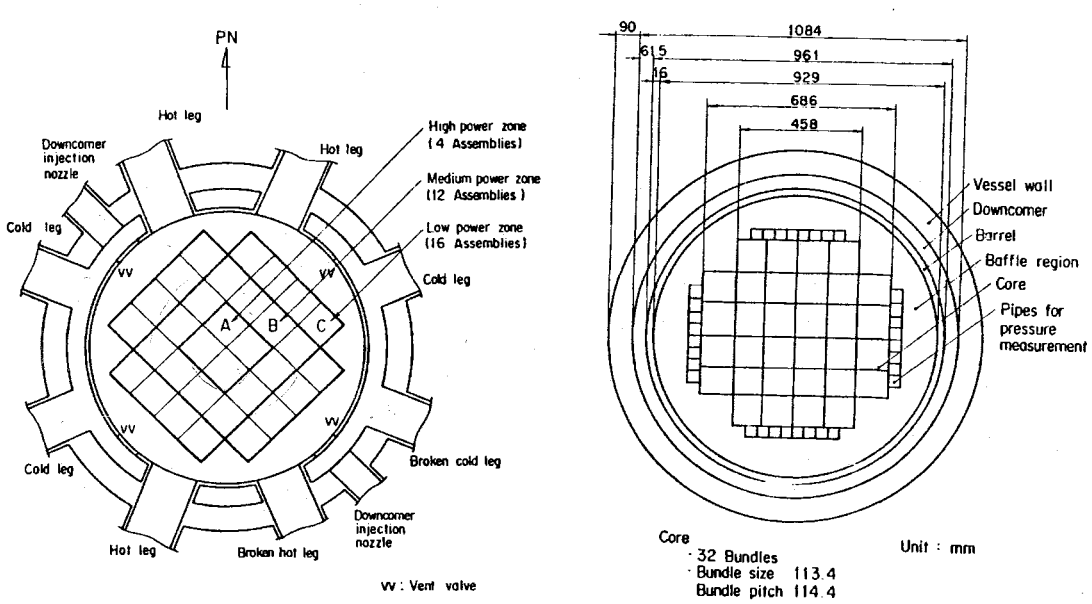

Figure 3-3 Core of the CCTF

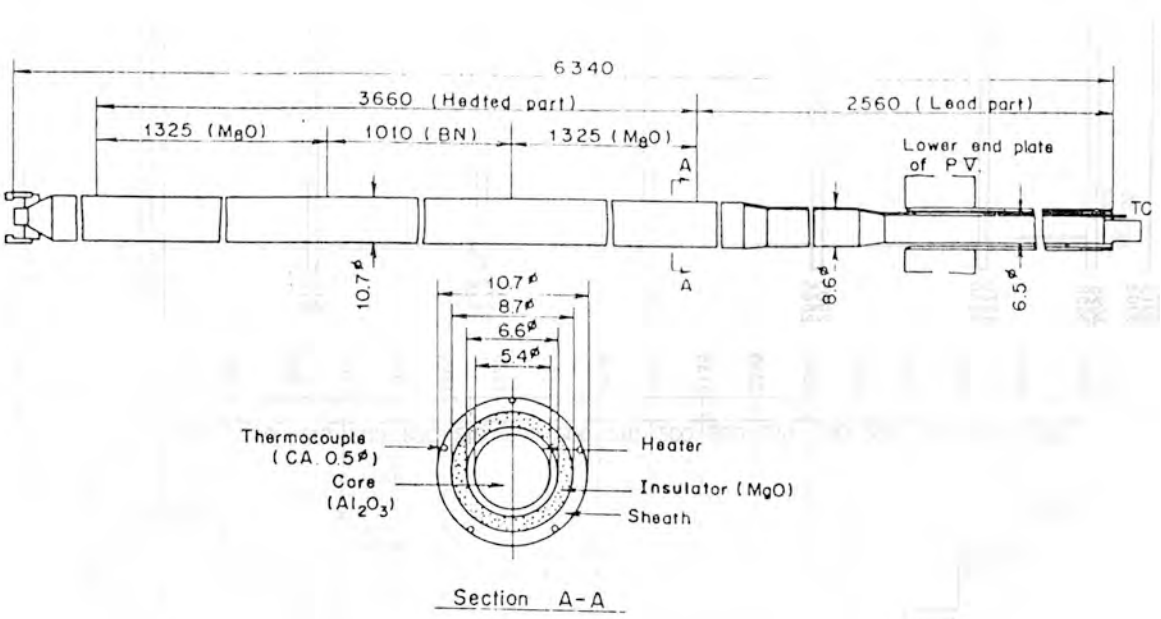

Figure 3-4 Heater Rod of the CCTF

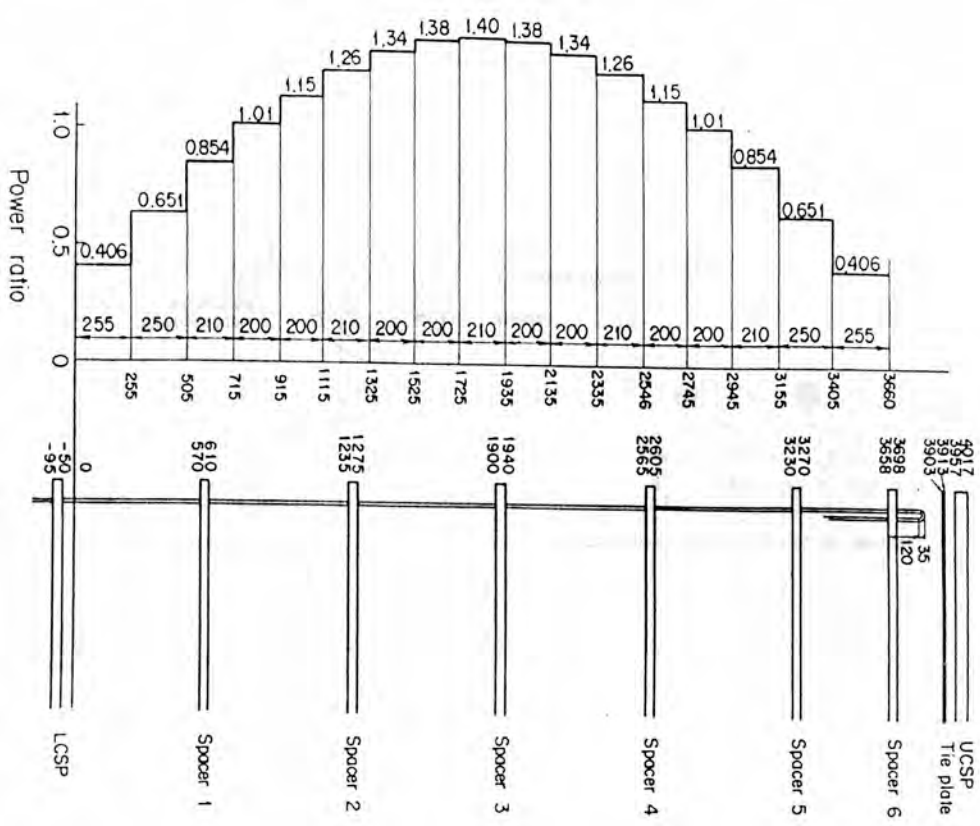

Figure 3-5 Axial Power Profile for the CCTF Core-II Tests

TS

Figure 3-6 RELAP5/MOD3.3/K Nodalization of the CCTF

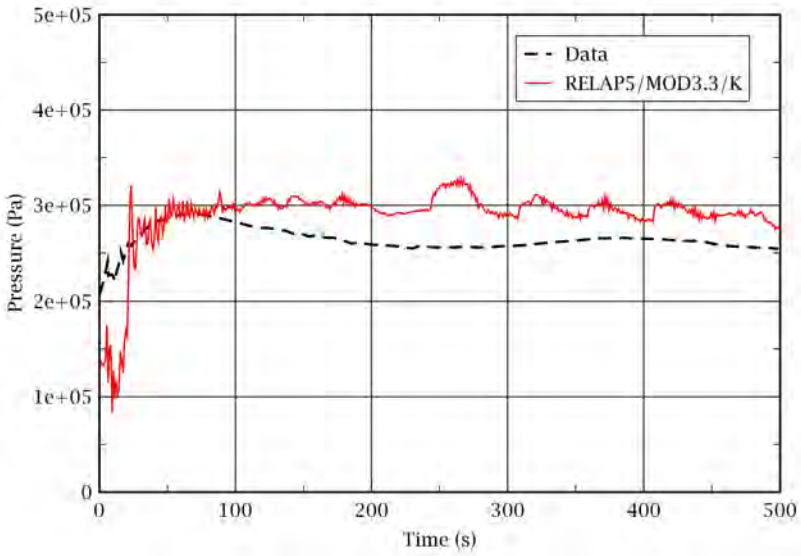

Figure 3-7 Upper Plenum Pressure: CCTF C2-4

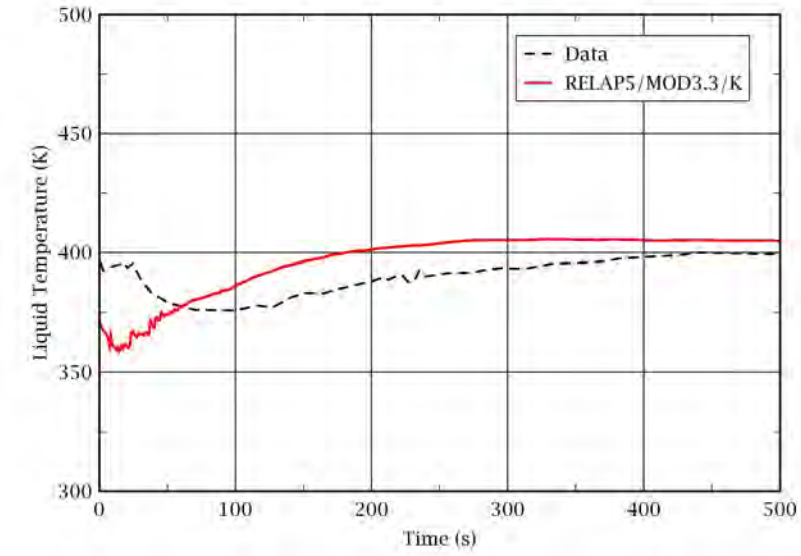

Figure 3-8 Core Inlet Fluid Temperature: CCTF C2-4

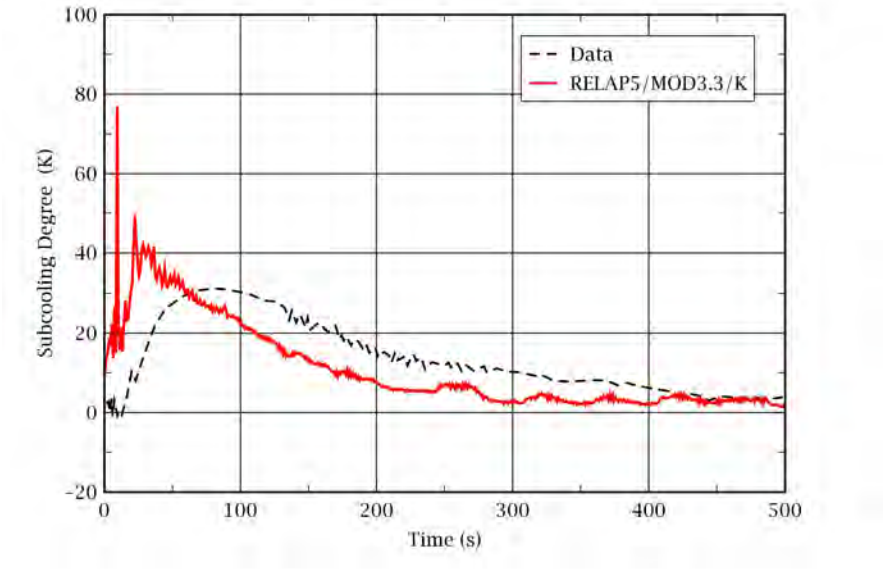

Figure 3-9 Subcooling of the Core Inlet Fluid: CCTF C2-4

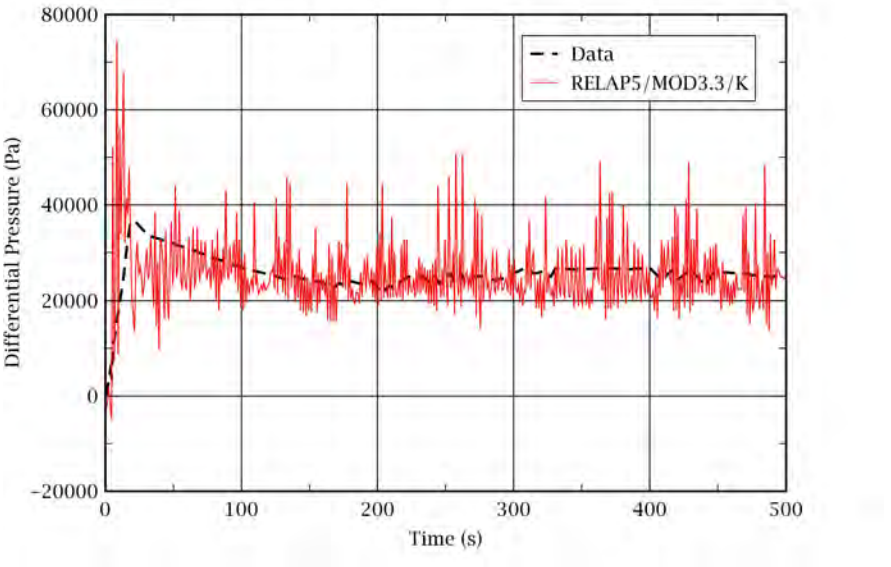

Figure 3-10 Intact Loop Differential Pressure: CCTF C2-4

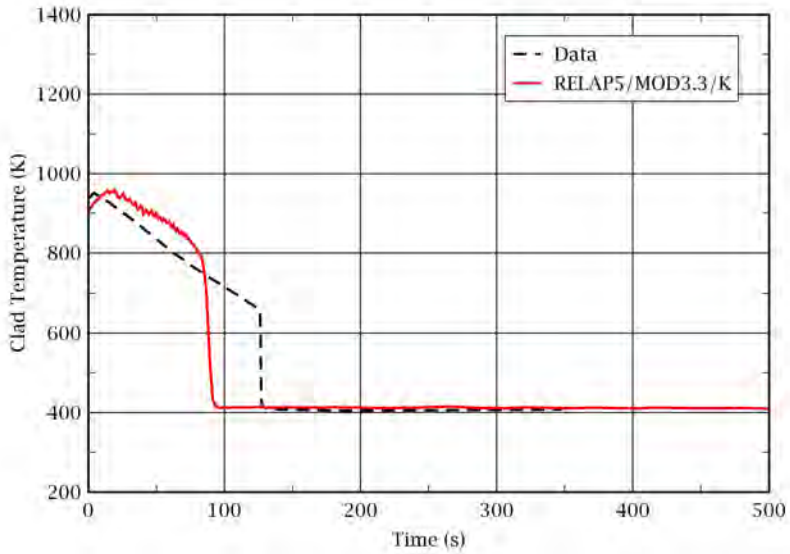

Figure 3-11 Rod Clad Temperature at 1.015 m from the Heater Rod Bottom: CCTF C2-4

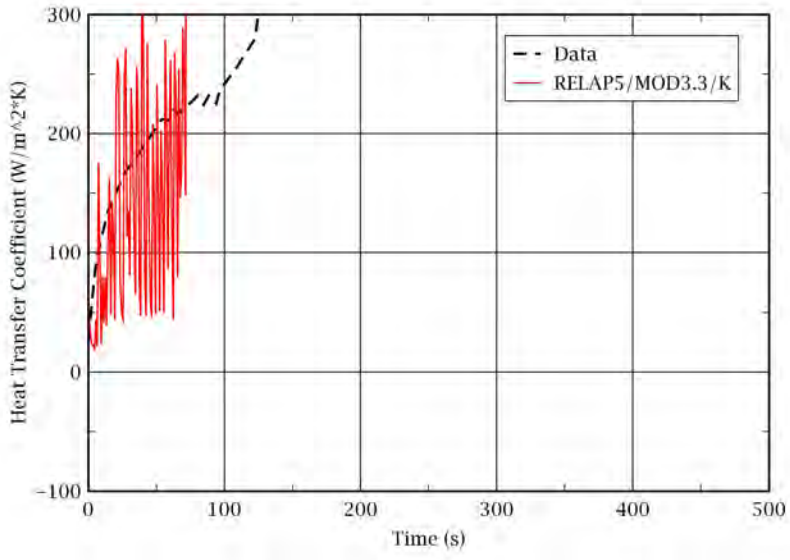

Figure 3-12 Heat Transfer Coefficient at 1.015 m from the Heater Rod Bottom: CCTF C2-4

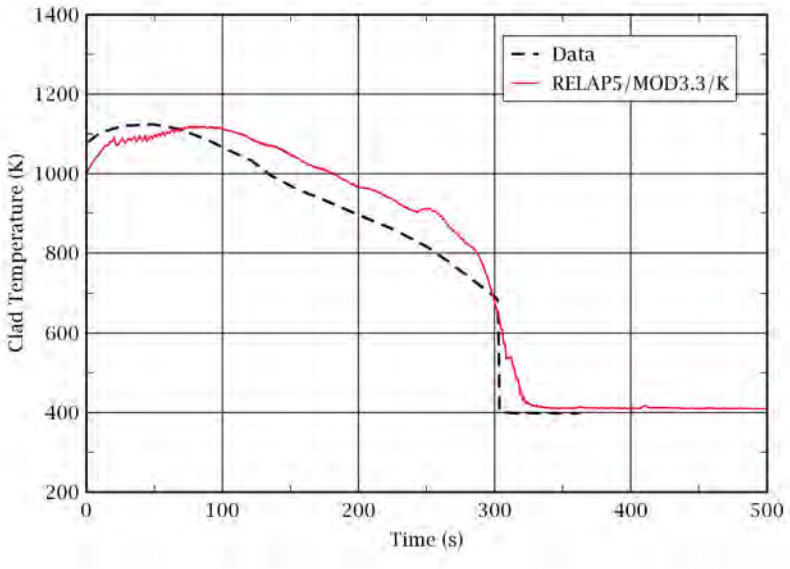

Figure 3-13 Rod Clad Temperature at 1.83 m from the Heater Rod Bottom: CCTF C2-4

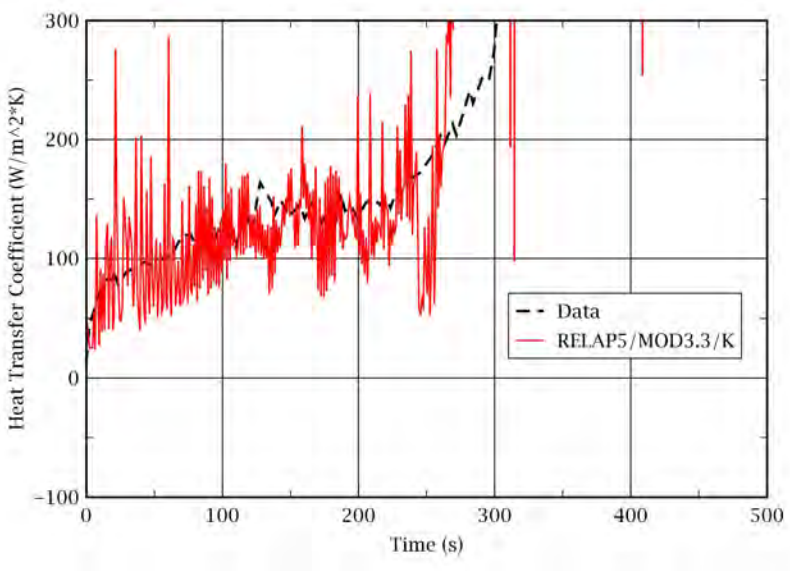

Figure 3-14 Heat Transfer Coefficient at 1.83 m from the Heater Rod Bottom: CCTF C2-4

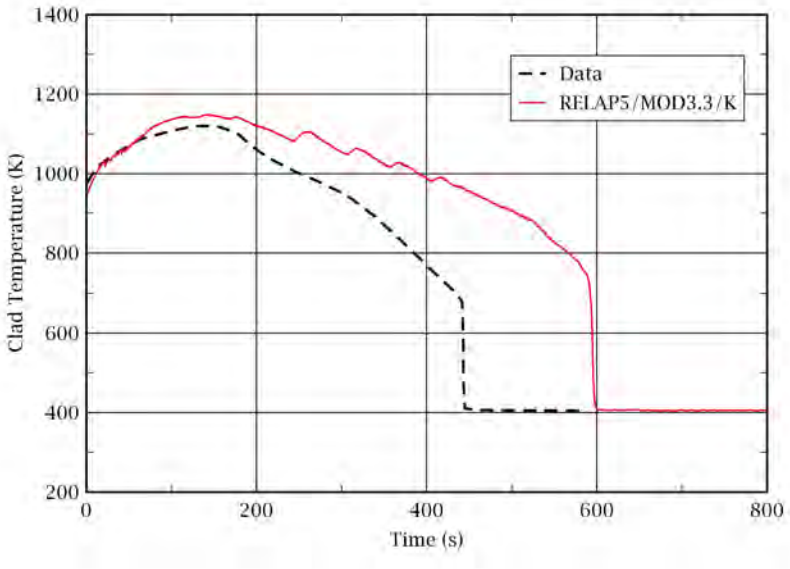

Figure 3-15 Rod Clad Temperature at 2.44 m from the Heater Rod Bottom: CCTF C2-4

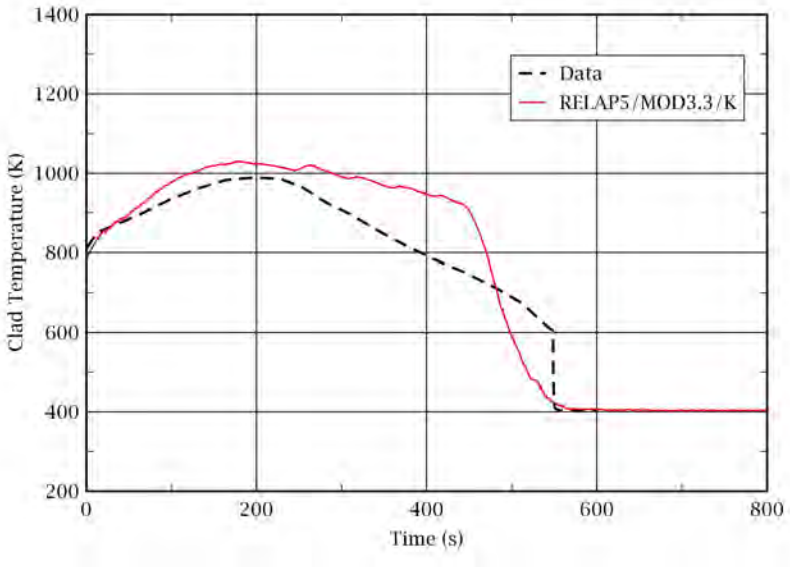

Figure 3-16 Rod Clad Temperature at 3.05 m from the Heater Rod Bottom: CCTF C2-4

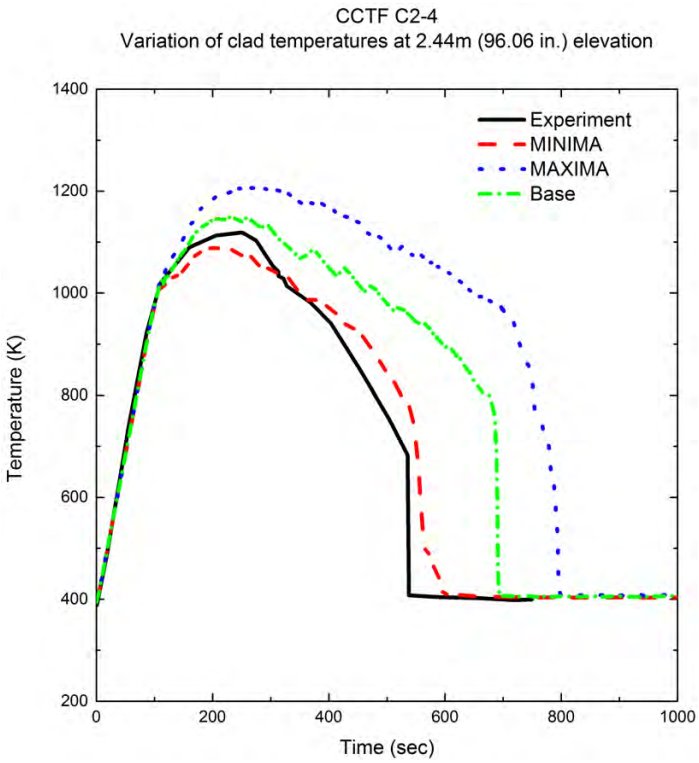

Figure 3-17 The Results of the SRS Calculations: CCTF C2-4

4. Code Assessment against NEPTUN

The RELAP5/MOD3.3/K is assessed against the NEPTUN reflood tests conducted at Eidge Institut fuer Reaktorforschung (EIR). Seven tests among a total 40 reflood tests conducted using the NEPTUN facility are selected to assess the capability of RELAP5/MOD3.3/K in predicting the reflood progression. The test number and test parameters of the selected seven tests are shown in Table 4-1.

4.1 NEPTUN Test Facility Description

The NEPTUN test facility was built to study reflooding in bundle geometries. Figure 4-1 shows an isometric view of the NEPTUN facility. The NEPTUN heater rod bundle consists of 33 electrically heated rods and four guide tubes. The bundle was placed in an insulated octagonal housing. The outer diameter of the heater rod was 10.7 mm (0.421 in), pitch-to-diameter was 1.33, and the heated length was 1.68 m (5.51 ft). The bundle contained five spacer grids which were axially located at equal distances. A cross section of the NEPTUN bundle is shown in Figure 4-2 and the dimensions of a heater rod are shown in Figure 4-3. The heater rods had a cosine axial power profile, as shown in Figure 4-4.

Rod cladding temperatures, fluid temperatures, and differential pressures were measured at eight elevations as shown in Figure 4-5. Each heater rod was instrumented with four to eight thermocouples placed inside of the cladding. The five heater rods located at a bundle center region were additionally instrumented with external thermocouples. There also were measurements of flooding water, fresh steam and exhaust steam mass flow rates, water carry over, absolute pressure, and heating power. The void fractions in the core were obtained from the measured absolute pressures and differential pressures. The upper plenum pressure was held constant during the experiments by a pressure control system. The specifications of the NEPTUN facility are shown in Table 4-2.

There exists no detailed quantification of the measurement uncertainty in the NEPTUN test facility. Thus, the errors of the test parameters were estimated using the measured values [4-1]. The obtained measurement errors and scattering of the data during the NEPTUN reflooding tests are shown in Table 4-3.

Six of the seven tests used for the code assessment were repeated tests to evaluate the effect of the external thermocouples. The effect of external thermocouples was reported as negligible, except to around 35 ^{o}C lower quench temperature and therefore four - nine seconds later quench times. The water entrainment was higher without external thermocouples. However, it was noticeable that the entrainment was dependent on the reflooding velocity. The entrainment was the same during experiments with 4.5 cm/s - 15 cm/s reflooding velocity. However, the effect of the external thermocouples became stronger as the reflooding velocity decreased. The entrainment was 5 % higher in the repetition test with 2.5 cm/s reflooding velocity and 33 % higher with 1.5 cm/s reflooding velocity. The differences of the data between the NEPTUN reflooding tests and repetition tests are shown in Table 4-4.

4.2 RELAP5/MOD3.3/K Model Description

The RELAP5/MOD3.3/K input model of the NEPTUN facility is shown in Figure 4-6.

The NEPTUN facility is simplified to the extent necessary for simulating the reflood process in the bundle test section. The test section is modeled with [ ]^{TS} consisting of [ ]^{TS} axial sub-volumes. The length of each sub-volume is set to [ ]^{TS} keeping consistency with a plant nodalization. Core inlet flow is simulated with [

]TS The test section outlet condition is modeled with [ ]TS

4.3 RELAP5/MOD3.3/K Simulation

Table 4-1 shows the test parameters of the seven tests selected for the RELAP5/MOD3.3/K assessment.

These tests were conducted at a system pressure 1 bar or 4 bar, flooding water subcooling of 11 °C or 78 °C, and initial cladding temperature of 757 °C or 867 °C. The flooding water velocity varied from 1.5 cm/s to 15 cm/s in these tests.

In this section, the results of simulations against Test 5050, 5051, and 5052 are discussed in detail. These three tests were conducted under the same conditions except flooding velocity. The results of simulations against the other four tests are considered in the code accuracy calculation.

4.3.1 NEPTUN Test 5050

NEPTUN Test 5050 was conducted under such conditions as a flooding velocity of 15 cm/s, flooding water subcooling of 78 °C, initial cladding temperature of 867 °C, and single rod power of 2.45 kW.

The rod clad temperatures calculated by RELAP5/MOD3.3/K are compared with the data at four different elevations corresponding to the measurement level 3, 4, 5, and 6, in Figure 4-7 through Figure 4-10. At all elevations, the RELAP5/MOD3.3/K predicts the clad temperatures well before the measured temperatures reach the quench time. However, the predicted rod quench times are later than the data in all elevations. This is mainly due to that the predicted rod quench temperatures are lower than the data. The maximum difference of rod quench time is observed at the measurement level 4. The predicted rod quench temperature is around 150 K lower than the data at the measurement level 4.

Figure 4-11 and Figure 4-12 show a comparison of the measured and predicted core collapsed level and the integrated mass of water carry over, respectively. The RELAP5/MOD3.3/K over-predicts the core collapsed level even though the code over-predicts the water carry-over. This is probably due to that the RELAP5/MOD3.3/K under-predicts steam generation in the core but over-predicts the water carry over per steam flow rate. However, the RELAP5/MOD3.3/K reasonably predicts the core collapsed level and water carry over considering that no accurate quantification of the measurement uncertainty was performed.

4.3.2 NEPTUN Test 5051

NEPTUN Test 5051 was conducted under identical test conditions to Test 5050, except for the flooding velocity. The flooding velocity of Test 5051 was 4.5 cm/s.

The rod clad temperatures calculated by RELAP5/MOD3.3/K are compared with the data at four different elevations corresponding to measurement levels 3, 4, 5, and 6 in Figure 4-13 through Figure 4-16. At all elevations, the RELAP5/MOD3.3/K predicts the clad temperatures fairly well before the measured temperatures reach the quench temperatures. However, the predicted rod quench times are later than the data in all elevations. As indicated before, this is mainly due to that the predicted rod quench temperatures are lower than the data. The predicted rod quench temperature is approximately 100 K lower than the data at the measurement level 4.

Figure 4-17 and Figure 4-18 show a comparison of the measured and predicted core collapsed level and integrated mass of water carry over, respectively. The RELAP5/MOD3.3/K predicts the core collapsed level fairly well until about 97 s. During this period, however, the RELAP5/MOD3.3/K

over-predicts water carry over. As described in the previous simulation, this is probably due to that the code over-predicts the water carry over per steam flow rate. The tendency of over-prediction of water carry over is stronger than predicted for Test 5050. However, the RELAP5/MOD3.3/K reasonably predicts the core collapsed level and water carry over considering that no accurate quantification of the measurement uncertainty was performed.

4.3.3 NEPTUN Test 5052

NEPTUN Test 5052 was conducted under identical test conditions to Test 5050, except for the flooding velocity. The flooding velocity of the Test 5052 was 2.5 cm/s.

The rod clad temperatures calculated by RELAP5/MOD3.3/K are compared with the data at four different elevations corresponding to measurement levels 3, 4, 5, and 6 in Figure 4-19 through Figure 4-22. At all elevations, the RELAP5/MOD3.3/K over-predicts the rod quench time, just like the other simulations provided in the previous sections. At measurement levels 4 and 6, the predicted clad temperatures turn around and decrease much faster than the data. At measurement levels 3 and 5, the RELAP5/MOD3.3/K predicts the rod clad temperatures very well until the measured temperatures reach the quench temperatures. As indicated in the previous simulations, this is mainly due to the fact that the predicted rod quench temperatures are lower than the data.

Figure 4-23 and Figure 4-24 show a comparison of the measured and predicted core collapsed level and integrated mass of water carry over, respectively. The RELAP5/MOD3.3/K predicts the core collapsed level fairly well, whereas the RELAP5/MOD3.3/K over-predicts water carry over. As described in the previous simulations, this is probably due to that the code over-predicts the water carry over per steam flow rate. The tendency of over-prediction of the water carry over is stronger than Test 5050 and Test 5051. However, the RELAP5/MOD3.3/K reasonably predicts the core collapsed level and water carry over considering that no accurate quantification of the measurement uncertainty was performed.

4.3.4 Assessment Results Summary

The capability of the RELAP5/MOD3.3/K in predicting the reflood progression was assessed against four NEPTUN tests. The assessment results show that the RELAP5/MOD3.3/K is capable of calculating the reflood process correctly, in general. The RELAP5/MOD3.3/K predicts the rod clad temperature well, whereas the RELAP5/MOD3.3/K over-predicts rod quench time because the code calculated rod quench temperature is lower than the data. The RELAP5/MOD3.3 predicts core collapsed water level reasonably well but the code over-predicts water carry over. The tendency of over-prediction of water carry over becomes stronger as flooding velocity decreases. This is consistent with the results of the repetition tests without external thermocouples because the external thermocouples are not modeled in the code simulations. In general, the RELAP5/MOD3.3/K reasonably predicts water carry over considering that no accurate quantification of the measurement uncertainty was performed.

4.4 Code Accuracy

Figure 4-25 shows the code accuracy evaluated using 14 test data obtained from the seven NEPTUN tests in Table 4-1. The highest and second highest measured clad temperatures of each test were compared with the predicted temperatures at corresponding elevations. The RELAP5/MOD3.3/K over-predicts clad temperature by [ ]^{TS} on average, with a standard deviation of [ ]^{TS}

4.5 SRS Calculations

SRS calculations were performed against seven NEPTUN tests in Table 4-1. [

]^{TS} The uncertainty parameters and distribution functions used for the SRS calculations against the NEPTUN tests are listed in Table 4-5.

Figures from Figure 4-26 to Figure 4-32 show the results of the SRS calculations against seven NEPTUN tests. In all SRS calculations, the third highest values of the calculated clad temperatures are higher than the measured PCTs confirming the data covering. Therefore, the number and the probability distribution functions of the selected code parameters are confirmed to be sufficient.

4.6 Conclusion

The capability of the RELAP5/MOD3.3/K in predicting the reflood progression was assessed against seven NEPTUN tests. The assessment results show that the RELAP5/MOD3.3/K is capable of calculating the reflood process correctly, in general. The RELAP5/MOD3.3/K over-predicts rod clad temperature as confirmed by the evaluation of code accuracy. The RELAP5/MOD3.3/K over-predicts rod quench time because the code calculated rod quench temperature is lower than the data. The RELAP5/MOD3.3 predicts core collapsed water level reasonably well but the code over-predicts water carry over. The tendency of the over-prediction of water carry over becomes stronger as flooding velocity decreases, showing the consistency with the results of the repetition tests without external thermocouples.

Data covering is confirmed in all SRS calculations against seven NEPTUN tests. This implies that the number and the probability distribution functions of the selected code parameters for the reflood heat transfer are sufficient to cover the measured PCTs.

References

[4-1] M. Richner, G. Th. Analytis, S. N. Aksan, “Assessment of RELAP5/MOD2, Cycle 36.02, Using NEPTUN Reflooding Experimental Data,” NUREG/IA-0054, NRC, 1992.

[4-2] H. Grutter, F. Stierli, S. N. Aksan, G. Varadi, “NEPTUN Bundle reflooding experiments: Test facility description,” EIR-report Nr.386, 1981.

Table 4-1 NEPTUN Tests Used for the RELAP5/MOD3.3/K Assessment

Test No.	Pressure (bar)	Flooding water		Single rod power (kW)	Maximum initial cladding temperature (^{o}C)
		Velocity (cm/s)	Subcooling (^{o}C)		
5036	4.1	1.5	11	2.45	757
5052	4.1	2.5	78	2.45	867
5051	4.1	4.5	78	2.45	867
5025	4.1	10.	78	2.45	757
5050	4.1	15.	78	2.45	867
5049	1.0	2.5	78	2.45	867
5056	4.1	2.5	78	4.19	867

Table 4-2 Specifications of the NEPTUN Facility

Parameters	Value
Max. bundle power	76 kW
Max. coolant flow	0.65 kg/s
Flooding rate	2 to 15 cm/s
Flooding water temperature	20 to 147 ^{o}C
System pressure	1 to 5 bar
Initial cladding temperature	Up to 900 ^{o}C
Heater rod	
Heated length	1,680 mm
Outer diameter	10.72 mm
Power distribution	Chopped cosine
Rod power (max.)	2.3 kW
Average heat flux	4.15 W/cm^2
Peak heat flux	6.35 W/cm^2
Peak linear heat rate	21.4 W/cm
Axial peaking factor	1.53
Rod arrangement; square pitch	14.3 mm
Guide tubes	
Outer diameter	13.87 mm

Table 4-3 Measurement Errors and Scattering of the Data during NEPTUN Reflood Tests

Quantity	Probable error	Largest scattering min. to max. of the data
Flooding water mass flow	± 5.3 %	
Flooding water temperature	± 0.5 ^{o}C	
Test section pressure	± 0.03 bar	0.42 bar during Test 5050
Rod power	± 1.8 %	
Collapsed water level	± 4 cm	
Void fraction	± 0.04	
Rod cladding temperature between all rods without external thermocouples	± 5 ^{o}C	48 ^{o}C during Test 5050 90 ^{o}C during Test 5036
Quench times between all rods without external thermocouples at measurement level 4 and 5	± 1.2 s	2.5 s during Test 5050 14.2 s during Test 5036

Table 4-4 Difference of the Data between NEPTUN Reflooding and Repetition Tests

Quantity	Largest scattering between original and repetition
Rod cladding temperature at the representative rod	20 ^{o}C between Test 5050 and repetition 90 ^{o}C between Test 5036 and repetition
Quench times of representative rods at measurement levels 4 and 5	4.2 s between Test 5050 and repetition 9.2 s between Test 5036 and repetition
Water entrainment	Identical during experiments with 4.5 - 15cm/s flooding velocity 5 % higher in repetition for experiments with 2.5 cm/s flooding velocity 33 % higher in repetition for experiments with 1.5 cm/s flooding velocity

Table 4-5 Parameters and Distribution Functions Used for the SRS Calculations: NEPTUN

TS

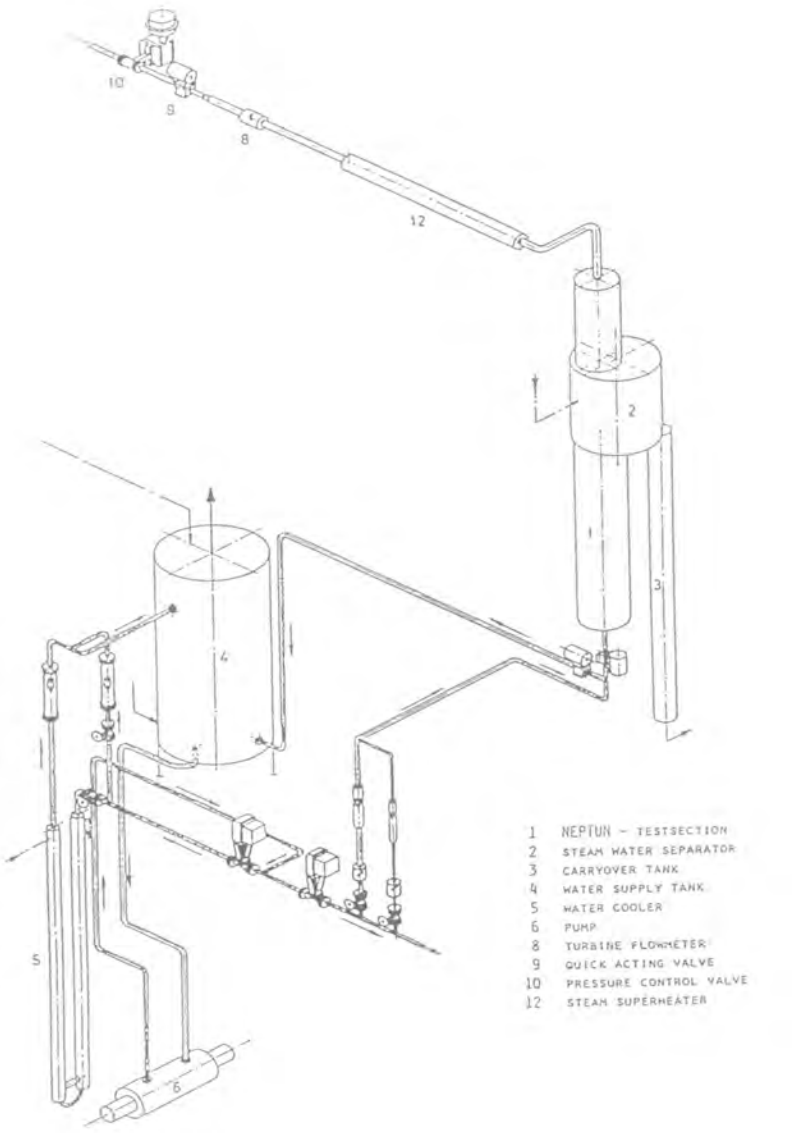

Figure 4-1 Schematic diagram of the NEPTUN

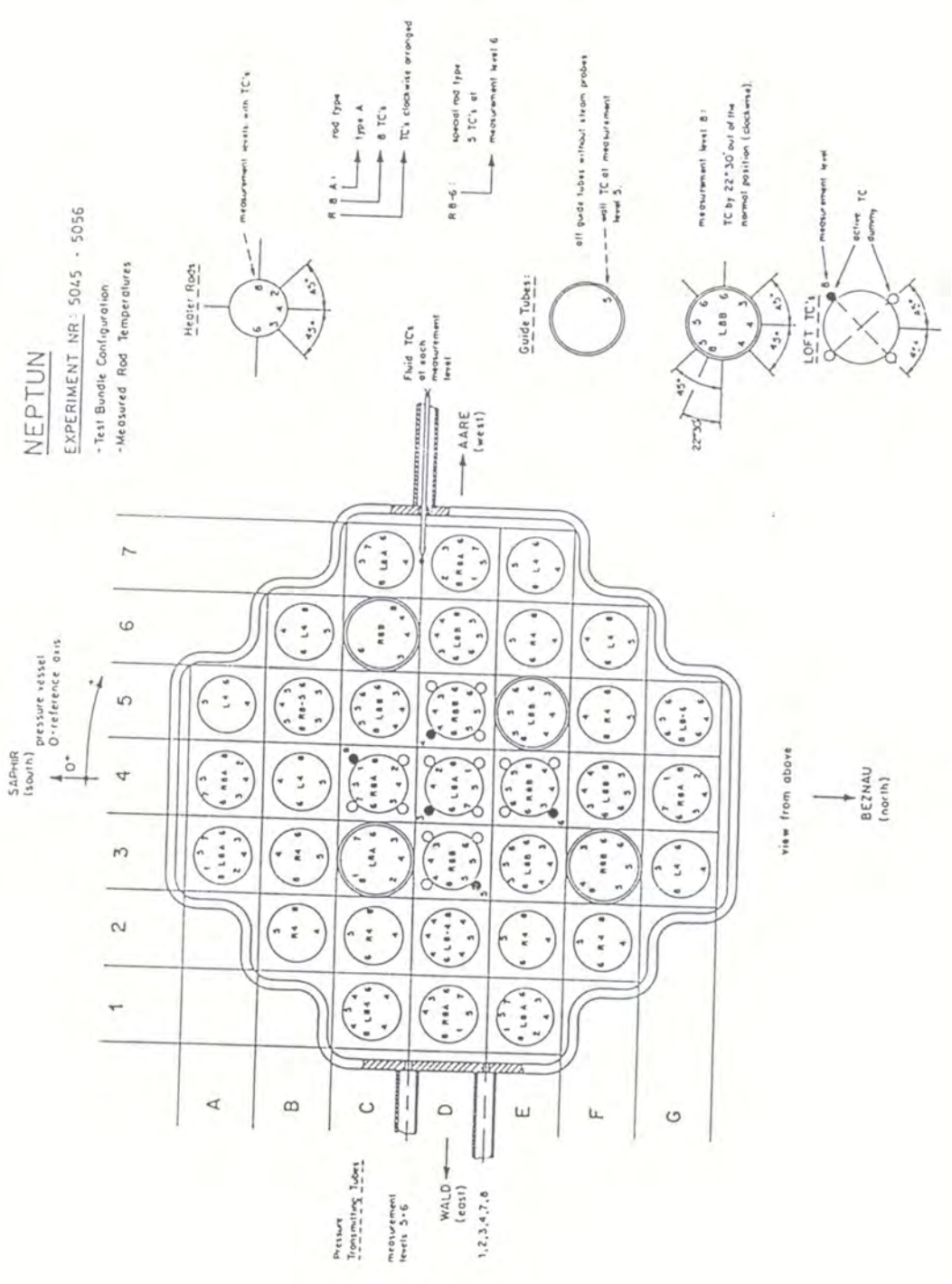

Figure 4-2 Configuration of the NEPTUN Bundle

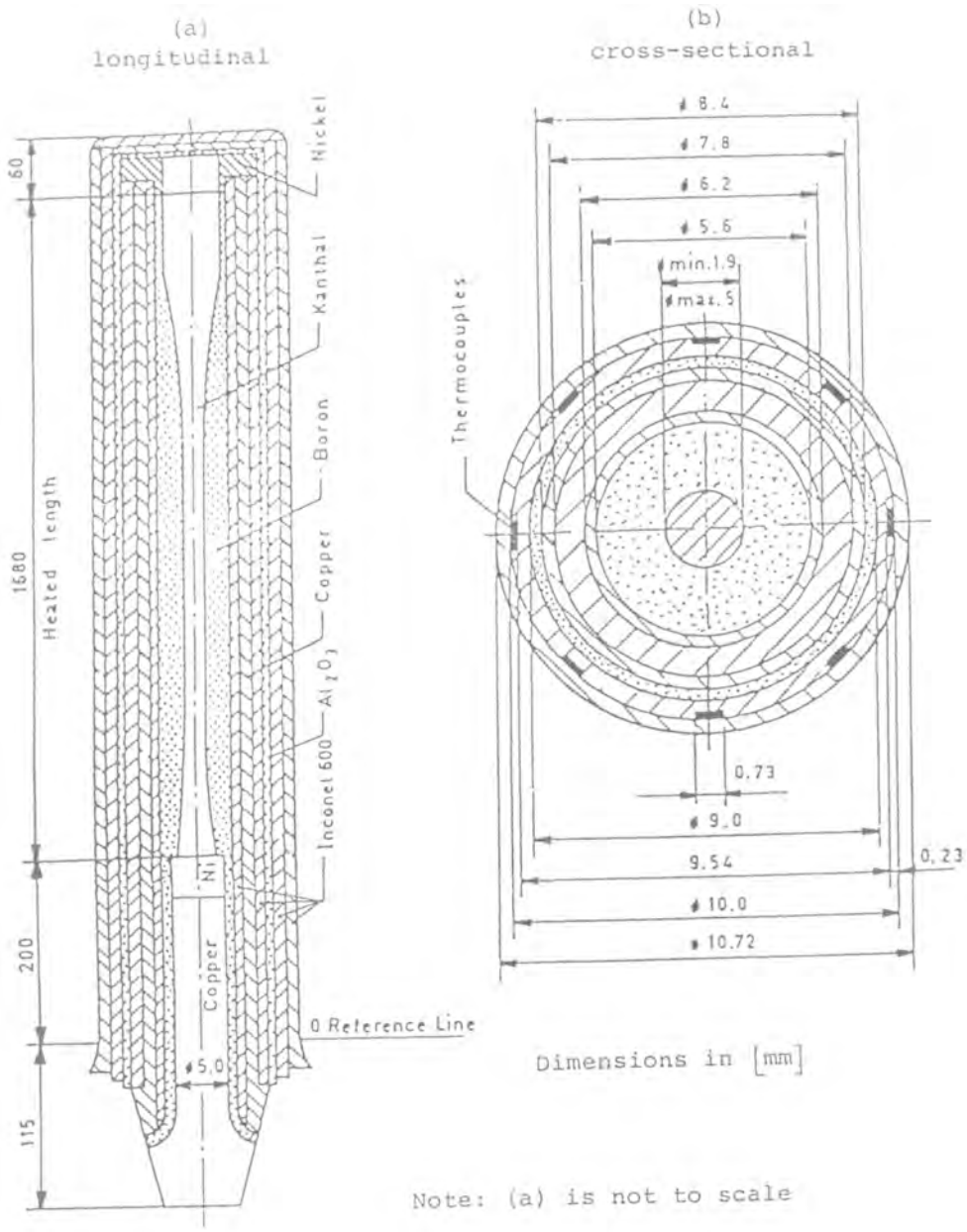

Figure 4-3 Geometry of the NEPTUN Heater Rod

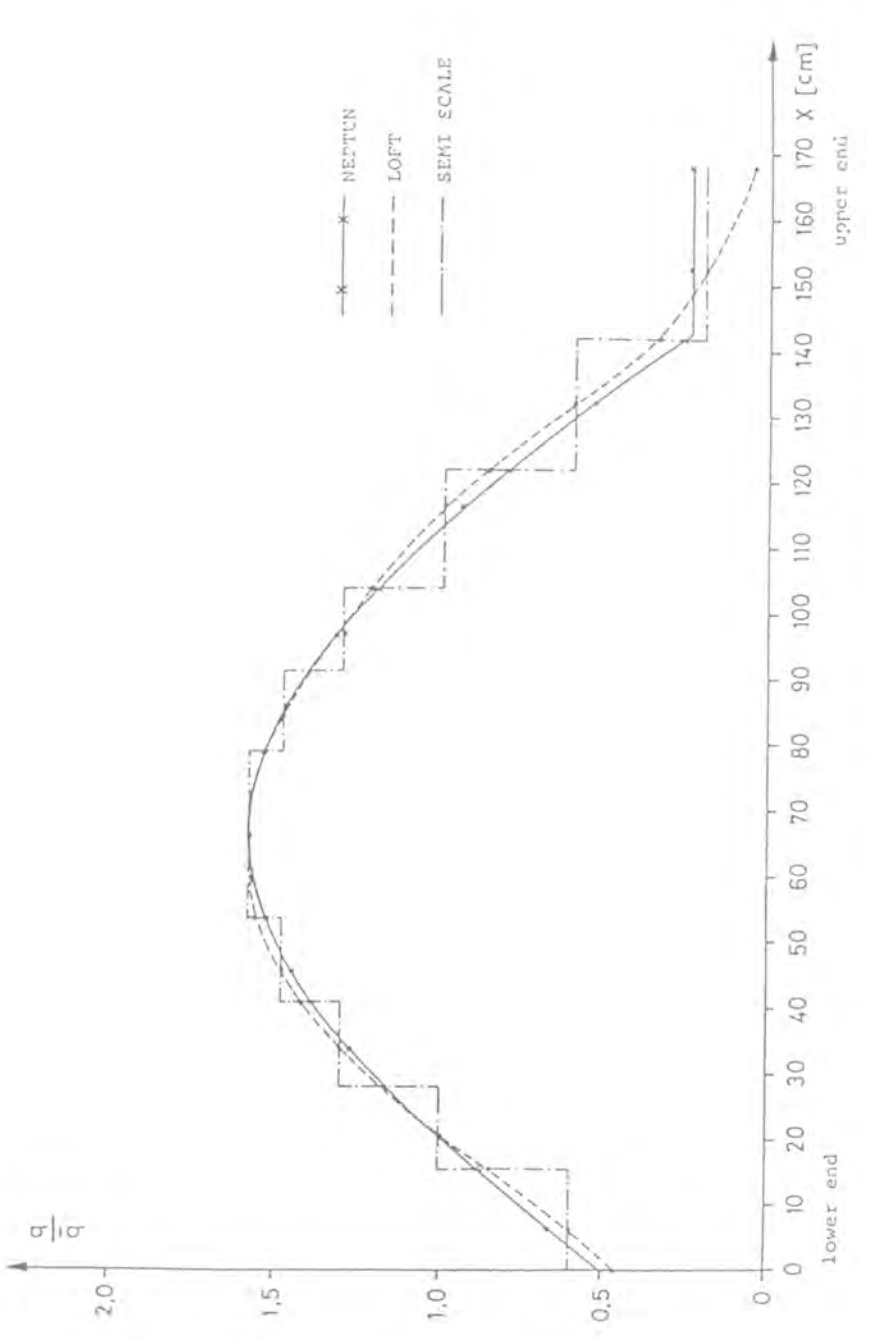

Figure 4-4 Axial Power Profile of the NEPTUN Heater Rod

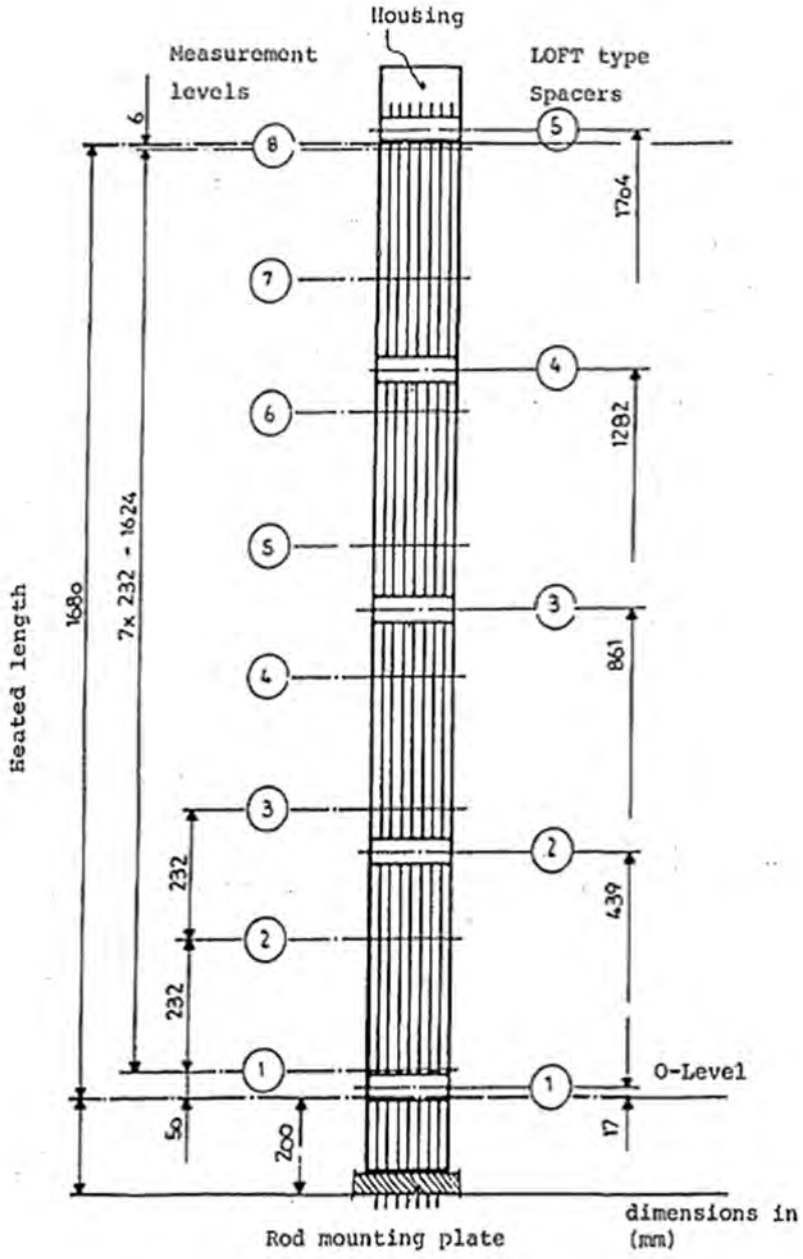

Figure 4-5 Axial Distribution of the Measurement Levels in the NEPTUN Facility

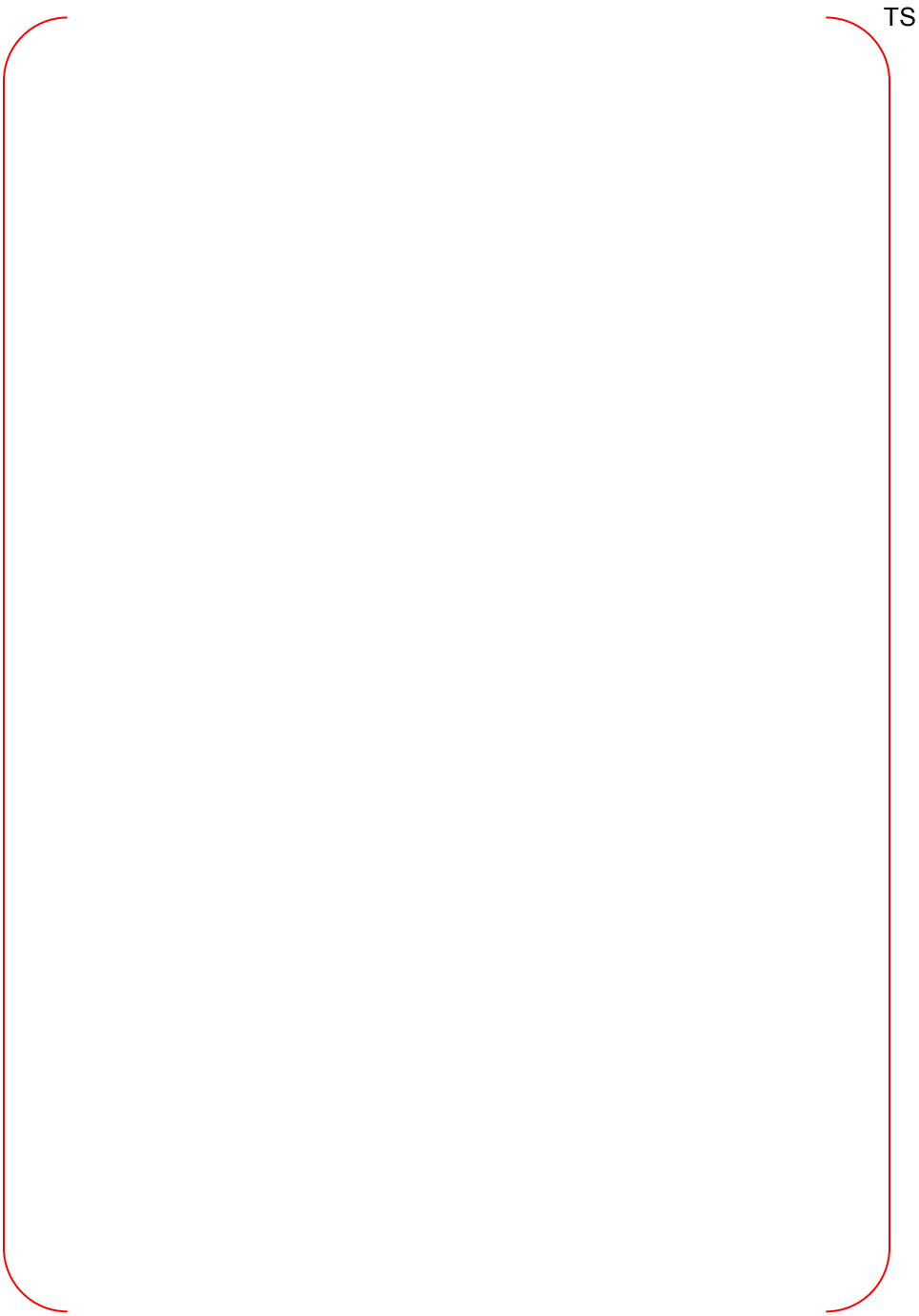

Figure 4-6 RELAP5/MOD3.3/K Nodalization of the NEPTUN Facility

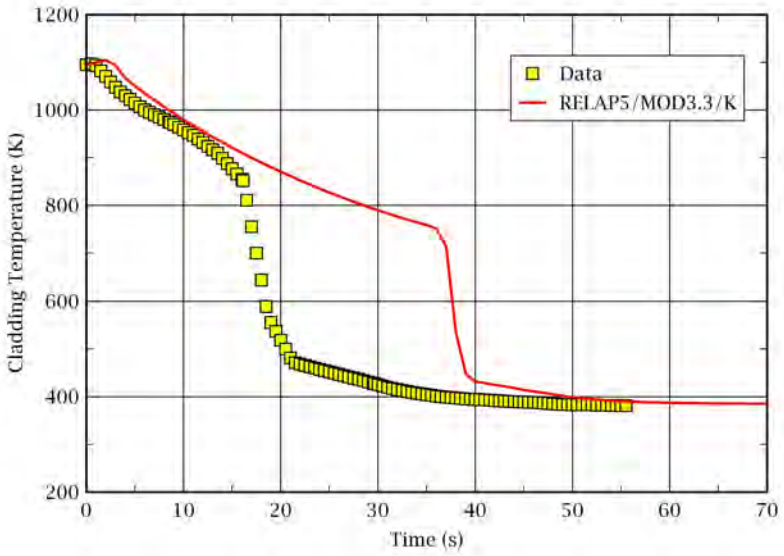

Figure 4-7 Rod Clad Temperatures at Measurement Level 3: Test 5050

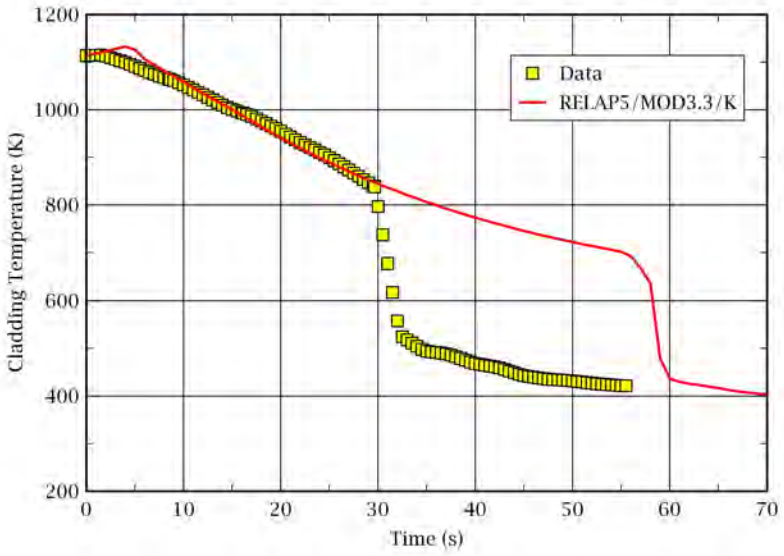

Figure 4-8 Rod Clad Temperatures at Measurement Level 4: Test 5050

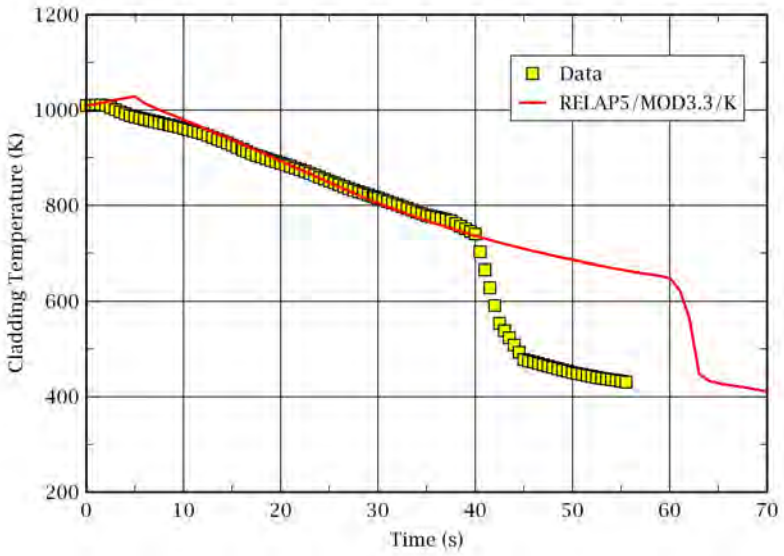

Figure 4-9 Rod Clad Temperatures at Measurement Level 5: Test 5050

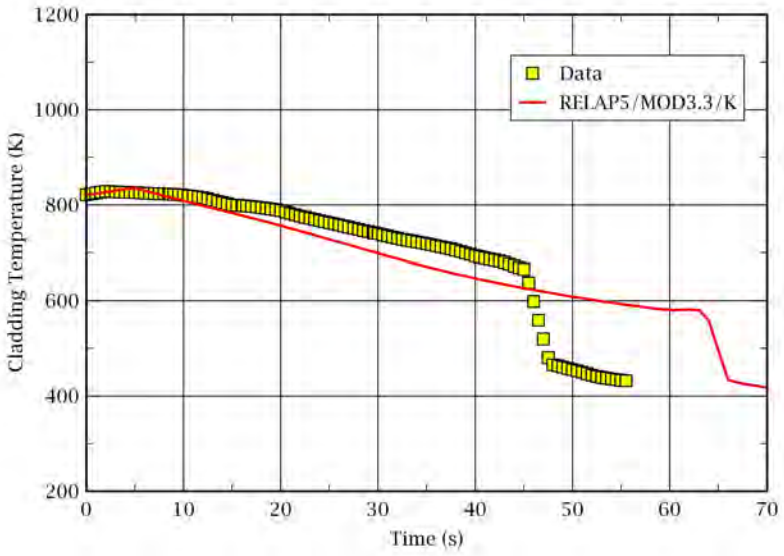

Figure 4-10 Rod Clad Temperatures at Measurement Level 6: Test 5050

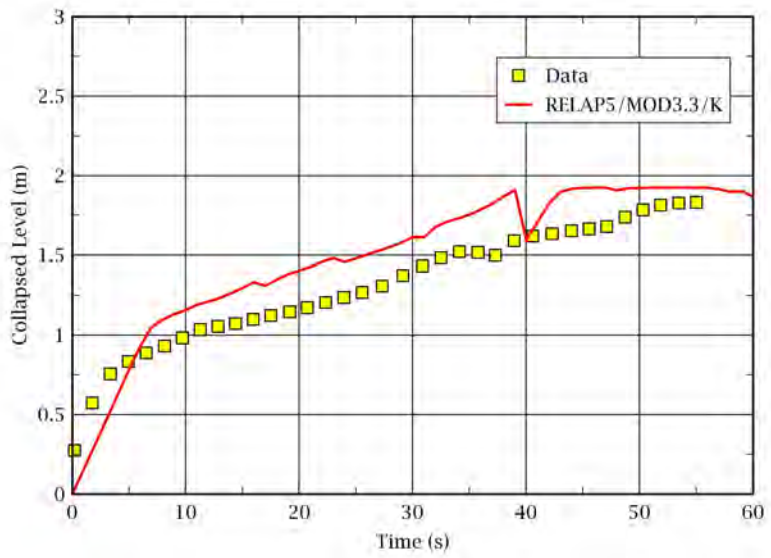

Figure 4-11 Collapsed Water Level in the Core: Test 5050

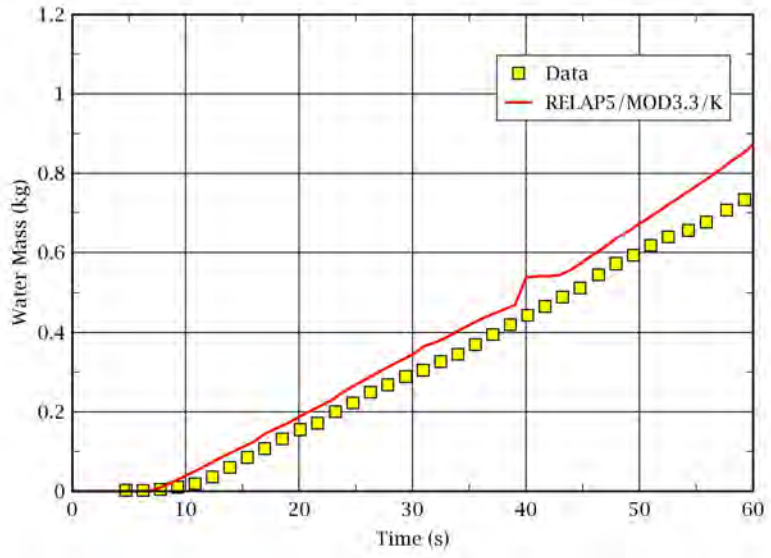

Figure 4-12 Water Carry-over: Test 5050

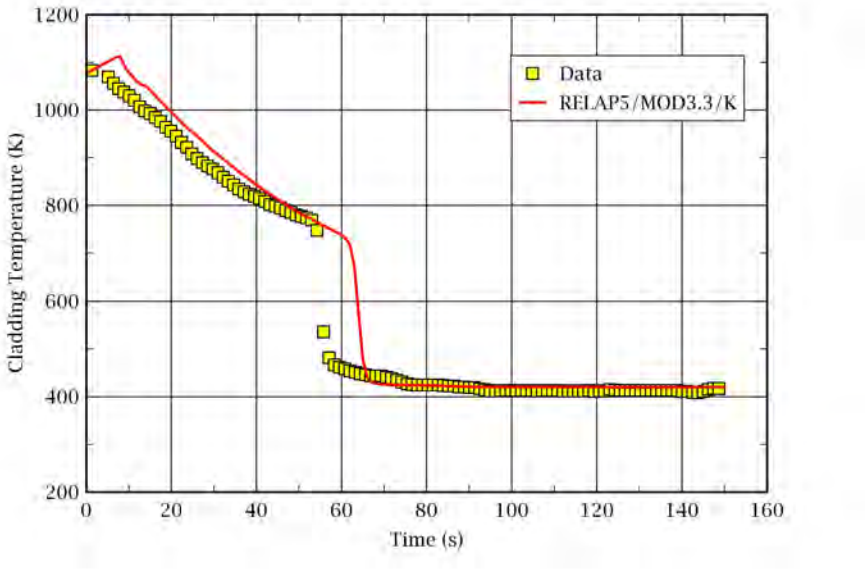

Figure 4-13 Rod Clad Temperatures at Measurement Level 3: Test 5051

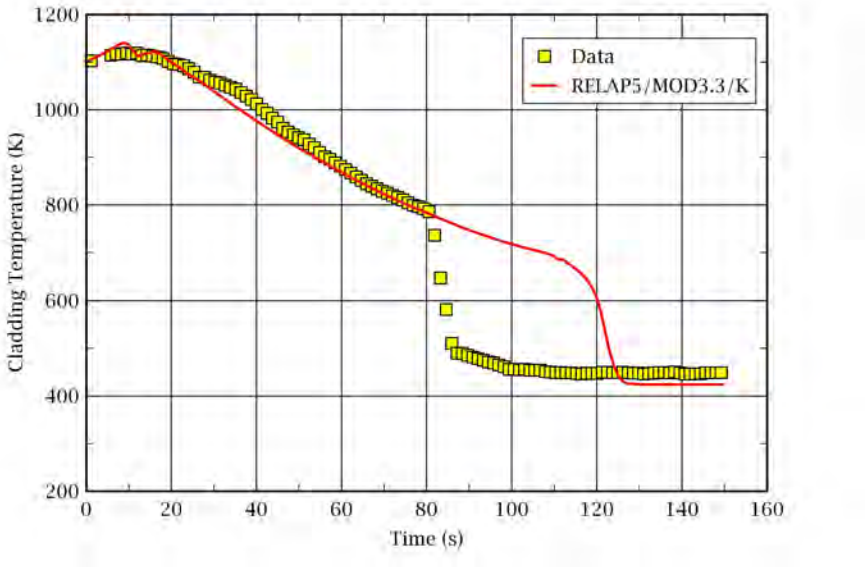

Figure 4-14 Rod Clad Temperatures at Measurement Level 4: Test 5051

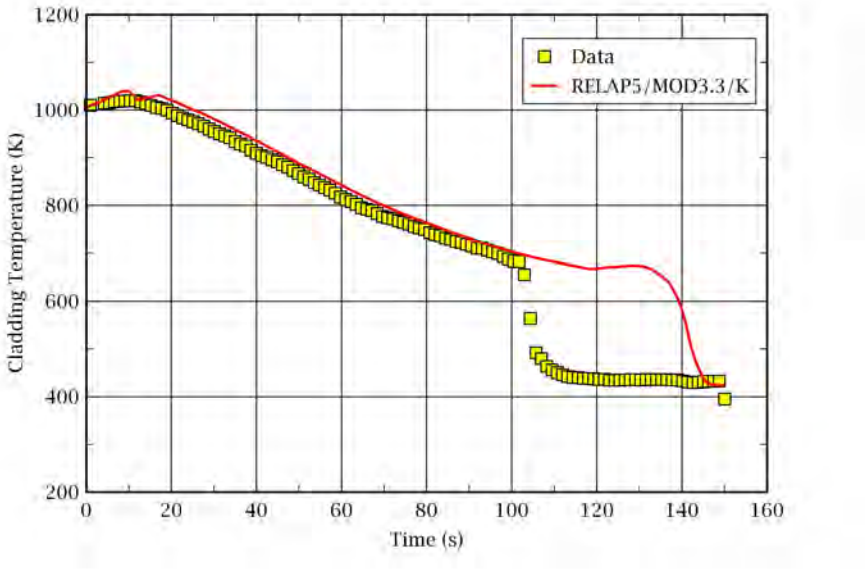

Figure 4-15 Rod Clad Temperatures at Measurement Level 5: Test 5051

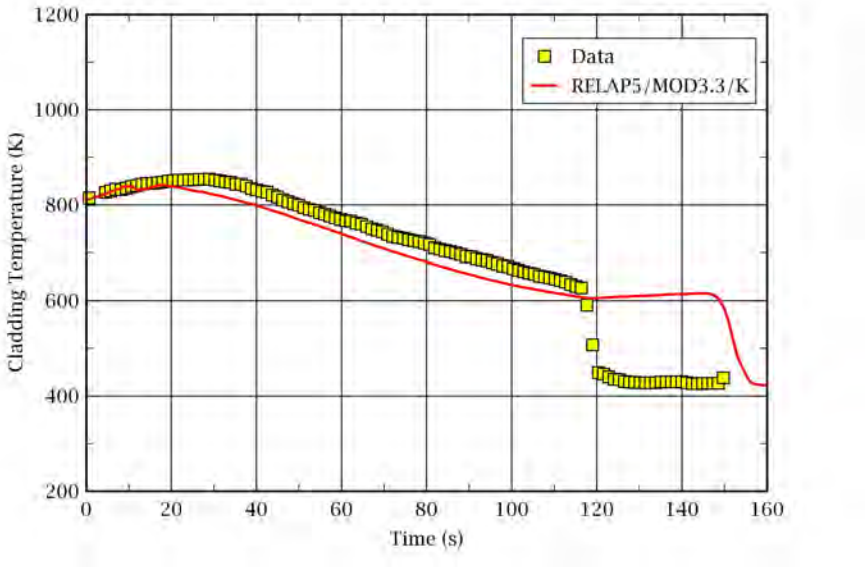

Figure 4-16 Rod Clad Temperatures at Measurement Level 6: Test 5051

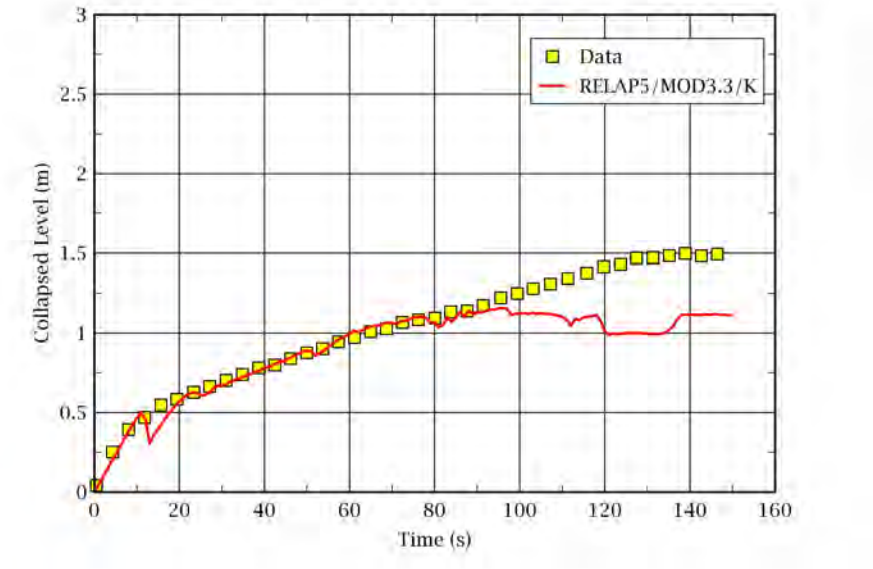

Figure 4-17 Collapsed Water Level in the Core: Test 5051

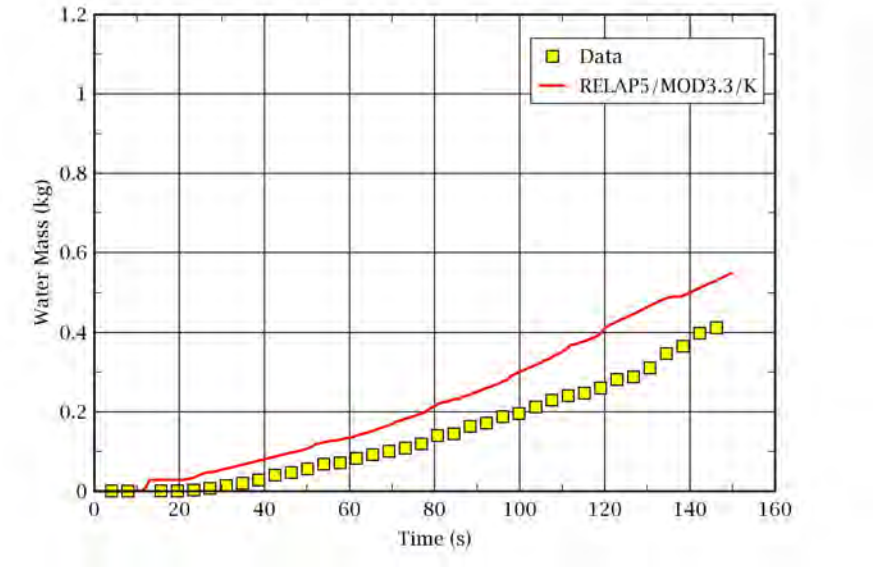

Figure 4-18 Water Carry-over: Test 5051

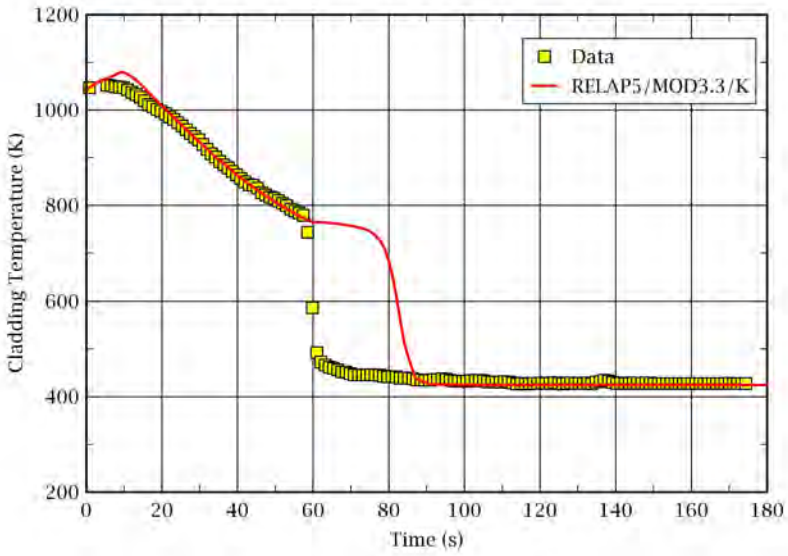

Figure 4-19 Rod Clad Temperatures at Measurement Level 3: Test 5052

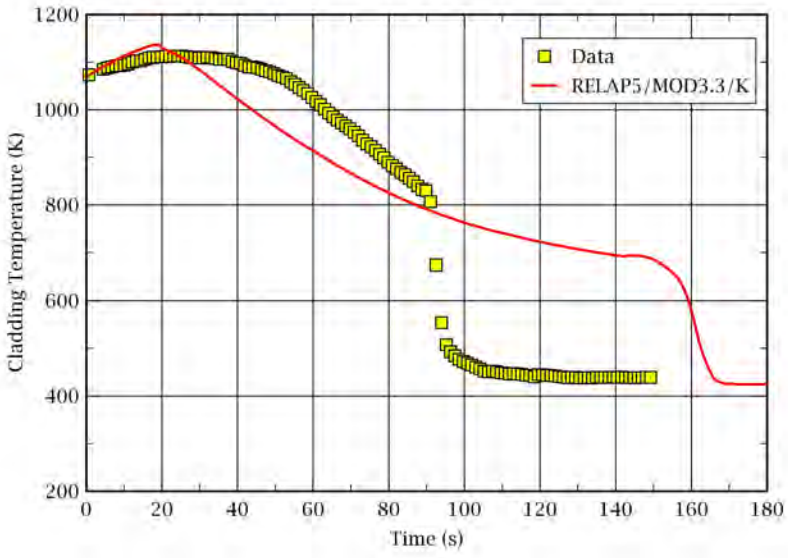

Figure 4-20 Rod Clad Temperatures at Measurement Level 4: Test 5052

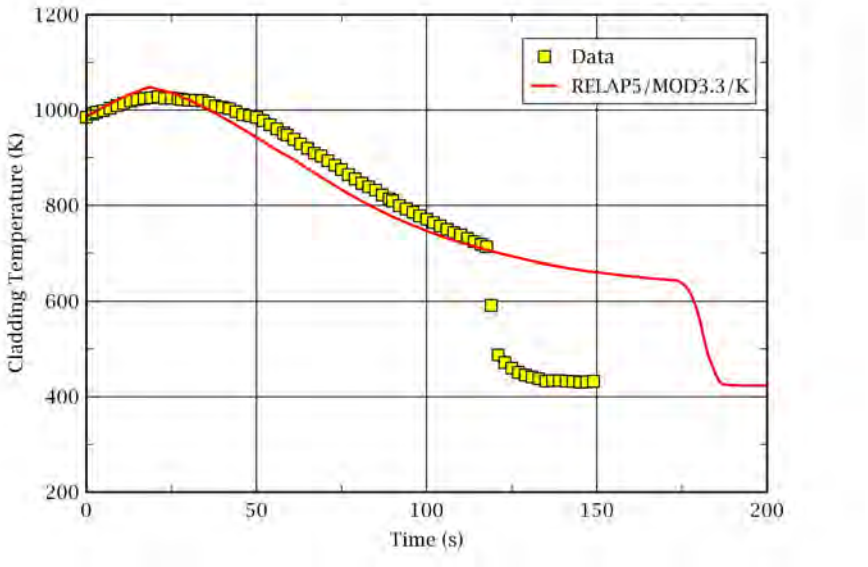

Figure 4-21 Rod Clad Temperatures at Measurement Level 5: Test 5052

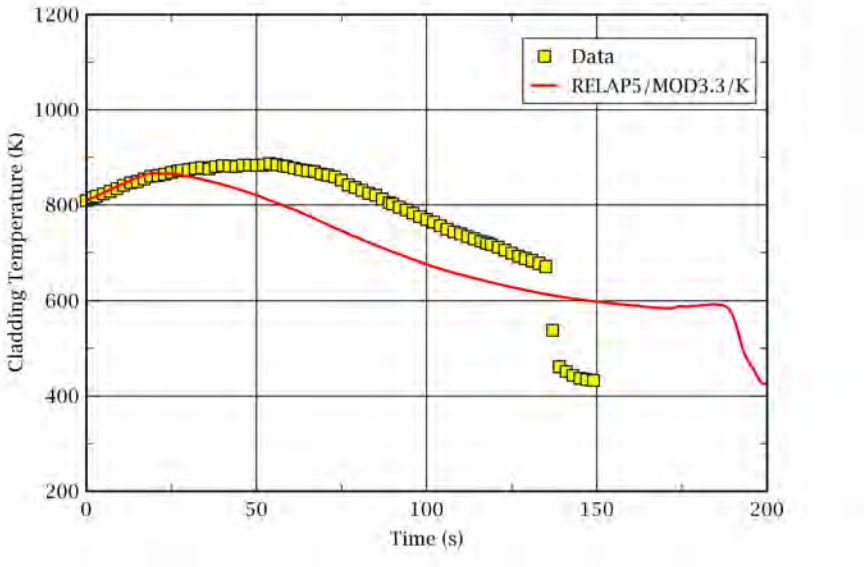

Figure 4-22 Rod Clad Temperatures at Measurement Level 6: Test 5052

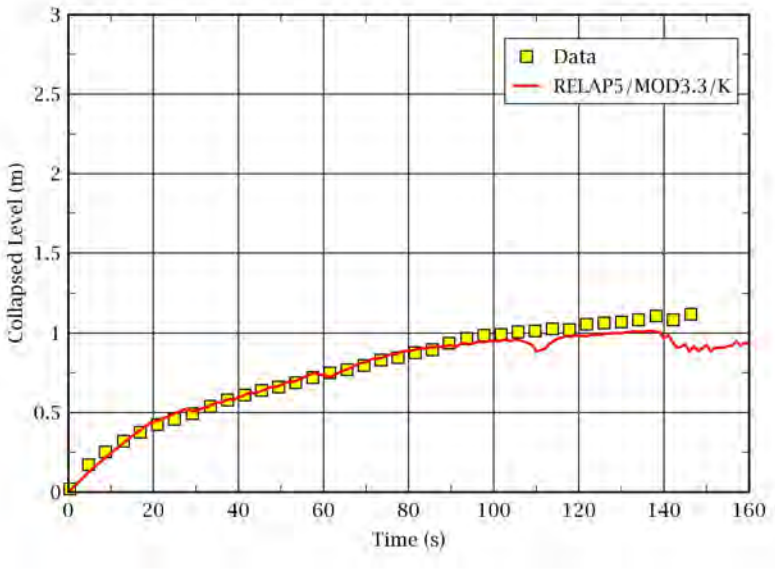

Figure 4-23 Collapsed Water Level in the Core: Test 5052

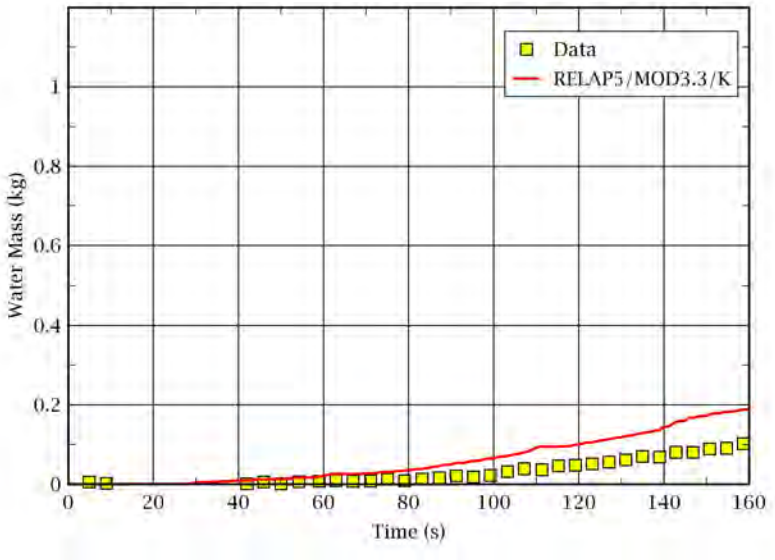

Figure 4-24 Water Carry-over: Test 5052

TS

Figure 4-25 Code Accuracy Calculated Using NEPTUN Test Data

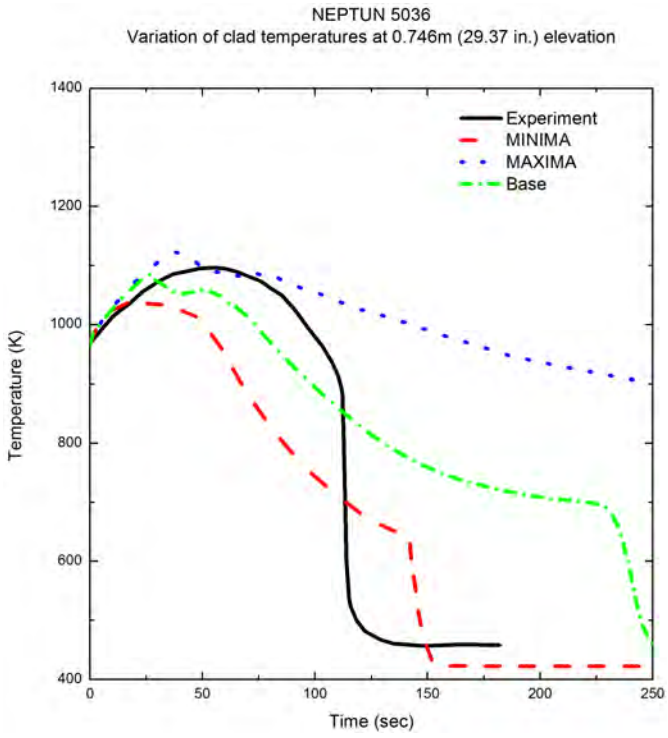

Figure 4-26 The Results of the SRS Calculations: Test 5036

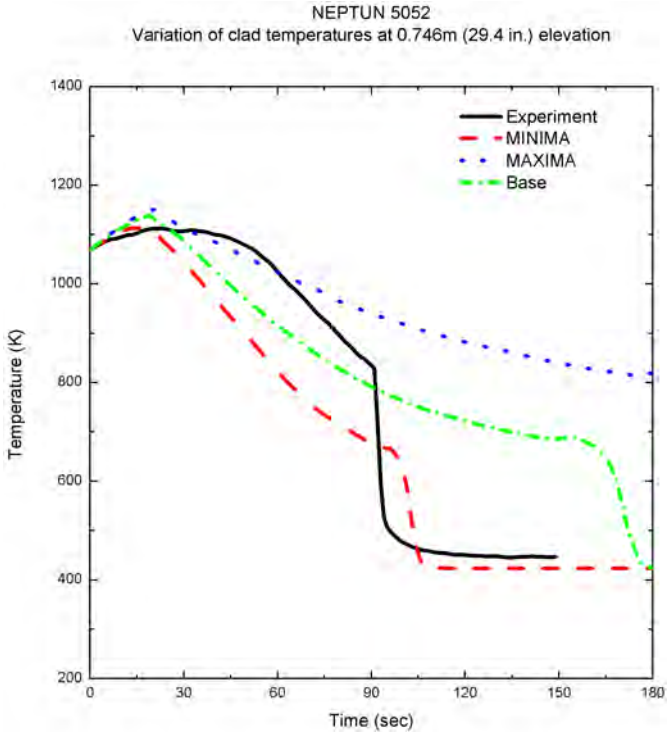

Figure 4-27 The Results of the SRS Calculations: Test 5052

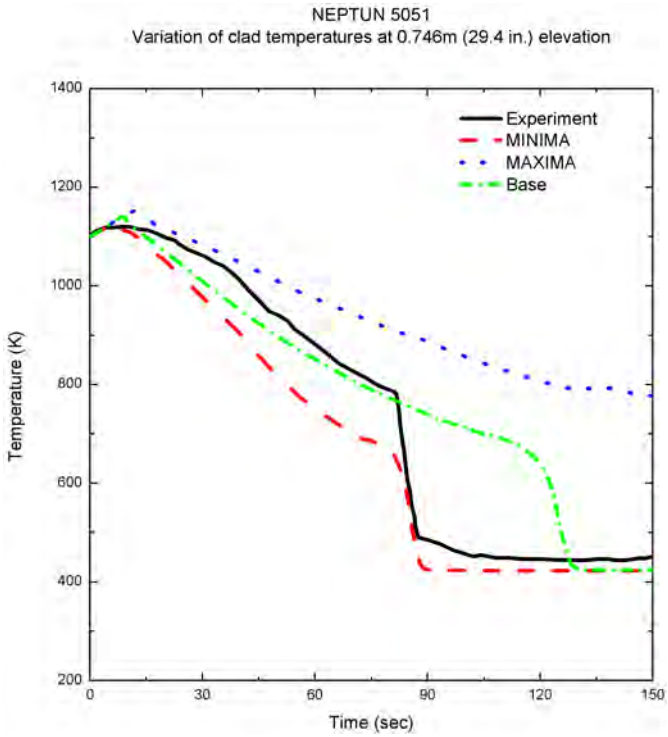

Figure 4-28 The Results of the SRS Calculations: Test 5051

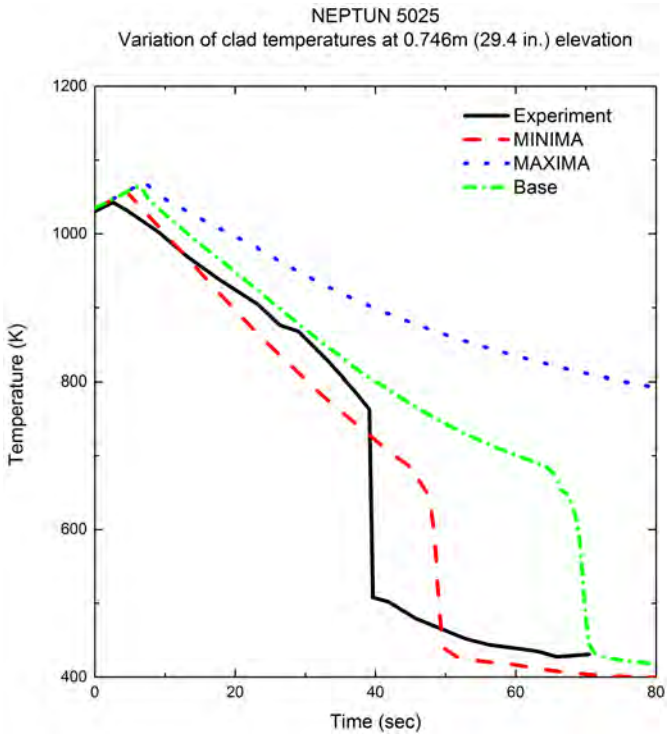

Figure 4-29 The Results of the SRS Calculations: Test 5025

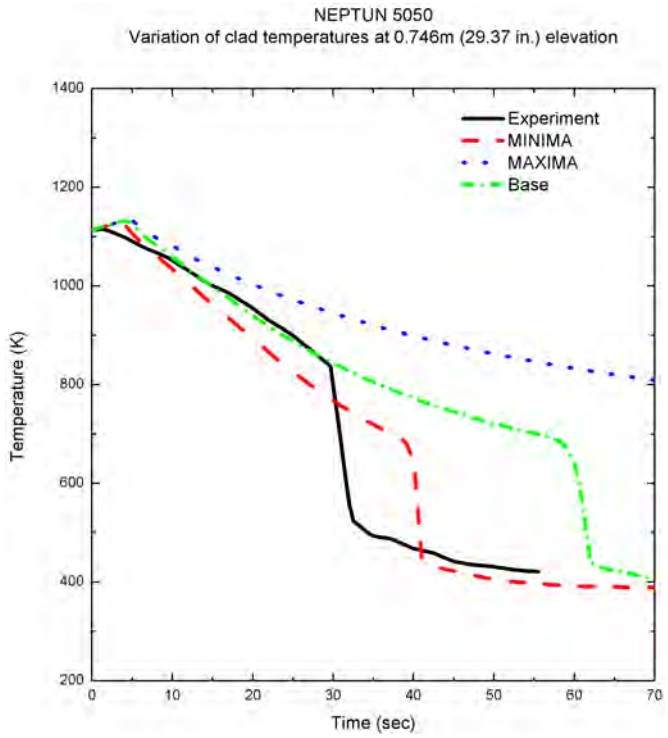

Figure 4-30 The Results of the SRS Calculations: Test 5050

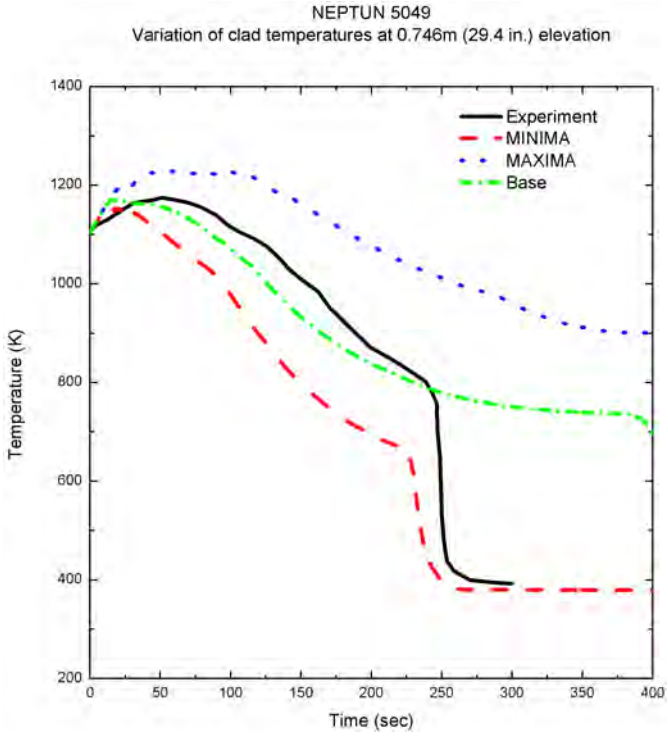

Figure 4-31 The Results of the SRS Calculations: Test 5049

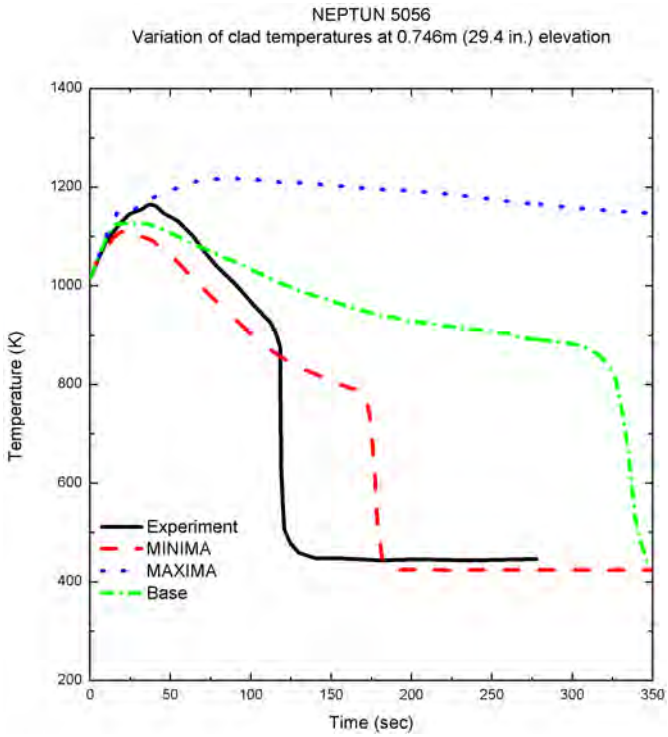

Figure 4-32 The Results of the SRS Calculations: Test 5056

5. Code Assessment against THTF

The Thermal-Hydraulic Test Facility (THTF) tests were part of the Oak Ridge National Laboratory (ORNL) PWR blowdown heat transfer separate effects program [5-1]. The objective of the program is to investigate the thermal-hydraulic phenomenon governing the energy transfer and transport processes that occur during a LOCA in a PWR system.

In this chapter, the capability of RELAP5/MOD3.3/K in predicting the blowdown progression is assessed against four blowdown tests conducted using the THTF facility.

5.1 Test Facility Description

The THTF facility, shown in Figure 5-1, consisted of the following major components:

- a test section with a 49-rod, 3.66 m long (12 ft) electrically heated core,
- a circulation loop comprised of three parallel heat exchangers with bypass, a pressurizer, a pump with bypass, and associated control valves,
- two rupture assemblies, and
- a pressure-suppression system

The heater rod bundle of the THTF facility contained 49 rods which consisted of 45 heater rods and 4 unheated rods. These rods were placed in 7x7 geometry. The heater rod had the outside diameter of 10.72 mm (0.422 in) and a chopped cosine axial power profile. The maximum power was 7.0 kW/ft and the ratio of maximum to average power was 1.67. The break configuration was 40 % inlet - 60 % outlet with a total break of 12.54 cm^2 (0.0135 ft^2). The main heat exchangers were operated to match the core power input. The design data of the THTF facility is summarized in Table 5-1. A cross-sectional view of the test section and the location of thermocouples in the bundle are shown in Figure 5-2 and Figure 5-3, respectively.

THTF blowdown tests began with opening two rupture disks simultaneously. The effluent from the primary system was ejected into the pressure suppression tank, which was maintained at atmospheric pressure. The primary coolant pump was tripped in coincident with the break initiation. However, full power (5.968 MW) was supplied until 2 s after the break initiation and then power was decayed exponentially with a time constant of 0.45 s until 5.8 s.

The instrument responses were recorded by a computer-controlled digital data acquisition system (CCDAS) or analog tape system. The measurement uncertainties are as follows:

- Pressure measurement uncertainty

  CCDAS: < +2.7 % of the measurement span

  Analog tape system: < +2.9 % of the measurement span

- Flow measurement uncertainty

  CCDAS: < 1.094 % of the measurement span

  Analog tape system: < 1.45 % of the measurement span

- Differential pressure measurement uncertainty

  CCDAS: < 1.07 % of the measurement span

  Analog tape system: < 1.43 % of the measurement span

- Density measurement uncertainty < 4 % of the measurement span

5.2 RELAP5/MOD3.3/K Model Description

The RELAP5/MOD3.3/K input model of the THTF facility is shown in Figure 5-4.

Modeling of the core was determined based on the previous simulation using the RELAP4 [5-1]. The core temperature variation in a radial direction was insignificant because the one-dimensional effect was dominant in the THTF tests. But the core was divided into three channels in the previous simulation using RELAP4. As a result, the outside channel temperature was predicted several hundred degrees lower than those of the center channel. [ ]^{TS} Therefore, the core is modeled with [ ]^{TS} in the simulation using the RELAP5/MOD3.3/K.

The primary loop is explicitly modeled. The heat structure of each component is also explicitly modeled. The pressure loss in the flow control valve was obtained by [ ]^{TS} The measured secondary side conditions, such as flow rate and fluid temperature, of the heat exchangers are set in the time dependent junctions and time dependent volumes as a function of time. The measured pump speed is also set in the input as a function of time.

5.3 RELAP5/MOD3.3/K Simulation

As indicated in Table 5-2, four tests are selected for RELAP5/MOD3.3/K assessment. The test conditions of these tests are almost the same, except for a system flow rate and power, as shown in Table 5-2. The system flow rate varies from 8.63E6 kg/m^2/hr to 12.2E6 kg/m^2/hr and the power varies from 80 kW/rod to 122 kW/rod.

In all simulations, the discharge coefficient of [ ]^{TS} is applied to the break junction. These discharge coefficients are [ ]^{TS} as determined in Step 8.2 of the CAREM.

In this section, the results of the simulation against THTF-105 are discussed in detail. Because the thermal-hydraulic behaviors of the THTF-151, the THTF-160, and the THTF-162 are similar with the THTF-105, the results of these tests are not discussed in detail, but the predicted clad temperatures are compared with the measured values.

5.3.1 THTF-105

THTF-105 was conducted under such conditions as a test section inlet temperature of 558 K, test section outlet temperature of 607 K, system pressure of 15.5 MPa, system flow rate of 12.2E6 kg/m^2/hr, and power of 122 kW/rod.

Break flow governs the system thermal-hydraulic behavior during the blowdown phase. However, because the data of the break flow is unavailable, the capability of the RELAP5/MOD3.3/K in predicting the break flow is judged based on the other predicted parameters such as differential pressures, pressures, and rod clad temperatures.

The predicted differential pressure at the pump inlet-outlet matches the experimental data well as shown in Figure 5-5. This implies that the RELAP5/MOD3.3/K predicts well the pump characteristics and flow behaviors in the cold leg during the transient.

The differential pressure at the inlet-outlet of the test section is shown in Figure 5-6. The flow reversal occurs in the core due to a negative differential pressure. The RELAP5/MOD3.3/K predicts earlier core flow reversal than the data, and the code over-predicts negative differential pressure until 8 s. In general, however, the general trend of the predicted differential pressure at the inlet-outlet of the test section is close to the measured data.

The pressure behaviors in the test section and pressurizer are shown in Figure 5-7 through Figure 5-9. The predicted pressure behaviors match the experimental data well. From these figures, the capability of the RELAP5/MOD3.3/K in predicting system hydraulics is confirmed.

Figure 5-10 shows a comparison of measured and calculated values of rod clad temperatures at 1.09 m (43 in) from the heated rod bottom. The RELAP5/MOD3.3/K predicts the rod clad temperature fairly well until around 7 s. The predicted temperature shows a quench behavior around 2 s later than the data. The predicted temperature after 7 s is higher than the data. However, the RELAP5/MOD3.3/K predicts well the highest rod clad temperature at this elevation.

Figure 5-11 shows a comparison of measured and calculated values of the rod clad temperatures at 1.96 m (77 in) from the heated rod bottom. The highest clad temperature was measured at this elevation. The RELAP5/MOD3.3/K over-predicts the highest measured temperature. This is due to that the predicted turn-around time is one second later than the data. The predicted rod quench time is later than the data with the same reason.

Figure 5-12 shows a comparison of measured and calculated values of rod clad temperatures at 3.18 m (125 in) from the heated rod bottom. The predicted rod temperature begins to heat-up at around 2.3 s whereas the measured value at around 5.3 s. This implies that the critical heat flux (CHF) is predicted to occur earlier than the data in the calculation. In both the test data and RELAP5/MOD3.3/K simulation, the increase of the rod clad temperature is insignificant at this elevation.

5.3.2 THTF-151, THTF-160, THTF-162

Because the thermal-hydraulic behaviors of THTF-151, THTF-160, and THTF-162 are similar with THTF-105, the results of these tests are not discussed in detail, but the predicted clad temperatures are compared with the measured values in Figure 5-13 through Figure 5-21.

For each test, the RELAP5/MOD3.3 calculated values of rod clad temperatures at three different elevations, such as 1.09 m (43 in), 1.96 m (77 in), and 3.18 m (125 in) from the heated rod bottom, are compared with the data.

The RELAP5/MOD3.3/K under-predicts the rod clad temperature at 1.09 m (43 in) from the heated rod bottom, in all simulations. However, the highest predicted clad temperature at 1.96 m (77 in) matches the data well, based on a comparison between the calculated value and the average measured value. The highest clad temperature (PCT) was measured at this elevation in all tests simulated in this section. The predicted temperatures at 1.96 m show a sharp decrease after turn-around time, in all simulations. At 1.09 m (43 in) from the heated rod bottom, the increase of the rod clad temperature is insignificant in both test data and RELAP5/MOD3.3/K simulations.

In general, the RELAP5/MOD3.3/K reasonably predicts rod clad temperatures, especially PCTs.

5.4 Code Accuracy

[

]TS

Figure 5-22 shows the code accuracy evaluated using [ ]TS test data. The RELAP5/MOD3.3/K over-predicts the rod clad temperature by [ ]TS on average with a standard deviation of [ ]TS

5.5 SRS Calculations

SRS calculations were performed against four THTF tests. [

]TS The uncertainty parameters and their distribution functions used for the SRS calculations are listed in Table 5-3.

Figures from Figure 5-23 through Figure 5-26 show the results of the SRS calculations against four tests. In all SRS calculations, the third highest values of the calculated clad temperatures are higher than the measured PCTs confirming the data covering. Therefore, the number and the probability distribution functions of the selected code parameters are confirmed to be sufficient.

5.6 Conclusion

The capability of the RELAP5/MOD3.3/K in predicting the blowdown progression was assessed against four THTF tests. The assessment results show that the RELAP5/MOD3.3/K is capable of calculating the blowdown process correctly, in general. The RELAP5/MOD3.3/K over-predicts rod clad temperature as confirmed by the evaluation of the code accuracy.

In all the SRS calculations against the four THTF tests, the data covering is confirmed. This implies that the number and the probability distribution functions of the selected code parameters for the blowdown heat transfer and the critical flow are sufficient to cover the measured PCTs.

References

[5-1] W.G. Craddick, et. al., “PWR Blowdown Heat Transfer Separate-Effects Program Data Evaluation Report: Heat Transfer for THTF Test Series 100,” NUREG/CR-0105 (ORNL/NUREG-45), Oak Ridge National Lab., 1978.

[5-2] “ORNL Rod Bundle Heat Transfer Test Data,” NUREG/CR-2525 Vol. 1-7 (ORNL/NUREG/TM-407), Oak Ridge National Lab., 1982.

[5-3] V.D. Clemons, M.D. White, P.A. Moore, R.A. Hedrick, “PWR Blowdown Heat Transfer Separate-Effects Program; Thermal-Hydraulic Test Facility Experimental Data Report for Test 103,” ORNL/NUREG/TM-187, Oak Ridge National Lab., 1978.

[5-4] D.M. Leon, M.D. White, R.A. Hedrick, “PWR Blowdown Heat Transfer Separate-Effects Program; Thermal-Hydraulic Test Facility Experimental Data Report for Test 151,” ORNL/NUREG/TM-188, Oak Ridge National Lab., 1978.

[5-5] D.M. Leon, M.D. White, R.A. Hedrick, “PWR Blowdown Heat Transfer Separate-Effects Program; Thermal-Hydraulic Test Facility Experimental Data Report for Test 153,” NUREG/CR-0278; ORNL/NUREG/TM-236, Oak Ridge National Lab., 1978.

[5-6] V.D. Clemons, M.D. White, R.A. Hedrick, “PWR Blowdown Heat Transfer Separate-Effects Program; Thermal-Hydraulic Test Facility Experimental Data Report for Test 155,” NUREG/CR-0279; ORNL/NUREG/TM-237, Oak Ridge National Lab., 1978.

[5-7] G.S. Massengill, M.D. White, “PWR Blowdown Heat Transfer Separate-Effects Program; Thermal-Hydraulic Test Facility Experimental Data Report for Test 157,” NUREG/CR-0280; ORNL/NUREG/TM-238, Oak Ridge National Lab., 1978

[5-8] V.D. Clemons, W.G. Craddick, R.M. Flanders, “PWR Blowdown Heat Transfer Separate-Effects Program; Thermal-Hydraulic Test Facility Experimental Data Report for Test 171,” NUREG/CR-0729; ORNL/NUREG/TM-277, Oak Ridge National Lab., 1980.

[5-9] V.D. Clemons, W.G. Craddick, M.D. White, “PWR Blowdown Heat Transfer Separate-Effects Program; Thermal-Hydraulic Test Facility Experimental Data Report for Test 160,” NUREG/CR-0730; ORNL/NUREG/TM-301, Oak Ridge National Lab., 1980.

[5-10] V.D. Clemons, W.G. Craddick, M.D. White, “PWR Blowdown Heat Transfer Separate-Effects Program; Thermal-Hydraulic Test Facility Experimental Data Report for Test 161,” NUREG/CR-0731; ORNL/NUREG/TM-302, Oak Ridge National Lab., 1980.

[5-11] V.D. Clemons, W.G. Craddick, M.D. White, “PWR Blowdown Heat Transfer Separate-Effects Program; Thermal-Hydraulic Test Facility Experimental Data Report for Test 162,” NUREG/CR-0732; ORNL/NUREG/TM-303, Oak Ridge National Lab., 1980.

[5-12] V.D. Clemons, W.G. Craddick, R.M. Flanders, “PWR Blowdown Heat Transfer Separate-Effects Program; Thermal-Hydraulic Test Facility Experimental Data Report for Test 163,” NUREG/CR-0732; ORNL/NUREG/TM-303, Oak Ridge National Lab., 1980.

[5-13] V.D. Clemons, W.G. Craddick, R.M. Flanders, “PWR Blowdown Heat Transfer Separate-Effects Program; Thermal-Hydraulic Test Facility Experimental Data Report for Test 164R,” NUREG/CR-0734; ORNL/NUREG/TM-305, Oak Ridge National Lab., 1980.

[5-14] V.D. Clemons, W.G. Craddick, M.D. White “PWR Blowdown Heat Transfer Separate-Effects Program; Thermal-Hydraulic Test Facility Experimental Data Report for Test 165,” NUREG/CR-0735; ORNL/NUREG/TM-306, Oak Ridge National Lab., 1980.

Table 5-1 Design Data of the THTF Facility

Design Parameters	Design Values
1. Heater Rod	
number (including 4 unheated rod)	49
diameter (in)	0.422
distance between centers	0.563
maximum/average power	1.67
2. Shroud Box	
inside dimension (in)	4×4
outside dimension (in)	6×5.5
3. Pressure Vessel	
inside diameter (in)	8.75
outside diameter (in)	10.75
length (in)	15
4. Primary System	
nominal pipe diameter (in)	4
total system volume (ft^3)	21.44
5. Pressurizer	
inside diameter (in)	10.5
length (ft)	11
steady state heat generation (kW)	24
normal water level	50%
6. Pump	
type	Bingham
stage	2
flow (gpm)	700
head (ft)	1940
pump power (kW)	450

Table 5-2 THTF Tests Used for the RELAP5/MOD3.3/K Assessment

Test Number	Inlet temperature (K)	Outlet temperature (K)	Pressure (MPa)	Mass flux (10^6 kg/m^2-hr)	Power (kW/rod)
105	558.0	607.0	15.5	12.2	122.0
151	558.2	606.5	15.7	11.2	122.0
160	558.3	608.1	15.5	8.63	80.0
162	558.3	597.8	15.8	11.2	100.0

Table 5-3 Parameters and Distribution Functions Used for the SRS Calculations: THTF

TS

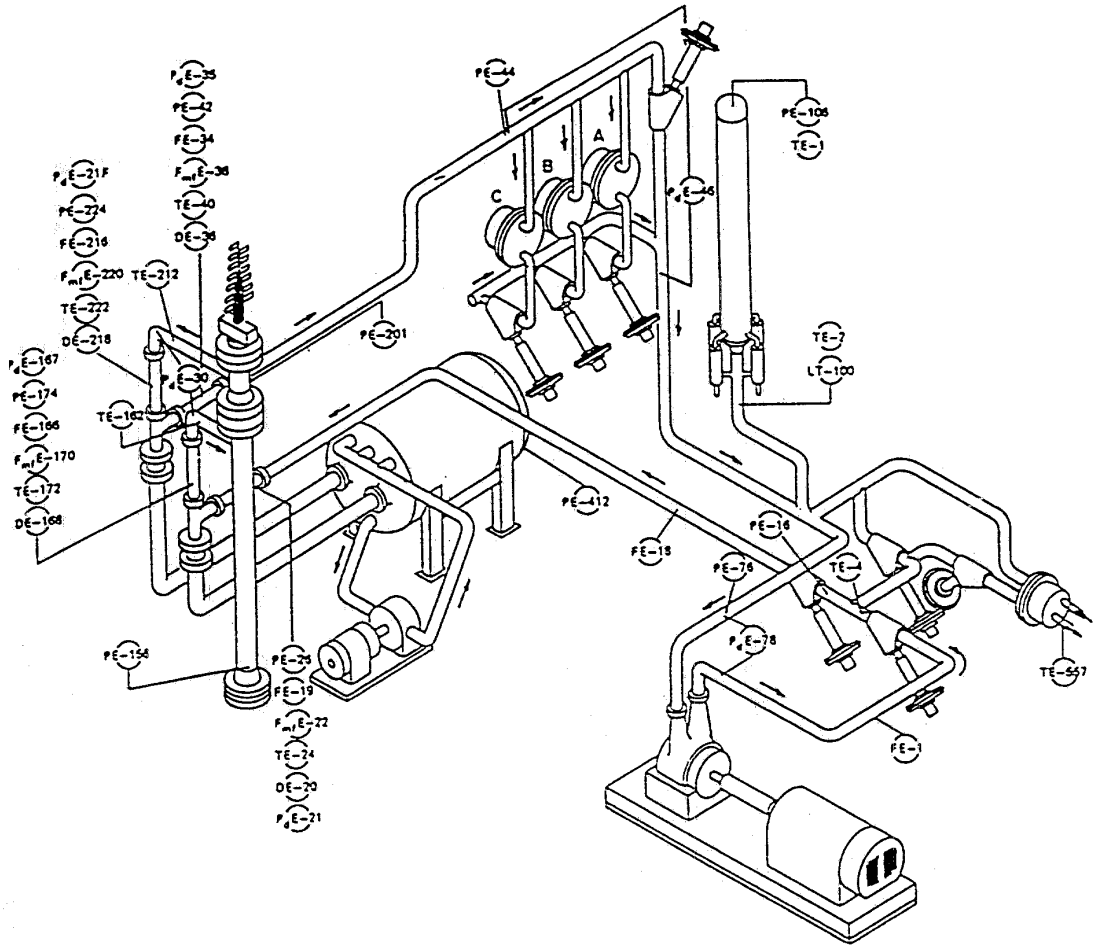

Figure 5-1 Configuration of the THTF

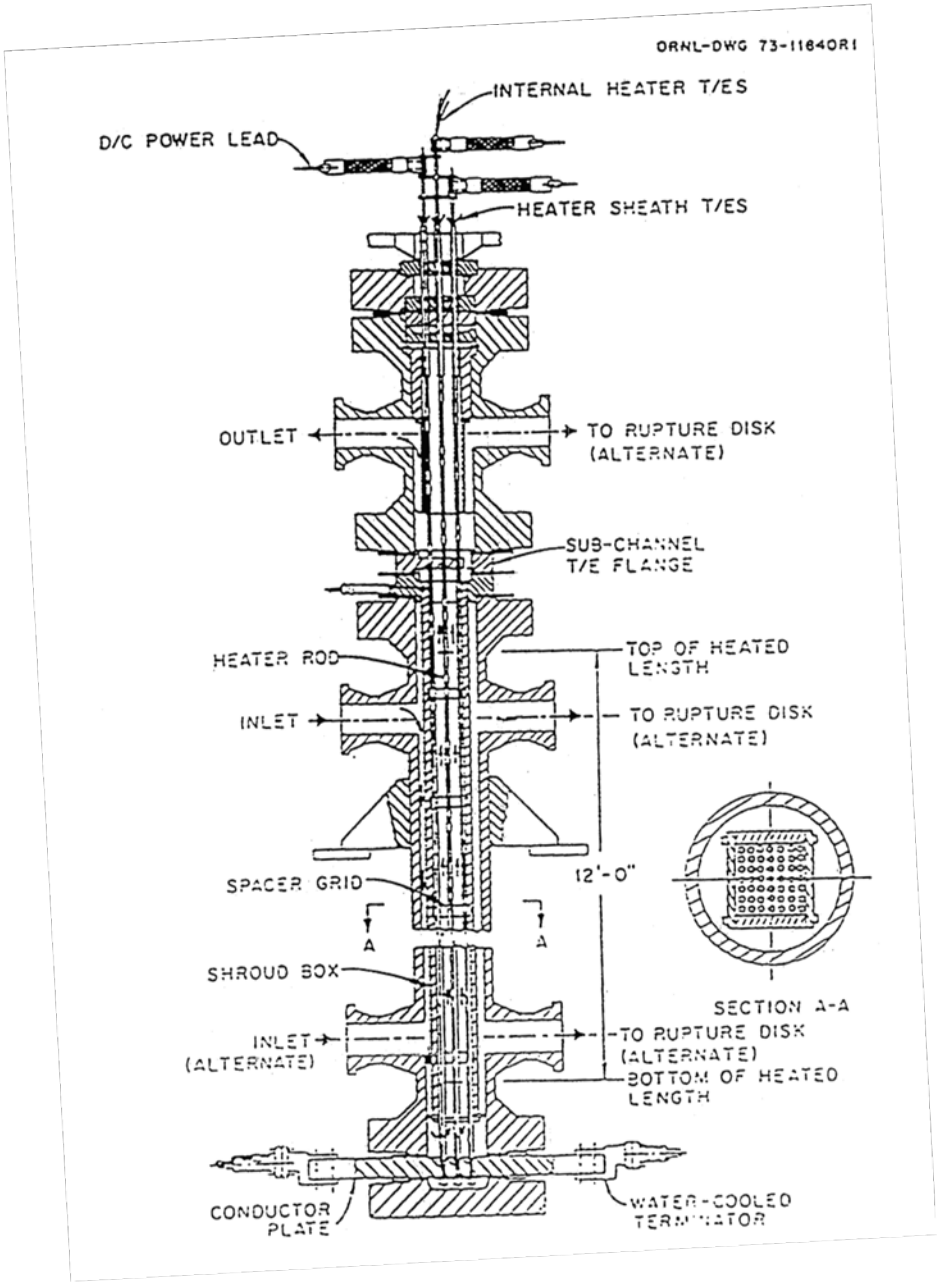

Figure 5-2 Test Section of the THTF

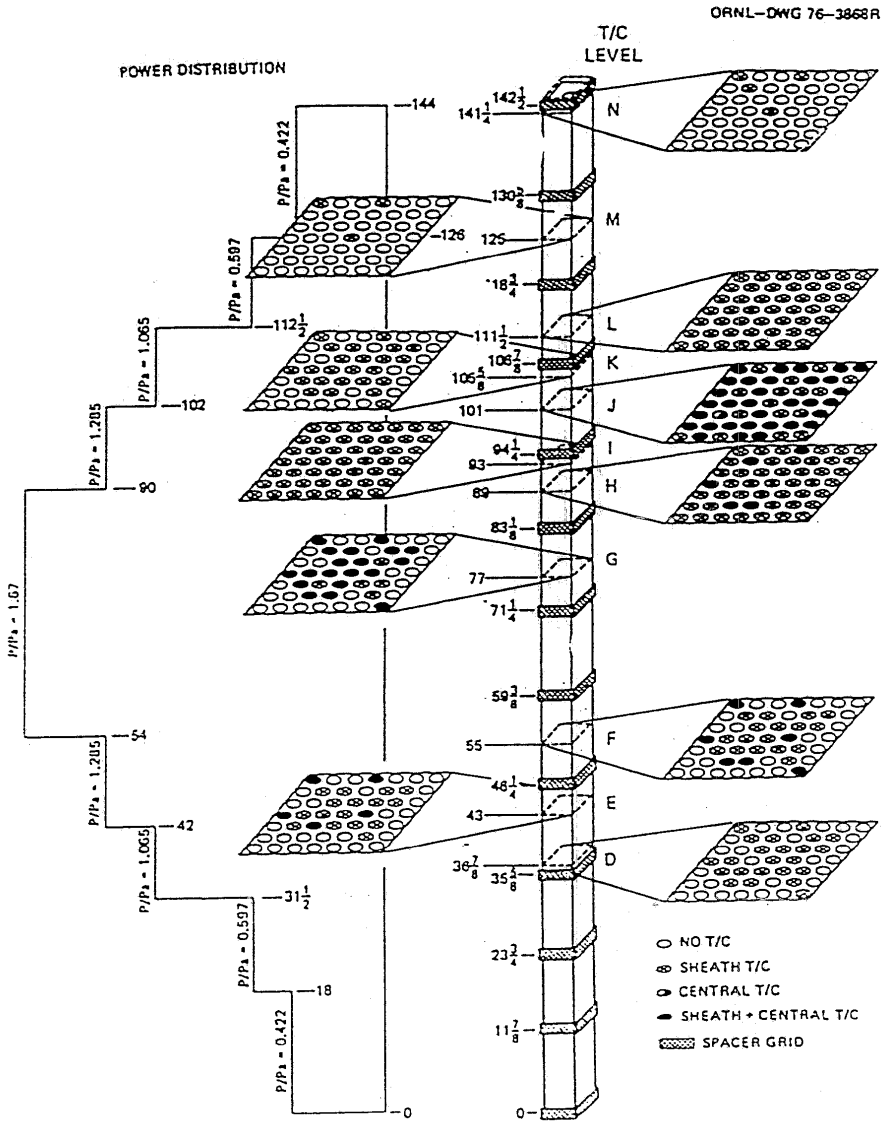

Figure 5-3 Thermocouple Locations in the Rod Bundle of the THTF

Figure 5-4 RELAP5/MOD3.3/K Nodalization of the THTF

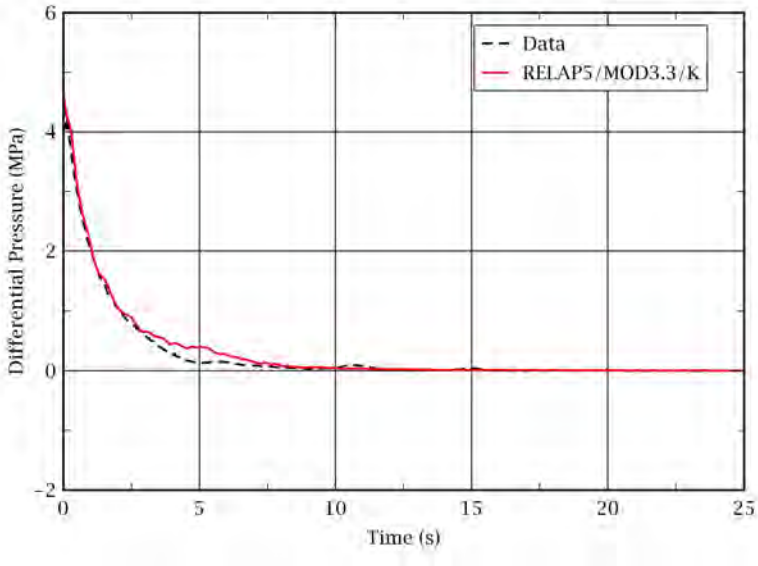

Figure 5-5 Differential Pressure at the Pump Inlet – Outlet: THTF-105

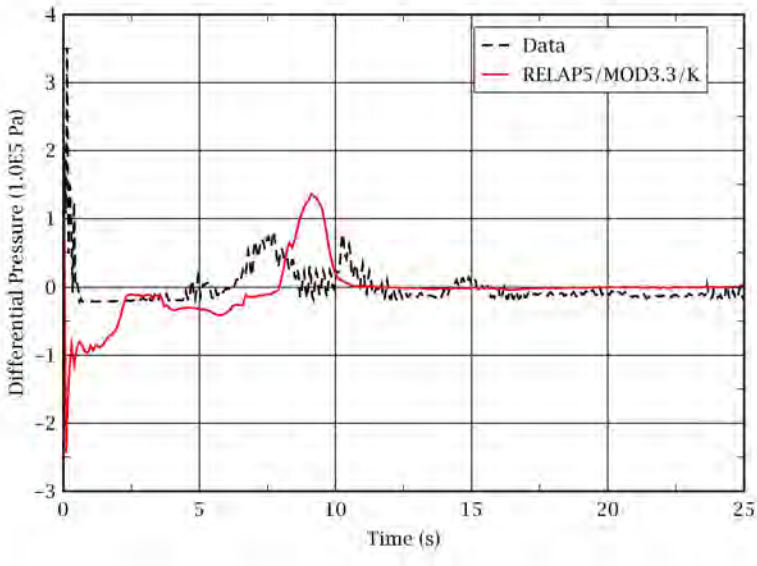

Figure 5-6 Differential Pressure at the Test Section Inlet – Outlet: THTF-105

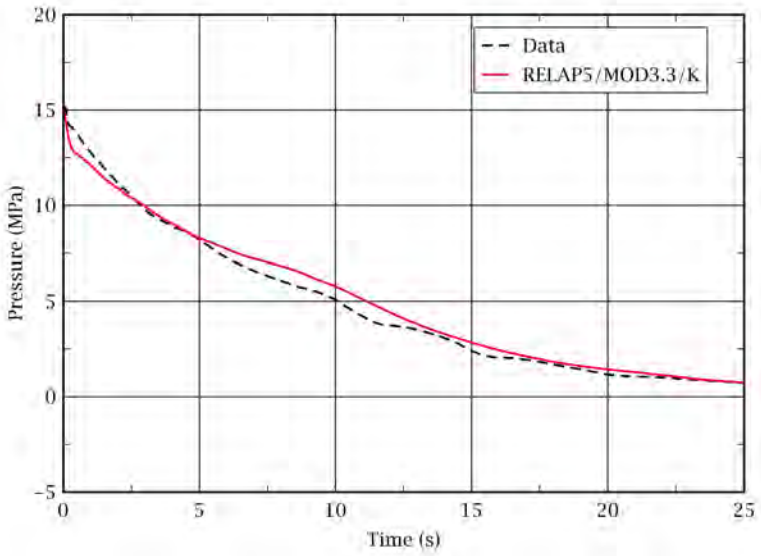

Figure 5-7 Pressure at the Pressurizer Top: THTF-105

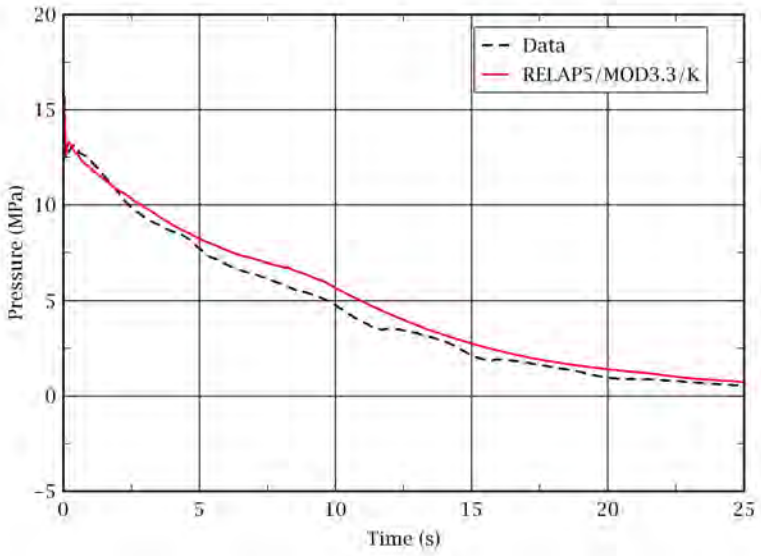

Figure 5-8 Pressure at the Test Section Inlet: THTF-105

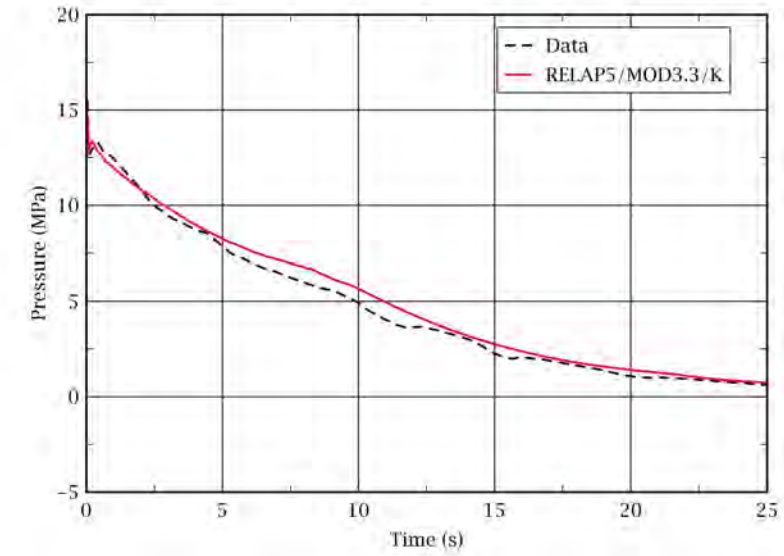

Figure 5-9 Pressure at the Test Section Outlet: THTF-105

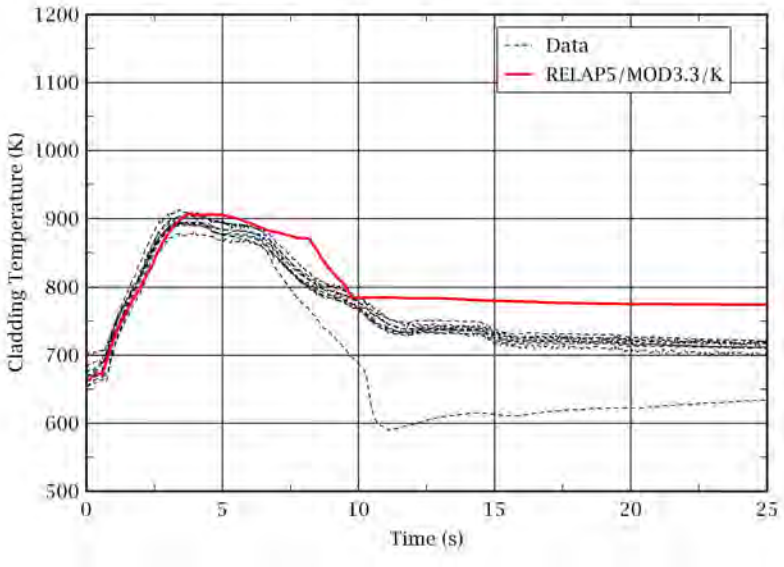

Figure 5-10 Rod Clad Temperatures at 43 in. from the Heated Bottom: THTF-105

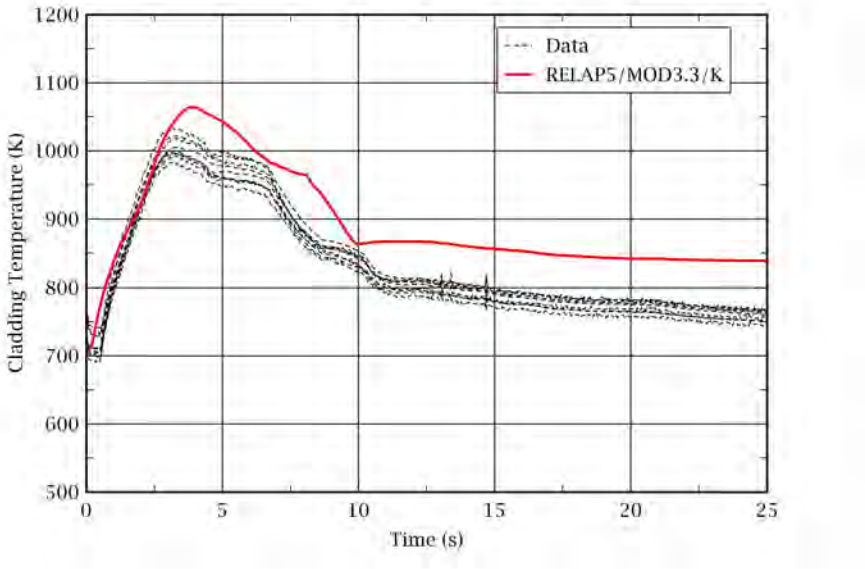

Figure 5-11 Rod Clad Temperatures at 77 in. from the Heated Bottom: THTF-105

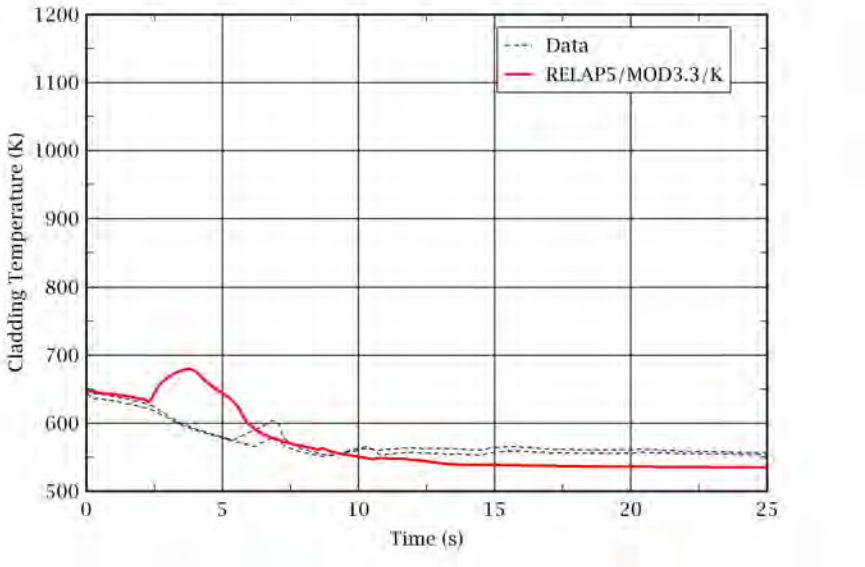

Figure 5-12 Rod Clad Temperatures at 125 in. from the Heated Bottom: THTF-105

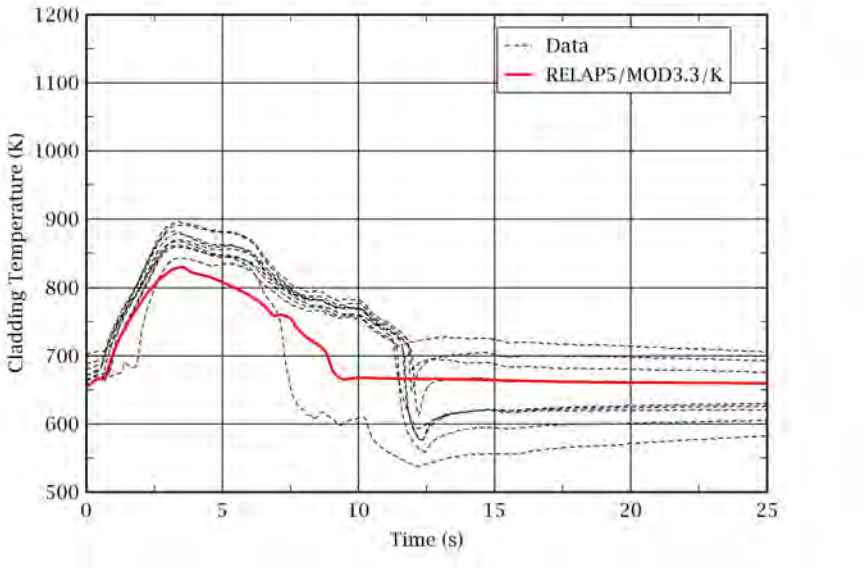

Figure 5-13 Rod Clad Temperatures at 43 in. from the Heated Bottom: THTF-151

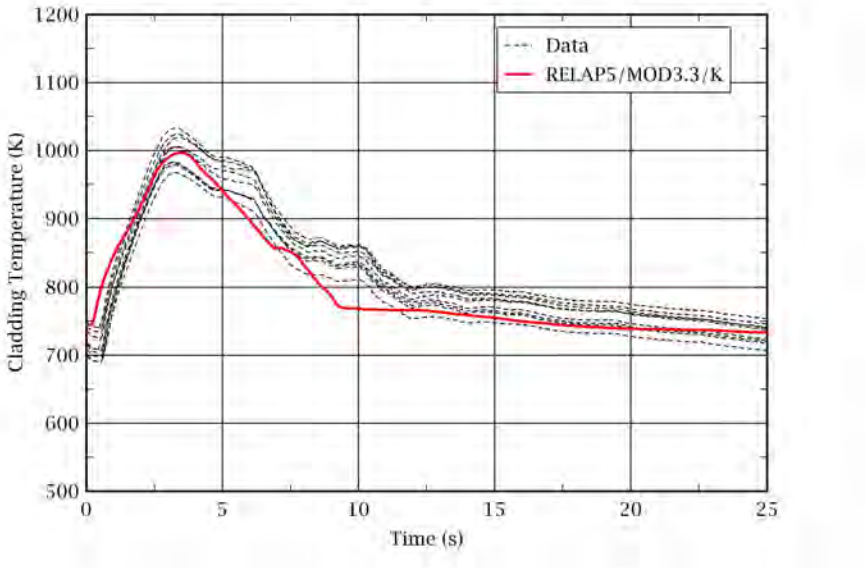

Figure 5-14 Rod Clad Temperatures at 77 in. from the Heated Bottom: THTF-151

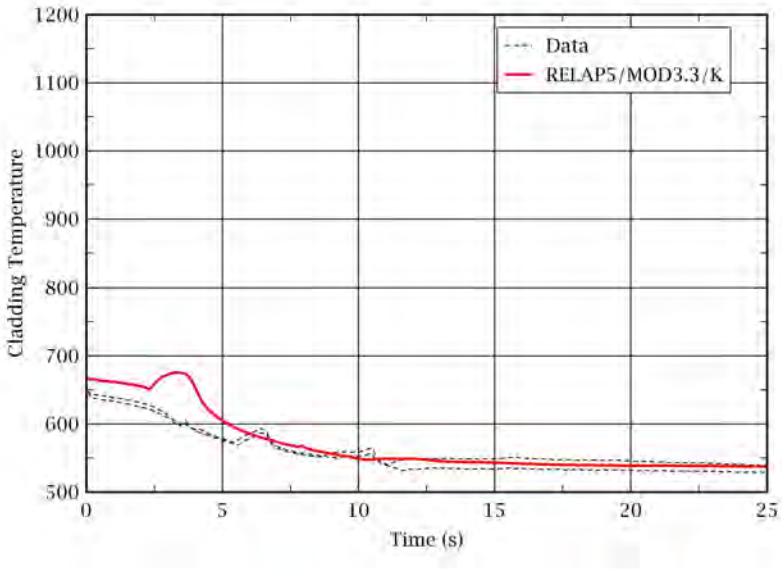

Figure 5-15 Rod Clad Temperatures at 125 in. from the Heated Bottom: THTF-151

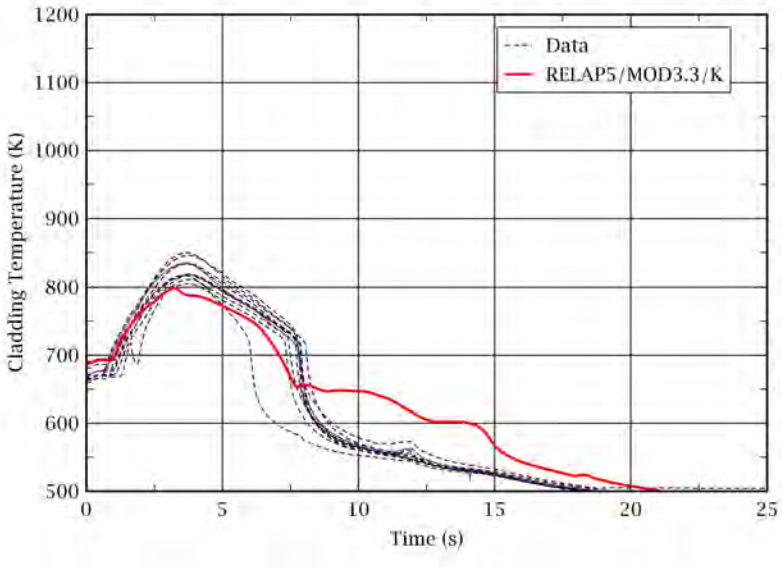

Figure 5-16 Rod Clad Temperatures at 43 in. from the Heated Bottom: THTF-160

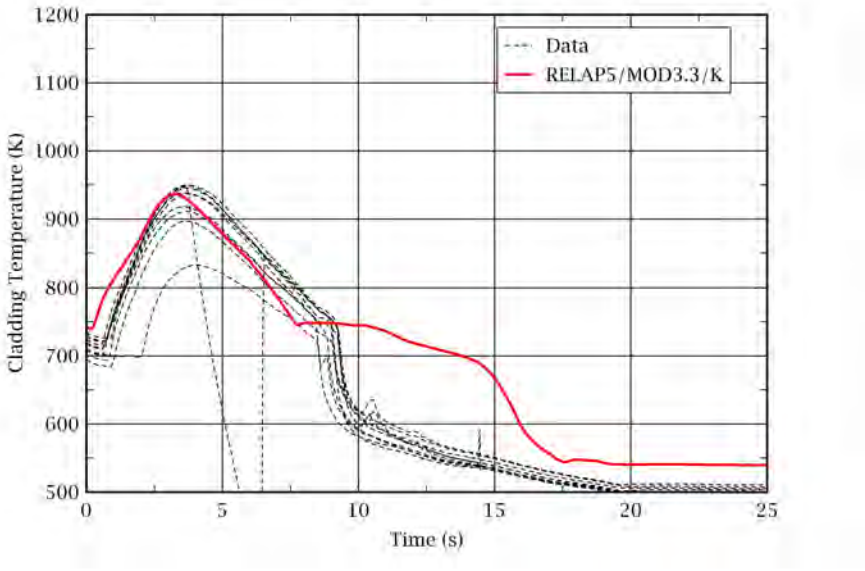

Figure 5-17 Rod Clad Temperatures at 77 in. from the Heated Bottom: THTF-160

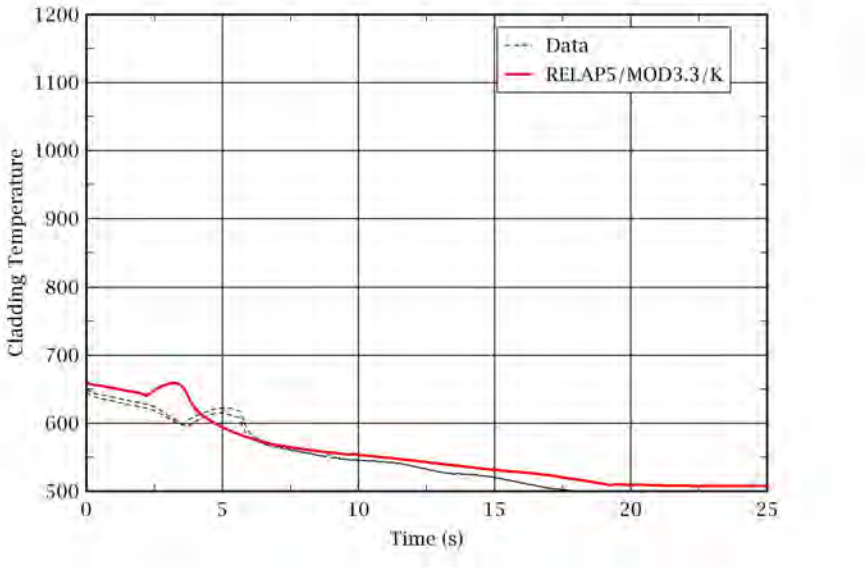

Figure 5-18 Rod Clad Temperatures at 125 in. from the Heated Bottom: THTF-160

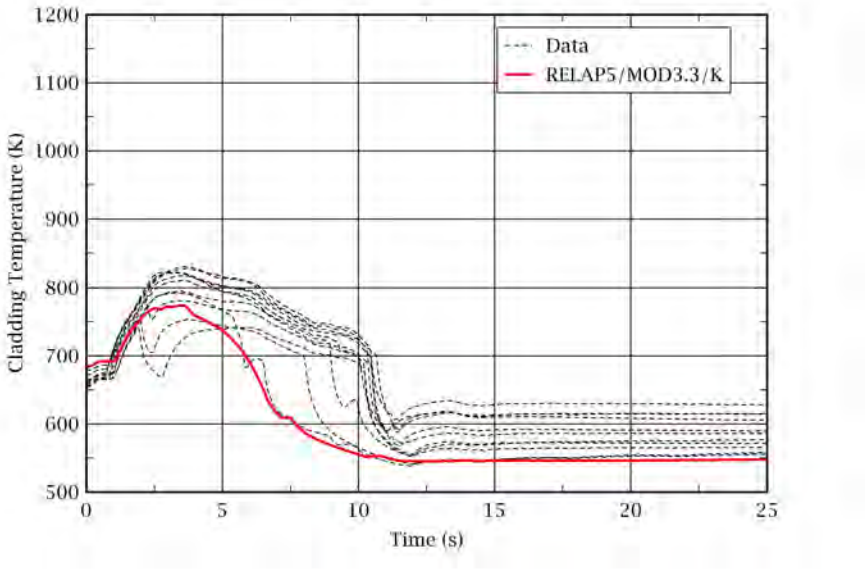

Figure 5-19 Rod Clad Temperatures at 43 in. from the Heated Bottom: THTF-162

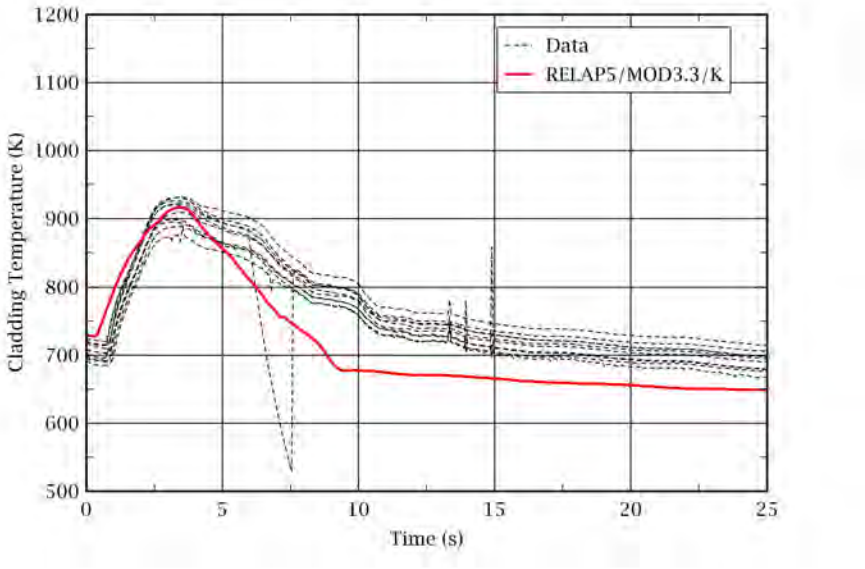

Figure 5-20 Rod Clad Temperatures at 77 in. from the Heated Bottom: THTF-162

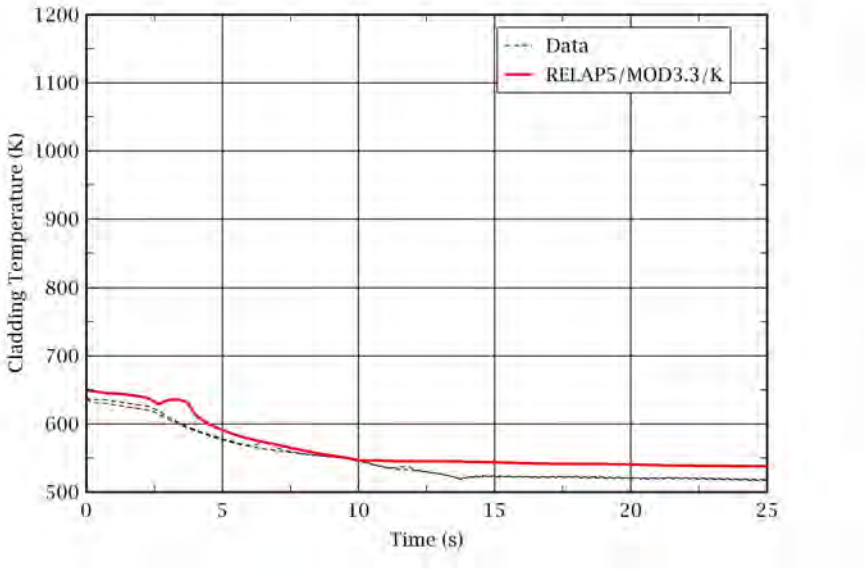

Figure 5-21 Rod Clad Temperatures at 125 in. from the Heated Bottom: THTF-162

TS

Figure 5-22 Blowdown Phase Code Accuracy Calculated Using THTF Test Data

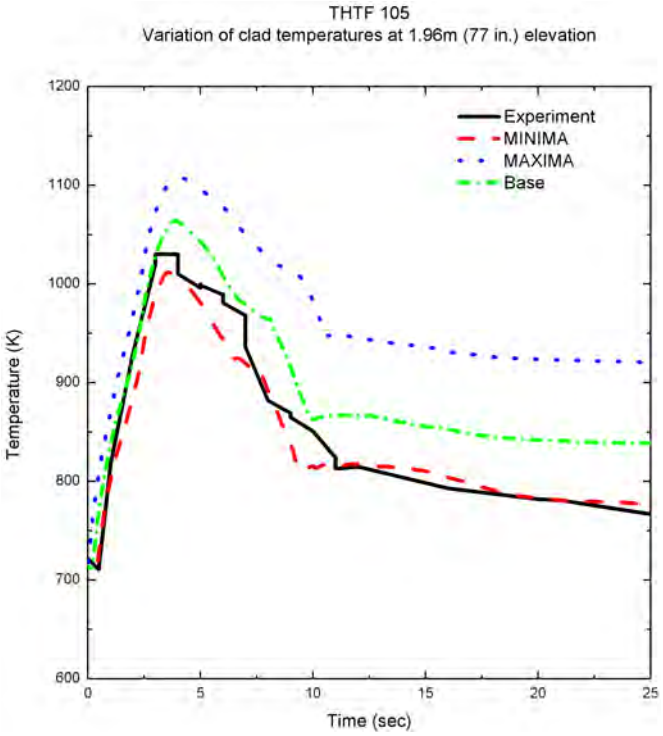

Figure 5-23 The Results of the SRS Calculations: THTF-105

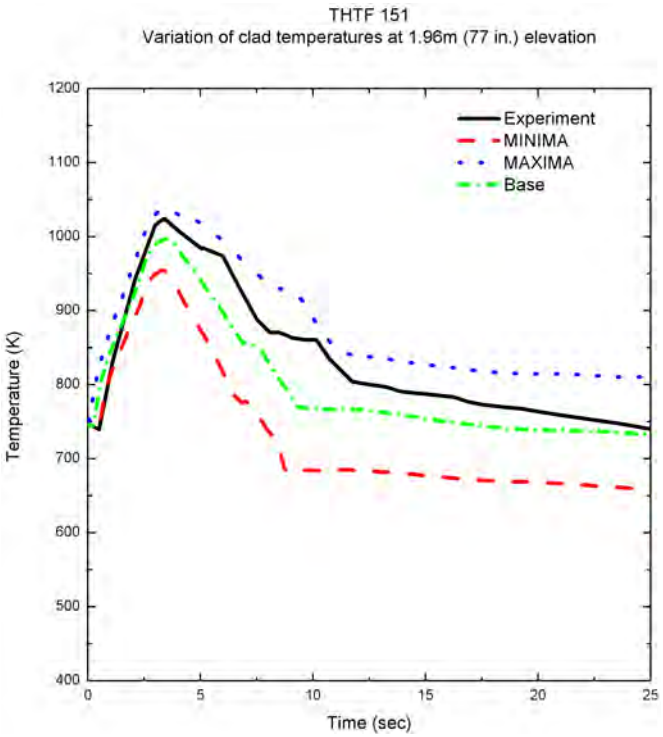

Figure 5-24 The Results of the SRS Calculations: THTF-151

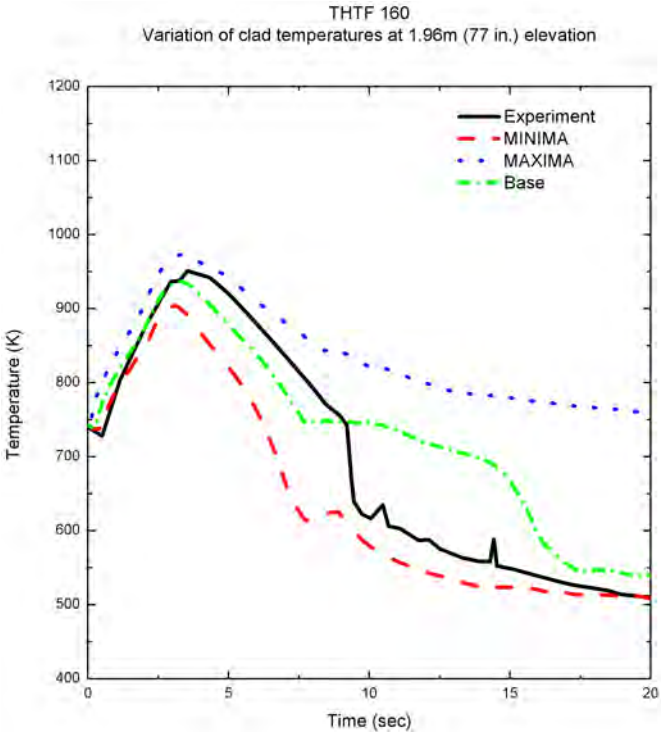

Figure 5-25 The Results of the SRS Calculations: THTF-160

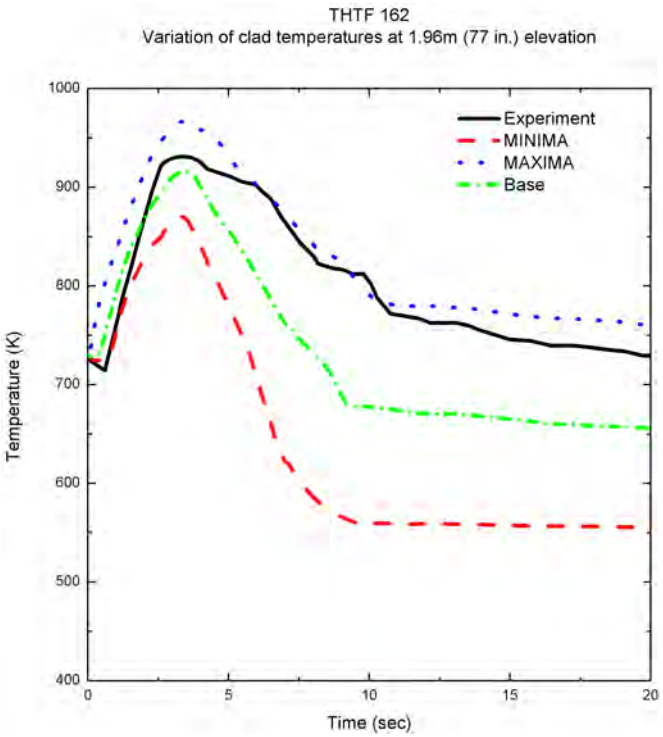

Figure 5-26 The Results of the SRS Calculations: THTF-162

6. Code Assessment against PKL-IIB5

The RELAP5/MOD3.3/K is assessed against Test IIB5 conducted by Siemens/KWU using the PrimärKreislauf (PKL) test facility [6-1]. Test IIB5 was carried out to study the thermal-hydraulic behavior of the primary system during a LBLOCA in a cold leg. This test covered the end-of-blowdown (EOB), the refill, and the reflood phase. Test IIB5 is selected to assess the capability of the RELAP5/MOD3.3/K in predicting the reflood progression.

6.1 PKL-IIB5

The PKL [6-1] was designed to simulate a Siemens/KWU 4-loop PWR. This facility was scaled 1:1 in height, 1:12 in diameter, and 1:145 in volume. The PKL test facility consisted of a complete primary circuit including a reactor pressure vessel (RPV), pressurizer (PZR), and main coolant loops. The primary loop consisted of one single intact loop, one doubled intact loop, and one broken loop. The doubled intact loop was a lumped loop including two intact single loops. Each loop had a fully scaled steam generator with U-tube geometry. The reactor vessel downcomer consisted of two separated pipes to simulate counter-current flow in the downcomer. A facility lay out of the PKL is shown in Figure 6-1.

The PKL-IIB5 test was conducted in 1985 to simulate a LBLOCA in a cold leg. Just before the break opens, conditioning water with a temperature of 523 K was injected into the upper head of the RPV and into two locations near the break to simulate the thermal hydraulic condition of the EOB phase. The injection of the conditioning water lasted for about three seconds. The reflood phase started with the activation of the accumulators (ACC) when the system pressure decreased to values below 2.6 MPa. The safety injection system (ACC and LPSI) injected only into the cold legs. The LPSI started to inject water at about 5 s after the break initiation.

The core simulator consisted of 314 electrically heated and 26 unheated rods. As shown in Figure 6-2, the heated and unheated rods were arranged within the core in three concentric radial zones according to the power level; 63 inner zone rods, 118 middle zone rods, and 133 outer zone rods. Configuration of the core is summarized in Table 6-1. The inner zone rods had 17 % and 30 % higher power per rod than the middle zone rods and outer zone rods, respectively. The heated rods had a chopped cosine axial power profile.

6.2 RELAP5/MOD3.3/K Model Description

The RELAP5/MOD3.3/K input model of the PKL test facility is shown in Figure 6-3.

The primary loop is modeled explicitly according to the facility configuration. The pressurizer is connected to the single intact loop.

The major components of the RPV, such as the core, downcomer, core bypass region, lower plenum, upper plenum and upper head, are explicitly modeled. The core region is [

]^{TS}

The upper plenum is modeled [

]^{TS}. The measured conditioning water injection and the safety injection are set as a function of time using time dependent volumes and time dependent junctions. Two water storage tanks are connected to the broken loop; one to the

pump-side and the other one to the RPV-side in order to model the loop conditioning water injection. One water storage tank is connected to the upper head in order to model the conditioning water injection to the upper head.

6.3 RELAP5/MOD3.3/K Simulation

Figure 6-4 shows a comparison of the measured and predicted core pressure. The RELAP5/MOD3.3/K predicts the core pressure behavior fairly well. The loop flow rate measured at the cross over leg in the broken loop is compared with the predicted value in Figure 6-5. Between 20 s and 40 s, the measurement shows that negative flow occurred due to the steam condensation by the safety injection water; whereas the code predicts almost no negative flow to occur. However, the predicted value matches the data well, in general.

Figure 6-6 shows a comparison of the measured and predicted core collapsed water level. Level 0.0 m in the figure indicates the bottom of the RPV. The safety injection system activates at 4.5 s and the core reflooding begins at around 32 s in the simulation. Both measured and predicted levels are very oscillatory. Between 50 s and 125 s, the average predicted level is slightly lower than the data. This is due to the fact that the RELAP5/MOD3.3/K over-predicts the entrainment in the core. After that, the predicted level matches the data well. Figure 6-7 shows a comparison of the measured and predicted collapsed water level in the upper plenum. In the simulation, the entrained water is accumulated in the upper plenum from about 42 s. The RELAP5/MOD3.3/K over-predicts the collapsed water level throughout the reflood period. In the experiment, it is supposed that a part of the entrained water was de-entrained at the upper core plate, and a part of the accumulated water in the upper plenum was de-entrained into the core. However, the code cannot predict the de-entrainment due to model deficiency. Thus, the main contributors of the over-prediction of the water level in the upper plenum are the over-prediction of the interfacial drag and the deficiency of the de-entrainment model. The over-prediction tendency of the entrainment becomes weaker as the reflood progresses.

Figure 6-8 and Figure 6-9 show a comparison of the measured and the predicted steam temperatures at the bottom and the top of the steam generator u-tubes, respectively. The RELAP5/MOD3.3/K over-predicts the steam temperatures before the reflood begins. However, the RELAP5/MOD3.3/K predicts the steam temperatures well, considering that the steam temperature measurements may have a large uncertainty.

Figure 6-10 shows a comparison of the measured and predicted differential pressure at the steam generator inlet and the outlet plenum. During the initial reflood period, between 42 s and 70 s, the predicted differential pressure is slightly lower than the data. This is mainly due to that the entrained water from the core is not introduced into the u-tubes, but is accumulated in the upper plenum during this time period. After 70 s, the RELAP5/MOD3.3/K over-predicts differential pressure at the steam generator. The higher differential pressure at the steam generator indicates that the steam binding phenomenon is stronger than the experiment.

Figure 6-11 and Figure 6-12 show a comparison of the measured and predicted rod clad temperatures at the middle zone and the inner zone, respectively. The measured temperatures are those at the elevation at which the highest temperature was observed. The RELAP5/MOD3.3/K predicts clad temperatures well during the initial five seconds. However, the code predicts 10 s earlier adiabatic heat-up of the rod than the data. Because of the conditioning water injection, the measured temperatures decrease by more than 60 K, whereas the predicted temperatures decrease by about 30 K. The under-prediction of the effect of the conditioning water on the clad temperatures is probably due to the fact that the conditioning water introduced into the core is entrained to the upper plenum earlier than the data. The predicted turn-around times are earlier than the data because the safety injection water is entrained to the hot region easily. After around 140 s, however, the code over-predicts the rod clad temperatures due to the over-prediction of the steam

binding effect. In both the middle zone and the inner zone, the highest predicted temperature is higher than the highest measured value.

6.4 SRS Calculations

SRS calculations were performed against the PKL-IIB5. [

]^{TS} The uncertainty parameters used in the SRS calculations are shown in Table 6-2.

Figure 6-13 shows the results of the SRS calculations against the PKL-IIB5. The third highest value of the calculated clad temperatures is higher than the measured PCT, confirming the data covering. Therefore, the number and the probability distribution functions of the selected uncertainty parameters are confirmed to be sufficient.

6.5 Conclusion

The capability of the RELAP5/MOD3.3/K in predicting the reflood progression was assessed against the PKL-IIB5. The assessment results show that the RELAP5/MOD3.3/K is capable of calculating the end-of-blowdown (EOB), the refill, and the reflood processes reasonably. The RELAP5/MOD3.3/K over-predicts the rod clad temperatures and the highest predicted temperature is higher than the highest measured temperature. The results of the SRS calculations against the PKL-IIB5 show that the measured PCT is covered by the calculated value. This implies that the number and the probability distribution functions of the selected [

]^{TS} are sufficient to cover the measured PCT.

References

[6-1] Schmidt, Umminger, Gueneysu, “Ergebnisse des Versuches IIB-5 aus der Testserie PKL IIB,” KWU, 1985.

[6-2] C. H. Ban, W. Hering, “Assessment of RELAP5 Reflood Models using PKL-IIB5 test,” IRS, FZK, 1999.

[6-3] V. Sanchez, C. H. Ban, “Status of Reflood Model Assessment in RELAP5/MOD3.2.2 Beta,” 14th CAMP meeting., Barioche, Argentina, 1999.

Table 6-1 Core Configuration for the PKL-IIB5

	Inner zone	Middle zone	Outer zone	Remarks
No. of rods	63	118	133	Total 314
Power fraction (kW)	313	502	510	
Rod power (W/rod)	4.97	4.25	3.83	Test condition
Axial power shape	Chopped cosine			

Table 6-2 Parameters and Distribution Functions Used for the SRS Calculations: PKL IIB5

TS

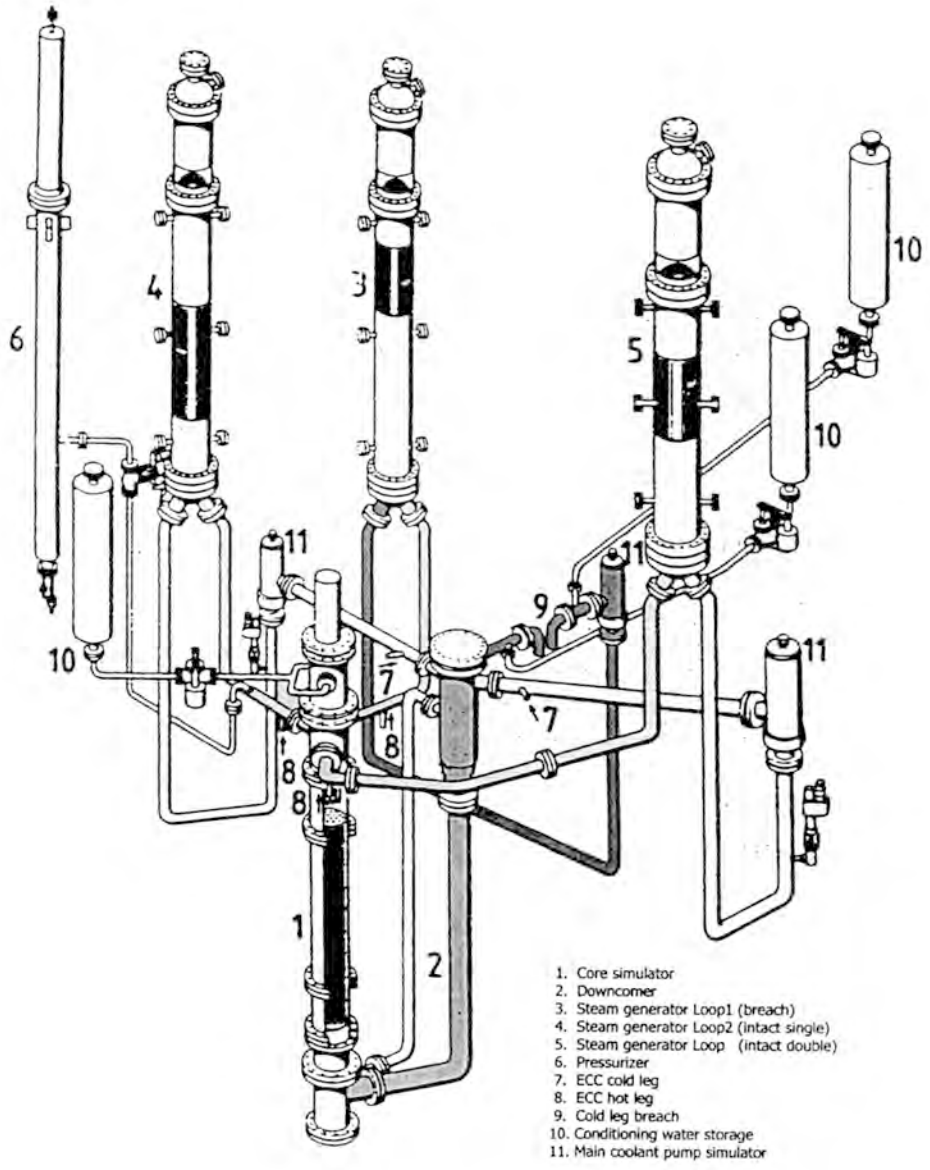

Figure 6-1 PKL Test Facility

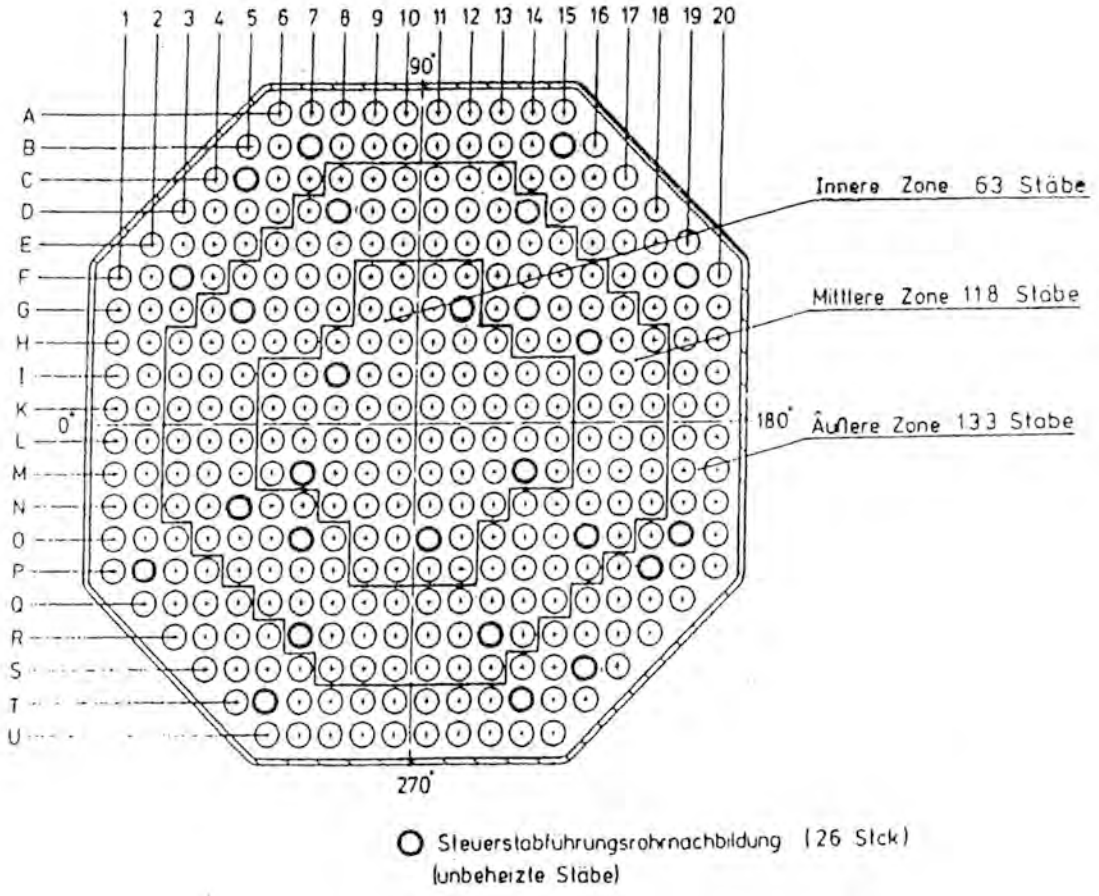

Figure 6-2 Core Configuration of the PKL Test Facility

TS

Figure 6-3 RELAP5/MOD3.3/K Nodalization of the PKL Test Facility

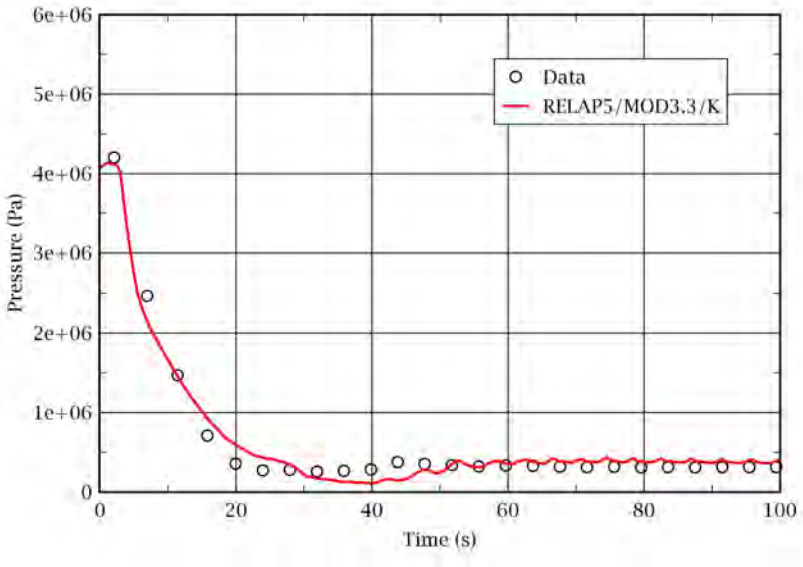

Figure 6-4 Core Pressure

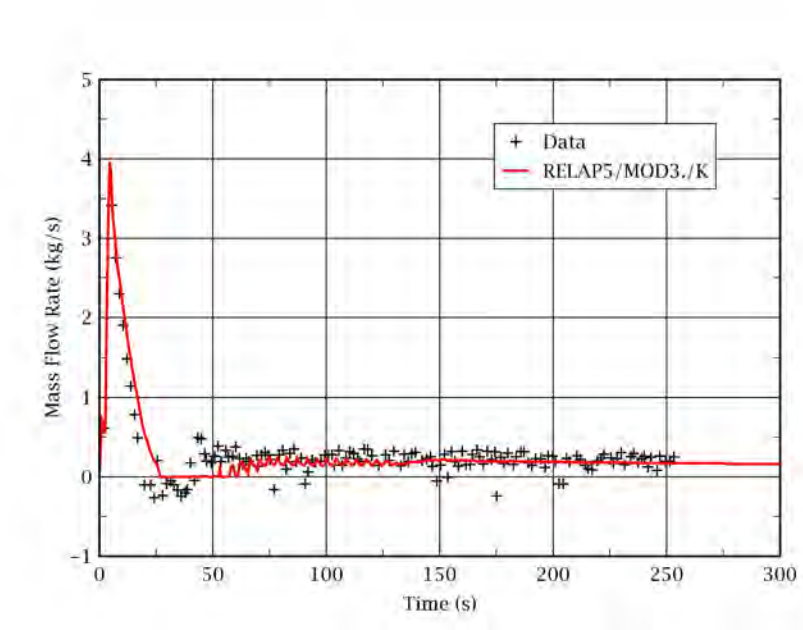

Figure 6-5 Loop Flow Rate (at Broken Loop Cross-over Leg)

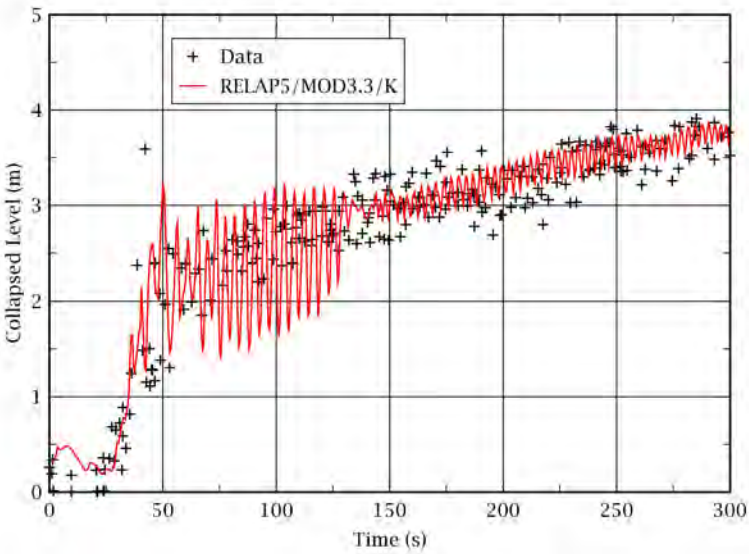

Figure 6-6 Core Collapsed Water Level

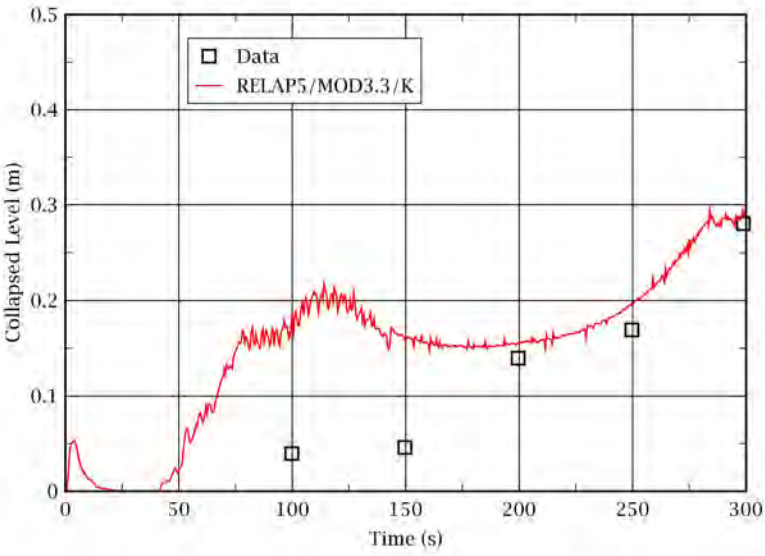

Figure 6-7 Upper Plenum Collapsed Water Level

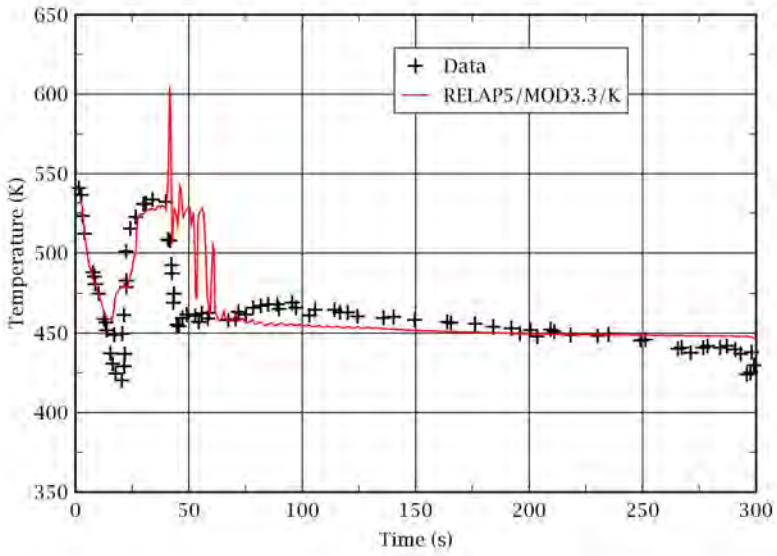

Figure 6-8 Steam Temperature at the Bottom of the U-tube

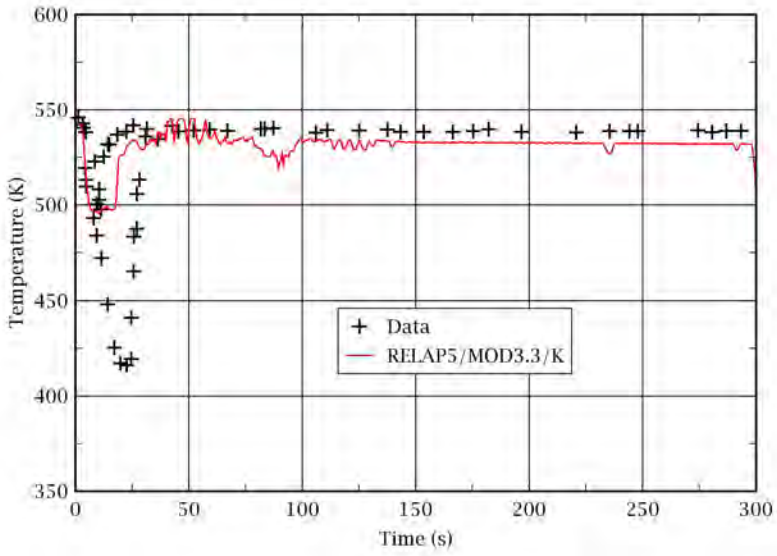

Figure 6-9 Steam Temperature at the Top of the U-tube

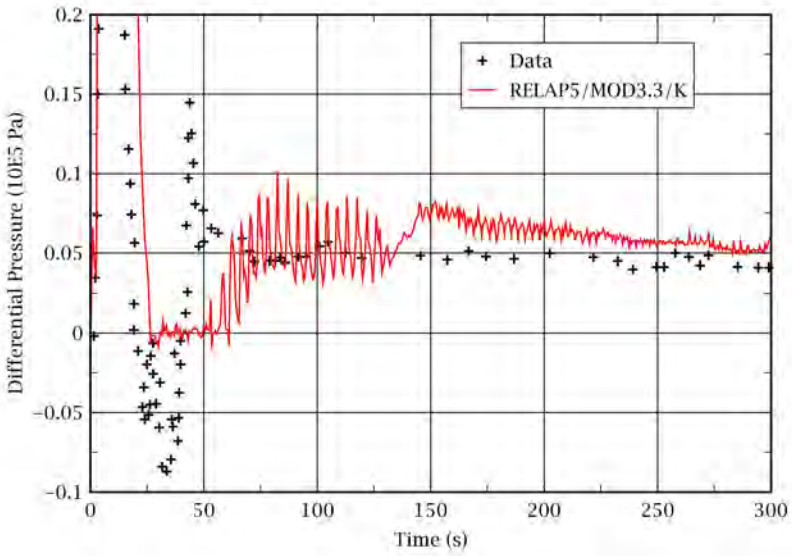

Figure 6-10 Differential Pressure at the Steam Generator Inlet-Outlet

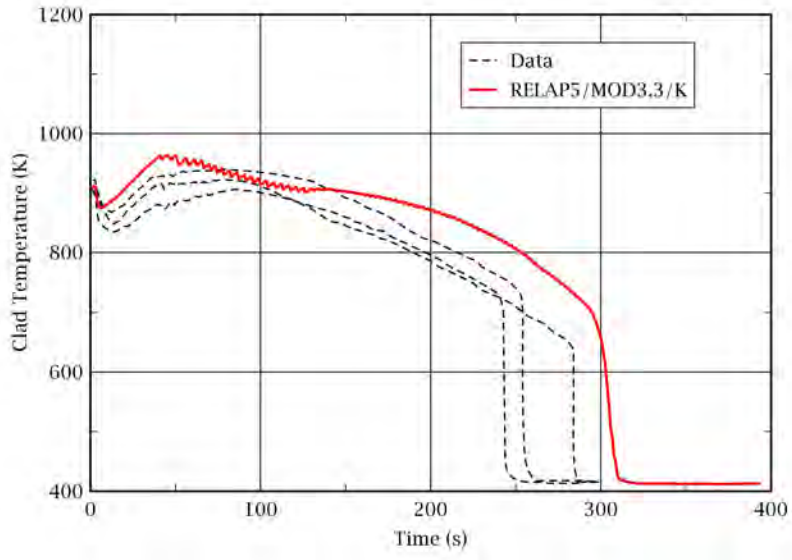

Figure 6-11 Rod Clad Temperature in the Middle Zone

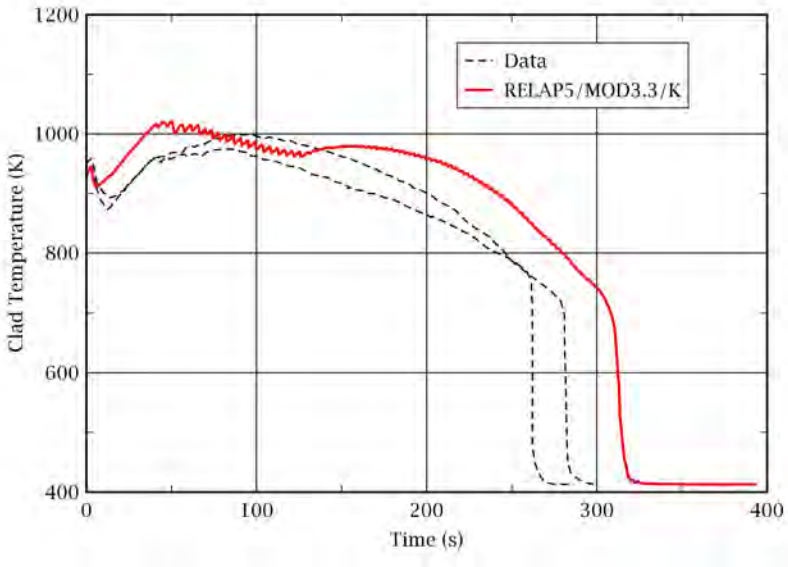

Figure 6-12 Rod Clad Temperature in the Inner Zone

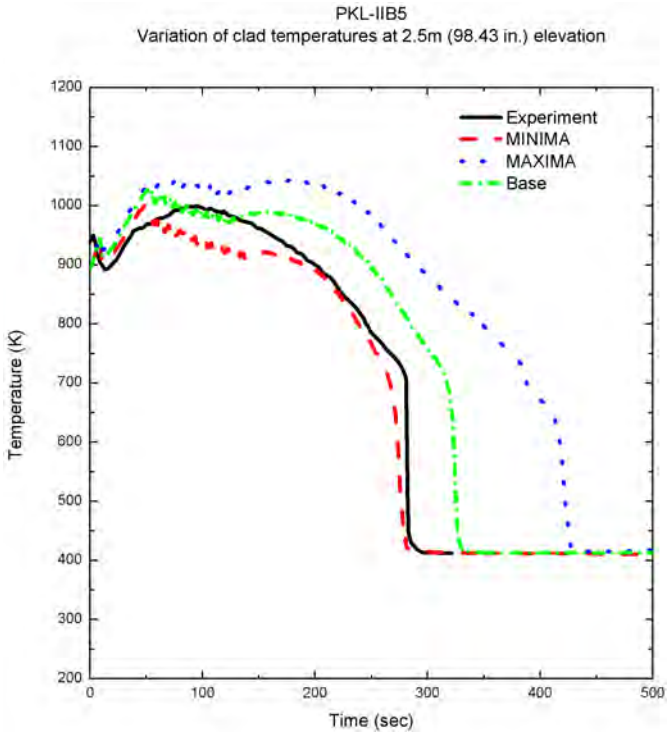

Figure 6-13 The Results of the SRS Calculations: PKL-IIB5

APPENDIX D

Assessment of RELAP5/MOD3.3/K against Integral-Effect Tests

Non-Proprietary

August 2018

Table of Contents

List of Tables

List of Figures

1. Introduction

The capability of the RELAP5/MOD3.3/K code to predict various thermal-hydraulic phenomena during a large break loss of coolant accident (LBLOCA) was assessed against various separate effect tests (SETs) and integral effect tests (IETs).

The purposes of the assessment are a) to examine the code's capability to accurately predict experimental data; b) to determine code accuracy; c) to determine probability distribution functions of the uncertainty parameters; d) to confirm the adequacy of the numbers of the uncertainty parameters and their ranges through checking the experimental data covering.

The code accuracy is used as a measure of the sufficiency of the set of uncertainty parameters. Via the code assessment, the capability of the code to predict the thermal-hydraulic phenomena is further confirmed and the parameters are determined in terms of probability distribution functions. 181 times of simple random sampling (SRS) calculations are performed for each experiment varying the values of the uncertainty parameters according to their distribution functions. Then it is checked whether the peak cladding temperature of the experiment can be covered by the third highest value of the calculations. In this way, sufficiency of the numbers and the ranges of the parameters are confirmed.

The code assessment against SETs is described in Appendix C. The definition and calculation method of code accuracy are also described in Appendix C.

This appendix describes the details of the code assessment against IETs

The IETs considered in the code assessment are;

- Four LOFT tests; L2-2, L2-3, L2-5 and LP-02-6
- One Semiscale test; S-06-3
- One LOBI test; A1-66

2. Code Assessment against LOFT

One of the most prominent reactor safety research facilities was the Loss-of-Fluid Test (LOFT) facility. Extensive research program were conducted at the LOFT including six nuclear large break loss of coolant accident (LOCA) experiments. The first nuclear experiment L2-2 was conducted with a maximum linear heat generation rate of 26.2 kW/m and with continuous primary coolant pump operation. Subsequent tests were conducted with larger power densities and variations in primary coolant pump operating conditions extending to an immediate trip at break initiation with a decoupling of the flywheels.

One of the most important phenomena observed in the LOFT transients is fuel cladding cooling/quench during blowdown. Extensive research concluded that this phenomenon was caused by system hydraulics in response to the operational characteristics of the primary coolant pumps relative to the transition from subcooled to saturated choked flow at the break.

Test L2-5 and LP-LB-1 incorporated pump characteristics which did not produce the early cooling/quench phenomena. The early cooling/quench phenomena was allowed to occur by intent in other tests. The significant finding from the six LOCA tests was that the cooling/quench phenomena would occur in all conditions except for a pump trip concurrent with break initiation and decoupling from the flywheels.

The thermal hydraulic computer code RELAP5/MOD3.3/K was assessed against four large break LOCA tests, L2-2, L2-3, L2-5, and LP-02-6, conducted in the LOFT facility. These four tests simulated a double ended guillotine break in a cold leg.

2.1 Test Facility Description

The LOFT integral test facility [2-1] was designed to simulate the major components and system responses of a PWR during a postulated LOCA. The facility consisted of five major systems which were extensively instrumented to measure system variables during the tests. The major five systems included; (a) the reactor vessel with the nuclear core, (b) primary coolant system, (c) secondary coolant system, (d) blowdown suppression system, and (e) emergency core cooling system (ECCS). The major components of the facility are shown in Figure 2-1.

The LOFT integral test facility was a 50 MWe PWR system and scaled to represent a 1/60-scale model of a typical 1,000 MWe commercial four-loop PWR. The reactor vessel of the facility consisted of an annular downcomer, a lower plenum, lower core support plates, a nuclear core, and an upper plenum. The unique feature of the LOFT facility was that the core had nuclear fuels (i.e., UO2 powered core). The nuclear core consisted of a total 1,300 unpressurized nuclear fuel rods arranged in five square and four triangular fuel modules as shown in Figure 2-2.

The fuel rods had an active length of 167.64 cm and fuel rod spacer grids at five locations. The LOFT fuel was designed to have the same physical and chemical properties as commercial fuel.

The primary coolant system consisted of an intact loop (with steam generator, two primary coolant pumps in parallel, a pressurizer and connecting piping) representing three unbroken loops of a four-loop PWR. A broken loop simulated the broken loop of a four-loop PWR during LOCA conditions. The broken loop consisted of a hot leg and a cold leg that connect the reactor coolant system to the pressure suppression system. Each leg consisted of a break plane orifice and a quick-opening blowdown valve. The broken loop hot leg also was equipped with steam generator and pump simulators.

The secondary system was designed to remove the heat transferred into the steam generator.

The blowdown suppression system simulated the containment backpressure in large PWRs during LOCA conditions. This system consisted of a large blowdown suppression tank, four suppression tank downcomers, nitrogen pressurization system, blowdown suppression tank spray system, a blowdown suppression tank header connected to the primary coolant system via the quick opening blowdown valves. To simulate the containment backpressure of a large PWR, predetermined initial conditions were established in the blowdown suppression tank.

The LOFT ECCS simulated the ECCS of a large PWR and consisted of the high-pressure injection system (HPIS), the low-pressure injection system (LPIS), and the accumulator. These systems were actuated to inject scaled amounts of ECC water and to simulate typical ECC delivery behavior in commercial PWRs. The LOFT facility had the capability of the ECC delivery to any of several locations including the intact loop hot or cold legs, the reactor vessel downcomer, lower plenum or upper plenum.

2.2 LOFT Test Descriptions

LOFT LBLOCA tests L2-2, L2-3, L2-5, and LP-02-6 are all double ended guillotine break tests in a cold leg. Tests L2-2 and L2-3 were identical except for increase in core power. Comparison of these tests was planned to investigate the effect of core power on system and ECC behavior during large cold leg break LOCAs. Tests L2-5 and LP-02-6 were to provide parametric investigations of the effect of loss of offsite power. Reactor power before the break initiation was 24.88, 36.7, 36.0 and 46.0 MWt for L2-2, L2-3, L2-5 and LP-02-6, respectively. The steady state operating conditions of each test are shown in Table 2-1.

An important boundary condition of LOFT L2-2 and L2-3 was continuous operation of primary coolant pumps. The primary coolant pumps were coasted down during LP-02-6. For L2-5, the primary coolant pumps were decoupled from their flywheels to provide a rapid pump deceleration.

Test L2-2

Test L2-2 was the first in a series of nuclear tests at LOFT. The basic objective of this test was to provide integrated system data on thermal-hydraulics and fuel behavior during a 200 % double ended break of a commercial PWR cold leg pipe. The test was initiated from a power level of 24.88 MW, yielding a maximum heat generation rate of 26.37 kW/m. Offsite power was assumed available in that the primary coolant pumps were left running at nearly normal speed. ECC water injected from the accumulator, HPIS, and LPIS to the intact loop cold leg. The ECC flow rates were adjusted to represent complete loss of ECC water injected to the broken loop and failure of one HPIS and LPIS injection train.

The test was initiated (0.0 s) by opening the quick-opening blowdown valves. The reactor was scrammed at 1.7 s. The HPIS and accumulator injection was initiated at 12 s and 18 s, respectively. The primary coolant pumps were tripped at 200 sec.

Test L2-3

The major objective of L2-3 was the same as Test L2-2. The facility configuration for this test was identical to that of L2-2, except for the core power level. The core power was 36.0 MW and the maximum heat generation rate was 39.0 kW/m.

The test was initiated (0.0 s) by opening the quick-opening blowdown valves. Reactor scram was completed 1.7 s, HPIS was initiated at 14 s, accumulator injection at 17 s at 4.18 MPa of system pressure, and LPIS at 29 s. The core reflood was started at 55 s. The primary coolant pumps operated throughout the test and were tripped at 200 s.

Test L2-5

The specific objectives of L2-5 were to determine if early core rewet occurs with immediate RCP coast down and to provide experimental data to demonstrate that 10 CFR 50 Appendix K assumptions result in a conservative prediction of peak cladding temperature. The configuration of the facility was almost identical to that of L2-2 or L2-3. The initial core power level was 36 MW and the maximum heat generation rate was 40.1 kW/m.

The test was initiated (0.0 s) by opening the quick-opening blowdown valves both in hot and cold leg. The reactor was scrammed on a low pressure (14.19 MPa) signal at 0.24 s. Following the scram, the operators tripped the primary coolant pumps at 0.94 s. This was done in order to provide an early rapid pump coast-down which would prevent the early core rewet phenomena and result in higher rod cladding temperatures. Accumulator injection was initiated at 16.8 s and the delayed ECC injection from HPIS and LPIS was started at 23.9 s and 37.3 s, respectively. The test was completed at the time of the end of LPIS injection, 107 s.

Test LP-02-6

The initial conditions for LP-02-6 were representative of USNRC licensing limits in commercial PWR and included loss of offsite power coincident with LOCA initiation and minimum ECC water injection. The test was initiated from a power level of 46.0 MW, yielding a maximum linear heat generation rate of 48.8 kW/m.

The test was initiated (0.0 s) by opening the quick-opening blowdown valves in the broken loop hot and cold legs. The reactor was scrammed automatically when the hot leg pressure reached 14.8 MPa at 0.1 s. The primary coolant pumps were tripped at 0.8 s and then allowed to coast-down naturally until 16.5 s when they were decoupled from their flywheels.

2.3 RELAP5/MOD3.3/K Model Description

The RELAP5/MOD3.3/K input models of LOFT facility is shown in Figure 2-3.

The reactor core is divided into [ ]^{TS} Active core of the fuel is divided into [ ]^{TS} axial volumes. Each volume has [ ]^{TS} The fuel rods in [ ]^{TS} are assumed to have the same normalized axial power shape. The normalized shape was calculated based on [ ]^{TS} This calculated shape was generally applied to the assessment calculations in this appendix except for the calculation for L2-5. The normalized axial power shape which was calculated based on L2-5 experimental data [2-4] was used for L2-5 calculation. Two power shapes are not much different each other. Axial power profile used for L2-2, L2-3, and LP-02-6 calculation is shown in Figure 2-4, for L2-5 calculation is shown in Figure 2-5. In both figures, 5H8 and 5M3 stand for the guide tubes of the center fuel assembly. The average powers of eight rods surrounding 5H8 and 5M3 were 93 % and 90 % of the hot rod power, respectively. 1C7 and 3C7 are the guide tubes of peripheral fuel assemblies. Interpolating the core power distributions at [

]^{TS}

The lateral flow between [ ]^{TS} Point reactor kinetics model is used to calculate the fission and decay power during the transient. The ANS 79 decay heat model is used for the calculation of decay heat release. Fuel rod gap conductance model is applied and [ ]^{TS}

The downcomer of LOFT reactor vessel has [

]TS

The break planes are modeled [
]TS the break initiation. The pressure transient of the blowdown suppression tank is modeled using the time dependent volumes at the end of the broken loop hot leg and cold leg.

The HPIS and LPIS are modeled [
]TS The steam generator secondary pressure is specified [
]TS the steam generator and feed-water flow is [
]TS Heat structures such as a steam generator vessel and U-tubes are explicitly modeled.

Test specific parameters such as reactor power, accumulator set-up pressure, reactor scram time, pump safety injection flow rate etc. are considered specifically in each test simulation.

2.4 RELAP5/MOD3.3/K Simulation

2.4.1 System Hydraulics

For each test simulation, the following parameters predicted by RELAP5/MOD3.3/K are presented and compared with data in Figure 2-6 to Figure 2-29.

- System pressure at the intact loop hot leg and pressurizer
- Mass flow rate at the broken loop cold leg
- Mass flow rate at the broken loop hot leg
- Accumulator injection flow rate
- Low pressure and high pressure safety injection flow rate
- Water levels in the reactor vessel

In all calculations, the intact loop hot leg and pressurizer pressures predicted by RELAP5/MOD3.3/K show a subcooled depressurization and a subsequent saturated depressurization. RELAP5/MOD3.3/K shows a slightly faster depressurization than the test data, but the predicted values reasonably match the data, in all test simulations.

The calculated broken loop cold leg mass flow rates compare well with the test data in all calculations, as shown in Figure 2-7, Figure 2-13, Figure 2-19, and Figure 2-25. For L2-2 and L2-3, RELAP5/MOD3.3/K under-predicts the mass flow rate between 6 s and 12 s. However, the predicted results are in reasonable agreement with the data considering the measurement uncertainty. The measurement uncertainties are ± 68.8 kg/s, ± 68.75, and ± 62.0 kg/s for L2-2, L2-3, and L2-5 respectively.

RELAP5/MOD3.3/K reasonably predicts the broken loop hot leg mass flow rate as shown in Figure 2-8, Figure 2-14, Figure 2-20, and Figure 2-26. In the case of L2-2, the predicted mass flow rate is slightly higher than the data. However, the general trend of the predicted values matches well the test data. The measurement uncertainties are ± 23.7 and ± 23.0 kg/s for L2-3 and L2-5, respectively.

The calculated accumulator injection flow rates are shown in Figure 2-9, Figure 2-15, Figure 2-21, and Figure 2-27. In the cases of L2-5 and LP-02-6, the predicted value is not compared with the data because the data is unavailable. For L2-2 and L2-3, because RELAP5/MOD3.3/K predicts a

slightly faster depressurization than the data, the earlier accumulator injection is predicted.

The calculated and measured HPIS and LPIS injection flow rates are shown in Figure 2-10, Figure 2-16, Figure 2-22, and Figure 2-28. In all calculations, RELAP5/MOD3.3/K cannot predict the reduction of LPIS flow rate observed 10 s after the injection initiation. However, the difference in the injection flow rate between the predicted and measured value is not significant compare to the accumulator injection flow rate. Moreover, the effect of this difference is negligible because most of the important events occurred before the reduction of LPIS injection flow rate. Generally, the predicted HPIS and LPIS injection flow rates reasonably match the data.

The calculated water levels in the core and the downcomer are shown in Figure 2-11, Figure 2-17, Figure 2-23, and Figure 2-29. For the cases of L2-2, L2-3 and LP-02-6, the core water level decreases rapidly during the initial 4 s and then increases again until 7 to 10 s. Because of this core level increase (i.e., positive core flow), the core is quenched during the blowdown period. This early cooling/quench phenomena was allowed to occur by intent in these experiments. RELAP5/MOD3.3/K reasonably predicts this early cooling/quench phenomena. The detailed description of the positive core flow behavior is presented in the following section. The core water level, then, decreases until the accumulator injection begins to reflood the core. As the core reflooding begins, both water levels in the core and the downcomer show oscillatory behaviors until about 60 s.

2.4.2 Core Flow during Blowdown; Test L2-2, L2-3 and LP-02-6

During the initial blowdown the flow out of the vessel through the cold leg break greatly exceeds the coolant flow into the downcomer from the intact loop cold leg. However, the break flow transitions from sub-cooled critical flow to saturated critical flow which reduces the magnitude of the break flow. Meanwhile the primary coolant pump at the intact loop cold leg still discharges sub-cooled liquid under normal operation or coast-down condition. Consequently, more liquid is being delivered to the downcomer than is expelled out of the downcomer. The additional liquid penetrates down to the lower plenum and up to the core resulting in a positive core flow [2-1].

The calculated mass flow rates at the intact and broken cold legs for the initial 10 s are shown in Figure 2-30 through Figure 2-32. RELAP5/MOD3.3/K reasonably predicts the phenomena observed during the initial blowdown period of test L2-2, L2-3 and LP-02-6. Integration of the core inlet mass flow rate calculated by RELAP5/MOD3.3/K is shown in Figure 2-33. Generally, the flow out of the core continues until about 4 s, after then, the positive core flow lasts until about 12 s. The accumulated liquid in the core between 4 s and 12 s is about 350 kg for LP-02-6, 220 kg for L2-2 and 240 kg for L2-3. For all calculations, this accumulated liquid in the core is larger than the amount obtained by subtracting the expelled liquid amount out of the downcomer from the delivered liquid amount to the downcomer. This implies that a portion of the liquid in the downcomer is carried to the core by the core up-flow behavior.

After 12 s, the flow out of the core continues until the safety injection flow recovers the positive flow at the core inlet. The accumulator injection is calculated to initiate at 15 s in all calculations.

2.4.3 Fuel Cladding Temperature

Test L2-2, L2-3 and LP-02-6

The comparisons of calculated and measured fuel rod cladding temperatures are shown in Figure 2-34 through Figure 2-42 for L2-2, in Figure 2-43 through Figure 2-51 for L2-3, and in Figure 2-52 through Figure 2-60 for LP-02-6. The cladding temperatures of the rods in the hot channel are compared with the corresponding measurement data in these figures. It should be noted that the LOFT external fuel thermocouples did not measure the rod cladding surface temperature accurately because of fin-cooling effect [2-1]. One axial core volume (i.e., node) of the calculations contains

one to three measurements.

For node 1 (i.e., the lowest core node), RELAP5/MOD3.3/K under-predicts the data measured at 0.051 m and 0.127 m (2 in. and 5 in.) from the bottom of the core in all three calculations, as shown in Figure 2-34, Figure 2-43, and Figure 2-52. RELAP5/MOD3.3/K favorably predicts the rod cladding temperature behavior near the bottom of the core.

The predicted node 2 temperatures are compared with the data measured at 2.032 m and 0.279 m (8 in. and 11 in.) from the bottom of the core, as shown in Figure 2-35, Figure 2-44, and Figure 2-53. The result of L2-2 calculation, the predicted first peak of the rod cladding temperature (i.e., blowdown peak) is higher than the data. RELAP5/MOD3.3.K predicts the second and third peak (i.e., reflood peaks) to occur later than the data. The results of L2-3 calculations that the predicted first heat-up and quench match well the data. However, RELAP5/MOD3.3/K does not properly calculate the second heat-up and quench. For the LP-02-6 calculation, the predicted first peak is slightly higher than the data. The predicted second peak is within two measured temperatures. In all three calculations, RELAP5/MOD3.3/K predicts well the early rod cooling/quench during blowdown which is one of the most important phenomena observed in LOFT transients.

For node 3, RELAP5/MOD3.3/K predicts very similar rod temperature behaviors with node 2 as shown in Figure 2-36, Figure 2-45, and Figure 2-54. In these figures, the predicted temperature is compared with the data measured at 0.381 m and 0.533 m (15 in. and 21 in.) from the bottom of the core. The results of L2-2 calculation show that the first peak is higher than the data. The second heat-up is predicted to occur several seconds later than the data. After blowdown, each measured temperature shows various heat-up and quench behavior due to different measurement locations. The rod temperature was heated-up and quenched once or two or three times during reflood while the predicted temperature shows two heat-up and quench behaviors. The predicted temperature is within the various measured data. Because a core node contains two or three measurement elevations, as described before, the prediction of RELAP5/MOD3.3/K seems to be reasonable. The results of L2-3 calculation show that the code predicts well the first heat-up and quench calculating slightly higher rod cladding temperature than the data. The code, however, under-predicts rod cladding temperature during reflood. The code predicts the second heat-up to occur 5 s later than the data while the code predicts the second quench to occur at least 5 s earlier than the data. For LP-02-6 calculation, RELAP5/MOD3.3/K predicts well both the first and second rod temperature heat-up and quench behavior.

The calculated node 4 temperatures are compared with the corresponding data in Figure 2-37, Figure 2-46, and Figure 2-55. The data measured at 0.610 m, 0.660 m, and 0.711 m (24 in., 26 in., and 28 in.) from the bottom of the core are used for the comparison. In the case of L2-2 calculation, RELAP5/MOD3.3/K over-predicts the first peak by 140 K. After blowdown, the measurements show various heat-up and quench behaviors due to different measurement locations. The second heat-up is predicted to occur later than the data and the predicted peak value is lower than the peak value of the measured data. Since the predicted temperature, however, is within the various measured data, the prediction of RELAP5/MOD3.3/K seems to be reasonable. In the result of L2-3 calculation, RELAP5/MOD3.3/K over-predicts the first peak by 70 K. The code predicts a delayed quench of the first heat-up and, consequently, a delayed second heat-up. RELAP5/MOD3.3/K under-predicts the rod cladding temperature during reflood. RELAP5/MOD3.3/K over-predicts the first peak by 100 K in the result of LP-02-6 calculation. However, the code predicts well the rod cladding temperature behavior during reflood. In all three calculations, RELAP5/MOD3.3/K predicts well the early cladding cooling/quench during blowdown.

The calculated node 5 temperatures are compared with the corresponding data in Figure 2-38, Figure 2-47, and Figure 2-56. The data measured at 0.762 m, 0.813 m, and 0.876 m are used for the comparison. In all three tests, the measured temperatures show very similar behaviors with the data used for the comparison of node 3 behavior. The calculated temperatures also show very similar trends with the node 3 results. Generally, the code over-predicts the blowdown peak and

under-predicts the reflood peaks.

Figure 2-39, Figure 2-48, and Figure 2-57 show a comparison of the predicted rod cladding temperature at node 6 with the corresponding measured data. The data measured at 0.940 m, 0.991 m, and 1.041 m (37 in., 39 in., and 41 in.) are used for the comparison. For L2-2 calculation, the code predicts the first heat-up to occur 3 s later than the data, consequently, resulting in lower rod cladding temperature behavior during blowdown. The data showed three heat-up and quench behaviors during reflood, which were caused by top-down quenching phenomena [2-8]. RELAP5/MOD3.3/K does not accurately predict these top-down quenching behaviors. For L2-3 calculation, the first peak is over-predicted by 30 K. During reflood, two of three measurements show three peaks while the code predicts one peak with the maximum temperature difference of 200 K. In the case of LP-02-6, the code over-predicts the first peak by 70 K. The measurements showed three types of rod cladding temperature behaviors according to the radial location of the rod while the predicted cladding temperature shows one heat-up and quench behavior during reflood. The predicted value encompasses all of the measurements.

The results of L2-2 calculation show that RELAP5/MOD3.3/K does not accurately predict the clad temperatures of node 7, 8, and 9, as shown in Figure 2-40, Figure 2-41, and Figure 2-42. Both blowdown peak and reflood peak(s) were observed at the elevations corresponding to node 7, 8, and 9. However, the code does not predict any considerable heat-up and quench behavior during the transients.

For L2-3 calculation, the predicted cladding temperatures at the upper core nodes (i.e., node 7, 8, and 9) are compared with the corresponding measured data in Figure 2-49, Figure 2-50, and Figure 2-51. The code predicts the blowdown peak of node 7 to occur 3 s later than the data resulting in under-prediction of the rod cladding temperature by 120 K. Three times rod heat-up and quench behaviors were observed during reflood while RELAP5/MOD3.3/K predicts rod heat-up and quench to occur once during reflood. The code predicts no considerable rod heat-up at node 8 and 9 during both blowdown and reflood.

For LP-02-6 calculation, the predicted cladding temperatures at the upper core nodes (i.e., node 7, 8, and 9) are compared with the corresponding measured data in Figure 2-58, Figure 2-59, and Figure 2-60. RELAP5/MOD3.3/K predicts well the first heat-up of node 7. Two of four measurements show decrease of the cladding temperature but no quenching during blowdown and the other two measurements show very short period of quenching. The code predicts a clear blowdown quenching behavior and the second heat-up to occur at 23 s. At node 8 and 9, the code predicts no considerable heat-up behavior.

Test L2-5

The comparisons of calculated and measured fuel rod cladding temperatures are shown in Figure 2-61 through Figure 2-69.

RELAP5/MOD3.3 predicts a relatively low heat-up at node 1. The predicted rod cladding temperature behavior at node 2 match well the data. Even though the predicted peak value is slightly lower than the data, the code predicts well not only a steep increase of the cladding temperature at the beginning of the transient but also rod quench time.

At node 3, the prediction match well the data except for rod quench time as shown in Figure 2-63. While RELAP5/MOD3.3/K predicts that the rod is quenched at around 75 s, the measurements show that rod quench is occurred between 54 s and 60 s. The predicted peak value is 20 K higher than the peak value of the measurements.

RELAP5/MOD3.3/K over-predicts rod cladding temperatures of node 4 and node 5 and the predicted temperature at each node encompasses all corresponding measurements. The general

trend of the predicted temperature behavior matches well the data. The code, however, significantly over-predicts rod quench time at these nodes.

The result of node 6 match well the data until 14 s. After then, the corresponding measurements to node 6 show a top-down quench during reflood, however, the code does not predict this behavior properly. Top-down quench during reflood, a multi-dimensional behavior, was observed between 14 s and 20 s. The code does not properly predict the second heat-up and quench behavior because of the improper prediction of the top-down quench.

For the upper core nodes, node 7, 8, and 9, the code does not properly calculate the first heat-up and quench. While the data shows a double heat-up at node 8 and 9, the code predicts one heat-up. The code predicts a longer time for the rods to quench during the reflood period.

The specific objectives of L2-5 were to determine if early core rewet occurs with immediate RCP coast-down. For the nodes 2, 3, 4, and 5, RELAP5/MOD3.3/K predicts well that early core rewet does not occur as observed during the test.

2.4.4 Code Accuracy

Code accuracy is defined as the statistical difference between calculated and measured peak cladding temperature (PCT), as described in Step 9.1 of this topical report. Because one value of the PCT is obtained from each test, measured cladding temperatures, both at the PCT location of a test and at neighboring locations where comparable cladding temperatures were measured, are compared with the predicted values at corresponding locations in order to obtain meaningful statistical code accuracy.

For the code accuracy calculation using the results of the assessments performed in this appendix, [

]TS

The standard deviation, σ, of the difference between the measured and calculated PCTs is calculated as follows:

$$dPCT = \sum \left(PCT_{\exp} - PCT_{cal} \right) / N \quad (1)$$

$$\sigma^2 = \left\{ \sum \left(PCT_{\exp} - PCT_{cal} \right)^2 - N \times dPCT^2 \right\} / N \quad (2)$$

where, N = the number of experimental data points

The blowdown phase code accuracy, which was calculated using the results of [ ]TS of L2-2, L2-3 and LP-02-6 calculations, is presented in Figure 2-70. RELAP5/MOD3.3/K over-predicts the clad temperatures by [ ]TS on average with a standard deviation of [ ]TS

The reflood phase code accuracy, which was calculated using the results of [ ]TS of L2-2, L2-3, L2-5 and LP-02-6, is presented in Figure 2-71. The code under-predicts the clad temperatures by [ ]TS on average with a standard deviation of [ ]TS during reflood.

2.5 SRS Calculations

181 times of simple random sampling (SRS) calculations were performed for each LOFT experiment considered in this report. The uncertainty parameters and their distribution functions used for the SRS calculation are listed in Table 2-2. [ ]^{TS} uncertainty parameters were used for all SRS calculations. Since the nuclear fuel rods were used in the LOFT tests, [

]^{TS} were considered in the SRS calculations. In addition to the [ ]^{TS} parameters, [ ]^{TS} parameters specific to LOFT tests such as [
]^{TS} were also considered. [

]^{TS} were used in the SRS calculations of each test.

Figures from Figure 2-72 through Figure 2-75 show the results of the SRS calculations against four LOFT experiments. In these figures, the measurement shown the highest cladding temperature is compared with the maxima and minima of the calculated results at the corresponding node. In all the SRS calculations, the third highest values of the calculated clad temperatures are higher than the measured PCTs confirming the data covering. Therefore, the number and the probability distribution functions of the selected code parameters are confirmed to be sufficient.

2.6 Conclusion

The capability of the RELAP5/MOD3.3/K in predicting thermal-hydraulic behaviors during a LBLOCA was assessed against four LOFT tests. The assessment results show that the code is capable of calculating thermal-hydraulic behaviors during a LBLOCA, in general. RELAP5/MOD3.3/K reasonably predicts the system pressure and the mass flow rates at the primary system pipes. The code predicts well the fuel cladding cooling/quench behaviors which was caused by system hydraulics in response to the operational characteristics of the primary coolant pumps.

RELAP5/MOD3.3/K over-predicts the rod clad temperature by [ ]^{TS} on average with a standard deviation of [ ]^{TS} during the blowdown period. The code under-predicts the clad temperatures by [ ]^{TS} on average with a standard deviation of [ ]^{TS} during the reflood period.

In all of the SRS calculations against four LOFT tests, the data covering was confirmed. This implies that the number and the probability distribution functions of the selected uncertainty parameters are sufficient to cover the measured PCTs.

References

[2-1] D.L. Reeder, “LOFT System and Test Description (5.5-ft Nuclear Core 1 LOCES),” NUREG/CR-0247; TREE-1208, 1978.

[2-2] S.M. Modro, et al., “Review of LOFT Large Break Experiments, OECD LOFT Project,” NUREG/IA-0028, 1989.

[2-3] P.G. Prassinos, et al., “Experiment Data Report for LOFT Power Ascension Experiment L2-3,” NUREG/CR-0792; TREE-1326, 1979.

[2-4] P.D. Bayless, et at., “Experiment Data Report for LOFT Large Break Loss-of-Coolant Experiment L2-5,” NUREG/CR-2826; EGG-2210, 1982.

[2-5] NRC/DRPS Reactor Safety Data Bank, ENCOUHTER, EGG-RTH-7285.

[2-6] D. Luebbesmeyer, “Post-Test-Analysis and Nodalization Studies of OECD LOFT Experiment LP-LB-1 with RELAP5 /MOD2 Cy 36-02,” NUREG/IA-0089, 1992.

[2-7] P. Coddington, C. Gill, “TRAC-PFI /MOD1 Calculations of LOFT Experiment LP-02-6,” NUREG/IA-0027; AEEW-M2464, 1992.

[2-8] C.L. Nalezny, “Summary of the Nuclear Regulatory Commission's LOFT Program Research Findings,” NUREG/CR-3005; EGG-2231, 1985.

Table 2-1 Initial Test Conditions

Parameter	L2-2	L2-3	L2-5	LP02-6
Mass flow rate (kg/s)	194.2	199 ±6.3	192.4 ±7.8	248.7 ±2.6
Pressure (MPa)	15.64	15.06 ±0.03	14.94 ±0.06	15.09 ±0.08
Cold leg temperature (K)	557.7	560.7 ±3	556.6 ±4.0	555.9 ±1.1
Hot leg temperature (K)	580.4	592.9 ±1.8	589.7 ±1.6	589.0 ±1.0
Reactor vessel power level (MW)	24.88	36.0 ±1.0	36.0 ±1.2	46.0 ±1.2
Maximum heat generation rate (kW/m)	26.37	39.0 ±3.0	40.1 ±3.0	48.8 ±3.6

Table 2-2 Parameters and Distribution Functions Used for the SRS Calculations: LOFT TS

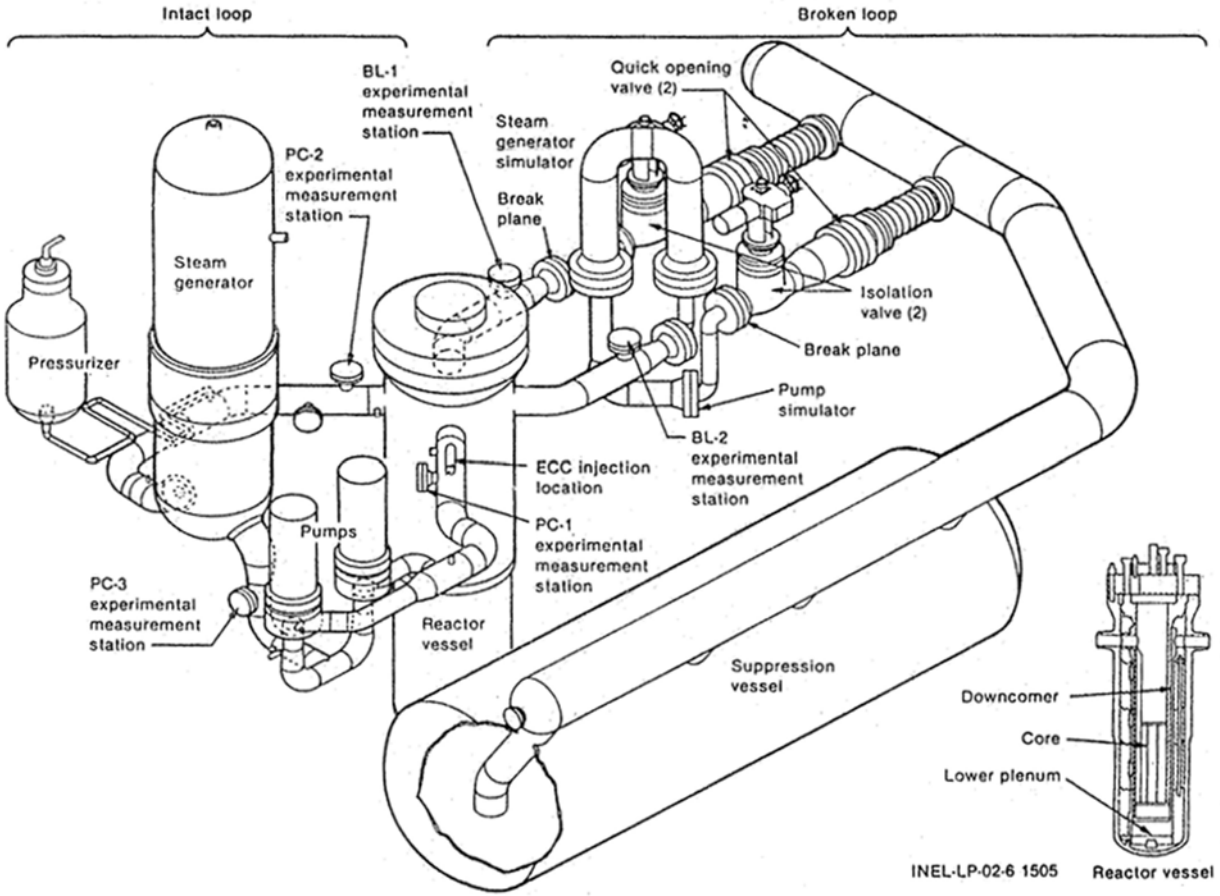

Figure 2-1 Schematic Diagram of the LOFT

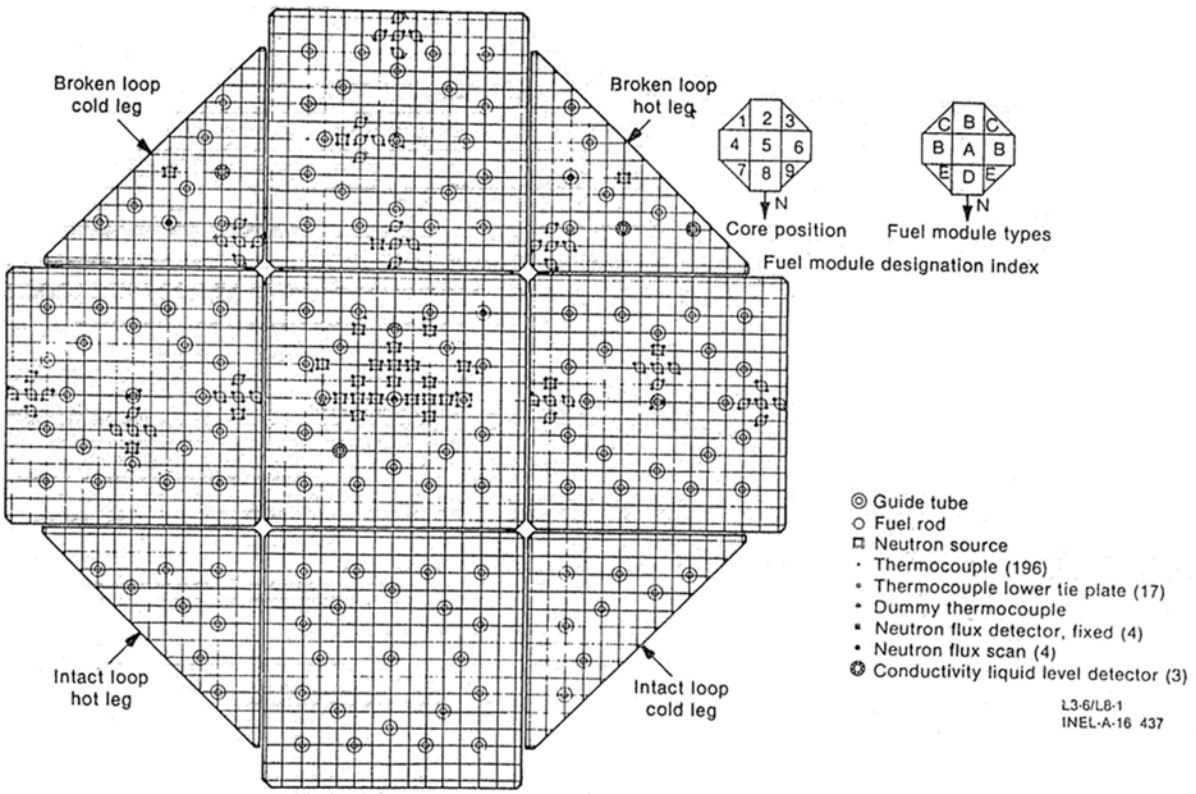

Figure 2-2 Core Configuration and Typical Instrumentation of the LOFT

Figure 2-3 RELAP5/MOD3.3/K Noding Diagram for the LOFT

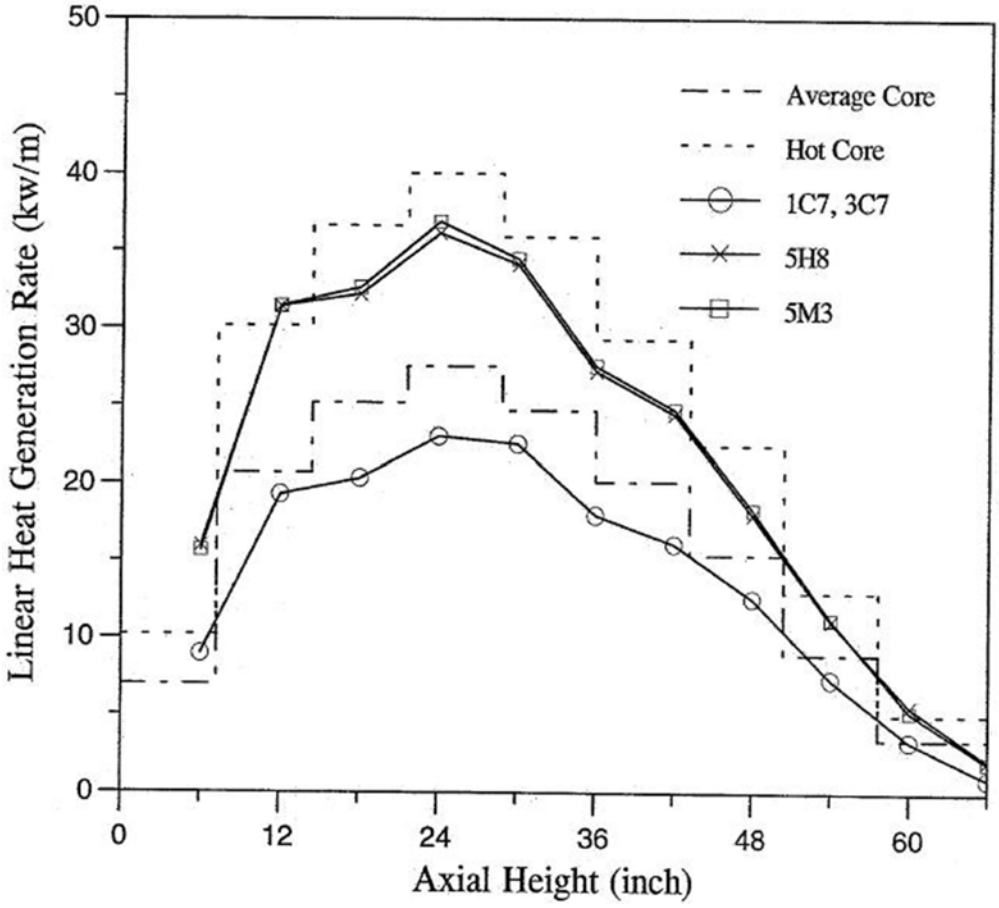

Figure 2-4 Axial Power Shape Used for the LOFT Test L2-2, L2-3 and LP-02-6 Calculations

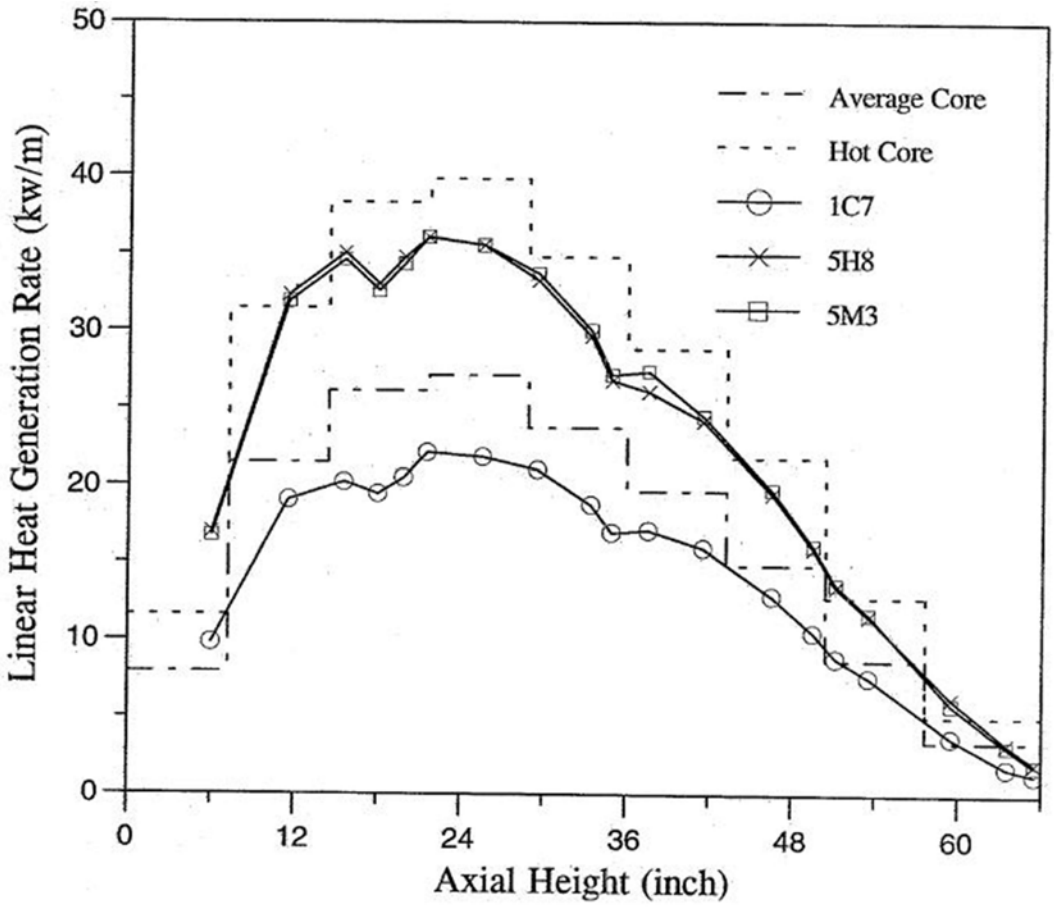

Figure 2-5 Axial Power Shape Used for the LOFT Test L2-5 Calculation

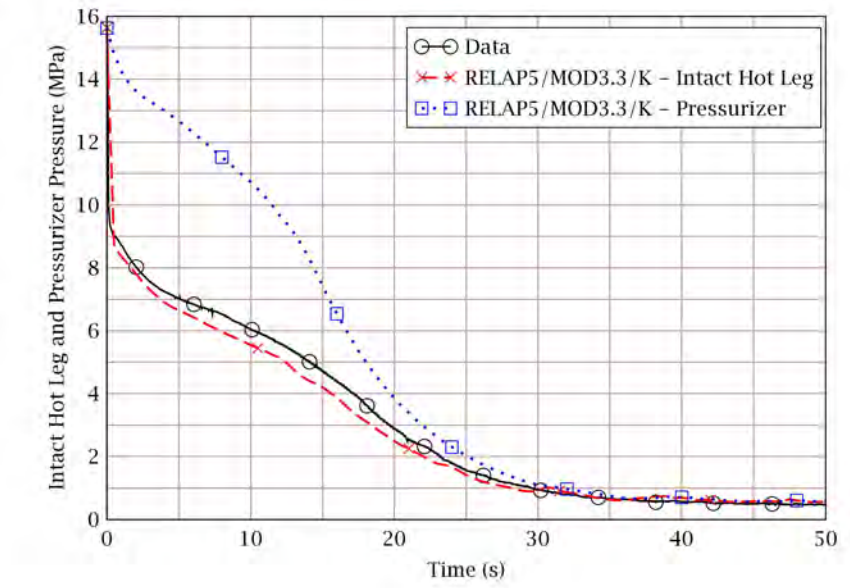

Figure 2-6 Intact Loop Hot Leg Pressure and Pressurizer Pressure: Test L2-2

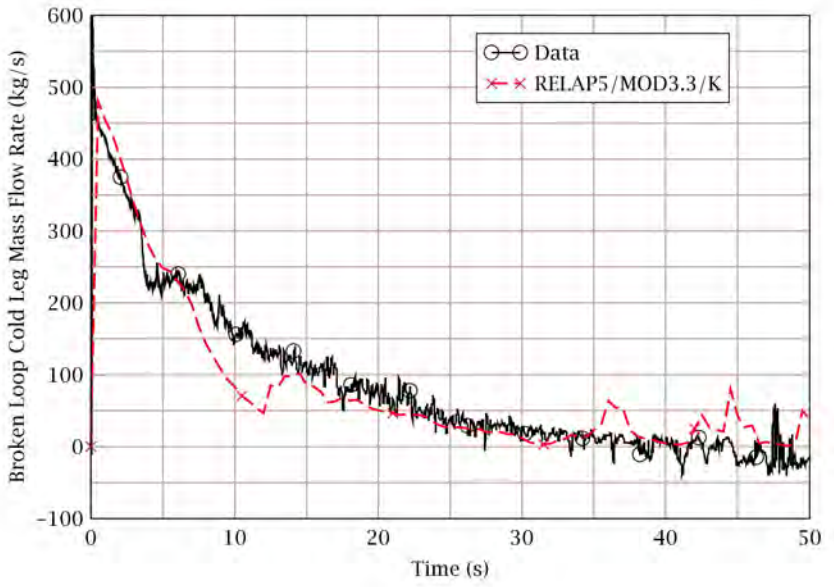

Figure 2-7 Broken Loop Cold Leg Mass Flow Rate: Test L2-2

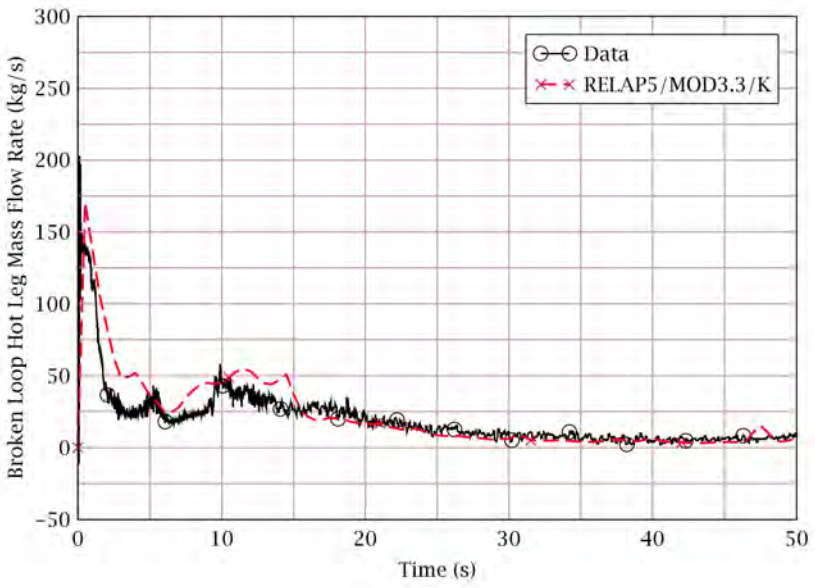

Figure 2-8 Broken Loop Hot Leg Mass Flow Rate: Test L2-2

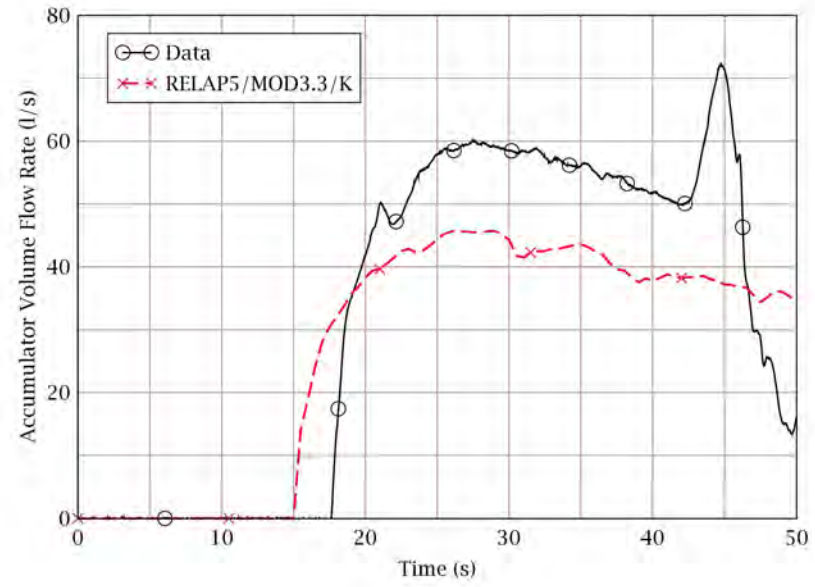

Figure 2-9 Accumulator Injection Flow Rate (volumetric): Test L2-2

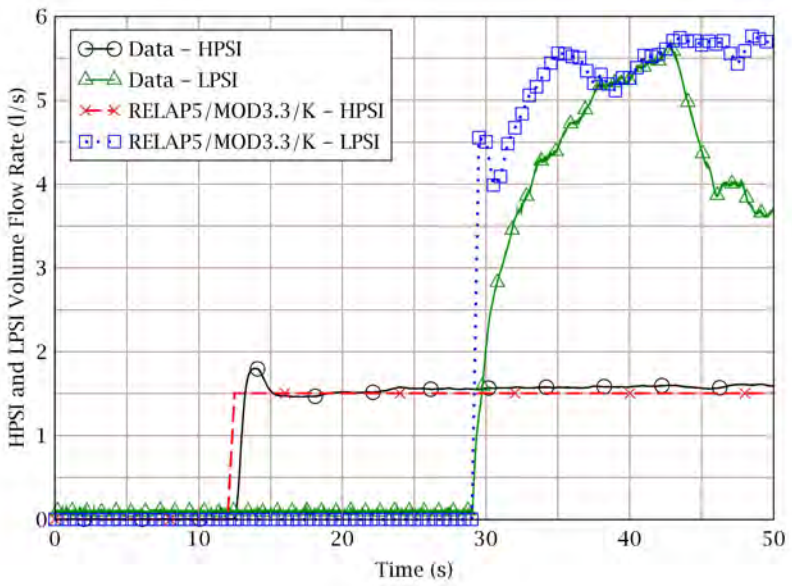

Figure 2-10 HPSI and LPSI Flow Rates (volumetric): Test L2-2

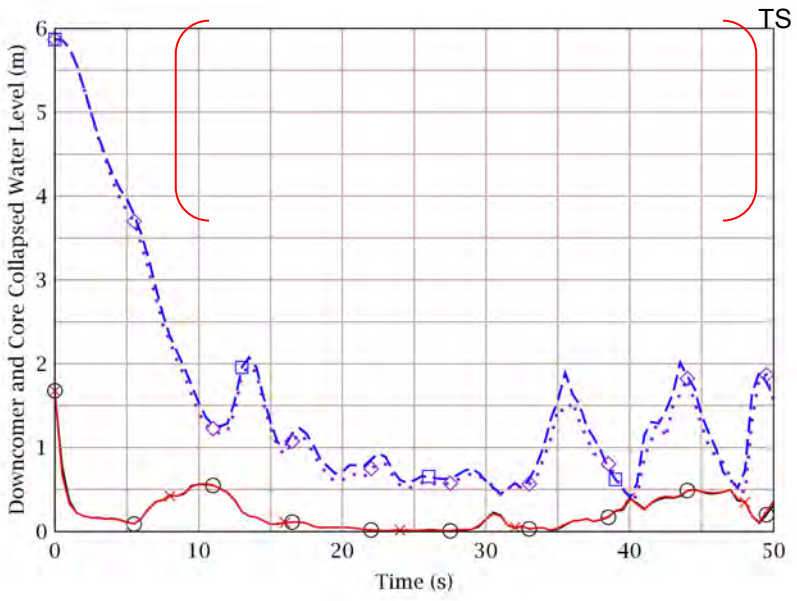

Figure 2-11 Downcomer and Core Collapsed Water Levels: Test L2-2

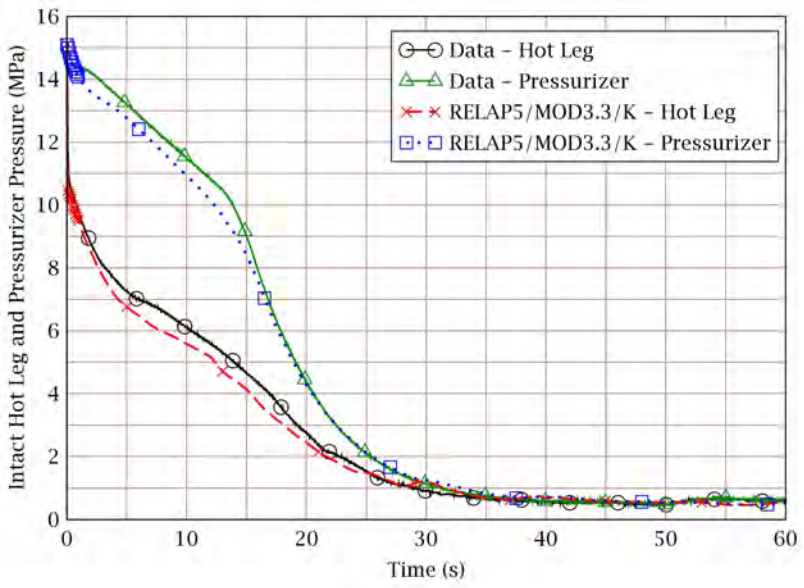

Figure 2-12 Intact Loop Hot Leg Pressure and Pressurizer Pressure: Test L2-3

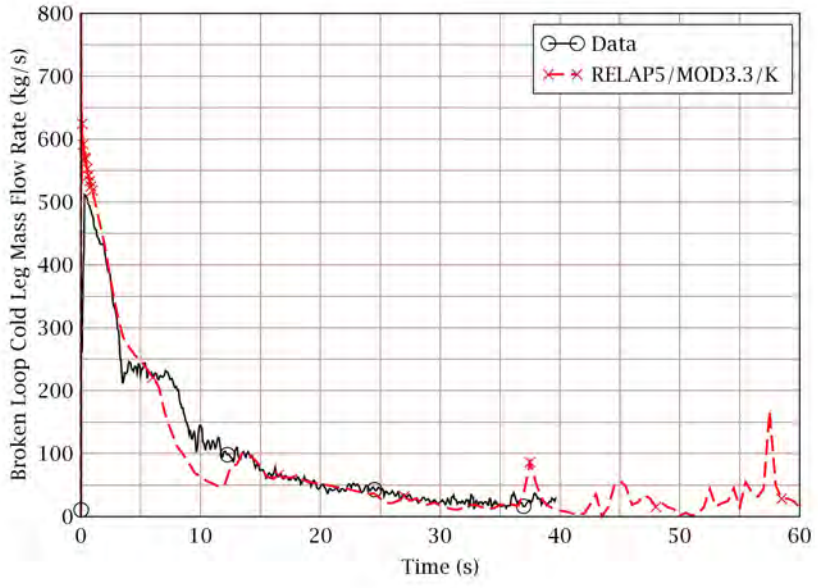

Figure 2-13 Broken Loop Cold Leg Mass Flow Rate: Test L2-3

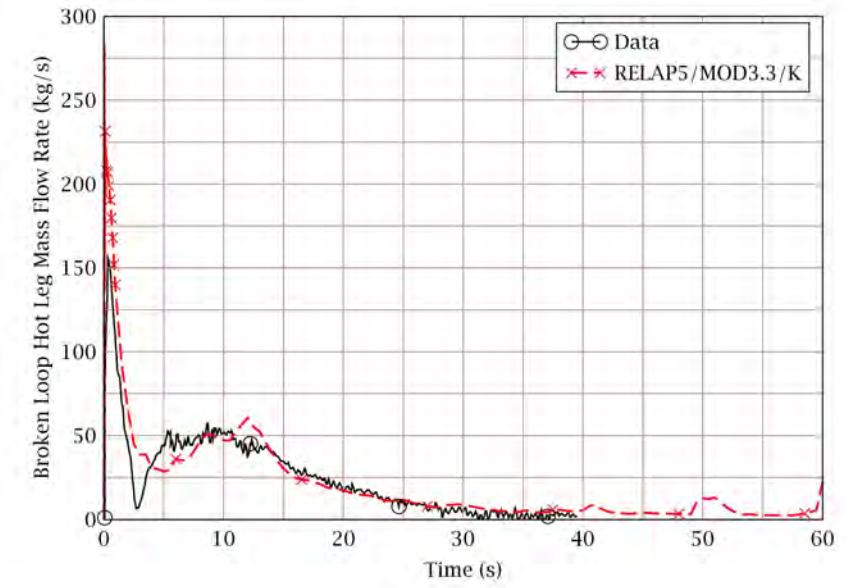

Figure 2-14 Broken Loop Hot Leg Mass Flow Rate: Test L2-3

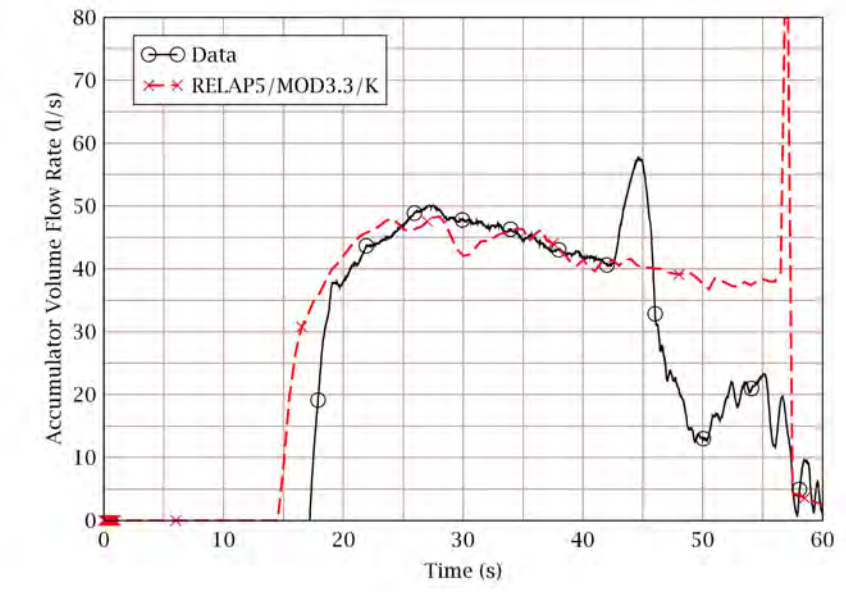

Figure 2-15 Accumulator Injection Flow Rate (volumetric): Test L2-3

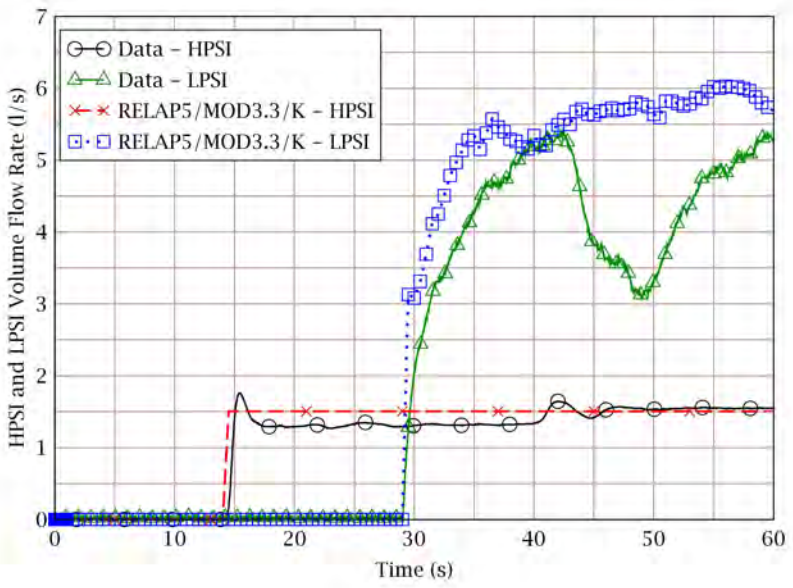

Figure 2-16 HPSI and LPSI Flow Rates (volumetric): Test L2-3

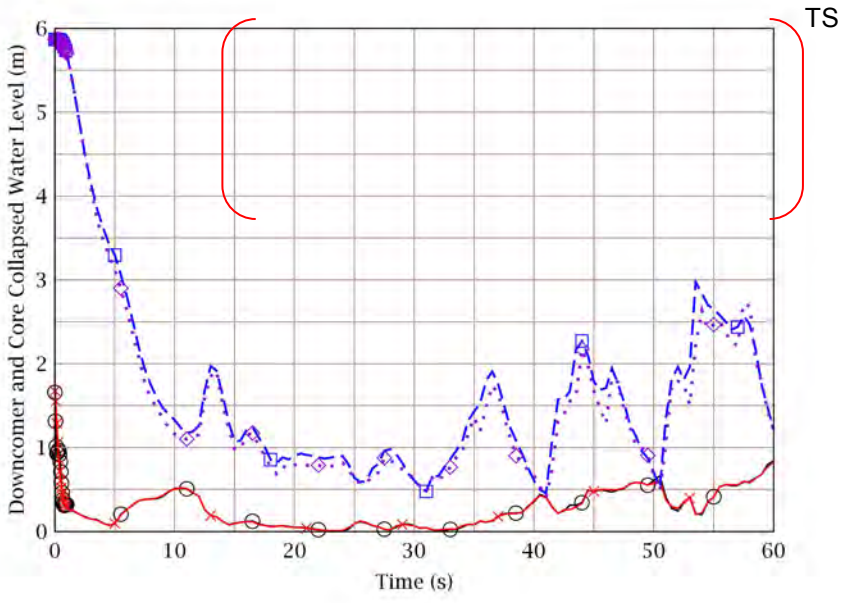

Figure 2-17 Downcomer and Core Collapsed Water Levels: Test L2-3

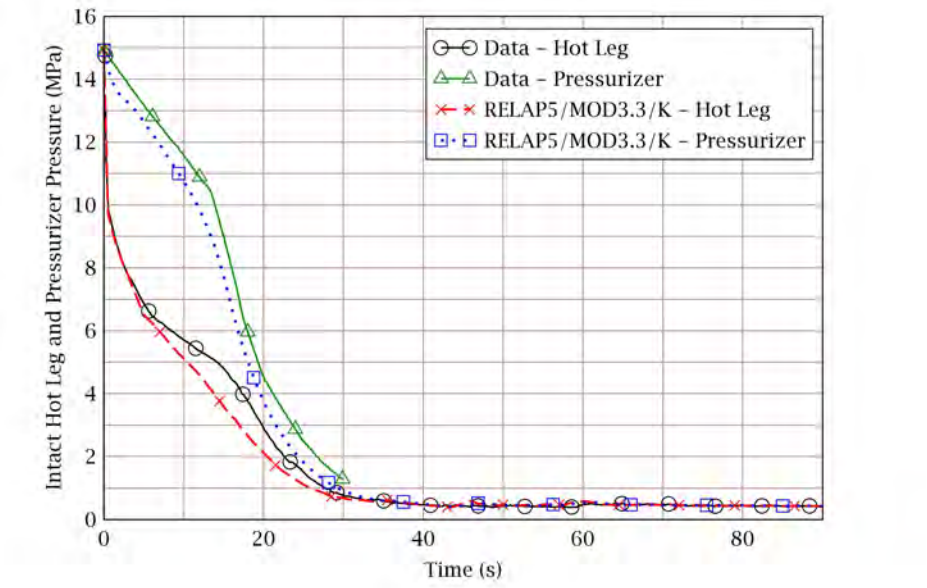

Figure 2-18 Intact Loop Hot Leg Pressure and Pressurizer Pressure: Test L2-5

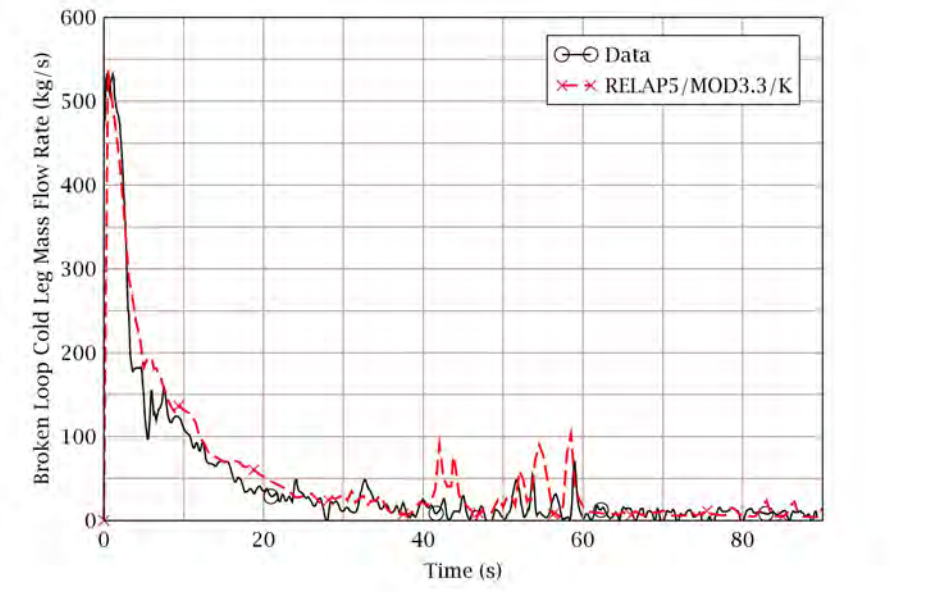

Figure 2-19 Broken Loop Cold Leg Mass Flow Rate: Test L2-5

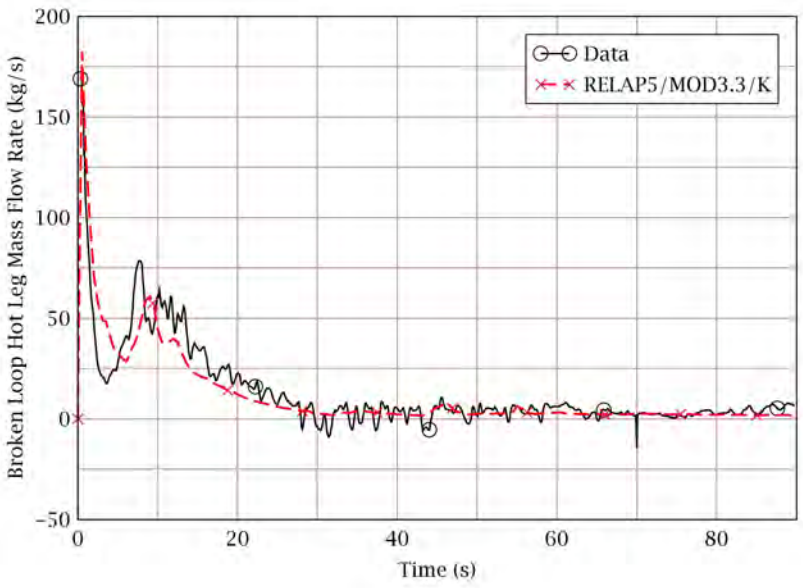

Figure 2-20 Broken Loop Hot Leg Mass Flow Rate: Test L2-5

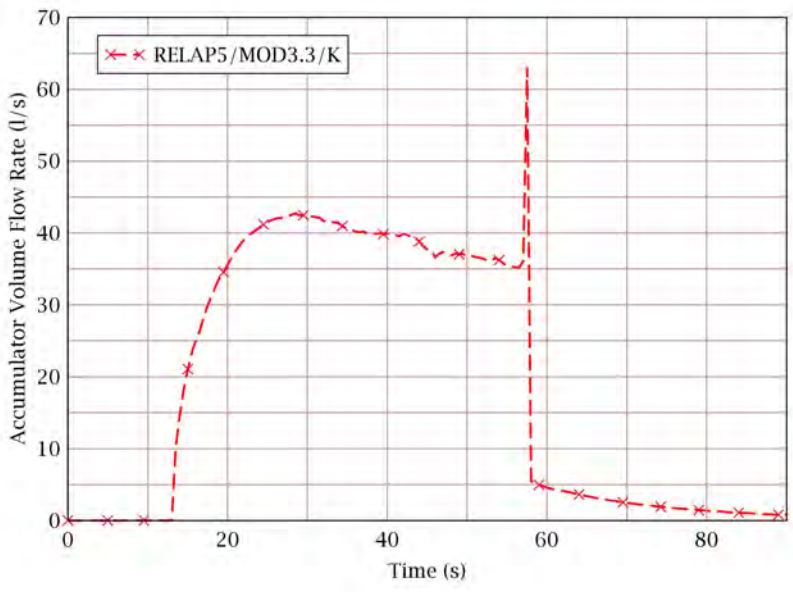

Figure 2-21 Accumulator Injection Flow Rate (volumetric): Test L2-5

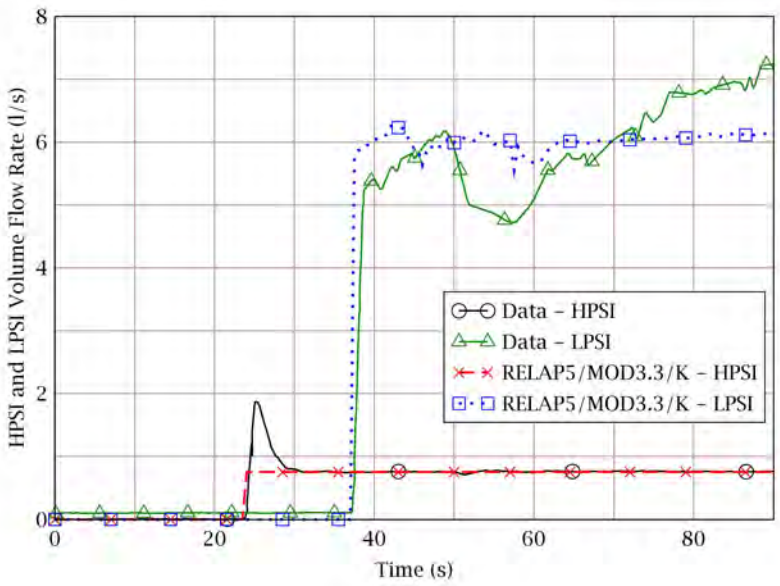

Figure 2-22 HPSI and LPSI Flow Rates (volumetric): Test L2-5

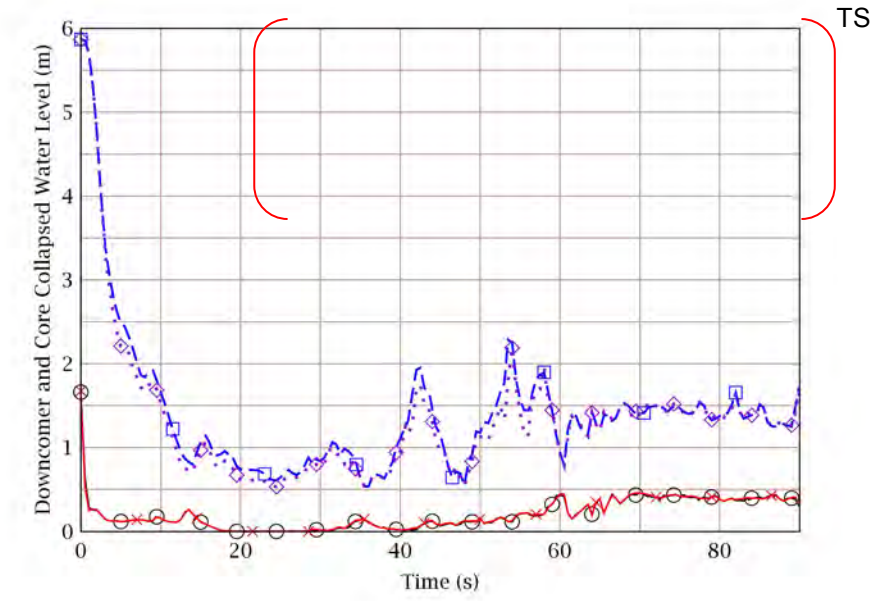

Figure 2-23 Downcomer and Core Collapsed Water Levels: Test L2-5

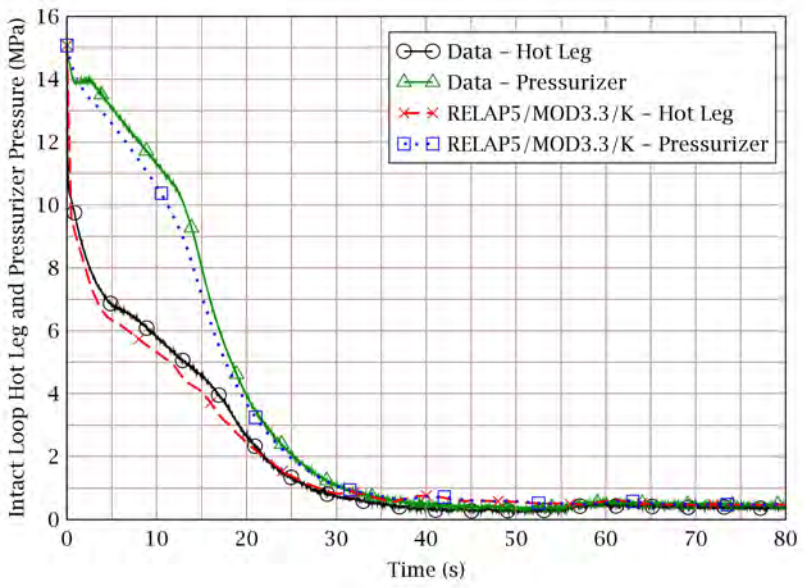

Figure 2-24 Intact loop Hot Leg and Pressurizer Pressure: Test LP-02-6

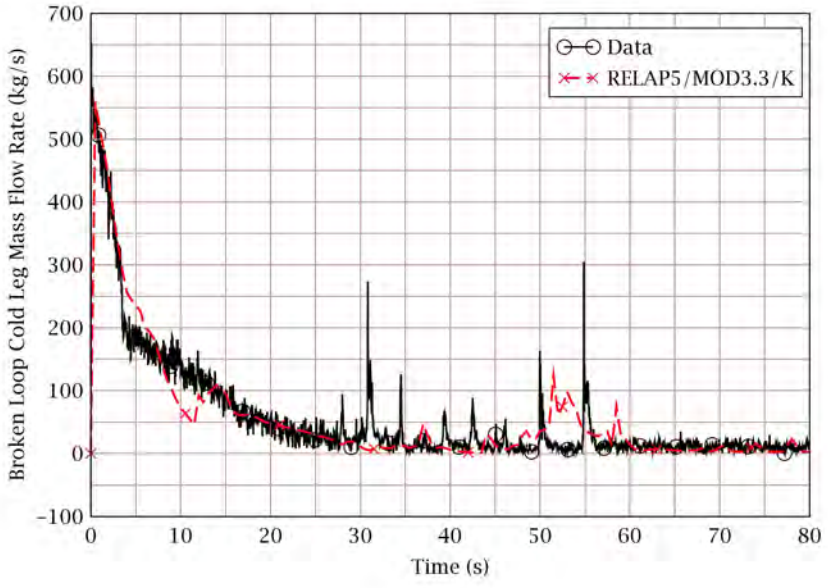

Figure 2-25 Broken Loop Cold Leg Mass Flow Rate: Test LP-02-6

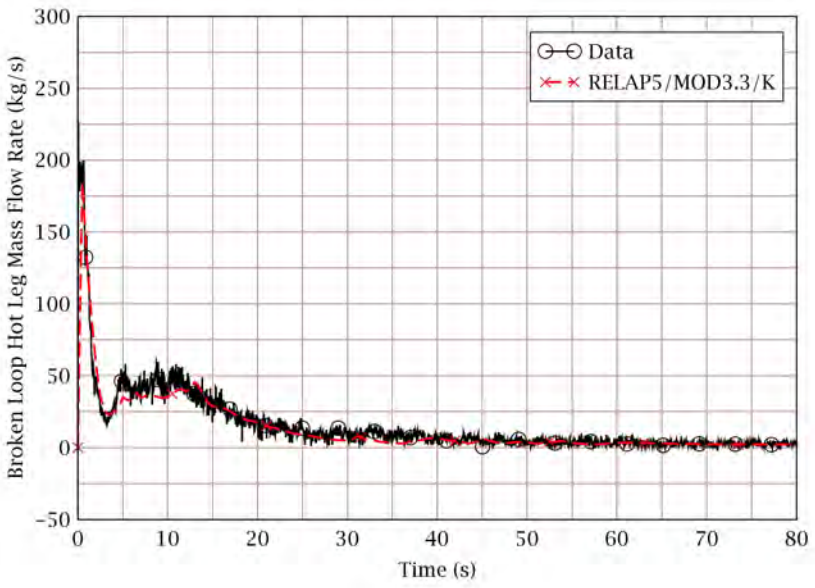

Figure 2-26 Broken Loop Hot Leg Mass Flow Rate: Test LP-02-6

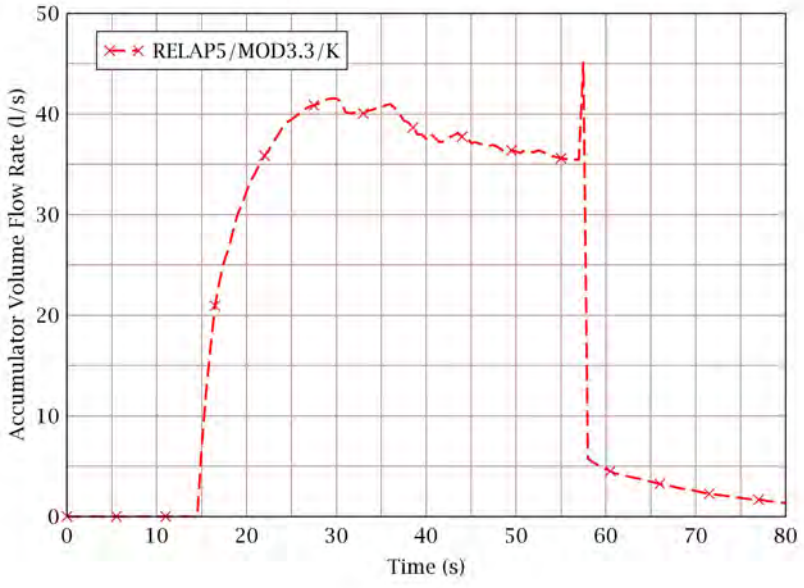

Figure 2-27 Accumulator Injection Flow Rate (volumetric): Test LP-02-6

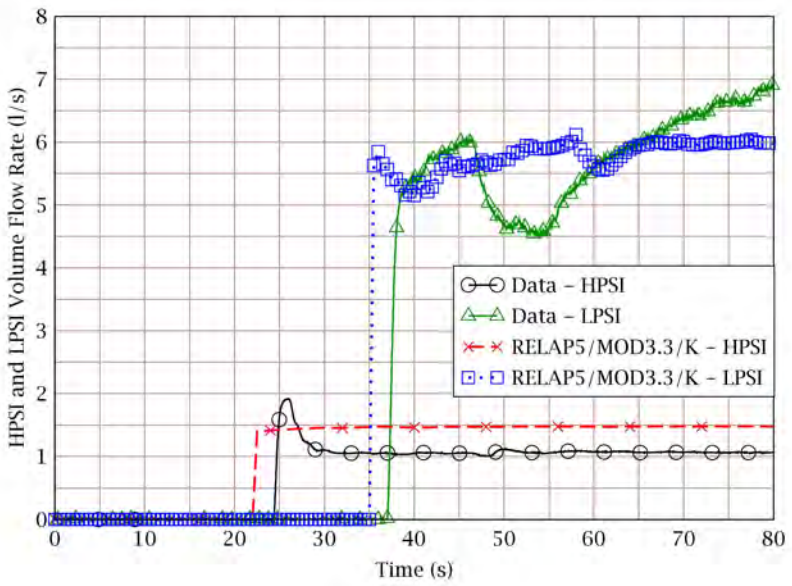

Figure 2-28 HPSI and LPSI Flow Rates (volumetric): Test LP-02-6

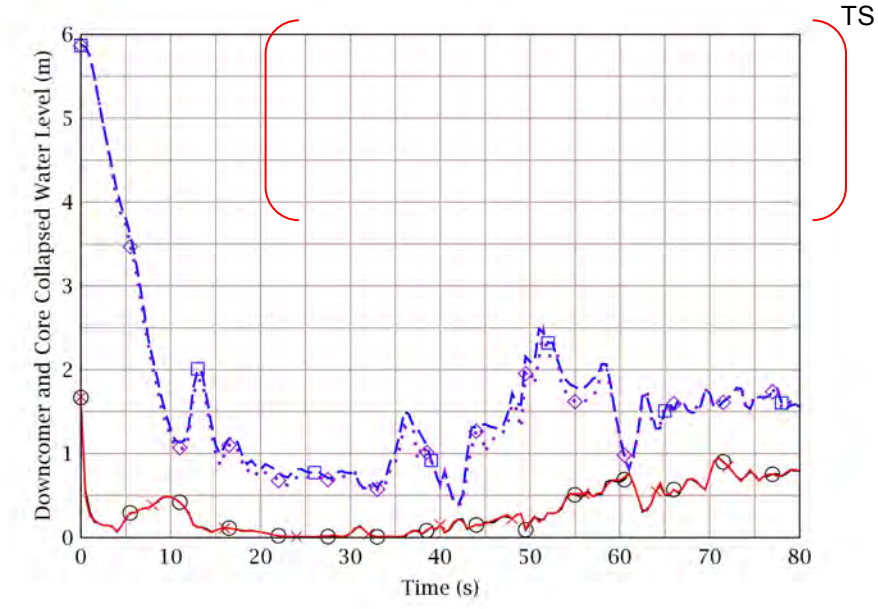

Figure 2-29 Downcomer and Core Collapsed Water Levels: Test LP-02-6

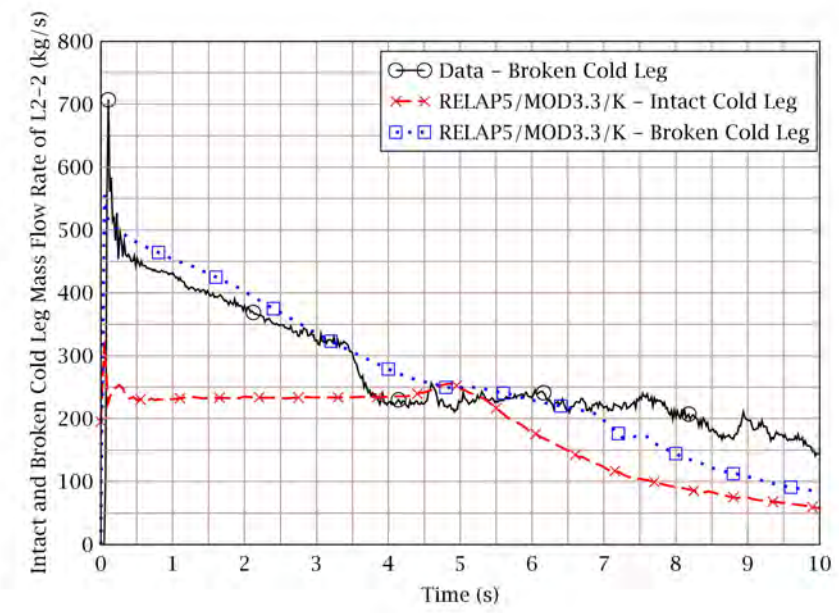

Figure 2-30 Intact and Broken Cold Leg Mass Flow Rates: Test L2-2

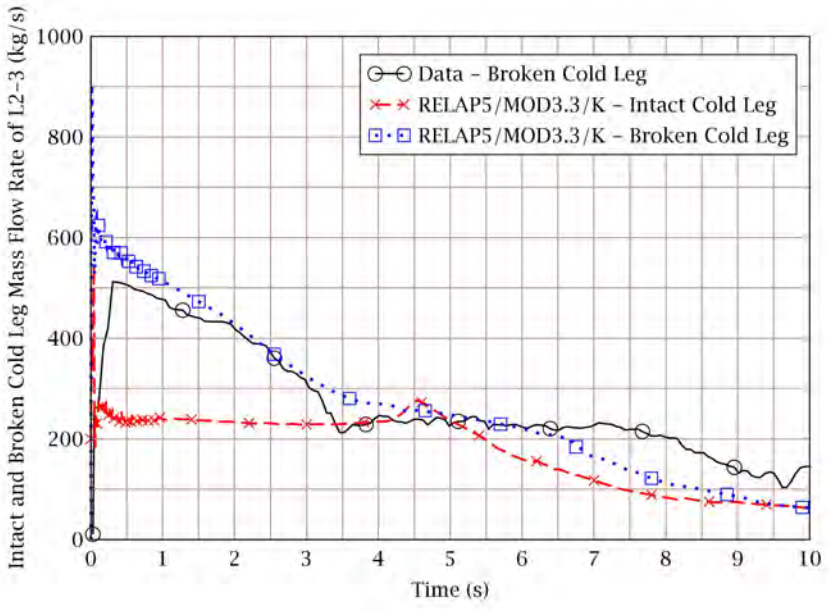

Figure 2-31 Intact and Broken Cold Leg Mass Flow Rates: Test L2-3

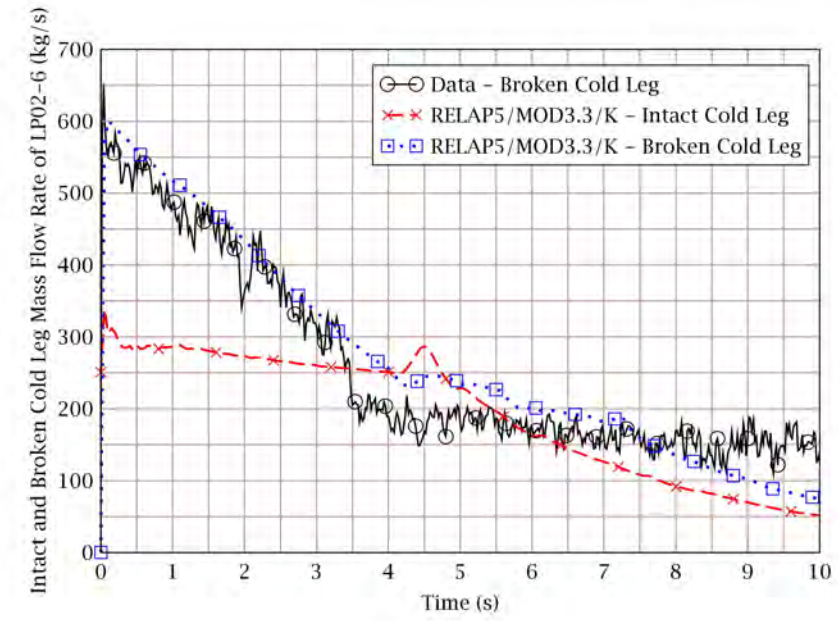

Figure 2-32 Intact and Broken Cold Leg Mass Flow Rates: Test LP-02-6

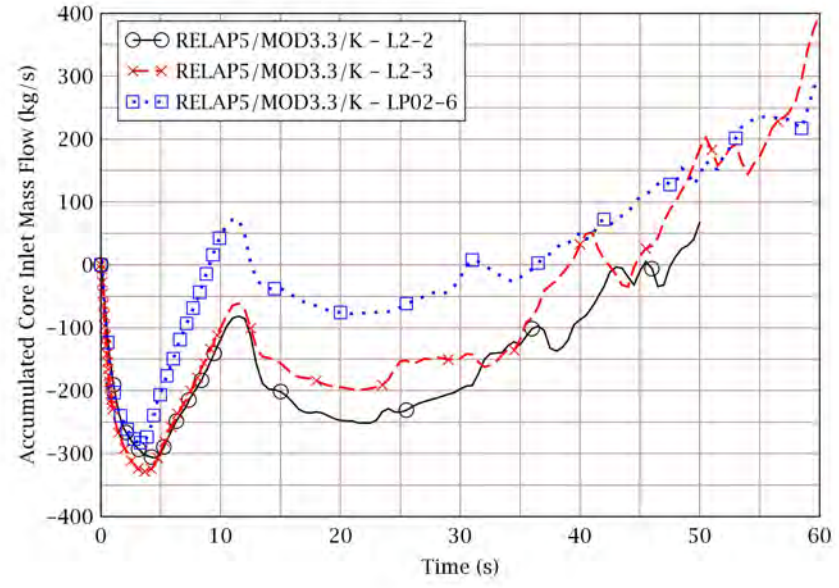

Figure 2-33 Accumulated Core Inlet Mass Flow: Tests L2-2, L2-3 and LP-02-6

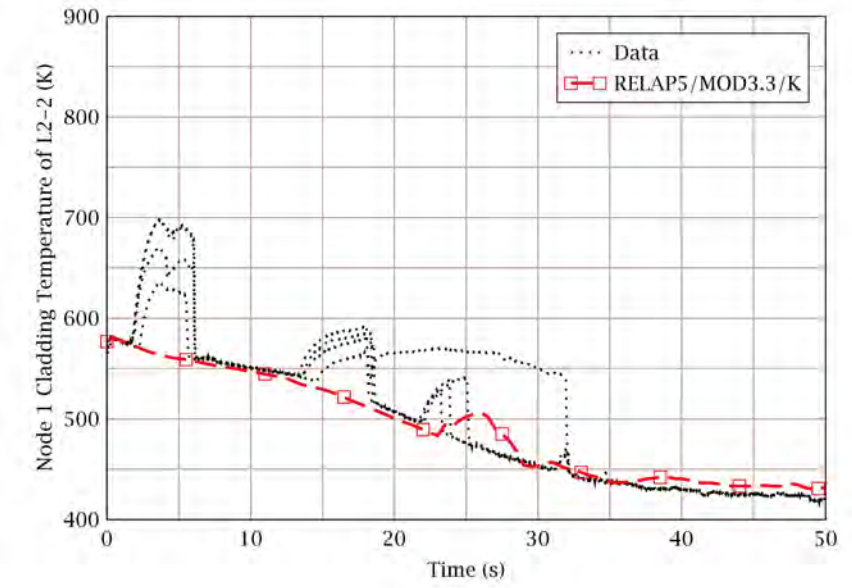

Figure 2-34 Rod Cladding Temperatures at Node 1: Test L2-2

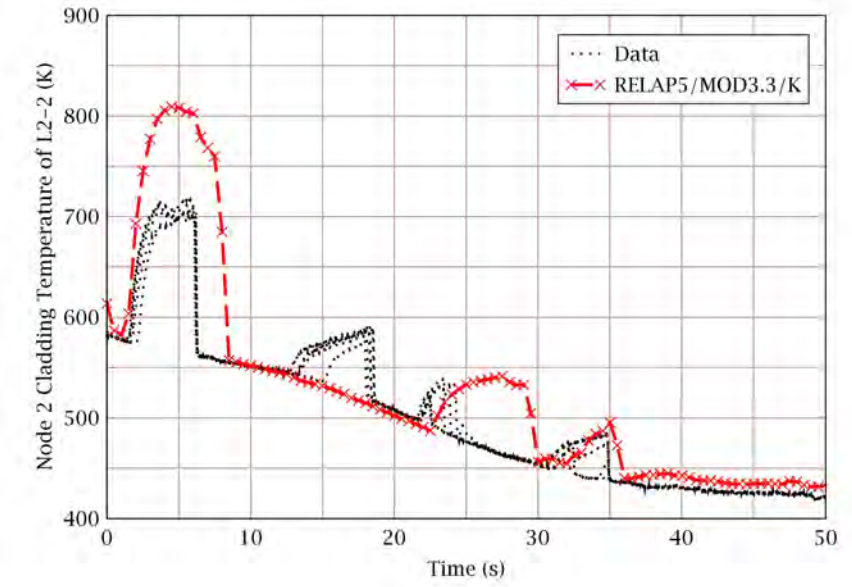

Figure 2-35 Rod Cladding Temperatures at Node 2: Test L2-2

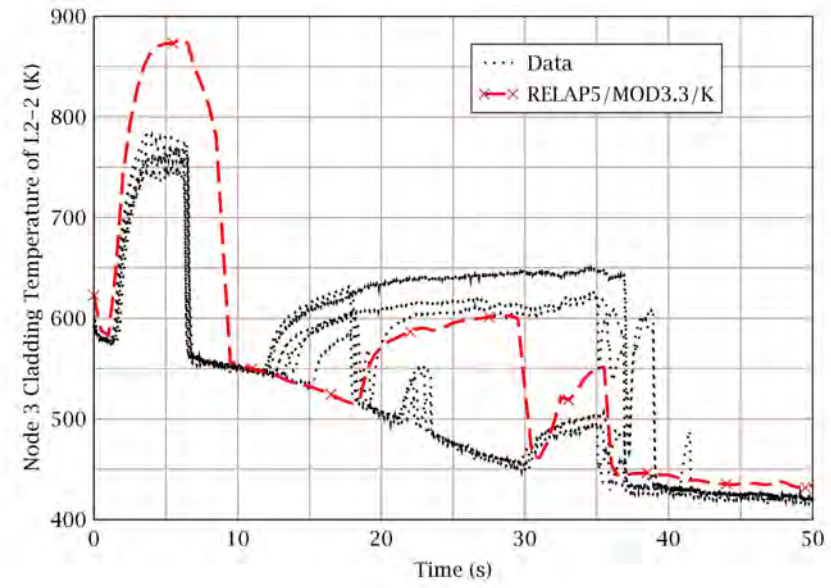

Figure 2-36 Rod Cladding Temperatures at Node 3: Test L2-2

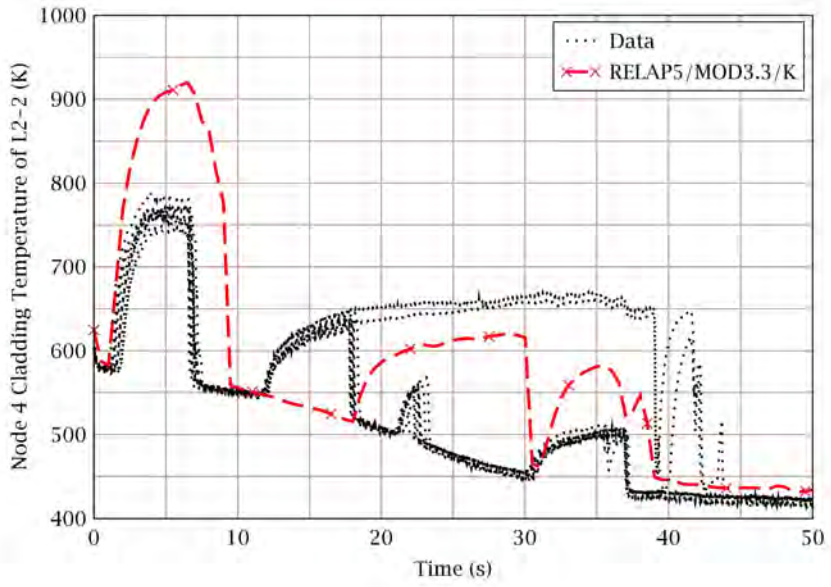

Figure 2-37 Rod Cladding Temperatures at Node 4: Test L2-2

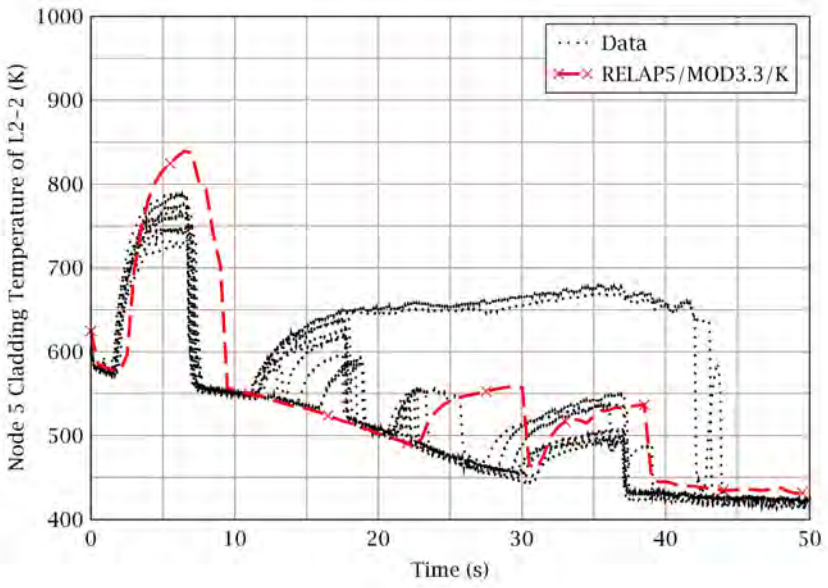

Figure 2-38 Rod Cladding Temperatures at Node 5: Test L2-2

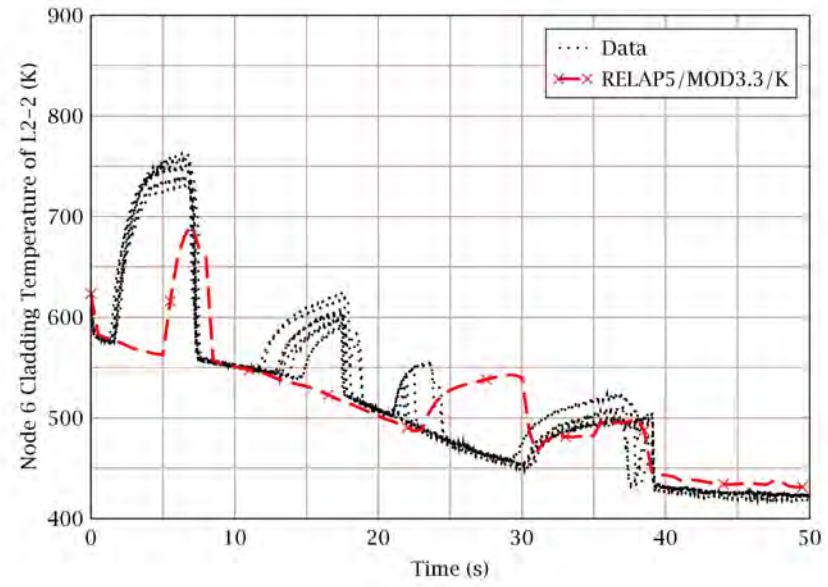

Figure 2-39 Rod Cladding Temperatures at Node 6: Test L2-2

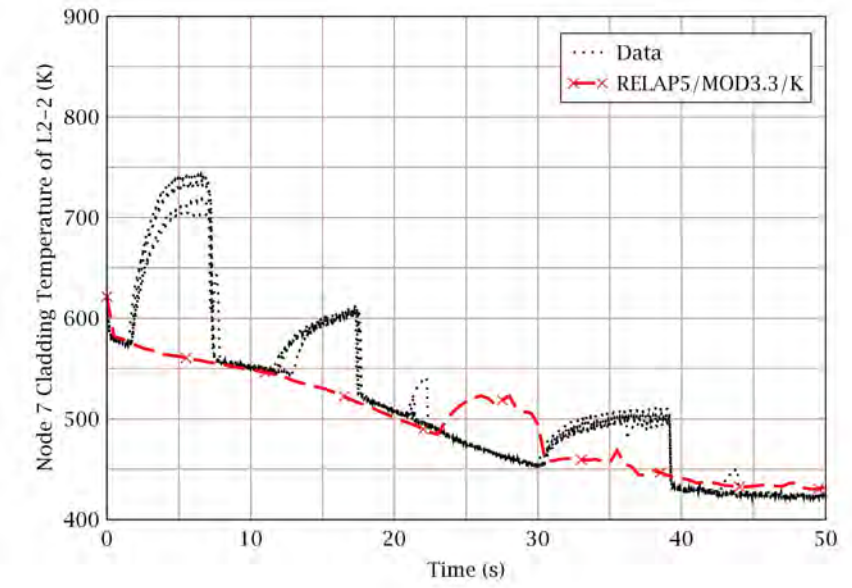

Figure 2-40 Rod Cladding Temperatures at Node 7: Test L2-2

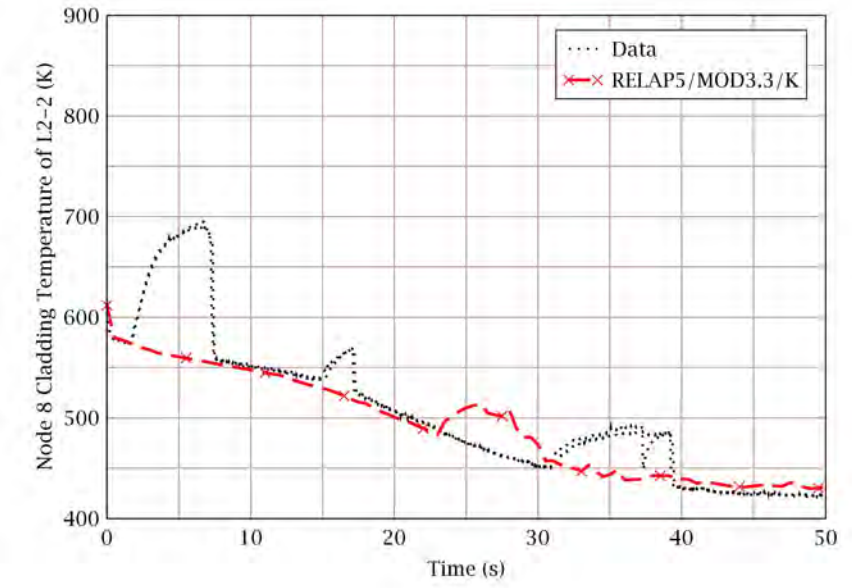

Figure 2-41 Rod Cladding Temperatures at Node 8: Test L2-2

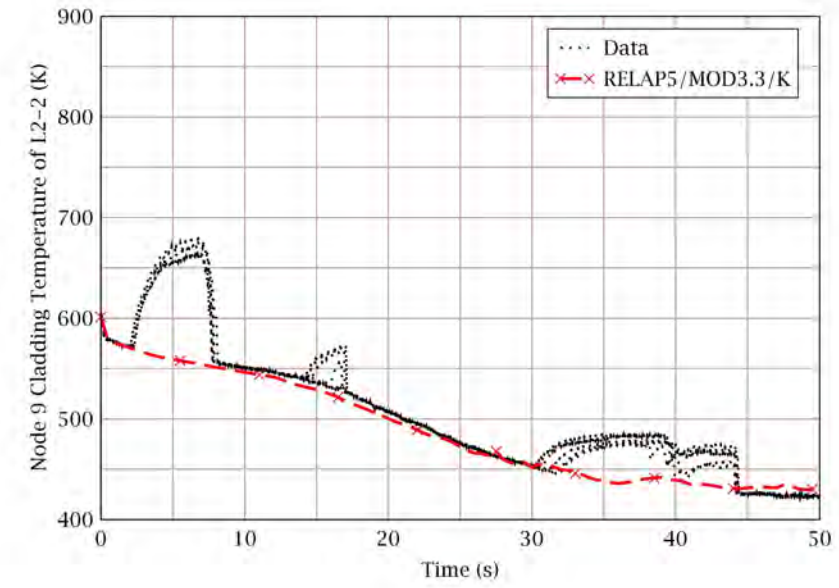

Figure 2-42 Rod Cladding Temperatures at Node 9: Test L2-2

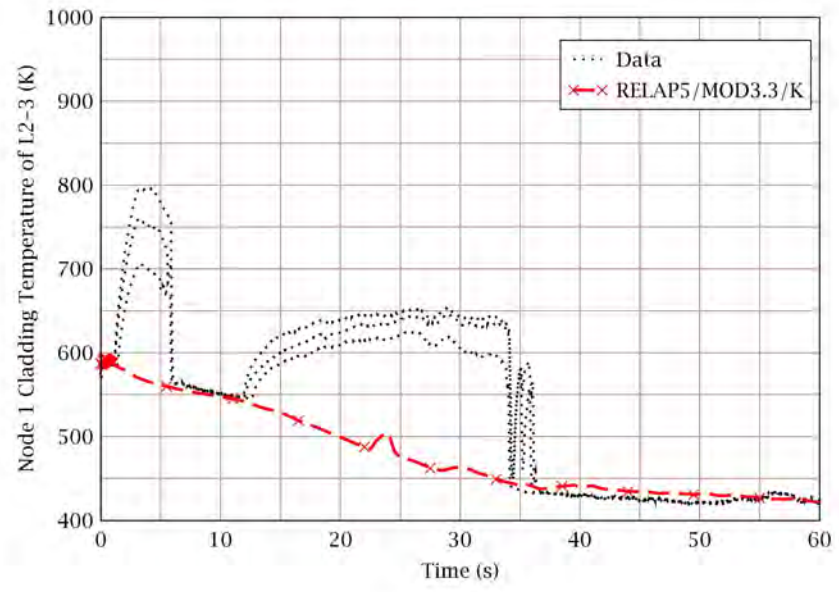

Figure 2-43 Rod Cladding Temperatures at Node 1: Test L2-3

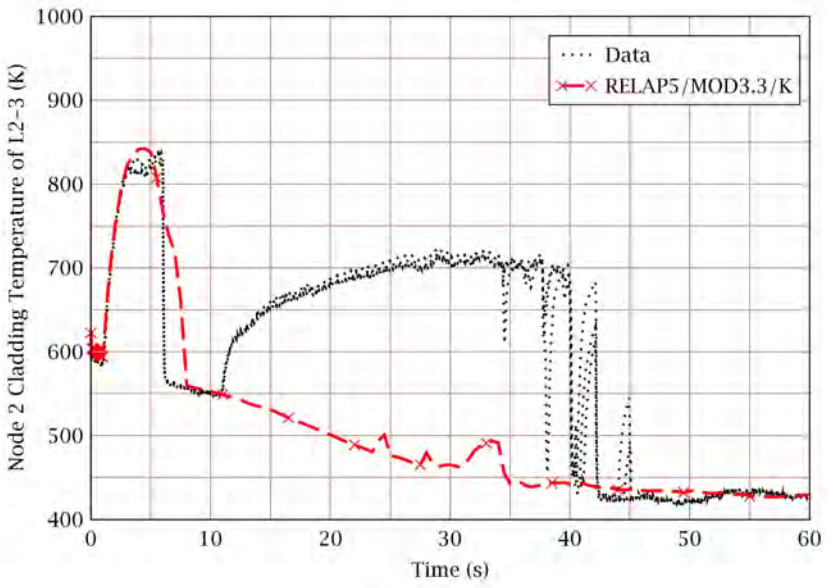

Figure 2-44 Rod Cladding Temperatures at Node 2: Test L2-3

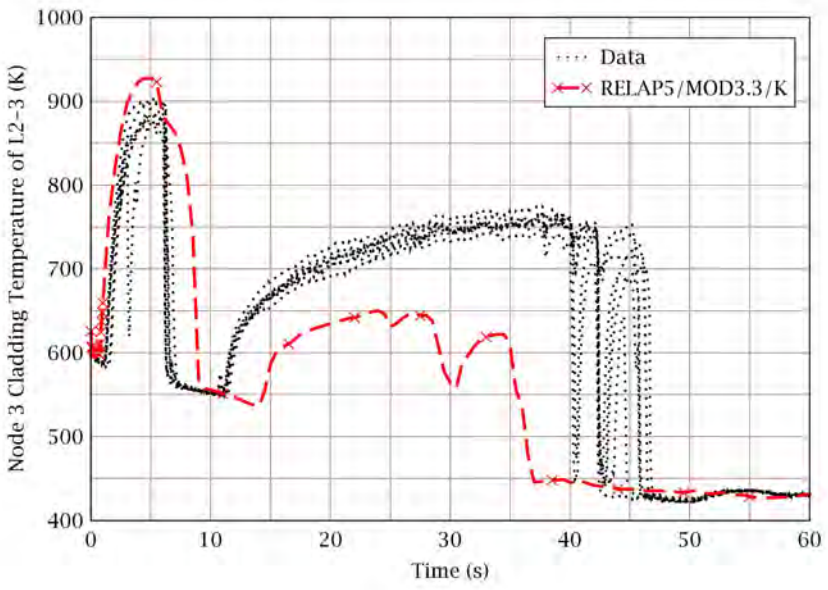

Figure 2-45 Rod Cladding Temperatures at Node 3: Test L2-3

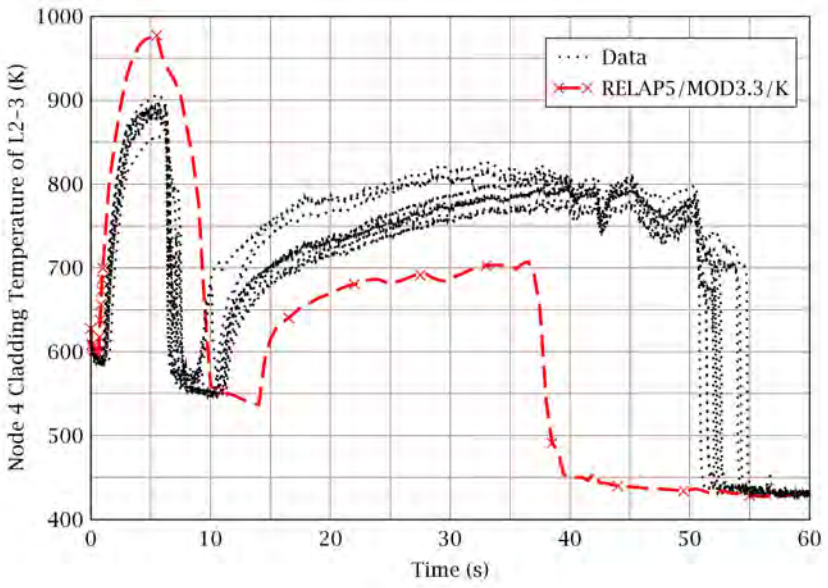

Figure 2-46 Rod Cladding Temperatures at Node 4: Test L2-3

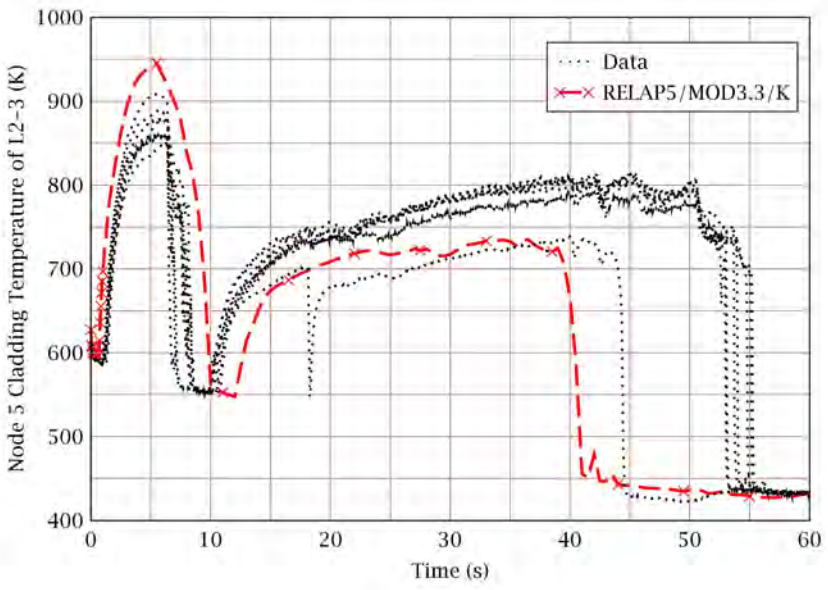

Figure 2-47 Rod Cladding Temperatures at Node 5: Test L2-3

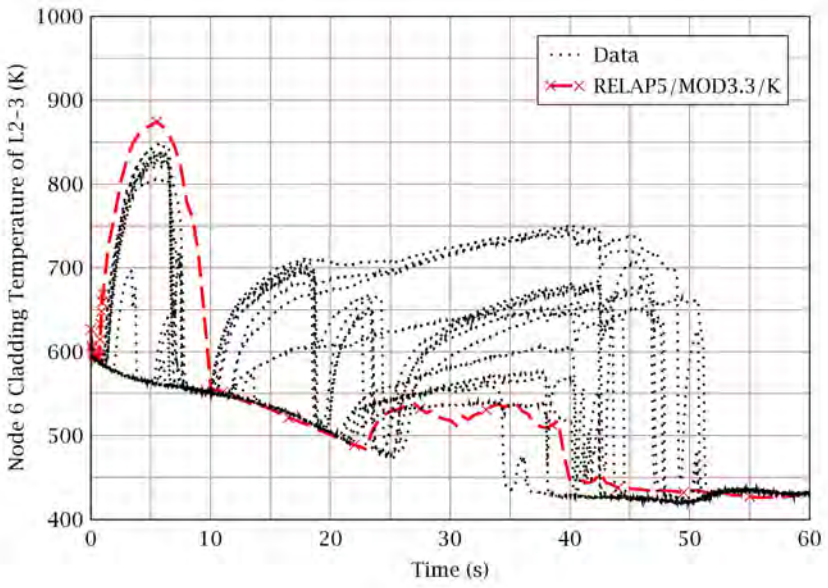

Figure 2-48 Rod Cladding Temperatures at Node 6: Test L2-3

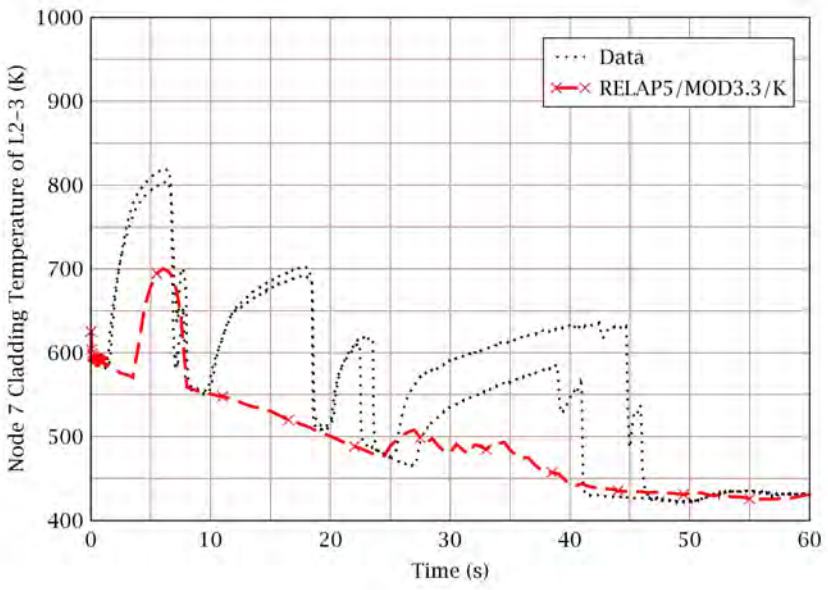

Figure 2-49 Rod Cladding Temperatures at Node 7: Test L2-3

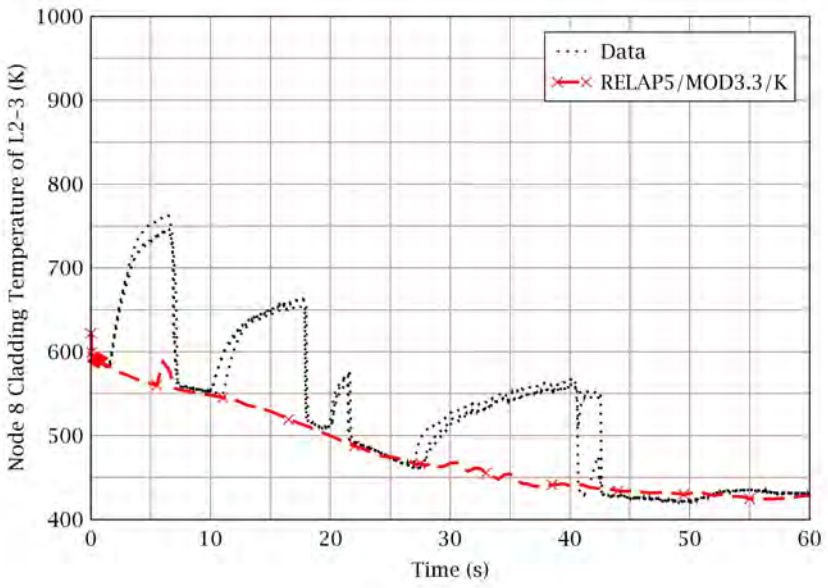

Figure 2-50 Rod Cladding Temperatures at Node 8: Test L2-3

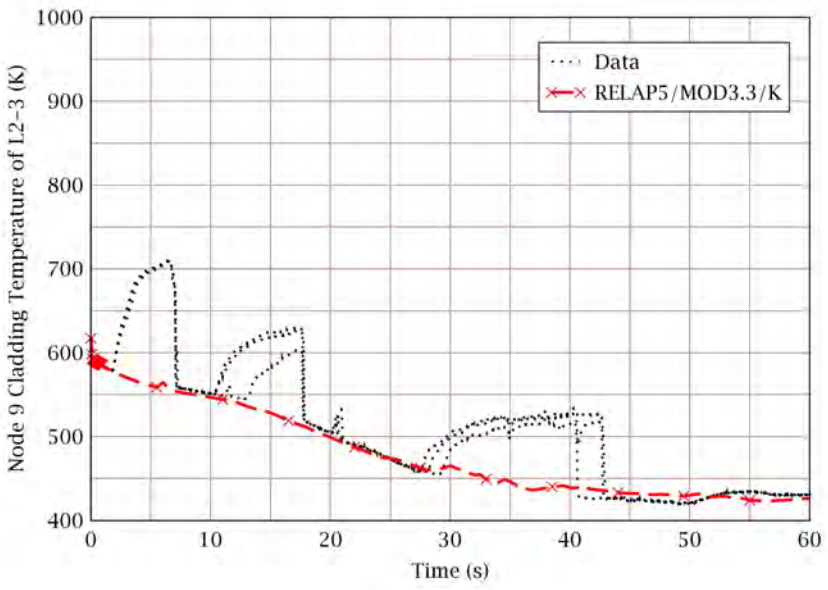

Figure 2-51 Rod Cladding Temperatures at Node 9: Test L2-3

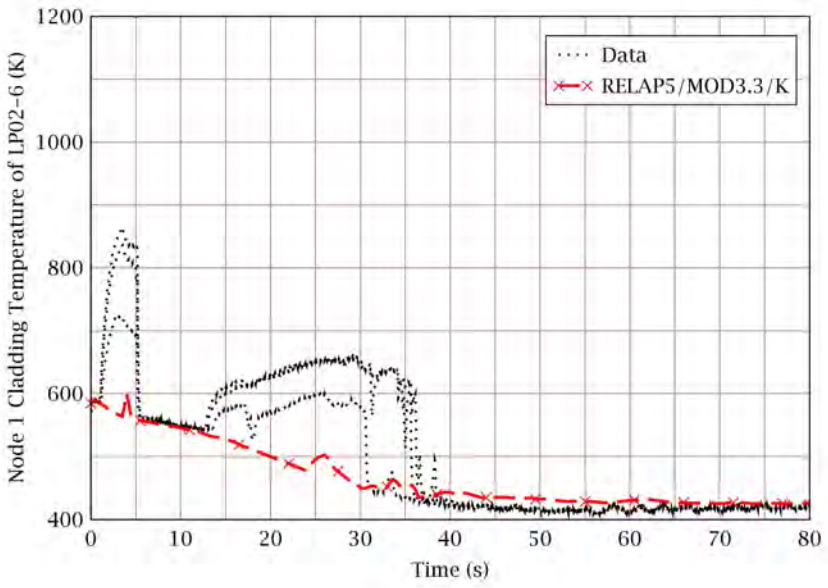

Figure 2-52 Rod Cladding Temperatures at Node 1: Test LP-02-6

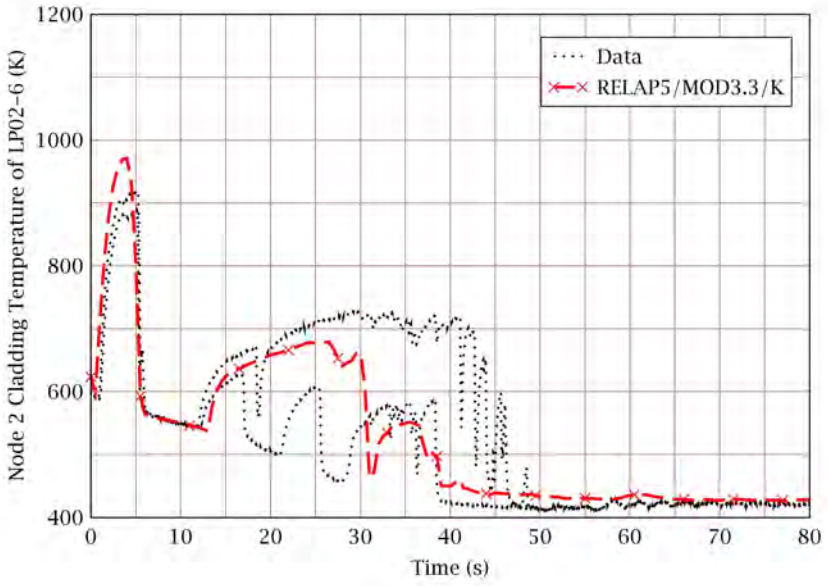

Figure 2-53 Rod Cladding Temperatures at Node 2: Test LP-02-6

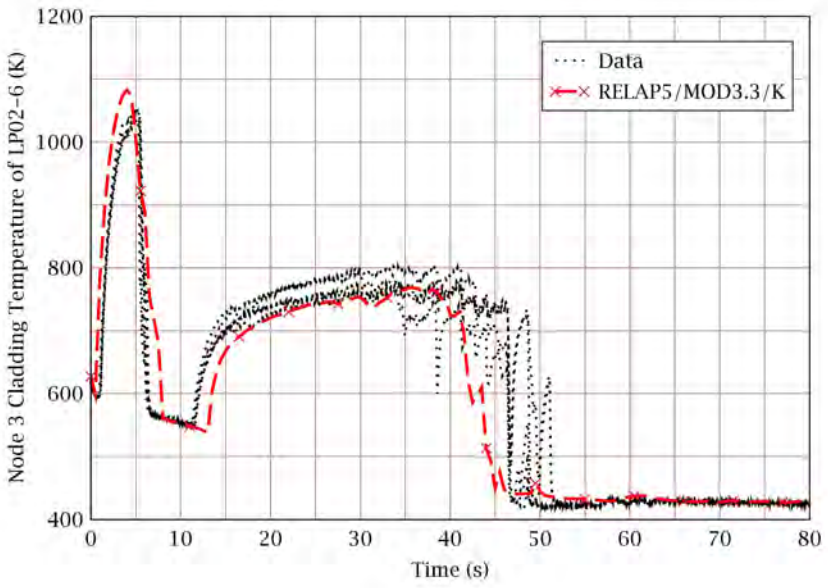

Figure 2-54 Rod Cladding Temperatures at Node 3: Test LP-02-6

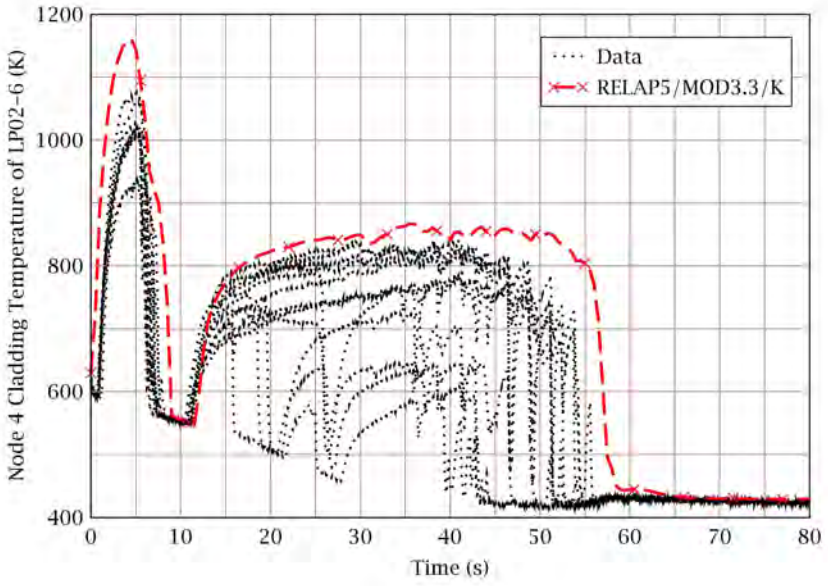

Figure 2-55 Rod Cladding Temperatures at Node 4: Test LP-02-6

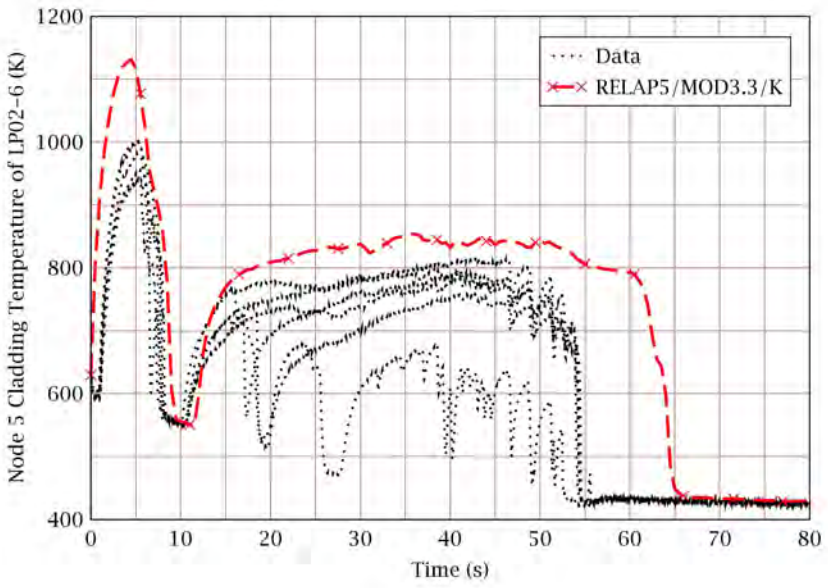

Figure 2-56 Rod Cladding Temperatures at Node 5: Test LP-02-6

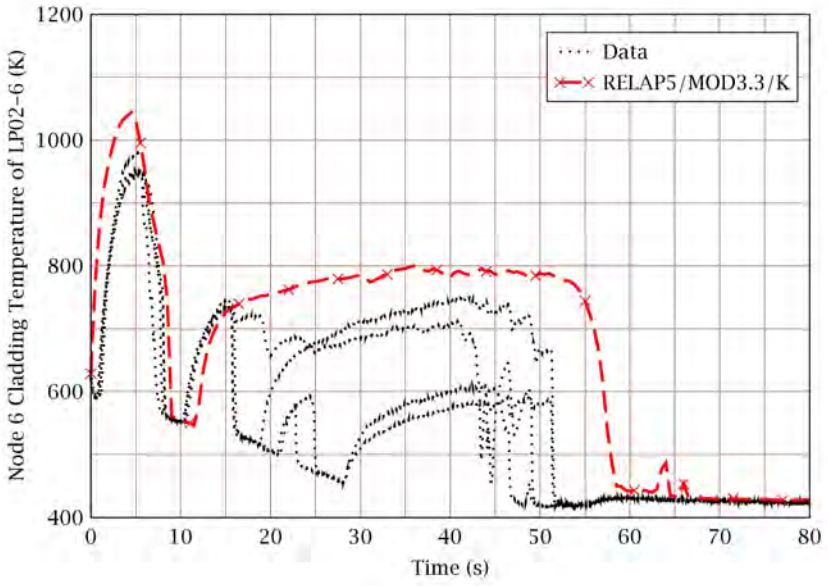

Figure 2-57 Rod Cladding Temperatures at Node 6: Test LP-02-6

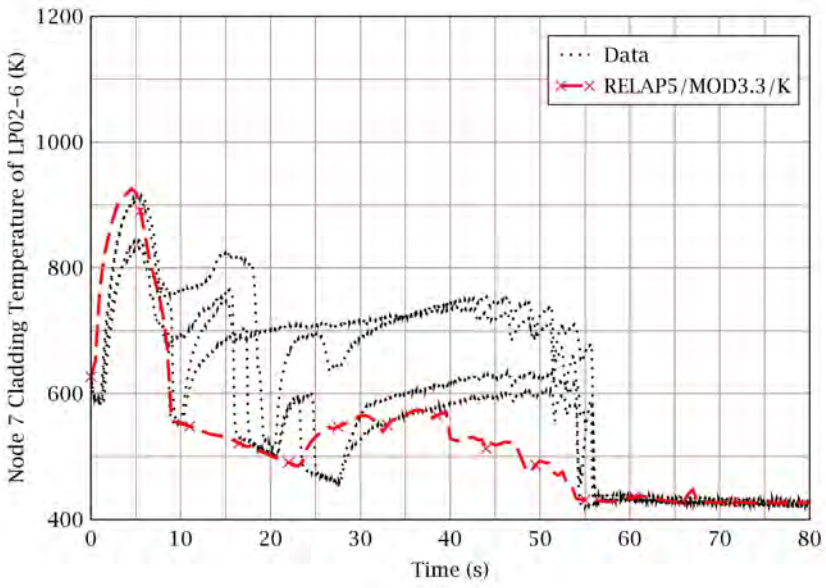

Figure 2-58 Rod Cladding Temperatures at Node 7: Test LP-02-6

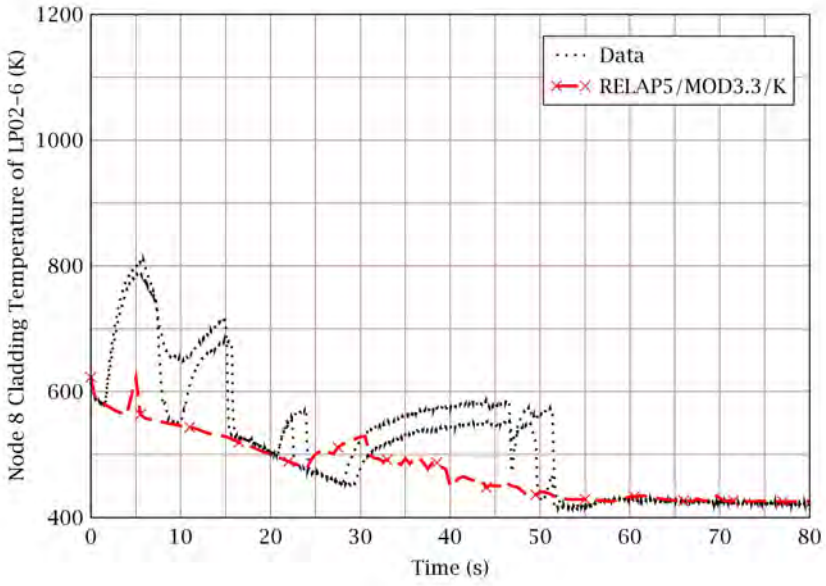

Figure 2-59 Rod Cladding Temperatures at Node 8: Test LP-02-6

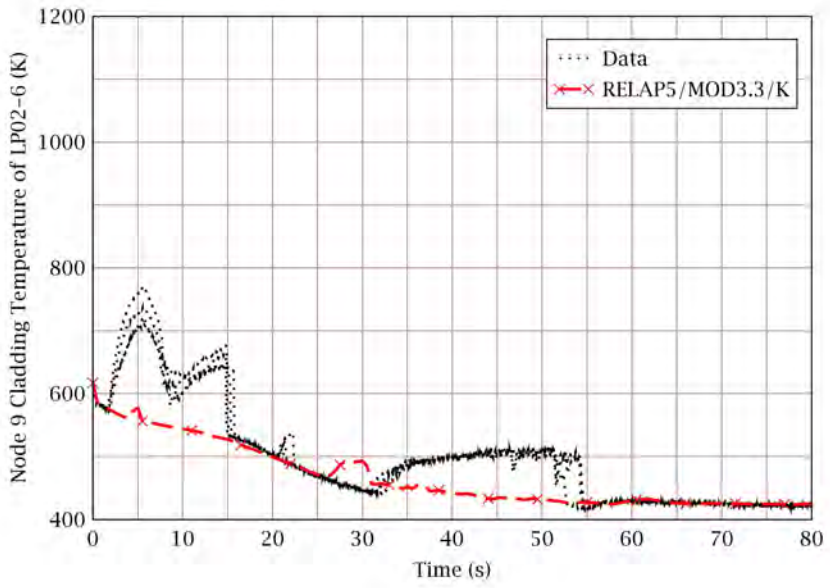

Figure 2-60 Rod Cladding Temperatures at Node 9: Test LP-02-6

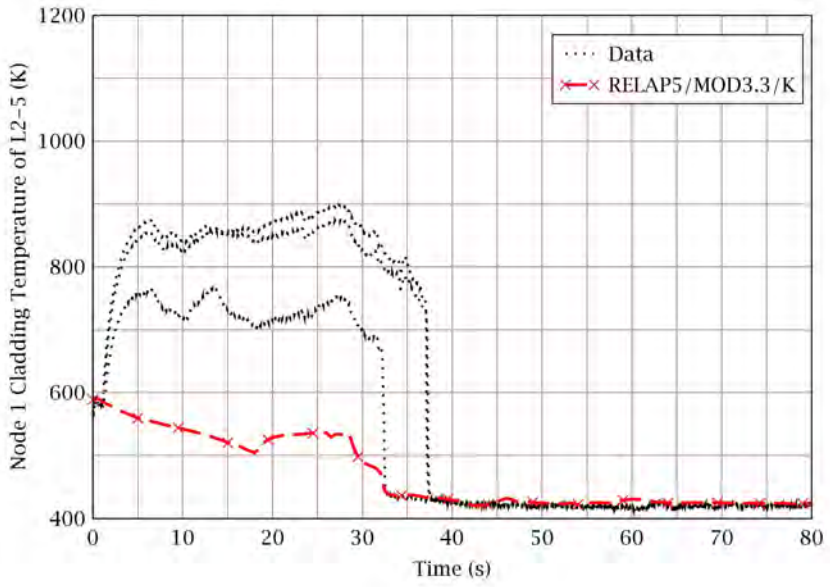

Figure 2-61 Rod Cladding Temperatures at Node 1: Test L2-5

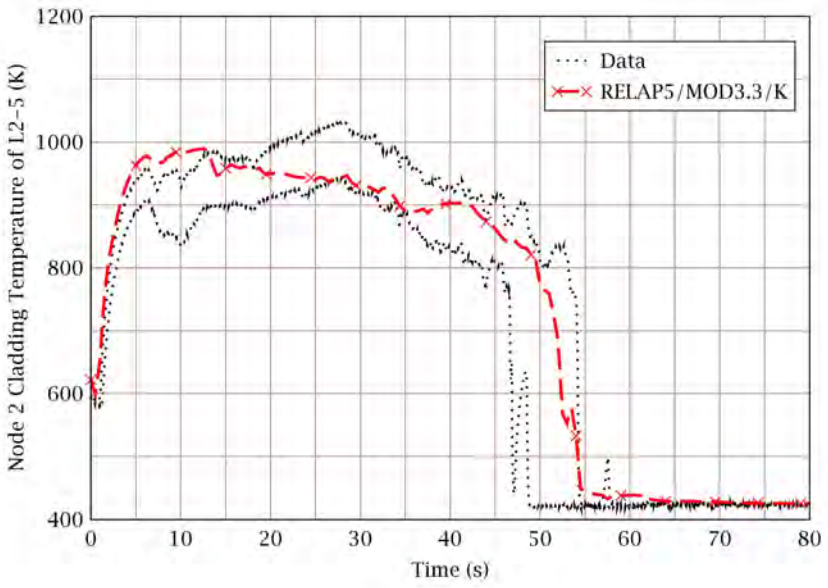

Figure 2-62 Rod Cladding Temperatures at Node 2: Test L2-5

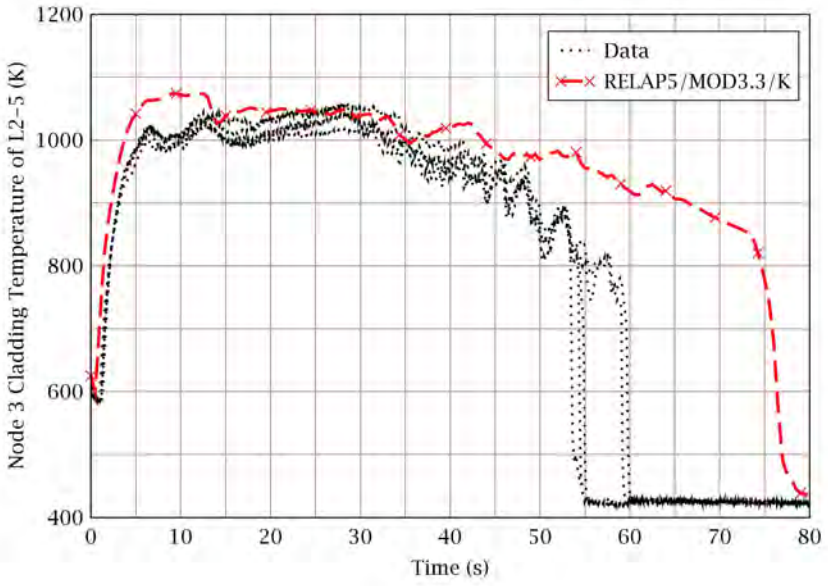

Figure 2-63 Rod Cladding Temperatures at Node 3: Test L2-5

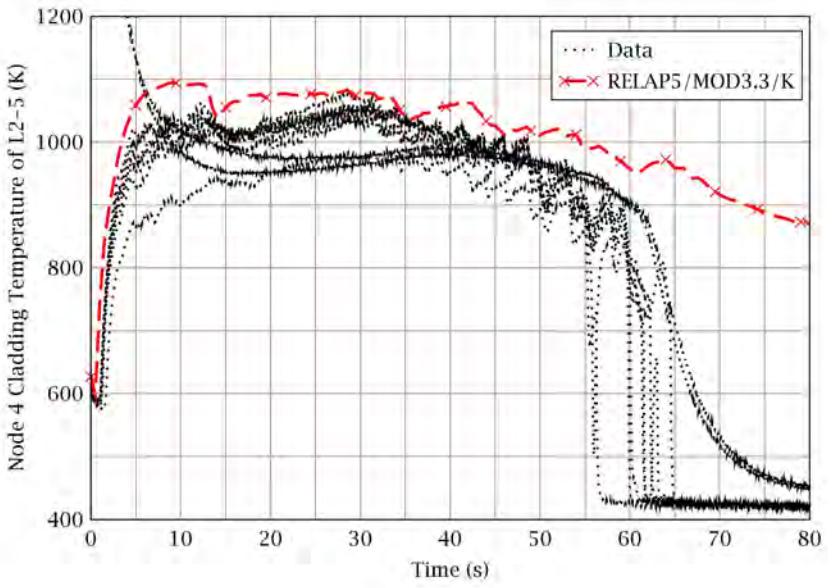

Figure 2-64 Rod Cladding Temperatures at Node 4: Test L2-5

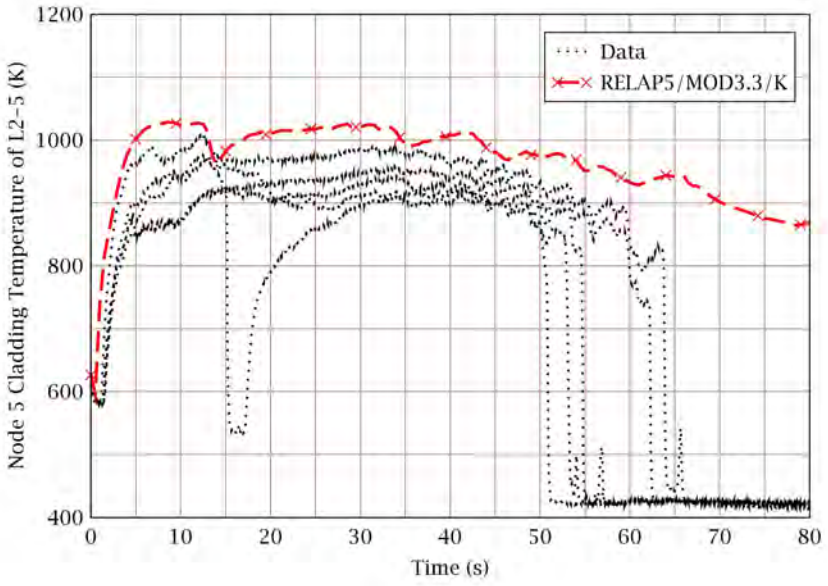

Figure 2-65 Rod Cladding Temperatures at Node 5: Test L2-5

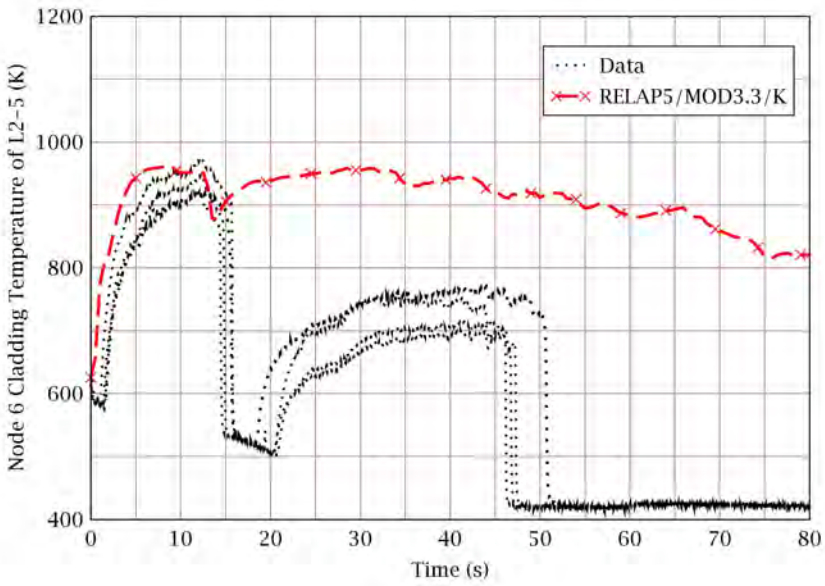

Figure 2-66 Rod Cladding Temperatures at Node 6: Test L2-5

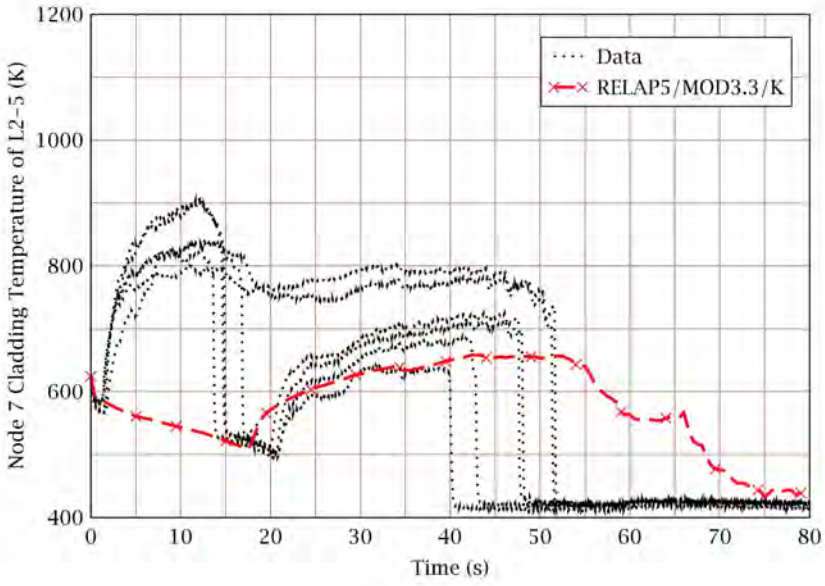

Figure 2-67 Rod Cladding Temperatures at Node 7: Test L2-5

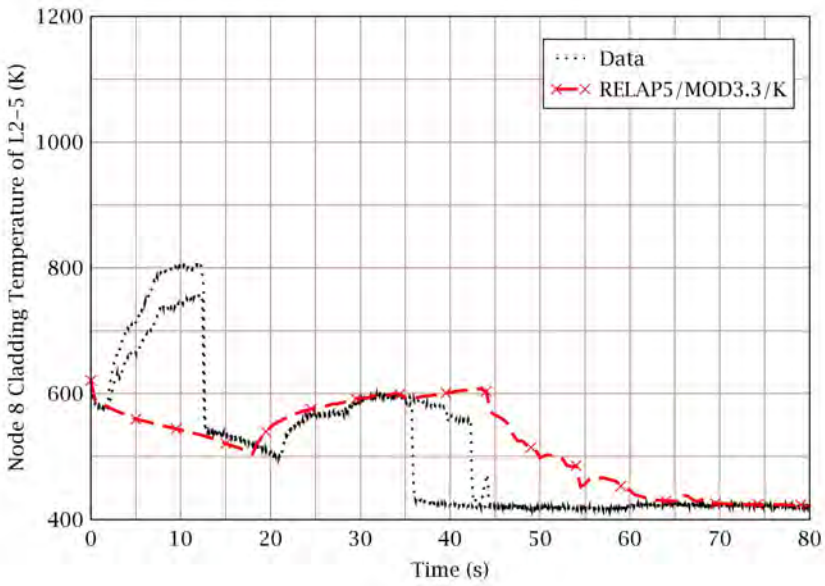

Figure 2-68 Rod Cladding Temperatures at Node 8: Test L2-5

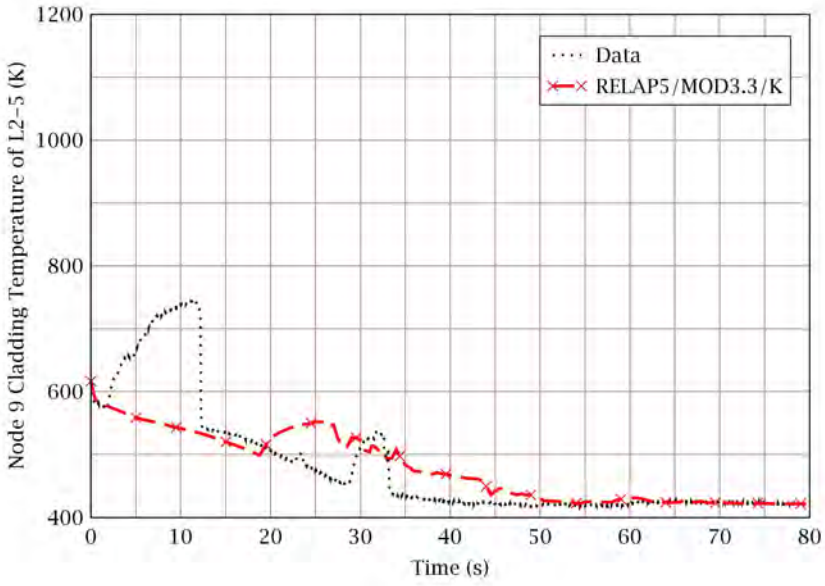

Figure 2-69 Rod Cladding Temperatures at Node 9: Test L2-5

TS

Figure 2-70 Blowdown Phase Code Accuracy Calculated Using the LOFT Test Data

TS

Figure 2-71 Reflood Phase Code Accuracy Calculated Using the LOFT Test Data

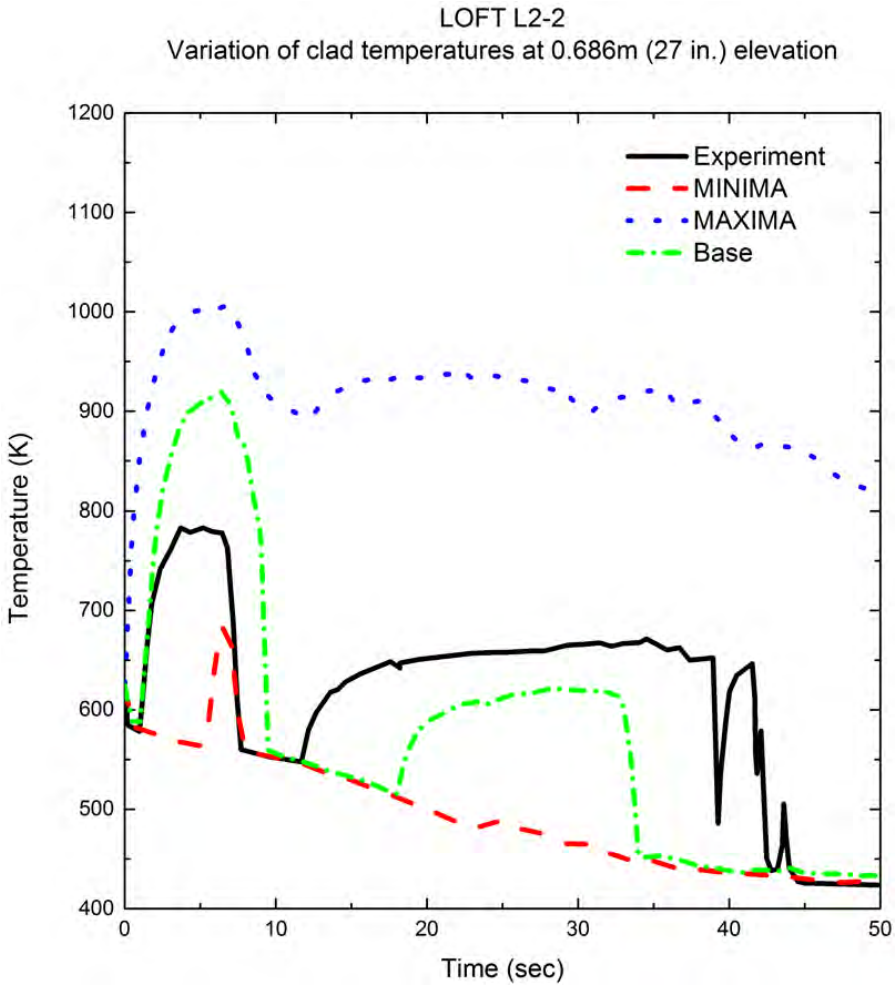

Figure 2-72 The Results of SRS Calculations: Test L2-2

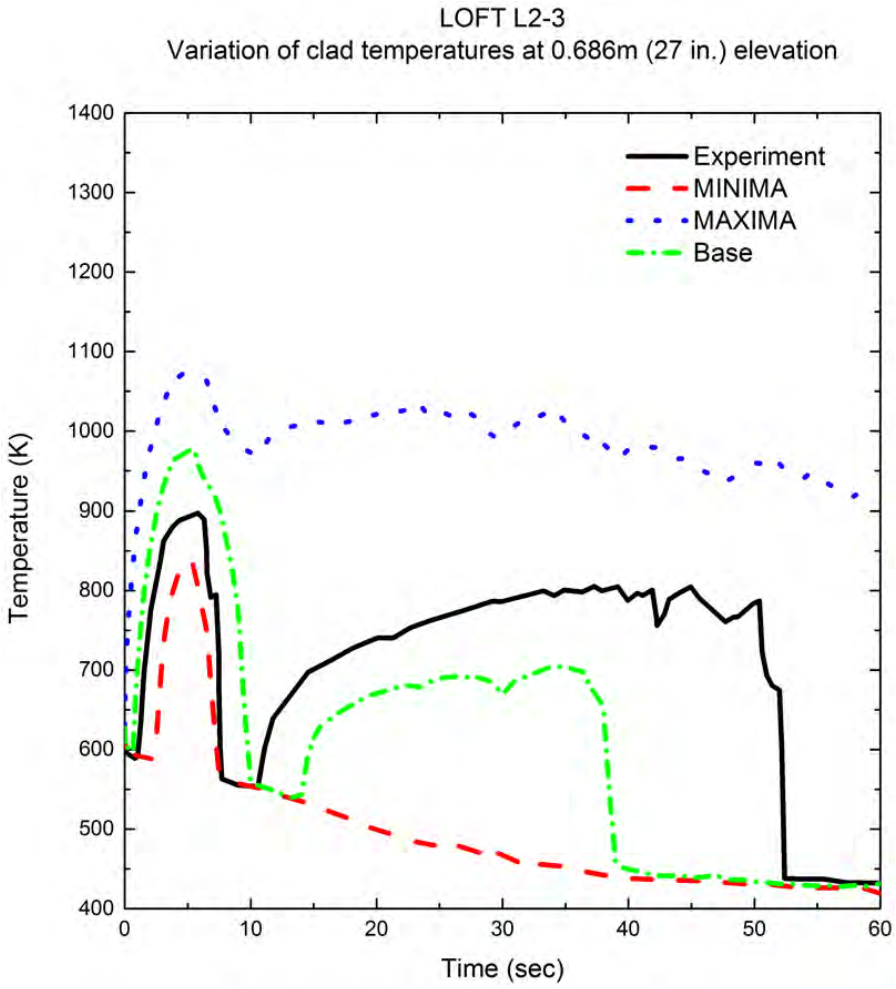

Figure 2-73 The Results of SRS Calculations: Test L2-3

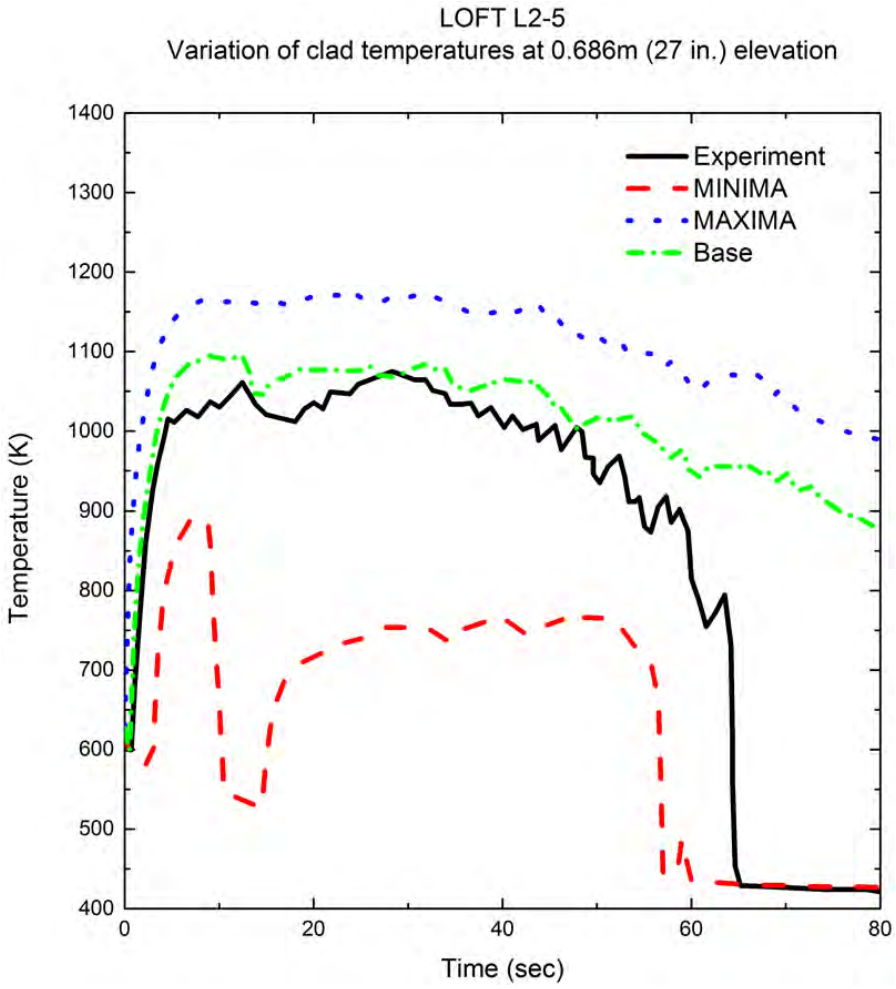

Figure 2-74 The Results of SRS Calculations: Test LOFT L2-5

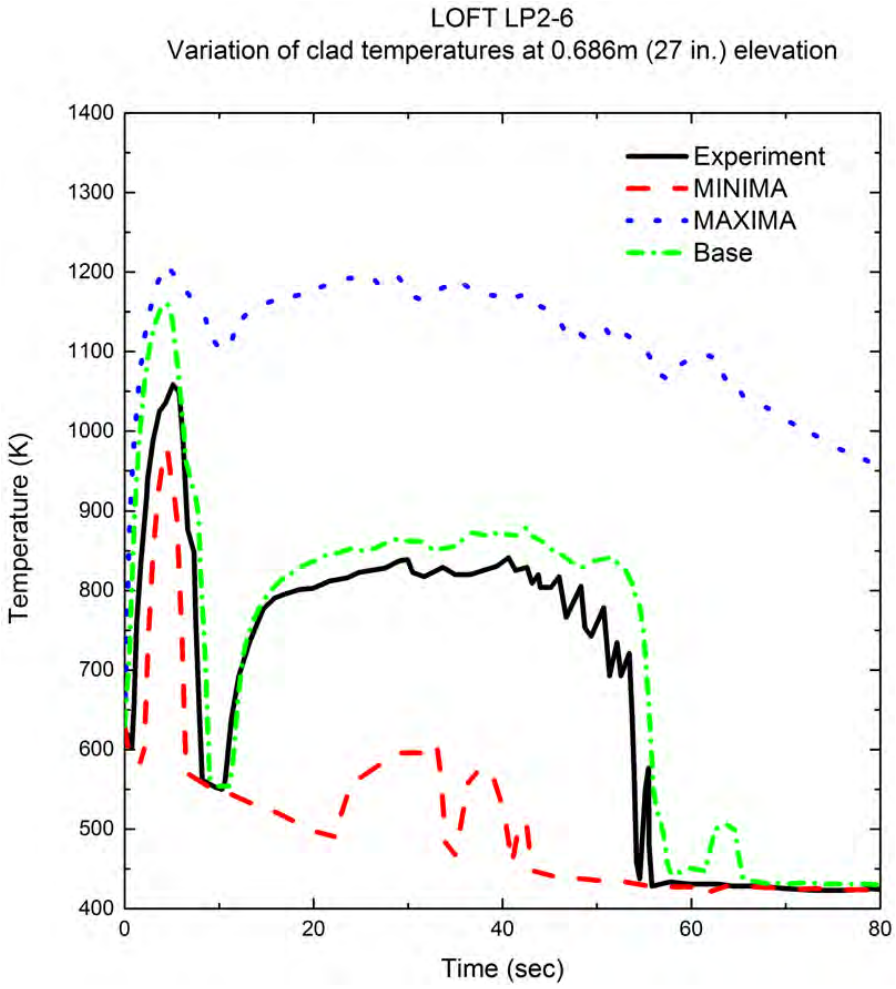

Figure 2-75 The Results of SRS Calculations: Test LP-02-6

3. Code Assessment against Semiscale S-06-3

This section describes RELAP5/MOD3.3/K assessment against test S-06-3 which was a portion of Mod-1 of the Semiscale experimental program. The Semiscale Mod-1 experiments were conducted by EG&G Idaho, Inc., for the United States Government. The program was sponsored by the Nuclear Regulatory Commission (NRC) and Department of Energy (DOE). The Semiscale Mod-1 facility was designed to simulate the Loss-of-Fluid-Test (LOFT). This modification investigated design basis accidents (200% double-ended offset shear breaks of the primary piping). The Mod-1 facility was used for a wide range of blowdown refill-reflood experiments as well as LOFT counterpart experiments. [3-1]

Test S-06-3 was one of the LOFT counterpart LBLOCA experiments (S-06 series) which were adjusted in an attempt to recreate LOFT phenomena such as early rewet during blowdown phase.

3.1 Test Facility Description

The Semiscale Mod-1 system consisted of a pressure vessel with simulated reactor internals which had 40 rods including 36 electrically heated rods; an intact loop with steam generator, pump, and pressurizer; a broken loop with simulated steam generator, simulated pump, simulated reflood bypass lines, LOFT counterpart nozzle, and two rupture assemblies; a pressure suppression system with header and auxiliary steam supply; suppression tank; and a coolant injection system with injection pumps, accumulators, and delivery piping. The intact loop simulated three operating loops of a commercial PWR, and the broken loop simulated a broken loop of a PWR during a LOCA. The exterior of the entire system and piping was thermally insulated. The detailed information for the Semiscale Mod-1 system is provided in reference [3-2].

The Semiscale Mod-1 system for cold leg break configuration is shown in Figure 3-1. The Mod-1 system broken loop was subjected to simulating a double-ended cold leg break through two rupture assemblies and two LOFT counterpart nozzles, each having a break area of 2.43 cm^2. In this broken loop, the pump and steam generator were simulated with flow resistance.

The electric heater rod matrix and plan view for Semiscale Mod-1 core is shown in Figure 3-2 and Figure 3-3, respectively. Test S-06-3 was performed to determine the maximum cladding temperature associated with a high-powered rod peak density of 39.4 kW/m, or 75 % of the maximum peak power density of 52.5 kW/m. The power density was 39.4 kW/m for four rods (rod D-4, D-5, E-4, and E-5), and 24.5 kW/m for 32 rods. The other four rods (rod C-4, D-6, E-3 and S-6) were unpowered to simulate LOFT passive rod locations. This configuration yielded a peaked power profile which simulates that of LOFT and provided a total core power of approximately 1.004 MW.

3.2 Test S-06-3 Description

Test S-06-3 was conducted with initial conditions of 15,769 kPa and 563 K (at the intact loop cold leg vessel inlet), core power of 1.004 MW, and 6.68 l/sec core inlet flow rate. This test simulated a double-ended guillotine cold leg break by simultaneous (within 10 ms) actuation of the rupture assemblies. After initiation of blowdown, power to the heated core was reduced to simulate the predicted heat flux response of nuclear fuel rods during a LOCA. Coolant injection from the high pressure injection system (HPIS) pump began at blowdown and continued until 300 s test termination time. Coolant injection from the accumulator started approximately 18.5 s after rupture at a system pressure of 4,200 kPa and continued to depletion at 68 s after blowdown. Low pressure coolant injection (LPIS) began 25.5 s after rupture at a system pressure of 1,900 kPa and continued until 300 s. The core power was tripped off at 300 s after rupture and the test was terminated.

3.3 RELAP5/MOD3.3/K Model Description

The RELAP5/MOD3.3/K input models of the Semiscale Mod-1 facility is shown in Figure 3-4.

A total of [
]TS axial nodes. The [

]TS

The lower plenum of the reactor vessel is modeled using [
]TS. The upper plenum of the reactor vessel is also modeled using [
]TS. The downcomer of the reactor vessel is [
]TS Each downcomer channel has [ ]TS axial volumes. [ ]TS

The vessel of the pressurizer connected to the intact loop is modeled using [
]TS For the steam generator of the intact loop, the primary side including inlet and outlet plenum is modeled using [
]TS For the modeling of the steam generator of the broken loop, [
]TS are used to model the primary side. The reactor coolant pump is modeled using PUMP component with adequate pressure loss coefficient.

Emergency core cooling system (ECCS) which consisted of HPIS, LPIS and accumulator are modeled using three sets of time-dependent volumes and junctions.

[ ]TS are used to model near pump and near vessel breaks. Two identical time-dependent volumes connected to each break are used to simulate the pressure suppression tank.

In addition to the system modeling, the following assumptions are made so that undesired calculation uncertainties can be avoided:

TS

The calculated steady state conditions achieved by using some initialization techniques are listed in Table 3-1 with the measured data [3-3]. The calculated initial conditions match well the data.

3.4 RELAP5/MOD3.3/K Simulation

This section provides the assessment results and measured data. The whole test can be into three phases, blowdown, refill and reflood. The blowdown phase is characterized by a fast system depressurization and finally the system is in equilibrium with the surroundings. During this phase most of fuel rods experience critical heat flux (CHF) due to rapid loss of reactor coolant. In the refill phase, owing to the injection of ECC water (ECCW), coolant begins to accumulate in the lower

plenum of reactor vessel. Once lower plenum is filled up, reflood phase begins. In this phase, since ECCW is injected continuously, core water level is increasing to the active core and finally all fuel rods are rewetted.

3.4.1 Blowdown Phase (0 ~ 35 s)

The calculated break mass flow rates at two ends of the breaks are compared in Figure 3-5 and Figure 3-6. RELAP5/MOD3.3/K slightly under-predicts the mass flow rate at the pump side break as shown in Figure 3-5 (or Figure 3-28). However, the code reasonably predicts the general trend of the data. The code predicts well the mass flow rate at the vessel side break before ECCW bypass begins, as shown in Figure 3-6 (or Figure 3-22).

Figure 3-7 (or Figure 3-29) shows a comparison of measured and calculated values of the pressurizer pressure. Even though the predicted pressure shows that the sharp decrease of the pressure occurs slightly later than the data, the general trend of the predicted result matches the data well. The calculated mass flow rate at the pressurizer surge line is compared with the data in Figure 3-8 (or Figure 3-30). The decrease of mass flow rate at the surge line implies that the inventory in the pressurizer is depleted. The predicted pressurizer depletion time is slightly later than the data and this causes that the sharp decrease of the pressure occurs slightly later than the data.

The intact loop cold leg and hot leg flow rates calculated by RELAP5/MOD3.3/K are compared with the data in Figure 3-9 (or Figure 3-31) and Figure 3-10 (or Figure 3-32), respectively. The calculated intact loop cold leg flow rate matches well the test data during blowdown phase. The calculated result of hot leg flow rate shows that the flow decrease rate is under-predicted and the reverse flow occurs later than the data.

The broken loop cold leg and hot leg flow rates predicted by RELAP5/MOD3.3/K are compared with the data in Figure 3-11 (or Figure 3-31) and Figure 3-12 (or Figure 3-34), respectively. The code predicts well both the cold leg and hot leg flow rates.

Figure 3-13 (or Figure 3-35) shows a comparison of measured and calculated values of the core inlet mass flow rate, and Figure 3-14 (or Figure 3-23) shows water level in the downcomer. As soon as the break opens, both of the measured and the calculated core inlet flow rates sharply decreases because the coolant flows out through the break. The code predicts well the core inlet mass flow rate. Water level in the downcomer also decreases sharply after the break opening and there is nearly no water at the end of blowdown phase. Even though the code predicts that the downcomer water level continuously decreases after 8 s, it reasonably predicts the general behavior of the downcomer water level.

The water level in the lower plenum is shown in Figure 3-15 (or Figure 3-24). Since the lower plenum is the lowest region of reactor pressure vessel, the water level varies relatively slowly. About 1/3 of the lower plenum height was filled with water at the end of blowdown phase of the test. RELAP5/MOD3.3/K reasonably predicts the water level behavior in the lower plenum. The code also predicts well the core water level as shown in Figure 3-16 (or Figure 3-27).

As soon as the test was started, the system pressure was sharply decreased and the core flow was decreased to 0.0 kg/s due to the flow stagnation in the core. This core flow behavior caused a rapid increase of the cladding temperatures of the high- and low-powered rods, as shown in Figure 3-17 (or Figure 3-25) and Figure 3-18 (or Figure 3-26). RELAP5/MOD3.3/K predicts well not only the occurrence time of CHF but also the general trends of the rod cladding temperature behavior of the high- and low-powered rods during the blowdown phase.

The predicted fluid temperatures in the lower plenum and upper plenum are compared with the data in Figure 3-19 (or Figure 3-36) and Figure 3-20 (or Figure 3-37), respectively. Superheated steam was observed in the reactor vessel and RELAP5/MOD3.3/K also predicts the generation of

superheated steam in the reactor vessel. The calculation results of generation time of superheated steam and degree of super-heating, however, show some discrepancies from the data. The fluid temperature in the lower plenum was observed to increase sharply at around 24 s. This implies that the direction of the core steam flow is reversed at this time. The reverse flow was resulted from the effect of the condensation caused by accumulator injection [3-2].

3.4.2 Refill Phase (35 ~ 75 s)

ECC bypass phenomena were observed twice during the test [3-3]. First ECC bypass occurred during blowdown period by count current flow limitation phenomena, and second ECC bypass occurred during refill phase by hot wall effect of reactor pressure vessel.

The predicted fluid density at the broken cold leg and the break mass flow rate from the reactor vessel side are compared with the measured data in Figure 3-21 and Figure 3-22 respectively, to investigate the prediction of ECC bypass phenomena of RELAP5/MOD3.3/K. The fluid density at the broken cold leg was observed to sharply increase when the accumulator injection began. Then, the fluid density was sharply decreased at 65 s when water levels in the lower plenum and downcomer started to increase. This implies that most of the ECC water injected from the accumulator was bypassed and did not penetrate into the downcomer until 65 s. This ECCW bypass phenomena is also confirmed by the mass flow measured at the vessel side break. The break mass flow increased when the accumulator injection began, after then it decreased gradually during this period. RELAP5/MOD3.3/K reasonably predicts ECCW bypass phenomena until 44 s. After that, however, the results of the code calculation show discrepancies from the test data. The predicted fluid density at the broken cold leg and break mass flow show that the code predicts no ECCW bypass between 44 s and 65 s. The main reason of no ECCW bypass is the over-prediction of steam condensation at the broken cold leg. The predicted broken cold pressure is lower than the suppression tank pressure due to the over-prediction of steam condensation, and this causes no break flow, consequently no ECCW bypass, from 44 s to 65 s. The downcomer and the lower plenum are filled with the ECCW 20 s earlier than the test data because no break flow is predicted, as shown in Figure 3-23 and Figure 3-24. The downcomer was filled with water at 71 s in the test. After 65 s, the predicted break mass flow begins to increase (Figure 3-22) because the system pressure increases as the core reflooding begins and the downcomer water level reaches to the bottom of the cold leg, as shown in Figure 3-23.

For both high- and low-powered rods, the cladding temperature was observed to increase continuously during the refill phase because there was no water entering the active core except a little droplets entrained by the up-going vapor [3-4], as shown in Figure 3-25 and Figure 3-26. RELAP5/MOD3.3/K reasonably predicts the rod temperature behavior. The turn-around of the cladding temperature, however, is predicted to occur earlier than the test data because the core reflooding begins earlier than the data in the calculation.

3.4.3 Reflood Phase (after 75 s)

RELAP5/MOD3.3/K predicts the core reflooding to begin around 20 s earlier than the test result as shown in Figure 3-24. Consequently, the cladding temperature starts to decrease from 59 s and the rods are quenched around 40 s earlier than the measured time, as shown in Figure 3-25 and Figure 3-26. However, RELAP5/MOD3.3/K reasonably predicts the trend of the cladding temperature behaviors, in general.

While the core water level was measured to decrease steadily after around 90 s, the predicted core water level starts to increase continuously after 90 s, as shown in Figure 3-27. From 65 s to 90 s, the code predicts that the broken cold leg is almost filled with ECCW and steam produced in the core does not easily flow out through the break causing the build-up of the system pressure. After the accumulator injection is ended at 90 s, however, the broken cold leg is filled with steam only and the build-up of the system pressure is released. Consequently, the core is easily reflooded and the core

water level begins to increase from 90 s in the calculation. Because quenching of the core occurs between 120 s and 140 s, the increase of the predicted core water level is accelerated after 120 s.

The highest cladding temperature of each measurement is compared with the calculated value at the corresponding node, as shown in Figure 3-38. Total 69 thermocouples were installed in high- and low-powered rods; nine for high-powered rods and 59 for low-powered rods. The code reasonably predicts the rod cladding temperatures and the predicted rod cladding temperatures are within the measured data ±100 K. The predicted rod quenching time is compared with the test data in Figure 3-39 and Figure 3-40 for high- and low-powered rods, respectively. For both rods, the code under-predicts rod quenching time in all elevations because of a favorable prediction of ECCW bypass phenomena during the refill phase. The code, however, reasonably predicts not only bottom-up quenching but also top-down quenching. Table 3-2 compares the measured sequence of events with the calculation results.

3.5 SRS Calculations

181 times of simple random sampling (SRS) calculations were performed against the Semiscale Test S-06-3. The uncertainty parameters and their distribution functions used for the SRS calculations are listed in Table 3-3. Total [ ]^{TS} uncertainty parameters for [ ]^{TS} were used for the SRS calculations.

Figure 3-41 shows the results of the SRS calculations; the measured cladding temperature behavior at the PCT elevation is compared with the maxima and minima of the predicted results at the corresponding elevation. The PCT of the Semiscale Test S-06-3 was observed to occur at 0.533 m (21 in.) from the bottom of the core. The third highest value of the calculated clad temperatures is higher than the measured PCT confirming the data covering. Therefore, the number and the probability distribution functions of the selected uncertainty parameters are confirmed to be sufficient.

3.6 Conclusion

The capability of RELAP5/MOD3.3/K in predicting thermal-hydraulic behaviors during a LBLOCA was assessed against the Semiscale Test S-06-3. The assessment results show that the code reasonably predicts the main parameters and phenomena observed during the test. The results of the assessment are summarized below:

(1) The code predicts well break flow rates during the blowdown period. The predicted break flow rates during the refill and reflood phases, however, show some discrepancies from the test data because the code over-predicts steam condensation at the broken cold leg.

(2) The code predicts well the water level behavior in the downcomer before the accumulator injection begins. After the accumulator injection begins, the code over-predicts the downcomer water level because the code favorably predicts ECCW bypass phenomena during the refill period. The code predicts that the lower plenum refill and the core reflood begin earlier than the measured time.

(3) The code predicts the rod cladding temperatures reasonably well even though the code under-predicts the rods quenching times.

(4) The data covering is confirmed through the SRS calculations. This implies that the number and the probability distribution functions of the selected uncertainty parameters are sufficient to cover the measured PCT.

References

[3-1] USNRC, “Summary of the Semiscale Program (1965-1986),” NUREG/CR-4945; EGC-2509, July 1987.

[3-2] E.M. Feldman and D.J. Olson, “Semiscale Mod-1 Program and System Description for the Blowdown Heat Transfer Tests (Test Series 2),” ANCR-1230, 1975.

[3-3] USNRC, “Experiment Data Report for Semiscale Mod-1 Test S-06-3 (LOFT Counterpart Test),” NUREG/CR-0251; Tree-1123, July 1978.

[3-4] USNRC, “Compendium of ECCS Research for Realistic LOCA Analysis,” NUREG-1230, April 1997.

Table 3-1 Comparison of Calculated and Measured Initial Conditions

Parameter	Measured value	Calculated value
Core power (MW)	1.004	1.004
Intact loop cold leg fluid temperature (K)	563.0	562.8
Intact loop hot leg fluid temperature (K)	598.0	598.3
Broken loop cold leg fluid temperature (K)	562.0	561.99
Broken loop hot leg fluid temperature (K)	591.0	591.6
Intact loop cold leg volumetric flow rate (l/s)	6.68	6.64
Pressurizer pressure (MPa)	15.769	15.767
Steam generator secondary side pressure (MPa)	6.55	6.53

Table 3-2 Sequence of Events

Accident	Measured value (seconds)	Calculated value (seconds)
Discharge starts	0.0	0.0
HPSI starts	0.0	0.0
Core power starts to decrease	1.27	1.27
Pressurizer empties	7.5	13.0
Accumulator starts to inject	18.5	18.5
PCT is reached	20.5	49.0
Downcomer interpenetration	42.5	-
Lower plenum water level starts to increase	60	34
Lower plenum is filled	71	54
Downcomer is filled	73	62
Accumulator stops to inject	90	90

Table 3-3 Parameters and Distribution Functions Used for the SRS Calculations: Semiscale S-06-3

TS

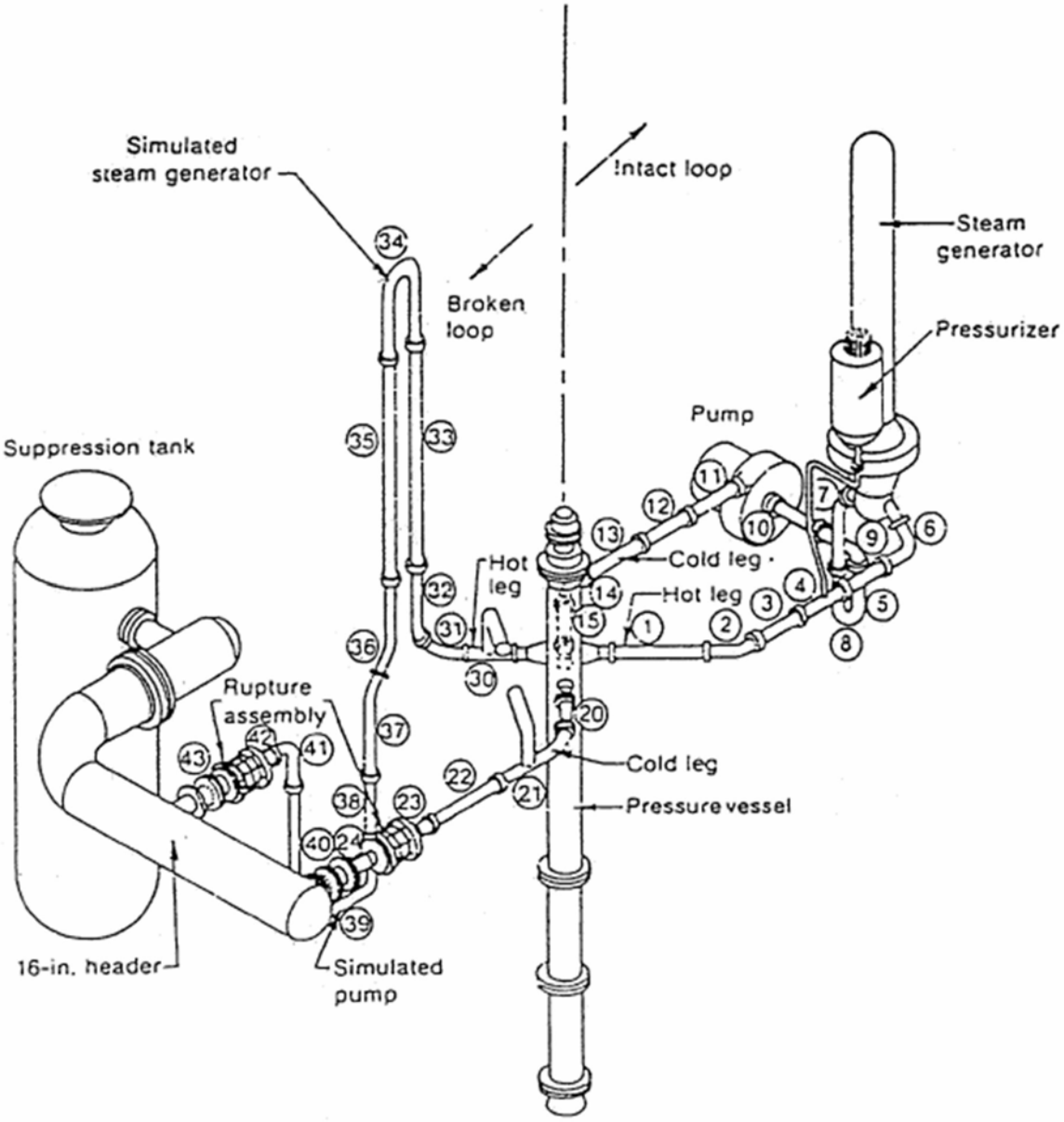

Figure 3-1 Semiscale Mod-1 System for Cold Leg Break Configuration

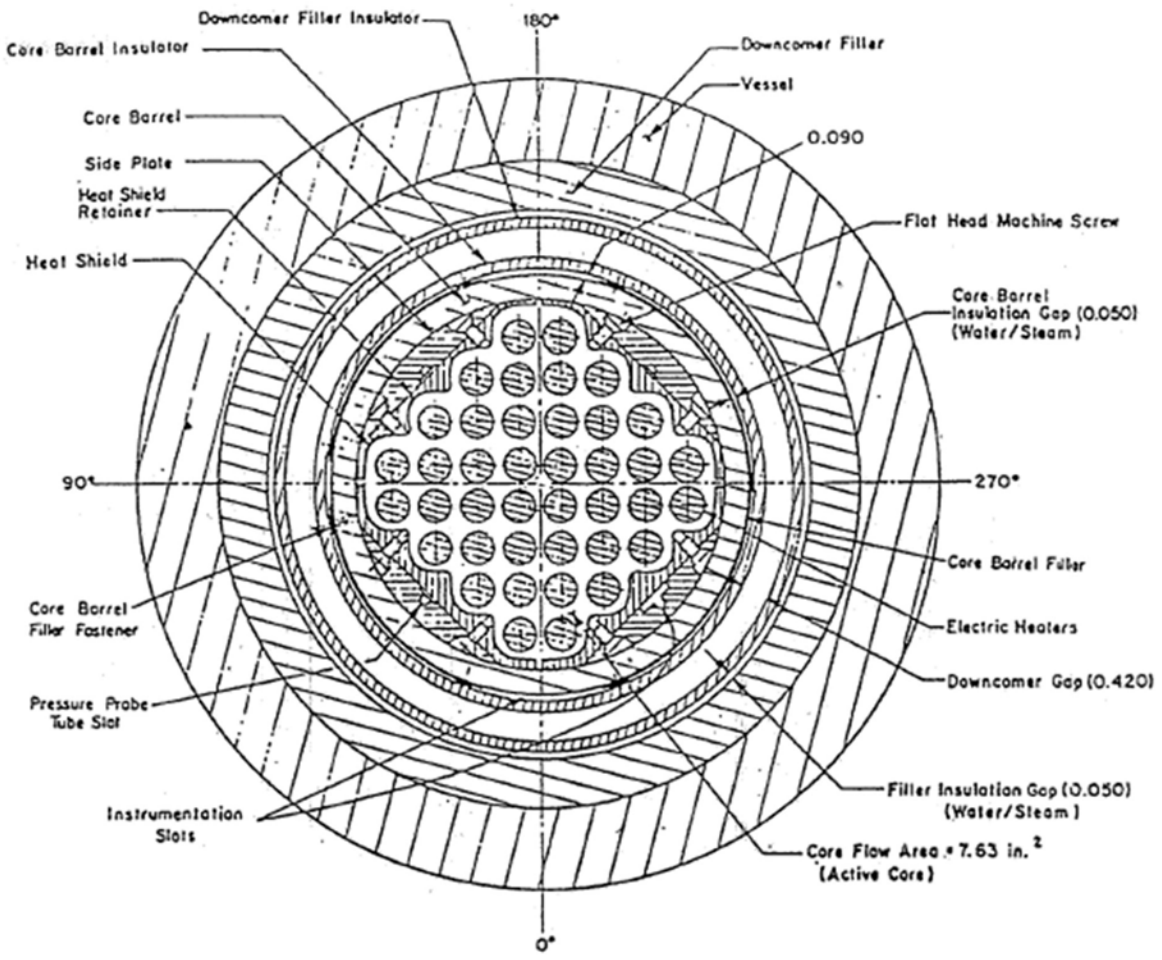

Figure 3-2 Electric Heater Rod Matrix for Semiscale Mod-1 Core

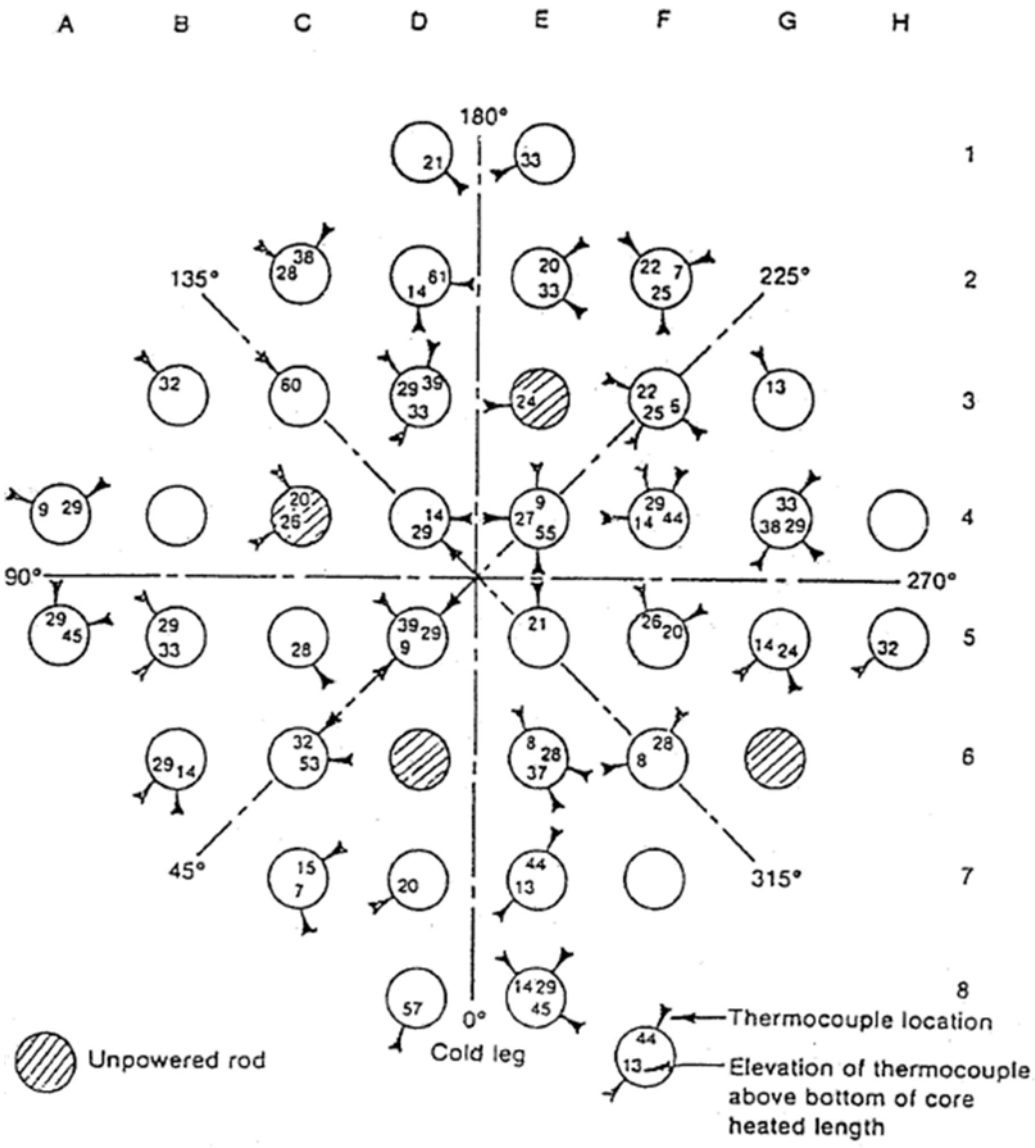

Figure 3-3 Semiscale Mod-1 Heated Core Plan View

TS

Figure 3-4 RELAP5/MOD3.3/K Nodalization of the Semiscale Mod-1

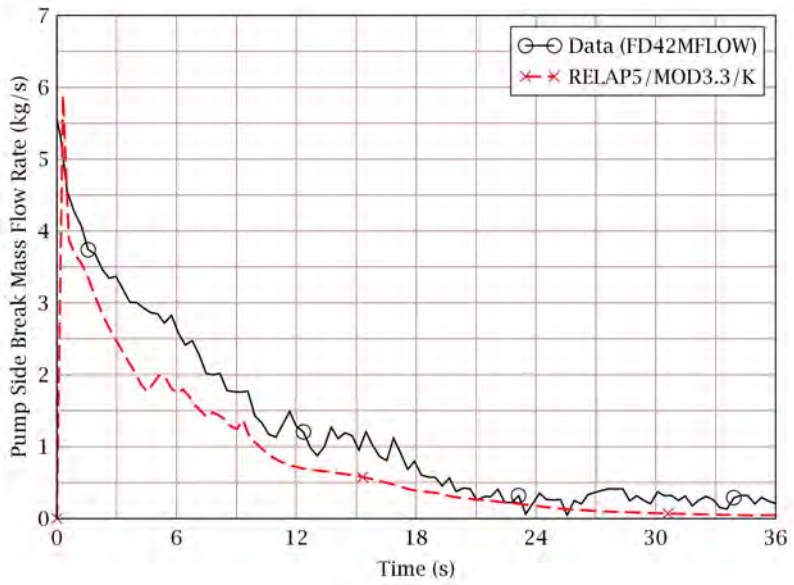

Figure 3-5 Pump Side Break Mass Flow Rate

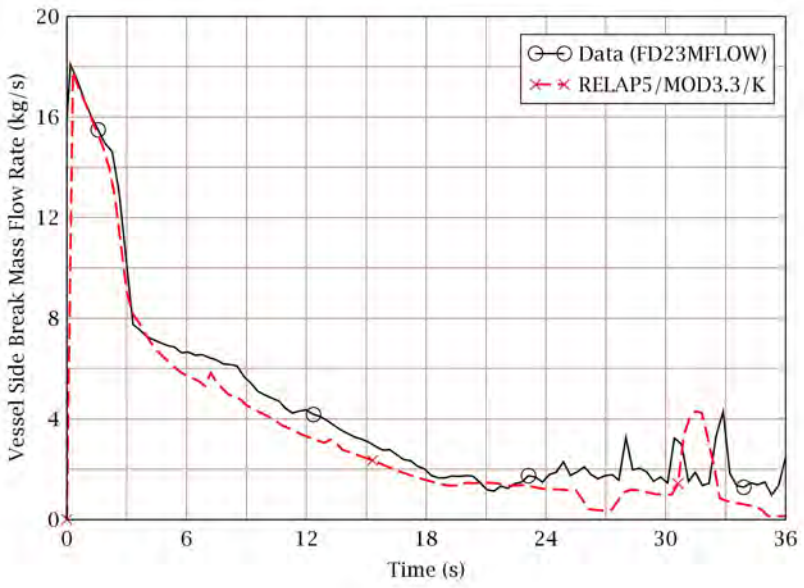

Figure 3-6 Vessel Side Break Mass Flow Rate

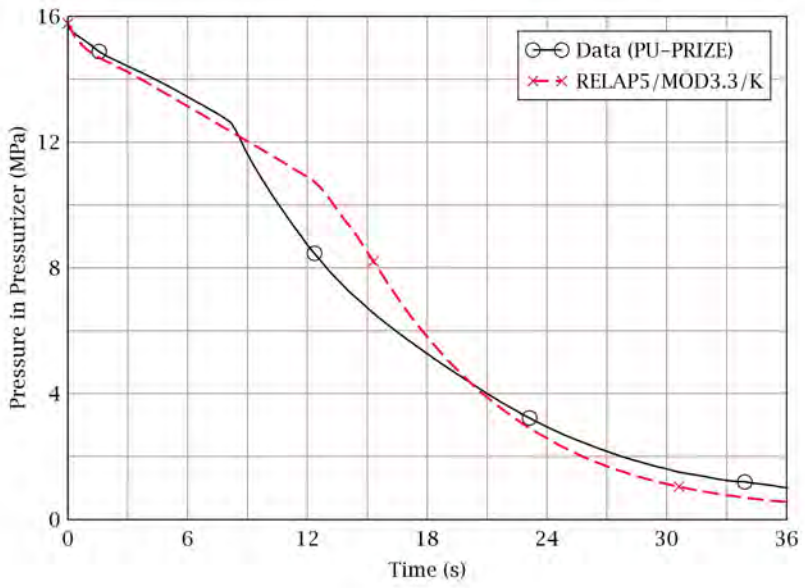

Figure 3-7 Pressure in Pressurizer

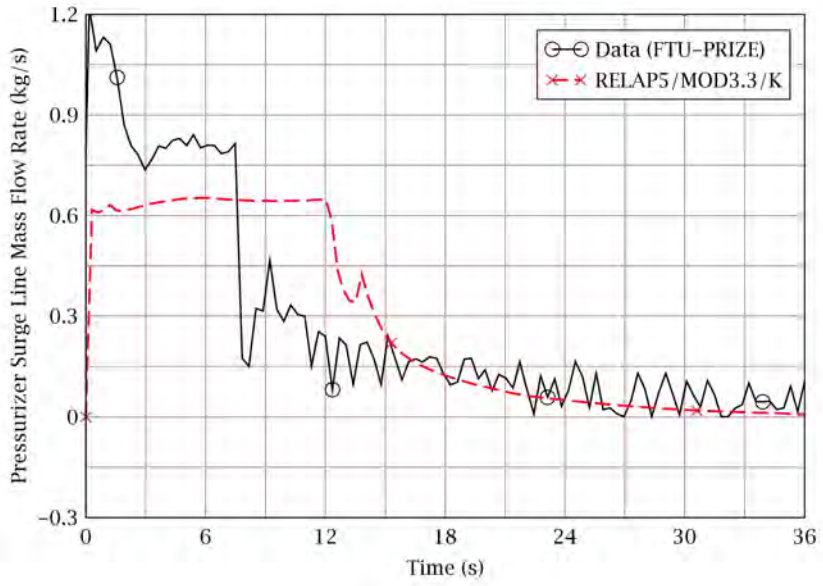

Figure 3-8 Pressurizer Surge Line Mass Flow Rate

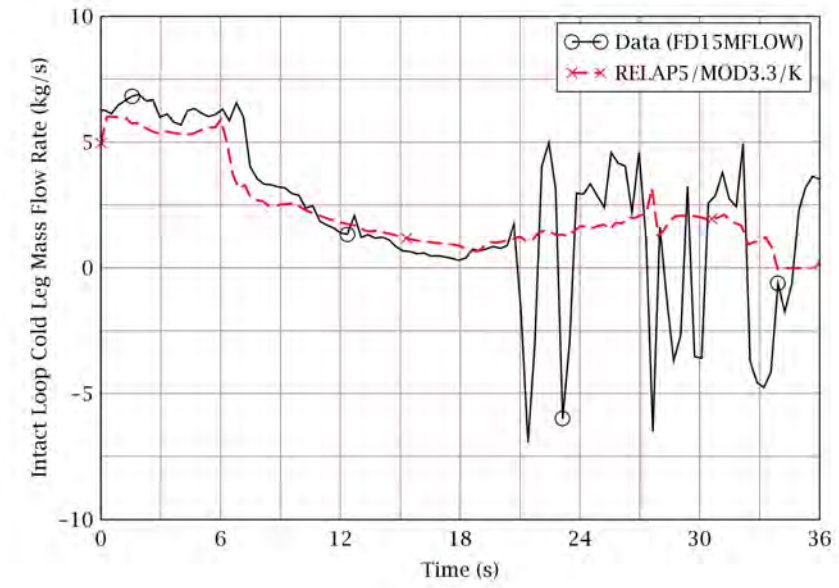

Figure 3-9 Intact Loop Cold Leg Mass Flow Rate

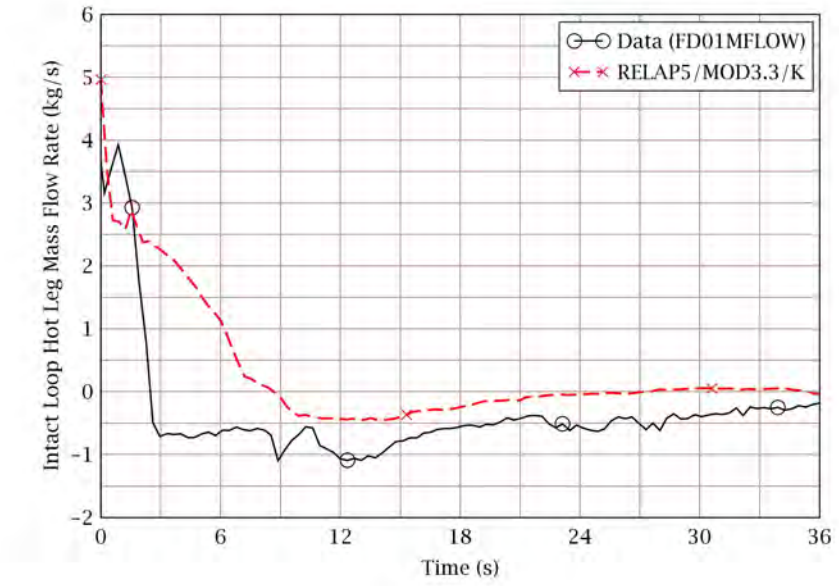

Figure 3-10 Intact Loop Hot Leg Mass Flow Rate

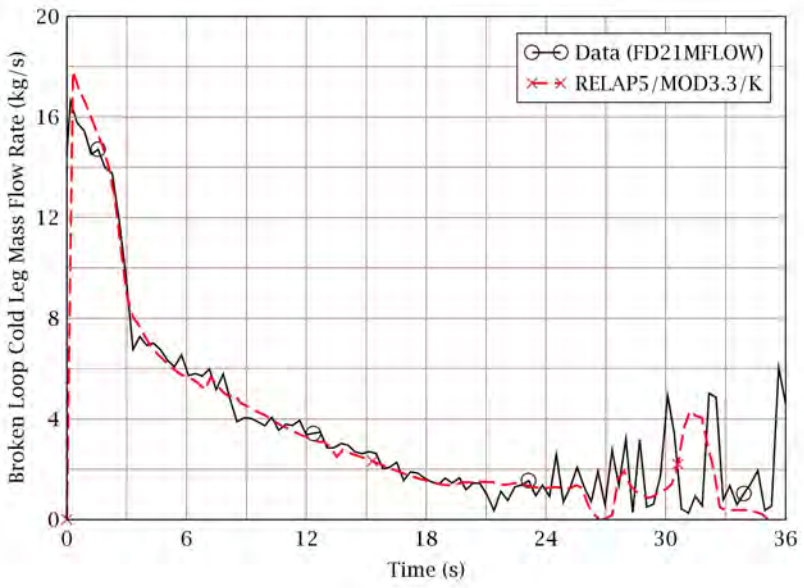

Figure 3-11 Broken Loop Cold Leg Mass Flow Rate

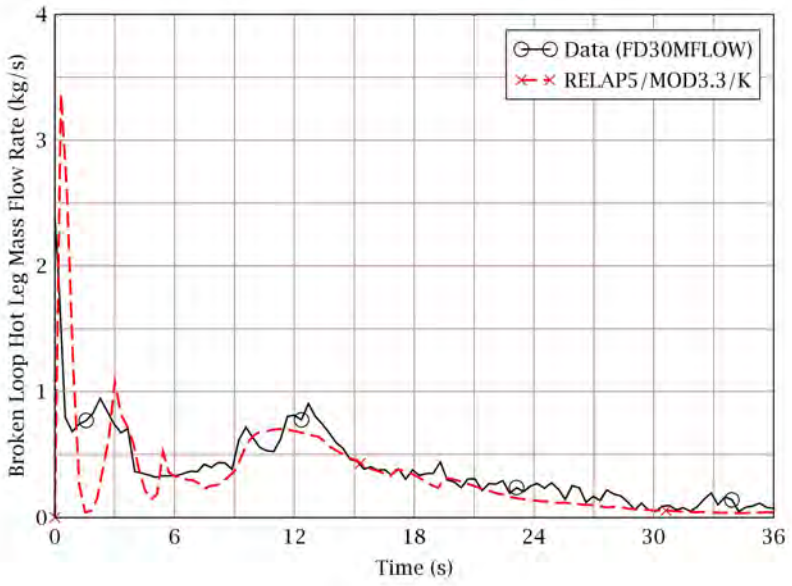

Figure 3-12 Broken Loop Hot Leg Mass Flow Rate

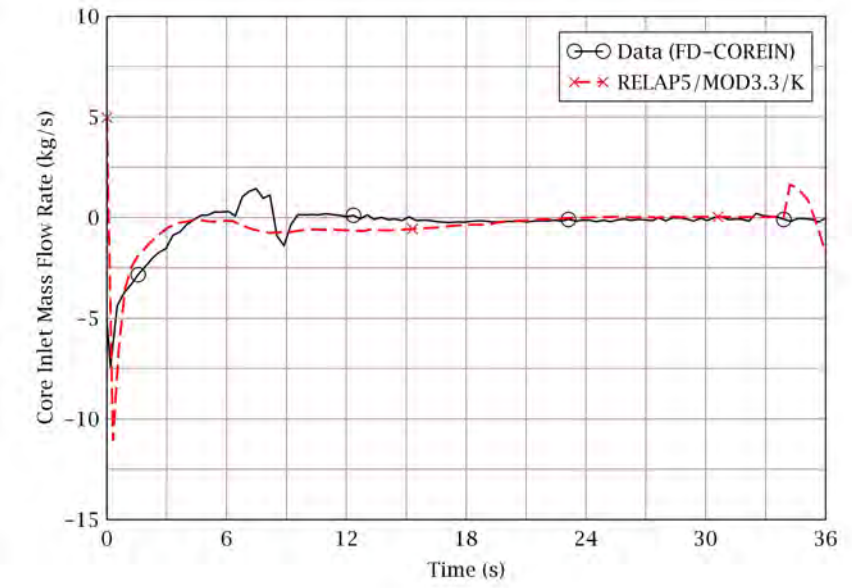

Figure 3-13 Core Inlet Mass Flow Rate

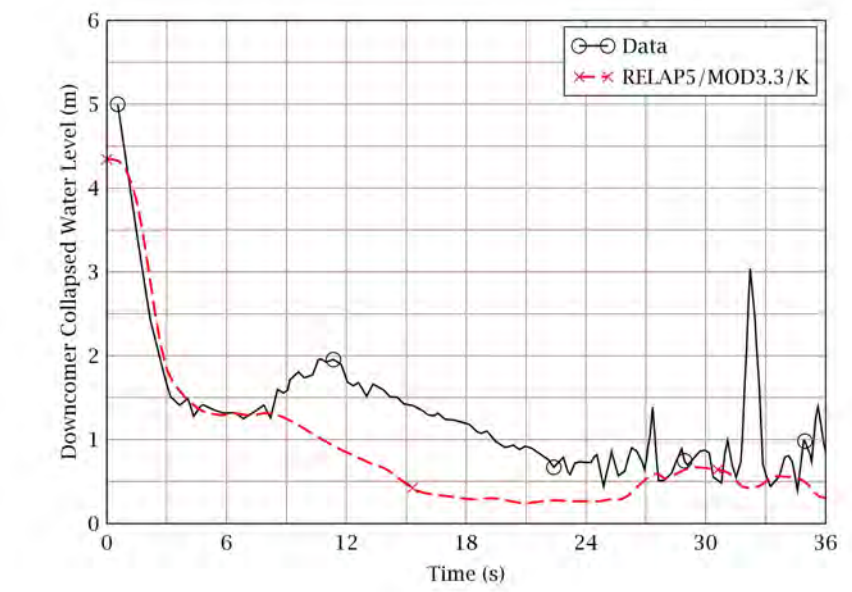

Figure 3-14 Downcomer Collapsed Water Level

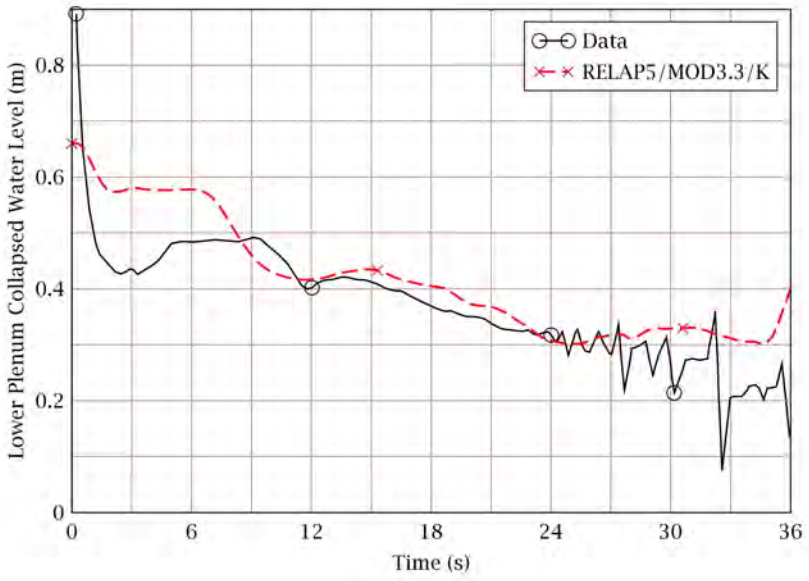

Figure 3-15 Lower Plenum Collapsed Water Level

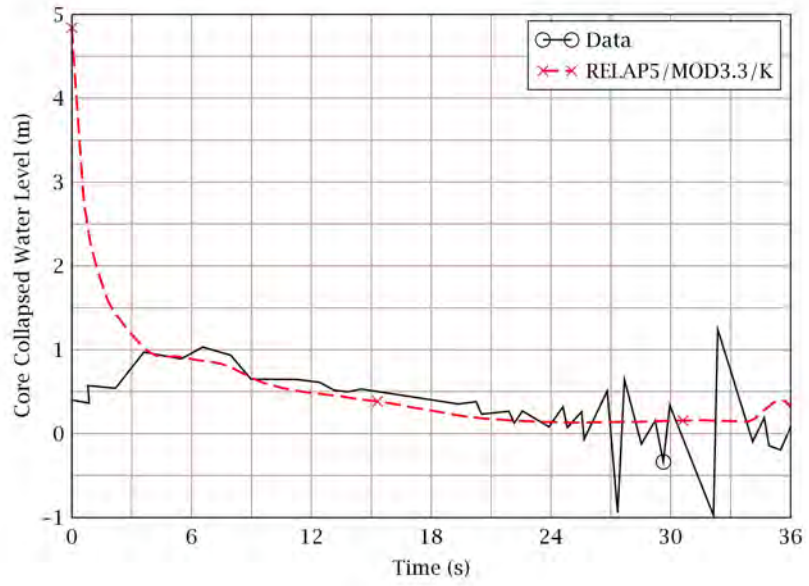

Figure 3-16 Core Collapsed Water Level

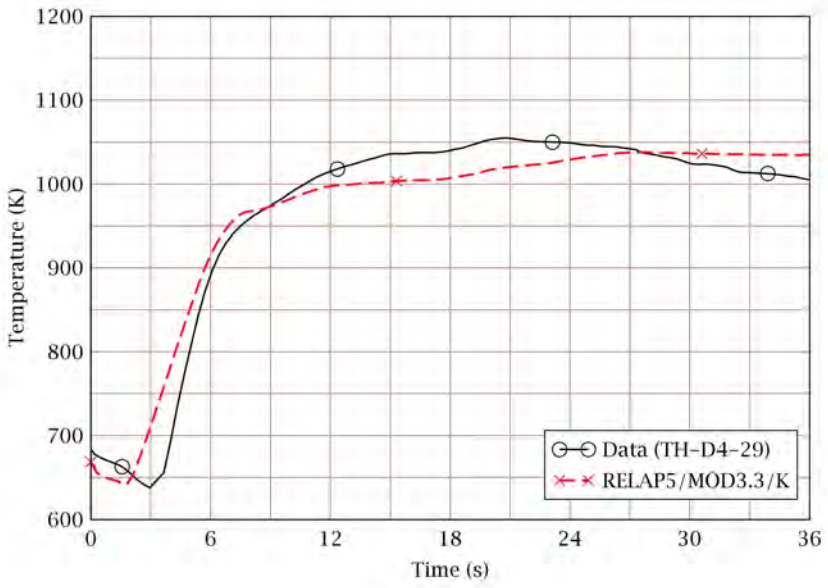

Figure 3-17 Cladding Temperature of High-Power Rods

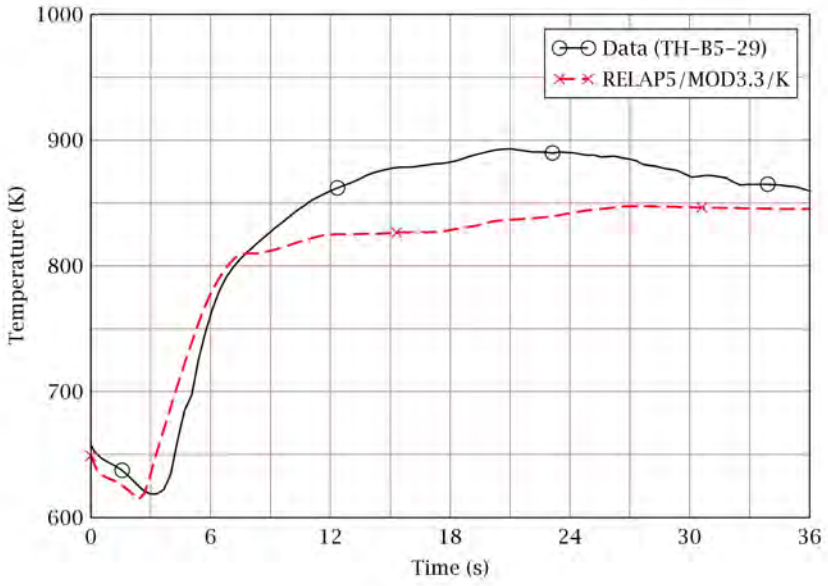

Figure 3-18 Cladding Temperature of Low-Power Rods

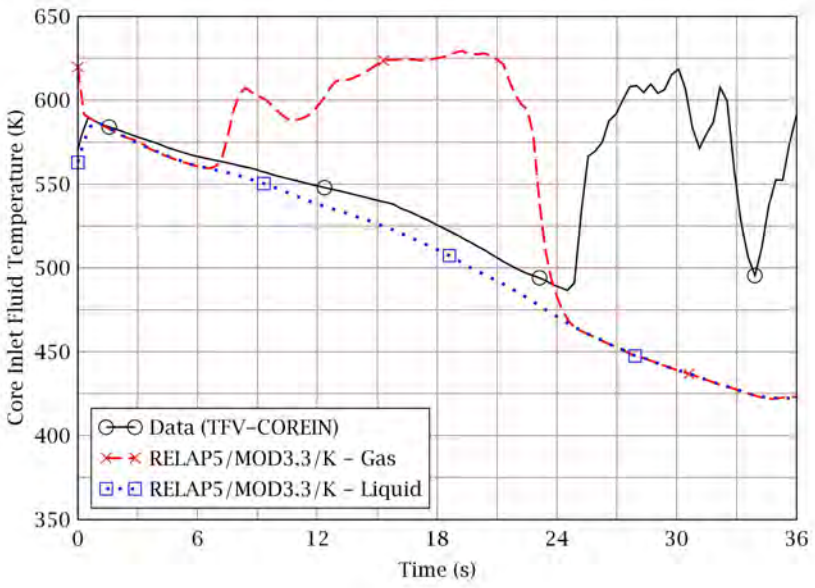

Figure 3-19 Lower Plenum Fluid Temperature

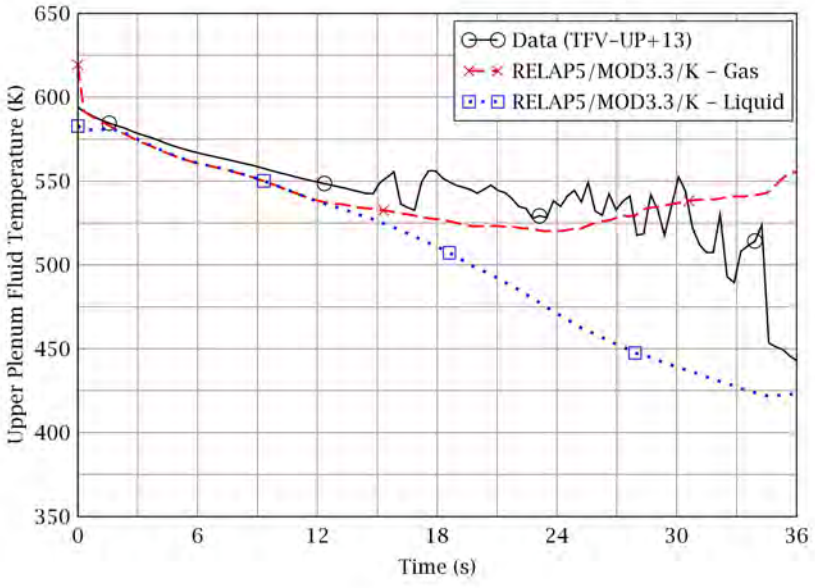

Figure 3-20 Upper Plenum Fluid Temperature

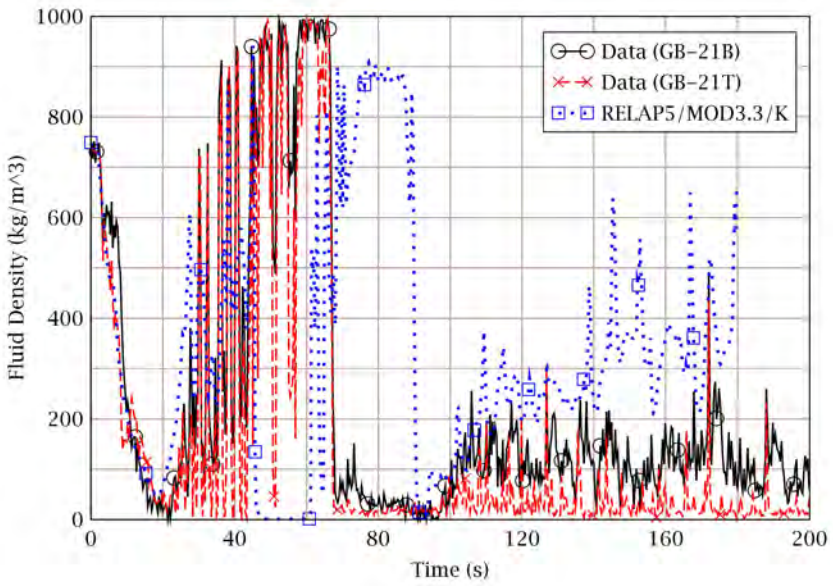

Figure 3-21 Fluid Density in Broken Loop Cold Leg

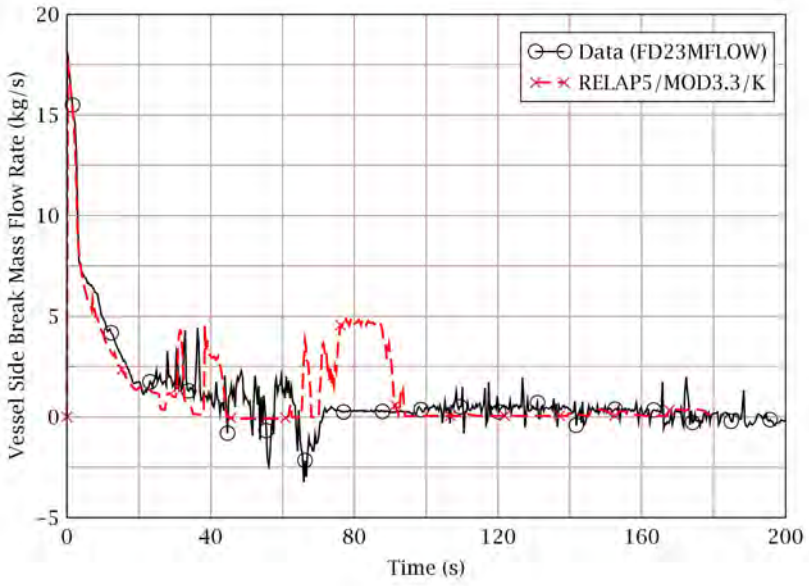

Figure 3-22 Vessel Side Break Mass Flow Rate

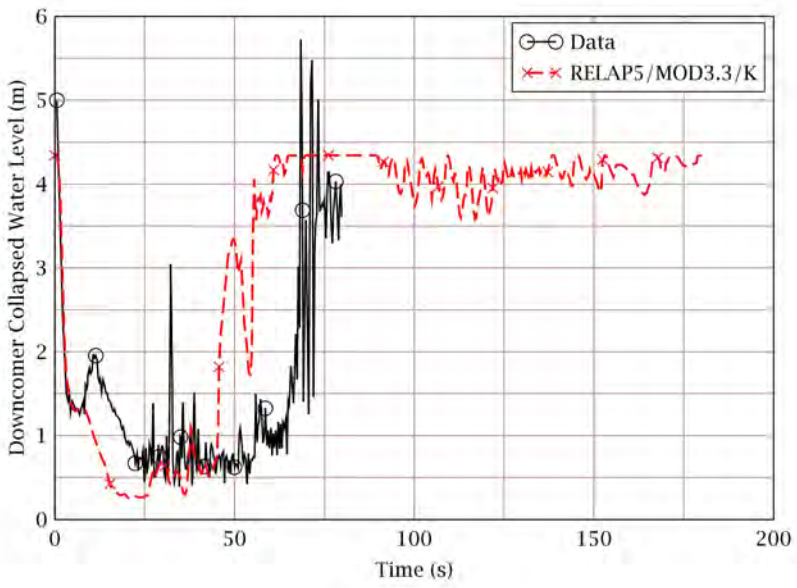

Figure 3-23 Downcomer Collapsed Water Level

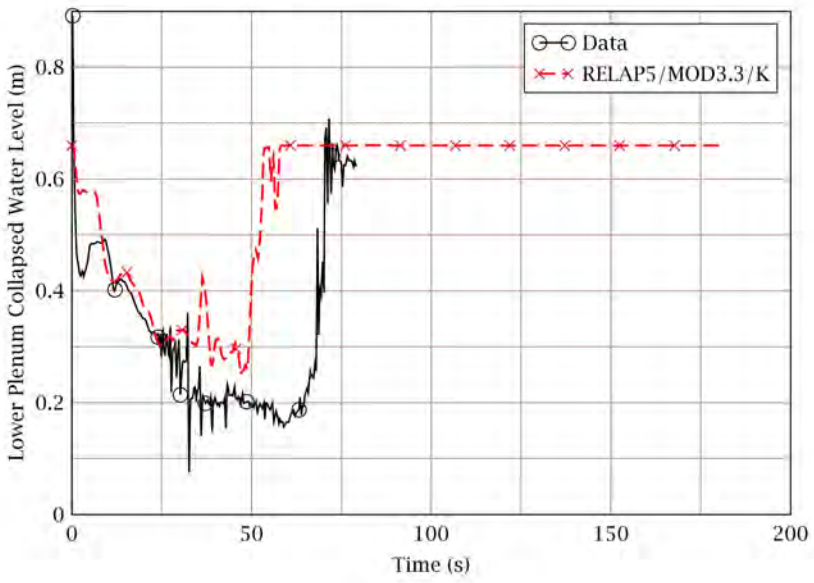

Figure 3-24 Lower Plenum Collapsed Water Level

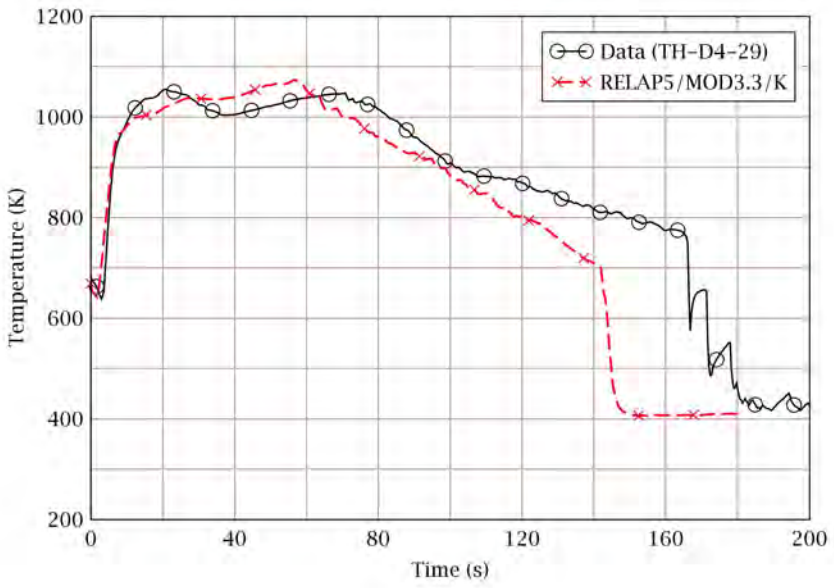

Figure 3-25 Cladding Temperature of High-Power Rods

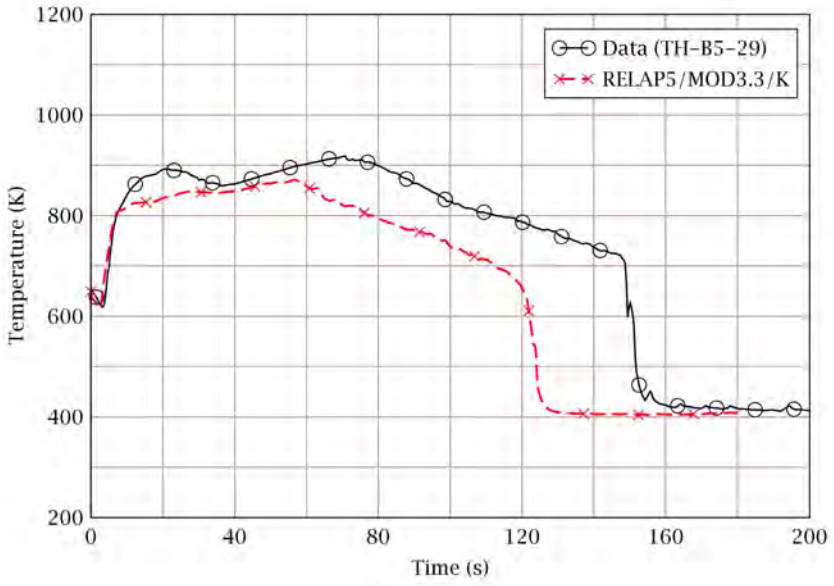

Figure 3-26 Cladding Temperature of Low-Power Rods

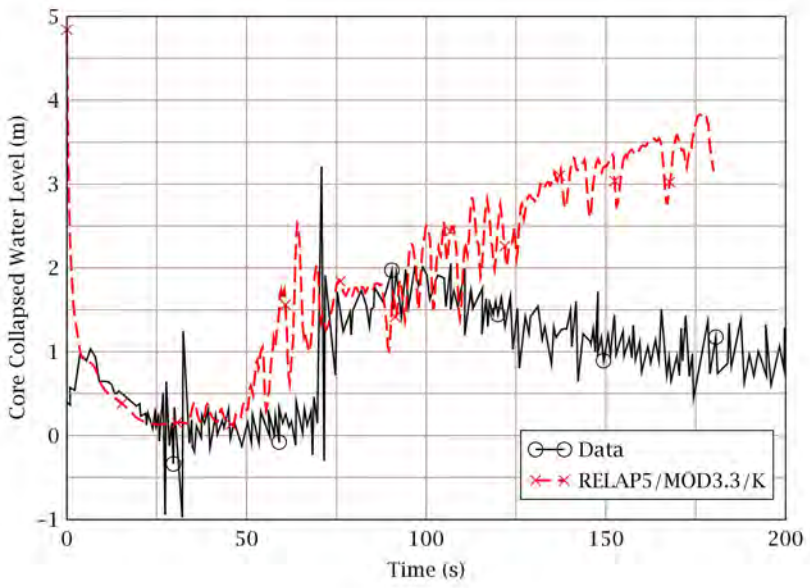

Figure 3-27 Core Collapsed Water Level

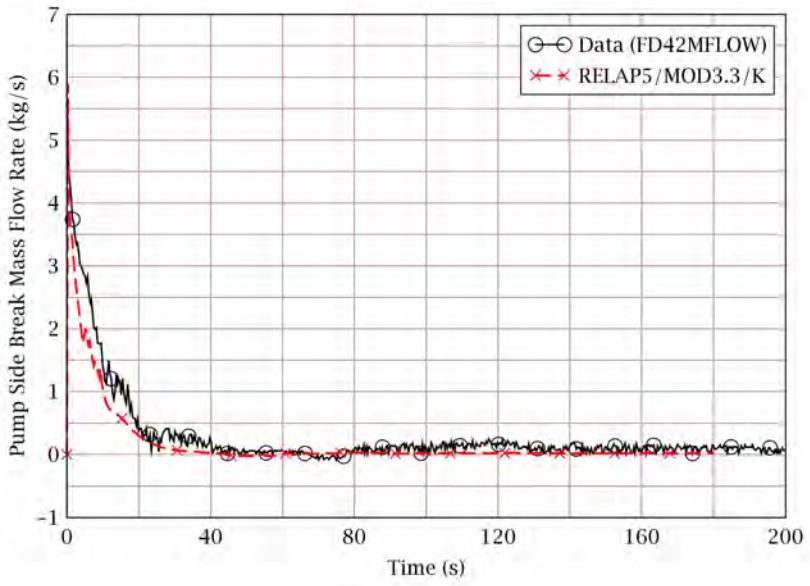

Figure 3-28 Pump Side Break Mass Flow Rate

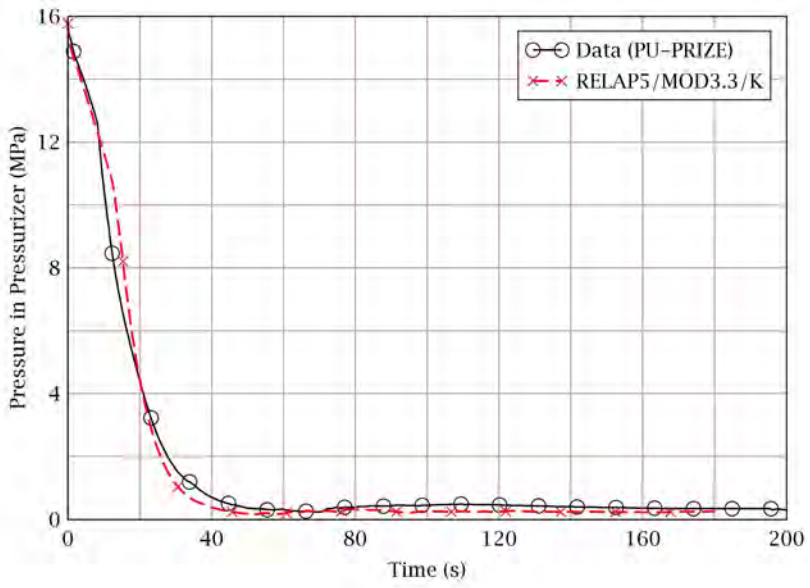

Figure 3-29 Pressure in Pressurizer

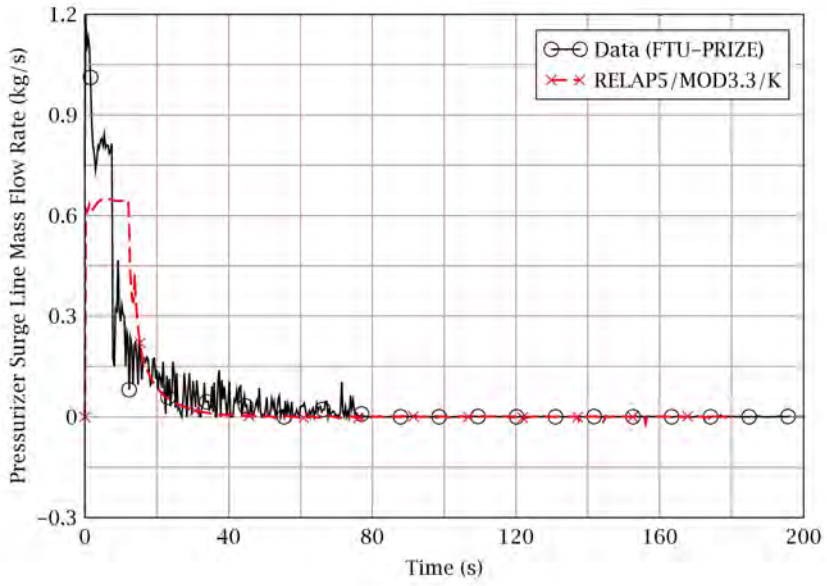

Figure 3-30 Pressurizer Surge Line Mass Flow Rate

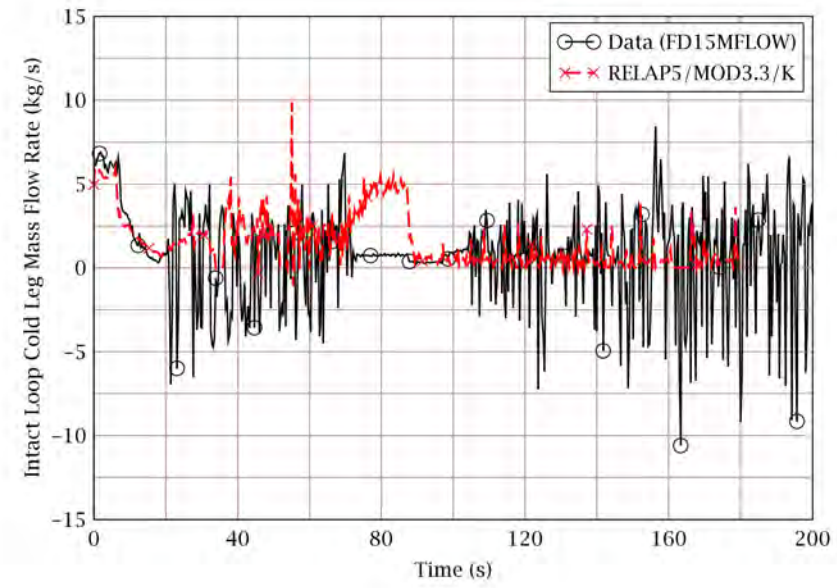

Figure 3-31 Intact Loop Cold Leg Mass Flow Rate

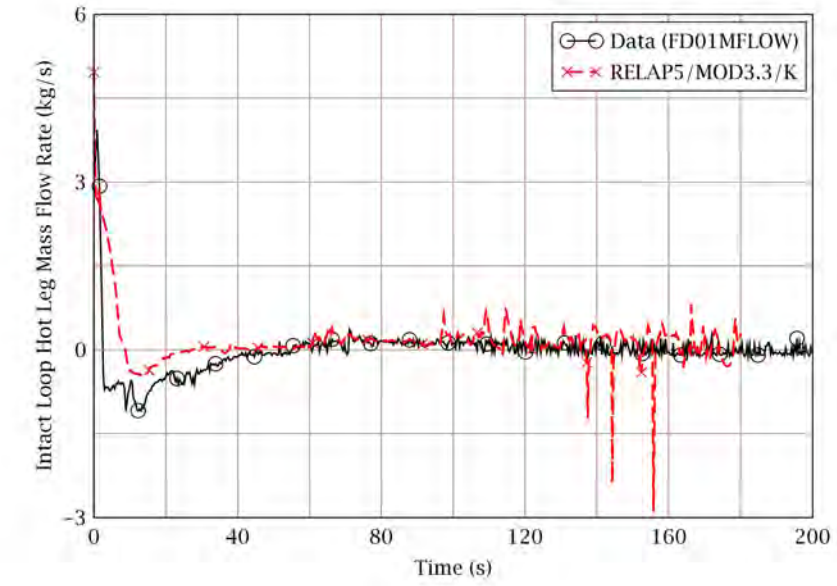

Figure 3-32 Intact Loop Hot Leg Mass Flow Rate

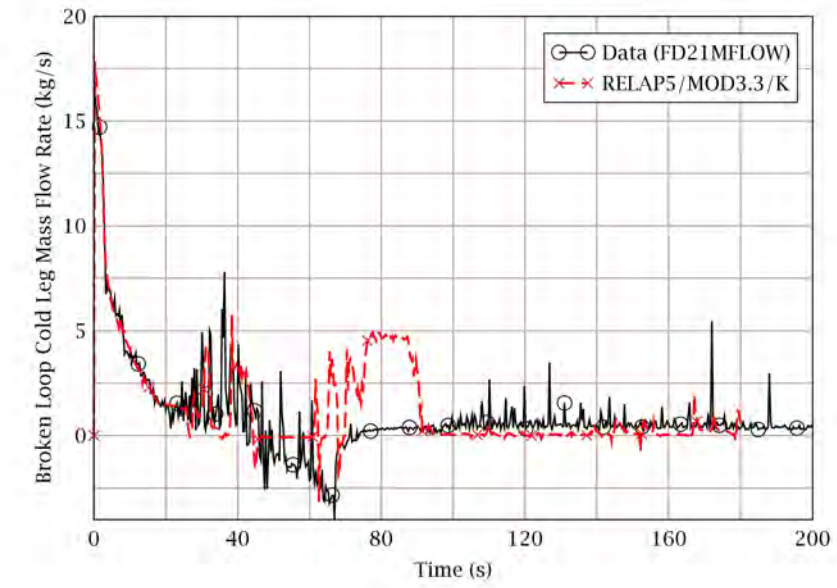

Figure 3-33 Broken Loop Cold Leg Mass Flow Rate

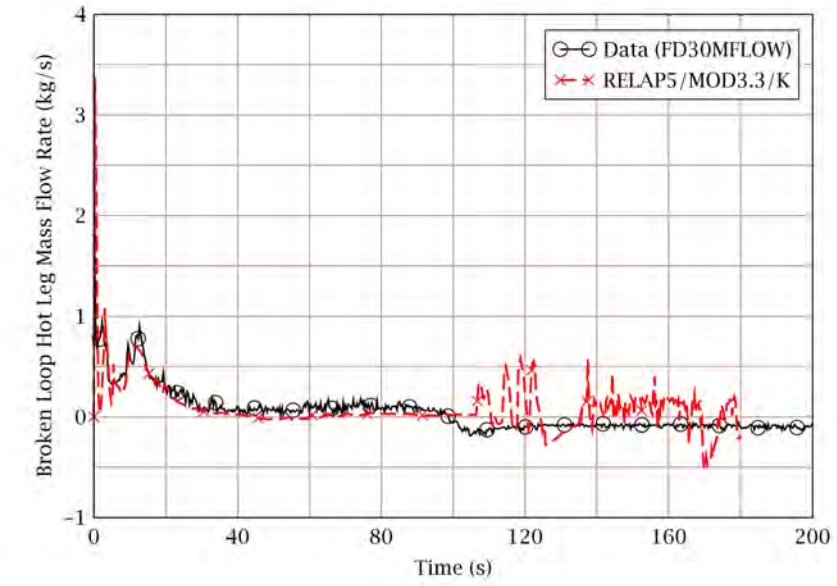

Figure 3-34 Broken Loop Hot Leg Mass Flow Rate

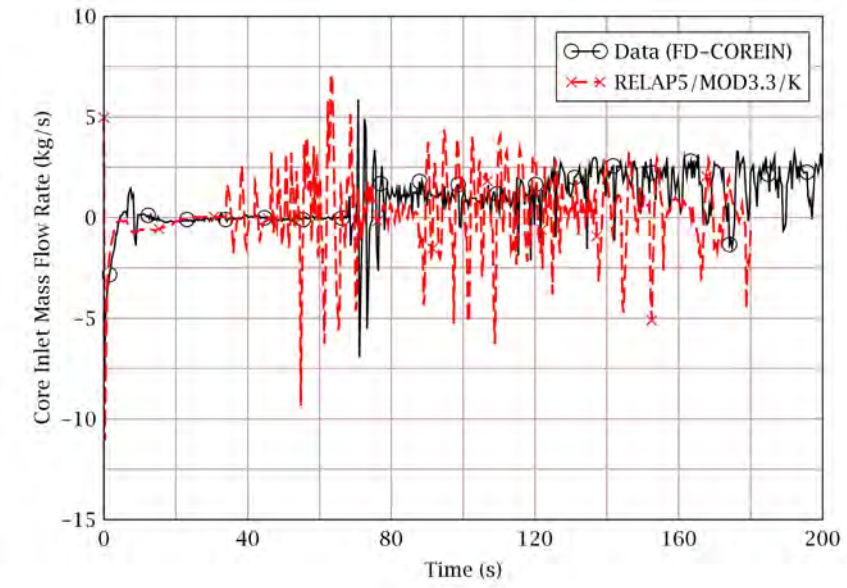

Figure 3-35 Core Inlet Mass Flow Rate

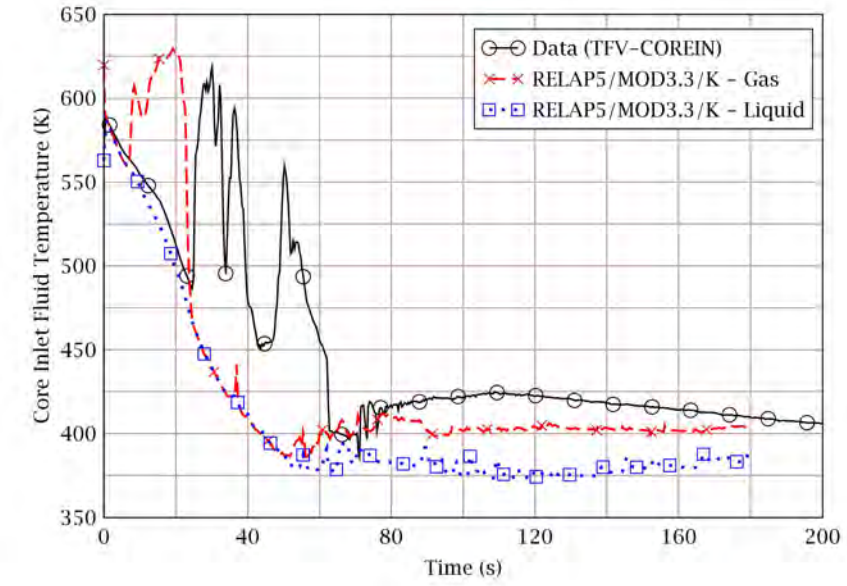

Figure 3-36 Lower Plenum Fluid Temperature

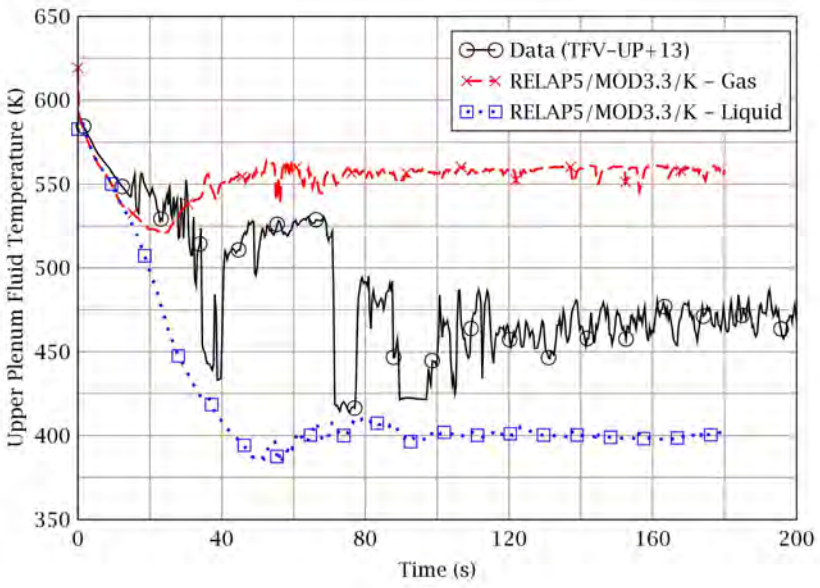

Figure 3-37 Upper Plenum Fluid Temperature

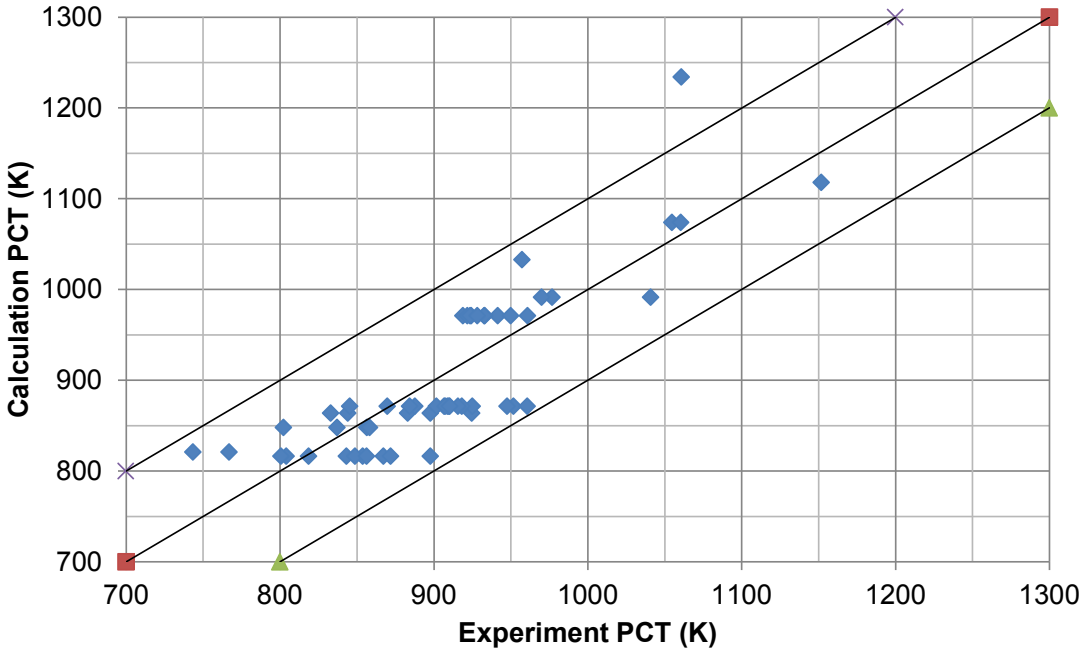

Figure 3-38 Comparison of Calculated Results and Test Results

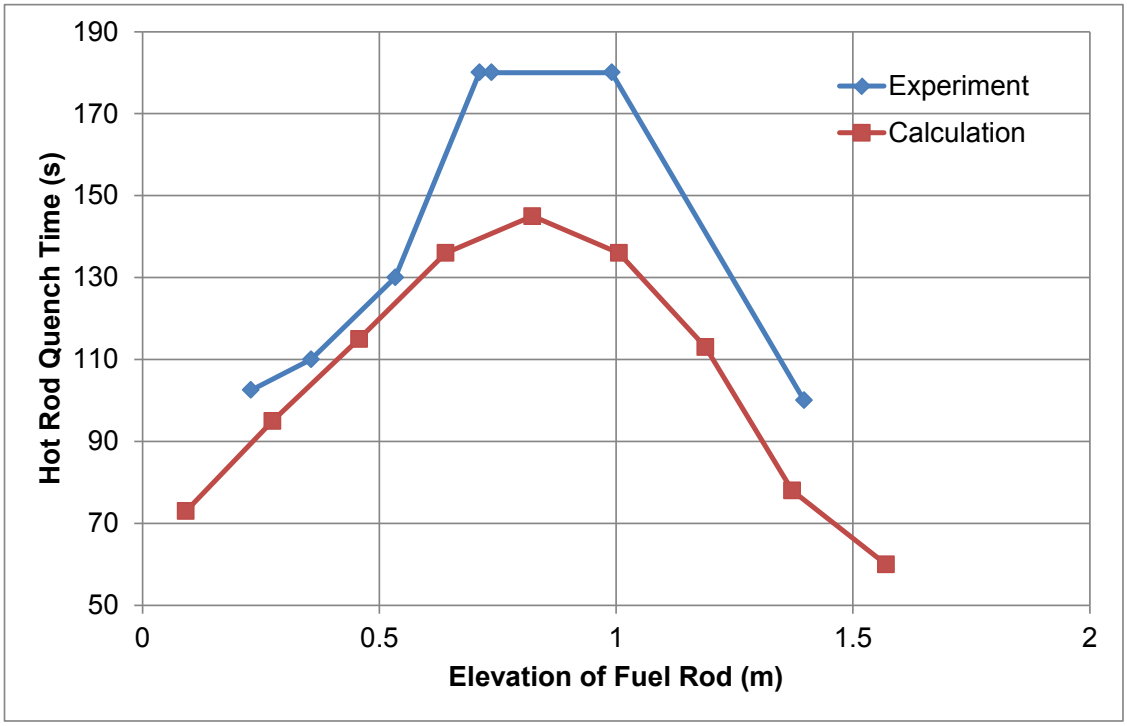

Figure 3-39 High-Power Rods Quenching Time

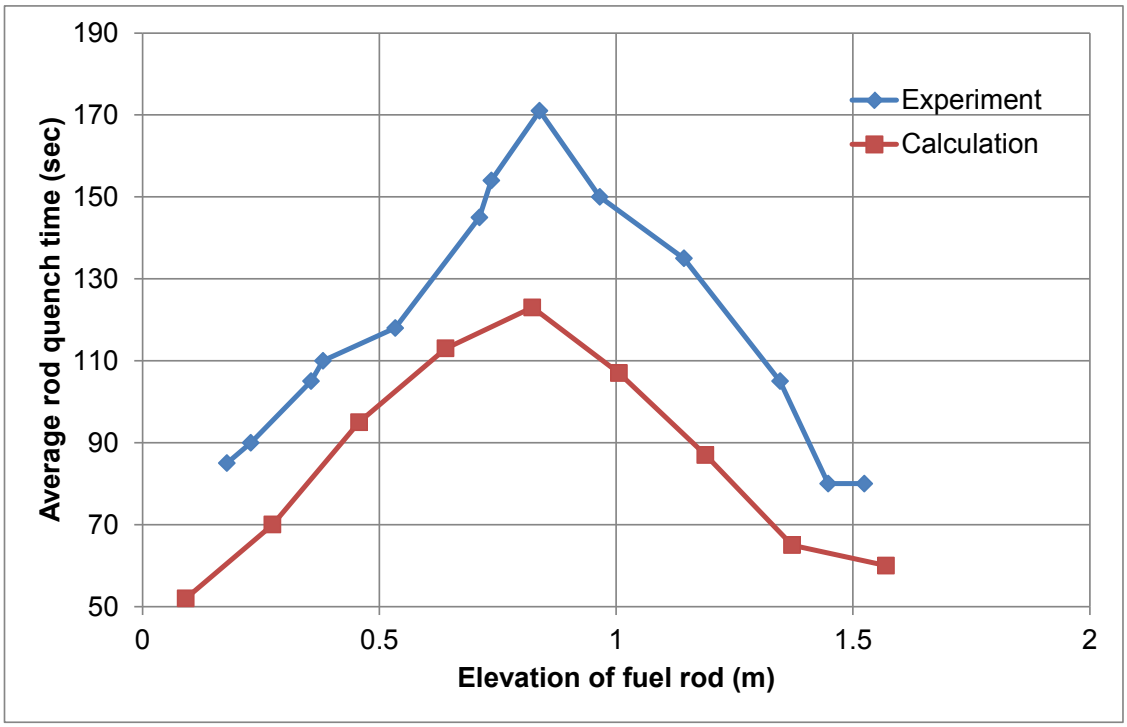

Figure 3-40 Low-Power Rods Quenching Time

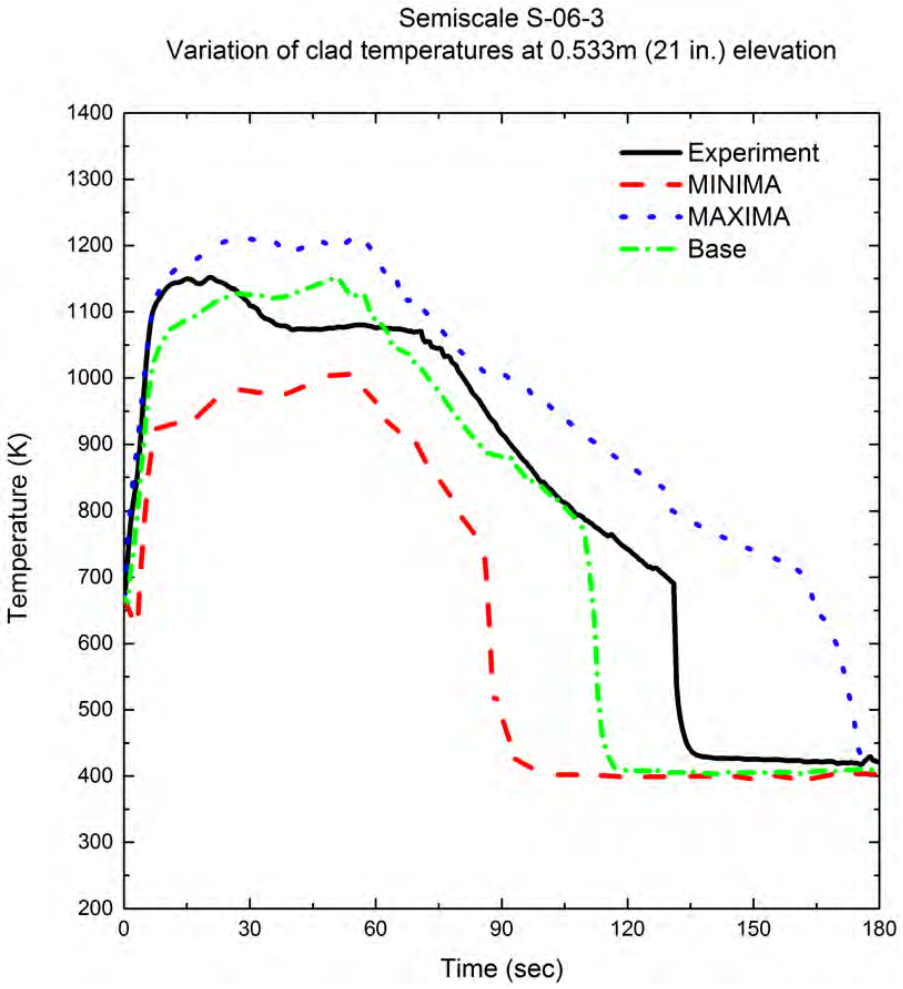

Figure 3-41 The Results of SRS Calculations: Semiscale S-06-3

4. Code assessment using LOBI A1-66 data

4.1 Introduction

The LOBI (LWR Off-normal Behavior Investigation) was a reactor thermal-hydraulic safety research program carried out by the Commission of the European Communities at the Ispra site of the Joint Research Center (JRC). The objective of the program was to investigate basic phenomenologies governing the thermal-hydraulic response of an integral system test facility for a range of PWR operational and accident conditions.

The LOBI experimental program included two parts; the MOD1 program and the MOD2 program. The LOBI-MOD1 test facility configuration was designed to meet the relevant requirements originating from the objectives of the experimental investigations of large and intermediate break Loss-of-Coolant Accidents (LOCA). The experimental program was performed in the framework of an R&D contract between the Commission of the European Communities and the former Bundesminister für Forschung und Technologie of the Federal Republic of Germany. A total of 28 tests were performed with this configuration. Test A1-66 was one of large break LOCA tests simulating a 200 % cold leg break.

In this chapter, the capability of RELAP5/MOD3.3/K in predicting the thermal-hydraulic behaviors during a large break LOCA was assessed against LOBI Test A1-66.

4.2 Test Facility and Descriptions

4.2.1 Test Facility

The LOBI facility shown in Figure 4-1, a full-power high pressure integral system test facility, was a 1/700 scale model of a four-loop PWR. The reference plant of the LOBI-MOD1 facility was Siemens-KWU 1300 MWe nuclear power plant. This facility had two primary loops, the intact loop representing three loops and the broken loop representing one loop of a four-loop PWR.

The reactor vessel consisted of the pressure vessel, the core barrel tube and the core simulator. The additional major components of the overall pressure vessel assembly were lower plenum, upper plenum, an annular downcomer and an externally mounted upper head simulator. The downcomer had a 50 mm gap width. After the execution of an initial test series and due to experimental evidences on the atypical influence of the large downcomer on the system thermal-hydraulic response, the 50 mm downcomer was replaced with a 12 mm downcomer.

Each of two primary loops consisted of a main coolant pump and a steam generator. The main coolant pumps were of the centrifugal type with a specific speed. The two pumps were equal in size and were therefore operated at two different speeds in order to yield the two different steady-state mass flows of 21 kg/s and 7 kg/s for the intact and broken loop at the same pressure head.

The pressurizer was designed to be geometrically similar to that of the reference plant, and it was scaled in volume but not in height.

The emergency core cooling system (ECCS) of the LOBI-MOD1 facility consisted of only the intermediate pressure accumulator system.

The reactor pressure vessel model contained an electrically heated rod bundle with 64 rods and a heated length of 3.9 m. The power input, the primary circuit coolant mass flow and volume were scaled down from the reactor values by a factor of 712, leading to a 5.24 MW heating power in the 8 x 8 heater rod bundle of the reactor pressure vessel model, to 28 kg/s core mass flow, and to 0.60 m^3 primary coolant volume. All the other most relevant quantities such as operating temperature and pressure, pressure drops and lengths of heat transfer surfaces were scaled 1/1. Also the absolute

heights and relative elevations of the individual system components were kept at reactor values.

The measurements of the main thermo-hydraulic parameters were performed at the boundaries of the principal loop components and at the important reactor pressure vessel sections. The measurement of the heater rod temperature is given in Figure 4-2 and Figure 4-3. The measurement instrumentation of the facility is described in the reference [4-1].

4.2.2 Test Descriptions

Test A1-66 was one of a series of three LOBI tests in which the ECC injection mode was studied. In these tests, a double-ended 2A break in the cold leg was simulated. The downcomer gap width was 12 mm. In test A1-66, ECC water was injected from the intact loop accumulator into the cold leg only. The pressurizer was connected to the intact loop. After blowdown initiation, the intact loop pump speed decreased to 72 % after about 8 s and remained constant. The broken loop pump speed diminished to 10 % after 3.0 seconds and reached zero speed after about 27 s.

With the normal run-up procedure the loop system was brought to the nominal stationary test conditions and then the blowdown was initiated. The stationary operation conditions are summarized in Table 4-1 with calculation results of steady state.

The boundary conditions for the test were as follows:

- The break valve at the reactor vessel side opened first. The instant of break opening start defines the blowdown time “zero”. The second break valve (pump side) had a delay of about 6 ms before opening.

- The break isolation valve closure started at blowdown initiation; closed after 0.9 s (switch-off signal, indicates end-of-closure position of the valve).

- The axial power distribution is given in Figure 4-4, and the core power after blowdown start was controlled as shown in Table 4-2.

- The pump speed time history in intact loop was controlled down to 72 % of nominal value over 7.7 s and then remained constant at this level. The broken loop pump was slowed down to about 10 % over 3.1 s and finally reached zero speed after 27 s.

- The feed water shut-off in the secondary system was started at blowdown initiation; the mass flows reduced reaching zero after about 10 s and 45 s in broken and intact loop steam generators respectively.

- The accumulator injection started at 18 s after blowdown in the intact loop cold leg. The loop pressure at this time was about 2.4 MPa.

4.3 Modeling Description of LOBI A1-66

The RELAP5/MOD3.3/K input models of the LOBI MOD1 test facility shown in Figure 4-5.

The active core is modeled using [ ]^{TS} axial volumes. The downcomer is also modeled using [

]^{TS} The pressurizer is connected to the intact loop. [ ]^{TS} are used in order to simulate a double ended break. The uniform core radial power distribution is modeled; and axial power distribution is shown in Figure 4-4. The electric heater rods are modeled using [ ]^{TS} heat structures, and the core power is modeled using [

]TS The pump velocity and the steam generator feed water are also [ ]TS

4.4 Results

Figure 4-6 to Figure 4-9 show a comparison of the calculated and measured pressure at the intact loop hot leg, intact loop cold leg, lower plenum, and the pressurizer, respectively. In these figures, the RELAP5/MOD3.3/K slightly under-predicts the system pressure decrease rate until around 15 s. This is mainly due to that the code under-predicts the break flow during the same period. However, the code predicts well the general trend of the system pressure behaviors.

The fluid velocity at each steam generator inlet is shown in Figure 4-10 and Figure 4-11. In both steam generator inlets, the calculated velocity is lower than the measured data. This is mainly due to that the code calculates flow area using the given node volume and elevation difference. The general trend of the calculated value, however, follows well the measured data.

Figure 4-12 and Figure 4-13 show fluid velocities at the pump outlet and the reactor vessel inlet of the broken loop, respectively. The calculated vessel inlet fluid velocity matches well the test data; while the calculated pump outlet fluid velocity much differ from the test data after 23 s. The measured velocity is maintained at 110 m/s between 13 s and 32 s, as shown in Figure 4-12. This implies that the upper measure limit of the instrumentation is 110 m/s. Because there is no thermal-hydraulic mechanism to maintain fluid velocity at 110 m/s after 23 s, it is considered that the difference between the measured and the calculated values results from the large uncertainty of the measurement rather than the code deficiency.

A comparison of the code calculated and the measured accumulator injection flow is shown in Figure 4-14. The predicted injection flow rate is in reasonable agreement with the data.

Figure 4-15 and Figure 4-16 show a comparison of the measured and the calculated fluid densities (i.e., mixture density of liquid and vapor) at the hot and cold legs of the intact loop, respectively. The code over-predicts fluid density at the intact loop hot leg because of under-prediction of the break flow until 15 s. The predicted fluid density at the intact loop cold leg reasonably matches the data. At the broken loop, the code over-predicts the hot leg fluid density and under-predicts the cold leg fluid density until 10 s because of under-prediction of the break flow, as shown in Figure 4-17 and Figure 4-18. The general trends of the code results, however, are in reasonable agreement with the data considering the measurement uncertainties.

Figure 4-19 through Figure 4-22 show a comparison of the code predicted and the measured fluid temperatures at the reactor vessel inlets and outlets of both loops. The code calculated vapor and liquid temperatures are compared with the measured mixture temperature. RELAP5/MOD3.3/K reasonably predicts the fluid temperatures. The measured mixture temperatures lie within the predicted liquid and vapor temperatures, in general.

Figure 4-23 through Figure 4-27 show a comparison of the predicted rod cladding temperatures and the corresponding test data. The comparison was made at the PCT location of the test and its neighboring locations where comparable cladding temperatures were measured. In general, the code over-predicts the rod cladding temperature. The tendency of over-prediction is stronger at higher elevations.

4.5 SRS Calculations

181 times of simple random sampling (SRS) calculations were performed against the LOBI Test A1-66. The uncertainty parameters and their distribution functions used for the SRS calculations are listed in Table 4-3. Total [ ]TS uncertainty parameters for [ ]TS were

used for the SRS calculations.

Figure 4-28 shows the results of the SRS calculations and the measured cladding temperature behavior at the PCT elevation. The measured PCT is compared with the maxima and minima of the predicted results at the corresponding elevation. The third highest value of the calculated clad temperatures is higher than the measured PCT confirming the data covering. Therefore, the number and the probability distribution functions of the selected uncertainty parameters are confirmed to be sufficient.

4.6 Conclusion

The capability of RELAP5/MOD3.3/K in predicting thermal-hydraulic behaviors during a LBLOCA was assessed against the LOBI A1-66. The assessment results show that the code reasonably predicts the main parameters and phenomena observed during the test.

The data covering is confirmed through the SRS calculations. This implies that the number and the probability distribution functions of the selected uncertainty parameters are sufficient to cover the measured PCT.

References

[4-1] E. Ohlmer, J. Sanders, “Expermental data report on LOBI test A1-66,” LQC 82-09, CCR Ispra, 1982.

[4-2] L. Piplies, N. Granner, “Quick look repoty on LOBI test A1-66,” LQC 82-09, CCR Ispra, 1982.

[4-3] H. Stadtke, “Prediction-Experment comparison report,” LQC 82-06, CCR Ispra, 1982.

[4-4] RELAP5/MOD3 code manual, NUREG/CR-5535; EGG-2596, 1995.

Table 4-1 LOBI A1-66 Test Initial and Boundary Conditions

	Experiment data	RELAP5 result	Unit
Primary side			
Mass flow rate: Intact loop	20.5	20.83	kg/s
Broken loop	6.9	6.06	kg/s
Pressure: Upper head	15. 4	15.6	MPa
Fluid temperature			
Intact loop vessel outlet	597.15	597.2	K
Intact loop vessel inlet	564.15	562.8	K
Broken loop vessel outlet	597.15	597.2	K
Broken loop vessel inlet	564.15	562.6	K
Pressurizer	618.15	618.5	K
Core thermal output	5.24	5.24	MW
Accumulator			
Gas pressure	2.7	2.7	MPa
Liquid temperature	303.15	303.15	K
Secondary side			
Main feed water mass flow rate:			
Intact loop	2.1	2.14	kg/s
Broken loop	0.64	0.72	kg/s
Pressure: Main steam line	5.7	6.05/6.25	MPa
Temperature			
Steam generator inlet	452.15	483.0	K
Steam generator outlet	545.15	549.3	K

Table 4-2 Core Power Degradation

Time after break (sec)	Power (5.24MW)
0.	100%
2.6	100%
2.61	30.6%
8.6	30.6%
8.61	22.0%
10.2	22.0%
10.21	14.5%
12.2	14.5%
12.21	8.2%
16.2	8.2%
16.21	4.9%
20.2	4.9%
20.21	3.4%
30.	3.4%
30.01	0.
100.	0.

Table 4-3 Parameters and Distribution Functions Used for the SRS Calculations: LOBI A1-66

TS

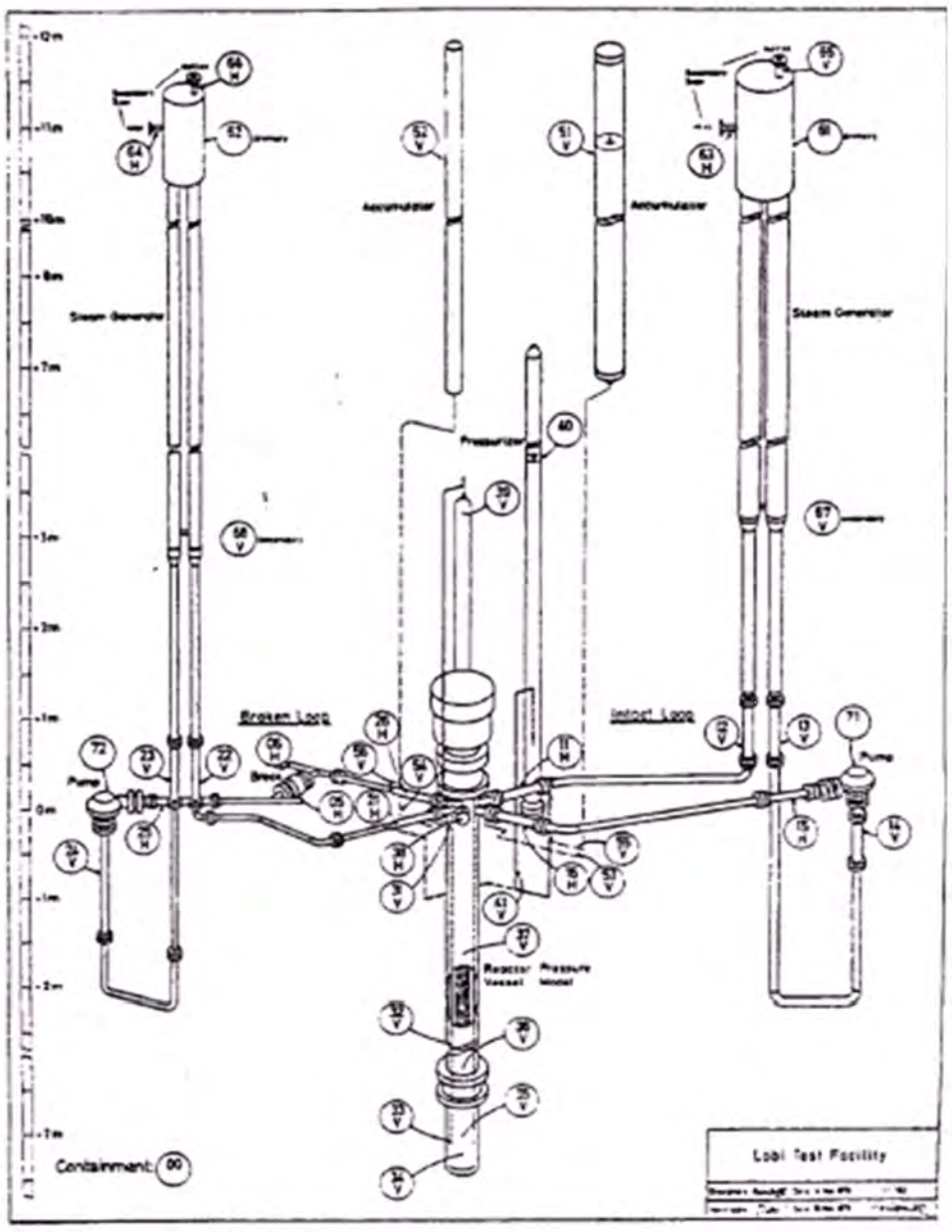

Figure 4-1 LOBI A1-66 Test Facility

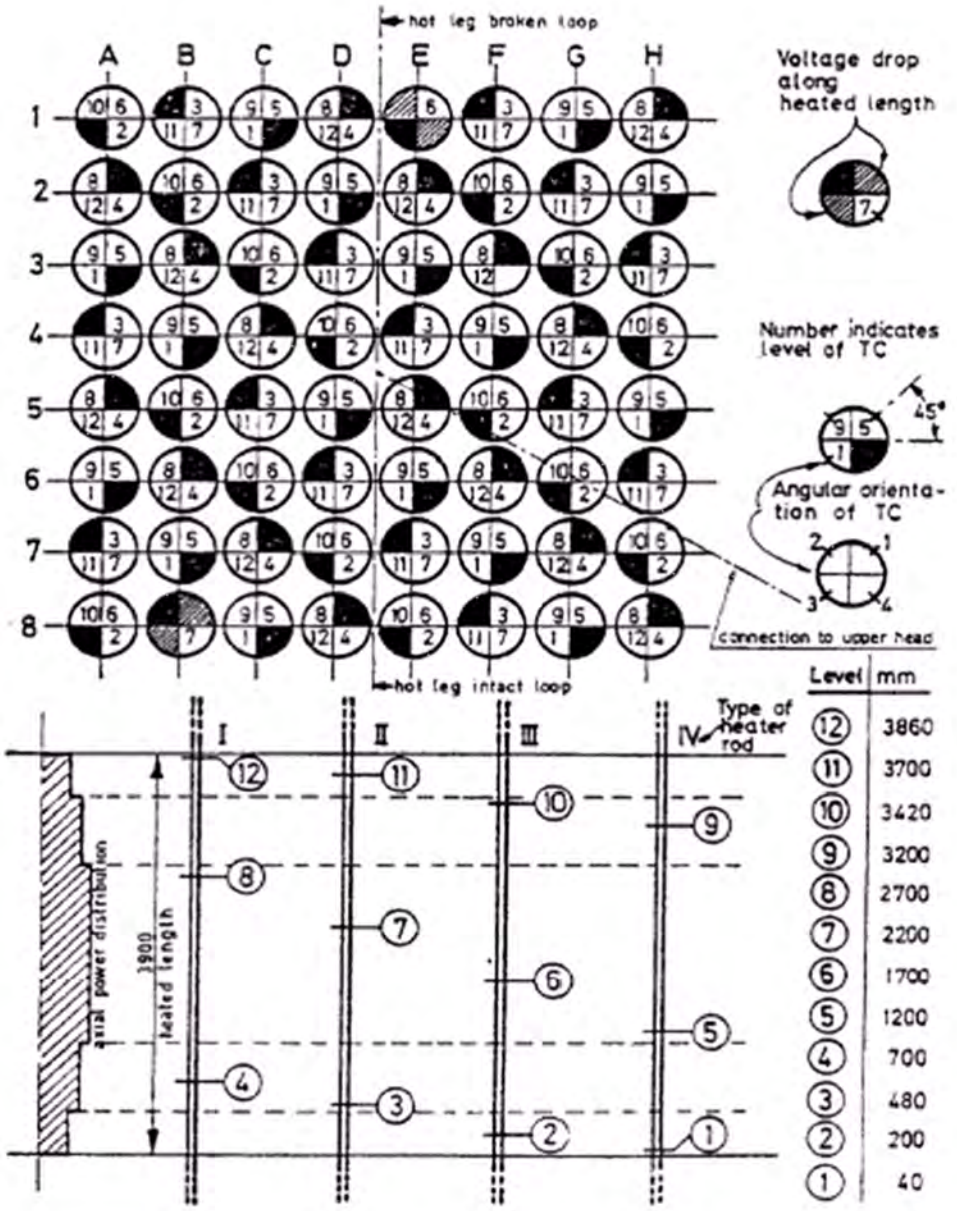

Figure 4-2 Thermocouple Elevation

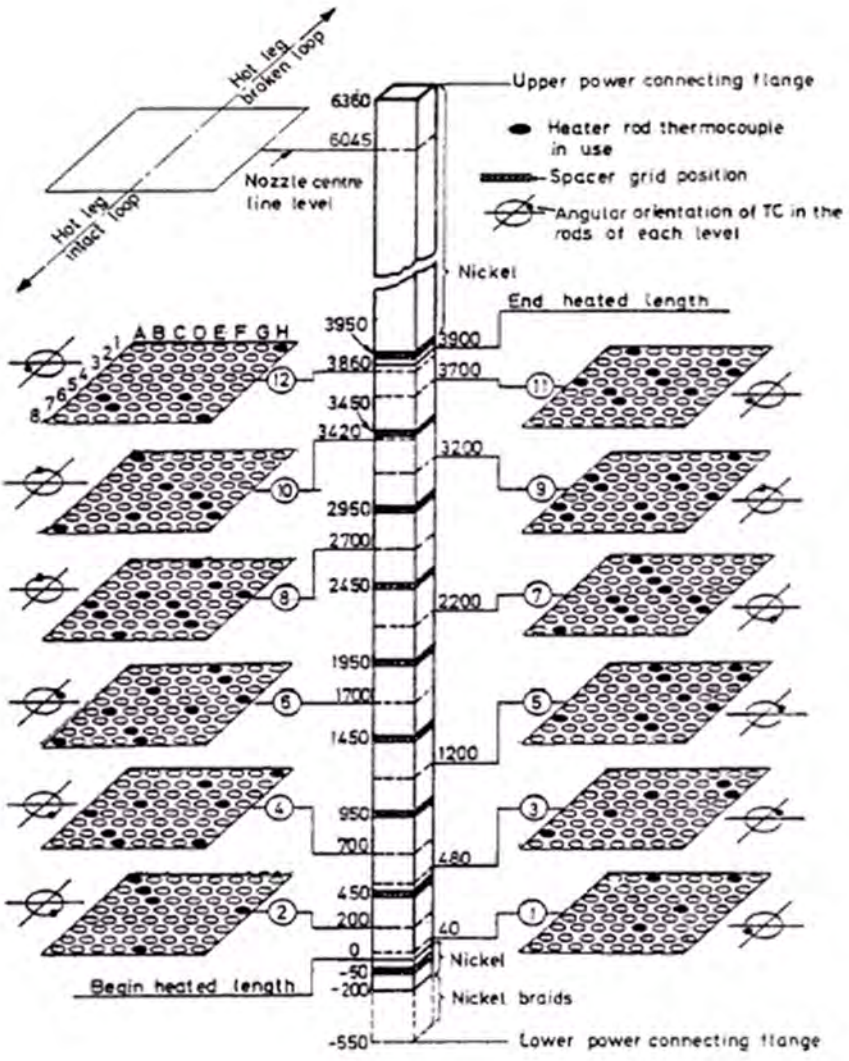

Figure 4-3 Location of Thermocouple in Electric Heater

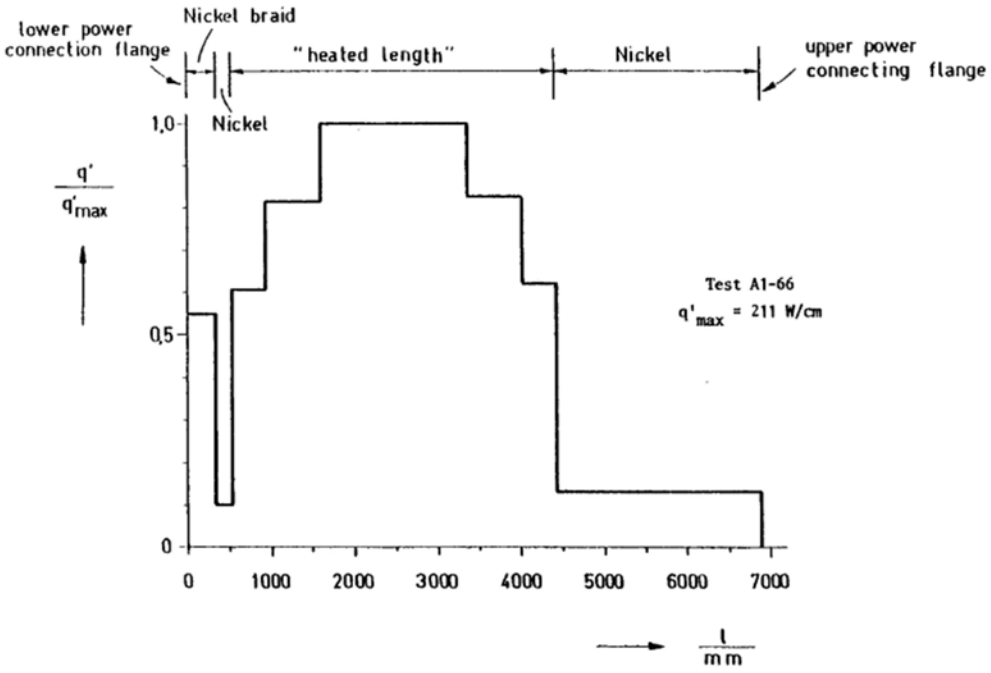

Figure 4-4 Axial Power Distribution

TS

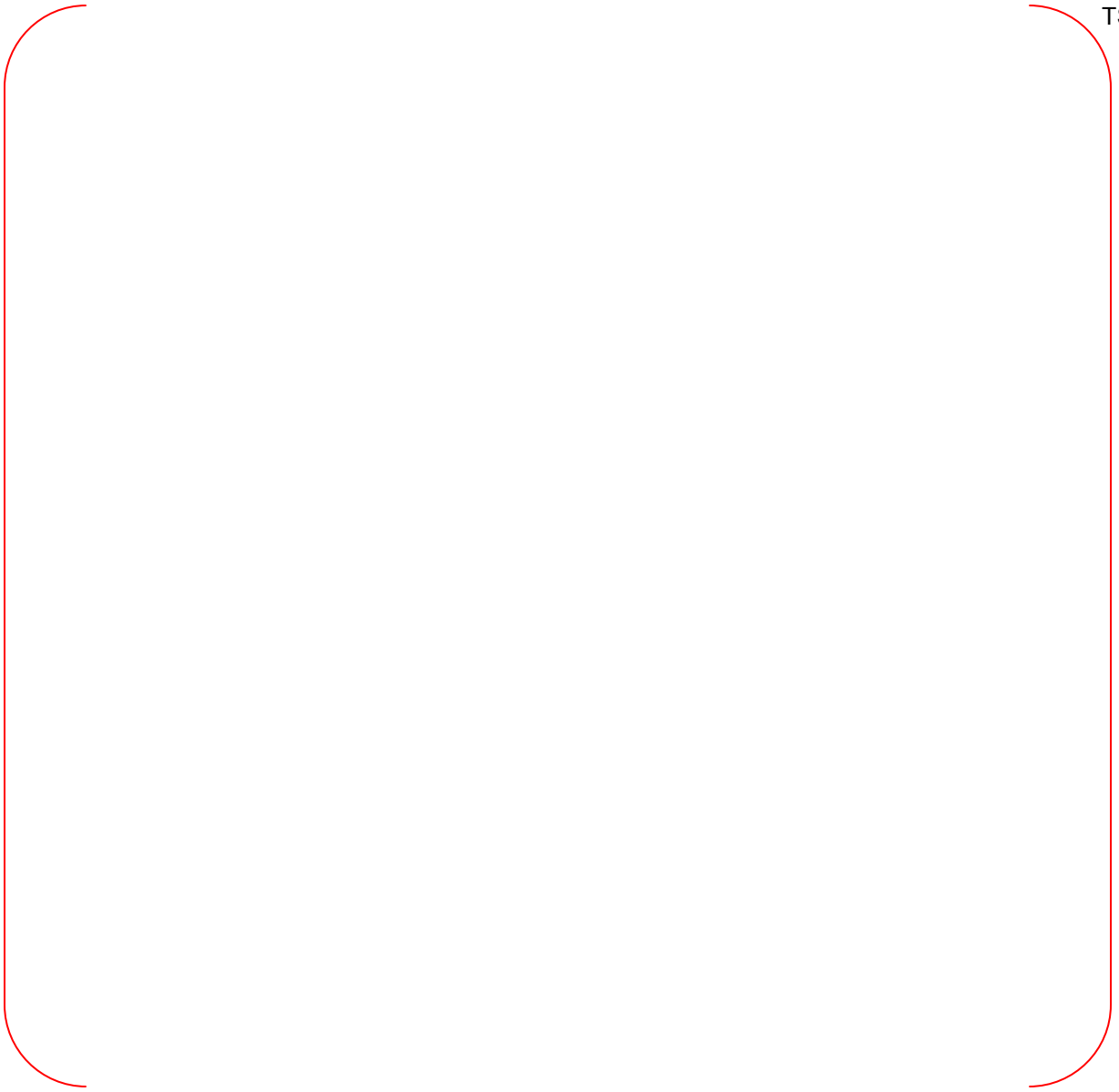

Figure 4-5 RELAP5/MOD3.3/K Nodalization of the LOBI MOD1 Facility

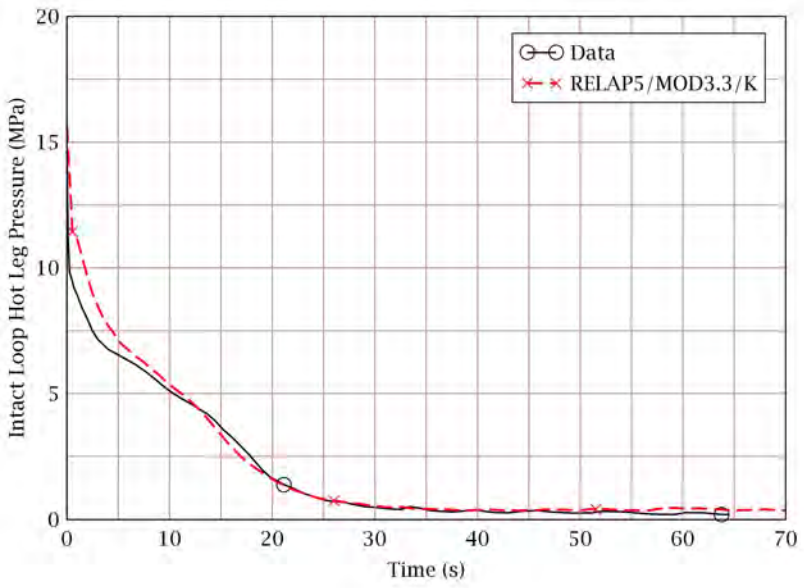

Figure 4-6 Intact Loop Hot Leg Pressure

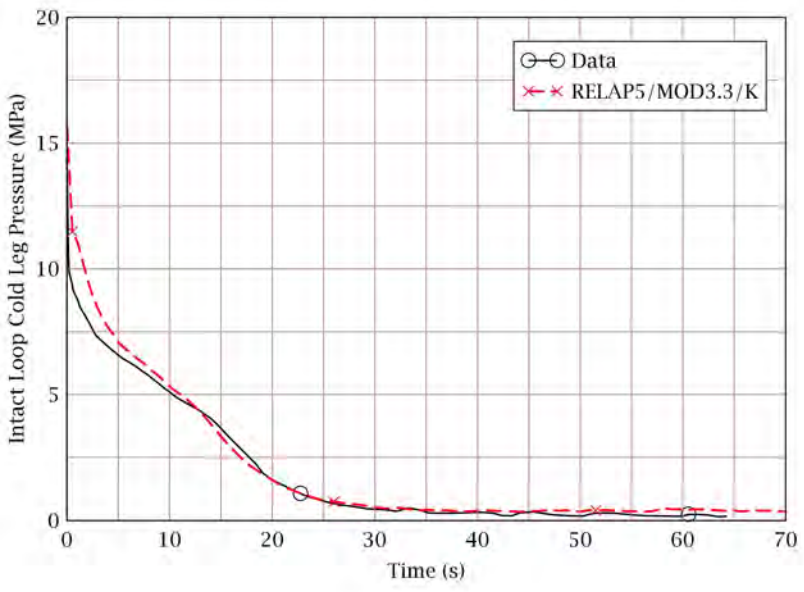

Figure 4-7 Intact Loop Cold Leg Pressure

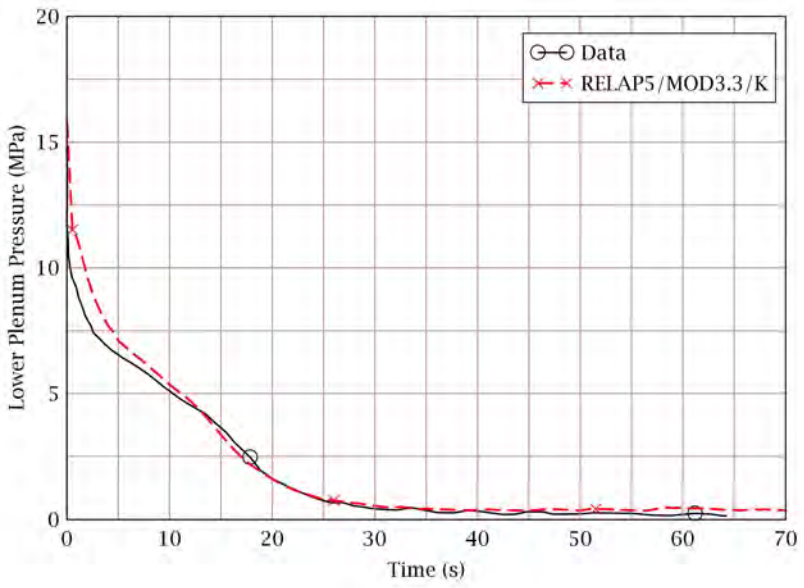

Figure 4-8 Lower Plenum Pressure

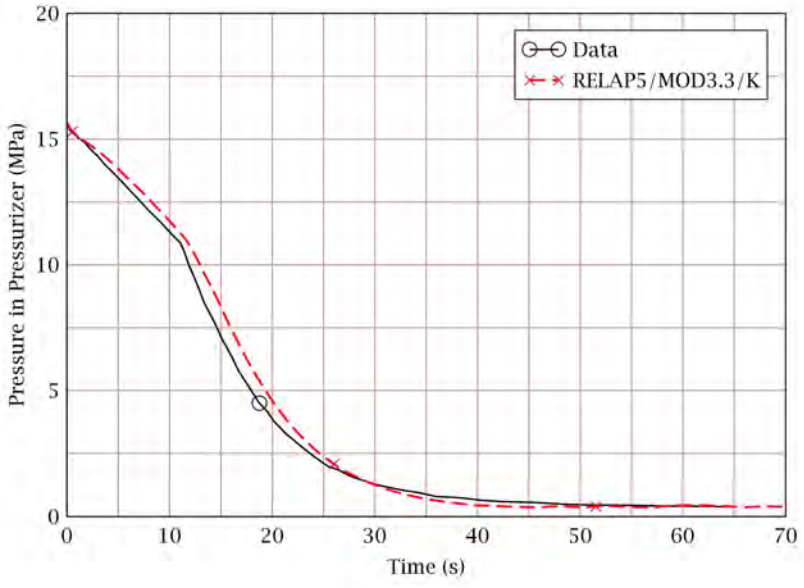

Figure 4-9 Pressure in Pressurizer

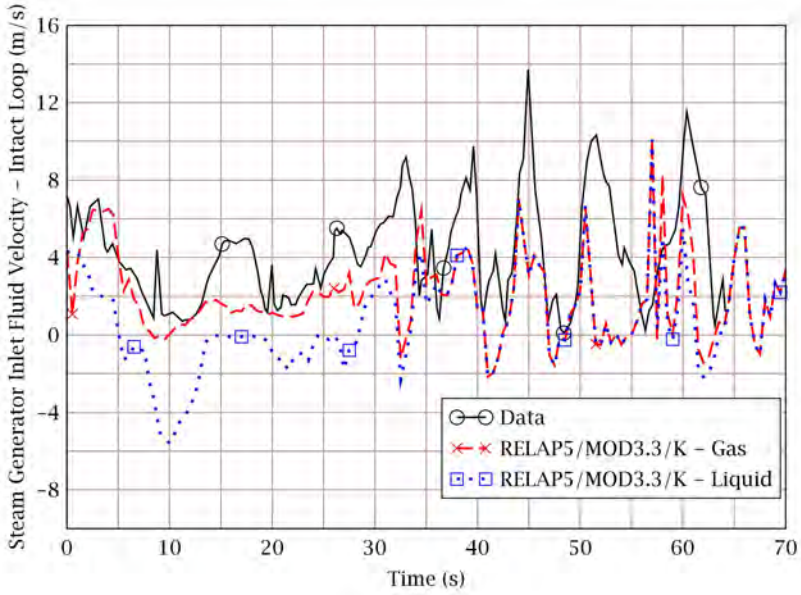

Figure 4-10 Intact Loop Steam Generator Inlet Fluid Velocity

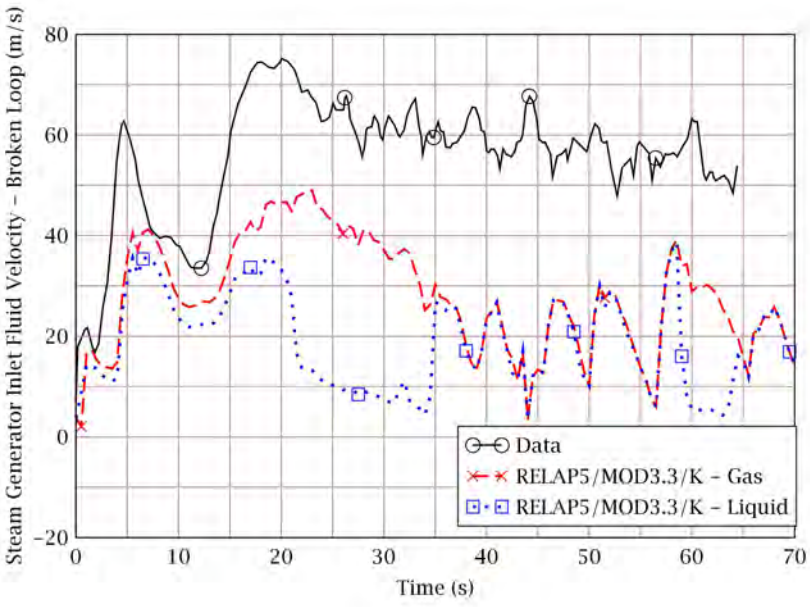

Figure 4-11 Broken Loop Steam Generator Inlet Fluid Velocity

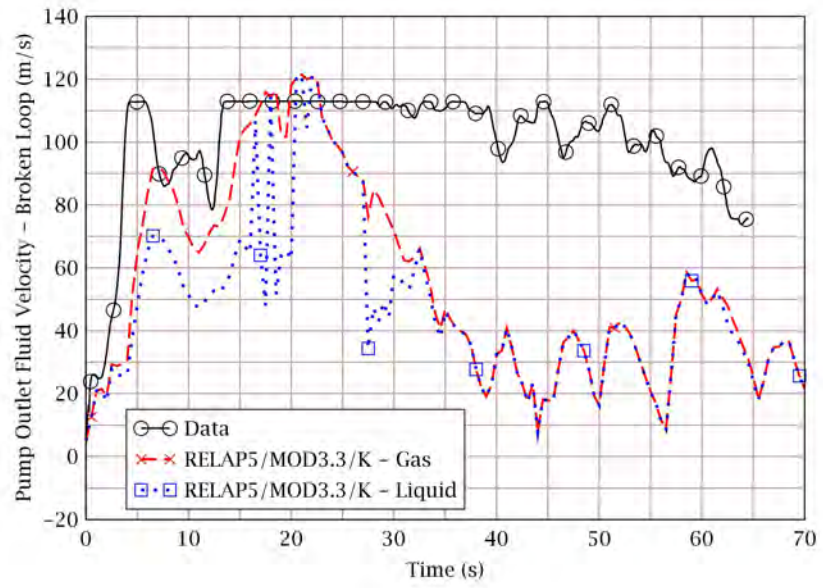

Figure 4-12 Broken Loop Pump Outlet Fluid Velocity

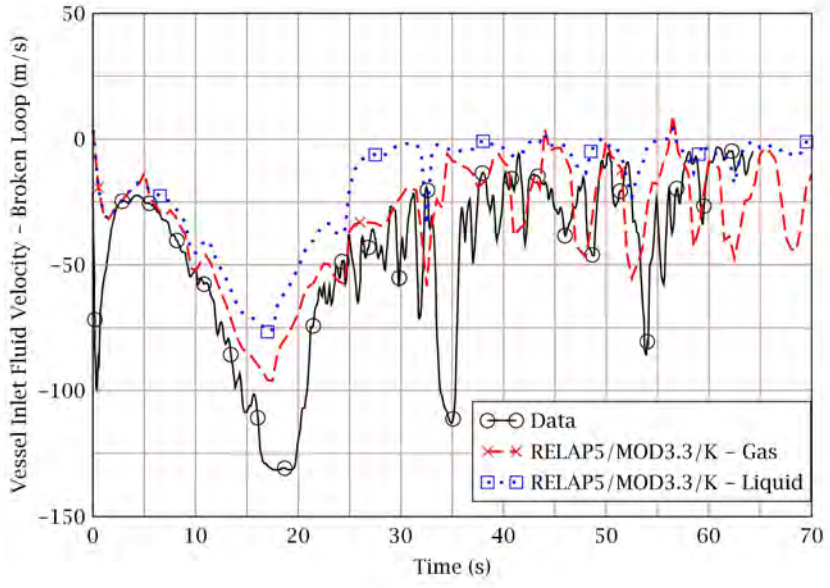

Figure 4-13 Broken Loop Vessel Inlet Fluid Velocity

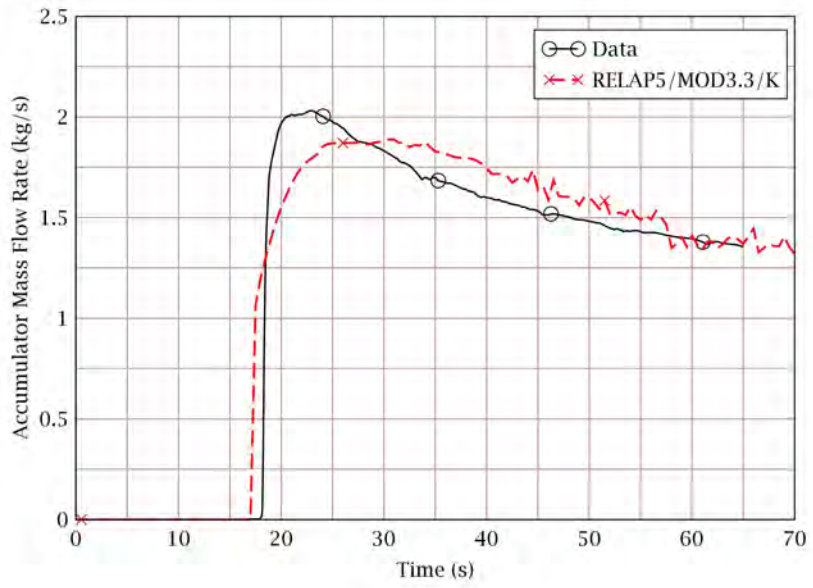

Figure 4-14 Accumulator Mass Flow Rate

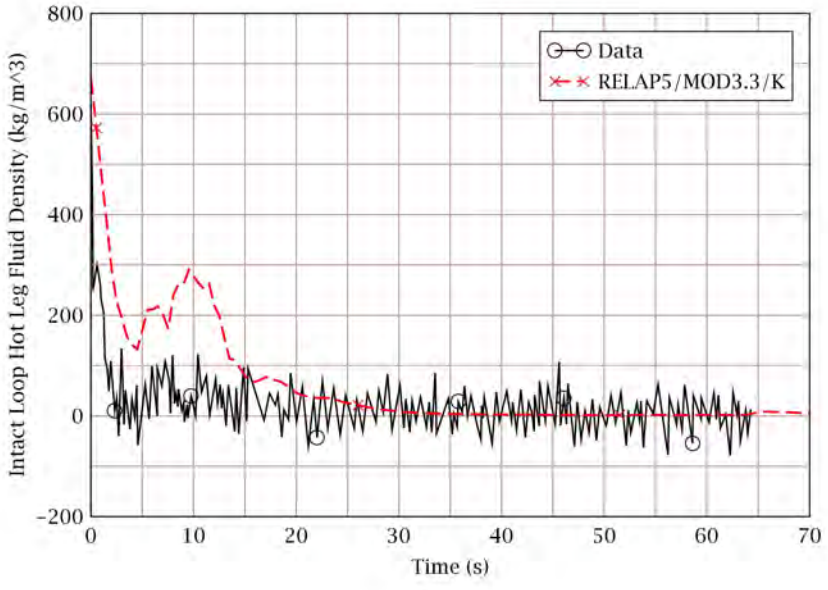

Figure 4-15 Intact Loop Hot Leg Fluid Density

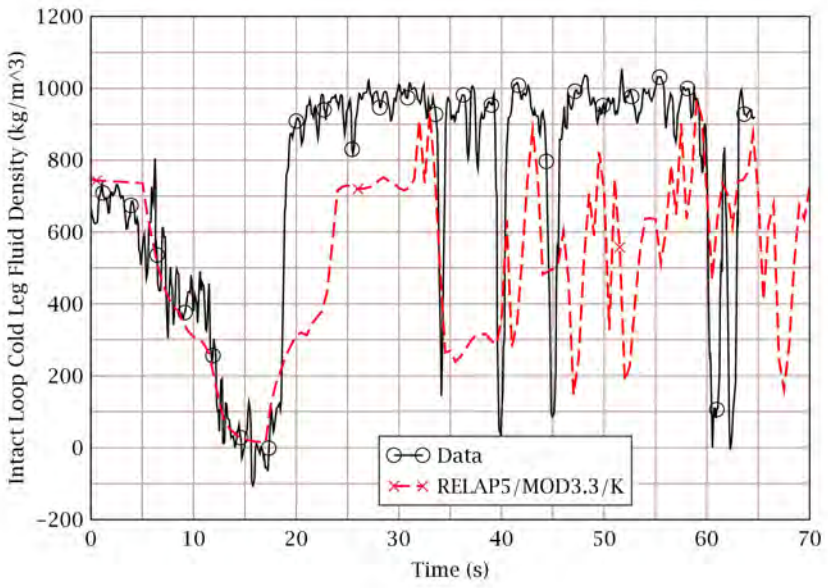

Figure 4-16 Intact Loop Cold Leg Fluid Density

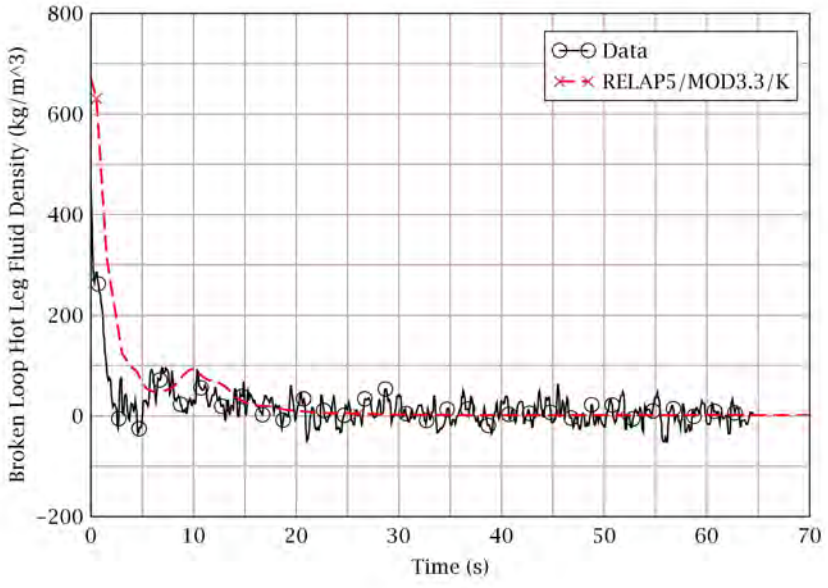

Figure 4-17 Broken Loop Hot Leg Fluid Density

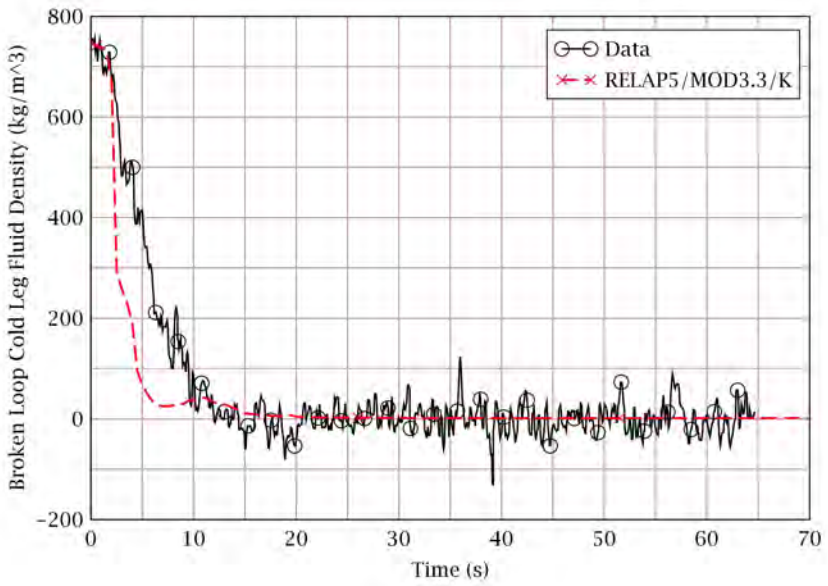

Figure 4-18 Broken Loop Cold Leg Fluid Density

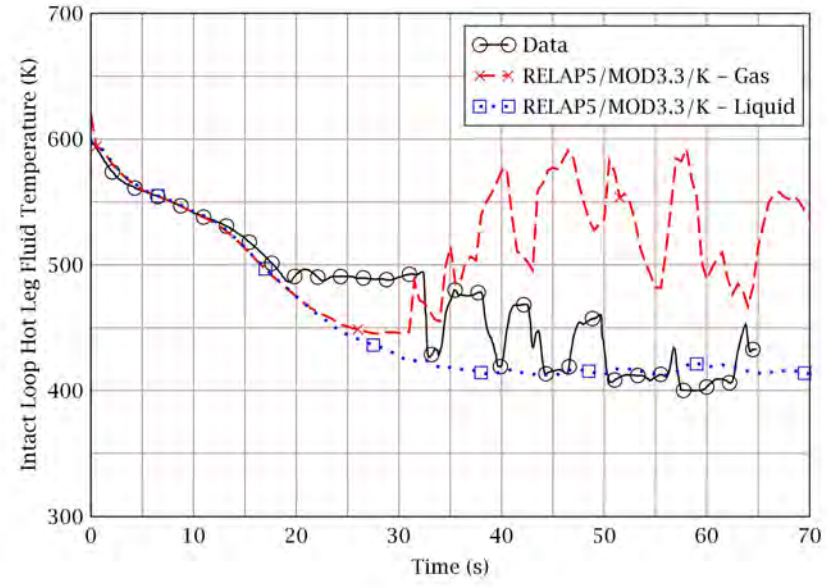

Figure 4-19 Intact Loop Hot Leg Fluid Temperature

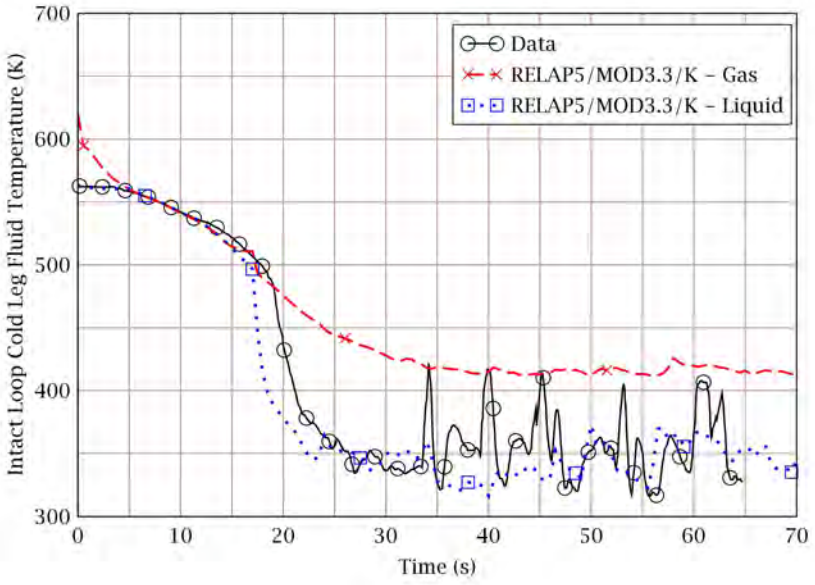

Figure 4-20 Intact Loop Cold Leg Fluid Temperature

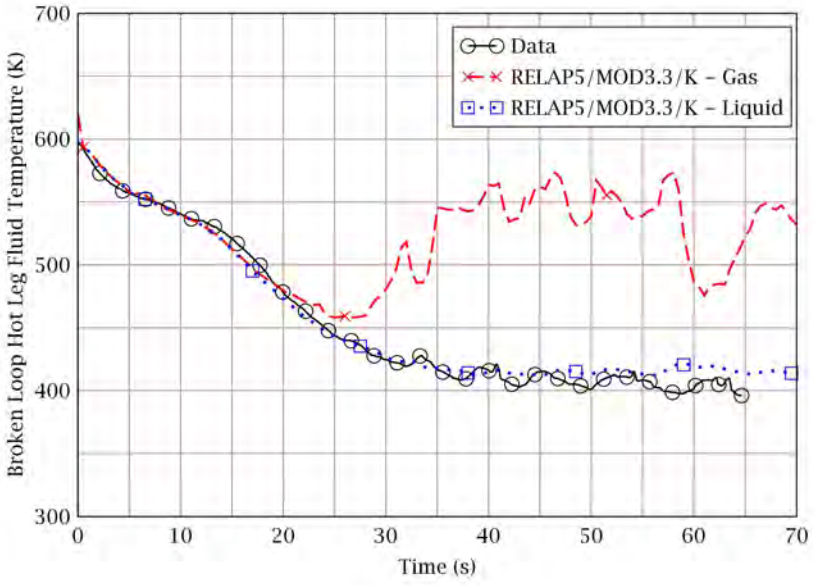

Figure 4-21 Broken Loop Hot Leg Fluid Temperature

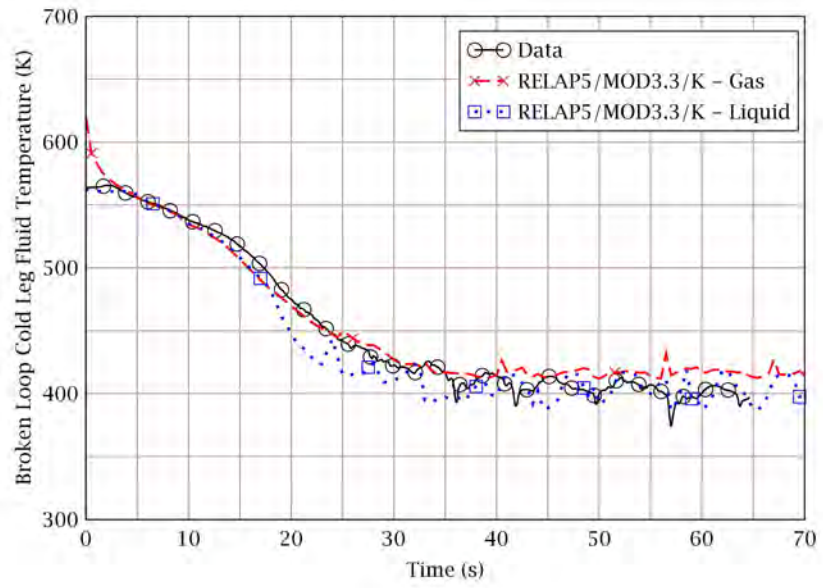

Figure 4-22 Broken Loop Cold Leg Fluid Temperature

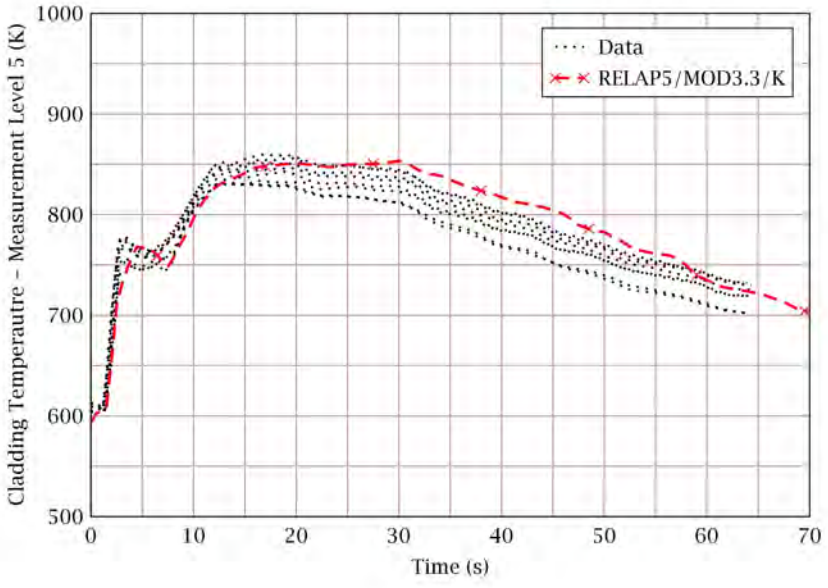

Figure 4-23 Heater Rod Cladding Temperature: Measurement Level 5

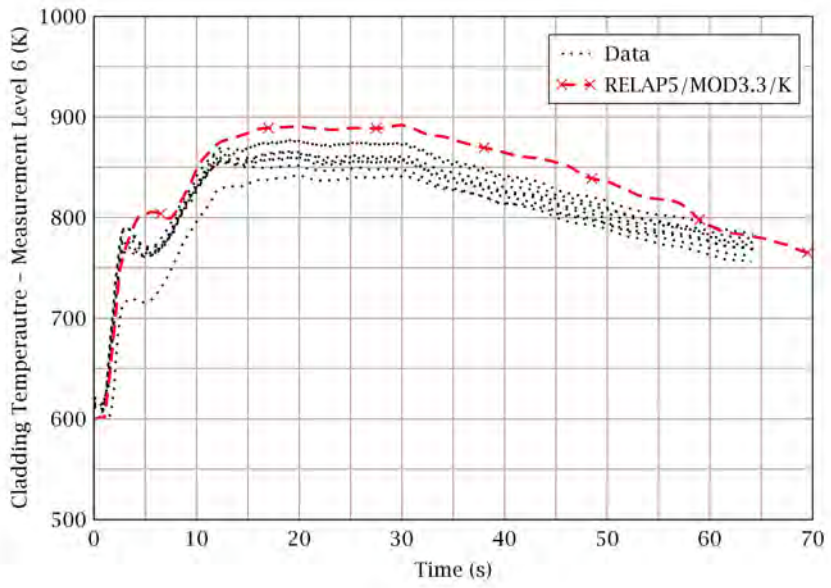

Figure 4-24 Heater Rod Cladding Temperature: Measurement Level 6

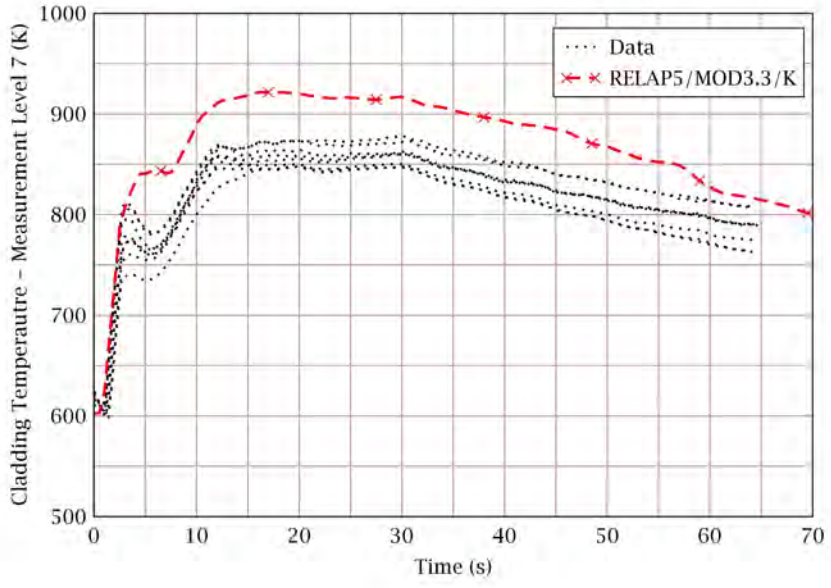

Figure 4-25 Heater Rod Cladding Temperature: Measurement Level 7

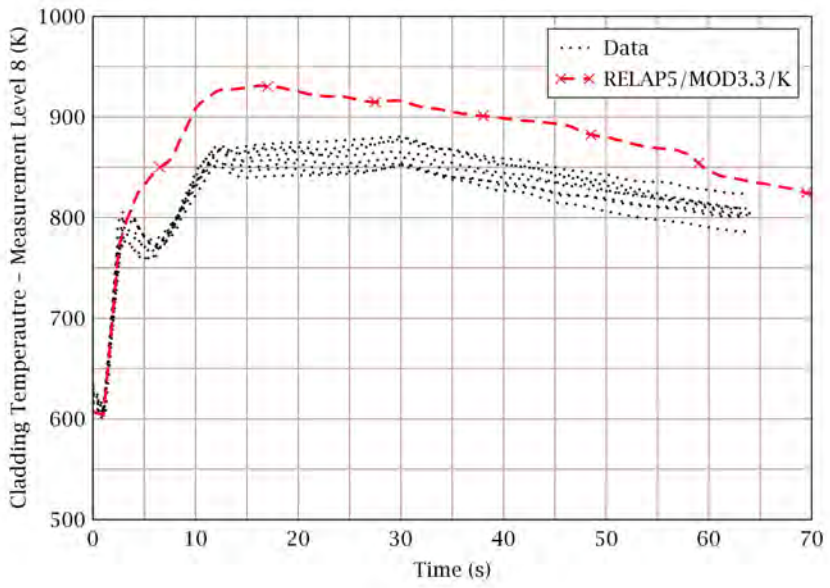

Figure 4-26 Heater Rod Cladding Temperature: Measurement Level 8

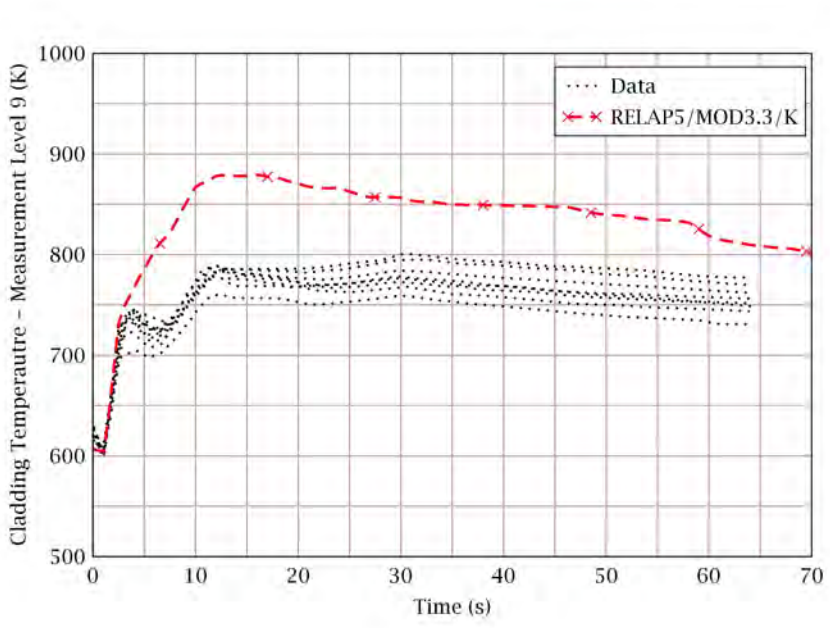

Figure 4-27 Heater Rod Cladding Temperature: Measurement Level 9

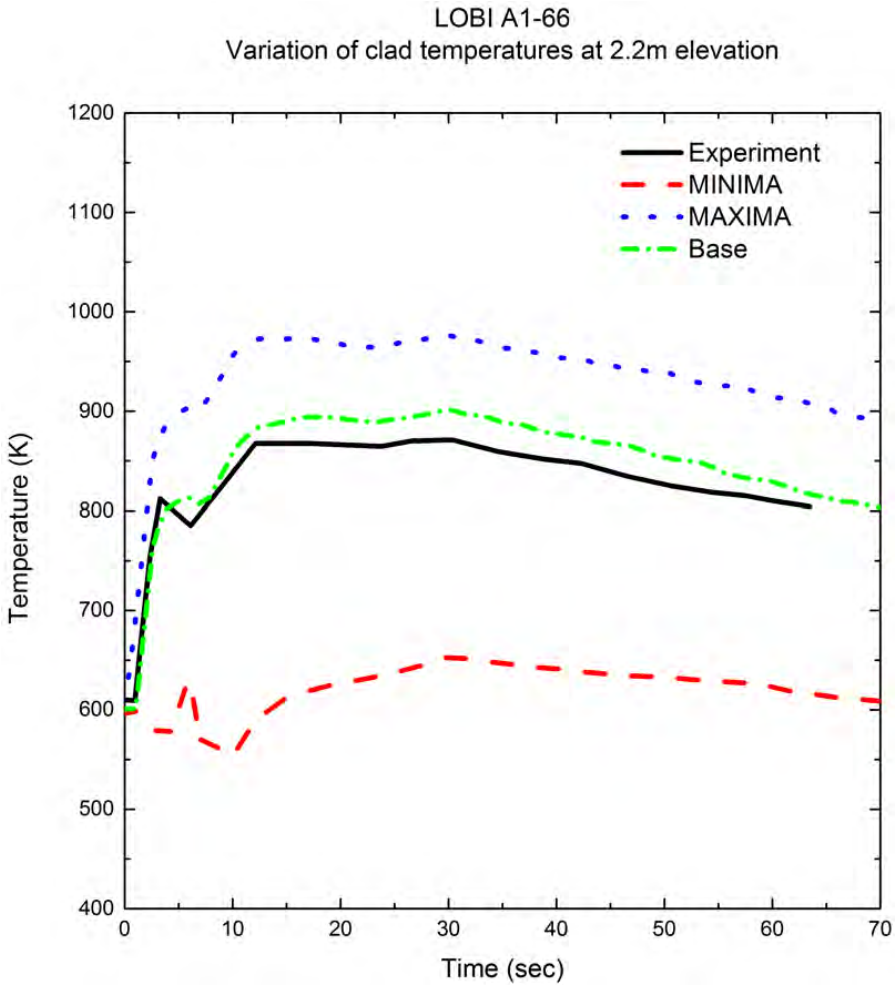

Figure 4-28 The Results of SRS Calculations: LOBI A1-66

5. Conclusions

Code accuracy, selected uncertainty parameters and their variations were confirmed by code assessment for the IETs.

181 SRS calculations were performed against all experiments considered in this appendix, even though the calculated PCT in base-case calculation was higher than the highest measured value. This was in order to understand and confirm the effect of selected uncertainty parameters and their variations

For all SRS calculations performed in this appendix, the calculated PCT exceeded the PCT of the experimental data. Therefore, it is confirmed that the number and the probability distribution functions of the selected parameters are sufficient to cover the measured PCTs in various IETs.

Non-Proprietary

SECTION C

Page intentionally left blank

KHNP Responses to Request for Additional Information No. 7425

Question TR Realistic Evaluation Methodology for LBLOCA of the APR1400-1

Provide a complete set of RELAP5 Mod 3.3 code manuals, including the theory manual, the input (user) manual, and the code qualification (benchmarking) manual. If these manuals are identical to published NUREG reports issued by the NRC, provide a list of these NUREG reports.

Response

RELAP5/MOD3.3 code manuals are identical to published NUREG reports issued by the NRC. The following is a list of these NUREG reports.

Volume Number	*Title*	*Report Number*	*Issued Date*
I	*RELAP5/MOD3.3 Code Manual Volume I: Code Structure, System Models, and Solution Methods*	*NUREG/CR-5535/Rev P3-Vol I*	*March, 2003*
II	*User's Guide and Input Requirements*	*NUREG/CR-5535/Rev P3-Vol II*	*March, 2006*
	Appendix A Input Requirements	*NUREG/CR-5535/Rev P3-Vol II App A*	*March, 2006*
III	*Developmental Assessment Problems*	*NUREG/CR-5535/Rev P3-Vol III*	*March, 2006*
VI	*Models and Correlations*	*NUREG/CR-5535/Rev P3-Vol IV*	*March, 2006*
V	*User's Guidelines*	*NUREG/CR-5535/Rev P3-Vol V*	*March, 2006*
VI	*Validation of Numerical Techniques in RELAP5/MOD3.0*	*NUREG/CR-5535/Rev P3-Vol VI*	*March, 2006*
VII	*Summaries and Reviews of Independent Code Assessment Reports*	*NUREG/CR-5535/Rev P3-Vol VII*	*March, 2006*
VIII	*Programmers Manual*	*NUREG/CR-5535/Rev P3-Vol VIII*	*March, 2006*

In addition to the inputs specified in RELAP5/MOD3.3 input manual, additional inputs are required for following calculations.

- *Quantification of uncertainty parameters*
  - *Uncertainty multiplier input cards are needed for 124 simple random sampling (SRS) calculations*
- *Calculation with CONTEMPT4/MOD5*
  - *Input cards are needed in order to activate and run CONTEMPT4/MOD5*
- *Evaluation of scale bias*
  - *Input cards are needed in order to activate scale bias calculations*

RELAP5/MOD3.3 was modified to accept additional inputs required for the above calculations.

The input requirements for the above calculations are as follow.

Input Data for Code Uncertainty Parameter Multiplier

The CAREM, realistic evaluation methodology for LBLOCA of the APR1400, selected total 30 uncertainty parameters. The uncertainty multipliers for [ ]^{TS}, can be input using RELAP5/MOD3.3 input cards specified in the input manual. But, the uncertainty multipliers for [ ]^{TS}, cannot be input using RELAP5/MOD3.3 input cards. Thus, additional input structures for code uncertainty parameters are needed. Table 1 shows [ ]^{TS} that need additional input data. The input cards for code uncertainty parameter multipliers are described below.

Table 1. Code Uncertainty Parameters

	TS

TS

TS

TS

Input Data for Coupled Run with CONTEMPT4/MOD5

TS

TS

Input Data for Bias Calculation

TS

Question TR Realistic Evaluation Methodology for LBLOCA of the APR1400-2

Provide a Compact Disk (CD) containing: (1) the complete RELAP5/MOD3.3/K source code subroutine listings; (2) the complied executable file(s); (3) the code input deck(s) developed for Shin-Kori (SKN), Unit 3 and Unit 4; (4) the model (node) diagram corresponding to the SKN input deck(s); and (5) the Parallel Virtual Machine (PCM) package used to link the CONTEMPT4/MOD5 with RELAP-5 code.

Response

A compact disk is provided separately.

(1) Most subroutines of RELAP5/MOD3.3/K are identical to those of released RELAP5/MOD3.3 (patch 03) by NRC. Total 51 subroutines were modified or added during the CAREM developmental phase. [

]^{TS} The subroutine list of the released RELAP5/MOD3.3 (patch 03) is presented in the code manual volume 8, Programmers Manual.

RELAP5/MOD3.3/K code was compiled in following environment.

- *OS: Windows NT server, 32bit*
- *Compiler: Compaq Visual Fortran 6.6B*

The folder structure of the compact disk containing RELAP5/MOD3.3/K source code files is as follows;

Folder Name	*Description*
Source code/Cenvrl	*Environment source files*
Source code/contempt/conta	*Released CONTEMPT4/MOD5 source files*
Source code/contempt/contl	*Modified or added source files for the CAREM*
Source code/contempt/ct4_exe	*Main function file of released CONTEMPT4/MOD5*
Source code/contempt/envrl	*Released CONTEMPT4/MOD5 environment source files*
Source code/relap5/envrl	*Released RELAP5/MOD3.3 environment source files*
Source code/relap5/kREM	*Modified or added source files for the CAREM*
Source code/relap5/selap	*Released RELAP5/MOD3.3 source files*

Table 2. List of RELAP5/MOD3.3/K Source Code Subroutines

TS

Table 2. List of RELAP5/MOD3.3/K Source Code Subroutines (Continued)

TS

(2) List of compiled RELAP5/MOD3.3/K code and libraries. These files are contained in "(2) Compiled files" folder.

Code	*File Name*	*Description*
RELAP5/MDO3.3/K	*Relap5m33p3k_dvi_compaq.exe*	*RELAP5 code execution file*
CONTEMPT4/MOD5	*contl.dll*	*CONTEMPT code DLL file*
Property Table for RELAP5/MOD3.3/K	*tpfh2onew*	*Water property file for RELAP*
Property Table for CONTEMPT4/MOD5	*tpfh2o*	*Water property file for CONTEMPT*
CONTEMPT4/MOD4 Input File	*inputc*	*CONTEMPT code input file*

(3) SKN34 input decks for the CAREM are contained in folder "(3) SKN34 inputs". In this folder, base and nominal input decks are provided in sub-folder "Base" and "Nominal", respectively. The base input decks do not consider any code uncertainty parameter and the code calculated values are used in RELAP5 calculations. [The nominal input decks use an arithmetic mean value of uncertainty range for each code uncertainty parameter.][TS]

(4)

(5)

(6)

(7) Figure 1 showed model diagram of SKN34, and graph file was contained in "(4) Model diagram" folder.

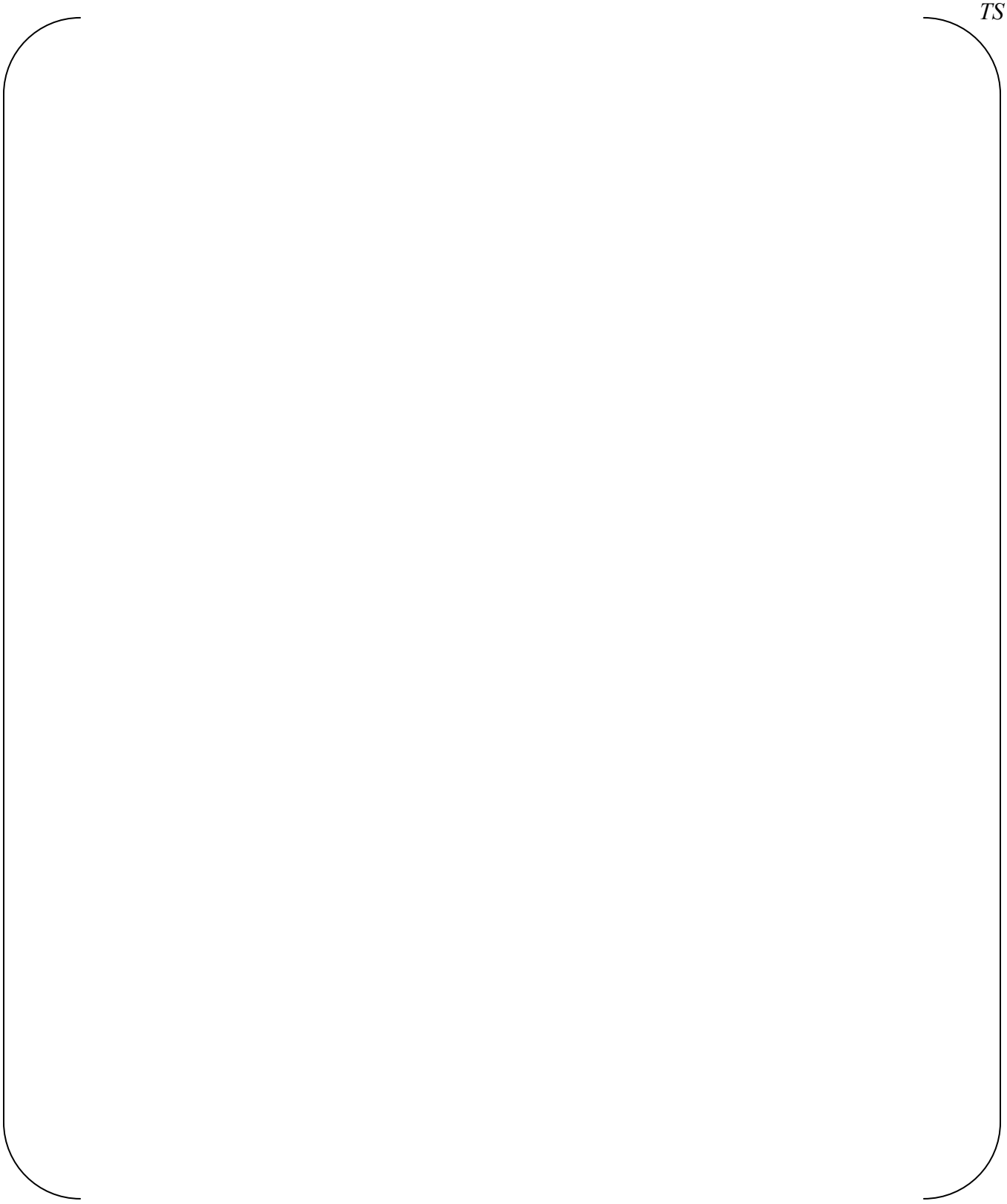

Figure 1 Model Diagram of SKN34

(8) CONTEMPT4/MOD5 is liked to RELAP5/MOD3.3/K using dynamic link library in Windows system. General information on the coupling of RELAP5/MOD3.3/K and CONTEMPT4/MOD5 are described in Appendix I of the CAREM topical report.

For the coupling code runs (RELAP5/MOD3.3/K and CONTEMPT4/MOD5), CONTEMPT DLL file (contl.dll) should be in the same folder with RELAP5/MOD3.3/K execution file. Two water property files (tpfh2o for CONTEMPT4/MOD5, tpfh2onew for RELAP5/MOD3.3) and input deck for CONTEMPT4/MOD5 (inputc) also should be in the same folder.

Question TR Realistic Evaluation Methodology for LBLOCA of the APR1400-3

Provide full size hard copies and PDF format files for a complete set of drawings of the reactor primary system, including the reactor pressure vessel, reactor core, cold leg and hot leg piping, steam generator, pressurizer, and the accumulator, as well as a diagram of the emergency core cooling system piping.

Response

Hard copies and PDF format files of the requested drawings are provided separately. Table 3 shows the list of drawings provided as hard copies and PDF format files.

Table 3. List of Drawings

Component	***PDF File Name***	***Project Drawing No.***	***Title***
Reactor Pressure Vessel	*MRDFD-140001M_1*	*9-431-Z-S-172-20*	*Reactor Vessel Arrangement & Installation*
	MRDFD-140001M_2	*9-431-Z-S-170-30*	*Reactor Vessel Closure Head Requirements*
	MRDFD-140001M_3	*9-732-Z-S-171-10*	*In-core Instrument Assembly*
	N11023-110CD-0101	*1-110-H-175-001C*	*Closure Head Ass'y for R/V*
	N11023-110CD-0102	*1-110-H-175-002C*	*Closure Head Machining for R/V*
	N11023-110CD-0103	*1-110-H-175-003C*	*Closure Head for R/V*
	N11023-110CD-0601	*1-110-H-175-004C*	*Closure Head Nozzles for R/V*
	N11023-110CD-0901	*1-110-H-175-005C*	*Closure Parts for R/V*
	N11023-110CD-1001	*1-110-H-175-006C*	*Closure Studs for R/V*
	N11023-110CD-1101	*1-110-H-175-007C*	*Closure Nuts & Washers for R/V*
	N11023-110CD-2101	*1-110-H-175-008C*	*Vessel Flange for R/V*
	N11023-110CD-2501	*1-110-H-175-009C*	*Inlet Nozzle for R/V*
	N11023-110CD-2601	*1-110-H-175-010C*	*Outlet Nozzle for R/V*
	N11023-110CD-2701	*1-110-H-175-011C*	*DVI Nozzle for R/V*
	N11023-110CD-2901	*1-110-H-175-012C*	*Monitor Tube for R/V*
	N11023-110CD-3101	*1-110-H-175-013C*	*Vessel Attachments for R/V*
	N11023-110CD-3201	*1-110-H-175-014C*	*Core Stabilizing Lugs for R/V*
	N11023-110CD-4101	*1-110-H-175-015C*	*Bottom Head for R/V*
	N11023-110CD-4201	*1-110-H-175-016C*	*Bottom Head Nozzles for R/V*
	N11023-110CD-6101	*1-110-H-170-001C*	*General Arrangement-Elevation*
	N11023-110CD-6102	*1-110-H-170-002C*	*General Arrangement-Sections*
	N11023-110CD-6201	*1-110-H-184-001C*	*External Interfaces*
	N11023-110CD-6202	*1-110-H-184-002C*	*External Interfaces*
	N11023-110CD-6203	*1-110-H-184-003C*	*External Interfaces*
	N11023-110CD-6204	*1-110-H-184-004C*	*Internal Interfaces*
	N11023-110CD-6205	*1-110-H-184-005C*	*Internal Interfaces*
	N11023-110CD-6501	*1-110-H-175-017C*	*Flow Baffle*
	N11023-110CD-6601	*1-110-H-175-018C*	*Surveillance Holders*
Steam Generators	*MRDFD-140001M_4*	*9-431-Z-S-172-11*	*Steam Generator Sliding Base Arrangement & Installation*
	MRDFD-140001M_5	*9-431-Z-S-172-12*	*Steam Generator Upper Supports Arrangement & Installation*
	N11023-160CD-0801	*1-160-H-175-001C*	*Steam Outlet Nozzle*
	N11023-160CD-0901	*1-160-H-175-002C*	*Dryer Supports*
	N11023-160CD-2801	*1-160-H-175-003C*	*Secondary Nozzles*
	N11023-160CD-2901	*1-160-H-175-004C*	*Vessel Supports*
	N11023-160CD-4101	*1-160-H-175-005C*	*Tubesheet Drilling*

Table 3. List of Drawings (Continued)

Component	***PDF File Name***	***Project Drawing No.***	***Title***
Steam Generators	*N11023-160CD-4102*	*1-160-H-175-006C*	*Lower Vessel Assembly*
	N11023-160CD-4103	*1-160-H-175-007C*	*Lower Vessel Assembly*
	N11023-160CD-4104	*1-160-H-175-008C*	*Handhole Access*
	N11023-160CD-4105	*1-160-H-175-009C*	*Feedwater Box*
	N11023-160CD-4106	*1-160-H-175-010C*	*Flow Distribution Plate*
	N11023-160CD-4601	*1-160-H-175-011C*	*Tubesheet*
	N11023-160CD-4701	*1-160-H-175-012C*	*Secondary Nozzles*
	N11023-160CD-5401	*1-160-H-175-013C*	*Primary Head*
	N11023-160CD-5701	*1-160-H-175-014C*	*Primary Divider Plates & Bars*
	N11023-160CD-5801	*1-160-H-175-015C*	*Primary Nozzles*
	N11023-160CD-5802	*1-160-H-175-016C*	*Primary Nozzles*
	N11023-160CD-6201	*1-160-H-170-001C*	*General Arrangement - Elevation*
	N11023-160CD-6202	*1-160-H-170-002C*	*General Arrangement - Sections*
	N11023-160CD-6203	*1-160-H-184-001C*	*Interfaces*
	N11023-160CD-6204	*1-160-H-184-002C*	*Interfaces*
	N11023-160CD-6205	*1-160-H-175-017C*	*Drawing Plan List*
	N11023-160CD-7101	*1-160-H-175-018C*	*Assembly of Tube Bundle*
	N11023-160CD-7102	*1-160-H-175-019C*	*External Attachements*
	N11023-160CD-7301	*1-160-H-175-020C*	*Steam Separators*
	N11023-160CD-7302	*1-160-H-175-021C*	*Steam Dryer Drains*
	N11023-160CD-7601	*1-160-H-175-022C*	*Primary Closure Parts*
	N11023-160CD-7602	*1-160-H-175-023C*	*Secondary Clolsure Parts*
	N11023-160CD-8501	*1-160-H-175-024C*	*Separator Support Plate*
	N11023-160CD-8601	*1-160-H-175-025C*	*Downcomer Feedwater Piping*
	N11023-160CD-8602	*1-160-H-175-026C*	*Recirculation Piping*
	N11023-160CD-8701	*1-160-H-175-027C*	*Shroud*
	N11023-160CD-8801	*1-160-H-175-028C*	*Tube Bundle Supports*
	N11023-160CD-8901	*1-160-H-175-029C*	*Upper Tube Supports*
	N11023-160CD-8902	*1-160-H-175-030C*	*Upper Tube Supports Details*
	N11023-160CD-9101	*1-160-H-175-031C*	*Tube Details*
	N11023-160CD-9401	*1-160-H-175-032C*	*Full Eggcrates*
	N11023-160CD-9402	*1-160-H-175-033C*	*Half Eggcrates*
	N11023-160CD-9403	*1-160-H-175-034C*	*Partial Eggcrates*
Pressurizer	*MRDFD-140001M_6*	*9-431-Z-S-172-40*	*Pressurizer Arrangement & Installation*
	N11023-170CD-0101	*1-170-H-175-001C*	*Top Head*
	N11023-170CD-0801	*1-170-H-175-002C*	*Spray Nozzle*
	N11023-170CD-0802	*1-170-H-175-003C*	*Manway*

Table 3. List of Drawings (Continued)

Component	***PDF File Name***	***Project Drawing No.***	***Title***
Pressurizer	*N11023-170CD-2901*	*1-170-H-175-004C*	*Vessel Attachments*
	N11023-170CD-5101	*1-170-H-175-005C*	*Bottom Head*
	N11023-170CD-5601	*1-170-H-175-006C*	*Support Skirt*
	N11023-170CD-5801	*1-170-H-175-007C*	*Surge Nozzle*
	N11023-170CD-6201	*1-170-H-170-001C*	*General Arrangement*
	N11023-170CD-6203	*1-170-H-184-001C*	*Interfaces*
	N11023-170CD-6204	*1-170-H-184-002C*	*Interfaces*
	N11023-170CD-6205	*1-170-H-175-008C*	*Drawing Plan List*
	N11023-170CD-7201	*1-170-H-175-009C*	*Instrument Nozzles*
	N11023-170CD-8401	*1-170-H-175-010C*	*Heaters and Sleeves*
	N11023-170CD-8601	*1-170-H-175-011C*	*Heater Supports*
Reactor Vessel Internals	*N11023-120CD-0001*	*1-120-H-175-001C*	*Reactor Internals Dimensional Assembly*
	N11023-120CD-0002	*1-120-H-175-002C*	*Reactor Internals Assembly*
	N11023-120CD-0101	*1-120-H-175-003C*	*Core Support Barrel Assembly*
	N11023-120CD-0201	*1-120-H-175-004C*	*Core Shroud/Lower Structure Assembly*
	N11023-120CD-0301	*1-120-H-175-005C*	*Upper Guide Structure Assembly*
	N11023-120CD-0401	*1-120-H-175-006C*	*Alignment Keys*
	N11023-120CD-0501	*1-120-H-175-007C*	*Socket Head Cap Screw*
	N11023-120CD-0601	*1-120-H-175-008C*	*Bill of Material*
	N11023-120CD-1001	*1-120-H-175-009C*	*Core Support Barrel*
	N11023-120CD-1401	*1-120-H-175-010C*	*Lifting Bolt Insert*
	N11023-120CD-2001	*1-120-H-175-011C*	*Core Shroud Assembly*
	N11023-120CD-2601	*1-120-H-175-012C*	*Guide Lug Inserts/ Dowel Pin*
	N11023-120CD-3001	*1-120-H-175-013C*	*Lower Support Structure/ Instrument Nozzle Assembly*
	N11023-120CD-3101	*1-120-H-175-014C*	*Lower Support Structure Assembly*
	N11023-120CD-3601	*1-120-H-175-015C*	*Insert Pins*
	N11023-120CD-3701	*1-120-H-175-016C*	*Instrument Nozzle Support Plate*
	N11023-120CD-3801	*1-120-H-175-017C*	*Instrumentation Nozzles*
	N11023-120CD-4001	*1-120-H-175-018C*	*Inner Barrel Assembly*
	N11023-120CD-4501	*1-120-H-175-019C*	*HJTC Upper Tube Assembly*
	N11023-120CD-4601	*1-120-H-175-020C*	*HJTC Lower Tube Assembly*
	N11023-120CD-5001	*1-120-H-175-021C*	*Upper Guide Structure Support Barrel Assembly*
	N11023-120CD-7001	*1-120-H-175-022C*	*Holddown Ring*

Table 3. List of Drawings (Continued)

Component	***PDF File Name***	***Project Drawing No.***	***Title***
Reactor Coolant Piping	*N11023-190CD-1102*	*1-190-H-175-001C*	*Closure Piping P-2,3,4,6,7,8,11,12,13,15,16,17*
	N11023-190CD-2801	*1-190-H-175-002C*	*Hot Leg Nozzles*
	N11023-190CD-2802	*1-190-H-175-003C*	*Cold Leg Nozzles*
	N11023-190CD-4101	*1-190-H-175-004C*	*Cold Leg Piping P-5*
	N11023-190CD-4102	*1-190-H-175-005C*	*Cold Leg Piping P-9*
	N11023-190CD-4103	*1-190-H-175-006C*	*Cold Leg Piping P-14*
	N11023-190CD-4104	*1-190-H-175-007C*	*Cold Leg Piping P-18*
	N11023-190CD-5801	*1-190-H-175-008C*	*Surge Line*
	N11023-190CD-6201	*1-190-H-184-001C*	*Interfaces*
	N11023-190CD-6202	*1-190-H-184-002C*	*Interfaces*
	N11023-190CD-6203	*1-190-H-184-003C*	*Interfaces*
	N11023-190CD-7101	*1-190-H-175-009C*	*Hot Leg Piping P-1*
	N11023-190CD-7102	*1-190-H-175-010C*	*Hot Leg Piping P-10*
	N11023-190CD-7201	*1-190-H-175-011C*	*Small Nozzles*
Safety Injection Tanks	*N11023-420CD-0010*	*1-420-H-175-001C*	*Outline Drawing for SIT*
ECCS Line	*MESFD-140001M*	*1-441-N-105-001*	*P&I Diagram Safety Injection/Shutdown Cooling System (1/4)*
	MESFD-140001M	*1-441-N-105-002*	*P&I Diagram Safety Injection/Shutdown Cooling System (2/4)*
	MESFD-140001M	*1-441-N-105-003*	*P&I Diagram Safety Injection/Shutdown Cooling System (3/4)*
	MESFD-140001M	*1-441-N-105-004*	*P&I Diagram Safety Injection/Shutdown Cooling System (4/4)*

Non-Proprietary

SECTION D

Page intentionally left blank

RESPONSE TO AUDIT ISSUES

APR1400 Topical Reports

Korea Electric Power Corporation / Korea Hydro & Nuclear Power Co., LTD

Docket No. PROJ0782

Review Section	**TR Realistic Evaluation Methodology for LBLOCA of the APR1400**
Application Section	**Topical Report: APR1400-F-A-TR-12004 Realistic Evaluation Methodology for Large-Break LOCA of the APR1400**
Issue Date	**08/13/2015**

Audit Issues No. 1

The abstract for the topical report states that the methodology does not cover the long-term performance of the emergency core cooling system (ECCS). All best-estimate ECCS methods are expected by the NRC to also include the long-term core cooling (LTCC) phase as is stated in the criteria provided by Title 10 of the *Code of Federal Regulations* (10 CFR) Part 50.46 (b). That requirement applies to the approved ECCS and evaluation models. The guidance of Regulatory Guide (RG) 1.157 also addresses this issue. The Applicant needs to be prepared to address and/or present the following:

a. The KHNP plans for revising all applicable statements in the topical report in order for the proposed KHNP methodology to fully address the LTCC in the topical report. This also applies to the revision in the topical report to fully describe the approach to modeling the LTCC functionally to meet the corresponding regulatory requirements.

b. Results of calculations to demonstrate LTCC phase of ECCS performance. The Applicant is requested to include details of the assumptions, input decks (for all relevant codes), and the methodology/computer codes used in arriving at the results.

Response

(a) & (b)

Topical report does not cover the so-called long term performance of an emergency core cooling system. It is covered by technical report of “Post-LOCA Long Term Cooling Evaluation Model,” and it was submitted in September of 2014. The abstract and references of topical report are modified to add information of above technical report as follows.

- Before Modifications

Abstract

The method evaluates the values to compare with the acceptance criteria of 10 CFR 50.46 (b) [3], but does not cover the so-called long term performance of an emergency core cooling system.

- After Modifications

Abstract

The method evaluates the values to compare with the acceptance criteria of 10 CFR 50.46 (b) [3], but does not cover the so-called long term performance of an emergency core cooling system. **The long term performance of an emergency core cooling system is covered by the other evaluation method described in reference [21].**

References

[21] “Post-LOCA Long Term Cooling Evaluation Model,” APR1400-F-A-NR-14003-P, Rev. 0, September 2014.

Impact on DCD

There is no impact on the DCD.

Impact on PRA

There is no impact on the PRA.

Impact on Technical Specifications

There is no impact on the Technical Specifications.

Impact on Technical/Topical/Environmental Report

Topical report will be revised as discussed above.

There is no impact on Technical or Environmental Report.

RESPONSE TO AUDIT ISSUES

APR1400 Topical Reports

Korea Electric Power Corporation / Korea Hydro & Nuclear Power Co., LTD

Docket No. PROJ0782

Review Section	**TR Realistic Evaluation Methodology for LBLOCA of the APR1400**
Application Section	**Topical Report: APR1400-F-A-TR-12004 Realistic Evaluation Methodology for Large-Break LOCA of the APR1400**
Issue Date	**08/13/2015**

Audit Issues No. 3

The guidance in RG 1.157, Section 3.1 establishes acceptable controls for the establishment of acceptable break sizes and types. The topical report Section 1 states that the report describes the methodology "...for large-break loss-of-coolant accidents (LBLOCA) for APR1400." The Applicant needs to clearly specify the range of break sizes, locations and types of breaks for which the methodology in the topical report will be used for licensing applications.

Response

The ranges of break sizes, locations and types in the topical report are described in the response to audit issue 6-a.

Impact on DCD

There is no impact on the DCD.

Impact on PRA

There is no impact on the PRA.

Impact on Technical Specifications

There is no impact on the Technical Specifications.

Impact on Technical/Topical/Environmental Report

There is no impact on any Technical, Topical, or Environmental Report.

RESPONSE TO AUDIT ISSUES

APR1400 Topical Reports

Korea Electric Power Corporation / Korea Hydro & Nuclear Power Co., LTD

Docket No. PROJ0782

Review Section	**TR Realistic Evaluation Methodology for LBLOCA of the APR1400**
Application Section	**Topical Report: APR1400-F-A-TR-12004 Realistic Evaluation Methodology for Large-Break LOCA of the APR1400**
Issue Date	**08/13/2015**

Audit Issues No. 4

Comparing Figure 1-1 in the topical report with Figure 1 of NUREG/CR-5249 it is noted that the step that determines whether a noding change is necessary is different in the two approaches. According to Figure 1-1 of the topical report, the determination of whether a noding change is required occurs after all the uncertainties and biases have been determined. It is unclear how this is accomplished and what metric will be used to determine if a nodalization change is warranted. It appears that decision of ‘noding change’ should be a part of the ‘covering ok’ decision in Figure 1-1 of the topical report, and it should follow more closely the NUREG/CR-5249 guidance. The Applicant will need to explain and provide additional rationale including the technical bases related to the process used to assess any changes to the noding in the evaluation model.

Response

Nodding change can be done anywhere along the steps between 8 and 12. But, if nodding change occurs, it is important to repeat the whole steps.

Impact on DCD

There is no impact on the DCD.

Impact on PRA

There is no impact on the PRA.

Impact on Technical Specifications

There is no impact on the Technical Specifications.

Impact on Technical/Topical/Environmental Report

There is no impact on any Technical, Topical, or Environmental Report.

RESPONSE TO AUDIT ISSUES

APR1400 Topical Reports

Korea Electric Power Corporation / Korea Hydro & Nuclear Power Co., LTD

Docket No. PROJ0782

Review Section	**TR Realistic Evaluation Methodology for LBLOCA of the APR1400**
Application Section	**Topical Report: APR1400-F-A-TR-12004 Realistic Evaluation Methodology for Large-Break LOCA of the APR1400**
Issue Date	**08/13/2015**

Audit Issues No. 5

The guidance in RG 1.157, Section 4.3.1 establishes acceptable controls for the utilization of conservative parameters in best estimate analysis. The topical report states that the methodology is best-estimate. However, the actual implementation of the methodology incorporates a mixture of best-estimate and conservative assumptions. The reason for the conservative treatment is provided for only certain parameters. The Applicant will need to provide the basis and justifications for the selecting the parameters to be treated conservatively instead of a best-estimate manner, involving the quantification and propagation of uncertainties.

Response

The phenomena treated conservatively are shown in the Table 1. The PIRT table in the topical report contains some errors and will be revised in association with audit issue no. 15. The part of the revised PIRT table is shown in Table 1 for conservatively treated phenomena. The basis and justification of the conservatism for each phenomenon are organized by components and are given below. According to regulatory guide 1.157, conservatism may be introduced by the following reasons.

1. The model simplification or conservatism has little effect on the result, and therefore the development of a better model is not justified.

2. The uncertainty of a particular model is difficult to determine, and only an upper bound can be determined.

3. The particular application does not require a totally best-estimate calculation, so a bias in the calculation is acceptable.

The category of conservatism of each phenomenon described below is also provided.

1) Containment

- Pressure and temperature history

The calculated peak cladding temperature must be very sensitive to the containment pressure and temperature during reflood period. In other words, if the containment pressure and temperature were considered as the uncertainty parameters, the calculated results (SRS) would vary widely. In practical application, the severe variation of the calculation result is not desirable. Therefore, the most conservative condition is imposed for the containment condition. In LBLOCA view point, the lower containment pressure and temperature, the more unfavorable for PCT calculation. The containment pressure and temperature condition is determined to have minimum pressure and temperature that can be obtained by CONTEMPT/MOD4, which is the conservative code with conservative user input. The category of conservatism of this belongs to Category 2.

2) SIT

- Gas discharge to piping

The nitrogen gas is injected just after the SIT injection ends. The SIT injection ends at the end of early reflood period. Thus the influence of the nitrogen gas is possible for period 3 and 4. The importance rank 5 is imposed for period 4, differently from the PIRT in the topical report. From the assessment against VAPER test, which is the full scale SIT-FD test, the gas discharge to piping phenomena is modeled to give the most conservative results. The details are well described in Appendix H of the topical report. The category of conservatism of this belongs to Category 3.

- SIT/Fluidic device high-flow delivery, low-flow delivery

The high- and low-flow deliveries of SIT-FD are treated conservatively by applying the most conservative combination of K-factors as discussed in Appendix H of the topical report. The other parameters related with SIT-FD such as inventory, pressure and temperature are treated as uncertainty parameters.

As the results of the various assessments in Appendix H of the topical report, it is concluded that the modeling difference does not produce significant changes in the injection flow rates on the plant calculation results. The conservative treatment of high-flow and low-flow deliveries in SIT/FD component belongs to Category 1.

3) Break

- Delta P (1-phase, 2-phase)

Delta P consideration at the break plane is given in Section 4.2.2.7 and 5.2.1.1 of the topical report. The break mass flow rate is influenced by Delta P at the break plane and discharge coefficients. From the Marviken test assessment, discharge coefficients are determined to be the best-estimate approach. Delta P is determined according to the flow condition of single-phase or two-phase flow. It is also influenced by the configuration of the break plane. By performing the break location sensitivity study, the most conservative break location is determined. The sensitivity calculation with varying break locations gives the cladding temperature variations and those results of cladding temperatures are always lower than the selected break location. The most conservative break location is cold leg (pump discharge line) break. The limiting break configuration and size is determined through the break spectrum and configuration sensitivity studies. As a result, the limiting break location, size and configuration is determined. Therefore, the uncertainty of Delta P is conservatively treated through the limiting break location, size and configuration considerations. Also, the uncertainty of loop Delta P is covered by RCP K-factor uncertainty. The conservative treatment of Delta P belongs to Category 3.

4) Reactor vessel upper head

- Upper head to upper plenum via upper guide structure support plate flow

The upper head water can flow down to the upper plenum and may affect the core cooling behavior during blowdown. This phenomenon is considered by the noding scheme. By performing several sensitivity studies on the nodalization of upper guide structure (UGS, the volume between upper guide structure support plate and inner vessel assembly), the noding that gives the most conservative result is determined. The limiting UGS noding is used for the plant calculation of the topical report. Figure 1 and Figure 2 show the conventional noding scheme and the most conservative noding scheme, respectively. Figure 3 shows the effect of the noding scheme on the cladding temperature. Although reflood PCT is changed more, the phenomenon is important for blowdown because the phenomenon is related with blowdown quenching. The category of conservatism of this phenomenon belongs to Category 2.

TS

Figure 1. The conventional noding diagram of UGS [ ]TS

TS

Figure 2. The most conservative noding diagram of UGS [ ]TS

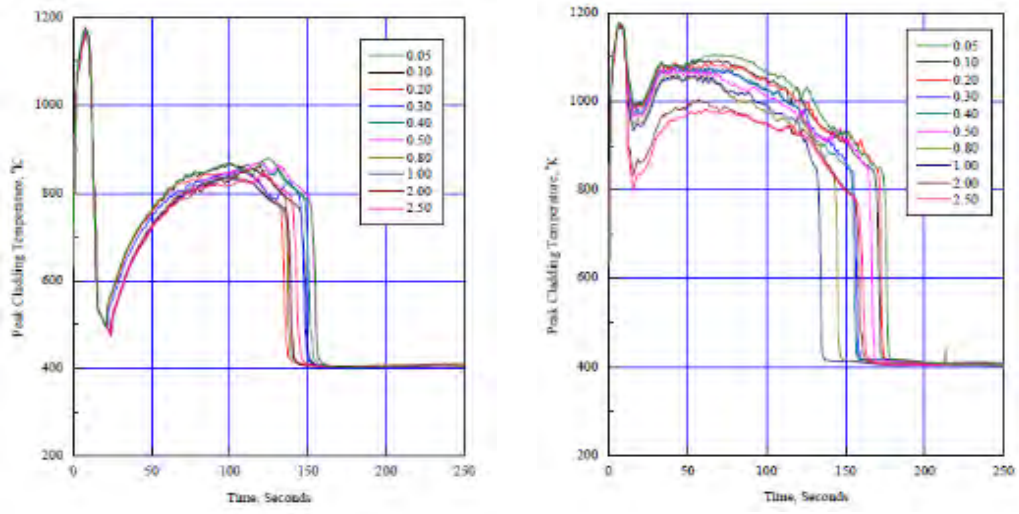

a) [ ]TS b) [ ]TS

Figure 3. The effect of the noding sensitivity

5) Reactor vessel core region

- Radiation heat transfer to surfaces, vapor & liquid

The radiation heat transfer to surfaces will always reduce the peak cladding temperature since the radiation heat transfer from fuel rod to other structures (e.g., the nearby fuels) will contribute to the cooling of the hot fuel at certain amount. The radiation heat transfer to surface to surface is neglected for conservatism. However, as described in the response to audit issue 37 (a) and (b), the radiation heat transfer to vapor and liquid is not neglected. The effect of radiation heat transfer to surfaces is shown in Figure 4 and shows the conservatism of the neglected radiation heat transfer assumption. Also refer to the response of the audit issue 37. The effect of the radiation heat transfer on PCT is about -22 K. The conservative treatment of this phenomenon belongs to Category 3.

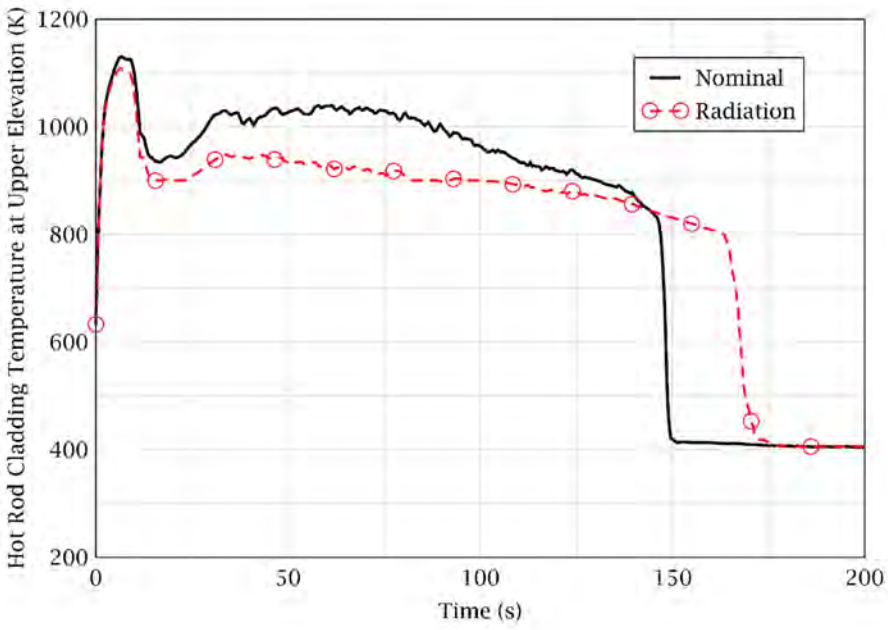

Figure 4. The effect of radiation heat transfer to surfaces on PCT

- Reactivity

As described Section 5.1.2 of the topical report, the most conservative moderator density vs. reactivity curve provided by the core design group is used to bound the uncertainty of the moderator density reactivity. This curve is made assuming non-uniform voiding and hot zero power. However, this curve causes unphysical power increase at the early stage of the transients, as pointed out by the staffs during the audit. Therefore the conservative curve at the hot full power condition will be used for the plant calculations. The topical report will be revised later. The category of conservatism of this phenomenon belongs to Category 2.

- Boron reactivity effect

The boron reactivity which gives negative reactivity is not considered for conservatism. The conservative treatment of this phenomenon belongs to Category 2.

- Fuel relocation into clad-ballooned region

As stated in section 4.2.2.1.1 of the topical report, clad ballooning has favorable effect on PCT because of the increased distance between cladding and fuel pellet. Fuel relocation into the clad

ballooning region can increase PCT but this phenomenon is not considered as uncertainty parameters due to the limited occurrences of the fuel relocation. It seems that the use of higher Fq in CAREM can encompass the uncertainty of this phenomenon. [

]TS The category of this conservatism treatment belongs to Category 3.

- Spacer grid heat transfer effects

As described in Sec 4.2.2.1.2 of the topical report, spacer grids of the fuel assembly usually have three effects on core cooling; (1) heat transfer enhancement by the agitation of the flow, (2) rewetting of spacer grids, and (3) breakup of entrained water drops into fine droplets. All three have favorable effects on core cooling. By neglecting the spacer grid heat transfer effects, the conservative cladding temperature is obtained. The phenomenon is treated conservatively because this belongs to Category 3.

6) Reactor vessel downcomer region

- Non-condensable gas effect

As described in Appendix H of the topical report, non-condensable gas behavior on Apr1400 is modeled using the model C. Non-condensable gas injection before end of SIT-FD was considered to be non-conservative due to the reduced amount of remaining non-condensable gas in the SIT dome during SIT-FD injection period. This issue is assessed in Appendix H and it is concluded that the non-condensable injection before end of SIT-FD should be neglected to be conservative. Moreover, non-condensable gas effect varies with the non-condensable injection rate from the SITs. The injection rate of non-condensable gas depends on the initial SIT pressure, water volume, and temperature. These are selected as uncertainty parameters to treat their uncertainties. This conservative treatment belongs to Category 3.

Table 1. Phenomena treated conservatively in CAREM

TS

Impact on DCD

There is no impact to the DCD.

Impact on PRA

There is no impact on the PRA.

Impact on Technical Specifications

There is no impact on the Technical Specifications.

Impact on Technical/Topical/Environmental Report

Topical report will be revised according to the PIRT revision as described in the attachment for the response of Audit Issue No. 14.

There is no impact on any Technical or Environmental Report.

RESPONSE TO AUDIT ISSUES

APR1400 Topical Reports

Korea Electric Power Corporation / Korea Hydro & Nuclear Power Co., LTD

Docket No. PROJ0782

Review Section	**TR Realistic Evaluation Methodology for LBLOCA of the APR1400**
Application Section	**Topical Report: APR1400-F-A-TR-12004 Realistic Evaluation Methodology for Large-Break LOCA of the APR1400**
Issue Date	**08/13/2015**

Audit Issues No. 6-a, c, d, and e

RG 1.157 specifies that breaks should be evaluated to include the range from "full double-ended" to small breaks. This range would include single and double-ended breaks. Furthermore, the guidance specifies that longitudinal split breaks should be considered as well. RG 1.157 also states that actual peaking factors and fuel conditions should be used. Section 3.1 (and its subsections) of the topical report discuss the limiting scenario that is used to determine the processes that must be addressed in the evaluation model. However, the criteria specified therein include break location and size only. Furthermore, Section 5.2.1.1 of the topical report describes the spectrum of cases evaluated as being [ ]^{TS}. A reference to a [ ]^{TS} is also provided without further discussion. The Applicant needs to:

a. Fully describe the spectrum of breaks that are applicable to analysis of APR1400 using the proposed methodology for licensing submittals. This includes a description of the break type (e.g., guillotine, double or single-ended, and longitudinal split), size, and location. Ensure that the size parameters are either quoted in measured units, or if in percentage, clearly describe that it is with respect to what dimension or pipe size.

c. Explain the modeling approach used (i.e., nodalization, discharge coefficient, etc.) for representing longitudinal split breaks.

d. Clarify whether any sensitivity calculations were performed to arrive at [ ]^{TS} If such sensitivity calculations have been performed, describe the results and highlight any differences. If such calculations have not been performed, justify the basis for their exclusion.

e. Describe whether the limiting break analysis included consideration for loop sensitivity (e.g., loops with and without the pressurizer). If such sensitivity calculations have been performed, describe the results and highlight any differences. If such calculations have not been performed, justify the basis for their exclusion.

Response

a)

CAREM is applicable to the following spectrum of break.

- Break location: primary loop piping such as RCP discharge leg (cold leg), RCP suction leg, hot leg.
- Break type: guillotine, double-ended and longitudinal split.
- Break size: 0.5 ft^2 ~ *100 % double ended.

*) 100 % break means 100 % of pipe cross sectional area. Thus, 100 % double-ended guillotine break has total 200 % break area of a pipe.

[

]TS

c)

Figure 1 shows slot break modeling method for the topical report. [

]TS

Slot break can be modeled several kinds of modeling methods. These modeling methods are described in response to audit issue 61-b ~ f with evaluation results of them.

d)

Break location sensitivity in the cold leg is not performed because there is no additional pressure loss coefficient in the cold leg. Thus, it can be thought that there is no significant differences in break locations in the cold leg (pump discharge line). Moreover, it is widely accepted that the break location near vessel is more limiting because it has more possibility to have ECC bypass or sweep-out of coolant than the other break locations in the cold leg.
[

]TS

Additional description for break location sensitivity within cold leg will be added in Section 3.1.1

of topical report as follows:

Break location sensitivity within the cold leg is not performed because of minimal effects of break location caused by insignificant friction and form pressure losses within the cold leg.

e)

The loop sensitivity is performed for two cases. Those are the cold leg break at the loop 1, where the pressurizer is not connected (without the pressurizer) and the cold leg break at the loop 2, where the pressurizer is connected (with the pressurizer) (See Figure 2).

Figure 3 shows calculation results with and without the pressurizer. [

]TS

Figure 3 and the description of loop sensitivity as followings will be added in the topical report as Figure 3-2 and Section 3.1.1, respectively.

Description:

For the limiting break location, i.e., a loop sensitivity study was performed to determine the conservative pressurizer location. As shown in Figure 3-2, the PCT was higher when the pressurizer was connected to the intact loop.

TS

Figure 1. Slot Break Modeling for the CAREM

Figure 2. RELAP5/MOD3.3/K Nodalization of the APR1400

Figure 3. Cladding Temperature Results of Sensitivity Study

Impact on DCD

There is no impact on the DCD.

Impact on PRA

There is no impact on the PRA.

Impact on Technical Specifications

There is no impact on the Technical Specifications.

Impact on Technical/Topical/Environmental Report

Topical report will be revised as discussed above.

There is no impact on Technical or Environmental Report.

RESPONSE TO AUDIT ISSUES

APR1400 Topical Reports

Korea Electric Power Corporation / Korea Hydro & Nuclear Power Co., LTD

Docket No. PROJ0782

Review Section	**TR Realistic Evaluation Methodology for LBLOCA of the APR1400**
Application Section	**Topical Report: APR1400-F-A-TR-12004 Realistic Evaluation Methodology for Large-Break LOCA of the APR1400**
Issue Date	**08/13/2015**

Audit Issues No. 6-b

RG 1.157 specifies that breaks should be evaluated to include the range from “full double-ended” to small breaks. This range would include single and double-ended breaks. Furthermore, the guidance specifies that longitudinal split breaks should be considered as well. RG 1.157 also states that actual peaking factors and fuel conditions should be used. Section 3.1 (and its subsections) of the topical report discuss the limiting scenario that is used to determine the processes that must be addressed in the evaluation model. However, the criteria specified therein include break location and size only. Furthermore, Section 5.2.1.1 of the topical report describes the spectrum of cases evaluated as being [ ]^{TS}. A reference to a [ ]^{TS} is also provided without further discussion. The Applicant needs to:

b. Describe the peaking factors and fuel conditions used in such determinations.

Response

Break sensitivity study and plant calculations in the Topical Report (TR) used actual peaking factors and fuel conditions.

For the sensitivity study, the limiting burnup at which fuel stored energy was maximum was determined first. Then actual fuel conditions at the limiting burnup were used in the calculations, except power peaking factors. Linear heat generation rate (LHGR) limit and a conservative radial peaking factor (Fr) which covers cycle-wise variation were used (see response to issue number 53a). The use of LHGR limit and conservative Fr will not change the sensitivity results.

[

]TS

Impact on DCD

There is no impact on the DCD.

Impact on PRA

There is no impact on the PRA.

Impact on Technical Specifications

There is no impact on the Technical Specifications.

Impact on Technical/Topical/Environmental Report

There is no impact on any Technical, Topical, or Environmental Report.

RESPONSE TO AUDIT ISSUES

APR1400 Topical Reports

Korea Electric Power Corporation / Korea Hydro & Nuclear Power Co., LTD

Docket No. PROJ0782

Review Section	**TR Realistic Evaluation Methodology for LBLOCA of the APR1400**
Application Section	**Topical Report: APR1400-F-A-TR-12004 Realistic Evaluation Methodology for Large-Break LOCA of the APR1400**
Issue Date	**08/13/2015**

Audit Issues No. 6-f

RG 1.157 specifies that breaks should be evaluated to include the range from “full double-ended” to small breaks. This range would include single and double-ended breaks. Furthermore, the guidance specifies that longitudinal split breaks should be considered as well. RG 1.157 also states that actual peaking factors and fuel conditions should be used. Section 3.1 (and its subsections) of the topical report discuss the limiting scenario that is used to determine the processes that must be addressed in the evaluation model. However, the criteria specified therein include break location and size only. Furthermore, Section 5.2.1.1 of the topical report describes the spectrum of cases evaluated as being [ ]^{TS}. A reference to a [ ]^{TS} is also provided without further discussion. The Applicant needs to:

f. Describe whether the limiting break analysis included consideration of the location of the available safety injection pump (SIP) trains with respect to the broken cold leg. (Previous tests (e.g., UPTF) with downcomer injection have shown that nearly all water injected through the nozzle located near the broken leg is lost through bypass.)

Response

Figure 1 shows RELAP5/MOD3.3/K code noding of DVI and downcomer. As discussed in Chapter 1 of topical report, two SIPs are assumed to be operable in the LBLOCA analysis. [

]TS

TS

Figure 1. Noding of DVI and Downcomer for APR1400

Impact on DCD

There is no impact on the DCD.

Impact on PRA

There is no impact on the PRA.

Impact on Technical Specifications

There is no impact on the Technical Specifications.

Impact on Technical/Topical/Environmental Report

There is no impact on any Technical, Topical, or Environmental Report.

RESPONSE TO AUDIT ISSUES

APR1400 Topical Reports

Korea Electric Power Corporation / Korea Hydro & Nuclear Power Co., LTD

Docket No. PROJ0782

Review Section	**TR Realistic Evaluation Methodology for LBLOCA of the APR1400**
Application Section	**Topical Report: APR1400-F-A-TR-12004 Realistic Evaluation Methodology for Large-Break LOCA of the APR1400**
Issue Date	**08/13/2015**

Audit Issues No. 6-g

RG 1.157 specifies that breaks should be evaluated to include the range from “full double-ended” to small breaks. This range would include single and double-ended breaks. Furthermore, the guidance specifies that longitudinal split breaks should be considered as well. RG 1.157 also states that actual peaking factors and fuel conditions should be used. Section 3.1 (and its subsections) of the topical report discuss the limiting scenario that is used to determine the processes that must be addressed in the evaluation model. However, the criteria specified therein include break location and size only. Furthermore, Section 5.2.1.1 of the topical report describes the spectrum of cases evaluated as being [ ]^{TS}. A reference to a [ ]^{TS} is also provided without further discussion. The Applicant needs to:

g. The topical report Section 3.1.2.1 states that the reactor coolant pumps (RCPs) are assumed to be tripped upon loss of offsite power (LOOP). Operational RCPs may impact the peak cladding temperature as well as the coolant inventory, because the flow from the intact loops can bypass the downcomer and eject coolant out of the break. Provide justification, using results of sensitivity calculations, for the assumption that the LOOP coincident with the break is limiting.

Response

When the loss of offsite power (LOOP) is not assumed, [

]TS

[

]TS

The uncertainty ranges of [

]TS

Figure 1 shows calculated cladding temperatures for with and without RCPs. The peak cladding temperatures (PCTs) with and without LOOP assumption are [ ]TS respectively, and PCTs for both cases [ ]TS And reflood PCTs for both cases with and without LOOP assumption are [ ]TS respectively.

The PCT with LOOP assumption occurred at heat structure node [ ]TS, whereas PCT without LOOP assumption occurred at heat structure node [ ]TS, which means the quenching time difference is caused by the PCT elevation.

Consequently, the LOOP assumption is more conservative than non-LOOP assumption based on the PCT results.

TS

Figure 1. Comparison of Cladding Temperatures for With and Without LOOP Assumption Cases

Impact on DCD

There is no impact on the DCD.

Impact on PRA

There is no impact on the PRA.

Impact on Technical Specifications

There is no impact on the Technical Specifications.

Impact on Technical/Topical/Environmental Report

There is no impact on any Technical, Topical, or Environmental Report.

RESPONSE TO AUDIT ISSUES

APR1400 Topical Reports

Korea Electric Power Corporation / Korea Hydro & Nuclear Power Co., LTD

Docket No. PROJ0782

Review Section	**TR Realistic Evaluation Methodology for LBLOCA of the APR1400**
Application Section	**Topical Report: APR1400-F-A-TR-12004 Realistic Evaluation Methodology for Large-Break LOCA of the APR1400**
Issue Date	**08/13/2015**

Audit Issues No. 6-h

RG 1.157 specifies that breaks should be evaluated to include the range from “full double-ended” to small breaks. This range would include single and double-ended breaks. Furthermore, the guidance specifies that longitudinal split breaks should be considered as well. RG 1.157 also states that actual peaking factors and fuel conditions should be used. Section 3.1 (and its subsections) of the topical report discuss the limiting scenario that is used to determine the processes that must be addressed in the evaluation model. However, the criteria specified therein include break location and size only. Furthermore, Section 5.2.1.1 of the topical report describes the spectrum of cases evaluated as being [ ]^{TS}. A reference to a [ ]^{TS} is also provided without further discussion. The Applicant needs to:

h. Provide information for all the activation signals used in the representative LBLOCA simulation and corresponding delay times. Justify the delay times used and provide results from sensitivity studies that consider the uncertainty in the delay times for reactor trip, RCP trip, SIP activation, etc.

Response

Basically, trip delay time is conservatively determined based on the design data as shown in Table 1.

[

]TS

Table 1. Delay Time in Design Data

TS

Table 2. Sequence of Trip Description for LBLOCA Analysis

TS

Impact on DCD

There is no impact to the DCD.

Impact on PRA

There is no impact on the PRA.

Impact on Technical Specifications

There is no impact on the Technical Specifications.

Impact on Technical/Topical/Environmental Report

There is no impact on any Technical, Topical, or Environmental Report.

RESPONSE TO AUDIT ISSUES

APR1400 Topical Reports

Korea Electric Power Corporation / Korea Hydro & Nuclear Power Co., LTD

Docket No. PROJ0782

Review Section	**TR Realistic Evaluation Methodology for LBLOCA of the APR1400**
Application Section	**Topical Report: APR1400-F-A-TR-12004 Realistic Evaluation Methodology for Large-Break LOCA of the APR1400**
Issue Date	**08/13/2015**

Audit Issues No. 07

NUREG/CR-5429, Section 2.1 establishes an acceptable approach for the documentation of the event sequence. Provide a table with the sequence of events and their timing for the limiting LBLOCA scenario described in Section 3.1.2 of the topical report.

Response

Sequence of events and their timing for the limiting LBLOCA scenario [ ]^{TS} are described in Table 1.

Table 1 Major Sequence of Events for the Limiting LBLOCA Scenario TS

Impact on DCD

There is no impact on the DCD.

Impact on PRA

There is no impact on the PRA.

Impact on Technical Specifications

There is no impact on the Technical Specifications.

Impact on Technical/Topical/Environmental Report

There is no impact on any Technical, Topical, or Environmental Report.

RESPONSE TO AUDIT ISSUES

APR1400 Topical Reports

Korea Electric Power Corporation / Korea Hydro & Nuclear Power Co., LTD

Docket No. PROJ0782

Review Section	**TR Realistic Evaluation Methodology for LBLOCA of the APR1400**
Application Section	**Topical Report: APR1400-F-A-TR-12004 Realistic Evaluation Methodology for Large-Break LOCA of the APR1400**
Issue Date	**08/13/2015**

Audit Issues No. 8

NUREG/CR-5429, Appendix B establishes an acceptable approach for the documentation of the timing of events. Section 3.1.2.1 of the topical report states that the blowdown period ends when a safety injection tank fluidic device (SIT-FD) injection is initiated at approximately 15 seconds after the break. Figure 5-12 of the topical report appears to illustrate this behavior. However, the SIT-FDs are connected via check valves to the downcomer. Due to the nature of a double-ended guillotine break, it is likely that the downcomer pressure decreases faster than the pressurizer pressure causing earlier initiation of SIT-FD injection. Such a sequence may affect the calculated peak cladding temperature (PCT). Demonstrate that such a situation does not exist, or if it does, characterize the impact on the behavior of the blowdown, reflood, and the resulting PCT.

Response

In the APR1400, SIT-FD is directly connected to the downcomer using check valves in order to operate passively when the downcomer pressure is decreased below the pressure of SIT-FD. In the code input, SIT-FDs are described to be connected to the downcomer using VALVE components which is the same in plant operation.

Impact on DCD

There is no impact on the DCD.

Impact on PRA

There is no impact on the PRA.

Impact on Technical Specifications

There is no impact on the Technical Specifications.

Impact on Technical/Topical/Environmental Report

There is no impact on any Technical, Topical, or Environmental Report.

RESPONSE TO AUDIT ISSUES

APR1400 Topical Reports

Korea Electric Power Corporation / Korea Hydro & Nuclear Power Co., LTD

Docket No. PROJ0782

Review Section	**TR Realistic Evaluation Methodology for LBLOCA of the APR1400**
Application Section	**Topical Report: APR1400-F-A-TR-12004 Realistic Evaluation Methodology for Large-Break LOCA of the APR1400**
Issue Date	**08/13/2015**

Audit Issues No. 09

NUREG/CR-5429, Appendix B establishes an acceptable approach for the documentation of the timing of events. Section 3.1.2 of the topical report states that the refill period ends when the mixture level reaches the bottom of active core. However, Section 3.1.2.2 of the topical report uses the terminology “water level” and “liquid level” to describe the end of the refill period. In addition, topical report Section 3.1.2.3 states that the early reflood period begins when the lower plenum is “completely filled with water.” Clarify the definition of the end of refill period, and plans to revise of the topical report to use consistent terminology throughout.

Response

The sentences (or phrases) of the topical report are corrected as follows.

Section No.	Before	After
3.1.2.2	The refill period begins when SIT-FD injection flow is initiated and ends when the water level in the lower plenum reaches the core inlet.	The refill period begins when SIT-FD injection flow is initiated and ends when ***the mixture level*** in the lower plenum reaches ***the bottom of the active core***.
3.1.2.2	At this stage, water levels in the downcomer and the lower plenum increase rapidly.	At this stage, ***mixture*** levels in the downcomer and the lower plenum increase rapidly.
3.1.2.2	The refill period ends when the liquid level in the lower plenum reaches the bottom of the active core.	The refill period ends when ***the mixture level in the vessel lower plenum reaches the bottom of the active core and remains full thereafter and conditions are established for continuously reflooding the core with coolant.***
3.1.2.3	The early reflood period begins when the lower plenum is completely filled with water and ends when the SIT-FD water is depleted.	The early reflood period begins ***when the mixture level in the lower plenum reaches the bottom of the active core*** and ends when the SIT-FD water is depleted.

The revised topical report will be submitted later.

Impact on DCD

There is no impact on the DCD.

Impact on PRA

There is no impact on the PRA.

Impact on Technical Specifications

There is no impact on the Technical Specifications.

Impact on Technical/Topical/Environmental Report

The revised topical report will be submitted later.

RESPONSE TO AUDIT ISSUES

APR1400 Topical Reports

Korea Electric Power Corporation / Korea Hydro & Nuclear Power Co., LTD

Docket No. PROJ0782

Review Section	**TR Realistic Evaluation Methodology for LBLOCA of the APR1400**
Application Section	**Topical Report: APR1400-F-A-TR-12004 Realistic Evaluation Methodology for Large-Break LOCA of the APR1400**
Issue Date	**08/13/2015**

Audit Issues No. 10

NUREG/CR-5429, Section 2.1 establishes an acceptable approach for the documentation of the event sequence. The Section 3.1.2.1 of the topical report describes the major phenomena occurring during the blowdown period. The end of the blowdown period is defined as the initiation of SIT-FD injection. However, the last paragraph of Section 3.1.2.1 of the topical report describes the phenomena that occurs when the four SIT-FD begin to inject water. If this is part of the refill period then the discussion is incorrectly located. Discuss plans to make appropriate changes to the description in Section 3.1.2.1 to ensure consistency with the definition of the accident period.

Response

The sentences in Section 3.1.2.1 and Section 3.1.2.2 of the topical report are corrected as follows.

Section No.	Before	After
3.1.2.1	Four SIT-FDs begin to deliver flow into the four DVI lines when the primary system pressure falls below their actuation set-point. The coolant flows through the DVI nozzles into the upper annulus and then begins to refill the reactor pressure vessel. Because the reactor coolant system is still depressurizing, some of the coolant entering the upper annulus is swept out to the break along with entrained liquid from the lower plenum and the downcomer. Although the break flow remains high, sufficient flow in the excess of the bypass is delivered downward into the downcomer and increases the downcomer water level. Then the coolant injected by the SIT-FDs eventually reaches the lower plenum.	Deleted
3.1.2.2	ECC water in the reactor vessel downcomer can flow down by gravity or be swept out to the break by the pressure differential and the upward-escaping steam flow that levitates the liquid. Reactor vessel walls and internals are large metal structures at temperatures above saturation. When subcooled ECC water comes into contact with the metal structures in the downcomer, steam is generated by nucleate boiling. This reduces the gravitational head of the fluid in the downcomer. The process of liquid penetration and sweep-out repeats in the downcomer and direct-contact condensation of steam on the subcooled ECC water continues in the upper annulus. Figure 3-5 gives a schematic of the two-phase primary coolant system 25 s after the break opens.	Four SIT-FDs begin to deliver flow into the four DVI lines when the primary system pressure falls below their actuation set-point. The coolant flows through the DVI nozzles into the upper annulus and then begins to refill the reactor pressure vessel. The reactor coolant system keeps depressurizing because some of the coolant entering the upper annulus is swept out to the break along with entrained liquid from the lower plenum and the downcomer. Although the break flow remains high, sufficient flow in the excess of the bypass is delivered downward into the downcomer and increases the downcomer water level. Eventually the coolant injected by the SIT-FDs reaches the lower plenum. Reactor vessel walls and internals are large metal structures at temperatures above saturation. When subcooled ECC

		water comes into contact with the metal structures in the downcomer, steam is generated by nucleate boiling. This reduces the gravitational head of the fluid in the downcomer. The process of liquid penetration and sweep-out repeats in the downcomer and direct-contact condensation of steam on the subcooled ECC water continues in the upper annulus. Figure 3-5 gives a schematic of the two-phase primary coolant system 25 s after the break opens.

In addition to this, we found the translation mistakes and then corrected it as follows (bold & italic).

Before	After
Four SIT-FDs begin to deliver flow into the four DVI lines when the primary system pressure falls below their actuation set-point. The coolant flows through the DVI nozzles into the upper annulus and then begins to refill the reactor pressure vessel***. Because the reactor coolant system is still depressurizing,*** some of the coolant entering the upper annulus is swept out to the break along with entrained liquid from the lower plenum and the downcomer. Although the break flow remains high, sufficient flow in the excess of the bypass is delivered downward into the downcomer and increases the downcomer water level. Then the coolant injected by the SIT-FDs eventually reaches the lower plenum.	Four SIT-FDs begin to deliver flow into the four DVI lines when the primary system pressure falls below their actuation set-point. The coolant flows through the DVI nozzles into the upper annulus and then begins to refill the reactor pressure vessel. ***The reactor coolant system keeps depressurizing because*** some of the coolant entering the upper annulus is swept out to the break along with entrained liquid from the lower plenum and the downcomer. Although the break flow remains high, sufficient flow in the excess of the bypass is delivered downward into the downcomer and increases the downcomer water level. Then the coolant injected by the SIT-FDs eventually reaches the lower plenum.

The revised topical report will be submitted later.

Impact on DCD

There is no impact on the DCD.

Impact on PRA

There is no impact on the PRA.

Impact on Technical Specifications

There is no impact on the Technical Specifications.

Impact on Technical/Topical/Environmental Report

The revised topical report will be submitted later.

RESPONSE TO AUDIT ISSUES

APR1400 Topical Reports

Korea Electric Power Corporation / Korea Hydro & Nuclear Power Co., LTD

Docket No. PROJ0782

Review Section	**TR Realistic Evaluation Methodology for LBLOCA of the APR1400**
Application Section	**Topical Report: APR1400-F-A-TR-12004 Realistic Evaluation Methodology for Large-Break LOCA of the APR1400**
Issue Date	**08/13/2015**

Audit Issues No. 11

NUREG/CR-5429, Appendix B establishes an acceptable approach for the documentation of the timing of events. Section 3.1.2.3 of the topical report describes the early reflood period as starting from ~38 s and ending at ~192 s. However, the text in the third paragraph of Section 3.1.2.3 states that “the maximum SIT-FD injection is reached during this period at around 30 s” which is inconsistent. Clarifications are needed.

Response

The sentence in Section 3.1.2.3 of the topical report is corrected as follows.

Before	After
Maximum SIT-FD injection flow is reached during this period at around 30 s.	Maximum SIT-FD injection flow is reached at around 30 s after the break.

The revised topical report will be submitted later.

Impact on DCD

There is no impact on the DCD.

Impact on PRA

There is no impact on the PRA.

Impact on Technical Specifications

There is no impact on the Technical Specifications.

Impact on Technical/Topical/Environmental Report

The revised topical report will be submitted later.

RESPONSE TO AUDIT ISSUES

APR1400 Topical Reports

Korea Electric Power Corporation / Korea Hydro & Nuclear Power Co., LTD

Docket No. PROJ0782

Review Section	**TR Realistic Evaluation Methodology for LBLOCA of the APR1400**
Application Section	**Topical Report: APR1400-F-A-TR-12004 Realistic Evaluation Methodology for Large-Break LOCA of the APR1400**
Issue Date	**08/13/2015**

Audit Issues No. 12

NUREG/CR-5429, Appendix B establishes an acceptable approach for the documentation of the timing of events. The liquid and void fractions in various RCS components at key times in the accident progression are depicted in Figures 3-3 through 3-8 of the topical report. According to the phenomena description in Sections 3.1.2.1 through 3.1.2.3 of the topical report, the SIT-FD water injection begins from ~15 seconds and ends at ~192seconds. However, Figures 3-5 through 3-8 of the topical report indicate that the SIT-FD is fully filled with water during this period. This is an inconsistency that needs to be addressed by making appropriate changes to Figures 3-5 to 3-8 to be consistent with the scenario description.

Response

Figure 3-5 through 3-8 of topical report will be modified to have consistency with the phenomena description as follows.

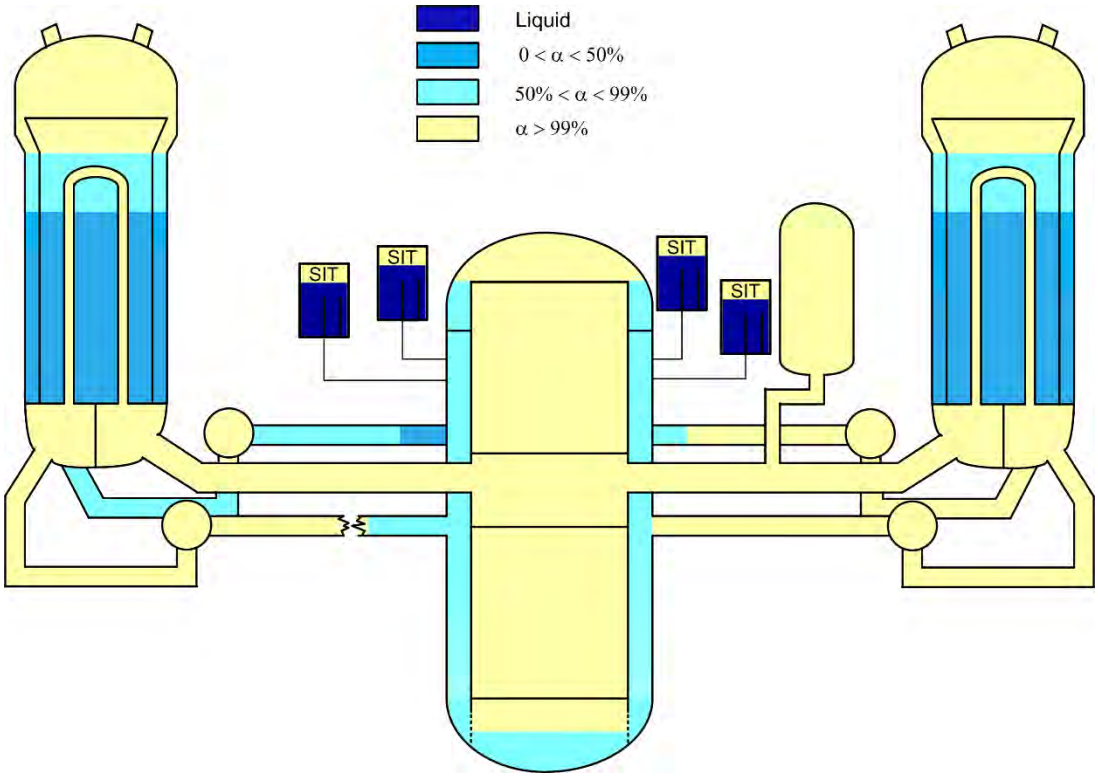

Figure 3-5. Calculated RCS Conditions, 25 s after the Break

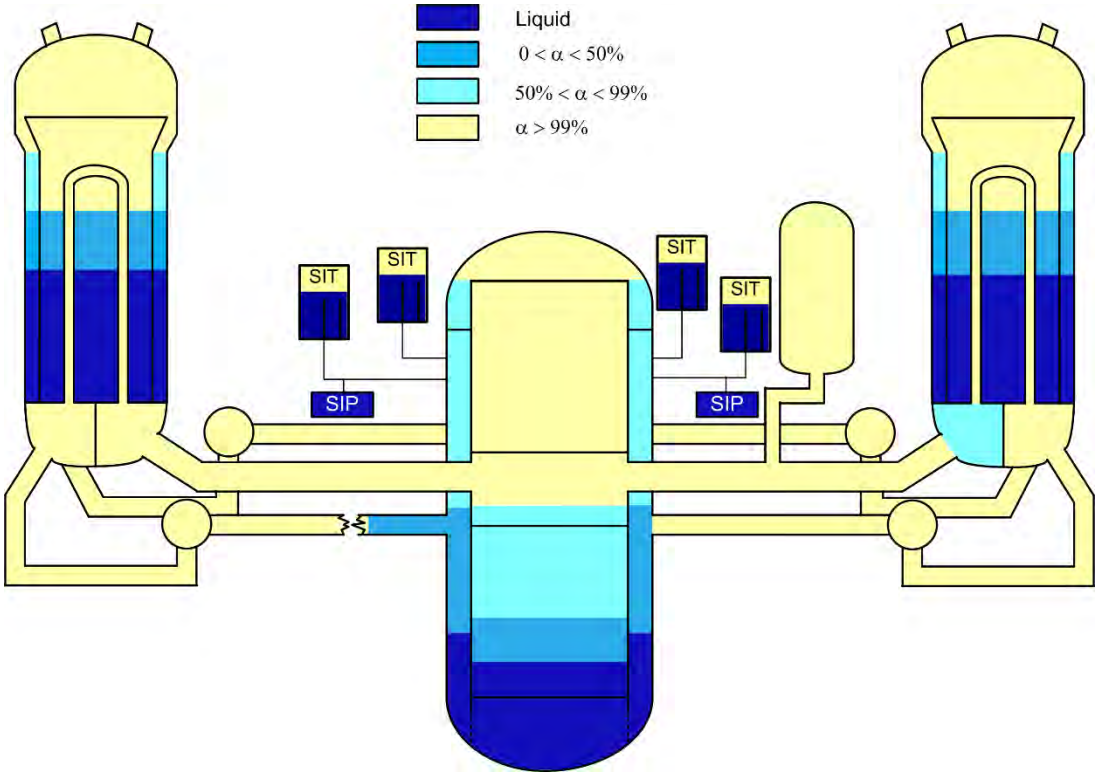

Figure 3-6. Calculated RCS Conditions, 62 s after the Break

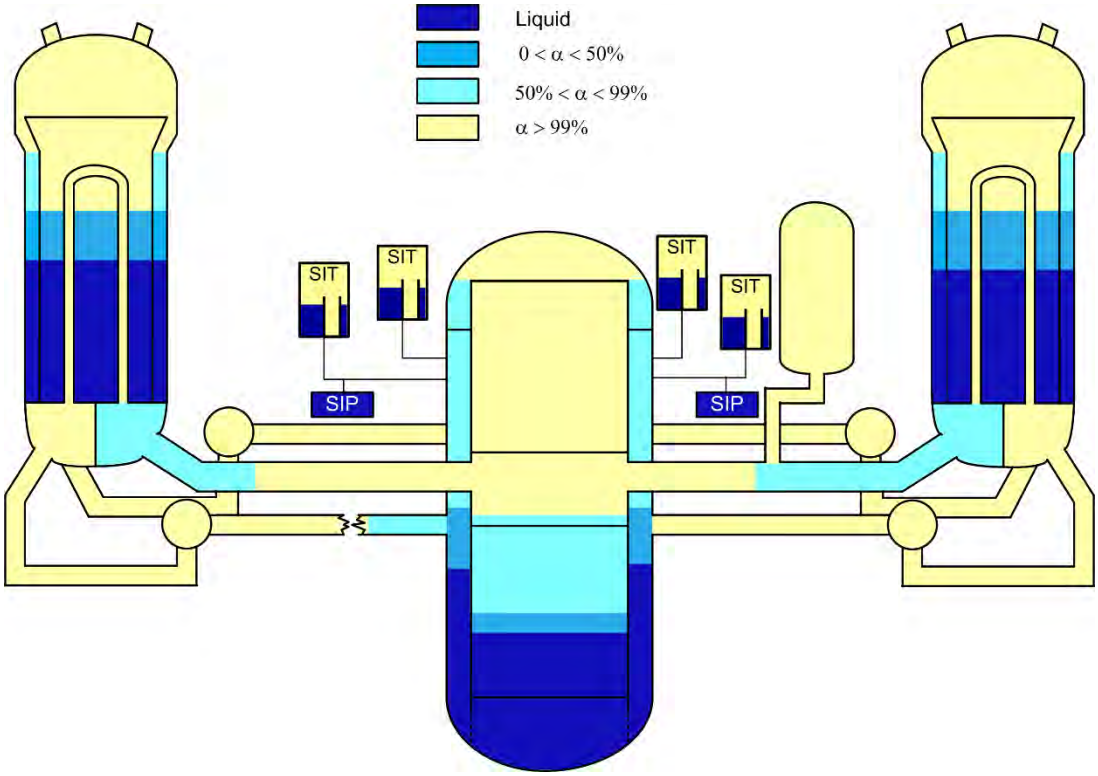

Figure 3-7. Calculated RCS Conditions, 92 s after the Break

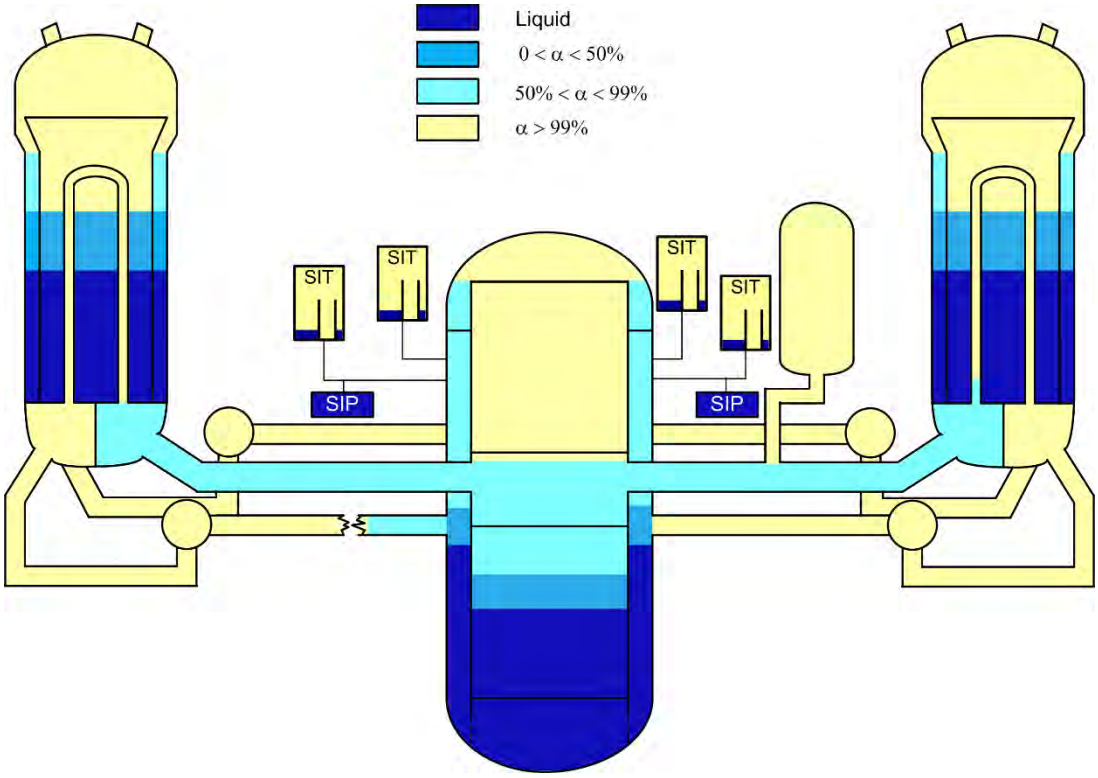

Figure 3-8. Calculated RCS Conditions, 150 s after the Break

Impact on DCD

There is no impact on the DCD.

Impact on PRA

There is no impact on the PRA.

Impact on Technical Specifications

There is no impact on the Technical Specifications.

Impact on Technical/Topical/Environmental Report

Topical report will be revised as discussed in this response.

There is no impact on Technical or Environmental Report.

RESPONSE TO AUDIT ISSUES

APR1400 Topical Reports

Korea Electric Power Corporation / Korea Hydro & Nuclear Power Co., LTD

Docket No. PROJ0782

Review Section	**TR Realistic Evaluation Methodology for LBLOCA of the APR1400**
Application Section	**Topical Report: APR1400-F-A-TR-12004 Realistic Evaluation Methodology for Large-Break LOCA of the APR1400**
Issue Date	**08/13/2015**

Audit Issues No. 13

RG 1.157 outlines guidance in many places that the results for best estimate calculations are to be considered acceptable provided their technical bases are demonstrated with appropriate data and analyses. However, some of the results provided in the topical report are unclear. Figure 3-2 of the topical report shows the normalized collapsed water level in the downcomer and the reactor core. It is essential to confirm that the following interpretations of Figure 3-2 are correct:

a. At the end of blowdown, approximately 25 percent of the initial core liquid volume remains in the core.

b. At the end of refill, approximately 5 percent of the initial core liquid volume remains in the core.

c. At the end of blowdown, approximately 30 percent of the initial lower plenum liquid volume remains in the lower plenum.

d. At the end of refill, approximately 20 percent of the initial lower plenum liquid volume is in the lower plenum.

e. In the late reflood period, approximately 35 percent of the initial core liquid volume is maintained in the core. Also, define what constitutes the lower downcomer relative to Figure 3-2 of the topical report.

Response

Figure 3-2 of the topical report shows the representative LBLOCA scenario which was calculated during the methodology development stage. In this figure, the active core level means the normalized water level from bottom of reactor vessel to the top upper guide structure (UGS). Because this may cause reader's confusion, Figure 3-2 of the topical report will be revised to the results of the nominal calculation as shown in Figure 1 of this response. The active core level in Figure 1 is the collapsed water level in the active fuel region.

The following responses are based on Figure 1.

Figure number of Figure 3-2 of topical report (Rev.0) is changed to Figure 3-3 in topical report (Rev.1) due to the editorial necessity.

a)

At the end of blowdown, the core water level decreases to approximately 3 % of the initial water level. This is because the primary coolant is rapidly expelled into the containment through the break due to the depressurization.

b)

The refill period ends when the mixture level in the lower plenum reaches the bottom of the active core. Therefore, there is no liquid in the active core region at the end of refill.

c)

The blowdown period ends when the SITs begin to inject ECC water. At the end of blowdown, approximately 24 % of the initial lower plenum water level remains in the lower plenum.

d)

At the end of refill, the collapsed water level in the lower plenum reaches approximately 95 % of the initial value. This means that the lower plenum fills up with two phase mixture.

e)

- In the late reflood period, the collapsed water level in the active core maintains at around 50 % of the initial value.

- Lower downcomer means the downcomer from the bottom of flow skirt to the bottom of loop pipe.

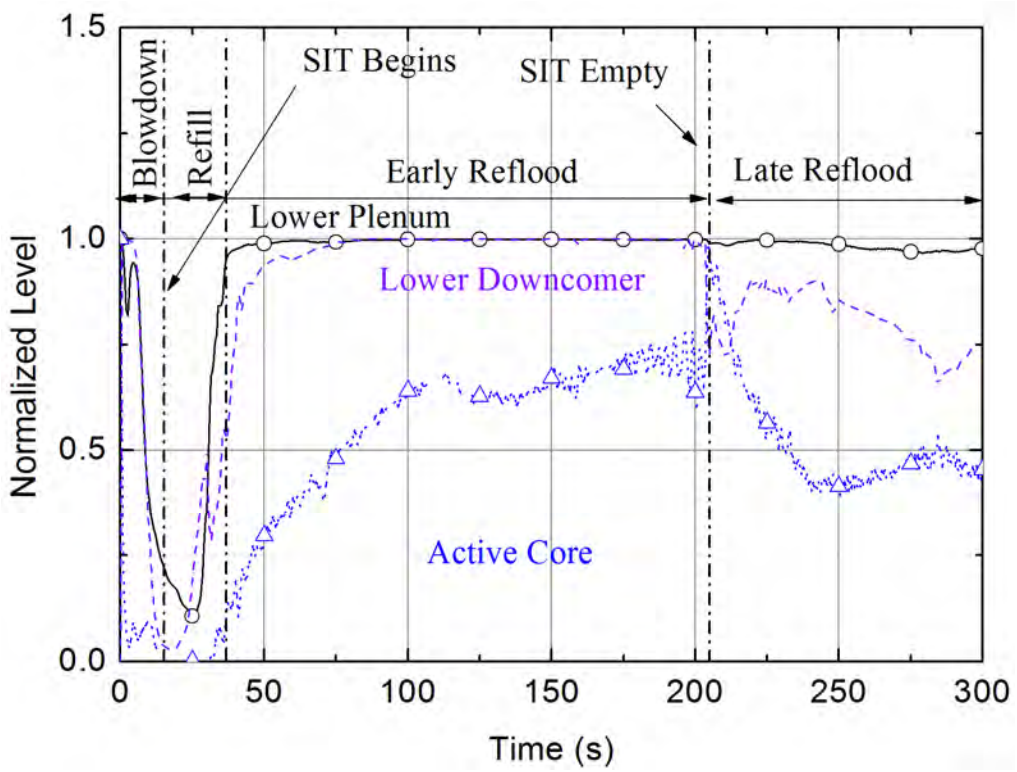

Figure 1. Normalized Collapsed Water Level in Downcomer and Core

Impact on DCD

There is no impact on the DCD.

Impact on PRA

There is no impact on the PRA.

Impact on Technical Specifications

There is no impact on the Technical Specifications.

Impact on Technical/Topical/Environmental Report

The revised topical report will be submitted later.

RESPONSE TO AUDIT ISSUES

APR1400 Topical Reports

Korea Electric Power Corporation / Korea Hydro & Nuclear Power Co., LTD

Docket No. PROJ0782

Review Section	**TR Realistic Evaluation Methodology for LBLOCA of the APR1400**
Application Section	**Topical Report: APR1400-F-A-TR-12004 Realistic Evaluation Methodology for Large-Break LOCA of the APR1400**
Issue Date	**08/13/2015**

Audit Issues No. 14

NUREG/CR-5429, Section 2.1 establishes an acceptable approach for the documentation of the phenomena identification and ranking table (PIRT). A large number (i.e., 83 parameters) of phenomena or processes are ranked 4 or higher in the APR1400 PIRT. However, the application of CAREM actually uses only 30 uncertainty parameters as shown in topical report Table 5-1.

a. A description of the process followed to determine the 30 uncertainty parameters that are actually ranged for the simple random sampling (SRS) calculations from the entire possible set (i.e., 83 parameters) based on the PIRT is needed.

b. An explanation and justification of the approach used (i.e., conservative or best estimate values) for the remaining parameters not included in the uncertainty analysis is needed.

Response (Rev.1)

a)

The presentation material attached [1] describes the entire process to determine the 30 uncertainty parameters out of the 82 phenomena/processes determined from the APR1400 PIRT. As described in the material, the phenomena already considered by other uncertainty parameters, phenomena treated conservatively and phenomena treated as biases are not considered as uncertainty parameters. The phenomena are considered to be treated conservatively when it is not easy to be included. Sensitivity calculations can be performed to determine the conservative case. When the sensitivity calculations are not possible, a parameter generally believed to reduce PCT when it is included in the calculation is not considered for conservatism. The APR1400 PIRT contains some errors mostly related to the definition of time periods and is revised in association with audit issue no. 15.

b)

The explanation and justification of the parameters are described in the topical report and these are summarized in Table 1 as follows. Among the 82 phenomena/processes in the APR1400 PIRT, two phenomena are not mentioned in the topical report. [

]^{TS} The SIT line and SI pump line merges at an expanded cross-sectional area pipe, thus the SIT injection cannot be interrupted by SI pump inherently. It has been found that the APR1400 PIRT contains errors as to the time period definitions, and the revised to the APR1400 PIRT is shown in the attached document [2]. The missing or insufficient rationale of the PIRT is reinforced in accordance with the revised PIRT.

Table 1. Description of each process/phenomena in the topical report (1/3)

TS

Table 2. Description of each process/phenomena in the topical report (2/3)

TS

Table 3. Description of each process/phenomena in the topical report (3/3)

TS

Reference

[1] Presentation Material, “PIRT to Uncertainty Parameter,” presented at the face to face meeting with NRC, 2016. 1. 12 ~ 2016. 1. 15. (Modifications are made in accordance to the reference [2]), Revision 1.

[2] Presentation Material, “APR1400 PIRT revision,” attached document of the response to the audit issue no. 15, July, 2016.

Impact on DCD

There is no impact to the DCD.

Impact on PRA

There is no impact on the PRA.

Impact on Technical Specifications

There is no impact on the Technical Specifications.

Impact on Technical/Topical/Environmental Report

Topical report is revised as discussed in this response.

There is no impact on Technical or Environmental Report.

Audit Issue No.14_Rev.1

Replace with next page Ŏ

Table 3-2 Phenomena Identification and Ranking Table (1/3) TS

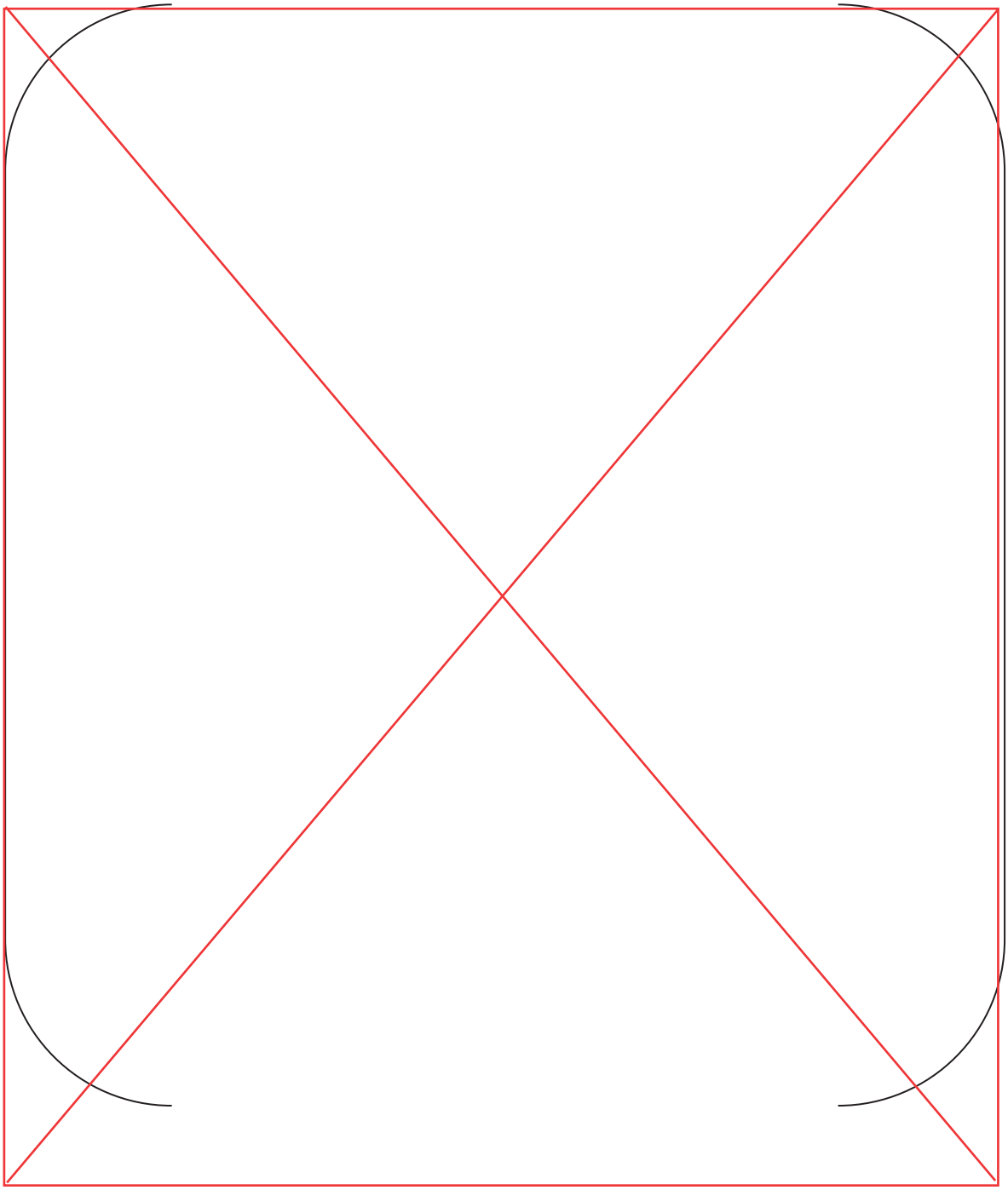

A

Table 3-2 Phenomena Identification and Ranking Table (1/3)

TS

Replace with next page B

Table 3-2 Phenomena Identification and Ranking Table (2/3) **TS**

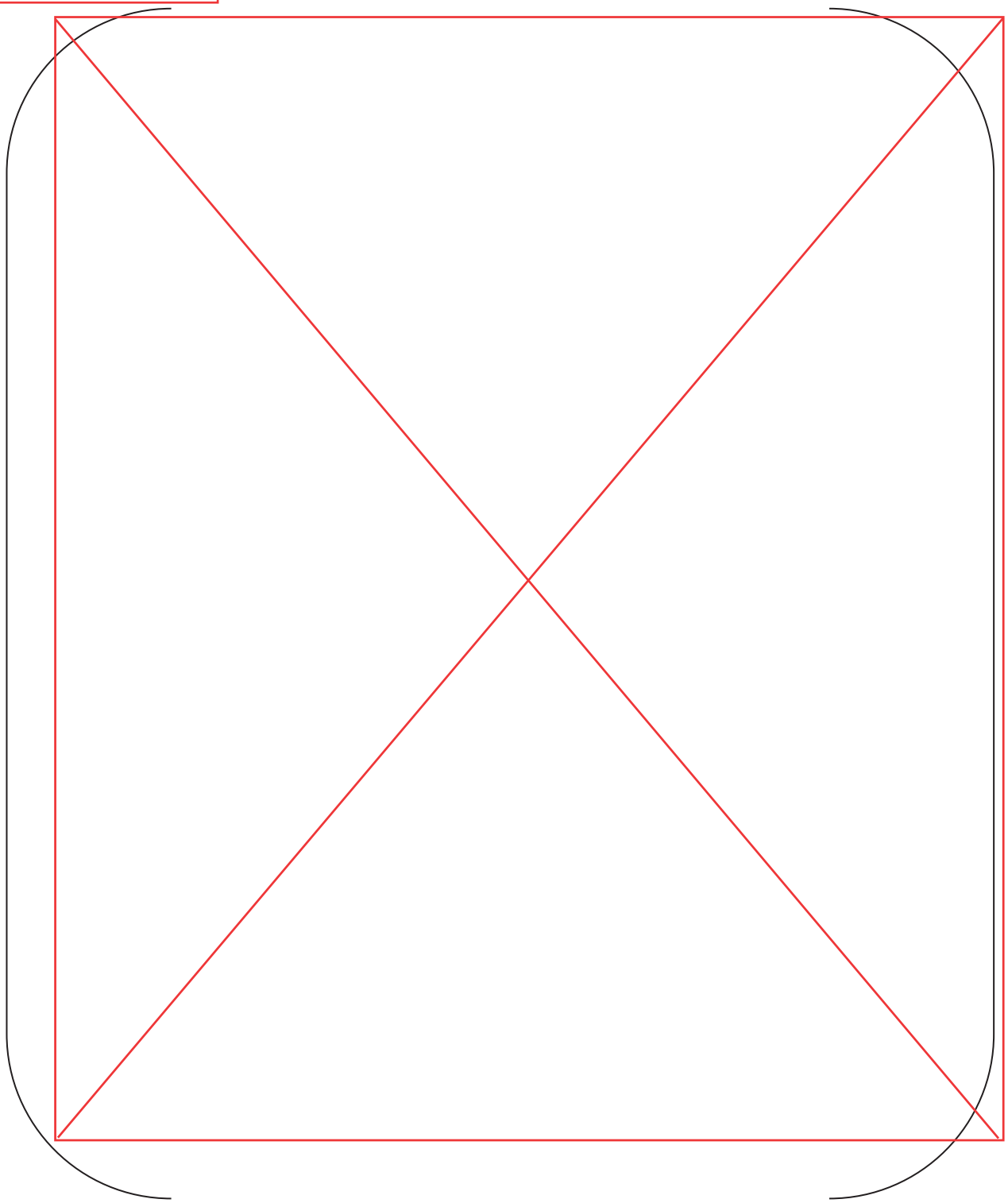

B

Table 3-2 Phenomena Identification and Ranking Table (2/3)

TS

Replace with next page C

Table 3-2 Phenomena Identification and Ranking Table (3/3) **TS**

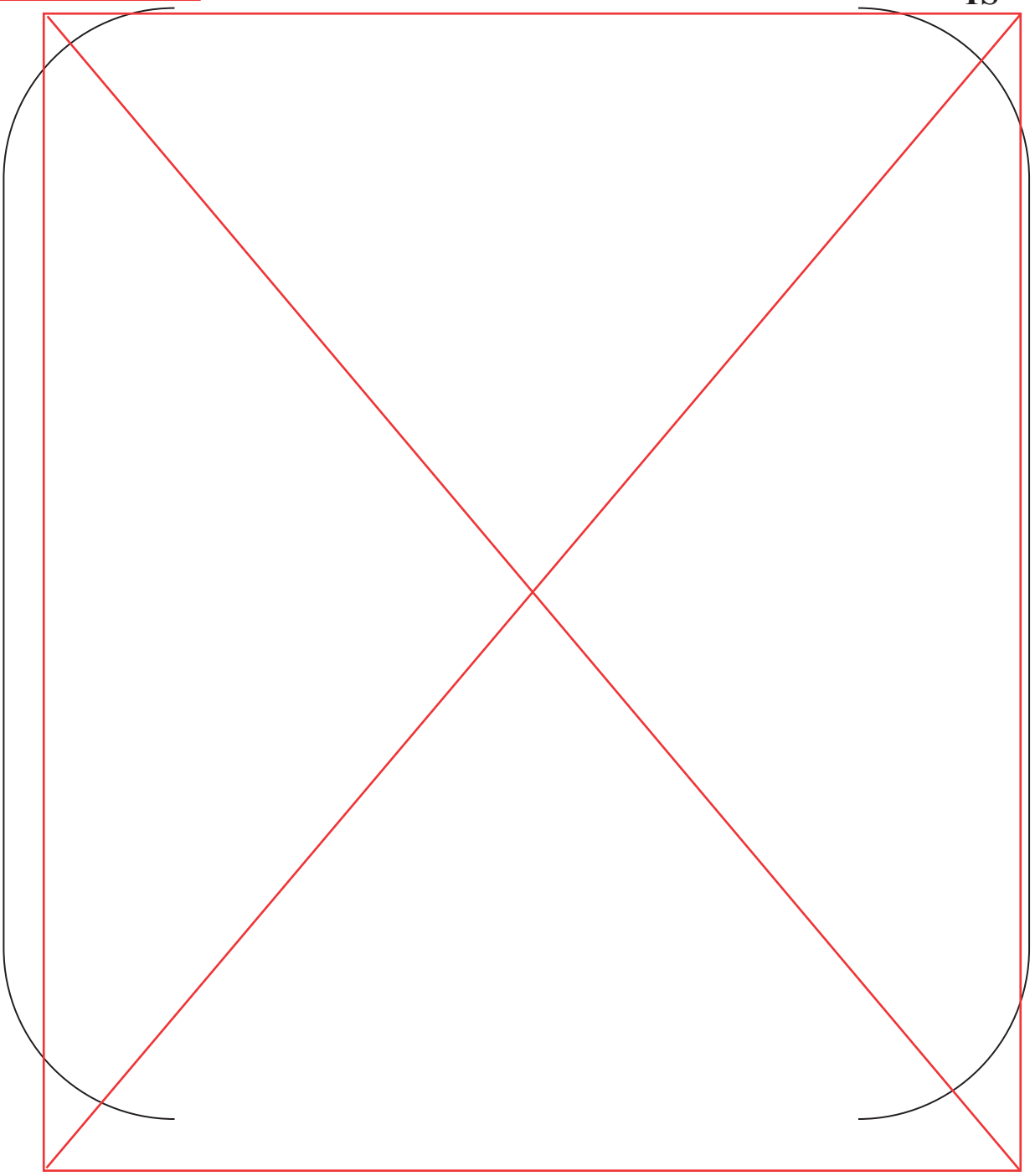

C

Table 3-2 Phenomena Identification and Ranking Table (3/3)

TS

1. Introduction

All the adjustments were reviewed by the peer review group consisting of six experts in nuclear reactor research and operation.

Phenomena identification and ranking table (PIRT) is used to identify major phenomena that occur during relevant accidents of the reference plant, and to prioritize the phenomena according to their effects on major safety parameters. PIRT is essential to understand the phenomena or processes that occur during the accident, and to determine code capability and uncertainty parameters.

APR1400

The PIRT for a large-break loss-of-coolant accident (LBLOCA) of APR1400 was developed based on the LBLOCA PIRT for "Korea Next Generation Reactor (KNGR)" by Wilson et al. 2001 [1]. KNGR was the name for ~~ARP1400~~ at its early developmental stage. KNGR PIRT was prepared by Idaho National Engineering and Environment Laboratory (INEEL) for Korea Institute of Nuclear Safety (KINS), the regulatory body of Korea. APR1400 PIRT has been established by adopting KNGR PIRT and reflecting the final design features of APR1400 and the results of the experiments specific to APR1400.

This appendix explains KNGR PIRT and its modifications. KNGR PIRT is explained in Chapter 2 and the adjustments of the rankings are explained in Chapter 3. The determined APR1400 PIRT is provided in Chapter 4.

~~and all the adjustments made was reviewed by the peer review process.~~

2. PIRT for "Korea Next Generation Reactor"

KNGR PIRT was prepared through 15 processes starting with defining the purpose of the PIRT and finishing with documenting the final PIRT. Figure 1 shows the development process of KNGR PIRT. The PIRT process used for KNGR is similar to those used in other preceding PIRT developments. Examples of prior PIRT efforts can be found in other references [2]-[8]. Applications of the process have repeatedly demonstrated that the collective knowledge of experts group significantly increase the probability of phenomena or processes of importance being identified. The KNGR PIRT panel has about 150 man-years of collective experience in nuclear reactor research and operation. The panel members were:

Dr. Brent E. Boyak (Los Alamos National Laboratory)

Dr. Bub-Dong Chung (Korea Atomic Energy Research Institute – KINS Representative)

Dr. Lawrence E. Hochreiter (Pennsylvania State University)

Dr. Jose N. Reyes (Oregon State University)

Mr. Gary E. Wilson (Idaho National Engineering and Environmental Laboratory – Panel Chairman)

The scenario selected for KNGR PIRT was an LBLOCA of a double-ended guillotine break in a cold leg with the assumptions of loss of off-site power and failure of one diesel generator. The assumptions led to the availability of only one, out of two, hydraulic division of the safety injection system. Each division included two safety injection pumps; and only two, out of four, safety injection pumps were credited in the scenario.

The relative importance of phenomena is time-dependent as an accident progresses. For KNGR PIRT, the panel divided the LBLOCA scenario into four temporal periods. These periods, termed blowdown (1), refill (2), reflood (3), and long-term cooling (4) were defined by the core and lower plenum liquid mass fractions as delineated in Table **1**. The numbers in parentheses were used as indices of the periods in the PIRT. The blowdown period begins when the break occurs and ends when the lower plenum begins to refill. The refill period ends when the liquid level in the vessel lower plenum approaches the core inlet and remains full thereafter. The reflood period ends when the entire core is quenched, that is, all fuel rod cladding temperatures are at or slightly above the

and Uncertainty" by B. Boyack et al. 1989 [3] were referenced. Sections 3.1 and 3.2 explain the modification of the four temporal periods and subsequent adjustment of the ranking, respectively.

3.1 Definition of Time Phases

The LBLOCA scenario of APR1400 is divided into four temporal periods. The definitions of each period are described in Table 4. The periods are termed blowdown (1), refill (2), early reflood (3), and late reflood (4). The numbers indicated in parentheses are used as indices in the PIRT to denote each period.

mixture

(1) The blowdown period starts when the break occurs and ends when SIT injection initiates.

(2) The refill period ends when the ~~liquid~~ level in the vessel lower plenum approaches the core inlet and remains full thereafter.

(3) The early reflood period ends when SITs are emptied.

(4) The late reflood period continues after SITs are emptied.

3.2 Adjustment of the Rankings

It is necessary to adjust the relative importance of phenomena or processes after modifying the definition of temporal periods. In addition, finalization of the APR1400 design and the findings of the experiments and code simulations, which have been performed after the development of KNGR PIRT, need to be reflected.

The same ranking scale used for the relative importance of phenomena or processes of KNGR PIRT, described in Table 2, is used for APR1400 PIRT. It should be ensured that the phenomena or processes of [ ]^{TS} are considered in the calculation. For these phenomena or processes, relevant uncertainty parameters were identified and their uncertainties were reflected in plant calculations in principle. In cases where the identification of uncertainty parameters was not probable, [ ]^{TS} Relevant uncertainty parameters for [ ]^{TS} were not identified. As described in Table 2, [ ]^{TS} allow modeling of the phenomena or processes with inaccuracy or moderate accuracy. As the RELAP5 code has best-estimate features, those phenomena or processes [ ]^{TS} can be modeled with moderate accuracy if the phenomena or processes are not ignored in the calculation. Modeling of these phenomena or processes includes [ ]^{TS}, and so on. Phenomena or processes of ranks lower than [ ]^{TS} are paid no attention.

Among the phenomena or processes of KNGR PIRT, those phenomena or processes, of which the importance ranking is equal to or higher than [ ]^{TS} in any temporal period, are considered when adjusting the rankings. This selection criterion was established in order to prevent omitting significantly important phenomena or processes. Phenomena or processes of [ ]^{TS} can be modeled by applying the models and correlations as they are in the code or by the nodalization capability of the RELAP5 code. The uncertainty of all the other phenomena or processes, or the combined effect of not-considered low ranked phenomena or processes can be accounted for in [ ]^{TS} of this method.

Modifications on KNGR PIRT are described below, item-by-item, along with the rationale. The indices for each time period used in the following tables are "1" for the blowdown, "2" for the refill, "3" for the early reflood, and "4" for the late reflood periods as described earlier.

Replace with next page D

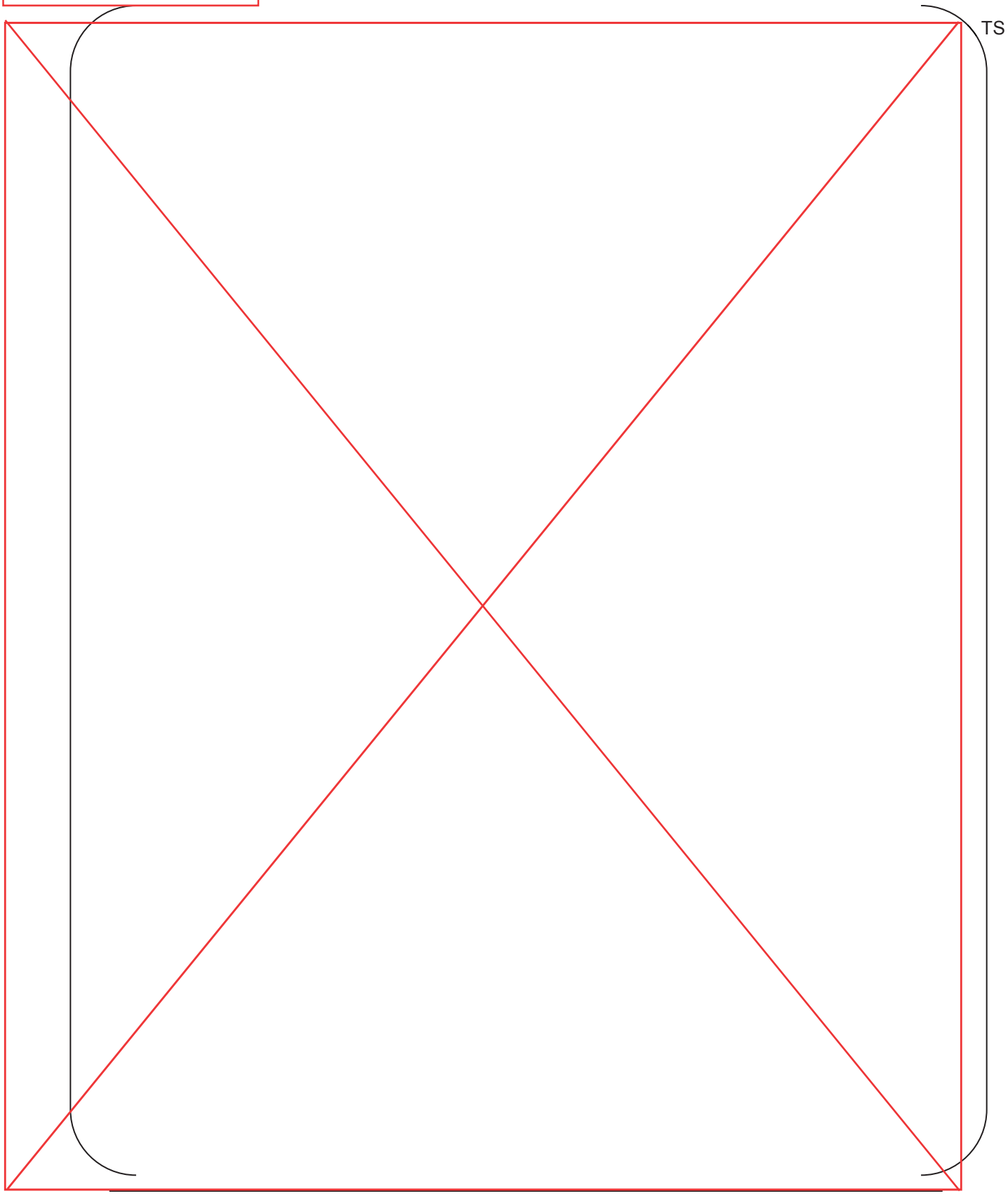

TS

TS

TS

TS

Replace with next page E

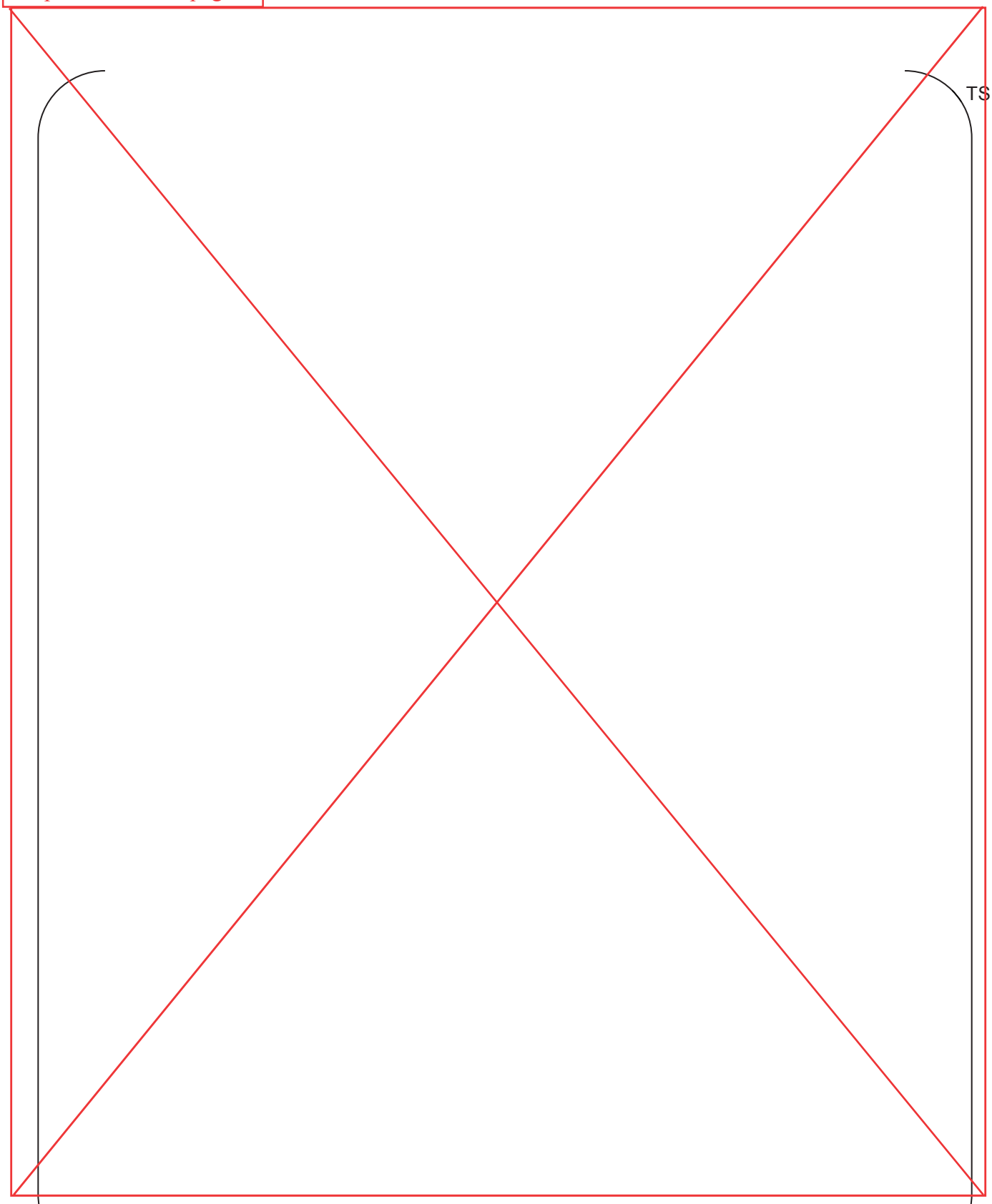

TS

%

TS

%

TS

%

TS

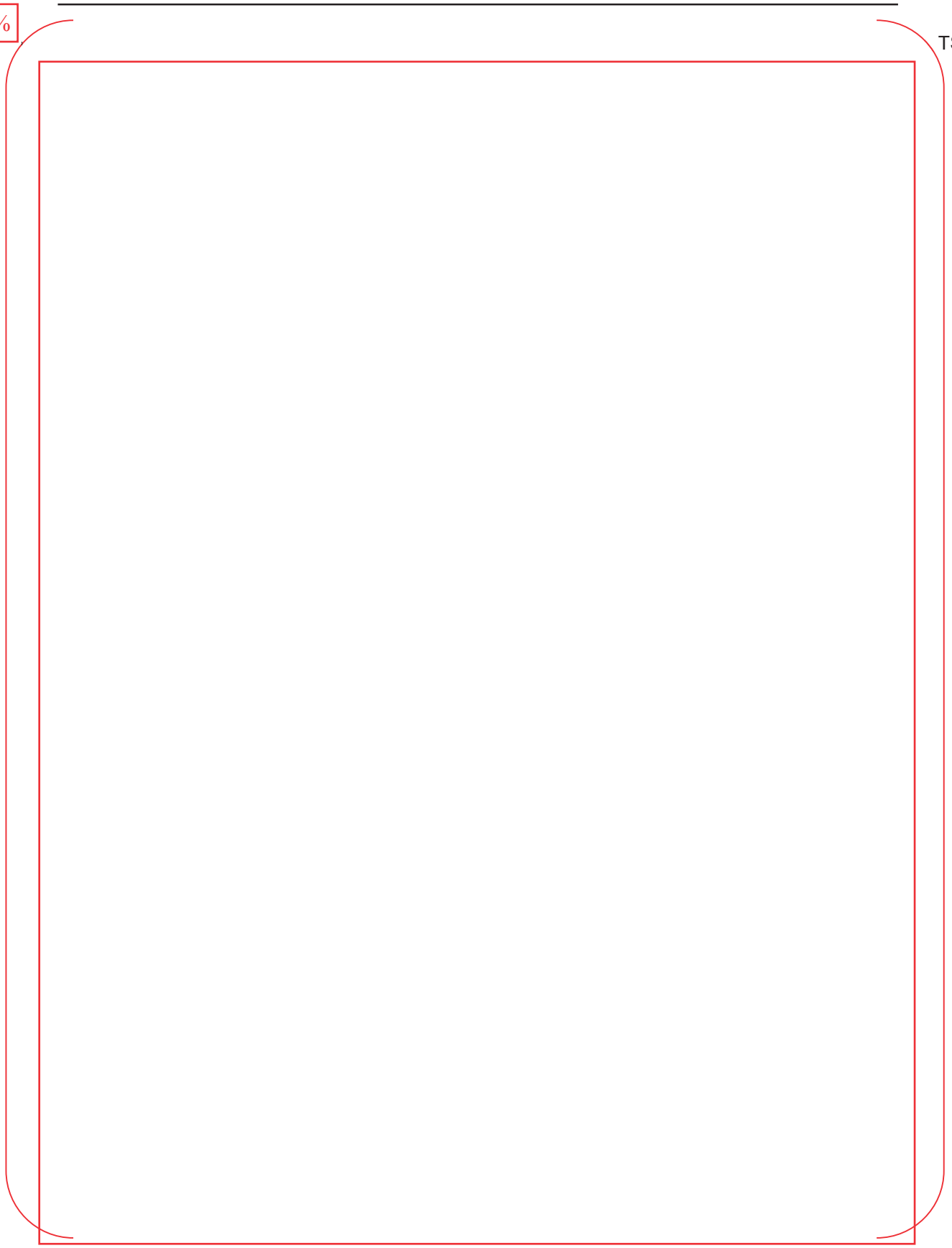

%

TS

Replace with next page F

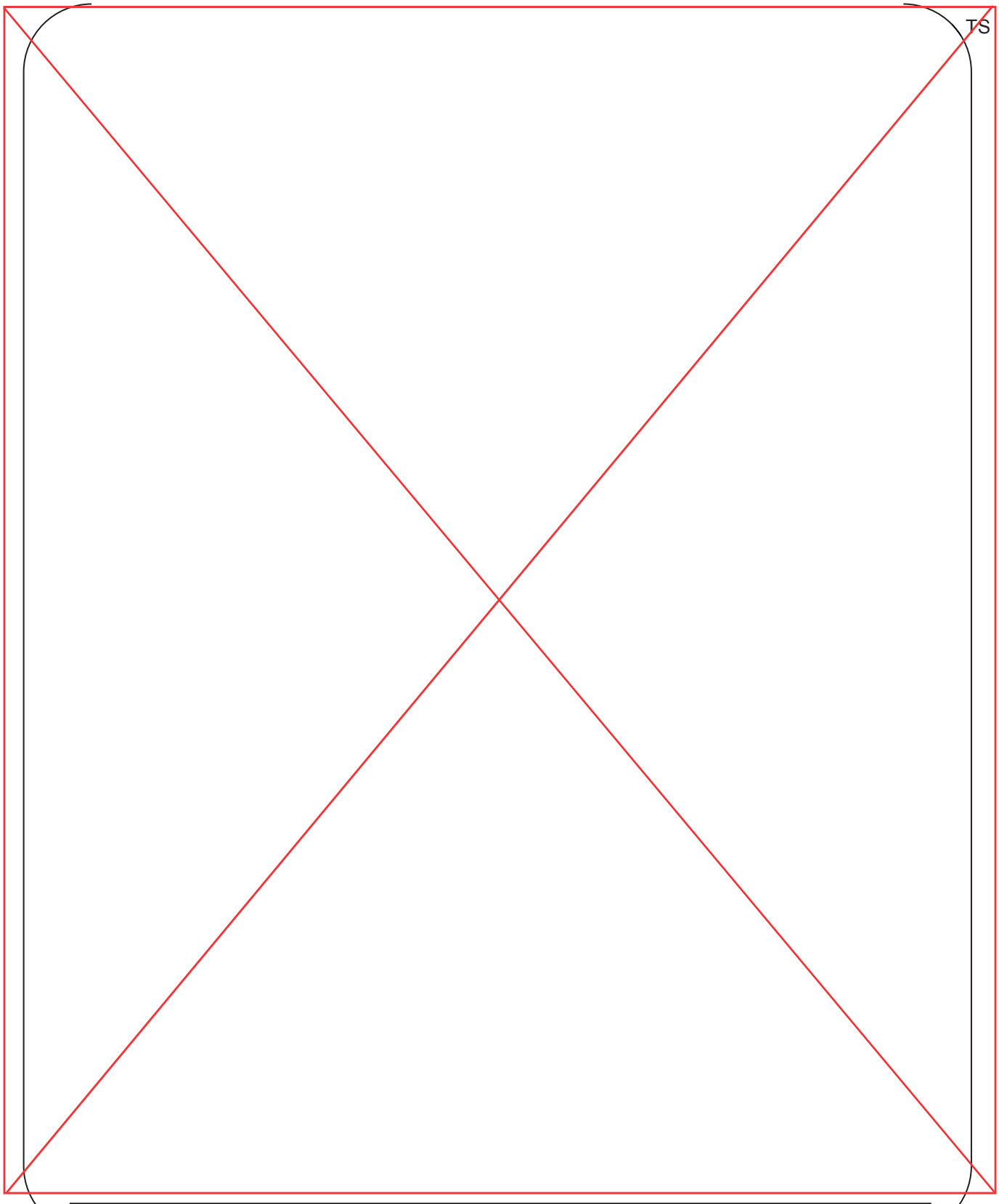

&

TS

&

TS

Replace with next page G

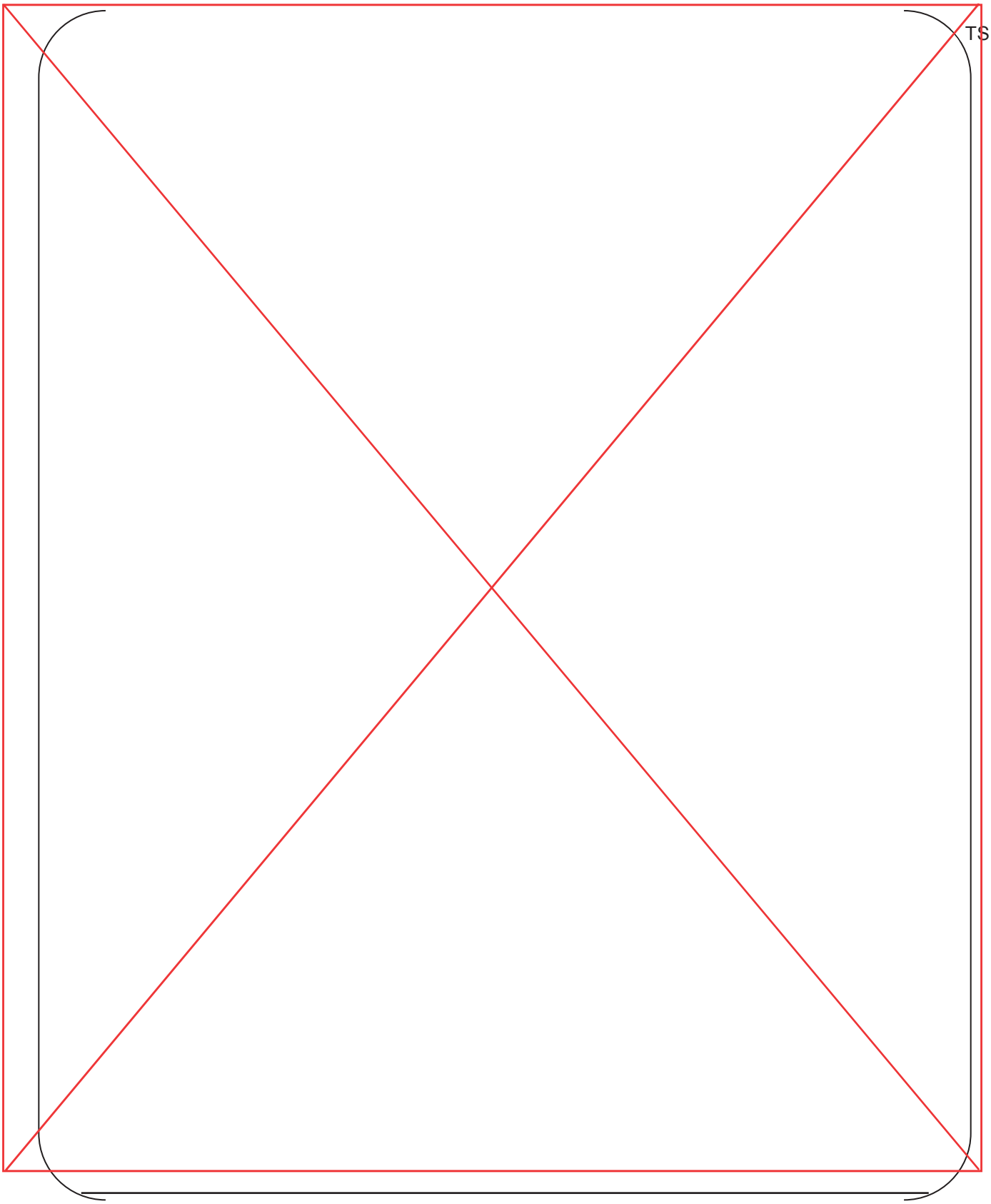

'

TS

'

TS

Replace with next page H

[ ]TS

4. PIRT for APR1400

APR1400 PIRT is described in Table 5. Findings from further code simulations and experiments performed after the preparation of KNGR PIRT are incorporated. Final features of the APR1400 design are also reflected. [ ]TS phenomena or processes from [ ]TS components are ranked as important. The number of phenomena or processes for each component is as follows:

[ ]TS

H

TS

(

TS

(

TS

(

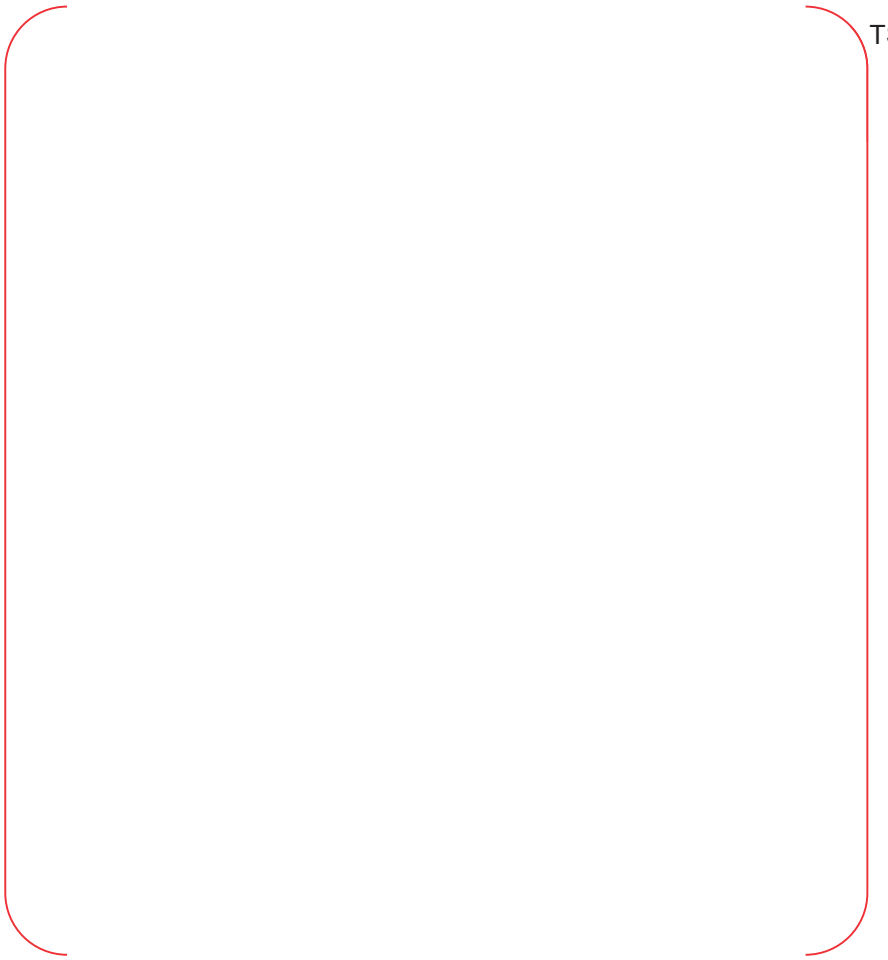

TS

Table 3 KNGR PIRT (1/8)

TS

Table 3 KNGR PIRT (3/8)

TS

Table 3 KNGR PIRT (4/8)

TS

Table 3 KNGR PIRT (5/8)

TS

Table 4 Definition of Time Phases for APR1400 PIRT

Phase (Number)*)	Starts at	Ends at
Blowdown (1)	Break initiation	Initiation of SIT injection
Refill (2)	~~End of blowdown~~	Initiation of core recovery (~~liquid~~ level at bottom fuel rod heated length)
Early Reflood (3)	~~End of refill~~	End of SIT injection
Late Reflood (4)	End of SIT injection	Stable core quench

Mixture

Initiation of SIT injection

Initiation of core recovery

*) The numbers indicated in parentheses are used as indices in the PIRT to denote each phase in that table.

Table 5 APR1400 PIRT (1/3)

TS

Table 5 APR1400 PIRT (2/3)

TS

Replace with next page ẇ

TS

Table 5 APR1400 PIRT (3/3)

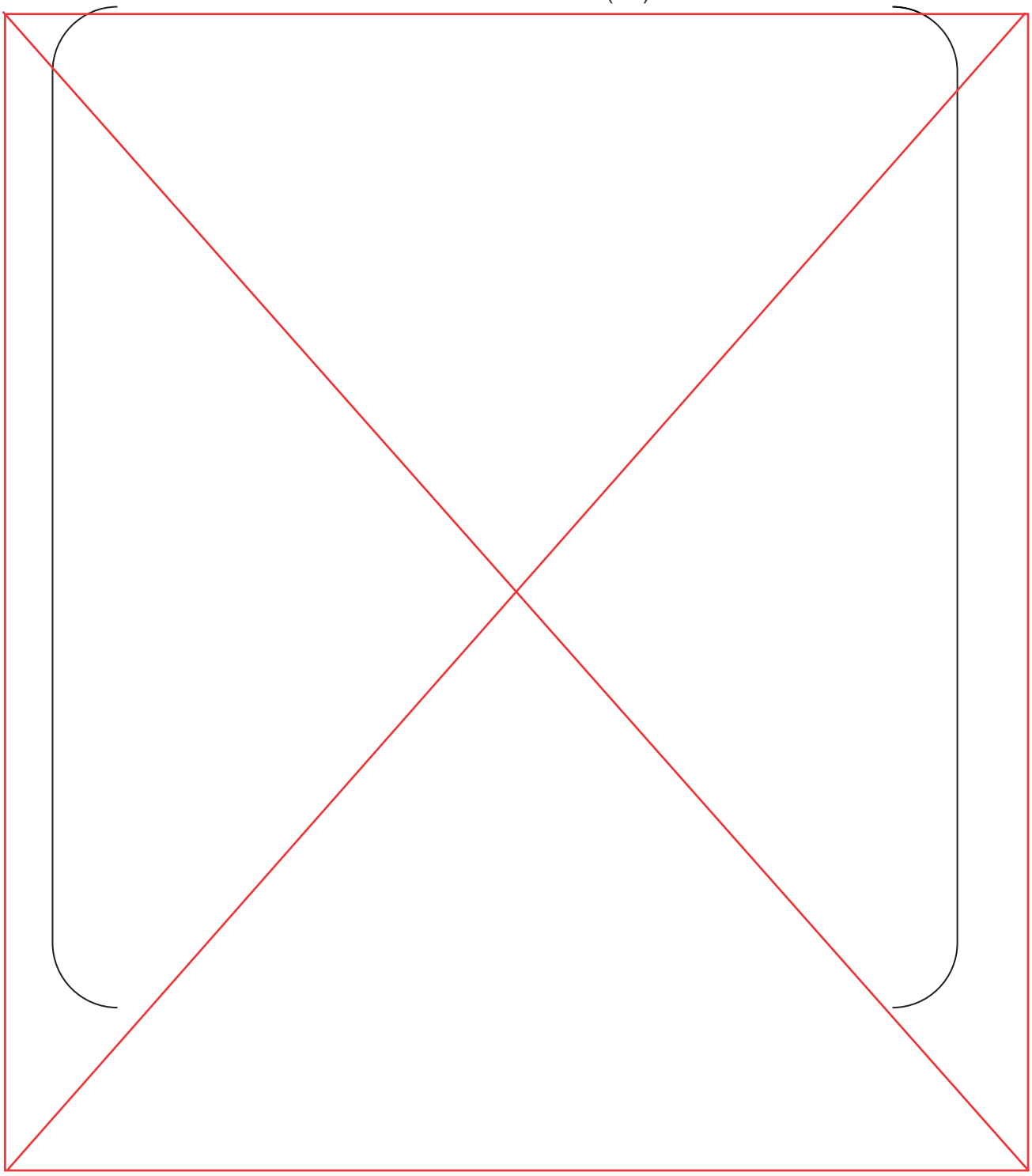

ẇ

TS

Table 5 APR1400 PIRT (3/3)

RESPONSE TO AUDIT ISSUES

APR1400 Topical Reports

Korea Electric Power Corporation / Korea Hydro & Nuclear Power Co., LTD

Docket No. PROJ0782

Review Section	**TR Realistic Evaluation Methodology for LBLOCA of the APR1400**
Application Section	**Topical Report: APR1400-F-A-TR-12004 Realistic Evaluation Methodology for Large-Break LOCA of the APR1400**
Issue Date	**08/13/2015**

Audit Issues No. 15

It appears that what is being termed the APR1400 PIRT in Table 3-2 and Table 5 of Appendix A of the topical report is actually a subset of the Korea Next Generation Reactor (KNGR) PIRT, shown in Table 3 in Appendix A, that includes only those phenomena from the KNGR PIRT (with modifications for APR1400) that are ranked 4 or higher during at least one of the accident periods. A complete PIRT, as described in NUREG/CR-5249 includes all the phenomena and their corresponding ranking. Both the KNGR and the APR1400 PIRTs lack a state-of-knowledge ranking for each phenomenon. In addition, according to RG 1.203, the PIRT generated to guide the evaluation model (EM) development process must be adequately documented. A complete documentation of the PIRT for APR 1400 that includes the rationale for the assigned ranks and state-of-knowledge is needed.

Response (Rev.1)

The APR1400 PIRT has been developed based on KNGR PIRT [1]. The presentation material attached [2] describes the changes from KNGR PIRT and the rationales for the changes. The APR1400 PIRT in the topical report will be revised to the document attached [3] where the rationales for the assigned ranks and state-of-knowledge column are added. The changes from KNGR PIRT are written in red and their rationales are reinforced.

Reference

[1] “Phenomena Identification and Ranking Tabulation Korean Next Generation Reactor Large Break Loss of Coolant Accident,“ KINS/INEEL, 2001

[2] Presentation Material, “PIRT to Uncertainty Parameter,” presented at the face to face meeting with NRC, 2016. 1. 12 ~ 2016. 1. 15. (Modifications are made in accordance to the reference [2]), Revision 1.

[3] Presentation Material, “APR1400 PIRT revision,” attached document of the response to the audit issue no. 15, July, 2016

Impact on DCD

There is no impact to the DCD.

Impact on PRA

There is no impact on the PRA.

Impact on Technical Specifications

There is no impact on the Technical Specifications.

Impact on Technical/Topical/Environmental Report

Topical report is revised according to the PIRT revision as described in the attachment for the response of Audit Issue No. 14.

There is no impact on any Technical or Environmental Report.

PIRT to Uncertainty Parameter

- Contents
  1. KNGR PIRT
  2. APR1400 PIRT
  3. Uncertainty parameter selection
     - General guide line
     - Uncertainty parameter selection from PIRT
     - Ranges of the parameters
     - Phenomena treated by bias
  4. Audit issues related with PIRT

PIRT to Uncertainty Parameter

- KNGR LBLOCA PIRT (WFO861702, 2001)
  - Former APR1400, KNGR (Korea Next Generation Reactor)
    - Developed by KINS/INEEL
    - Internationally recognized panel members: Dr. Brent E. Boyack (LANL), Dr. Bub-Dong Chung (KAERI), Dr. Lawrence E. Hochreiter (PSU), Dr. Jose N. Reyes (OSU), Mr. Gary E. Wilson (INEEL)
    - Time period definition
      1: Blowdown (break ~ lower plenum begins to refill)
      2: Refill (~ mixture level approaches the core inlet)
      3: Reflood (~ initial core quenched)
      4: long-term cooling period (~ stable core quenched)

PIRT to Uncertainty Parameter

- KNGR LBLOCA PIRT (WFO861702, 2001)
  - Constitutes of
    - PIRT KNGR LBLOCA (main body)
    - Description of process/phenomena used in the PIRT (Appendix A)
    - Importance Ranking, Knowledge-Level and Rationales LBLOCA PIRT for the KNGR (Appendix B)
    - Summary of KNGR RELAP5 LBLOCA Sensitivity Calculations (Appendix C)
    - TRAC-M Simulations of LBLOCA in the KNGR (Appendix D)
    - Curriculum Vitae for KNGR PIRT panel (Appendix E)

PIRT to Uncertainty Parameter

- KNGR LBLOCA PIRT (WFO861702, 2001)
  - KNGR LBLOCA PIRT table
- APR1400 PIRT
  - Some modifications made for APR1400 PIRT
    - Definition of time periods modified
      1. blowdown (~ SIT injection initiates)
      2. refill (~ level approaches the core inlet)
      3. early reflood (~ SITs empty)
      4. late reflood (SITs empty ~)
    - SIT flow path, IRWST water level, IRWST-SIP flow, Pressurizer stored energy, etc… are modified
    - Due to better knowledge, change in the definition of time phases, corrections…

PIRT to Uncertainty Parameter

- Adjustment of rankings modified

TS

PIRT to Uncertainty Parameter

- Adjustment of rankings modified

TS

PIRT to Uncertainty Parameter

- Adjustment of rankings modified

TS

PIRT to Uncertainty Parameter

- Adjustment of rankings modified

TS

PIRT to Uncertainty Parameter

- Adjustment of rankings modified

TS

PIRT to Uncertainty Parameter

- Adjustment of rankings modified

TS

PIRT to Uncertainty Parameter

- Adjustment of rankings modified

TS

PIRT to Uncertainty Parameter

- Adjustment of rankings modified

TS

PIRT to Uncertainty Parameter

- Adjustment of rankings modified

TS

PIRT to Uncertainty Parameter

- Adjustment of rankings modified

TS

PIRT to Uncertainty Parameter

- Adjustment of rankings modified

TS

PIRT to Uncertainty Parameter

- Adjustment of rankings modified

TS

PIRT to Uncertainty Parameter

- Adjustment of rankings modified

TS

PIRT to Uncertainty Parameter

- Adjustment of rankings modified

TS

PIRT to Uncertainty Parameter

- Adjustment of rankings modified

TS

PIRT to Uncertainty Parameter

- Adjustment of rankings modified

TS

PIRT to Uncertainty Parameter

- Adjustment of rankings modified

TS

PIRT to Uncertainty Parameter

- Adjustment of rankings modified

TS

PIRT to Uncertainty Parameter

- Adjustment of rankings modified

TS

PIRT to Uncertainty Parameter

- Adjustment of rankings modified

TS

PIRT to Uncertainty Parameter

- Adjustment of rankings modified

TS

PIRT to Uncertainty Parameter

- Adjustment of rankings modified

TS

PIRT to Uncertainty Parameter

- Adjustment of rankings modified

TS

PIRT to Uncertainty Parameter

- Adjustment of rankings modified

TS

PIRT to Uncertainty Parameter

- Adjustment of rankings modified

TS

PIRT to Uncertainty Parameter

- Adjustment of rankings modified

TS

PIRT to Uncertainty Parameter

- Adjustment of rankings modified

TS

PIRT to Uncertainty Parameter

- Adjustment of rankings modified

TS

PIRT to Uncertainty Parameter

- Adjustment of rankings modified

TS

PIRT to Uncertainty Parameter

- Adjustment of rankings modified

TS

PIRT to Uncertainty Parameter

- Adjustment of rankings modified

TS

PIRT to Uncertainty Parameter

- Adjustment of rankings modified

TS

PIRT to Uncertainty Parameter

- Adjustment of rankings modified

TS

PIRT to Uncertainty Parameter

- Adjustment of rankings modified

TS

PIRT to Uncertainty Parameter

- Adjustment of rankings modified

TS

PIRT to Uncertainty Parameter

- Adjustment of rankings modified

TS

PIRT to Uncertainty Parameter

- Adjustment of rankings modified

TS

PIRT to Uncertainty Parameter

- Adjustment of rankings modified

TS

PIRT to Uncertainty Parameter

- Adjustment of rankings modified

TS

PIRT to Uncertainty Parameter

- Adjustment of rankings modified

TS

PIRT to Uncertainty Parameter

- Adjustment of rankings modified

TS

PIRT to Uncertainty Parameter

- Adjustment of rankings modified

TS

PIRT to Uncertainty Parameter

- Adjustment of rankings modified

TS

PIRT to Uncertainty Parameter

- Adjustment of rankings modified

TS

PIRT to Uncertainty Parameter

- Adjustment of rankings modified

TS

PIRT to Uncertainty Parameter

- Adjustment of rankings modified

TS

PIRT to Uncertainty Parameter

- Adjustment of rankings modified

TS

PIRT to Uncertainty Parameter

- Adjustment of rankings modified

TS

PIRT to Uncertainty Parameter

- Adjustment of rankings modified

TS

PIRT to Uncertainty Parameter

- Adjustment of rankings modified

TS

PIRT to Uncertainty Parameter

- Adjustment of rankings modified

TS

PIRT to Uncertainty Parameter

- Adjustment of rankings modified

TS

PIRT to Uncertainty Parameter

- APR1400 LBLOCA PIRT (as described in Appendix A of the ToR)

TS

Continued to next page

PIRT to Uncertainty Parameter

- APR1400 LBLOCA PIRT (Appendix A of Topical Report) TS

APR1400 LBLOCA PIRT (1/3)

Non-Proprietary

APR1400 LBLOCA PIRT (2/3)

Non-Proprietary

APR1400 LBLOCA PIRT (3/3)

Non-Proprietary

PIRT to Uncertainty Quantification

- General guideline
  - In CAREM, all phenomena of importance (≥ 4) should be considered by each uncertainty parameters (UCP) and their uncertainty ranges, in principle. (e.g. 1 to 1 match)
  - However, there are some exceptions such as…

    (1) Phenomena already considered by other UCP

    ex) Flashing in the core ⇨ depressurization of RCS ⇨ treated as the uncertainty of critical flow, break size, etc.

    (2) Phenomena treated conservatively

    ex) Radiation to surroundings ⇨ conservative when not considered

    (3) Phenomena treated as bias

    ex) ECC bypass during refill

PIRT to Code Parameters (1/7)

APR1400 LBLOCA PIRT (ToR)

TS

- Descriptions: Sections in ToR.
- (R) considered in other parameter, (C) conservatively treated, (B) bias
- (Y) handled by uncertainty parameter

PIRT to Code Parameters (2/7)

- APR1400 LBLOCA PIRT (ToR)

TS

PIRT to Code Parameters (3/7)

- APR1400 LBLOCA PIRT (ToR)

TS

PIRT to Code Parameters (4/7)

➢ APR1400 LBLOCA PIRT (ToR)

TS

PIRT to Code Parameters (5/7)

- APR1400 LBLOCA PIRT (ToR)

TS

PIRT to Code Parameters (6/7)

- APR1400 LBLOCA PIRT (ToR)

TS

PIRT to Code Parameters (7/7)

TS

Final Uncertainty Parameter Selection

- Total 82 phenomena → 27 uncertainty parameter
- In addition to the parameters selected from PIRT,

TS

- Distribution of the uncertainty parameter is assumed as either normal or uniform. (Uniform is used when the knowledge level is low for conservatism.)

Final Uncertainty Parameter Selection

➢ As a results,

[ ] TS

- Bias evaluation performed for the high (reflood) PCT cases and added
- Uncertainty from all PIRT phenomena/process are considered in the final calculation of the safety parameters, i.e., PCT, PLO, …

Distributions and Ranges of the Uncertainty Parameters (1/2)

TS

Distributions and Ranges of the Uncertainty Parameters (2/2)

TS

Thank you for your attention

Non-Proprietary

APR1400 LBLOCA PIRT
Revision 1

2016. 7.

Acronyms

APR1400	Advanced Power Reactor 1400
CCF	Counter Current Flow
CHF	Critical Heat Flux
CL	Cold Leg
DC	Downcomer
DVI	Direct Vessel Injection
ECC	Emergency Core Coolant
FD	Fluidic Device
HL	Hot Leg
IR	Importance Ranking
KL	Knowledge Level
LP	Lower Plenum
PCT	Peak Cladding Temperature
PZR	Pressurizer
NC	Non-condensible
RCS	Reactor Coolant System
SG	Steam Generator
SIP	Safety Injection Pump
SIT	Safety Injection Tank
SIT-FD	Safety Injection Tank with Fluidic Device
UP	Upper Plenum

added

Definition of IR and KL

- Same definition with KNGR PIRT [1] is used

Importance Ranking

Importance Ranking (IR)	Meaning
5	Highest of the high in importance
4	High importance
3	Moderate importance
2	Low importance
1	Lowest of the low in importance

Knowledge Level

Knowledge-Level (KL)	Meaning
5	Fully Known. Small uncertainty.
4	Known. Moderate uncertainty.
3	Partially Known. Large uncertainty.
2	Very Limited Knowledge. Uncertainty cannot be characterized.
1	Totally Unknown.

added

General guide lines of KNGR PIRT[1]

- IR and KL was determined from votes by PIRT panel, and there are general guide lines for the ranks.
- The general guide lines for the IR and KL are described in slide 4 and 5.

Changes for APR1400 PIRT

- After SIT-FD design is completed, it is revealed that the time period definition based on the SIT injection is more useful than that of KNGR PIRT.
- The general IR and KL changes as well as the change in the definition of time period are described in slide 6 through 8.

added

IR General Descriptors, pp. 17 of Reference [1], also pp. A-13 of Appendix A of ToR

Rank	General Descriptors
5	a. Highest of the high b. Experimental simulations and analytical modeling, with high degree of accuracy, is critical
4	a. High influence on FOM b. Needs to be experimentally present[1] and/or analytically modeled[2] with high degree of accuracy c. Approximately one –half the importance of rank 5
3	a. Moderate influence on FOM b. Needs to be experimentally present and/or analytically modeled with moderate degree of accuracy c. Approximately one –half the importance of rank 4
2	a. Low influence on (or importance to) FOM b. Needs to be experimentally present and/or analytically modeled, but high uncertainty or inaccuracy is acceptable c. Approximately one –half the importance of rank 3
1	a. Lowest of the low in importance b. Very low influence on (or importance to) FOM c. Approximately one –half the importance of rank 2
IS	A system, component or process/phenomena may be active; however, its influence on the FOM is insignificant and may be ignored
NA	A system, component or process/phenomena is not active or present

[1]: As used here, “experimentally present” relates to test facilities used to simulate the reactor

[2]: Likewise, “analytically modelled” relates to models and computer codes used to simulate the reactor

added

KL Relationships (General rationale of KL in KNGR PIRT), pp. 19 or pp. B2 of Reference [1]

Knowledge-Level (KL)	Meaning
5	Stored energy release for well-defined geometries is ranked at level 5. Stored energy release in pellets with cracks is an exception.
5	Flashing phenomenon is well known.
5	Reactivity parameters are well known.
5	Oxidation kinetics is well known. There is more uncertainty when double-sided oxidation is being considered.
5	Single-Phase pressure-drop in simple geometries.
4	One-Phase pressure-drop in complex geometries.
4	Two-Phase pressure-drop in simple geometries.
3	Two-Phase pressure-drop in complex geometries.
3	Multi-dimensional flow knowledge is ranked 3 because of the effects of complex geometry and the complications caused by multiple fluid streams, condensation, entrainment and de-entrainment.
3-4	Level in components is ranked between 3 and 4 depending on flow paths.
Note	Transient dynamic phenomena have a lower knowledge level than quasi-steady behavior for same phenomena. (e.g., blowdown phase versus long term cooling phase).

added

Change in the definition of time period

Definition of time period (KNGR)

Time period	Definition
Blowdown (1)	Break initiation ~ Initiation of lower plenum refill
Refill (2)	Initiation of lower plenum refill ~ Initiation of core recovery (liquid level at bottom of fuel rod heated length)
Reflood (3)	End of refill ~ Initial core quench
Long-term cooling (4)	Initial core quench ~ Stable core quench

Downcomer boiling was considered as being important and this is the reason for division of reflood period to reflood and long-term cooling periods.

Definition of time period (APR1400)

Time period	Definition
Blowdown (1)	Break initiation ~ Initiation of SIT injection
Refill (2)	Initiation of SIT injection ~ Initiation of core recovery (mixture level at the bottom of fuel rods)
Early Reflood (3)	End of refill ~ End of SIT injection
Late Reflood (4)	End of SIT injection ~ Stable core quench

Time period change have been made due to practical application, better knowledge on phenomena:
- Initiation of lower plenum refill is not easy to determine and changed to SIT injection initiation.
- Division of Initial core quench and long-term cooling is not meaningful any more. It is required to confirm the core quench behavior when the SI is not sufficient(late reflood).

IR adjustment due to time period change

added

- Blowdown
  - "SIT injection" is NOT included during blowdown period in APR1400 PIRT
    - ECC injection during blowdown does not occur
    - The rank of phenomena related with SIT or ECC interaction become "NA"
- Refill
  - "Early SIT injection" is included during refill period in APR1400 PIRT
    - The blowdown period importance rank of KNGR PIRT is used as the rank for the refill period of APR1400 PIRT
- Early reflood, late reflood
  - Massive NC gas release does NOT occur during early reflood period in APR1400 PIRT
    - The earliest massive NC gas release occurs during late reflood period
    - However, NC gas release due to vortex motion of SIT-FD can occur during early reflood period
  - Full Scale SIT-FD experiment was performed
    - Sufficient amount of ECC is guaranteed during early reflood, IR during early period can be lowered.

KL change due to design completion

added

- SIT-FD
  - Full-scale VAPER test has been performed
    - Knowledge levels of phenomena related with SIT-FD, such as level, flow deliveries and noncondensable gas are increased to 5.

TS

References

[1] “Phenomena Identification and Ranking Tabulation Korean Next Generation Reactor Large Break Loss of Coolant Accident”, WFO861702, KINS/INEEL, January 2001.

RESPONSE TO AUDIT ISSUES

APR1400 Topical Reports

Korea Electric Power Corporation / Korea Hydro & Nuclear Power Co., LTD

Docket No. PROJ0782

Review Section	**TR Realistic Evaluation Methodology for LBLOCA of the APR1400**
Application Section	**Topical Report: APR1400-F-A-TR-12004 Realistic Evaluation Methodology for Large-Break LOCA of the APR1400**
Issue Date	**08/13/2015**

Audit Issues No. 16

Section 3.12.1 of RG 1.157 states that “the containment pressure used for evaluating cooling effectiveness during the post-blowdown phase of a LOCA should be calculated in a best-estimate manner and should include the effects of containment heat sinks.” According to Section 3.4 of the topical report, the APR1400 LBLOCA methodology calls for the coupling of RELAP5/MOD3.3/K with CONTEMPT4/MOD5 for the LBLOCA. As a result, the adequacy of CONTEMPT4/MOD5 also needs to be determined. Table 3-2 of the topical report (also Table 3 in Appendix A from which Table 3-2 is derived) contain and rank the generic processes such as [ ]^{TS} for the containment component. However, the ranking of such generic processes is insufficient for adequacy determination. Individual phenomena that impact these general processes (e.g., “condensation heat transfer,” “impact of non-condensable gases,” “droplet heat and mass transfer,” etc.) need to be included and ranked in the PIRT to determine the code adequacy and uncertainty following the SRP Section 15.0.2, Revision 0, and NUREG/CR-5249 guidance. A complete PIRT for the containment phenomena is required. Also, provide an explanation of how the containment is treated statistically.

Response

[

]TS They satisfy the associated technical standard in the following manner.

TS

TS

Impact on DCD

There is no impact on the DCD.

Impact on PRA

There is no impact on the PRA.

Impact on Technical Specifications

There is no impact on the Technical Specifications.

Impact on Technical/Topical/Environmental Report

There is no impact on any Technical, Topical, or Environmental Report.

RESPONSE TO AUDIT ISSUES

APR1400 Topical Reports

Korea Electric Power Corporation / Korea Hydro & Nuclear Power Co., LTD

Docket No. PROJ0782

Review Section	**TR Realistic Evaluation Methodology for LBLOCA of the APR1400**
Application Section	**Topical Report: APR1400-F-A-TR-12004 Realistic Evaluation Methodology for Large-Break LOCA of the APR1400**
Issue Date	**08/13/2015**

Audit Issues No. 17

NUREG/CR-5429, Section 2.1 establishes an acceptable approach for the documentation of the PIRT. The following concerns are related to Table 3-2 of the topical report:

a. A more detailed explanation of the phenomena [ ]TS along with a justification for their respective importance rankings is needed. This needs to include a discussion of how these phenomena (ranked 4 or higher) are modeled and how the uncertainty in these parameters is determined and included in the analysis.

b. According to the Table 3-1 of the topical report, the end of blowdown period is defined as the initiation of SITs-FD injection. As a result, the process or phenomena associated with SIT-FD are not present during the blowdown period. However, some of phenomena for the SIT-FD are ranked during the blowdown period in Table 3-2 of the topical report. The basis for the importance rankings assigned to the SIT-FD phenomena during the blowdown period is needed.

c. Section 3.1.2.3 of the topical report provides the phenomena descriptions during the early reflood period. [ ]TS

Based on the accident period definition, the gas discharge should be initiated after the SIT-FD water has depleted at the end of the early reflood period. The same comment also holds for the ranking of the [ ]TS The basis for the stated importance rankings is needed.

d. [ ]TS According to the accident period definition, SIT-FD do not inject until the beginning of period 2. Therefore, provide the rationale for the rank of 3 for period 2 and the rank of 5 for period 1, for both the above mentioned phenomena. The ranking for these phenomena is important because they are treated with a bias during the accident.

e. [

]TS

f. Provide an explanation for not considering downcomer boiling during the refill period.

g. [

]TS

h. According to Table 3-2 of the topical report, non-condensable gas is only expected to be influential in the reactor vessel downcomer component during the early reflood period. However, a relatively large amount of non-condensable gas is transferred from SIT to the downcomer after the depletion of SIT water inventory, the late reflood period. Provide an explanation of the current ranking for the cited phenomenon.

i. [

]TS Table 5-1 the topical report shows that this parameter is part of the uncertainty analysis. Provide the rationale for not including the form loss through the RCPs.

Response

a) ~ h)

The APR1400 PIRT has some mistakes in the PIRT modification process based on the KNGR PIRT, especially with regard to the change in time period definitions. The APR1400 PIRT will be revised to the attached documents of audit issue no. 15. The audit issues a) through h) include the issues related to the nitrogen gas injection phenomenon and its effectiveness in time period, therefore those issues can be cleared up following the modification of the APR1400 PIRT in association with the response to audit issue no. 15.

i)

[

]TS The limiting break determination process is described in Section 3.1.1 and 5.2.1.1 of the topical report. The additional information is available in the response to the audit issue no. 61 (b)~(f) as well.

Impact on DCD

There is no impact on the DCD.

Impact on PRA

There is no impact on the PRA.

Impact on Technical Specifications

There is no impact on the Technical Specifications.

Impact on Technical/Topical/Environmental Report

Topical report will be revised as discussed in this response. Revised PIRT is described in the attachment for the response of Audit Issue No. 14.

There is no impact on Technical or Environmental Report.

As the primr, y system depressuri/ es, flashing oc1urs first in the hot regions of the system, such as the upper plenum, hot leg, pressuri/ e,r and core, and then proceeds to the relatively cold regions, such as the lower plen.- , do2 ncomer, and cold legs. Ǒ3tensi! e ! oiding oc1urs i all areas of the reactor pressure ! essel. . 1leate boiling develops in the 1ore. Fission +o2 er, whi1h is 1r l1ulated by the kinetics - odel, drops to the level of decr y heat due to the voiding in the core. The flashing also reduces the primr, y syste- depressurization rate.

) hen the criti1r l heat flux (CHF) condition is rer1 hed in the core, heat transfer - ode changes fro- ˝.1 leate boiling to post-CHF heat transfer regi- es (i.e., transitio˝ boiling, film boiling, a˝ d fo,1ed 1o! ection to ! r por). Fuel rod cladding tem+eratures increase rapidly due to the degradi˜ g rod-to-fluid heat transǾer" The increase of the rod claddi˜ g temperatures during the early blo2 down period is terminated by Ǿllowing reasons8

- The core po2 er decreases rapidly due to the insertion of negative reacti! ity resulting from the ! oiding of the core.
- Rod-to-fluid heat transǾer enhances due to the do2˝ 2 ard flo2 in the core r0ter the flo2 stagnation.
- The large 1oolr˝ t inventory in the . pper guide st,.1 tures 6(9 S) and the .++ er her d - o! es to2 r rd the top of the core 4y two paths; through the U9 S drainage holes i the U9 S bottom plate that is between the UGS and the .+ per plenum, and through the guide tube pi+es that terminate in the upper inactive core.

As the low press. ri/ er press. re set-point is reached, the reactor is tripped. Reactor 1oolant p.- ps (RCPs) are modeled to trip and coast down from the beginning o0the ac1ident ass. - ing loss-of-ofǾsite-po2 er" As the primr, y system pressure continues to de1rease, flashing develops i the cold regions of the system. Resultant ! oiding i the RCP degrades its +.- pi˜ g performr˝1 e. Break flow rate decreases rapidly as the flo2 regi- e changes fro- s.41 ooled to saturated criticr l Ǿow at the brer5 .

Four SIT-FDs begin to deliver flow i to the Ǿb., DVI lines when the primr, y syste- press. re fr lls belo2 their actuation set-point. The coolant flo2 s through the D=I no/ / les into the upper r˝ ulus and then begins to refill the reactor pressure ! essel" ẇecause the reactor coolant system is still depress. rizing, some of the coolant entering the .+ per annulus is swept out to the break along with entrained liquid f,om the lower plenum and the do2˝1 omer" Although the break flo2 remains high, sufǾcient flo2 i the excess of the by+ass is deli! ered do2˝ ward into the do2 nco- e, and increases the do2 ncomer wr ter level" Then the coolr˝ t injected by the SIT-FDs event.r lly reaches the lower ple˝ .- .

3.1.2"2 Refill

The reǾll period begins when SIT-F& injection flo2 is initir ted r˝ d ends 2 hen the water level in the lo2 er plenum reaches the ~~core inlet~~. Refill begins at r, ound 15 s and ends at aro. nd 3A s.

bottom of the active core

~~ECC water in the reactor vessel downcomer can flow do2 n 4y gra! ity or be s2 e+t out to the brer5 4y the press. re diǾerential and the .+ 2r ,d-escapi˜ g steam flow that levitates the liquid.~~ Reactor ! essel walls and internals a,e large metal structures at temperatures abo! e saturation.) hen s.41 ooled ECC water 1omes into contact 2 ith the metal structures in the do2 nco- en˜ stea- is generated by˝.1 leate boili˜ g. This reduces the gravitatior l head of the fluid in the do2˝ comer. The process of liquid penetration and s2 ee+-out reper ts in the do2 ncomer and direct-contact 1ondensatio˝ of steam on the subcooled ECC water continues in the .++ er annulus. Figure 3-5 gives a schemati1 of the t2 o-phase primr, y coolant system 25 s after the break opens"

The depressuri/ ation of the system 2 anes as the diǾerential pressure bet2 een the reactor coolr nt

system (RCS) and the contai- ent reduces. Ġwing to the gradual reduction of flashing and break 0lo2, the rate of li>. id penet,ation ĩ to the lower plenu- increases.) ith the dec,easing steam flow rate, ŎKK) 4ypass is insig ̃i0cant and most of it flo2s do2 ̃ward to fill the do21 omer and the lo2er plenum. At this stage, ~~water~~ le! els in the downco- er and the lo2er ple ̃.- increase rapidly.

Heatup, whi1h is al- ost adiabatic, continues in the core during this period 4ecause there is no in! entory to cool the core.

mixture

mixture

The re0ll period ends 2he ̃ the ~~liquid~~ le! el in the lower ple ̃.- reaches the botto- o0the active core.

and remains full thereafter and conditions are established for continuously reflooding the core with coolant.

3.1.2"* Early R~~e~~

The early ,e0lood period begins when the lower plen. - ~~is co +letely 0lled with water~~ a ̃d e ̃ds when the SIT-FD 2ater is depleted. This period begins at around 38 s

reaches the bottom of the active core

the mixture level in

7, and Figure 3-8. These figures The early reflooding process is sho2n in ~~i~~

respe1tively +rovide sche- atics of coolr nt distributions at C2 s when “high flow” is injected from the SIT-FDs, at 92 s when “low flow” is injected from SIT-FDs, and at 150 s when the entire 1ore is quenched. Modeling of SIT-FD is explained in Section 4.2.1. The “high flow” and the “low flow” of SIT-FD are exemplified in Figure 5-14 and further described in Section 5.2.1. Aro. nd the begi ̃ing of the early reflood period, SIPs begin to inject 2ater"

Initially, the core reflood is quite rapid because:

- the do2 ̃comer re- ai ̃s filled with water 4y the ECC ĩ jection,
- the high 0lo2 ĩ jectio ̃ o0: IT-FD co ̃ti ̃. es,
- loop steam 0low rate is low and therefore the hydraulic resistance in the loop is lo2r and
- there is no se! ere steam binding.

after the break

Maxi- . - SIT-F& injection flo2 is reached ~~during this +eriod~~ at around 30 s. High flo2 injection of the SIT-FD conti ̃ues until around 66 s, then the flo2 through the stand-pipe beco- es unavailable and only the flow through the fluidi1-de! i1e is +ossible. During the high flo2 injection, do2ncomer and core li>. id levels increase rapidly" ᵛs the do2 ̃ 1o- er liquid level a++,oaches the level of the cold legs, much of the coolant spills out of the break and the ! essel side break flow tends to increase.) hen the water le! el in the SIT-FD decreases to below the top of the stand pi+e, the lo2 0low injection begins.) ater le! els in the downcomer and core decrease slightly but the levels increase again within arou ̃d 10 s, maintaining downco- er water le! el abo! e the le! el of the cold legs. It appears that the co- bined S+P r ̃d SIT-FD flo2s are suf01ient to maintain the 2ater le! el in the do2ncomer and to retard 1ore heatu+"

In the core, heat transfer regimes encompass the enti,e spectrum, such as single phase liquid 1onvection, nucleate boili ̃g, transition boiling, 0lm boiling, a ̃d single phase !r por convection.

Due to droplet de-entrainment at the f. el alignment plate a ̃d spr1 er grids, local quenching could occ., . Vr por ! elocities and liquid entrainment in the central region of the core are higher due to the higher po2er of this region. The entrained liquid co. ld have a cooling ef0ect on the .++ er region of the core. Some of the e ̃trained liquid is de-entrained at the f. el alignment plate r ̃d the remainder is cr,, ied into the upper ple ̃.- 0or- ing a t2o-phase +ool. Liquid f,om the pool cr n reenter the lo2 po2ered regions of the core through the fuel alig ̃- ent plate due to the lo2er !r +or velocities in those regions. Therefore, a three-dimensional flo2 pattern 1an occur: water flo2s from low to high po2ered regions in the core, 2hile the flo2 is in the opposite di,ection in the upper plen.- . Liquid 0lo- the upper ple ̃.- pool mr y be further entrai ̃ed r ̃d carried o! er into the hot legs and ster-

generators"

As reflooding progresses up2 ard from the lo2 er core region, more liquid is entrained to the upper ple .- and the level of the two-phase - i3ture in the pool 1r n reach the hot leg.) hen the entrained liquid reaches the (-tubes of the steam generators, it is vr+ ori/ ed 4y reverse her t transfer fro- the secondary side to the primr, y side. Due to the vapori/ ation in the U-tubes, hot side pressure increases and this causes steam binding whi1h dete,iorates the refloodi g of the 1ore. Because the steam generation rate in the 1ore decreases due to the lo2 er reflood ,r te, liquid e trai- ent r d the steam binding ef0ect decrease, 1r using the reflood rate to i crease agr i" Through this cy1licr l process, the enti,e core e! entually becomes reflooded. The increase of core pressure due to the steam binding causes - r nometric os1illations between levels in the do21 omer and the core.

The early ,eflood period ends when SIT-FDs are emptied.

3.1.2.4 Late Reflood

The late reflood period begins when SIT-FDs are emptied. ECC water is supplied only 4y : <Ps during this period.

The water level in the do2 1o- er decreases somewhat as the SIT flo2 stops at the begi ing of this late reflood, r d falls 4elow the le! el of the cold legs. Then, the core water le! el becomes stabili/ ed. Liquid le! els i the do2 comer and 1ore be1o- e balanced ~~withi around 20 s~~ as shown in Figure 3-2. Due to the de1reased flo2 of coolant i to the do2 ncomer, liquid temperature i the do2 comer can increase to near sat. ration temperature due to the residual hea during this period structures, that is, ! essel walls in the do2 ncome,. Boiling can occur on the surface of the walls depending on the conditions" As enough ŎKK) is provided 4y t2 o :<Ps, the possibility of the do2 ncomer boili g is success0ully suppressed and the 1ore is found to remain amenable to cooling.

Because the entire core re- ains in a quenched state during this period, the stea- generation in the 1ore is not signi01ant eno. gh to cause a y severe ŎKK) by+ass. The core is found to be kept in r 1oolable 1ondition as shown in Figure 3-B"

3.2 Nuclear Power Plant Selection 6: tep 27

:# 3 and 4 2 ere selected as a reference. The main features are described in Chapter 1.

" Phenomena Identi01r tion and Ran5ing Table (Step *7

Phenomena identification a d ,r5 ing tr 4le (PIRT7is . sed to identi0y the major phenomena or processes that oc1., during the accident and to prioriti/ e them according to their ef0ects on primr, y safety co ce, "

The PIRT of Y PR1400 LwkGKY is based on “KN9 R P<RT"” KN9 R is i itialis- 0or “Korea Next 9 eneration Reacto,;” and it was ARP1400’s name during its developmental stage" The PIRT 2 as prepared by INŎČk in 2001[5] for KINS. Fo., characteristi1 ti- e periods of blo2 down, refill, early reflood, r d lr te reflood are s. - - arized in Tr ble 3-1. Y .- eric val. e is assig ed to each +hase as show below8

1: Blowdo2

2: Refill

3: Early reflood

4: Late reflood

Tƒ ble 3-1 Definition of Ti- e Periods

Period (Number)[L7]	Starts at	Ends at
Blowdown (1)	ẇ,eak initiatiǒ	˂ itiatiǒ o0:<T inʔe1tiǒ
Refill (27	End of blowdoʔǒ	Initiation of core recovery (~~liquid~~ level at the bottom of the f. el rods7
Early Re0ood (*7	End of refill	Ǒ d of SIT injectiǒ
Late Reflood (4)	Ǒ d of SIT injectiǒ	Stable core quench

mixture

[L7]The n.- bers indicated ï parentheses are used as indi1es in the PIRT table to denote each phase in that table.

RESPONSE TO AUDIT ISSUES

APR1400 Topical Reports

Korea Electric Power Corporation / Korea Hydro & Nuclear Power Co., LTD

Docket No. PROJ0782

Review Section	**TR Realistic Evaluation Methodology for LBLOCA of the APR1400**
Application Section	**Topical Report: APR1400-F-A-TR-12004 Realistic Evaluation Methodology for Large-Break LOCA of the APR1400**
Issue Date	**08/13/2015**

Audit Issues No. 18

The guidance in RG 1.157, Section 3.12.2 establishes acceptable controls for the calculation of mixture level in best estimate analysis. Table 3-2 of the topical report ranks [ ]^{TS} Since the RELAP5 fluid nodes are basically homogenous, a description of the approach (i.e., fine nodalization, level tracking, etc.) used to determine the mixture level in the APR1400 RELAP5/MOD3.3/K model is needed to better understand the PIRT and the reported results.

Response

As described in the section 4.2.2.1.2 of the topical report, [

]TS

The nodalization of the reactor vessel is important since this might affect those related processes. Section 4.2.1 of the topical report describes the reactor pressure vessel nodalizations, where the nodalizations of the each part of the vessel are described. Specifically, the core is modeled using [

]TS In fact, the fluid volume of RELAP5 is not “homogeneous”, but stratified option is used as a default option. Therefore, the basic function of the mixture level option, which considers the gas and two-phase mixture separately when the vertical flow stratification occurs, is reflected all the calculations in the topical report. It is expected that the mixture level option would not show significant differences from the stratification option.

In CAREM, the same noding scheme should be applied for all experimental assessment calculations and the plant calculation as well. The core noding determined above is applied to all code accuracy calculations. The peak cladding temperature predictions by the code are compared against the measured values and revealed that the code accuracy is very high. Based on this, it can be deduced that the current noding scheme is able to predict the mixture level reasonably well.

Impact on DCD

There is no impact on the DCD.

Impact on PRA

There is no impact on the PRA.

Impact on Technical Specifications

There is no impact on the Technical Specifications.

Impact on Technical/Topical/Environmental Report

There is no impact on any Technical, Topical, or Environmental Report.

RESPONSE TO AUDIT ISSUES

APR1400 Topical Reports

Korea Electric Power Corporation / Korea Hydro & Nuclear Power Co., LTD

Docket No. PROJ0782

Review Section	**TR Realistic Evaluation Methodology for LBLOCA of the APR1400**
Application Section	**Topical Report: APR1400-F-A-TR-12004 Realistic Evaluation Methodology for Large-Break LOCA of the APR1400**
Issue Date	**08/13/2015**

Audit Issues No. 19

NUREG/CR-5429, Section 2.1 establishes an acceptable approach for the documentation of the computer codes and associated interfaces. Table 3-5 of the topical report does not provide the entire picture of the presence of models and correlations in RELAP5/MOD3.3/K and CONTEMPT4/MOD5. Therefore:

a. A clear statement of all the phenomena that are treated by biases in Section 3.6.1 is needed.

Response

The phenomenon mentioned in Section 3.6.1 of the topical report as [

]TS RELAP5 describes two-phase flow using two-fluid, two-field equations, therefore, the [

]TS

There are two types of [

]TS

All phenomena that are treated as biases in the topical report are summarized in Table 1. The PIRT shown in Table 1 is modified from the PIRT in the topical report due to some errors that have been included. The complete modified APR1400 PIRT is given in association with audit issue no. 15.

Table 1. Modified APR1400 PIRT treated by biases TS

TS

Impact on DCD

There is no impact on the DCD.

Impact on PRA

There is no impact on the PRA.

Impact on Technical Specifications

There is no impact on the Technical Specifications.

Impact on Technical/Topical/Environmental Report

Topical report will be revised according to the PIRT revision.

There is no impact on any Technical or Environmental Report.

RESPONSE TO AUDIT ISSUES

APR1400 Topical Reports

Korea Electric Power Corporation / Korea Hydro & Nuclear Power Co., LTD

Docket No. PROJ0782

Review Section	**TR Realistic Evaluation Methodology for LBLOCA of the APR1400**
Application Section	**Topical Report: APR1400-F-A-TR-12004 Realistic Evaluation Methodology for Large-Break LOCA of the APR1400**
Issue Date	**08/13/2015**

Audit Issues No. 19

NUREG/CR-5429, Section 2.1 establishes an acceptable approach for the documentation of the computer codes and associated interfaces. Table 3-5 of the topical report does not provide the entire picture of the presence of models and correlations in RELAP5/MOD3.3/K and CONTEMPT4/MOD5. Therefore:

b. Table 3-5 of the topical report needs to include a column providing the status of the existence of model (“yes/no”) in RELAP5/MOD3.3/K and CONTEMPT4/MOD5 for each of the listed phenomenon.

Response

Second column of Table 3-5 in topical report shows important phenomena and processes related to each component. Third column shows the existing models in RELAP5/MOD3.3/K and CONTEMPT4/MOD5.

Impact on DCD

There is no impact on the DCD.

Impact on PRA

There is no impact on the PRA.

Impact on Technical Specifications

There is no impact on the Technical Specifications.

Impact on Technical/Topical/Environmental Report

There is no impact on any Technical, Topical, or Environmental Report.

RESPONSE TO AUDIT ISSUES

APR1400 Topical Reports

Korea Electric Power Corporation / Korea Hydro & Nuclear Power Co., LTD

Docket No. PROJ0782

Review Section	**TR Realistic Evaluation Methodology for LBLOCA of the APR1400**
Application Section	**Topical Report: APR1400-F-A-TR-12004 Realistic Evaluation Methodology for Large-Break LOCA of the APR1400**
Issue Date	**08/13/2015**

Audit Issues No. 20

The guidance in RG 1.157, Section 2.1.2 establishes acceptable controls for the calculation of the effects of noncondensible gases in best estimate analysis. In addition, NUREG/CR-5249 (pg. 68) explicitly addresses the bias due to dissolved nitrogen. The RELAP5/MOD3.3 code does not model dissolved nitrogen in the liquid and therefore, the predicted reflood peak cladding temperature does not reflect its effect. An assessment and documentation of the effect of dissolved nitrogen on the PCT is needed.

Response

Dissolved nitrogen release from SIT-FD was evaluated in Section 5.2 of Reference [1]. This report conservatively estimates mass and volume flow rate of dissolved nitrogen from SIT-FD and analyzes their effects on the fluidic device K-factors as shown in Figure 5.2-1 and Figure 5.2-2 of Reference [1]. The estimated mass and volume flow rate results of dissolved nitrogen are relatively small compared with those of ECCW from the SIT-FD. Especially, since SIT-FD of APR1400 has large amount of ECCW during high injection period, the impact of dissolved nitrogen on the refill phase duration can be insignificant.

In this response, sensitivity calculation is performed to evaluate dissolved nitrogen effects on the refill phase using APR1400 LBLOCA input deck. The amount of dissolved nitrogen is calculated based upon a few conservative assumptions that nitrogen gas is fully saturated in the water of SIT-FDs (nitrogen gas can be fully dissolved only near the water surface), amount of dissolved nitrogen in the water is proportional to partial pressure of nitrogen gas, and all dissolved nitrogen is released when the water from SIT-FDs is discharged through the DVI nozzle. In this calculation, pressure change in the tank is not considered and larger amount of dissolved nitrogen is released than the evaluated in Reference [1] to make the effects of dissolved nitrogen on downcomer hydraulics clearly and the conservative ECCW bypass phenomena.

Solubility of nitrogen gas at 303.15 K and atmospheric pressure is about 17 mg per one kilo-gram of water [2]. [

]TS

Four time-dependent volumes and junctions are used to simulate dissolved nitrogen gas release, and each set of time-dependent volume and junction installed at the same position of DVI. The amount of released nitrogen gas is controlled by control variable of RELAP and it refer to mass flow rates of SIT-FDs.

Most of the LBLOCA analysis results show that refill is ended at about 33 sec after break, thus, this study focuses on the time frame between initiation of break and 50 sec after.

Figure 1 shows the total dissolved nitrogen gas release rate from four SIT-FDs. The peak mass flow rate of dissolved nitrogen is about 2.7 kg/s, and this value exceeds the maximum value of Reference [1] as described above. This is intended to demonstrate the apparent effect of dissolved nitrogen on ECCW bypass.

Figure 2 shows core collapsed water level. Bottom of active core is about 2.5 m, and collapsed water level reaches that elevation at about 35 seconds in common. It means dissolved nitrogen gas has no effects on the refill phase duration. Since discharged water mass flow rate from SIT-FDs is large enough, dissolved nitrogen effects are negligible and this results is consistent with the above description.

Figure 3 shows accumulated break liquid mass flow through vessel side break to investigate ECCW bypass. Accumulated liquid break mass flow rates of both cases are similar, and it means that dissolved nitrogen effects on ECCW bypass are also insignificant.

As discussed above, the dissolved nitrogen has no effects during refill phase because dissolved

nitrogen gas release rate is relatively small and large amount of ECCW from SIT-FD are injected during APR1400 LBLOCA.

After 50 sec, the downcomer is filled and maintained with ECCW from SIT-FDs even though the dissolved nitrogen gas released, as shown in Figure 4. Therefore, the dissolved nitrogen gas has minimal effects on the core cooling and it can be concluded that additional bias on dissolved nitrogen is not considered in APR1400 LBLOCA analysis.

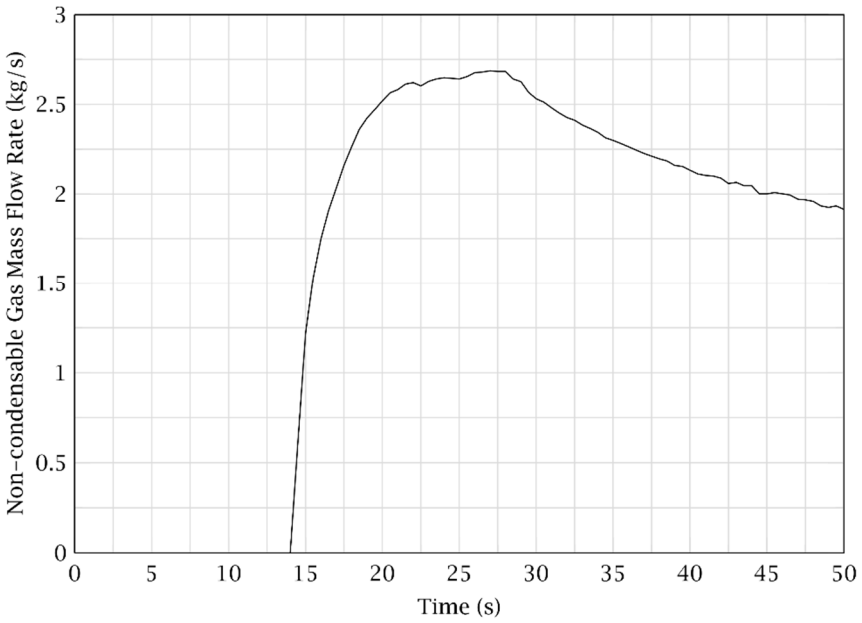

Figure 1. Total Nitrogen Gas Release Rate from Four SIT-FDs

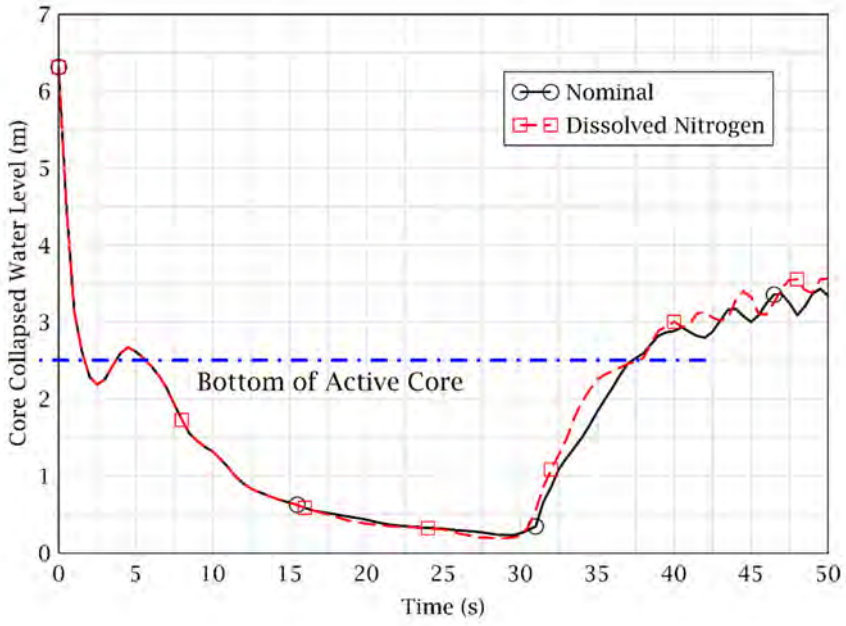

Figure 2. Core Collapsed Water Level

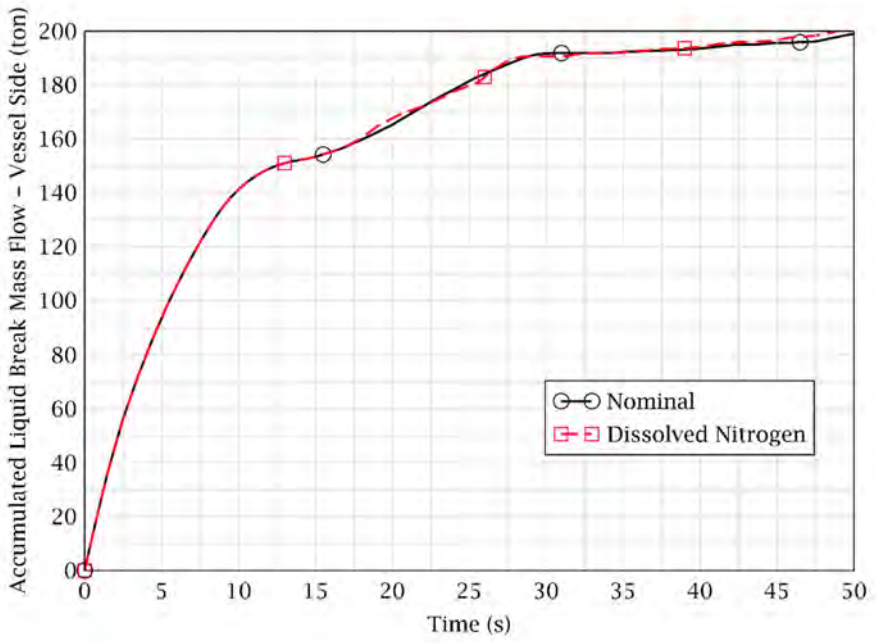

Figure 3. Accumulated Break Liquid Mass Flow Rate

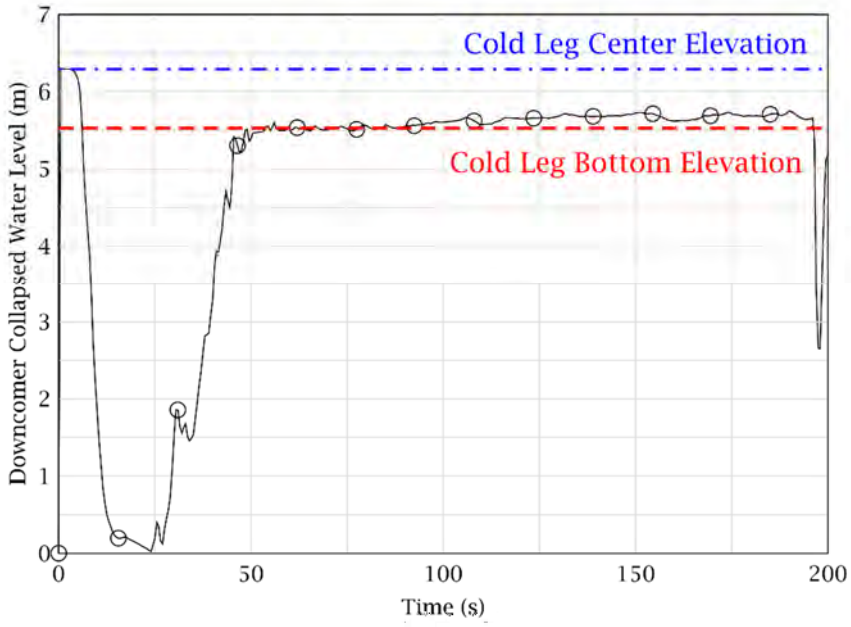

Figure 4. Downcomer Collapsed Water Level Result of Dissolved Nitrogen Injection Case

Reference

[1] KHNP, “Fluidic Device Design for the APR1400,” APR1400-Z-M-TR-12003-P, Rev. 0, December, 2012.

[2] Nikolay Ivanov Kolev, “Multiphase Flow Dynamics 4: Nuclear Thermal Hydraulics,” Springer, page 409, Fig. 11.6.

Impact on DCD

There is no impact on the DCD.

Impact on PRA

There is no impact on the PRA.

Impact on Technical Specifications

There is no impact on the Technical Specifications.

Impact on Technical/Topical/Environmental Report

There is no impact on any Technical, Topical, or Environmental Report.

RESPONSE TO AUDIT ISSUES

APR1400 Topical Reports

Korea Electric Power Corporation / Korea Hydro & Nuclear Power Co., LTD

Docket No. PROJ0782

Review Section	**TR Realistic Evaluation Methodology for LBLOCA of the APR1400**
Application Section	**Topical Report: APR1400-F-A-TR-12004 Realistic Evaluation Methodology for Large-Break LOCA of the APR1400**
Issue Date	**08/13/2015**

Audit Issues No. 21-a and b

NUREG/CR-5429, Section 2.1 establishes an acceptable approach for the documentation of the computer codes and associated interfaces. Address the following concerns related to Section 3.4 and Appendix B of the topical report:

a. Section 3.4 and Appendix B give the impression that all the changes made to the original RELAP5/MOD3.3 code are described in Appendix B. However, in response to prior requests for additional information (RAIs), documented in APR1400-F-A-RA-14001-P, it appears that additional changes have been made to RELAP5/MOD3.3, including the ability to input uncertainty variables. A complete characterization of all changes made to RELAP5/MOD3.3 for inclusion in Appendix B is needed.

b. A list of all changes that have been made to the original CONTEMPT5/MOD4 source code for the present application is needed.

Response a and b

As to Appendix B of the topical report, it only described model and error changes to the RELAP5/MOD3.3/K code which would affect the calculation results. Other than that, all the modifications made to the RELAP5/MOD3.3/K and CONTEMPT4/MOD5 codes were written down and managed in separated reports for each code. The modification reports are written in Korean and controlled by software management system.

Impact on DCD

There is no impact on the DCD.

Impact on PRA

There is no impact on the PRA.

Impact on Technical Specifications

There is no impact on the Technical Specifications.

Impact on Technical/Topical/Environmental Report

There is no impact on any Technical, Topical, or Environmental Report.

RESPONSE TO AUDIT ISSUES

APR1400 Topical Reports

Korea Electric Power Corporation / Korea Hydro & Nuclear Power Co., LTD

Docket No. PROJ0782

Review Section	**TR Realistic Evaluation Methodology for LBLOCA of the APR1400**
Application Section	**Topical Report: APR1400-F-A-TR-12004 Realistic Evaluation Methodology for Large-Break LOCA of the APR1400**
Issue Date	**08/13/2015**

Audit Issues No. 22-a

RG 1.157 outlines in many places that the results from best estimate calculations are to be considered acceptable provided their technical basis is demonstrated with appropriate data and analyses. Section 3.4 and Appendix B of the topical report discuss [

]^{TS} Appendix C provides a list of the FLECHT-SEASET tests for comparison to RELAP5/MOD3.3/K calculations, most of which have flooding rates larger than 25 cm/s. Address the following:

a. Provide results from the examination of the [ ]^{TS} against data from low flooding rate tests such as test 31805 and/or test 34006.

Response

As discussed in Appendix B, [

]TS

Code modification for [ ]TS is performed onto the original RELAP5/MOD3.3 code. And code assessments for the FLECHT-SEASET test 31805 and 34006 are performed.

Figure 1 and Figure 2 show the calculation results of the code with [ ]TS for test 31805 and 34006 with original calculation results of RELAP5/MOD3.3 code (named as current version), respectively. Since PCTs of both tests occurred at 78 inch elevation in common, calculation results of heat structure node [ ]TS are compared. And all measurement data installed at the same elevation of 78 inches in the test facility are presented. As shown in these figures, code modification for [ ]TS

TS

Figure 1. Effect of [ ]TS; FLECHT-SEASET Test 31805

TS

Figure 2. Effect of [ ]TS; FLECHT-SEASET Test 34006

Impact on DCD

There is no impact on the DCD.

Impact on PRA

There is no impact on the PRA.

Impact on Technical Specifications

There is no impact on the Technical Specifications.

Impact on Technical/Topical/Environmental Report

There is no impact on any Technical, Topical, or Environmental Report.

RESPONSE TO AUDIT ISSUES

APR1400 Topical Reports

Korea Electric Power Corporation / Korea Hydro & Nuclear Power Co., LTD

Docket No. PROJ0782

Review Section	**TR Realistic Evaluation Methodology for LBLOCA of the APR1400**
Application Section	**Topical Report: APR1400-F-A-TR-12004 Realistic Evaluation Methodology for Large-Break LOCA of the APR1400**
Issue Date	**08/13/2015**

Audit Issues No. 22-b

RG 1.157 outlines in many places that the results from best estimate calculations are to be considered acceptable provided their technical basis is demonstrated with appropriate data and analyses. Section 3.4 and Appendix B of the topical report discuss [

]^{TS} Appendix C provides a list of the FLECHT-SEASET tests for comparison to RELAP5/MOD3.3/K calculations, most of which have flooding rates larger than 25 cm/s. Address the following:

b. Figure 5-16 of the topical report shows the liquid velocity at the core inlet for the base case calculation. Provide the transient history (from 50 seconds onwards) for the liquid velocity at the core inlet for the base case calculation in sufficient detail to enable assessing the general flooding rate.

Response

Figure 1 shows the liquid velocity at the core inlet from 25 to 300 seconds of the base (nominal) calculation.

In Appendix C of the topical report, the flooding rates of FLECHT-SEASET tests for RELAP5/MOD3.3/K assessment are from 1.5 cm/s to 16.58 cm/s. Table 1 shows Table 2-1 of the Appendix C and the incorrect flooding rates will be revised.

Table 1 FLECHT-SEASET Tests Used for RELAP5/MOD3.3/K Assessment

Group	Run No.	System Pressure	Rod Temperature	Rod Power	Flooding Rate	Coolant Inlet Temperature	PCT* Elevation	PCT	Radial Power Distribution
		MPa	K	kW/m	cm/s	K	m (in)	K	-
Flooding Rate	31203 (1)	0.28	1145.15	2.3	38.4 → 3.84	325.15	1.93 (76)	1310.15	Uniform
	31302	0.28	1142.15	2.3	76.5 → 7.65	325.15	1.70 (67)	1205.15	Uniform
	31504 (2)	0.28	1136.15	2.3	24.6 → 2.46	324.15	1.98 (78)	1423.15	Uniform
	31701	0.28	1145.15	2.3	155 → 15.5	326.15	1.78 (70)	1196.15	Uniform
	31805	0.28	1144.15	2.3	21 → 2.1	324.15	1.98 (78)	1505.15	Uniform
System Pressure	31504	same as (2)							
	32013	0.41	1160.15	2.3	26.4 → 2.64	339.15	1.93 (76)	1444.15	Uniform
	34209	0.14	1162.15	2.4	27.2 → 2.72	305.15	1.98 (78)	1434.15	Uniform
Initial Clad Temperature	30518	0.28	529.15	2.3	38.9 → 3.89	325.15	1.98 (78)	926.15	Uniform
	30817	0.27	804.15	2.3	38.9 → 3.89	326.15	1.98 (78)	1105.15	Uniform
	31203	same as (1)							
	34420	0.27	1392.15	2.4	38.9 → 3.89	324.15	1.83 (72)	1480.15	Uniform
Initial Rod Peak Power	31021	0.28	1152.15	1.3	38.6 → 3.86	325.15	1.78 (70)	1214.15	Uniform
	31203	same as (1)							
	34524	0.28	1151.15	3	39.9 → 3.99	325.15	1.83 (72)	1477.15	Uniform
Others	31108	0.13	1144.15	2.3	79 → 7.9	306.15	1.78 (70)	1211.15	Uniform
	32235	0.14	1161.15	2.3	165.8/24.9/15.7 → 16.58/2.49/1.57	304.15	1.98 (78)	1419.15	Uniform
	32333	0.28	1162.15	2.3	162/21 → 16.2/2.1	326.15	1.93 (76)	1421.15	Uniform
	33338	0.28	1144.15	2.3/1.3	5.9/0.807 kg/s	325.15	1.78 (70)	1198.15	Uniform
	34006	0.27	1155.15	1.3	15 → 1.5	324.15	1.98 (78)	1436.15	Uniform

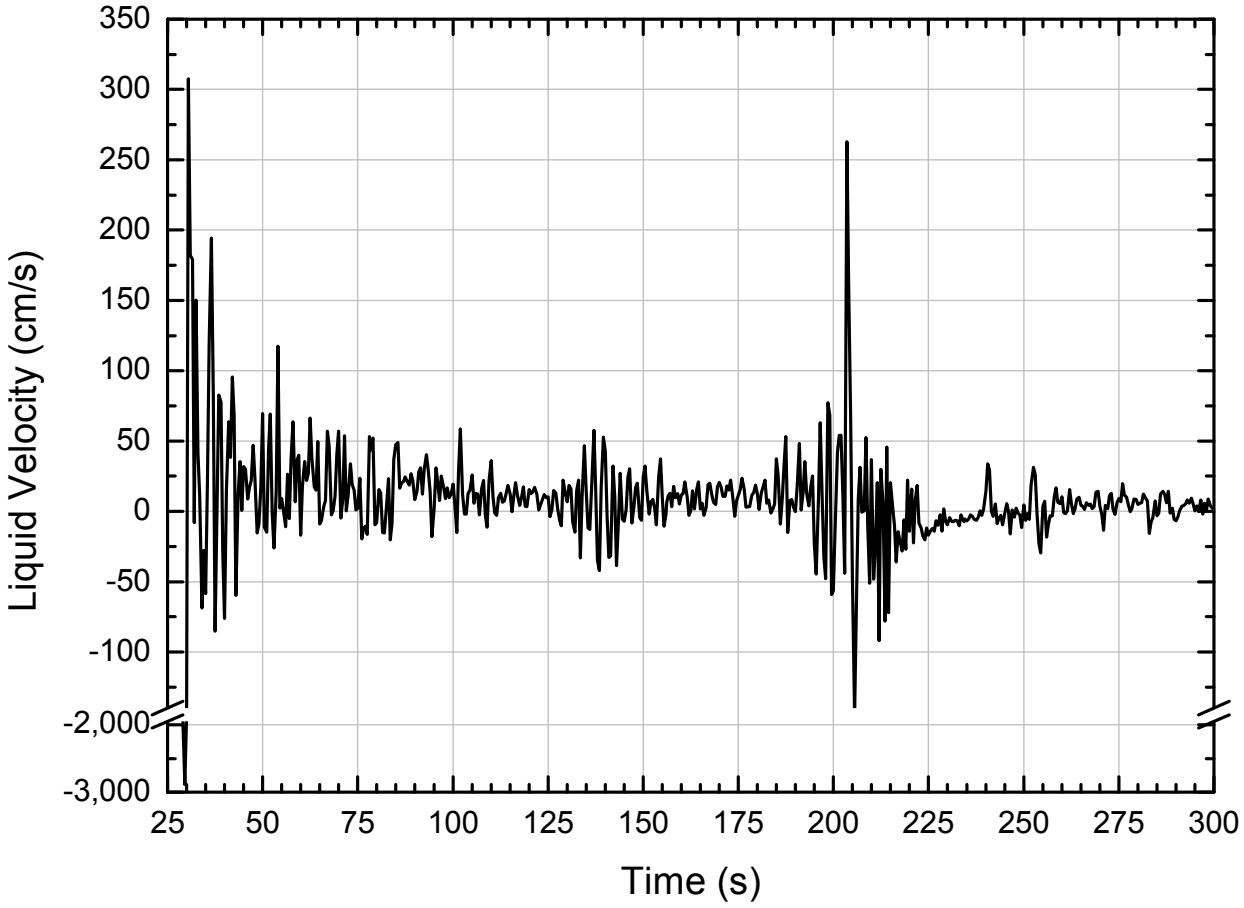

Figure 1. Liquid Velocity at the Core Inlet

Impact on DCD

There is no impact on the DCD.

Impact on PRA

There is no impact on the PRA.

Impact on Technical Specifications

There is no impact on the Technical Specifications.

Impact on Technical/Topical/Environmental Report

Topical report will be revised as discussed in this response.

There is no impact on Technical or Environmental Report.

RESPONSE TO AUDIT ISSUES

APR1400 Topical Reports

Korea Electric Power Corporation / Korea Hydro & Nuclear Power Co., LTD

Docket No. PROJ0782

Review Section	**TR Realistic Evaluation Methodology for LBLOCA of the APR1400**
Application Section	**Topical Report: APR1400-F-A-TR-12004 Realistic Evaluation Methodology for Large-Break LOCA of the APR1400**
Issue Date	**08/13/2015**

Audit Issues No. 23-a

The guidance in RG 1.157, Section 2.1.2 establishes acceptable controls regarding the accuracy of computational models in best estimate analysis. Section 3.4 and Appendix B of the topical report discuss the modification [ ]TS Figures 11 and 12 of Appendix B provide comparisons of the cladding temperature calculated with the modified code against the data for FLECHT-SEASET tests 31108 and 31504, respectively. The high flooding rate test (31108) shows an excellent comparison to the quench time at the PCT location. The low flooding rate test (31504) shows an under-prediction of the cladding temperature at the peak location and a delay in the quench time. Figure 14 of Appendix B provides a comparison of the calculated heat transfer coefficient against the data for test 31504. However, Figure 14 of Appendix B only shows the comparison beyond 200 seconds. Address the following:

a. Provide the heat transfer coefficient comparison for the time period of 50 to 200 seconds against the data for test 31504.

Response

Heat transfer coefficient predicted by the code for the time period of 50 to 200 sec is compared against the data for test 31504 in the following Figure 1. The heat transfer coefficient values of test 31504 are calculated from Equation 9 of Appendix B of the topical report.

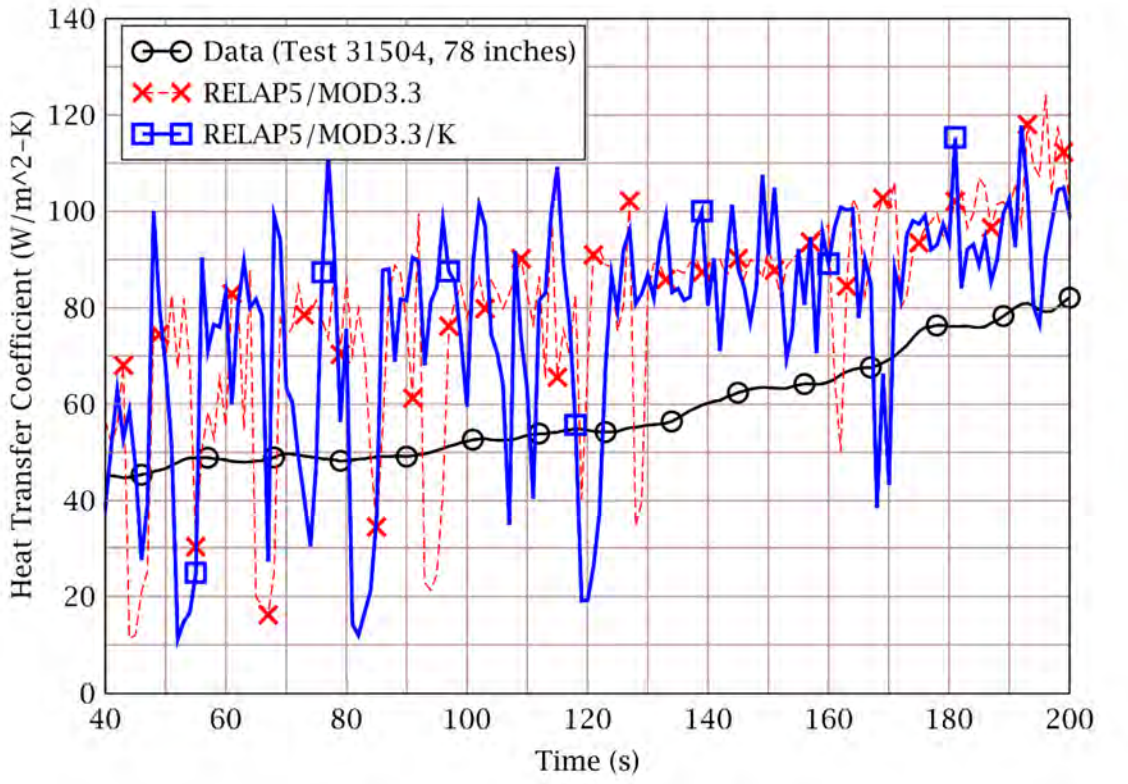

Figure 1. Heat Transfer Coefficient Comparison

Impact on DCD

There is no impact on the DCD.

Impact on PRA

There is no impact on the PRA.

Impact on Technical Specifications

There is no impact on the Technical Specifications.

Impact on Technical/Topical/Environmental Report

There is no impact on any Technical, Topical, or Environmental Report.

RESPONSE TO AUDIT ISSUES

APR1400 Topical Reports

Korea Electric Power Corporation / Korea Hydro & Nuclear Power Co., LTD

Docket No. PROJ0782

Review Section	**TR Realistic Evaluation Methodology for LBLOCA of the APR1400**
Application Section	**Topical Report: APR1400-F-A-TR-12004 Realistic Evaluation Methodology for Large-Break LOCA of the APR1400**
Issue Date	**08/13/2015**

Audit Issues No. 23-b

The guidance in RG 1.157, Section 2.1.2 establishes acceptable controls regarding the accuracy of computational models in best estimate analysis. Section 3.4 and Appendix B of the topical report discuss the modification [ ]TS Figures 11 and 12 of Appendix B provide comparisons of the cladding temperature calculated with the modified code against the data for FLECHT-SEASET tests 31108 and 31504, respectively. The high flooding rate test (31108) shows an excellent comparison to the quench time at the PCT location. The low flooding rate test (31504) shows an under-prediction of the cladding temperature at the peak location and a delay in the quench time. Figure 14 of Appendix B provides a comparison of the calculated heat transfer coefficient against the data for test 31504. However, Figure 14 of Appendix B only shows the comparison beyond 200 seconds. Address the following:

b. Provide the RELAP5/MOD3.3K calculated mass flow rates (liquid/vapor) for the elevation at which the peak temperature occurs for tests 31108 and 31504.

Response

The liquid and vapor mass flow rates for the elevation at which the peak temperature occurs for test 31108 are given in Figure 1 and 2, respectively. The peak temperature occurs at [ ]^{TS} node in test 31108, thus the junction number [ ]^{TS}, which is the nearest junction from the node is plotted. Time period of 0 to 200 s are employed consistently with the test period.

The liquid and vapor mass flow rates for the test 31504 are shown in Figure 3 and 4, respectively. In these Figures, the junction number [ ]^{TS} is plotted for the time period of 0 to 400 s due to the same reason as the above.

In those figures above, hot channel data are presented in common.

TS

Figure 1. Liquid Mass Flow Rate at [ ]TS Junction for Test 31108

TS

Figure 2. Vapor Mass Flow Rate at [ ]TS Junction for Test 31108

TS

Figure 3. Liquid Mass Flow Rate at [ ]TS Junction for Test 31504

TS

Figure 4. Vapor Mass Flow Rate at [ ]TS Junction for Test 31504

Impact on DCD

There is no impact on the DCD.

Impact on PRA

There is no impact on the PRA.

Impact on Technical Specifications

There is no impact on the Technical Specifications.

Impact on Technical/Topical/Environmental Report

There is no impact on any Technical, Topical, or Environmental Report.

RESPONSE TO AUDIT ISSUES

APR1400 Topical Reports

Korea Electric Power Corporation / Korea Hydro & Nuclear Power Co., LTD

Docket No. PROJ0782

Review Section	**TR Realistic Evaluation Methodology for LBLOCA of the APR1400**
Application Section	**Topical Report: APR1400-F-A-TR-12004 Realistic Evaluation Methodology for Large-Break LOCA of the APR1400**
Issue Date	**08/13/2015**

Audit Issues No. 23-c

The guidance in RG 1.157, Section 2.1.2 establishes acceptable controls regarding the accuracy of computational models in best estimate analysis. Section 3.4 and Appendix B of the topical report discuss the modification [ ]TS Figures 11 and 12 of Appendix B provide comparisons of the cladding temperature calculated with the modified code against the data for FLECHT-SEASET tests 31108 and 31504, respectively. The high flooding rate test (31108) shows an excellent comparison to the quench time at the PCT location. The low flooding rate test (31504) shows an under-prediction of the cladding temperature at the peak location and a delay in the quench time. Figure 14 of Appendix B provides a comparison of the calculated heat transfer coefficient against the data for test 31504. However, Figure 14 of Appendix B only shows the comparison beyond 200 seconds. Address the following:

c. Provide results from the examination of the final combined heat transfer coefficient compared with data for FLECHT-SEASET test 31805 and/or test 34006.

Response

Figure 1 and Figure 2 show calculated cladding temperature at 78 inches against experimental data for test 31805 and 34006, respectively. In the figures, calculated data are [ ]^{TS} node results of hot channel heat structure which includes 78 inches measurement elevation.

Figure 3 and Figure 4 show calculated heat transfer coefficients at the same node against experimental data for test 31805 and 34006, respectively. Since several measurements are installed at the same elevation in the test, several heat transfer coefficients are obtained. Thus, average, maxima, and minima values of test data are presented in those figures.

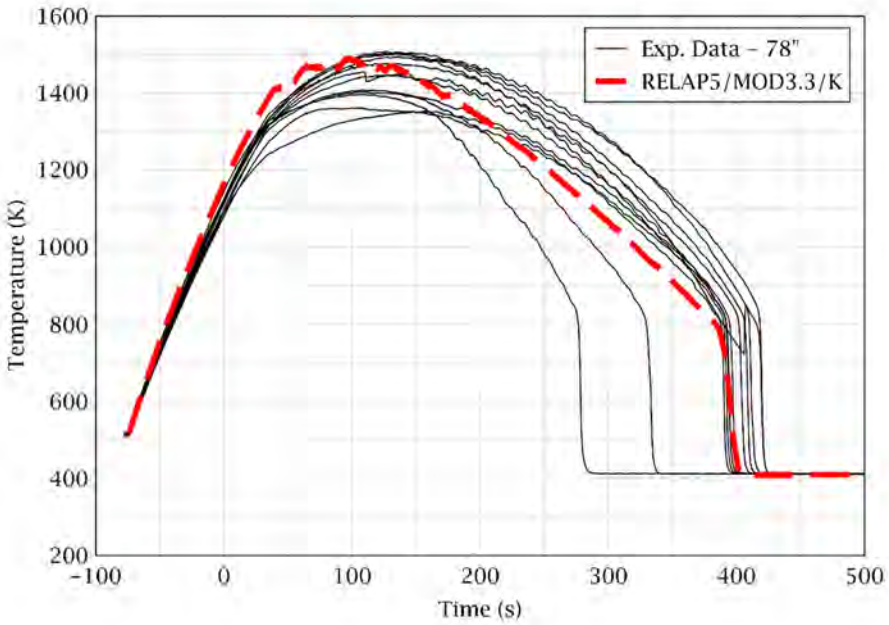

Figure 1. Cladding Temperature Comparison for Test 31805

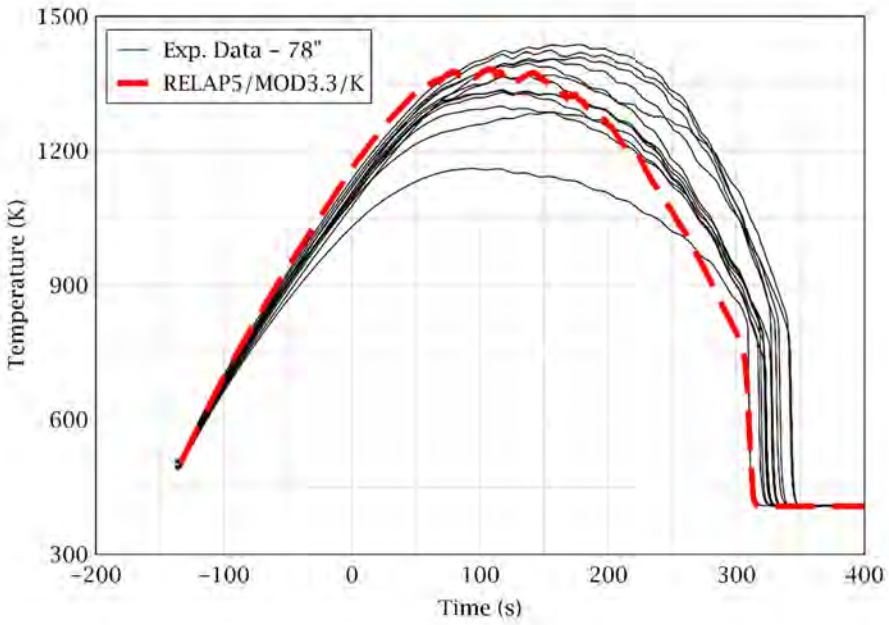

Figure 2. Cladding Temperature Comparison for Test 34006

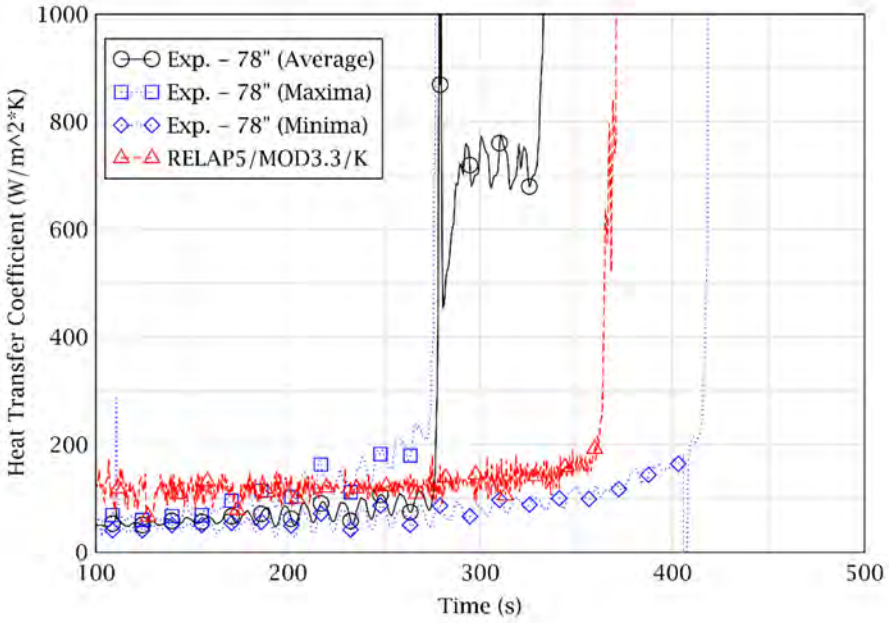

Figure 3. Heat Transfer Coefficient Comparison for Test 31805

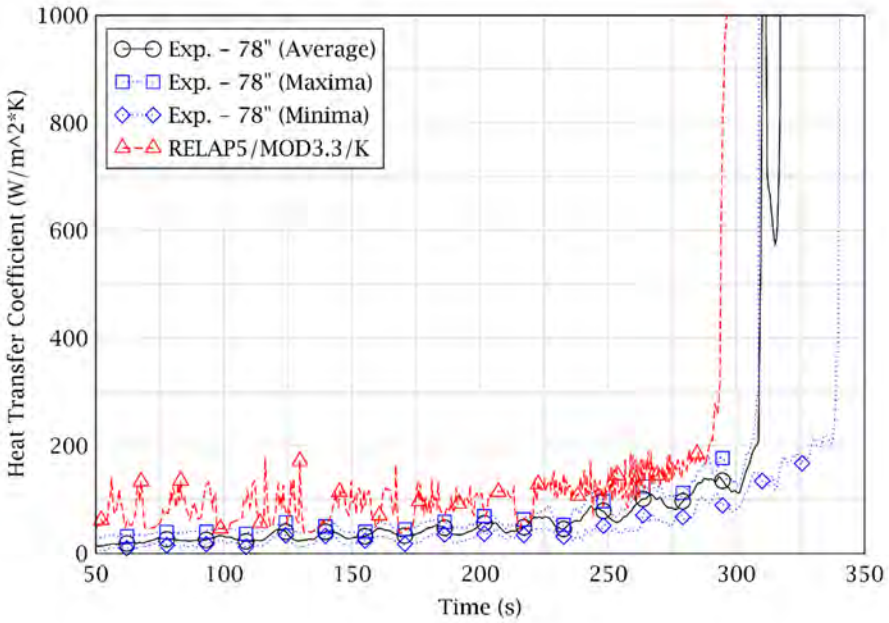

Figure 4. Heat Transfer Coefficient Comparison for Test 34006

Impact on DCD

There is no impact on the DCD.

Impact on PRA

There is no impact on the PRA.

Impact on Technical Specifications

There is no impact on the Technical Specifications.

Impact on Technical/Topical/Environmental Report

There is no impact on any Technical, Topical, or Environmental Report.

RESPONSE TO AUDIT ISSUES

APR1400 Topical Reports

Korea Electric Power Corporation / Korea Hydro & Nuclear Power Co., LTD

Docket No. PROJ0782

Review Section	**TR Realistic Evaluation Methodology for LBLOCA of the APR1400**
Application Section	**Topical Report: APR1400-F-A-TR-12004 Realistic Evaluation Methodology for Large-Break LOCA of the APR1400**
Issue Date	**08/13/2015**

Audit Issues No. 23-d

The guidance in RG 1.157, Section 2.1.2 establishes acceptable controls regarding the accuracy of computational models in best estimate analysis. Section 3.4 and Appendix B of the topical report discuss the modification [ ]^{TS} Figures 11 and 12 of Appendix B provide comparisons of the cladding temperature calculated with the modified code against the data for FLECHT-SEASET tests 31108 and 31504, respectively. The high flooding rate test (31108) shows an excellent comparison to the quench time at the PCT location. The low flooding rate test (31504) shows an under-prediction of the cladding temperature at the peak location and a delay in the quench time. Figure 14 of Appendix B provides a comparison of the calculated heat transfer coefficient against the data for test 31504. However, Figure 14 of Appendix B only shows the comparison beyond 200 seconds. Address the following:

d. The code modification [

]^{TS} based on Figure 5 of Appendix B. Assuming the flow rate is accurately predicted, the underprediction of heat transfer should translate into an over-prediction of the cladding temperature. However, the cladding temperature is under-predicted for the low reflood rate test (Figure 12 of Appendix B) implying that another mechanism may be responsible. This is also true for test 34006 as shown in Appendix C. If the APR1400 calculated flooding rate is low, the calculated cladding temperature will be lower than that calculated if a better or more realistic heat transfer coefficient is utilized. A justification for the code modification that enables a best-estimate representation is needed.

Response

As described in the response to audit issue number 23-c, RELAP5/MOD3.3/K code predicts heat transfer coefficient (HTC) higher than FLECHT-SEASET test 31805 and 34006 during the film boiling region whereas, the results of the test 31108 which has relatively high reflood rate show low HTC and high PCT as expected. The under-prediction of cladding temperature for test 34006 is caused by over-prediction of HTC when the maximum data is compared only. However, when all measurement data are compared with code result, it is concluded that core predicts cladding temperature reasonably well. And also, in spite of these under-predictions of the maximum cladding temperatures for low reflood rate tests, the SRS calculations of FLECHT-SEASET tests show that the code predictions with uncertainty parameters can cover the experimental data well.

On the other hand, as discussed in the response to the audit issue number 22-b, predicted reflood rate of the APR1400 nominal case is about 10 cm/s during early reflood period. This value is high compared to FLECHT-SEASET test conditions, hence, it is expected that code predicts clad temperature properly.

Impact on DCD

There is no impact on the DCD.

Impact on PRA

There is no impact on the PRA.

Impact on Technical Specifications

There is no impact on the Technical Specifications.

Impact on Technical/Topical/Environmental Report

There is no impact on any Technical, Topical, or Environmental Report.

RESPONSE TO AUDIT ISSUES

APR1400 Topical Reports

Korea Electric Power Corporation / Korea Hydro & Nuclear Power Co., LTD

Docket No. PROJ0782

Review Section	**TR Realistic Evaluation Methodology for LBLOCA of the APR1400**
Application Section	**Topical Report: APR1400-F-A-TR-12004 Realistic Evaluation Methodology for Large-Break LOCA of the APR1400**
Issue Date	**08/13/2015**

Audit Issues No. 23-e

The caption for Figure 12 in Appendix B is incorrect. It refers to FLECHT-SEASET Test 31504 instead of 31108.

Response

The caption for Figure 12 in Appendix B is corrected as follows.

Before	After
Figure 12 Comparison of Rod Cladding Temperature; FLECHT-SEASET ***31108***	Figure 12 Comparison of Rod Cladding Temperature; FLECHT-SEASET ***31504***

The revised topical report will be submitted later.

Impact on DCD

There is no impact on the DCD.

Impact on PRA

There is no impact on the PRA.

Impact on Technical Specifications

There is no impact on the Technical Specifications.

Impact on Technical/Topical/Environmental Report

The revised topical report will be submitted later.

RESPONSE TO AUDIT ISSUES

APR1400 Topical Reports

Korea Electric Power Corporation / Korea Hydro & Nuclear Power Co., LTD

Docket No. PROJ0782

Review Section	**TR Realistic Evaluation Methodology for LBLOCA of the APR1400**
Application Section	**Topical Report: APR1400-F-A-TR-12004 Realistic Evaluation Methodology for Large-Break LOCA of the APR1400**
Issue Date	**08/13/2015**

Audit Issues No. 24

The guidance in RG 1.157, Section 2.1.2 establishes acceptable controls regarding the accuracy of computational models in best estimate analysis. Appendix B of the topical report states that the [

]^{TS} Provide the basis for performing the modification [

]^{TS} to that of the earlier version. Include discussion of the accuracy of the models.

Response

Volume I, Chapter 4.11 of reference [1] describes [ ]TS of RELAP5/MOD3.3. [

]TS

Code manual mentions that [ ]TS of RELAP5/MOD3.3 code is based on a [ ]TS Whereas, any reasonable reason for modification of [ ]TS isn't mentioned. Thus, it is determined to modify [ ]TS In addition, it is considered that code modification for [ ]TS has limited effects because [ ]TS are adjusted to the analysis results of [ ]TS in the CAREM, that is, [ ]TS doesn't change.

Reference

[1] “RELAP5/MOD3.3 Code Manual Volume I: Code Structure, System Models, and Solution Methods,” NUREG/CR-5535, Rev P3, U.S.NRC, March 2003.

[2] “RELAP5/MOD3.3 Code Manual Volume IV: Models and Correlations,” NUREG/CR-5535, Rev P3, U.S.NRC, March 2006.

Impact on DCD

There is no impact on the DCD.

Impact on PRA

There is no impact on the PRA.

Impact on Technical Specifications

There is no impact on the Technical Specifications.

Impact on Technical/Topical/Environmental Report

There is no impact on any Technical, Topical, or Environmental Report.

RESPONSE TO AUDIT ISSUES

APR1400 Topical Reports

Korea Electric Power Corporation / Korea Hydro & Nuclear Power Co., LTD

Docket No. PROJ0782

Review Section	**TR Realistic Evaluation Methodology for LBLOCA of the APR1400**
Application Section	**Topical Report: APR1400-F-A-TR-12004 Realistic Evaluation Methodology for Large-Break LOCA of the APR1400**
Issue Date	**08/13/2015**

Audit Issues No. 25

NUREG/CR-5429, Section 2.1.4 discusses controls over code versions and changes that could affect best estimate calculations. The effects of the modifications to RELAP5/MOD/3.3 have been demonstrated using either SET data (from the FLETCH- SEASET tests) or APR1400 plant simulations in Appendix B. The APR1400 simulations show the comparison of results before and after a particular modification [ ]^{TS} is made. However, a comparison of results for either the APR1400 plant or an integral test using RELAP5/MOD3.3 and RELAP5/MOD3.3/K (with all changes present in the frozen code version) is missing. Provide such a comparison.

Response

Figure 1 ~ Figure 4 show cladding temperature comparisons of high power region calculated by RELAP5/MOD3.3 and modified RELAP5/MOD3.3 (RELAP5/MOD3.3/K) for LOFT L2-2 test. Code inputs for each code are different because user input for [ ]TS is modified to match [ ]TS described in Appendix B of the topical report. But the other user input data are the same.

In these figures, blowdown PCTs are similar with each other because initial fuel average temperatures are similar and major code modifications have effects on reflood period. And reflood PCTs are also similar with each other, but reflood quenching time is delayed in common.

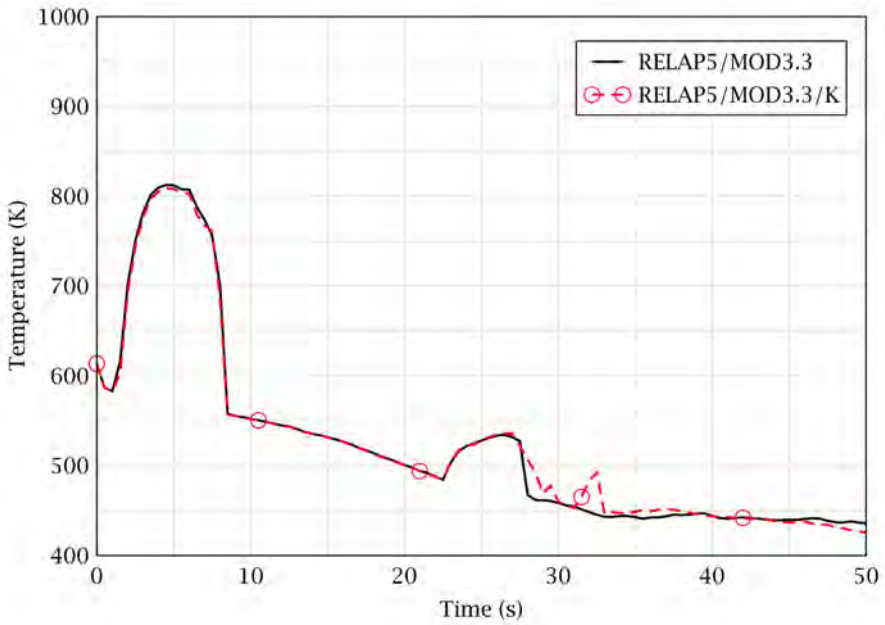

Figure 1. Cladding Temperature Comparison of Node 2 Elevation for LOFT L2-2 Test

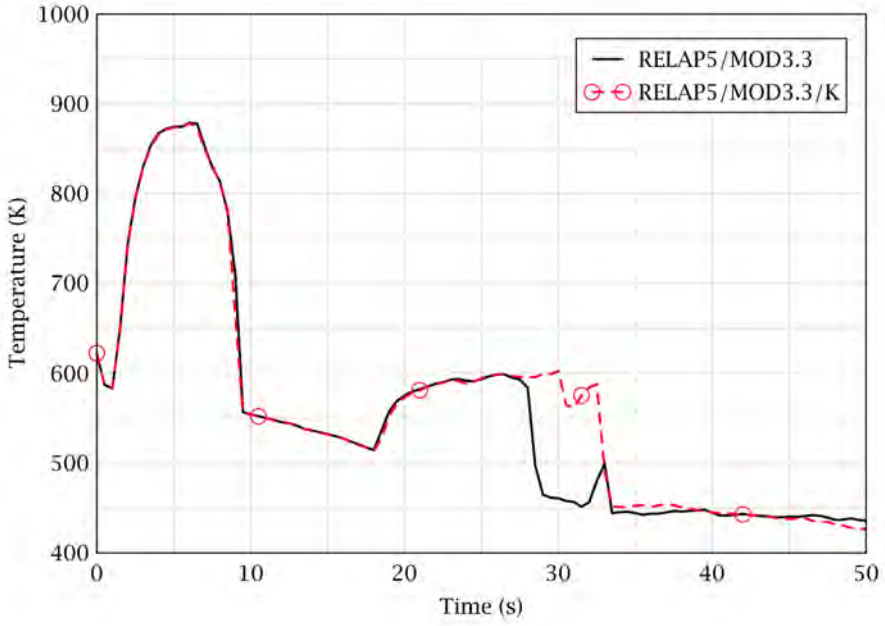

Figure 2. Cladding Temperature Comparison of Node 3 Elevation for LOFT L2-2 Test

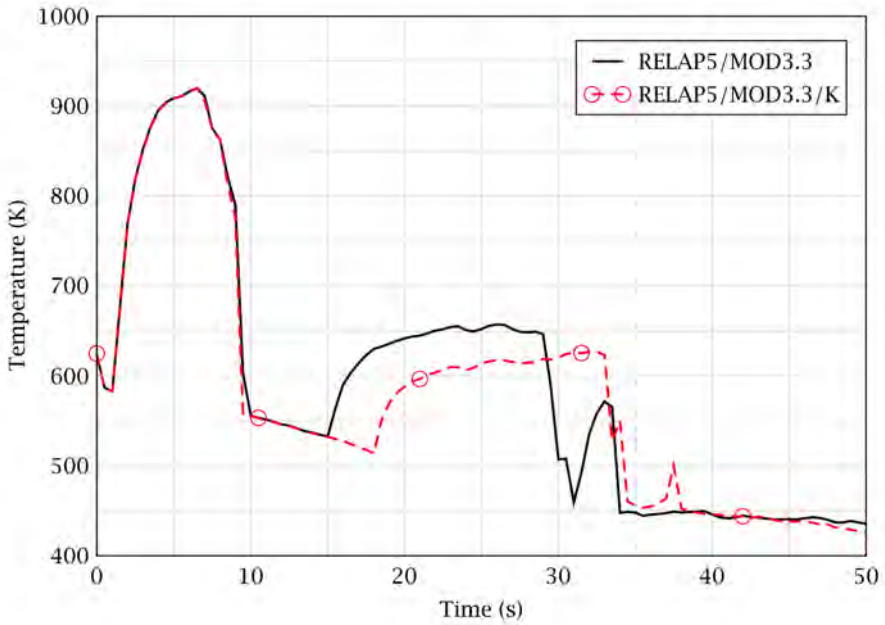

Figure 3. Cladding Temperature Comparison of Node 4 Elevation for LOFT L2-2 Test

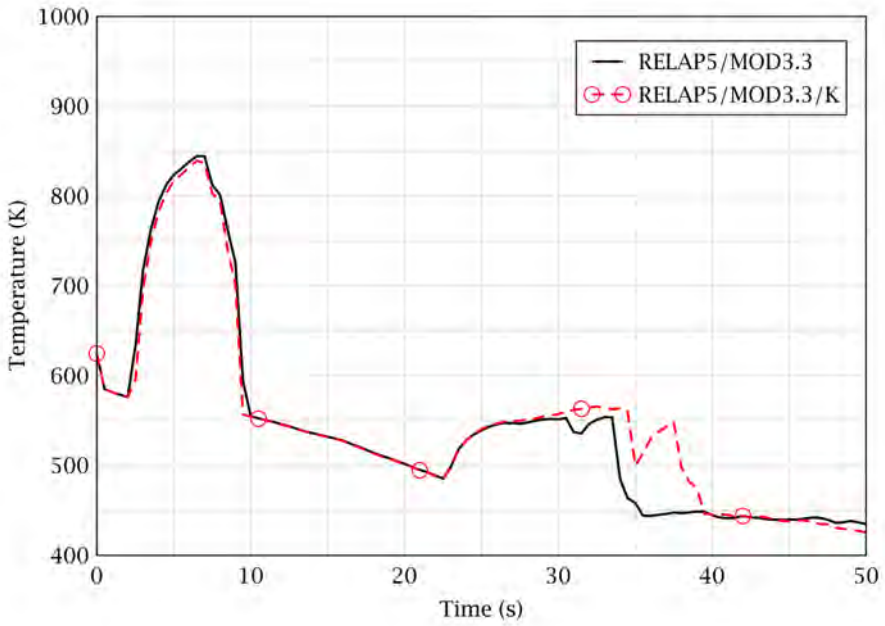

Figure 4. Cladding Temperature Comparison of Node 5 Elevation for LOFT L2-2 Test

Impact on DCD

There is no impact on the DCD.

Impact on PRA

There is no impact on the PRA.

Impact on Technical Specifications

There is no impact on the Technical Specifications.

Impact on Technical/Topical/Environmental Report

There is no impact on any Technical, Topical, or Environmental Report.

RESPONSE TO AUDIT ISSUES

APR1400 Topical Reports

Korea Electric Power Corporation / Korea Hydro & Nuclear Power Co., LTD

Docket No. PROJ0782

Review Section	**TR Realistic Evaluation Methodology for LBLOCA of the APR1400**
Application Section	**Topical Report: APR1400-F-A-TR-12004 Realistic Evaluation Methodology for Large-Break LOCA of the APR1400**
Issue Date	**08/13/2015**

Audit Issues No. 26

SRP 15.0.2 Section 2.5 requires that the EM be placed under a quality assurance program that meets the requirements of 10 CFR 50 Appendix B. Confirm that the RELAP5/MOD3.3/K EM for LBLOCA is controlled in this manner. Also provide details of the code modification quality assurance program in place to confirm that the changes to RELAP5/MOD3.3 are correctly implemented and that the remainder of the source code is not altered. Furthermore, explain the use of the term “frozen” and how this affects the current submittal and future use in various licensing calculations.

Response

Design procedure enclosed is used for the control of the design computer code and meets the requirements of 10 CFR 50 Appendix B. The RELAP5/MOD3.3/K is controlled by the configuration management system for design computer code. The captured picture for configuration management system is also enclosed.

The terminology ‘frozen’ comes from NUREG/CR-5249, which states “frozen code does not allow model enhancements and code improvements during the analysis period”. The frozen code is applied to the current submittal and future use in licensing calculations.

Impact on DCD

There is no impact on the DCD.

Impact on PRA

There is no impact on the PRA.

Impact on Technical Specifications

There is no impact on the Technical Specifications.

Impact on Technical/Topical/Environmental Report

There is no impact on any Technical, Topical, or Environmental Report.

한전원자력연료

설 계 관 리 절 차 서

DESIGN CONTROL PROCEDURE

제 목 : 설계 전산코드 관리

SUBJECT : Design computer code control

A4(210x297)

TS

TS

TS

TS

TS

TS

Non-Proprietary

TS

TS

RESPONSE TO AUDIT ISSUES

APR1400 Topical Reports

Korea Electric Power Corporation / Korea Hydro & Nuclear Power Co., LTD

Docket No. PROJ0782

Review Section	**TR Realistic Evaluation Methodology for LBLOCA of the APR1400**
Application Section	**Topical Report: APR1400-F-A-TR-12004 Realistic Evaluation Methodology for Large-Break LOCA of the APR1400**
Issue Date	**08/13/2015**

Audit Issues No. 27-a

NUREG/CR-5429, Section 2.2.2 discusses issues related to model nodalization. Address the following issues regarding nodalization of the APR1400:

a. Section 4.2.1 of the topical report states that the APR1400 nodalization of the reactor vessel "...follows the typical pressurized water reactor nodalization..." Provide additional details to support this assertion. Furthermore, as specified by RG 1.157, provide a reference for the documentation related to the nodalization sensitivity studies that were performed in order to determine the final APR1400 RELAP5 nodalization that will be used for licensing calculations.

Response

In order to determine the nodalization of the APR1400 plant, CAREM refers to the code assessments related to the nodalization, nodalization examples and the code user guideline and those are described in Reference [1] and [2]. Also, code assessments using SET and IET of the assessment matrix are considered. The applicability of the selected nodalization is also confirmed by the experimental assessments described in Appendices of the topical report.

In addition to that, Audit Issues No. 27 contained several questions related to the nodalization for APR1400 plant, and our responses to each question includes a basis to select reactor vessel nodalization and the results of the sensitivity study. The specific nodalization and its supporting details can be found in our responses to the audit issues and reference as follows.

- Downcomer nodalization: Audit Issues No. 27-b and c
- [ ]^{TS}: Audit Issues No. 27-d and e
- Core axial nodalization: Audit Issues No. 27-g
- Nodalization below the downcomer skirt: Audit Issues No. 27-h
- Axial nodalization of the upper downcomer: Audit Issues No. 27-j
- Upper guide structure: Reference [3]

Reference

[1] RELAP5/MOD3.3 Code Manual Volume III: Developmental Assessment Problems," Nuclear Systems Analysis Division, March 2006.

[2] "RELAP5/MOD3.3 Code Manual Volume V: User's Guideline," Nuclear Systems Analysis Division, March 2006.

[3] "Modification of LBLOCA Best-Estimate Evaluation Methodology of APR1400 Typ3 Nuclear Power Plants (2012)," KNF-TR-SGA-12005, KNF, September 2012.

Impact on DCD

There is no impact on the DCD.

Impact on PRA

There is no impact on the PRA.

Impact on Technical Specifications

There is no impact on the Technical Specifications.

Impact on Technical/Topical/Environmental Report

There is no impact on any Technical, Topical, or Environmental Report.

RESPONSE TO AUDIT ISSUES

APR1400 Topical Reports

Korea Electric Power Corporation / Korea Hydro & Nuclear Power Co., LTD

Docket No. PROJ0782

Review Section	**TR Realistic Evaluation Methodology for LBLOCA of the APR1400**
Application Section	**Topical Report: APR1400-F-A-TR-12004 Realistic Evaluation Methodology for Large-Break LOCA of the APR1400**
Issue Date	**08/13/2015**

Audit Issues No. 27-b, c

NUREG/CR-5429, Section 2.2.2 discusses issues related to model nodalization. Address the following issues regarding nodalization of the APR1400:

b. [ ]TS have been chosen to represent the downcomer based on [ ]TS However, no information is provided as to what phenomena were investigated. Moreover, the ECCS bypass is introduced [ ]TS and is not dependent on the nodalization of the downcomer. List the applicable phenomena considered.

c. No evidence is provided to support the assertion that the selected nodalization for the downcomer [ ]TS requested in part (b) as asserted in the topical report. Address this concern.

Response

In modeling the downcomer, a multi-channel downcomer modeling technique is used where, [ ]TS in CAREM. The reason for this is to preserve [ ]TS explicitly. It is required to model the downcomer by azimuthally divided [ ]TS of the APR1400. Figure 1 shows the nodalization of reactor vessel downcomer in a circumferential direction. The reason for this is to [

]TS which may occur during refill and reflood periods. The [ ]TS addressed in the topical report would be the ECCS bypass. The ECC bypass ratio, level at the downcomer, break flow, etc. are the phenomena of concerns. Since [

]TS

The assertions on the selected nodalization for the downcomer are performed by adjusting the consistent nodalization scheme in modeling various experimental facilities. Consequently, the code calculation results show reasonably good predictions of the experimental results.

TS

Figure 1. Nodalization of Reactor Vessel Downcomer in a Circumferential Direction

Impact on DCD

There is no impact on the DCD.

Impact on PRA

There is no impact on the PRA.

Impact on Technical Specifications

There is no impact on the Technical Specifications.

Impact on Technical/Topical/Environmental Report

There is no impact on any Technical, Topical, or Environmental Report.

RESPONSE TO AUDIT ISSUES

APR1400 Topical Reports

Korea Electric Power Corporation / Korea Hydro & Nuclear Power Co., LTD

Docket No. PROJ0782

Review Section	**TR Realistic Evaluation Methodology for LBLOCA of the APR1400**
Application Section	**Topical Report: APR1400-F-A-TR-12004 Realistic Evaluation Methodology for Large-Break LOCA of the APR1400**
Issue Date	**08/13/2015**

Audit Issues No. 27-d

NUREG/CR-5429, Section 2.2.2 discusses issues related to model nodalization. Address the following issues regarding nodalization of the APR1400:

d. RG 1.157 states that "…one-dimensional approximations to three-dimensional phenomena will be considered if those approximations are properly justified." [

]TS The lower power peripheral fuel assemblies are also not represented separately. It is unclear how this nodalization was selected over other options and how it can model multidimensional phenomena (e.g., "upper plenum to core counter-current flows (CCF)" in topical report Table 3-2). Provide the basis for the selected nodalization with respect to capturing the multidimensional phenomena occurring in the core.

Response

[

]TS

Multidimensional flows can be broadly classified into two phenomena. First, higher vapor velocities and liquid entrainment occur in the higher power region of the core. The entrained liquid from the core is carried into the upper plenum, where it is de-entrained, forming a two phase pool. The liquid from the pool can reenter the lower power region of the core due to the lower vapor velocities in those regions. [

]TS The modeling of the core is not intended to consider the multidimensional phenomena of the core, but to consider the harsh condition that may occur in the nearest region of the hottest rod. In case of APR1400 plant, multidimensional phenomena is not significant from the following reasons.

- [
-
-

]TS

Figure 1 shows the mass flow rate at the hot channel exit and it can be seen that some down flow occurs during reflood period. In order to confirm the effect of the down flow, sensitivity calculation was performed by limiting the down flow. For the limitation of the down flow, the reverse K-factor of the junction connecting the hot channel exit and upper plenum was assumed to be very large value. Figure 2 through 4 compare the mass flow rate at the core exit, heat transfer mode and cladding surface temperature at the PCT node respectively. During the reflood period, the heat transfer mode is film boiling until core quench. During film boiling period, heat transfer between wall and liquid is very low because the liquid does not contact directly to the wall. Therefore, even though there is some down flow at the upper region of the hot channel, it does not affect the cladding temperature as shown in Figure 4.

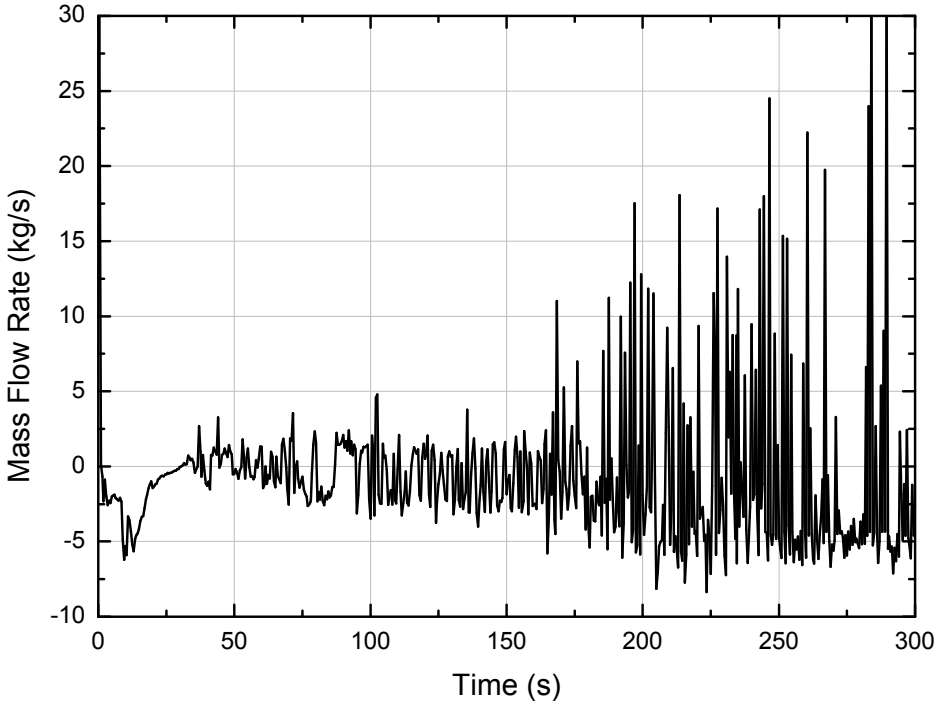

Figure 1. Mass Flow Rate at Hot Channel Exit – Original Calculation

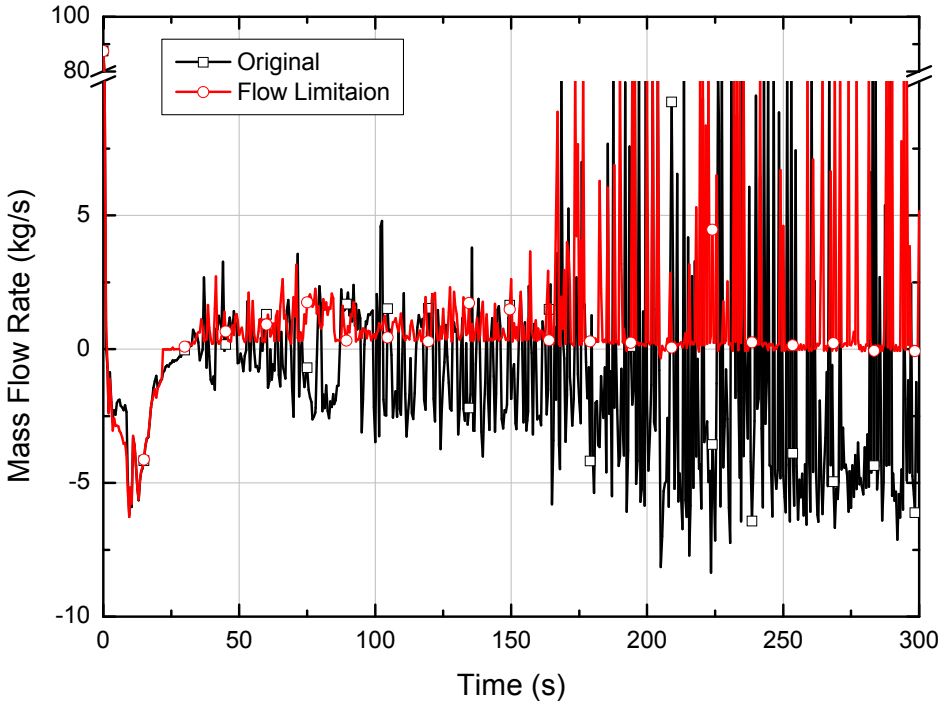

Figure 2. Comparison of Mass Flow Rate – Original vs. Flow Limitation

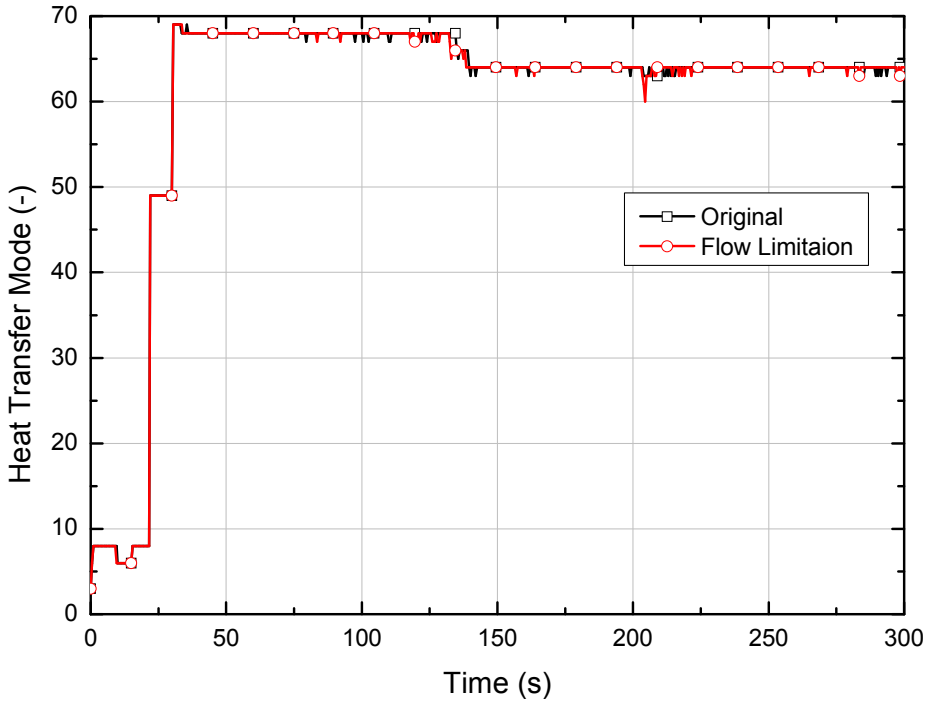

Figure 3. Comparison of Heat Transfer Mode – Original vs. Flow Limitation

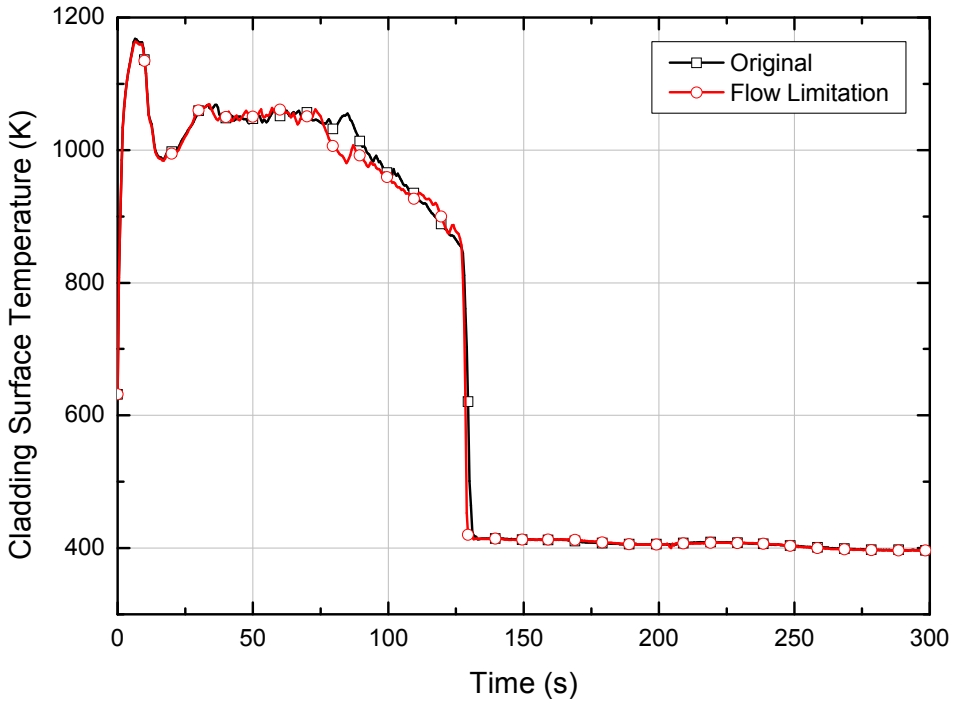

Figure 4. Comparison of Cladding Surface Temperature – Original vs. Flow Limitation

Impact on DCD

There is no impact on the DCD.

Impact on PRA

There is no impact on the PRA.

Impact on Technical Specifications

There is no impact on the Technical Specifications.

Impact on Technical/Topical/Environmental Report

There is no impact on any Technical, Topical, or Environmental Report.

RESPONSE TO AUDIT ISSUES

APR1400 Topical Reports

Korea Electric Power Corporation / Korea Hydro & Nuclear Power Co., LTD

Docket No. PROJ0782

Review Section	**TR Realistic Evaluation Methodology for LBLOCA of the APR1400**
Application Section	**Topical Report: APR1400-F-A-TR-12004 Realistic Evaluation Methodology for Large-Break LOCA of the APR1400**
Issue Date	**08/13/2015**

Audit Issues No. 27-e

NUREG/CR-5429, Section 2.2.2 discusses issues related to model nodalization. Address the following issues regarding nodalization of the APR1400:

e. Section 4.3.1.1 of NUREG/CR-5249 discusses the use of different nodalizations in the core to evaluate the hot channel bias. The topical report does not document or discuss such sensitivity studies. The selected nodalization may also overestimate the cross-flow into the hot assembly from the surrounding assemblies which is non-conservative for PCT calculation. Provide the basis for the selected radial nodalization of the core and upper plenum.

Response

As described in the response to the audit issue no. 76, [the two channel core model of CAREM is adequate to model the core and also includes some conservatism coming from using the higher Fr value for hot bundle. In addition, the two channel core modeling is adequately confirmed by various code assessments as described in Appendices of the topical report.]^{TS}

In this response, sensitivity calculation is performed to confirm the above. Four assemblies surrounding the hot assembly are explicitly modeled as surrounding channel in the sensitivity calculation. [

]^{TS}

[

]^{TS}

[

]^{TS}

In case of upper plenum, the adequate modeling of the upper plenum is quite arguable during reflood period and is treated by a bias in CAREM as described in the Section 4.2.3.2 of the topical report.

Table 1. Fr Values for Hot Pin, Hot Assembly, and Surrounding Assemblies

[ ]TS

[ ]TS

Figure 1. Schematic Diagram for Current [ ]TS

TS

Figure 2. Sensitivity Calculation Results

Impact on DCD

There is no impact on the DCD.

Impact on PRA

There is no impact on the PRA.

Impact on Technical Specifications

There is no impact on the Technical Specifications.

Impact on Technical/Topical/Environmental Report

There is no impact on any Technical, Topical, or Environmental Report.

RESPONSE TO AUDIT ISSUES

APR1400 Topical Reports

Korea Electric Power Corporation / Korea Hydro & Nuclear Power Co., LTD

Docket No. PROJ0782

Review Section	**TR Realistic Evaluation Methodology for LBLOCA of the APR1400**
Application Section	**Topical Report: APR1400-F-A-TR-12004 Realistic Evaluation Methodology for Large-Break LOCA of the APR1400**
Issue Date	**08/13/2015**

Audit Issues No. 27-f

NUREG/CR-5429, Section 2.2.2 discusses issues related to model nodalization. Address the following issues regarding nodalization of the APR1400:

f. Cross-flow through the junctions in the core depends on the associated flow areas and loss coefficients. Provide an explanation of the calculation approach used to determine these parameters and how their uncertainties are represented.

Response

Because the areas of core cross flow junctions are determined by reactor core geometry, the [ ]TS

The uncertainty of the cross flow junction loss coefficient was [ ]TS The followings are quoted from reference [1].

The power of the peripheral bundles is lower than the power of central bundles. This radial core power profile causes so called chimney effect (refer to Figure 1). As a result of this chimney effect, heat transfer to flow is enhanced in the high power region and degraded in the low power region. However, since PCT occurs in the high power region, the net effect is a decrease in PCT.

The loss coefficients of cross flow junctions are determined as follows;

[

]TS

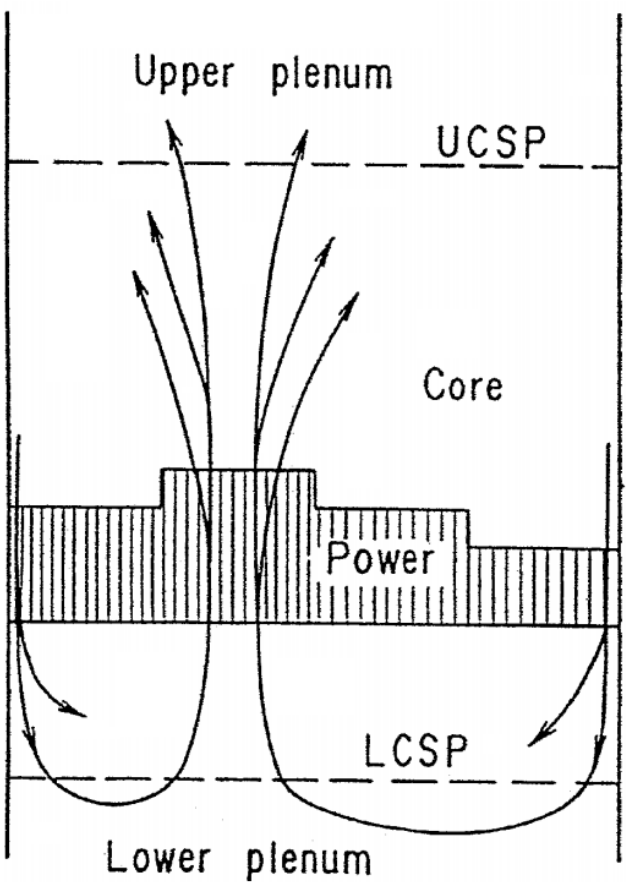

Figure 1. Multi-Dimensional Behavior in Core with a Non-Uniform Radial Power Profile [1]

References.

[1] “2D/3D Program Work Summary Report,” NUREG/IA-0126, June 1993.

[2] I. E. Idelchick, “Handbook of Hydraulic Resistance,” 2nd Edition.

Impact on DCD

There is no impact on the DCD.

Impact on PRA

There is no impact on the PRA.

Impact on Technical Specifications

There is no impact on the Technical Specifications.

Impact on Technical/Topical/Environmental Report

There is no impact on any Technical, Topical, or Environmental Report.

RESPONSE TO AUDIT ISSUES

APR1400 Topical Reports

Korea Electric Power Corporation / Korea Hydro & Nuclear Power Co., LTD

Docket No. PROJ0782

Review Section	**TR Realistic Evaluation Methodology for LBLOCA of the APR1400**
Application Section	**Topical Report: APR1400-F-A-TR-12004 Realistic Evaluation Methodology for Large-Break LOCA of the APR1400**
Issue Date	**08/13/2015**

Audit Issues No. 27-g

NUREG/CR-5429, Section 2.2.2 discusses issues related to model nodalization. Address the following issues regarding nodalization of the APR1400:

g. The froth level is typically important in determining the quench front progression. This requires accurate calculations of the fluid quality and heat release in a control volume and the mass flow rate and steam flow rate through a control volume. Provide an explanation of the basis for the core axial nodalization and the uncertainty associated with it. Also provide an assessment of the Courant limits on the nodalization.

Response

The nodalization of the plant should be modeled in detail to simulate the design characteristics and the major phenomena, however, extremely detailed modelling is hard to achieve due to practical and economic reasons. In principle the nodalization of the plant can be seen as one of uncertainty parameters, however, it is empirically known that quantifying the uncertainty costs a lot and user dependency is significant. Therefore, the standard nodalization for plant calculations is selected and it is applied to both code assessment and plant calculation. Through this, the uncertainty of nodalization can be reflected to the plant calculation.

The length of core nodes needs to be small enough to be able to detail the major thermal-hydraulic phenomena as long as it does not impede the practicality of the plant calculation. The core axial nodalization of CAREM is modeled on the basis of assessment against [ ]^{TS} of which the rod lengths are the same as the fuel rod length of the conventional plant.

In case of test facility which has the same core length as the plant, the distortion of the thermal-hydraulic behavior in the core due to the scale down is prevented by assuming the power-to-flow area ratio similar to the value of the fuel assembly. Thus, the measuring positions of the test facilities against axial direction of the core is important reference in determining the nodding for plant. In the CAREM, the active length of the fuel rod is modeled using [

]^{TS}

Figure 1 shows comparison of Courant limit and time step of plant calculation. As shown in Figure 1, it is confirmed that the time step used in plant calculation is always lower than Courant limit.

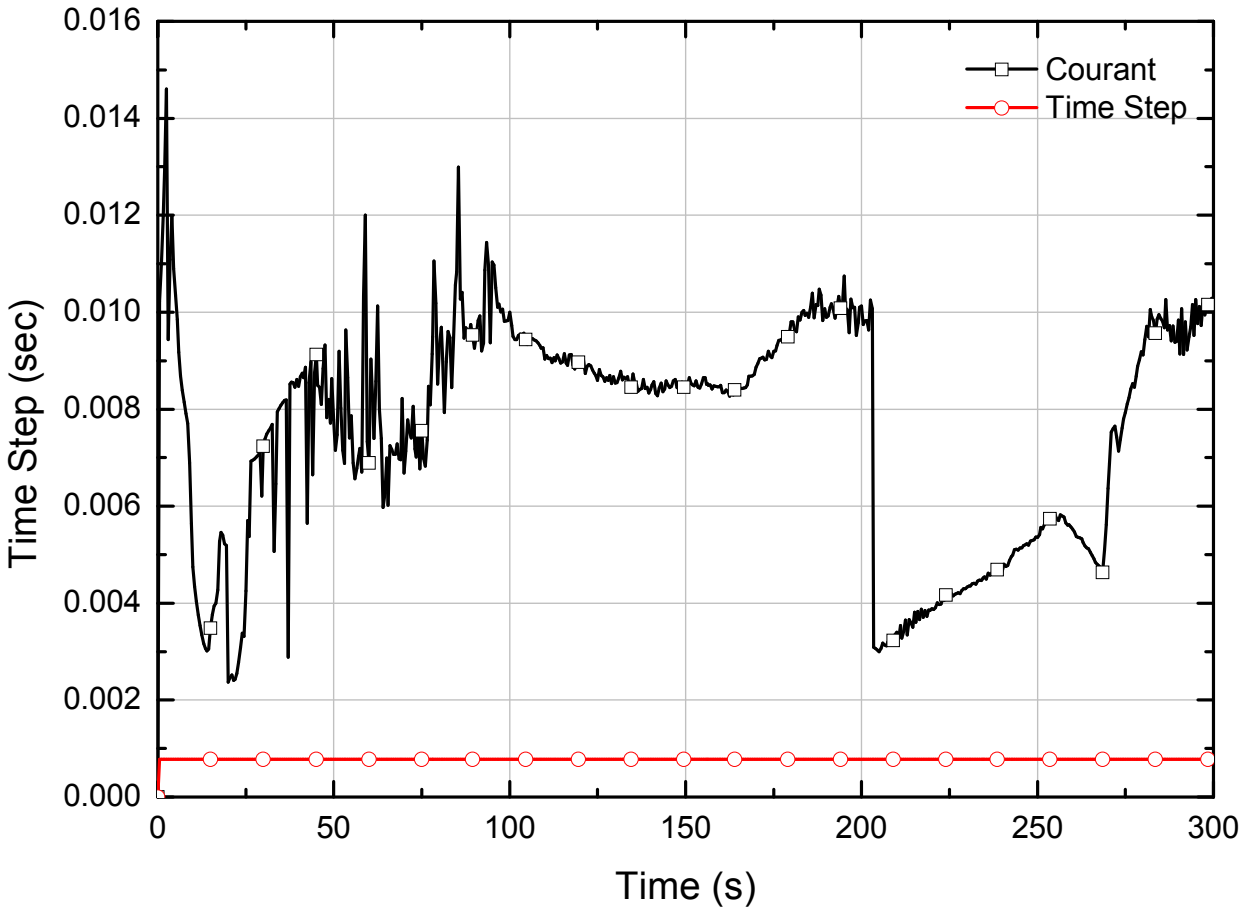

Figure 1. Courant Limit and Time Step of Plant Calculation

Impact on DCD

There is no impact on the DCD.

Impact on PRA

There is no impact on the PRA.

Impact on Technical Specifications

There is no impact on the Technical Specifications.

Impact on Technical/Topical/Environmental Report

There is no impact on any Technical, Topical, or Environmental Report.

RESPONSE TO AUDIT ISSUES

APR1400 Topical Reports

Korea Electric Power Corporation / Korea Hydro & Nuclear Power Co., LTD

Docket No. PROJ0782

Review Section	**TR Realistic Evaluation Methodology for LBLOCA of the APR1400**
Application Section	**Topical Report: APR1400-F-A-TR-12004 Realistic Evaluation Methodology for Large-Break LOCA of the APR1400**
Issue Date	**08/13/2015**

Audit Issues No. 27-h

NUREG/CR-5429, Section 2.2.2 discusses issues related to model nodalization. Address the following issues regarding nodalization of the APR1400:

h. According to NUREG/CR-5249 (see Figure 18 in NUREG/CR-5249), analysis results from the simulation of a pressurized-water reactor (PWR) LBLOCA showed that at least two nodes are required in the lower plenum below the downcomer skirt to adequately model the sweep-out effect which is [ ]^{TS} It appears that the APR1400 nodalization models the region below the downcomer skirt [ ]^{TS} Provide justification for the selected nodalization.

Response

During blowdown period, flashing occurs due to the rapid depressurization and it causes generation of the vapor in the lower plenum. Figure 1 shows the liquid temperature and the saturation temperature at the lower plenum. The liquid temperature is greater than saturation temperature between 6 seconds and 30 seconds. Because of this, the vapor is generated in the lower plenum as shown in Figure 2.

The lower plenum region (below the downcomer skirt) of APR1400 plant is [ ]^{TS} In order to find out the sensitivity of the lower plenum noding on the sweep out, the volume below the flow skirt is modeled by [ ]^{TS} And the noding of lower plenum is shown in Figure 3. Figure 4 shows comparison of the vapor flow rate from the lower plenum to downcomer using the ToR noding and the new noding. The comparison of PCTs calculated using [ ]^{TS} is presented in Figure 5. As shown in Figures, the calculation results of two models are very similar. Based on these results, it is found that the impact of lower plenum noding is not significant in APR1400. The different effect of lower plenum noding from NUREG/CR-5249 would be resulted from the difference in lower plenum geometry such as flow skirt.

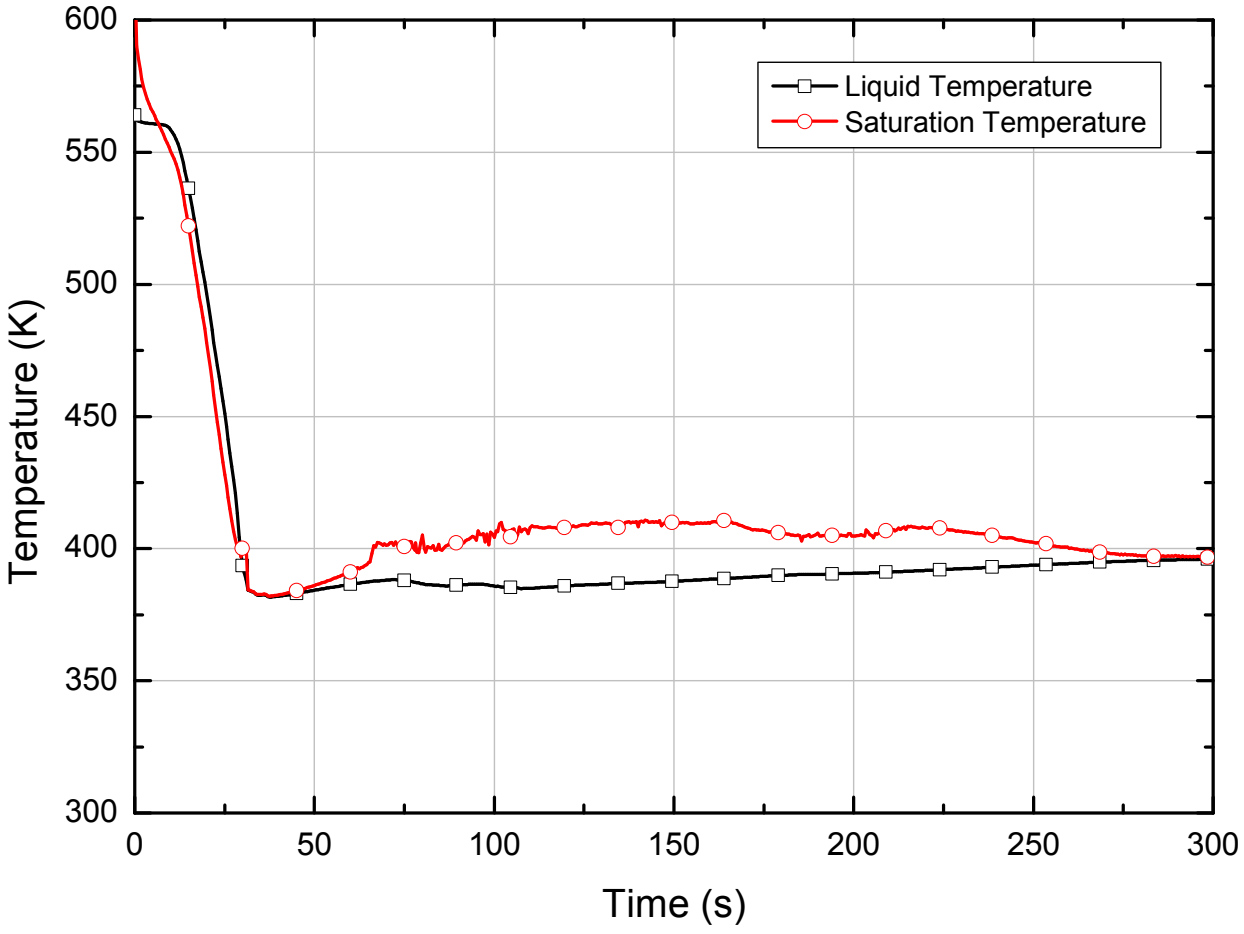

Figure 1. Liquid and Saturation Temperature at the Lower Plenum

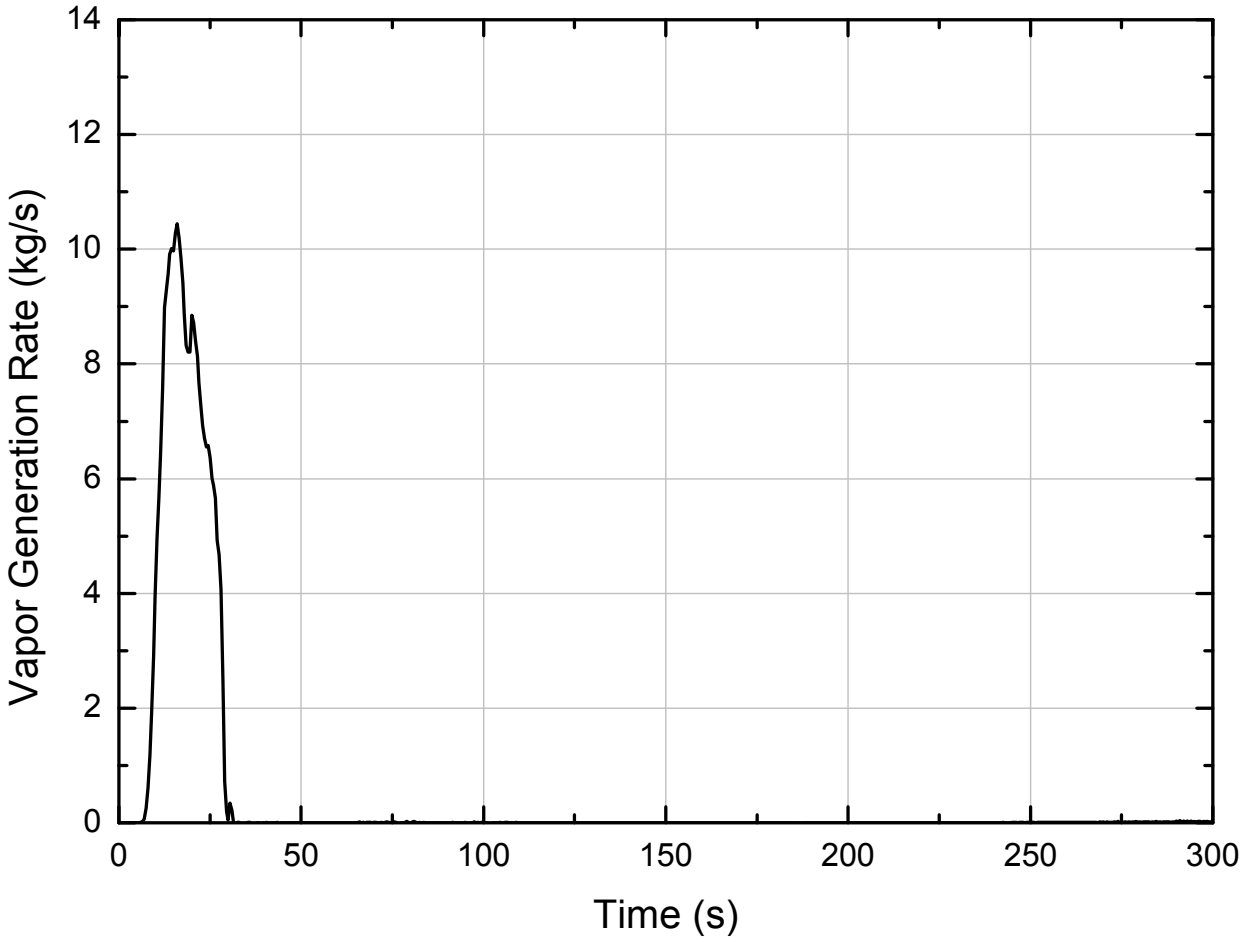

Figure 2. Vapor Generation at the Lower Plenum

TS

Figure 3. Noding Diagram of the Lower Plenum

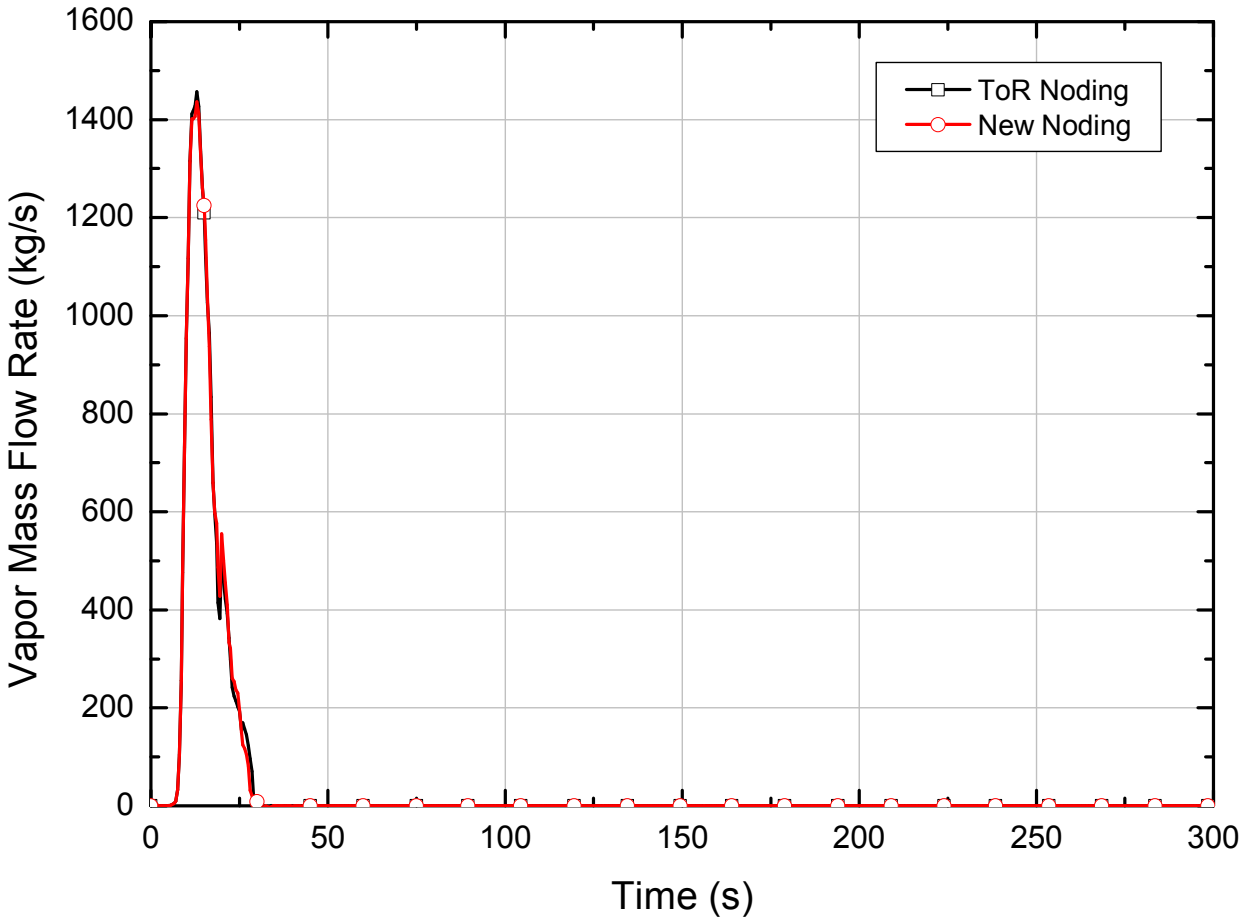

Figure 4. Vapor Mass Flow Rate from Lower Plenum to Downcomer

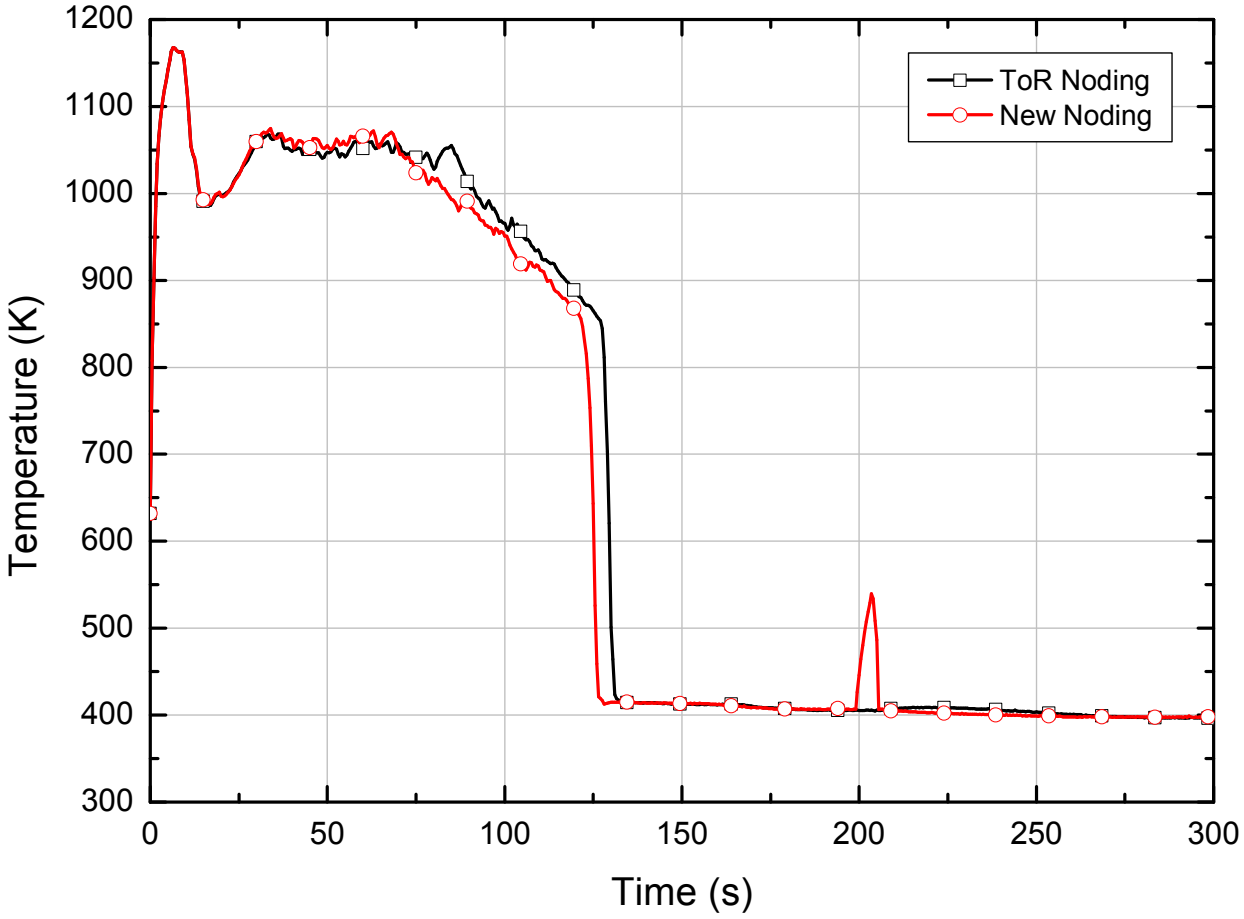

Figure 5. Hottest Rod Temperature

Impact on DCD

There is no impact on the DCD.

Impact on PRA

There is no impact on the PRA.

Impact on Technical Specifications

There is no impact on the Technical Specifications.

Impact on Technical/Topical/Environmental Report

There is no impact on any Technical, Topical, or Environmental Report.

RESPONSE TO AUDIT ISSUES

APR1400 Topical Reports

Korea Electric Power Corporation / Korea Hydro & Nuclear Power Co., LTD

Docket No. PROJ0782

Review Section	**TR Realistic Evaluation Methodology for LBLOCA of the APR1400**
Application Section	**Topical Report: APR1400-F-A-TR-12004 Realistic Evaluation Methodology for Large-Break LOCA of the APR1400**
Issue Date	**08/13/2015**

Audit Issues No. 27-i

NUREG/CR-5249, Section 2.2.2 discusses issues related to model nodalization. Address the following issues regarding nodalization of the APR1400.

i. According to RG 1.157 Section 3.5 the break location and ECCS injection point are areas of high fluid velocity and complex fluid flow and contain phenomena that are often difficult to calculate. The results of these calculations are often highly dependent on noding. Justify the nodalization selected for the APR1400 broken cold leg and provide results from relevant sensitivity studies to assess the impact of nodalization changes in the break discharge region (i.e., based on the Marviken data)

Response

Figure 1 illustrates Marviken test nodalization. To determine the break nozzle nodalization, sensitivity study was performed with varying the number of volumes [1]. As a result, the two-phase critical flow rates are [ ]TS Therefore the [ ]TS was adopted for the nozzle. With this nodalization, the evaluation was performed and the best estimated discharge coefficients of [ ]TS were determined [1].

Meanwhile, [ ]TS to minimize the impact on the critical mass flux under subcooled conditions in the Marviken test [2]. As described above, since the Marviken test nozzle is represented by [ ]TS

In Figure 2, Case 02 shows plant break nodalization in the topical report. The discharge coefficients of [ ]TS are also applied to the plant calculation. [ ]TS of the break is presented in Table 1. [ ]TS However, nodding sensitivity (Case 01 in Figure 2) shows that the [ ]TS does not impose critical impact on the calculated result (Figure 3). Consequently, the final nodalization of the break discharge nozzle in the Marviken facility is identical to that of the plant break modeling.

Table 1 Length to Diameter Ratio for APR1400 Plant Nodalization

TS

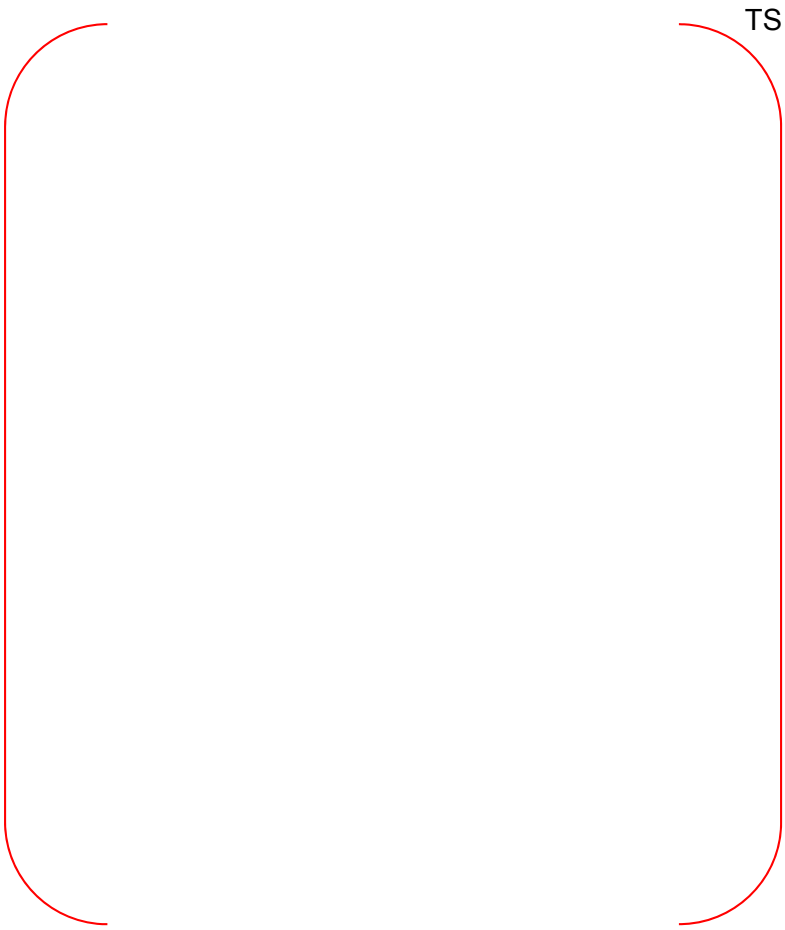

Figure 1 Nodalization (Marviken Test Facility)

Figure 2 Nodalization (APR1400 Broken Cold Leg)

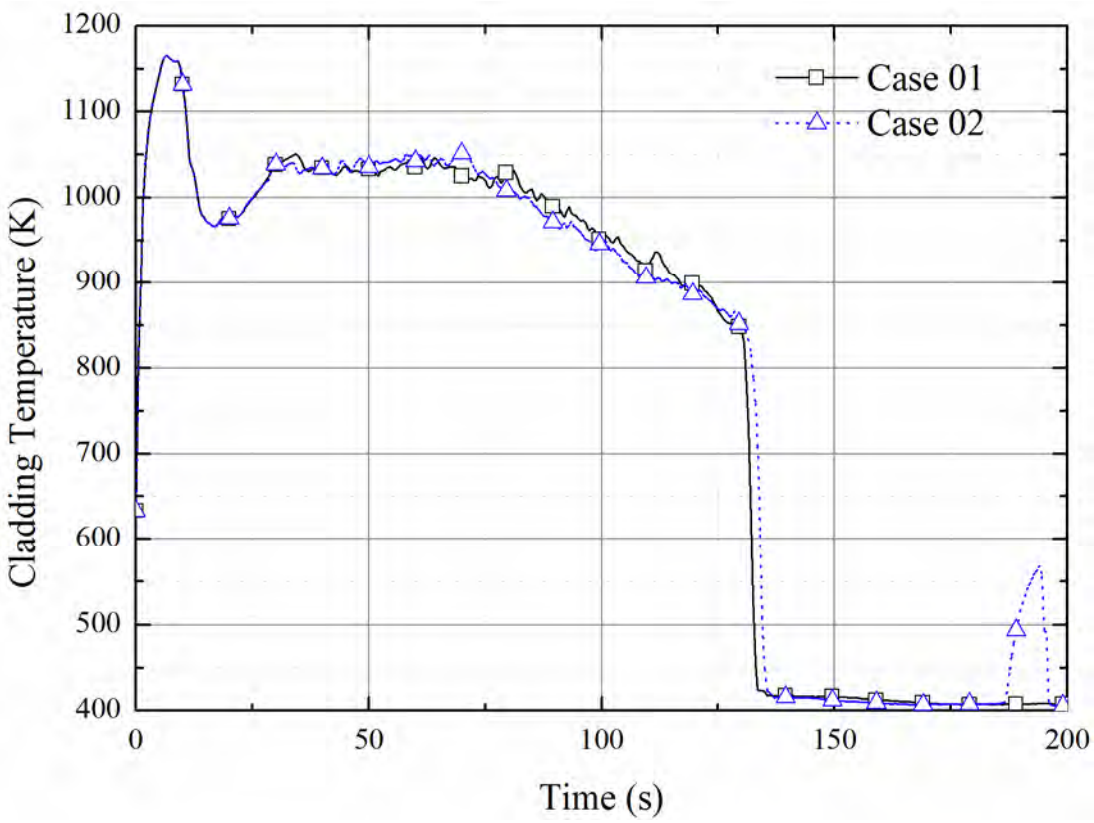

Figure 3 Cladding Temperature at the PCT Node

References

[1] S.Y. Lee, “Uncertainty Quantificiation of RELAP5/MOD3/KAERI Critical Flow Model using Marviken Experiment Data,” KAERI/TR-437/94, Oct. 1994.

[2] S.Levy, Inc., “Critical Flow Data Review and Analysis,” EPRI-NP 2192 Project 14385-1, Jan. 1982.

Impact on DCD

There is no impact on the DCD.

Impact on PRA

There is no impact on the PRA.

Impact on Technical Specifications

There is no impact on the Technical Specifications.

Impact on Technical/Topical/Environmental Report

There is no impact on any Technical, Topical, or Environmental Report.

RESPONSE TO AUDIT ISSUES

APR1400 Topical Reports

Korea Electric Power Corporation / Korea Hydro & Nuclear Power Co., LTD

Docket No. PROJ0782

Review Section	**TR Realistic Evaluation Methodology for LBLOCA of the APR1400**
Application Section	**Topical Report: APR1400-F-A-TR-12004 Realistic Evaluation Methodology for Large-Break LOCA of the APR1400**
Issue Date	**08/13/2015**

Audit Issues No. 27-j

NUREG/CR-5429, Section 2.2.2 discusses issues related to model nodalization. Address the following issues regarding nodalization of the APR1400:

j. RG 1.157 Section 3.5 discusses nodalization near the ECCS injection point and states that "…sufficient sensitivity studies should be performed on the noding and other important parameters to ensure that the calculations provided realistic results." Appendix E of the topical report discusses tests performed in the ATLAS facility to study direct vessel injection (DVI) performance relative to emergency core cooling water bypass and downcomer boiling. Describe or refer to the sensitivity studies performed to assess the selected nodalization near the ECCS injection point using the ATLAS test results.

Response

j)

As described in Section 4.2.1 of the topical report, downcomer is [
]TS
The nodalization for the ATLAS test follows the same nodalization concept by modeling the downcomer with [ ]TS Direct vessel injection (DVI) nozzle is located at [ ]TS above the center of cold leg in ATLAS facility. Thus, axial nodalization of upper downcomer (C130 ~ C136, C140 ~ C146 as shown in Figure 3-3 of Appendix E) is determined to [ ]TS Downcomer gap width is fixed by the geometric configuration.

Based on the above nodalization concept, [ ]TS Sensitivity calculation for ATLAS test 15 is performed using [ ]TS of the volume that ranges from [ ]TS

Figure 1 shows integrated break mass flow rates of [ ]TS and the one marked with circles means nominal case. Figure 2 shows ECC bypass ratio results calculated by dividing integrated liquid phase break mass flow by integrated total safety injection (SI) mass flow. Since integrated liquid break mass flow results are similar to each other, ECC bypass ratio results are consequently similar.

Figure 3 shows clad temperature results of [ ]TS Clad temperature behaviors of all cases are similar, and the PCT difference between the maximum and minimum data is about 15 K. But there seems [ ]TS

Consequently, [ ]TS has insignificant effects on the ECC bypass and clad temperature behavior.

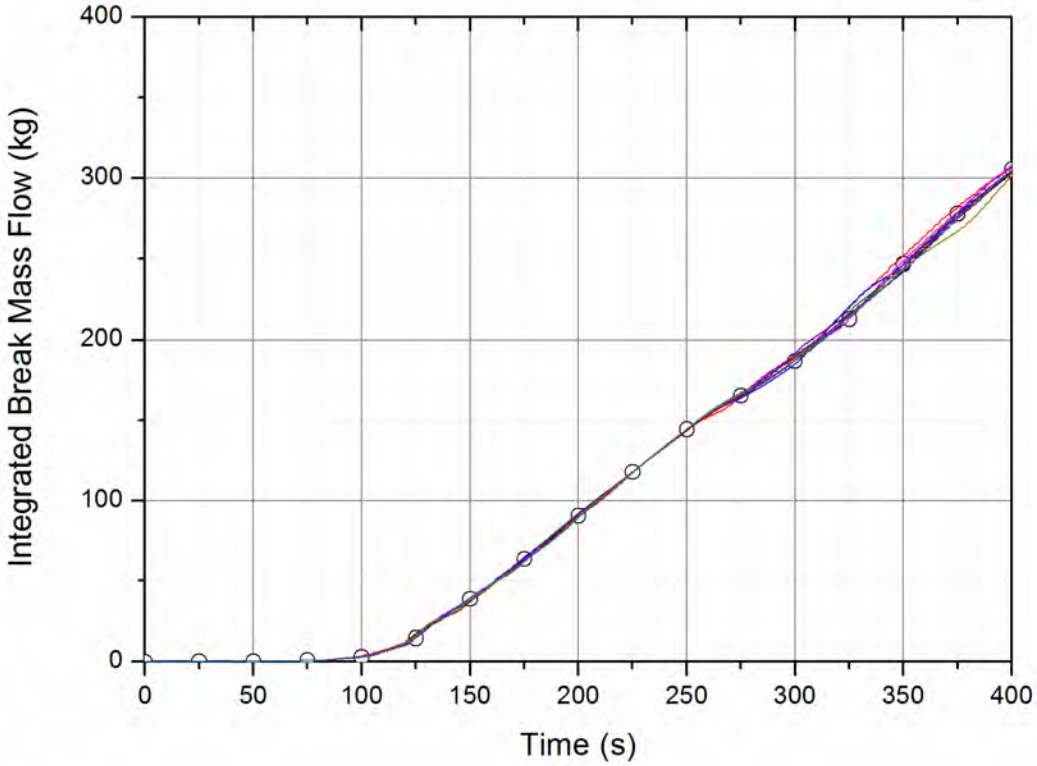

Figure 1. Integrated Break Mass Flow Results for [ ]TS

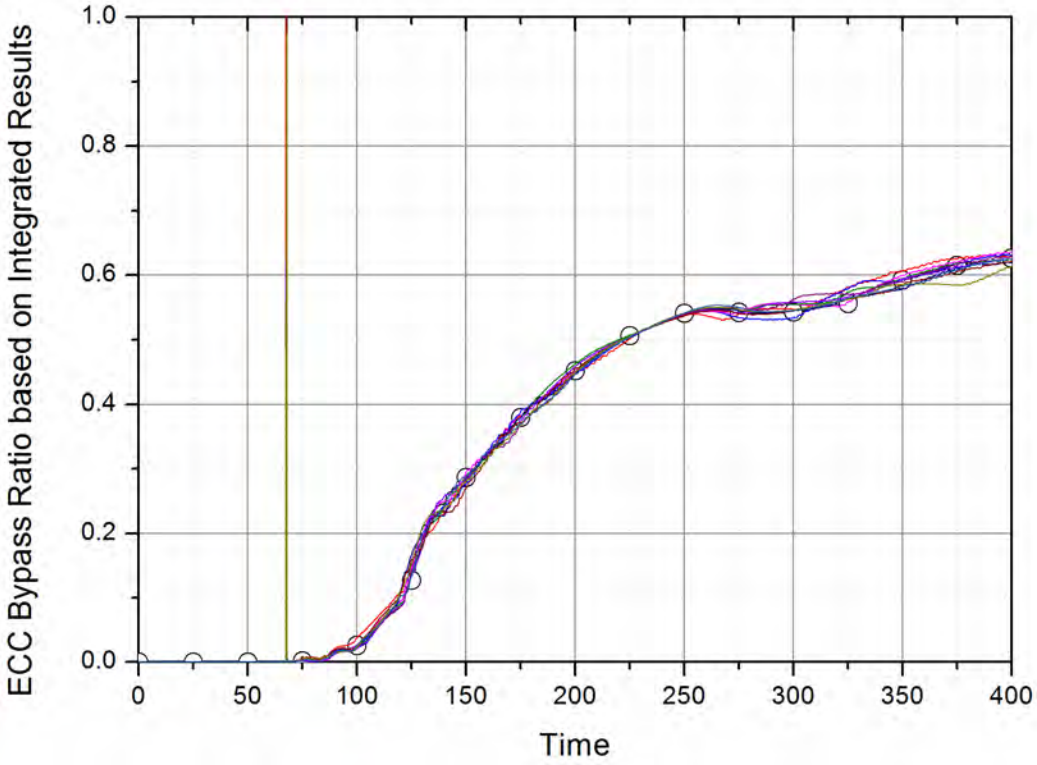

Figure 2. ECC Bypass Ratio Results for [ ]TS

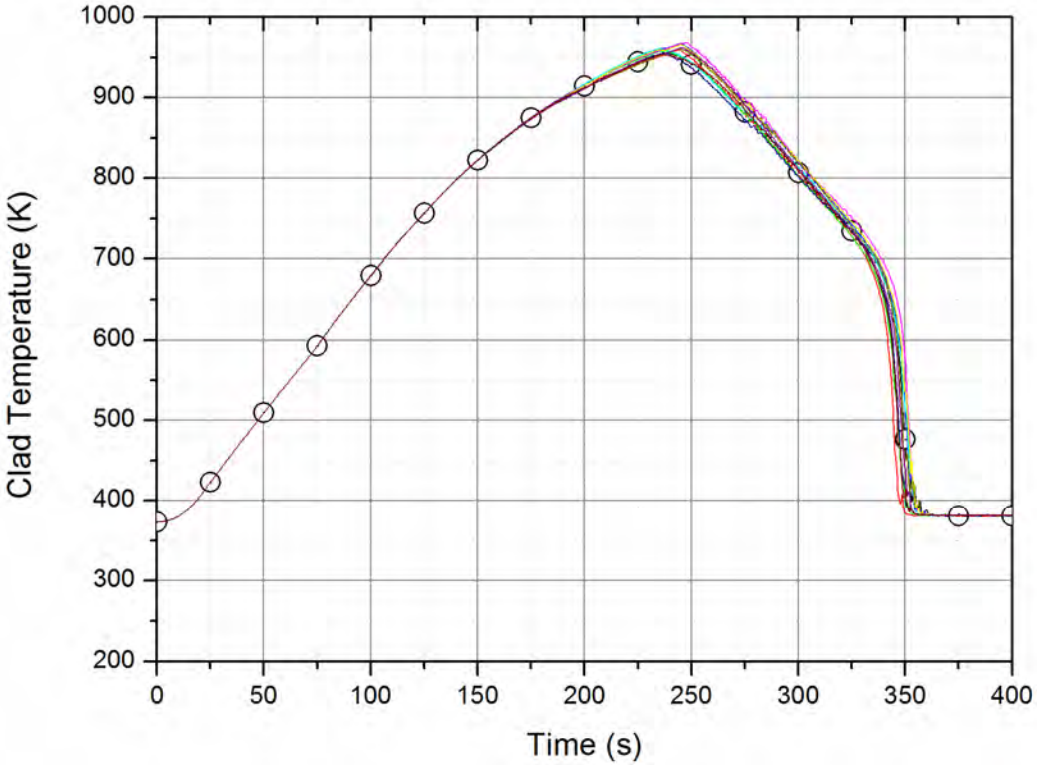

Figure 3. Clad Temperature Results for [ ]TS

TS

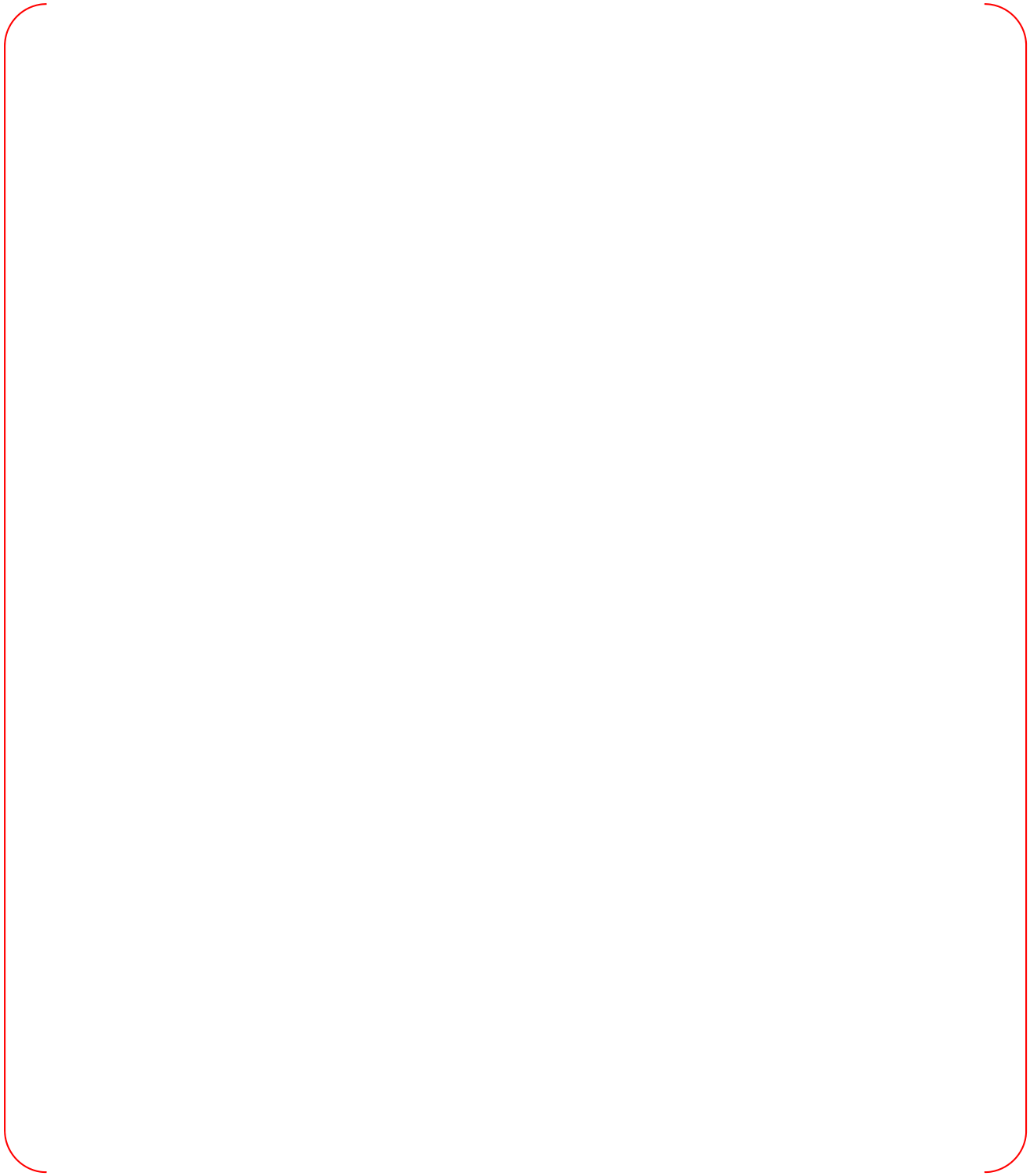

Figure 4. Drawing of Downcomer to Lower Plenum for APR1400 [1]

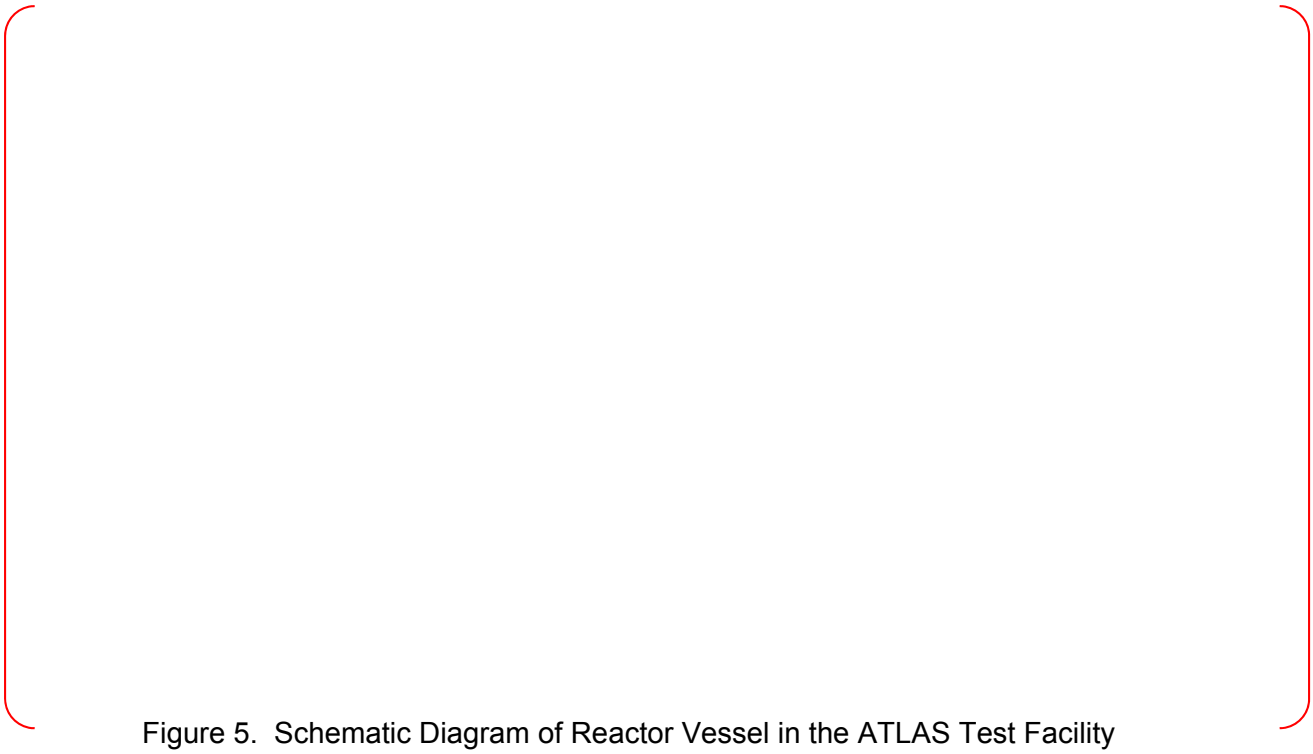

Figure 5. Schematic Diagram of Reactor Vessel in the ATLAS Test Facility

Reference

[1] Drawings, “Reactor Vessel: Flow Baffle,”1-110-H-175-017C, Doosan Heavy industries & Construction, December 2011.

Impact on DCD

There is no impact on the DCD.

Impact on PRA

There is no impact on the PRA.

Impact on Technical Specifications

There is no impact on the Technical Specifications.

Impact on Technical/Topical/Environmental Report

There is no impact on any Technical, Topical, or Environmental Report.

RESPONSE TO AUDIT ISSUES

APR1400 Topical Reports

Korea Electric Power Corporation / Korea Hydro & Nuclear Power Co., LTD

Docket No. PROJ0782

Review Section	**TR Realistic Evaluation Methodology for LBLOCA of the APR1400**
Application Section	**Topical Report: APR1400-F-A-TR-12004 Realistic Evaluation Methodology for Large-Break LOCA of the APR1400**
Issue Date	**08/13/2015**

Audit Issues No. 27-k

NUREG/CR-5429, Section 2.2.2 discusses issues related to model nodalization. Address the following issues regarding nodalization of the APR1400:

k. In order to adequately simulate the depletion time of the pressurizer and liquid drainage during the blowdown period, the nodalization of the pressurizer surge line should be consistent with the actual plant geometry. However, the description for the pressurizer surge line nodalization is not provided in Section 4.2.1 of the topical report. According to the RELAP5 base model input deck, the surge line is modeled using a single inclined hydraulic component. Additionally, the loss coefficient through surge line pipe is set to be computed by the code which neglects the turns and orientation changes in the line. Justify the selected nodalization and loss coefficients including any references to nodalization sensitivity studies comparing the pressurizer flow into upper plenum against the available special effects tests and/or integral effects tests data.

Response

1) Nodalization of surge line

The surge line of pressurizer is modeled as a SNGLVOL component as show in Figure 1 and the detailed information of surge line are as follows.

[

]TS

In order to predict the depletion of pressurizer, the pressurizer and surge line are modeled as PIPE component with [ ]TS and SNGLVOL component respectively to reflect the assessment result against LOFT test. Figure 2 shows the pressurizer level. It is confirmed that the calculation result using this nodalization is adequately predicted comparing to the result of LOFT test. Based on the result, the nodalization of pressurizer and surge line mentioned above is used in the plant calculation.

2) Loss coefficient of surge line

The pressurizer surge line is modeled by SNGLVOL component and the geometric loss coefficient including the effect of elbows, entrance/exit nozzles and others (flow screen, thermal sleeve, etc) for the insurge/outsurge flow is used at the branch region (310 component) which connecting hot leg and surge line pipes. The loss coefficient of surge line is as follows:

nominal max min

[

]TS

The nominal values are applied for surge line K-factor above. It may need to confirm the sensitivity study for conservativeness. The sensitivity study results of loss coefficient are shown in Table 1. The depletion time of the pressurizer is almost same in accordance with change of loss coefficient. Based on this result, the effect of loss coefficient of surge line is not significant.

3) Nodalization sensitivity

The drawings of pressurizer surge line for APR1400 are illustrated in Figure 3. The surge line

piping is composed of [
]TS Figure 4 shows the nodalization of surge line used in CAREM and the new nodalization consistent with actual plant geometry. In case of the new pressurizer surge line modeling reflecting the actual plant geometry, the surge line is modeled by PIPE component with [
]TS The results of nodalization sensitivity show no significant difference in the hydrodynamic behavior as shown in Figure 5 to Figure 8.

Table 1. Depletion Time of the Pressurizer

	Nominal	Max	Min
Empty Time (sec)	25.0	25.6	24.8

Figure 1. Nodalization of Pressurizer Surge Line

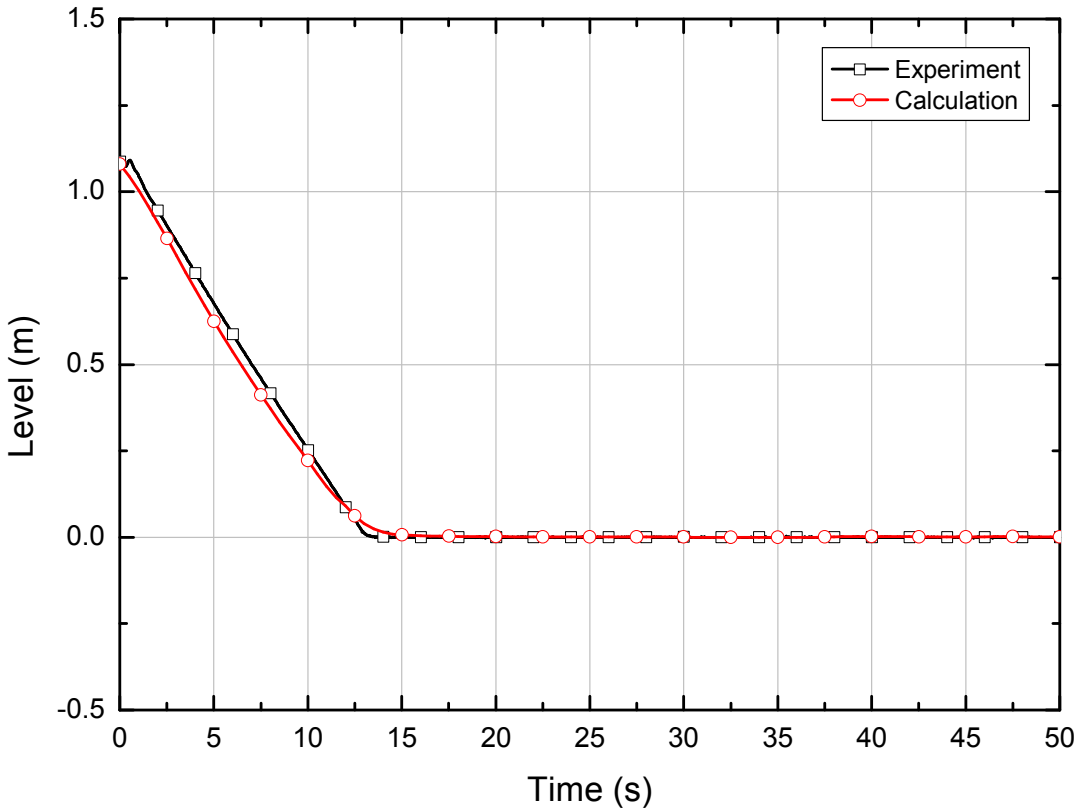

Figure 2. Pressurizer Level

TS

Figure 3. Drawings of Pressurizer Surge Line for APR1400

TS

Figure 4. Schematics of Pressurizer Surge Line Nodalization

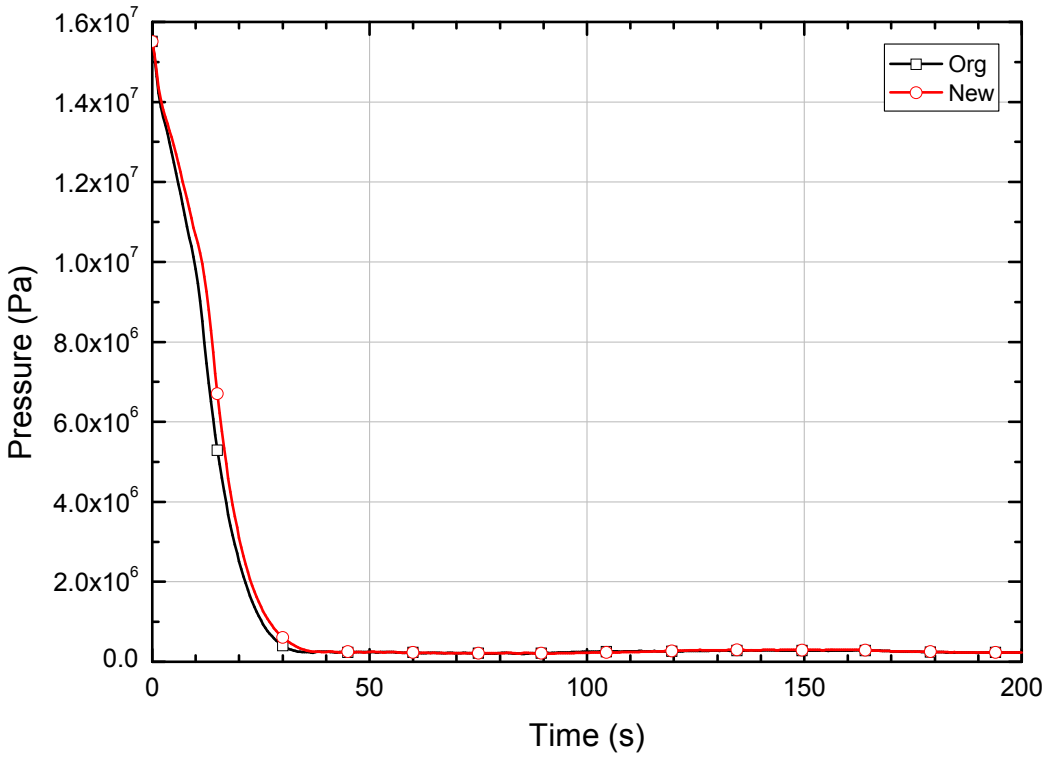

Figure 5. Nodalization Sensitivity – Pressurizer Pressure

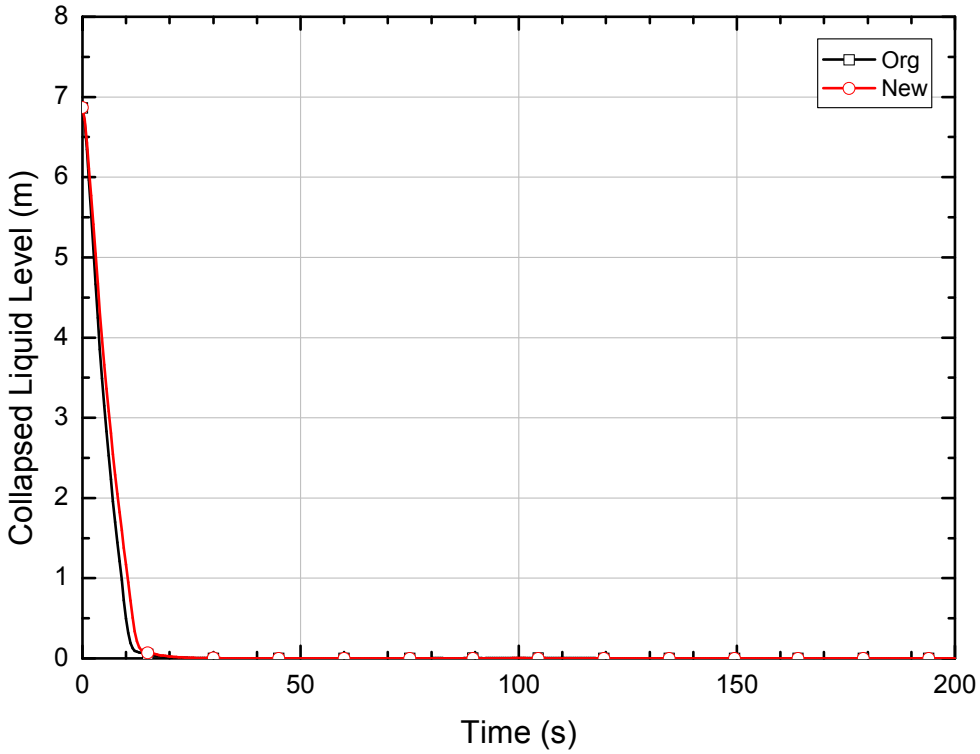

Figure 6. Nodalization Sensitivity – Pressurizer Level

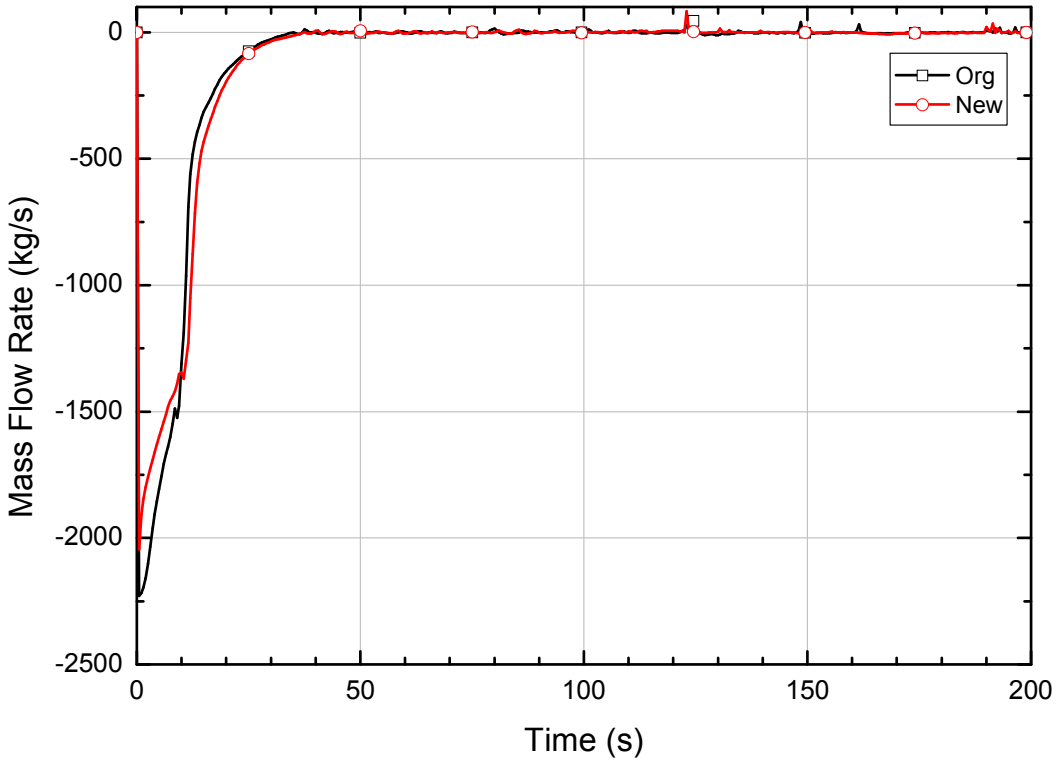

Figure 7. Nodalization Sensitivity – Mass Flow Rate between Surge Line and Hot Leg

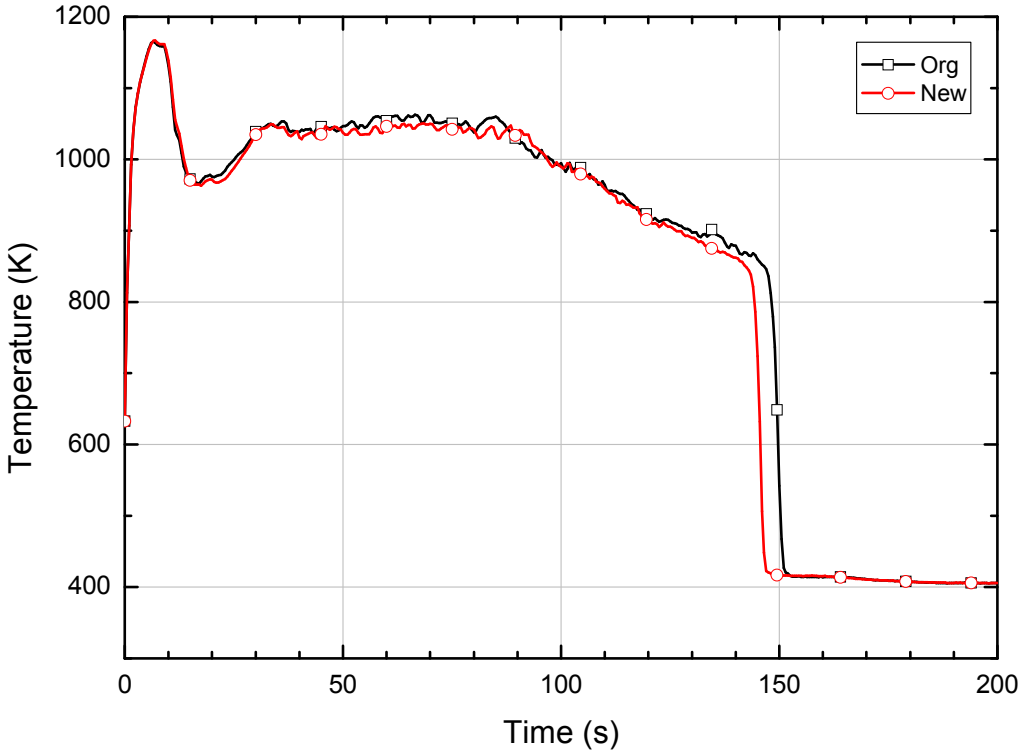

Figure 8. Nodalization Sensitivity – Cladding Temperature at PCT Node

Impact on DCD

There is no impact on the DCD.

Impact on PRA

There is no impact on the PRA.

Impact on Technical Specifications

There is no impact on the Technical Specifications.

Impact on Technical/Topical/Environmental Report

There is no impact on any Technical, Topical, or Environmental Report.

RESPONSE TO AUDIT ISSUES

APR1400 Topical Reports

Korea Electric Power Corporation / Korea Hydro & Nuclear Power Co., LTD

Docket No. PROJ0782

Review Section	**TR Realistic Evaluation Methodology for LBLOCA of the APR1400**
Application Section	**Topical Report: APR1400-F-A-TR-12004 Realistic Evaluation Methodology for Large-Break LOCA of the APR1400**
Issue Date	**08/13/2015**

Audit Issues No. 27-I

NUREG/CR-5429, Section 2.2.2 discusses issues related to model nodalization. Address the following issues regarding nodalization of the APR1400:

I. Discuss the differences in the nodalization of the upper guide support structure region between the RELAP5 nodalizations shown in Figure 4-1 of the topical report, and Figure 17 in Appendix B. Identify, with justification, the nodalization that will be used for licensing calculations.

Response

Nodalization of Figure 4-1 in the topical report will be used for licensing calculations.

Figure 17 in Appendix B is used only to study sensitivities for code modifications. Nodalization of Figure 17 in Appendix B was used during developing phase of the CAREM.

However, it is reasonable to use same nodalization for all sensitivity study. Therefore, revision of topical report will be included re-calculation results of sensitivity study using same nodalization of APR1400.

Impact on DCD

There is no impact on the DCD.

Impact on PRA

There is no impact on the PRA.

Impact on Technical Specifications

There is no impact on the Technical Specifications.

Impact on Technical/Topical/Environmental Report

Topical report will be revised as discussed above.

There is no impact on Technical or Environmental Report.

Replace with next page A

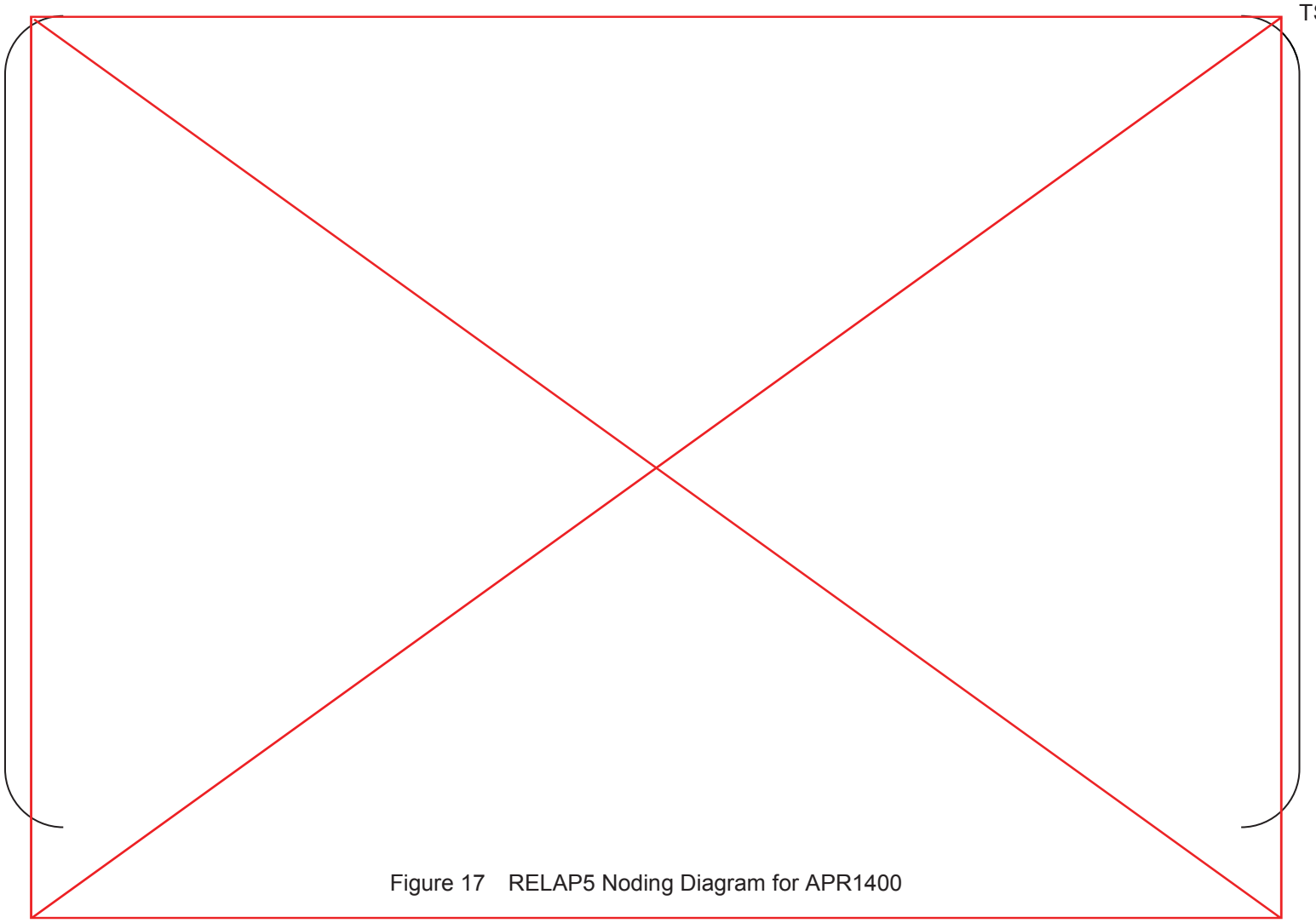

Figure 17 RELAP5 Noding Diagram for APR1400

A

TS

Figure 17 RELAP5 Noding Diagram for APR1400

Replace with next page B

[ ]TS

Figure 18 Comparison of [ ]TS

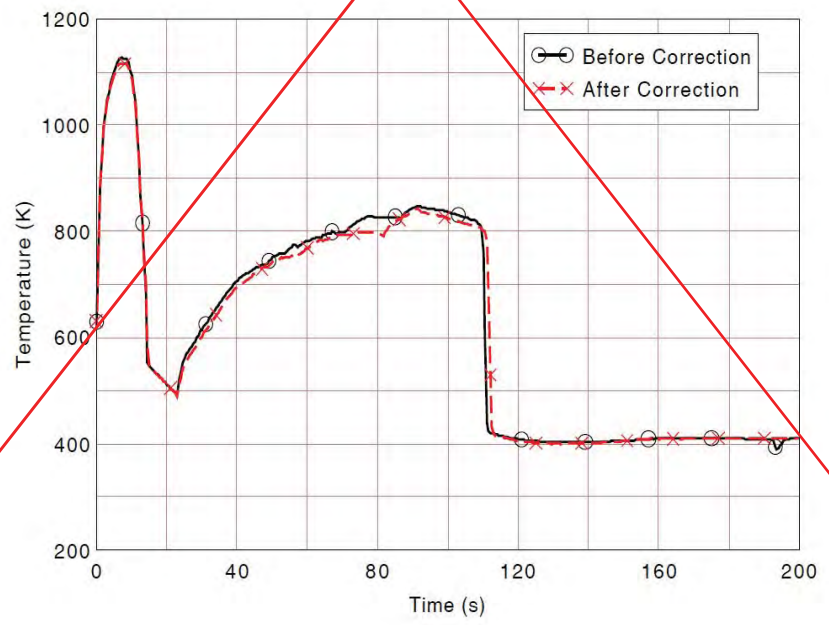

Figure 19 Effect of the [ ]TS

B

TS

Figure 18 Comparison of [ ]TS

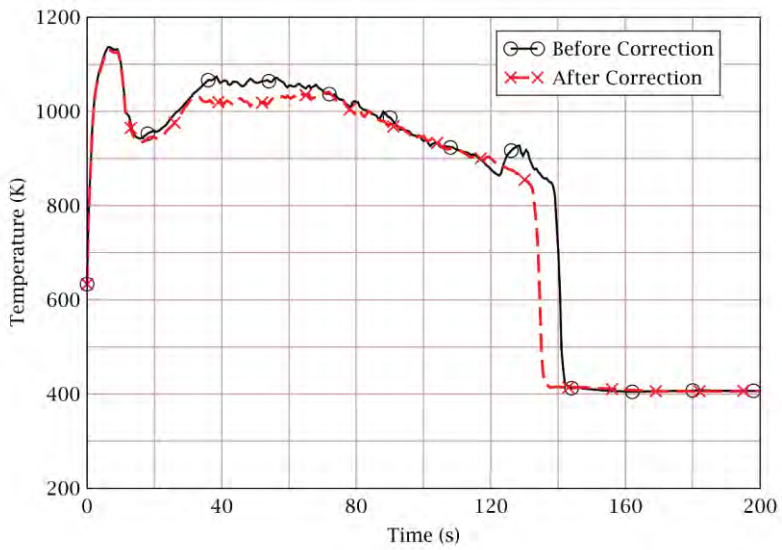

Figure 19 Effect of the [ ]TS

Replace with next page C

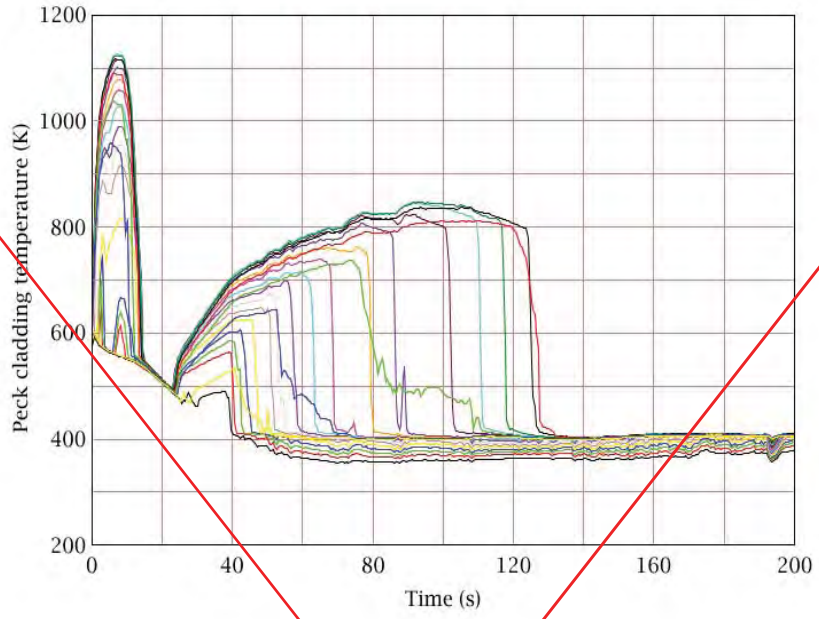

Figure 20 Cladding Temperatures at [ ]^{TS} Axial Nodes of the Hottest Rod; Before Modification

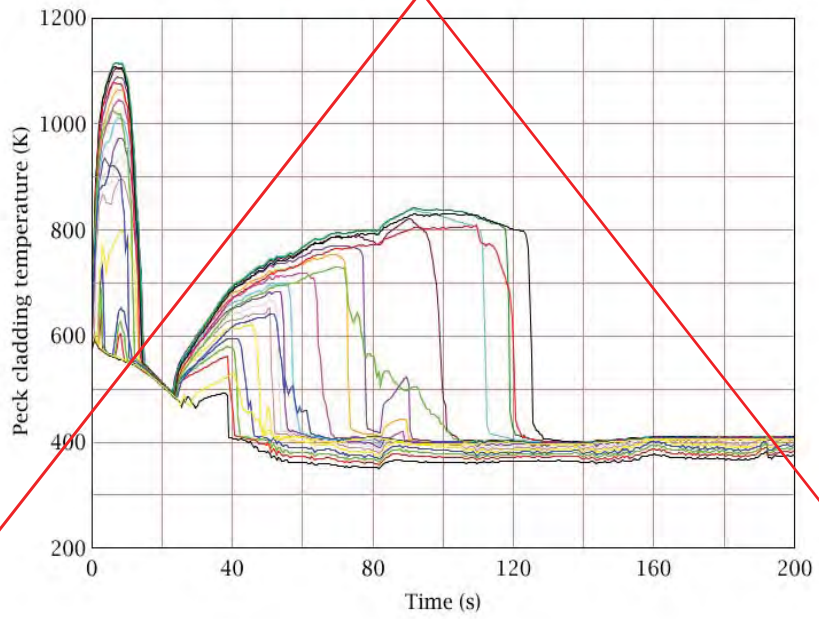

Figure 21 Cladding Temperatures at [ ]^{TS} Axial Nodes of the Hottest Rod; After Modification

C

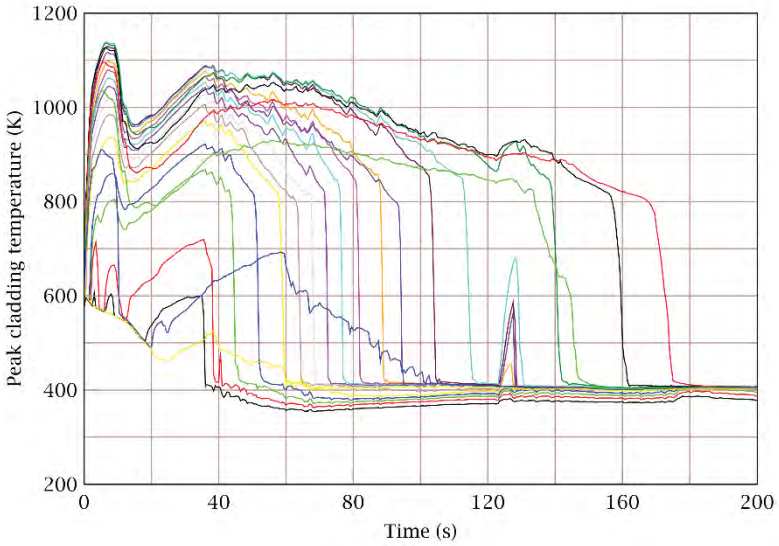

Figure 20 Cladding Temperatures at [ ]^{TS} Axial Nodes of the Hottest Rod; Before Modification

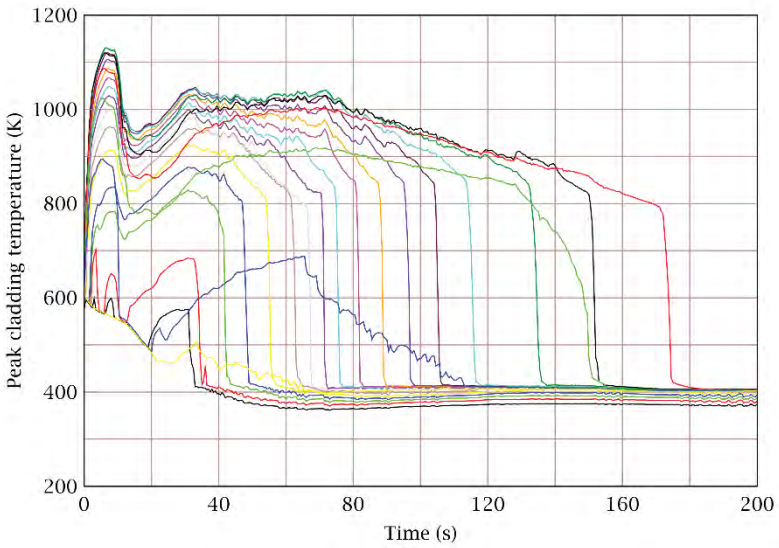

Figure 21 Cladding Temperatures at [ ]^{TS} Axial Nodes of the Hottest Rod; After Modification

Replace with next page ˇ

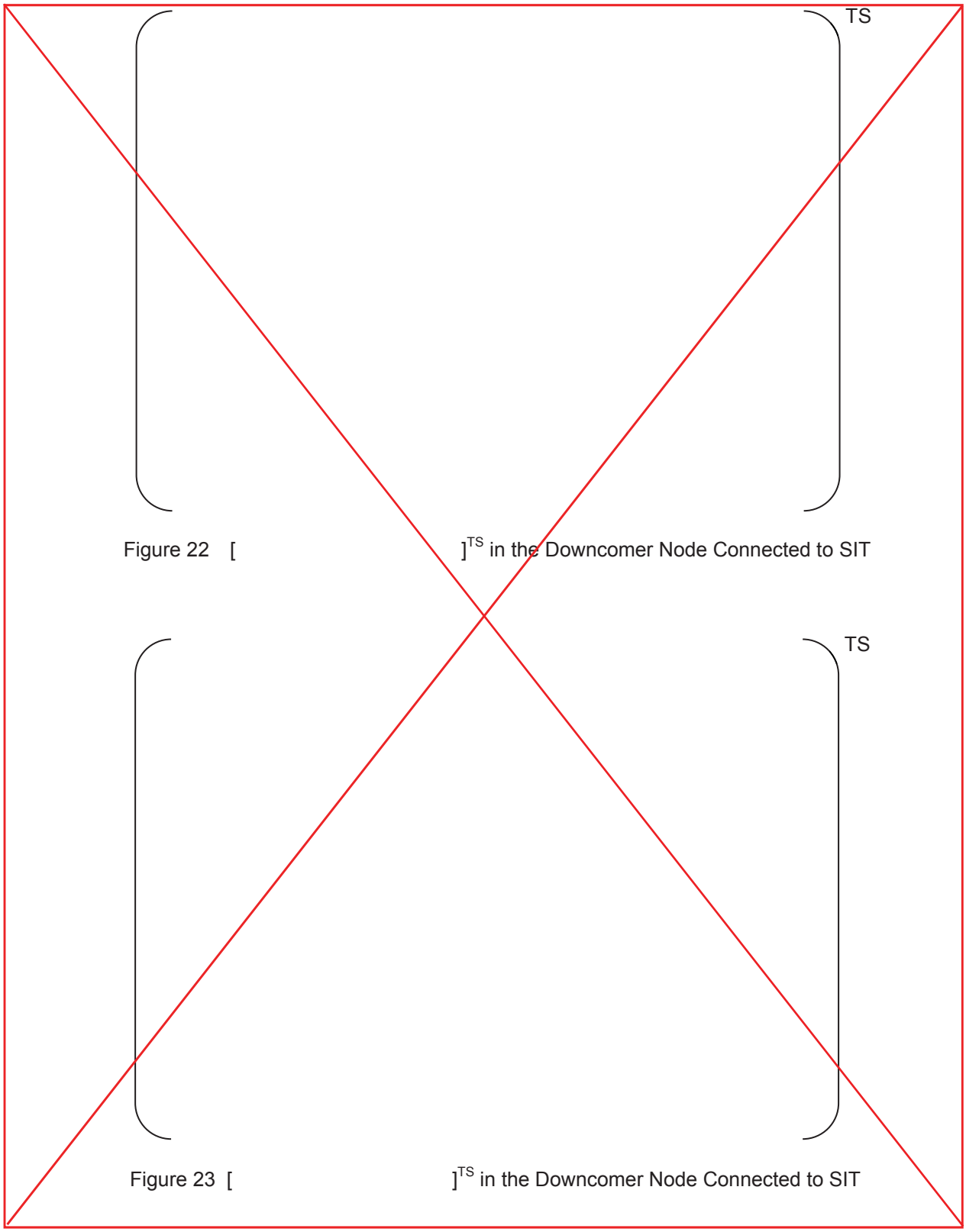

Figure 22 [ ]^{TS} in the Downcomer Node Connected to SIT

Figure 23 [ ]^{TS} in the Downcomer Node Connected to SIT

˘

TS

Figure 22 [ ]TS in the Surge-line of SIT-FD

TS

Figure 23 [ ]TS in the Surge-line of SIT-FD

Replace with next page ″

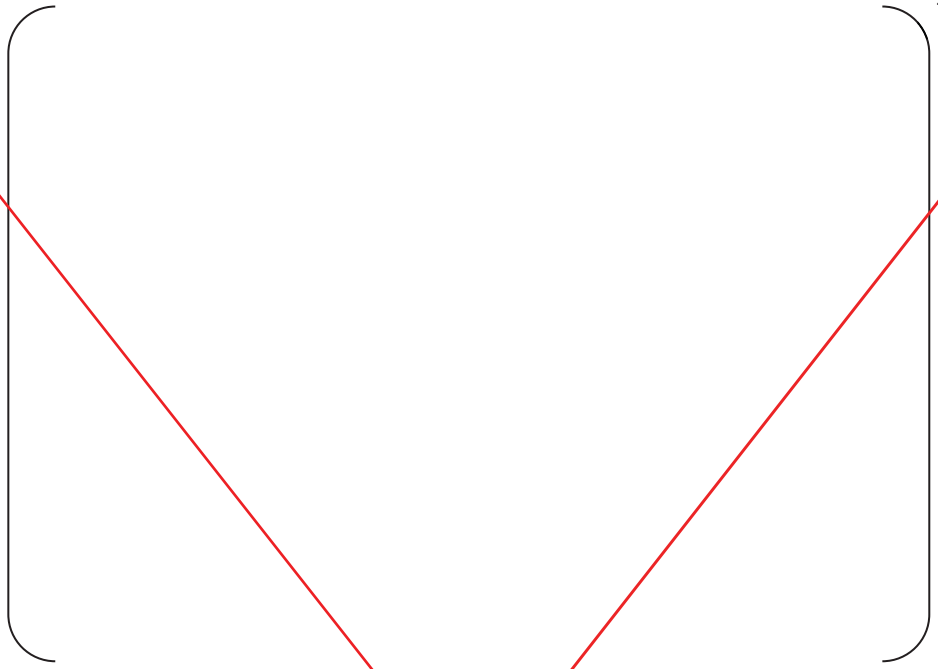

Figure 24 [ ]^{TS} in an Upper Downcomer Node

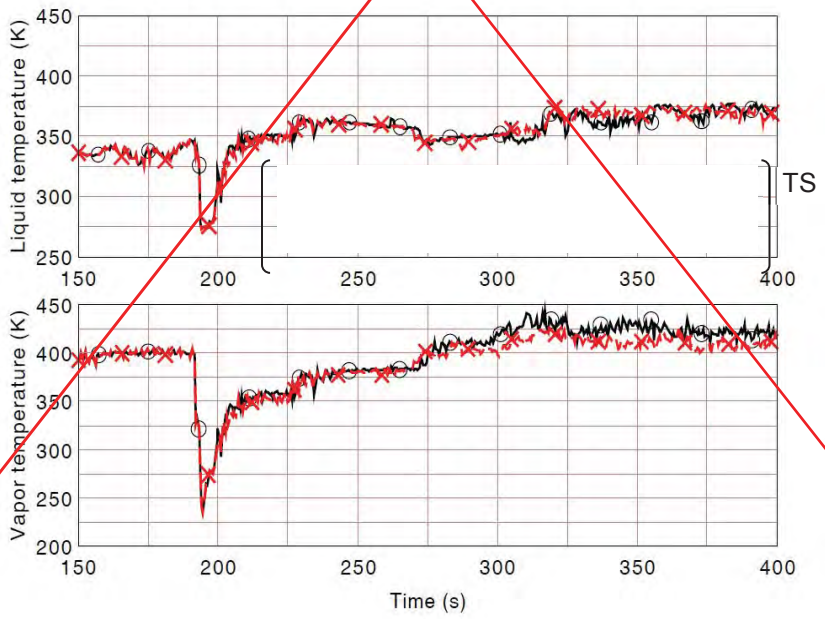

Figure 25 Liquid and Vapor Temperatures in an Upper Downcomer Node

"

TS

Figure 24 [ ]TS in an Upper Downcomer Node

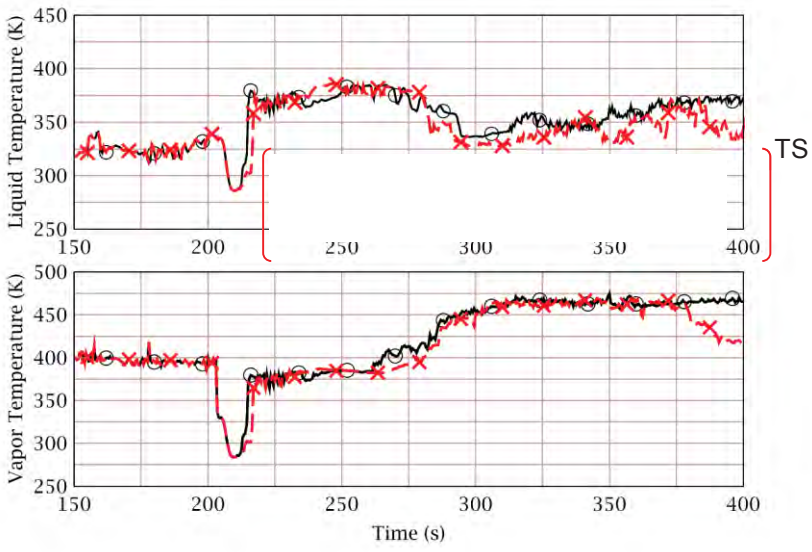

TS

Figure 25 Liquid and Vapor Temperatures in an Upper Downcomer Node

Replace with next page °

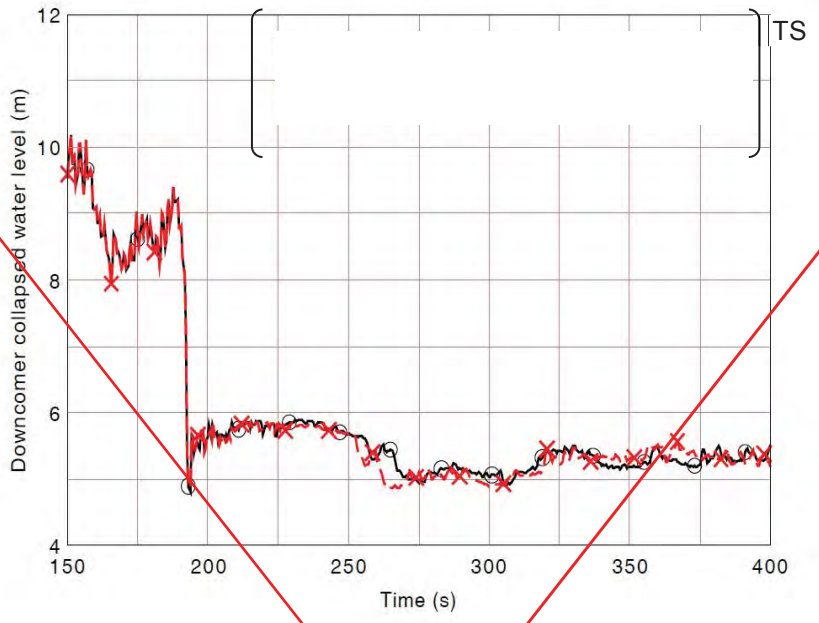

Figure 26 Collapsed Water Level in the Downcomer

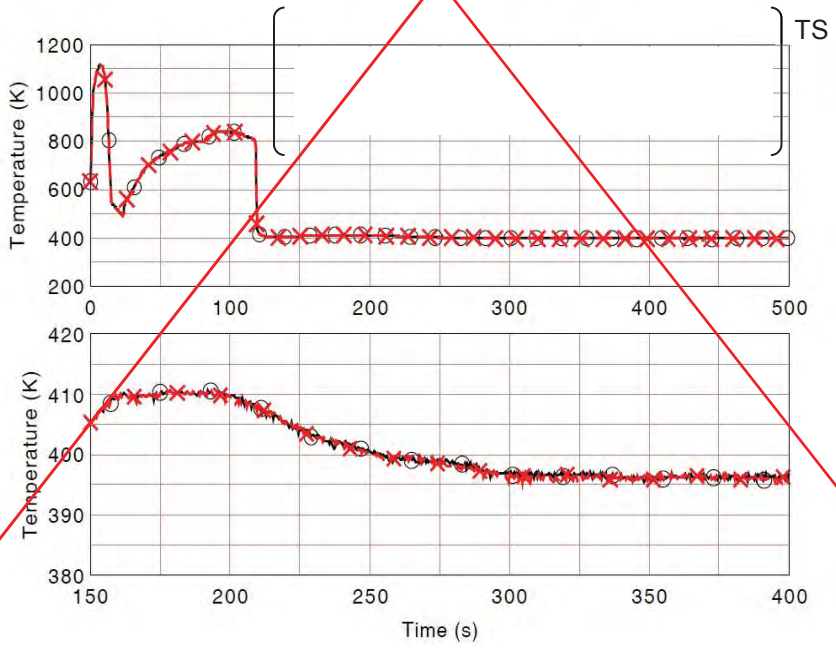

Figure 27 Comparison of the Cladding Temperature of the Hottest Rod

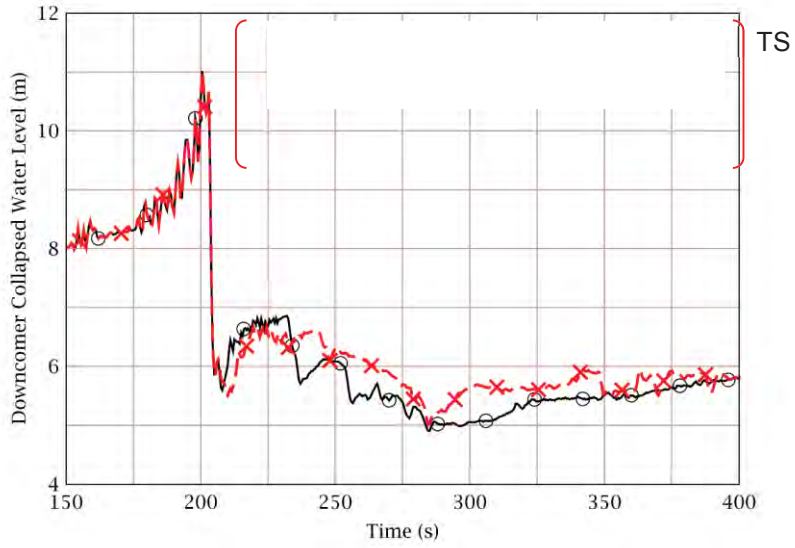

Figure 26 Collapsed Water Level in the Downcomer

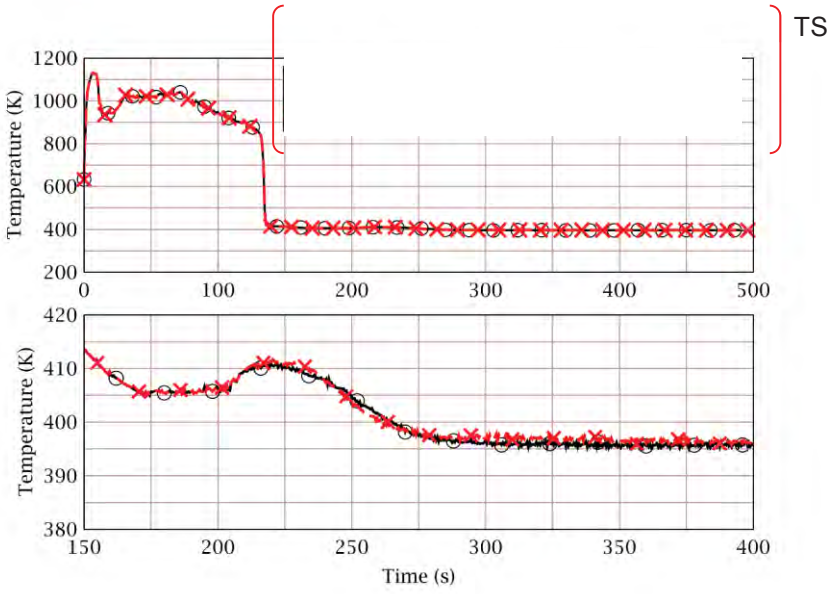

Figure 27 Comparison of the Cladding Temperature of the Hottest Rod

RESPONSE TO AUDIT ISSUES

APR1400 Topical Reports

Korea Electric Power Corporation / Korea Hydro & Nuclear Power Co., LTD

Docket No. PROJ0782

Review Section	**TR Realistic Evaluation Methodology for LBLOCA of the APR1400**
Application Section	**Topical Report: APR1400-F-A-TR-12004 Realistic Evaluation Methodology for Large-Break LOCA of the APR1400**
Issue Date	**08/13/2015**

Audit Issues No. 27-m

NUREG/CR-5429, Section 2.2.2 discusses issues related to model nodalization. Address the following issues regarding nodalization of the APR1400:

m. Differences are noted in the nodalization of the vessel between the APR1400 plant shown in Figure 4-1 of the topical report and the ATLAS facility shown in Figure 3-3 of Appendix E. These differences include the nodalization of the downcomer, lower plenum, upper plenum and the upper plenum to dome connection. Explain the reasons for the noted differences.

Response

m)

Major nodalization differences between APR1400 and ATLAS test facility are found in three parts: lower downcomer to lower plenum, lower plenum and upper plenum.

Lower Downcomer to Lower Plenum

Nodalization difference between APR1400 and ATLAS test is caused by geometric differences. Downcomer of APR1400 is separated by flow skirt from the lower plenum and lower head space below the bottom of downcomer exists as shown in Figure 1. On the other hand, [ ]TS Consequently, nodalization follow physical geometry of the component, thereby nodalization of [ ]TS that of the APR1400.

Lower Plenum

As described in previous paragraph, nodalization difference is caused by geometric difference.

Upper Plenum

[

]TS However, since ATLAS tests assessed in Appendix E were designed to investigate thermal hydraulic behavior during reflood period, [

]TS

TS

Figure 1. Drawing of Downcomer to Lower Plenum for APR1400 [1]

TS

Figure 2. Schematic Diagram of Reactor Vessel in the ATLAS Test Facility

Reference

[1] Drawings, “Reactor Vessel: Flow Baffle,”1-110-H-175-017C, Doosan Heavy industries & Construction, December 2011.

Impact on DCD

There is no impact on the DCD.

Impact on PRA

There is no impact on the PRA.

Impact on Technical Specifications

There is no impact on the Technical Specifications.

Impact on Technical/Topical/Environmental Report

There is no impact on any Technical, Topical, or Environmental Report.

RESPONSE TO AUDIT ISSUES

APR1400 Topical Reports

Korea Electric Power Corporation / Korea Hydro & Nuclear Power Co., LTD

Docket No. PROJ0782

Review Section	**TR Realistic Evaluation Methodology for LBLOCA of the APR1400**
Application Section	**Topical Report: APR1400-F-A-TR-12004 Realistic Evaluation Methodology for Large-Break LOCA of the APR1400**
Issue Date	**08/13/2015**

Audit Issues No. 28

The guidance in RG 1.157, Section 4 establishes acceptable controls for the estimation of calculational uncertainty. Section 4.2.2.1.1 of the topical report states that the uncertainty of fuel thermal conductivity is based on the information from MATPRO (Version 11, Rev. 1, 1980). However, Section 2.3 of NUREG/CR-7024 provides the latest comparison of fuel thermal conductivity models against available experimental data. Section 2.3.2 of NUREG/CR-7024 provides a higher uncertainty for the MATPRO fuel thermal conductivity correlation for both un-irradiated and irradiated fuel as compared to that in Section 4.2.2.1.1 of the topical report. Section 2.3.2 of NUREG/CR-7024 states that the MATPRO fuel thermal conductivity correlation has a bias in the prediction of data from un-irradiated and irradiated uranium oxide fuel. Address the discrepancy between the uncertainty cited in the topical report and the assessment in NUREG/CR-7024, and justify the value used in the topical report.

Response

MATPRO [1] which was referred from CSAU presented standard error for UO2 as ±0.20 W/(m·K). [

]TS Therefore, it is believed to have the conservative results when the MATPRO data is applied.

[

]TS

References

[1] NUREG-CR-0497, “MATPRO-Version 11 (Revision 1), A Handbook of Material Properties for Use in the Analysis of Light Water Reactor Fuel Rod Behavior,” Feb. 1980.

[2] NUREG-CR-0497, “MATPRO-Version 11 (Revision 2), A Handbook of Material Properties for Use in the Analysis of Light Water Reactor Fuel Rod Behavior,” 1981.

[3] NUREG-CR-7024, “Material Property Correlations: Comparisons between FRAPCON-3.4, FRAPTRAN 1.4, and MATPRO,” Mar. 2011.

[4] PNNL-19418, “FRAPCON-4.0: A Computer Code for the Calculation of Steady-State, Thermal-Mechanical Behavior of Oxide Fuel Rods for High Burnup,” U.S.NRC, September 2015.

Impact on DCD

There is no impact on the DCD.

Impact on PRA

There is no impact on the PRA.

Impact on Technical Specifications

There is no impact on the Technical Specifications.

Impact on Technical/Topical/Environmental Report

Topical report will be modified to consider TCD effects. Additional technical report will be submitted for TCD consideration.

There is no impact on Environmental Report.

RESPONSE TO AUDIT ISSUES

APR1400 Topical Reports

Korea Electric Power Corporation / Korea Hydro & Nuclear Power Co., LTD

Docket No. PROJ0782

Review Section	**TR Realistic Evaluation Methodology for LBLOCA of the APR1400**
Application Section	**Topical Report: APR1400-F-A-TR-12004 Realistic Evaluation Methodology for Large-Break LOCA of the APR1400**
Issue Date	**08/13/2015**

Audit Issues No. 29

The guidance in RG 1.157, Section 4 establishes acceptable controls for the estimation of calculational uncertainty. The guidance in RG 1.157, Section 3.3.1 establishes acceptable controls regarding the calculation of clad swelling and rupture. Section 4.2.2.1.1 of the topical report states that the uncertainty in [ ]TS According to Section 9.3 of Volume 4 of the RELAP5/MOD3.3 manual, [ ]TS in the code, derived from FRAP-T6, considers "...elastic deformation of cladding under the differential pressure..." A few lines later the manual states that "...clad ballooning is not included in the [ ]TS Address the following issues:

a. Describe the methods used by RELAP5/MOD3.3 to calculate clad ballooning, fuel pellet fragmentation, and relocation.

b. Describe how ballooned cladding affects long term core coolability.

c. Describe how the ballooning model alters the calculated [ ]TS

d. Provide the rationale for not utilizing the uncertainty in the existing [ ]TS

e. Provide evidence that the selected uncertainty in the cladding rupture model bounds the uncertainty in [ ]TS calculation.

f. Manufacturing tolerance for gas composition, initial backfill pressure, and the uncertainty associated with fission gas production, will also affect the potential ranges of cladding temperature independent of the swelling and rupture, particularly if rupture is not calculated to occur. Describe how the chosen approach treats the gap gas uncertainty component of [ ]TS

Response

a)

The RELAP5 dynamic gap conductance model is a simplified deformation model generated from FRAP-T6 as described in reference [1]. The gap conductance is calculated by the following equation.

$$h_g = \frac{k_g}{N}\sum_{n=1}^{N}\frac{1}{t_n+3.2(R_F+R_C)+(g_1+g_2)}$$ Equation (4.11-1) of reference [1]

where

h_g = conductance through the gas in the gap [W/m^2-K]

n = number of a circumferential segment

N = total number of circumferential segments = 8

k_g = thermal conductivity of gas [W/m-K]

t_n = width of fuel-cladding gap at the midpoint of the n-th circumferential segment [m]

R_F = surface roughness of the fuel [m]

R_C = surface roughness of the cladding [m]

g_1, g_2 = temperature jump distance terms for fuel and cladding

The width of the fuel-cladding gap at any given circumferential segment is calculated by the following equation.

$$t_n = t_g + \left[-1 + \left(\frac{2n-1}{N}\right)\right] t_0$$ Equation (4.11-2) of reference [1]

where

t_g = circumferentially averaged fuel-cladding gap width [m]

t_0 = as-fabricated fuel-cladding gap width [m]

Cladding deformation is considered in the variable of t_g, this variable is calculated by the following equation.

$$t_g = t_0 - u_F + u_C$$ Equation (4.11-8) of reference [1]

where

u_F = radial displacement of the fuel pellet surface [m]

u_C = radial displacement of cladding inner surface [m]

Radial displacement of cladding inner surface (u_C) can be divided into three parts; thermal expansion, creepdown, and elastic deformation unless plastic deformation isn't occur. If plastic deformation occurs, plastic deformation result is added to this variable.

Plastic deformation of cladding occurs when average cladding temperature exceeds plastic temperature, and plastic temperature is calculated by following equation.

$T_{plas} = T_r - 70$ $T_r < 700$

$T_{plas} = T_r - 70 - 0.14(T_r - 700)$ $700 < T_r < 1300$

$T_{plas} = T_r - 155$ $1300 < T_r$

Equation (4.14-5) of reference [1]

The rupture temperature (T_r) is defined as follows.

$$T_r = 3960 - \left(\frac{20.4 \cdot S}{1+H}\right) - \left(\frac{8.51 \times 10^6 S}{100(1+H)+2790 \cdot S}\right)$$ Equation (4.14-4) of reference [1]

where

S = cladding hoop stress [kpsi]

H = max[(heating rate) / (28 C/s), 1.0]

If the deformation model is active and average cladding temperature exceeds plastic temperature, total cladding strain which is sum of the thermal strain, elastic strain, and plastic strain is calculated by the following equation.

$$E_p = 0.25 E_{rup} \exp[-0.0153(T_r - T_C)]$$ Equation (4.14-3) of reference [1]

where

E_p = plastic hoop strain before rupture

E_{rup} = cladding strain at rupture

T_c = average cladding temperature [^oC]

When average cladding temperature exceeds rupture temperature, rod rupture occurs.

These clad deformation model doesn't alter the flow area of the fluid cell and the geometric changes in the heat structures. The geometry changes enter the conduction solution only by affecting the value being calculated for gap conductance [1].

Clad ballooning is considered in the RELAP5/MOD3.3 code as mentioned above, but code does not have fuel pellet fragmentation and relocation models. And those are not considered in the CAREM.

b)

As discussed in the previous response (a), ballooned cladding affects gap width, and it decreases gap conductance. However, geometry changes caused by ballooned cladding does not alter any other parameters which have influence on the RELAP5 hydraulic solution.

c)

Described in a).

In the CAREM, steady state gap conductance data which are calculated by fuel performance code is used for the initial condition of the fuel. [

]TS

[

]TS

d) and e)

Cladding deformation can be divided into two categories: elastic and plastic deformation.

[

]TS

f)

[

]TS

Reference

[1] "RELAP5/MOD3.3 Code Manual Volume I: Code Structure, System Models, and Solution Methods," NUREG/CR-5535/Rev P3-Vol I, U.S.NRC, March 2003.

[2] D. A. Powers, R. O. Meyer, "Cladding Swelling and Rupture Models for LOCA Analysis," NUREG -0630, U.S.NRC, March 1980.

Impact on DCD

There is no impact on the DCD.

Impact on PRA

There is no impact on the PRA.

Impact on Technical Specifications

There is no impact on the Technical Specifications.

Impact on Technical/Topical/Environmental Report

There is no impact on any Technical, Topical, or Environmental Report.

RESPONSE TO AUDIT ISSUES

APR1400 Topical Reports

Korea Electric Power Corporation / Korea Hydro & Nuclear Power Co., LTD

Docket No. PROJ0782

Review Section	**TR Realistic Evaluation Methodology for LBLOCA of the APR1400**
Application Section	**Topical Report: APR1400-F-A-TR-12004 Realistic Evaluation Methodology for Large-Break LOCA of the APR1400**
Issue Date	**08/13/2015**

Audit Issues No. 30-a

The guidance in RG 1.157, Section 3.3.1 establishes acceptable controls regarding the calculation of clad oxidation. Section 4.2.2.1.1 of the topical report describes the uncertainty in the cladding oxidation. The document "KHNP Responses to Request for Additional Information No. 1-7425" (page 4 of 23) describes the input for the uncertainty in the cladding oxidation reaction. Address the following issues:

a. The description implies that the uncertainty will be [ ]TS The rationale provided is that [ ]TS However, the acceptance criterion applies to core-wide cladding oxidation, and in addition, RG 1.157 does not distinguish between oxidation in different rods for best-estimate analysis. Therefore, justify the basis for [ ]TS

Response (Rev.1)

The core-wide cladding oxidation is in reality, related with the maximum hydrogen generation of 10 CFR 50.46(b). In CAREM, [

]TS

In the topical report, calculation results of the maximum hydrogen generation for APR1400 are considerably lower than the acceptance criteria. [

]TS

[

]TS

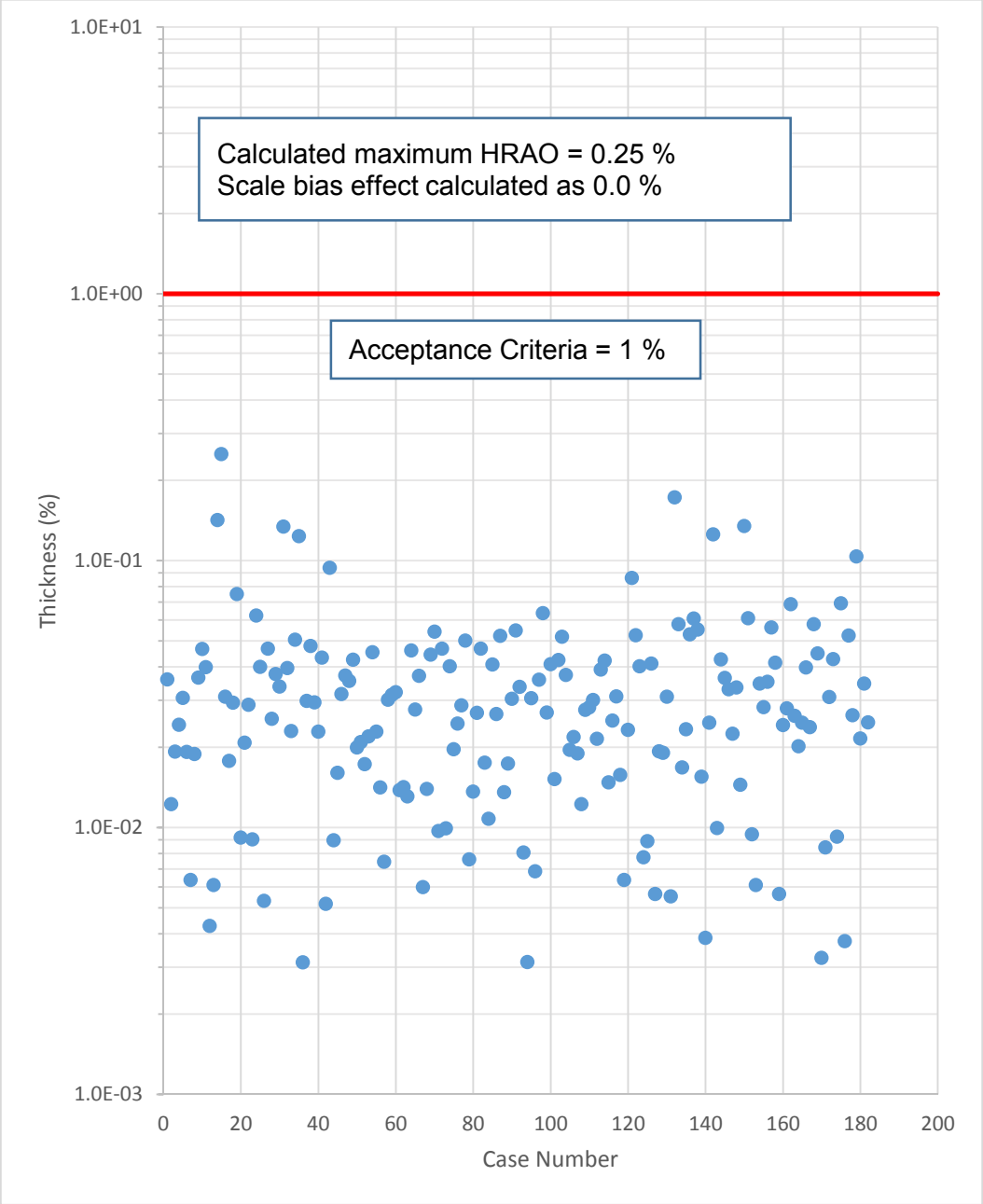

Figure 1. Hot Rod Hydrogen Generation

Impact on DCD

There is no impact on the DCD.

Impact on PRA

There is no impact on the PRA.

Impact on Technical Specifications

There is no impact on the Technical Specifications.

Impact on Technical/Topical/Environmental Report

Topical report was revised.

There is no impact on any Technical or Environmental Report.

RESPONSE TO AUDIT ISSUES

APR1400 Topical Reports

Korea Electric Power Corporation / Korea Hydro & Nuclear Power Co., LTD

Docket No. PROJ0782

Review Section	**TR Realistic Evaluation Methodology for LBLOCA of the APR1400**
Application Section	**Topical Report: APR1400-F-A-TR-12004 Realistic Evaluation Methodology for Large-Break LOCA of the APR1400**
Issue Date	**08/13/2015**

Audit Issues No. 30-b

The guidance in RG 1.157, Section 3.3.1 establishes acceptable controls regarding the calculation of clad oxidation. Section 4.2.2.1.1 of the topical report describes the uncertainty in the cladding oxidation. The document “KHNP Responses to Request for Additional Information No. 1-7425” (page 4 of 23) describes the input for the uncertainty in the cladding oxidation reaction. Address the following issues:

b. According to Section 3.2.5 of RG 1.157, “For rods calculated to rupture their cladding during the loss-of-coolant accident, the oxidation of the inside of the cladding should be calculated in a best-estimate manner.” A discussion of how this requirement is met in CAREM is needed.

Response

The reaction of zirconium and steam in RELAP5/MOD3.3/K code is treated using the correlation developed by Cathcart. As described in Section 4.13 of reference [1], the metal-water reaction model is coupled with the fuel rod deformation model so that if a rod ruptures, the inside of the cladding can react with steam and the oxidation of the inside of the cladding is calculated.

Reference

[1] RELAP5/MOD3.3 Code Manual, Vol. 1: Code Structure, System Models, And Solution Methods, July 2003.

Impact on DCD

There is no impact on the DCD.

Impact on PRA

There is no impact on the PRA.

Impact on Technical Specifications

There is no impact on the Technical Specifications.

Impact on Technical/Topical/Environmental Report

There is no impact on any Technical, Topical, or Environmental Report.

RESPONSE TO AUDIT ISSUES

APR1400 Topical Reports

Korea Electric Power Corporation / Korea Hydro & Nuclear Power Co., LTD

Docket No. PROJ0782

Review Section	**TR Realistic Evaluation Methodology for LBLOCA of the APR1400**
Application Section	**Topical Report: APR1400-F-A-TR-12004 Realistic Evaluation Methodology for Large-Break LOCA of the APR1400**
Issue Date	**08/13/2015**

Audit Issues No. 31

The guidance in RG 1.157, Section 4 establishes acceptable controls for the estimation of calculational uncertainty. Section 4.2.2.1.1 of the topical report provides the uncertainty for the Dittus-Boelter correlation for the liquid-phase forced convection heat transfer by citing “various references.” Provide the references used to determine the uncertainty as well as the results used to determine the standard deviation for this parameter.

Response

Dittus-Boelter correlation has been broadly used to calculate the various kinds of single-phase fluids, and its validity has been demonstrated. Reference [1] summarizes the evaluation results as follows.

TS

[

]TS

References

[1] “Development of PCT Uncertainty Quantification Methodology, Assessment of Separate Models and Construction of Thermal-Hydraulic Data Banks for Establishment of the Korean ECCS Evaluation Model,” KINS/GR-011, 1990.12.

[2] R.A. Dimmena et. Al., “RELAP5/MOD2 Models and Correlations,” NUREG/CR-5194, EGG-2561-R4, 1988.

[3] J.A. Malina and E.M.Sparrow, “Variable-Property, Constant-Property, and Entrance Region Heat Transfer results for Turbulent Flow of Water and TI in a Circular Tube,” Chem. Eng. Sci., Vol. 19, 1964.

[4] C. A. Sleichjev and M. W. Rouse, “ A convenient correlation for heat transfer to constant and variable property fluids in turbulent pipe flow,” Int. J. Heat Mass Transfer, Vol. 18, 1975.

Impact on DCD

There is no impact on the DCD.

Impact on PRA

There is no impact on the PRA.

Impact on Technical Specifications

There is no impact on the Technical Specifications.

Impact on Technical/Topical/Environmental Report

There is no impact on any Technical, Topical, or Environmental Report.

RESPONSE TO AUDIT ISSUES

APR1400 Topical Reports

Korea Electric Power Corporation / Korea Hydro & Nuclear Power Co., LTD

Docket No. PROJ0782

Review Section	**TR Realistic Evaluation Methodology for LBLOCA of the APR1400**
Application Section	**Topical Report: APR1400-F-A-TR-12004 Realistic Evaluation Methodology for Large-Break LOCA of the APR1400**
Issue Date	**08/13/2015**

Audit Issues No. 32

The guidance in RG 1.157, Section 3.8 establishes acceptable controls for the calculation of critical heat flux. Section 4.2.2.1.2 of the topical report states that the nucleate boiling heat transfer coefficient is calculated in RELAP5/MOD3.3 based on the Chen correlation, and it goes on to cite the RELAP5/MOD3.3 code manual for the average error of 21.1 percent for saturated nucleate boiling and ± 40 percent for subcooled nucleate boiling. However, the reviewers find that the maximum average error using the Chen correlation for saturated nucleate boiling is 15.7 percent according to Table 4.2-4 of Volume 4 of the RELAP5/MOD3.3 manual. Furthermore, the range of errors using the Chen correlation for subcooled nucleate boiling is given as +180 percent to -60 percent in the Section 4.2.3.2.3 of Volume 4 of the RELAP5/MOD3.3 manual. Provide the basis and details of the source(s) used to determine the values listed in Section 4.2.2.1.2 of the topical report for the uncertainty in the Chen correlation.

Response

Table 1 shows the average deviations for the saturated and the sub-cooled nucleate boiling heat transfer coefficient in RELAP5/MOD3.3 code manual and topical report (ToR) with the reference document of RELAP5/MOD3.1 code manual [1].

The RELAP5/MOD3.3 code manual does not contain the code assessment for Chen correlation but model basis. Meanwhile, RELAP5/MOD3.1 code manual contains both the model basis and the code assessment for Chen correlation. In the sections of model basis and the code assessment describe the uncertainty range of Chen correlation. However, the ranges in both sections are different from each other. The topical report uses the uncertainty ranges for Chen correlation obtained from the code assessment which is written in the RELAP5/MOD3.1 code manual.

Table 1. Average deviations for the nucleate boiling heat transfer coefficient

1) Saturated nucleate boiling		Avg. Deviation [%]
ToR		21.1
RELAP5/MOD3.3 manual (Vol. 4, Table 4.2-4)		Max. 15.7
RELAP5/MOD3.1 manual (Vol. 4)	Assessment (Section 4.2.3.1.3)	21.1
	Model Basis (Section 4.2.3.1.1)	Max. 15.7
2) Sub-cooled nucleate boiling		Avg. Deviation [%]
ToR		±40
RELAP5/MOD3.3 manual (Vol. 4, Section 4.2.3.2.3)		+180 to -60
RELAP5/MOD3.1 manual (Vol. 4)	Assessment (Section 4.2.3.2.3)	±40
	Model Basis (Section 4.2.3.2.1)	+180 to -60

References

[1] “RELAP5/MOD3 Code Manual Vol. 4, Model and Correlations (Draft),” NUREG/CR-5535, EGG-2596, 1990. 06.

Impact on DCD

There is no impact on the DCD.

Impact on PRA

There is no impact on the PRA.

Impact on Technical Specifications

There is no impact on the Technical Specifications.

Impact on Technical/Topical/Environmental Report

There is no impact on any Technical, Topical, or Environmental Report.

RESPONSE TO AUDIT ISSUES

APR1400 Topical Reports

Korea Electric Power Corporation / Korea Hydro & Nuclear Power Co., LTD

Docket No. PROJ0782

Review Section	**TR Realistic Evaluation Methodology for LBLOCA of the APR1400**
Application Section	**Topical Report: APR1400-F-A-TR-12004 Realistic Evaluation Methodology for Large-Break LOCA of the APR1400**
Issue Date	**08/13/2015**

Audit Issues No. 33

The guidance in RG 1.157, Section 3.8 establishes acceptable controls for the calculation of critical heat flux. Section 4.2.2.1.2 of the topical report discusses the comparison of the performance of the Groeneveld lookup table, shown in Figure 4-2 for the “high-pressure and high-flow critical heat flux” phenomenon. Demonstrate that the system conditions encountered during the limiting LBLOCA are covered by the 1993 data points that were used for comparison. In addition, clarify whether the 1993 data points represent data from steady-state tests or include transient critical heat flux (CHF) tests as well.

.

Response

Table 1 shows the experimental conditions of the CHF data (shown in Figure 4-2 of the topical report) with APR1400 LBLOCA conditions. The system conditions were obtained from the calculation of 100 % double ended guillotine break at a cold leg.

From Table 1, all of the steady and transient conditions are covered by the experimental conditions. Low flow region (0.5 – 10 kg/m^{2}s) exists, though, where the transient calculation result below the data range. The CHF at low flow region (below a mass flux of 100 kg/m^{2}s [2]) is calculated by the modified Zuber correlation.

Table 1. Ranges of Experimental Data and Calculations (Steady and Transient)

	Exp. Data [1]	Calc. (Steady State)	Calc. (Transient State)
Pressure [MPa]	0.1~20.0	15.9	0.19~15.9
Mass flux [kg/m^{2}s]	10.0~18600.0	3488.5	0.5~3499.6
Quality [-]	-0.097~0.988	0.0	0.0~0.90

References

[1] “RELAP5/MOD3 Code Manual Vol. 4, Model and Correlations (Draft),” NUREG/CR-5535, EGG-2596, page 4.2-82, 1990. 06.

[2] “RELAP3.3 MOD3.3 Code Manual Vol. 4, Models and Correlations,” NUREG/CR-5535, Rev. P3, page 211~212, 2006. 03.

Impact on DCD

There is no impact on the DCD.

Impact on PRA

There is no impact on the PRA.

Impact on Technical Specifications

There is no impact on the Technical Specifications.

Impact on Technical/Topical/Environmental Report

There is no impact on any Technical, Topical, or Environmental Report.

RESPONSE TO AUDIT ISSUES

APR1400 Topical Reports

Korea Electric Power Corporation / Korea Hydro & Nuclear Power Co., LTD

Docket No. PROJ0782

Review Section	**TR Realistic Evaluation Methodology for LBLOCA of the APR1400**
Application Section	**Topical Report: APR1400-F-A-TR-12004 Realistic Evaluation Methodology for Large-Break LOCA of the APR1400**
Issue Date	**08/13/2015**

Audit Issues No. 34-a

The guidance in RG 1.157, Section 3.8 establishes acceptable controls for the calculation of critical heat flux. Address the following regarding the two CHF correlations when the RELAP5/MOD3.3 reflood model is activated:

a. Provide the mass flux limits and transition criterion for the CHF calculated from the lookup table and from the modified Zuber correlation when the reflood model is activated.

Response

Mass flux limits are described in Section 4.4.5.4 of reference [1]. Modified Zuber CHF correlation is used to calculate CHF for low mass flux region, whereas CHF of high mass flux region is obtained by Groeneveld lookup table. Mass flux limits for above two region is below.

Above than 200 kg/m^{2}s:	Groeneveld lookup table
Below than 100 kg/m^{2}s:	Modified Zuber correlation

Linear interpolation of modified Zuber CHF and Groeneveld lookup table is used in intermediate region between a mass flux of 100 and 200 kg/m^{2}s.

Reference

[1] “RELAP5 MOD3.3 Code Manual Volume IV: Models and Correlations,” NUREG/CR-5535, Rev P3, U.S.NRC, March 2006.

Impact on DCD

There is no impact to the DCD.

Impact on PRA

There is no impact on the PRA.

Impact on Technical Specifications

There is no impact on the Technical Specifications.

Impact on Technical/Topical/Environmental Report

There is no impact on any Technical, Topical, or Environmental Report.

RESPONSE TO AUDIT ISSUES

APR1400 Topical Reports

Korea Electric Power Corporation / Korea Hydro & Nuclear Power Co., LTD

Docket No. PROJ0782

Review Section	**TR Realistic Evaluation Methodology for LBLOCA of the APR1400**
Application Section	**Topical Report: APR1400-F-A-TR-12004 Realistic Evaluation Methodology for Large-Break LOCA of the APR1400**
Issue Date	**08/13/2015**

Audit Issues No. 34-b

The guidance in RG 1.157, Section 3.8 establishes acceptable controls for the calculation of critical heat flux. Address the following regarding the two CHF correlations when the RELAP5/MOD3.3 reflood model is activated:

b. Indicate whether the conditions in the representative LBLOCA during the early reflood period fall in the transition region. Furthermore, explain how separate uncertainties in the high- and low-flow CHF calculations can capture the uncertainty in the transition region where interpolation is used.

Response

Figure 1 shows calculated result of core collapsed water level for nominal case, and it can be found that end of refill or start of early reflood is around 36 seconds after break. Figure 2 shows total SI mass flow rate from the four SIT-FDs. All SIT-FDs are depleted at around 203 seconds, it means the end of early reflood is around 203 seconds after break. Thus, early reflood period can be defined as 36 ~ 203 seconds for nominal case.

Figure 3 shows calculated CHF values, black line data with circle symbols are calculated by modified Zuber CHF correlation, red dotted line data with rectangular symbols are calculated by Groeneveld lookup table, and blue dotted line data with diamond symbols are final CHF values. By the definition of early reflood period, calculated CHF data are presented for time period of 40 ~ 200 seconds. Modified Zuber CHF correlation is used for almost all of early reflood period.

Modified Zuber CHF correlation is used to calculate CHF if mass flux is lower than 100 kg/m^{2}s. Whereas, Groeneveld lookup table is used when mass flux is larger than 200 kg/m^{2}s. And interpolated value is used between mass flux ranges of 100 ~ 200 kg/m^{2}s. In the interpolated region, [

]^{TS}

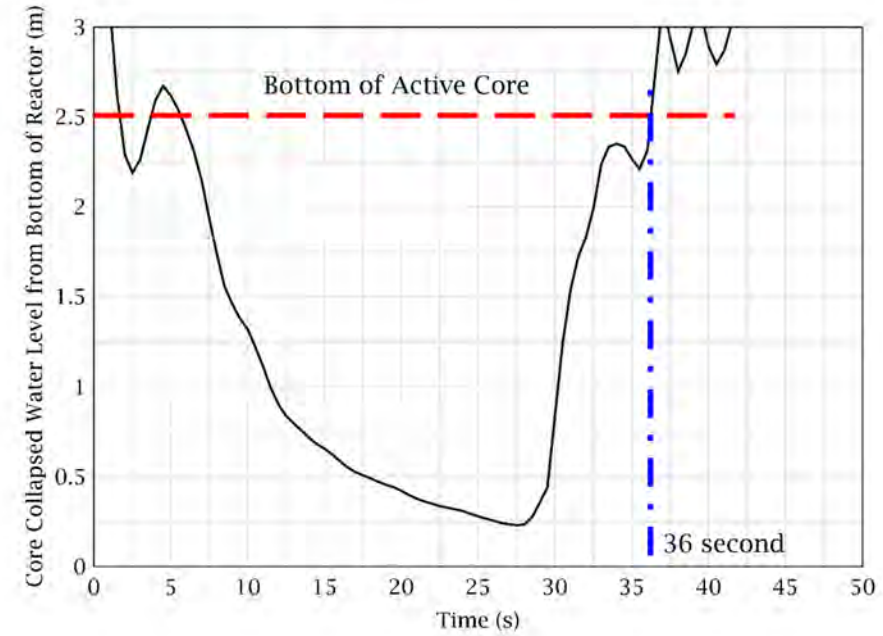

Figure 1. Core Collapsed Water Level

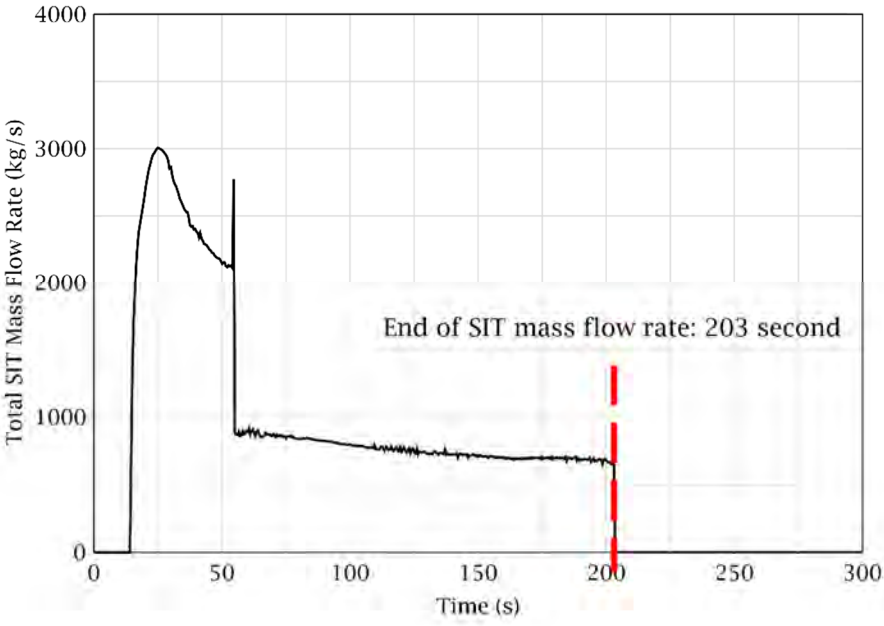

Figure 2. Total SI Mass Flow Rate from four SIT-FDs

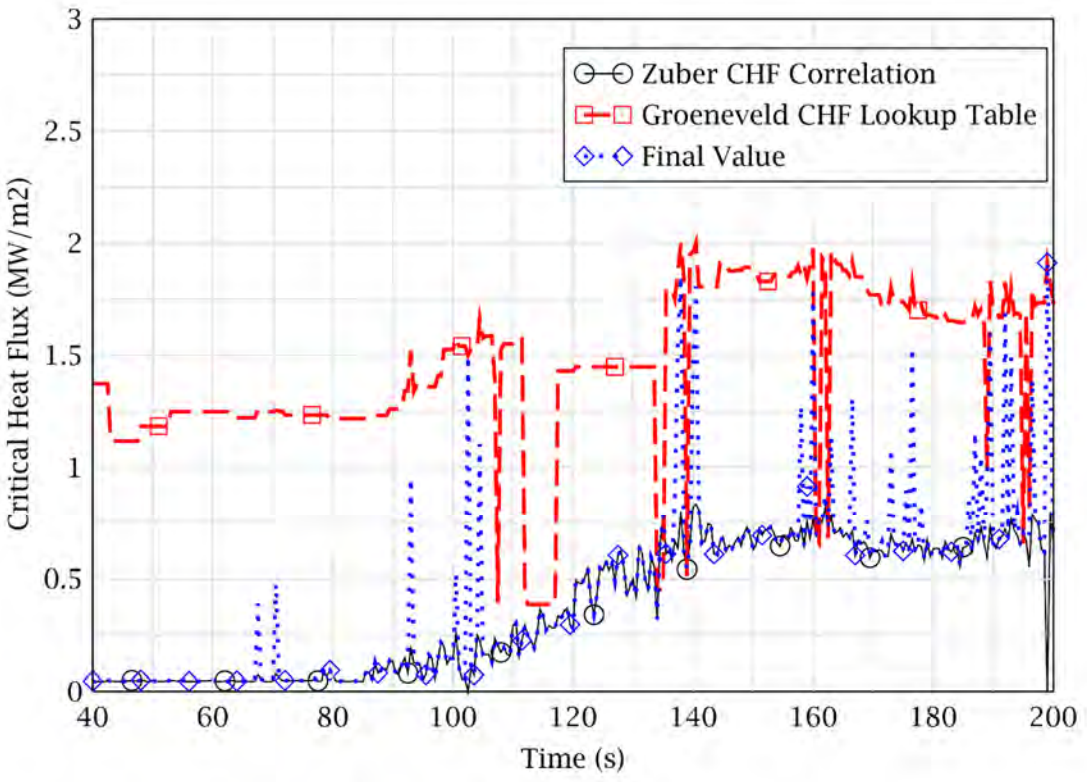

Figure 3. Comparison of Calculated CHF Values

Impact on DCD

There is no impact on the DCD.

Impact on PRA

There is no impact on the PRA.

Impact on Technical Specifications

There is no impact on the Technical Specifications.

Impact on Technical/Topical/Environmental Report

There is no impact on any Technical, Topical, or Environmental Report.

RESPONSE TO AUDIT ISSUES

APR1400 Topical Reports

Korea Electric Power Corporation / Korea Hydro & Nuclear Power Co., LTD

Docket No. PROJ0782

Review Section	**TR Realistic Evaluation Methodology for LBLOCA of the APR1400**
Application Section	**Topical Report: APR1400-F-A-TR-12004 Realistic Evaluation Methodology for Large-Break LOCA of the APR1400**
Issue Date	**08/13/2015**

Audit Issues No. 35

The guidance in RG 1.157, Section 4 establishes acceptable controls for the estimation of calculational uncertainty. Section 4.2.2.1.2 of the topical report discusses the uncertainty for the "film boiling heat transfer" phenomenon. Address the following regarding the corresponding uncertainty determination:

a. The assessments presented in Appendix C of the topical report compare the prediction of the overall film boiling heat transfer correlation in RELAP5/MOD3.3/K against experimental data, so that the resulting uncertainty in the prediction can be determined. Explain the reason for the current approach of using uncertainties for the individual correlations (e.g., Bromley and Forslund-Rohsenow [F-R]) instead of the uncertainty range based on the overall film boiling heat transfer prediction by RELAP5/MOD3.3/K. Justify use of the Forsland-Rohsenow correlation and any modifications made in its application.

b. Section 4.2.2.1.2 of the topical report cites NUREG/CR-5249 as the basis for determining the uncertainty range for the F-R heat transfer correlation. However, Section 4.1 of NUREG/CR-5249 (pg. 82, second paragraph), the range of multipliers (0.75 – 1.5) used in NUREG/CR-5249 is for the total film boiling heat transfer. The impact of only the F-R correlation is captured via a bias as noted in Section 4.1 of NUREG/CR-5249 (pg. 82, second paragraph) and described in Section 4.3.1.2 and Table 37 of NUREG/CR-5249. Justify the range for the F-R correlation in Section 4.2.2.1.2 of the topical report [ ]TS

c. Section 4.2.2.1.2 of the topical report states that the study documented in the topical report Reference [16] showed that the experimental data was [ ]TS As described in Appendix B of the topical report, [

]TS Explain how the performance of only the Bromley correlation was determined from the RELAP5/MOD3.3 comparisons for use in the uncertainty analysis.

d. Section 4.2.2.1.2 of the topical report states that the study documented in the topical report Reference [16] showed that [ ]TS The topical report proceeds to assign, without any explanation, the standard deviation for the Bromley correlation based on the lower end of this prediction range. Provide the corresponding justification.

Response

a)

The Forslund-Rohsenow correlation is developed for dispersed film boiling conditions, whereas the Bromley correlation is developed for pool boiling conditions. That is, experimental conditions developed for these correlations are different even though these conditions belong to the film boiling region. So, it is natural to have different uncertainty ranges and distribution functions for the above two correlations, and reasonable to consider individual uncertainty for them. The basic approach of the CAREM is that a specific parameter of an individual correlation for major phenomena is selected as an uncertainty parameter. Consequently, it is determined that uncertainty of each correlation (Bromley and Forslund-Rohsenow) should be considered.

b), c) and d)

Uncertainty ranges and distribution functions of the above two correlations are selected based on the literature survey and sensitivity calculations.

As stated in the RELAP5 code manual, the wall-to-fluid heat transfer mechanisms are conduction across a vapor film blanket next to a heated wall, convection to flowing vapor and between the vapor and droplets, and radiation across the film to a continuous liquid blanket or dispersed mixture of liquid droplets and vapor. [

]TS

More detail, the conduction heat transfers during reflood and non-reflood period are considered separately. The conduction heat transfer coefficient in the non-reflood period is obtained by the modified Bromley correlation, whereas, the conduction heat transfer coefficient in the reflood period is obtained by [

]TS The radiation heat transfer coefficient to the droplet and convection heat transfer coefficient to the vapor are added to the calculated conduction heat transfer coefficient.

Figure 1 shows the heat transfer coefficients calculated by [

]TS As shown in Figure 1, which is the result from nominal case of plant calculation, it can be stated that the heat transfer coefficient of [ ]TS is mainly used during the reflood period. Whereas, the heat transfer coefficient of the modified Bromley correlation affects blowdown period because the modified Bromley correlation is only used to calculate conduction heat transfer coefficient in film boiling heat transfer mode.

In the CAREM, the uncertainty parameter range for the modified Bromley correlation is determined to have standard deviation of [ ]TS And for the Forslund-Rohsenow correlation, the uncertainty parameter range is from [ ]TS as stated below.

- Forslund-Rohsenow

  [

  ]TS

- Modified Bromley

[

]TS

The rationales of uncertainty parameter ranges of modified Bromley correlation are obtained from RELAP5/MOD3.3 manual and Reference [16] of the topical report. Those of Forslund-Rohsenow correlation are obtained from [1]. The RELAP5/MOD3.3 code manual describes that the film boiling heat transfer coefficients using the modified Bromley correlation cover all data within ± 18 % deviation. However, Reference [16] of the topical report shows following conclusions for uncertainty of film boiling.

[

]TS

It can be concluded from the results of Reference [16] of the topical report that the standard deviation from Reference [16] is much larger than the one from RELAP5/MOD3.3.

The above results have some limitations: [

]TS Therefore, the result for reflood period cannot be used for the selection of the present parameter.

As we can see from the above, the standard deviations obtained from RELAP5 manual and Reference [16] of the topical report are different each other as 0.18 and [ ]TS, respectively. Since the distribution of uncertainty parameter obtained from the two literature are different, the broader range values is employed as the distribution of the modified Bromley correlation. In the CAREM, uncertainty parameter ranges are designed as 1.96 times of standard deviation for the uncertainty parameter with normal distribution. In the topical report, the standard deviation of the modified Bromley correlation is [ ]TS. By assuming [ ]TS times of standard deviation in SRS calculation for conservatism, this value of the standard deviation meets the 1.96 times of the [ ]TS, which is the broader range requirement. It was also confirmed by data coverage

check in appendix C and D of the topical report.

In case of the Forslund-Rohsenow correlation, it is stated in [1] that the correlation has a bias and varies from 0.75 to 1.5. Another sensitivity calculation against FLECHT-SEASSET test was performed using RELAP5/MOD3.3/K. Total 17 test data of FLECHT-SEASET described in appendix C of the topical report were used, and only Forslund-Rohsenow correlation was used to calculate the conduction heat transfer coefficient for the film boiling of the reflood period. As shown in Figure 1, it could be expected that the sensitivity results are similar with the code assessment results using RELAP5/MOD3.3/K code described in appendix C because calculated values of Forslund-Rohsenow correlation are dominant in the reflood period. Figure 2 shows comparison of the experimental data and the sensitivity results. This figure shows all measurement data installed at the same elevation of peak cladding temperature measurement for each test. As a result, [

]TS

Reference

[1] “Quantifying Reactor Safety Margins: Application of Code Scaling, Applicability, and Uncertainty Evaluation Methodology to a Large-Break, Loss-of-Coolant Accident,” NUREG/CR-5249, U.S.NRC, December 1989.

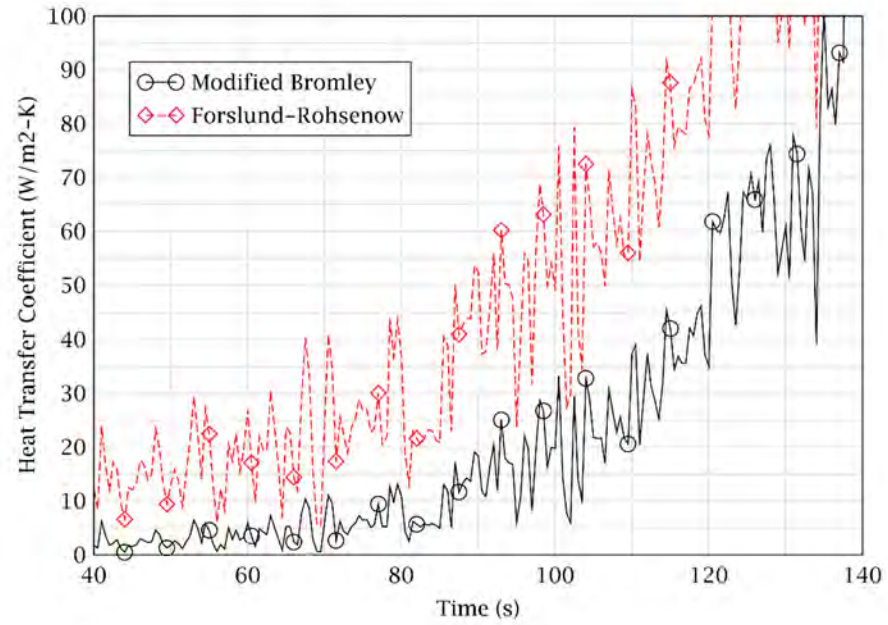

Figure 1. Calculated Heat Transfer Coefficients Comparison

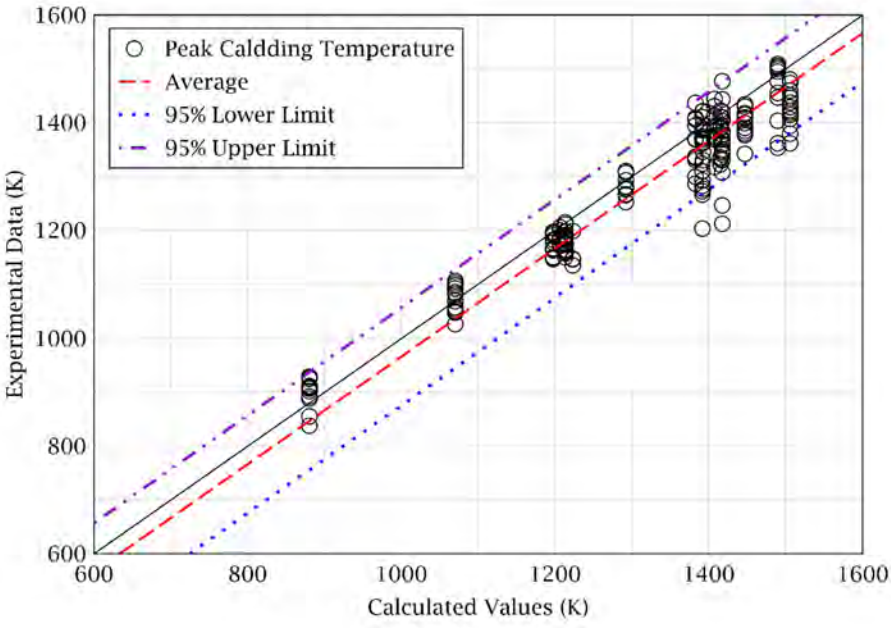

Figure 2. Comparison of Experimental Data and Predicted Values

Impact on DCD

There is no impact on the DCD.

Impact on PRA

There is no impact on the PRA.

Impact on Technical Specifications

There is no impact on the Technical Specifications.

Impact on Technical/Topical/Environmental Report

There is no impact on any Technical, Topical, or Environmental Report.

RESPONSE TO AUDIT ISSUES

APR1400 Topical Reports

Korea Electric Power Corporation / Korea Hydro & Nuclear Power Co., LTD

Docket No. PROJ0782

Review Section	**TR Realistic Evaluation Methodology for LBLOCA of the APR1400**
Application Section	**Topical Report: APR1400-F-A-TR-12004 Realistic Evaluation Methodology for Large-Break LOCA of the APR1400**
Issue Date	**08/13/2015**

Audit Issues No. 36

NUREG/CR-5429, Section 2.1 establishes an acceptable process for the documentation of PIRT. Section 4.2.2.1.2 of the topical report discusses the phenomenon of spacer grid heat transfer which carries a rank of [ ]^{TS} in the APR1400 PIRT (topical report Table 3-2). It is stated that "RELAP5/MOD3.3/K does not have a model to address these heat transfer enhancement effects of the spacer grids. The deficiency of the spacer grid model would result in a conservative prediction of the cladding temperatures." The FLECHT-SEASET test bundle incorporates spacer grids. It would be expected therefore that the RELAP5/MOD3.3/K simulations would over-predict the cladding temperature test data. However, Figure 8 of Appendix B shows that for the low flooding rate test 31504 the cladding temperature at the 78-inch elevation is under-predicted. Appendix C provides a comparison of RELAP5/MOD3.3/K simulations of 17 FLECHT-SEASET tests. Most of those tests were at high flooding rates. At the 72-inch and 96-inch elevation, several cases were under-predicted. In addition, three of the four low flooding rate cases (less than 30 cm/sec) tended to be under-predicted. Furthermore, most of the RELAP5/MOD3.3/K calculated results show unusual behavior for rod quenching at the various elevations – the rod cladding temperature rapidly drops followed by a declining plateau and then a final temperature drop to quenching. The above discussion indicates that even though the RELAP5/MOD3.3/K calculations do not include the effects of modeling the spacer grids, the cladding temperature calculation is non-conservative for several cases. Therefore, describe the code calculated physical phenomena providing the cladding cooling in the noted results.

Response

Grid Effect

The spacer grids of the fuel assembly usually have three effects on core cooling; (1) heat transfer enhancement by the agitation of the flow, (2) rewetting of spacer grids, and (3) breakup of entrained water drops into fine droplets. All three have favorable effects on core cooling. RELAP5/MOD3.3/K does not have a model to address these heat transfer enhancement effects of the spacer grids. The deficiency of the spacer grid model would result in a conservative prediction of the cladding temperatures.

Heat transfer effect of different grid type is described in Reference 1. According to the reference, the droplet breakup and convective enhancement for the grid with mixing vanes are greater than those for the grid without mixing vanes. Since FLECHT-SEASET tests have no mixing vanes, the grid effect is relatively not significant.

Peak Cladding Temperature

The peak cladding temperature of FLECHT-SEASET tests is defined as the maximum value among the measured temperatures at the same elevation. In considering this, the RELAP5 code predicts the cladding temperature behavior of the tests appropriately in general, and the peak cladding temperatures are within the measurement deviation range as shown in Appendix C.

When the values calculated by code are lower than the tests data, SRS calculations are performed. And it was confirmed that the maximum value of SRS calculations covered the maximum tests data.

124 times of SRS calculations were performed for each test case and Figures 2-93 to Figure 2-109 of Appendix C show the results of the SRS calculations against 17 FLECHT-SEASET tests. In all SRS calculations, data covering was confirmed and the third highest values of the calculated cladding temperatures were higher than the measured PCTs.

Quenching

The calculated temperature at a specified elevation is obtained by interpolating the two adjacent node center values. The interpolated rod cladding temperature drops twice after the turn-around time, because one of the two node center temperatures quenches later than the other one.

Reference

[1] “Compendium of ECCS Research for Realistic LOCA Analysis,” NUREG-1230, R4, December 1988.

Impact on DCD

There is no impact on the DCD.

Impact on PRA

There is no impact on the PRA.

Impact on Technical Specifications

There is no impact on the Technical Specifications.

Impact on Technical/Topical/Environmental Report

There is no impact on any Technical, Topical, or Environmental Report.

RESPONSE TO AUDIT ISSUES

APR1400 Topical Reports

Korea Electric Power Corporation / Korea Hydro & Nuclear Power Co., LTD

Docket No. PROJ0782

Review Section	**TR Realistic Evaluation Methodology for LBLOCA of the APR1400**
Application Section	**Topical Report: APR1400-F-A-TR-12004 Realistic Evaluation Methodology for Large-Break LOCA of the APR1400**
Issue Date	**08/13/2015**

Audit Issues No. 37a, b, and d

The guidance in RG 1.157, Section 3.9.1 establishes acceptable controls regarding the calculation of radiation heat transfer. Section 4.2.2.1.2 of the topical report states that [

]TS

Address the following concerns about this statement:

a. As mentioned in Appendix B, the prediction by RELAP5/MOD3.3/K using [ ]TS is added to the convective vapor and radiation heat transfer to determine the total heat transfer. In addition, Appendix C makes no mention of [ ]TS in the comparison of RELAP5/MOD3.3/K predictions against experimental data. Clarify whether [ ]TS as part of CAREM and therefore, [ ]TS in the film boiling heat transfer calculation.

b. Clarify whether the code used for the assessments documented in Appendices B and C of the topical report includes radiation heat transfer, especially for the film boiling heat transfer calculation.

d. The APR1400 PIRT assigns a rank of [ ]TS or lower for the “radiation heat transfer to the surfaces, vapor and liquid” phenomenon. Based on the definition of the importance rankings, it is implied that the phenomenon is calculated in the code. [

]TS

Response

(a) & (b)

RELAP5/MOD3.3 code has radiation heat transfer model, and it can be divided into wall-to-wall and wall-to-fluid radiation models. Wall-to-wall radiation model in the RELAP5/MOD3.3 code can be activated by user input, whereas wall-to-fluid radiation is considered using additional radiation model.

Film boiling heat transfer coefficient of RELAP5/MOD3.3/K code is predicted by maximum of [ ]TS calculated values. And radiation heat transfer to the droplet and convection heat transfer to the vapor are added to the calculated film boiling heat transfer coefficient.

Descriptions in the topical report mean that [ ]TS in the CAREM. Thus, it means [ ]TS is considered by the code.

It is conservative method to [ ]TS Heat transfer by convection and film boiling is dominant comparing with radiation heat transfer. Thus, convection heat transfer and film boiling heat transfer were determined as uncertainty parameters.

(d)

See the response to 37-(a) and (b).

Impact on DCD

There is no impact on the DCD.

Impact on PRA

There is no impact on the PRA.

Impact on Technical Specifications

There is no impact on the Technical Specifications.

Impact on Technical/Topical/Environmental Report

There is no impact on any Technical, Topical, or Environmental Report.

RESPONSE TO AUDIT ISSUES

APR1400 Topical Reports

Korea Electric Power Corporation / Korea Hydro & Nuclear Power Co., LTD

Docket No. PROJ0782

Review Section	**TR Realistic Evaluation Methodology for LBLOCA of the APR1400**
Application Section	**Topical Report: APR1400-F-A-TR-12004 Realistic Evaluation Methodology for Large-Break LOCA of the APR1400**
Issue Date	**08/13/2015**

Audit Issues No. 37 (c)

The guidance in RG 1.157, Section 3.9.1 establishes acceptable controls regarding the calculation of radiation heat transfer. Section 4.2.2.1.2 of the topical report states that [ ]TS

Address the following concerns about this statement:

c. [ ]TS in Section 4.2.2.1.2 of the topical report is called "conservative." [ ]TS may actually be non-conservative. Justify [ ]TS

Response

(c)

As discussed in response to 37-(a) and (b), [ ]TS is calculated, whereas [ ]TS Thus, it only needs to examine the effects of [ ]TS However, it is clear that [ ]TS that is, it tends to decrease cladding temperature.

A sensitivity study for [ ]TS

Figure 1 through Figure 3 show cladding temperatures of hot rod for lower, center, and upper elevations. As discussed in topical report, [ ]TS

Figure 4 through Figure 6 show cladding temperatures of core average rod for lower, center, and upper elevations. As shown in these figures, it can confirm that core average rod cladding temperature tends to increase by [ ]TS

Figure 7 shows core collapsed water level. [ ]TS

Figure 8 through Figure 10 show vapor phase temperatures of hot channel for lower, center, and upper elevation, and Figure 11 through Figure 13 show those of average channel. As shown in these figures, there are insignificant differences on vapor phase temperature between nominal and [ ]TS Consequently, it can be concluded that the decrease in cladding temperature of hot rod is caused by [ ]TS

Figure 1. Hot Rod Cladding Temperature at Lower Elevation

Figure 2. Hot Rod Cladding Temperature at Center Elevation

Figure 3. Hot Rod Cladding Temperature at Upper Elevation

Figure 4. Average Rod Cladding Temperature at Lower Elevation

Figure 5. Hot Rod Cladding Temperature at Center Elevation

Figure 6. Hot Rod Cladding Temperature at Upper Elevation

TS

Figure 7. Core Collapsed Water Level

TS

Figure 8. Hot Channel Vapor Phase Temperature at Lower Elevation

Figure 9. Hot Channel Vapor Phase Temperature at Center Elevation

Figure 10. Hot Channel Vapor Phase Temperature at Upper Elevation

Figure 11. Average Channel Vapor Phase Temperature at Lower Elevation

Figure 12. Average Channel Vapor Phase Temperature at Center Elevation

TS

Figure 13. Average Channel Vapor Phase Temperature at Upper Elevation

Impact on DCD

There is no impact on the DCD.

Impact on PRA

There is no impact on the PRA.

Impact on Technical Specifications

There is no impact on the Technical Specifications.

Impact on Technical/Topical/Environmental Report

There is no impact on any Technical, Topical, or Environmental Report.

RESPONSE TO AUDIT ISSUES

APR1400 Topical Reports

Korea Electric Power Corporation / Korea Hydro & Nuclear Power Co., LTD

Docket No. PROJ0782

Review Section	**TR Realistic Evaluation Methodology for LBLOCA of the APR1400**
Application Section	**Topical Report: APR1400-F-A-TR-12004 Realistic Evaluation Methodology for Large-Break LOCA of the APR1400**
Issue Date	**08/13/2015**

Audit Issues No. 38

The guidance in RG 1.157, Section 4 establishes acceptable controls for the estimation of uncertainties. Section 4.2.2.1.2 of the topical report states that the uncertainty in the interfacial drag and heat transfer models is captured via [ ]^{TS} Address the following concerns about [ ]^{TS}:

a. It is unclear what is being achieved by the uncertainty on [ ]^{TS} because the impact on entrainment from the upper plenum resulting in steam binding is captured via a separate assessment that does not include [ ]^{TS}. In addition, results showing the actual impact of [ ]^{TS} have not been provided. Therefore, it is difficult to determine the purpose of the selected uncertainty and whether the selection and the ranges are appropriate. Justify the selection of [ ]^{TS}.

b. The purpose of the ranging of parameters is to capture the uncertainty in the code prediction by comparisons against relevant experimental data. Such an approach has not been followed to determine the uncertainty in the interfacial drag and heat transfer models. The range of uncertainty selected for [ ]^{TS} is based on code manuals rather than on the comparison against interfacial drag or heat transfer data (i.e., tests listed in the Table 4-4 of the topical report). Furthermore, comparisons against data also reveal the impact of code features such as level tracking. These code features can potentially impact the predicted entrainment and therefore, the uncertainty in the predictions. Justify the values used for the uncertainty in the interfacial drag and heat transfer in the topical report.

c. Section 6.1.3.1 of Volume 4 of RELAP5/MOD3.3 manual states that [ ]^{TS} is 3.0 and that for post-CHF droplets is 12.0. These values are also stated on page 46 in Volume 4 of RELAP5/MOD3.3 manual. These [ ]^{TS} values appear to represent a range. Provide details of the source(s) for [ ]^{TS} that is documented in Section 4.2.2.1.2 of the topical report.

Response

a)

As described in Section 4.2.2.1.2 of the topical report, [ ]TS to describe the uncertainty of interfacial drag and heat transfer in the core region.

Entrainment of droplets is a major source of heat transfer for the fuel. In RELAP5, a [ ]TS is used to calculate the droplet size and the droplet size is used in the calculation of the interfacial area. The interfacial area is used in the calculation of both interfacial drag and heat transfer. Therefore, in order to represent the uncertainty of the interfacial drag and heat transfer in the core region during the reflood period, [ ]TS is selected as a code parameter.

b) and c)

The uncertainty ranges of individual parameters can be determined from information such as experimental data, reference documents, engineering judgments and code calculations as discussed in Chapter 4 of the topical report. The uncertainty range and distribution function of [ ]TS are determined using the following reference documents.

RELAP5/MOD3.3 code uses various correlations to evaluate interfacial heat transfer and drag for various conditions. And these correlations needed droplet diameter to calculate interfacial heat transfer area and projection area. In the code, [ ]TS is defined and used to evaluate droplet diameter. In the reference [1] and [2], it can be found that representative [ ]TS for various correlations and their conditions are used. In CAREM, various representative [ ]TS are considered as uncertainty of [ ]TS. And following values of [ ]TS described in reference [1] and [2] are considered.

TS

[ ]

As discussed above, [ ]TS are considered for various conditions in reference [1] and [2]. The uncertainty range of [ ]TS is assumed to have the same possibility within the uncertainty range.

In the CAREM, overall impacts of the uncertainty parameters related with the reflood

phenomena in the core region were evaluated by code assessment against SETs as discussed in Appendix C.

Reference

[1] "COBRA/TRAC – A Thermal-Hydraulics Code for Transient Analysis of Nuclear Reactor Vessels and Primary Coolant System, Volume 1, Revision4," NUREG/CR-3046, PNL-4385, March 1983.

[2] "RELAP5/MOD3.3 Code Manual Volume IV: Models and Correlations," NUREG/CR-5535/Rev P3-Vol IV, Information Systems Laboratories, Inc., March 2006.

Impact on DCD

There is no impact on the DCD.

Impact on PRA

There is no impact on the PRA.

Impact on Technical Specifications

There is no impact on the Technical Specifications.

Impact on Technical/Topical/Environmental Report

There is no impact on any Technical, Topical, or Environmental Report.

RESPONSE TO AUDIT ISSUES

APR1400 Topical Reports

Korea Electric Power Corporation / Korea Hydro & Nuclear Power Co., LTD

Docket No. PROJ0782

Review Section	**TR Realistic Evaluation Methodology for LBLOCA of the APR1400**
Application Section	**Topical Report: APR1400-F-A-TR-12004 Realistic Evaluation Methodology for Large-Break LOCA of the APR1400**
Issue Date	**08/13/2015**

Audit Issues No. 39

The guidance in RG 1.157, Section 3.11 establishes acceptable controls regarding the calculation of flow distribution. Provide the reason for flashing in the downcomer to be treated using a different approach (i.e., ECCS bypass bias) in Section 4.2.2.2 of the topical report as compared to flashing elsewhere in the RCS (e.g., uncertainty in break flow and system pressure).

Response

[

]TS The complexity made the downcomer phenomena impossible to be separated and the downcomer phenomena were considered as being merged altogether. [

]TS

However, the phenomenon “Flashing” need not to be treated as part of bias but seems to be included in the uncertainties of other parameters, just like the way that the flashing in the other components was treated due to the knowledge level shown in Table 1. The reason why the uncertainty of “Flashing” is treated by the uncertainties of other parameters is because of the calculation method of the RELAP5 code. In RELAP5, flashing is not considered by a correlation, but as a result of governing equations and state equations. [

]TS

In summary, the uncertainty of the flashing is considered by the uncertainty of critical flow, interfacial heat transfer, interfacial drag, etc. The uncertainties of the interfacial heat transfer and interfacial drag model during blowdown period are considered as being not important due to the low value in the importance rank from the PIRT. In CAREM, the uncertainty of the flashing is considered by the uncertainties in break flow and initial pressure as described in Section 4.2.2.1.2 of the topical report. The descriptions in Section 4.2.2.2 of the topical report will be revised in the future.

Table 1. The flashing in the downcomer phenomenon in the reference [5] of the topical report TS

Impact on DCD

There is no impact on the DCD.

Impact on PRA

There is no impact on the PRA.

Impact on Technical Specifications

There is no impact on the Technical Specifications.

Impact on Technical/Topical/Environmental Report

Topical report will be revised as mentioned above. Revised PIRT is described in the attachment for the response of Audit Issue No. 14.

There is no impact on any Technical or Environmental Report.

The increase of the vapor temperature above the saturation temperature is governed by the heat transfer from the hot core structures. Vapor superheating is not a cause but a result of the core heat. Therefore the uncertainty of vapor superheating can be described by the uncertainties of core heat transfer parameters. Core heat transfer parameters are already described above. There is no need to determine an additional parameter for vapor superheating.

Interfacial Heat Transfer

Interfacial heat transfer is strongly dependent on the interface area between the phases. The volumetric interface area is often calculated as a function of droplet diameter. The droplet diameter is determined by the Weber number in RELAP5/MOD3.3. Selection of the [ ]^{TS} as an uncertainty parameter for interfacial heat transfer is probable. And it has another advantage of describing the uncertainty of interfacial drag as well, because the drag is also dependent on the interfacial area. Therefore, the [ ]^{TS} is selected as a code parameter to describe the uncertainty of interfacial drag and heat transfer. By referring to the code manuals of COBRA-TF and RELAP5, the uncertainty range of the [ ]^{TS} has been determined. The maximum and minimum values of the [K]^{TS}, respectively. A [ ]^{TS}.

- Parameter; [

]^{TS}

Countercurrent Flow at Top Nozzles

Except for the blowdown period, countercurrent flow is frequently calculated at the top nozzles of the fuel assemblies. At the top nozzles, steam flows upward while liquid flows downward. This countercurrent flow can affect the probable water accumulation at the upper plenum. Upflowing steam from the core can entrain the water in the upper plenum ultimately into the steam generator u-tubes. Because the steam generator secondary side is hotter than the primary side during reflood, the entrained droplets evaporate and the steam becomes superheated in the u-tubes. This droplet evaporation and steam superheating phenomena result in steam binding. The effect of steam binding on peak clad temperature is quantified as a separate bias in Section 4.2.3. Therefore, the uncertainty parameter for this countercurrent flow at the fuel assembly top nozzles is not determined.

4.2.2.2 Code Parameters and Their Ranges for Phenomena in the Reactor Vessel

4.2.2.2.1 Reactor Vessel Downcomer

As summarized in CSAU [1], the downcomer is one of the components where scale distortion is inevitable in scaled-down test facilities. Many facilities, especially when power-to-volume scaling is applied, preserve the height of the prototype but reduce the diameter of fluid volumes considerably. Due to a large height-to-diameter ratio, the facilities become tall and skinny. Consequently the downcomer not only has a narrow gap but also has a very large surface-to-volume ratio. These distortions will affect the ECC bypass process which is a consequence of many complex processes such as condensation, ~~flashing~~, interface momentum transfer, entrainment, de-entrainment, single- and two-phase pressure drops. The ECC bypass is also affected by multidimensional and countercurrent flow phenomena in the downcomer. Therefore, the phenomena or processes

observed in scaled facilities become atypical to those occurring in the full-scale power plant. Therefore, the observations cannot be directly applied to full-scale power plants. As there is no one code parameter that characterizes the ECC bypass phenomenon, it is necessary to evaluate the ECC bypass as a separate bias.

four

"flashing,"

12

Except for these ~~three~~ processes or phenomena of "vessel stored energy release," "boiling in the downcomer," and "non-condensable gas effect," ~~13~~ among16 important processes or phenomena of the downcomer identified in Table 3-2 are treated in the evaluation of scale bias in Section 4.2.3.

Vessel Stored Energy Release and Boiling in the Downcomer

If enough cooling water is not supplied, the downcomer water would lose its subcooling and begin to boil. This is especially true in the late reflood period where SIPs only provide the emergency core cooling water. Therefore in order to describe the uncertainty of downcomer boiling, we need to consider the amount of ECCW supply and the wall stored energy. The SIP injection flow rate is treated as one of the plant parameters in Section 5.1.5. Wall stored energy can be described by material properties such as the heat capacity and conductivity. The material properties of the reactor vessel wall are dependent on the system design of the power plant. Therefore, the uncertainties of the material properties are described in Section 5.1.6.

[ ]^{TS}.

Direct Vessel Injection Jet Flow

DVI jet impingement produces dispersed droplets and affects the ECC bypass. This phenomenon is an attributor to the ECC bypass. Code parameter relevant to this phenomenon is not determined, and the effect is evaluated as a scale bias in Section 4.2.3.

Flashing

~~This phenomenon is an attributor to the ECC bypass. Code parameter relevant to this phenomenon is not determined and the effect is evaluated as a scale bias in Section 4.2.3.~~

Level

As described in Section 4.2.2.1.2, the uncertainty of the flashing phenomenon is represented by the uncertainties of the break flow model and system pressure.

This phenomenon is an attributor to the ECC bypass. Code parameter relevant to this phenomenon is not determined and the effect is evaluated as a scale bias in Section 4.2.3.

Entrainment and De-entrainment

These processes are attributors to ECC bypass. Code parameters relevant to these processes are not determined and the effects are evaluated as a scale bias in Section 4.2.3.

Multidimensional Flow, Condensation, Countercurrent Flow, and Bulk Mixing

These processes or phenomena are attributors to ECC bypass. Code parameters relevant to these are not determined and the effects are evaluated as a scale bias in Section 4.2.3.

Single- and Two-phase Pressure Drop

This phenomenon is an attributor to ECC bypass. Code parameter relevant to this phenomenon is not determined and the effect is evaluated as a scale bias in Section 4.2.3.

Non-condensable Gas Effect

Non-condensable gas in the downcomer is mainly nitrogen from SIT after the depletion of its water

inventory. The nitrogen increases downcomer pressure because its pressure is higher than the downcomer pressure at its appearance time. The higher pressure pushes down the downcomer water column into the core and enhances core reflood. On the other hand, the nitrogen might affect the condensation in the downcomer. Ingression of the nitrogen into the core is not probable or considerable because of the existence of the water column in the downcomer. [

]^{TS}

The release of non-condensable gas from the SIT after the depletion of the SIT water is dependent on the SIT pressure, nitrogen volume and temperature. These SIT parameters are dependent on the safety system design of the NPP. Therefore, the uncertainties of these SIT parameters are treated as plant input parameters, and are discussed in Section 5.1.

4.2.2.2.2 Reactor Vessel Lower Plenum

As summarized in the CSAU [1], the lower plenum is one of the components where scale distortion is inevitable in the scaled-down test facilities. The phenomena or processes observed in scaled facilities become atypical to those occurring in the full-scale power plant. Therefore, it is necessary to evaluate the effects of the phenomena or processes except for those which code parameters can be determined.

Stored Energy Release and Boiling

The initial steady-state energy is released by conduction during the transient from the reactor vessel lower plenum walls. Consequently, boiling and vapor generation can occur in the lower plenum due to the energy release from the internal structures and the vessel wall. The parameters governing these phenomena are the material properties, such as heat capacity and conductivity, of the vessel lower plenum wall. The material of the reactor vessel lower plenum wall is dependent on the system design of the NPP. Therefore, the uncertainties of these governing parameters are treated as plant input parameters, and are discussed in Section 5.1.

Level

This phenomenon is an attributor to, or a result of, ECC bypass. Code parameters relevant to this phenomenon are not determined, and the effect is evaluated as a scale bias in Section 4.2.3.

Multidimensional Flow, Entrainment, and Bulk Mixing

Multidimensional flow, entrainment (i.e., sweep-out) and bulk mixing have an impact on the initiation time of core reflooding because these phenomena govern the water level in the lower plenum and the ECC bypass during the refill period. Therefore, the uncertainties of these phenomena can be described by a separate bias evaluation of the ECC bypass. Bias evaluation is described in detail in Section 4.2.3.

4.2.2.2.3 Reactor Vessel Upper Plenum

Flashing

As described in Section 4.2.2.1.2, the uncertainty of the flashing phenomenon is ~~replaced~~ represented by the uncertainties of the break flow model and system pressure.

Level

As described in Section 4.2.2.1.2, no specific code parameter for the water level has been identified because the water level is dependent on all the other phenomena.

RESPONSE TO AUDIT ISSUES

APR1400 Topical Reports

Korea Electric Power Corporation / Korea Hydro & Nuclear Power Co., LTD

Docket No. PROJ0782

Review Section	**TR Realistic Evaluation Methodology for LBLOCA of the APR1400**
Application Section	**Topical Report: APR1400-F-A-TR-12004 Realistic Evaluation Methodology for Large-Break LOCA of the APR1400**
Issue Date	**08/13/2015**

Audit Issues No. 40

The guidance in RG 1.157, Section 3.11 establishes acceptable controls regarding the calculation of flow distribution. [

]^{TS} Explain these phenomena are sampled in the calculations.

Response

The phenomena mentioned in this issue are not sampled in the calculation, but treated as biases. The descriptions for each bias are in Section 4.2.3 of the topical report. The components of the test facilities designed according to “power-to-volume” scaling can cause a bias due to scale distortions. Phenomena that can be affected from these scale distortions are treated as biases which are evaluated from the assessments against full-scale experimental facilities.

All phenomena that are treated as biases in the topical report are summarized in Table 1. The phenomena treated as biases are those phenomena that the code capability is not confirmed to be used. Downcomer, lower plenum, and upper plenum of test facilities which are designed to "power-to-volume" scaling are known as the components that can cause bias due to scale distortions. Also, these components have strong importance in multi-dimensional characteristics during certain periods, which is difficult to model by 1-dimensional RELAP5. The PIRT shown in Table 1 is revised from the PIRT of the topical report due to some errors that have been included. The complete modified PIRT will be given in association with audit issue no. 15. For each PIRT item, the bias used in the evaluation of the PIRT item is listed in the Table 1. [

]TS

Table 1. PIRT items treated by biases TS

TS

Impact on DCD

There is no impact on the DCD.

Impact on PRA

There is no impact on the PRA.

Impact on Technical Specifications

There is no impact on the Technical Specifications.

Impact on Technical/Topical/Environmental Report

Topical report will be revised according to the PIRT revision as described in the attachment for the response of Audit Issue No. 14.

There is no impact on any Technical or Environmental Report.

RESPONSE TO AUDIT ISSUES

APR1400 Topical Reports

Korea Electric Power Corporation / Korea Hydro & Nuclear Power Co., LTD

Docket No. PROJ0782

Review Section	**TR Realistic Evaluation Methodology for LBLOCA of the APR1400**
Application Section	**Topical Report: APR1400-F-A-TR-12004 Realistic Evaluation Methodology for Large-Break LOCA of the APR1400**
Issue Date	**08/13/2015**

Audit Issues No. 41

The guidance in RG 1.157, Section 4 establishes acceptable controls for the estimation of uncertainties. Address the following questions about the uncertainty determination for critical flow described in Section 4.2.2.7.1 of the topical report.

a. NUREG/CR-5249 proposes that the nodalization for the plant should follow that used to establish the uncertainty ranges. Explain whether the final nodalization of the break discharge location in the Marviken facility used for the break flow uncertainty determination was identical to that for the plant deck.

b. Based on Figure 4-6 of the topical report, it appears that RELAP5 shows underprediction for two-phase break flow in excess of 4500 kg/s even with the adjusted discharge coefficient. Provide the range of two-phase discharge flow for the APR1400 design based on integral tests and plant calculations.

Response

a)

As described in Audit Issue No. 27-i, the final nodalization of the break discharge location in the Marviken facility is regarded to be identical to that for the plant deck.

b)

Figure 1 illustrates the break flow rates near pump side and vessel side as a consequence of the APR1400 plant calculation. As shown in Figure 1, the break flow rates for both sides during the blowdown period are above 4,500 kg/s unlike with the other LOCA periods. Considering the break junction void fraction in Figure 2, such two-phase discharge flow ranges exist between about 1,600 ~ 15,000 kg/s (0 ~ 15 s, pump side) and 260 ~ 25,500 kg/s (0 ~ 243 s, vessel side), respectively.

[

]TS

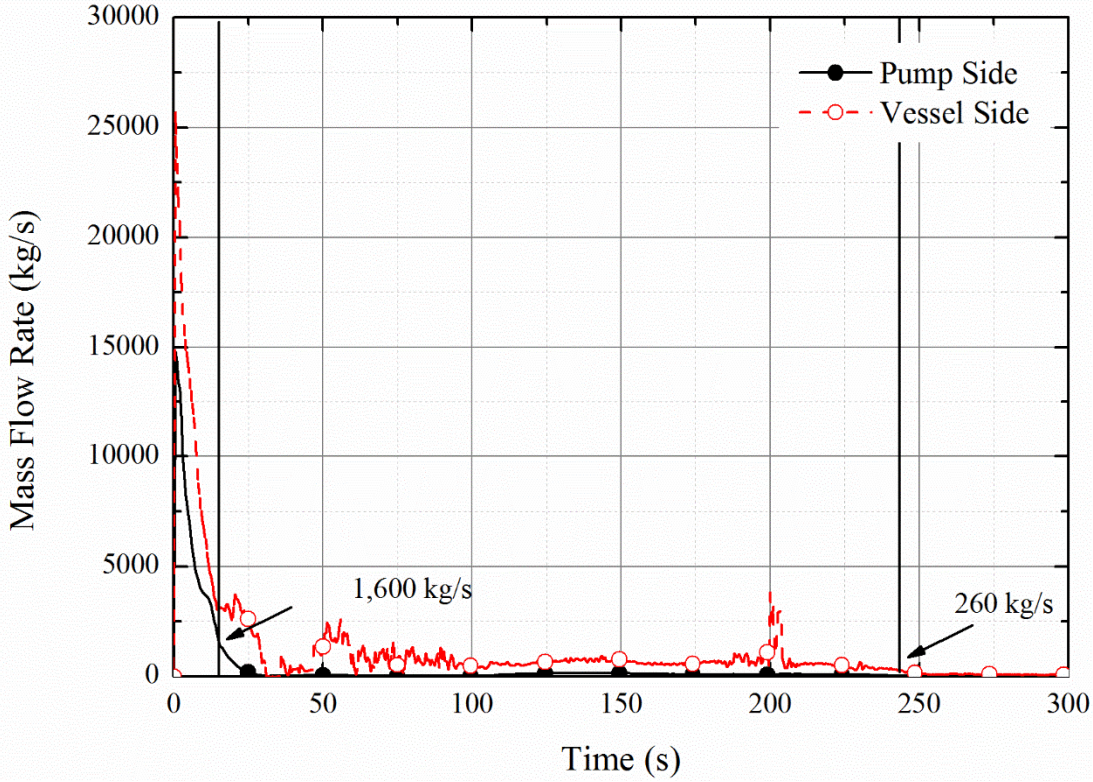

Figure 1. Break Flow Rate at a Pump and a Reactor Vessel

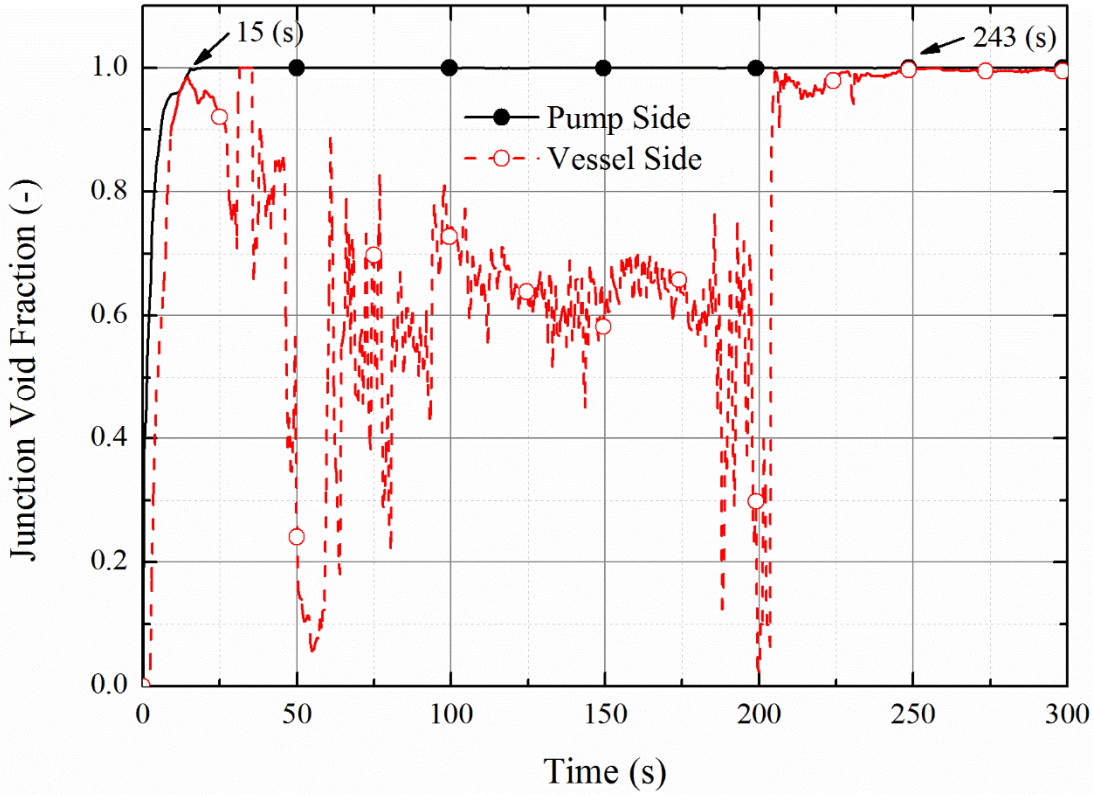

Figure 2. Break Junction Void Fraction

TS

Figure 3. Two-phase Critical Flow Rate using [ ]TS

Impact on DCD

There is no impact on the DCD.

Impact on PRA

There is no impact on the PRA.

Impact on Technical Specifications

There is no impact on the Technical Specifications.

Impact on Technical/Topical/Environmental Report

There is no impact on any Technical, Topical, or Environmental Report.

RESPONSE TO AUDIT ISSUES

APR1400 Topical Reports

Korea Electric Power Corporation / Korea Hydro & Nuclear Power Co., LTD

Docket No. PROJ0782

Review Section	**TR Realistic Evaluation Methodology for LBLOCA of the APR1400**
Application Section	**Topical Report: APR1400-F-A-TR-12004 Realistic Evaluation Methodology for Large-Break LOCA of the APR1400**
Issue Date	**08/13/2015**

Audit Issues No. 42

The guidance in RG 1.157, Section 4 establishes acceptable controls for the estimation of uncertainties. Section 4.2.2.7.1 of the topical report states that the break mass flow rate is influenced by the pressure drop along the break flow path. Instead of sampling the break mass flow rate, in Section 5.2.1.1 of the topical report the limiting break is determined. Section 5.2.1.1 and Table 5-1 of the topical report do not mention whether the loss coefficients in the break flow paths (on both sides of the break) were varied during sensitivity studies. [

]^{TS} Clarify the uncertainty evaluation.

Response

[

]TS It is also stated that the flow rate is determined by either critical flow or the flow area and the single and two-phase form, acceleration and friction losses in the flow path in the break plane. The importance level of the phenomenon during blowdown is “not applicable”, since the break flow during blowdown would be dependent on the critical flow.
[

]TS

In CAREM, the discharge coefficients are determined by assessment against Marviken test. [

]TS Then, the limiting break condition is found instead of considering the uncertainty of the break location, type and size. Since the worst break condition is used, the uncertainty evaluation of the break condition is basically not required. However, there are concerns related with the flow resistance uncertainty.

[

]TS Also, the plant input making process of CAREM includes the checking of the steady state pressure differences with the designed values. Therefore, the uncertainty of the loop flow resistance is essentially very small.

Impact on DCD

There is no impact on the DCD.

Impact on PRA

There is no impact on the PRA.

Impact on Technical Specifications

There is no impact on the Technical Specifications.

Impact on Technical/Topical/Environmental Report

There is no impact on any Technical, Topical, or Environmental Report.

RESPONSE TO AUDIT ISSUES

APR1400 Topical Reports

Korea Electric Power Corporation / Korea Hydro & Nuclear Power Co., LTD

Docket No. PROJ0782

Review Section	**TR Realistic Evaluation Methodology for LBLOCA of the APR1400**
Application Section	**Topical Report: APR1400-F-A-TR-12004 Realistic Evaluation Methodology for Large-Break LOCA of the APR1400**
Issue Date	**08/13/2015**

Audit Issues No. 43

The guidance in RG 1.157, Section 3.12.1 establishes acceptable controls for the calculation of containment pressure. Section 4.2.2.7.2 of the topical report states that [

]^{TS}. However, there is no description of the CONTEMPT inputs (i.e., for heat transfer surface area, the wall condensation model, etc.), including results of sensitivity calculations that demonstrate [

]^{TS}. Provide justification for [

]^{TS}

Response

As described in response to Audit Issue No. 16, user input is [ ]TS. Therefore, it is not necessary to perform sensitivity calculations that [ ]TS

Impact on DCD

There is no impact on the DCD.

Impact on PRA

There is no impact on the PRA.

Impact on Technical Specifications

There is no impact on the Technical Specifications.

Impact on Technical/Topical/Environmental Report

There is no impact on any Technical, Topical, or Environmental Report.

RESPONSE TO AUDIT ISSUES

APR1400 Topical Reports

Korea Electric Power Corporation / Korea Hydro & Nuclear Power Co., LTD

Docket No. PROJ0782

Review Section	**TR Realistic Evaluation Methodology for LBLOCA of the APR1400**
Application Section	**Topical Report: APR1400-F-A-TR-12004 Realistic Evaluation Methodology for Large-Break LOCA of the APR1400**
Issue Date	**08/13/2015**

Audit Issues No. 44

The guidance in RG 1.157, Section 3.12.1 establishes acceptable controls for the calculation of containment pressure. According to “KHNP Responses to Request for Additional Information No. 1-7425” (pg. 7 of 23) for the APR1400 LBLOCA analysis, “...TPEAK is set to 0 (zero) and CONTEMPT4/MOD5 dynamic-link library (contl.dll) is loaded when RELAP5/MOD3.3 starts reflood calculation (reflood heat structures enter to reflood mode). The coupled code sets TPEAK to the time reflood calculation starts.” The explanation implies that the coupling between the codes does not commence till the early reflood period. Explain how the containment backpressure is determined and supplied to RELAP5 for the accident period before early reflood.

Response

[

]TS Detailed description on the user input card is written in Section A10.1 of reference [1].

[

]TS The loading time is at about 22 s after break in nominal calculation results of APR1400 as shown in Figure 1. Because the early reflood period begins at around 38 s as discussed in Section 3.1.2.3 of topical report, it can be confirmed that CONTEMPT4/MOD5 is loaded during refill period.

Representative containment pressure is used for LBLOCA analysis of APR1400 before the CONTEMPT4/MOD5 loading time as shown in Figure 2. Representative containment pressure data were determined to have lower value than those calculated by Appendix K model (COMPERC-II [2]). And the representative containment pressure data are entered by user input. However, the representative containment pressure is meaningless because critical flow phenomena occur until around 20 s as shown in Figure 3. Therefore, it is reasonable to use the representative containment pressure before the CONTEMPT4/MOD5 loading.

RELAP5/MOD3.3/K stores released mass and energy data for liquid, vapor, and non-condensable gas phase through the breaks until the CONTEMPT4/MOD5 loading, and the stored data are transferred to the CONTEMPT4/MOD5 code right after the loading time. And then, CONTEMPT4/MOD5 calculates containment pressure from the beginning of break to the loading time. After the loading of CONTEMPT4/MOD5, RELAP5/MOD3.3/K and CONTEMPT4/MOD5 work as boundary condition for each other at every calculation time step of RELAP5/MOD3.3/K.

Reference

[1] "RELAP5/MOD3.3 Code Manual Volume II: Appendix A Input Requirements," NUREG/CR-5535, Rev P3, App A, U.S.NRC, March 2006.

[2] CENPD-134P, COMPERC-II, "A Program for Emergency Refill-Reflood of the Core," August, 1974.

CENPD-134P, Supplement 1, COMPERC-II, "A Program for Emergency Refill-Reflood of the Core (Modifications)," February, 1975.

CENPD-134P, Supplement 2, COMPERC-II, "A Program for Emergency Refill-Reflood of the Core," June, 1985.

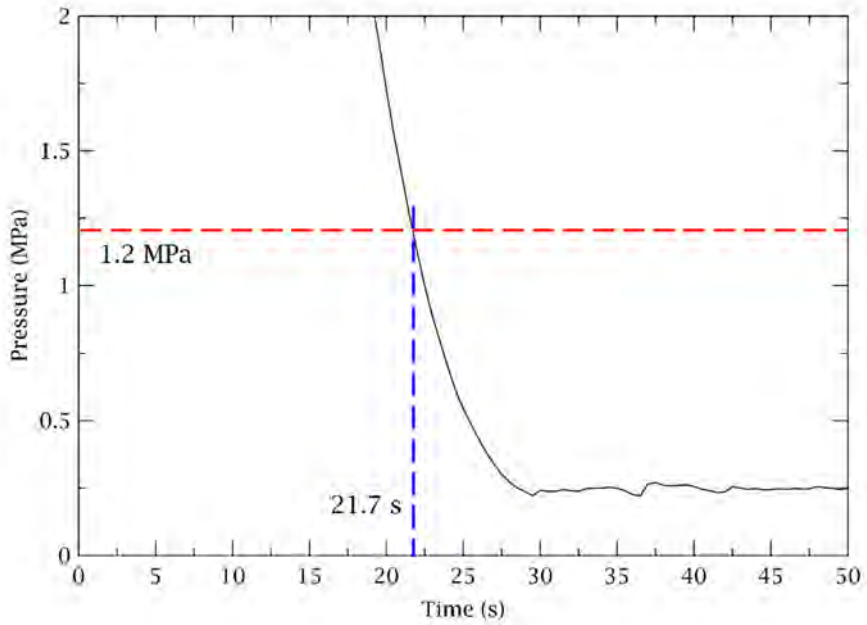

Figure 1. Average Core Channel Pressure

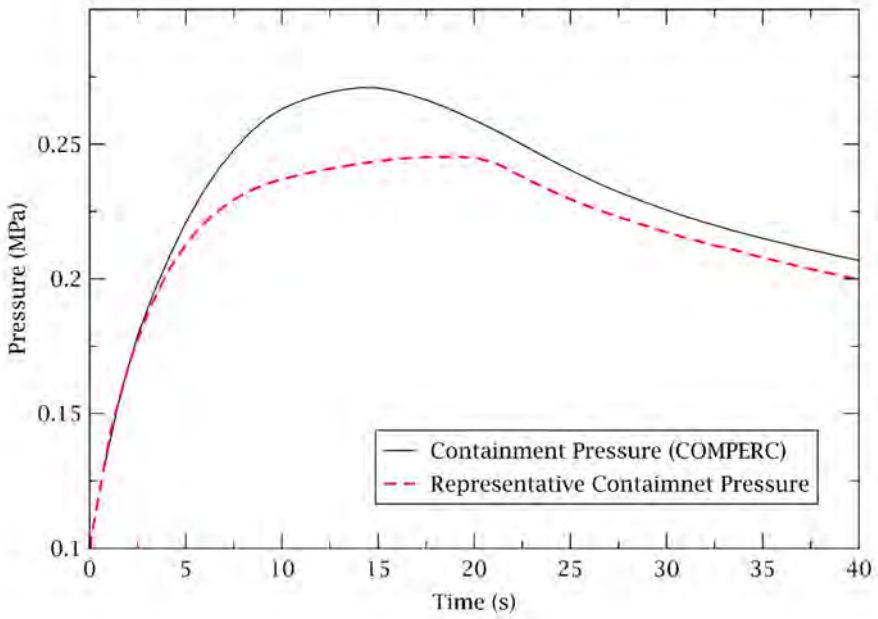

Figure 2. Comparison of Representative Containment Pressure and COMPERC Results

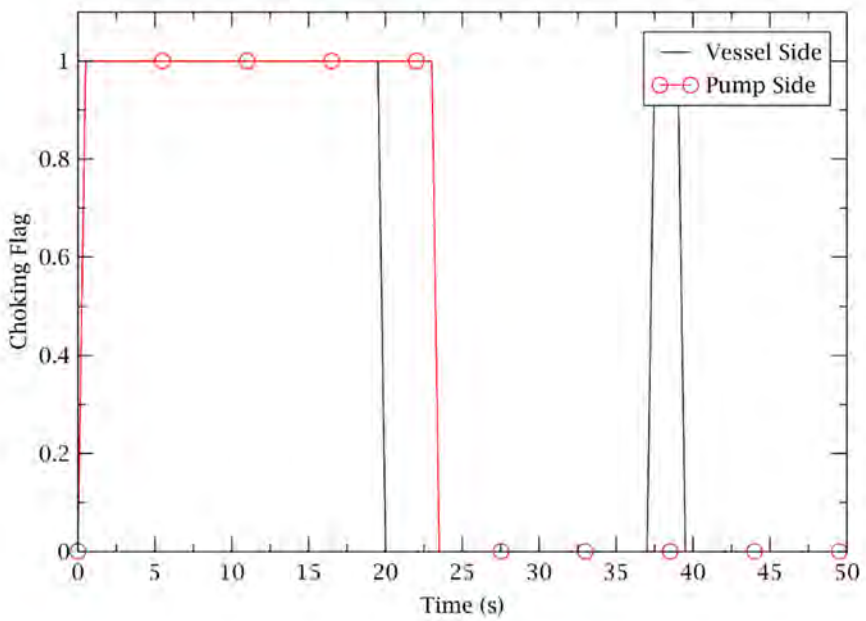

Figure 3. Critical Flow Flag at Break Valves

Impact on DCD

There is no impact on the DCD.

Impact on PRA

There is no impact on the PRA.

Impact on Technical Specifications

There is no impact on the Technical Specifications.

Impact on Technical/Topical/Environmental Report

There is no impact on any Technical, Topical, or Environmental Report.

RESPONSE TO AUDIT ISSUES

APR1400 Topical Reports

Korea Electric Power Corporation / Korea Hydro & Nuclear Power Co., LTD

Docket No. PROJ0782

Review Section	**TR Realistic Evaluation Methodology for LBLOCA of the APR1400**
Application Section	**Topical Report: APR1400-F-A-TR-12004 Realistic Evaluation Methodology for Large-Break LOCA of the APR1400**
Issue Date	**08/13/2015**

Audit Issues No. 45

The guidance in RG 1.157, Section 3.4.2 establishes acceptable controls for the calculation of bypass flow. Address the following concerns about [ ]^{TS} determination discussed in Section 4.2.3.1 of the topical report:

a. The actual implementation of [ ]^{TS} in the code calculations is unclear. It cannot be determined whether [ ]^{TS}. A clarification is needed about the approach used to incorporate [ ]^{TS} in the code during the blowdown, early and late reflood periods.

Response

[
]TS Separately from this, the ECC bypass during the early and late reflood periods is accounted from the assessments against [
]TS. Results of the code assessment against these reflood tests show that the RELAP5/MOD3.3/K code conservatively calculates ECC bypass during reflood. Therefore, [
]TS.

Impact on DCD

There is no impact on the DCD.

Impact on PRA

There is no impact on the PRA.

Impact on Technical Specifications

There is no impact on the Technical Specifications.

Impact on Technical/Topical/Environmental Report

There is no impact on any Technical, Topical, or Environmental Report.

RESPONSE TO AUDIT ISSUES

APR1400 Topical Reports

Korea Electric Power Corporation / Korea Hydro & Nuclear Power Co., LTD

Docket No. PROJ0782

Review Section	**TR Realistic Evaluation Methodology for LBLOCA of the APR1400**
Application Section	**Topical Report: APR1400-F-A-TR-12004 Realistic Evaluation Methodology for Large-Break LOCA of the APR1400**
Issue Date	**08/13/2015**

Audit Issues No. 45

The guidance in RG 1.157, Section 3.4.2 establishes acceptable controls for the calculation of bypass flow. Address the following concerns about [ ]^{TS} determination discussed in Section 4.2.3.1 of the topical report:

b. Provide the assessment results of [ ]^{TS} is appropriate, should be provided.

Response

The purpose of [

]TS

TS

Figure 1 Liquid mass through breaks

TS

Figure 2 Liquid Mass Extracted

Impact on DCD

There is no impact on the DCD.

Impact on PRA

There is no impact on the PRA.

Impact on Technical Specifications

There is no impact on the Technical Specifications.

Impact on Technical/Topical/Environmental Report

There is no impact on any Technical, Topical, or Environmental Report.

RESPONSE TO AUDIT ISSUES

APR1400 Topical Reports

Korea Electric Power Corporation / Korea Hydro & Nuclear Power Co., LTD

Docket No. PROJ0782

Review Section	**TR Realistic Evaluation Methodology for LBLOCA of the APR1400**
Application Section	**Topical Report: APR1400-F-A-TR-12004 Realistic Evaluation Methodology for Large-Break LOCA of the APR1400**
Issue Date	**08/13/2015**

Audit Issues No. 45

The guidance in RG 1.157, Section 3.4.2 establishes acceptable controls for the calculation of bypass flow. Address the following concerns about [ ]^{TS} determination discussed in Section 4.2.3.1 of the topical report:

c. The selected test, [ ]^{TS} during the refill period initiates from a system pressure of 1200 kPa (i.e., 1.2 MPa). The refill period in APR1400 begins, based on the results in Figure 5-12 of the topical report, when the system pressure is approximately 6 MPa. Therefore, [ ]^{TS} may not capture a large portion of the depressurization transient and the resulting ECCS bypass during the APR1400 refill period. Discuss the applicability of [ ]^{TS}.

Response

The initial conditions of [ ]TS test were determined from the TRAC analysis of US PWR and starts at 1.2MPa, while the SIT injection in APR1400 starts at 6 MPa. The beginning of the SIT injection is only dependent on the setpoint of SIT, hence is different due to the design differences between reference plant of [ ]TS and APR1400. Although the SIT injection starts at 6 MPa, the RCS pressure still drops rapidly after the injection of SIT, and at about 25 sec the RCS pressure becomes below 1.2 MPa, which is consistent to the initial condition of [ ]TS. The period between 6 MPa and 1.5 MPa still has the strong characteristic of blowdown and therefore not adequate to be considered as the ECC bypass for refill. Also, as shown in the figures below, though the SIT injection starts at 14 sec, the ECCS during that period does not get into the downcomer until 25 sec. In conclusion, it is adequate to use [ ]TS.

[ ]TS

Figure 1. APR1400 Downcomer Bottom Volume Liquid Volume Fraction [ ]TS

[ ]TS

Figure 2. APR1400 Downcomer Bottom Volume Liquid Volume Fraction [ ]TS

Impact on DCD

There is no impact on the DCD.

Impact on PRA

There is no impact on the PRA.

Impact on Technical Specifications

There is no impact on the Technical Specifications.

Impact on Technical/Topical/Environmental Report

There is no impact on any Technical, Topical, or Environmental Report.

RESPONSE TO AUDIT ISSUES

APR1400 Topical Reports

Korea Electric Power Corporation / Korea Hydro & Nuclear Power Co., LTD

Docket No. PROJ0782

Review Section	**TR Realistic Evaluation Methodology for LBLOCA of the APR1400**
Application Section	**Topical Report: APR1400-F-A-TR-12004 Realistic Evaluation Methodology for Large-Break LOCA of the APR1400**
Issue Date	**08/13/2015**

Audit Issues No. 45

The guidance in RG 1.157, Section 3.4.2 establishes acceptable controls for the calculation of bypass flow. Address the following concerns about the ECCS bypass bias determination discussed in Section 4.2.3.1 of the topical report:

d. UPTF-21A and -21B involve downcomer injection of ECCS. Justify the selection of UPTF-4A with cold leg injection for determination of the ECCS bypass bias over the tests with a configuration similar to that in APR1400.

Response

The ECC bypass during end-of-blowdown and refill period is mainly dependent on the flow mixing behavior below the cold leg bottom. Also, due to the high elevation of the DVI injection in the APR1400 design, the distance that the steam and ECC water are expected to contact until they go through broken cold leg is almost the same as that of CLI plant. Therefore, it has been considered that the ECC injection type is less important in comparison to the depressurization process.

There are UPTF-21A and -21B tests targeted to investigate the ECC bypass mechanism during end-of-blowdown with DVI injection, however, the test configurations of those tests are not exactly the same as the LBLOCA conditions during end-of-blowdown and refill period; the broken hot leg break valve and the pump simulators were closed. The initial pressure in primary system and containment simulator was set at approximately 0.3 MPa, thus the depressurization process was not investigated through the tests. In other words, UPTF-21A, -21B tests are tests to investigate steady-state downcomer CCFL behavior only with DVI geometry, where the steam flow rates injected from the core simulator were determined from the end-of-blowdown and refill condition, respectively.

In conclusion, UPTF-4A test is the only UPTF test, which simulated the transient ECC bypass during end-of-blowdown and refill period. Therefore, it is the only possible test to quantify the ECC bypass bias during the period.

Impact on DCD

There is no impact on the DCD.

Impact on PRA

There is no impact on the PRA.

Impact on Technical Specifications

There is no impact on the Technical Specifications.

Impact on Technical/Topical/Environmental Report

There is no impact on any Technical, Topical, or Environmental Report.

RESPONSE TO AUDIT ISSUES

APR1400 Topical Reports

Korea Electric Power Corporation / Korea Hydro & Nuclear Power Co., LTD

Docket No. PROJ0782

Review Section	**TR Realistic Evaluation Methodology for LBLOCA of the APR1400**
Application Section	**Topical Report: APR1400-F-A-TR-12004 Realistic Evaluation Methodology for Large-Break LOCA of the APR1400**
Issue Date	**08/13/2015**

Audit Issues No. 45

The guidance in RG 1.157, Section 3.4.2 establishes acceptable controls for the calculation of bypass flow. Address the following concerns about [ ]^{TS} determination discussed in Section 4.2.3.1 of the topical report:

e. NUREG/CR-5249 recommends that the nodalization selected for the nuclear plant be consistent with that used for selected test facilities. The UPTF nodalization shown in Appendix F of the topical report is different (i.e., the downcomer axial and azimuthal nodalization) as compared to that selected for APR1400. Discuss the differences between the nodalizations and its impact on the conclusions from the UPTF simulations.

Response

Although the downcomer modeling of UPTF tests is not exactly the same as that of the APR1400 and the UPTF, the principle ideas employed in modeling [ ]TS are consistent.

In modeling a downcomer, [ ]TS. In UPTF, there are 4 hot legs and 4 cold legs, while 2 hot legs and 4 cold legs are in the APR1400. In order to preserve the [ ]TS.

The difference in axial nodalization of the downcomer is mainly due to the noding convenience that is coming from the geometrical difference between the APR1400 and UPTF facility, e.g. the downcomer gap width variation in axial direction. It is easier to model the downcomer with the constant area volumes than to model it with the varying area ones. However, [ ]TS are similar and also the connections to the cold legs are consistent in both nodalizations by having the same normal connections.

The upper plenum nodalization of UPTF in Appendix F is different from the APR1400 nodalization. The nodalization is based on the upper plenum noding scheme developed for the analysis of other nuclear power plants in Korea which have the UPI type injection. In this modeling, every upper plenum structure is modeled using pipes and multi-junction components, hence, very complicated. This noding scheme was employed because the upper plenum SI mixing phenomena were considered to be important. In the APR1400 modeling, the detailed investigations on these phenomena are not necessary and it is decided not to use [ ]TS. The UPTF nodalization in Appendix F is [ ]TS. In the assessment of UPTF-21D test, the impact of the modeling differences does not seem significant because the complicated upper plenum noding may only affect the flow behavior in the upper plenum, which would be very limited in DVI injection test, such as UPTF-21D.

An additional assessment of UPTF-21D with [ ]TS as shown in Figure 5 is conducted and the results are shown in Figure 6 and 7. The downcomer level and the break flow show that the code results are slightly more conservative than the test results. The conclusion from the assessment is consistent with the one in the topical report.

TS

Figure 1. Azimuthal Modeling of UPTF Downcomer

TS

Figure 2. Azimuthal Modeling of APR1400 Downcomer

TS

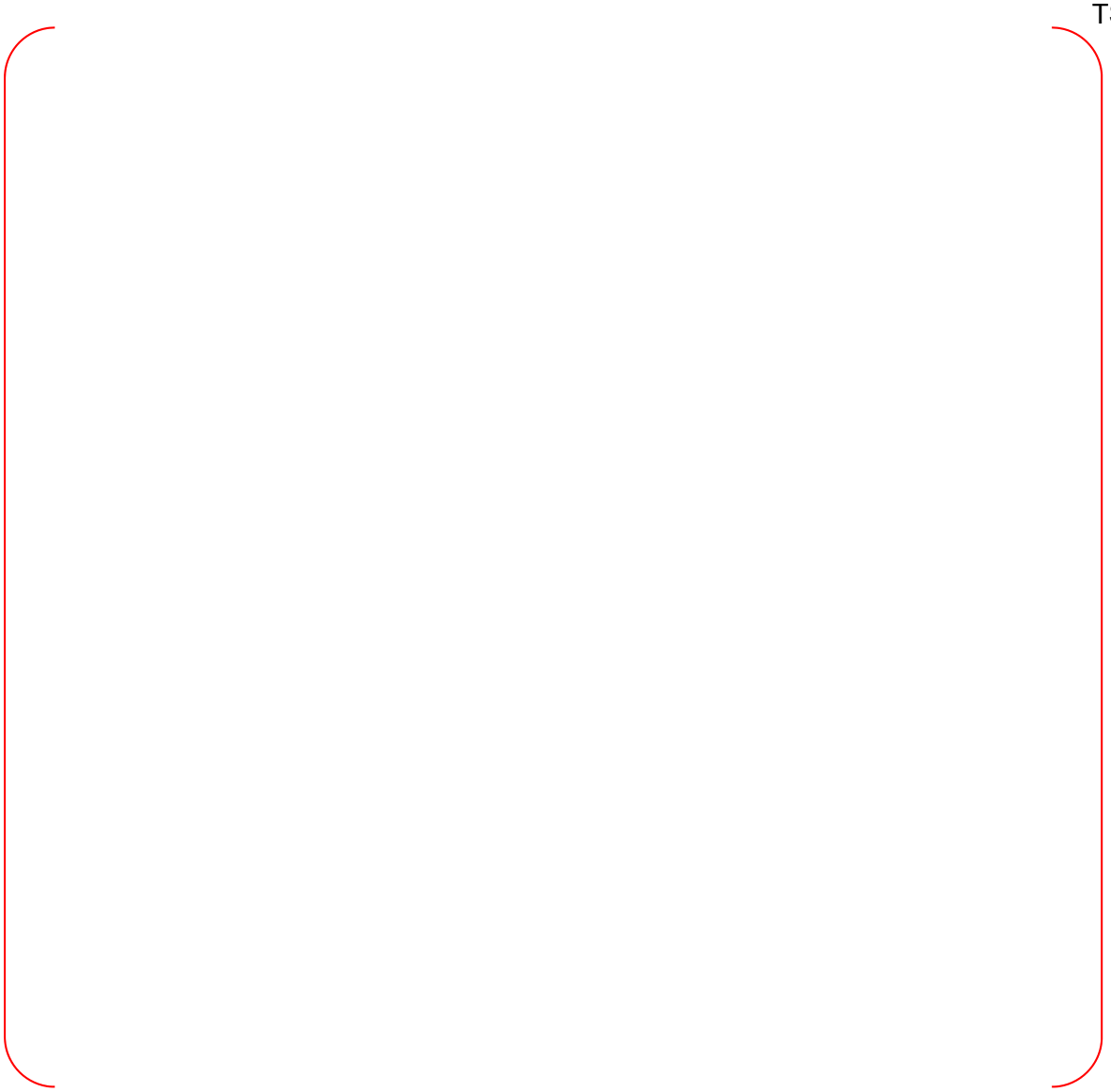

Figure 3. UPTF Axial Vessel Modeling (Topical Report)

TS

Figure 4. APR1400 Axial Vessel Modeling (Modified)

TS

Figure 5. UPTF Axial Vessel Modeling (Simpler Upper Plenum Noding)

Figure 6. Downcomer Water Level

TS

Figure 7. Break Flow Mass Flow Rate

Impact on DCD

There is no impact to the DCD.

Impact on PRA

There is no impact on the PRA.

Impact on Technical Specifications

There is no impact on the Technical Specifications.

Impact on Technical/Topical/Environmental Report

Topical report will be revised.

There is no impact on any Technical or Environmental Report.

RESPONSE TO AUDIT ISSUES

APR1400 Topical Reports

Korea Electric Power Corporation / Korea Hydro & Nuclear Power Co., LTD

Docket No. PROJ0782

Review Section	**TR Realistic Evaluation Methodology for LBLOCA of the APR1400**
Application Section	**Topical Report: APR1400-F-A-TR-12004 Realistic Evaluation Methodology for Large-Break LOCA of the APR1400**
Issue Date	**08/13/2015**

Audit Issues No. 45-f

The guidance in RG 1.157, Section 3.4.2 establishes acceptable controls for the calculation of bypass flow. Address the following concerns about the ECCS bypass bias determination discussed in Section 4.2.3.1 of the topical report:

f. ATLAS Tests 9, 11 and 15 are included to determine the ECCS bypass bias during the reflood period. However, the figures for Tests 9 and 11 in Appendix E are provided only from 200 seconds after the beginning of the accident. The results from the period before 200 seconds were adjusted to match the measured conditions. The results for ATLAS Test 15 shown in Figures 3-19 and 3-20 in Appendix E of the topical report reveal that RELAP5/MOD3.3/K over-predicts the downcomer and core collapsed water levels for the period from 38 seconds to 150 seconds (early reflood). Provide justification for the neglect of this non-conservatism in the ECCS bypass prediction during the early reflood period.

Audit Issues No. 85

The guidance in RG 1.157, Section 3.16.2 establishes acceptable controls for the data comparisons necessary to justify best estimate models. The Applicant asserts in Section 3.1 of the topical report Appendix E that the abnormalities observed in Tests 9, 11, and 15 are not expected to occur in the APR1400 plant. However, the purpose of integral tests is to demonstrate the expected behavior of the plant. Therefore, stating that certain phenomena observed in the tests are not expected in the plant, defeats the purpose of the tests. In addition, the Applicant's rationale for not expecting the anomalous behavior in the plant is unconvincing. As an example, it is stated that the difference between the lower and upper downcomer wall temperatures is not expected to exist in the plant "...because of the existence of continuous flow in the downcomer..." but such flow will also exist in the test facility which does exhibit the temperature difference. Please justify the representativeness of the selected ATLAS tests and their use for assessment purposes.

Response to 45-f

[

]TS

Response to 85

As described in Chapter 2 of Appendix E, ATLAS test facility was designed to investigate major phenomena related to the DVI of the ECCW, such as downcomer boiling and ECCW bypass. Target plant of the ATLAS test facility is APR1400.

Downcomer boiling phenomenon can occur during refill and reflood periods. The effects of downcomer boiling on the thermal hydraulic behavior is relatively insignificant because large amount of ECCW is injected during refill and early reflood periods. [

]^{TS} Two uncertainty parameters are selected for downcomer boiling phenomenon in CAREM, and uncertainty parameter ranges and distribution functions are determined by the assessment of ATLAS tests.

ECCW bypass phenomenon is evaluated by assessing against various experiment data including ATLAS test data, and it is treated by bias because it is related to many complex phenomena as described in Section 4.4.1 of the topical report.

TS

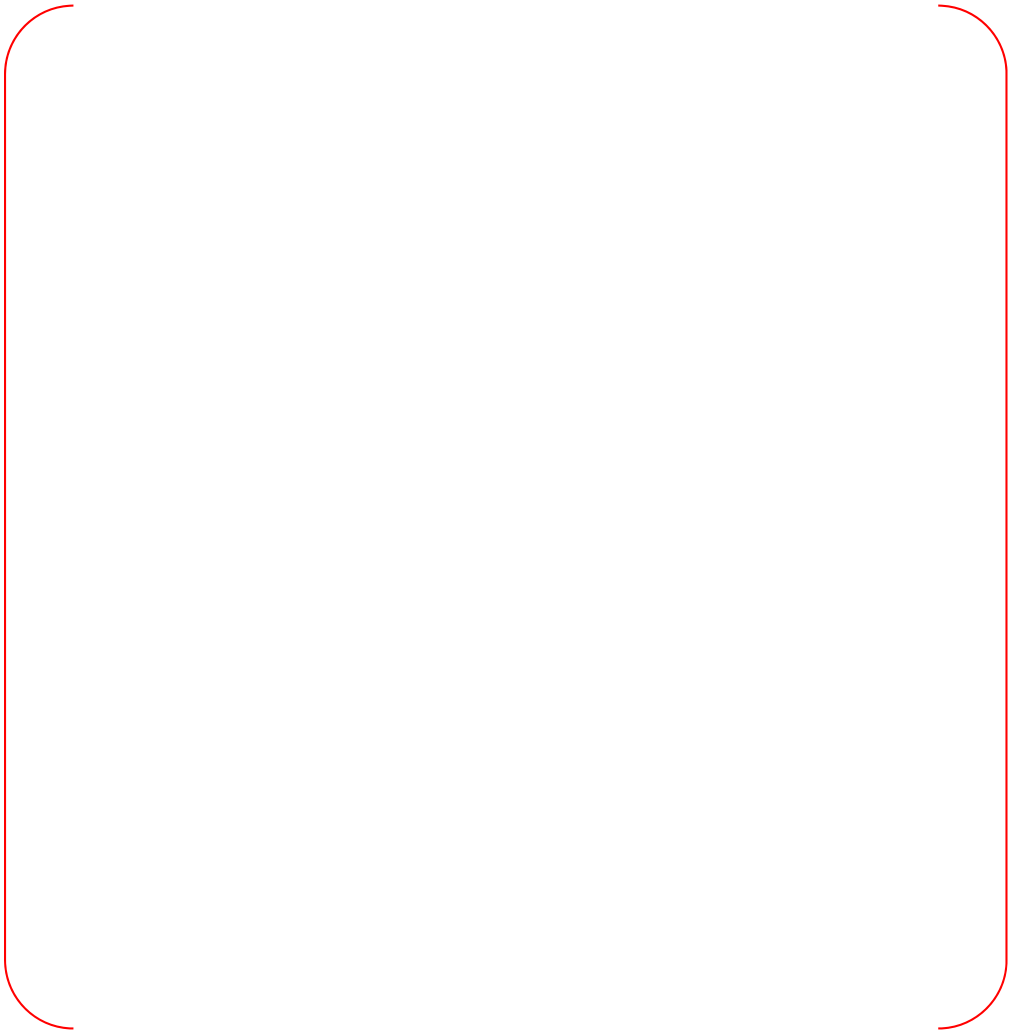

Figure 1. Heat Flux Comparison of Lower Downcomer

Reference

[1] “ATLAS Project Experimental Data/Information Transfer; Quick-Look Data Report of LB-CL-15,” ATLAS-QLR-LB-CL-15, Revision 5, October 2008.

Impact on DCD

There is no impact on the DCD.

Impact on PRA

There is no impact on the PRA.

Impact on Technical Specifications

There is no impact on the Technical Specifications.

Impact on Technical/Topical/Environmental Report

There is no impact on any Technical, Topical, or Environmental Report.

RESPONSE TO AUDIT ISSUES

APR1400 Topical Reports

Korea Electric Power Corporation / Korea Hydro & Nuclear Power Co., LTD

Docket No. PROJ0782

Review Section	**TR Realistic Evaluation Methodology for LBLOCA of the APR1400**
Application Section	**Topical Report: APR1400-F-A-TR-12004 Realistic Evaluation Methodology for Large-Break LOCA of the APR1400**
Issue Date	**08/13/2015**

Audit Issues No. 45-g

The guidance in RG 1.157, Section 3.4.2 establishes acceptable controls for the calculation of bypass flow. Address the following concerns about [ ]^{TS} determination discussed in Section 4.2.3.1 of the topical report:

g. None of the descriptions of the models for APR1400, MIDAS or UPTF that are used to determine [ ]^{TS} mention the use of a counter-current flow limitation (CCFL) correlation in the downcomer. Clarify whether any such correlation was used and if so, describe the resulting impact on [ ]^{TS}.

Response

CCFL model is [

]TS

[ ]TS the results for test assessment (MIDAS, UPTF)
[ ]TS are conservatively calculated in terms of reflood ECC bypass.

Impact on DCD

There is no impact on the DCD.

Impact on PRA

There is no impact on the PRA.

Impact on Technical Specifications

There is no impact on the Technical Specifications.

Impact on Technical/Topical/Environmental Report

There is no impact on any Technical, Topical, or Environmental Report.

RESPONSE TO AUDIT ISSUES

APR1400 Topical Reports

Korea Electric Power Corporation / Korea Hydro & Nuclear Power Co., LTD

Docket No. PROJ0782

Review Section	**TR Realistic Evaluation Methodology for LBLOCA of the APR1400**
Application Section	**Topical Report: APR1400-F-A-TR-12004 Realistic Evaluation Methodology for Large-Break LOCA of the APR1400**
Issue Date	**08/13/2015**

Audit Issues No. 46

The guidance in RG 1.157, Section 3.4.2 establishes acceptable controls for the calculation of bypass flow. The expression for the bypass fraction shown in Section 2.1 of Appendix F appears to be incorrect. M_water_out is defined as the liquid flow rate discharged through the lower plenum which would be indicative of the amount that has not been bypassed in the test. Confirm and if necessary, provide the correct the expression. Also confirm that the bypass fractions shown in Figures 2-3, 2-7 and 2-8 in Appendix E are correctly calculated and compared.

Response

[ ]TS The M_{water_out} is the measured liquid flow rate discharged through the lower plenum.

In MIDAS tests, the downcomer water level is maintained at the predetermined constant value. The liquid flow rate discharged through the lower plenum which would be indicative of the amount that has not been bypassed in the test. That is, the liquid flow rate through the lower plenum can be calculated by following equation.

[ ]TS

The expression for the bypass fraction above is obtained from the mass balance.

Even though the typos in the topical report, Figure 2-3, 2-7 and 2-8 of Appendix E are calculated correctly based on the above modified equation. Therefore, these figures do not need to be modified.

Impact on DCD

There is no impact on the DCD.

Impact on PRA

There is no impact on the PRA.

Impact on Technical Specifications

There is no impact on the Technical Specifications.

Impact on Technical/Topical/Environmental Report

Topical report will be revised as mentioned above.

There is no impact on Technical or Environmental Report.

Replace with next page A

labeled 'ECCW Injection Nozzle', is the DVI injection nozzle number through which ECCW was injected. The major test results are also depicted in Figure 2-3 and Figure 2-4.

The bypass fraction and the condensation ratio were calculated as follows:

$$\text{Bp\_fraction} = \frac{M_{Water\_out}}{M_{SI\_in}+M_{Condensate}} \quad (1)$$

$$\text{Cond\_ratio} = \frac{M_{Condensate}}{M_{Steam\_in}} \quad (2)$$

Where, M_{SI_in} (kg/s) was the total ECCW injection flow rate, M_{Water_out} (kg/s) is the liquid flow rate discharged through the lower plenum, M_{Steam_in} is the steam injection flow rate, and $M_{Condensate}$ (kg/s) is the condensation rate which is calculated as follows:

$$M_{Condensate} = M_{Steam\_in} - M_{Steam\_out} \quad (3)$$

Where, M_{Steam_out} (kg/s) is the steam flow rate discharged through the break.

The total steam injection flow rate used in the tests was ranged [ ]^{TS}. Table 2-4 presents the scaled MIDAS test conditions and corresponding APR1400 conditions.

The ECCW bypass fractions measured in 15 tests are presented in Figure 2-3 as a function of the total steam injection flow rate. In the cases of one SIP injection through DVI-4 (located nearby the broken cold leg), the DVI-4 injection tests Test 110 through Test 114, the bypass fraction abruptly increased as the total steam injection flow rate increased. The maximum bypass fraction reached almost [ ]^{TS}. It was also observed that very steep increases of the bypass fraction became weakened as the steam flow rate increased. A similar tendency was also observed in the tests that ECCW injected through both DVI-2 and DVI-4 (Test 100 through Test 108; two SIPs operated). The bypass fraction converged into an asymptotic value of about [ ]^{TS} as the steam flow rate increased. In the case of one SIP injection through DVI-2 (located on the opposite side of the broken cold leg), Test 109, the bypass fraction was only [ ]^{TS}; even though the steam flow rate was as high as [ ]^{TS}. These test results indicate that most of the ECCW injected through the DVI-2 nozzle, which was the farthest from the broken cold leg, penetrated into the lower plenum, and that most of the ECCW injected through the DVI-4 nozzle, which was closest to the broken cold leg, bypassed through the break.

Figure 2-4 shows the condensation ratio as a function of the total steam injection flow rate. The condensation ratio is defined as a condensed fraction of the total steam flow rate. The condensation ratio decreased as the total steam injection flow rate increased. For the DVI-2 or DVI-4 injection tests (one SIP operated), the condensation rate was about half of the condensation rate for DVI-2 and DVI-4 injection tests (2 SIPs operated) under the same total steam injection flow rate. This is because the condensation rate is almost proportional to the ECCW injection flow rate, as shown in Table 2-4.

2.2 Code Assessment

2.2.1 RELAP5/MOD3.3/K Model Description

The RELAP5/MOD3.3/K input model of the MIDAS facility is shown in Figure 2-5 and Figure 2-6.

The downcomer is modeled [ ]^{TS}. Each channel of the upper downcomer region (i.e., the region above the cold leg) is modeled [ ]^{TS}. DVI-4, which is the closest DVI nozzle to the break, is connected to Volume 130-2. DVI-2, which is the farthest DVI nozzle from the break, is connected to Volume 140-2. Each channel of the lower downcomer region (i.e., the region below the cold leg) is modeled [

A

labeled 'ECC, Injection Nˆ 11le', is the DVI injectiˆ n nˆ 11le number ˜˜5ˆ3 gh whi0h ECC, 6 as injected. " he major test results are also depi0ted in Fi˙ ure # 3 and Fi˙ ure 2-4.

" ˘ e bypass f5action and the condensation 5atio 6 ere calculated as fˆ llˆ 6 s:

$$Bp_{fraction} = 1 - \frac{M_{Water\_out}}{M_{SI\_in} + M_{Condensate}} \qquad :˛;$$

$$Cond\_ratio = \frac{M_{Condensate}}{M_{Steam\_in}} \qquad :\#;$$

, ˘ ere, M_{SI_in} (kg/s) was the total ECC, injection flˆ w rate, M, ater_ou˘ (kg/s) is the liquid flo6 rate discharged thro3˙ h the lower plenum, M_{Steam_in} is the steam injection flˆ w rate, and $M_{Condensate}$ (kg/s) is the condensation rate 6˘ ich is calculated as follˆ 6 s:

$$M_{Condensate} = M_{Steam\_in} - M_{Steam\_out} \qquad :-;$$

, ˘ ere, M Steam_o3˘ (kg/s) is the steam flˆ6 rate discharged thro3˙ h the break%

" he bypass f5action is defined by using the li@3id flow rate discharged thro3˙ h the lˆ 6 er plenum. " he li@3d flo6 rate discharged t˘5ˆ3 gh the lˆ 6 er plen34 is the same as accu4 ulated li@3d rate to do6 ncomer that is the sum4 ation of ECC, injectiˆ n rate with consideration ˆ8 bypass and steam condensatiˆ n, since dˆ 6 ncˆ4 er water le$el is constantly 4 ain˘ained.

The total steam injection flow rate used in the tests was ranged A B˂. Table # 4 presents the scaled MIDAS test conditions and corresponding APR1400 conditions.

" he ECCW bypass f5actions 4 easured in 15 tests are presented in Figure # 3 as a function of the total steam injectiˆ n flow rate. In the cases of one <.P injection ˜˜5ˆ3 gh D2. 4 (located nearby ˘he broken cold leg), the D2. 4 injectiˆ n tests " est 110 through " est 114, the by7ass f5action abruptly increased as the total steam injection flow rate increased. The maximum bypass fraction reached almost [KKKKB˂KKKKwas also observed that very steep increases of the bypass fraction became weakened as the steam 8ˆ w rate increased. A similar tendency was also obser$ed in the tests that ECCW injected through both DVI-2 and DVI-4 (Test 100 through Test 108; two SIPs operated). The bypass fraction converged into an asymptotic value of about AKKKKB˂KKasKthe steam flow rate increased. In the case of one SIP injection through DVI-2 (located on the opposite side of the broken cold leg), Test 109, the bypass fraction was only [KKB˂KKeven though the steam flow rate was as high as AKKKKKKKKKKKKKKKB˂KKTheseKtestKresultsKindicateKthat most of the ECCW injected through the)2. 2 nozzle, which 6 as the farthest from the broken cold leg, penetrated into the lower plenum, and that most of the ECCW injected through the DVI-4 nozzle, which was closest to the broken cold leg, bypassed through the break.

Figure # 4 sho6 s the condensation 5atio as a function ˆ 8the total steam injection flo6 rate%" ˘ e 0ondensatiˆ n 5atio is defined as a 0ˆ ndensed 85actiˆ n ˆ 8the total steam 8low rate. " ˘ e condensatiˆ n ratio decreased as the total stea4 injection flˆ w rate in0reased. For ˜˘ e D2. 2 or DVI-4 injection tests (one <.˝ operated), t˘ e condensation rate was about hal8of the condensation rate for)2 . 2 and D2. 4 injection tests :# SIPs operated) under the same total steam injectiˆ n flˆ 6 rate. " his is because the condensation 5ate is al4 ˆ st proportional to the ECC, injectiˆ n flˆ w rate, as sho6 n in " able 2-4.

#%# Code Assessment

#%#%˛ REL ˝ 5/MOD- %-K Mˆ del Des05ption

" ˘ e RELA˝C /MOD3.-?K input model of the MI) < facility is shown in Figure # 5 and Figure 2-H%

RESPONSE TO AUDIT ISSUES

APR1400 Topical Reports

Korea Electric Power Corporation / Korea Hydro & Nuclear Power Co., LTD

Docket No. PROJ0782

Review Section	**TR Realistic Evaluation Methodology for LBLOCA of the APR1400**
Application Section	**Topical Report: APR1400-F-A-TR-12004 Realistic Evaluation Methodology for Large-Break LOCA of the APR1400**
Issue Date	**08/13/2015**

Audit Issues No. 47

The guidance in RG 1.157, Section 3.11 establishes acceptable controls regarding the calculation of core flow distribution. Section 4.2.2.1.2 of the topical report states that the uncertainty in the high importance phenomenon of [ ]^{TS} is not determined because it is included in the steam binding bias. Flow through the top nozzles is a complex multidimensional process with liquid down flow through the lower power outer assemblies and steam and entrained liquid up flow through the central higher power assemblies. Bias in the steam binding process is not directly related to the uncertainty in the countercurrent flow at the top nozzles. Demonstrate how the bias in the steam binding process bounds the uncertainty in countercurrent flow at the top nozzles or provide the bases for neglecting the relevant uncertainty.

Response

The meaning of the term “top nozzle” is to be understood as a component that has the smallest flow area along the flow path from core to upper plenum. The term “tie plate” is used for the following discussions according to the term used in the 2D/3D research project. [

]TS

CCFL is discussed on the junctions between node 170 and node 180 in the same figure. CCFL on the tie plate has been studied in UPTF-10C test. The results of the study are well described in the reference [1]. Figure 4.4.1 of the reference [1] depicts the CCFL phenomena occurring on the tie plate. Part of the figure and summary is redrawn in Figure 1 for the clarification of the following discussions. Reference [1] also describes the CCFL phenomena as “the steam/water up-flow from the core and the water fallback through the tie plate being uniform across the vessel”.

The phenomena mentioned in the question as, “a complex multidimensional process with liquid down flow through the lower power outer assemblies and steam and entrained liquid up flow through the central higher power assemblies”, is the recirculation process that may occur during the core reflood. It is not the CCFL phenomena, which were studied by UPTF-10C test, but the recirculation phenomena that will effectively help the cooling of the core. In the CAREM, it is not allowed by modeling single flow path at tie the plate.

The current nodding of core is a conservative approach for PCT by essentially removing the favorable recirculation process.

Returning to the CCFL phenomena, CCFL on tie plate is very complicated hydraulic phenomena. As shown in Figure 1, CCFL phenomena consist of three flow streams, the steam and water up-flow from the core and the water fallback. REALP5 has two fluid flow fields. Therefore, it is not easy to correctly model the CCFL phenomena with RELAP5. RELAP5 treats CCFL with a general model that allows the user to select the Wallis form, the Kutateladze form, or a form in between the Wallis and Kutateladze forms[2].

In general, experiments on CCFL are well correlated with the Kutateladze number as shown in Figure 1. Most important thing to check is the limiting gas velocity, $v_{s,Limit}$, above which no down-flow is possible.

$$K_x^* = \frac{\dot{M}_x}{\rho_x A_{tie}} \left(\frac{(\rho_x)^{\frac{1}{2}}}{\left(g\sigma(\rho_w - \rho_s)\right)^{\frac{1}{4}}} \right)$$

$$\sigma = 0.0002822(Pa \cdot s) @ 100^o C \; liquid$$

$$\rho_w = 958.4(kg/m^3) @ 100^o C$$

$$\rho_s = 0.59(kg/m^3) @ 1bar = 1.651(kg/m^3) @ 3bar$$

$$K_{s,}^*@3bar = v_s \left(\frac{(\rho_s)^{\frac{1}{2}}}{\left(g\sigma(\rho_w - \rho_s)\right)^{\frac{1}{4}}} \right) = \frac{v_s(1.651)^{.5}}{\left(9.8 \times 0.0002822 \times (958.4 - 1.651)\right)^{0.25}} = \frac{1.285 v_s}{1.275} = 1.0 v_s$$

$K_{s,Limit}^* = 4.0$, From Figure 1

$$v_{s,Limit}@3bar = \frac{4.0}{1.0} = 4.0(m/s)$$

$$v_{s,Limit}@1bar = \frac{4.0}{0.6} = 6.7(m/s)$$

As exemplified in the above calculations, $v_{s,Limit}$ is 6.7 m/s. The steam velocity at the tie plate for APR-1400 is shown in Figure 2. It is always greater than 6.7 m/s during the reflood period, between 70 sec and 200 sec. The steam and liquid flow at the tie plate are shown in Figure 3. The liquid flow is generally upward in all reflood period except the time period between 170 ~ 250 sec, which is consistent with the $v_{s,Limit}$ consideration. Thus, the code predicts thermal hydraulic behavior on the tie plate reasonably even without CCFL model.

One more concern of the CCFL is its implementation in the code. Since the CCFL changes the flow, RELAP5 implements it by changing the momentum equations (refer to reference [3], section 3.4.7). The implemented CCFL models are validated mainly through steady state experiments. But the flow during the reflood period is very oscillatory. There is a strong tendency that the implemented CCFL model in RELAP5 amplifies the oscillation during the reflood. This tendency is the same as that with critical flow model used on the internal junctions. In general, any model that manipulates the momentum equations during its implementation makes it difficult to get a stable solution. Considering this situation, CAREM does not use CCFL option on the tie plate junctions.

RELAP5 in CAREM over-predicts the water carry-over rate from core to upper plenum. These facts are shown in the assessments of FLECHT-SEASET (Reference [4], Appendix P, pp. P-11) and NEPTUN (Topical Report, Appendix C, section 4.3.4).

The flow regime in upper plenum during reflood period is mainly annular or annular/mist type. There is no model for the de-entrainment by internal structures in upper plenum. Therefore, liquid flow from upper plenum to hot leg depends on the liquid volume fraction of upper plenum and it usually over predicts. Liquid volume left in upper plenum is under predicted. Such a process can be found in the result of UPTF-10B simulation (Reference [4], Appendix P, pp. P-13). As a result of these series of process, liquid flow to steam generator is excessive and ensuing steam binding is too excessive. It is necessary to implement a de-entrainment model in the upper plenum to solve the problem.

An effective de-entrainment model can be constructed by controlling the droplet fraction in annular flow regime. Reducing the droplet fraction to 10 % of the RELAP5 prediction value makes the liquid fraction in upper plenum close to the UPTF-10B experimental value (Reference [4], Appendix P, pp. P-13).

Lastly, there are only limited experiments that can be used for assessing the behavior of the droplet reaching to steam generator. Due to the lack of experimental data, the problem dealing with the behavior of droplet transferred to steam generator is decided to be treated as a bias. The method is to evaporate all liquid drops that pass through steam generator. By reducing the droplet size and increasing heat transfer coefficients, it is possible to make all drops evaporate in steam generator.

In summary;

1. Steam velocity at the tie plate is greater than CCFL limit velocity, CCFL option is not

needed. Due to the unstable behavior of the CCFL option, the CCFL option is not recommendable on the tie plate junction. Therefore, it is not used in the CAREM.

2. RELAP5 in the CAREM over-predicts the water carry-over rate from core to upper plenum. But it is used as it is in the CAREM. This is a conservative approach with respect to PCT.

3. An effective upper plenum de-entrainment model is constructed by controlling the droplet fraction in annular flow regime using UPTF-10B experiment. It is treated as a bias.

4. The behavior of droplet transferred to steam generator is treated as a bias.

Using the above processes, the CCFL phenomena at the tie plate, upper plenum de-entrainment phenomena, and the behavior of the droplet in the steam generator, during the reflood period, are treated conservatively as biases.

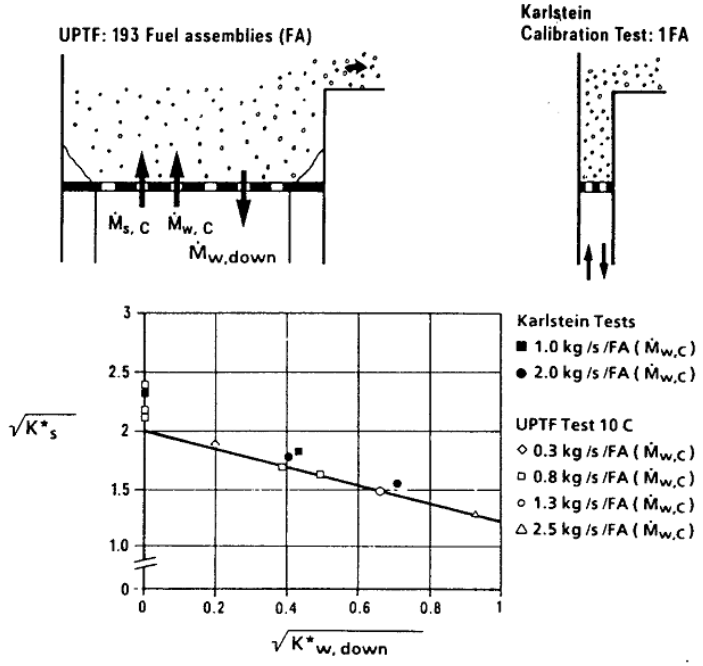

COUNTERCURRENT FLOW OF SATURATED STEAM AND WATER AT THE TIE PLATE

FIGURE 4.4-1

Figure 1. Figure 4.4-1 of the reference [1]

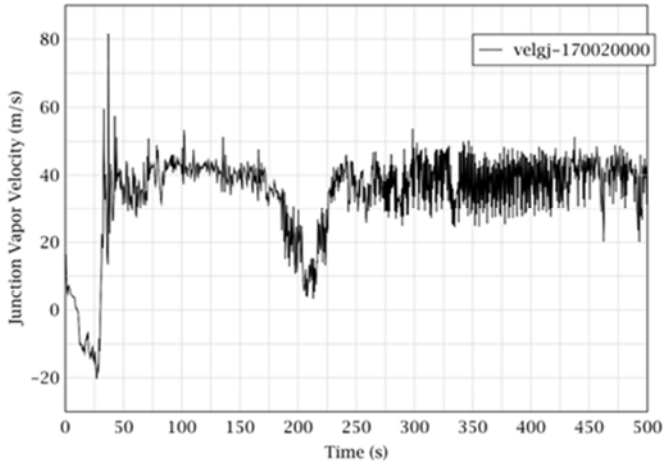

Figure 2. Steam Velocity at Tie-Plate

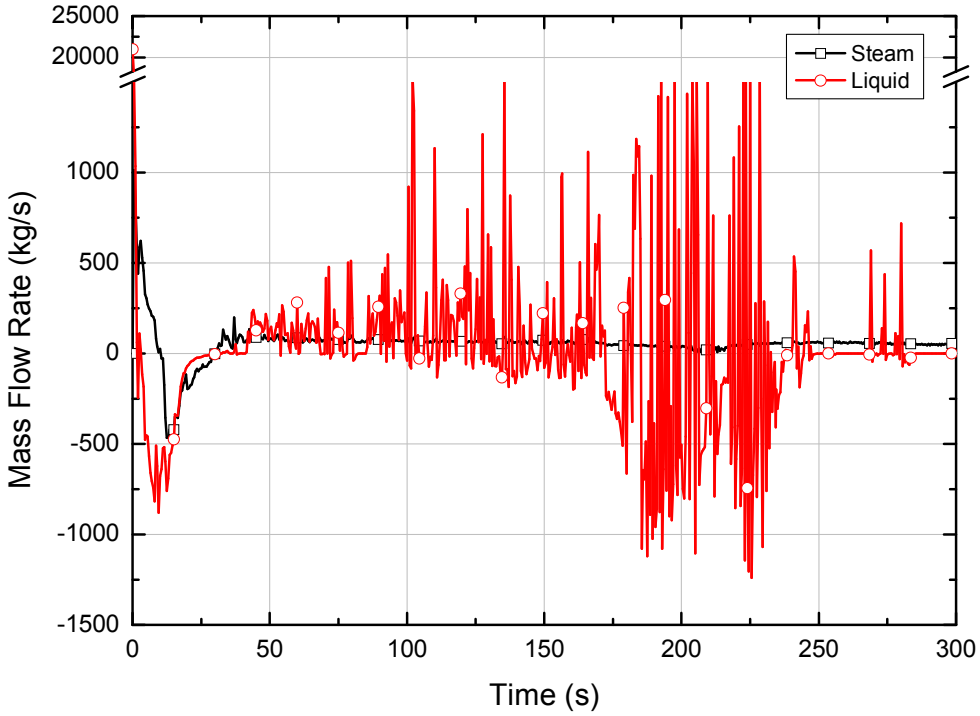

Figure 3. Steam and Liquid Flow Rate through the Tie Plate

References

[1] "2D/3D Program Work Summary Report," NUREG/IA-0126, GRS-100, MPR-1345, 1993.

[2] "RELAP5/MOD3.3 Code Manual Volume IV: Models and Correlations," Nuclear Systems Analysis Division, March 2006.

[3] "RELAP5/MOD3.3 Code Manual Volume I: Code Structure, System Models, and Solution Methods", Nuclear Systems Analysis Division, March 2003.

[4] "Topical Report for the Realistic Evaluation of Emergency Core Cooling System", TR-KHNP-0002, 2002. (Appendix P Evaluation of Steam Binding Using UPTF and PKL Test)

Impact on DCD

There is no impact on the DCD.

Impact on PRA

There is no impact on the PRA.

Impact on Technical Specifications

There is no impact on the Technical Specifications.

Impact on Technical/Topical/Environmental Report

There is no impact on any Technical, Topical, or Environmental Report.

RESPONSE TO AUDIT ISSUES

APR1400 Topical Reports

Korea Electric Power Corporation / Korea Hydro & Nuclear Power Co., LTD

Docket No. PROJ0782

Review Section	**TR Realistic Evaluation Methodology for LBLOCA of the APR1400**
Application Section	**Topical Report: APR1400-F-A-TR-12004 Realistic Evaluation Methodology for Large-Break LOCA of the APR1400**
Issue Date	**08/13/2015**

Audit Issues No. 48

The guidance in RG 1.157, Section 3.11 establishes acceptable controls regarding the calculation of steam or two-phase fluid interaction with injection flow. Address the following concerns about [ ]^{TS} determination discussed in Section 4.2.3.2 of the topical report:

a. Results from a past assessment using RELAP5/MOD3.1 have been cited. However, that is not the code version being utilized for the KHNP analyses. Indicate whether RELAP5/MOD3.3/K has been used to confirm that the results cited are applicable.

Response

In the topical report, the applicability of results cited is not confirmed using RELAP5/MOD3.3/K directly, but it is expected to be acceptable because of the similar code predictability of the RELAP5/MOD3.3/K against the older version. These have been inferred from the code accuracy results, which were described in [1] and [2]. There, the code prediction by newer version shows similar or more conservative (larger calculated value) results.

In order to confirm the code applicability of RELAP5/MOD3.3/K, the assessment against [ ]^{TS} The results are consistent with that of RELAP5/MOD3.1 as shown in Figure 1, where the calculated [ ]^{TS}.

TS

Figure 1. The new assessment result of [ ]TS with RELAP5/MOD3.3/K with and without [ ]TS

References

[1] TR-KHNP-0018(Proprietary), “Topical Report for the LBLOCA Best-Estimate Evaluation Methodology of the APR1400 Type Nuclear Power Plants”, 2010. 8.

[2] TR-KHNP-0002(Proprietary), “Topical Report for the Realistic Evaluation of Emergency Core Cooling System, Volume 1: Description of Best Estimate Methodology for Large Break LOCA”, 2002. 12.

Impact on DCD

There is no impact on the DCD.

Impact on PRA

There is no impact on the PRA.

Impact on Technical Specifications

There is no impact on the Technical Specifications.

Impact on Technical/Topical/Environmental Report

There is no impact on any Technical, Topical, or Environmental Report.

RESPONSE TO AUDIT ISSUES

APR1400 Topical Reports

Korea Electric Power Corporation / Korea Hydro & Nuclear Power Co., LTD

Docket No. PROJ0782

Review Section	**TR Realistic Evaluation Methodology for LBLOCA of the APR1400**
Application Section	**Topical Report: APR1400-F-A-TR-12004 Realistic Evaluation Methodology for Large-Break LOCA of the APR1400**
Issue Date	**08/13/2015**

Audit Issues No. 48

The guidance in RG 1.157, Section 3.11 establishes acceptable controls regarding the calculation of steam or two-phase fluid interaction with injection flow. Address the following concerns about [ ]^{TS} determination discussed in Section 4.2.3.2 of the topical report:

b. It is expected that the predicted entrainment from the upper plenum will be a strong function of nodalization in the core and the upper plenum regions. Describe the nodalization of these components for the comparison against [ ]^{TS}. In case the nodalization for the core and upper plenum for comparison against [ ]^{TS} is different from that for APR1400, justify the applicability of the nodalization used for APR1400 calculations.

Response

The upper plenum nodings of [ ]TS and APR1400 are shown in the following figure.

TS

In APR1400, the upper plenum is [

]TS

Impact on DCD

There is no impact on the DCD.

Impact on PRA

There is no impact on the PRA.

Impact on Technical Specifications

There is no impact on the Technical Specifications.

Impact on Technical/Topical/Environmental Report

There is no impact on any Technical, Topical, or Environmental Report.

RESPONSE TO AUDIT ISSUES

APR1400 Topical Reports

Korea Electric Power Corporation / Korea Hydro & Nuclear Power Co., LTD

Docket No. PROJ0782

Review Section	**TR Realistic Evaluation Methodology for LBLOCA of the APR1400**
Application Section	**Topical Report: APR1400-F-A-TR-12004 Realistic Evaluation Methodology for Large-Break LOCA of the APR1400**
Issue Date	**08/13/2015**

Audit Issues No. 48

The guidance in RG 1.157, Section 3.11 establishes acceptable controls regarding the calculation of steam or two-phase fluid interaction with injection flow. Address the following concerns about [ ]TS determination discussed in Section 4.2.3.2 of the topical report:

c. The implementation of [ ]TS in RELAP5/MOD3.3/K is shown in Slide 18 of 29 of APR1400-F-A-RA-14001-P. Use of inconsistent activation times for [

]TS may lead to different results and render the assessment inapplicable. Clarify whether the activation time implemented in RELAP5/MOD3.3/K is consistent with that used for [ ]TS. If the activation times are different, a justification needs to be provided.

Response

[

]TS activation time should be matched phenomenologically, not the absolute time itself, because [ ]TS should be considered in that interested specific period. Therefore, the start of the reflood is used as [ ]TS.

Impact on DCD

There is no impact on the DCD.

Impact on PRA

There is no impact on the PRA.

Impact on Technical Specifications

There is no impact on the Technical Specifications.

Impact on Technical/Topical/Environmental Report

There is no impact on any Technical, Topical, or Environmental Report.

RESPONSE TO AUDIT ISSUES

APR1400 Topical Reports

Korea Electric Power Corporation / Korea Hydro & Nuclear Power Co., LTD

Docket No. PROJ0782

Review Section	**TR Realistic Evaluation Methodology for LBLOCA of the APR1400**
Application Section	**Topical Report: APR1400-F-A-TR-12004 Realistic Evaluation Methodology for Large-Break LOCA of the APR1400**
Issue Date	**08/13/2015**

Audit Issues No. 48-d

The guidance in RG 1.157, Section 3.11 establishes acceptable controls regarding the calculation of steam or two-phase fluid interaction with injection flow. Address the following concerns about [ ]TS determination discussed in Section 4.2.3.2 of the topical report:

d. The implementation of [ ]TS in RELAP5/MOD3.3/K is shown in Slide 19 of 29 of APR1400-F-A-RA-14001-P which states that this feature is activated at [ ]TS. This selection of the activation time for this portion of [ ]TS. According to Table 3-5 of the topical report, the PIRT assigns a rank of [ ]TS. [ ]TS is expected to be more important during the early reflood period due to the higher rates of flow and entrainment. Justify the selected activation timing for [ ]TS.

Response

Due to the reasons described in the response of the audit issue No. 71, the activation timing for [ ]TS.

Impact on DCD

There is no impact on the DCD.

Impact on PRA

There is no impact on the PRA.

Impact on Technical Specifications

There is no impact on the Technical Specifications.

Impact on Technical/Topical/Environmental Report

There is no impact on any Technical, Topical, or Environmental Report.

RESPONSE TO AUDIT ISSUES

APR1400 Topical Reports

Korea Electric Power Corporation / Korea Hydro & Nuclear Power Co., LTD

Docket No. PROJ0782

Review Section	**TR Realistic Evaluation Methodology for LBLOCA of the APR1400**
Application Section	**Topical Report: APR1400-F-A-TR-12004 Realistic Evaluation Methodology for Large-Break LOCA of the APR1400**
Issue Date	**08/13/2015**

Audit Issues No. 49

The guidance in RG 1.157, Section 3.16.1 establishes acceptable controls regarding the calculation of acceptance criteria. In Section 4.3.1.1 of the topical report, the one-sided 95 percent limit of blowdown PCT is specified as [ ]^{TS}, and it is calculated using [ ]^{TS}. However, the one-sided 95 percent limit of reflood PCT is calculated as [ ]^{TS}. Moreover, the calculation for the blowdown period is inconsistent with the expression in Section 4.3.1 of the topical report. Provide the reason for the discrepancy in the approaches used for blowdown and reflood PCT calculations in Section 4.3.1.1.

Response

Description for blowdown code accuracy in Section 4.3.1.1 and Figure 4-7 is wrong. The equation of one-sided 95 percent limit [ ]TS is correct, but calculation results of [ ]TS is wrong. Therefore, description and Figure 4-7 of topical report will be modified as follows.

Description:

When all [ ]TS data sets are considered, the RELAP5 code is found to over-predict the measured data by [ ]TS.

Figure:

TS

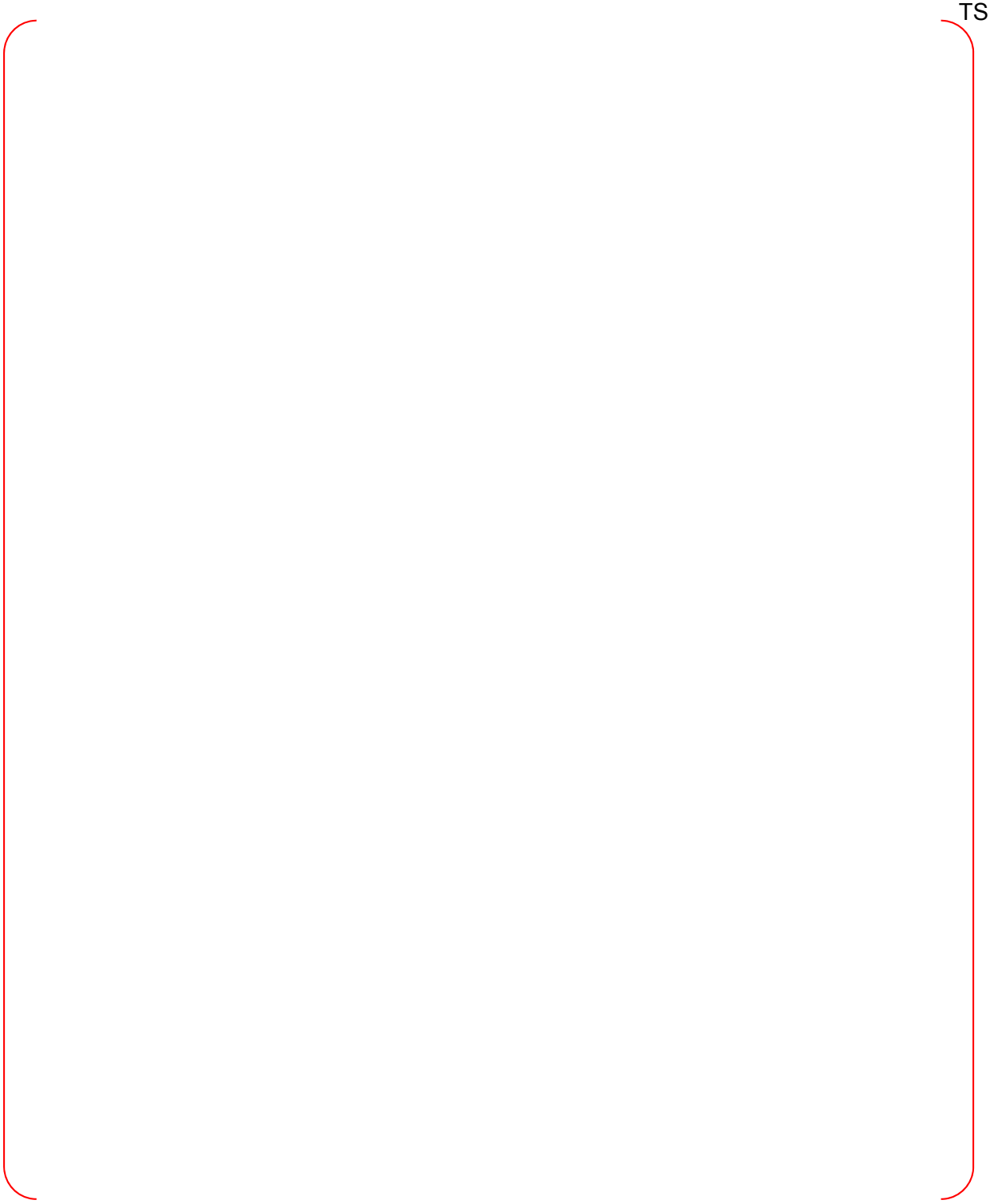

Figure 4-7. Code Accuracy during Blowdown Phase

Impact on DCD

There is no impact on the DCD.

Impact on PRA

There is no impact on the PRA.

Impact on Technical Specifications

There is no impact on the Technical Specifications.

Impact on Technical/Topical/Environmental Report

Topical report will be revised as discussed in this response.

There is no impact on Technical or Environmental Report.

RESPONSE TO AUDIT ISSUES

APR1400 Topical Reports

Korea Electric Power Corporation / Korea Hydro & Nuclear Power Co., LTD

Docket No. PROJ0782

Review Section	**TR Realistic Evaluation Methodology for LBLOCA of the APR1400**
Application Section	**Topical Report: APR1400-F-A-TR-12004 Realistic Evaluation Methodology for Large-Break LOCA of the APR1400**
Issue Date	**08/13/2015**

Audit Issues No. 50-a and b

The guidance in RG 1.157, Section 4 establishes acceptable controls for the estimation and propagation of uncertainties. Address the following concerns about the “coverage check” discussed in Section 4.3.2 of the topical report.

a. Explain how the limited number of parameters for uncertainty variation in the blowdown and reflood “coverage check”’ was chosen from the list of all phenomena with [ ]^{TS} during these periods.

b. The “coverage check” uses a small subset of parameters for uncertainty variation. However, a larger set of parameters is actually used in the best-estimate plant calculations. Explain how it is ensured that inclusion of the additional uncertainty parameters does not change the results and alter the conclusions of the “coverage check.” Further, if such a demonstration has been accomplished, describe the change in the limiting PCT.

Response to (a) and (b)

All uncertainty parameters can be consistently considered for blowdown and reflood coverage check. It is obvious that larger number of uncertainty parameters results in wider uncertainty variation, i.e., higher cladding temperature.

Meanwhile, it is not needed to consider the uncertainty parameters related to reflood phenomena for the blowdown coverage check, and vice versa. Some uncertainty parameters involved with both blowdown and reflood phenomena are commonly used for the blowdown and reflood coverage check. In addition, both uncertainty parameters related to blowdown and reflood phenomena are considered for IETs. If the effects of test specific uncertainty are not negligible [

]^{TS}, those uncertainties are additionally considered.

Impact on DCD

There is no impact on the DCD.

Impact on PRA

There is no impact on the PRA.

Impact on Technical Specifications

There is no impact on the Technical Specifications.

Impact on Technical/Topical/Environmental Report

There is no impact on any Technical, Topical, or Environmental Report.

RESPONSE TO AUDIT ISSUES

APR1400 Topical Reports

Korea Electric Power Corporation / Korea Hydro & Nuclear Power Co., LTD

Docket No. PROJ0782

Review Section	**TR Realistic Evaluation Methodology for LBLOCA of the APR1400**
Application Section	**Topical Report: APR1400-F-A-TR-12004 Realistic Evaluation Methodology for Large-Break LOCA of the APR1400**
Issue Date	**08/13/2015**

Audit Issues No. 50-c

The guidance in RG 1.157, Section 4 establishes acceptable controls for the estimation and propagation of uncertainties. Address the following concerns about the “coverage check” discussed in Section 4.3.2 of the topical report.

c. Clarify whether [ ]^{TS} was included in the performance of the “coverage checks” for reflood period when compared to integral test data.

Response

The purpose of “coverage checks” is to confirm the adequacy of the number of uncertainty parameters and the uncertainty range of each parameter. [

]TS

Impact on DCD

There is no impact on the DCD.

Impact on PRA

There is no impact on the PRA.

Impact on Technical Specifications

There is no impact on the Technical Specifications.

Impact on Technical/Topical/Environmental Report

There is no impact on any Technical, Topical, or Environmental Report.

RESPONSE TO AUDIT ISSUES

APR1400 Topical Reports

Korea Electric Power Corporation / Korea Hydro & Nuclear Power Co., LTD

Docket No. PROJ0782

Review Section	**TR Realistic Evaluation Methodology for LBLOCA of the APR1400**
Application Section	**Topical Report: APR1400-F-A-TR-12004 Realistic Evaluation Methodology for Large-Break LOCA of the APR1400**
Issue Date	**08/13/2015**

Audit Issues No. 51

The guidance in RG 1.157, Section 4 establishes acceptable controls for the estimation of uncertainties. The following issues are related to the distribution-free statistics method described in Section 4.3.2 of the topical report:

a. It appears that the method described in Section 4.3.2 is similar to the formulation of Guba, Makai and Pál based on order statistics (Reliability Engineering and System Safety, Vol. 80, Issue 3, pp.217-232, June 2003). Confirm or provide a reference for the method used in the topical report.

b. Section 4.3.2 states that the third highest result of 124 random calculations provides the 95/95 limit. In case the method in the topical report uses order statistics (see part (a) of this issue), it is unclear whether the approach employed in the topical report is the single parameter uncertainty evaluation with the third estimator grade or the multiple parameter uncertainty evaluation with three parameters. Both approaches require 124 random calculations. Clarify the method used in CAREM.

c. In case the distribution-free statistics method is based on the single parameter uncertainty evaluation for the PCT, the approach used to determine the limiting values of local cladding oxidation and hydrogen generation is not clear. It is not possible to determine whether the limiting values of local cladding oxidation and hydrogen generation are those that correspond to the calculations resulting in the limiting PCT or are derived from separate 124 random calculations for each of those two parameters. Explain and justify the approach used.

d. In case the distribution-free statistics method is based on the multiple parameter uncertainty evaluation with three parameters, such a method assumes that the parameters are continuous and independent. During LBLOCA calculations bursting of cladding may be predicted to occur resulting in a discontinuous increase in the cladding temperature. In addition, the local and the core-wide cladding oxidation and hydrogen generation values are dependent on the corresponding cladding temperature. Clarify whether the methodology described in the topical report is limited to pre-burst conditions

or justify the applicability of the assumption of the continuity of the parameters in the event of cladding burst. Further, justify the assumption of the independence of the three parameters (e.g., PCT, cladding oxidation and hydrogen generation).

Response (Rev.1)

(a) ~ (d)

[

]TS

- From reference [1];

Let us choose the first row of the sample matrix, and arrange its elements in order of increasing magnitude, $y_1(1), y_1(2), \ldots y_1(N)$. Select from these $y_1(r_1)$ as L_1 and $y_1(s_1) > y_1(r_1)$ as U_1: Let $i_1, i_2, \ldots, i_{s_1-r_1-1}$ stand for the original column indices of elements $y_1(r_1+1), y_1(r_1+2), \ldots y_1(s_1-1)$: In the next step, choose the second row, the N observed values of the output variable y_2 and arrange the part $y_{2i_1}, y_{2i_2}, \ldots y_{2_{s_1-r_1-1}}$ of its elements in increasing order to obtain $y_2(1) < y_2(2) < \cdots < y_2(s_1-r_1-1)$. From among these, $y_2(r_2)$ and $y_2(s_2)$ are selected for L_2 and U_2 and evidently $r_2 \geq r_1, s_2 \leq s_1 - r_1 - 1$: We continue this imbedding procedure to the last row of the sample matrix and define a p-dimensional volume $V_p = \{|L_1, U_1, | \times |L_2, U_2| \times \ldots \times |L_p, U_p|\}$, where $L_j = y_j(r_j), U_j = y_j(s_j)$, and $r_j \geq r_{j-1} \geq \cdots \geq r_1$, while $r_j < s_j \leq s_{j-1} - r_{j-1} - 1, \ \forall j = 2 \ldots p$.

….

Theorem 4. In the case of p independent output variables with continuous joint density function $g(y_1, \ldots y_p)$, it is possible to construct p-pairs of random intervals $[L_j, U_j]_{j=1\ldots p}$ such that the probability of the inequality

$$\int_{L_1}^{U_1} \ldots \int_{L_p}^{U_p} g(y_1, \ldots y_p) dy_1 \ldots dy_p > \gamma$$

is free of g and is given by

$$Prob\left\{\int_{L_1}^{U_1} \ldots \int_{L_p}^{U_p} g(y_1, \ldots y_p) dy_1 \ldots dy_p > \gamma\right\} =$$

$$\beta = 1 - I(\gamma, s_p - r_p, N - s_p + r_p + 1) \qquad (1)$$

Here,

$$s_p \leq s_{p-1} - r_{p-1} - 1 \leq s_1 - \sum_{j=1}^{p-1}(r_j + 1) \qquad (2)$$

$$r_p \geq r_{p-1} \ldots \geq r_1 \qquad (3)$$

Proof of Theorem 4 is given in Appendix D….

Furthermore, if $r_1 = r_2 = \cdots = r_p = 0$ and $s_p = N - p + 1$, then one obtains the following one-sided confidence level.

$$\beta = 1 - I_\gamma(N - p + 1, p) = I_{1-\gamma}(p, N - p + 1) = \sum_{j=p}^{N} \binom{N}{j} (1-\gamma)^j \gamma^{N-j}$$

$$= 1 - \sum_{j=0}^{p-1} \binom{N}{j} (1-\gamma)^j \gamma^{N-j} \qquad (4)$$

- [ ]TS

[

]TS

- It is strongly recommended [2] that the estimation of the upper limits should be higher than the first order with the following arguments.

When the upper tolerance limit approaches regulatory acceptance criteria, e.g. 1200°C PCT, the number of code runs may be increased to 150 or 200 calculations instead of the 59 code runs needed, using Wilks' formula at the first order for the estimation of a α = 95% one-sided tolerance limit with a confidence level β of 95%. This would be advisable for two reasons:

1) With increasing sample size the uncertainty results will be less dispersed, and consequently more converged (less conservative), and

2) The sensitivity results will be more reliable.

[

]TS

Table 1. Ordering of parameters during estimating confidence level

TS

Reference

[1] Reliability Engineering and System Safety, Vol. 80, Issue 3, pp.217-232, June 2003

[2] H. Glaser, “BEMUSE Phase VI Report, Status report on the area, classification of the methods, conclusions and recommendations”, NEA/CSNI/R(2011)4, 28-Mar-2011; (https://www.oecd-nea.org/nsd/docs/2011/csni-r2011-4.pdf).

Impact on DCD

There is no impact on the DCD.

Impact on PRA

There is no impact on the PRA.

Impact on Technical Specifications

There is no impact on the Technical Specifications.

Impact on Technical/Topical/Environmental Report

Topical report is changed based on this response.

There is no impact on Technical or Environmental Report.

data by [ ]TS. The one-sided 95 % limit of blowdown PCT is [ ]TS.

4.3.1.2 Reflood Code Accuracy

In the evaluation of the reflood code accuracy, 27 separate effect tests (i.e., 17 FLECHT-SEASET tests, 7 NEPTUN tests, and 3 ATLAS tests) and 7 integral effect tests (i.e., LOFT L2-2, L2-3, L2-5, LP-02-6, CCTF C2-4, PKL-IIb5, and Semiscale S-06-3) are considered.

The maximum clad temperatures of NEPTUN were measured at various locations of No. 3, 4, and 5 in general depending on experimental conditions. These locations correspond to 0.512 m, 0.744 m, and 0.976 m elevations from the bottom of the 1.68 m effective length. The two highest measurements from each NEPTUN test and their calculational correspondents are considered in this evaluation. Code assessment calculation against NEPTUN is described in Appendix C. In the case of FLECHT-SEASET, three data sets, one at a PCT location and two at neighboring measurement locations, are considered. Calculated temperatures are taken from the results given in Appendix C. Measurements of the FLECHT-SEASET experiments are concentrated at the central part of the core. Three elevations correspond to one or two nodes in the calculation.

In the case of ATLAS, the three highest measurements from each test and their correspondents are considered. ATLAS Tests 9 and 15 showed the three highest temperatures at 1.066 m, 1.271 m, and 1.329 m elevations from the bottom of the 1.905 m active core, while they were measured at 0.953 m, 1.066 m, and 1.329 m elevations in Test 11. Corresponding node numbers are 12, 14, and 15 for test 9 and 15, and 11, 12, and 15 for Test 11. Calculated values are taken from calculations in Appendix E. In the case of CCTF C2-4, the measured peak value at 2.44 m (96 in.) and its correspondent are considered. In the case of PKL-IIb5, the measured peak value at 2.5 m (98 in.) elevation and a comparable peak value at 1.95 m (77 in.), and their correspondents, are considered. In the case of Semiscale S-06-3, the measured peak value at 0.74 m (29 in.) and the neighboring measurement at 0.71 m (28 in.) are selected and compared with their calculational correspondents.

Figure 4-8 shows the reflood code accuracy evaluated using [ ]TS data sets. The code over-predicts the clad temperatures by [ ]TS.

4.3.2 Check Data Covering (Step 9.2)

Data covering is checked to confirm the variety, number, and ranges of code uncertainty parameters. If the code uncertainty is quantified using all the code uncertainty parameters in accordance with the bottom-up approach of NUREG-1230 [19], this checking process may not be necessary. In the top-down approach, however, it is necessary to confirm the number of uncertainty parameters with respect to the practicality of the method. Identification and ranking of the phenomena and subsequent selection of uncertainty parameters are dependent on the subjective decision of experts in the field. Accordingly, the objective basis of the determination of the number and the ranges of the parameters needs to be provided.

In principle, this covering check is performed for all the experiments considered in the code accuracy evaluation, especially for the cases where code predictions are lower than the measured peak values. A set of uncertainty parameters confirmed by this covering check can produce the uncertainty encompassing code accuracy.

~~Distribution-free statistics is utilized in this checking. The probability that N random samples are all within a certain percentile p is p^N. The probability that one of N samples exceeds p percentile and the others fall within p percentile is~~

[ ]TS

The probability that two of them N samples exceeds p percentile is

[ ]TS

Hence the probability that at most two of N samples exceeds p percentile is

[ ]TS

The complement of the above probability,

[ ]TS

means the probability that at least three of N samples exceed p percentile.

The confidence level q is calculated by

[ ]TS

If $p = q = 0.95$, the minimum number of samples (N) is calculated as 124 in order to obtain at least three samples exceeding 95 percentile at 95% confidence level. This means that three results (i.e., the highest, the second highest, and the third highest results) drawn from the domain of 124 LBLOCA calculations exceed 95 percentile tolerance limit at 95 % confidence level. Therefore, the third highest result of 124 random calculations is an estimate of the 95 percentile tolerance limit at 95 % confidence level. [

]TS

4.3.2.1 Check Blowdown Covering

Simple-random sampling (SRS) calculations were performed against the test data obtained from THTF, LOFT, and LOBI in order to check whether the calculations can cover the measured blow-down PCTs.

The eight code uncertainty parameters used for checking the blowdown covering against the THTF tests are: [

]TS. Because the LOFT and LOBI tests were integral effect tests performed for whole transients of the LBLOCA, other code parameters, which are used during the reflood period, and some system parameters are additionally considered for these tests. The effects of additional code parameters on the blowdown calculation are minimal. Uncertainty parameters used for checking the covering against each test are listed in Appendices C and D for the THTF, and LOBI and LOFT, respectively.

A set of uncertainty parameters is randomly sampled 124 times along their probability distribution functions, and the same numbers of calculations are performed. SRS calculations and measured data from the THTF Test 105 and Test 160 are compared in Figure 4-9 and Figure 4-10, respectively. Out of four sets of THTF SRS calculations in Appendix C, the above two are excerpted for examples, as they have the highest and the lowest rod power. Squared markings represent the upper-bound of the measurement. It is confirmed that the [

]TS

data by [ ]TS. The one-sided 95 % limit of blowdown PCT is [ ]TS.

4.3.1.2 Reflood Code Accuracy

This page is replaced with page B.

In the evaluation of the reflood code accuracy, 27 separate effect tests (i.e., 17 FLECHT-SEASET tests, 7 NEPTUN tests, and 3 ATLAS tests) and 7 integral effect tests (i.e., LOFT L2-2, L2-3, L2-5, LP-02-6, CCTF C2-4, PKL-IIb5, and Semiscale S-06-3) are considered.

The maximum clad temperatures of NEPTUN were measured at various locations of No. 3, 4, and 5 in general depending on experimental conditions. These locations correspond to 0.512 m, 0.744 m, and 0.976 m elevations from the bottom of the 1.68 m effective length. The two highest measurements from each NEPTUN test and their calculational correspondents are considered in this evaluation. Code assessment calculation against NEPTUN is described in Appendix C. In the case of FLECHT-SEASET, three data sets, one at a PCT location and two at neighboring measurement locations, are considered. Calculated temperatures are taken from the results given in Appendix C. Measurements of the FLECHT-SEASET experiments are concentrated at the central part of the core. Three elevations correspond to one or two nodes in the calculation.

In the case of ATLAS, the three highest measurements from each test and their correspondents are considered. ATLAS Tests 9 and 15 showed the three highest temperatures at 1.066 m, 1.271 m, and 1.329 m elevations from the bottom of the 1.905 m active core, while they were measured at 0.953 m, 1.066 m, and 1.329 m elevations in Test 11. Corresponding node numbers are 12, 14, and 15 for test 9 and 15, and 11, 12, and 15 for Test 11. Calculated values are taken from calculations in Appendix E. In the case of CCTF C2-4, the measured peak value at 2.44 m (96 in.) and its correspondent are considered. In the case of PKL-IIb5, the measured peak value at 2.5 m (98 in.) elevation and a comparable peak value at 1.95 m (77 in.), and their correspondents, are considered. In the case of Semiscale S-06-3, the measured peak value at 0.74 m (29 in.) and the neighboring measurement at 0.71 m (28 in.) are selected and compared with their calculational correspondents.

Figure 4-8 shows the reflood code accuracy evaluated using [ ]TS data sets. The code over-predicts the clad temperatures by [ ]TS.

4.3.2 Check Data Covering (Step 9.2)

Data covering is checked to confirm the variety, number, and ranges of code uncertainty parameters. If the code uncertainty is quantified using all the code uncertainty parameters in accordance with the bottom-up approach of NUREG-1230 [19], this checking process may not be necessary. In the top-down approach, however, it is necessary to confirm the number of uncertainty parameters with respect to the practicality of the method. Identification and ranking of the phenomena and subsequent selection of uncertainty parameters are dependent on the subjective decision of experts in the field. Accordingly, the objective basis of the determination of the number and the ranges of the parameters needs to be provided.

In principle, this covering check is performed for all the experiments considered in the code accuracy evaluation, especially for the cases where code predictions are lower than the measured peak values. A set of uncertainty parameters confirmed by this covering check can produce the uncertainty encompassing code accuracy.

Distribution-free statistics is utilized in this checking [23]. Let us choose the first row of the sample matrix, and arrange its elements in order of increasing magnitude, $y_1(1), y_1(2), \ldots y_1(N)$. Select from these $y_1(r_1)$ as L_1 and $y_1(s_1) > y_1(r_1)$ as U_1: Let $i_1, i_2, \ldots, i_{s_1-r_1-1}$ stand for the original column indices of elements $y_1(r_1+1), y_1(r_1+2), \ldots y_1(s_1-1)$: In the next step, choose the second row, the

N observed values of the output variable y_2 and arrange the part $y_{2i_1}, y_{2i_2}, \ldots y_{2_{s_1-r_1-1}}$ of its elements in increasing order to obtain $y_2(1) < y_2(2) < \cdots < y_2(s_1 - r_1 - 1)$. From among these, $y_2(r_2)$ and $y_2(s_2)$ are selected for L_2 and U_2 and evidently $r_2 \geq r_1, s_2 \leq s_1 - r_1 - 1$: We continue this imbedding procedure to the last row of the sample matrix and define a p-dimensional volume $V_p = \{|L_1, U_1, | \times |L_2, U_2| \times \ldots \times |L_p, U_p|\}$, where $L_j = y_j(r_j), U_j = y_j(s_j)$, and $r_j \geq r_{j-1} \geq \cdots \geq r_1$, while $r_j < s_j \leq s_{j-1} - r_{j-1} - 1, \ \forall j = 2 \ldots p$.

This page is replaced with page B.

Theorem.

In the case of p independent output variables with continuous joint density function $g(y_1, \ldots y_p)$, it is possible to construct p-pairs of random intervals $[L_j, U_j]_{j=1\ldots p}$ such that the probability of the inequality

$$\int_{L_1}^{U_1} \ldots \int_{L_p}^{U_p} g(y_1, \ldots y_p) dy_1 \ldots dy_p > \gamma$$

is free of g and is given by

$$Prob\left\{\int_{L_1}^{U_1} \ldots \int_{L_p}^{U_p} g(y_1, \ldots y_p) dy_1 \ldots dy_p > \gamma\right\} =$$

$$\beta = 1 - I(\gamma, s_p - r_p, N - s_p + r_p + 1) \quad (4\text{-}1)$$

Here,

$$s_p \leq s_{p-1} - r_{p-1} - 1 \leq s_1 - \sum_{j=1}^{p-1}(r_j + 1) \quad (4\text{-}2)$$

$$r_p \geq r_{p-1} \ldots \geq r_1 \quad (4\text{-}4)$$

Furthermore, if $r_1 = r_2 = \cdots = r_p = 0$ and $s_p = N - p + 1$, then one obtains the following one-sided confidence level.

$$\beta = 1 - I_\gamma(N - p + 1, p) = I_{1-\gamma}(p, N - p + 1) = \sum_{j=p}^{N} \binom{N}{j} (1 - \gamma)^j \gamma^{N-j}$$

$$= 1 - \sum_{j=0}^{p-1} \binom{N}{j} (1 - \gamma)^j \gamma^{N-j} \quad (4\text{-}4)$$

It is strongly recommended that the estimation of the upper limits should be higher than the first order with the following arguments [24].

When the upper tolerance limit approaches regulatory acceptance criteria, e.g. 1200°C PCT, the number of code runs may be increased to 150 or 200 calculations instead of the 59 code runs needed, using Wilks' formula at the first order for the estimation of a α = 95% one-sided tolerance limit with a confidence level β of 95%. This would be advisable for two reasons:

- With increasing sample size the uncertainty results will be less dispersed, and consequently more converged (less conservative), and
- The sensitivity results will be more reliable.

Firstly, for uncertainty analysis, it is possible to use Wilks' formula for example at the order 3 (124 runs) up to 5 (181 runs) for percentile α and confidence β unchanged, which may reduce the effect of conservatism of tolerance limits from a small number of code runs. The dispersion of the estimated tolerance limit in conservative direction tending to substantially overestimate the 95%-quantile one is originally interested in. On the other hand, the underestimation of the 95% percentile with 5% probability decreases when the order of Wilks' formula is increased.

Secondly the results of sensitivity analysis will become more reliable, particularly for less important parameters, because the variances of the estimators of the sensitivity measures will decrease and spurious (artificial) correlations between independent input parameters will appear less frequently when sample sizes increase. The issue of the number of code runs required for a proper sensitivity analysis is independent of that required by Wilks' formula. For example and unlike Wilks' formula, mainly for Regression Coefficients, the number of code runs should be (significantly) higher than the number of input parameters.

This page is replaced with page B.

TS

4.3.2.1 Check Blowdown Covering

Simple-random sampling (SRS) calculations were performed against the test data obtained from

B

CAREM uses the non-parametric order statistics to estimate the uncertainty propagation.

CAREM provides three values (i.e., peak cladding temperature, peak local oxidation, and core-wide hydrogen generation) for the comparison with the acceptance criteria of 10 CFR 50.46(b). As a results, there are three code output parameters of interest.

As described in reference [23], the equation used to determine the number of computer code runs needed for three parameters, assuming a one-sided tolerance interval is given below

$$\beta = \sum_{j=0}^{N-p} \binom{N}{j} \gamma^{j} \gamma^{N-j} \qquad (4\text{-}1)$$

where, β: confidence level

γ: probability

N: number of computer code runs

p: number of output parameters

For the case where p=3, and a 95 % probability and 95 % confidence level, the number of computer code runs (N) becomes 124. In this case, the extreme values (rank=1) are used as upper tolerance limits. However, the application of extreme values would cause following issues [24];

- The extreme values are subject to large variability.
- The sensitivity results will be less reliable.

Based on the above arguments, CAREM adopts p=5 instead of p=3 with 3rd order PCT, 1st order PLO, and 1st order CWO. Inserting p=5, γ=0.95, and β=0.95 to Equation 4-1 yields the necessary sample size which is 181.

Consequently, 3rd order value for PCT and 1st order values for CWO and PLO of 181 SRS calculations are chosen for licensing values in CAREM.

[18] American National Standard Decay Heat Power in Light Water Reactors, ANSI/ANS-5.1-1979.

[19] D. F. Ross et al., “Compendium of ECCS Research for Realistic LOCA Analysis,” USNRC, NUREG-1230, April 1987.

[23] Reliability Engineering and System Safety, Vol. 80, Issue 3, pp.217-232, June 2003.

[24] H. Glaser, "BEMUSE Phase VI Report, Status report on the area, classification of the method, conclusions and recommendations," NEA/CSNI/R(2011)4, March 2011.

RESPONSE TO AUDIT ISSUES

APR1400 Topical Reports

Korea Electric Power Corporation / Korea Hydro & Nuclear Power Co., LTD

Docket No. PROJ0782

Review Section	**TR Realistic Evaluation Methodology for LBLOCA of the APR1400**
Application Section	**Topical Report: APR1400-F-A-TR-12004 Realistic Evaluation Methodology for Large-Break LOCA of the APR1400**
Issue Date	**08/13/2015**

Audit Issues No. 52-a

The guidance in RG 1.157, Section 4 establishes acceptable controls for the estimation of uncertainties. In addition, NUREG/CR-5249 describes the process for formulation of uncertainty distributions. Address the following questions about the statistical treatment of uncertainties in CAREM:

a. RG 1.157 states that “the methodology used to obtain an estimate of the overall calculation uncertainty at the 95 percent probability limit should be provided and justified.” Provide the justification for the use of the distribution free statistical approach.

Response

See the response for Audit issue no. 51.a.

Impact on DCD

There is no impact on the DCD.

Impact on PRA

There is no impact on the PRA.

Impact on Technical Specifications

There is no impact on the Technical Specifications.

Impact on Technical/Topical/Environmental Report

There is no impact on any Technical, Topical, or Environmental Report.

RESPONSE TO AUDIT ISSUES

APR1400 Topical Reports

Korea Electric Power Corporation / Korea Hydro & Nuclear Power Co., LTD

Docket No. PROJ0782

Review Section	**TR Realistic Evaluation Methodology for LBLOCA of the APR1400**
Application Section	**Topical Report: APR1400-F-A-TR-12004 Realistic Evaluation Methodology for Large-Break LOCA of the APR1400**
Issue Date	**08/13/2015**

Audit Issues No. 52

The guidance in RG 1.157, Section 4 establishes acceptable controls for the estimation of uncertainties. In addition, NUREG/CR-5249 describes the process for formulation of uncertainty distributions. Address the following questions about the statistical treatment of uncertainties in CAREM.

b. The example of the process shown in NUREG/CR-5249 indicates that mean value of the effect for each of the uncertainties on the blowdown and reflood portions is calculated. The sum of all the 95th percentiles relative to the mean are added to obtain the summed biases. The summed biases are then added to 95th percentile of the response surface produced from the calculation of the mean peak cladding temperatures from the uncertainty of high influence parameters. Table 5-4 through 5-7 of the topical report provide the determination of the biases for application in the CAREM process. Describe how the CAREM process provides the 95th percentile for the bias determination.

c. RG 1.157 indicates that the uncertainty can vary over time during the transient, and states that “In evaluating the code uncertainty, it will be necessary to evaluate the code’s predictive ability over several time intervals, since different processes and phenomena occur at different intervals. For example, in large-break loss-of-coolant accident evaluations, separate code uncertainties may be required for the peak cladding temperature during the blowdown and post-blowdown periods. Justification for treating these uncertainties individually or methods for combining them should be provided.” It is not clear how the temporal differences in the bias and uncertainty are treated in the CAREM methodology. Provide the basis and the process for determination and application of the bias and uncertainty during the blowdown and reflood (early and late) periods.

Response

b)

Although the bias evaluation in NUREG/CR-5249 seems to provide 95th percentile for the bias determination, only the bias related with hot channel could give the 95th percentile consideration. In CAREM, almost the same approaches as NUREG/CR-5249 are used for the estimation of biases. The biases in CAREM are evaluated from [ ]TS. The thermal-hydraulic conditions that can affect the PCT are observed and evaluated in the assessment of [ ]TS. The evaluated bias is considered as shown in Table 5-4 through 5-7 for practically all of the SRS cases. For example, [ ]TS. Here, 95th percentile of the bias does not need to be evaluated in CAREM, because the bias is considered for practically all of the SRS cases. Thus, the maximum biases neglecting the minus biases are considered for the final scaled bias evaluation for conservatism.

c)

The temporal differences in the biases are treated depending on the importance rankings defined in APR1400 PIRT. If one bias is considered to be important for certain period, the bias is only activated for that time period.

[

]TS

All of the biases need not consider the uncertainties due to the application of the biases estimated. The estimated biases from test assessment are applied for practically all of the SRS cases, thus the most conservative estimation of biases are obtained as the result of the final bias evaluation. In conclusion, the conservative approaches to apply biases are employed in CAREM.

Impact on DCD

There is no impact on the DCD.

Impact on PRA

There is no impact on the PRA.

Impact on Technical Specifications

There is no impact on the Technical Specifications.

Impact on Technical/Topical/Environmental Report

There is no impact on any Technical, Topical, or Environmental Report.

RESPONSE TO AUDIT ISSUES

APR1400 Topical Reports

Korea Electric Power Corporation / Korea Hydro & Nuclear Power Co., LTD

Docket No. PROJ0782

Review Section	**TR Realistic Evaluation Methodology for LBLOCA of the APR1400**
Application Section	**Topical Report: APR1400-F-A-TR-12004 Realistic Evaluation Methodology for Large-Break LOCA of the APR1400**
Issue Date	**08/13/2015**

Audit Issues No. 53-a

The guidance in RG 1.157, Section 4.3.1 establishes acceptable controls for the utilization of conservative parameters in best estimate analysis. Provide the following details:

a. Explain the determination of the radial peaking factor (Fr) for [ ]^{TS} in the LBLOCA analysis.

Response (Rev. 1)

Radial peaking factor (Fr) for [ ]TS was determined based on nuclear design data for APR1400. The most limiting Fr at [

]TS

[

]TS

Impact on DCD

There is no impact on the DCD.

Impact on PRA

There is no impact on the PRA.

Impact on Technical Specifications

There is no impact on the Technical Specifications.

Impact on Technical/Topical/Environmental Report

There is no impact on any Technical, Topical, or Environmental Report.

RESPONSE TO AUDIT ISSUES

APR1400 Topical Reports

Korea Electric Power Corporation / Korea Hydro & Nuclear Power Co., LTD

Docket No. PROJ0782

Review Section	**TR Realistic Evaluation Methodology for LBLOCA of the APR1400**
Application Section	**Topical Report: APR1400-F-A-TR-12004 Realistic Evaluation Methodology for Large-Break LOCA of the APR1400**
Issue Date	**08/13/2015**

Audit Issues No. 53-b

The guidance in RG 1.157, Section 4.3.1 establishes acceptable controls for the utilization of conservative parameters in best estimate analysis. Provide the following details:

b. Describe how the power shape and peaking factor (Fq) were determined for the base case calculation.

Response (Rev. 1)

Power Peaking Factor

The range of Fq variation for [ ]TS as shown in Figure 1. The variation is for the initial core of the SKN 3 and 4. However, the maximum of [ ]TS the linear heat generation rate (LHGR) limit of the technical specifications.

[

]TS

Power Shape

The procedure of determining the power shape is described in Section 5.1.1 of the topical report.

TS

TS

Therefore, the power shape of the base case calculation made in accordance with the above procedure is shown in Figure 7.

TS

Figure 1. [ ]TS

TS

Figure 2. [ ]TS

TS

Figure 3. [

]TS

TS

Figure 4. [ ]TS

TS

Figure 5. [ ]TS

TS

Figure 6. [ ]TS

TS

Figure 7. [ ]TS

Impact on DCD

There is no impact on the DCD.

Impact on PRA

There is no impact on the PRA.

Impact on Technical Specifications

There is no impact on the Technical Specifications.

Impact on Technical/Topical/Environmental Report

There is no impact on any Technical, Topical, or Environmental Report.

RESPONSE TO AUDIT ISSUES

APR1400 Topical Reports

Korea Electric Power Corporation / Korea Hydro & Nuclear Power Co., LTD

Docket No. PROJ0782

Review Section	**TR Realistic Evaluation Methodology for LBLOCA of the APR1400**
Application Section	**Topical Report: APR1400-F-A-TR-12004 Realistic Evaluation Methodology for Large-Break LOCA of the APR1400**
Issue Date	**08/13/2015**

Audit Issues No. 54

The guidance in RG 1.157, Section 4.3.1 establishes acceptable controls for the utilization of conservative parameters in best estimate analysis. [

]^{TS} Explain how this will be applied for operational cycles to ensure adequate conservatism.

Response

The variation of peaking factors at the limiting burn-up (BOC) of initial core is as follows;

- [ ]TS
- [ ]TS

[

]TS

The maximum of peaking factors at the equilibrium cycles is as follows;

- [ ]TS
- [ ]TS

[

]TS

Radial peaking factor uncertainty of hot pin is assumed as 4 %, which is the value used in nuclear design. Radial peaking factor uncertainty of hot assembly is introduced to cover the cycle-wise variation, and it is calculated as 12 %.

Impact on DCD

There is no impact on the DCD.

Impact on PRA

There is no impact on the PRA.

Impact on Technical Specifications

There is no impact on the Technical Specifications.

Impact on Technical/Topical/Environmental Report

Topical report will be revised to modify typo described in this response.

There is no impact on Technical and Environmental Report.

[

,°-

+

]°-

Hot Assem/ ly Po0 er

[

,°-

[

,°-

Hot Pin Power Peaking Fa3tor

+

,°-

° he technic l speci53 tions of the S# 6 and 4 pres31/ e the LHGR li. it as one o5the limiting 3onditions 5or operation. ° he LHGR limit is defined as the product o5Fq and the 3ore ! erage LHGR. ° he average L$7 R at rated power is 5.:˙ 2 k) ;ft. The Fq co11esponding to the L$7 R limit 16": 2) ;51 is 2.428 (i"e., ˇ6": kW;51 di! ided by * ":˙ 2 k) ;51>. Therefore the range of Fq is extended to the limit o5the technic l speci53 tion o5˜" ˆ˜ 8. ° he dist1i/ 8tion 5unction of ˛ q is 3onservatively ass8. ed to be uni5o1. .

- ˇ 1 . eter; hot pin power peaking factor (Fq)

  Distribution 5unction; uni5orm

  Mean value; ˜"ˇ< ˆ

  Mini.8 m ! l8e@"Aˆ ˙

  M ?i.8 m ! l8e@"ˆ ˜ <

*"ˇ"˜ Reactivity ˛ eed/ 3 2 Related P 1 . eters

Boid Reactivity

° he negative reactivity of the moderator rapidly reduces reactor power during the t1ansient. Because the RELAˇ*; MO&6"6;K models the moderator density 1e 3 tivity whi3h corresponds to the ! oid reacti! ity, it is necessa1y to treat the uncertainty of the moderator density reactivity. ° he . oderator density reactivity is dependent on the moderator temperature coe55icients (MTC>@M° C in! olves ! 1ious core 4 1 . eters. ° his means that there is no one code p 1 . eter that 3haracteri3es the moderator density reactivity. ° herefore, the uncertainty of the moderator density reactivity is treated conservatively. The core design provides two conservative moderator density reactivity curves for the LOCA analysis as shown in Figure 4-4. [

RESPONSE TO AUDIT ISSUES

APR1400 Topical Reports

Korea Electric Power Corporation / Korea Hydro & Nuclear Power Co., LTD

Docket No. PROJ0782

Review Section	**TR Realistic Evaluation Methodology for LBLOCA of the APR1400**
Application Section	**Topical Report: APR1400-F-A-TR-12004 Realistic Evaluation Methodology for Large-Break LOCA of the APR1400**
Issue Date	**08/13/2015**

Audit Issues No. 55

The guidance in RG 1.157, Section 4.3.1 establishes acceptable controls for the utilization of conservative parameters in best estimate analysis. The guidance in RG 1.157, Section 4 establishes acceptable controls for the estimation of calculational uncertainty. Section 5.1.2 of the topical report discusses the reactivity feedback related parameters and the corresponding uncertainty. There is no discussion of the fuel temperature reactivity and its uncertainty. Explain whether the Doppler reactivity contribution is considered in the model input. If so, provide and justify the values used and the corresponding uncertainty.

Response

The PIRT for a LBLOCA of APR1400 was developed based on the LBLOCA PIRT for KNGR. Those phenomena whose importance rankings are higher than equal to [4]^{TS} in any temporal period are counted among the phenomena or processes of KNGR PIRT. The APR1400 PIRT is discussed in Table 5 of Appendix A. [

]^{TS}.

However, the Doppler reactivity is used as RELAP5 input. In RELAP5, one or more pairs of numbers are entered to define Doppler reactivity as a function of volume average fuel temperature.

[

]^{TS}

To simulate the non-linear feedback, the Doppler temperature coefficient (DTC) is defined as the following input.

W1(R) Temperature (K)

W2(R) Reactivity (Dollars = $\Delta\rho/\beta_{eff}$)

[

]TS

Table 1. Reactivity vs. Fuel Temperature for APR1400 (SKN3/4) Cycle 1
(Corresponding to Least Negative Doppler Coefficient)

TS

Table 2. Reactivity vs. Fuel Temperature for APR1400 (SKN3/4) Cycle 1
(Corresponding to Most Negative Doppler Coefficient)

TS

Table 3. Doppler Reactivity Table Used in Plant Calculation TS

References

[1] 3L186-NE-DD012, Rev. 01, “Design Data for Safety Analysis for SHINKORI Nuclear Units 3&4,” 2009. 6. 29.

Impact on DCD

There is no impact on the DCD.

Impact on PRA

There is no impact on the PRA.

Impact on Technical Specifications

There is no impact on the Technical Specifications.

Impact on Technical/Topical/Environmental Report

There is no impact on any Technical, Topical, or Environmental Report.

RESPONSE TO AUDIT ISSUES

APR1400 Topical Reports

Korea Electric Power Corporation / Korea Hydro & Nuclear Power Co., LTD

Docket No. PROJ0782

Review Section	**TR Realistic Evaluation Methodology for LBLOCA of the APR1400**
Application Section	**Topical Report: APR1400-F-A-TR-12004 Realistic Evaluation Methodology for Large-Break LOCA of the APR1400**
Issue Date	**08/13/2015**

Audit Issues No. 56-a, b and c

The guidance in RG 1.157, Section 3.3 establishes acceptable controls for the determination of thermal/physical parameters. Section 5.1.3 of the topical report provides details of indirectly capturing the [ ]TS Address the following:

a. Section 5.1.3 states that [ ]TS Although this is technically reasonable, justification has not been provided for the selected range of [ ]TS Demonstrate the selected range of [ ]TS is either related to gap temperatures of interest based on burn-up and operational cycle or to available data.

b. The mean value and the [ ]TS are determined using a fuel performance code that is not referenced. The fuel performance analysis code may have its own effect on the uncertainty in [ ]TS Provide details of the uncertainty in the calculation of [ ]TS in the fuel performance analysis code, and describe how any such uncertainty is accounted for.

c. Provide the actual values of the [ ]TS that are determined and are used in the analysis.

Response (Rev. 1)

a) ~ c)

As described in the topical report, initial fuel rod conditions from the fuel performance analysis code (FATES3B) are reflected to RELAP5. And LBLOCA analysis with TCD will not treat [ ]TS

Fuel average temperatures including centerline temperatures will be modeled by [ ]TS And calculated fuel average and centerline temperatures will be confirmed with fuel performance analysis code (FATES3B) results which are [ ]TS The limiting burnup for average rod is selected as average burnup of [ ]TS, and burnup for hot pin and hot assembly will be selected based on the burnup sensitivity results.

Impact on DCD

There is no impact on the DCD.

Impact on PRA

There is no impact on the PRA.

Impact on Technical Specifications

There is no impact on the Technical Specifications.

Impact on Technical/Topical/Environmental Report

Topical report will be changed to consider TCD effects. Additional technical report for TCD consideration will be released.

There is no impact on Environmental Report.

RESPONSE TO AUDIT ISSUES

APR1400 Topical Reports

Korea Electric Power Corporation / Korea Hydro & Nuclear Power Co., LTD

Docket No. PROJ0782

Review Section	**TR Realistic Evaluation Methodology for LBLOCA of the APR1400**
Application Section	**Topical Report: APR1400-F-A-TR-12004 Realistic Evaluation Methodology for Large-Break LOCA of the APR1400**
Issue Date	**08/13/2015**

Audit Issues No. 56-d

The guidance in RG 1.157, Section 3.3 establishes acceptable controls for the determination of thermal/physical parameters. Section 5.1.3 of the topical report provides details of indirectly capturing the range of [ ]TS Address the following:

d. The current [ ]TS in Section 5.1.3 is inconsistent with the current [ ]TS in Table 5-1. Address this inconsistency.

Response (Rev. 1)

The [ ]TS However, [ ]TS

Impact on DCD

There is no impact on the DCD.

Impact on PRA

There is no impact on the PRA.

Impact on Technical Specifications

There is no impact on the Technical Specifications.

Impact on Technical/Topical/Environmental Report

Topical report will be revised to consider TCD effects. Additional technical report for TCD consideration will be released.

There is no impact on Environmental Report.

RESPONSE TO AUDIT ISSUES

APR1400 Topical Reports

Korea Electric Power Corporation / Korea Hydro & Nuclear Power Co., LTD

Docket No. PROJ0782

Review Section	**TR Realistic Evaluation Methodology for LBLOCA of the APR1400**
Application Section	**Topical Report: APR1400-F-A-TR-12004 Realistic Evaluation Methodology for Large-Break LOCA of the APR1400**
Issue Date	**08/13/2015**

Audit Issues No. 57

The guidance in RG 1.157, Section 4 establishes acceptable controls for the estimation of uncertainties. Address the following regarding the pump degradation multiplier uncertainty in Section 5.1.4:

a. Explain and justify the pump degradation multiplier uncertainty.

b. The minimum (and therefore, the mean) value of the head and torque degradation multiplier provided in Section 5.1.4 is different from that listed in Table 5-1. In addition, the range of pump resistance in Table 5-1 and Appendix J (page J-2) is also inconsistent. Address these inconsistencies.

c. [

]^{TS} Explain:

i. The inconsistency between the mean of zero and the lower and upper bounds of the uniform distribution.

ii. The application of the distribution provided in the topical report for the pump degradation multiplier.

Response

a)

Pump degradation multiplier is used to model a pump performance for 2-phase flow and it is divided into the 2-phase head multiplier and 2-phase torque multiplier as follows.

$$H = H_{1\phi} - M_H\left(\alpha_g\right)\left(H_{1\phi} - H_{2\phi}\right) \qquad \text{Eq. (1)}$$

$$\tau = \tau_{1\phi} - M_\tau\left(\alpha_g\right)\left(\tau_{1\phi} - \tau_{2\phi}\right) \qquad \text{Eq. (2)}$$

where,

H = the total pump head

$H_{1\phi}$ = the single-phase pump head

$H_{2\phi}$ = the fully degraded pump head

M_H = the head degradation multiplier (or the 2-phase head multiplier)

$\tau_{1\phi}$ = the single-phase pump torque

$\tau_{2\phi}$ = the fully degraded pump torque

M_τ = the torque degradation multiplier (or the 2-phase torque multiplier)

α_g = the vapor fraction

Pump degradation is expressed via two-phase multiplier curves. And pump degradation multiplier uncertainty ranges were determined based on the following findings of reference [11].

1) Figure 1 shows the variations of two phase head multiplier of CE pump by system pressure as shown in Figure 3.IV-9 of reference [11] in the topical report. In this figure, it can be found that two phase head multiplier widely varies by system pressure at the same void fraction.

2) Figure 2 shows two phase head multiplier variations of WEC 93A pump which is evaluated by SECY-83-472 method. In this figure, two phase head multiplier could have from 0.1 ~ 1.0 for almost of all void fraction ranges.

3) Table 1 shows standard deviations of two phase head multiplier presented in CSAU. The maximum standard deviation of two phase head multiplier is 0.319.

Based on the above findings, it was concluded that pump two head multiplier has uncertainty ranges from 0.0 to 1.0 in reference [11]. This range means that pump two head multiplier can

cover from fully degraded pump head to single phase pump head. Uniform distribution is assumed because experimental data are insufficient to quantify their uncertainties. Also, two phase torque multiplier is assumed to have the same behavior with two phase head multiplier because head and torque multipliers are applied using the same form of equation. Consequently, following uncertainties for the pump degradation multipliers were determined.

- Parameter: pump two-phase head multiplier

[

]TS

- Parameter: pump two-phase torque multiplier

[

]TS

b)

Those are typing errors in which the mean and the minimum values are swapped each other. Therefore the topical report will be corrected as follows.

- Parameter: pump two-phase degradation multiplier

[

]TS

The values of pump resistance in Appendix J (page 2) are also incorrect. Therefore those will be corrected into the minimum and maximum values in Table 5-1 of the topical report as follows.

- Parameter: pump resistance (or pump K-factor)

[

]TS

However, the correct pump degradation and resistance uncertainty ranges are used in the plant SRS calculations in Appendix J of the topical report.

c-i)

See response to audit issue number 57-b.

c-ii)

As previously mentioned in the response to audit issue number 57-b, the mean and the minimum values are swapped each other. However, the plant SRS calculations of the topical report used the correct pump degradation uncertainty ranges.

Table 1. The Uncertainty of Pump Two Phase Head Multiplier in the CSAU

TS

TS

Figure 1. Two Phase Head Multiplier Variations of CE Pump by System Pressure

TS

Figure 2. Two Phase Head Multiplier Variation of WEC 93A Pump by Void Fraction

Impact on DCD

There is no impact on the DCD.

Impact on PRA

There is no impact on the PRA.

Impact on Technical Specifications

There is no impact on the Technical Specifications.

Impact on Technical/Topical/Environmental Report

Topical report will be revised as discussed in this response.

There is no impact on Technical or Environmental Report.

+ ultiplier val, es are relati! ely lo/ er at low void f.actions; the other is for such pu+ - s such as the ' W -, + - , CREARE ai.3water pump, Semis1 le p,+ - , and the p,+ p used 0or CE e! luation + odel, of / hich he d multiplier ! lues - proach nearly ˇ" 0 above the 30 % void f.action. Sensitivity studies were performed using the Byron-Jackson and the Semiscale pump data. These data are the representative pump data of each pump group. [

;˚4 . [

KKKKKKK;˚4KKKKKKKKK

- ˇ . + eter; pump two-phase degradation multi- lier

:

;˚4

"ˇ" 4 0ety Injection 4ystem Related ˇ . + eters

ˇ . + eters associated with the safety injection system 1an be divided into 4<° parameters and S<ˇ - . + eters. S<° parameters include water ! olume, water temperature, and nitrogen gas pressure. 4<ˇ - . + eters include IR) 4T w ter te+ - e.ature and injection 0o/ rate.

[

;˚4

- Parameter; [

;˚4

- Parameter; [

;˚4

- Parameter; [

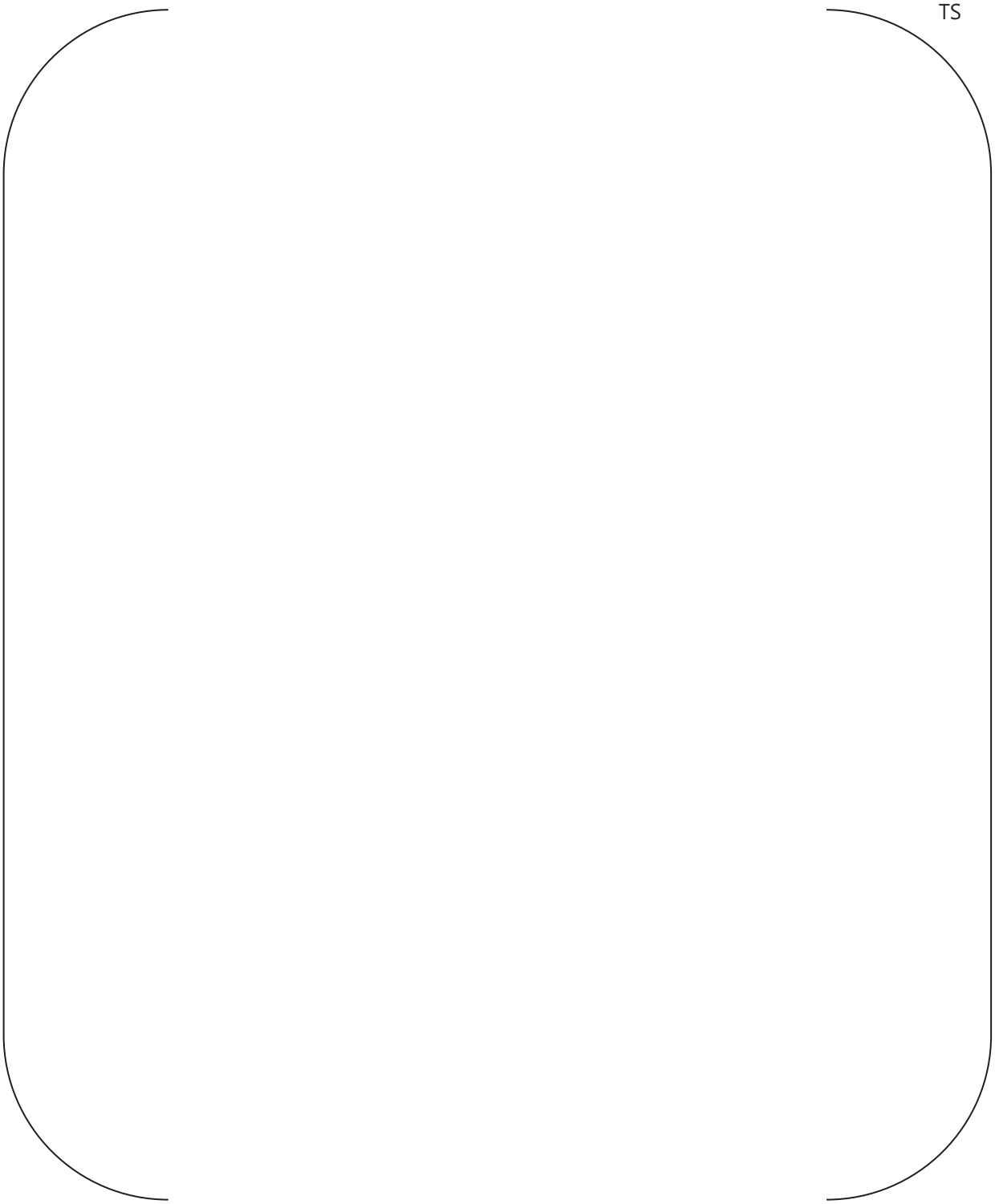
TS

RESPONSE TO AUDIT ISSUES

APR1400 Topical Reports

Korea Electric Power Corporation / Korea Hydro & Nuclear Power Co., LTD

Docket No. PROJ0782

Review Section	**TR Realistic Evaluation Methodology for LBLOCA of the APR1400**
Application Section	**Topical Report: APR1400-F-A-TR-12004 Realistic Evaluation Methodology for Large-Break LOCA of the APR1400**
Issue Date	**08/13/2015**

Audit Issues No. 58

The guidance in RG 1.157, Section 3.8 establishes acceptable controls for the calculation of critical heat flux. [ ]TS It is unclear what the minimum value means since it is expected that the “dial” implies a multiplier. The distribution encompasses a value of 0.0 and the implication of that value is also unclear. [

]TS

Response

In CAREM, 1.96 times standard deviation is required to cover 95 % of the uncertainty parameter range for normal distribution. In the SRS calculation, however, 3.09 times the standard deviation is used to cover 99.9 % of normal distribution for conservatism. [ ]TS

Calculated CHF is used to determine heat transfer mode whether it is post CHF or pre CHF. Thus, minus value of CHF results in determination of post CHF heat transfer mode. Since post CHF heat transfer mode predicts low heat transfer coefficient, it can be expected that minus value of CHF multiplier increases cladding temperature.

[ ]TS

However, minus value of CHF multiplier has no physical meaning. Therefore, it should be limited by certain low value. In this methodology, zero value is determined as lower limit of CHF multiplier. All SRS results for experiments and APR1400 in topical report will be revised.

TS

Figure 1. Cladding Temperatures for Various CHF Multipliers

Impact on DCD

There is no impact on the DCD.

Impact on PRA

There is no impact on the PRA.

Impact on Technical Specifications

There is no impact on the Technical Specifications.

Impact on Technical/Topical/Environmental Report

Topical report will be revised as discussed above.

There is no impact on Technical or Environmental Report.

Table 5-1 Distributions and Ranges of the Uncertainty Parameters

TS

RESPONSE TO AUDIT ISSUES

APR1400 Topical Reports

Korea Electric Power Corporation / Korea Hydro & Nuclear Power Co., LTD

Docket No. PROJ0782

Review Section	**TR Realistic Evaluation Methodology for LBLOCA of the APR1400**
Application Section	**Topical Report: APR1400-F-A-TR-12004 Realistic Evaluation Methodology for Large-Break LOCA of the APR1400**
Issue Date	**08/13/2015**

Audit Issues No. 59

The guidance in RG 1.157, Section 4.3.1 establishes acceptable controls for the utilization of conservative parameters in best estimate analysis. Table 5-2 lists some of the containment parameters used in the APR1400 RELAP5/MOD3.3/K calculation. Provide the basis for the containment parameters and any other assumptions used in the analysis regarding the passive heat sinks and the activation and operation of containment sprays.

Response

Table 1 shows major containment parameters used in the LBLOCA analysis of APR1400.

[

]TS

Table 1. Major Input Parameters for Containment

TS

Table 2. Uchida Heat Transfer Coefficients (h_{Uchida})

TS

Impact on DCD

There is no impact on the DCD.

Impact on PRA

There is no impact on the PRA.

Impact on Technical Specifications

There is no impact on the Technical Specifications.

Impact on Technical/Topical/Environmental Report

There is no impact on any Technical, Topical, or Environmental Report.

RESPONSE TO AUDIT ISSUES

APR1400 Topical Reports

Korea Electric Power Corporation / Korea Hydro & Nuclear Power Co., LTD

Docket No. PROJ0782

Review Section	**TR Realistic Evaluation Methodology for LBLOCA of the APR1400**
Application Section	**Topical Report: APR1400-F-A-TR-12004 Realistic Evaluation Methodology for Large-Break LOCA of the APR1400**
Issue Date	**08/13/2015**

Audit Issues No. 60

RG 1.157 guidance expresses in many places that results from best estimate calculations will be considered acceptable provided their technical basis is demonstrated with appropriate data and analyses. However, some of the results provided in the topical report are unclear. Figures 5-12 to 5-25 provide some transient information for the base case calculation. In order to understand the details of the base case transient, provide the following additional transient information:

a. Break mass flow rate from 25 to 125 seconds

b. Downcomer void fractions for the control volumes in [ ]^{TS}

c. [ ]^{TS} inlet liquid mass flow rate from 30 to 130 seconds

d. [ ]^{TS} inlet vapor mass flow rate from 30 to 130 seconds

e. [ ]^{TS} inlet liquid mass flow rate from 175 to 225 seconds

f. [ ]^{TS} inlet vapor mass flow rate from 175 to 225 seconds

g. [ ]^{TS} inlet liquid mass flow rate from 30 to 130 seconds

h. [ ]^{TS} inlet vapor mass flow rate from 30 to 130 seconds

i. [ ]^{TS} inlet liquid mass flow rate from 175 to 225 seconds

j. [ ]^{TS} inlet vapor mass flow rate from 175 to 225 seconds

k. [ ]^{TS} outlet liquid and vapor flow

l. [ ]^{TS} outlet liquid and vapor flow

m. Downcomer flow below the cold leg [ ]^{TS}

n. Void fraction in the upper plenum

Response

Figure 1 shows break mass flow rate from 25 to 125 seconds (in response to item a).

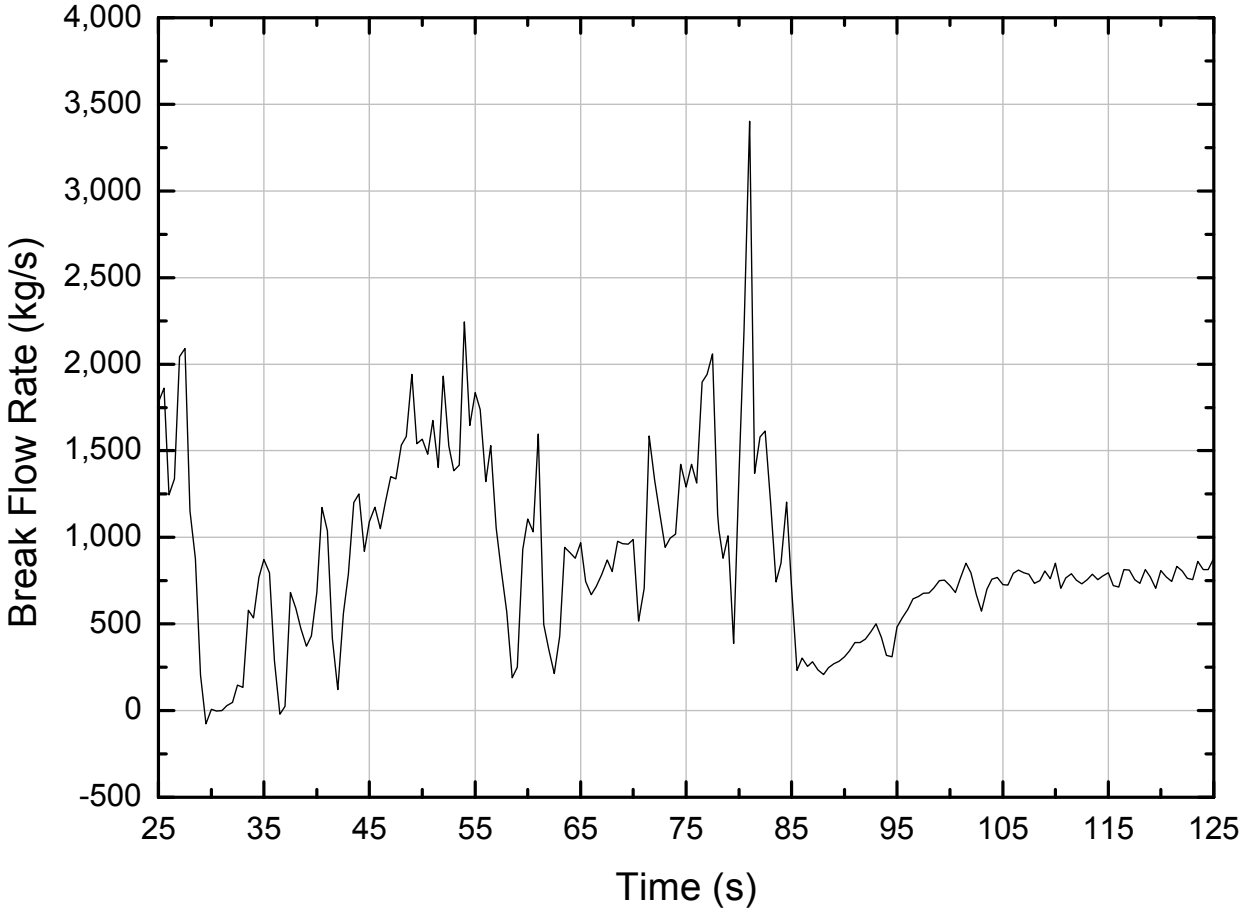

Figure 1. Total Break Mass Flow Rate

The nodalization of downcomer is composed of [

]TS

TS

Figure 2. RELAP5 Nodalization of the Reactor Vessel

TS

Figure 3. [ ]TS

TS

Figure 4. [ ]TS

TS

Figure 5. [ ]TS

TS

Figure 6. [ ]TS

TS

Figure 7. [ ]TS

TS

Figure 8. [ ]TS

Figure 9 shows [ ]TS inlet liquid mass flow rate from 30 to 130 seconds (in response to item c).

TS

Figure 9. [ ]TS

Figure 10 shows [ ]TS inlet vapor mass flow rate from 30 to 130 seconds (in response to item d).

TS

Figure 10. [ ]TS

Figure 11 shows [ ]TS inlet liquid mass flow rate from 175 to 225 seconds (in response to item e).

TS

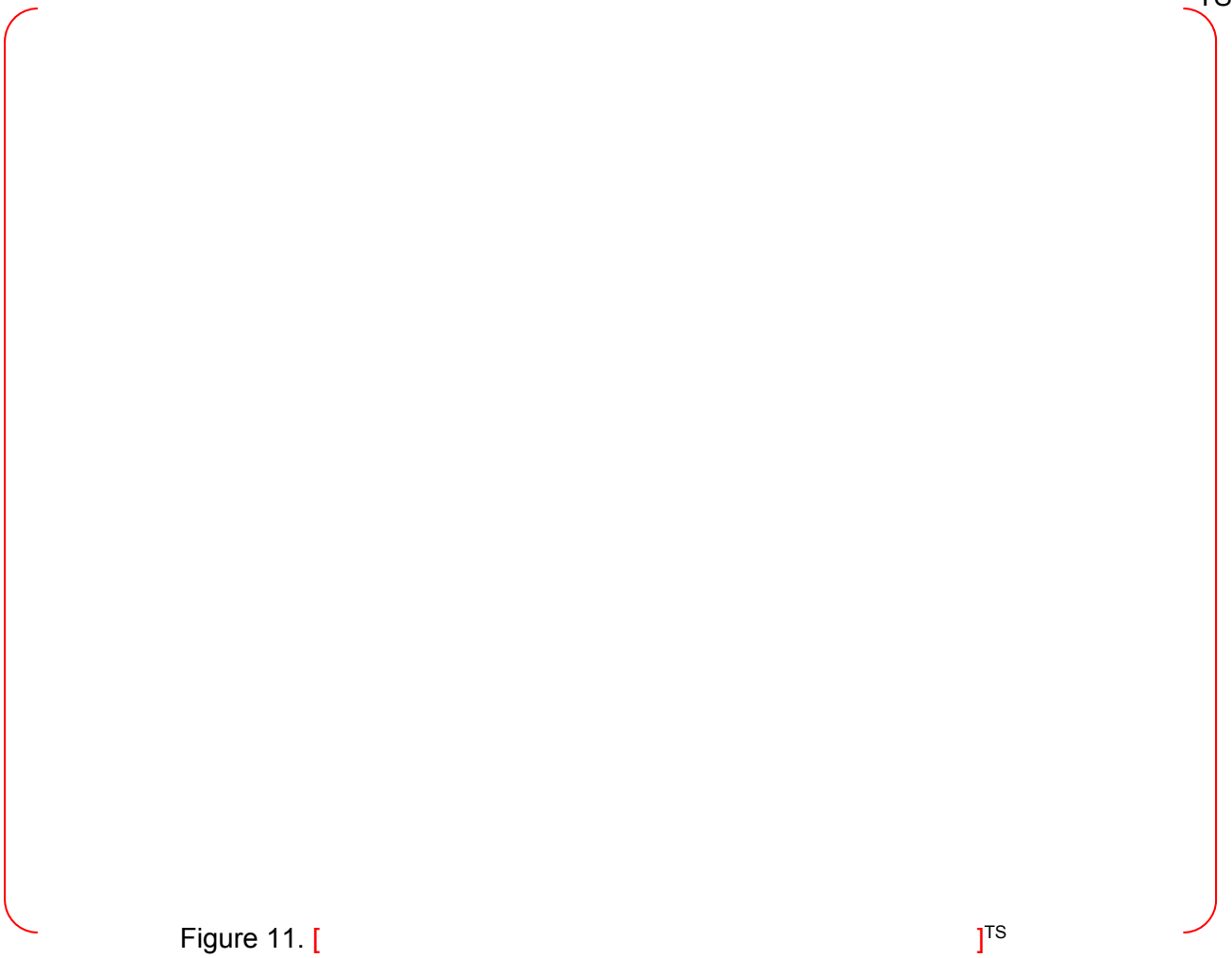

Figure 11. [ ]TS

Figure 12 shows [ ]TS inlet vapor mass flow rate from 175 to 225 seconds. The vapor flow rate from 175 to 225 seconds is almost zero (in response to item f).

TS

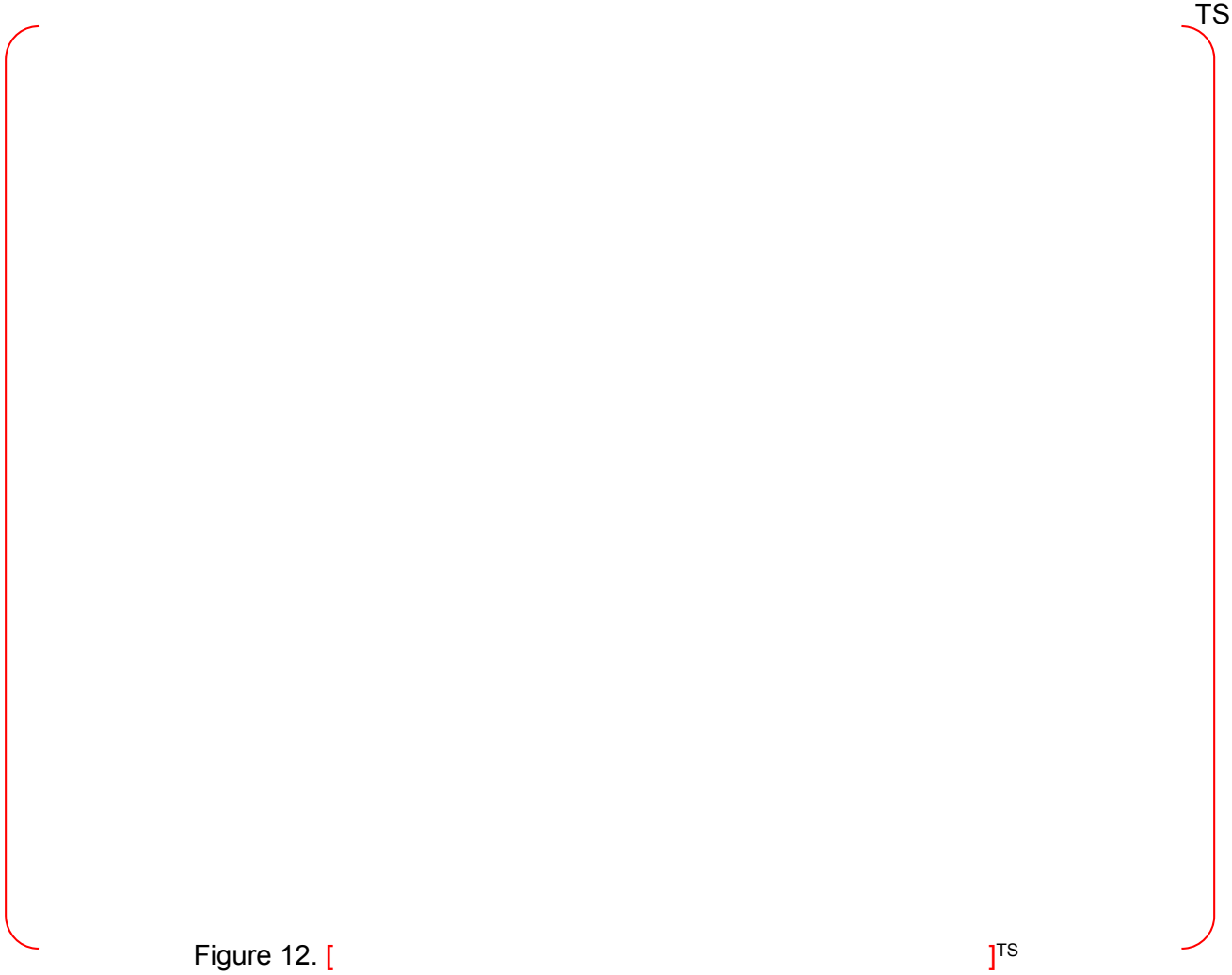

Figure 12. [ ]TS

Figure13 shows [ ]TS inlet liquid mass flow rate from 30 to 130 seconds (in response to item g).

TS

Figure 13. [ ]TS

Figure 14 shows [ ]TS inlet vapor mass flow rate from 30 to 130 seconds (in response to item h).

TS

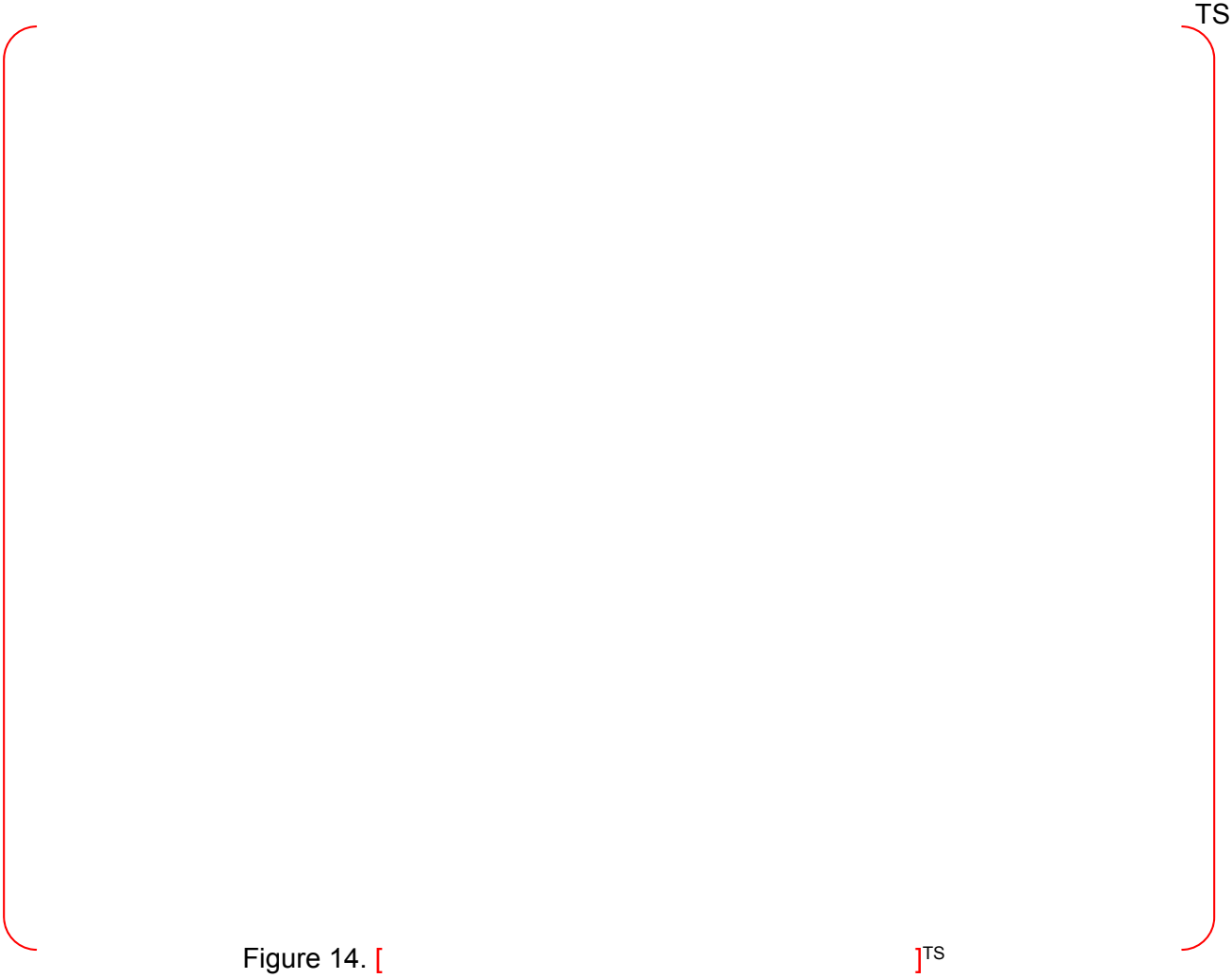

Figure 14. [ ]TS

Figure 15 shows [ ]TS inlet liquid mass flow rate from 175 to 225 seconds (in response to item i).

TS

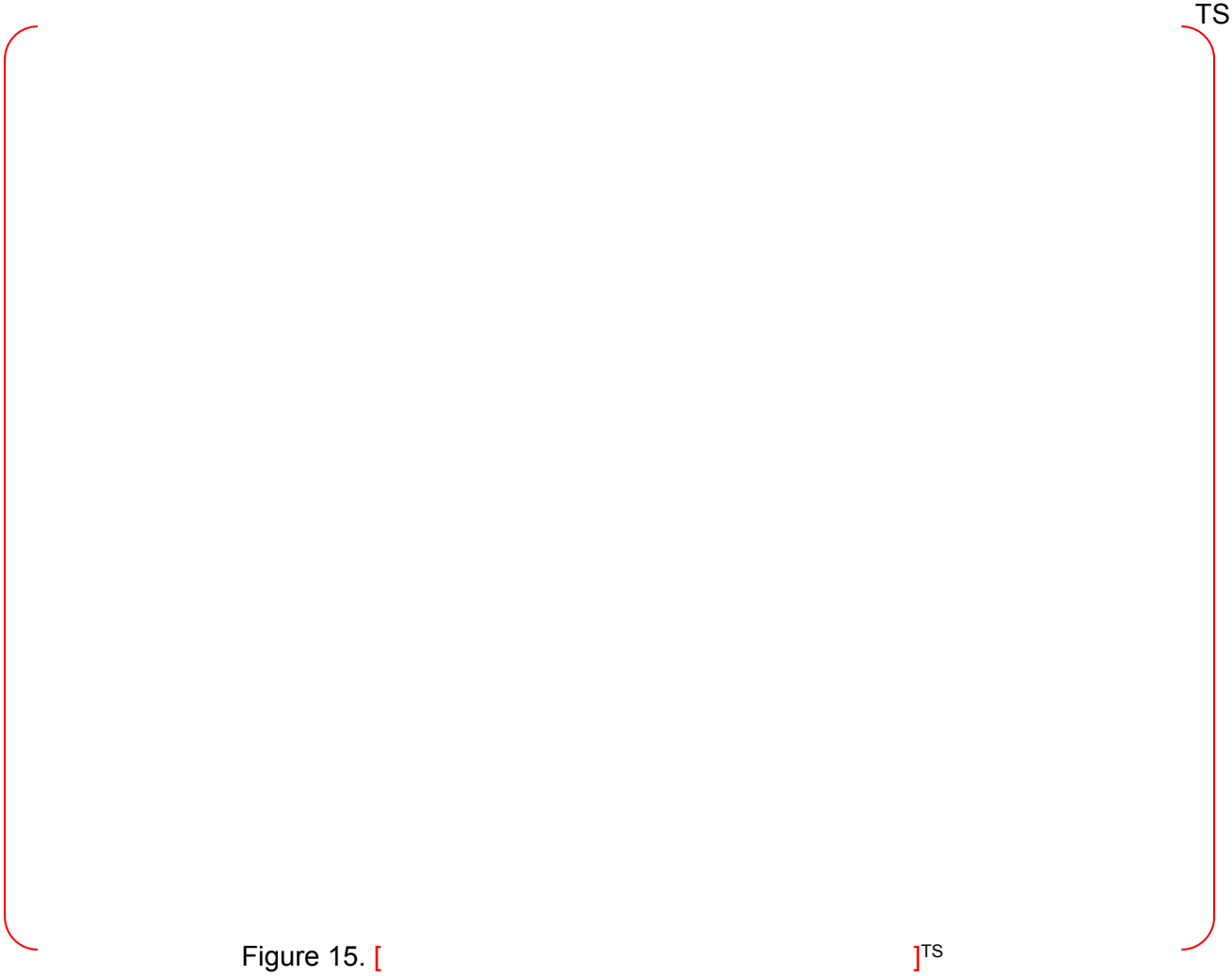

Figure 15. [ ]TS

Figure 16 shows [ ]TS inlet vapor mass flow rate from 175 to 225 seconds. The vapor flow rate from 175 to 225 seconds is almost zero (in response to item j).

TS

Figure 16. [ ]TS

Figure 17 and Figure 18 show [ ]TS outlet liquid and vapor flow rate respectively (in response to item k).

TS

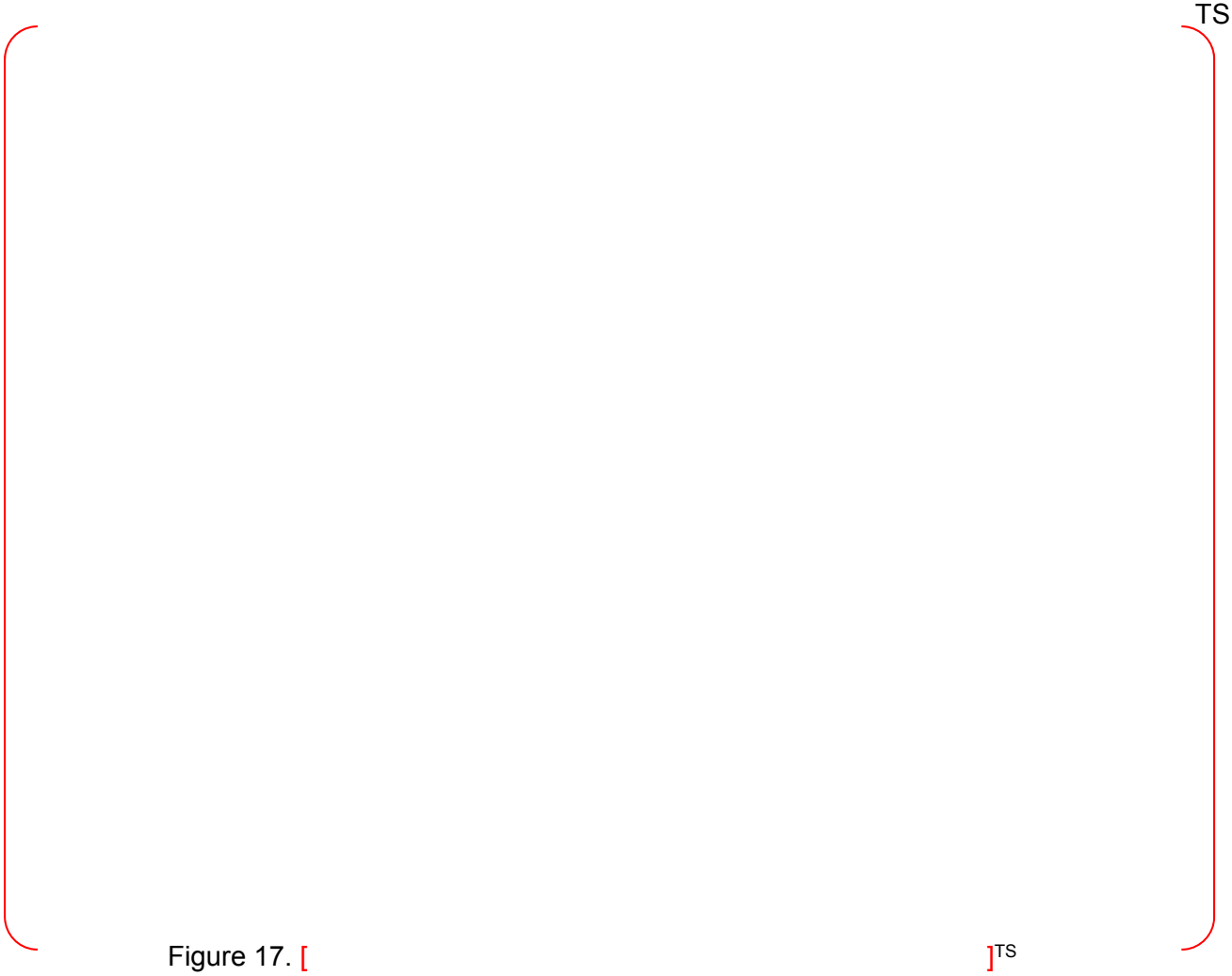

Figure 17. [ ]TS

TS

Figure 18. [ ]TS

Figure 19 and Figure 20 show [ ]TS outlet liquid and vapor flow rate respectively (in response to item l).

TS

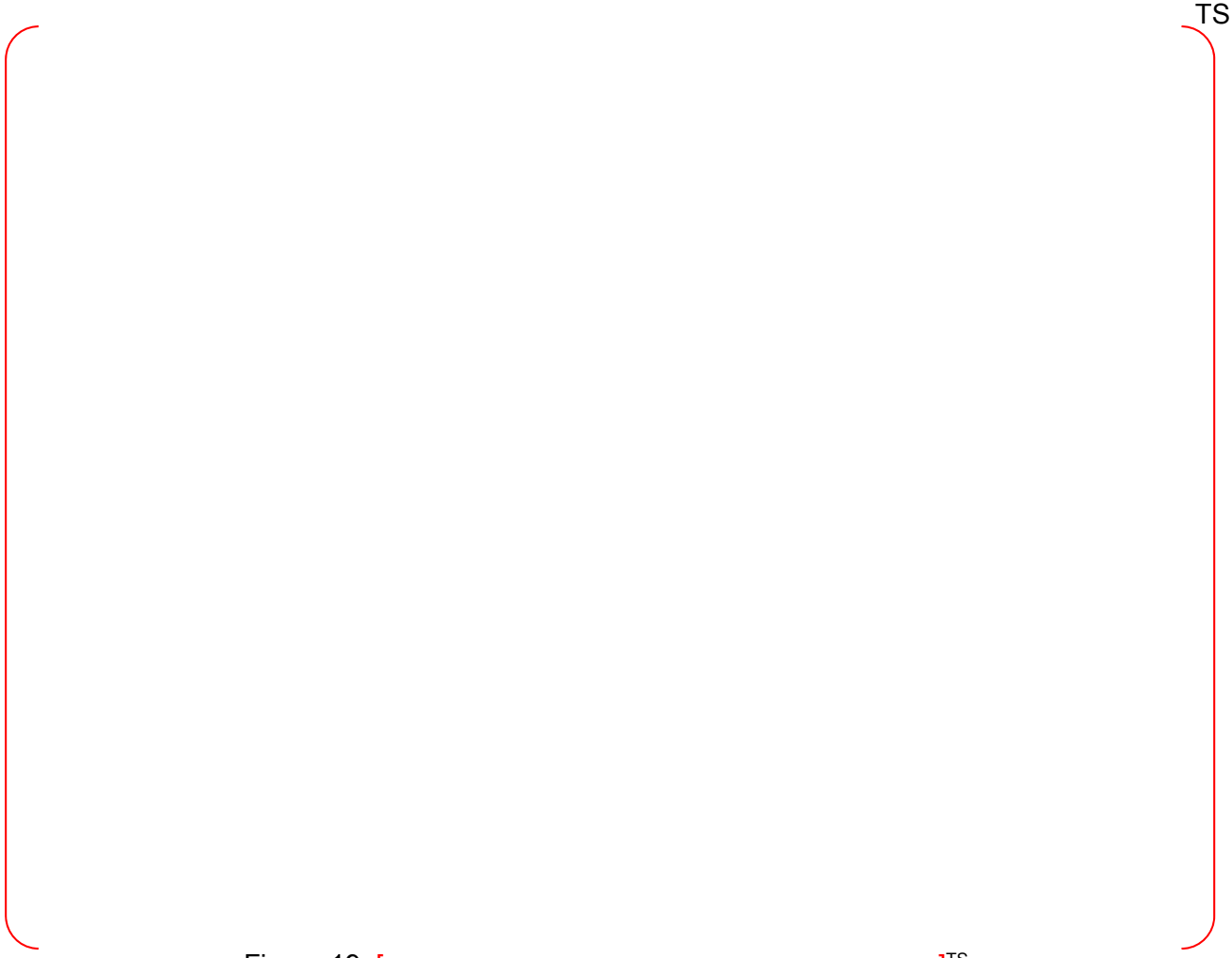

Figure 19. [ ]TS

TS

Figure 20. [ ]TS

Figure 21 to Figure 26 show downcomer flows of [ ]TS respectively (in response to item m). The nodalization of downcomer is composed of [ ]TS

Figure 21. [ ]TS

TS

TS

Figure 22. [ ]TS

TS

Figure 23. [ ]TS

TS

Figure 24. [ ]TS

TS

Fgure 25. [ ]TS

TS

Figure 26. [ ]TS

Figure 27 shows void fraction in the upper plenum (in response to item n).

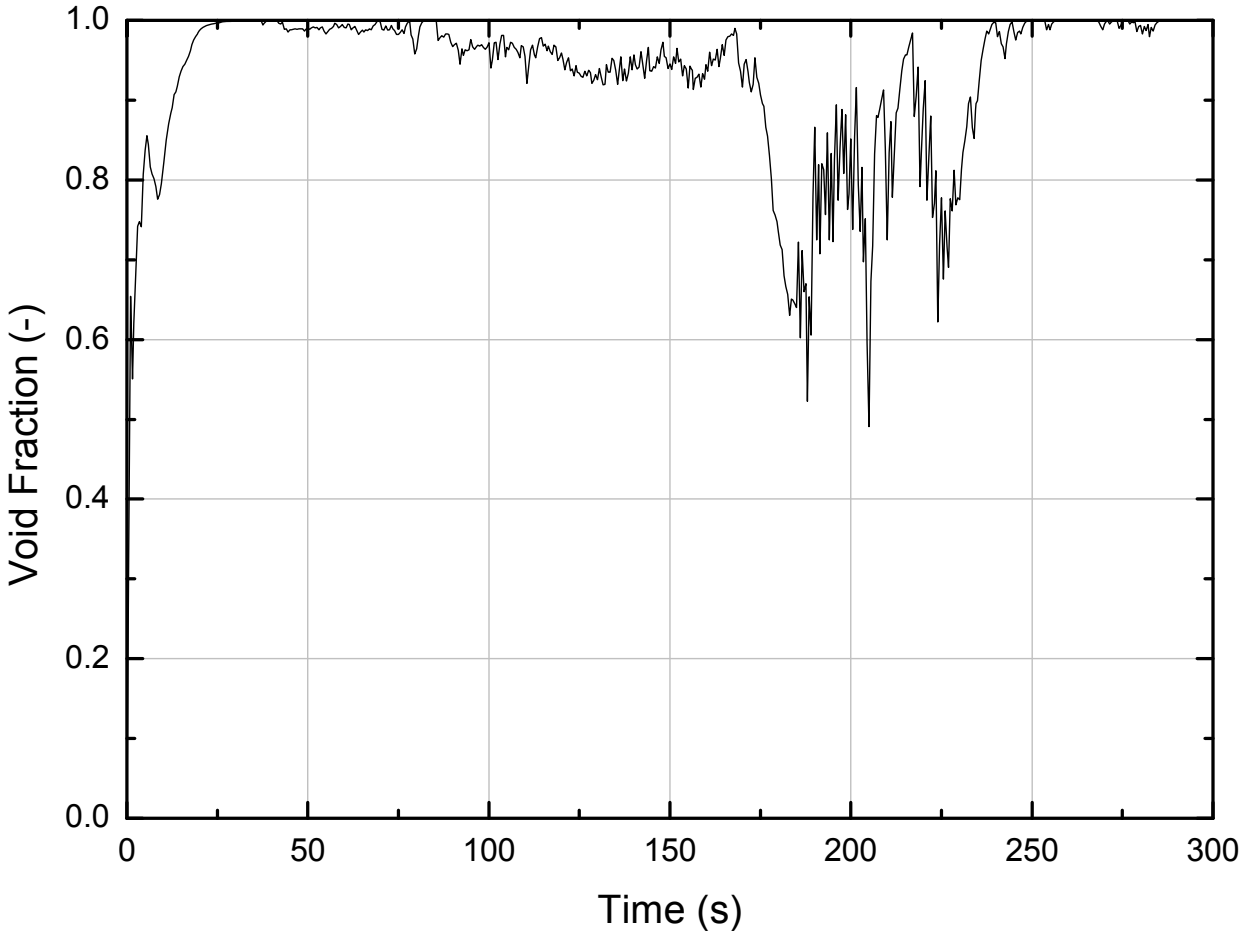

Figure 27. Void Fraction in the Upper Plenum

Impact on DCD

There is no impact on the DCD.

Impact on PRA

There is no impact on the PRA.

Impact on Technical Specifications

There is no impact on the Technical Specifications.

Impact on Technical/Topical/Environmental Report

There is no impact on any Technical, Topical, or Environmental Report.

RESPONSE TO AUDIT ISSUES

APR1400 Topical Reports

Korea Electric Power Corporation / Korea Hydro & Nuclear Power Co., LTD

Docket No. PROJ0782

Review Section	**TR Realistic Evaluation Methodology for LBLOCA of the APR1400**
Application Section	**Topical Report: APR1400-F-A-TR-12004 Realistic Evaluation Methodology for Large-Break LOCA of the APR1400**
Issue Date	**08/13/2015**

Audit Issues No. 61-a

The guidance in RG 1.157, Section 3.1 establishes acceptable controls for the establishment of acceptable break sizes and types. Section 5.2.1.1 of the topical report provides information regarding the selection of the limiting break. Address the following concerns:

a. Provide the calculated PCT and corresponding elevation during the blowdown period and the reflood period for the 100 percent and 80 percent guillotine break cases.

Response

Calculation results of blowdown and reflood PCTs are presented in Table 1.

Table 1. PCT results of DEG 100 % and 80 % TS

Impact on DCD

There is no impact on the DCD.

Impact on PRA

There is no impact on the PRA.

Impact on Technical Specifications

There is no impact on the Technical Specifications.

Impact on Technical/Topical/Environmental Report

There is no impact on any Technical, Topical, or Environmental Report.

RESPONSE TO AUDIT ISSUES

APR1400 Topical Reports

Korea Electric Power Corporation / Korea Hydro & Nuclear Power Co., LTD

Docket No. PROJ0782

Review Section	**TR Realistic Evaluation Methodology for LBLOCA of the APR1400**
Application Section	**Topical Report: APR1400-F-A-TR-12004 Realistic Evaluation Methodology for Large-Break LOCA of the APR1400**
Issue Date	**08/13/2015**

Audit Issues No. 61-b ~ f

The guidance in RG 1.157, Section 3.1 establishes acceptable controls for the establishment of acceptable break sizes and types. Section 5.2.1.1 of the topical report provides information regarding the selection of the limiting break. Address the following concerns:

b. Since the reflood PCT for [ ]TS, provide the basis for NOT examining the 90 percent and 70 percent guillotine break cases.

c. Since the rod quenching for [ ]TS, describe the phenomena resulting in [ ]TS.

d. Based on the information on Figure 5-10 of the topical report, [ ]TS. Provide information to justify that the 180 percent, 160 percent, 140 percent, etc., CLS break PCT will be bounded by the guillotine break.

e. Based on Figure 5-9, the 100 percent guillotine break is selected as the limiting case because its blowdown PCT is the maximum as compared to [ ]TS. However, the reflood PCT for [ ]TS. If various uncertainties and biases are factored in, it is likely that the reflood PCT for the 80 percent guillotine break resulting from the application of distribution free statistics may be limiting. Provide evidence that such a situation does not exist.

f. The CAREM methodology permits the determination of the limiting break type, location and size with a 95th percentile tolerance at a 95 percent confidence level using the simple random sampling process to sample across break locations (cold leg or pump suction leg), break types (DECLG or split) and break sizes/areas. This is the only

method that provides a 95/95 basis that the limiting break type, location, and area are determined. To justify that the calculations performed are representative of the spectrum of break sizes and locations, provide the results of a calculation using the simple random sampling method considering the variation in the break type, location, and area. Also provide confirmation that split breaks continue to remain bounded when a random selection of break areas for the split break and the DECLG are used.

Response to Audit Issue 61-b, d, e and f

In response to the audit issue No. 61-b, d, e and f, the followings are discussed.

Break Location Sensitivity

Figure 1 shows comparison of calculation results for [

]TS In this figure, both break areas are fixed to have 100 % of broken pipe cross-sectional area.

[

]TS

Therefore, CAREM does not quantify PCT uncertainties for [

]TS

Break Type Sensitivity

Break type sensitivity calculation is performed with the selected break location. Slot break and DEG break are considered. In case of slot break, several modeling methods are evaluated.

Figure 3 shows three kinds of slot break noding. [

]TS

In the topical report, model B is only used to determine limiting break type because model B has been selected as limiting slot break modeling for conventional nuclear power plants. But, it is concluded that various modeling methods for slot break should be evaluated to respond to this audit issue.

Figure 4 compares PCTs calculated using model A, B and C with DEG break result. This figure shows that DEG break is still limiting break type.

Break Area Sensitivity for Slot Break

The slot break area sensitivity is performed using 'Model C – Bottom' case since it shows relatively high blowdown and reflood PCTs and has the latest reflood quenching time.

Figure 5 shows comparison of cladding temperature results for various slot break areas with that of 100 % DEG break case. Slot break areas from [ ]TS. Since the calculation results [ ]TS But, PCT results of 100 % DEG break case are still higher than those of slot break cases for both blowdown and reflood. Therefore, the PCT of DEG break covers those of slot breaks.

Break Area for DEG Break

To determine the limiting break area, [ ]TS are evaluated in the topical report. To support the appropriateness of the limiting break size selection logic of the topical report, it is determined to perform the simple random sampling (SRS) calculation with break area as one of the uncertainty parameters. DEG in the cold leg is assumed as limiting break location and type for this SRS calculation. In this SRS calculation, break area ranging from [ ]TS of the cold leg area are considered, and uniform distribution function is assumed to have same possibility for all break areas.

Figure 6 shows SRS calculation results for break area as one of the uncertainty parameters (Case A) with SRS calculation results of the topical report (Case B). The third PCT of Case A is [ ]TS. The third PCTs of two calculation cases are similar but the PCT of the topical report occurs during blowdown period while the PCT of Case A occurs during reflood period. Quenching time of Case B is longer than that of Case A. In conclusion, the SRS calculation in the topical report (100 % cold leg area as limiting break area) bound the SRS calculation when the break area is considered as the uncertainty parameter.

Response to Audit Issue 61-c

[

]TS

Figure 1. Comparison of Break Location Sensitivity Results

Figure 2. RELAP5/MOD3.3/K Nodalization of the APR1400

TS

Figure 3. Three Kinds of Slot Break Modeling

Figure 4. Comparison of Slot Break Model Results

Figure 5. Calculation Results for Various Slot Break Areas

Figure 6. Comparison of SRS Calculation Results with and without Break Area

Figure 7. Comparison of Core Collapsed Water Level

Impact on DCD

There is no impact on the DCD.

Impact on PRA

There is no impact on the PRA.

Impact on Technical Specifications

There is no impact on the Technical Specifications.

Impact on Technical/Topical/Environmental Report

There is no impact on any Technical, Topical, or Environmental Report.

RESPONSE TO AUDIT ISSUES

APR1400 Topical Reports

Korea Electric Power Corporation / Korea Hydro & Nuclear Power Co., LTD

Docket No. PROJ0782

Review Section	**TR Realistic Evaluation Methodology for LBLOCA of the APR1400**
Application Section	**Topical Report: APR1400-F-A-TR-12004 Realistic Evaluation Methodology for Large-Break LOCA of the APR1400**
Issue Date	**08/13/2015**

Audit Issues No. 62

RG 1.157 guidance expresses in many places that results from best estimate calculations will be considered acceptable provided their technical basis is demonstrated with appropriate data and analyses. However, some of the results provided in the topical report are unclear. The base case calculation of the APR1400 plant applying the best-estimate operating conditions is shown in Figures 5-12 through 5-28. The water level in the reactor vessel is mainly determined by the balance of inlet (ECCS) and outlet mass flow (break flow). During late reflood period, ECCS water is supplied by SIPs with constant flow rate (see Figure 5-14), while the break flow in Figure 5-13 decreases to almost zero beyond 250 seconds. Based on these results, the mass balance is expected to cause continuous water level recovery in the reactor core region after 250 seconds. However, the water levels in the core and downcomer region, shown in Figure 5-15, are constant and gradually decreasing, respectively, beyond 250 seconds. Provide an explanation for the observed behavior.

Response

Figure 1 shows the collapsed water level in the downcomer and the active core. Figure 2 shows the total break and total SI flow rate.

Before SIT is depleted (at about 200 seconds), the downcomer water level is maintained higher than the height of cold leg due to the excessive SI flow rate. After depletion of SIT, the downcomer water level is decreased to the cold leg elevation. From this point, the steam generated in the core is discharged smoothly through the break and the steam flow can carry the water in the downcomer out the break. Also ECC bypass flow increases. Based on this, as shown in Figure 2, the break flow rate increases after 200 seconds. After about 250 seconds (the time that the pressure balance between core and downcomer is maintained), core and downcomer water levels are maintained constant. Note that, the entire core is quenched at 190 seconds.

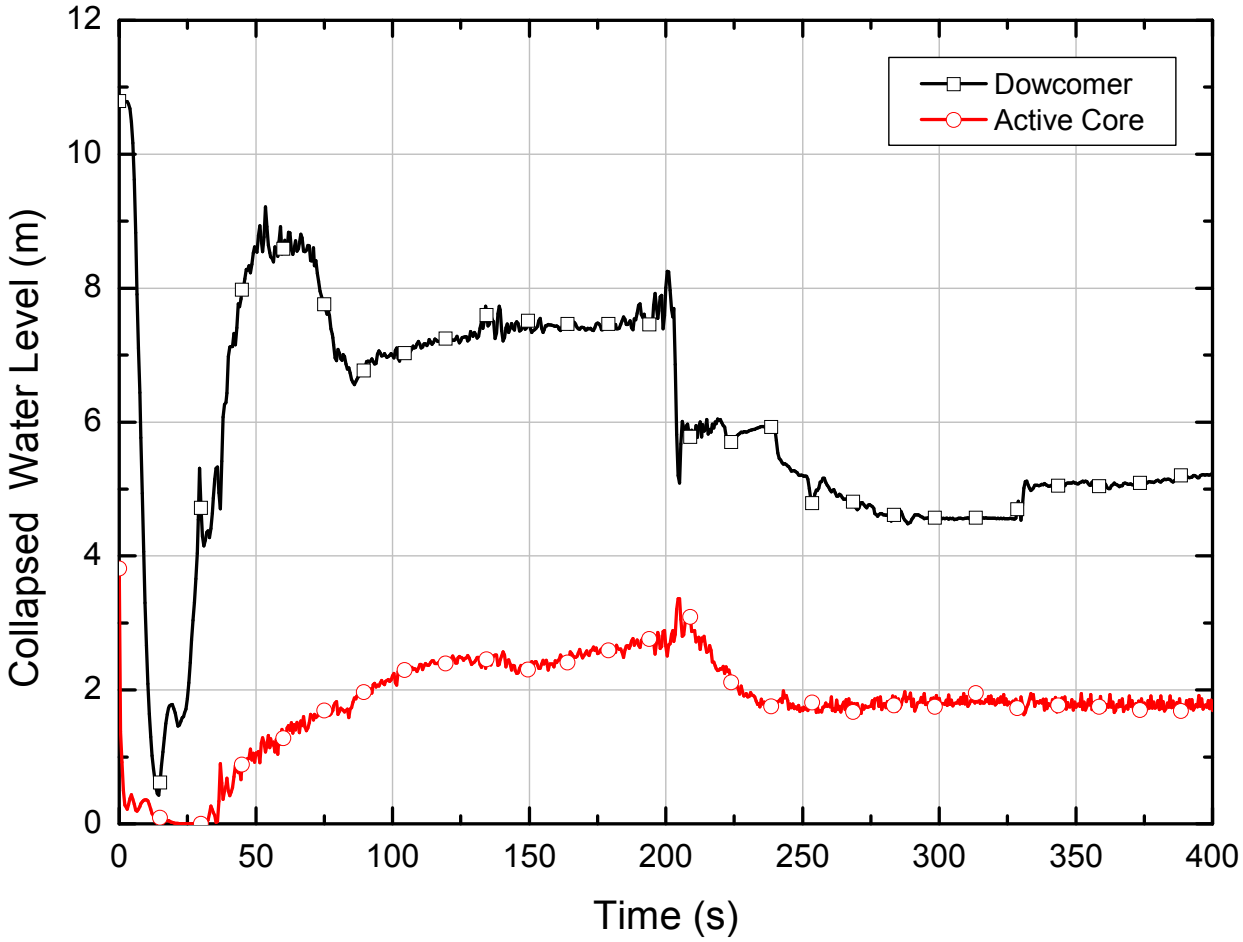

Figure 1. Collapsed Water Level in the Downcomer and Active Core

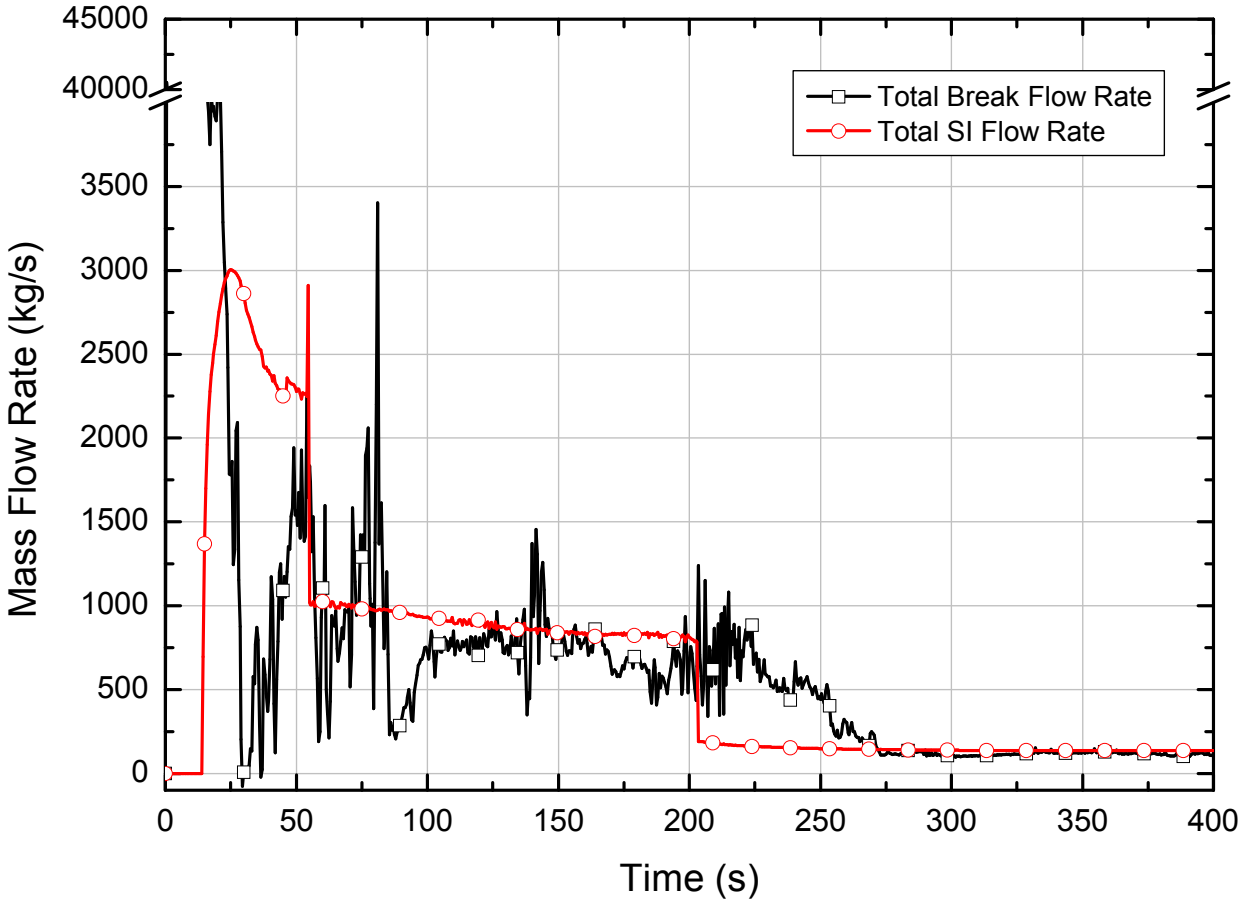

Figure 2. Total Break and Total SI Flow Rate

Impact on DCD

There is no impact on the DCD.

Impact on PRA

There is no impact on the PRA.

Impact on Technical Specifications

There is no impact on the Technical Specifications.

Impact on Technical/Topical/Environmental Report

There is no impact on any Technical, Topical, or Environmental Report.

RESPONSE TO AUDIT ISSUES

APR1400 Topical Reports

Korea Electric Power Corporation / Korea Hydro & Nuclear Power Co., LTD

Docket No. PROJ0782

Review Section	**TR Realistic Evaluation Methodology for LBLOCA of the APR1400**
Application Section	**Topical Report: APR1400-F-A-TR-12004 Realistic Evaluation Methodology for Large-Break LOCA of the APR1400**
Issue Date	**08/13/2015**

Audit Issues No. 63

The guidance in RG 1.157, Section 4 establishes acceptable controls for the estimation of calculational uncertainty. Section 5.2.2 of the topical report discusses the use of simple random sampling approach to perform 124 calculations using the distributions of the uncertainty parameters listed in Table 5-1. Describe the model or method that is utilized to perform the random selection of samples and provide justification that the sampling process is unbiased.

Response

Following reference is a guide for CAREM.

H. Glaser, “BEMUSE Phase VI Report, Status report on the area, classification of the methods, conclusions and recommendations”, NEA/CSNI/R(2011)4, 28-Mar-2011; (https://www.oecd-nea.org/nsd/docs/2011/csni-r2011-4.pdf),

Following statements are found in section 7.2; “It is also important to note that the model outcome sample values $Y_1 \ldots Y_N$ from which the tolerance intervals/limits are determined must constitute a random sample of the model outcome Y in the statistical sense, i.e. they must be realizations of stochastically independent and identically distributed random variables $Y_1 \ldots Y_N$. This is ensured if the underlying input parameter sample is generated according to the simple random sampling (SRS) principle. Other types of parameter selection procedures like Latin Hypercube Sampling or Importance Sampling, etc. may therefore not be appropriate for tolerance intervals or tolerance limits”.

Also it (in section 7.7) strongly recommends the simple random sampling technique to get a random sample. There is no concern about the bias with the simple random sampling process in the reference.

To get the random sample, open source computer program, LHS, is used (G. D. Wyss, K. H. Jorgensen, “A User’s Guide to LHS: Sandia’s Latin Hypercube Sampling Software”, SAND98-0210, February 1998).

Simple random sampling is performed using the option “random sampling” in the LHS code that will cause LHS to perform pure Monte Carlo sampling to generate random sample.

Impact on DCD

There is no impact on the DCD.

Impact on PRA

There is no impact on the PRA.

Impact on Technical Specifications

There is no impact on the Technical Specifications.

Impact on Technical/Topical/Environmental Report

There is no impact on any Technical, Topical, or Environmental Report.

RESPONSE TO AUDIT ISSUES

APR1400 Topical Reports

Korea Electric Power Corporation / Korea Hydro & Nuclear Power Co., LTD

Docket No. PROJ0782

Review Section	**TR Realistic Evaluation Methodology for LBLOCA of the APR1400**
Application Section	**Topical Report: APR1400-F-A-TR-12004 Realistic Evaluation Methodology for Large-Break LOCA of the APR1400**
Issue Date	**08/13/2015**

Audit Issues No. 64

RG 1.157 guidance expresses in many places that results from best estimate calculations will be considered acceptable provided their technical basis is demonstrated with appropriate data and analyses. However, some of the results provided in the topical report are unclear. Provide the values and plots for the three highest PCTs predicted via the plant SRS calculations documented in Section 5.2.2.

Response

Figure 1 shows the three highest PCT results from the plant SRS calculations. The first and second highest PCTs are [
]TS. The third highest PCT is [
]TS.

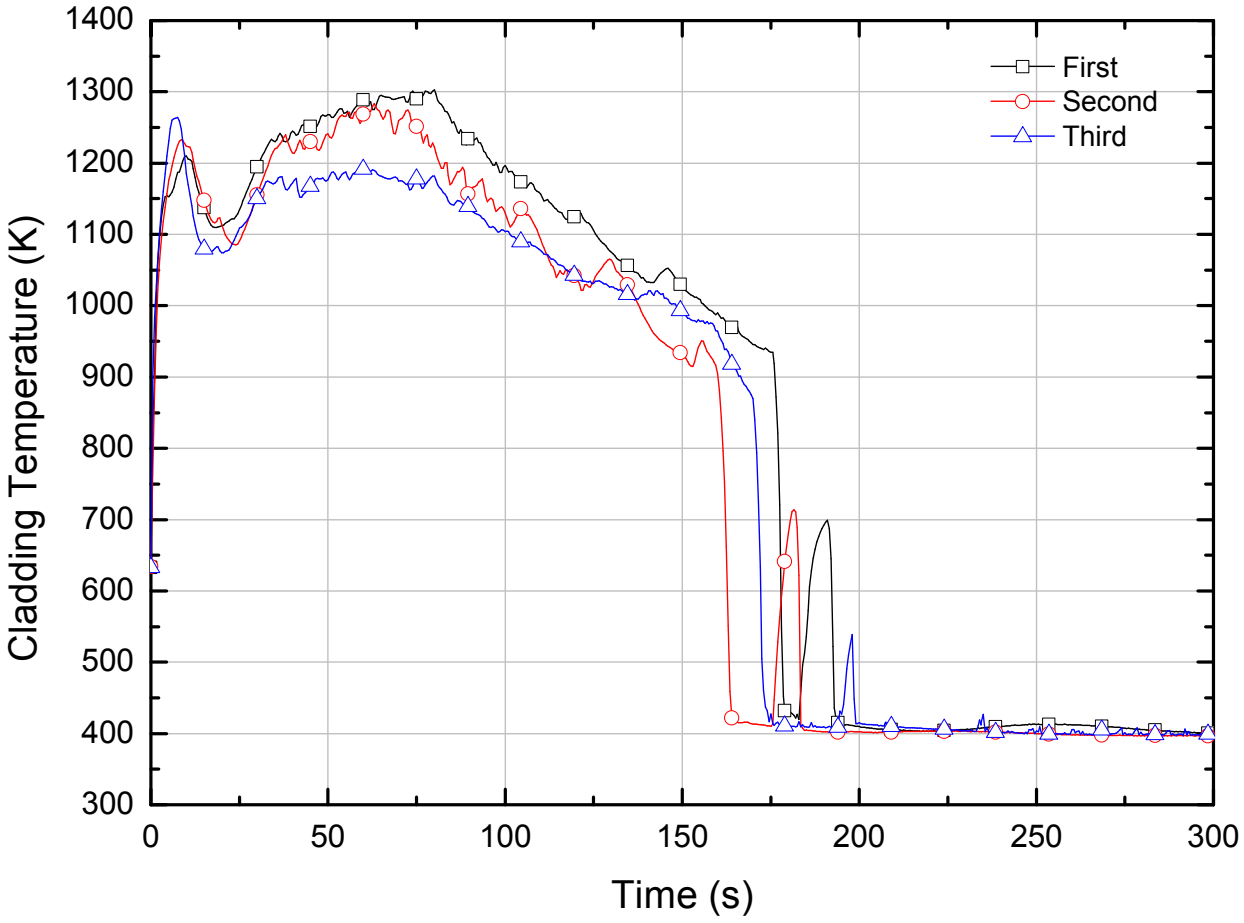

Figure 1. Three highest PCTs result from the SRS calculation

Impact on DCD

There is no impact on the DCD.

Impact on PRA

There is no impact on the PRA.

Impact on Technical Specifications

There is no impact on the Technical Specifications.

Impact on Technical/Topical/Environmental Report

There is no impact on any Technical, Topical, or Environmental Report.

RESPONSE TO AUDIT ISSUES

APR1400 Topical Reports

Korea Electric Power Corporation / Korea Hydro & Nuclear Power Co., LTD

Docket No. PROJ0782

Review Section	**TR Realistic Evaluation Methodology for LBLOCA of the APR1400**
Application Section	**Topical Report: APR1400-F-A-TR-12004 Realistic Evaluation Methodology for Large-Break LOCA of the APR1400**
Issue Date	**08/13/2015**

Audit Issues No. 65

The guidance in RG 1.157, Section 4 establishes acceptable controls for the estimation of uncertainties, including the determination of biases. The selection of the cases for evaluation of scale bias in Section 5.2.3 of the topical report is “...based on previous experiences...” Provide details of the referenced “experiences” and the basis for the selection of the cases. Also confirm that the case with the highest second peak is captured in the set that is used for the evaluation of the scale bias.

Response

In the CAREM, as stated in the section 4.3.2 in the topical report, 124 combinations of the uncertainty parameters are used to quantify the uncertainty of the PCT prediction. In those combinations, two cases with two highest PCTs are not considered as valid results.

In the topical report, the set for bias calculation is selected based on the cases whose [

]TS.

[ ]TS the scale bias cases is determined based on “the previous experiences” which means licensing experience in Korea. In addition, considering that [ ]TS as indicated in Table 5-8, [ ]TS the scale bias cases seems fairly reasonable to evaluate bias effects.

The sentences in Section 5.2.3 of the topical report will be corrected for typo and modified for better understanding as follows.

Section No.	Before	After
5.2.3	Based on the previous experiences, [ ]TS are selected for the scale bias calculations. [ ]TS	Based on the previous experiences, [ ]TS are selected for the scale bias calculations. [ ]TS

The revised topical report will be submitted later.

Impact on DCD

There is no impact on the DCD.

Impact on PRA

There is no impact on the PRA.

Impact on Technical Specifications

There is no impact on the Technical Specifications.

Impact on Technical/Topical/Environmental Report

Topical report will be revised as discussed in this response.

There is no impact on Technical or Environmental Report.

RESPONSE TO AUDIT ISSUES

APR1400 Topical Reports

Korea Electric Power Corporation / Korea Hydro & Nuclear Power Co., LTD

Docket No. PROJ0782

Review Section	**TR Realistic Evaluation Methodology for LBLOCA of the APR1400**
Application Section	**Topical Report: APR1400-F-A-TR-12004 Realistic Evaluation Methodology for Large-Break LOCA of the APR1400**
Issue Date	**08/13/2015**

Audit Issues No. 66

The guidance in RG 1.157, Section 4 establishes acceptable controls for the estimation of uncertainties and determination of biases. Elaborate and provide reason(s) for Cases 9 and 105 in Tables 5-5 and 5-6 that show no influence from any of the biases.

Response

Table numbers of Tables 5-5 and 5-6 in the topical report (Rev.0) are changed to Tables 5-6 and 5-7 in the topical report (Rev.1), respectively. As discussed in RAI-8510 and Audit Issue number 51, SRS calculation for APR1400 is re-performed considering several input modifications, 181 sampling times, and TCD consideration. Following Tables 1 and 2 shown in this response include recalculation results and represent Tables 5-6 and 5-7 in the revised topical report (Rev.1).

Table 1. Biases from the ECC Bypass TS

TS

Table 2. Biases from the De-entrainment in the Upper Plenum

Impact on DCD

There is no impact on the DCD.

Impact on PRA

There is no impact on the PRA.

Impact on Technical Specifications

There is no impact on the Technical Specifications.

Impact on Technical/Topical/Environmental Report

Topical report is revised as discussed in this response.

There is no impact on Technical or Environmental Report.

RESPONSE TO AUDIT ISSUES

APR1400 Topical Reports

Korea Electric Power Corporation / Korea Hydro & Nuclear Power Co., LTD

Docket No. PROJ0782

Review Section	**TR Realistic Evaluation Methodology for LBLOCA of the APR1400**
Application Section	**Topical Report: APR1400-F-A-TR-12004 Realistic Evaluation Methodology for Large-Break LOCA of the APR1400**
Issue Date	**08/13/2015**

Audit Issues No. 67-a

The guidance in NUREG/CR-5429, Section 2.1 establishes acceptable controls for the ranking and documentation of the PIRT. Appendix A of the topical report provides the modification to the PIRT ranking of the in-containment refueling water storage tank (IRWST). [ ]TS. Address the following:

a. The end of the late reflood period is not clearly specified. Provide the definition for the end of the late reflood period and therefore, the beginning of the long term cooling period, in the analysis.

Response

The end of late reflood is not specifically defined in LBLOCA topical report. LBLOCA analysis is performed until the time core quenching is stable, which typically can be established before the SIT-FD empty. Technically Long Term Cooling (LTC) calculation can begin when stable quenching is established, typically beginning of late reflood or later.

[

]TS

[1] “Fluidic Device Design for the APR1400, Rev.0”, APR1400-Z-M-TR-12003-P, Rev.0, KHNP

TS

Figure 1. Boil-off Rate Resulting from 1.2 x ANS79 Decay Heat

Impact on DCD

There is no impact on the DCD.

Impact on PRA

There is no impact on the PRA.

Impact on Technical Specifications

There is no impact on the Technical Specifications.

Impact on Technical/Topical/Environmental Report

There is no impact on any Technical, Topical, or Environmental Report.

RESPONSE TO AUDIT ISSUES

APR1400 Topical Reports

Korea Electric Power Corporation / Korea Hydro & Nuclear Power Co., LTD

Docket No. PROJ0782

Review Section	**TR Realistic Evaluation Methodology for LBLOCA of the APR1400**
Application Section	**Topical Report: APR1400-F-A-TR-12004 Realistic Evaluation Methodology for Large-Break LOCA of the APR1400**
Issue Date	**08/13/2015**

Audit Issues No. 67-b and c

The guidance in NUREG/CR-5429, Section 2.1 establishes acceptable controls for the ranking and documentation of the PIRT. Appendix A of the topical report provides the modification to the PIRT ranking of the in-containment refueling water storage tank (IRWST). [ ]^{TS}. Address the following:

b. To confirm sufficiency, provide the volume of the IRWST and indicate the amount of water that was depleted at the end of the late reflood period.

c. Explain how suction is provided to the SIPs when the IRWST inventory is exhausted.

Response 67-b and c

The minimum normal operation water volume of IRWST is [ ]TS.

The detail information about in-containment water storage system (IWSS) is described in Chapter 6.8 in DCD [1]. [

]TS

[1] KEPCO, KHNP, “APR1400 Design Control Document Tier 2”, December 2014, APR1400-K-FS-14002-NP, Rev.0

Impact on DCD

There is no impact on the DCD.

Impact on PRA

There is no impact on the PRA.

Impact on Technical Specifications

There is no impact on the Technical Specifications.

Impact on Technical/Topical/Environmental Report

There is no impact on any Technical, Topical, or Environmental Report.

RESPONSE TO AUDIT ISSUES

APR1400 Topical Reports

Korea Electric Power Corporation / Korea Hydro & Nuclear Power Co., LTD

Docket No. PROJ0782

Review Section	**TR Realistic Evaluation Methodology for LBLOCA of the APR1400**
Application Section	**Topical Report: APR1400-F-A-TR-12004 Realistic Evaluation Methodology for Large-Break LOCA of the APR1400**
Issue Date	**08/13/2015**

Audit Issues No. 68

The guidance in NUREG/CR-5429, Section 2.1 establishes acceptable controls for the documentation of the ranking rationale for the PIRT. Page A-5 of Appendix A provides the rationale for the change to PIRT ranking of the stored energy release from pressurizer. However, it is unclear whether the stored energy release is actually modeled or simply lumped into the pressure uncertainty. The rationale for the ranking change states, [

]^{TS} In such a case, no stored heat transfer is expected. Explain the modeling of pressurizer wall heat structures and clarify whether the pressurizer vessel stored energy release is explicitly represented in the calculation through transient heat transfer to the fluid.

Response

The pressurizer is modeled to transfer vessel stored energy to the fluid through the transient calculation because pressurizer wall heat structures are modeled.

Impact on DCD

There is no impact on the DCD.

Impact on PRA

There is no impact on the PRA.

Impact on Technical Specifications

There is no impact on the Technical Specifications.

Impact on Technical/Topical/Environmental Report

There is no impact on any Technical, Topical, or Environmental Report.

RESPONSE TO AUDIT ISSUES

APR1400 Topical Reports

Korea Electric Power Corporation / Korea Hydro & Nuclear Power Co., LTD

Docket No. PROJ0782

Review Section	**TR Realistic Evaluation Methodology for LBLOCA of the APR1400**
Application Section	**Topical Report: APR1400-F-A-TR-12004 Realistic Evaluation Methodology for Large-Break LOCA of the APR1400**
Issue Date	**08/13/2015**

Audit Issues No. 69

NUREG/CR-5429, Section 2.1 discusses the process for the documentation of the PIRT. Page A-6 of Appendix A provides the modification to PIRT ranking of [ ]^{TS} The rationale for the change states [ ]^{TS} Explain what is meant by the phrase [ ]^{TS} with respect to this issue.

Response

In the SBLOCA or long term cooling situation, the water accumulation in the crossover leg can affect the fluid motion. This is a so called loop seal clearing phenomena. It can be general or realistic. However, in LBLOCA situation, the fluid does not exist at the cross-over leg during whole period of interest for most applications. The phrase [

]^{TS} therefore, the assumption is not realistic.

Impact on DCD

There is no impact on the DCD.

Impact on PRA

There is no impact on the PRA.

Impact on Technical Specifications

There is no impact on the Technical Specifications.

Impact on Technical/Topical/Environmental Report

There is no impact on any Technical, Topical, or Environmental Report.

RESPONSE TO AUDIT ISSUES

APR1400 Topical Reports

Korea Electric Power Corporation / Korea Hydro & Nuclear Power Co., LTD

Docket No. PROJ0782

Review Section	**TR Realistic Evaluation Methodology for LBLOCA of the APR1400**
Application Section	**Topical Report: APR1400-F-A-TR-12004 Realistic Evaluation Methodology for Large-Break LOCA of the APR1400**
Issue Date	**08/13/2015**

Audit Issues No. 70

NUREG/CR-5429, Section 2.1 discusses the process for the documentation of the PIRT. Appendix A provides the modification to the ranking for the phenomenon [ ]^{TS} Fluid in the upper head and the flashing behavior in the upper head may have a significant effect on the LBLOCA transient response. To understand the bases for the change of the influence rank discussed above, provide the temperature of the upper head fluid and describe the flow process to and from the upper head during the LBLOCA.

Response

[

]TS which is described in Appendix A of the topical report as the modified PIRT from KNGR PIRT.

TS

Impact on DCD

There is no impact on the DCD.

Impact on PRA

There is no impact on the PRA.

Impact on Technical Specifications

There is no impact on the Technical Specifications.

Impact on Technical/Topical/Environmental Report

There is no impact on any Technical, Topical, or Environmental Report.

RESPONSE TO AUDIT ISSUES

APR1400 Topical Reports

Korea Electric Power Corporation / Korea Hydro & Nuclear Power Co., LTD

Docket No. PROJ0782

Review Section	**TR Realistic Evaluation Methodology for LBLOCA of the APR1400**
Application Section	**Topical Report: APR1400-F-A-TR-12004 Realistic Evaluation Methodology for Large-Break LOCA of the APR1400**
Issue Date	**08/13/2015**

Audit Issues No. 71

NUREG/CR-5429, Section 2.1 discusses the process for the documentation of the PIRT. Appendix A provides the modification to the ranking for the phenomenon of [

]^{TS} In the early reflood period the safety injection flow is higher and the amount of liquid entrainment is likely higher than in the late reflood period. Therefore, the steam binding effect is expected to be more important during the early reflood period. Provide the transient results for the steam flow, entrained liquid through the top nozzles, and the vapor and liquid flow into the steam generator inverted U-tubes. These are intended to confirm the Applicant's conclusions on the influence of the phenomenon.

Response

Figure 1 shows the steam and liquid flow rate through the top nozzles. Figure 2 shows the vapor and liquid flow rate into the steam generator inverted U-tubes.

[

]TS

Flooding Rate

Reflood begins as water enters the core from the lower plenum. During the reflood period, part of the water injected into the vessel flows through the downcomer and lower plenum to core. In the core, the water is accumulated, vaporized to steam, or entrained by the steam flow exiting the core. The water entrained by the steam flow is either de-entrained at or above the top nozzle, or carried over to the hot legs and steam generators. Water entrained into the steam generators vaporizes by reverse heat transfer from the secondary side of the steam generators causing a pressure increase in the upper plenum. The pressure increase reduces the flooding rate. [

]TS

[ ]TS

The entrained droplets evaporate and the steam becomes superheated in the u-tubes. This droplet evaporation and steam superheating phenomena result in steam binding. In CAREM, the effect of steam binding is evaluated [ ]TS. As the RELAP5 code does not include a model to describe mechanical de-entrainment due to the internal structures in the upper plenum, [

]TS

The reflood during the FD-SIT injection period, the excessive entrainment from the core is expected due to the high safety injection penetration into the core. The RELAP5/MOD3.1/K which was used for the earlier version of CAREM was assessed against FLECHT/SEASET series test and found that the entrainment coming out of core is [ ]TS higher than the experimental data on average[1]. RELAP5/MOD3.3/K of the present TR shows [

]TS

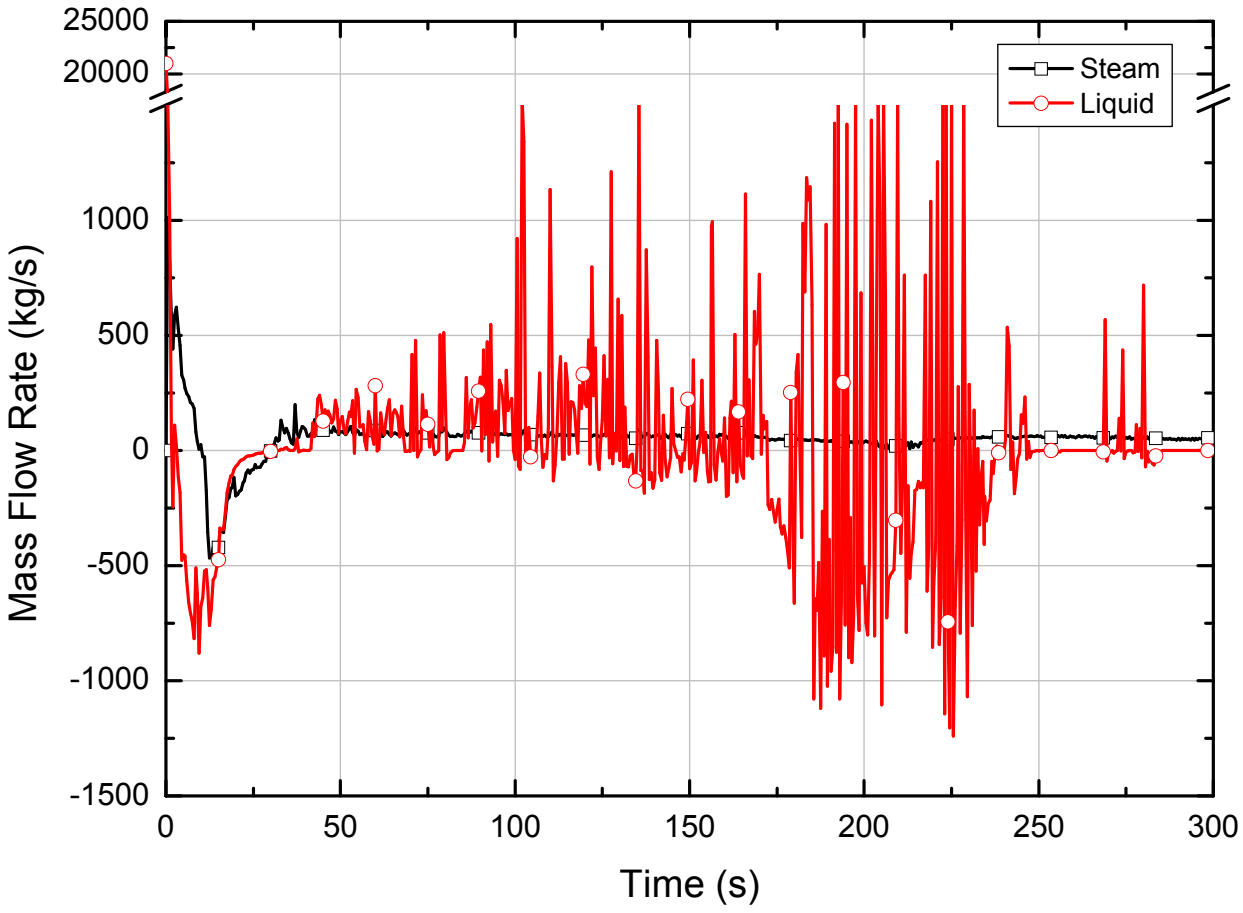

Figure 1. Steam and Liquid Flow Rate through the Top Nozzle

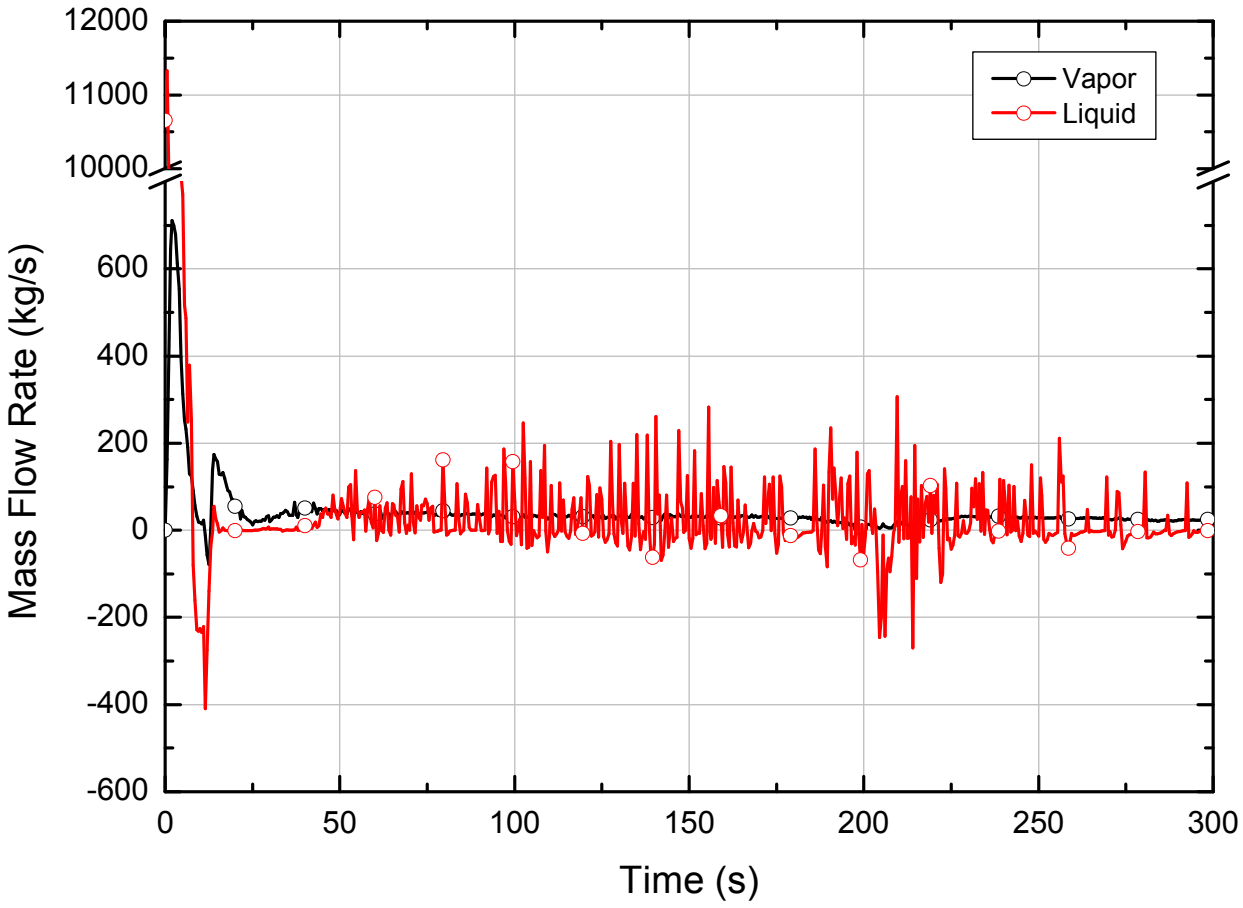

Figure 2. Vapor and Liquid Flow Rate into the SG Inverted U-tube

Reference

[1] Topical Report, “The best evaluation methodology for the Emergency Core Cooling System,”TR-KHNP-002, KEPRI/KHNP, December 2002.

Impact on DCD

There is no impact on the DCD.

Impact on PRA

There is no impact on the PRA.

Impact on Technical Specifications

There is no impact on the Technical Specifications.

Impact on Technical/Topical/Environmental Report

There is no impact on any Technical, Topical, or Environmental Report.

RESPONSE TO AUDIT ISSUES

APR1400 Topical Reports

Korea Electric Power Corporation / Korea Hydro & Nuclear Power Co., LTD

Docket No. PROJ0782

Review Section	**TR Realistic Evaluation Methodology for LBLOCA of the APR1400**
Application Section	**Topical Report: APR1400-F-A-TR-12004 Realistic Evaluation Methodology for Large-Break LOCA of the APR1400**
Issue Date	**08/13/2015**

Audit Issues No. 72

NUREG/CR-5429, Section 2.1 discusses the process for the documentation of the PIRT and associated ranking of various phenomena. [

]^{TS} Section 3.3.1 of RG 1.157 states that the calculation of the swelling and cladding rupture should be included in the analysis and performed in a best-estimate manner. The blockage may reduce the cladding temperature but that would not appear to decrease the importance of the effect of blockage on the physical response. The calculated cladding temperature transient should reflect the cooling effects of cladding swelling. Confirm that RELAP5/MOD3.3/K can calculate fuel cladding swelling and rupture. Further, confirm that the calculated effect of swelling and rupture on fluid flow and cladding temperature calculations reflects that effect into the fuel channel blockage.

Response

RELAP5/MOD3.3 code has cladding deformation model described in Section 4.14 of reference [1]. An empirical cladding deformation model from FRAT-T6 has been incorporated into RELAP5. In this model, cladding strain by thermal, elastic, and plastic deformation is estimated, and rupture strain and blockage are predicted by NUREG-0630[2] data.

Cladding deformation model in the RELAP5/MOD3.3 code is used to calculate dynamic gap conductance model. If flow blockage option is activated and rod rupture occurs, flow blockage by additional pressure loss coefficients (K-factors) to the neighborhood junctions is considered.

Consequently, RELAP5/MOD3.3 code has a capability to calculate fuel cladding swelling and rupture, and it can also consider flow blockage effect when rod rupture occurs. However, geometry changes caused by fuel rod swelling (before rod rupture) does not cause the fuel channel blockage.

Reference

[1] “RELAP5/MOD3.3 Code Manual Volume I: Code Structure, System Models, and Solution Methods,” NUREG/CE-5535, Rev. P3-Vol I, U.S.NRC, March 2003.

[2] “Cladding Swelling and Rupture Models for LOCA Analysis,” NUREG-0630, U.S.NRC, March 1980.

Impact on DCD

There is no impact to the DCD.

Impact on PRA

There is no impact on the PRA.

Impact on Technical Specifications

There is no impact on the Technical Specifications.

Impact on Technical/Topical/Environmental Report

There is no impact on any Technical, Topical, or Environmental Report.

RESPONSE TO AUDIT ISSUES

APR1400 Topical Reports

Korea Electric Power Corporation / Korea Hydro & Nuclear Power Co., LTD

Docket No. PROJ0782

Review Section	**TR Realistic Evaluation Methodology for LBLOCA of the APR1400**
Application Section	**Topical Report: APR1400-F-A-TR-12004 Realistic Evaluation Methodology for Large-Break LOCA of the APR1400**
Issue Date	**08/13/2015**

Audit Issues No. 73-a

NUREG/CR-5429, Section 2.1 discusses the process for the documentation of the PIRT and associated ranking of various phenomena. Appendix A provides the modification to the ranking for the phenomenon “stored energy release” for the lower plenum and downcomer components. In order to concur with the modified influence ranking, provide the following information:

a. Transient results for the energy release from the lower plenum metal structures as a function of time, the enthalpy (or fluid temperature and void fraction, if saturated) as a function of time, and the stored energy of the lower plenum metal structures as a function of time for the base case calculation discussed in Section 5.2.1.3.

Response

The lower plenum is from the bottom of vessel to active core inlet as shown in Figure 1. Figure 2 shows the energy release from the lower plenum metal structures. Figure 3 shows enthalpy of the fluid at the lower plenum. The stored energy of the lower plenum metal structures is expressed as the volume average temperature of the lower plenum (Figure 4).

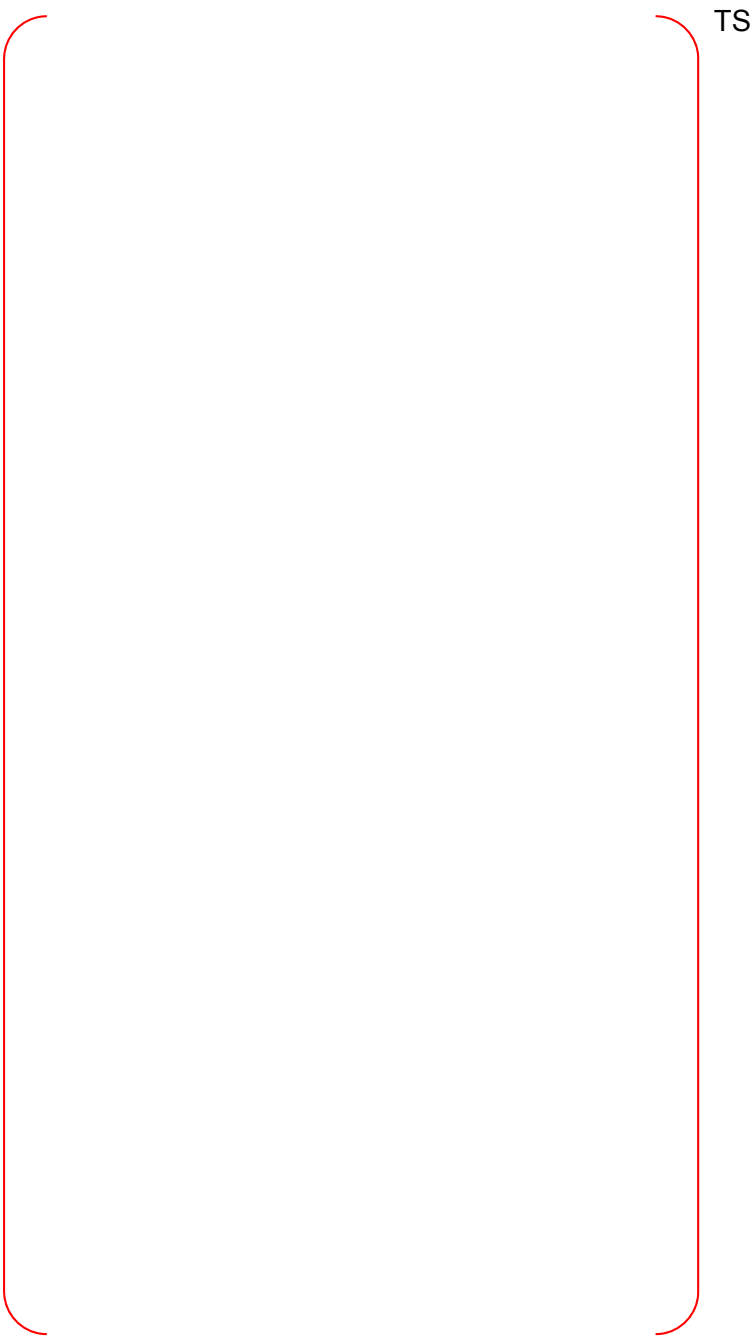

Figure 1. Nodalization of the Reactor Vessel (The Red Boxes are Lower Plenum Region)

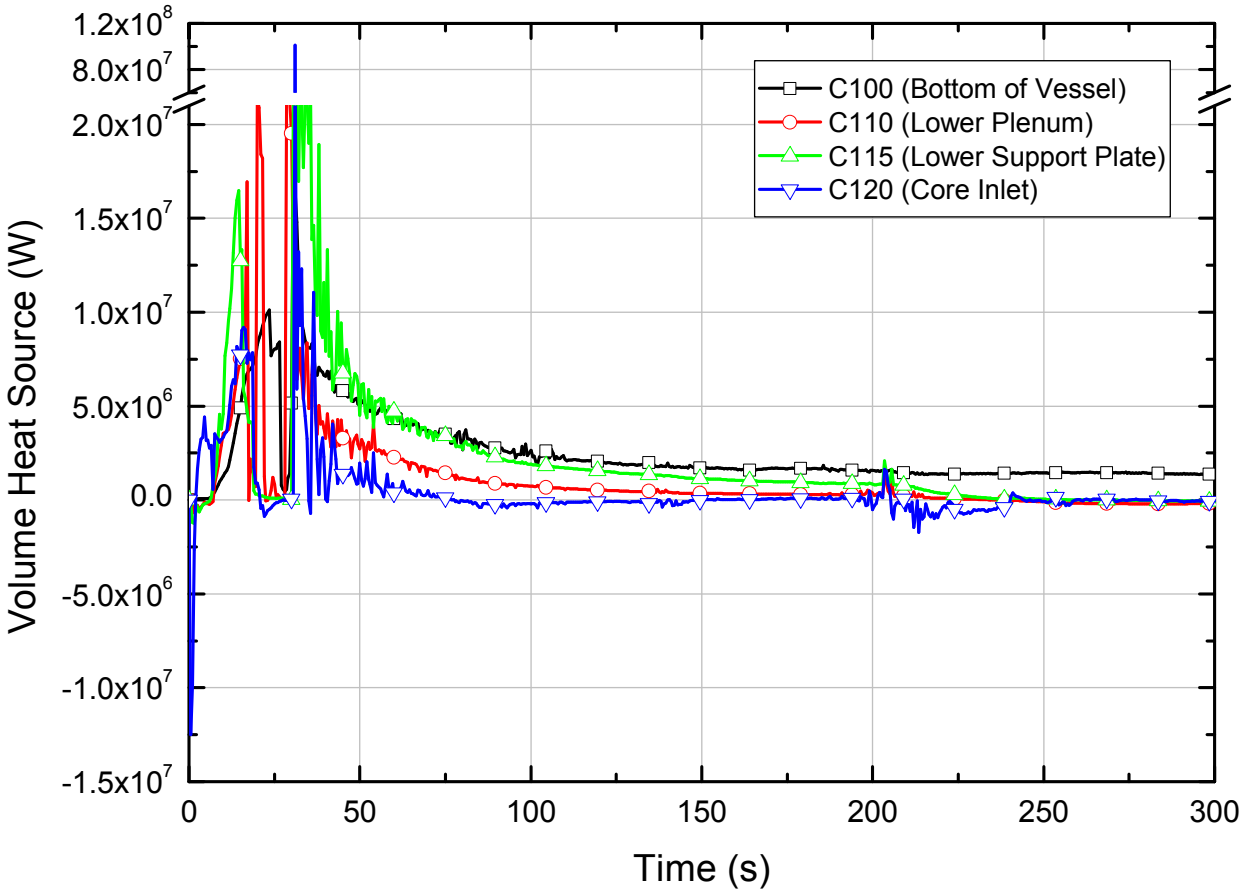

Figure 2. Energy Release from the Lower Plenum Metal Structures

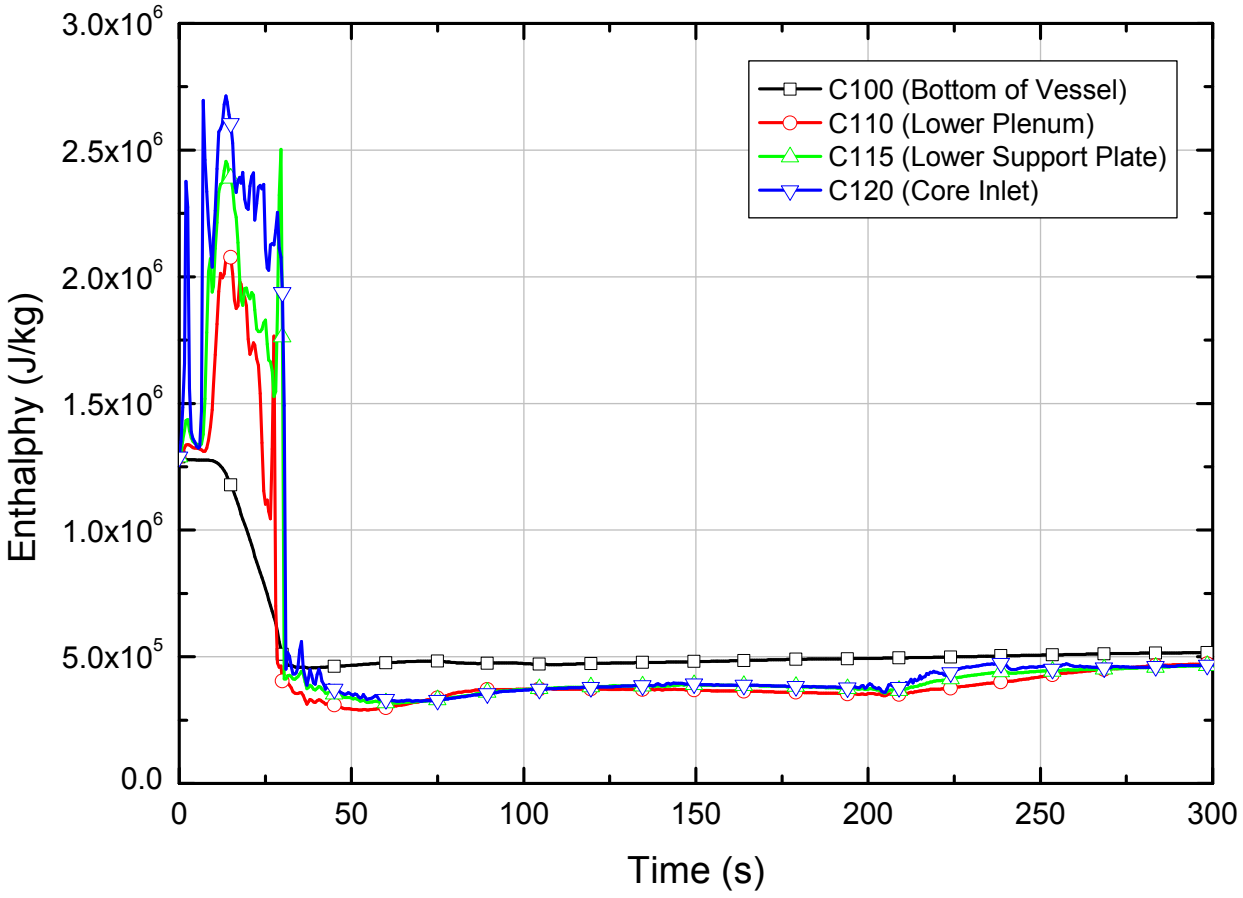

Figure 3. Enthalpy of Fluid at the Lower Plenum

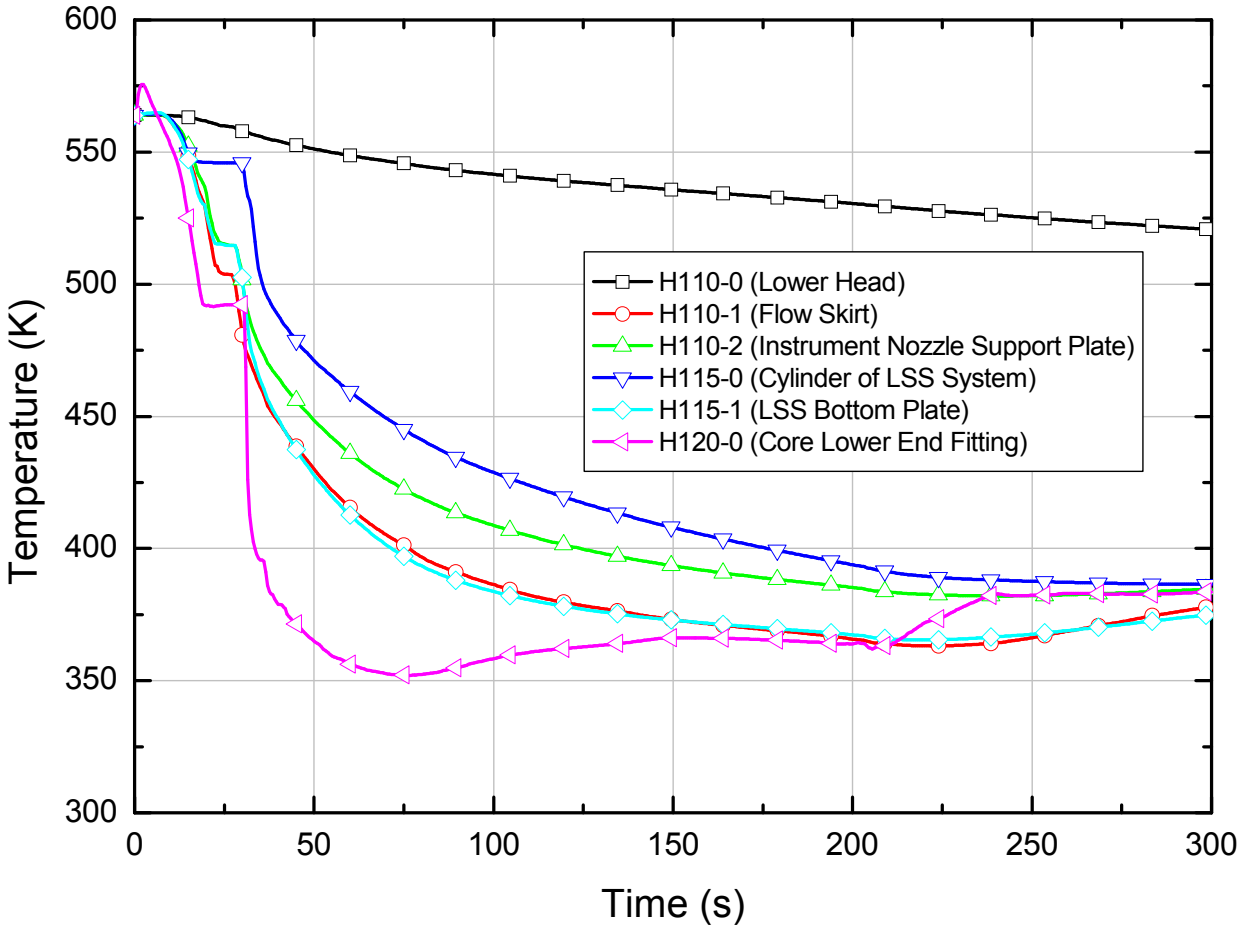

Figure 4. Volume Average Temperature of the Lower Plenum Metal Structures
(LSS: Lower Support Structure)

Impact on DCD

There is no impact on the DCD.

Impact on PRA

There is no impact on the PRA.

Impact on Technical Specifications

There is no impact on the Technical Specifications.

Impact on Technical/Topical/Environmental Report

There is no impact on any Technical, Topical, or Environmental Report.

RESPONSE TO AUDIT ISSUES

APR1400 Topical Reports

Korea Electric Power Corporation / Korea Hydro & Nuclear Power Co., LTD

Docket No. PROJ0782

Review Section	**TR Realistic Evaluation Methodology for LBLOCA of the APR1400**
Application Section	**Topical Report: APR1400-F-A-TR-12004 Realistic Evaluation Methodology for Large-Break LOCA of the APR1400**
Issue Date	**08/13/2015**

Audit Issues No. 73-b

NUREG/CR-5429, Section 2.1 discusses the process for the documentation of the PIRT and associated ranking of various phenomena. Appendix A provides the modification to the ranking for the phenomenon “stored energy release” for the lower plenum and downcomer components. In order to concur with the modified influence ranking, provide the following information:

b. Transient results for the energy release from the reactor vessel downcomer metal structures, core barrel and thermal shield metal structures as a function of time, the enthalpy of the fluid (or temperature) as a function of time, and the stored energy of the downcomer, core barrel and thermal shield metal structures as a function of time for the base case calculation discussed in Section 5.2.1.3.

Response

The reactor vessel downcomer and core barrel metal structures are shown in Figure 1. Figure 2 shows sum of the energy release from the reactor vessel downcomer metal structures and core barrel metal structures. Figure 3 shows enthalpy of the fluid at the downcomer. The stored energy of the downcomer and core barrel metal structures is expressed as the volume average temperature of the downcomer and core barrel metal structures (Figure 4). The downcomer is composed of [ ]^{TS} Therefore, the average values of [ ]^{TS} in the same elevation are presented in Figure 3 and Figure 4.

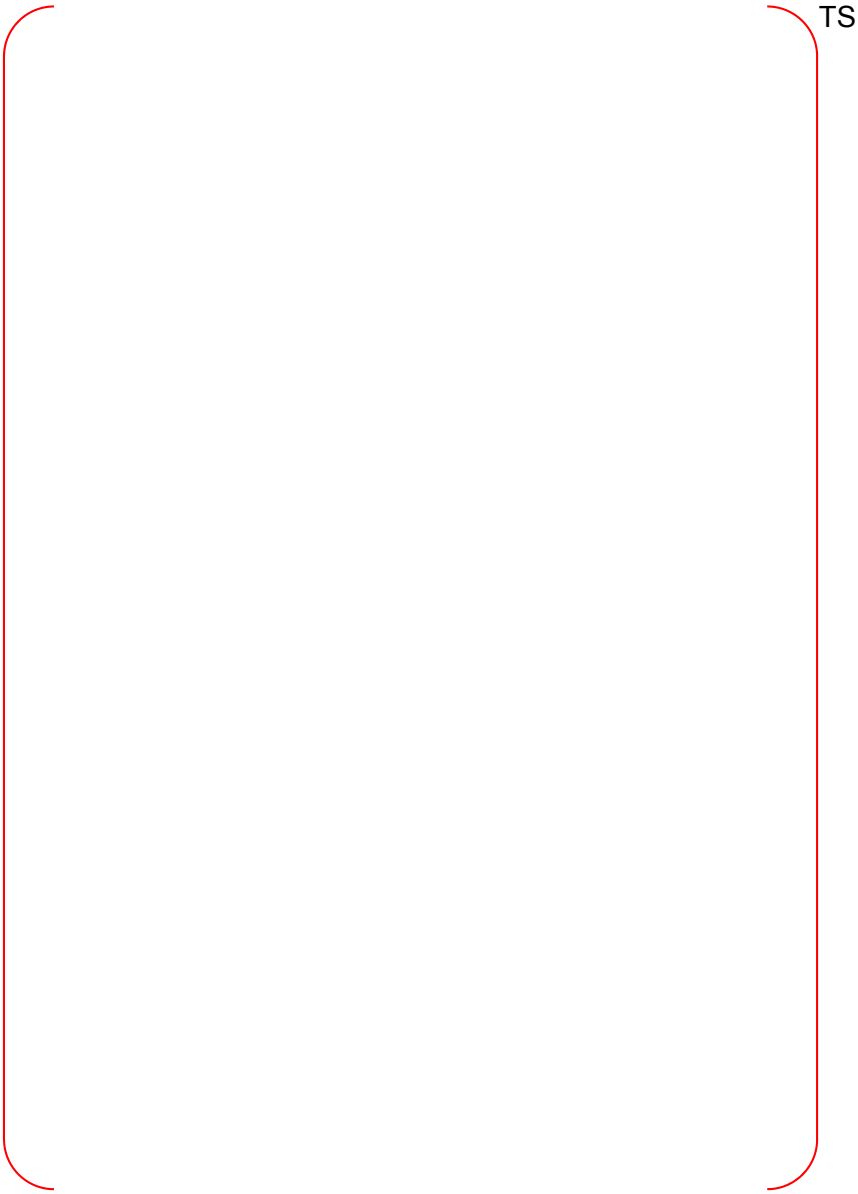

Figure 1. Nodalization of the Reactor Vessel

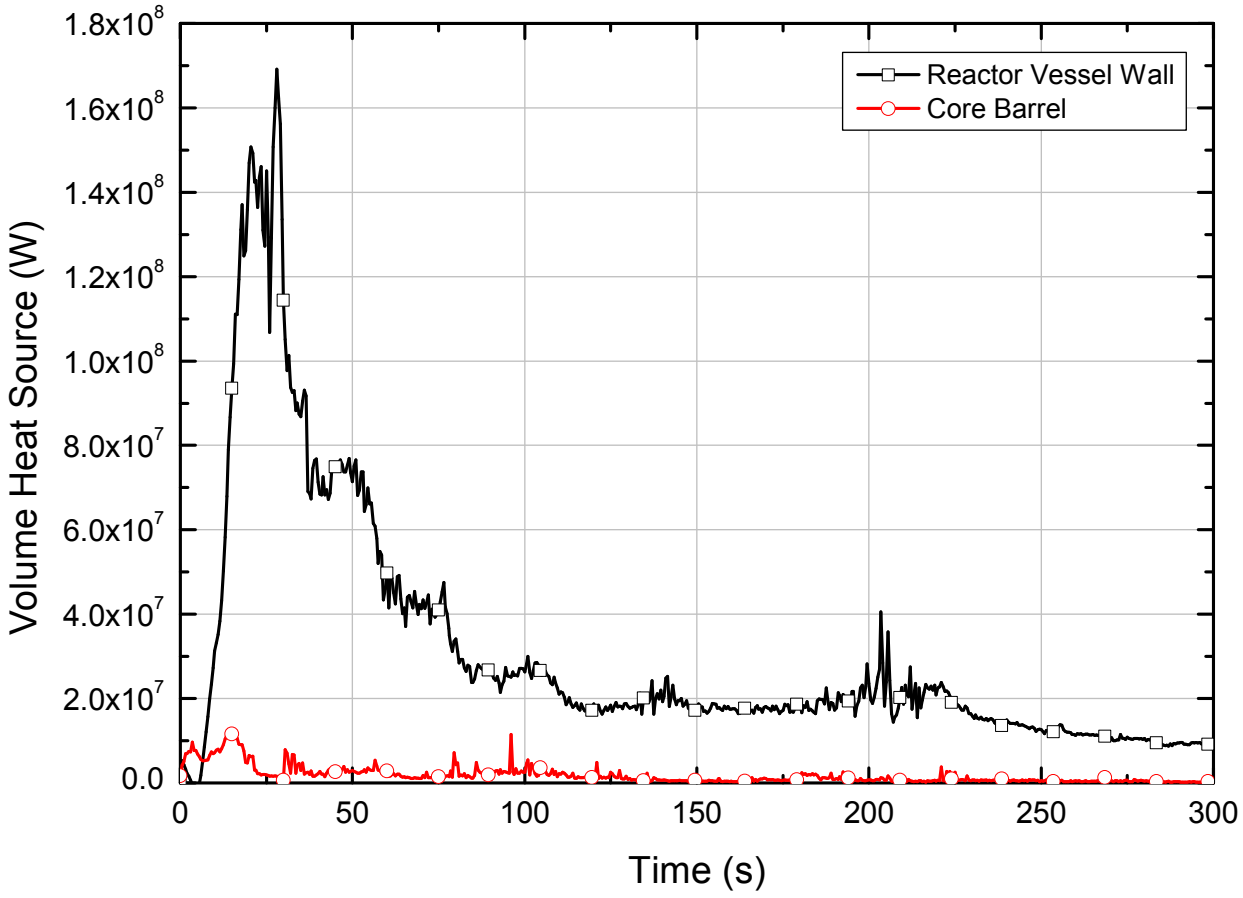

Figure 2. Energy Release from the Reactor Vessel Wall and Core Barrel Structures

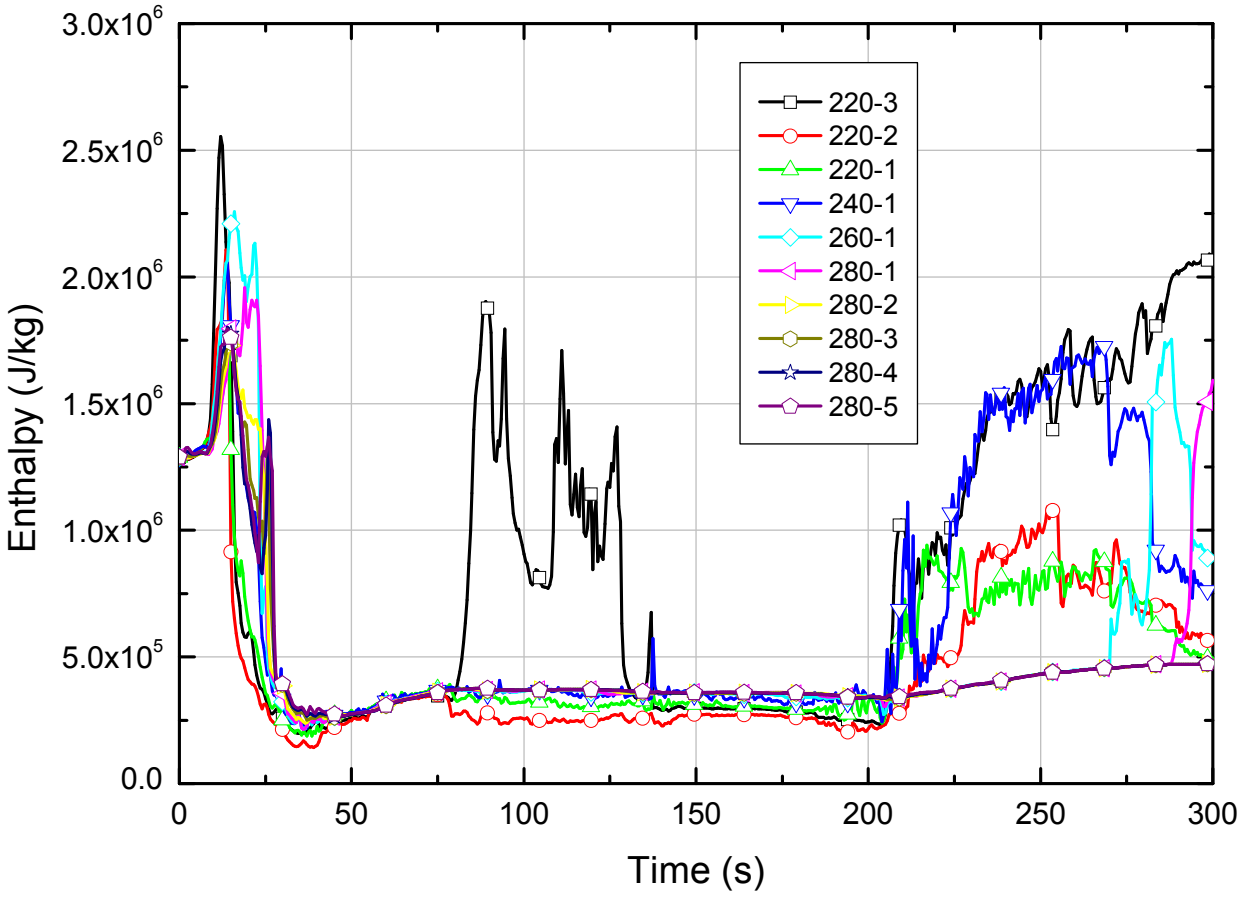

C220: Upper annulus from center of loop to top of annulus
C240: 1/2 of downcomer annulus region from bottom of UGS to top of FAP elevations
C260: Annulus region from the top of active core to the top of FAP
C280: Downcomer annulus from the top of active core region to flow skirt hole

Figure 3. Enthalpy of Fluid at the Downcomer

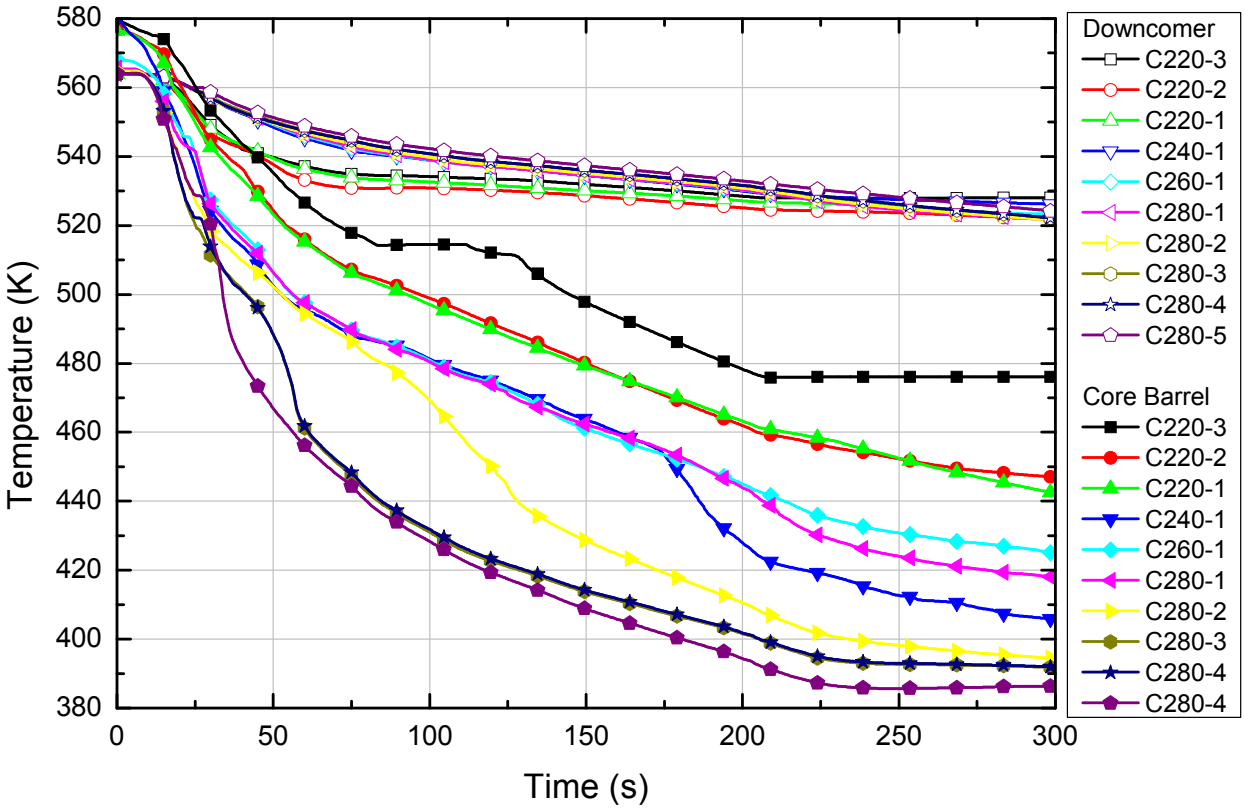

Figure 4. Volume Average Temperature of the Downcomer and Core Barrel Metal Structures

Impact on DCD

There is no impact on the DCD.

Impact on PRA

There is no impact on the PRA.

Impact on Technical Specifications

There is no impact on the Technical Specifications.

Impact on Technical/Topical/Environmental Report

There is no impact on any Technical, Topical, or Environmental Report.

RESPONSE TO AUDIT ISSUES

APR1400 Topical Reports

Korea Electric Power Corporation / Korea Hydro & Nuclear Power Co., LTD

Docket No. PROJ0782

Review Section	**TR Realistic Evaluation Methodology for LBLOCA of the APR1400**
Application Section	**Topical Report: APR1400-F-A-TR-12004 Realistic Evaluation Methodology for Large-Break LOCA of the APR1400**
Issue Date	**08/13/2015**

Audit Issues No. 73-c

NUREG/CR-5429, Section 2.1 discusses the process for the documentation of the PIRT and associated ranking of various phenomena. Appendix A provides the modification to the ranking for the phenomenon “stored energy release” for the lower plenum and downcomer components. In order to concur with the modified influence ranking, provide the following information:

c. The outside boundary conditions used for the heat structures representing the vessel wall in the downcomer region and the lower head are not specified in the topical report. The RELAP5 base model uses an insulated boundary condition for these regions. The selection of the boundary condition affects the stored energy release to the fluid in the downcomer and the lower head. Justify the outer surface boundary conditions used for the lower head and vessel wall in the downcomer region in the APR1400 RELAP5/MOD3.3/K model, and if external cooling of the reactor pressure vessel (RPV) lower head can impact this boundary condition.

Response

External cooling of the reactor pressure vessel (RPV) lower head is not modeled in the APR1400 analysis.

The outer surface boundary conditions used for the lower head and vessel wall in the downcomer region are [ ]TS The heat structure number is [ ]TS The details are as follows:

TS

Impact on DCD

There is no impact on the DCD.

Impact on PRA

There is no impact on the PRA.

Impact on Technical Specifications

There is no impact on the Technical Specifications.

Impact on Technical/Topical/Environmental Report

There is no impact on any Technical, Topical, or Environmental Report.

RESPONSE TO AUDIT ISSUES

APR1400 Topical Reports

Korea Electric Power Corporation / Korea Hydro & Nuclear Power Co., LTD

Docket No. PROJ0782

Review Section	**TR Realistic Evaluation Methodology for LBLOCA of the APR1400**
Application Section	**Topical Report: APR1400-F-A-TR-12004 Realistic Evaluation Methodology for Large-Break LOCA of the APR1400**
Issue Date	**08/13/2015**

Audit Issues No. 74

NUREG/CR-5429, Section 2.1 discusses the process for the documentation of the PIRT and associated ranking of various phenomena. Provide the rationale for [ ]^{TS} to the coast down phenomenon in the RCP component for the blowdown period in Table 3 of Appendix A.

Response

In the CAREM, the reactor coolant pumps (RCPs) are shutoff when LBLOCA occurs due to assumption of loss of offsite power. RCP coast down starts at this time. Since there is no electric power supplied to the RCPs during the transient, stored energy of RCP fly wheel is spent by hydraulic and friction torques. However, almost all of liquid is vaporized in few seconds caused by rapid depressurization even if RCP is located in intact loop side, and then RCP degradation effects are increased significantly whereas RCP coastdown effects are relatively decreased. [

]TS

Impact on DCD

There is no impact on the DCD.

Impact on PRA

There is no impact on the PRA.

Impact on Technical Specifications

There is no impact on the Technical Specifications.

Impact on Technical/Topical/Environmental Report

There is no impact on any Technical, Topical, or Environmental Report.

RESPONSE TO AUDIT ISSUES

APR1400 Topical Reports

Korea Electric Power Corporation / Korea Hydro & Nuclear Power Co., LTD

Docket No. PROJ0782

Review Section	**TR Realistic Evaluation Methodology for LBLOCA of the APR1400**
Application Section	**Topical Report: APR1400-F-A-TR-12004 Realistic Evaluation Methodology for Large-Break LOCA of the APR1400**
Issue Date	**08/13/2015**

Audit Issues No. 75-a

The guidance in NUREG/CR-5429, Section 2.1.4 establishes acceptable controls over code versions and changes that could affect best estimate calculations. The RELAP5/MOD3.3/K source code has been provided in response to a previous NRC RAI. Address the following concerns:

a. The file “gapcon.f” for the RELAP5/MOD3.3/K code (in the folder Question-2\(1) Source code\relap5\kREM from the response CD) contains several changes that are in addition to the single line mentioned in Section 1.4 of Appendix B. Examples of such changes include lines 51-53, lines 73-81 and line 233 in the file “gapcon.f.” Explain the purpose and function of these additional changes.

Response

Gap conductance is one of the uncertainty parameters in the CAREM. RELAP5/MOD3.3 code doesn't have minor or major edit for gap conductance data, so RELAP5/MOD3.3 code is modified to write gap conductance data as well as pellet radius as major edit. Modified lines which are not mentioned in Appendix B exist for additional major edit to identify current heat structure number.

Line 38 ~ 39

Global and local variables are defined in these modified lines.

[ ] TS

Line 51 ~ 53

Local real variables are defined and defined real variables are connected with global memory array (fa array).

[ ] TS

Line 73 ~ 81

This modifications are made to identify current heat structure number if current heat structure is one of the fuel rod heat structures which are put in by additional user input card of 41000N00 described in Section 1.4.2 of response document for RAI no. 7425. However, identified current heat structure number information is not used in this sub-routine, that information is used another sub-routine.

[ ] TS

TS

Line 183

Calculated pellet radius is stored to local real variable of ‘pellet’. And pellet radius data is printed as major edit data.

TS

Line 213 ~ 214

This modifications are described in Appendix B.

TS

Line 233

Calculated gap conductance data is stored to local variable of ‘gpcond’. And gap conductance data is printed as major edit data.

[ ] TS

Reference

[1] "RELAP5/MOD3.3 Code Manual Volume I: Code Structure, System Models, and Solution Methods," NUREG/CR-5535, Rev P3, U.S.NRC, March 2003.

Impact on DCD

There is no impact on the DCD.

Impact on PRA

There is no impact on the PRA.

Impact on Technical Specifications

There is no impact on the Technical Specifications.

Impact on Technical/Topical/Environmental Report

There is no impact on any Technical, Topical, or Environmental Report.

RESPONSE TO AUDIT ISSUES

APR1400 Topical Reports

Korea Electric Power Corporation / Korea Hydro & Nuclear Power Co., LTD

Docket No. PROJ0782

Review Section	**TR Realistic Evaluation Methodology for LBLOCA of the APR1400**
Application Section	**Topical Report: APR1400-F-A-TR-12004 Realistic Evaluation Methodology for Large-Break LOCA of the APR1400**
Issue Date	**08/13/2015**

Audit Issues No. 75-b

The guidance in NUREG/CR-5429, Section 2.1.4 establishes acceptable controls over code versions and changes that could affect best estimate calculations. The RELAP5/MOD3.3/K source code has been provided in response to a previous NRC RAI. Address the following concerns:

b. The RELAP5/MOD3.3/K source code has been provided in response to a previous NRC RAI. The source code in the files “fidisv.f” and “fidis2.f” for RELAP5/MOD3.3/K (in the folder Question-2\(1) Source code\relap5\kREM from the response CD) does not contain the changes listed in lines (f) and (h) of Section 1.3 of Appendix B. The source code in the two files still shows the old logic with “dcon(2)” thereby restricting the droplet diameter to 1.5 mm. Address this discrepancy and its implication on the discussion and the results in the topical report.

Response

[

]TS

Following modified lines are written in ‘fidisv.f’, and similar code modifications are written in ‘fidis2.f’.

‘fidisv.f’ Sub-routine Line 146 ~ 161

[

]TS

Impact on DCD

There is no impact on the DCD.

Impact on PRA

There is no impact on the PRA.

Impact on Technical Specifications

There is no impact on the Technical Specifications.

Impact on Technical/Topical/Environmental Report

Topical report will be revised as discussed in this response.

There is no impact on Technical or Environmental Report.

[ ]TS

1.4 Modification of [ ]TS

[ ]TS

RESPONSE TO AUDIT ISSUES

APR1400 Topical Reports

Korea Electric Power Corporation / Korea Hydro & Nuclear Power Co., LTD

Docket No. PROJ0782

Review Section	**TR Realistic Evaluation Methodology for LBLOCA of the APR1400**
Application Section	**Topical Report: APR1400-F-A-TR-12004 Realistic Evaluation Methodology for Large-Break LOCA of the APR1400**
Issue Date	**08/13/2015**

Audit Issues No. 76

The guidance in NUREG/CR-5249, Section 2.0, discusses issues related to model nodalization. Figure 17 of Appendix B shows the RELAP-5 nodalization of the primary system. [

]^{TS} Provide justifications regarding this core radial nodalization. If a different nodalization is to be used, justify why it will provide conservative or realistic predictions of the core heat transfer behavior.

Response

[

]TS Moreover, in CAREM, the conservative Fr (radial peaking factor) is applied to hot bundle. The conservative radial peaking factor for the hot bundle is described in response to audit issue no. 54.

Impact on DCD

There is no impact on the DCD.

Impact on PRA

There is no impact on the PRA.

Impact on Technical Specifications

There is no impact on the Technical Specifications.

Impact on Technical/Topical/Environmental Report

There is no impact on any Technical, Topical, or Environmental Report.

RESPONSE TO AUDIT ISSUES

APR1400 Topical Reports

Korea Electric Power Corporation / Korea Hydro & Nuclear Power Co., LTD

Docket No. PROJ0782

Review Section	**TR Realistic Evaluation Methodology for LBLOCA of the APR1400**
Application Section	**Topical Report: APR1400-F-A-TR-12004 Realistic Evaluation Methodology for Large-Break LOCA of the APR1400**
Issue Date	**08/13/2015**

Audit Issues No. 77

The guidance in RG 1.157, Section 4 establishes acceptable controls for the estimation of uncertainties. Table 2-2 in Appendix C shows the parameters and distribution functions used for SRS calculations for FLECHT-SEASET tests. Explain how the uncertainty range and distribution for flooding rate and power were determined. Explain the implication of negative power and flooding rate and how these are handled in the calculations.

Response

Measurement uncertainties of total power and volumetric flow rate (turbine meter) as one sigma level are as follows:

[ ] TS

Since liquid phase velocity is used as boundary condition using time-dependent junction, volumetric flow rate should be changed to velocity using core area (0.0156 m^2).

[ ] TS

In the CAREM, sampling uncertainty ranges are calculated by [ ]TS
Thus, sampling uncertainty ranges for power and liquid phase velocity (reflooding rate) are as follows:

[ ] TS

The above calculated uncertainty ranges for power and reflooding rate are determined and the normal distribution function is assumed for power and reflooding rate in common since the measurement uncertainty data described in reference [2-1] of Appendix C are the standard deviations for each measurement.

The rod power in Table 2-1 in the Appendix C of the topical report is the linear heat generation rate of a rod, while the uncertainty of the power obtained above is the uncertainty of the total power. Also the unit of the flooding rates in Table 2-1 in the Appendix C is mistakenly used as cm/s, which should have been used as mm/s. This will be fixed in the future revision of the topical report.

The sampled values for power and reflooding rate are variation from nominal values of the total power and reflood rate which are boundary conditions of each test. Thus, the sampled values are added to the nominal values of the total power and reflood rate.

Impact on DCD

There is no impact on the DCD.

Impact on PRA

There is no impact on the PRA.

Impact on Technical Specifications

There is no impact on the Technical Specifications.

Impact on Technical/Topical/Environmental Report

There is no impact on any Technical, Topical, or Environmental Report.

RESPONSE TO AUDIT ISSUES

APR1400 Topical Reports

Korea Electric Power Corporation / Korea Hydro & Nuclear Power Co., LTD

Docket No. PROJ0782

Review Section	**TR Realistic Evaluation Methodology for LBLOCA of the APR1400**
Application Section	**Topical Report: APR1400-F-A-TR-12004 Realistic Evaluation Methodology for Large-Break LOCA of the APR1400**
Issue Date	**08/13/2015**

Audit Issues No. 78

The guidance in RG 1.157, Section 4 establishes acceptable controls for the estimation of uncertainties. Clarify the uncertainty limits (e.g., 2 times standard deviation) used for the parameters with normal distribution during the SRS sampling in Appendix C.

Response

For the SRS sampling of the uncertainty variables with normal distribution, the uncertainty range of [ ]^{TS} is used in order to include as much uncertainty range as possible.

On the other hand, for the sampling with uniform distribution, the uncertainty range of [ ]^{TS} is used. In this case, σ means the standard deviation but μ means the deviation of one-sided limitation.

Impact on DCD

There is no impact on the DCD.

Impact on PRA

There is no impact on the PRA.

Impact on Technical Specifications

There is no impact on the Technical Specifications.

Impact on Technical/Topical/Environmental Report

There is no impact on any Technical, Topical, or Environmental Report.

RESPONSE TO AUDIT ISSUES

APR1400 Topical Reports

Korea Electric Power Corporation / Korea Hydro & Nuclear Power Co., LTD

Docket No. PROJ0782

Review Section	**TR Realistic Evaluation Methodology for LBLOCA of the APR1400**
Application Section	**Topical Report: APR1400-F-A-TR-12004 Realistic Evaluation Methodology for Large-Break LOCA of the APR1400**
Issue Date	**08/13/2015**

Audit Issues No. 79

The guidance in RG 1.157, Section 4 establishes acceptable controls for the estimation of uncertainties. Section 4.5 of Appendix C states that "...the selected code parameters and distribution functions for the NEPTUN test are the same as those used in the SRS calculations against FLECHT-SEASET tests." However, Table 4-5 of Appendix C lists only 8 parameters compared with the 12 parameters used for the FLECHT-SEASET tests. Confirm this apparent inconsistency.

Response

See the response to audit issue number 50-a.

Impact on DCD

There is no impact on the DCD.

Impact on PRA

There is no impact on the PRA.

Impact on Technical Specifications

There is no impact on the Technical Specifications.

Impact on Technical/Topical/Environmental Report

There is no impact on any Technical, Topical, or Environmental Report.

RESPONSE TO AUDIT ISSUES

APR1400 Topical Reports

Korea Electric Power Corporation / Korea Hydro & Nuclear Power Co., LTD

Docket No. PROJ0782

Review Section	**TR Realistic Evaluation Methodology for LBLOCA of the APR1400**
Application Section	**Topical Report: APR1400-F-A-TR-12004 Realistic Evaluation Methodology for Large-Break LOCA of the APR1400**
Issue Date	**08/13/2015**

Audit Issues No. 80

The guidance in RG 1.157, Section 3.16.2 establishes acceptable controls for the data comparisons necessary to justify best estimate models. RG 1.157 states that "…best estimate code calculations should be compared with applicable experimental data (e.g., separate effects tests…". Appendix C presents the results of comparisons against FLECHT- SEASET tests. These selected tests utilize a cosine power distribution. [

]^{TS} Provide the results or a reference for the calculations performed for the FLECHT-SEASET tests that utilize skewed power distributions or provide the bases justifying the applicability of the selected tests.

Response

The objective of data comparisons in RG 1.157, Section 3.16.2 is to ensure that the code predicts realistic behavior of SET well. In addition, this section states that the uncertainty analysis is required to ensure that a major bias does not exist in the code and rarely affects code calculation result.

FLECHT-SEASET is a reflood experiment to observe thermal-hydraulic phenomena in the bundle test section during the reflood phase. The experiments were performed with assuming cosine power shape [1]. In Appendix C, FLECHT-SEASET is adopted to ensure that code predicts thermal-hydraulic phenomena, such as cladding temperature, vapor temperature, and differential pressure, accurately during the reflood phase. In addition, the axial variation of FLECHT-SEASET test data is well predicted by the code as described in Appendix C both qualitatively and quantitatively. [

]TS

[

]TS

[1] M.J. Loftus. et al., “PWR FLECHT SEASET Unblocked Bundle, Forced and Gravity Reflood Task Data Report,” EPRI NP-1459, NUREG/CR-1532, WCAP-9699, 1981

Figure 1. Axial Power Shape Comparison

Impact on DCD

There is no impact to the DCD.

Impact on PRA

There is no impact on the PRA.

Impact on Technical Specifications

There is no impact on the Technical Specifications.

Impact on Technical/Topical/Environmental Report

There is no impact on any Technical, Topical, or Environmental Report.

RESPONSE TO AUDIT ISSUES

APR1400 Topical Reports

Korea Electric Power Corporation / Korea Hydro & Nuclear Power Co., LTD

Docket No. PROJ0782

Review Section	**TR Realistic Evaluation Methodology for LBLOCA of the APR1400**
Application Section	**Topical Report: APR1400-F-A-TR-12004 Realistic Evaluation Methodology for Large-Break LOCA of the APR1400**
Issue Date	**08/13/2015**

Audit Issues No. 81

NUREG-0800, Section 15.0.2 establishes review guidance related to the documentation of the evaluation model. Provide the input decks used for the RELAP5/MOD3.3/K assessments against the ATLAS tests 9, 11, and 15 described in Section 3 of Appendix E.

Response

As described in Appendix E of topical report, code assessment for the ATLAS test 09 and 11 are focused on the experiment data after 200 s and 210 s, respectively. Code calculations conducted from time 0 s to 200 s and 210 s for ALTAS Test 09 and 11 were done just for adjusting thermal-hydraulic conditions at 200 s and 210 s. And restart option of RELAP5/MOD3.3/K code was used to calculate after 200 s and 210 s. On the other hand, code assessment for the ATLAS Test 15 was conducted from 0 s to the end of the test.

Therefore, two input files for each ATLAS test 09 and 11 are required, and only one file is needed for ATLAS test 15 as follows.

ATLAS test 09:

1. ATLAS9-090320-annulus-t2.i Input file for 0 to 200 s

2. t_ATLAS09-090320-annulus_t2_126.i Input file for 200 s to end of test

   Code calculation using input file for 200 s to the end of the test needs restart file of calculation result using input file for 0 to 200 s.

ATLAS test 11:

1. ATLAS11-090923-annulus.i Input file for 0 to 210 s

2. t_ATLAS11-090923-annulus_126.i Input file for 210 s to end of test

   Code calculation using input file for 210 s to the end of test needs restart file of calculation result using input file for 0 to 210 s.

ATLAS test 15:

1. ATLAS-LB15-U10_126

Input decks for ATLAS test assessment will be submitted in face-to-face meeting because ERR system has no download function.

Impact on DCD

There is no impact on the DCD.

Impact on PRA

There is no impact on the PRA.

Impact on Technical Specifications

There is no impact on the Technical Specifications.

Impact on Technical/Topical/Environmental Report

There is no impact on any Technical, Topical, or Environmental Report.

RESPONSE TO AUDIT ISSUES

APR1400 Topical Reports

Korea Electric Power Corporation / Korea Hydro & Nuclear Power Co., LTD

Docket No. PROJ0782

Review Section	**TR Realistic Evaluation Methodology for LBLOCA of the APR1400**
Application Section	**Topical Report: APR1400-F-A-TR-12004 Realistic Evaluation Methodology for Large-Break LOCA of the APR1400**
Issue Date	**08/13/2015**

Audit Issues No. 82

NUREG-0800, Section 15.0.2 establishes review guidance related to the documentation of the evaluation model. The scaling of the ATLAS facility is briefly discussed in Section 2.1 of Appendix E. Describe how the metal mass to fluid volume ratio was scaled in order to correctly capture the stored energy release and the downcomer boiling phenomena.

Response

NUREG-0800, Section 15.0.2 establishes review guidance related to the documentation of the evaluation model. The scaling of the ATLAS facility is briefly discussed in Section 2.1 of Appendix E of the topical report. Descriptions of how the metal mass to fluid volume ratio was scaled in order to correctly capture the stored energy release and the downcomer boiling phenomena are as follows.

For the reactor pressure vessel downcomer with an annular shape, the metal mass to fluid volume ratio is proportional to volume ratio and can be expressed by

[ ]TS

where D_i, D_o is the downcomer inner and outer diameter, respectively. L is the height, and t is the vessel thickness. The ratio of the metal mass to fluid volume can be expressed by, assuming the same metal property

[ ]TS

where G is the downcomer gap defined as (D_o-D_i), the subscript R indicates a ratio of a model to a prototype. In order to preserve the stored energy release from the downcomer wall to fluid in the scaled-down model, the ratio, $(t/G)_R$, should be kept to be unit in an ideal condition. It implies that the diameter of the downcomer and the wall thickness should be reduced by the same scaling ratio. However, in the as-built design of ATLAS, the downcomer diameter was intentionally enlarged to have a gap enough to simulate the cap bubble rising in the downcomer region and the wall thickness was increased to be able to withstand high pressure conditions according to the requirement of the ASME B&PV Code, Section VIII, Division II. Consequently, the ratio $(t/G)_R$ of ATLAS becomes [ ]TS It means that the ATLAS downcomer wall has larger stored energy per unit fluid volume than the prototype plant by a factor of [ ]TS A summary of the comparison of the major scaling values is given in Table 1. These scaling conditions provide more conservative condition particularly when the downcomer boiling phenomena are simulated in the ATLAS facility.

Table 1. Summary of the major parameters of the ATLAS facility

TS

Impact on DCD

There is no impact on the DCD.

Impact on PRA

There is no impact on the PRA.

Impact on Technical Specifications

There is no impact on the Technical Specifications.

Impact on Technical/Topical/Environmental Report

There is no impact on any Technical, Topical, or Environmental Report.

RESPONSE TO AUDIT ISSUES

APR1400 Topical Reports

Korea Electric Power Corporation / Korea Hydro & Nuclear Power Co., LTD

Docket No. PROJ0782

Review Section	**TR Realistic Evaluation Methodology for LBLOCA of the APR1400**
Application Section	**Topical Report: APR1400-F-A-TR-12004 Realistic Evaluation Methodology for Large-Break LOCA of the APR1400**
Issue Date	**08/13/2015**

Audit Issues No. 83

The guidance in RG 1.157, Section 3.16.2 establishes acceptable controls for the data comparisons necessary to justify best estimate models. Section 2.2 of Appendix E states that the conditions at the start of the reflood period of the APR1400 LBLOCA were given as the initial and boundary conditions. Presumably, these conditions are determined based on code calculations. Confirm this understanding and clarify whether RELAP5/MOD3.3/K is used to determine the initial conditions. If so, describe the assessments used to validate the code's prediction of the phenomena during the blowdown period. Include details about the accuracy of code prediction of depressurization, levels and break flow discharge during the blowdown period against corresponding data.

Response

The initial and boundary conditions of the ATLAS tests at the start of the reflood period of the APR1400 LBLOCA were obtained by [ ]TS However, the code prediction during blowdown and refill periods is not different from RELAP5/MOD3.3/K because [ ]TS Therefore, the code assessments for blowdown period in Appendix C and D of the topical report is valid for checking the adequateness of the code used in determination of the initial condition of the ATLAS tests.

Impact on DCD

There is no impact on the DCD.

Impact on PRA

There is no impact on the PRA.

Impact on Technical Specifications

There is no impact on the Technical Specifications.

Impact on Technical/Topical/Environmental Report

There is no impact on any Technical, Topical, or Environmental Report.

RESPONSE TO AUDIT ISSUES

APR1400 Topical Reports

Korea Electric Power Corporation / Korea Hydro & Nuclear Power Co., LTD

Docket No. PROJ0782

Review Section	**TR Realistic Evaluation Methodology for LBLOCA of the APR1400**
Application Section	**Topical Report: APR1400-F-A-TR-12004 Realistic Evaluation Methodology for Large-Break LOCA of the APR1400**
Issue Date	**08/13/2015**

Audit Issues No. 84

The guidance in RG 1.157, Section 3.16.2 establishes acceptable controls for the data comparisons necessary to justify best estimate models. Figures 2-9 and 2-15 of Appendix E show the SIT-FD injection rate (high- and low-flow) for the ATLAS tests 9 and 11. The tests start from the reflood period and therefore, as shown in Figure 2-6 of Appendix E, a portion of the SIT-FD flow is not considered. Explain how the time at which SIT-FD injection occur and therefore, the injection rate in the tests is determined. Also explain the reason for the difference in the injection rate between the four SITs as seen in Figure 2-9 and especially, for Figure 2-15.

Response

As described in the response of audit issue no. 83, the initial condition of the reflood test and the injection rate of the SIT-FD in the ATLAS tests were determined using the [ ]^{TS} The condition determined by the code is experimentally achieved as follows.

As the main objective of the ATLAS tests 9 and 11 was to simulate the reflood phase only, the initial portion of the SIT-FD flow during the refill period was excluded in the ATLAS tests as shown in Figure 2-6 of Appendix E. The initial condition of the ATLAS reflood test was obtained along a series of preparation steps: (1) filling, (2) heating, (3) steady state, (4) draining, (5) break open, (6) power restart, (7) SIT injection, and (8) SIP injection.

In the draining step among them, when the water level in the core and downcomer region reached at specified levels, the core power increased linearly from 0 to specified heater powers. The power maintained at a specified value until the maximum heater rod surface temperature reached a specified surface temperature of 450 ^{o}C, which generated a SIT injection signal. The specified core and downcomer levels for test 9 and 11 were [ ]^{TS}, respectively. The specified core powers for test 9 and 11 were [ ]^{TS}, respectively.

From the code predictions to determine the initial condition of the tests, it was assumed that the reflood period started [ ]^{TS} When the reflood period was triggered [ ]^{TS}, the core power was controlled to follow the specified ANS73 decay curve multiplied by 1.2 (in the case of test 9) and the ANS79 curve multiplied by 1.02 (in the case of test 11), respectively.

The injection rates between the four SITs seen in Figure 2-9 and Figure 2-15 of Appendix E show a little differences with each other. Mainly these differences come from the small differences in the orifice diameter and the opening of flow control valves. Although extensive preliminary tests were done for four SITs in order to obtain a consistent injection behavior, small differences in the orifice hole size, initial water level, initial SIT pressure and pressure drop across the flow control valve resulted in such a difference in the actual test. Such differences among four SITs are within reasonably acceptable range, taking into account of the inherent characteristics of the most integral effect tests.

Impact on DCD

There is no impact on the DCD.

Impact on PRA

There is no impact on the PRA.

Impact on Technical Specifications

There is no impact on the Technical Specifications.

Impact on Technical/Topical/Environmental Report

There is no impact on any Technical, Topical, or Environmental Report.

RESPONSE TO AUDIT ISSUES

APR1400 Topical Reports

Korea Electric Power Corporation / Korea Hydro & Nuclear Power Co., LTD

Docket No. PROJ0782

Review Section	**TR Realistic Evaluation Methodology for LBLOCA of the APR1400**
Application Section	**Topical Report: APR1400-F-A-TR-12004 Realistic Evaluation Methodology for Large-Break LOCA of the APR1400**
Issue Date	**08/13/2015**

Audit Issues No. 86

The guidance in RG 1.157, Section 3.16.2 establishes acceptable controls for the data comparisons necessary to justify the applicability of the best estimate models. Table 1 of Appendix G provides the downcomer boiling test conditions. Describe how these test conditions correspond to those that would exist in the APR1400 during the late reflood period. Include the transient time at which the test wall heat fluxes correspond to the downcomer/core barrel heat fluxes, expected temperature/pressure of the downcomer coolant, and the expected scaled high pressure safety injection flow at these times.

Response

The basis of selected test conditions for the DOBO is described in reference [1]. The reference states that the experimental condition was obtained by applying Table 1 to RELAP5 results. The test condition was determined from the RELAP5 analysis results at 250 seconds after the initiation of an LBLOCA. [

]^{TS} In the test, the ECC water injected via a DVI nozzle into the test section simulates the penetrating water from the cold-leg level to the lower downcomer region in the APR1400. Therefore, the temperature of the injected ECC water was maintained the same as that of the ECC water where the mixture level exists in the downcomer of the APR1400. [

]^{TS} In the test, the heat flux was changed to cover this range.

Since this test was performed in the development phase of APR1400, the test conditions such as system pressure, ECC flow rate, and wall heat flux might differ from the current APR1400 LBLOCA conditions. Nonetheless, the DOBO is a quasi-steady state test and observes boiling mechanism and fluid distribution with assumption that coolant boiling occurs by residual heat of the wall. The assessment in Appendix G is only used to confirm whether the code can appropriately predict boiling occurrence, boiling location, and fluid distribution in the downcomer with boiling condition. Boiling occurrence in the plant is not the point of this assessment.

Table 1 Scaling Ratio of the DOBO Facility

Parameter	Scaling Law	
	Scaling Ratio	DOBO
Elevation	1	1
Gap Size Ratio	1	1
Width Ratio	l_R	1/47.08
Area Ratio	a_R	1/47.08
Volume Ratio	a_R	1/47.08
Velocity Ratio	1	1
Flow Rate Ratio	a_R	1/47.08
Gravity Ratio	1	1
Pressure Ratio	1	1
Temperature Ratio	1	1

Reference

[1] B.J. Yun, et al., “Downcomer Boiling Phenomena during the Reflood Phase of a Large-Break LOCA for the APR1400,” Nuclear Engineering and Design 238, 2008, 2064-2074

Impact on DCD

There is no impact on the DCD.

Impact on PRA

There is no impact on the PRA.

Impact on Technical Specifications

There is no impact on the Technical Specifications.

Impact on Technical/Topical/Environmental Report

There is no impact on any Technical, Topical, or Environmental Report.

RESPONSE TO AUDIT ISSUES

APR1400 Topical Reports

Korea Electric Power Corporation / Korea Hydro & Nuclear Power Co., LTD

Docket No. PROJ0782

Review Section	**TR Realistic Evaluation Methodology for LBLOCA of the APR1400**
Application Section	**Topical Report: APR1400-F-A-TR-12004 Realistic Evaluation Methodology for Large-Break LOCA of the APR1400**
Issue Date	**08/13/2015**

Audit Issues No. 87

The guidance in RG 1.157, Section 3.16.2 establishes acceptable controls for the data comparisons necessary to justify the applicability of the best estimate models. Provide the fluid volume temperatures and the void fractions for each of the control volumes in both stacks of the dual stack RELAP5 model (i.e., two channel modeling) for the downcomer boiling test.

Response

Figure 1 and Figure 2 show the fluid volume temperature and the void fractions for each of the control volumes in both stacks of the dual stack RELAP5 model for the downcomer boiling test.

TS

Figure 1. Fluid Temperature of Control Volumes for Dual Stack RELAP5 Model

TS

Figure 2. Void Fraction of Control Volumes for Dual Stack RELAP5 Model

Impact on DCD

There is no impact to the DCD.

Impact on PRA

There is no impact on the PRA.

Impact on Technical Specifications

There is no impact on the Technical Specifications.

Impact on Technical/Topical/Environmental Report

There is no impact on any Technical, Topical, or Environmental Report.

RESPONSE TO AUDIT ISSUES

APR1400 Topical Reports

Korea Electric Power Corporation / Korea Hydro & Nuclear Power Co., LTD

Docket No. PROJ0782

Review Section	**TR Realistic Evaluation Methodology for LBLOCA of the APR1400**
Application Section	**Topical Report: APR1400-F-A-TR-12004 Realistic Evaluation Methodology for Large-Break LOCA of the APR1400**
Issue Date	**08/13/2015**

Audit Issues No. 88

The guidance in RG 1.157, Section 3.16.2 establishes acceptable controls for the data comparisons necessary to justify the applicability of the best estimate models. Differences are noted in the details of the total, liquid and therefore, gas volume for each SIT- FD between the RELAP5 base input model and the VAPER facility. [

]TS

a. Provide the technical specification values for the total volume, the initial volume of liquid and the liquid volume below the standpipe and the gas volume of a single SIT-FD.

b. Justify the use of the volumes cited in the VAPER facility and the applicability of the corresponding data to the APR1400 plant.

Response

a)

The design data of APR1400 SIT-FD are slightly different with those of VAPER facility. The design data of APR1400 SIT-FD, VAPER, and RELAP5 Input of the topical report are summarized in Table 1.

SIT-FD for the APR1400

SIT-FD geometry data and nominal data of initial conditions for APR1400 are as follows.

[

]TS

As mentioned above, internal volume does not consider any structures installed in the tank. If internal structure is considered and calculate inside volume as three parts (top elliptical, cylinder above fluidic upper plat, and bottom elliptical below fluidic device upper plate) separately, free volumes for three parts are below.

[

]TS

Bottom elliptical below fluidic device upper plate is assumed as dead volume which means that liquid volume in the dead volume is not available. Therefore, total available free volume can be calculated as below.

[ ]TS

Since it is assumed that mass flow rate of SIT-FD is changed when liquid level of the SIT-FD decreases below the top of the standpipe, liquid volume below the standpipe can be calculated by sum of standpipe inner, standpipe outside, and fluidic device inside volumes as follow.

[

]TS

Since SIT-FD is modeled using two valves in RELAP5 as described in Appendix H, the operation of valves require overlap region for stability of code calculation. Thus, following values to close or open the valve are used.

[

]TS

Since nominal liquid volume means available liquid volume, gas volume in the SIT-FD can be calculated using total free volume and nominal liquid volume.

[ ]TS

SIT-FD for the VAPER Test

Total water in the SIT-FD of Table 1-2 in Appendix H is reference condition and water volume inside of fluidic device is not considered. Initial conditions for the VAPER test were calculated as follows.

[

]TS

Above total water volume includes dead zone water volume, specifically water volume below the top of FD (a) includes dead zone water volume. [

]TS

[

]TS The longer stand pipe height in APR1400 is designed to extend small flow injection period and is advantageous for safety in comparison to the VAPER test. The difference of stand pipe height causes the difference of water volume below top of stand pipe.

On the other hand, the effects of stand pipe height were investigated by the VAPER test facility, and the results show that the effects of stand pipe height on the pressure loss coefficient of SIT-FD are insignificant as described in reference [5].

b)

As mentioned previous response a), available water volume difference between VAPER tests and APR1400 is caused by stand pipe height. And the effects of stand pipe height to the pressure loss coefficient of SIT-FD are insignificant as described in reference [5]. Therefore, it is concluded that the VAPER test data are applicable to the APR1400 analysis.

Table 1. The Design Data of SIT-FD and RELAP5 Input Values TS

Reference

[1] “APR1400 Design Control Document Tier 2: Chapter 6 Engineered Safety Features,” APR1400-K-X-FS-14002-NP, Rev 0, KEPCO & KHNP, December 2014.

[2] “Fluid System and Component Engineering Design Data for Plant Safety, Containment and Performance Analyses,” 11A60-FS-DD012, Rev 2, KEPCO E&C, November 2014.

[3] “Input Modifications for APR1400,” APR1400-F-A-TM-12030-P, Rev 0, KNF, December 2012.

[4] KAERI, “Fluidic Device Performance Test Using the VAPER Test Facility,” VAPER-QLR-005-rev01, July 2004.

[5] KHNP, “Fluidic Device Design for the APR1400,” APR1400-Z-M-TR-12003-P Rev. 0, 2012.

Impact on DCD

There is no impact on the DCD.

Impact on PRA

There is no impact on the PRA.

Impact on Technical Specifications

There is no impact on the Technical Specifications.

Impact on Technical/Topical/Environmental Report

There is no impact on any Technical, Topical, or Environmental Report.

RESPONSE TO AUDIT ISSUES

APR1400 Topical Reports

Korea Electric Power Corporation / Korea Hydro & Nuclear Power Co., LTD

Docket No. PROJ0782

Review Section	**TR Realistic Evaluation Methodology for LBLOCA of the APR1400**
Application Section	**Topical Report: APR1400-F-A-TR-12004 Realistic Evaluation Methodology for Large-Break LOCA of the APR1400**
Issue Date	**08/13/2015**

Audit Issues No. 89

The guidance in RG 1.157, Section 3.16.2 establishes acceptable controls for the data comparisons necessary to justify the applicability of the best estimate models. Appendix H Section 1.3.1 briefly discusses the air release behavior for Cases 01-01 through 01-03 referring to Figure 1-7 of Appendix H. That figure shows two peaks in the air release behavior. Section 1.3.2 of Appendix H discusses the air release behavior for Case 01-04 referring to Figure 1-11 of the same Appendix.

a. Provide the physical reason(s) for the double-peaked behavior of air release for Cases 01-01 through 01-03.

b. Provide a discussion of the noncondensible transport, the impact on the flow pattern, and the effect on the heat transfer.

Response

a)

In the SIT-FD, there is no flow path through the supply port after the water level drops below the top of the stand pipe, and the pressure drop occurs only through the control ports. The water level inside the stand pipe becomes lower than the water level in the SIT to compensate for the pressure drop and to balance the pressure difference between the vortex chamber and the top of the SIT. As a result, the water in the stand pipe becomes depleted before the water in the SIT is completely discharged.

The air in the SIT can be released through the stand pipe and vortex chamber when the water level in the stand pipe drops down to the top of the supply nozzles in the vortex chamber, which corresponds to the time of about 100 sec in Figure 1-7 of Appendix H.

It is expected that the flow in the vortex chamber changes from single phase water swirling flow to two-phase air-water swirling flow after the inception of the air release at around 100 sec. The two-phase swirling flow in the vortex chamber is so much complicated that even up-to-date CFD analysis has great difficulty in predicting the precise behavior.

The air release rate is governed by the pressure drop characteristics in the vortex chamber. Both the water level and pressure in the SIT decrease as time elapses following the air release. The decrease in the water level affects the opening ratio of the supply nozzles in the vortex chamber, which probably promotes the air release rate up to a certain degree. On the other hand, the decrease in the SIT pressure definitely reduces the air release rate. The first peak at around 125 sec resulted from the balance of the above two factors.

The second peak starts from around 160 sec, which corresponds to the time when the water in the SIT becomes completely depleted. That is, the air in the SIT is released not only from the stand pipe and supply nozzles but also from the control ports and control nozzles, and the flow in the vortex chamber becomes single phase flow of air. The air release rate is determined by the pressure difference between the SIT and the downstream piping of the SIT. The air release is terminated at around 195 sec when the pressure difference becomes insignificant.

Figures 1 ~ 3 illustrate the structure of the APR1400 SIT-FD and the vortex chamber in the Fluidic Device of the APR1400 SIT.

b)

The noncondensable transport phenomenon is described in the response to the current issue a.

The air release behavior of the SIT-FD can affect the ECC bypass behavior due to the condensation decrease by noncondensable gas existence. However, the effect on the flow pattern and heat transfer in the downcomer region will become negligible soon, because the noncondensable gas introduced to the downcomer will vanish eventually.

In general, the downcomer water level can be pushed down abruptly by the noncondensable gas release after the depletion of the SIT water. This will enhance the core quenching and thus, may have some effects on the core quenching behavior. The noncondensable gas release from the conventional SIT would be more favorable to the core quenching.

The noncondensable transport is hard to simulate using the system code such as RELAP5 and even using the up-to-date CFD analysis. However, the impact of noncondensable gas release behavior observed in VAPER test are evaluated in the modeling of the SIT-FDs as described in Appendix H of the topical report.

Table 1 Test Matrix for additional LBLOCA tests

TS

TS

Figure 1 Structure of the APR1400 SIT installed with the Fluidic Device

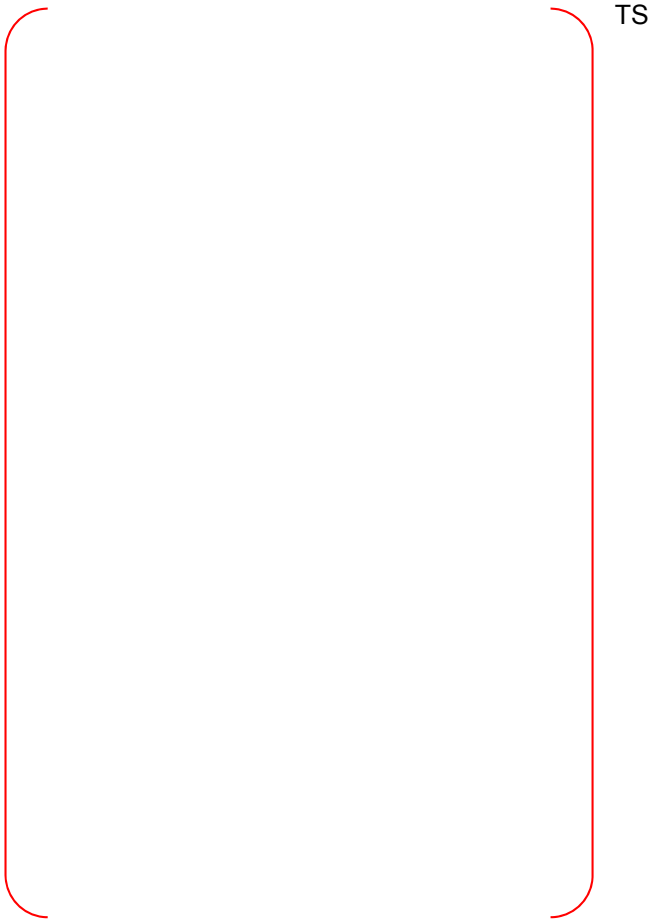

Figure 2 Structure of the Fluidic Device

Figure 3 Typical flow pattern in the vortex chamber at small injection flow rate condition

Impact on DCD

There is no impact on the DCD.

Impact on PRA

There is no impact on the PRA.

Impact on Technical Specifications

There is no impact on the Technical Specifications.

Impact on Technical/Topical/Environmental Report

There is no impact on any Technical, Topical, or Environmental Report.

RESPONSE TO AUDIT ISSUES

APR1400 Topical Reports

Korea Electric Power Corporation / Korea Hydro & Nuclear Power Co., LTD

Docket No. PROJ0782

Review Section	**TR Realistic Evaluation Methodology for LBLOCA of the APR1400**
Application Section	**Topical Report: APR1400-F-A-TR-12004 Realistic Evaluation Methodology for Large-Break LOCA of the APR1400**
Issue Date	**08/13/2015**

Audit Issues No. 90 a through g

The guidance in RG 1.157, Section 3.16.2 establishes acceptable controls for the data comparisons necessary to justify the applicability of the best estimate models. Address the following concerns regarding the SIT-FD tests and K-factor determination discussed in Appendix H:

a. The Section 5.1.5 of the topical report states that [ ]^{TS} The range selected for the sensitivities, as documented in Section 3 of Appendix H, is narrow as compared to the scatter in the experimental results shown in Figure 1-2 of Appendix H for the high and low-injection period. The scatter in the low-flow K-factor for the experimental results is [ ]^{TS} These K-factors are much higher than the design values which are supposed to bound the K-factor for the SIT-FD. Explain the rationale and basis for the selection of the SIT-FD K-factors.

b. Figure 1-2 in Appendix H shows the selected SIT-FD K-factor values based on the sensitivity calculations. [ ]^{TS} is lower than that shown in Figure 1-2 of Appendix H. Justify the use of the lower K factor for the APR1400 plant calculations.

c. Table 3-1 of Appendix H defined the “K” sensitivity study range and also the fluidic device high flow and low flow loss coefficient design requirements. Demonstrate that either the manufacturing tolerance of the device will result in loss coefficients within the defined range, or, the bounding K values based on LOCA analyses can greatly cover the K value uncertainties due to the manufacturing tolerance.

d. Figure 1-2 in Appendix H shows a large number of data points and large variations in the K-factor determination. However, Figure 1-5 of Appendix H does not show a similar number of data points and variation for the SIT-FD level. Explain the reason for these differences.

e. The initial SIT-FD water temperature for the VAPER tests listed in Table 1-3 of Appendix H is 5°C to 6°C which is lower than the operating temperature range of 10°C to 50°C according to Table 6.3.2-1 of the APR1400 DCD. Provide the justification for such a low initial SIT-FD water temperature. Also discuss the impact of the initial water temperature on the non-condensable gas release behavior near the end of SIT injection in the test.

f. According to Table 1-2 of Appendix H, the exit pressure for the SIT-FD in the VAPER tests (e.g., the stock tank pressure) is atmospheric for all tests. The RPV pressure during a LBLOCA is higher than atmospheric pressure at the time of SIT injection. This is also demonstrated by the results of the Applicant's simulation studies (see Figure 5-12 of the topical report). Therefore, the exit pressure boundary condition in the VAPER tests (especially Cases 01-01 through 01-03) results in a higher pressure difference between the SIT tank and the exit as compared to that during a LBLOCA. Provide the rationale for the selected boundary pressures in the tests as compared to the prototypical pressure boundary conditions, and the impact of the low pressure in the test on the SIT-FD high and low-flow delivery and K-factor determination in Appendix H Figure 1-2.

g. Figure 3-1 of Appendix H shows noticeable variation of the maximum SIT-FD flow which is not reflected in the PCT prediction shown in Figure 3-5 in Appendix H. However, the ECCS bypass bias does not appear to be factored into the sensitivity in Section 3 of Appendix H. Clarify whether the ECCS bypass bias was included in the SIT-FD K-factor sensitivities.

Response

a)

The K-factor ranges for high and low flow injection are determined by the requirements of the SIT-FD described in reference [1], and the VAPER test aims to verify whether the performance of the fluidic device satisfies the requirements.

Experimental data in Figure 1-2 of Appendix H are measured for whole test period, so the variations of the experimental data are caused by oscillation of the measurement data. Thus, it is reasonable to use averaged K-factor values of all tests for high and low flow injection region separately to confirm the performance of the fluidic device. [

]TS

In Appendix H, it is concluded that averaged experiment results satisfied the requirements of the SIT-FD and the representative K-factor values described in Section 1.2 of Appendix H provided reasonable code assessment results on the VAPER tests.

b)

The K-factor is calculated by following equation.

[ ] TS Equation (4.3-2) of Reference [1]

where, K_{FD}: pressure loss coefficient of the FD

ΔP_{FD}: pressure drop across the FD (Pa)

U_{SI}: area averaged velocity of SIT water (m/s)

A_{Pipe}: cross-sectional area of the SIT discharge line (m^2)

The K-factors for the APR1400 SIT-FD are different from those of the VAPER test because of different pipe area. The relation between K-factor for the APR1400 and K-factor for the VAPER test is as follows:

[ ] TS

Equation (4-4) of Reference [4] in the topical report

Hence, [

]TS

c)

The K-factor ranges of the SIT-FD in Appendix H are determined based on the design requirements described in reference [1]. The requirements include the K-factor specification of

the fluidic device and also the pressure loss coefficient of the surgeline to the RPV. The K-factor specification should include the uncertainty of the K-factor due to the manufacturing tolerance, because this is the requirement of the manufactured SIT-FD. Therefore, it is concluded that the determined K-factor ranges based on the requirement can cover uncertainties due to the manufacturing tolerance.

d)

Figure 1-6 of Appendix H does not contain whole experimental data because of readability of figure and experimental data of SIT water level has small variations.

e)

The effects of the temperature variations on the performance of the fluidic device are negligible because the variations of water properties for operating temperature ranges are not significant. Therefore water temperature was not considered as initial condition for the test.

Initial water temperature can affect the heat transfer to the non-condensable gas during SIT-FD injection. It is natural that low initial water temperature has low heat transfer rate to the gas phase, thus gas pressure near the end of SIT-FD injection could be lower than that of relatively high temperature water case. However, since the gas phase temperature during SIT-FD injection decreases much lower than the initial water temperature, the effects of initial water temperature on the behavior of non-condensable gas release are not significant.

f)

As shown in Table 1-3 of Appendix H, Case-01-04 test is conducted to evaluate the impact of pressure difference on the K-factors of the SIT-FD. Calculated K-factors for all test cases are presented in reference [1], and it shows that pressure difference has insignificant effects on the K-factors for both of high and low injection periods.

g)

Since this sensitivity study does not focus on the total PCT quantification but the effects of the SIT-FD K-factors to the PCT, the ECC bypass bias is not factored.

Reference

[1] “Fluidic Device Design for the APR1400,” APR1400-Z-M-TR-12003-P, Rev. 0, KHNP, December 2012.

Impact on DCD

There is no impact on the DCD.

Impact on PRA

There is no impact on the PRA.

Impact on Technical Specifications

There is no impact on the Technical Specifications.

Impact on Technical/Topical/Environmental Report

There is no impact on any Technical, Topical, or Environmental Report.

RESPONSE TO AUDIT ISSUES

APR1400 Topical Reports

Korea Electric Power Corporation / Korea Hydro & Nuclear Power Co., LTD

Docket No. PROJ0782

Review Section	**TR Realistic Evaluation Methodology for LBLOCA of the APR1400**
Application Section	**Topical Report: APR1400-F-A-TR-12004 Realistic Evaluation Methodology for Large-Break LOCA of the APR1400**
Issue Date	**08/13/2015**

Audit Issues No. 90-h

The guidance in RG 1.157, Section 3.16.2 establishes acceptable controls for the data comparisons necessary to justify the applicability of the best estimate models. Address the following concerns regarding the SIT-FD tests and K-factor determination discussed in Appendix H:

h. Describe the type and number of valves in the line connecting the SIT-FD to the RPV in the actual APR1400 plant. Furthermore, explain whether all the valves have been represented in the VAPER tests. If not, justify the exclusion of the valves and their corresponding loss coefficients in determining the SIT-FD K-factor and injection rate.

Response

The following Figure 1 (Figure 6.3.2-1 in Tier 2 DCD) shows the P&ID of the line connecting the SIT-FD to the RPV in the APR1400 plant. [ ]TS.
The actual APR1400 plants, Shin-Kori Unit 3 and 4 built in Korea, have the same configuration.

The total K-factor is [
]TS The K-factor of the piping line can be evaluated without difficulty based on the previous experiences in designing the nuclear power plant. However, the SIT-FD is the component which was firstly adopted in the APR1400, and the flow structure inside the Fluidic Device is complicated. Therefore, the K-factor of SIT-FD was validated using a full scale test facility, VAPER.

The purpose of the VAPER tests is to validate the K-factor of SIT-FD and [
]TS

TS

Figure 1. P&ID of the line connecting the SIT-FD to the RPV

Impact on DCD

There is no impact on the DCD.

Impact on PRA

There is no impact on the PRA.

Impact on Technical Specifications

There is no impact on the Technical Specifications.

Impact on Technical/Topical/Environmental Report

There is no impact on any Technical, Topical, or Environmental Report.

RESPONSE TO AUDIT ISSUES

APR1400 Topical Reports

Korea Electric Power Corporation / Korea Hydro & Nuclear Power Co., LTD

Docket No. PROJ0782

Review Section	**TR Realistic Evaluation Methodology for LBLOCA of the APR1400**
Application Section	**Topical Report: APR1400-F-A-TR-12004 Realistic Evaluation Methodology for Large-Break LOCA of the APR1400**
Issue Date	**08/13/2015**

Audit Issues No. 91

The guidance in RG 1.157, Section 3.16.2 establishes acceptable controls for the data comparisons necessary to justify the applicability of the best estimate models. Appendix H describes the assessment of RELAP5/MOD3.3/K for the performance of the safety injection tank with the fluidic device installed. Address the following concerns:

a. Figure 1-6 of Appendix H shows the experimental data for the water level (as well as three RELAP5/MOD3.3/K models) as a function of time for three tests in the VAPER test facility. Based on the stand pipe height in Table 1-1 in Appendix H, the water level falls below the top of the standpipe at approximately 50 seconds. However, the rate of water level decrease is seen to change at approximately 35 seconds. Explain this change.

b. Figure 1-7 of Appendix H shows that gas is released beginning at about 105 seconds while the SIT-FD tank level is approximately 1.9 m. Provide a description of the fluid and gas flow patterns in the SIT-FD tank from approximately 100 seconds to 225 seconds.

c. It is difficult to discern between the actual data and the analysis calculations in Figures 1-6 through 1-13 of Appendix H. Provide a comparison of the prediction of each model against the experimental data separately to confirm the Applicant's conclusions.

Response

a)

The disagreement occurred from the difference in the definition of the two levels. The definitions of the two levels are as follows;

- [ ]TS
- [ ]TS

There is another source of the disagreement coming from the Coriolis effect; the fluid is rotating when it sinks due to the Coriolis force. Therefore, the level of the water varies in radial direction due to the characteristics of rotating fluid motion. In the most of the nuclear thermal-hydraulic applications, the Coriolis force is not significant compared to other forces. However, in the specific situation with SIT, the effect of the Coriolis effect become more important. As a result, the water level at the center is lower than that at the near wall. Since the DP tab is installed at the tank wall, actual water level could be lower than the measured data.

The change of water injection rate in the test starts to occur when the water level drops around 5.5 m and it ends when the water level is below around 4.8 m as shown in Figure 1-2 of Appendix H. [ ]TS. Considering the two sources of disagreement stated above, the SIT water level matches with the stand pipe height reasonably well.

b)

When the water level is higher than the top of the standpipe, water can flow through both supply and control ports installed in the fluidic device as shown in Figure 2.2-2 of Reference [1]. Since the standpipe is filled with non-condensable gas at around 100 sec, some of the non-condensable gas can be entrained into vortex chamber of the fluidic device at this time exhibiting gas flow rate from the SIT. After that, water injection flow rate decreases continuously, so drag force to the entrained non-condensable gas by liquid flow is decreased, whereas, buoyancy force of entrained non-condensable gas in the vertical part of surgeline becomes relatively dominant. Non-condensable gas release behavior during 125 sec ~ 150 sec is the result of force balance between drag and buoyancy forces. And non-condensable gas release rate increases after about 150 sec because non-condensable gas can be injected to the stock tank directly. Since experimental data of SIT water level shown in Figure 1-6 of Appendix H includes dead zone volume level, the level no longer decreases after around 160 sec. It means that SIT is empty at this time. Non-condensable gas release rate ends at around 200 sec because pressure in the SIT reaches atmospheric condition at this time as shown in Figure 1-8 of Appendix H.

c)

Figure 1 ~ 4 show SIT water level results for each model separately which is shown in Figure 1-6 of Appendix H.

Figure 5 ~ 8 show air release rate results for each model separately which is shown in Figure 1-7 of Appendix H.

Figure 9 ~ 12 show SIT pressure results for each model separately which is shown in Figure 1-8 of Appendix H.

Figure 13 ~ 16 show liquid mass flow rate results for each model separately which is shown in Figure 1-9 of Appendix H.

Figure 17 ~ 20 show SIT water level results for each model separately which is shown in Figure 1-10 of Appendix H.

Figure 21 ~ 24 show air mass flow rate results for each model separately which is shown in Figure 1-11 of Appendix H.

Figure 25 ~ 28 show SIT pressure results for each model separately which is shown in Figure 1-12 of Appendix H.

Figure 29 ~ 32 show liquid mass flow rate results for each model separately which is shown in Figure 1-13 of Appendix H.

Figure 1. SIT Water Level: Test Case-01-01 ~ Case-01-03 (Model A)

Figure 2. SIT Water Level: Test Case-01-01 ~ Case-01-03 (Model B)

Figure 3. SIT Water Level: Test Case-01-01 ~ Case-01-03 (Model C)

Figure 4. SIT Water Level: Test Case-01-01 ~ Case-01-03 (Model D)

Figure 5. Air Release Rate: Test Case-01-01 ~ Case-01-03 (Model A)

Figure 6. Air Release Rate: Test Case-01-01 ~ Case-01-03 (Model B)

Figure 7. Air Release Rate: Test Case-01-01 ~ Case-01-03 (Model C)

Figure 8. Air Release Rate: Test Case-01-01 ~ Case-01-03 (Model D)

Figure 9. Pressure at Top of the Tank: Test Case-01-01 ~ Case-01-03 (Model A)

Figure 10. Pressure at Top of the Tank: Test Case-01-01 ~ Case-01-03 (Model B)

Figure 11. Pressure at Top of the Tank: Test Case-01-01 ~ Case-01-03 (Model C)

Figure 12. Pressure at Top of the Tank: Test Case-01-01 ~ Case-01-03 (Model D)

Figure 13. Liquid Mass Flow Rate: Test Case-01-01 ~ Case-01-03 (Model A)

Figure 14. Liquid Mass Flow Rate: Test Case-01-01 ~ Case-01-03 (Model B)

Figure 15. Liquid Mass Flow Rate: Test Case-01-01 ~ Case-01-03 (Model C)

Figure 16. Liquid Mass Flow Rate: Test Case-01-01 ~ Case-01-03 (Model D)

Figure 17. SIT Water Level: Test Case-01-04 (Model A)

Figure 18. SIT Water Level: Test Case-01-04 (Model B)

Figure 19. SIT Water Level: Test Case-01-04 (Model C)

Figure 20. SIT Water Level: Test Case-01-04 (Model D)

Figure 21. Air Mass Flow Rate: Test Case-01-04 (Model A)

Figure 22. Air Mass Flow Rate: Test Case-01-04 (Model B)

Figure 23. Air Mass Flow Rate: Test Case-01-04 (Model C)

Figure 24. Air Mass Flow Rate: Test Case-01-04 (Model D)

Figure 25. Pressure at Top of the Tank: Test Case-01-04 (Model A)

Figure 26. Pressure at Top of the Tank: Test Case-01-04 (Model B)

Figure 27. Pressure at Top of the Tank: Test Case-01-04 (Model C)

Figure 28. Pressure at Top of the Tank: Test Case-01-04 (Model D)

Figure 29. Liquid Mass Flow Rate: Test Case-01-04 (Model A)

Figure 30. Liquid Mass Flow Rate: Test Case-01-04 (Model B)

Figure 31. Liquid Mass Flow Rate: Test Case-01-04 (Model C)

Figure 32. Liquid Mass Flow Rate: Test Case-01-04 (Model D)

Impact on DCD

There is no impact on the DCD.

Impact on PRA

There is no impact on the PRA.

Impact on Technical Specifications

There is no impact on the Technical Specifications.

Impact on Technical/Topical/Environmental Report

There is no impact on any Technical, Topical, or Environmental Report.

RESPONSE TO AUDIT ISSUES

APR1400 Topical Reports

Korea Electric Power Corporation / Korea Hydro & Nuclear Power Co., LTD

Docket No. PROJ0782

Review Section	**TR Realistic Evaluation Methodology for LBLOCA of the APR1400**
Application Section	**Topical Report: APR1400-F-A-TR-12004 Realistic Evaluation Methodology for Large-Break LOCA of the APR1400**
Issue Date	**08/13/2015**

Audit Issues No. 92

The guidance in RG 1.157, Section 2.1.2 establishes acceptable controls for the calculation of the effects of noncondensible gases on the results of best estimate analysis. The sensitivity of PCT to non-condensable gas injection is documented in Section 2.1 of Appendix H. As part of Case 2 sensitivity studies, the non-condensable gas release from Model D is input to the calculation as a table. Describe how the temperature of the injected gas is represented in the calculations for the Case 2 sensitivities. Further, describe the local pressure and condensation effects of the injected gas and whether these translate into a decrease in the collapsed water level in the lower downcomer and a corresponding increase in the core collapsed water level (Figures 2-4 and 2-5 of Appendix H).

Response

The calculation results of Model D shows gas temperature decrease to 250 K at around 180 sec and recovery to the average value of 420 K as shown in Figure 1. However, Case 2 in Appendix H uses a constant value of 300 K as the gas phase temperature due to the two reasons: very low temperature of gas phase frequently causes calculation failure and the effects of gas phase temperature are insignificant.

Figure 2 through Figure 4 show sensitivity calculation results of various constant non-condensable gas temperatures. Representative constant non-condensable gas temperatures of 274 K, 300 K and 350 K are selected and the sensitivity calculation is performed for Case 2 with SIT-FD Model A in Section 2 of Appendix H. Figure 2 through Figure 4 show the sensitivity results of downcomer level, core level and clad temperature. Although there are small differences among the results, no particular tendency is observed and overall behaviors are generally similar to each other. Therefore, the effects of non-condensable gas temperature are negligible.

Figure 5 shows the calculation results of the pressure sensitivity at the injection point of DVI. In this figure, definitions of ‘Model A’, ‘Case 1’ and ‘Case 2’ in the legend are the same as those of Appendix H. Since non-condensable gas starts to release at around 180 sec, downcomer pressure increases at this time. And the pressure increment pushes down the water level of the downcomer, thus increase the level in the core region. Pressure behaviors of other modeling methods described in Appendix H are similar to Figure 5.

Figure 6 shows comparison of vapor generation rate resulted in the upper downcomer. Minus value means vapor condensation, and the result shows that non-condensable gas decreases vapor condensation. It means that non-condensable gas tends to decrease vapor condensation and decrement of vapor condensation is one of the factors that increase downcomer pressure.

Consequently, local pressure increment is caused directly by non-condensable gas release and indirectly by subsequent decrement of vapor condensation. And increment of downcomer pressure increases driving force of ECCW to the core region.

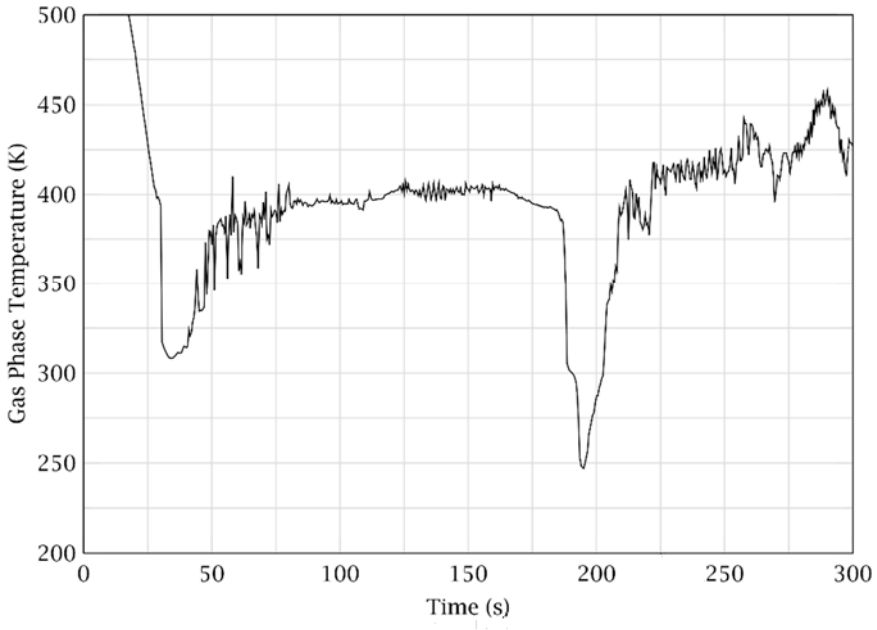

Figure 1. Gas Phase Temperature

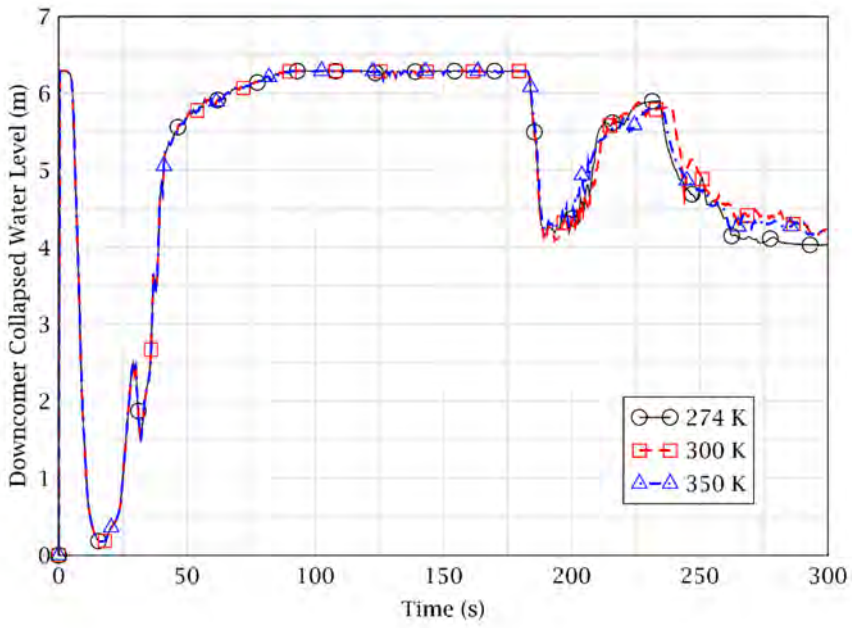

Figure 2. Comparison of Downcomer Collapsed Water Levels

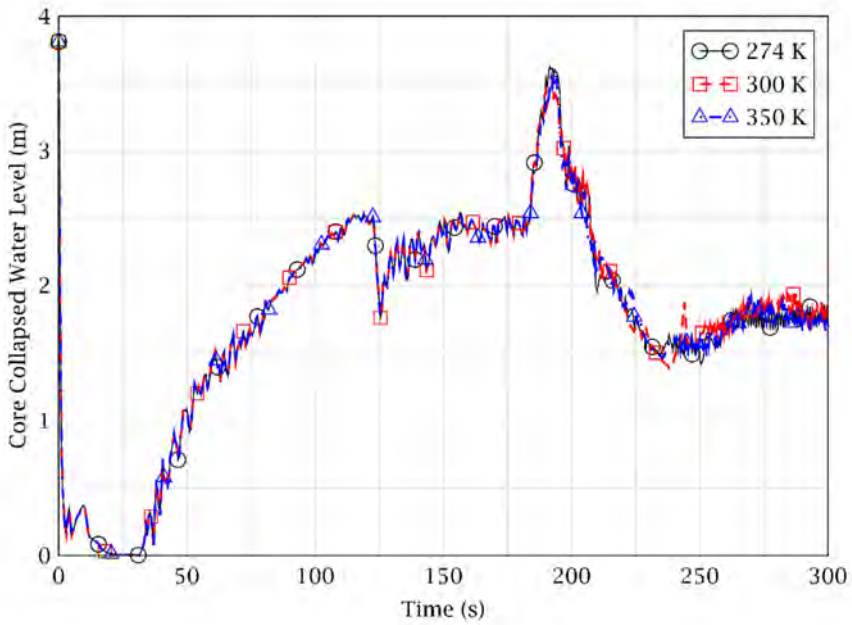

Figure 3. Comparison of Core Collapsed Water Levels

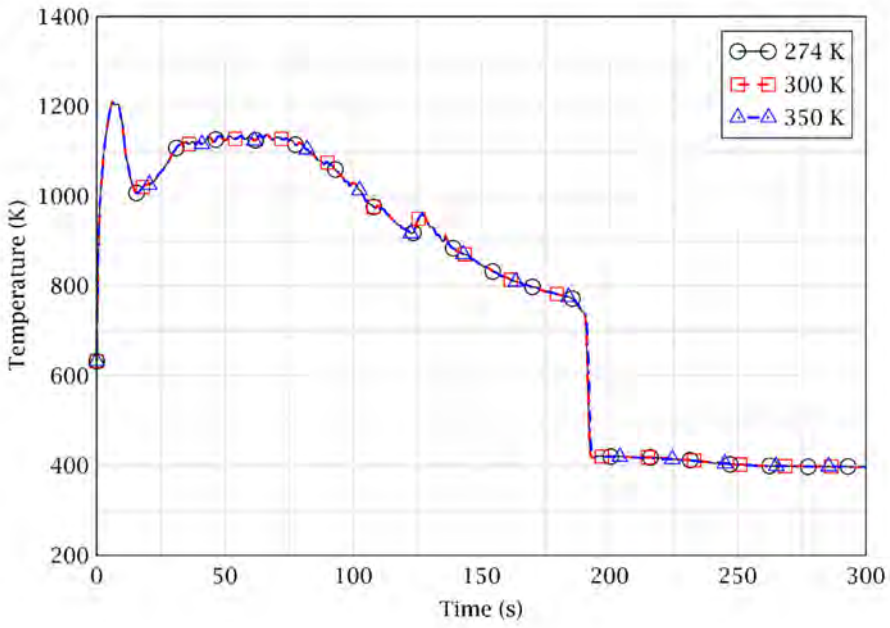

Figure 4. Comparison of Clad Temperatures

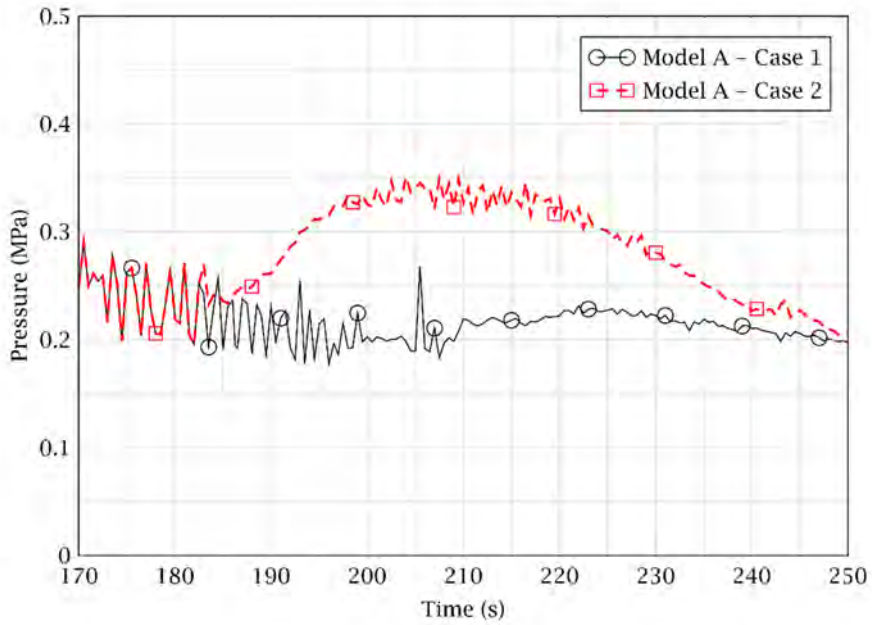

Figure 5. Comparison of Downcomer Pressure Results

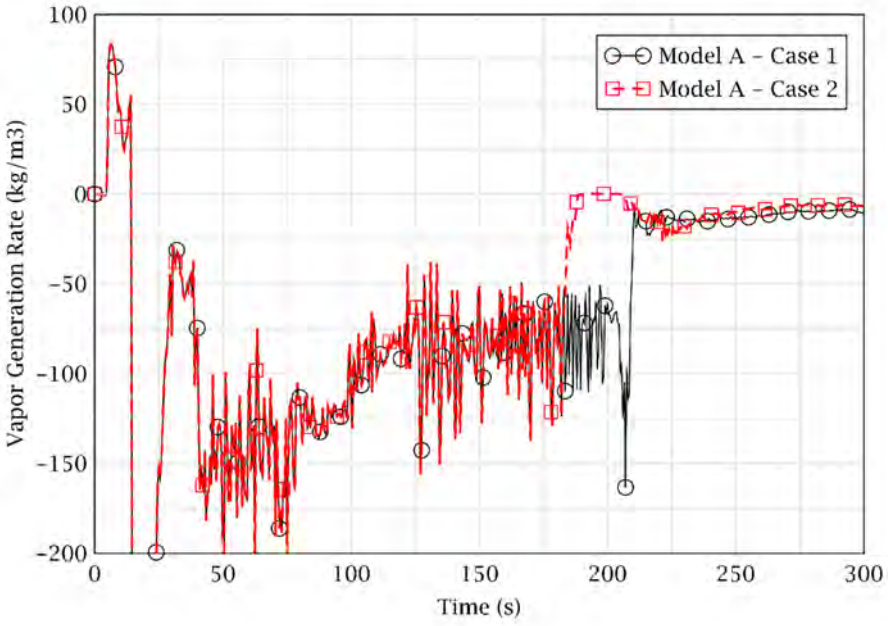

Figure 6. Comparison of Vapor Generation Rates in Upper Downcomer

Impact on DCD

There is no impact on the DCD.

Impact on PRA

There is no impact on the PRA.

Impact on Technical Specifications

There is no impact on the Technical Specifications.

Impact on Technical/Topical/Environmental Report

There is no impact on any Technical, Topical, or Environmental Report.

RESPONSE TO AUDIT ISSUES

APR1400 Topical Reports

Korea Electric Power Corporation / Korea Hydro & Nuclear Power Co., LTD

Docket No. PROJ0782

Review Section	**TR Realistic Evaluation Methodology for LBLOCA of the APR1400**
Application Section	**Topical Report: APR1400-F-A-TR-12004 Realistic Evaluation Methodology for Large-Break LOCA of the APR1400**
Issue Date	**08/13/2015**

Audit Issues No. 93

The guidance in RG 1.157, Section 4 establishes acceptable controls for the estimation of uncertainties. The uncertainty ranges for various parameters used in the actual demonstration calculations used to determine the limiting PCT for a LBLOCA are shown in Appendix J (page J-2). The ranges for the pressurizer pressure, fuel thermal conductivity, and the power peaking factor (Fq) provided in Appendix J are inconsistent with the corresponding ranges listed in Table 5-1 of the topical report. Address these inconsistencies and their impact on the demonstration calculations.

Response

Table 1 attached in this response represents Table 5-1 in the topical report, and the following Table 2 contains page 2 in Appendix J. The [ ]TS in Table 2 was applied to demonstration calculation of the current version of the topical report.

However, LBLOCA analysis with TCD effects will be used [

]TS

Other inconsistencies except [ ]TS are typos.

Reference

[1] “FRAPCON-4.0: A Computer Code for the Calculation of Steady-State, Thermal-Mechanical Behavior of Oxide Fuel Rods for High Burnup,” PNNL-19417, Vol. 1, Rev. 2, U.S.NRC, September 2015.

Table 1. Distributions and Ranges of the Uncertainty Parameters

TS

Table 2. Sampling Output in Appendix J

TS

Impact on DCD

There is no impact on the DCD.

Impact on PRA

There is no impact on the PRA.

Impact on Technical Specifications

There is no impact on the Technical Specifications.

Impact on Technical/Topical/Environmental Report

Topical report will be revised as discussed in this response.

There is no impact on Technical or Environmental Report.

°able 5-1 Distributions and Ranges of the Uncertainty ˇ - 1 eters

TS

title - APR1400 CAREM Topical Report

TS

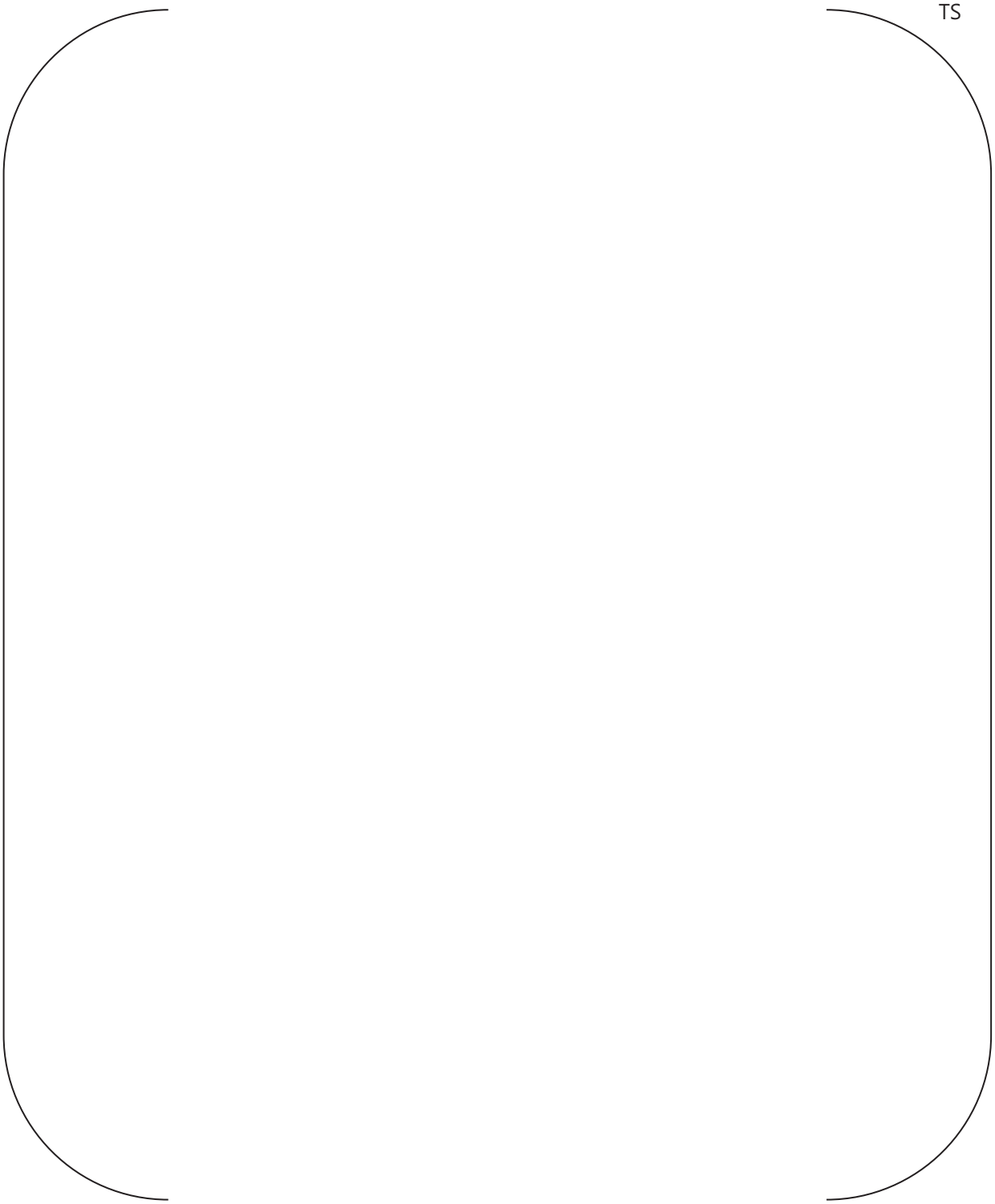

RESPONSE TO AUDIT ISSUES

APR1400 Topical Reports

Korea Electric Power Corporation / Korea Hydro & Nuclear Power Co., LTD

Docket No. PROJ0782

Review Section	**TR Realistic Evaluation Methodology for LBLOCA of the APR1400**
Application Section	**Topical Report: APR1400-F-A-TR-12004 Realistic Evaluation Methodology for Large-Break LOCA of the APR1400**
Issue Date	**08/13/2015**

Audit Issues No. 94

The guidance in NUREG-0800, Section 15.0.2 establishes acceptable controls for the documentation of the evaluation model. Provide the following documents cited in the topical report and in APR1400-F-A-EC-13012-P:

a. “Performance Verification Test for APR1400 Fluidic Device,” A03NJ02, KAERI, February 2005.

b. “Phenomena Identification and Ranking Tabulation Korean Next Generation Reactor Large Break Loss of Coolant Accident,” KINS/INEEL, 2001.

c. “The Best Evaluation Methodology for the Emergency Core Cooling System,” TR-KHNP-002, KEPRI/KHNP, December 2002.

d. “Development of PCT Uncertainty Quantification Methodology, Assessment of Separate Models and Construction of Thermal-Hydraulic Data Banks for Establishment of the Korean ECCS Evaluation Model,” KINS/GR-011, December 1990.

e. Nuclear Technology, V.148, 3, 2004.

f. Nuclear Technology, V.158, 2007.

g. Annals of Nuclear Energy, Vol. 38 (2011), p.1053-1064.

h. “Fluidic Device Design for the APR1400,” APR1400-Z-M -TR-12003-P Rev.0, 2012.

Response

a)

Document mentioned is a proprietary material of Korea Atomic Energy Research Institute, and this material was submitted to U.S.NRC as a proprietary material.

b) and d)

Documents mentioned are proprietary materials of Korea Institute of Nuclear Safety, and these materials were submitted to U.S.NRC as proprietary materials.

c)

Document mentioned is proprietary material of Korea Hydro & Nuclear Power, and this material was submitted to U.S.NRC as a proprietary material.

e), f), and g)

Documents mentioned are papers, and these papers are available in the web site of each journal with subscription fee.

h)

Document mentioned is topical report for safety injection tank equipped with fluidic device, and this report was submitted to U.S.NRC. Non-proprietary version of this report is available in ADAMS with accession number of ML13107A008.

Impact on DCD

There is no impact on the DCD.

Impact on PRA

There is no impact on the PRA.

Impact on Technical Specifications

There is no impact on the Technical Specifications.

Impact on Technical/Topical/Environmental Report

There is no impact on any Technical, Topical, or Environmental Report.

RESPONSE TO AUDIT ISSUES

APR1400 Topical Reports

Korea Electric Power Corporation / Korea Hydro & Nuclear Power Co., LTD

Docket No. PROJ0782

Review Section	**TR Realistic Evaluation Methodology for LBLOCA of the APR1400**
Application Section	**Topical Report: APR1400-F-A-TR-12004 Realistic Evaluation Methodology for Large-Break LOCA of the APR1400**
Issue Date	**08/13/2015**

Audit Issues No. 95

The guidance in RG 1.157, Section 3.8 establishes acceptable controls for the calculation of critical heat flux. Section 4 of the technical report (APR1400-F-C-NR-12001-P) discusses the development of the CHF correlation for the 16x16 PLUS7 fuel assemblies that is to be used for APR1400 analysis. RG 1.157 states “Research has shown that CHF is highly dependent on the fuel rod geometry, local heat flux, and fluid conditions.” [

]TS

Response

System pressure during LBLOCA experiences from about 16 MPa to atmospheric pressure, thus CHF data or correlation which is used in LBLOCA analysis should cover the above pressure ranges. [

]TS

Reference

[1] “KCE-1 Critical Heat Flux Correlation for PLUS7 Thermal Design,” APR1400-F-C-TR-12002-NP, Rev.0, KHNP / KNF, November 2012.

Impact on DCD

There is no impact on the DCD.

Impact on PRA

There is no impact on the PRA.

Impact on Technical Specifications

There is no impact on the Technical Specifications.

Impact on Technical/Topical/Environmental Report

There is no impact on any Technical, Topical, or Environmental Report.

RESPONSE TO AUDIT ISSUES

APR1400 Topical Reports

Korea Electric Power Corporation / Korea Hydro & Nuclear Power Co., LTD

Docket No. PROJ0782

Review Section	**TR Realistic Evaluation Methodology for LBLOCA of the APR1400**
Application Section	**Topical Report: APR1400-F-A-TR-12004 Realistic Evaluation Methodology for Large-Break LOCA of the APR1400**
Issue Date	**08/13/2015**

Audit Issues No. 96

The guidance in RG 1.157, Section 4 establishes acceptable controls for the estimation of uncertainties. The “inlet factor” or form loss coefficient for the limiting channel is identified as one of the uncertainty parameters for minimum departure from nucleate boiling ratio determination in Section 5.2 of the technical report (APR1400-F-C-NR-12001-P, Rev. 0). The uncertainty in the inlet form loss coefficient for the hot channel is expected to be important in the calculation of the reflood PCT. Justify the reason for not including this parameter in the APR1400 LBLOCA uncertainty analysis and the PIRT described in the topical report (APR1400-F-A-TR-12004-P, Rev. 0).

Response

During the reflood period, the quality of the vapor is high and the flow rate is comparatively low. The pressure difference due to the geometry is not so significant because of the low fluid velocity. Therefore, [

]TS

Impact on DCD

There is no impact on the DCD.

Impact on PRA

There is no impact on the PRA.

Impact on Technical Specifications

There is no impact on the Technical Specifications.

Impact on Technical/Topical/Environmental Report

There is no impact on any Technical, Topical, or Environmental Report.

RESPONSE TO AUDIT ISSUES

APR1400 Topical Reports

Korea Electric Power Corporation / Korea Hydro & Nuclear Power Co., LTD

Docket No. PROJ0782

Review Section	**TR Realistic Evaluation Methodology for LBLOCA of the APR1400**
Application Section	**Topical Report: APR1400-F-A-TR-12004 Realistic Evaluation Methodology for Large-Break LOCA of the APR1400**
Issue Date	**08/13/2015**

Audit Issues No. 97

The list of acronyms in the topical report does not contain all the acronyms used in the topical report (e.g., EDG, SI, etc. are missing). An updated list of all acronyms or abbreviations needs to be supplied.

Response

The page for list of acronyms in topical report will be updated as follows.

Acronyms

ACC	***Activation of the Accumulators***
AO	Axial Offset
BE	Best Estimate
BOC	***beginning of cycle***
CAMP	***Code Application Maintenance Program***
CAREM	Code-Accuracy-based Realistic Evaluation Methodology
CCDAS	***Computer-Controlled Digital Data Acquisition System***
CCF	Counter-Current Flow
CHF	Critical Heat Flux
CLI	Cold Leg Injection
CSAU	Code Scaling, Applicability and Uncertainty
CWO	Core Wide Oxidation
DG	Diesel Generator
DNB	Departure from Nucleate Boiling
DOE	***Department of Energy***
DP	***Differential Pressure***
DVI	Direct Vessel Injection
ECC	Emergency Core Cooling
ECCS	Emergency Core Cooling System
ECCW	Emergency Core Cooling Water
EDG	***Emergency Diesel Generator***
EIR	***Eidge Institut fuer Reaktorforschung***
EOB	***End of Blowdown***
EPRI	***Electric Power Research Institute***
FD	Fluidic Device
HPIS	***High-Pressure Injection System***
HPSI	High-Pressure Safety Injection
HTC	***Heat Transfer Coefficient***
ICAP	***International Code Assessment and Application Program***
IET	***Integral Effect Test***
INEEL	***Idaho National Engineering and Environment Laboratory***
INEL	***Idaho National Engineering Laboratory***
IRWST	In-containment Refueling Water Storage Tank
JAERI	***Japan Atomic Energy Research Institute***
JRC	***Joint Research Center***
KAERI	***Korea Atomic Energy Research Institute***
KNGR	***Korea Next Generation Reactor***
LBLOCA	Large-Break Loss-of-Coolant Accident
LHGR	***Linear Heat Generation Rate***
LOCA	Loss-of-Coolant Accident
LPCI	***Low-Pressure Coolant Injection***
LPIS	***Low-Pressure Injection System***
LPSI	Low-Pressure Safety Injection
LPSIP	***Low-Pressure Safety Injection Pump***
MSIV	***Main Steam Isolation Valve***
MSLB	***Main Steam Line Break***
MTC	***Moderator Temperature Coefficient***
ORNL	***Oak Ridge National Laboratory***

PCT	Peak Cladding Temperature
PIRT	Phenomena Identification and Ranking Table
PLO	Peak Local Oxidation
POSRV	***Pilot Operated Safety Relief Valve***
PSI	***Paul Scherrer Institute***
PWR	Pressurized-Water Reactor
PZR	***Pressurizer***
RCP	Reactor Coolant Pump
RCS	Reactor Coolant System
RPV	Reactor Pressure Vessel
SBLOCA	***Small Break Loss-of-Coolant Accident***
SET	***Separate Effect Test***
SG	***Steam Generator***
SGTR	***Steam Generator Tube Rupture***
SI	***Safety Injection***
SIP	Safety Injection Pump
SIS	***Safety Injection System***
SIT	Safety Injection Tank
SKN	***Shin-Kori Nuclear Power Plant***
SRS	Simple-Random Sampling
UGS	***Upper Guide Structure***
UH	***Upper Head***
USNRC	***United States Nuclear Regulatory Commission***
WH	***Westinghouse Corporation***

Impact on DCD

There is no impact on the DCD.

Impact on PRA

There is no impact on the PRA.

Impact on Technical Specifications

There is no impact on the Technical Specifications.

Impact on Technical/Topical/Environmental Report

Topical report will be revised as discussed in this response.

There is no impact on Technical or Environmental Report.

RESPONSE TO AUDIT ISSUES

APR1400 Topical Reports

Korea Electric Power Corporation / Korea Hydro & Nuclear Power Co., LTD

Docket No. PROJ0782

Review Section	**TR Realistic Evaluation Methodology for LBLOCA of the APR1400**
Application Section	**Topical Report: APR1400-F-A-TR-12004 Realistic Evaluation Methodology for Large-Break LOCA of the APR1400**
Issue Date	**08/13/2015**

Audit Issues No. 98

There is a typographical error in the second paragraphs of Section 3.3 of the topical report and Section 1 of Appendix A. The current text incorrectly states “ARP1400” instead of “APR1400.” Also the second paragraph of Section 3.6.2 of the topical report, “CONTEPT4” should read “CONTEMPT4” and in Section 3.6.3 where “CONTEPM4” should read “CONTEMPT4.”

Response

Typos will be corrected and reflected in the future revision of the topical report as follows.

Section No.	Before	After
3.3	The PIRT of APR1400 LBLOCA is based on “KNGR PIRT.” KNGR is initialism for “Korea Next Generation Reactor;” and it was ***ARP***1400’s name during its developmental stage.	The PIRT of APR1400 LBLOCA is based on “KNGR PIRT.” KNGR is initialism for “Korea Next Generation Reactor;” and it was ***APR***1400’s name during its developmental stage.
App. A 1	KNGR was the name for ***ARP***1400 at its early developmental stage.	KNGR was the name for ***APR***1400 at its early developmental stage.
3.6.2	A proper constitutive equation or relation needs to be determined based on code assessment calculations against the database. Typical constitutive equations of the RELAP5/MOD3.3/K and ***CONTEPT4/MOD5*** are listed in Table 3 5 together with the related important phenomena and processes.	A proper constitutive equation or relation needs to be determined based on code assessment calculations against the database. Typical constitutive equations of the RELAP5/MOD3.3/K and ***CONTEMPT4/MOD5*** are listed in Table 3 5 together with the related important phenomena and processes.
3.6.3	In order to obtain accurate and stable solutions of the governing and constitutive equations, consistency, completeness, and well-posedness should be theoretically established and justified through validation calculations. The validity of the numerical methods of RELAP5 and ***CONTEMP4*** were justified by the assessment calculations against various numerical problems, and by separate and integral effect tests. [7][8][9][10]	In order to obtain accurate and stable solutions of the governing and constitutive equations, consistency, completeness, and well-posedness should be theoretically established and justified through validation calculations. The validity of the numerical methods of RELAP5 and ***CONTEMPT4*** were justified by the assessment calculations against various numerical problems, and by separate and integral effect tests. [7][8][9][10]

Impact on DCD

There is no impact on the DCD.

Impact on PRA

There is no impact on the PRA.

Impact on Technical Specifications

There is no impact on the Technical Specifications.

Impact on Technical/Topical/Environmental Report

Topical report will be revised as discussed in this response.

There is no impact on Technical or Environmental Report.

RESPONSE TO AUDIT ISSUES

APR1400 Topical Reports

Korea Electric Power Corporation / Korea Hydro & Nuclear Power Co., LTD

Docket No. PROJ0782

Review Section	**TR Realistic Evaluation Methodology for LBLOCA of the APR1400**
Application Section	**Topical Report: APR1400-F-A-TR-12004 Realistic Evaluation Methodology for Large-Break LOCA of the APR1400**
Issue Date	**08/13/2015**

Audit Issues No. 99

The topical report Table 4-4 lists “RELAP5 document” as the entry in the second column “Tests (SET)” for a couple of phenomena. List the full document reference and to the actual tests used for the assessment.

Response

The table 4-4 in the topical report will be modified in the future revision of topical report as shown in Table 1 of this response.

In Table 1, test assessments, which have "※)" mark in the Table 1, are conducted in this topical report whereas, the others are conducted in RELAP5 code manual.

Table 1. RELAP5/MOD3.3 Model and Tests Used for the Assessment

RELAP5 MOD3.3 Model / Parameter	Tests (SET) → *Tests*
Gap conductance	Power burst
Core decay heat model	***RELAP5 document → 1979 ANS Standard for Decay Heat Power in Light Water Reactors***
Critical flow model	Marviken
Two-phase pump head multiplier	CE pump, CREARE, Semiscale pump, W_pump, LOFT pump, Byron-Jackson, B&W
Two-phase pump torque multiplier	Semiscale
Critical heat flux, Vapor generation, Non-equilibrium heat transfer	Bennet experiment 5358, 5294, 5394 Royal Institute of Technology (RIT) Test 261 ORNL Bundle CHF Test 3.07.9B, 3.07.9N, 3.07.9W
Subcooled boiling	Christensen Subcooled boiling Test 15, Shoukri Subcooled Boiling Experiment
Dittus-Boelter Liquid/Vapor HTC	McAdams-Frost, Larsen and Ford, Kreith, Heineman, Morris-Whitman, Slecher-Rouse
Chen nucleate boiling HTC	Dengler-Addoms, Schrock-Grossman, Sani, Bennett et al, Wright
Chen transition boiling heat flux	B&W, Bennett, Bennett & Kearsey, Bertoletti, Bishop, Era, Jansson, Herkenrath
Bromley film boiling HTC	***RELAP5 document → ADI data*** ¶)
Pressurizer model	MIT Pressurizer Test ST4
Interphase drag model	Dukler Air-Water Tests, FROJA, FRIGG, CISE, Kasai et al, ORNL TLTA, GEC TLTA, Hall et al, FLECHT-SEASET※), THETIS, FIST, Hughes, Carrier, ORNL THTF※), AERE Harwell, GE, Marviken, Petrick
Accumulator model	LOFT Accumulator blowdown test, VAPER※)
ECC bypass	UPTF※), CREARE, MIDAS※), ATLAS※)
Downcomer boiling	DOBO※), ATLAS※)
Steam generator heat transfer	ATLAS※)
Overall reflood phenomena	FLECHT-SEASET※), NEPTUN※), CCTF※), PKL※), ATLAS※)
Overall blowdown phenomena	THTF※)
Overall LOCA phenomena	LOFT※), Semiscale※), LOBI※)

※) Tests used for the code assessment conducted in this report.

¶) Data tables are on file with the American Documentation Institute, Washington, D.C. Test conditions are described in page 132 of Reference [1].

Reference

[1] "RELAP5/MOD3.3 Code Manual Volume 4: Models and Correlations," NUREG/CR-5535, Rev P3, March 2006.

Impact on DCD

There is no impact on the DCD.

Impact on PRA

There is no impact on the PRA.

Impact on Technical Specifications

There is no impact on the Technical Specifications.

Impact on Technical/Topical/Environmental Report

Table 4-4 of the topical report will be revised to Table 1 of this response.

There is no impact on Technical or Environmental Report.

Non-Proprietary

SECTION E

Page intentionally left blank

RESPONSE TO REQUEST FOR ADDITIONAL INFORMATION

APR1400 Design Certification

Korea Electric Power Corporation / Korea Hydro & Nuclear Power Co., LTD

Docket No. 52-046

RAI No.:	**399-8510**
SRP Section:	**15.06.05 – Loss of Coolant Accidents Resulting From Spectrum of Postulated Piping Breaks Within the Reactor Coolant Pressure Boundary**
Application Section:	**15.6.5**
Date of RAI Issue:	**02/03/2016**

Question No. 15.06.05-6

Provide additional information regarding the choice of assumptions with respect to LOOP in context of a LBLOCA

Regulatory Basis:

NUREG-0800, Section 15.6.5, requires that the evaluation of a LBLOCA address whether the appropriate break locations, break sizes, and initial conditions were selected in a manner that conservatively predicts the consequences of the LOCA for evaluating ECCS performance; and whether an adequate analysis of possible failure modes of ECCS equipment and the effects of the failure modes on the ECCS performance have been provided. For postulated break sizes and locations, the reactor systems review includes the postulated initial reactor core and reactor system conditions, the postulated sequence of events including time delays prior to and after emergency power actuation, the calculation of the power, pressure, flow and temperature transients, the functional and operational characteristics of the reactor protective and ECCS systems in terms of how they affect the sequence of events, and operator actions required to mitigate the consequences of the accident.

Technical Basis:

The applicant states that LOOP is assumed at the beginning of the LBLOCA transient evaluation and that the reactor coolant pumps (RCPs) are assumed to coast down. Additionally, the applicant takes no credit for control element assembly (CEA) insertion at the same time the power is lost to the RCPs.

Question:

1. Has loss of RCP flow been demonstrated to be more limiting than the same event with the

RCPs operating?

2. With the assumption of LOOP, why is no credit taken for CEA insertion at the same time the power is lost to the RCPs? (CEA insertion and turbine trip are delayed until the low pressure trip).

3. Has the stuck/windmilling flow resistance (both flow directions) for the RCPs been measured as part of a test program and are these data used to develop the homologous curves used in RELAP5/MOD/3.3K?

Response

1)

Figure 1, provided below, shows the calculated clad temperatures for with and without operation of the RCPs. The peak clad temperature (PCT) without operation of the RCPs is [ ]^{TS}, and PCT with operation of the RCPs is [ ]^{TS}. And reflood PCTs for both cases are [ ]^{TS} for without and with operation of RCPs, respectively.

The PCT without operation of the RCPs occurred at the 14th heat structure node, whereas the PCT with operation of RCPs occurred at the 15th heat structure node. Thus, the quench time difference is caused by the PCT elevation.

Consequently, the loss of RCP flow case was determined to be the more limiting case based on the PCT results.

2)

During LBLOCA condition, vaporization in the core rapidly increases due to depressurization of the RCS. According to the moderator density vs. reactivity design of the APR1400 used in the analysis, negative reactivity occurs due to increase of the void fraction in the core. For this reason, the core power is rapidly decreasing whether CEA insertion is credited or not.

A plant calculation with and without CEA insertion was performed and is shown in Figures 2 and 3. When CEA insertion is not credited, core power from the fuel rods is higher than the CEA insertion credited case as shown in Figure 2. The higher core power causes higher PCT as shown in Figure 3. The LBLOCA analysis model does not credit CEA insertion and confirms the performance of ECCS for the APR1400 under this severe thermal hydraulic condition.

3)

In the homologous curves, zero pump speed data for forward and reverse flow are produced by considering stuck flow resistance or a locked rotor K-factor. And zero torque data are produced by considering windmilling flow resistance. Pump homologous curve data are obtained from the pump test and this curve data are used in LBLOCA analysis.

TS

Figure 1. Comparison of Clad Temperatures for With and Without Pump Operation

TS

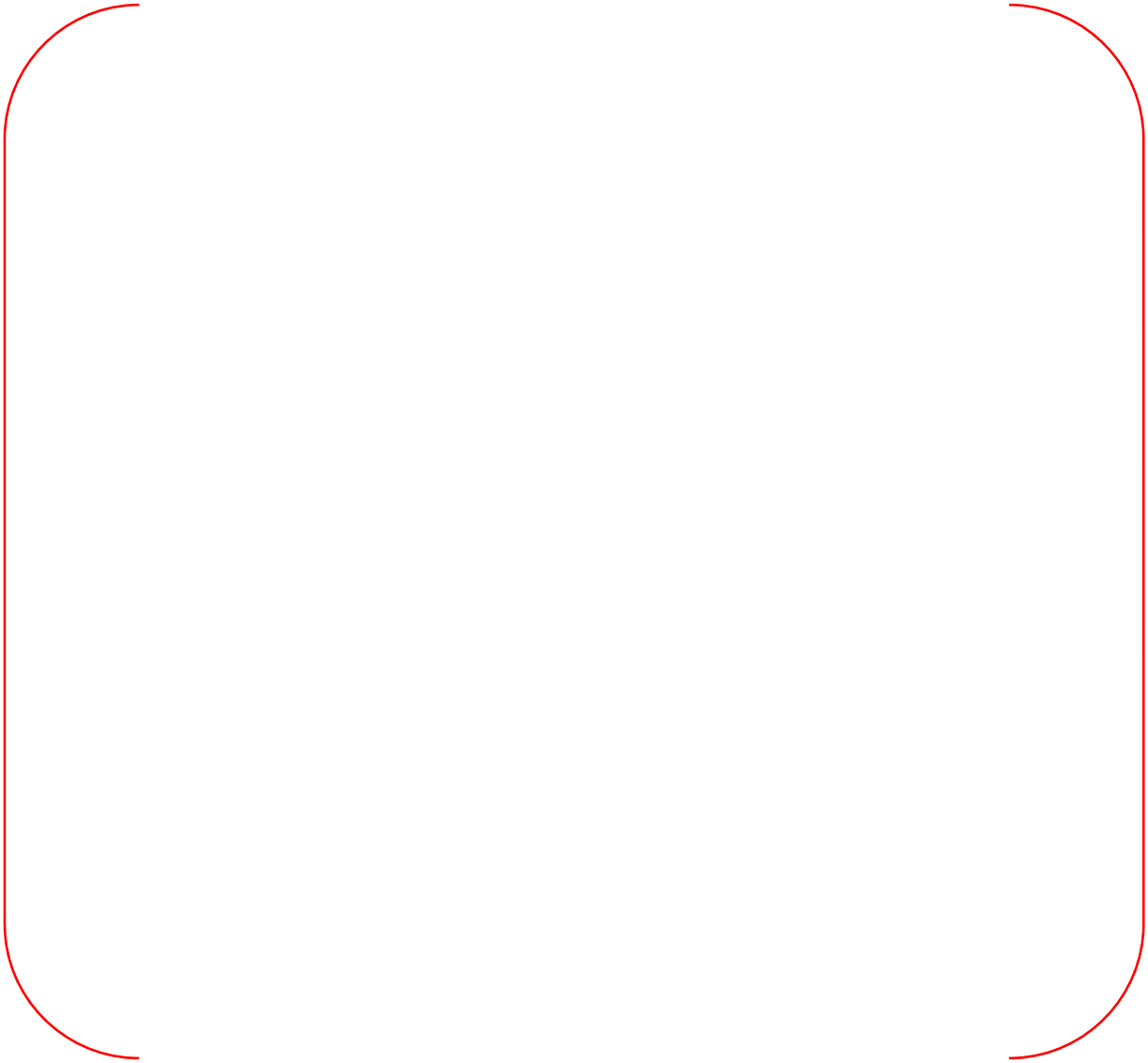

Figure 2. Comparison of Normalization Total Core Power for With and Without CEA Insertion

TS

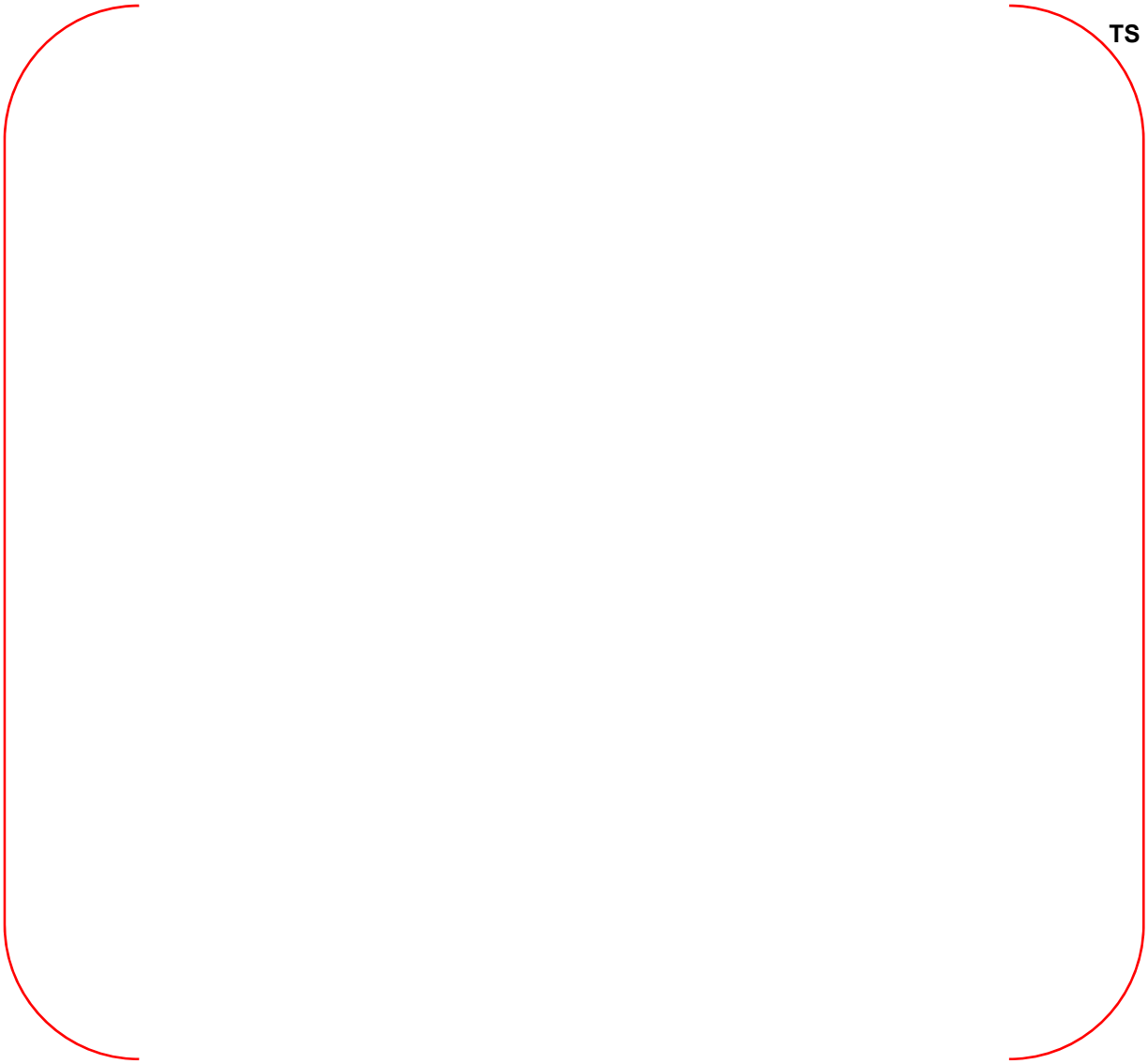

Figure 3. Comparison of Cladding Temperature for With and Without CEA Insertion

Impact on DCD

There is no impact on DCD.

Impact on PRA

There is no impact on PRA.

Impact on Technical Specifications

There is no impact on Technical Specifications.

Impact on Technical/Topical/Environmental Report

There is no impact on any Technical, Topical, or Environmental Report.

REVISED RESPONSE TO REQUEST FOR ADDITIONAL INFORMATION

APR1400 Design Certification

Korea Electric Power Corporation / Korea Hydro & Nuclear Power Co., LTD

Docket No. 52-046

RAI No.:	**399-8510**
SRP Section:	**15.06.05 – Loss of Coolant Accidents Resulting From Spectrum of Postulated Piping Breaks Within the Reactor Coolant Pressure Boundary**
Application Section:	**15.06.05**
Date of RAI Issue:	**02/03/2016**

Question No. 15.06.05-7

Provide an evaluation of the potential for fuel failure during the initial power spike in the LBLOCA evaluation (Fig 15.6.5-5)

Regulatory Basis:

NUREG-0800, Section 15.6.5, requires that the evaluation of a LBLOCA address:

- Design basis radiological consequence analyses associated with design basis accidents per NUREG-0800, Section 15.0.3.3.
- Fuel failure modes and burst correlations are evaluated for compliance with 10 CFR 50.46 as part of its fuel design review per NUREG-0800, Section 4.2required to mitigate the consequences of the accident.

Technical Basis:

The LBLOCA reactor power response (Figure 15.6.5-5 of the APR1400 DCD) shows normalized power increasing to 1.7 times nominal in the first 0.5 sec of a 100 percent double-ended guillotine LBLOCA transient. Values approaching 1.8 times nominal are seen for 60 percent double-ended cases (Figure15.6.5-13). This behavior is not as expected for this event, since core depressurization and voiding usually result in the insertion of significant negative reactivity.
The power increase is suspected to be due to the moderator reactivity curve being used (this curve is taken from the RELAP5/MOD3.3K input file).
Such a large increase in power may cause fuel failures.
It is recognized that this conservative reactivity versus density curve was developed for the analysis of other events evaluated in Chapter 15 which are assessed using a conservative (versus best estimate plus uncertainty) basis. This conservatism results in the inclusion of

positive moderator reactivity feedback which is not allowed per the Technical Specifications. However, the use of the conservative curve in the best estimate application leads to large power excursions.

Question:

1. A verification and an explanation for the shape and magnitude (positive reactivity at some densities) of the curve. In particular, the increase in reactivity with decreasing moderator density for densities above 500 kg/m^3.

2. A justification for the use of the conservative curve in a best estimate plus uncertainty evaluation.

3. An explanation for the rapid increase in reactor power during the first 0.5 sec of the LBLOCA transient, and

4. An evaluation of fuel performance during this spike in power to determine if the fuel fails due to PCMI or fuel melt.

Response – Rev. (1)

1)

Figure 1 shows a curve of reactivity vs. moderator density used in the LOCA evaluation. The value of the density coefficient used corresponds to a 0 MTC for the small break events and $+0.5\times10^{-4}$ Δρ/°F for the large breaks (Table 4.3-3 of the APR1400 DCD).

As moderator temperature increases or pressure decreases, the moderator density decreases reducing the amount of moderator in the core. Decreasing moderation leads MTC to become more negative. But the amount of soluble boron is also reduced when the moderator density decreases. Reducing neutron absorption of boron leads to a positive effect on reactivity.

The higher boron in the MDC curve corresponding to $+0.5\times10^{-4}$ Δρ/°F MTC causes positive reactivity with decreasing moderator density compared with a MDC curve corresponding to 0 MTC.

2)

The maximum positive limit of MTC is 0.0 Δk/k/˚F at 100% RTP (LCO 3.1.3). The realistic MTC value for full power operation is negative. But the moderator density coefficient corresponding to 0.5×10^{-4} Δρ/°F MTC is used for the large break LOCA to conservatively account the non-uniform voiding. It is not the realistic value, but a very conservative one.

3)

The major cause of the rapid power spike is due to the positive reactivity with decreasing moderator density during the early phase of LBLOCA transient. Figure 2 shows the normalized core power during 1.0 × Double-ended Guillotine Break in Pump Discharge Leg (same case as

Figure 15.6.5-5 of the APR1400 DCD) using the density coefficient of 0 MTC. In this case, there is almost no power excursion.

4)

The melting temperature of uranium dioxide pellets is 2,804 °C (5,080 °F) for unirradiated fuel and decreases by 32 °C (58 °F) per 10,000 MWD/MTU (Section 4.4.1.2 of the APR1400 DCD). The highest fuel temperature in the large breaks analyzed is [ ]^{TS}, which is lower than the fuel melting temperature limit.

The current LBLOCA evaluation is based on an unrealistic positive MDC. For realistic evaluation, a sensitivity study using 0 MTC demonstrates that there is no power excursion. Therefore it is not necessary to perform an evaluation of fuel performance due to PCMI.

The re-analysis of large break LOCA using realistic density coefficient and 181 SRS(Simple Random Sampling) calculations with the additional application of thermal conductivity degradation (TCD) effect was performed. DCD revision which includes the results of re-analysis is provided.

DCD revision also contains the increased data number of the containment time table applied to transfer mass and energy data (M/E data) from RELAP5 to CONTEMPT4 which reads the transferred data at given time points. During the large break LOCA the containment pressure rapidly increases after RCS piping break because of high M/E release from the break and gradually decreases over time with the operations of containment spray and cooling fan.

After performing the analyses before the revision, time reading points tended to over-estimate the M/E data in the minimum containment pressure analysis. When coupling the RELAP and CONTEMPT codes it was found that denser data reading time points resulted in better convergence of the M/E data and more conservative results in the estimation of containment pressure. Sensitivity studies showed that using denser data points made visible changes to the results, e.g. going from 29 time steps to 100 time steps. However, when evaluating the combined effects with or without TCD and MDC, with keeping time steps constant (29), the results indicated that there were negligible differences between the Rev. 1 and Rev. 2 results of the minimum containment pressure analysis.

Figure 3 shows the comparison of containment pressure curves for the different time table numbers in the minimum containment pressure analysis. Specifically, the red solid line (Rev.1_29 time table) represents the result from the case of 29 time table number with previous MDC curve with no TCD input application. The blue dash-dot line (Rev.2_100 time table) represents the final containment pressure analysis results with using a 100 time table number including TCD input and revised MDC curve. The black dotted line (Rev.2_29 time table) represents the same case as the final analysis results (blue line) however it represents results at a reduced time table number of 29.

The input differences of the containment pressure comparison analysis shown in Figure 3 are summarized in Table 1. The input of ‘Rev.2_100 Time Table’ is applied to current revised LBLOCA analysis of DCD sections 6.2.1.5 and 15.6.5.

Table 1. Major Input Differences for Containment Pressure Comparison

Legends in Figure 3	TCD Inputs	MDC Revision	Containment Time Table
Rev. 1_29 Time Table	None	None	29
Rev. 2_29 Time Table	✓	✓	29
Rev. 2_100 Time Table	✓	✓	100

Figure 1. Reactivity vs. Moderator Density for LOCA Evaluation

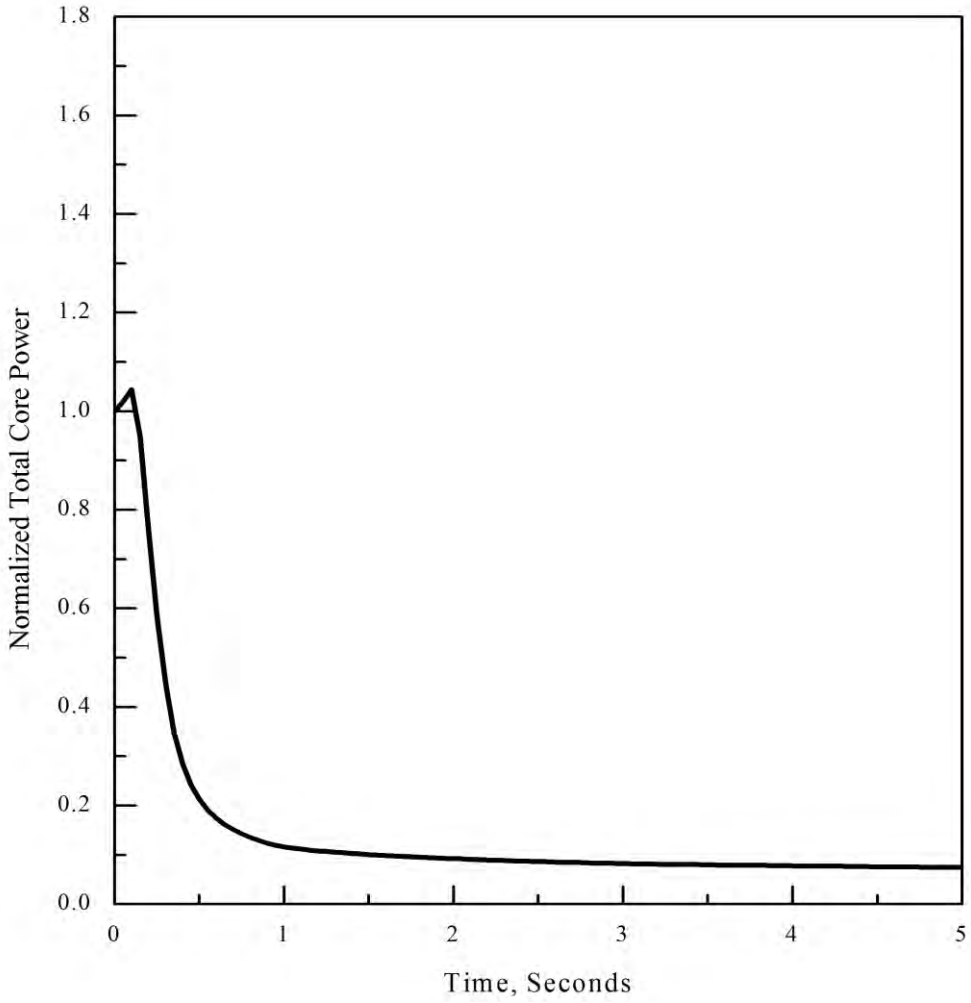

Figure 2. Normalized Core Power using Density Coefficient Corresponds to 0 MTC

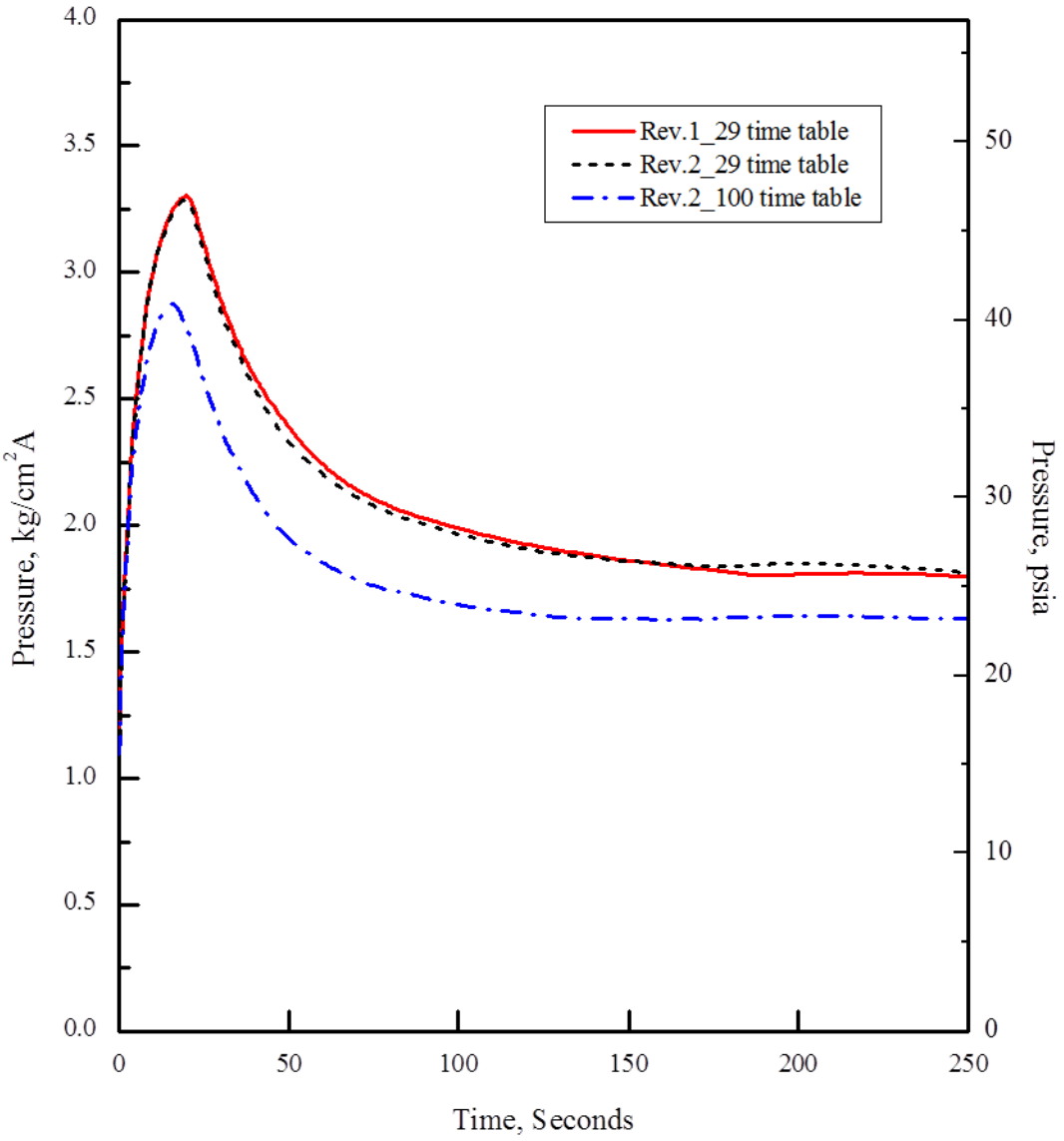

Figure 3. Comparison of Containment Pressure Curves for Different Time Table Numbers

Impact on DCD

The re-analysis of large break LOCA is performed for Question No.15.06.05-7. The DCD revisions for Section 6.2.1.5 and 15.6.5 are attached.

The original response indicates future incorporation of DCD changes. The changes that were proposed in the markup of original response to this RAI are still valid for the response of Revision 1.

Impact on PRA

There is no impact on the PRA.

Impact on Technical Specifications

There is no impact on the Technical Specifications.

Impact on Technical/Topical/Environmental Reports

There is no impact on any Technical, Topical, or Environment Report.

RESPONSE TO REQUEST FOR ADDITIONAL INFORMATION

APR1400 Design Certification

Korea Electric Power Corporation / Korea Hydro & Nuclear Power Co., LTD

Docket No. 52-046

RAI No.:	**399-8510**
SRP Section:	**15.06.05 – Loss of Coolant Accidents Resulting From Spectrum of Postulated Piping Breaks Within the Reactor Coolant Pressure Boundary**
Application Section:	**15.6.5**
Date of RAI Issue:	**02/03/2016**

Question No. 15.06.05-8

LBLOCA evaluation with a stuck check valve in the SIT

Regulatory Basis:

General Design Criterion (GDC) 35, as it relates to demonstrating that the ECCS would provide abundant emergency core cooling to satisfy the ECCS safety function of transferring heat from the reactor core following any loss of reactor coolant at a rate that (1) fuel and clad damage that could interfere with continued effective core cooling would be prevented, and (2) clad metal water reaction would be limited to negligible amounts. The analysis should consider the possibility of a single failure.

Technical Basis:

It is not clear that the applicant has considered the potential for a check valve in the SIT to stick. The single failure could occur prior to, or at any time during, the design basis event for which the safety system is required to function.

Question:

Provide a LBLOCA evaluation with a stuck check valve in the SIT (potential single failure). If no evaluation exists, provide a justification for not considering this potential failure.

Response

General Design Criterion (GDC) 35 in 10 CFR 50 Appendix A explains as follows:

“Criterion 35- Emergency core cooling. A system to provide abundant emergency core cooling shall be provided. The system safety function shall be to transfer heat from the reactor core following any loss of reactor coolant at a rate such that (1) fuel and clad damage that could interfere with continued effective core cooling is prevented and (2) clad metal-water reaction is limited to negligible amounts.

Suitable redundancy in components and features, and suitable interconnections, leak detection, isolation, and containment capabilities shall be provided to assure that for onsite electric power system operation (assuming offsite power is not available) and for offsite electric power system operation (assuming onsite power is not available) the system safety function can be accomplished, assuming a single failure.”

10 CFR 50 Appendix A also states about single failures as follows:

“Single failures of passive components in electric systems should be assumed in designing against a single failure. The conditions under which a single failure of a passive component in a fluid system should be considered in designing the system against a single failure are under development.”

From GDC 35 and the statements about single failures in 10 CFR 50 Appendix A, single failure of check valve in SIT which is a passive component does not need to be considered.

Impact on DCD

There is no impact on DCD.

Impact on PRA

There is no impact on the PRA.

Impact on Technical Specifications

There is no impact on the Technical Specifications.

Impact on Technical/Topical/Environmental Reports

There is no impact on any Technical, Topical, or Environment Report.

RESPONSE TO REQUEST FOR ADDITIONAL INFORMATION

APR1400 Design Certification

Korea Electric Power Corporation / Korea Hydro & Nuclear Power Co., LTD

Docket No. 52-046

RAI No.:	**399-8510**
SRP Section:	**15.06.05 – Loss of Coolant Accidents Resulting From Spectrum of Postulated Piping Breaks Within the Reactor Coolant Pressure Boundary**
Application Section:	**15.06.05**
Date of RAI Issue:	**02/03/2016**

Question No. 15.06.05-9

Regulatory Basis:

Title 10 of the Code of Federal Regulations, Part 50.46 requires an analysis of ECCS performance following loss of coolant accidents. The calculational framework used for the evaluation of the ECCS system in terms of core short term behavior and long term cooling performance are referred to as an evaluation model. It includes one or more computer programs, the mathematical models used, the assumptions and correlations included in the program, the procedure for selecting and treating the program input and output information, the specification of those portions of the analysis not included in computer programs, the values of parameters, and all other information necessary to specify the calculational procedure.

The evaluation model used by the applicant must comply with the acceptance criteria for ECCS given in 10 CFR 50.46. The following questions pertain to the RELAP5/MOD3.3 and CONTEMP4/MOD5 programs which comprise the APR1400 Evaluation Model:

1. The version of RELAP5/MOD3.3 used in these analyses has known errors in the Groeneveld (1986) tables implementation. These errors were corrected in RELAP5/MOD3.3 Patch04 in October, 2010. Additionally, the Groeneveld (2006) tables were updated in a later RELAP5/MOD3.3 version (incremental version3.3kg).

   If the applicant has not corrected these errors in the version used to perform the analyses in DCD Section 15.6.5, provide an assessment of the effect of these errors. Note that because these results will be used in a CSAU/BEPU analysis, it is not sufficient to determine if the results are conservative. As a minimum, the effect of the errors should affect the uncertainty in the analysis results.

2. When using the coupled codes RELAP5 and CONTEMPT with a one-to-one time step correspondence, it is correct to use fluid, vapor and non-condensable flows as calculated by each code. However, if either of the codes uses more than one time step to reach the next coupling time, it is necessary to provide the integral of some properties over the coupling time interval (fluid enthalpy, vapor enthalpy, fluid mass flow, vapor mass flow and air mass flow) not just the last times step values. If this is not done, these properties are not conserved.

   Explain how the passed quantities are defined to ensure conservation of mass and energy.

3. In the LBLOCA Topical Report, it is stated that the break flow is underpredicted for the LOBI experiments. There are multiple critical flow models in RELAP5/MOD3.3 for subcooled and saturated critical flow. Please specify which correlation was used in each flow regime. For example, was the Henry-Fauske (recommended) or the default Ransom-Trapp model used? What discharge factors were used in the chosen model and how were they determined?

4. It is well known that RELAP5 convects an incorrect amount of energy into the downstream volume connected to a junction. There is a junction flag (the e flag) that can be used to correct this. This is only an issue at the breaks where the pressure change across the junction is large.

   Provide justification that break flow is correctly treated in this regard. Otherwise, containment pressures will be too low.

5. Due to the location of the break and the location of the pressurizer, there will be times during the transient that flow and thermal conditions from each loop will be different. Assuming that the inlet plenum nodalization in the full plant model is the same as that used in the topical report, the inlet plenum is modeled as a single volume. This implies that there is complete mixing of the flows from each loop and that the core inlet conditions are therefore uniform across the core.

   Please justify that the use of a single volume, hence uniform inlet conditions, is based on some experimental data or explain if loop-to-loop mixing is accounted for using some other model?

6. The modeling of the reactor vessel in the downcomer region and the thermal shield on the other side of the downcomer are critical to the prediction of downcomer filling during the refill and reflood phases. Since rapid temperature transients caused by fluid heating (or cooling) the walls initially only affects the surface of the metal and does not involve all of the metal mass. It is crucial to choose a “good” mesh spacing to capture accurately these effects. There are modeling guidelines based on the component Biot Number in the RELAP5-3D manuals to provide help on the development of an accurate mesh spacing.

Please provide a discussion of the adequacy of the mesh size selected for the analyses.

7. For the LOBI experiments discussed in the LBLOCA Methodology Topical Report, late in the transient, the RELAP5 based Engineering Model predicts 150K superheat in both hot legs and the intact loop cold leg. This seems to be unrealistically high.

   Is the same level of vapor superheat seen in the full plant model? If so, are there modeling adjustments that can be made to reflect more closely the experimental data? How was this uncertainty handled in the final evaluation?

8. In the early reflood phase, there are series of cyclic events that involve steam binding caused by reverse heat transfer in the steam generation. Subsequent lower reflood rates in the core are followed by increased steam generation in the core. Through this cyclical process, the core is eventually reflooded. The cyclical behavior involves a number of complex and interrelated processes. Has the ability of RELAP5/MOD3.3 to model these types of phenomena been demonstrated through comparisons to test data or other methods?

9. In the analysis of the LOFT test in the LBLOCA topical report the applicant notes: “For all calculations, this accumulated liquid in the core is larger than the amount obtained by subtracting the expelled liquid amount out of the downcomer from the delivered liquid amount to the downcomer. This implies that a portion of the liquid in the downcomer is carried to the core by the core up-flow behavior.” RELAP5 has a tendency to accumulate “mass error” particularly in two-phase regions. When the mass error is large relative to the change in mass of interest, it often masks the actual behavior of the system. The mass error can usually be reduced by using smaller time steps and/or renodalizing the region where the mass error is occurring.

   Provide justification that the mass error for full plant evaluation as well as the LOFT test results ensure that the conclusions remain correct and that mass error is not influencing the conclusions.

10. During the early reflood phase, it is stated that the entrained liquid travels to the upper plenum where it is de-entrained and accumulates in the upper plenum where it subsequently flows down through the lower power (cooler) assemblies. This sets up a three-dimensional flow pattern (essentially a Natural Circulation flow path up the hot assemblies and down the cooler assemblies).

    Since RELAP5/MOD3.3 is a set of one-dimensional models, how is the model constructed to capture these three-dimensional phenomena and how is the model qualified/validated?

Response

1)

Groeneveld CHF lookup table of RELAP5/MOD3.3 has errors reported as follows.

Related sub-routine: chftab.ff

Description: In April 2010, an IRUG member reported an error in the RELAP5-3D implementation of the Groeneveld critical heat flux (CHF) look up table after comparing the coding in subroutine CHFTAB to the 1986 paper. A subsequent, more detailed review by RELAP5-3D developers revealed 41 errors or inconsistencies, some of which were minor (e.q., difference in the last digit due to round off for interpolated values), and some of which were significant. These errors affect all RELAP5 versions since and including RELAP5/MOD3 version 3.0 and all RELAP5-3D versions.

Development code version: 3.3in

Complete date: 25, August, 2010

Based on the above code modification information, CHF lookup table data file (chftab.ff) of RELAP5/MOD3.3/K is changed to the modified CHF lookup table data file (RELAP5/MOD3.3 Patch 4).

Figure 1-1 and Figure 1-2 show code accuracy results for RELAP5/MOD3.3/K (topical report code) and modified CHF lookup table data of RELAP5/MOD3.3/K (modified code) against THTF, LOFT and LOBI test data. Figure 1-1 shows calculation results using the topical report code, but it differs from Figure 4-7 of the topical report because Figure 4-7 of the topical report contains an error. Figure 4-7 will be replaced with Figure 1-1 of this response. Comparison results of the code accuracy show that the effect of the error modification on the Groeneveld lookup table data is evaluated within [ ]^{TS}.

Figure 1-3 and Figure 1-4 show plant SRS calculation results for the topical report code and the modified code. Overall quench times for both results are similar and the third highest (95/95 confidence level) PCT values are the same as [ ]^{TS}.

TS

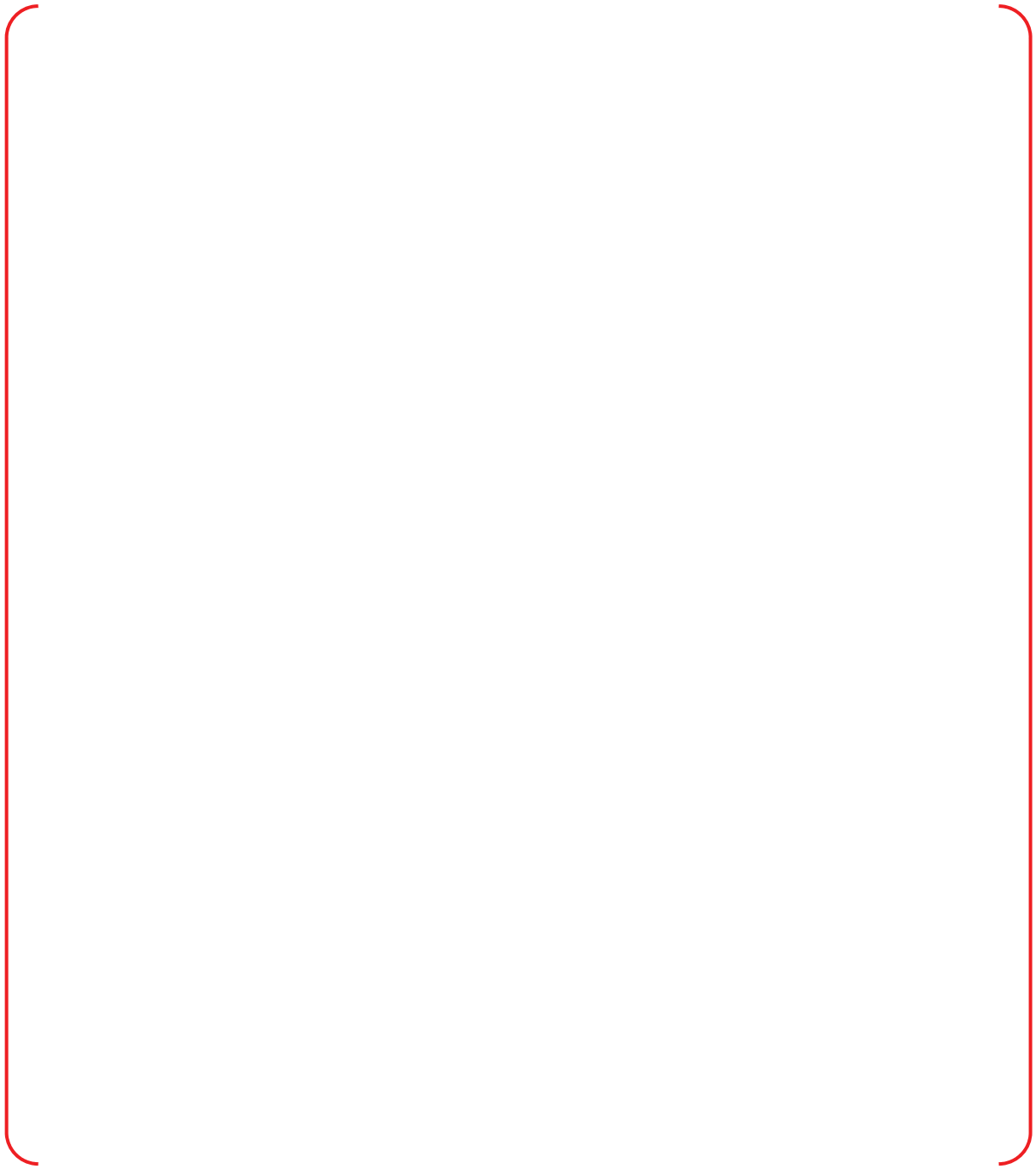

Figure 1-1. Code Accuracy of RELAP5/MOD3.3/K for Blowdown Phase

TS

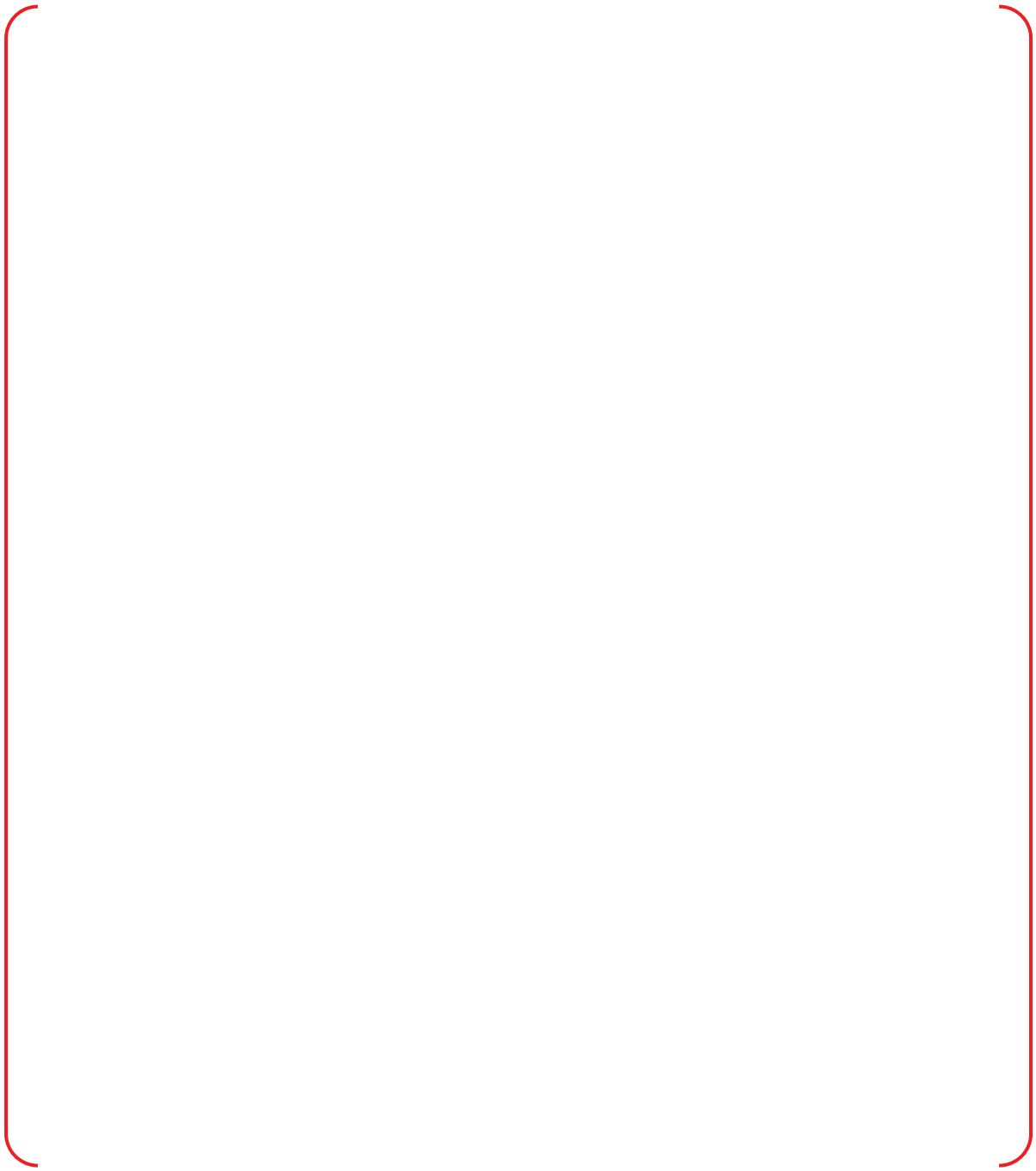

Figure 1-2. Code Accuracy of Modified RELAP5/MOD3.3/K for Blowdown Phase

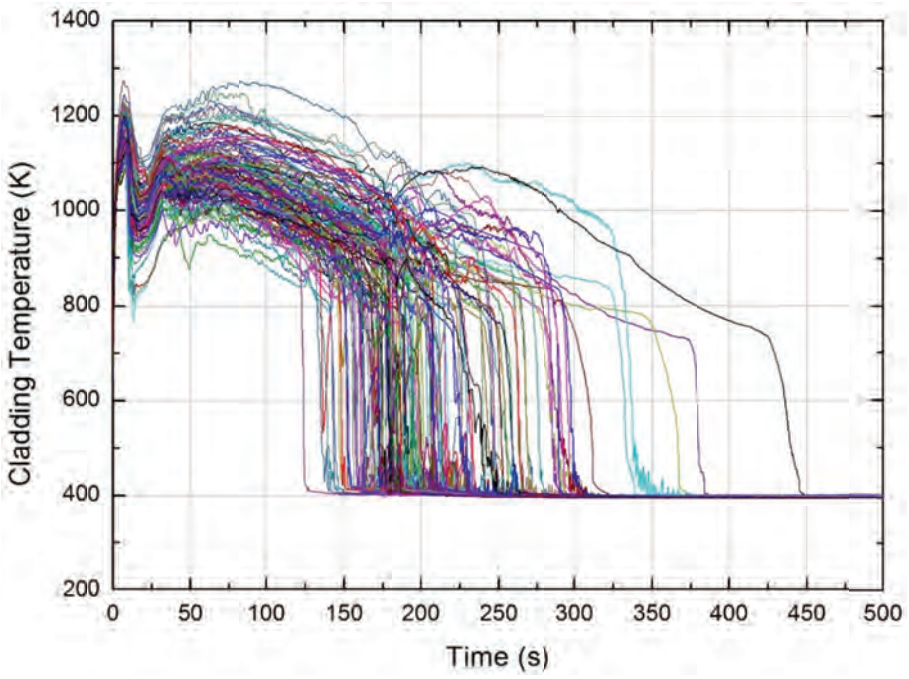

Figure 1-3. SRS Calculation Results of RELAP5/MOD3.3/K

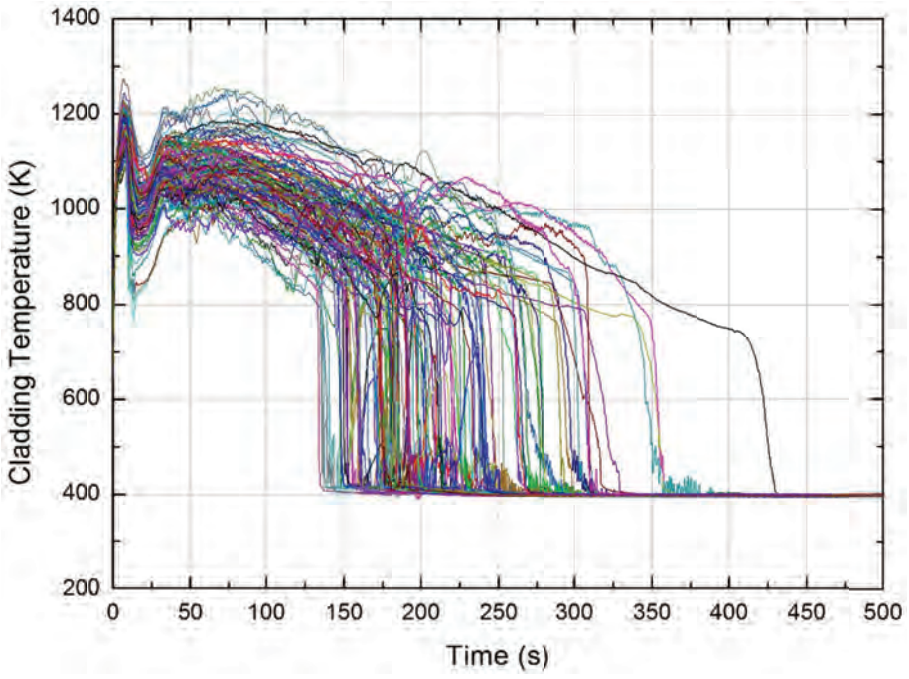

Figure 1-4. SRS Calculation Results for of Modified RELAP5/MOD3.3/K

2)

[ ]TS.
RELAP5 calculates total released mass and energy data for liquid, vapor and non-condensable gas through the breaks [ ]TS. Then, the CONTEMPT code calculates containment pressure [ ]TS. After the loading of CONTEMPT, RELAP5 and CONTEMPT exchange mass, energy, and pressure data for every calculation time step of RELAP5.

3)

As described in Section 4.2.2.7.1 of the topical report, Ransom-Trapp critical flow model is used in CAREM, and discharge coefficients for subcooled single-phase and two-phase were obtained based on the code assessment against MARVIKEN tests. The results of the assessment show that the Ransom-Trapp critical flow model [ ]TS for the subcooled single-phase critical flow and [ ]TS for the two-phase critical flow. Therefore, discharge coefficients for subcooled single-phase and two-phase were determined as [ ]TS respectively to match the calculated results with experimental data.

4)

A sensitivity study of the e-flag option in the junction at the break was performed for the plant base case to evaluate the effect of the e-flag junction. Figure 4-1 shows the containment pressure with activated e-flag option and de-activated e-flag option, respectively. Containment pressures for those two cases do not have significant differences. Discharged mass with de-activated e-flag option is larger than that with activated e-flag option at 500 sec, by 0.2 %, as shown in Figure 4-2, thus it can be considered negligible. Therefore, it is confirmed that the e-flag option does not have a significant effect on the calculation for the amount energy of the downstream volume.

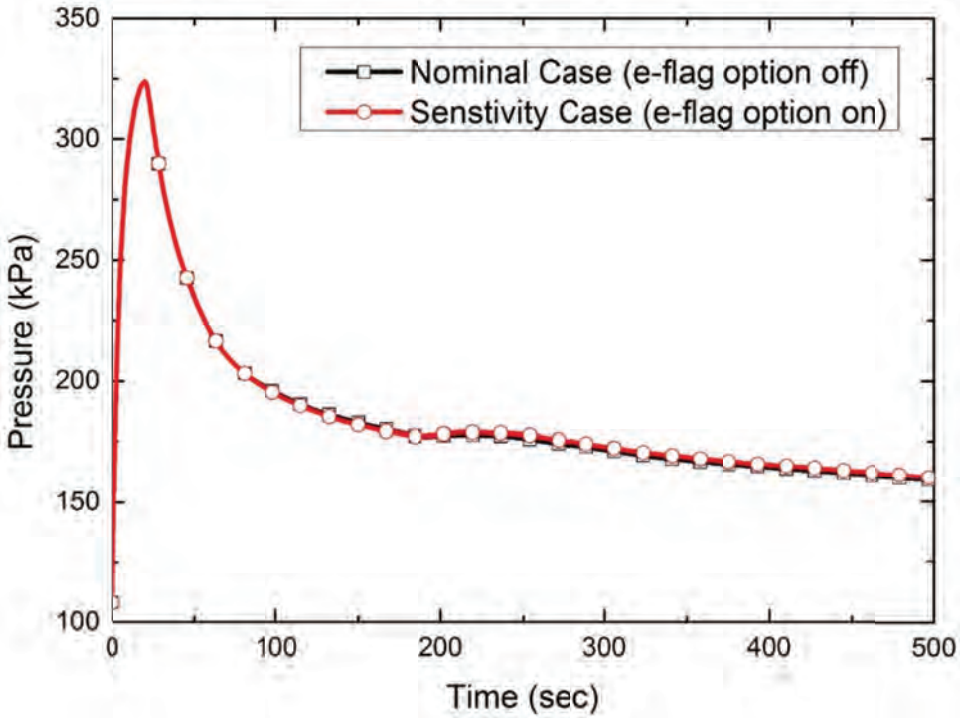

Figure 4-1. Containment Pressure

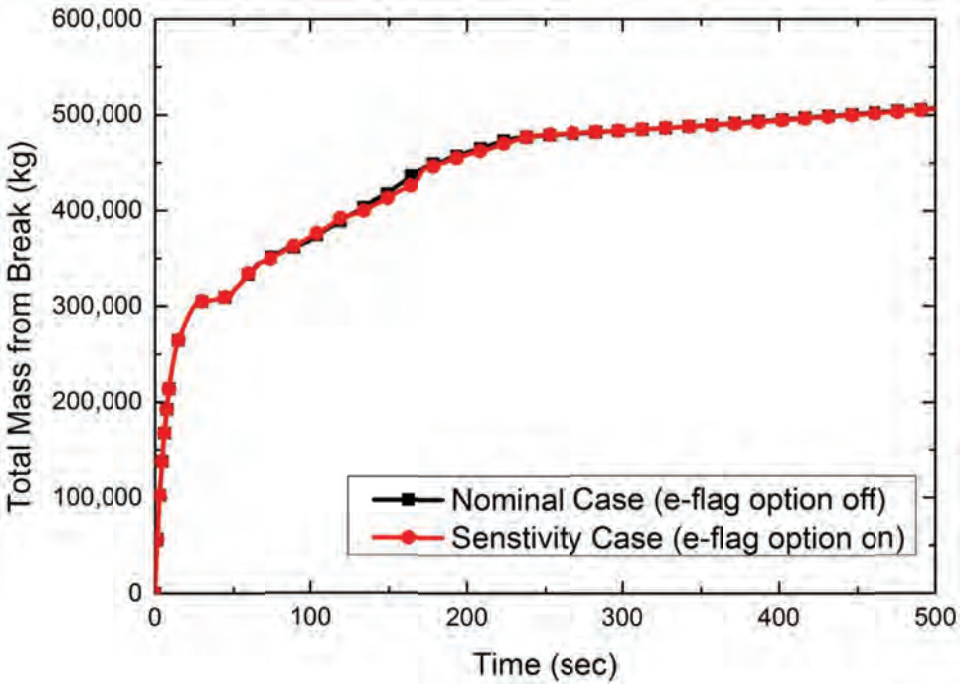

Figure 4-2. Discharged Mass from the Break

5)

The flow path of the coolant in the reactor vessel is shown in Figure 5-1. The flow rate between inlet plenum and each loop in the APR1400 plant is almost uniform because the coolant from the each loop flows through the flow skirt and lower support plate holes.

The flow skirt is a cylindrical structure with a number of holes as shown in Figure 5-2. This structure enhances the occurrence of mixing in the lower plenum, thus it uniformly distributes the inlet flow. The coolant from the flow skirt flows into the core through the lower support structure. The lower support structure is composed of the cylinder, support beam and bottom plate, as presented in Figure 5-3; the bottom plate has holes for flow distribution.

Therefore, even though non-uniform flow from the downcomer [ ]^{TS} enters into the lower plenum, the flow is redistributed uniformly and then the uniform flow enters into the core because of the complex structures such as flow skirt and lower support structure. Based on this, the inlet plenum of the APR1400 plant is modeled [ ]^{TS}.

TS

Figure 5-1. Flow Path of the Coolant in the Reactor Vessel

TS

Figure 5-2. Flow Skirt of APR1400

TS

Figure 5-3. Lower Support Structure and In-Core Instrumentation Nozzle Assembly

6)

The downcomer wall of the APR1400 plant is composed of [ ]TS. In CAREM, in order to model the downcomer wall, [ ]TS presented in Figure 6-1. The RELAP5-3D code manual in Reference [6-1] requires that a mesh point be placed at the interface between two heat structure compositions. Thus, as shown in Figure 6-1, [

]TS.

The performance of different mesh layout strategies is a strong function of the Biot number. The Biot number represents the ratio of convective and conductive heat transfer and is given by:

$$\mathrm{Bi} = \frac{hL}{k}$$

Where h is the convective heat transfer coefficient, L is the thickness of the wall, and k is the thermal conductivity of the wall material. The Biot number has a significant effect on the mesh size, and the line in Figure 6-2 shows the recommended maximum relative surface node size (β_{max}). The equation for the recommended maximum surface node size is given by:

$$\frac{1}{\beta_{max}} = 0.338Bi + 5.2$$

In the calculation for the APR1400 plant, the current mesh interval size is allowable since the surface node ($\beta = \frac{1}{2}\delta_1/L$, $\frac{1}{2}\delta_1$ is one half of the first mesh interval size, L is the wall thickness) is always lower than β_{max} during the transient as illustrated in Figure 6-3.

In Reference [6-1], in order to perform the accurate calculation of the temperature gradients, the use of the graduated or spatially variable mesh point intervals with smaller mesh point intervals near the surface in contact with the fluid is recommended. The current nodalization of the APR1400 plant is shown in Figure 6-1, and the sensitivity study for analysis of the mesh layout strategies was performed. The nodalization of the downcomer wall used in the sensitivity study is shown in Figure 6-4.

Through the sensitivity study for mesh size of the downcomer wall, it is confirmed that the current noding transfers more heat to the fluid than the variable mesh (Figure 6-5). However, the differences are not significant. And, more heat transferred to the fluid is conservative from the viewpoint of downcomer boiling. Consequently, the current nodalization for the downcomer wall of the APR 1400 plant as shown in Figure 6-1 is used for the LBLOCA analysis.

TS

Figure 6-1. Heat Structure Mesh Point for Downcomer Wall of APR1400 Plant

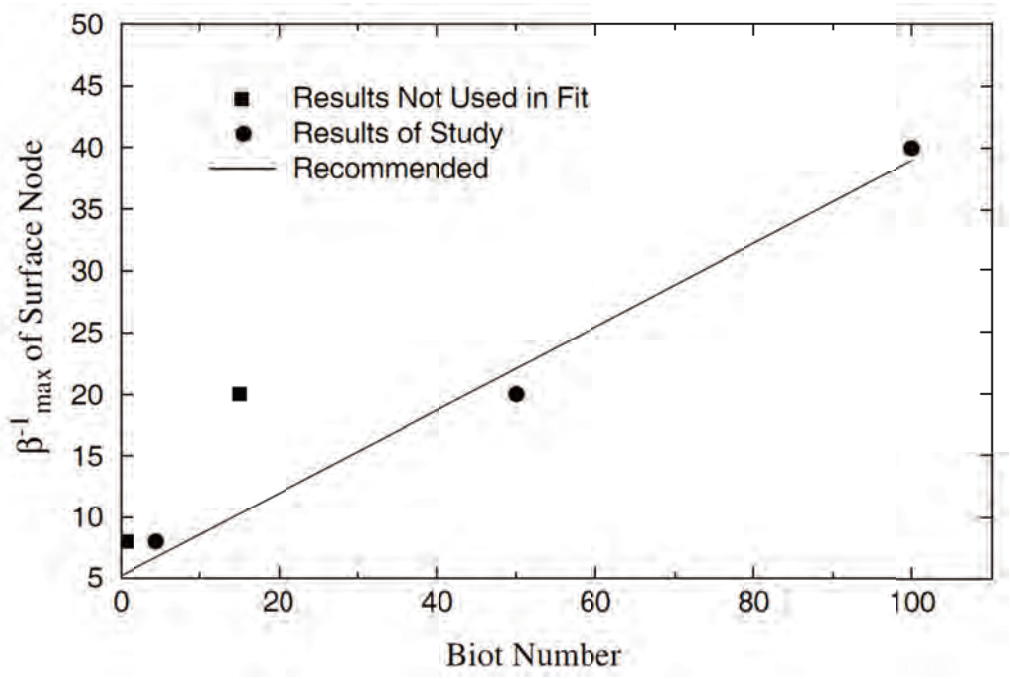

Figure 6-2. Effect of Biot Number on Suggested Surface Node Size

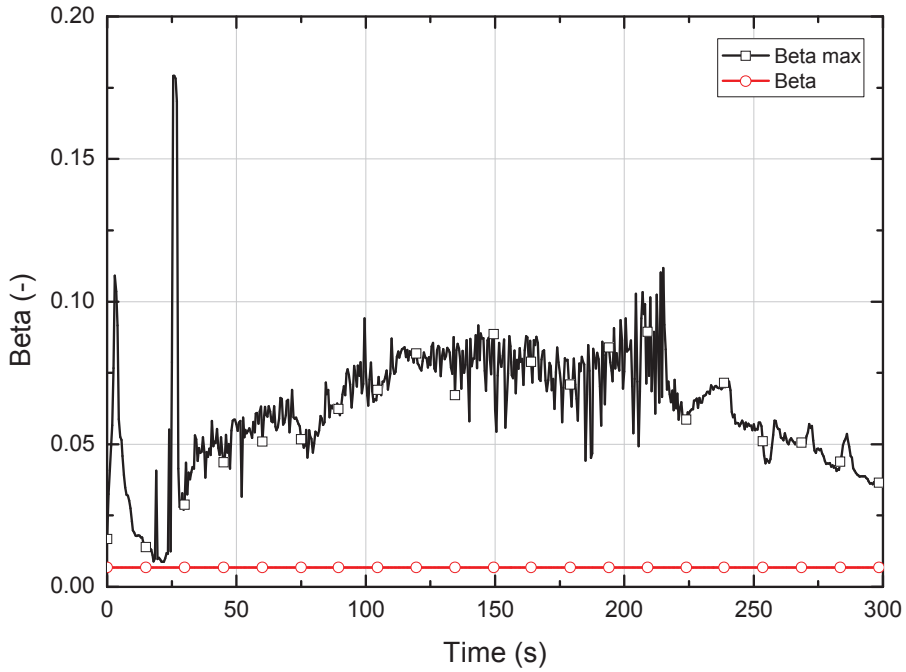

Figure 6-3. Maximum Acceptable Surface Node Size for APR1400 Plant Calculation

TS

Figure 6-4. Nodalization Strategies of Downcomer Wall

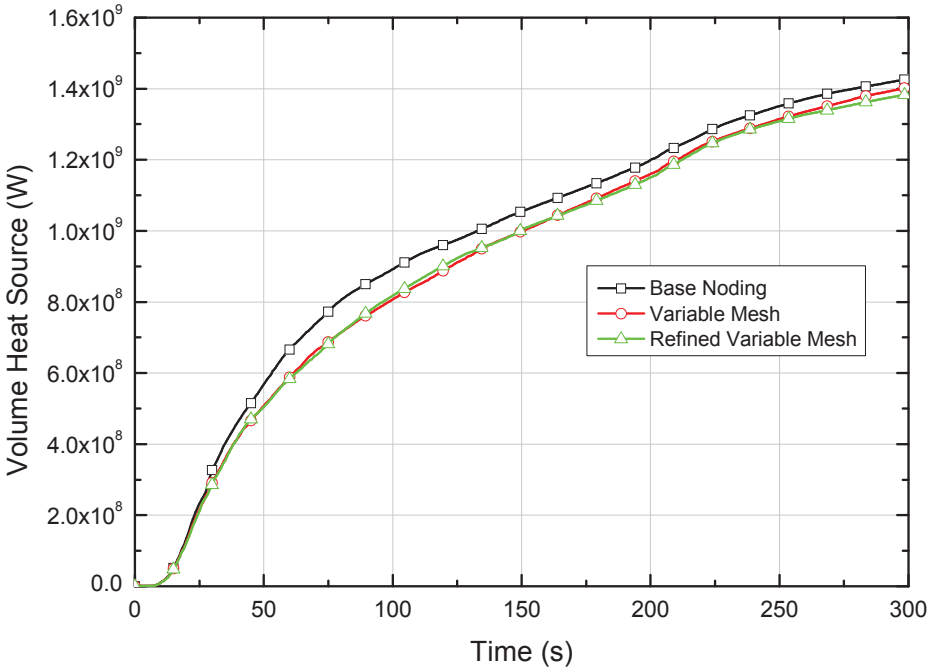

Figure 6-5. Total Volume Heat Source from the Downcomer Wall to the Fluid

Reference

[6-1] "RELAP5-3D Code manual Volume V: User's Guidelines," INEEL-EXT-98-008347, INEEL, July 2002.

7)

Figure 7-1 and Figure 7-2 show the calculation results of the intact loop hot and cold leg fluid temperatures for the APR1400, respectively. The reflood period initiates about 30 sec after the break, and superheated vapor comes out from the core, and superheated vapor comes out until 70 sec. However, the temperature difference between the liquid and vapor phases in Figure 7-1 is smaller than the 150 K observed in the LOBI assessment results, and the vapor temperature eventually drops to a liquid temperature at about 70 sec after the break because the core water level is increased. The cold leg fluid temperatures also show similar behavior, but the temperature difference is bigger than that of the hot leg because of the reverse heat transfer phenomenon in the steam generator.

The LOBI A1-66 test was designed to investigate the thermal hydraulic behavior of the system during the blowdown and refill periods, and the core inlet safety injection flow rate is not enough to cause entrainment of droplets to the hot leg. It makes superheated vapor in the hot leg. Superheated vapor continuously flows in from the core, whereas inflow of liquid phase is almost zero at about 30 sec after the break as shown in Figure 7-3. At this time the code calculates the liquid temperature as saturation temperature and vapor temperature as superheated temperature, all of which is coming from the core. For the cold leg in the LOBI assessment results, the temperature difference of liquid and vapor phases increases at 18 sec after the break because the safety injection from the SIT starts at this time. The liquid temperature drops below the saturation temperature because of the low temperature of the SIT injection water, whereas the vapor temperature maintains saturation temperature.

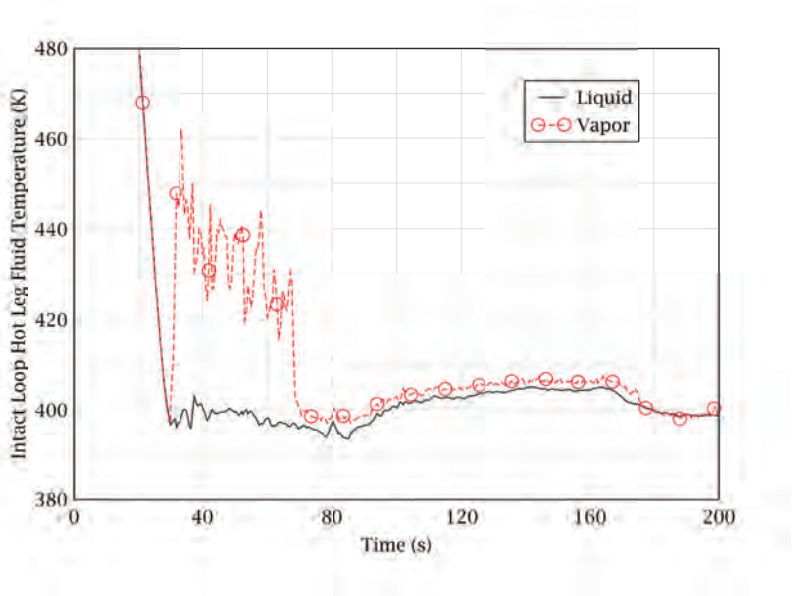

Figure 7-1. Calculation Result of Intact Hot Leg Fluid Temperature for APR1400

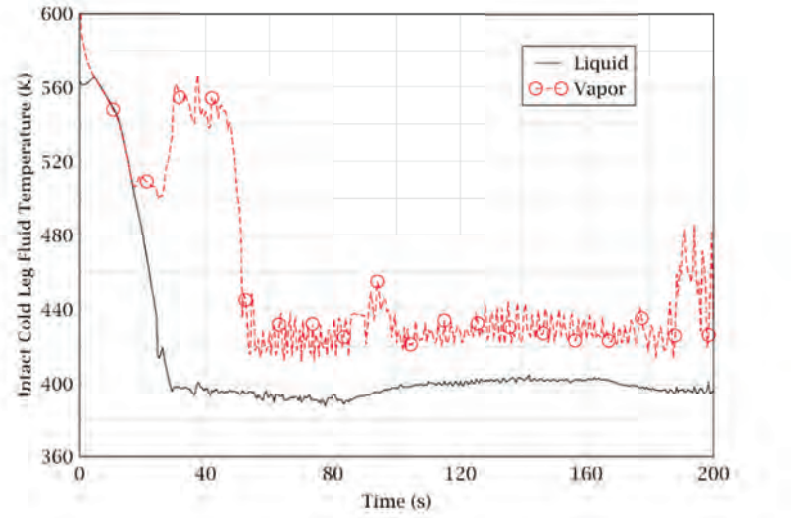

Figure 7-2. Calculation Result of Intact Cold Leg Fluid Temperature for APR1400

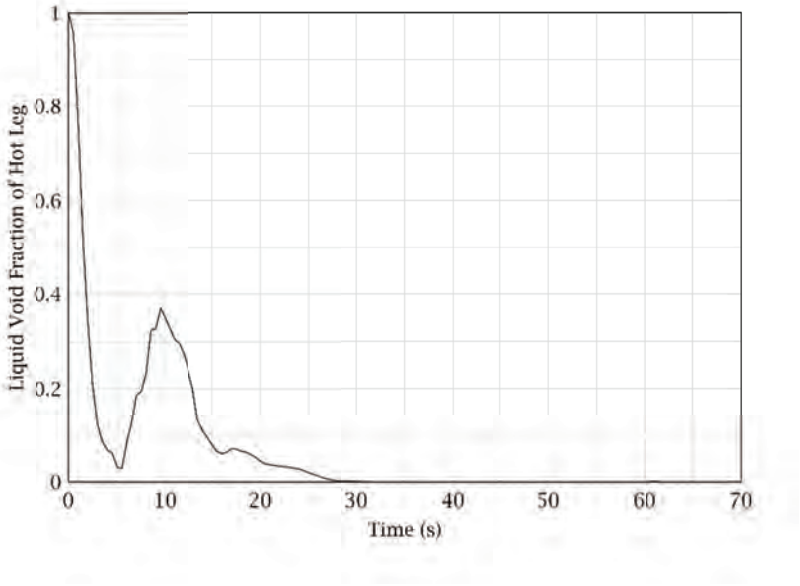

Figure 7-3. Calculation Results of Hot Leg Liquid Fraction for LOBI A1-66

8)

Code capability for the reflood phenomena was evaluated and described in Appendix C, D, and E of the topical report. The ATLAS test is used to confirm the code capability for the cyclic behavior.

The ATLAS test facility was designed to investigate thermal hydraulic behaviors of the APR1400. Therefore, the ATLAS test data and assessment results are determined to analyze the cyclic behavior of the core.

As shown in Figure 3-19 and Figure 3-20 of Appendix E, resorting to only collapsed water level data in the core and downcomer is [

]^{TS}. Therefore, the pressure difference between upper head and downcomer is investigated directly.

Figure 8-1 and Figure 8-2 show test and code calculated data on the pressure difference between the upper head and downcomer for ATLAS test 15. In test 15, [

]^{TS}. This pressure difference behavior is observed several times in Figure 8-1.

To confirm the code predictability for the cyclical behavior described above, it needs to be confirmed whether the code can predict the pressure difference behavior. Figure 8-2 shows the code predicted result of the pressure difference between the upper head and downcomer. [

]^{TS}.

Consequently, it is concluded based on the code assessment results of the ATLAS test that RELAP5/MOD3.3/K have the capability to predict cyclical behavior in the core and downcomer.

TS

Figure 8-1. Pressure Difference between Upper Head and Downcomer for ATLAS Test 15

TS

Figure 8-2. Code Predicted Pressure Difference between Upper Head and Downcomer for ATLAS Test 15

9)

In the RELAP5 code, two types of mass errors are computed as described in Reference [9-1]. If either K_m or K_{rms} is larger than 8×10^{-3}, the time step is repeated with one half of the time step size. The maximum of K_m or K_{rms} for all volumes can be found in minor edit (ERRMAX, current estimate of the truncation mass error fraction). The mass error fraction for the APR1400 plant and the LOFT test calculation are shown in Figure 9-1. As shown in Figure 9-1, the mass error is always lower than 8×10^{-3} during the transient.

Figure 9-2 and Figure 9-3 show the mass errors in all systems for the APR1400 plant and the LOFT test calculation. The total system masses at the start of each calculation are about [ ]^{TS} respectively, and the total system masses at the end of each calculation are about [ ]^{TS} respectively. The mass error for the APR1400 plant and the LOFT test are represented in Figure 9-4 and Figure 9-5. Since the mass error for the plant and the LOFT test calculation (300 kg and 1.5 kg respectively) are very low compared with total system mass, the effect on the calculation result is negligible.

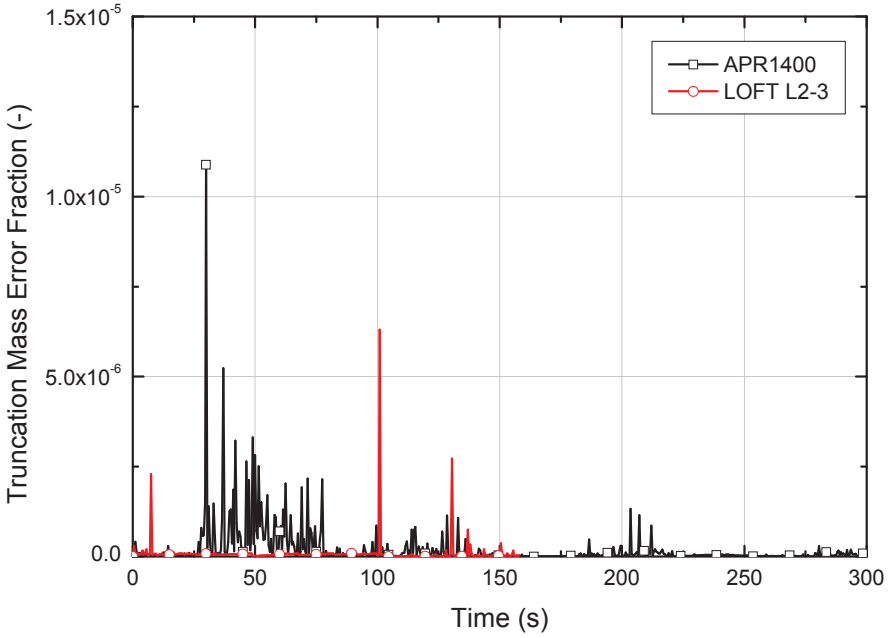

Figure 9-1. Truncation Mass Error Fraction for APR1400 Plant and LOFT L2-3 Test

TS

Figure 9-2. Total Mass in All the Systems of APR1400

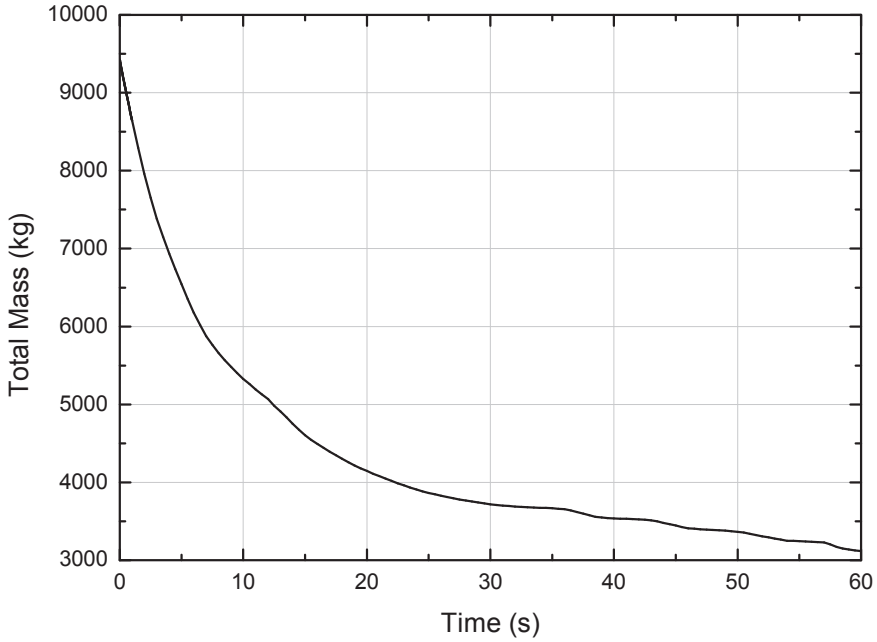

Figure 9-3. Total Mass in All the Systems of LOFT L2-3 test

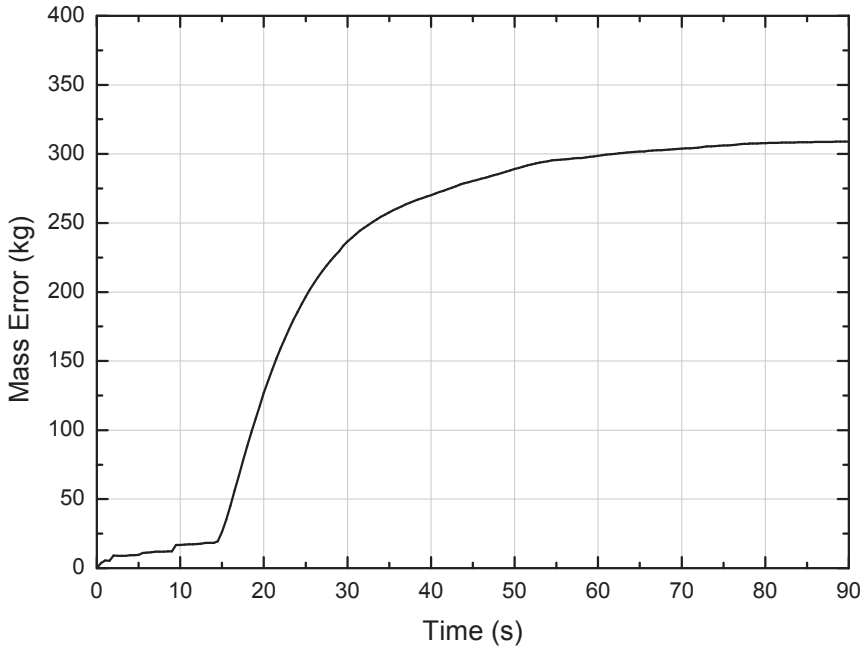

Figure 9-4. Mass Error in All the Systems of APR1400

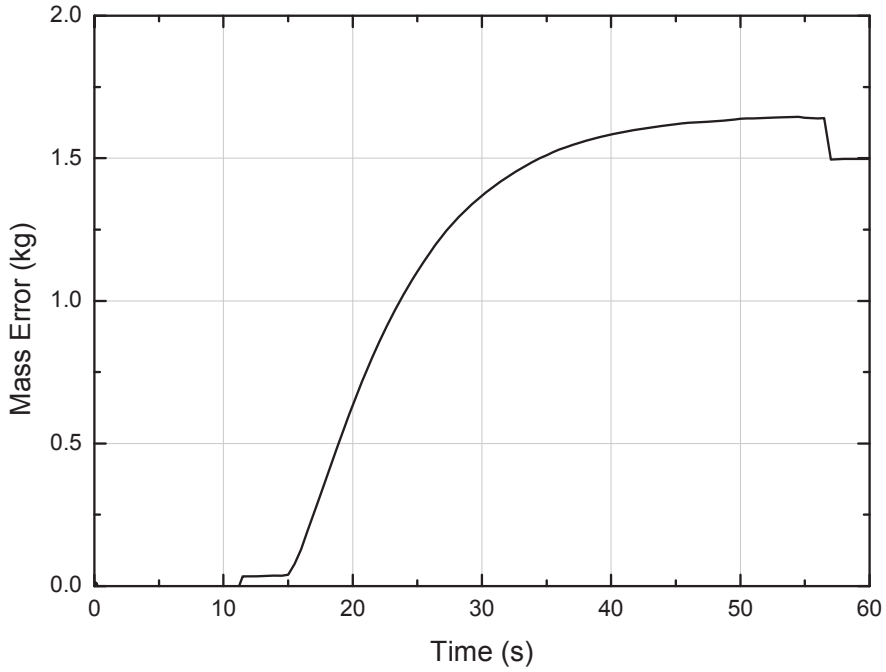

Figure 9-5. Mass Error in All the Systems of LOFT L2-3

Reference

[9-1] "RELAP5/MOD3.3 Code Manual Volume 1: Code Structure, System Models, and Solution Methods," NUREG/CR-5535, Information Systems Laboratories, March 2003.

10)

Predictability and conservatism of [ ]TS were assessed against various SETs and IETs and the assessment results are described in Appendix C, D, and E of the topical report. Therefore, it can be concluded that the applicability of [ ]TS was confirmed.

As to the multi-dimensional flow in the core, [ ]TS. However, the current core nodalization is applicable for the APR1400 because [ ]TS.

In general, experiments on CCFL are well correlated with the Kutateladze number as shown in Figure 10-1. Most important thing to check is the limiting gas velocity, $v_{s,Limit}$, above which no liquid fall back is possible.

[ ]TS

[

]TS

Consequently, chances of such liquid fall back causing multi-dimensional thermal hydraulic behavior are [

]TS thermal hydraulic behavior for the APR1400 LBLOCA analysis.

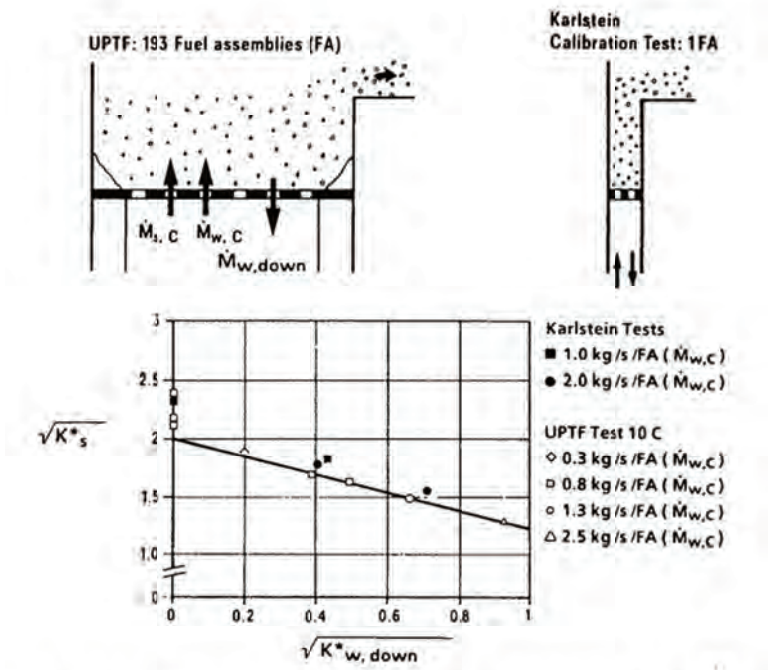

COUNTERCURRENT FLOW OF SATURATED STEAM AND WATER AT THE TIE PLATE

FIGURE 4.4-1

Figure 10-1. Figure 4.4-1 of the reference [10-1]

TS

Figure 10-2. Steam Velocity at Tie-Plate

TS

Figure 10-3. Steam and Liquid Flow Rate through the Tie Plate

TS

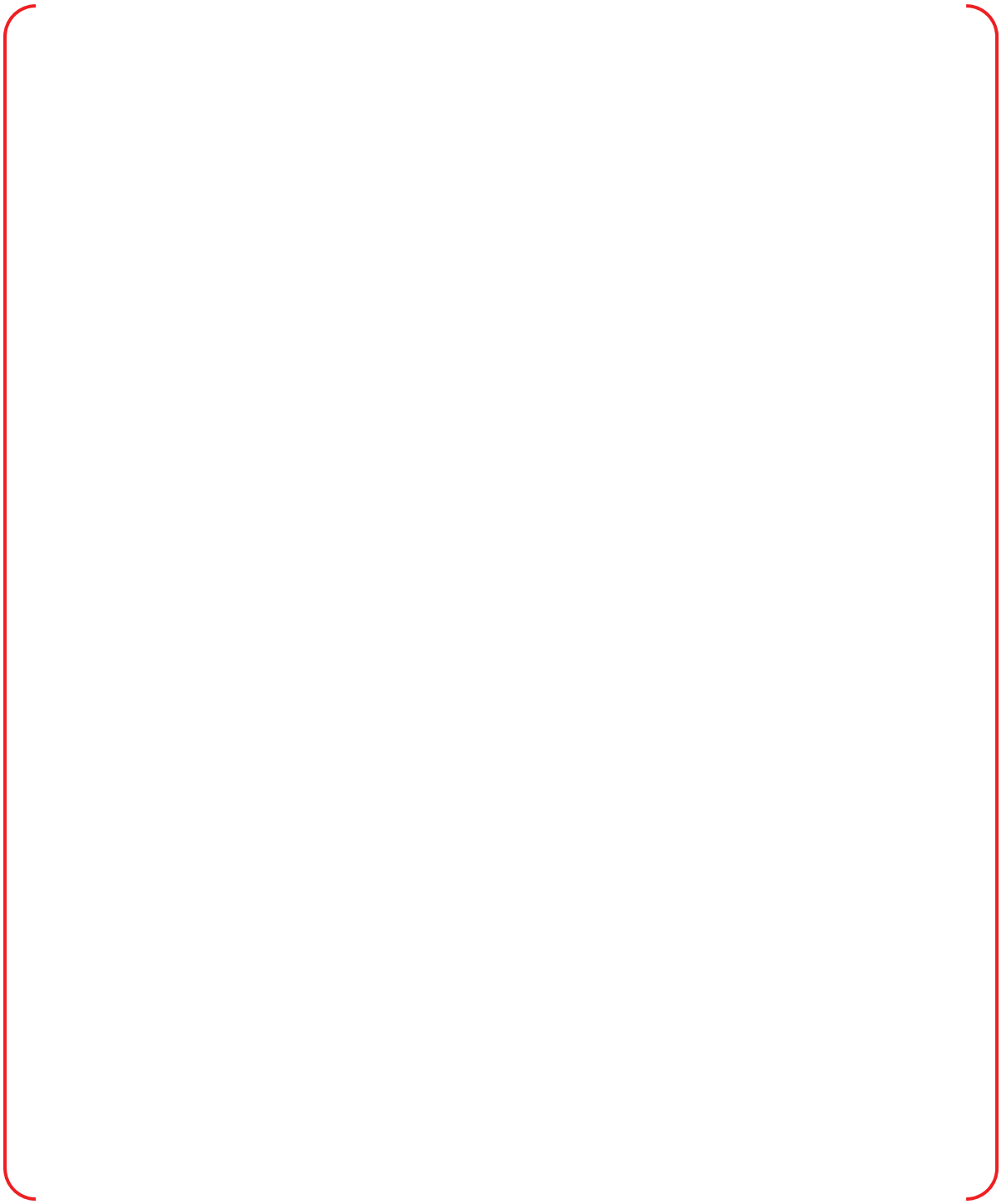

Figure 10-4. Core Nodalization to Capture Multi-Dimensional Flow

TS

Figure 10-5. Quadratic View of Core Fuel Assemblies

TS

Figure 10-6. Collapsed Water Levels of Upper Plenum Volumes

TS

Figure 10-7. Accumulated Liquid Mass Flow Rate from Low Power Channel and Average Channel to Upper Plenum

Reference

[10-1] “2D/3D Program Work Summary Report,” NUREG/IA-0126, GRS-100, MPR-1345, 1993.

Impact on DCD

There is no impact on the DCD.

Impact on PRA

There is no impact on the PRA.

Impact on Technical Specifications

There is no impact on the Technical Specifications.

Impact on Technical/Topical/Environmental Reports

Topical report (APR1400-F-A-TR-12004) will be revised as attached markup.

There is no impact on Technical or Environment Report.

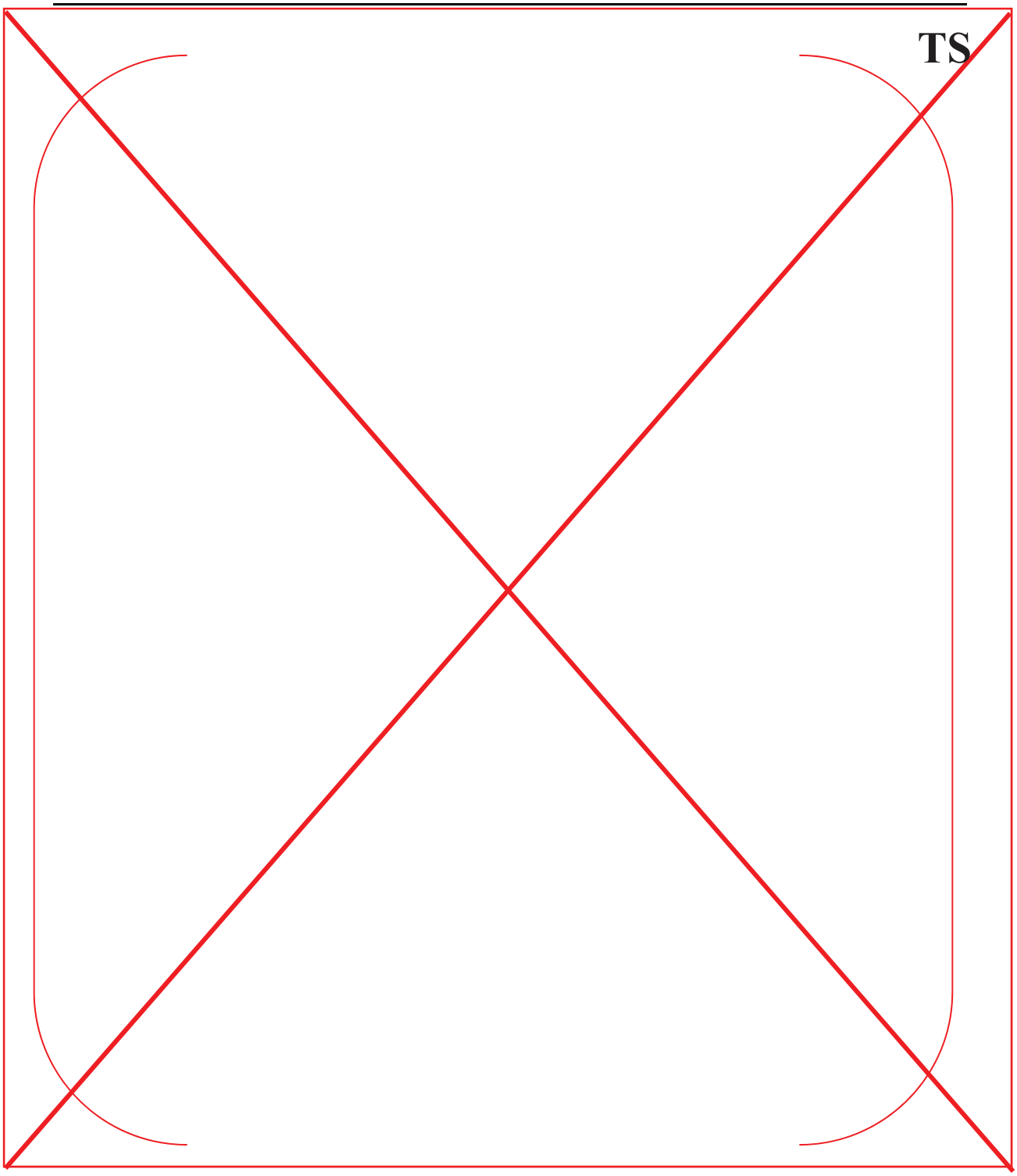

Figure 4-7 Code Accuracy during Blowdown Phase

TS

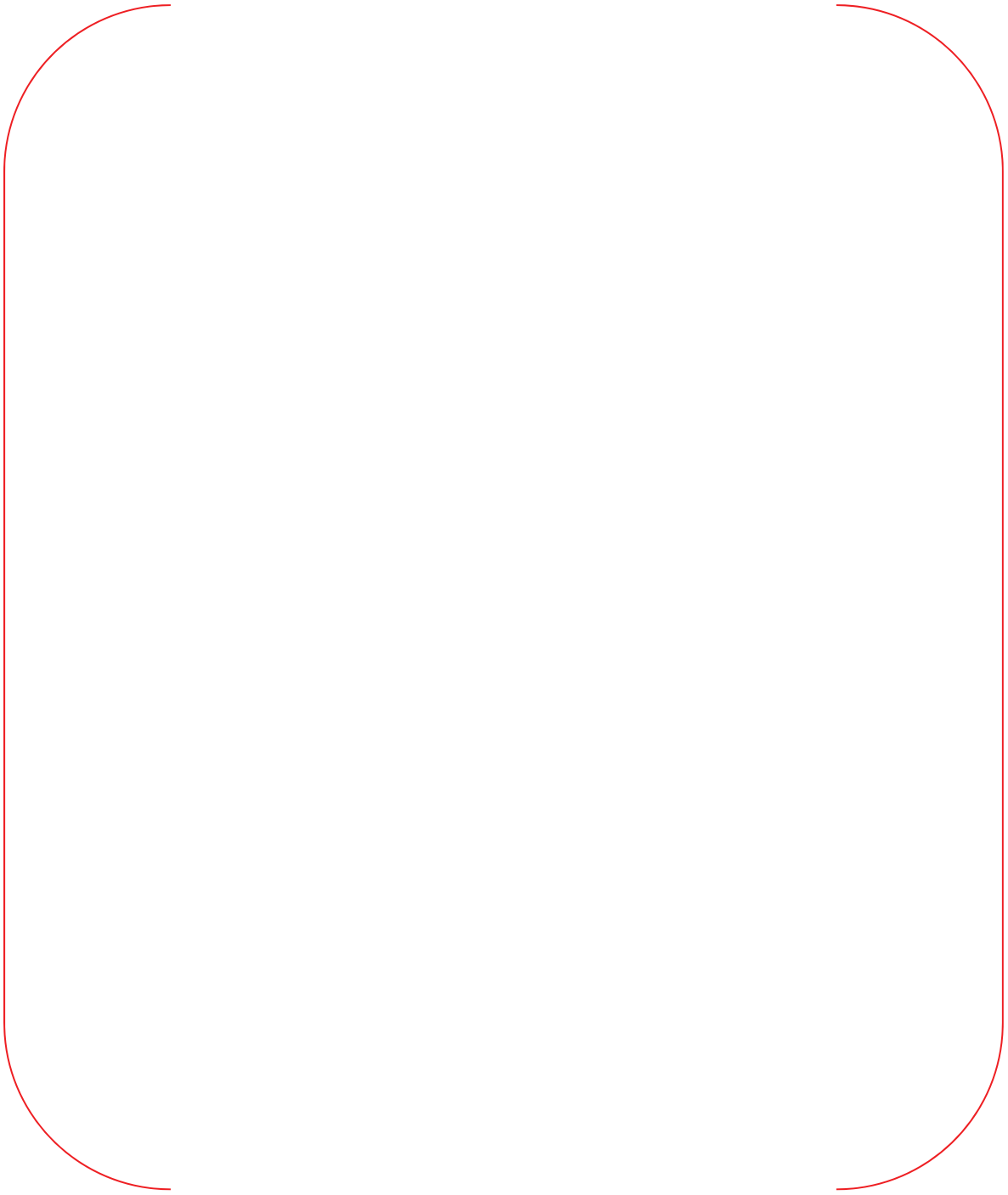

Figure 4-7 Code Accuracy during Blowdown Phase

Non-Proprietary

SECTION F

Page intentionally left blank

REVISED RESPONSE TO REQUEST FOR ADDITIONAL INFORMATION

APR1400 Topical Reports

Korea Hydro & Nuclear Power Co., LTD

Docket No. PROJ 0782

RAI No.:	**7-8567**
SRP Section:	**TR Realistic Evaluation Methodology for LBLOCA of the APR1400**
Application Section:	**Topical Report APR1400-F-A-TR-12004 Realistic Evaluation Methodology for Large-Break LOCA of the APR1400**
Date of RAI Issue:	**04/07/2016**

Question No. APR1400-4

10 CFR 50.46(a) states that the evaluation model for calculating the emergency core cooling system performance must adequately account for uncertainty in the calculated results. Section 15.0.2 of the standard review plan (NUREG-0800) states the uncertainty analysis must address all important sources of code uncertainty, including the mathematical models in the code and user modeling.

The phenomena identification and ranking table for the APR1400 large break loss of coolant accident identifies the cold leg to containment flow path as being a significant parameter during the refill and reflood phases. The friction and form losses associated with the cold leg to containment flow path are not included in the uncertainty parameters. This has caused NRC staff to question whether the treatment of uncertainty of these significant parameters is suitably conservative. NRC staff requests that KHNP justify their treatment of uncertainty associated with the cold leg to containment flow path in the refill and reflood phases.

10 CFR 50.46(a) states that the evaluation model for calculating the emergency core cooling system performance must adequately account for uncertainty in the calculated results. Section 15.0.2 of the standard review plan (NUREG-0800) states that the major sources of uncertainty must be addressed consistent with the results of the accident sequence identification process. In the development of the phenomena identification and ranking table (PIRT) for analysis of the APR1400 large break loss of coolant accident, [ ]^{TS} phenomena or processes were ranked as important. The topical report identifies [ ]^{TS} uncertainty parameters to be sampled. NRC staff is questioning whether the selection of uncertainty parameters adequately addresses the important phenomena identified in the PIRT. NRC staff requests the following additional information:

1. Explain how the sampled uncertainty parameters (identified in Table 5-1 of the topical report) were selected.

2. Explain how all the important phenomena identified in the PIRT are covered by the selected uncertainty parameters.

Response – (Rev.1)

1)

The entire process to determine the uncertainty parameters out of the selected phenomena/processes derived from the APR1400 PIRT were described in Attachment 1 of response to Audit Issue number 15 (Rev.1, ML17345A961). As described in the material, the phenomena already considered by [ ]TS, are not considered as uncertainty parameters. The APR1400 PIRT in the topical report contains some errors mostly related to the definition of time periods and will be revised.

2)

The explanation and justification of the parameters are described in the topical report and these are summarized in Table 1below. Among the [ ]TS phenomena/processes in the APR1400 PIRT, two phenomena are not mentioned in the topical report. One is the [ ]TS The [ ]TS It has been found that the APR1400 PIRT contains errors as to the time period definitions, and the revision to the APR1400 PIRT was submitted in Attachment 2 of response to Audit Issue number 15. The missing or insufficient rationale of the PIRT is reinforced in accordance with the revised PIRT. As described in the response to Question 1 above), the phenomena [ ]TS are not considered as uncertainty parameters.

(1) Phenomena treated by other uncertainty parameters

TS

TS

TS

TS

TS

TS

Table 1. Description of each process/phenomena in the topical report (1/3) TS

Table 1. Description of each process/phenomena in the topical report (2/3)

TS

Table 1. Description of each process/phenomena in the topical report (3/3)

TS

Table 2. Phenomena treated conservatively in CAREM

TS

Table 3. Modified APR1400 PIRT treated by biases

TS

TS

TS

Figure 1. The conventional noding diagram of UGS [ ]TS

TS

Figure 2. The most conservative noding diagram of UGS [ ]TS

Figure 3. The effect of the noding sensitivity

Figure 4. The effect of radiation heat transfer to surfaces on PCT

Reference

[1] "Korea Hydro & Nuclear Power Co., Ltd – Submittal of Revised Response to LBLOCA Audit Issues", Attachment 1 of Response to Audit Issue Number 15, Rev.1, ML17345A961, December 19 2017.

[2] "Korea Hydro & Nuclear Power Co., Ltd – Submittal of Revised Response to LBLOCA Audit Issues", Attachment 2 of Response to Audit Issue Number 15, Rev.1, ML17345A961, December 19 2017.

Impact on DCD

There is no impact on the DCD.

Impact on PRA

There is no impact on the PRA.

Impact on Technical Specifications

There is no impact on the Technical Specifications.

Impact on Technical/Topical/Environmental Reports

Topical report (APR1400-F-A-TR-12004) was revised and submitted (ML17240A221) based on the Attachments 1 and 2 of response to Audit Issue number 15.

There is no impact on Technical or Environment Report.

RESPONSE TO REQUEST FOR ADDITIONAL INFORMATION

APR1400 Topical Reports

Korea Hydro & Nuclear Power Co., LTD

Docket No. PROJ 0782

RAI No.:	**7-8567**
SRP Section:	**TR Realistic Evaluation Methodology for LBLOCA of the APR1400**
Application Section:	**Topical Report APR1400-F-A-TR-12004 Realistic Evaluation Methodology for Large-Break LOCA of the APR1400**
Date of RAI Issue:	**04/07/2016**

Question No. APR1400-5

10 CFR 50.46(a) states that the evaluation model for calculating the emergency core cooling system performance must adequately account for uncertainty in the calculated results. Section 15.0.2 of the standard review plan (NUREG-0800) states the uncertainty analysis must address all important sources of code uncertainty, including the mathematical models in the code and user modeling, such as nodalization.

Section 4.2.1 of topical report APR1400-F-A-TR-12004, Rev. 0 discusses the radial nodalization of the core. The discussion in the topical report does not discuss the assessment of the radial nodalization, which has caused NRC staff to question if the nodalization can capture the multidimensional effects in a realistic or suitably-conservative manner. NRC requests that KHNP provide additional justification for the radial nodalization used in the large break loss of coolant accident analyses.

Response

In CAREM, the core is [ ]TS as shown in Figure 4-1 of the topical report. In order to model the harsh conditions [

]TS Appendix C and D of the topical report describes the code assessment results against SETs and IETs. The core nodalizations of the SETs and IETs are modeled [ ]TS, thus are consistent with those of the APR1400 plant and RELAP5 predicts the cladding temperature of those tests well.

Multidimensional flows can be broadly characterized by two phenomena. First, high vapor velocities and liquid entrainment occur in the hot power region of the core. The entrained liquid from the core is carried into the upper plenum and entrained liquid is de-entrained by structures of the upper plenum and forming a two phase pool. The liquid from the pool can reenter the low power region of the core due to the low vapor velocities in those regions. Second is the transverse flow between the channels by the difference in the core power between the hot and low powered region.

The first phenomenon of multidimensional flow was evaluated in response to RAI 399-8510 (response to the question number 15.06.05-9 has been submitted in May). Evaluation results show [

]TS

Therefore, current nodalization, [ ]TS, is applicable to the analysis of LBLOCA of APR1400.

The second phenomenon of multidimensional flow is [ ]TS As mentioned above, [

]TS is considered for APR1400 as follows.

[

]TS

[

]TS

Consequently, [ ]TS nodalization is applicable to APR1400 LBLOCA analysis.

Impact on DCD

There is no impact on the DCD.

Impact on PRA

There is no impact on the PRA.

Impact on Technical Specifications

There is no impact on the Technical Specifications.

Impact on Technical/Topical/Environmental Reports

Topical report (APR1400-F-A-TR-12004) will be revised as attached markup.

There is no impact on Technical or Environment Report.

[

]TS

[

]TS

Hot Assembly Power

[

]TS

[

]TS

Hot Pin Power Peaking Factor

[

]TS

The technical specifications of the SKN 3 and 4 prescribe the LHGR limit as one of the limiting conditions for operation. The LHGR limit is defined as the product of Fq and the core average LHGR. The average LHGR at rated power is 5.602 kW/ft. The Fq corresponding to the LHGR limit 13.6 kW/ft is 2.428 (i.e., 13.6 kW/ft divided by 5.602 kW/ft). Therefore the range of Fq is extended to the limit of the technical specification of 2.428. The distribution function of Fq is conservatively assumed to be uniform.

- Parameter; hot pin power peaking factor (Fq)

  Distribution function; uniform

  Mean value; 2.184

  Minimum value; 1.940

  Maximum value; 2.428

5.1.2 Reactivity Feedback Related Parameters

Void Reactivity

The negative reactivity of the moderator rapidly reduces reactor power during the transient. Because the RELAP5/MOD3.3/K models the moderator density reactivity which corresponds to the void reactivity, it is necessary to treat the uncertainty of the moderator density reactivity. The moderator density reactivity is dependent on the moderator temperature coefficients (MTC); MTC involves various core parameters. This means that there is no one code parameter that characterizes the moderator density reactivity. Therefore, the uncertainty of the moderator density reactivity is treated conservatively. The core design provides two conservative moderator density reactivity curves for the LOCA analysis as shown in Figure 4-4. [

RESPONSE TO REQUEST FOR ADDITIONAL INFORMATION

APR1400 Topical Reports

Korea Hydro & Nuclear Power Co., LTD

Docket No. PROJ 0782

RAI No.:	**7-8567**
SRP Section:	**TR Realistic Evaluation Methodology for LBLOCA of the APR1400**
Application Section:	**Topical Report APR1400-F-A-TR-12004 Realistic Evaluation Methodology for Large-Break LOCA of the APR1400**
Date of RAI Issue:	**04/07/2016**

Question No. APR1400-6

10 CFR 50.46(a) states that the evaluation model for calculating the emergency core cooling system performance must adequately account for uncertainty in the calculated results. Section 15.0.2 of the standard review plan (NUREG-0800) states the uncertainty analysis must address all important sources of code uncertainty, including the mathematical models in the code and user modeling.

The phenomena identification and ranking table for the APR1400 large break loss of coolant accident identifies the cold leg to containment flow path as being a significant parameter during the refill and reflood phases. The friction and form losses associated with the cold leg to containment flow path are not included in the uncertainty parameters. This has caused NRC staff to question whether the treatment of uncertainty of these significant parameters is suitably conservative. NRC staff requests that KHNP justify their treatment of uncertainty associated with the cold leg to containment flow path in the refill and reflood phases.

Response

The phenomena “cold leg to containment flow path” is defined in reference [4] of the topical report as [

]TS

In CAREM, the discharge coefficients are determined by assessment against the [ ]TS test. In the determination of the discharge coefficients, it is believed that [

]TS Then, the limiting break condition is found instead of considering the uncertainty of the break location, type and size. Since the worst break condition is used, the uncertainty evaluation of the break condition is not required. However, there are concerns related with the flow resistance uncertainty.

These concerns can be treated by the uncertainty parameter for [ ]TS , which is already used in CAREM and is described in Section 5.1.7 of the topical report. The uncertainty parameter is intended to consider the uncertainty of [

]TS Also, the plant input making process of CAREM includes the checking of the steady state pressure differences with the designed values.
[ ]TS

Impact on DCD

There is no impact on the DCD.

Impact on PRA

There is no impact on the PRA.

Impact on Technical Specifications

There is no impact on the Technical Specifications.

Impact on Technical/Topical/Environmental Reports

There is no impact on any Technical, Topical, or Environment Report.

RESPONSE TO REQUEST FOR ADDITIONAL INFORMATION

APR1400 Topical Reports

Korea Hydro & Nuclear Power Co., LTD

Docket No. PROJ 0782

RAI No.:	**7-8567**
SRP Section:	**TR Realistic Evaluation Methodology for LBLOCA of the APR1400**
Application Section:	**Topical Report APR1400-F-A-TR-12004 Realistic Evaluation Methodology for Large-Break LOCA of the APR1400**
Date of RAI Issue:	**04/07/2016**

Question No. APR1400-7

10 CFR 50.46(a) states that the evaluation model for calculating the emergency core cooling system (ECCS) performance must include sufficient supporting justification to show that the analytical technique realistically describes the behavior of the reactor system during a loss- of-coolant accident.

Evaluation of ECCS bypass included a comparison against data from the upper plenum test facility (UPTF). KHNP selected test UPTF-4A, with cold leg injection, to determine the ECCS bypass bias during the refill phase. Tests UPTF-21A and UPTF-21B involve downcomer injection of the ECCS. Because the APR1400 utilizes direct vessel injection, NRC staff is questioning if test UPTF-4A is the appropriate choice for determining ECCS bypass bias. NRC staff requests that KHNP justify their selection of the UPTF-4A test, with cold leg injection, to determine ECCS bypass bias during the refill phase in their evaluation model.

Response

The ECC bypass during the end-of-blowdown and refill period is mainly dependent on the flow mixing behavior below the cold leg bottom. Therefore, it has been considered that the ECC injection type is less important in comparison to the depressurization process. Also, the test configurations of UPTF-21A, -21B tests are not exactly the same as the LBLOCA conditions during the end-of-blowdown and refill period; the broken hot leg break valve and the pump simulators were closed. The initial pressure in the primary system and containment simulator was set at approximately 0.3 MPa, thus the depressurization process was not investigated through the tests. In other words, UPTF-21A, -21B tests are the tests for steady-state downcomer CCFL tests with DVI geometry and the steam flow rates injected from the core simulator were determined from the end-of-blowdown and refill condition, respectively.

Impact on DCD

There is no impact on the DCD.

Impact on PRA

There is no impact on the PRA.

Impact on Technical Specifications

There is no impact on the Technical Specifications.

Impact on Technical/Topical/Environmental Reports

There is no impact on any Technical, Topical, or Environment Report.

SPONSE TO REQUEST FOR ADDITIONAL INFORMATION

APR1400 Topical Reports

Korea Hydro & Nuclear Power Co., LTD

Docket No. PROJ 0782

RAI No.:	**7-8567**
SRP Section:	**TR Realistic Evaluation Methodology for LBLOCA of the APR1400**
Application Section:	**Topical Report APR1400-F-A-TR-12004 Realistic Evaluation Methodology for Large-Break LOCA of the APR1400**
Date of RAI Issue:	**04/07/2016**

Question No. APR1400-8

10 CFR 50.46(a) states that the evaluation model for calculating the emergency core cooling system (ECCS) performance must include sufficient supporting justification to show that the analytical technique realistically describes the behavior of the reactor system during a loss-of-coolant accident.

Evaluation of ECCS bypass included a comparison against data from the advanced thermal-hydraulic test loop for accident simulation (ATLAS). For ATLAS Test 15, downcomer wall temperatures and collapsed liquid levels in the core and downcomer region appear to show that RELAP is under-predicting ECCS bypass. This has caused NRC staff to question whether the evaluation model can capture ECCS bypass during reflood in a suitably conservative way. NRC staff requests the following information of KHNP:

1. Explain the cause of RELAP5 over-predicting the collapsed liquid level in the core and downcomer for ATLAS Test 15.

2. Explain how the evaluation model for large break loss-of-coolant accident analysis captures the phenomena of ECCS bypass in a suitably conservative way.

Response

1)

As discussed in Appendix E of the topical report, the result of the initial period (the period before 200 sec after the beginning of the test) of the ATLAS tests include [

]TS

Therefore, it was concluded that the test results of initial period in ATLAS test 9 and 11 are neglected.

However, it was determined to assess whole test period for the ATLAS test 15 because the initial condition of test 15 is adjusted to have a [

]TS And it has low flow rate of ECCW as boundary condition. These conditions decrease [ ]TS compared to the test results of the other tests. Therefore, the ATLAS test 15 is assessed by the code for the whole reflood test period, and ECCW bypass phenomenon during the whole reflood period is evaluated.

Consequently, the water level and ECCW bypass of the initial period are [

]TS, thus it is concluded that RELAP5/MOD3.3/K code conservatively predicts water level and ECCW bypass during general reflood period.

2)

Code predictability on the ECCW bypass phenomenon is evaluated by experimental data of ATLAS, MIDAS and UPTF as described in Appendix E and F of the topical report, and it is concluded that ECCW bypass during the refill period is considered [

]TS

Code assessment on the ECCW bypass during reflood period is performed using ATLAS, MIDAS and UPTF-21D test data.

Impact on DCD

There is no impact on the DCD.

Impact on PRA

There is no impact on the PRA.

Impact on Technical Specifications

There is no impact on the Technical Specifications.

Impact on Technical/Topical/Environmental Reports

There is no impact on any Technical, Topical, or Environment Report.

RESPONSE TO REQUEST FOR ADDITIONAL INFORMATION

APR1400 Topical Reports

Korea Hydro & Nuclear Power Co., LTD

Docket No. PROJ 0782

RAI No.:	**7-8567**
SRP Section:	**TR Realistic Evaluation Methodology for LBLOCA of the APR1400**
Application Section:	**Topical Report APR1400-F-A-TR-12004 Realistic Evaluation Methodology for Large-Break LOCA of the APR1400**
Date of RAI Issue:	**04/07/2016**

Question No. APR1400-9

10 CFR 50.46(a) states that the evaluation model for calculating the emergency core cooling system performance must adequately account for uncertainty in the calculated results. Section 15.0.2 of the standard review plan (NUREG-0800) states the uncertainty analysis must address all important sources of code uncertainty, including the mathematical models in the code and user modeling.

Section 5.1.4 of topical report APR1400-F-A-TR-12004-P, Rev. 0, discusses the treatment of the uncertainty associated with the pump two-phase degradation multiplier. The topical report states that the pump is assumed to be [

]^{TS} This has caused NRC staff to question the treatment of uncertainty associated with pump two-phase performance. Additionally, the mean value provided for the distribution function is stated to be below the minimum value for the distribution. NRC staff requests the following additional information:

1. Provide justification for the chosen uncertainty range for the pump two-phase pump degradation multiplier.

2. Correct the information in Section 5.1.4 regarding the distribution.

Response

1)

Pump degradation multiplier is used to model a pump performance for 2-phase flow and it is divided into the 2-phase head multiplier and 2-phase torque multiplier as follows.

$$H = H_{1\Phi} - M_H(\alpha_g)\left(H_{1\Phi} - H_{2\Phi}\right) \qquad \text{Eq. (1)}$$

$$\tau = \tau_{1\Phi} - M_\tau(\alpha_g)\left(\tau_{1\Phi} - \tau_{2\Phi}\right) \qquad \text{Eq. (2)}$$

where,

H = the total pump head

$H_{1\Phi}$ = the single-phase pump head

$H_{2\Phi}$ = the fully degraded pump head

M_H = the head degradation multiplier (or the 2-phase head multiplier)

$\tau_{1\Phi}$ = the single-phase pump torque

$\tau_{2\Phi}$ = the fully degraded pump torque

M_τ = the torque degradation multiplier (or the 2-phase torque multiplier)

α_g = the vapor fraction

Pump degradation is expressed via two-phase multiplier curves. [

]TS

Based on the sensitivity studies as described in Section 5.1.4 of topical report, [

]TS

- Parameter; pump two-phase degradation multiplier

[

]TS

2)

The topical report will be corrected as follows:

- Parameter; pump two-phase degradation multiplier

[

]TS

Impact on DCD

There is no impact on the DCD.

Impact on PRA

There is no impact on the PRA.

Impact on Technical Specifications

There is no impact on the Technical Specifications.

Impact on Technical/Topical/Environmental Reports

Topical report (APR1400-F-A-TR-12004) will be revised as attached markup.

There is no impact on Technical or Environment Report.

multiplier values are relatively lower at low void fractions; the other is for such pumps such as the B&W pump, CREARE air/water pump, Semiscale pump, and the pump used for CE evaluation model, of which head multiplier values approach nearly 1.0 above the 30 % void fraction. Sensitivity studies were performed using the Byron-Jackson and the Semiscale pump data. These data are the representative pump data of each pump group. [

]TS

- Parameter; pump two-phase degradation multiplier
- [

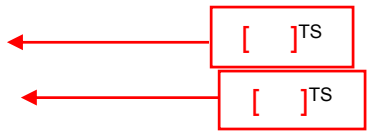

]TS

5.1.5 Safety Injection System Related Parameters

Parameters associated with the safety injection system can be divided into SIT parameters and SIP parameters. SIT parameters include water volume, water temperature, and nitrogen gas pressure. SIP parameters include IRWST water temperature and injection flow rate.

[

]TS

- Parameter; [

]TS

- Parameter; [

]TS

- Parameter; [

Appendix E

Assessment of RELAP5/MOD3.3/K against APR1400 Reflood Tests

Non-Proprietary

August 2018

Table of Contents

List of Tables

List of Figures

1. Introduction

The ATLAS (Advanced Thermal-hydraulic Test Loop for Accident Simulation), a thermal-hydraulic integral effect test facility, was designed and manufactured to analyze transient and accident conditions of the APR1400 and the OPR1000. It is a 1/2 reduced height and 1/288 volume scaled test facility based on the design features of the APR1400. Several tests for the reflood phase of a large break (LB) loss of coolant accident (LOCA) have been conducted with the ATLAS.

This appendix describes the assessment of RELAP5/MOD3.3/K code against the APR1400 LBLOCA tests performed using the ATLAS test facility. Three tests simulated a large break LOCA of the APR1400; ATLAS LB-CL-09 (Test 09), LB-CL-11 (Test 11), and LB-CL-15 (Test 15) were used for the code assessment. The major phenomena related to the direct vessel injection (DVI) of the emergency core cooling water (ECCW), such as boiling of the downcomer inventory and ECCW bypass, were investigated in these tests.

The details of the ATLAS test facility and the test results are described in Chapter 2. The code assessment against the ATLAS LBLOCA tests is described in Chapter 3. The capability of RELAP5/MOD3.3/K in predicting ECCW bypass and downcomer boiling phenomena is described in Chapter 4.

2. Overview of the ATLAS LBLOCA Tests

The APR1400 LBLOCA experiments were performed in the ATLAS test facility to investigate major phenomena related to the direct vessel injection of the ECCW. For the simulation of APR1400 LBLOCA, total 14 tests were performed including seven parametric effect tests (i.e., Test 01-Test 07). The other tests (i.e., Test 08-Test 14) simulated the entire reflood phase of the APR1400 LBLOCA. In addition to these tests, two additional tests (i.e., Test 14B and Test 15) were conducted to investigate the reflood phenomena. The purpose of these tests were; to obtain the information on the main phenomena such as ECCW bypass, downcomer boiling, steam binding and so on; and to understand the main phenomena of the APR1400 by analyzing the test results.

Among the ATLAS LBLOCA tests, the representative tests of Test 09, Test 11, and Test 15 are selected in order to assess the capability of RELAP5/MOD3.3/K code in predicting the reflood progression.

2.1 ATLAS Test Facility

A schematic diagram and a 3-dimensional view of the ATLAS facility are presented in Figure 2-1 and Figure 2-2, respectively. The ATLAS test facility is an IET facility which simulates the entire systems of a nuclear power plant and consists of the fluid system, the instrumentation and control system, the data processing system, the power supply system, and the subsystems. The ATLAS has the same two-loop features as the APR1400. The ATLAS test facility was designed according to the scaling method suggested by Ishii-Kataoka in order to simulate many experimental scenarios as close as possible to the actual reference plant. The major scaling factors are presented in Table 2-1. The ATLAS was scaled down as 1/2 in length, 1/12 in diameter, 1/144 in area, 1/288 in volume, and $1/\sqrt{2}$ in time, compared to the APR 1400. The detailed information on the design and scaling factor of the ATLAS test facility are presented in Reference [1].

The ATLAS facility consists of the primary system, secondary system, safety injection system, break simulator system, containment simulating system, auxiliary system, and heat loss compensating system. The primary system includes a reactor vessel, two hot legs, four cold legs, a pressurizer, four reactor coolant pumps, and two steam generators. The secondary system consists of main steam system, main feedwater system, auxiliary feedwater system, and auxiliary devices. The heat loss compensating system compensates heat loss of the primary system and the safety injection system. The safety injection system consists of four trains of SIT-FDs (Safety Injection Tank equipped with a Fluidic Device), four trains of SIPs (Safety Injection Pumps), shutdown cooling pumps, low pressure SIPs, and shutdown cooling heat exchangers for shutdown cooling operation. The break simulation system consists of break simulation lines which can simulate the LBLOCA, DVI line break, SBLOCA (Small Break Loss-of-Coolant Accident), SGTR (Steam Generator Tube Rupture), MSLB (Main Steam Line Break) and so on. Each break simulation line consists of a quick opening valve, a break nozzle, and instruments. The containment simulating system has a function of collecting the break flow and maintaining a specified containment back-pressure.

The ATLAS has more than 1,200 instruments in order to catch important phenomena of tests. Among the extensive instruments, the locations of the instruments for measuring the water levels of the reactor pressure vessel are shown in Figure 2-3.

As shown in Figure 2-4, the core simulator has 390 electric heater rods which are divided concentrically into 3 groups (Group-1, Group-2, and Group-3). Group-1, -2, and -3 heater rods are located in inner, middle, and outer regions of the heater bundle respectively. Group-1, -2, and -3 have 102, 138, and 150 heater rods, respectively. The cross-sectional location of the thermocouples in the core heater bundles are shown in this figure. The axial location of the

thermocouples for fuel rod and core fluid temperature, spacer grids, and level transmitters are shown in Figure 2-5.

2.2 Test Initial and Boundary Conditions

This section describes the initial and boundary conditions of the ATLAS tests selected for the code assessment.

The ATLAS Tests 09 and 11 were to investigate various thermal hydraulic phenomena during the reflood phase. The ATLAS Test 09, which was an experiment to investigate the thermal hydraulic phenomena during the entire reflood phase, was performed under the conservative conditions; 1.2 times of the ANS-73 decay heat curve was used for the core decay heat, and the containment pressure was set to 0.10 MPa. In this test, the worst single failure of a safety injection system (i.e., one emergency diesel generator failure) was assumed. In addition to this assumption, another one SIP was assumed to fail due to loss of the cooling capacity of component cooling system after several hours later one emergency diesel generator failure. Thus four SITs and two SIPs were operated in these tests. The scaled-down safety injection flow rates are shown in Figure 2-6. The conditions at the start of the reflood period of the APR1400 LBLOCA were given as initial and boundary conditions. The initial conditions were achieved by draining the inventory in the primary system by using vent valves. After the draining of the primary system, operator actions were focused on the achievement of the initial conditions for the reflood tests (e.g., the downcomer wall temperature, the collapsed water levels in the downcomer, lower plenum and core, etc.). When the reactor vessel water level, downcomer wall temperature, and heater rod temperature matched their target values, the tests were started by injecting ECCW from the four SITs. During the injection of ECCW from the SITs, the reflood period started when the lower plenum water level reached to the bottom of the active core. The test procedures and the safety injection flow rates of the ATLAS Test 11 were the same as the Test 09 in general. However, it was performed under the best estimate conditions; the core decay heat was 1.02 times of the ANS-79 decay heat curve, and the containment pressure was set to 0.20 MPa.

The ATLAS Test 15 was a separate effect test to investigate the reflood phenomena with only four SIP injection from DVI nozzles. The test procedure of the Test 15 was almost the same as the Test 09 and Test 11.

The initial and boundary conditions of the ATLAS tests 09, 11 and 15 are presented in Table 2-2. The sequences of the major events during the tests 09, 11 and 15 are presented in Table 2-3. In this table, 'Time (DAS)' means the time after the start of measurements and 'Time (Reflood)' means time after the start of the reflood. For the Test 09 and 11, the SIT injection started 2 s before the reflood beginning time and the SIP injection started 15 s after the reflood beginning time.

2.3 Test Results

The major results of the tests 09, 11 and 15 are presented in this section. The detailed information on the test results can also be found in References [2], [3] and [4].

2.3.1 ATLAS Test 09

The pressure behavior of the primary system is shown in Figure 2-7, and the collapsed water levels of the downcomer and the core are shown in Figure 2-8. The primary system pressure increased abruptly when the safety injection water was injected from the SITs. The safety injection flow rates from the SITs and SIPs are shown in Figure 2-9 with the scaled-down safety injection flow rate of the APR1400. The main reason for the pressure increase was due to the [ ]^{TS} and the core heater rods to the coolant inventory in the downcomer and the core. The pressure increased

again at around 2,050 s in DAS time. This second pressure increase was mainly due to that [

]TS. [

]TS The more detailed analysis of the measured water levels is presented in Chapter 3.

The cladding temperatures of the rods in Group 1 are presented in Figure 2-10. In the ATLAS Test 09, the cladding temperatures of the rods in the Group 1 showed higher values than those in Group 2 and Group 3. The highest cladding temperature was [

]TS

The reactor vessel wall (alternatively called as downcomer wall) temperatures and fluid temperatures measured at lower downcomer region below the cold leg elevation are shown in Figure 2-11. The inner surface (facing to the downcomer) temperature of the reactor vessel wall drastically decreased to water temperature as soon as the injected water from the SITs introduced into the lower downcomer because the thermocouples to measure inner surface temperature of the reactor vessel wall were contacted with the safety injection water from the SITs. Because the outer surface of the reactor vessel wall was isolated, the outer surface (facing to the atmosphere) temperatures of the reactor vessel wall gradually decreased due to heat conduction to the inside.

Figure 2-12 shows the accumulation of the break mass flow rate discharged from the vessel side break plane. The accumulations of the break mass flow rate obtained using two methods are shown in this figure; one is the accumulation of the measured break flow rate and the other is accumulation of the break flow rate obtained from the mass balance using the injected water and the vessel inventory. [

]TS

2.3.2 ATLAS Test 11

The pressure behavior of the primary system is shown in Figure 2-13, and the collapsed water levels of the downcomer and the core are shown in Figure 2-14. The primary system pressure behavior of the Test 11 showed a very similar trend with that observed in Test 09. Whereas, the measured primary pressure was higher than that of the Test 09 because the simulated containment back pressure was around twice of that of Test 09. [

]TS because the saturation temperature of the water inventory in the downcomer increased due to the higher containment back pressure. The trivial downcomer boiling was observed from 1,620 s to 1,720 as shown in Figure 2-14. The safety injection flow rate simulated during Test 11 is shown in Figure 2-15.

The cladding temperatures of the rods in Group 1 are presented in Figure 2-16. The cladding temperatures of the rods in the Group 1 showed higher values than those in the other groups. [

]TS. The rod clad quenching time was faster than Test 09 by 350 s because water levels in the downcomer and the core increased earlier than Test 09 [ ]TS The cladding temperatures were [ ]TS This

implies that the effect of the downcomer boiling phenomena on the core reflood was minimal in Test 11.

The reactor vessel wall temperatures and fluid temperatures measured at the lower downcomer region are shown in Figure 2-17. The wall temperature behavior was fairly similar with Test 09. The accumulations of the break flow rates obtained using the two methods are shown in Figure 2-18. The break flow was less than that of Test 09.

2.3.3 ATLAS Test 15

Test 15 was designed to investigate the reflood phenomena in APR1400; only four SIPs injected ECCW during the test. The downcomer wall temperature was set at 150 ^{o}C. The initial and boundary conditions of the ATLAS Test 15 are presented in Table 2-2 .

Figure 2-19 shows the pressure behavior of the system primary side, and Figure 2-20 presents the collapsed water levels of the downcomer and the core. The primary side pressure was initially maintained at the containment back pressure of 0.1 MPa. After the start of the SIPs injection at 1,243 s, the primary system pressure started to increase due to the evaporation of the injected ECCW in the downcomer. After then, the system pressure gradually increased as the core reflooding began and the containment simulator pressure increased. Figure 2-21 shows the ECCW injection rate from the four SIPs. The downcomer and core water levels increased gradually after the ECCW injection. In general, the downcomer water level was higher than the core water level.
[

]^{TS}; the downcomer and core water levels gradually increased during the test.

The cladding temperatures of the rods in Group 1 are presented in Figure 2-22. The observed cladding temperature behaviors were fairly similar with those of another reflood tests such as the FLECHT-SEASET tests. The highest cladding temperature of [ ]^{TS} The entire core was quenched at 1,520 s.

The reactor vessel wall temperatures and fluid temperatures measured at the lower downcomer region are shown in Figure 2-23. The wall temperature behaviors were similar with the other two tests. The accumulations of the break flow rates obtained using the two methods are shown in Figure 2-24. The break flow was less than those of the other two tests since the core power was smaller than the other tests and the SITs were not simulated in this test.

Table 2-1 Major Scaling Factors of the ATLAS Test Facility

Parameter	Scaling law	ATLAS design
Length	l_{OR}	1/2
Diameter	d_{OR}	1/12
Area	d_{OR}^2	1/144
Volume	$l_{OR}d_{OR}^2$	1/288
Core temperature rise	ΔT_{OR}	1
Velocity	$l_{OR}^{1/2}$	$1/\sqrt{2}$
Time	$l_{OR}^{1/2}$	$1/\sqrt{2}$
Power/Volume	$l_{OR}^{-1/2}$	$\sqrt{2}$
Heat flux	$l_{OR}^{-1/2}$	$\sqrt{2}$
Core power	$l_{OR}^{1/2}d_{OR}^2$	1/203.6
Flow rate	$l_{OR}^{1/2}d_{OR}^2$	1/203.6
Pressure drop	l_{OR}	1/2

Table 2-2 Initial and Boundary Conditions of the ATLAS Tests

TS

Table 2-3 Sequence of Events of the ATLAS Tests

TS

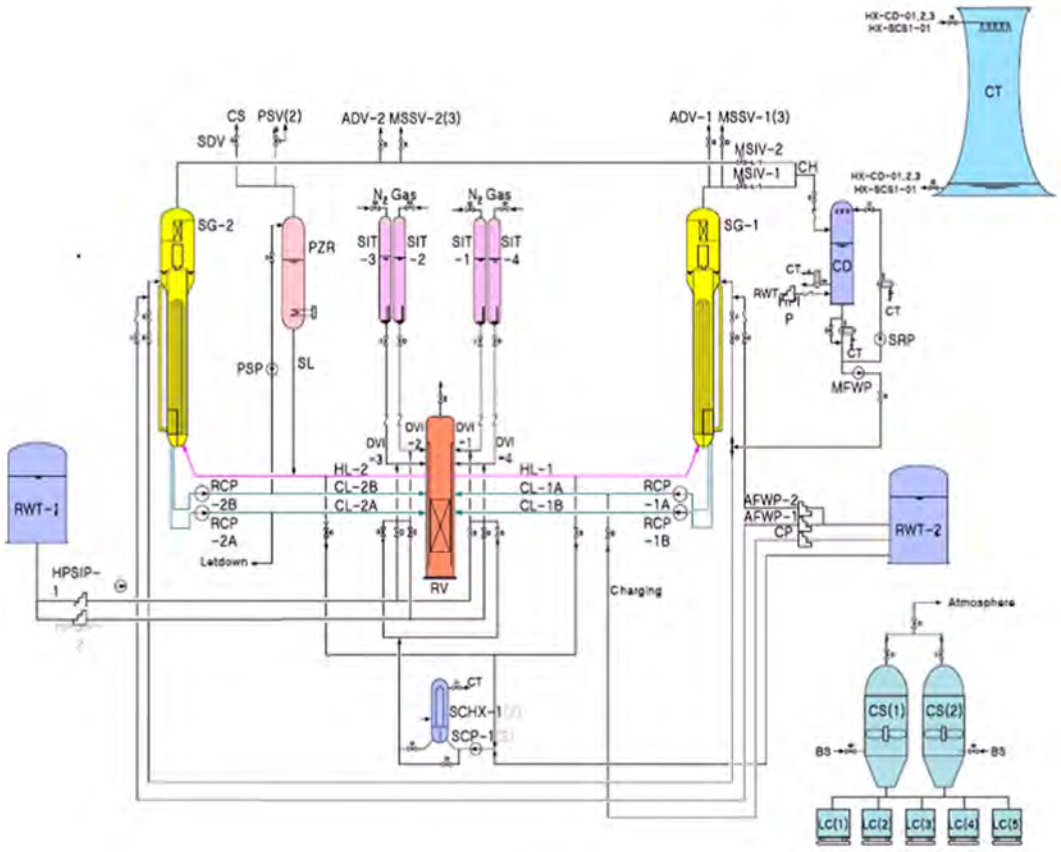

Figure 2-1 Schematic diagram of the ATLAS Test Facility

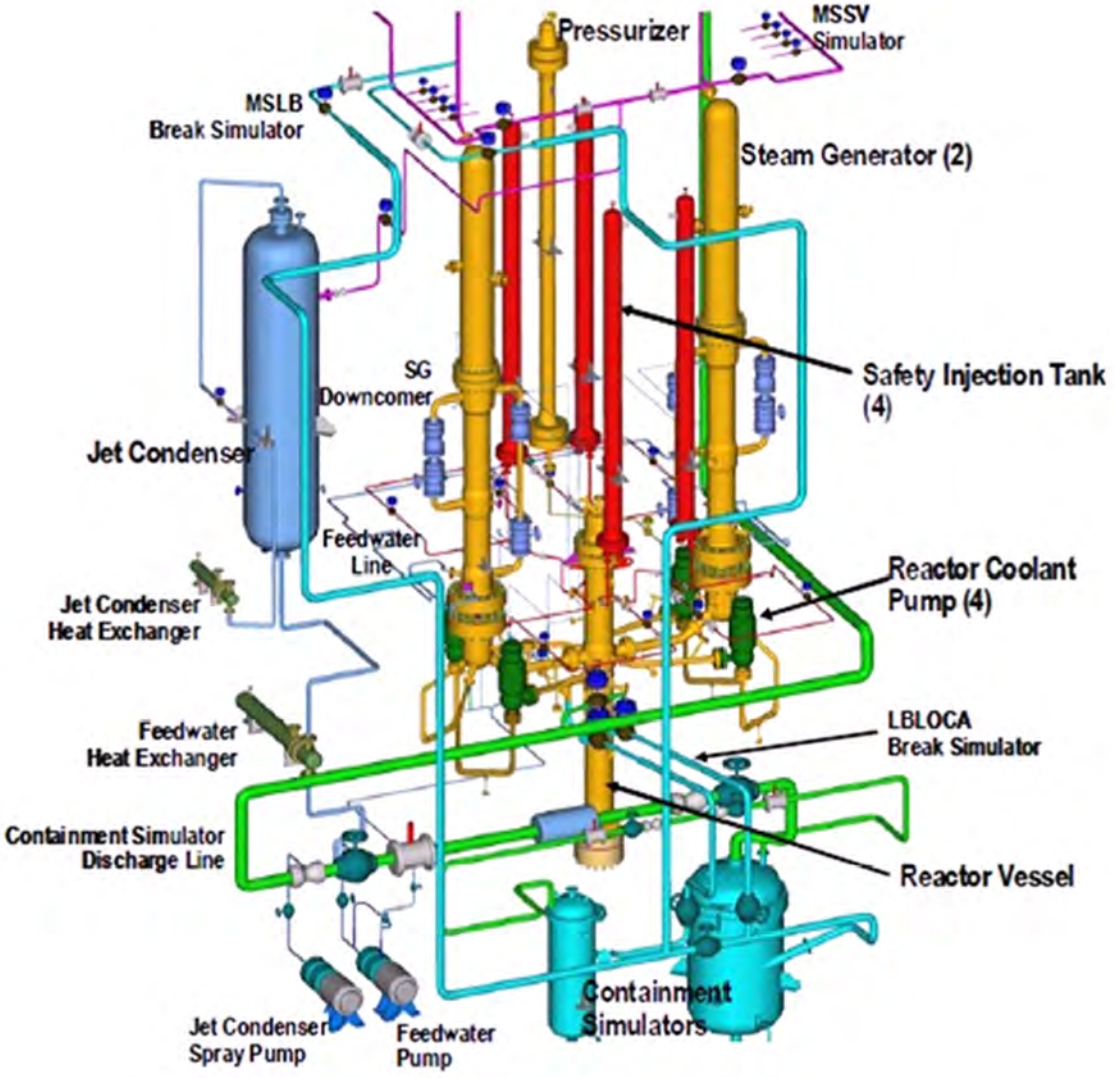

Figure 2-2 3-D View of the ATLAS Test Facility

TS

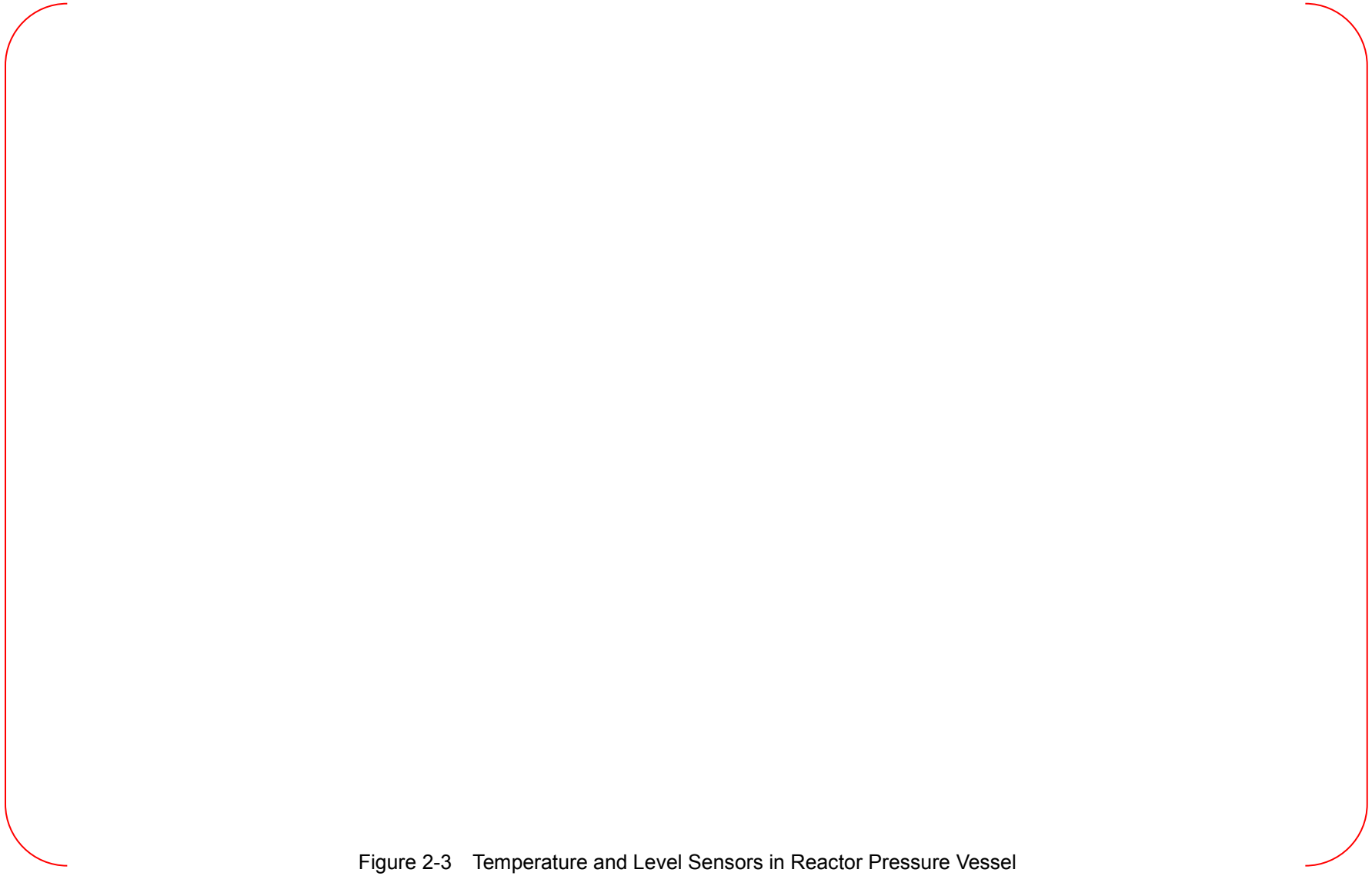

Figure 2-3 Temperature and Level Sensors in Reactor Pressure Vessel

Figure 2-4 Temperature and Level Sensors in Reactor Pressure Vessel

Figure 2-5 Temperature and Level Sensors in the Core

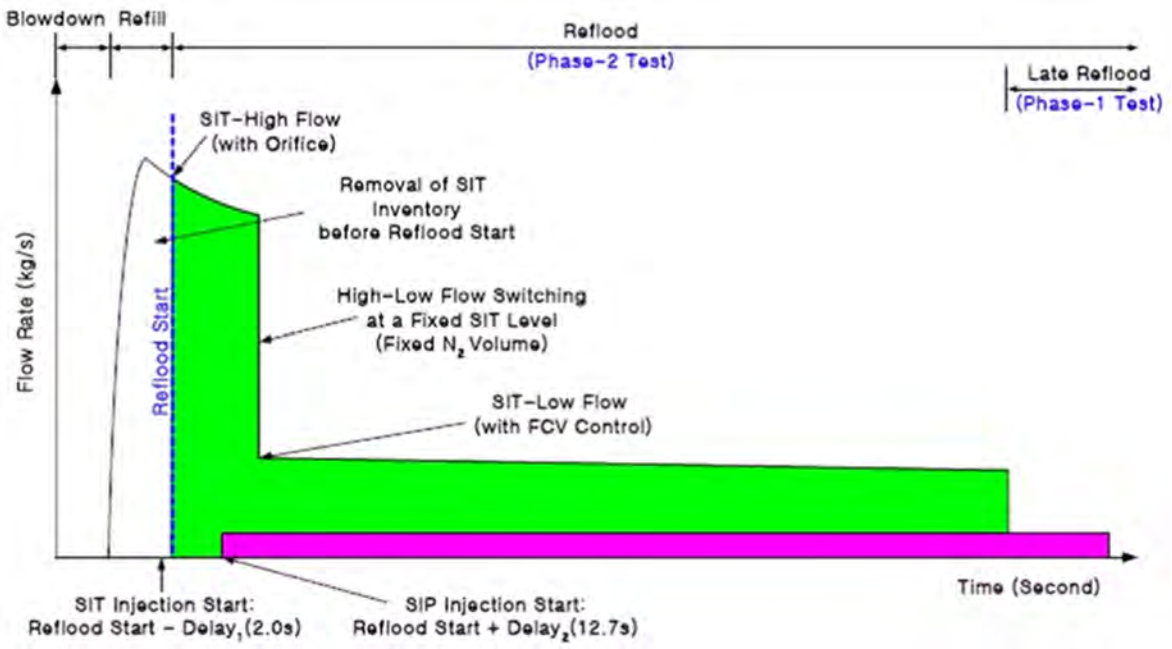

Figure 2-6 ECCW Mass Flow Rate for Test 09 and Test 11

TS

Figure 2-7 Primary System Pressure Behavior: Test 09

TS

Figure 2-8 Collapsed Water Levels in the Downcomer and the Core: Test 09

TS

Figure 2-9 Measured ECCW Mass Flow Rate: Test 09

Figure 2-10 Axial Distribution of Cladding Temperatures (Group 1): Test 09

Figure 2-11 Wall and Fluid Temperatures in the Lower Downcomer: Test 09

TS

Figure 2-12 Accumulated Break Flow: Test 09

TS

Figure 2-13 Primary System Pressure Behavior: Test 11

TS

Figure 2-14 Collapsed Water Levels in the Downcomer and the Core: Test 11

TS

Figure 2-15 Measured ECCW Mass Flow Rate: Test 11

Figure 2-16 Axial Distribution of Cladding Temperatures (Group 1): Test 11

Figure 2-17 Wall and Fluid Temperature in the Lower Downcomer: Test 11

Figure 2-18 Accumulated Break Flow: Test 11

Figure 2-19 Primary System Pressure Behavior: Test 15

TS

Figure 2-20 Collapsed Water level in the Downcomer and the Core: Test 15

TS

Figure 2-21 Measured ECCW Mass Flow Rate: Test 15

TS

Figure 2-22 Axial Distribution of Cladding Temperatures (Group 1): Test 15

TS

Figure 2-23 Wall and Fluid Temperature in the Lower Downcomer: Test 15

TS

Figure 2-24 Accumulated Break Flow: Test 15

3. RELAP5/MOD3.3/K Code Assessment against ATLAS Tests

This chapter describes the assessment of RELAP5/MOD3.3/K code against the ATLAS Test 09, 11, and 15. The capability of the code to predict the major phenomena (i.e., ECCW bypass, downcomer boiling, core heat transfer, and so on) are investigated. In Section 3.1, the target and the measured initial conditions are compared each other based on the scaling factors applied to the tests, and the results of three tests are evaluated also. The code assessment against three ATLAS LBLOCA tests is presented in Section 3.2.

3.1 Test Data Evaluation

Heat transfer from the downcomer wall

The ATLAS was scaled down as 1/2 in length, 1/12 in diameter, 1/144 in area, 1/288 in volume, 1/204 in flow rain, and $1/\sqrt{2}$ in velocity and time, compared to the APR 1400. Therefore, the heat transfer area of the downcomer wall (i.e., reactor vessel wall) ratio of the ATLAS facility to the APR1400 is as follows;

$$A = \pi DL, \quad \left(A_m / A_p\right)_{ATLAS} = \left(DL\right)_m / \left(DL\right)_p = \frac{D_m}{D_p} \cdot \frac{L_m}{L_p} = a_R^{1/2} \cdot l_R \qquad \text{(Equation 3-1)}$$

where, D = Inner diameter of the reactor vessel wall
L = Length of downcomer
m, p = Model and reference plant; m stands for model and p stands for prototype

In Equation 3-1, the downcomer heat transfer area ratio is represented as a multiplication of the length ratio and the square root of the area ratio.

By assuming that the amount of the wall heat transfer per injected mass flow rate is conserved, the following equation is obtained under the ideal condition.

$$\frac{\left(q/w\right)_m}{\left(q/w\right)_p} = \frac{\left[hA\Delta T/\left(\rho Av\right)\right]_m}{\left[hA\Delta T/\left(\rho Av\right)\right]_p} = \frac{\left(Av\right)_p A_m}{\left(Av\right)_m A_p} = 1 \qquad \text{(Equation 3-2)}$$

where, q = Heat transfer rate
w = Injected water mass flow rate
h = Heat transfer coefficient
A = Area
T = Temperature
ρ = Injected water density
v = Injected water velocity

If Equation 3-2 is rearranged for the area ratio, the following equation is obtained.

$$\left(\frac{A_m}{A_p}\right)_{Ideal} = \left(\frac{A_m}{A_p}\right)\left(\frac{v_m}{v_p}\right) = a_R l_R^{1/2} \qquad \text{(Equation 3-3)}$$

The Equation 3-2 means the surface area ratio of model to prototype under the ideal condition.

[

]TS

TS

[

]TS

[

]TS

Initial condition of the downcomer wall temperature

The axial distribution of the inner and outer surface temperatures of the reactor vessel wall (i.e., downcomer wall) measured at the test start time is shown in Figure 3-1 and Figure 3-2, respectively. As mentioned above, the target value of the initial outer surface temperature of the downcomer wall was 205 °C for Test 09 and Test 11. In these tests, the initial surface temperatures of the lower downcomer wall match well the target temperature in general. [

]TS

[

]TS

Thermal hydraulic behavior in the downcomer

[

]TS

3.2 Code Assessment

The RELAP5/MOD3.3/K input model of the ATLAS test facility is shown in Figure 3-3. [

]TS

Each loop has one hot leg, one steam generators, two pumps, and two cold legs; totally two loops are modeled as is the ATLAS test facility. The steam generator U-tube region is [ ]TS By designating both sides of the U-tubes as convective heat transfer boundaries, it is possible to simulate the heat transfer between primary and secondary sides.

The ECCW injection is modeled using TMDPJUN and TMDPVOL components.

The identical nodalization scheme except for ECCW injection is applied to the APR1400 nodalization. The detailed nodalization scheme is described in the main body of this topical report.

3.2.1 Code Assessment against Test 09 and Test 11

[

]TS

[

]TS

[

]TS

[

]TS

The measured values of the core power and the safety injection flow rate were used as the boundary conditions of the restart calculation, as shown in Figure 3-4 through Figure 3-7.

Table 3-1 and Table 3-2 show the comparison between the wall surface temperatures of the downcomer wall [ ]TS and the corresponding measured data. Table 3-3 and Table 3-4 show the comparison between the predicted fluid temperatures in the downcomer and the measured data. Since the RELAP5/MOD3.3/K calculates liquid and vapor temperatures separately, both liquid and vapor temperatures are presented in Table 3-3 and Table 3-4. The inner and outer surface temperatures of the downcomer wall are almost the same with the measured data. [ ]TS There is insignificant differences in the wall temperatures between the code results and the measured data because the nodal center elevations differ from the instrumentation locations. The fluid temperatures are also very similar to the measured data. [

]TS

[

]TS

The above explanation for the code assessment [

]TS

[

]TS

Figure 3-9 and Figure 3-10 show the accumulated break mass flow, Figure 3-11 and Figure 3-12 show the downcomer collapsed water level, and Figure 3-13 and Figure 3-14 show the core collapsed water level of each test. These figures show that, for both Test 09 and Test 11, the RELAP5/MOD3.3/K code predicts well the break flow, the core water level, and the downcomer water level. [

]TS

Figure 3-15 and Figure 3-16 show the pressures in the downcomer and the core, and pressure difference between the core and the downcomer, for Test 09 and Test 11, respectively. [

]TS The pressure difference between the downcomer and the core, however, are almost the same with the measured data. This is the reason that code predicts well the core water level because the core water level is determined by the pressure difference between the core and the

downcomer. For Test 11, the code slightly under-predicts the pressure difference between the downcomer and the core.

Figure 3-17 and Figure 3-18 show the cladding temperature behavior at the elevation where the highest value was measured, for Test 9 and Test 11 respectively. The code conservatively over-predicts the measured data for Test 09, even the predicted core water level match well the test data. This implies that the code under-predicts reflood heat transfer coefficients, consequently over-predicts the cladding temperatures. For Test 11, the code predicted cladding temperature matches well the test data.

In summary, the assessment of the RELAP5/MOD3.3/K against the ATLAS Test 09 and Test 11 shows that the RELAP5/MOD3.3/K is capable of calculating the reflood thermal hydraulic behaviors including the rod cladding temperatures correctly. It is also confirmed that the code has the capability to [ ]^{TS} Therefore, the code's capability of simulating the APR1400 LBLOCA reflood process is confirmed through this assessment.

3.3 Code Assessment against Test 15

The code assessment against Test 15 was performed for entire test period. The assessment results are shown in Figure 3-19 through Figure 3-25. Time 0.0 in these figures corresponds to 1,174 s of DAS time.

Figure 3-19 and Figure 3-20 show the water levels in the core and the downcomer, respectively. The code predicts that the downcomer and the core collapsed water levels start to increase as soon as the SIT-FDs inject ECCW, whereas the measured downcomer and core collapsed water levels increased after a few seconds delay. [

]^{TS} In general, theRELAP5/MOD3.3/K predicts the system water level behaviors reasonably well.

Figure 3-21 shows the cladding temperature behavior measured at the elevation where the highest value was observed and the predicted cladding temperature at the corresponding elevation. The RELAP5/MOD3.3/K predicts fairly well the measured test data.

Figure 3-22 through Figure 3-25 show the downcomer wall temperature comparisons at various elevations. It should be noted that; 1) the temperature measurement locations do not exactly match the center elevations of the corresponding heat structures, 2) the code predicted value is the average value of the corresponding heat structure.

Figure 3-22 shows the inner and outer surface temperatures of the reactor vessel wall measured at 4.2756 m from the reactor vessel bottom with the predicted values at the corresponding node. The measurement elevation is just below of the DVI nozzle elevation of 4.4416 m from the reactor vessel bottom. The measured inner surface temperature drastically decreased as soon as the safety injection water was injected, consequently the outer surface temperature gradually decreased due to the heat conduction inside the wall.[

]^{TS}

Figure 3-23 shows the inner and outer surface temperatures of the reactor vessel wall measured at 2.9736 m from the reactor vessel bottom with the predicted values at the corresponding node. The measurement elevation is just below of the cold leg center elevation of 3.3906 m from the reactor vessel bottom. The code well predicts the trend of the wall temperature behavior at this elevation.
[ ]^{TS}

At 2.1396 m and 1.3056 m from the reactor vessel bottom, the code predicted wall temperatures match relatively well the measured data, as shown in Figure 3-24 and Figure 3-25, respectively.

In summary, the assessment of the RELAP5/MOD3.3/K against the ATLAS Test 15 shows that the RELAP5/MOD3.3/K is capable of calculating the reflood thermal hydraulic behaviors including the rod cladding temperatures correctly, in general, although there is a deficiency. [

]TS

Therefore, the code's capability of simulating the APR1400 LBLOCA reflood process is confirmed through this assessment.

Table 3-1 The Comparison of the RPV Wall Temperatures [ ]TS

TS

Table 3-2 The Comparison of the RPV Wall Temperatures [ ]TS

TS

Table 3-3 The Comparison of the Downcomer Fluid Temperature [ ]TS

TS

Table 3-4 The Comparison of the Downcomer Fluid Temperature [ ]TS

TS

Figure 3-1 Axial Distribution of RPV Wall Inner Surface Temperature: Test 09, 11 and 15

Figure 3-2 Axial Distribution of RPV Wall Outer Surface Temperature: Test 09, 11 and 15

TS

Figure 3-3 RELAP5/MOD3.3/K Nodalization of the ATLAS Test Facility

Figure 3-4 Core Power: Test 09

Figure 3-5 Core Power: Test 11

Figure 3-6 ECCW Injection Flow Rate: Test 09

Figure 3-7 ECCW Injection Flow Rate: Test 11

TS

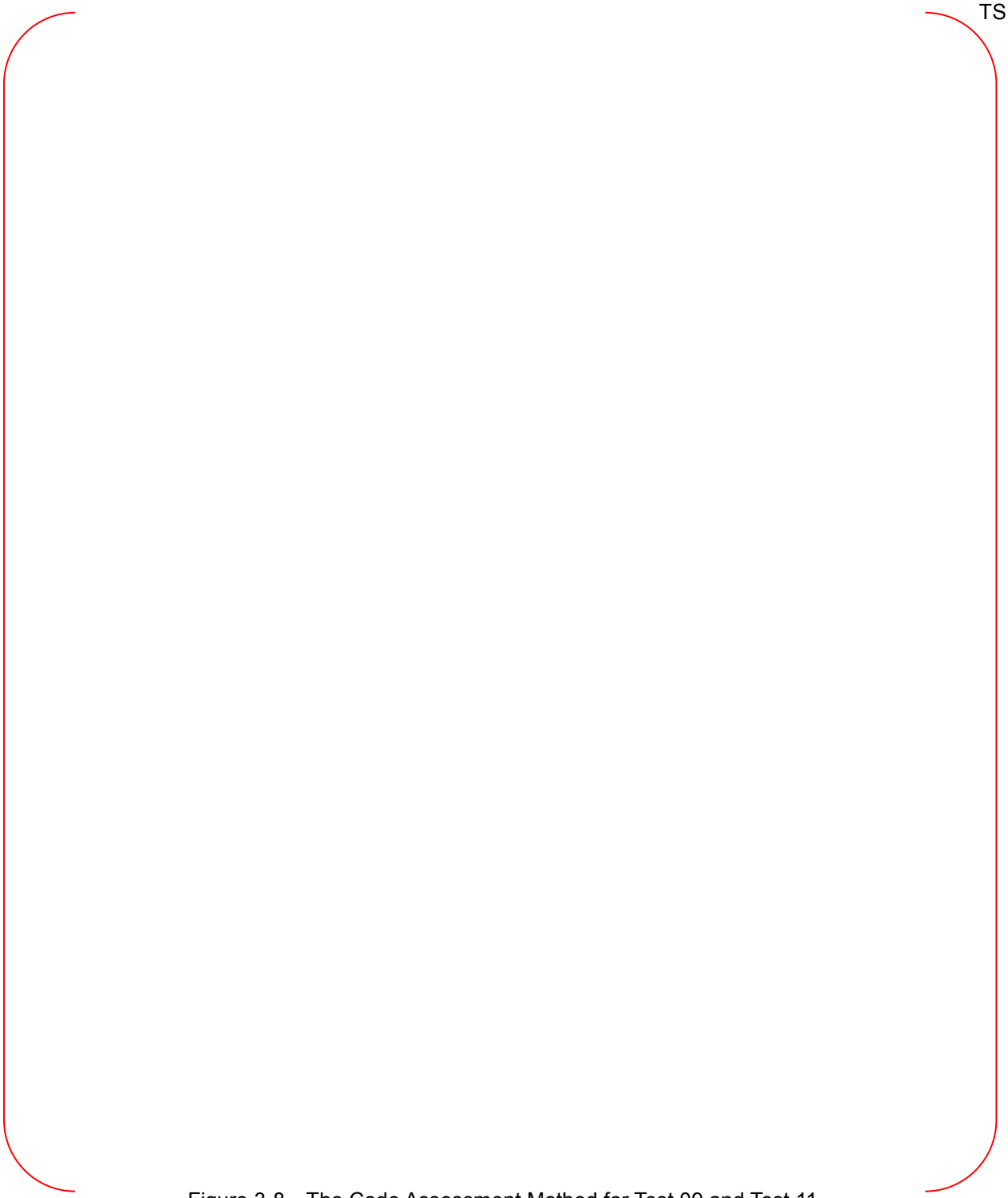

Figure 3-8 The Code Assessment Method for Test 09 and Test 11

Figure 3-9 Accumulated Break Flow: Test 09

Figure 3-10 Accumulated Break Flow: Test 11

TS

Figure 3-11 Downcomer Collapsed Water Level: Test 09

TS

Figure 3-12 Downcomer Collapsed Water Level: Test 11

Figure 3-13 Core Collapsed Water Level: Test 09

Figure 3-14 Core Collapsed Water Level: Test 11

Figure 3-15 Downcomer and Core Pressure: Test 09

Figure 3-16 Downcomer and Core Pressure: Test 11

Figure 3-17 Peak Cladding Temperature: Test 09

Figure 3-18 Peak Cladding Temperature: Test 11

Figure 3-19 Core Collapsed Water Level: Test 15

Figure 3-20 Downcomer Collapsed Water Level: Test 15

Figure 3-21 Peak Cladding Temperature: Test 15

Figure 3-22 Downcomer Wall Temperatures at 4.2756 m from the RPV Bottom: Test 15

Figure 3-23 Downcomer Wall Temperatures at 2.9736 m from the RPV Bottom: Test 15

Figure 3-24 Downcomer Wall Temperatures at 2.1396 m from the RPV Bottom: Test 15

Figure 3-25 Downcomer Wall Temperatures at 1.3056 m from the RPV Bottom: Test 15

4. RELAP5/MOD3.3/K Capability of Predicting ECCW Bypass and Downcomer Boiling Phenomena

The ability of predicting the thermal hydraulic behaviors of LBLOCA, particularly the ECCW bypass and the downcomer boiling phenomena during reflood period is important to the RELAP5/MOD3.3/K, since these phenomena are the major parameters determining the rod cladding temperatures. This chapter describes the RELAP5/MOD3.3/K capability to predict ECCW bypass and downcomer boiling phenomena based on the assessment against the ATLAS Test 09, Test 11 and Test 15.

4.1 ECCW Bypass

In the ATLAS tests, the ECCW bypass ratio was calculated as follows [2][3][4];

$$R_{ECCW\ bypass} = \frac{W_{LC}}{W_{ECCW}}$$

where, W_{LC} is the liquid break flow rate and W_{ECCW} is the total injected ECCW flow rate.

Because W_{LC} includes the amount of the condensed steam, the calculated ECCW bypass ratio is always higher than the actual value.

As described in Chapter 2.3, the break mass flow rate obtained using two methods are; one is the accumulation of the measured break flow rate and the other is accumulation of the break flow rate obtained from the mass balance using the injected water and the vessel inventory. [

]^{TS}

[

]^{TS}

ATLAS Test 09

Figure 4-1 shows the instant ECCW bypass ratios evaluated using the break flow rates obtained from the mass balance method. The ECCW bypass ratio [ ]^{TS}. The accumulation of the bypassed flow is shown in Figure 4-2. Time 346 s in this figure corresponds to 2,200 s in DAS time. The average bypass ratio, [ ]^{TS}.

The instant bypass ratio predicted by RELAP5/MOD3.3/K is shown in Figure 4-3. Time 346 s in this figure corresponds to DAS time 2,200 s. The predicted instant ECCW bypass ratio [ ]^{TS}, showing slightly higher ECCW bypass ratio than the test data. The predicted average bypass ratio, [ ]^{TS}.

ATLAS Test 11

[

]TS

The instant ECCW bypass ratio obtained using the mass balance method is presented in Figure 4-5. On average, the ECCW bypass ratio was [ ]TS. The accumulation of the measured ECCW bypass flow is presented in Figure 4-6. Time 300 s in this figure corresponds to DAS time 1,698 s. The average bypass ratio, [ ]TS.

The instant bypass ratio predicted by RELAP5/MOD3.3/K is shown in Figure 4-7. The predicted instant ECCW bypass ratio [ ]TS. The predicted average bypass ratio, [

]TS.

ATLAS Test 15

The instant ECCW bypass ratio obtained using the mass balance method is presented in Figure 4-9. On average, the instant ECCW bypass ratio was [ ]TS. The accumulation of the measured ECCW bypass flow is presented in Figure 4-10. Time 0.0 s in this figure corresponds to DAS time 1,174 s. The average bypass ratio was calculated using the accumulated ECCW bypass flow, and was [ ]TS.

The instant bypass ratio predicted by RELAP5/MOD3.3/K is shown in Figure 4-11. The averaged value of the predicted instant ECCW bypass ratio is [ ]TS. The predicted average bypass ratio, calculated using the accumulated ECCW bypass flow in Figure 4-12, was calculated [ ]TS.

4.2 Downcomer Boiling

[

]TS

Figure 4-13 shows comparisons of measured and predicted values of water levels in the downcomer and the core. [

]TS

RELAP5/MOD3.3/K well predicts water level behaviors in the downcomer and core [ ]TS. [ ]TS. The water level decreased more in the predictions, compared to the test data.

Figure 4-14 and Figure 4-15 show comparisons of measured and predicted behaviors of the inner and outer surface temperatures of the downcomer wall, respectively, and Figure 4-16 shows a comparison of measured and predicted values of the accumulated break flow. The RELAP5/MOD3.3/K code predicts the downcomer wall temperature behaviors and break flow fairly well [ ]TS

Therefore, it can be concluded that the RELAP5/MOD3.3/K code well predicts the overall thermal hydraulic behaviors [ ]TS

4.3 Uncertainty Parameters for the Downcomer Boiling

As described in Chapter 3 of this appendix, the RELAP5/MOD3.3/K code assessment against ATLAS Test 09 was performed [ ]TS [

]TS

Figure 4-17 shows the effect of the downcomer wall temperature on the downcomer and the core water level. When the downcomer wall temperatures values measured in the test were used as the initial condition for the restart calculation, the predicted downcomer and core levels were slightly lower than the test data. Whereas, when the downcomer wall temperatures obtained from the initial transient calculation were used, the predicted downcomer water level was higher than the measured value, showing a maximum 0.5 m difference, compared with the other case. [

]TS

[

]TS

To confirm the adequacy of the parameter selection and to determine the range of the uncertainty of the selected parameter, [

]TS, were reviewed. During the

modification, [

]TS, respectively. [

]TS

Figure 4-18 shows the downcomer water level. In the upper part of Figure 4-18, two different calculation results are presented with the experimental data. In the figure, one calculation result that is represented as [

]TS [

]TS. In the lower part of Figure 4-18, another two different calculation results are presented with the experimental data. [

]TS

Figure 4-19 shows the core water level in the same way as in Figure 4-18. Figure 4-18 and Figure 4-19 show that the calculation results with [

]TS. [

]TS

Figure 4-20 through Figure 4-23 show the downcomer wall temperature at different elevations in the four cases described in Table 4-1. [

]TS

Figure 4-24 through Figure 4-28 show the accumulated heat flux at each downcomer wall elevation. [

]TS

The measured and the calculated PCTs are shown in Figure 4-29 and it is noted that the RELAP5/MOD3.3/K code predicts PCT more conservatively than the experimental data in all calculations. [

]TS

[

]TS

[

]TS

[

]TS

4.4 SRS Calculations

In the previous section, the parameters that govern the downcomer boiling phenomena were selected and their uncertainty ranges were determined. This section describes the 181 SRS calculations that were performed for ATLAS Test 09 and Test 15, using the selected uncertainty parameters. The SRS calculations for [

]TS

Table 4-2 shows the parameters and their uncertainty ranges used in the 181 SRS calculations. The uncertainty parameters considered in the SRS calculations are [

]TS

The SRS calculation results of ATLAS Test 09 and Test 15; shown in Figure 4-30 and Figure 4-31; sufficiently cover the test results. Therefore, the adequacy of the selected parameters, including the parameters related to downcomer boiling, and their uncertainty ranges were confirmed to be sufficient to cover the measured cladding temperatures.

Table 4-1 The Four Cases Considered in the Sensitivity Study

TS

Table 4-2 Parameters and Their Uncertainty Ranges Used for the SRS Calculations

TS

Figure 4-1 ECCW Bypass Ratio (Test Data); Test 09

Figure 4-2 Accumulation of the Bypassed ECCW (Test Data); Test 09

Figure 4-3 ECCW Bypass Ratio (RELAP5 Result); Test 09

Figure 4-4 Accumulation of the Bypassed ECCW (RELAP5 Result); Test 09

Figure 4-5 ECCW Bypass Ratio (Test Data); Test 11

Figure 4-6 Accumulation of the Bypassed ECCW (Test Data); Test 11

Figure 4-7 ECCW Bypass Ratio (RELAP5 Result); Test 11

Figure 4-8 Accumulation of the Bypassed ECCW (RELAP5 Result); Test 11

Figure 4-9 ECCW Bypass Ratio (Test Data); Test 15

Figure 4-10 Accumulation of the Bypassed ECC2 (Test Data); Test 15

Figure 4-11 ECCW Bypass Ratio (RELAP5 Result); Test 15

Figure 4-12 Accumulation of the Bypassed ECCW (REALP5 Result); Test 15

Figure 4-13 Water Level Behavior in the Downcomer and Core; Test 09

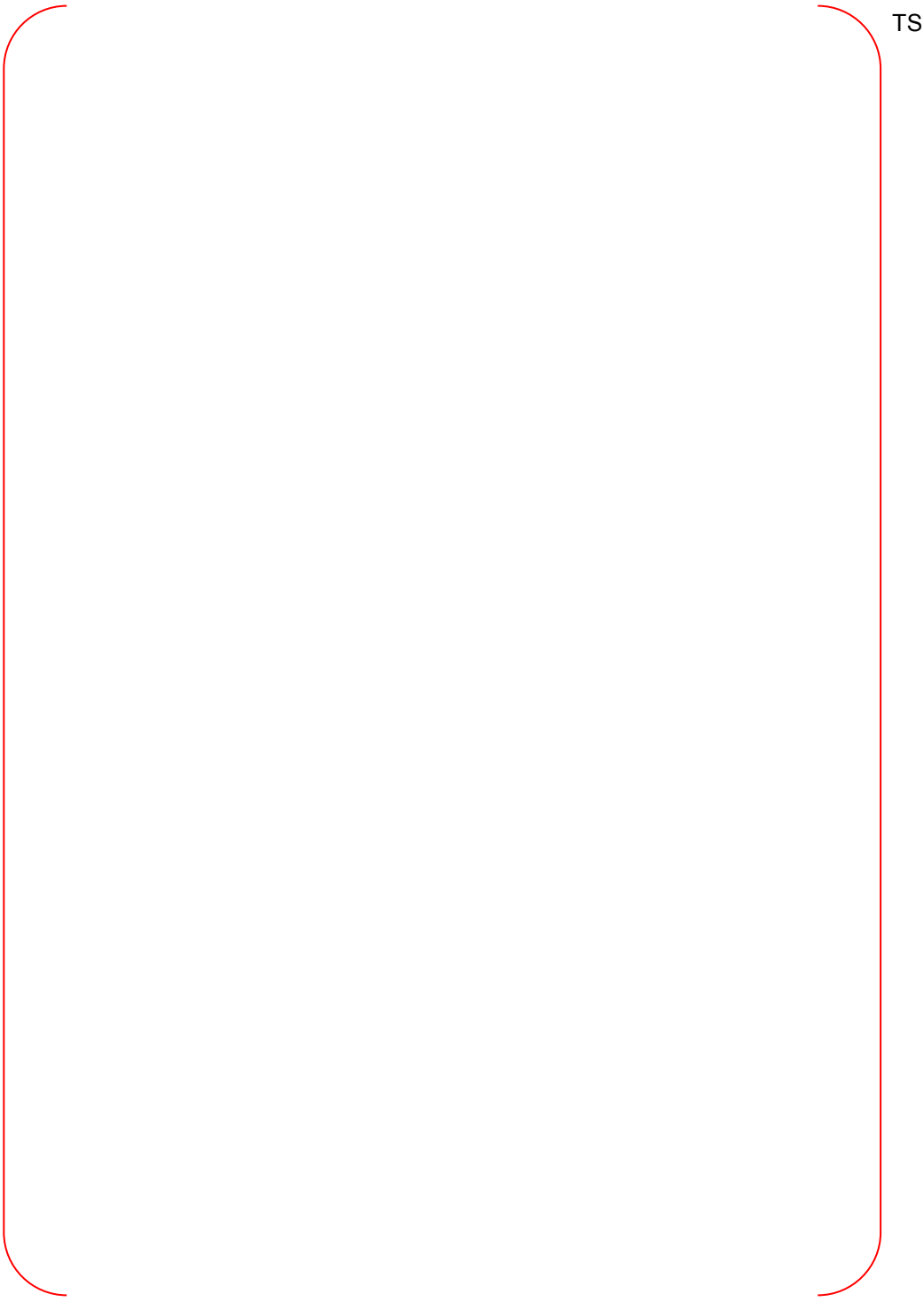

Figure 4-14 Outer Surface Temperature of the Downcomer Wall; Test 09

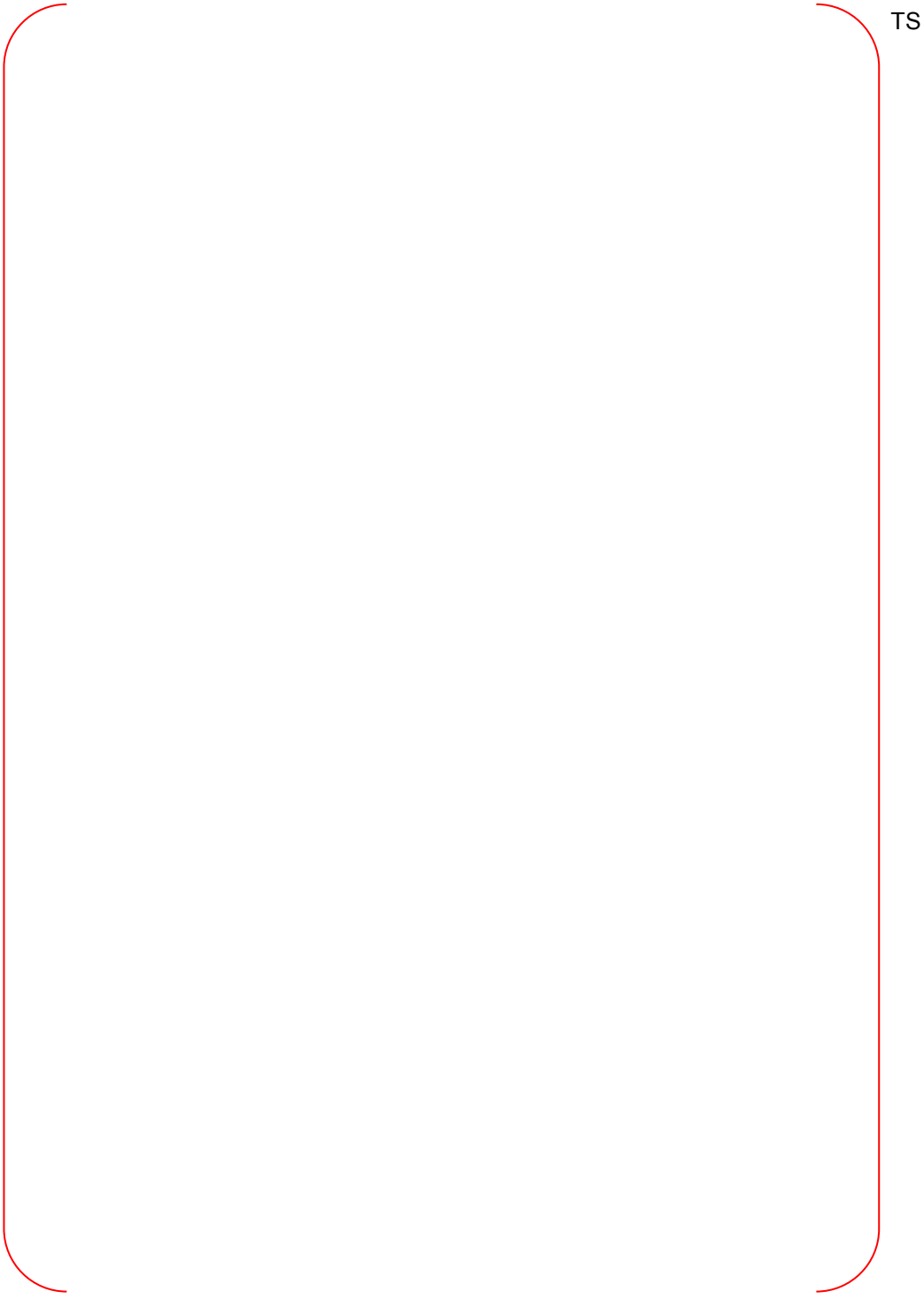

Figure 4-15 Inner Surface Temperature of the Downcomer Wall; Test 09

Figure 4-16 Accumulated Break Flow; Test 09

Figure 4-17 The Effect of the Wall Temperature on the Water Levels; Test 09

TS

Figure 4-18 [ ]TS

TS

Figure 4-19 [ ]TS

TS

Figure 4-20 [ ]TS

TS

Figure 4-21 [ ]TS

TS

Figure 4-22 [ ]TS

TS

Figure 4-23 [ ]TS

TS

Figure 4-24 [ ]TS

TS

Figure 4-25 [ ]TS

TS

Figure 4-26 [

]TS

TS

Figure 4-27 [

]TS

TS

Figure 4-28 [

]TS

TS

Figure 4-29 The Comparison of Peak Cladding Temperatures: Test 09

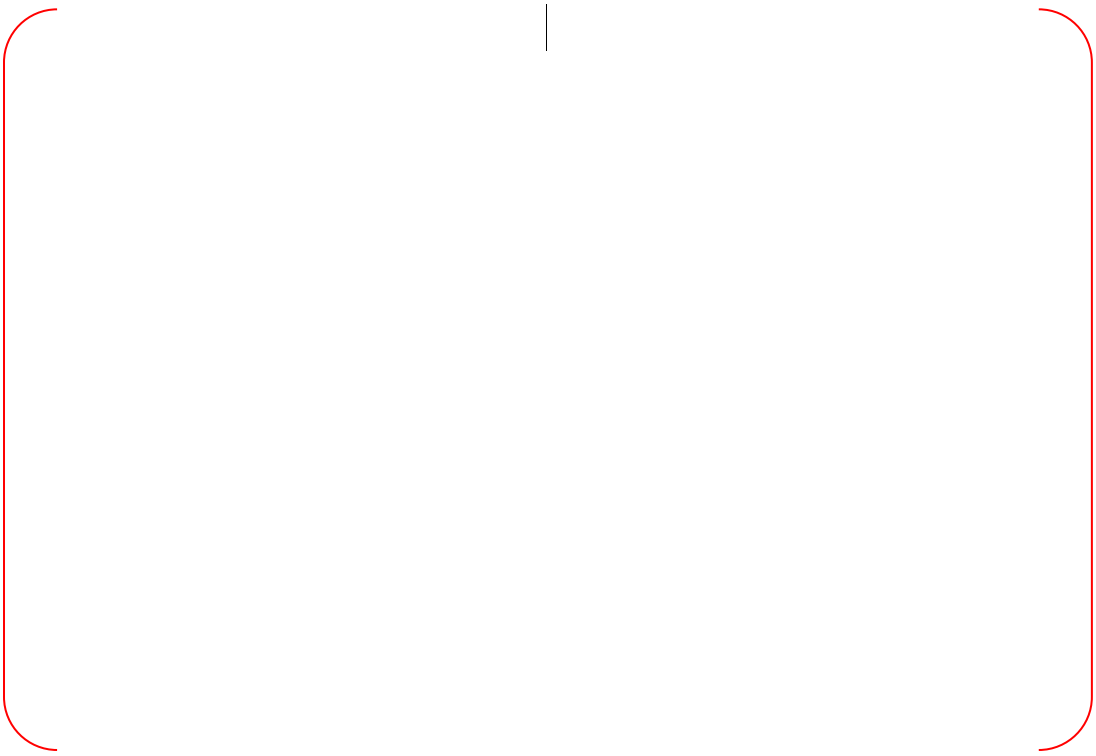

Figure 4-30 The Results of the 181 SRS calculations; Test 09

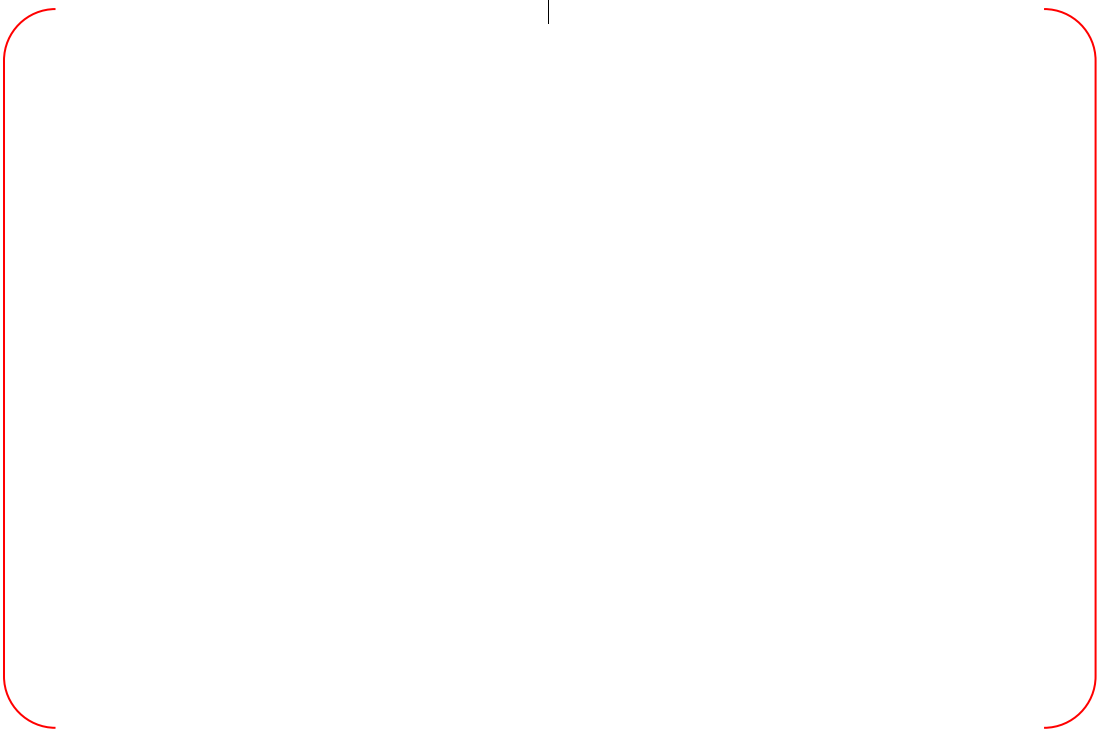

Figure 4-31 The Results of the 181 SRS calculations; Test 15

5. Conclusion

In this Appendix, the capability of RELAP5/MOD3.3/K to predict the thermal hydraulic phenomena during the reflood phase was confirmed by the assessment against ATLAS tests 09, 11, and 15.

The results showed that RELAP5/MOD3.3/K conservatively predicts ECCW bypass, which is a main interest for DVI plants, and also that the code reasonably predicts downcomer boiling phenomenon. [

]TS

References

[1] “Basic Design Calculation of the ATLAS Fluid System,” KAERI/TR-3333/2007, KAERI, March 2007.

[2] “Quick-look Data Report of LB-CL-09,” ATLAS-QLR-LB-CL-09, KAERI, November 2008.

[3] “Quick-look Data Report of LB-CL-11,” ATLAS-QLR-LB-CL-11, KAERI, November 2008.

[4] “Quick-look Data Report of LB-CL-15,” ATLAS-QLR-LB-CL-15, KAERI, October 2008.

Appendix F

Assessment of RELAP5/MOD3.3/K against ECCW Bypass Tests

Non-Proprietary

August 2018

Table of Contents

List of Tables

List of Figures

1. Introduction

Emergency core cooling water (ECCW) bypass is an important phenomenon in a hypothetical loss-of-coolant accident (LOCA). This appendix addresses ECCW bypass during the late reflood period in particular, since only the safety injection pump (SIP) flow is available during this period.

This appendix examines the ability of the RELAP5/MOD3.3/K code to predict the ECCW bypass during the late reflood period. The RELAP5/MOD3.3/K code was assessed against the data obtained from tests conducted using the Multi-dimensional Investigation in Downcomer Annulus Simulation (MIDAS) and the Upper Plenum Test Facility (UPTF).

2. MIDAS ECCW Bypass Tests

The Korea Atomic Energy Research Institute (KAERI) conducted the ECCW bypass tests [2-1][2-2] using the MIDAS facility to study the ECCW bypass phenomena which can occur in the direct vessel injection (DVI) system during the late reflood period. Only SIPs supplied the ECCW during the late reflood period. The tests were conducted in steam and water condition. The MIDAS was a scaled-down facility of APR1400. It had 1/5 height, 1/24 flow area, and 1/54 flow rate of APR1400. Table 2-1 provided the scaling law applied to the MIDAS design. The temperature and pressure conditions of the MIDAS tests were maintained the same as the APR1400. The schematic diagram of the MIDAS facility was shown in Figure 2-1. The portion above the “Level 4,491 mm” was a test section, and the lower part was a drain system. The test section was comprised of two concentric pipes. The outer diameter of the inner pipe is 834.8 mm, and the inner diameter of the outer pipe is 938.8 mm. Relative locations of the four cold legs, two hot legs, and four DVI nozzles are shown in Figure 2-2.

The main parameters measured were the downcomer water level, the coolant temperature distribution in the downcomer, and flow rates at DVI nozzles and cold legs. The ECCW bypass fraction and condensation ratio in the downcomer were calculated from the measured parameters.

In order to assess the RELAP5/MOD3.3/K code’s ability to predict the ECCW bypass during the late reflood period, 15 MIDAS tests were simulated. Test conditions of the 15 tests are presented in Table 2-2. The ECCW was injected through one or two DVI nozzles to simulate one or two SIPs injection. Test conditions are further detailed in the following.

2.1 MIDAS Test Description

The MIDAS test facility was composed of the downcomer, the core simulator, three intact cold legs, broken cold leg, steam-water separator, containment simulator, steam supplier, and the ECCW supplier. Steam produced in the core was simulated using the steam supplier and was injected through three intact cold legs. In Figure 2-2, three intact cold legs are marked as CL-1, CL-2, and CL-3. The broken cold leg is marked as BL. HL-1 and HL-2 indicated two hot legs. The DVI nozzle number 1, 2, 3 and 4 (DVI-1, 2, 3, 4) were located above the CL-1, 2, 3 and BL, respectively. The DVI nozzle number 2 (DVI-2) was located above CL-2 which was located on the opposite side of the broken cold leg. The DVI nozzle number 4 (DVI-4) was located above the broken cold leg (BL). Four DVI nozzles were arranged at an angle of 90 degree.

The following ECCW injection was simulated in the MIDAS tests.

- DVI-2&4 injection (Test 100 ~ Test 108)
  - ECCW injection through DVI-2 and DVI-4; 2 SIPs operated
- DVI-2 injection (Test 109)
  - ECCW injection only through DVI-2 (opposite side of the BL); 1 SIP operated
- DVI-4 injection (Test 110 ~ Test 114)
  - ECCW injection only through DVI-4 (BL side); 1 SIP operated

Table 2-3 provided major test results with the total steam and ECCW flow rates. In this table, ‘Steam_in’ is the total steam flow rate injected through three intact cold legs and ‘SI_in’ is the total ECCW injection flow rate. The meaning of ‘Bp_fraction’ and ‘Cond_ratio’ are the data-derived ECCW bypass fraction and condensation ratio in the downcomer, respectively. The last column,

labeled 'ECCW Injection Nozzle', is the DVI injection nozzle number through which ECCW was injected. The major test results are also depicted in Figure 2-3 and Figure 2-4.

The bypass fraction and the condensation ratio were calculated as follows:

$$\mathrm{Bp_{fraction}} = 1 - \frac{M_{Water\_out}}{M_{SI\_in}+M_{Condensate}} \quad (1)$$

$$\mathrm{Cond\_ratio} = \frac{M_{Condensate}}{M_{Steam\_in}} \quad (2)$$

Where, M_{SI_in} (kg/s) was the total ECCW injection flow rate, M_{Water_out} (kg/s) is the liquid flow rate discharged through the lower plenum, M_{Steam_in} is the steam injection flow rate, and $M_{Condensate}$ (kg/s) is the condensation rate which is calculated as follows:

$$M_{Condensate} = M_{Steam\_in} - M_{Steam\_out} \quad (3)$$

Where, M_{Steam_out} (kg/s) is the steam flow rate discharged through the break.

The liquid flow rate discharged through the lower plenum, M_{Water_out}, is the same as accumulated liquid rate to the downcomer that is the summation of ECCW injection rate with consideration of bypass and steam condensation, since the downcomer water level is constantly maintained.

The total steam injection flow rate used in the tests was ranged [ ]^{TS}. Table 2-4 presents the scaled MIDAS test conditions and corresponding APR1400 conditions.

The ECCW bypass fractions measured in 15 tests are presented in Figure 2-3 as a function of the total steam injection flow rate. In the cases of one SIP injection through DVI-4 (located nearby the broken cold leg), the DVI-4 injection tests Test 110 through Test 114, the bypass fraction abruptly increased as the total steam injection flow rate increased. The maximum bypass fraction reached almost [ ]^{TS}. It was also observed that very steep increases of the bypass fraction became weakened as the steam flow rate increased. A similar tendency was also observed in the tests that ECCW injected through both DVI-2 and DVI-4 (Test 100 through Test 108; two SIPs operated). The bypass fraction converged into an asymptotic value of about [ ]^{TS} as the steam flow rate increased. In the case of one SIP injection through DVI-2 (located on the opposite side of the broken cold leg), Test 109, the bypass fraction was only [ ]^{TS}; even though the steam flow rate was as high as [ ]^{TS}. These test results indicate that most of the ECCW injected through the DVI-2 nozzle, which was the farthest from the broken cold leg, penetrated into the lower plenum, and that most of the ECCW injected through the DVI-4 nozzle, which was closest to the broken cold leg, bypassed through the break.

Figure 2-4 shows the condensation ratio as a function of the total steam injection flow rate. The condensation ratio is defined as a condensed fraction of the total steam flow rate. The condensation ratio decreased as the total steam injection flow rate increased. For the DVI-2 or DVI-4 injection tests (one SIP operated), the condensation rate was about half of the condensation rate for DVI-2 and DVI-4 injection tests (2 SIPs operated) under the same total steam injection flow rate. This is because the condensation rate is almost proportional to the ECCW injection flow rate, as shown in Table 2-4.

2.2 Code Assessment

2.2.1 RELAP5/MOD3.3/K Model Description

The RELAP5/MOD3.3/K input model of the MIDAS facility is shown in Figure 2-5 and Figure 2-6.

The downcomer is modeled [ ]^{TS}. Each channel of

the upper downcomer region (i.e., the region above the cold leg) is modeled [ ]TS. DVI-4, which is the closest DVI nozzle to the break, is connected to Volume 130-2. DVI-2, which is the farthest DVI nozzle from the break, is connected to Volume 140-2. Each channel of the lower downcomer region (i.e., the region below the cold leg) is modeled [ ]TS. The drain valve is modeled using a TRIP VALVE that opens if the water level of the lower downcomer becomes higher than a set point. Figure 2-6 shows the relative position of four cold legs, two hot legs, and DVI nozzles in the modeling. Cold leg number 1 (CL-1), 2 (CL-2), and 3 (CL-3) are azimuthally 60^{o}, 180^{o}, and 240^{o} away from the broken cold leg (CL-4), respectively. Two hot legs which penetrate the downcomer were located between CL-1 and CL-2, and between CL-3 and CL-4.

The downcomer regions, where the cold legs are connected to, [ ]TS. Time-dependent volume and junction components (i.e., TMDPVOL and TMDPJUN) are used to simulate steam flow rates. The separator, which is located downstream of the broken cold leg, is not modeled explicitly; but the measured separator pressure is simulated using a TMDPVOL component. Each cold leg is connected to the downcomer (Node 750, 752, 760, and 762) [ ]TS.

2.2.2 Assessment Results

Figure 2-7 shows a comparison of the predicted values versus the measured values of the ECCW bypass fraction. It shows that the RELAP5/MOD3.3/K code conservatively over-predicts the ECCW bypass fraction over the entire range. The degree of RELAP5/MOD3.3/K's over-prediction increases as the measured value decreases. This indicates that RELAP5/MOD3.3/K over-predicts the ECCW bypass fraction, especially when the steam injection flow rate is low.

Predicted and measured, the ECCW bypass fractions as a function of the steam flow rate are compared in Figure 2-8. The RELAP5/MOD3.3/K over-predicts the bypass fractions over the entire range of the steam flow rate. This tendency is stronger for the low steam injection flow rate condition. On the other hand, when the steam flow rate is high, the degree of over-prediction is reduced. For the highest steam flow rate case among the tests that two SIPs injected ECCW through DVI-2 and DVI-4, the measured and the predicted bypass fractions are about [ ]TS, respectively. In the DVI-4 injection cases, the maximum measured bypass fraction is [ ]TS, and the corresponding code prediction is [ ]TS. For the DVI-2 injection case, the code under-predicts the test data; however, the degree of under-prediction is insignificant.

Figure 2-9 or Figure 2-10 shows a comparison of the steam condensation ratio between the predicted and the measured values. The RELAP5/MOD3.3/K predicts flow regimes of upper downcomer nodes as "annular-mist". Even though the annular-mist regime of RELAP5 is developed for vertical or horizontal tube (internal) flows, the code predicts the trend of condensation ratio well over the entire range of the test. This is mainly due to that that the code shows differences from the test data in prediction of the effects of jet impingement, breakup of the jet into droplets, and consequential interfacial condensation. The predicted condensation ratio is generally lower by about 0.1 except for the DVI-2 injection case. The code over-predicts the condensation ratio of the DVI-2 injection case.

As discussed above, even though the RELAP5/MOD3.3/K over-predicts the ECCW bypass and under-predicts the condensation ratio, the code well predicts the general trend of the bypass and condensation. And the code prediction is found to be conservative with respect to the availability of the emergency core cooling water regardless of the number of available SIPs and their injection locations.

References

[2-1] MIDAS-QLR-007, “Direct Vessel Injection Test Using the MIDAS Test Facility-ECC Direct Bypass Test,” KAERI, June 2001.

[2-2] MIDAS-QLR-009, “Direct Vessel Injection Test Using the MIDAS Test Facility-ECC Direct Bypass Test,” KAERI, August 2001.

Table 2-1 Scaling Ratio of the MIDAS Facility

Parameter	Ratio
Length	L
Area	$(L)^2$
Velocity	$(L)^{0.5}$
Flow rate	$(L)^{2.5}$
Temperature & Pressure	1.0

L=1/4.9295

Table 2-2 Test Conditions of the MIDAS Tests

TS

Table 2-3 MIDAS Test Results – Bypass and Condensation Ratio

TS

Note:

Steam_in: Total steam flow rate injected into the intact cold legs,
Bp_fraction: Bypass fraction,
SI_in: Total ECCW flow rate
Cond_ratio: Condensation ratio

Table 2-4 MIDAS Test Conditions and Corresponding APR1400 Conditions

TS

Note:

Steam_in: Total steam flow rate injected into the intact cold legs
SI_in: Total ECCW flow rate

TS

Figure 2-1 Schematic Diagram of the MIDAS Test Facility

TS

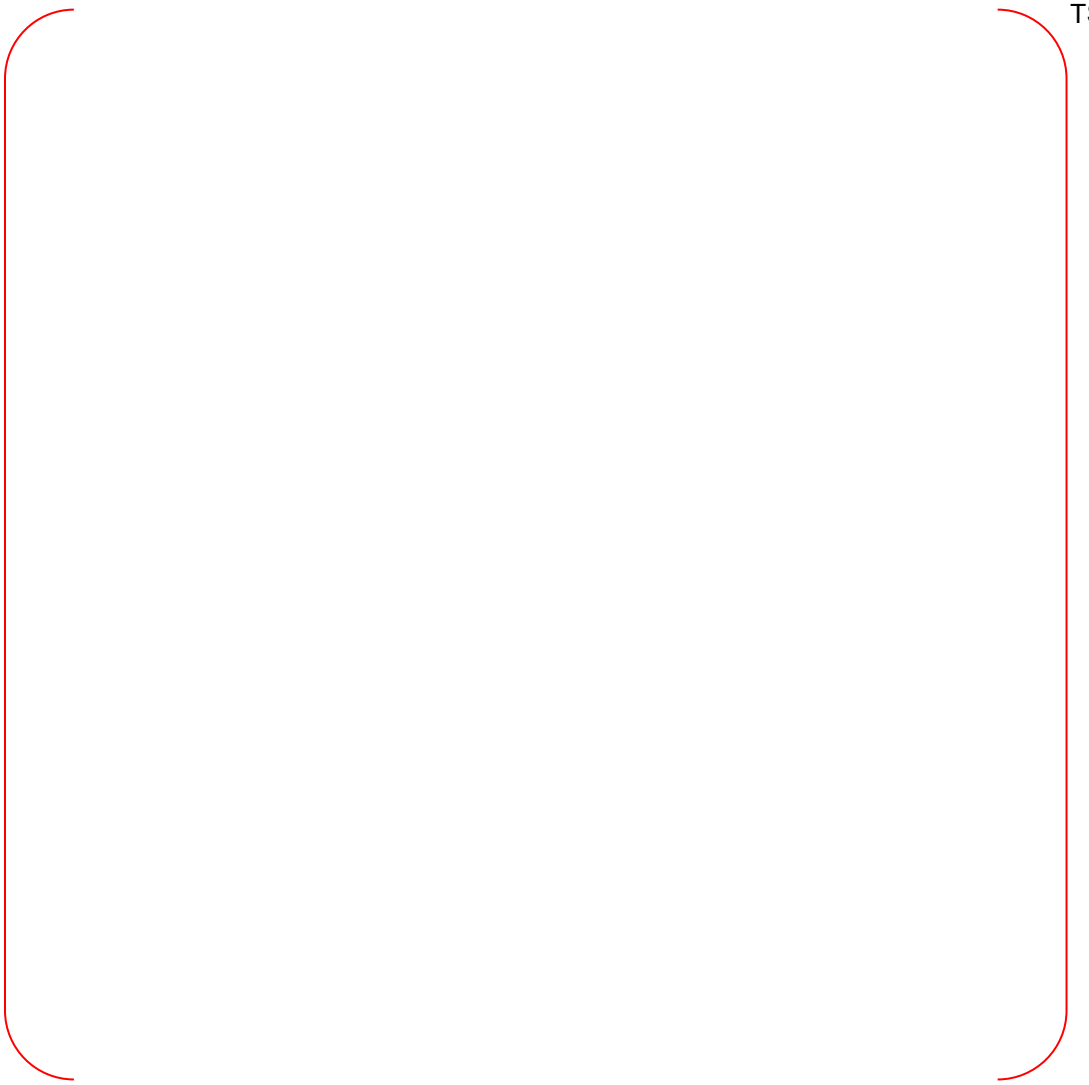

Figure 2-2 The Position of the DVI Nozzles and Primary Piping in the MIDAS Test Facility

Figure 2-3 ECCW Bypass Fraction obtained from the MIDAS Tests

TS

Figure 2-4 Steam Condensation Ratio obtained from MIDAS Tests

T
S

Figure 2-5 RELAP5/MOD3.3/K Nodalization of the MIDAS Test Facility

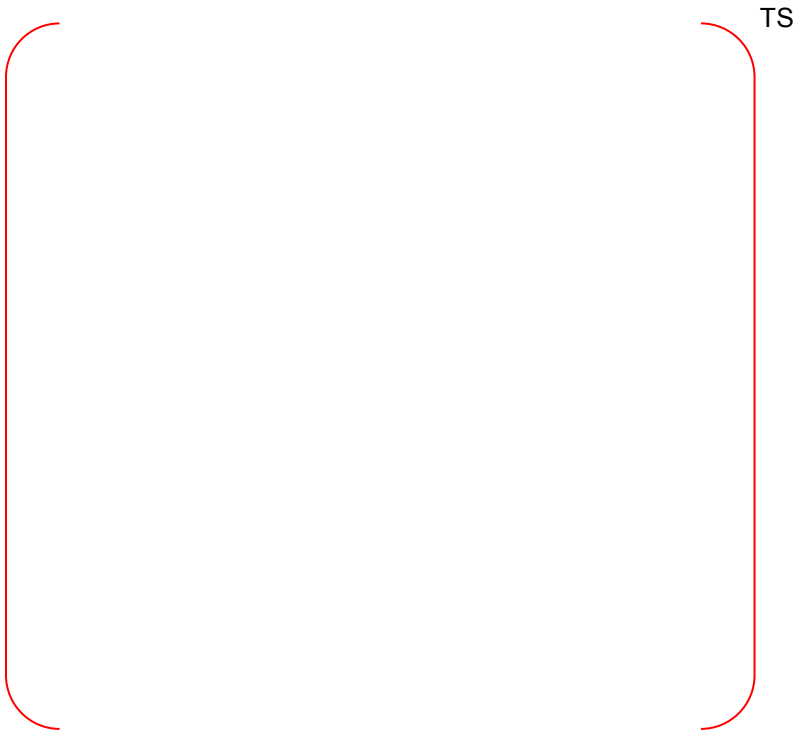

Figure 2-6 Cross Sectional View of RELAP5/MOD3.3/K Nodalization for the MIDAS Test Facility

TS

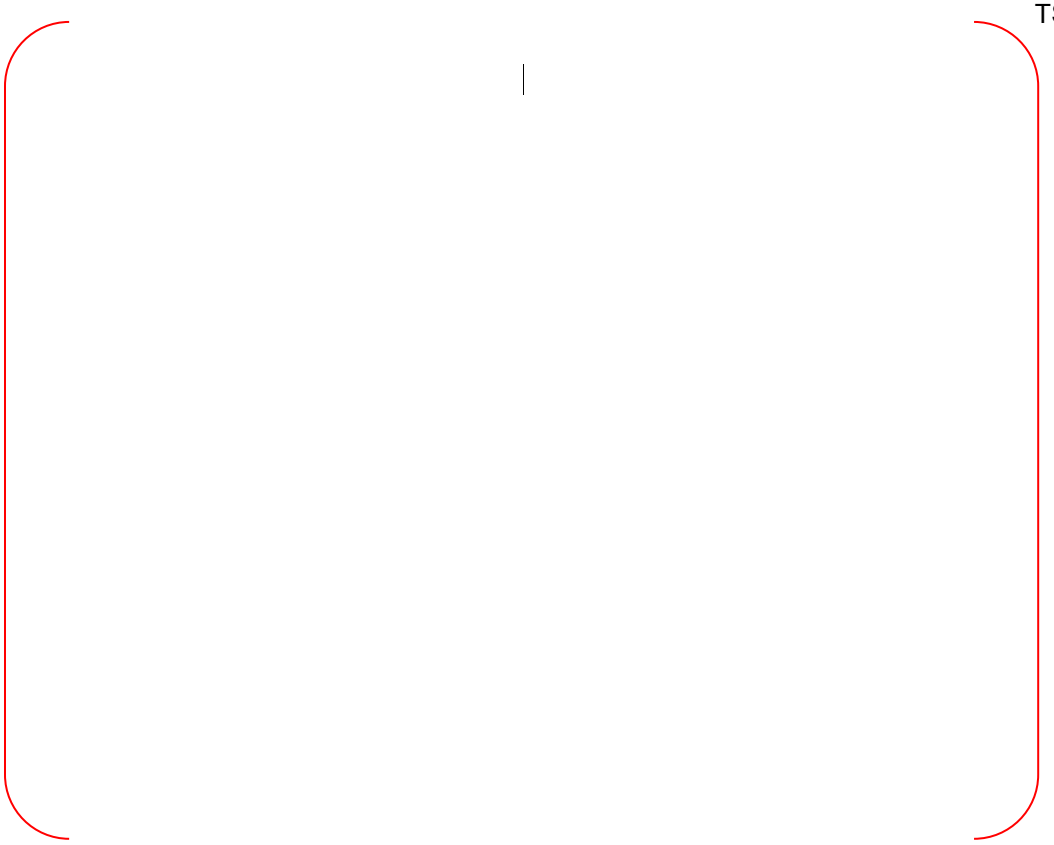

Figure 2-7 Comparison of the Predicted and the Measured ECCW Bypass Fraction

TS

Figure 2-8 Variation of ECCW Bypass Fraction according to Steam Flow Rate

Figure 2-9 Comparison of the Predicted and the Measured Condensation Ratio

TS

Figure 2-10 Variation of Steam Condensation Ratio according to Steam Flow Rate

3. UPTF ECCW Bypass Test

The Upper Plenum Test Facility (UPTF) tests were performed as a part of the international joint research program [3-1][3-2] to investigate the thermal hydraulic phenomena during the postulated accidents in PWRs. Under this program, various hot leg and cold leg breaks were simulated; and various ECCW injection configurations (i.e., ECCW injection through nozzles in the hot leg, cold leg, downcomer, and in the upper plenum) were also simulated.

In this chapter, RELAP5/MOD3.3/K code was assessed against UPTF Test 21-D to examine the code's ability to predict ECCW bypass. UPTF Test 21-D simulated ECCW injection through the two direct vessel injection (DVI) nozzles in the downcomer.

3.1 UPTF Test Facility and Test 21-D

3.1.1 Test Facility Description

The UPTF was the full scale test facility which modeled the 3,900 MWt four loop PWR to investigate the multi-dimensional behavior of the steam and liquid in the downcomer, upper plenum and loops during the end of the blowdown phase as well as during the refill and reflood phase of the hot leg or cold leg break. One of the four primary loops could simulate a hot leg or a cold leg break (i.e., three intact loops and one broken loop). The facility contained all major components with the exception of the nuclear core, active pumps, steam generators, and containment. The core, steam generators, reactor coolant pumps and containment were represented by simulators to account for the thermal hydraulic behavior in these components during a large break LOCA. The schematic diagram of the facility is shown in Figure 3-1.

The reactor vessel consisted of the upper plenum internals, dummy fuel assemblies, core simulator, lower plenum internals, downcomer, and so on. The detailed configuration of the reactor vessel is shown in Figure 3-2. The geometric dimensions of the reactor vessel were nearly the same with that of the reactor vessel of the reference PWR except for the wall thickness. The wall thickness of the reactor vessel was reduced to correspond to the necessary operating pressure loading.

The upper plenum had actual reactor dimensions, and contained 61 control rod guide tubes and 16 support columns. In the core barrel above the hot leg, eight vent valves were mounted for the simulation of ABB and B&W PWRs. The vent valves were locked or unlocked depending on the type of test. The core and the upper plenum were separated by the upper core plate, whose detail configuration is shown in Figure 3-3.

The core region contained the core simulator and 193 dummy fuel assemblies. The steam generation in an actual core was simulated by the core simulator. The schematic diagram and core-wide arrangement of the core simulator are shown in Figure 3-4 and Figure 3-5, respectively. The core simulator consisted of 17 injection pipes for both steam and water injection. These injection pipes were subdivided into 193 steam and water injection nozzles. Each injection nozzle was located at the bottom of each dummy fuel assembly. The steam and water injected into the core simulator flowed into the upper plenum passing through the dummy assemblies.

The drain system to control the entire mass balance was installed in the lower plenum of the reactor vessel. The downcomer gap width was 0.25 m. The diameter of the reactor vessel was 4.87 m. Four cold leg nozzles and four hot leg nozzles had 0.75 m diameters and they were located 9.12 m above the bottom of the reactor vessel. Two DVI nozzles had diameters of 0.308 m and were located 9.47 m above the bottom of the reactor vessel. The DVI nozzle elevation was higher than the cold leg by 0.35 m.

Each of the three intact loops contained the steam generator simulator to simulate the PWR steam

generator. They were designed to be able to measure the water amount carried into the simulators and simulate the steam generator responses to the carryover while preserving the flow resistance of the reference steam generators. Water carryover was measured by separating the water from the steam flow using a set of 31 two-stage cyclone separators.

The pump simulator simulated the flow resistance of a rotating or locked rotor of a reactor coolant pump with adjustable valves.

3.1.2 UPTF Test 21-D Description

The major objective of the UPTF Test 21 was to study the thermal hydraulic behavior of the two phase flow during the end of the blowdown, refill and reflood periods of a large break LOCA in a cold leg, with ECCW injection through DVI nozzles. This test was divided into four sub-phases; A, B, C, and D. Phases A and B were conducted to investigate behaviors in the downcomer at the end of blowdown and refill periods. In Phases A and B, the core simulator injected steam only and a high amount of accumulator flow was injected through the DVI nozzles. Phases C and D were for the reflood conditions. Phase C was to investigate the phenomena of de-entrainment in the upper plenum and entrainment into the steam generator.

Phase D (UPTF Test 21-D), which is used for the RELAP5/MOD3.3/K code assessment, was to study the water level, sweep-out by entrainment, and ECCW bypass in the downcomer during the reflood period. Figure 3-6 shows the system configuration for the Test 21-D. This test was conducted under the quasi-steady state. Steam generation in the primary side of the steam generators was simulated by injecting steam into the steam generator simulators. This steam flowed into the intact cold legs, the downcomer, and then finally discharged into the containment simulator through the break. The reactor coolant pump simulators were partly open and the K-factor for the pump was set to 20.

The UPTF Test 21-D was divided into four sub-phases, D-I, D-II, D-III, and D-IV, based on the steam injection flow rate. These four sub-phase tests were continuously conducted by varying the steam injection flow rate. Table 3-1 shows the test conditions for each sub-phase. The ECCW injection flow rate was 120 kg/s per DVI nozzle throughout the entire four sub-phases. The steam flow rate injected to each loop was 33 kg/s, 30 kg/s, 25 kg/s, and 20 kg/s for the sub-phases D-I, D-II, D-III, and D-IV respectively. Drainage from the lower plenum of the reactor vessel was 120 kg/s. The containment pressure was maintained at about 250 kPa during the entire sub-phase. The initial downcomer water level of each sub-phase was maintained at the level higher than 6 m from the bottom of the reactor vessel. At the beginning of sub-phase D-III and D-IV, saturated water was injected to increase the downcomer water level.

3.2 RELAP5/MOD3.3/K Model Description

The RELAP5/MOD3.3/K input model of the UPTF is shown in Figure 3-7. Four coolant flow paths and the reactor vessel are modeled explicitly. The reactor vessel is divided into azimuthal, radial, and axial nodes, according to the actual geometry. The radial node of the reactor vessel consists of [ ]^{TS}.

The reactor vessel downcomer is modeled with [ ]^{TS}. The downcomer is connected with four cold leg nozzles (Nodes 110, 114, 710, and 714). The upper plenum of the reactor vessel was connected with four hot legs by hot leg nozzles (Nodes 116, 118, 716 and 718). Two DVI nozzles are connected to the downcomer.

The reactor vessel lower plenum is divided into [ ]^{TS}. The dummy fuel region is modeled with [ ]^{TS}. The upper plenum region, from the top of the dummy fuel assemblies to the bottom of the upper core support plate, is modeled with

[ ]^{TS}. The upper head is modeled with [ ]^{TS}.

Four loops are modeled identically, except for the break simulation section of the broken cold leg. The nodalization of each loop includes the hot leg, steam generator, pump suction leg, pump, and cold leg nodes. The broken cold leg is connected to the containment simulator by a valve. The steam generator simulator is modeled using various components including the 'SEPARATER'.

3.3 RELAP5/MOD3.3/K Simulation

Figure 3-8 shows a comparison of the predicted and the measured total break flow. For phases D-I and D-II, the predicted total break flow is similar to the test data. For the phases D-III and D-IV, however, the code predicts much higher total break flow than the test data.

The predicted downcomer water levels of the broken cold leg side and the opposite side are compared with the data in Figure 3-9. The downcomer water level on the broken cold leg side is higher than that of the opposite side, as observed in the test. This is due to that the steam introduced from the intact cold legs flows to the broken cold leg entraining water in the downcomer.

The predicted subcooling of the inventory in the broken cold leg side downcomer (Node 130-1) is compared with that on the opposite side (Node 730-1) in Figure 3-10. While the inventory of the broken cold leg side downcomer has almost no subcooling, the inventory on the opposite side has a considerable amount of subcooling. This means that the ECCW injected near the broken cold leg is almost discharged through the break; and large amounts of the ECCW injected from the opposite side of the broken cold leg penetrates into the lower downcomer. The same ECCW behavior was observed during the test. The code predicts well the observed behavior of the ECCW.

Figure 3-11 shows a comparison of the predicted and the measured average downcomer water level. The downcomer water level did not vary considerably as the steam flow rate decreased during the first three sub-phases of the test. Considerable increase in downcomer level was observed during the fourth sub-phase as shown in the figure. This increment in downcomer level during the last sub-phase was occurred due to the decrease of steam flow rate caused the decrease of lateral flow field and ECCW bypass. The prediction of code is comparable with the measurement for all of the sub-phase; and the predicted levels are lower than the measured levels in most of all sub-phases. The downcomer water level can be considered as the final result for the various thermal hydraulic phenomena in the downcomer, such as the ECCW bypass, sweep-out by entrainment, and steam condensation. Henceforth, the under-prediction of the downcomer water level implies that the code conservatively predicts the ECCW bypass and the behavior of the downcomer water level.

As discussed above, the RELAP5/MOD3.3/K code reasonably predicts the major phenomena observed during the UPTF Test 21-D; especially the code conservatively over-predicts the ECCW bypass.

References

[3-1] NUREG/IA-0126, GRS-100, MPR-1345, “International Agreement Report, 2D/3D Program Work Summary Report,” U.S. NRC, June 1993.

[3-2] NUREG/IA-0127, GRS-101, MPR-1346, “International Agreement Report, Reactor Safety Issues Resolved by the 2D/3D Program,” U.S. NRC, July 1993.

Table 3-1 Initial and Boundary Conditions of the UPTF 21-D

Parameter \ Sub-phase	D-I	D-II	D-III	D-IV
Initial conditions (Test vessel)				
Time (sec)	58	193	319	450
Pressure (kPa)	282	276	263	257
Downcomer water level (m)	6.2	6.2	6.2	7.1
Wall temperature (K)	401	404	406	408
Fluid temperature (K)	399	401	401	399
Test conditions				
Containment pressure (kPa)	250	250	250	250
Steam mass flow rate, Intact loop (kg/s)	33	30	25	20
ECCW/Nozzle (kg/s)	120	120	120	120
ECCW temperature (K)	303	303	303	303
Lower plenum drain mass flow rate (kg/s)	120	120	120	120

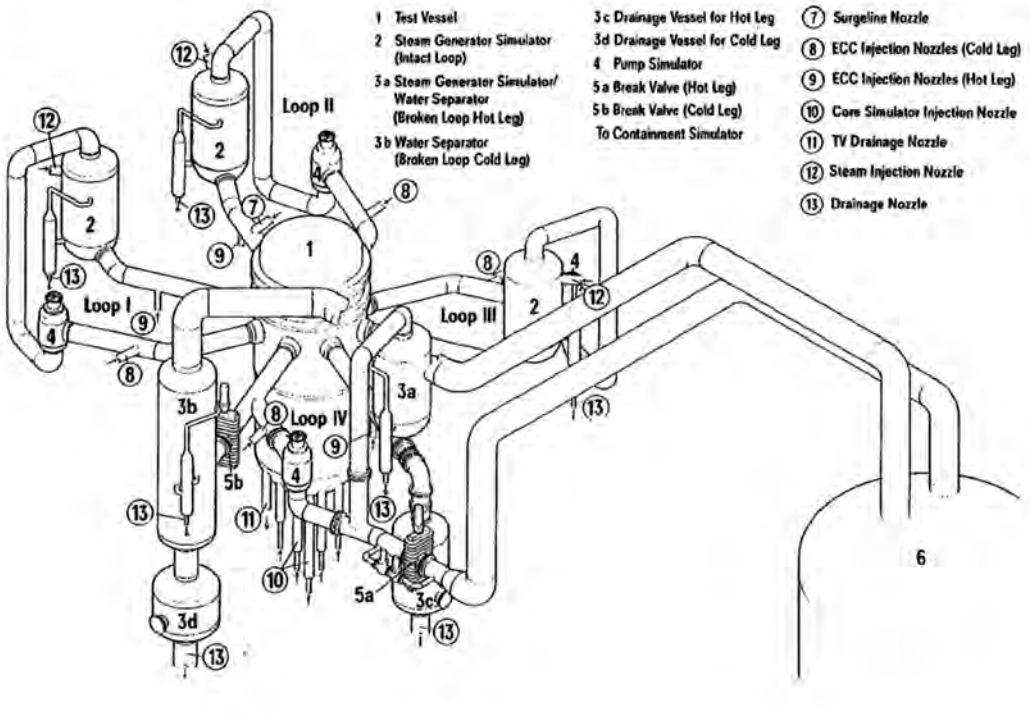

Figure 3-1 Schematic Diagram of the UPTF

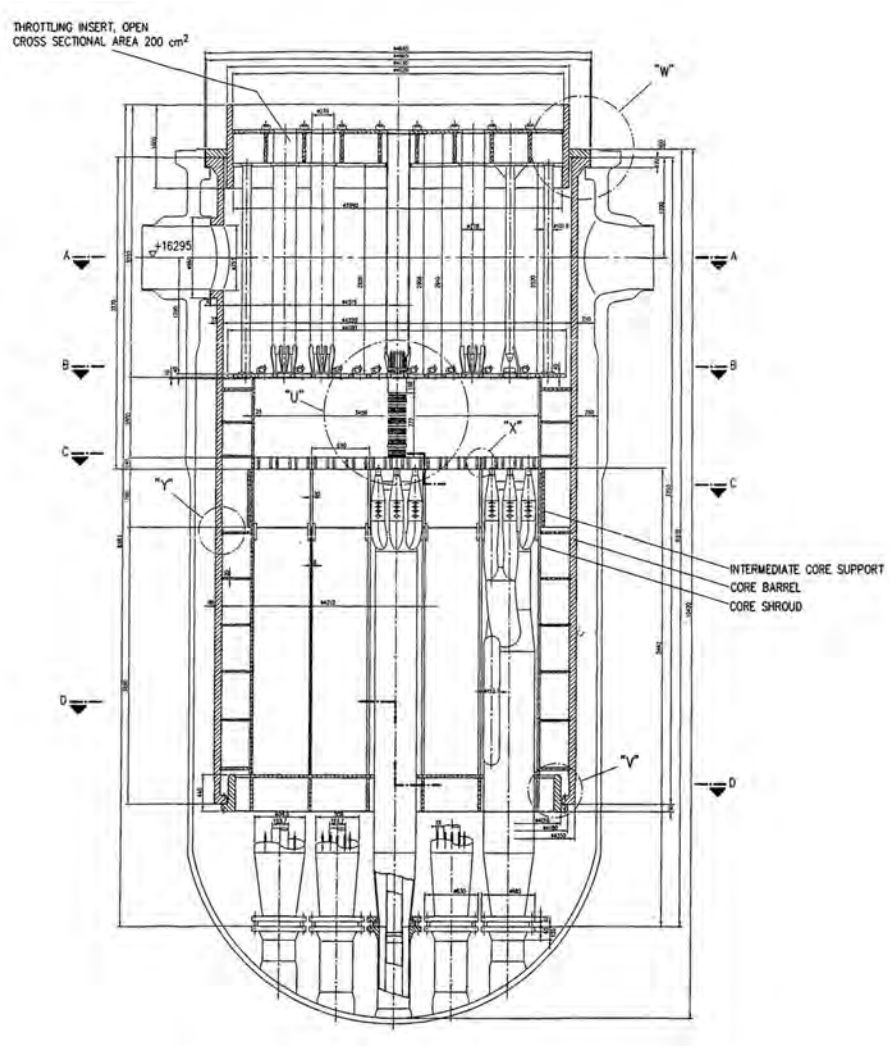

Figure 3-2 UPTF Reactor Vessel

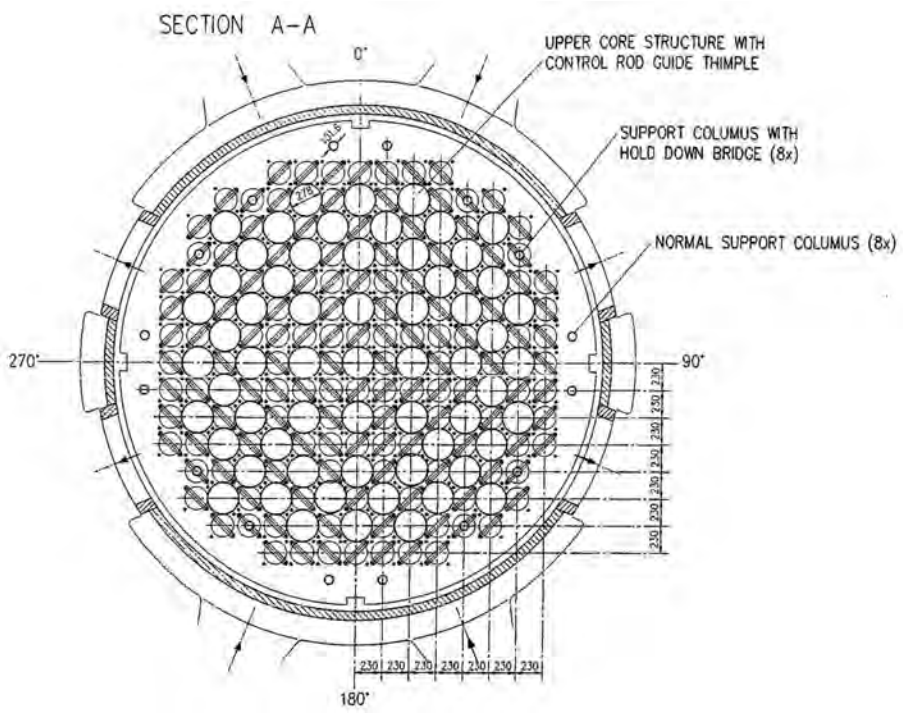

Figure 3-3 UPTF Upper Core Plate

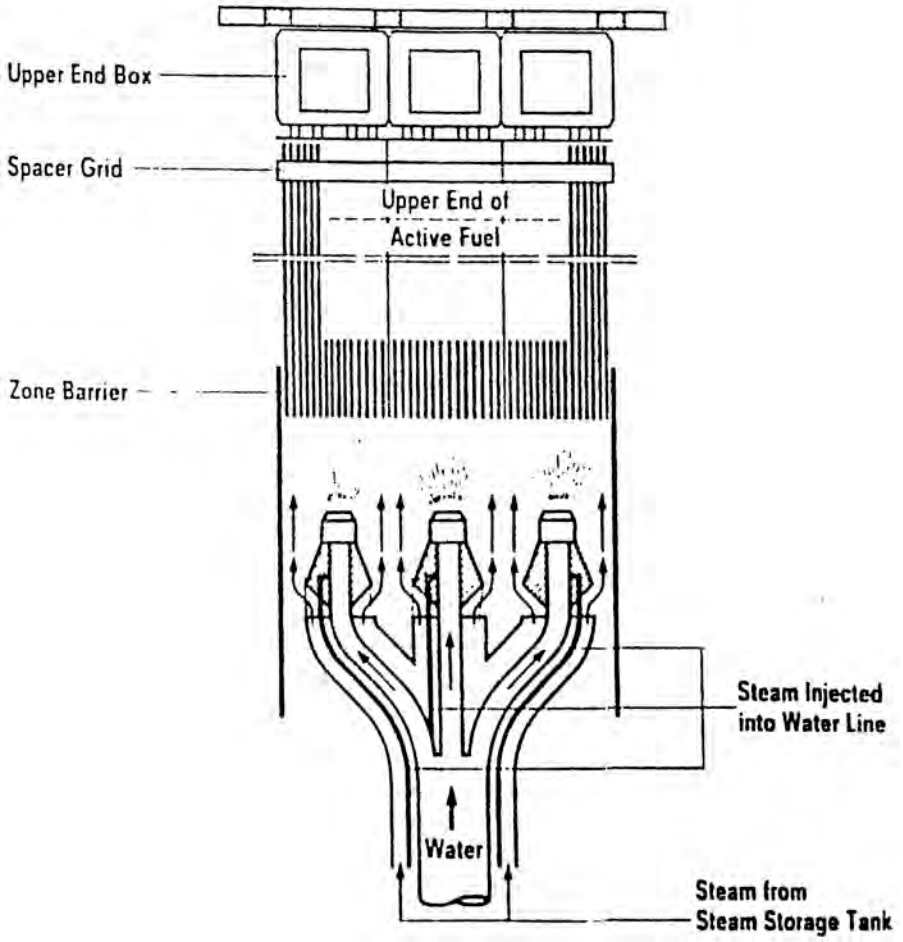

Figure 3-4 UPTF Core Simulator

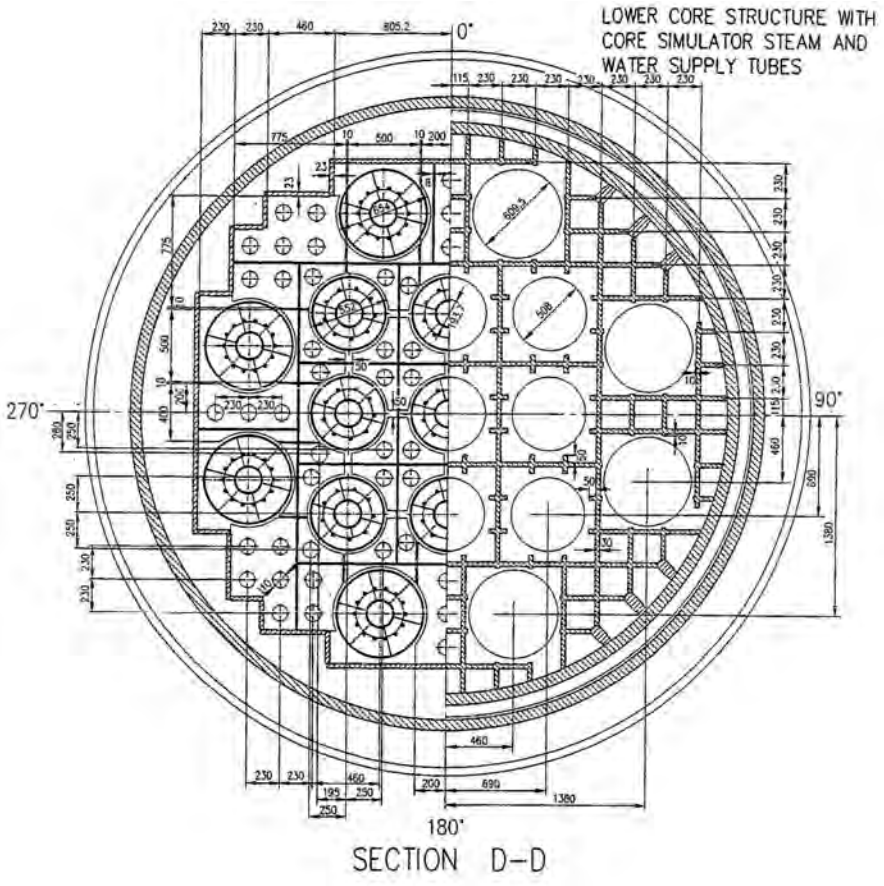

Figure 3-5 The Arrangement of the UPTF Core Simulator

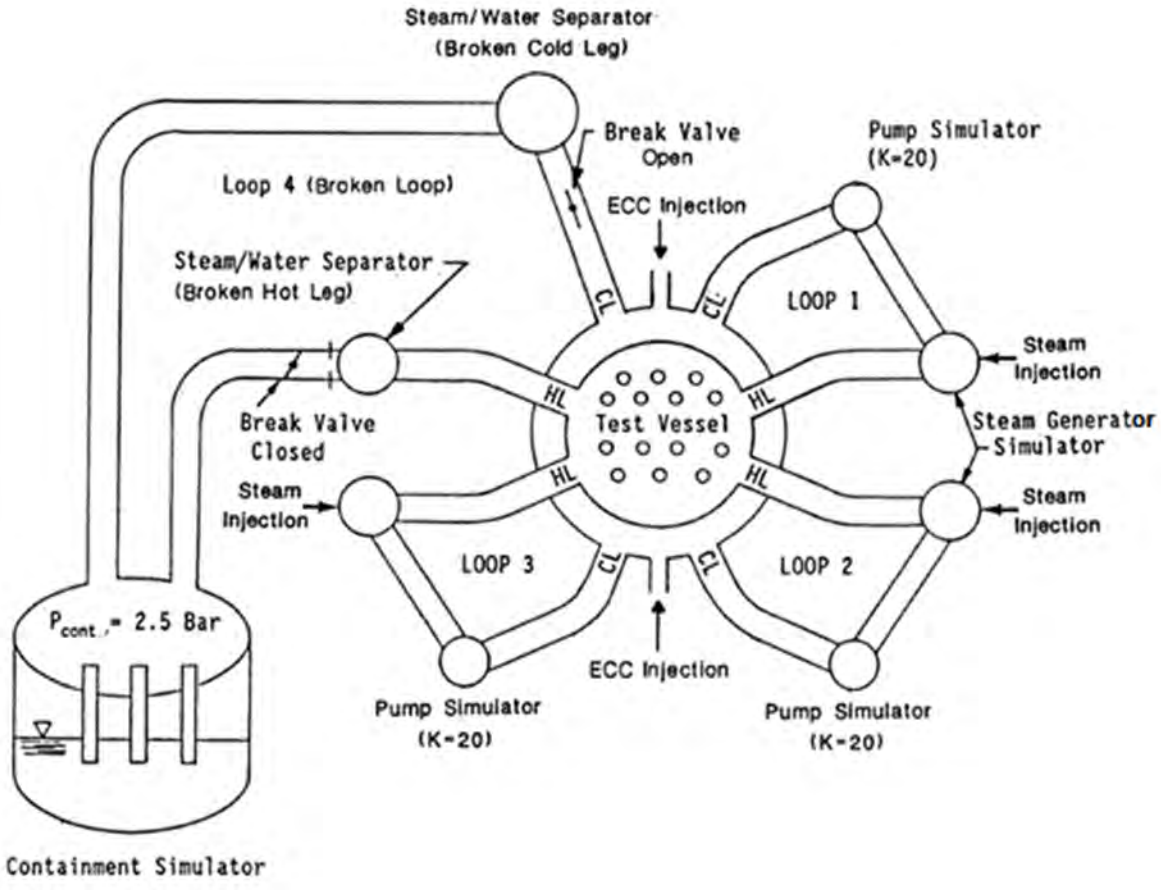

Figure 3-6 System Configuration for the UPTF Test 21-D

TS

Figure 3-7 RELAP5 Nodalization of the UPTF Test 21-D

TS

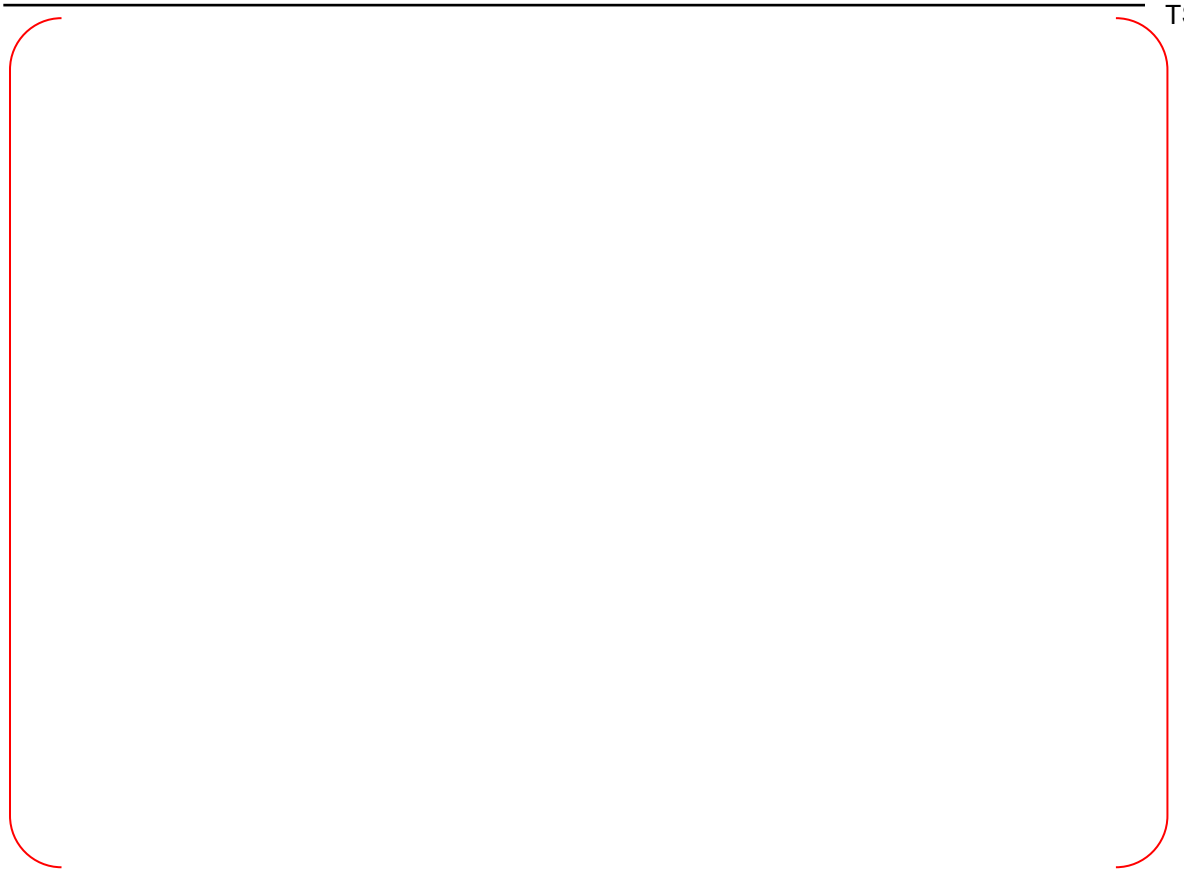

Figure 3-8 Comparison of the Predicted and the Measured Break Flow: UPTF-21D

TS

Figure 3-9 Predicted Downcomer Collapsed Water Level: UPTF-21D

TS

Figure 3-10 Predicted Subcooling of the Downcomer Coolant: UPTF-21D

TS

Figure 3-11 Comparison of the Predicted and the Measured Downcomer Water Level: UPTF-21D

4. Conclusion

In this appendix, the RELAP5/MOD3.3/K code's capability to predict the ECCW bypass was assessed against the MIDAS tests and the UPTF Test 21-D.

The assessment results show that the RELAP5/MOD3.3/K reasonably predicts the thermal hydraulic behaviors which could occur in the downcomer under the conditions of direct vessel injection (DVI) of ECCW. The results of the assessment against the MIDAS tests show that the RELAP5/MOD3.3/K over-predicts the ECC bypass conservatively. The results of the assessment against the UPTF test 21-D confirm that the code over-predicts the ECCW bypass. The code's over-prediction of ECCW bypass is also confirmed in Appendix E of this topical report.

[

]TS

Appendix G

Assessment of RELAP5/MOD3.3/K against Downcomer Boiling Tests

Non-Proprietary

August 2018

Table of Contents

List of Tables

List of Figures

1. Introduction

The Loss-of-Coolant Accident (LOCA) is analyzed in many cases, as assuming to occur at the full power operating condition of the reactor. In this case, all the metal structures of the primary system piping, reactor vessel, core barrel, and so on are assumed to be at the relevant temperatures of a full power condition in a steady state calculation. As the accident progresses, most of the metal structures are cooled down by expelling coolant and cold emergency core cooling water. The temperature difference between the metal structures and the coolant becomes negligible and there is no considerable concern about the heat transfer between them.

However, downcomer boiling needs careful attention to be paid. Downcomer boiling means that the water in the downcomer heats up to the saturation temperature and begins boiling. Because the thickness of the reactor vessel wall is more than 20 centimeters, it can still contain enough energy in it, even after the blowdown period, to still reach the boiling point. This is true even though the temperature of the reactor vessel wall is saturated. If it begins to boil, the coolant which may usually be in a liquid state becomes a two-phase mixture. If this happens, it will then lower the hydraulic head of the downcomer water, which is the driving force for reflooding the core, and can cause an adverse effect on the core cooling. This can have a critical impact to the successful cooling of the core in a LOCA condition.

Usually, the downcomer water is the mixture of the reactor-coolant remnant after the blowdown, and of the cold emergency core cooling water. The temperature may be lower than the saturation temperature, especially in the early phase of the reflood. This subcooling needs to be maintained in order to avoid the saturation of downcomer water and subsequent boiling. Because of the probable temperature difference between the water and the wall of the downcomer, a certain degree of local boiling is inevitable. But there is a need to avoid bulk boiling throughout the downcomer. In order to suppress the global downcomer boiling, a large enough amount of subcooled water is required from the safety injection system. Because only safety injection pumps are available during the late reflood period of APR1400 LBLOCA, the possibility of downcomer boiling cannot be ignored. This is a necessity to confirm the ability of RELAP5/MOD3.3/K to predict the downcomer boiling phenomena.

Thus, this appendix describes the ability of the RELAP5/MOD3.3/K to predict the downcomer boiling phenomena. The RELAP5/MOD3.3/K was assessed against the data obtained from the downcomer boiling (DOBO) tests. The DOBO tests simulated a constant downcomer wall heat flux with time to cause downcomer boiling artificially, whereas the downcomer wall temperature decreases during the APR1400 LBLOCA.

2. Downcomer Boiling (DOBO) Test

2.1 DOBO Test Description

The Korea Atomic Energy Research Institute (KAERI) conducted the downcomer boiling tests in the DOBO facility [1][2] to investigate the thermal hydraulic behavior in the downcomer region.

The schematic of the facility is shown in Figure 1. The test section was designed to simulate a high temperature wall of the reactor pressure vessel between the elevations of the cold leg and flow skirt. As described in reference [2], the test section had a heated rectangular cross-section which adopted the full pressure, height, and downcomer gap width. The circumferential length of the test section was reduced to 1/47.08 of the APR1400 under the assumption that there is no preference of downcomer boiling in the azimuthal direction. The simulated azimuthal angle of the test section corresponded to 7.65 degrees. Because this angle was small enough to be assumed as having no curvature, the rectangular channel was used for the test section. The downcomer wall was heated by the electrical heaters to achieve a steady-state constant heat flux condition. Windows were installed over the entire test section for visual observation. The heat flux which might be released from the core support barrel wall was reflected to the heat flux of the reactor pressure vessel wall. The steam vent was located at the top of the rectangular test section. The drain pipe was installed at the bottom of the test section to keep the mixture level. The injection nozzle of the emergency core cooling water was installed at the upper part of the test section.

The major parameters were the wall heat flux, the water temperature, and the void fraction. Average void fractions in various levels were obtained by converting differential pressure measured at corresponding levels. Degrees of subcooling of the water were measured at the top and bottom of the test section.

The test procedure was as follows:

- The coolant was heated up to the target temperature by the preheater, and was injected through the coolant inlet nozzle.
- When the water level in the test section reached target value, heaters were operated to supply constant power and the bottom drain valve was opened.

Table 1 provides test conditions of four tests conducted in DOBO. The principal parameter is the wall heat flux.

Figure 2 shows a schematic diagram of the downcomer boiling which was visually observed through the window. The observed bubble behavior can be roughly divided into three regions. In the lower region of the test section, the onset of nucleate boiling (ONB in Figure 2) occurred and the bubbly boundary layer developed. The detachment of the bubbles from the wall, and sliding along the wall were also observed. It should be noted that the amount of void formation was negligible. OSV in Figure 2 stands for onset of void where void fraction is noticeable. In the middle part of the test section, the swirling turbulent flow induced by periodic lateral or downward bubble flow was observed. The average void fraction was less than a few percent. A well-mixed bulk boiling occurred in the upper region of the test section. The higher bubble population was observed at the higher elevation of the test section, in general. Figure 3 shows the measured axial void distribution in the test section. The void fraction of the lower test section, from the bottom of the test section to two meters high; was almost zero, because there was no boiling, or limited subcooled boiling began in this region. In the upper test section above the subcooled boiling region, void fraction increased along the height of the test section. The amount of void was also proportional to the heat fluxes from the wall.

Figure 4 shows the void fraction averaged for the full span of the test section with respect to heat flux from the wall. It is obvious that the average void fraction is proportional to the wall heat flux.

2.2 Code Assessment against DOBO Tests

This section describes the results of the code assessments to evaluate the ability of the RELAP5/MOD3.3/K to predict the downcomer boiling phenomena.

The RELAP5/MOD3.3/K input model of the DOBO facility is shown in Figure 5. [

]^{TS} Figure 6 shows a comparison of the predicted and measured void fractions. The RELAP5/MOD3.3/K code over-predicts the void fractions in all of the axial nodes for all test cases. While the measurements showed the survival of the subcooled ECCW, the calculations also showed almost no subcooling at the bottom of the test section. Figure 7 shows the comparison between the measured and predicted subcooling at the bottom of the test section. Applying [

]^{TS} of Figure 5, there is almost no chance for the ECCW to maintain the subcooling at the bottom of the test section.

We did an additional sensitivity study using [ ]^{TS} as shown in Figure 8. The purpose of the sensitivity study was to examine whether the prediction could be improved when [ ]^{TS} was not applied. The transverse gap of the downcomer was [

]^{TS}. With this configuration, the subcooling at the bottom of the test section was well predicted as shown in Figure 9. Temperatures calculated at the two control volumes at the bottom of the test section were averaged and the degree of subcooling was calculated for each test. Figure 10 shows the void fraction profile along the height for each test. The void fractions of the two control volumes; at the same elevation; were also averaged in Figure 10. Using [

]^{TS}, it was possible to predict the degree of subcooling at the bottom, very well. In the case of the void fraction profile though, [ ]^{TS} only resulted in better prediction in the lower part of the test section. The improvement at the higher elevation was not as good. This is due to the fact that the variation of the void fraction along the height, as shown in Figure 2, cannot be exactly predicted using the [ ]^{TS}. In order to capture the axial variations of the void fractions exactly, it may be necessary to [

]^{TS}

Rather than doing a further study of the detailed modeling, two different modeling results were compared. [ ]^{TS} results of Figure 6 and Figure 7 are definitely conservative with respect to the hydrostatic head of the downcomer water, which is a driving force of the core reflood. [

]^{TS} of the test section is applied, it is costly and invokes a technical difficulty. Usually, water volumes in system codes should be confined in tubes or channels of solid walls. [

]^{TS}

Because the results of [

]^{TS} to relevant calculations for power plants and experiment facilities.

[

]^{TS}, and the applicability of RELAP5 to those kinds of channels.

3. Conclusion

The ability of the RELAP5/MOD3.3 code to predict downcomer boiling phenomena was examined in this appendix. The RELAP5/MOD3.3/K code was assessed against the data obtained from the DOBO tests.

The assessment results revealed that the downcomer boiling phenomena were conservatively predicted, if the downcomer is modeled [ ]^{TS}. Accordingly, the reactor pressure vessel downcomer of the APR1400 should be modeled [ ]^{TS} of the downcomer boiling phenomena.

Table 1 Downcomer Boiling Test Conditions

TS

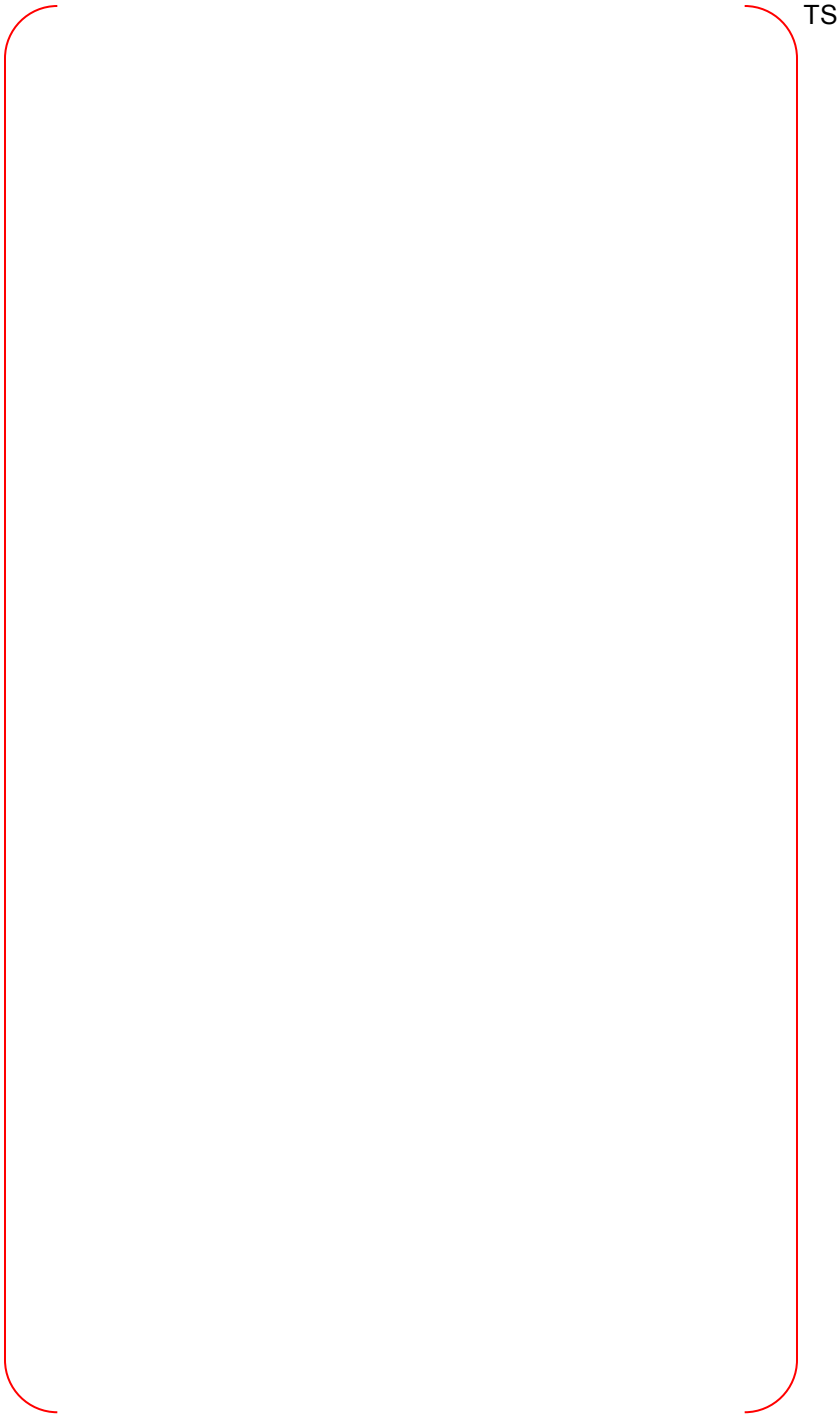

Figure 1 Downcomer Boiling Test Facility of KAERI

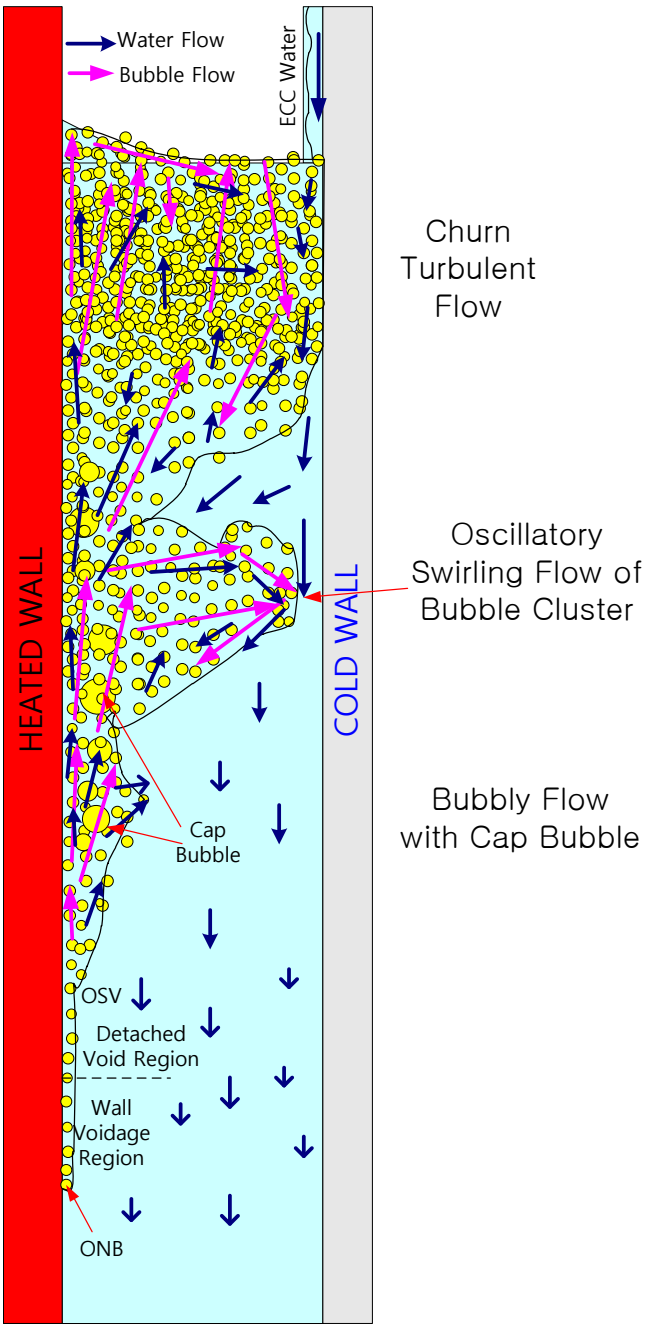

Figure 2 Illustration of typical downcomer boiling

Figure 3 Measured Void Fractions, by Height, for Each Heat Flux Condition

TS

Figure 4 Average Void Fraction of the Test Section for Each Heat Flux Condition

TS

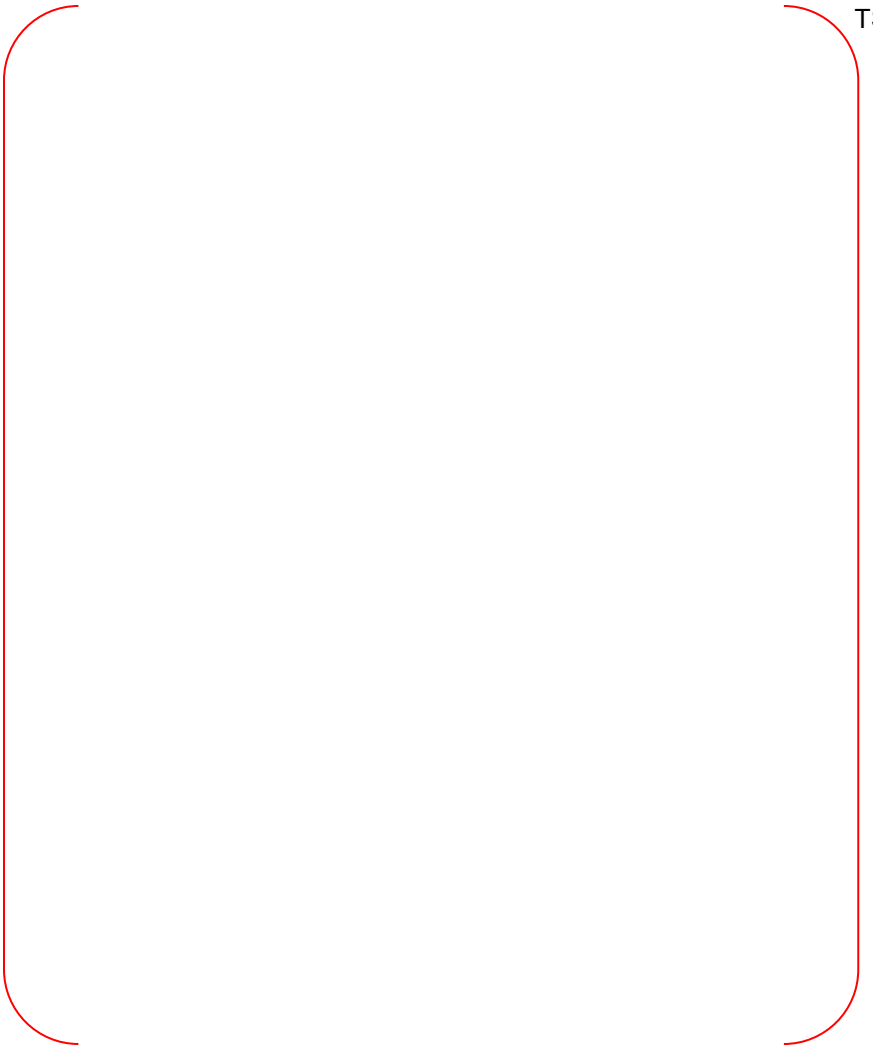

Figure 5 [ ]TS of DOBO Test Facility

Figure 6 Comparison of the Elevation-Wise Void Fractions; Between the Measured and Predicted; [ ]TS

TS

Figure 7 Comparison of the Subcooling at the Bottom of the Test Section; Between the Measured and Predicted; [ ]TS

TS

Figure 8 [ ]TS of DOBO Test Facility

Figure 9 Comparison of the Subcooling at the Bottom of the Test Section; Between the Measured and Predicted; [ ]TS

TS

Figure 10 Comparison of the Elevation-Wise Void Fractions; Between the Measured and Predicted; [ ]TS

References

[1] B. J. Yun, et al., “Investigation of the downcomer boiling phenomena during the reflood phase of a postulated large-break LOCA in the APR1400,” v. 156, Nuclear Technology, Oct. 2006.

[2] B. J. Yun, et al., “Downcomer boiling phenomena during the reflood phase of a large-break LOCA for the APR1400,” 238, Nuclear Engineering and Design, 2008.

Appendix H

Assessment of RELAP5/MOD3.3/K against Fluidic-Device-Installed Safety Injection Tank Tests

Non-Proprietary

August 2018

Abstract

The APR1400 newly employs safety injection tanks equipped with fluidic devices (SIT-FD), which distinguishes it from other typical pressurized water reactors (PWRs). The fluidic device is installed inside the SIT and passively controls the water injection flow rate from the SIT. The SIT-FD injects water at a high flow rate during the blowdown and refill periods, and at a low flow rate during the reflood period. This is a unique characteristic of the SIT-FD. Since the SIT-FD has a unique water injection characteristic, a SIT modeling, which can appropriately simulate the SIT-FD, is required instead of the conventional modeling using the ACCUM component in the RELAP5/MOD3.3/K code.

Therefore, in this appendix, several modeling methods, which can appropriately simulate SIT-FD are suggested and are assessed against the SIT-FD performance tests conducted using the full-scale test facility VAPER.

Three kinds of modeling methods, Model A, B, and C, were suggested and assessed against the VAPER test data in Chapter 1. Assessment results show that all modeling methods have capability to predict ECCW injection behavior of SIT-FD but, non-condensable gas release behavior which occurs before the end of SIT-FD injection could not be predicted properly by all modeling methods. To evaluate effects of non-condensable gas release which occurs before the end of SIT-FD injection, Model D was additionally devised and assessed in this chapter. In Model D, the logical flow path K-factor adjustment method was developed to predict the non-condensable gas behavior observed in the VAPER tests.

In Chapter 2, the investigation on the effects of non-condensable gas release which occurs before the end of SIT-FD injection was performed for the APR1400. Model A ~ C were considered in this investigation and the non-condensable gas release behavior predicted by Model D was used as boundary condition. As a result of the sensitivity calculation, the effects of non-condensable gas release before the end of SIT-FD injection have tendency to cause earlier core quenching. Therefore, it is concluded that non-condensable gas release behavior which occurs before the end of SIT-FD injection can be ignored for conservatism. Consequently, Model C is determined as the representative modeling of SIT-FD based on the conclusions of Chapter 1 and 2.

In Chapter 3, a sensitivity study of pressure loss coefficients (K-factor) was performed for the K-factor ranges of design requirements for the large and small flow injections. Based on the results of this sensitivity study, the representative K-factors for large and small flow injection have been selected for the APR1400 LBLOCA analysis.

Table of Contents

List of Tables

List of Figures

1. Code Assessment against VAPER Tests

One of the advanced safety features of the APR1400 is the safety injection tank equipped with fluidic device (SIT-FD). Each of the four SITs of the APR1400 has a fluidic device, which passively controls the injection flow rate into the reactor vessel system during the refill and reflood phases of a loss of coolant accident (LOCA).

In LOCA analyses using the RELAP5 code, SIT is usually modeled with the ACCUM component. However, the ACCUM component model regards SIT as a lumped volume so that it cannot be directly applied to the modeling of the SIT-FD of the APR1400. In this chapter, therefore, several models for the SIT-FD are suggested and assessed.

Since the FD is a new type of safety equipment, a full scale test facility, valve performance evaluation rig (VAPER), was built and various tests were conducted. The suggested models for the SIT-FD were assessed using the results from VAPER tests

Section 1.1 describes the general descriptions and test conditions of the VAPER tests. Section 1.2 discusses RELAP5 models for simulating SIT-FD. The assessment results of the suggested models are presented in Section 1.3.

1.1 VAPER Test

1.1.1 Test Facility Description

The performance of the SIT-FD was evaluated and verified at the full scale test facility VAPER. The schematic diagram of the VAPER facility is shown in Figure 1-1. VAPER is consisted of the SIT, fluidic device, compressed air supply system, safety injection (SI) water discharge pipe line, SI water supply and recirculation system, stock tank, and a data acquisition and control system. The fluidic device was installed at the bottom of the tank. At the discharge pipe, a quick opening valve was installed, and discharged water and gas were collected in a stock tank, which was maintained at atmospheric pressure.

[

]^{TS}. The fluidic device of the VAPER facility had almost the same geometrical shape and size as the fluidic device of APR1400. The major dimensions of the fluidic device are summarized in Table 1-1.

Major parameters measured in the tests were SIT water level, gas pressure and temperature, water level in the stand pipe, and pressure drop across the fluidic device. The discharged water mass flow rate was calculated using the measured SIT water level. The discharged gas mass flow rate was also estimated with the measured gas pressure assuming polytrophic gas expansion. The initial water level and level change in the SIT were measured by a differential pressure transmitter. The pressure of the SIT and the temperature of the compressed air in the SIT were measured by a pressure transmitter and a thermocouple at the top of the SIT, respectively. The pressure drop across the fluidic device was measured by a differential pressure transmitter. The level change in the stand pipe was measured by a differential pressure transmitter.

The design data of APR1400 SIT-FD are slightly different from those of VAPER facility. The design data of APR1400 SIT-FD, VAPER, and RELAP5 input of the topical report are summarized in Table 1-2. Tank volume is the same, however available water volumes of VAPER and APR1400 SIT-FD are different due to change in stand pipe height. The stand pipe height of VAPER test is 4.066 m

whereas, that of APR1400 SIT-FD is 4.59 m. The longer stand pipe height in APR1400 is designed to extend small flow injection period with the same large flow injection water volume and is advantageous for safety in comparison to the VAPER test. Meanwhile, the effects of stand pipe height were investigated with the VAPER test facility, and the results showed that the effects of stand pipe height on the pressure loss coefficient of SIT-FD are insignificant as described in reference [1].

1.1.2 Test Conditions

Four cases of tests were carried out to verify the performance of the SIT-FD at the VAPER facility. Case-01 and Case-02 correspond to the standard fluidic device tests. That is, the fluidic device in Case-01 and Case-02 had almost the same geometrical dimensions as the fluidic device of the APR1400. [

]^{TS}

Four Case-01 tests, Case-01-01 through Case-01-04, were selected for the RELAP5/MOD3.3/K code assessment. Three identical tests, Case-01-01 through Case-01-03, were conducted under the reference test conditions in order to check the repeatability of the test results. [

]^{TS} The reference conditions of the Case-01 tests are shown in Table 1-3.

Detailed information on the SIT and FD installed in the VAPER facility is provided in Reference [1].

1.2 Modeling of the SIT-FD

As mentioned above, four Case-01 tests were used for the RELAP5/MOD3.3/K assessment and test conditions of these tests are summarized in Table 1-4.

The data-derived pressure loss coefficient (K-factor) of the fluidic device is shown in Figure 1-2 as a function of the SIT water level. The data-derived K-factor was determined based on the pressure drop across the fluidic device measured in four Case-01 tests. [

]^{TS}. The average and input values of RELAP5/MOD3.3/K are also shown in this figure.

Based on the VAPER test results, four input models were studied to simulate the SIT-FD and its flow injection characteristics. Case A is a detailed modeling [

]^{TS}. Cases B and C are [

]^{TS}. In addition to these three input models, Case D was studied in order to only predict gas release phenomenon from the SIT-FD.

Model A; [ ]^{TS}

The RELAP5/MOD3.3/K nodalization of Model A for the VAPER facility is shown in Figure 1-3. [

]^{TS} to simulate large and small flow injection and gas release. Gas, water volume above the top of the stand pipe, and the stand pipe were modeled [

]^{TS}. [

]^{TS} The surge line pipe was modeled with the PIPE component (C160), which has three volumes, and the stock tank

was modeled with a TMDPVOL (C170) component. The quick opening valve, which is located between the stock tank and surge line pipe, was modeled with one VALVE (V165) component.

[ ]TS Figure 1-2 shows the measured, averaged, and code input values of the K-factor. [ ]TS.

Model B; [ ]TS

The Model B nodalization of the VAPER facility is shown in Figure 1-4. [ ]TS The surge line pipe, stock tank, and quick opening valve were modeled in the same way used in Model A. [ ]TS

Model C; [ ]TS

Figure 1-5 shows Model C nodalization for VAPER. [ ]TS

Model D; [ ]TS

[ ]TS The effects of non-condensable gas in the APR1400 LOCA will be evaluated in Chapter 2.

1.3 Assessment Results

Two cases of RELAP5/MOD3.3 calculations were performed, one was for Case-01-01 through Case-01-03 tests and the other was for Case-01-04. For each case, three calculations were performed using the models suggested in the previous section. The reference conditions specified in Table 1-3 were used as input for RELAP5/MOD3.3/K except for the Case-01-04 test, which was performed under approximately half of the reference SIT pressure.

1.3.1 Case-01-01, Case-01-02, and Case-01-03

SIT water level

The SIT water levels predicted by the four models are compared with the test data in Figure 1-6. The SIT water level decreased steeply when the quick opening valve was opened at approximately 4 s then the water level gradually decreased after the water level reached the top of the stand pipe at approximately 30 s. Test data showed that the SIT water level was approximately 0.7 m at the end of the test due to the measurement elevation located at the SIT bottom. However, there was no water actually available above the bottom of the fluidic device. The volume between the FD bottom and the SIT bottom was not modeled in the calculations. The levels calculated by Model A and D well match the data, whereas the values predicted by models B and C deviate from the data after approximately 100 s. The water levels calculated by models B and C decrease more sharply than the data after 100 s. This is because models B and C do not properly predict air release behavior. For tests Case-01-01 through Case-01-03, air was injected with water from approximately 100 s whereas models B and C predicted that air would be released after SIT water is exhausted at approximately 148 s, as shown in Figure 1-7. Thus, the water injection flow rate predicted by models B and C were higher than the data after 100 s, resulting in a faster decrease of water level than the data.

Air release

Air release behaviors predicted by the four models are compared with the test data in Figure 1-7. Test results showed that air release began at approximately 100 s. Model A and Model D well predict the air release beginning time. The air release rate predicted by Model A, however, showed a little qualitative difference from the data. Model D predicted the air release behavior fairly well because this model arbitrarily adjusts the [ ]^{TS} to produce the measured air release rate. Meanwhile, Model B and Model C predicted that gas release starts after all the water in the tank is exhausted.

Pressure

The measured SIT pressure is compared with the calculations results in Figure 1-8. The SIT pressure was measured at the upper side of the tank. The results of the calculations well match the data until 100 s. After 100 s, however, the predicted values were higher than the data in all calculations. For Model B and Model C, the degree of pressure over-prediction was higher than those of the other models because these models predicted that air release begins after SIT water is exhausted. However, general SIT pressure behaviors predicted by the four models match the data reasonably.

Water injection flow rate

Water injection flow rates calculated by the four models are compared with the data in Figure 1-9. The measured injection flow rate decreased sharply when the water level reached the top of the stand pipe at approximately 30 s and then small flow injection started at approximately 40 s. After approximately 100 s, discharged mass flow rate gradually decreased because air started to release. All four models reasonably well predicted a peak flow rate and the general behavior of the large flow injection. The flow rate turning point was also well predicted by all models, except for Model C. For Model C, the flow rate turning point was calculated to occur slightly after than that from the data. [ ]^{TS}. The injection flow rate changes to low flow rate without a transition period between large and small flow injection periods when the SIT water volume above the top of the stand pipe and water volume inside the stand pipe are exhausted. Meanwhile the other models control the injection flow rate when the SIT water level reaches the top of the stand pipe and simulate the transition period between large and small flow injection periods. This difference in modeling methods results in a late flow rate turning point in Model C. Because Model A and Model D can reasonably simulate air release, the water injection flow rate predicted by Model A and Model D well match the data after 100 s. For Model B and Model C, however, the injection flow rate was higher than the data and

sharply reached zero when the SIT water was exhausted since these models predict air release behavior differently from the data.

1.3.2 Case-01-04

SIT water level

The SIT water levels predicted by four models are compared with the test data in Figure 1-10. The SIT water level predicted by Model B and Model C decreases faster than that from the data while Model A well predicts the experiment data. All models reasonably predict the tank level behavior.

Air release

Air release behaviors predicted by the four models are compared with the test data in Figure 1-11. Test data showed that air release began at approximately 175 s and reached the maximum flow rate at approximately 210 s. The air release behavior of Case-01-04 is very similar to that of conventional SITs, unlike the other three tests. In other words, air release in Case-01-04 started when the SIT water inventory was almost exhausted. The only difference between Case-01-04 and the other three tests is the SIT pressure. The SIT pressure of Case-01-04 was approximately half of the reference pressure. This implies that the pressure difference between the SIT and the stock tank of Case-01-04 is very similar to the pressure difference between the SIT and the reactor coolant system (RCS) during a hypothetical LOCA in APR1400. Due to this reason, the gas release behavior during a hypothetical LOCA in APR1400 is expected to be similar to that of Case-01-04.

Model A reasonably predicts the air release beginning time, however, the air release rate predicted by this model shows a little qualitative difference from the data. Models B and C predicted that air release begins after all the water in the tank is exhausted. The general trend of gas release behavior predicted by models B and C was similar to the test data. Model D predicts air release behavior relatively well. [

]^{TS}

Pressure

The predicted SIT pressure is compared with the measured data in Figure 1-12. All four models reasonably predicted the general behavior of the SIT pressures. All models well predicted tank pressure until approximately 20 s, the large flow injection period. After approximately 20s, all models over-predicted the SIT pressure showing the same tendency with the results from previous assessments against the other three tests. This over-prediction of the SIT pressure is due to the under-prediction of the high injection flow rate as described below. The initial pressure difference between the measured and predicted SIT pressure was maintained until the end of the test.

Water injection flow rate

Figure 1-13 shows a comparison between the predicted and measured liquid mass flow rate. All models slightly under-predicted flow rates during the large flow injection period. Model C predicted the flow rate change to occur slightly later than that of the test data, due to the modeling characteristics. However, the other models predict well the flow rate changing time. All models well predict the injection flow rate during the small flow injection period. Model B and Model C slightly over-predicted flow rates after air release that begins at approximately 175 s. However, the deviation from the data was not significant.

1.4 Conclusion

In this chapter, several models that simulate the liquid and gas injection behaviors observed in VAPER tests are suggested. The model assessment results show that models A, B, and C reasonably predict the injection flow rates, pressure drop in the tank, and water level behaviors during both the large and small flow injection periods. Air release behaviors predicted by these three models, however, show discrepancies from the test data. [

]TS

Table 1-1 Main Dimensions of the Fluidic Device

TS

Table 1-2 The Design Data of SIT-FD for APR1400 and VAPER Test and RELAP5 Input Values

TS

Table 1-3 Reference Test Conditions for VAPER Case-01 Tests

TS

Table 1-4 Test Conditions of Case-01 Tests

TS

TS

Figure 1-1 Schematic Diagram of the VAPER Facility

Figure 1-2 Measured FD K-factor

Figure 1-3 Model A for VAPER Facility

Figure 1-4 Model B for VAPER Facility

Figure 1-5 Model C for VAPER Facility

Figure 1-6 SIT Water Level: Test Case-01-01 ~ Case-01-03

Figure 1-7 Air Release Rate: Test Case-01-01 ~ Case-01-03

Figure 1-8 Pressure at Top of the Tank: Test Case-01-01 ~ Case-01-03

Figure 1-9 Liquid Mass Flow Rate: Test Case-01-01 ~ Case-01-03

Figure 1-10 SIT Water Level: Test Case-01-04

Figure 1-11 Air Mass Flow Rate: Test Case-01-04

Figure 1-12 Pressure at Top of the Tank: Test Case-01-04

Figure 1-13 Liquid Mass Flow Rate: Test Case-01-04

2. APR1400 Sensitivity Calculations

The assessment results of the three models for SIT-FD, models A, B, and C, show that these models can reasonably predict SIT-FD injection characteristics, such as large and small flow injection, water level in the tank, and pressure, [ ]^{TS} as described in the previous chapter.

This chapter describes two sensitivity studies; one was performed to investigate the effects of non-condensable gas release on the thermal-hydraulic behavior of the APR1400 RCS, the other was performed to determine a SIT-FD model for the APR1400 LBLOCA analysis.

The sensitivity studies were performed on the limiting break size of a double-ended guillotine break in a cold leg, with the assumptions of loss of off-site power and failure of one diesel generator. Figure 2-1 shows the RELAP5 input model for APR1400 used in the sensitivity studies.

2.1 Sensitivity Study of Non-condensable Gas Effect

As discussed in the previous chapter, [ ]^{TS} Model D has been confirmed to be capable of reasonably predicting non-condensable gas release behavior. Therefore, [ ]^{TS}

In this section, the results of the following calculation cases are compared to investigate the effects of non-condensable gas release before the end of SIT-FD injection.

Case 1: Calculations using SIT-FD Model A (or B or C)

Case 2: Calculations using SIT-FD Model A (or B or C) and [ ]^{TS}

For Case 2 calculations, because [ ]^{TS}

Figure 2-2 shows the non-condensable gas release behavior [ ]^{TS}. [ ]^{TS}

Non-condensable gas release

The non-condensable gas release behavior is shown in Figure 2-3. In each graph, the solid black line is the result of the Case 1 calculation and dotted red line is the result of the Case 2 calculation. The trends of gas release behavior predicted by models A, B, and C are very similar to those observed in the assessment against VAPER tests using the same models. As expected, however, non-condensable gas behaviors predicted by models A, B, and C, show an apparent discrepancy from the result of Case 2, which is believed to be reality.

Water injection flow rate

Figure 2-4 shows a comparison of the water injection flow rates between Case 1 and Case 2 calculations. There was almost no difference between the results of Case 1 and Case 2 calculations. This is an obvious result since the water injection flow rate is not affected until non-condensable gas release begins. The water injection flow rates in Case 1 and Case 2 show the same results even after non-condensable gas release. [

]TS

Lower downcomer and core collapsed water level

The collapsed water level in the lower downcomer and core are shown in Figure 2-5 and Figure 2-6 respectively. The reactor vessel bottom elevation was used as the reference elevation in these figures. In both cases, the downcomer water level sharply decreases when non-condensable gas release begins. This is because the discharged gas increases the downcomer pressure and this in turn suppresses water level. [

]TS Consequently, the core water level of Case 2 increases higher than that of Case 1 when non-condensable gas is released from the SIT. The general water level behaviors in the downcomer and core, however, are very similar in both cases.

Peak cladding temperature

Figure 2-7 shows a comparison of the cladding temperatures predicted by Case 1 and Case 2 calculations at the PCT location. Before non-condensable gas was released, there was no difference in cladding temperature behavior between Case 1 and Case 2 calculations. After then, the cladding temperature of Case 2 was quenched earlier than in Case 1 except Case 2 with Model C. For Case 1 and Case 2 with Model C, there is no obvious difference in rod quenching. However, Case 2 with Model C shows that non-condensable gas release causes lower cladding temperature than that of Case 1 with Model C at around 180 s. Therefore, it concluded that non-condensable gas release before the end of SIT-FD has an effects to decrease fuel rod temperature and cause earlier rod quenching time.

Sensitivity study results summary

The APR1400 sensitivity calculations were performed to investigate the effects of non-condensable gas release behavior on the thermal-hydraulic behavior of the RCS. In the sensitivity calculations, models A, B, C, and D were used to simulate the SIT-FD.

The results of the sensitivity calculations show that the non-condensable gas release before the end of SIT-FD injection causes early fuel rod quenching.

2.2 Determination of SIT-FD Model for APR1400 Calculations

This section describes the determination of the SIT-FD model for APR400 LBLOCA calculations.

As described in Chapter 1, the assessment results of models A, B, and C against VAPER tests show that these models can reasonably predict water injection characteristics of the SIT-FD [

]TS. From the results of the previous section 2.1, non-condensable gas release behavior [

]TS. [

]TS Consequently, the final SIT-FD model for the APR1400 LBLOCA

calculations was selected as the one that gave the most conservative effects on thermal-hydraulic behavior and PCT among the three models, even though the difference in the results was not significant.

For the determination of the SIT-FD model, the results of three APR1400 calculations, which Model A or B or C is applied to, are compared below.

Water injection flow rate

Figure 2-8 shows a comparison of calculation results of the water injection flow rate. The peak flow rate predicted by Model A was higher than those predicted by other models; however, the differences in the peak flow rate predicted in the three models were insignificant. In calculations using models A and B, the water flow rate decreased relatively smoothly during the transition period between large and small flow injection periods. In the calculation using Model C, the water injection flow rate instantly decreased and changed to low flow rate, due to the model characteristics described in Chapter 1. The predicted low flow rates were almost the same in the three models, except for the depletion time of the SIT inventory. The result of the calculation using Model C showed the earliest depletion of the SIT inventory due to a longer large flow injection period than in other calculations. The latest depletion of the SIT inventory was predicted by Model B. Unlike the other cases, the water injection flow rate predicted by Model A decreased relatively smoothly at around SIT inventory depletion time [ ]^{TS}

Non-condensable gas release

Non-condensable gas release behaviors predicted by the three calculations are compared in Figure 2-9. The calculations using models B and C predicted that non-condensable gas release begins after the depletion of the SIT inventory. [ ]^{TS} The trends of gas release behavior predicted by the three calculations were very similar with those predicted in the assessment against VAPER tests using the same SIT-FD models.

Lower downcomer and core collapsed water level

The lower downcomer collapsed water level is shown in Figure 2-10. Downcomer collapsed water level increased quickly and reached the cold leg elevation during the large flow injection period. The water level was maintained during the small flow injection period.

All models predicted similar downcomer collapsed water level behaviors before 210 s, even though Model C predicted a longer large flow injection period. After 210 s, the downcomer collapsed water level predicted by each model showed some differences, but the general trend of the predicted downcomer water level was very similar among the models.

The predicted core collapsed water levels were almost the same until approximately 75 s as shown in Figure 2-11 because the injection flow rates were almost the same before 50 s as shown in Figure 2-8. After 75 s, the core water levels predicted in the three calculations showed some differences. This is due to the effect of the difference in large flow injection end time on the core water level, which appears from 75 s. In all calculations, the core collapsed water level decreased after the SIT inventory was depleted. In general, the core water levels predicted by the three models show similar trends.

Rod cladding temperature

The predicted cladding temperature behavior of the hottest rod is compared in Figure 2-12. The differences among the three models in predicting rod cladding temperature behavior were negligible. But, Model C predicted relatively higher reflood PCT than in the other models.

Summary

The results of the sensitivity study described in this section show that all three models predict very similar SIT-FD injection behaviors, and the differences are insignificant. In the thermal-hydraulic behaviors of the system, calculation results of each model show some differences but these are also insignificant.

2.3 Conclusion

As described in Chapter 1, the suggested SIT-FD models have difficulty in predicting non-condensable gas release behavior, except for Model A, which is a very detailed nodalization using general hydraulic components. In this chapter, therefore, two sensitivity studies were performed to investigate the effects of non-condensable gas release behavior on the thermal-hydraulic behavior of the APR1400 RCS and to determine a SIT-FD model for the APR1400 LBLOCA analysis.

The results of model assessment in Chapter 1 and sensitivity studies in this chapter show that all suggested models can be applied to APR1400 LBLOCA calculations. This is because these models reasonably predict water injection flow rates during large and small flow injection periods. In addition, the sensitivity study results also show that an early release of non-condensable gas before depletion of SIT inventory could result in favorable effects on the fuel rod quenching behavior.

Therefore, Model C was selected as the final SIT-FD model for the APR1400 LBLOCA analysis because this model is not only enough to represent injection flow characteristics of the SIT-FD but also enough to remain economical.

Figure 2-1 RELAP5/MOD3.3/K Nodalization for APR1400

Figure 2-2 Non-Condensable Gas Release Behavior Calculated by Model D

TS

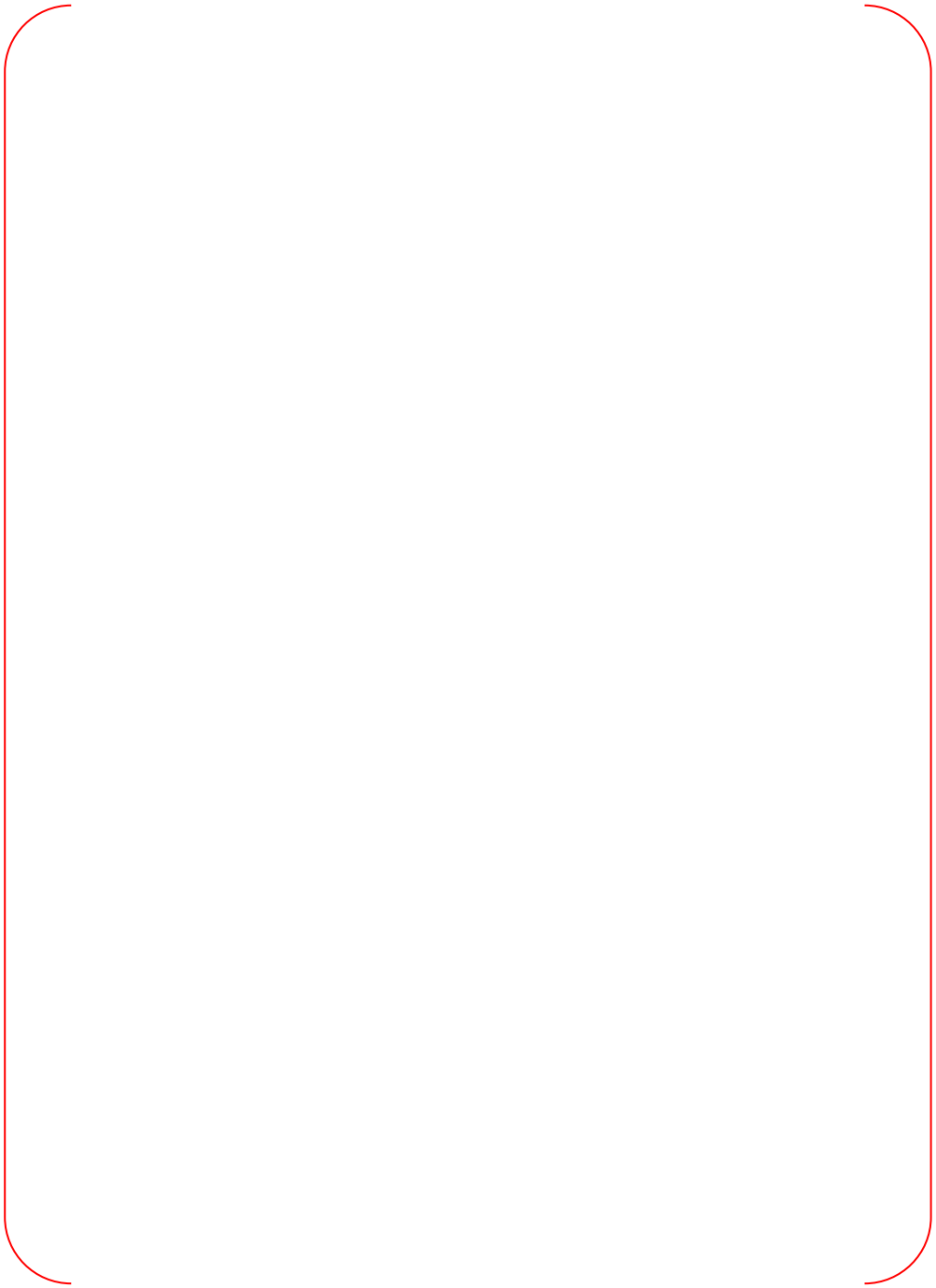

Figure 2-3 Non-Condensable Gas Release Behavior

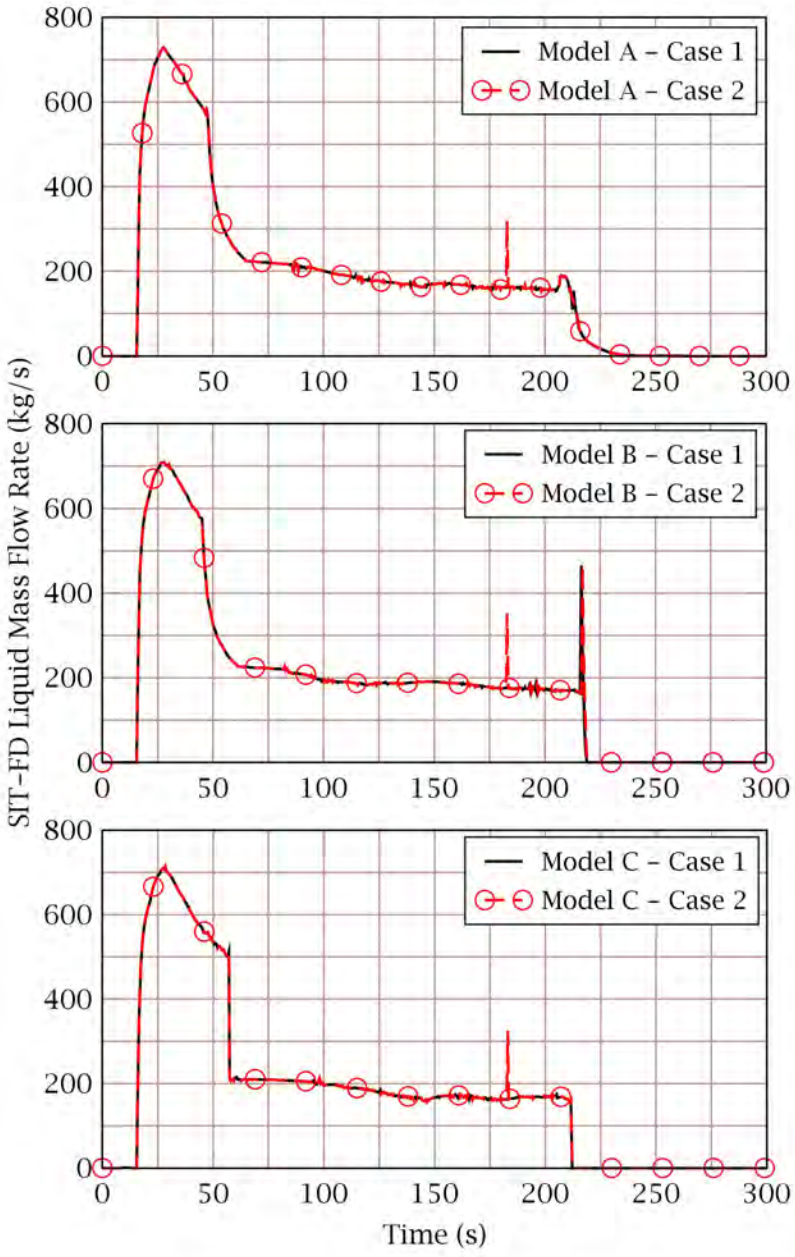

Figure 2-4 Water Injection Flow Rate from SIT-FD

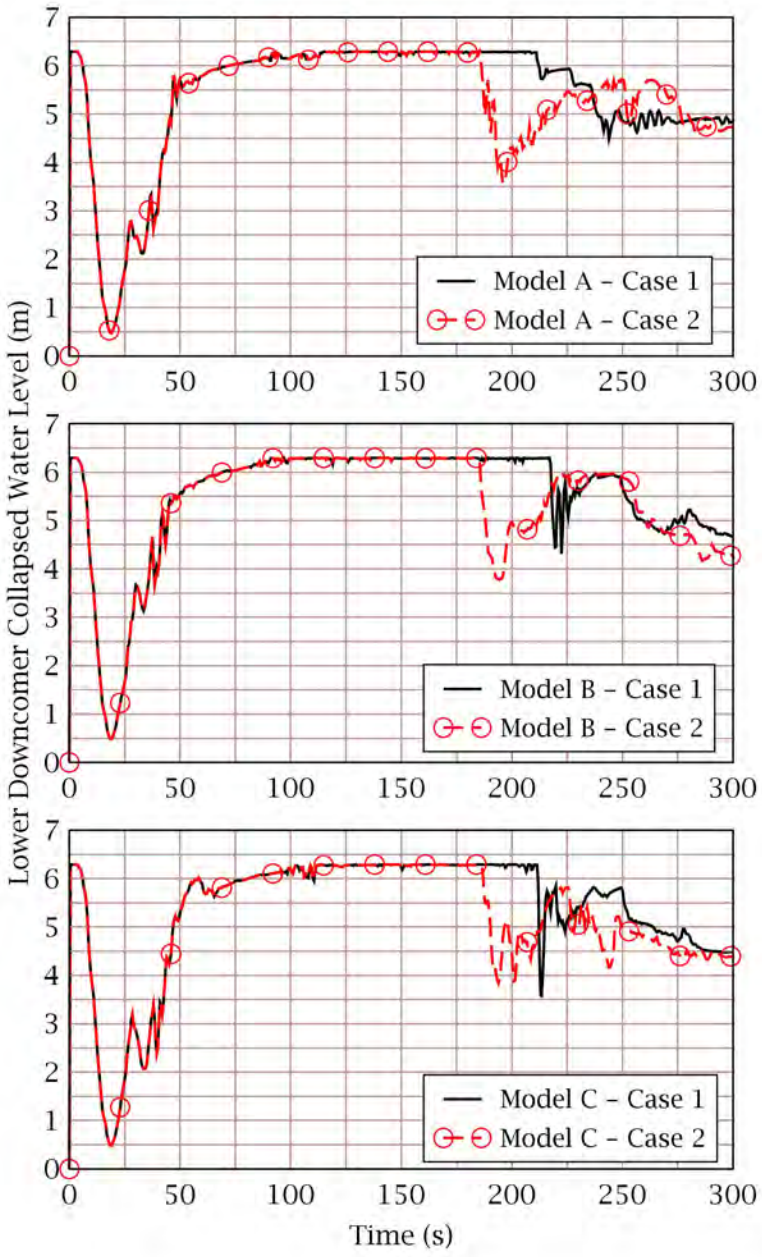

Figure 2-5 Lower Downcomer Collapsed Water Level

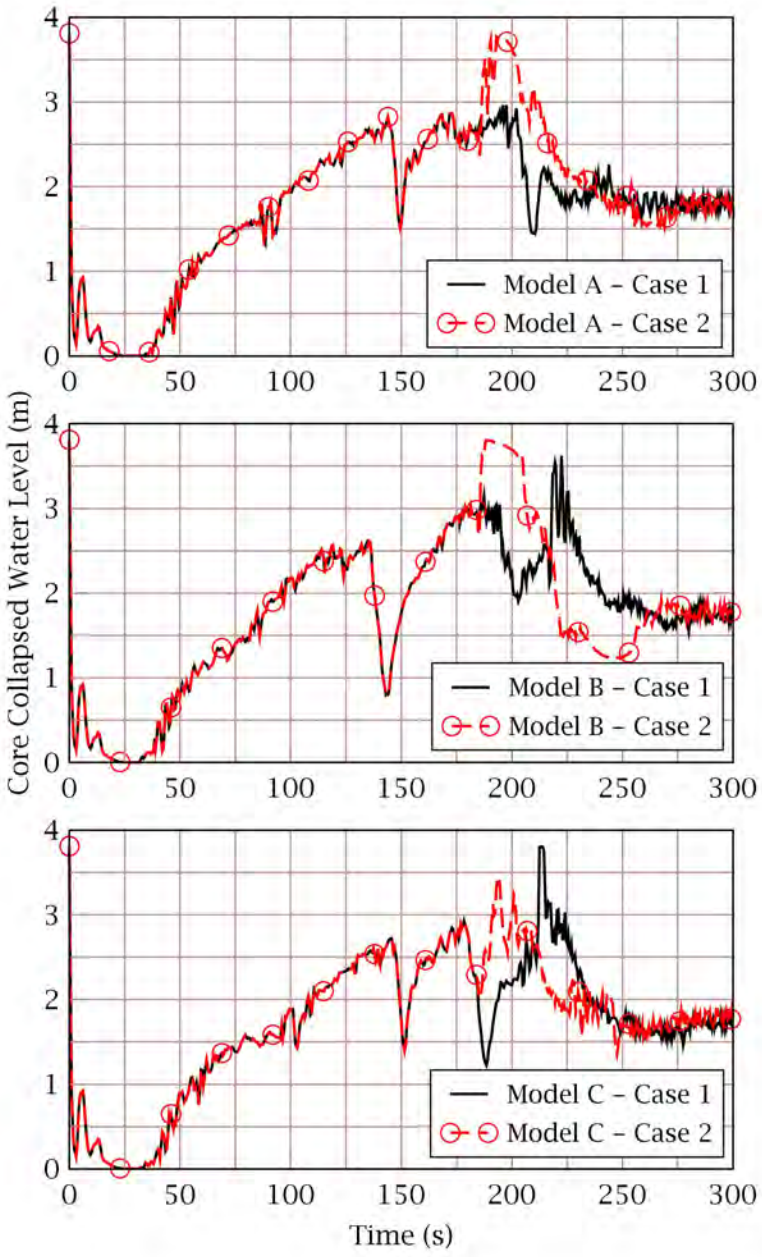

Figure 2-6 Core Collapsed Water Level

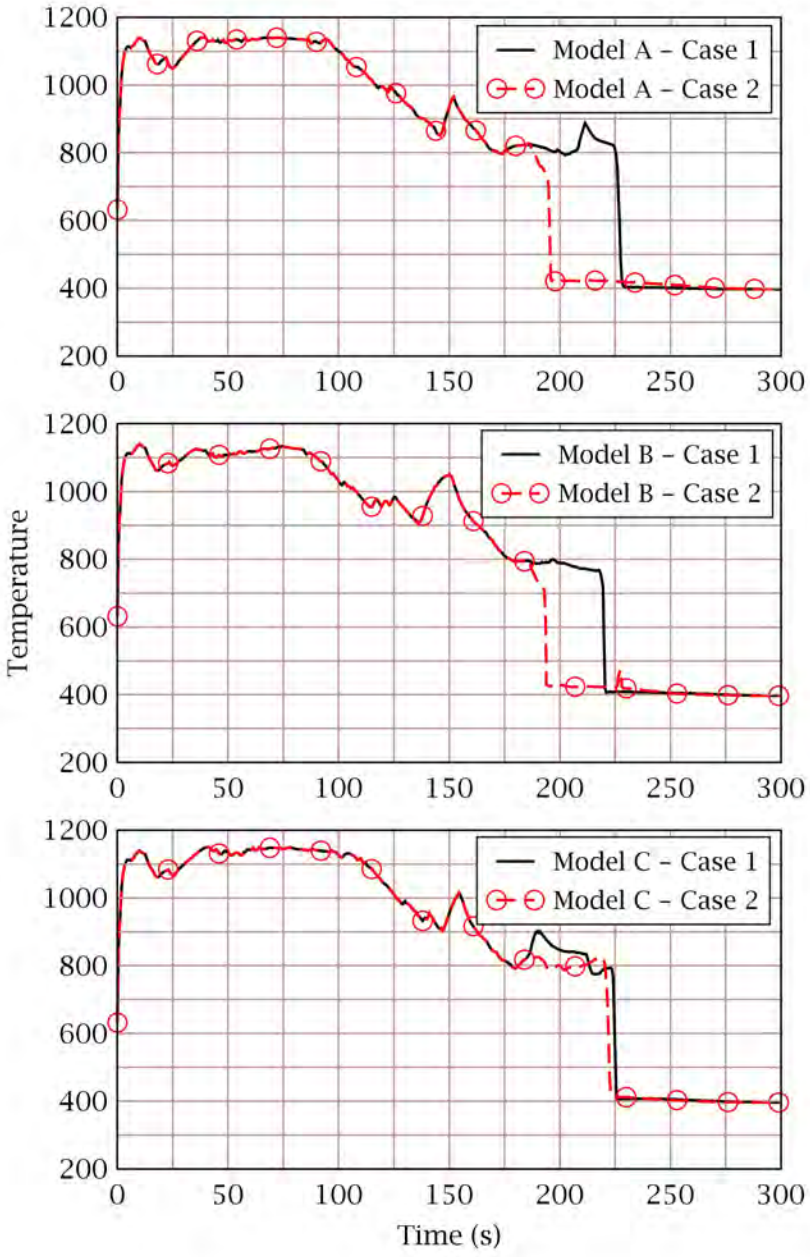

Figure 2-7 Rod Cladding Temperature at PCT Node

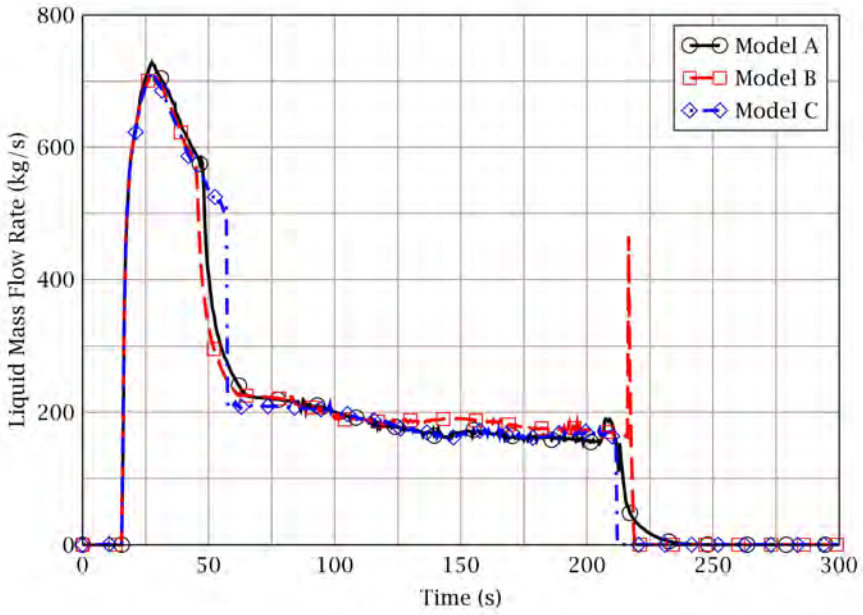

Figure 2-8 Water Injection Flow Rate

TS

Figure 2-9 Non-Condensable Gas Release Rate

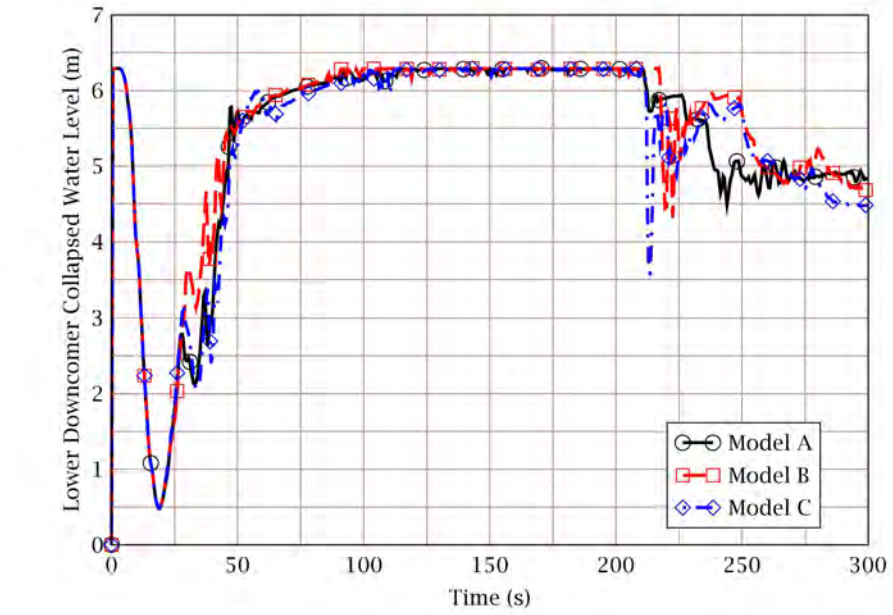

Figure 2-10 Lower Downcomer Collapsed Water Level

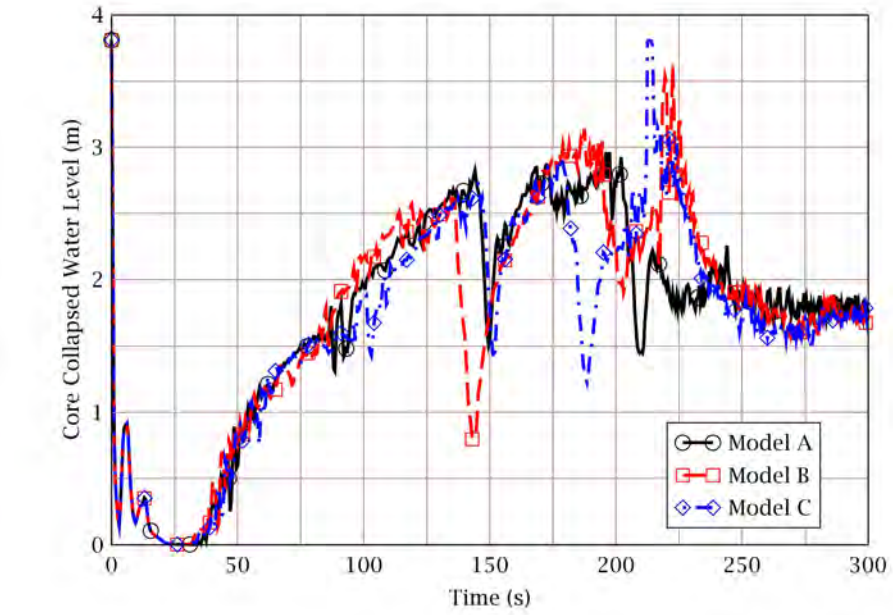

Figure 2-11 Core Collapsed Water Level

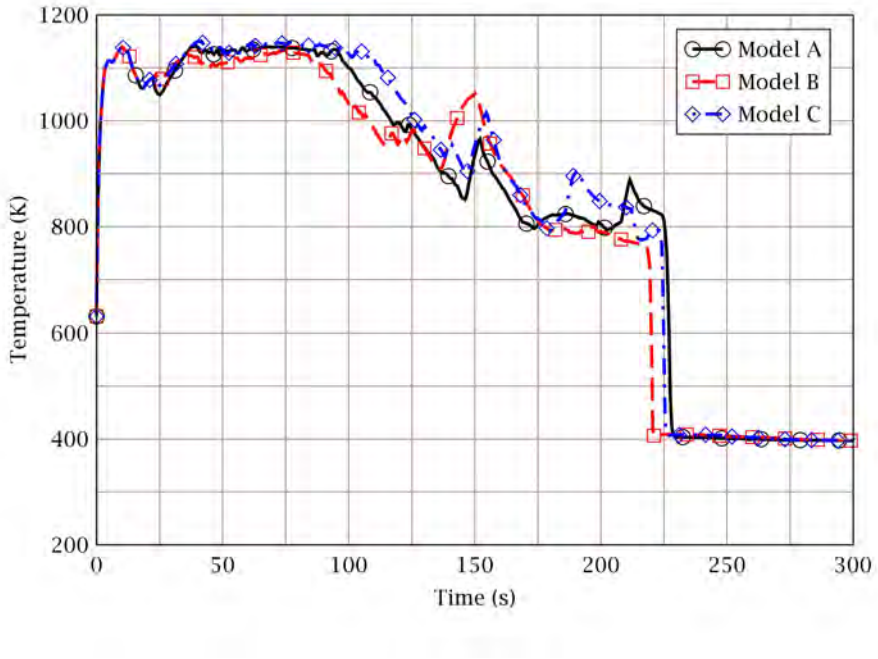

Figure 2-12 Rod Cladding Temperature of the Hottest Rod

3. Determination of the Limiting K-factors for Injection Flow

As described in the main body and Appendix A of this topical report; eight phenomena or processes are ranked as important for the SIT-FD. [

]TS

The uncertainty range for the K-factors of large and small flow delivery can be determined using the results of VAPER tests. [

]TS However, the liming K-factors were selected through the evaluation of the K-factors [

]TS

Because the limiting K-factors are selected within the ranges of the design requirements that cover the measured K-factors in VAPER tests, uncertainty in the peak cladding temperature due to the K-factors will be conservatively bounded in plant calculations.

The K-factor ranges of the design requirements are;

- 10 ~ 25 : for large flow injection period
- 80 ~ 120 : for small flow injection period

Table 3-1 shows the evaluation matrix for the K-factors. All possible combinations of two values among the mean, minimum, and maximum values of the K-factor ranges were considered in the matrix to simulate various large and small flow injections. Based on the matrix, five evaluation calculations were performed. The SIT-FD was simulated using Model C, which was selected as the final SIT-FD model for the APR1400 LBLOCA analysis. All other input models except K-factors are the same in the five calculations.

The liquid injection flow rates predicted by the five calculations are compared in Figure 3-1. The peak injection flow rates were approximately [ ]TS, respectively, when the minimum, nominal, and maximum K-factors were applied during the large flow injection period. In the cases of calculation with the maximum K-factor, the large flow injection period was approximately [ ]TS longer than in the minimum K-factor cases. The low injection flow rate was higher than in the other cases when the minimum K-factor was applied during the small flow injection period. The maximum difference in low injection flow rate is about [ ]TS For the calculations with the maximum K-factor during the small flow injection period, the injection duration was approximately [ ]TS longer than in the minimum K-factor cases. The total injection period was the longest when the maximum K-factors were applied in both large and small flow injection periods since the injection flow rate was lower than the other cases.

Figure 3-2 shows a comparison of the collapsed water level in the lower downcomer below the bottom of the cold leg. The collapsed water level was predicted to increase similarly in all cases. However, the collapsed water levels with the maximum K-factor for large flow injection increased relatively slower than the others, regardless of the K-factor value for small flow injection.

The liquid volume fraction of the lowest volume of the active core is shown in Figure 3-3 to compare the core reflooding time. The core reflooding time was very similar regardless of the K-factors. The maximum difference in core reflooding time was within 3 s.

Figure 3-4 shows the core collapsed water level. The results of all calculations showed a similar trend until 75 s after the break. After 75 s, however, there was no obvious trend in the core water level. This is due to the complex thermal-hydraulic phenomena that occur in the core. In all calculations, the downcomer collapsed water level reached near the cold leg elevation after 75 s, as shown in Figure 3-2. It can be inferred that the difference in the core water level behavior after 75 s was not caused by the difference in the SIT-FD injection flow rate because the downcomer water levels (i.e., a driving force to reflood the core) were very similar to each other after 75 s.

The cladding temperature behavior of the hottest rod is shown in Figure 3-5. The blowdown PCTs were the same in all calculations, because the blowdown PCTs occur before the initiation of SIT-FD injection. The variation of reflood PCTs was estimated as below 10 K, and the highest reflood PCT was predicted with the minimum K-factors for both of large and small flow injection periods.

As discussed above, the effect of injection flow rate variation according to K-factor on the system thermal hydraulic behavior is evaluated. Consequently, the minimum values of K-factor ranges for large and small flow injections were selected to use for the APR1400 LBLOCA analysis.

Table 3-1 K-factor Matrix for the Sensitivity Study

TS

TS

Figure 3-1 SIT-FD Liquid Injection Flow Rate

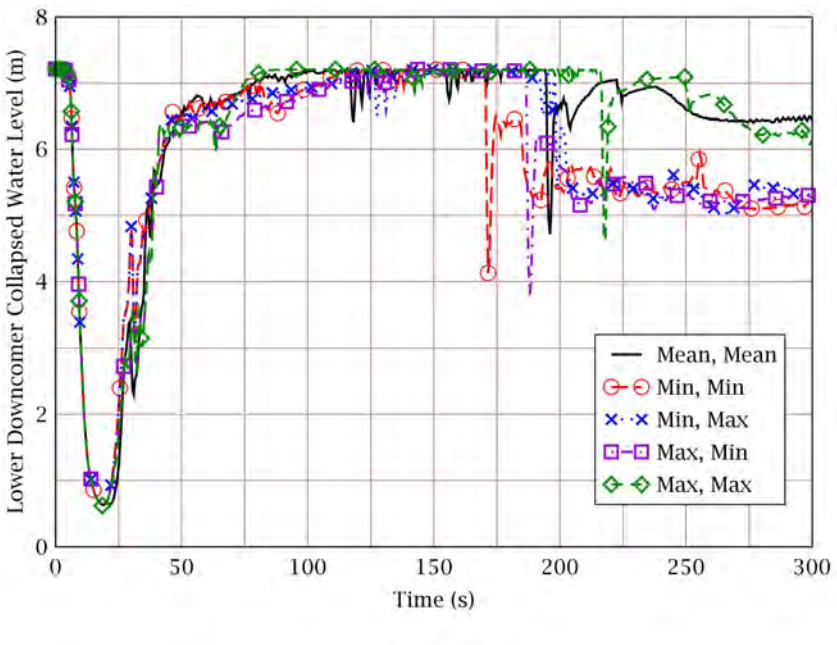

Figure 3-2 Lower Downcomer Collapsed Water Level

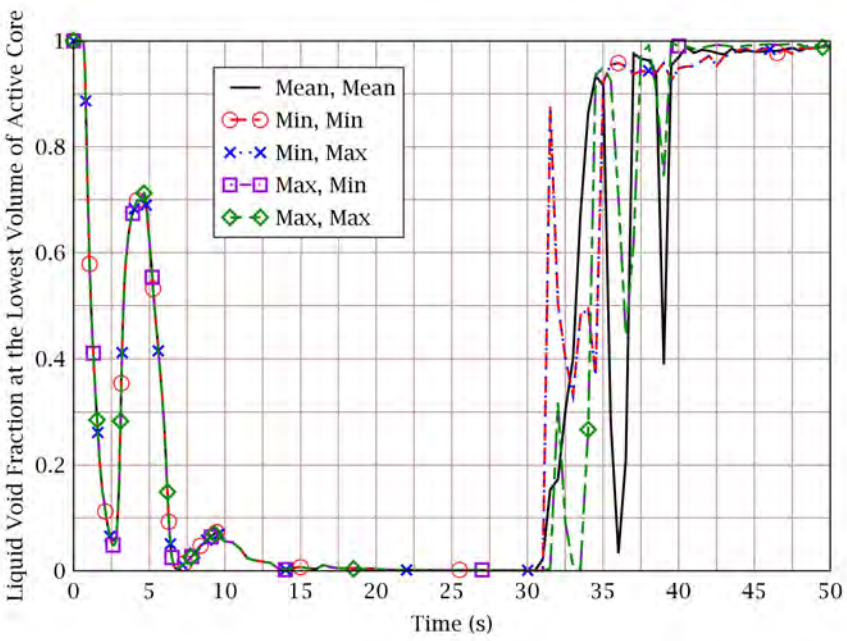

Figure 3-3 Liquid Volume Fraction of the Lowest Node of the Active Core

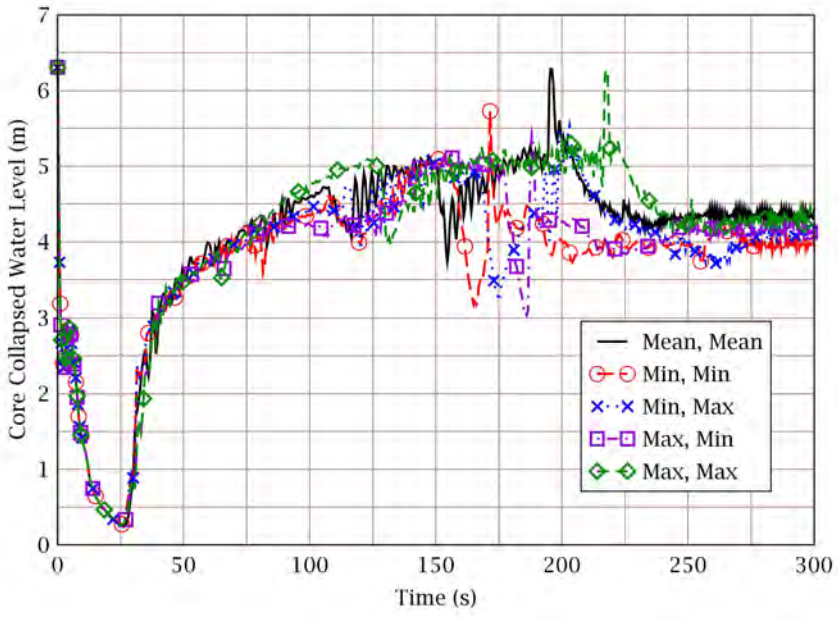

Figure 3-4 Core Collapsed Water Level

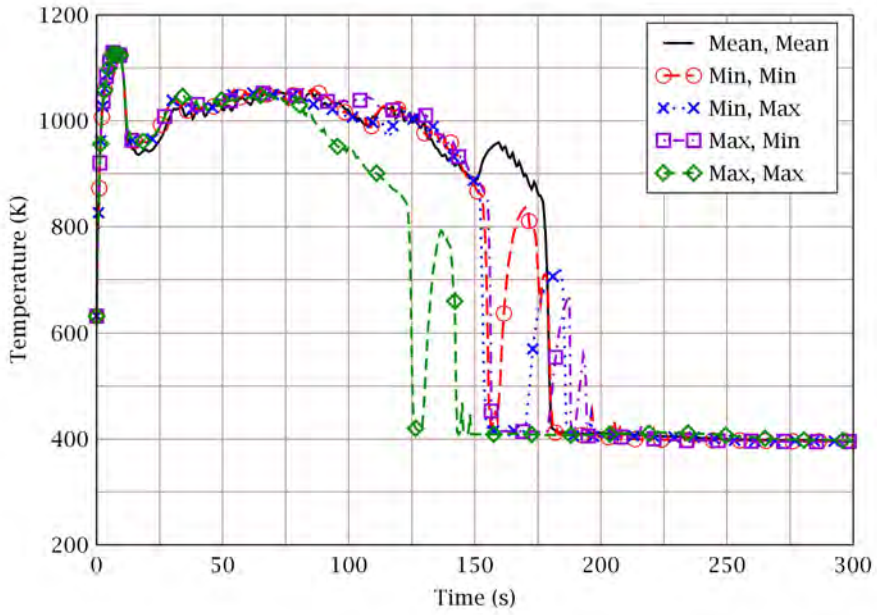

Figure 3-5 Rod Cladding Temperature

4. Conclusion

As new conceptual equipment, the fluidic device (FD), is adopted in APR1400, a new modeling method to simulate SIT-FD injection behavior is required for the APR1400 LBLOCA analysis. In this appendix, various models are suggested to determine the most appropriate SIT-FD model. The suggested models were assessed against the experiment data obtained from a full scale test facility, VAPER.

The predictive capability of the suggested models has been confirmed by comparing the calculated injection flow rate, tank water level, and pressure with the test data. [

]^{TS}

From the sensitivity study to select the SIT-FD model for APR1400 LBLOCA analysis, a simple SIT-FD model (Model C) was selected. [

]^{TS}

The representative K-factors for large and small flow injections were determined instead of quantifying the uncertainty of injection flow rates. The determined K-factors for APR1400 LBLOCA analyses are 10 and 80 for the large flow injection and the small flow injection, respectively. These representative K-factors are the minimum values of the K-factor ranges for large and small flow injection specified in the SIT-FD design requirements.

References

[1] KHNP, " Fluidic Device Design for the APR1400," APR1400-Z-M -TR-12003-P Rev.0, 2012.

[2] USNRC, "Quantifying Reactor Safety Margins; Application of Code Scaling, Applicability and Uncertainty Evaluation Methodology to a Large Break Loss of Coolant Accident," NUREG/CR-5249, October 1989.

[3] KAERI, "Fluidic Device Performance Test Using the VAPER Test Facility," VAPER-QLR-005-rev01, July 2004.

[4] "APR1400 Design Control Document Tier 2: Chapter 6 Engineered Safety Features," APR1400-K-FS-14002-NP, Rev 0, KEPCO & KHNP, December 2014.

APPENDIX I

Coupling RELAP5/MOD3.3/K and CONTEMPT4/MOD5

Non-Proprietary

August 2018

Abstract

As per regulatory guide 1.157 [1], the containment pressure used for evaluating cooling effectiveness during the post-blowdown phase of a loss of coolant accident (LOCA) should be calculated in a best-estimate manner and should include the effects of containment heat sinks and the effects of the operation of all pressure reducing equipment assumed to be available in a realistic LOCA analysis. However, the RELAP5/MOD3.3 code adopted in CAREM for the thermal-hydraulic calculation of the reactor coolant system does not have the capability to calculate the realistic behavior of containment pressure. Therefore, CAREM adopts the CONTEMPT4/MOD5 [2] code for a realistic calculation of containment pressure.

During a LOCA, the mass and energy discharged from the reactor coolant system govern thermal-hydraulic behaviors such as atmospheric pressure and containment temperature. Meanwhile, the containment pressure acts as the back-pressure of the reactor coolant system. In other words, the conditions of the reactor coolant system and the containment system act as boundary conditions to each other. Consequently, it is essential for a realistic calculation of a LOCA to calculate simultaneously the thermal-hydraulic behaviors of the reactor coolant system and the containment system considering information exchange between the two systems. Therefore, CONTEMPT4/MOD5 was coupled to RELAP5/MOD3.3 by utilizing the dynamic link library and CAREM uses this coupled code for a realistic calculation of a LOCA of the APR1400.

The containment pressure calculated using the coupled code showed good agreement with the pressure calculated through iterative calculations exchanging the results of the separate calculations of RELAP5/MOD3.3 and CONTEMPT4/MOD5. This appendix describes the details of the coupling of RELAP5/MOD3.3 and CONTEMPT4/MOD5 and the validation of the coupled code.

Table of Contents

List of Figures

1. Coupling of RELAP5/MOD3.3 and CONTEMPT4/MOD5

It is essential for a realistic calculation of a loss of coolant accident (LOCA) to calculate simultaneously the thermal-hydraulic behaviors of the reactor coolant system (RCS) and the containment system, considering information exchange between the two systems. However, the system code RELAP5/MOD3.3 adopted in CAREM does not have the capability to calculate the realistic behavior of containment pressure. Therefore, CAREM adopts the CONTEMPT4/MOD5 code for a realistic calculation of the containment pressure.

The RELAP5/MOD3.3 code was developed for best-estimate transient simulations of light water reactor coolant systems during postulated accidents. This code employs a two-fluid model to simulate the flow behavior of a two-phase steam-water mixture that can contain non-condensable components in the steam phase and/or a soluble component in the water phase. The two-fluid equations consist of the continuity, momentum, and energy equation for each phase. Constitutive relations are also incorporated for closure of the equations. These relations include state-of-the-art physical models for interfacial mass transfer, interfacial forces, liquid and vapor wall drag, wall and interfacial heat transfer, and the thermodynamic properties of water. The numerical solution scheme used in RELAP5/MOD3.3 is a semi-implicit scheme using a staggered grid and donor cell concept.

CONTEMPT4/MOD5 is a multi-compartment/multi-junction containment system analysis code. A compartment is divided into the vapor region and the liquid pool region. The vapor region is considered to be a homogeneous mixture of non-condensable gases and water in both the liquid and vapor state, while the liquid pool region is filled only with liquid phase of water. The inter-compartment junction flow is calculated by the nozzle model or the orifice model. The thermodynamic properties of mixture are calculated at the end of each time step. Vapor region mass and the energy of a compartment are affected by interactions with the liquid pool region, heat transfer through structures, leakage or flow via junctions, pressure suppression systems, safeguard systems such as fans and sprays, and tabular mass and energy additions inputted by the user. Basically an explicit numerical solution scheme is used, but an implicit scheme is partially used in the particular junctions at which flow oscillations are numerically induced.

Martin [3] coupled RELAP5 and CONTAIN using parallel processing via a parallel virtual machine (PVM) software. The Korea Atomic Energy Research Institute (KAERI) coupled the MARS system code and CONTEMPT4/MOD5/PCCS using the dynamic link library (DLL) technique [4] based on the previous experience of merging RELAP5 and CONTEMPT4/MOD5 into a unified version capable of simultaneous analysis for both RCS and containment systems by using the concept of process control in the UNIX system. Since CAREM adopts 124 simple random sampling calculations to quantify the uncertainty of the safety criteria, code execution on a WINDOWS PC system is more economical than using other systems. Therefore, CONTEMPT4/MOD5 was coupled to RELAP5/MOD3.3 by a very similar way with the coupling of MARS and CONTEMPT4 [4].

A dynamic link library is a collection of data, source, and object codes collected in the same manner as a static library. Data and code in a dynamic link library are loaded into the same address space as the data and code of the program that call them. However, variables and routines declared in the program and DLL are not shared unless one uses special complier directives for interfacing. These features enable the compiler and linker to map the correct portions of the address space so that the data and routines can be shared. The coupling of the two codes using DLL enables the coupled code to preserve the inherent features of each code, to maintain the integrity of each code independently, and to keep simpler coupled code structures. Only minor coding changes are necessary for data communications.

1.1 Configuration of the Coupled Code System

The configuration of the coupled code system is shown in Figure 2. The configuration of the coupled

code is quite similar with the MARS-CONTEMPT coupled code [4] because the backbone of the MARS code is RELAP5. RELAP5/MOD3.3 works as a main driver program while CONTEMPT4 works as associated routines. Because both codes have input processing and an initialization process using their own input and steam tables before the start of transient calculation, the CONTEMPT4 code is divided into three major parts to synchronize with the main driver, RELAP5/MOD3.3. Some additional modifications are necessary to share data with RELAP5/MOD3.3 using special compiler directives for interfacing. The Compaq Visual Fortran compiler was used to make the source code to control the dynamic link library with the interfacing routine names and arguments. All interfacing routines and variables of the CONTEMPT code were identified. The following Digital Visual Fortran statements are examples to specify interfacing routines;

TS

[

]TS

[

]TS

TS

1.2 Coupling with RELAP5/MOD3.3

Coupling with the RELAP5/MOD3.3 code is realized by calling the DLL routines at the appropriate calculation step. RELAP5/MOD3.3 calls the containment input process and initialization routines during the RELAP5/MOD3.3 input process and initialization process respectively. During the transient, the RELAP5/MOD3.3 calculation should be performed by sharing data with CONTEMPT DLL.

Because the numerical solution procedures of RELAP5/MOD3.3 and CONTEMPT4/MOD5 significantly differ from each other, as described above, implicit coupling is not appropriate and explicit coupling is much simpler than implicit coupling. Therefore, RELAP5/MOD3.3 and CONTEMPT4/MOD5 were coupled explicitly.

In the RELAP5/MOD3.3 code, [

]^{TS}. The CONTEMPT DLL routine calculates thermal properties such as total pressure, liquid and vapor enthalpy, quality, etc. of the vapor region of the compartment adjacent to the break. These properties are transferred to RELAP5/MOD3.3 through the interface module. RELAP5/MOD3.3 updates [

]^{TS}. The mass and energy discharge rates of the liquid, steam, and non-condensable gases calculated by RELAP5/MOD3.3 using the conditions of [

]^{TS} are transferred to the CONTEMPT routines through the interface routine. The overall scheme is shown in Figure 1.

CONTEMPT4/MOD5 provides for a variety of boundary conditions or intrinsic heat conduction correlations to solve heat transfer at heat conducting structures. The tabular form of the heat transfer coefficients, otherwise, can be inputted to solve heat conduction. During the blowdown period, the Tagami correlation is used to solve heat conduction. The Tagami correlation requires the total released energy during the blowdown period in order to calculate heat transfer coefficients. Therefore, CONTEMPT4 routines do not perform any calculations until the total released energy during the blowdown period is provided by RELAP5/MOD3.3. In other words, RELAP5/MOD3.3 performs calculation without the containment back-pressure information during the blowdown period. At the end of the blowdown period, the integrated total energy and mass and energy release rate calculated by RELAP5/MOD3.3 during the blowdown period are transferred to the CONTEMP5 routines to calculate containment pressure during the blowdown period. This approach is reasonable because the critical break flow, which is independent from the containment back-pressure, is assumed during the blowdown period. Since the end time of the blowdown period should be determined to follow this procedure, the end time of blowdown was defined as the reflood starting time determined by RELAP5/MOD3.3.

After the end time of blowdown, RELAP5/MOD3.3 and CONTEMPT4 perform their calculations in turns. Since the RELAP5/MOD3.3 time step is smaller than that of CONTEMPT4 in general, the two codes exchange their results at every RELAP5/MOD3.3 time step for finer calculations.

2. Verification of the Coupled Code

The verification of coupling was performed for the APR1400 LBLOCA transients. The input model of APR1400 is shown in Figure 2. The results of the calculations using the coupled code were compared with those of the iterative runs of each standalone code, RELAP5/MOD3.3 and CONTEMPT4/MOD5. The iterative calculations of the standalone codes were performed in the following manner:

1. perform APR1400 LBLOCA analysis using RELAP5/MOD3.3, with a constant containment back pressure simulated using the time-dependent volume component

2. perform the CONTEMPT4/MOD5 calculation using the tabulated discharged mass and energy discharge rates obtained from the RELAP5/MOD3.3 calculation of Step 1

3. perform the RELAP5/MOD3.3 calculation using the containment conditions obtained from the CONTEMPT4/MOD5 calculation of Step 2

4. repeat Step 2 and Step 3 until the containment pressure is converged

The containment pressure calculated using the coupled code is compared with the results of the iterative calculations using the standalone codes, RELAP5/MOD3.3 and CONTEMPT4/MOD5, in Figure 3. The constant containment pressure of 1.5 bar was used in the RELAP5/MOD3.3 calculation to acquire the mass and energy discharge rates for the first interactive calculation. As the iterative calculations are repeated, the calculated containment pressure becomes close to the result of the coupled code. After three iterative calculations, the calculated containment pressure becomes almost identical to the result of the coupled code.

The containment gas-phase temperature calculated using the coupled code is compared with the results of the iterative calculations in Figure 4. The gas-phase temperature becomes almost identical to the result of the coupled code calculation after three iterative calculations.

Accumulated break mass flow rates are compared in Figure 5. Before around 30 seconds, there are almost no differences among the results due to the critical flow phenomenon. After 30 seconds, the accumulated break mass flow of the iterative calculations becomes almost identical to the result of the coupled code calculation after three iterative calculations.

Based on the above results, it can conclude that the strategy and method of code coupling are validated.

3. Conclusion

CONTEMPT4/MOD5 was coupled to RELAP5/MOD3.3 by utilizing the dynamic link library (DLL) for a realistic calculation of containment pressure. These two codes were coupled explicitly to minimize code modifications and to preserve the inherent features of each code. RELAP5/MOD3.3 works as a main driver program while CONTEMPT4 works as associated routines.

The RELAP5/MOD3.3 code simulates the containment as [ ]^{TS} connected to the break(s), and the CONTEMPT DLL routine calculates the thermal properties of the vapor region of the compartment adjacent to the break. The results of the main driver RELAP5/MOD3.3 and the CONTEMPT DLL routine are exchanged through the interface routine to update boundary conditions or the heat source/sink.

The verification of the coupling was performed by comparing the results of the coupled code and the iterative calculations using the standalone codes. The results of the iterative calculation using the RELAP5/MOD3.3 and CONTEMPT4/MOD5 codes were converged to the results of the coupled code, showing the validity of the coupling strategy and method.

TS

Figure 1 Configuration of the Merged Code System

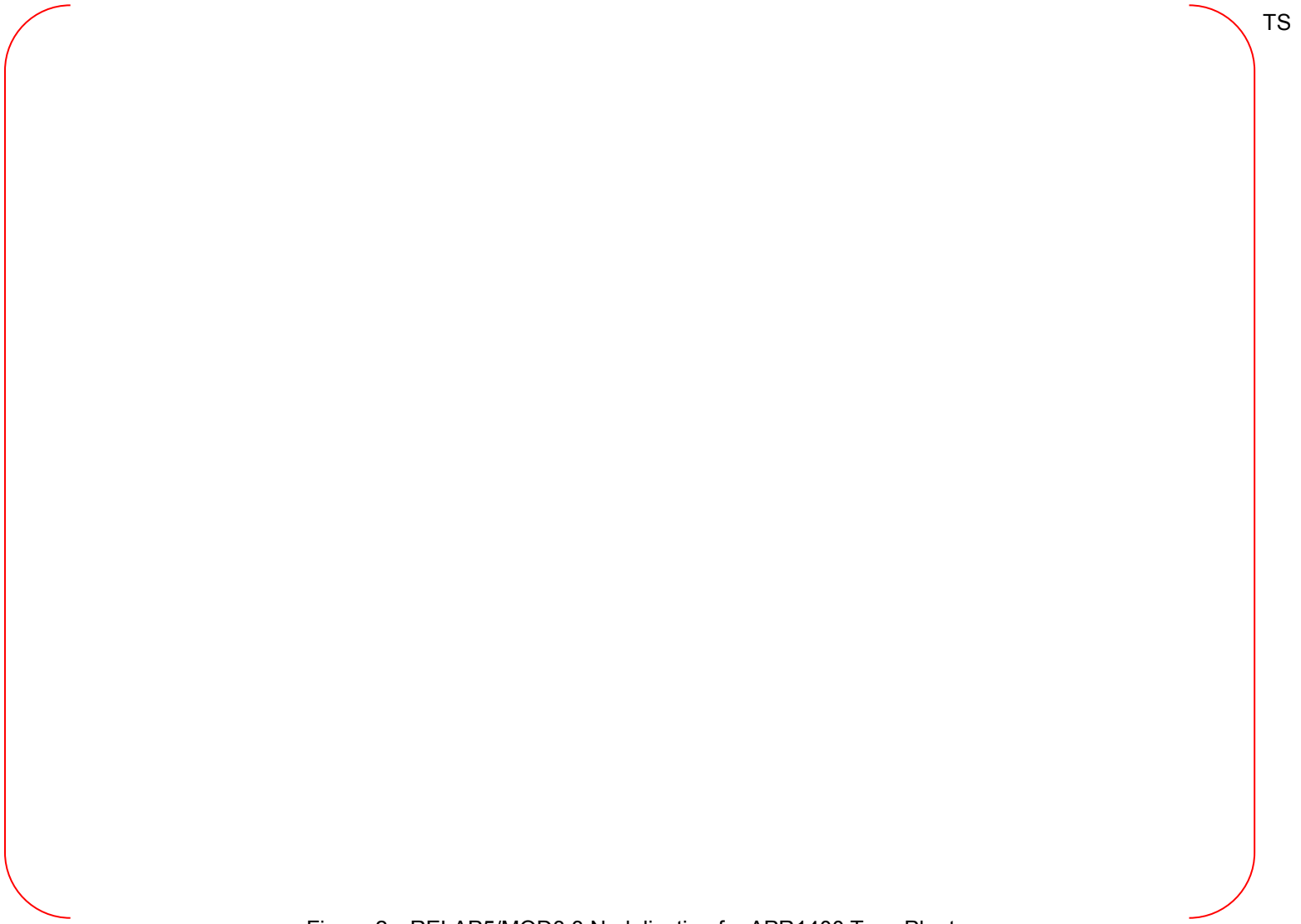

Figure 2 RELAP5/MOD3.3 Nodalization for APR1400 Type Plants

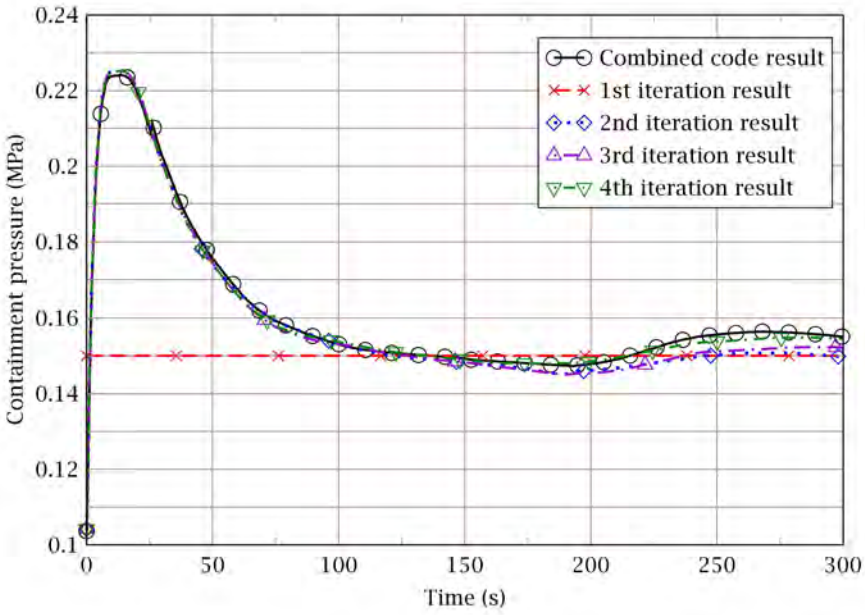

Figure 3 Comparison of Containment Pressure Results

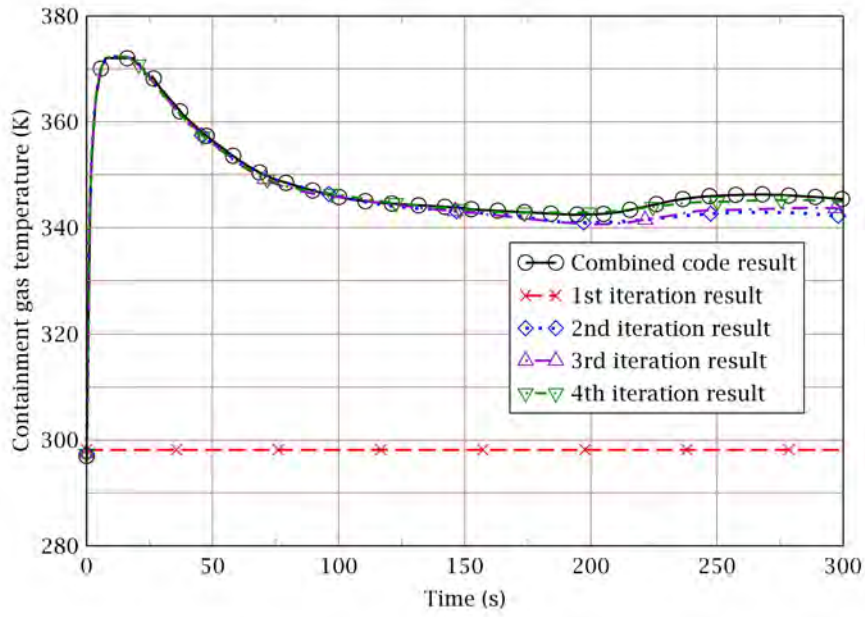

Figure 4 Comparison of Containment Gas Temperature Results

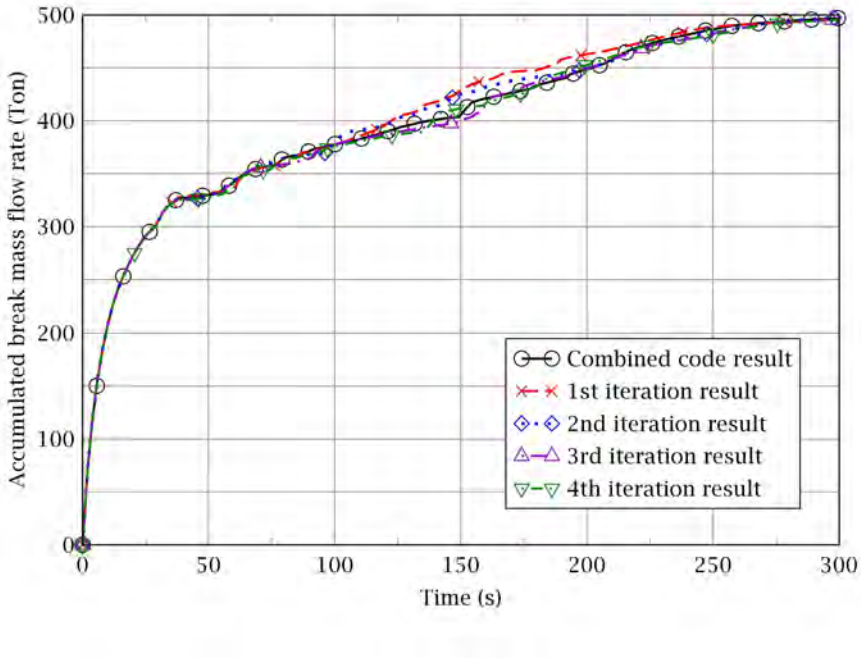

Figure 5 Comparison of Accumulated Break Mass Flow Rate Results

References

[1] "Best-estimate Calculations of Emergency Core Cooling System Performance," Regulatory Guide 1.157, U.S. Nuclear Regulatory Commission, 1989.

[2] "CONTEMPT4/MOD5: An Improvement to CONTEMPT4/MOD4 Multi-compartment containment System Analysis Program for Ice Containment Analysis," NUREG/CR-4001, BNL-NUREG-51894, Brookhaven National Laboratory, 1984.

[3] "RELAP5/CONTAIN Coupling," RELAP5 International Users Seminar, R.P. Martin, Idaho Falls, 1993.

[4] "MARS 1.3 System Analysis Code Coupling with CONTEMPT4/MOD5/PCCS Containment Analysis Code using Dynamic Link Library," Proceedings of the Korean Nuclear Society Autumn Meeting, Bub Dong Chung, et al., 1998.

Appendix J

Sampled Uncertainty Parameter Values for 181 Plant Calculations

Non-Proprietary

August 2018

1

TS

title - skn 3/4 krem topical report

variable	distribution	range	label	TS

TS

TS

TS

TS

TS

TS

TS

TS

TS

TS

TS

TS

TS

TS

TS

TS

TS

TS

TS

TS

TS

TS

TS

TS

TS

TS

TS

TS

TS

TS

TS

TS

TS

APPENDIX K

Break and Burnup Sensitivity Study

Non-Proprietary

August 2018

Table of Contents

List of Tables

List of Figures

1. Introduction

The limiting break location, type, and size are determined by break spectrum analysis. In addition, the limiting pressurizer location as well as burnup is determined by sensitivity study. This appendix describes above sensitivity studies and their results.

The break locations of hot leg, cold leg, and pump suction leg are considered, and the break types of double-ended guillotine (DEG) and slot are considered. In addition, the pressurizer locations of intact and broken loops are evaluated. Finally, the break sizes with selected burnup cases are evaluated. Above sensitivities are performed step by step, thus, the limiting break case and burnup are determined based on the results of the final step.

A burnup sensitivity is performed to consider UO_2 fuel pellet thermal conductivity degradation (TCD) effects. [ ]^{TS} are selected based on the radial fall-off (RFO) curve data described in reference [1]. The RFO curve data are relative values by the maximum value and a unit value is maintained until [ ]^{TS}. And then RFO curve data decreases with burnup increases gradually. Thus, burnup cases are selected mainly around the burnup of [ ]^{TS}. In the case of break size, the break sizes of 100, 80, and 60 % of pipe area are considered.

The burnup and break size sensitivity are evaluated [ ]^{TS}. Thus, [ ]^{TS}. Total [ ]^{TS} cases are evaluated and the case which has the highest PCT is determined as the limiting break size and burnup.

2. Break Spectrum with Burnup Sensitivity

A sensitivity case which has the highest PCT is determined as the limiting case in this break spectrum with burnup sensitivity. The break spectrum with burnup sensitivity is performed by following steps:

1. Break Location Sensitivity
   - The break locations of hot leg, cold leg, and pump suction leg are evaluated in order to determine the limiting break location.
2. Break Type Sensitivity
   - In order to determine the limiting break type, the break types of DEG and slot breaks are evaluated at the limiting break location determined in step 1.
3. Pressurizer Location Sensitivity
   - The limiting location of pressurizer is determined by considering pressurizer location in intact loop and broken loop based on the result of step 1 and 2.
4. Break Size and Burnup Sensitivity
   - At the limiting conditions determined in step 1 through 3, the break sizes of 100, 80, and 60 % of pipe area are evaluated for all selected burnup cases in order to determine the limiting break size and burnup.

The limiting break configuration and burnup determined through the above sensitivity studies are applied to the simple random sampling (SRS) calculations.

Section 2.1 through 2.3 describes the break location, type, and pressurizer location sensitivities. Section 2.4 describes the selection of target burnups, initialization methods, and results for burnup sensitivity.

2.1 Break Location Sensitivity Study

The break locations of hot leg, cold leg, and pump suction leg are considered for this sensitivity. The nominal case is used as the base case. All input values are the same in three calculations except for break location.

Figure 1 and Figure 2 show the noding of break region in case of hot leg break and pump suction leg break, respectively. The break noding for cold leg break is shown in Figure 4-1 of this topial report.

Figure 3 compares the results of cladding temperatures calculated at three different break locations. The cold leg break shows the highest PCT and is determined as the limiting break location. [

]^{TS}.

The break location sensitivity within [

]^{TS}.

2.2 Break Type Sensitivity Study

The DEG and slot breaks in cold leg are considered to determine the limiting break type. Figure 4 shows a noding diagram for slot break, and Figure 5 shows the calculation results. The blowdown PCTs of both cases are almost the same, whereas the reflood PCT of DEG break is higher than that of slot break. Therefore, DEG in cold leg is determined as the limiting break type.

2.3 Location of Pressurizer Sensitivity Study

In order to determine the limiting location of a pressurizer, two cases were studied; 1) pressurizer is connected to the hot leg volume number 310 in the intact loop, 2) pressurizer is connected to the hot leg volume number 410 in the broken loop. Even there is no significant differences in cladding temperature during the blowdown period, the reflood PCT of case 1 (pressurizer in the intact loop) is higher than that of case 2, as shown in Figure 6. Therefore, the pressurizer is determined to be located at the intact loop.

2.4 Break Size and Burnup Sensitivity Study

This section describes the sensitivity study to determine the limiting break size and burnup at the limiting conditions obtained in the above sensitivity studies.

2.4.1 Selection of Target Burnups and Break Sizes

The sensitivity target burnups of the hot rod and hot assembly heat structures are selected based on the radial fall-off (RFO) data described in reference [1] in order to consider TCD effects. For this sensitivity study, the [ ]^{TS} of reference [1] is used. Table 1 compares [ ]^{TS}. As shown in Table 1, the RFO data are relative values by the maximum value and a unit value is maintained until [ ]^{TS}. And then the RFO data decreases with burnup increases gradually. Thus, target burnups need to be selected at around the [ ]^{TS} where PCT is expected to occur. In this sensitivity study, total nine burnups shown in Table 1 are selected for hot rod and hot assembly heat structures.

For the average rod heat structure burnup, the core average burnup of [ ]^{TS} is assumed. It is because [

]^{TS}.

In case of break size, the break sizes of 100, 80, and 60 % of pipe area are considered.

2.4.2 Initialization of Fuel Rod Heat Structures

The initial conditions of fuel rods in RELAP5 are modeled using the FATES-3B results with TCD penalty, hereafter, referred to as “fuel rod interface data”. The details of fuel rod interface data are described in reference [1]. The fuel rod conditions in RELAP5 steady state are initialized using the following procedure to match the fuel rod interface data;

Step 1 Burnup dependent fuel rod input models for RELAP5 steady state calculations are prepared using the fuel rod interface data.

Step 2 RELAP5 steady state calculatios are performed using the input models obtained from Step 1.

Step 3 [ ]^{TS}

[ ]TS

Figure 7 through Figure 16 show the comparison of gap width between the calculated values through the above iterative procedure and the interface data at selected burnups. In these figures, zero gap width means that fuel pellet contacts with cladding inner surface. [ ]TS The burnup of average rods is [ ]TS. It is concluded that the calculated gap width data predict well the interface data, since the differences are relatively small.

Figure 17 through Figure 26 show the comparison of the FCTs between the calculated and interface data at selected burnups. The calculated FCTs are close to or higher than the interface data. The calculated FCTs of average rods are [ ]TS because of the same reason described in gap width case.

2.4.3 Determination of the Limiting Break Size and Burnup

The sensitivity study is performed using three break sizes of 100, 80, and 60 % of cold leg area and nine burnups selected in Section 2.4.1. Table 2 shows the results of [ ]TS and the highest PCT occurs at the break size of 100 % and the burnup of 27,000 MWd/MTU.

Consequently, the limiting break size and burnup are determined as 100 % of cold leg area and 27,000 MWd/MTU burnup.

3. Input Preparation for SRS Calculations

The initialization of fuel rod heat structures can be achieved for each case of 181 SRS calculations by processing iterative steps described in Section 2.4.2. The [ ]TS using polynomial curve fitting line, however, is applied to 181 SRS calculations for effective RELAP5 runs.

3.1 Determination of Polynomial Curve Fitting Line

The polynomial curve fitting line is determined using the [ ]TS in Section 2.4.2. The same polynomial curve fitting line is used for the both of hot rod and hot assembly heat structures. The polynomial curve fitting line for average rods is obtained separately based on the [ ]TS. The second order polynomial curve fitting lines are obtained as shown in Figure 27 and Figure 28, and equations are follows.

[ ]TS

If roughness input value calculated by above equations has [ ]TS.

3.2 Applicability of Polynomial Curve Fitting Line

The applicability of the polynomial curve fitting line obtained in Section 3.1 is confirmed by comparing the steady state calculation results of SRS calculations with FCTs of the fuel rod interface data. [

]TS

Based on the above iterative procedure, the distribution of the calculated FCTs are adjusted to be located around or higher than those of fuel rod interface data.

Figure 29 and Figure 30 show the comparisons of calculated FCTs in steady state 181 SRS calculations and the interface data for hot rod and average rods, respectively. In case of hot rod, [ ]TS. And it is concluded that conservative FCTs are predicted because [ ]TS. The calculated FCTs of average rods also show conservative results. Therefore, it can be concluded that the polynomial curve fitting lines are applicable for LBLOCA analysis.

4. Conclusion

The limiting break location, type, and pressurizer location are determined by break sensitivity studies. In addition, the limiting burnup and size are determined by sensitivity study with considering TCD effects. This appendix describes above sensitivity studies and their results.

The DEG break at cold leg with the pressurizer location in intact loop is determined as the limiting break configuration. For the burnup and break size sensitivity study using the limiting break configuration, total [ ]^{TS} are evaluated and the highest PCT is occurred at the break size of 100 % cold leg area and the burnup of 27,000 MWd/MTU.

Consequently, the 100 % of DEG break at cold leg with 27,000 MWd/MTU are determined as the limiting break and burnup which will be applied to 181 SRS calculations.

Table 1 Selected Burnup Cases and RFO Data

TS

Note: RFO data are relative values by the maximum value.

Table 2 Results of Break Size and Burnup Sensitivity

TS

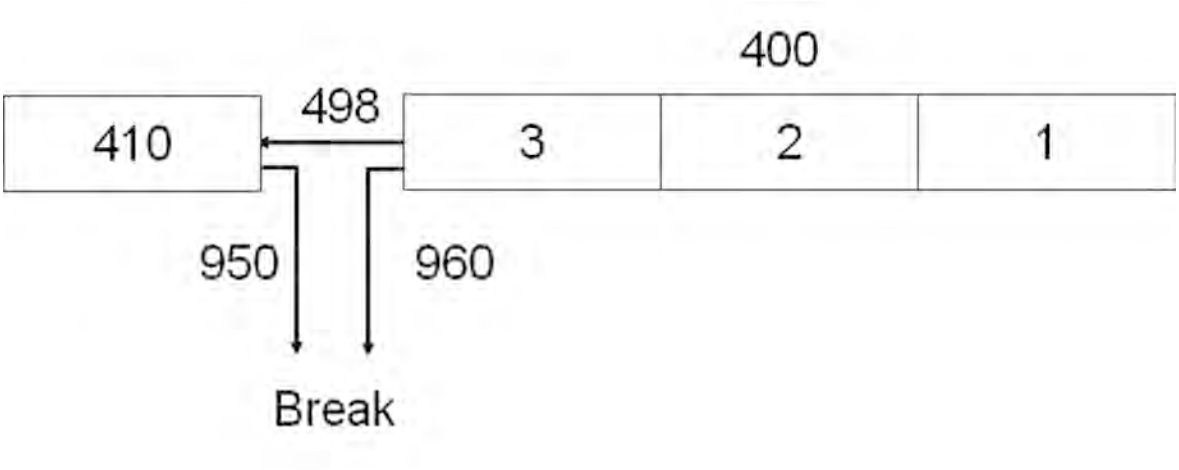

Figure 1 Noding Diagram for Hot Leg Break

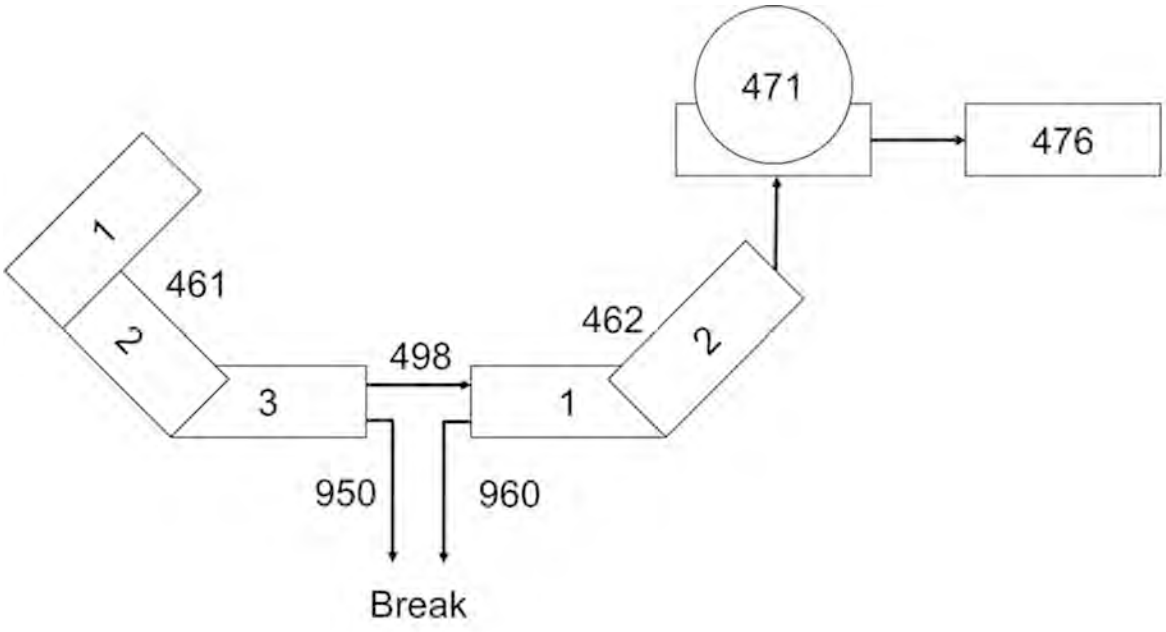

Figure 2 Noding Diagram for Pump Suction Leg Break

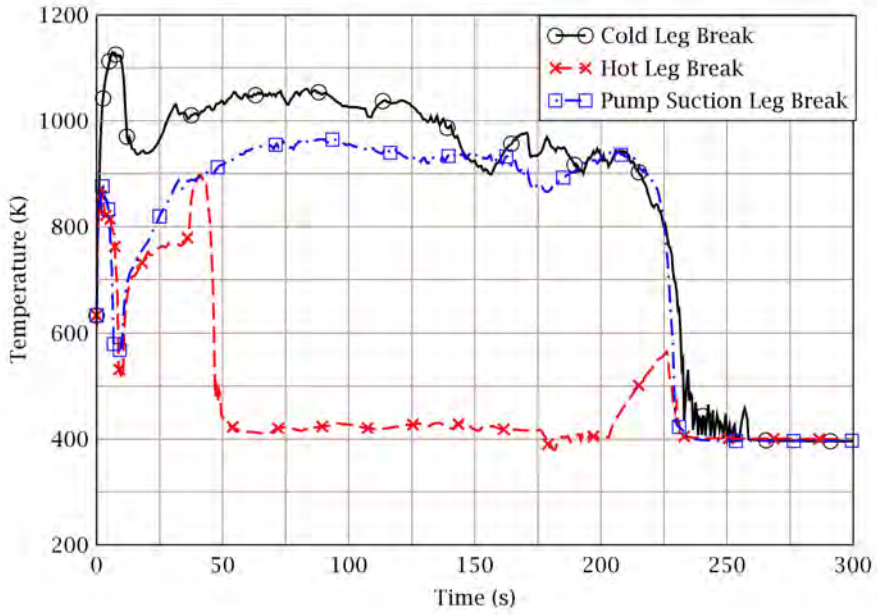

Figure 3 Cladding Temperature Results of Break Location Sensitivity

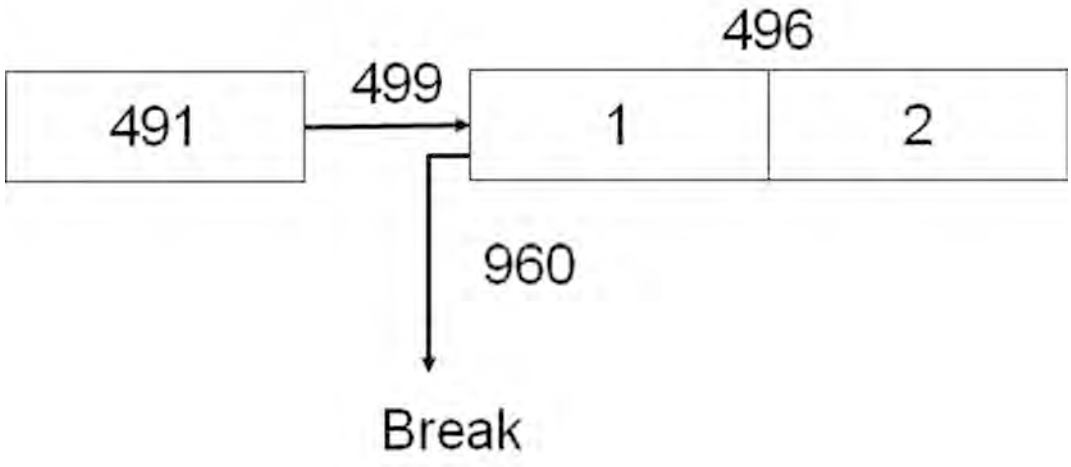

Figure 4 Noding Diagram for Slot Break

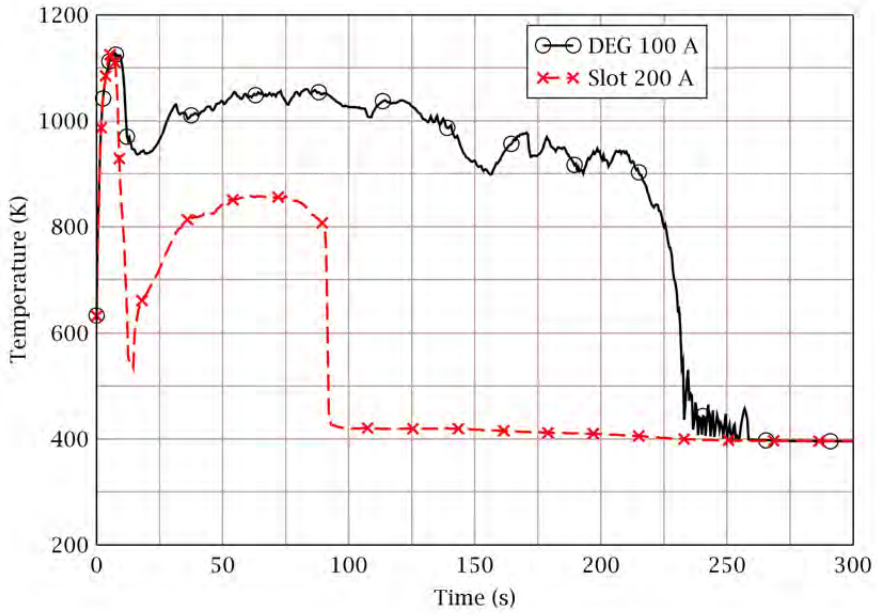

Figure 5 Cladding Temperature Results of Break Type Sensitivity

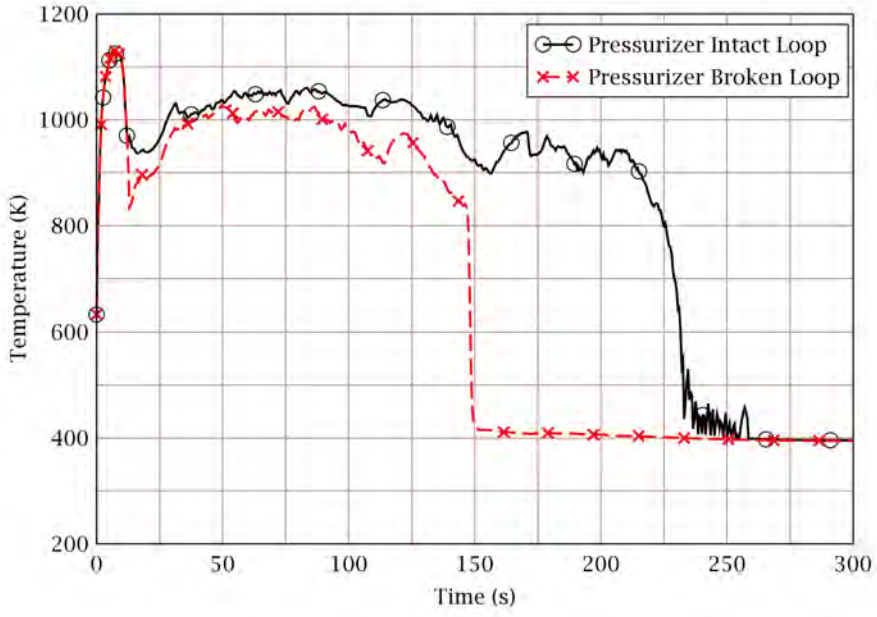

Figure 6 Cladding Temperature Results of Pressurizer Location Sensitivity

TS

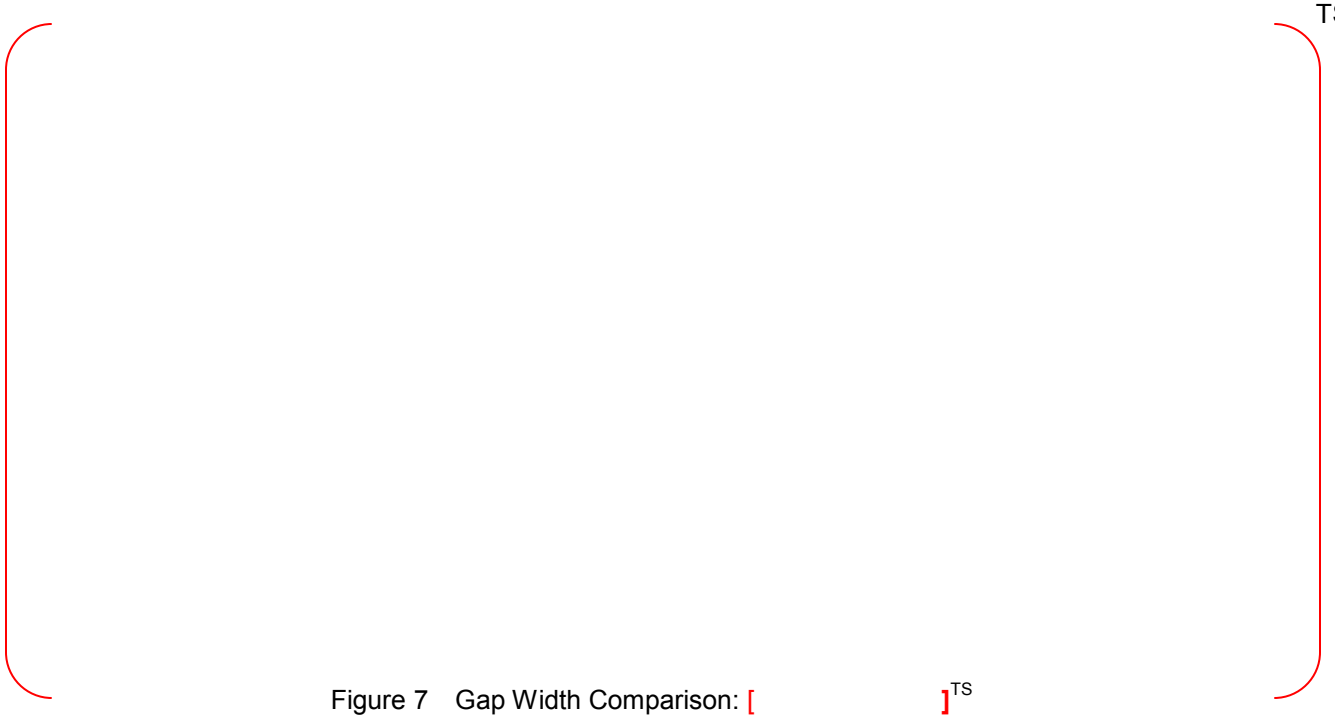

Figure 7 Gap Width Comparison: [ ]TS

TS

Figure 8 Gap Width Comparison: [ ]TS

TS

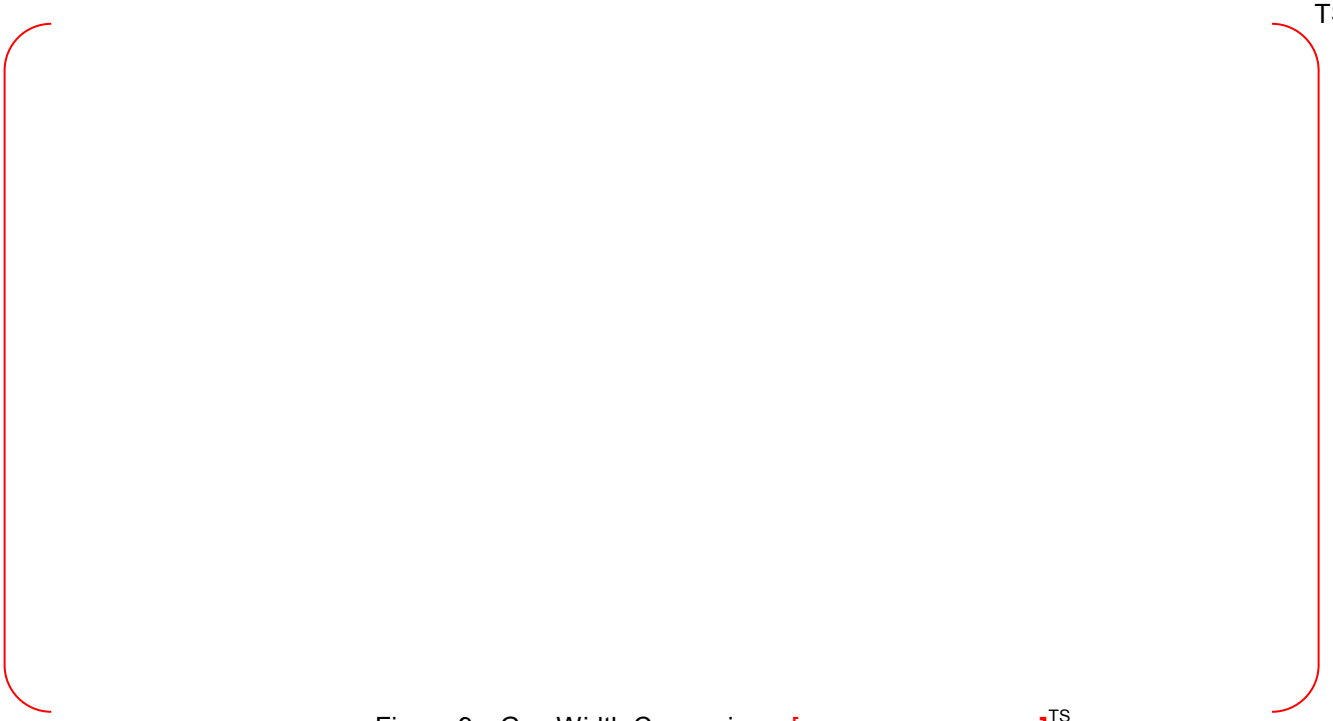

Figure 9 Gap Width Comparison: [ ]TS

TS

Figure 10 Gap Width Comparison: [ ]TS

TS

Figure 11 Gap Width Comparison: [ ]TS

TS

Figure 12 Gap Width Comparison: [ ]TS

TS

Figure 13 Gap Width Comparison: [ ]TS

TS

Figure 14 Gap Width Comparison: [ ]TS

TS

Figure 15 Gap Width Comparison: [ ]TS

TS

Figure 16 Gap Width Comparison for Average Rods: [ ]TS

TS

Figure 17 FCT Comparison: [ ]TS

TS

Figure 18 FCT Comparison: [ ]TS

TS

Figure 19 FCT Comparison: [ ]TS

TS

Figure 20 FCT Comparison: [ ]TS

TS

Figure 21 FCT Comparison: [ ]TS

TS

Figure 22 FCT Comparison: [ ]TS

TS

Figure 23 FCT Comparison: [ ]TS

TS

Figure 24 FCT Comparison: [ ]TS

TS

Figure 25 FCT Comparison: [ ]TS

TS

Figure 26 FCT Comparison for Average Rods: [ ]TS

TS

Figure 27 Approximated Polynomial Curve Fitting Line for Hot Rods

TS

Figure 28 Approximated Polynomial Curve Fitting Line for Average Rods

TS

Figure 29 FCTs of Steady State SRS Calculation for Hot Rod

TS

Figure 30 FCTs of Steady State SRS Calculation for Average Rods

References

[1] Topical Report, "PLUS7 Fuel Design for the APR1400," APR1400-F-M-TR-13001-P-A, August 2018.

Page intentionally left blank